University of Salford MANCHESTER

Mitigation of Gas and Vapour Cloud Explosions using Fine Water Sprays

Volume I of III

By

Stephen Andrew Johnston, M.Sc. MIGEM

Submitted in accordance with the requirements for the degree of Doctor of Philosophy

Department of Gas and Petroleum Engineering

School of Computing, Science and Engineering

University of Salford

February 2015

CONTENTS

CHAPTER 3

LITERATURE REVIEW : FUNDAMENTALS AND UTILISATION OF FINE SPRAYS IN EXPLOSION MITIGATION

CHAPTER 4

APPARATUS, PROCEDURES AND METHODS OF DATA PROCESSING

CHAPTER 5

RESULTS AND DISCUSSIONS

CHAPTER 6

VALIDATION OF COMPUTATIONAL FLUID DYNAMICS (CFD) AND SUITABILITY FOR USE AS A FUTURE DESIGN TOOL

CHAPTER 7

CONCLUSIONS AND RECOMMENDATIONS

Accompanying CD Volume (VOLUME III)

LIST OF FIGURES

Chapter 2

Chapter 3

Chapter 4

Chapter 5

Chapter 6

Chapter 7

LIST OF TABLES

Chapter 2

Chapter 3

Chapter 4

Chapter 5

Chapter 6

LIST OF EQUATIONS

Chapter 2

Chapter 3

Chapter 4

Chapter 5

Chapter 6

DEDICATED TO MY FAMILY

I would like to thank all of my amazing family for all of their tremendous support and understanding. My absence from several family occasions and events was also required to finally complete this thesis, and for this I am truly thankful for your tolerance and encouragement.

To Kristina, Emma and Sophie, my three beautiful daughters, I am so proud of the women that you have become and love you with all of my heart and can't wait to share your future happiness with you.

To my wife Lucia, your endless love, reassurance and total backing throughout this program has given me the inspiration and commitment to finally complete this research. Not only have you been beside me (literally) during the many hours of proof reading, but you have been alongside me as my devoted 'other half' for the past thirty something years.

Thank you.

ACKNOWLEDGEMENTS

It would not have me possible to complete this Doctoral thesis without support of several colleagues, that I am proud to also call friends.

Firstly, to my core supervisor Professor G.G. Nasr, for his passion and dedication to research, which is reinforced by his many wealthy years of industry experience and innovation. Thank you for the encouraging texts, emails and sound bites of advice (or Ghasemism's) received, often during the weekend and frequently late in the evening. Your students, the department, the University and Industry owe a great deal of gratitude to your knowledge and devotion.

I would also like to thank several people in Professor G.G. Nasr's team, including, Dr. Martin Burby for his knowledge, advice and guidance on CFD analysis and PDA techniques, also Dr Amir Nourian for his experience in spray imaging.

From industry, I would like to thank Gary Tomlin and his team from G.L Noble Denton for access to FLACS CFD software, to some previous research papers and for the kind invitation to attend the Vapour Cloud Explosion course and simulations at their Spadeadam test centre.

Finally, I would like to thank my work colleague Keith Rimmer for introducing me to macro's, one of the 'I.T. brigades' little secret weapons that helped with the repetitive processing of data and imagery.

Thank you colleagues and friends.

DECLARATION

"**I STEPHEN ANDREW JOHNSTON**, declare that this thesis is submitted in fulfilment of the requirements for the degree of Doctor of Philosophy (PhD) at the University of Salford. The work described in this thesis is my own work.

Any Section, part or phrasing of more than thirty words that is copied from any other work or publication, has been clearly referenced at the point of use and fully described in the references Section of this thesis."

Stephen A Johnston (Candidate)

………………………………….. February 2015

Professor G.G. Nasr (Supervisor)

………………………………….. February 2015

NOMENCLATURE

A	Projected or Cross-sectional area, e.g. of spray (m^2)
C	Discharge coefficient of nozzle (dimensionless)
CO	Carbon Monoxide
CO_2	Carbon Dioxide
C/F	Counter flow
C_D	Drag Coefficient (dimensionless)
C_p	Specific Heat Capacity
D	Diameter of particle or droplet (µm or m)
D_{10}	Linear mean diameter of particle or droplet (µm or m)
D_{20}	Area mean diameter of particle or droplet (µm or m)
D_{30}	Volume mean diameter of particle or droplet (µm or m)
D_{32}	Sauter mean diameter of particle or droplet (µm or m)
d	Diameter of orifice, jet or chamber (µm, mm or m)
E	Activation Energy
E.R.	Equivalence ratio (ϕ)
F	Force, e.g. drag force on a particle (N)
FA	Flame acceleration
Fw	Water volume fraction (%)
H_2O	Water
Jw	Water volume flux (L/min)
K	K-factor = $Q/\sqrt{P}$
kPa	KiloPascals (1000 Pa)
L	Length (m)
Ld	Mean droplet separation (m)
N_2	Nitrogen
M	Mass
m	Mass flow rate (kg/s)
MPa	MegaPascals (1,000,000 Pa)
ms	Millisecond (1/1000th of a second)
N	Number of particles (dimensionless)
N_2	Nitrogen
Pa	Pascal (unit of pressure)

$P_{(abs)}$	Pressure (absolute) (Pa or bar)
P/F	Parallel flow
$P_{(gauge)}$	Pressure (gauge) (Pa or bar)
Q	Volume flow rate (at NTP) (m^3/s)
Q_f	Liquid volume flux ($m^3/s/m^2$)
Q_w	Water volume flow rate (m^3/s or in)
q	Heat transfer rate (W $/m^2$)
$r_{(se)}$	Radius of spray envelope (m)
Re	Reynolds number (dimensionless)
S	Span of size distribution
S_f	Flame speed (m/s)
S_g	Flow rate of unburned mixture (m^3/h)
T	Total measurement time (s)
T	Temperature (K)
ΔT	Temperature difference (K)
t	Time (s)
t	Flame thickness
U	Burning velocity (m/s)
U	Velocity (m/s)
S_u	Burning velocity (m/s)
V	Volume (m^3)
v	Normalised volume distribution of droplets (μm^{-1} or m^{-1} according to dimensions used for D)
We	Weber number ($We = \rho \Delta U^2 D/\sigma$, or $\rho \Delta U^2 d/\sigma$) (dimensionless)
X/F	Cross flow
Θ	Cone angle (degrees or ^{o})
ρ	Liquid density (kg/m)
σ	Surface tension (kg/s)
μm	Micron (1/1000th of a metre)
ϕ	Equivalence ratio
$\%$	Percentage
π	Pi

ABBREVIATIONS AND ACRONYMS

AFI	Advancing front and inflation
ANSI	American National Standards Institute
BL	Boundary layer
BOC	British Oxygen Company
BSI	British Standards Institute
BSP	British Standard Pipe
BVM	Burning velocity model
CFD	Computational fluid dynamics
CSA	Cross sectional area
DAQ	Data acquisition
DS	Downstream
ECFM	Extended coherent flame model
EDM	Eddy dissipation model
FDM	Fluid dependent model
FPS	Frames per second
HP	High pressure
HVLP	High volume, low pressure
LDA	Laser Doppler anemometry
LVHP	Low volume, high pressure
LEL	Lower explosive limit
LFL	Lower flammability limit
FAR	Fuel air ratio
FPMR	Flame propagation and mitigation rig
FRC	Finite rate chemistry
HD	High definition
HMA	Helicoil mitigation apparatus
HR	High resolution
HRS	High resolution scheme
HT	High tension
ID	Internal, or inside diameter
IGEM	Institution of Gas Engineers and Managers
MESG	Maximum experimental safe gap

MCM	Mitigation curtain module
NC	Normally closed
NO	Normally open
OD	Outside diameter
PD	Pressure transducer
PDA	Phase Doppler anemometry
PDF	Probability density function
PMMA	Polymethyl-Methacrylate
PR	Petroleum research
PTRG	Petroleum technology research group
RA	Research assistant
RNG	Renormalised group
RSM	Reynolds stress model
RTD	Resistance temperature detectors
SMD	Sauter mean diameter
SRA	Spill return atomiser
SRG	Spray research group
TAB	Taylor analogy breakup
TAR	Theoretical air requirement
TC	Thermocouple
UEL	Upper explosive limit
UFL	Upper flammability limit
UVCE	Unconfined vapour cloud explosion
VCE	Vapour cloud explosion
UGE	Unconfined gas explosion
VCE	Vapour cloud explosion

DEFINITION OF TERMS

The following glossary of terms and expressions provides useful descriptions of terms and expressions used within this thesis. A great debt of gratitude is expressed to all authors listed in the references.

Blast wave

The air wave set in motion by an explosion.

BLEVE

Boiling Liquid Expanding Vapour Explosion. An explosion due to 'flashing' of liquids when a vessel with a high vapour pressure fails.

Burn or Burning rate

The amount of fuel consumed by the combustion process per unit time (i.e. kg/s).

Burning velocity

Velocity of a flame normal to the flame front.

Combustion

The burning of a gas, liquid, or solid in which fuel is oxidised; involves heat release and often light emission.

Deflagration

A combustion wave propagating at *subsonic velocity* relative to the unburned gas immediately ahead of the flame.

Detonation

A combustion wave propagating at *supersonic velocity* relative to the unburned gas immediately ahead of the flame.

Endothermic or endothermicity

Relating to a chemical reaction that is associated with, and receives heat from the surroundings.

Exothermic of exothermicity

Relating to a chemical change that is associated with the release of heat.

Explosion

An event leading to a rapid increase of pressure. An explosion that produces heat, is known as a *thermal explosion*.

Equivalence ratio

Stoichiometric air : fuel ratio, divided by actual air : fuel ratio. (ϕ)

Flame speed

Velocity of a flame relative to a stationary observer.

Flash point

The minimum temperature at which a liquid fuel gives off sufficient vapour to form a flammable mixture with air, near the surface of the liquid or within the vessel used.

Gas Explosion

A process where combustion of a premixed gas cloud is causing rapid increase of pressure.

Laminar flow

Non-turbulent streamline flow in parallel layers (laminae).

Lower Flammability Limit (LFL)

Normally expressed as the percentage of gas in air by volume, this is the lower limit where below this value a flame will not propagate beyond the region of the ignition source.

Thermocouple

A device consisting of two dissimilar metals that produces an electrical potential difference when heated. The voltage produced is proportional to temperature.

Turbulent flow

Flow in which the local velocity and pressure at any point varies erratically.

Triggered system

A mitigation or control measure that is initiated by an event or build to such an event, which is normally associated and ‘triggered’ by a means of prompt detection i.e. pressure sensors or fuel gas detection.

Reynolds number

A dimensionless number used in fluid dynamics that gives a measure of the ratio of inertial to viscous forces.

Stoichiometric

A quantitative relationship, usually expressed as the ratio between two or more chemical substances undergoing a physical or chemical change.

Unconfined Vapour Cloud Explosion (UVCE)

This is where a combustion wave travels through a flammable vapour cloud in an area unconfined by boundaries i.e. walls, floor, roof.

Upper Flammability Limit (UFL)

Normally expressed as the percentage of gas in air by volume, this is the upper limit where above this value a flame will not propagate beyond the region of the ignition source.

Vapour Cloud Explosion (VCE)

This is where a combustion wave travels through a flammable vapour cloud. The overpressure development is related directly to the level of confinement and instantaneous flame speed.

ABSTRACT

For the past fifty years or so, there has been a great deal of interest in the use of water based explosion suppression systems, designed to mitigate or reduce the impact of thermal explosions and their consequential overpressures, which may be as high as 2MPa in outdoor environments. This level of interest has been heightened in more recent years due to a number of high loss explosion events including, Flixborough, UK (1974), Piper Alpha, North Sea (1998) and Buncefield, UK (2005).

All of the previous research has focused on the suppression and mitigation proficiency of existing or new water deluge systems, which deploy sprays containing droplets $200 \leq D_{32} \leq 1000\mu m$. Where a high speed flame propagates through a region of spray containing such droplets, the flow ahead of the flame will hydrodynamically break up the droplets into fine mist, which in turn will act as a heat sink in the flame, with a resulting degree of suppression. These studies concluded that in most cases, existing deluge systems contributed to a global reduction in flame speed and thus caused a decrease in the resultant damaging overpressures.

This present study however, is focused on the mitigation of slow moving deflagrations with resulting speeds of ≤30m/s. A flame travelling at such low relative speeds will not possess the inertia to inflict secondary atomisation by hydrodynamic break up. Consequently, the droplets within the spray must be small enough to extract heat in the short finite moments that the flame and droplets interact (approximately 0.03ms for a representative 1mm thick flame front). Previous theoretical studies have suggested that droplets, D_{32}, in the order of 10μm - 20μm will be required to successfully mitigate combustion without relying on further droplet break up. To date, there have been no other published experimental studies in this area.

An innovative high pressure atomiser known as a Spill Return Atomiser (SRA) was selected, which contained a unique swirl chamber and was originally developed for decontamination and disinfection. The efficient atomisation of the SRA produced fine sprays containing droplets, D_{32}, 15μm - 20μm. A series of ‘cold trials’ were conducted to further develop the single SRA, which manifested in the creation of several exclusive single and multiple spray options in counter, parallel and cross flow, with the direction of the propagating flame. These new configurations were supplied with deionised water at a liquid pressure of 13MPa and were qualitatively analysed using High Definition (HD) imagery and quantitatively characterised using non-intrusive laser techniques. During the development stages of this study the SRA spray cone angle was increased from 34.7˚ to 49.2˚and the exit orifice flow rate was raised from 0.295 L/min to 1.36 L/min. The increase in flow rate provided a number of spray options ranging from $17 \leq D_{32} \leq 29\mu m$, with liquid volume flux of 0.011 $cm^3/s/cm^2$ - 0.047$cm^3/s/cm^2$ and mean droplet velocity of 0m/s - 21.4m/s, with the resulting characteristics giving way to complete explosion mitigation qualities.

The second phase of this study was to conceive, design and build a suitable apparatus capable of producing slow representative flame speeds within the range of 5 m/s - 30m/s. In excess of 250 mitigation ‘hot trials’ were performed using the unique conformations produced during the ‘cold trials’, whereby a configuration consisting of 4 x SRA’s in cross flow (X/F) configuration, successfully and repeatedly, completely mitigated homogeneous methane-air mixtures throughout the whole flammable range E.R. $0.5 \leq (\phi) 1.0 \leq 1.69$ (5 - 15%), with flame speeds ranging from 5 - 30m/s. The combined spray configuration consisted of four SRA’s which were 105mm apart and each opposed by 120˚, thus providing a total spray region of 315mm (spray centre to centre). As the sprays did not overlap or converge, the liquid volume flux remained as 0.047$cm^3/s/cm^2$.

With droplets, D_{32}, ≤30μm generally requiring impact velocities of approximately ≥142.83m/s to break up further, the flame speeds experienced in these trials of ≤30m/s would not have caused hydrodynamic break up of the droplets in the sprays. Therefore, due to the flame speeds and drop sizes utilised in this study, the droplets entering the flame front would have been in their original form.

Although some comparisons were made using the experimental data with Computational Fluid Dynamics (CFD), it proved to be an extremely complicated phenomenon. This was due to the presence and interaction of the complexities of the combustion process and other variables such as water droplet dynamics and heat transfer modes. As such, a set of recommendations have therefore been proposed in pursuing this work in future projects.

JOURNAL PUBLICATION (to be authorised)

Due to the sensitive nature of this study, a moratorium has been placed on this thesis by the University of Salford. Therefore, it has not been possible to publish any of the content from this Doctoral thesis due to the restrictions in place.

However, a survey of appropriate publications, including impact factor and readership has been carried out and a journal publication has been produced in draft form, in readiness to be submitted following the subsequent relaxation of the moratorium.

Details of the survey of various publications, author information pack and draft journal paper are provided in Appendix 1 (See CD of Appendices, Volume III).

CHAPTER 1

INTRODUCTION

1.1 Overview

Regrettably gas and vapour cloud explosions will always occur. This is partly due to the reactivity and flammability of the species and the increased risk of likelihood caused by contributing factors, including engineering and human failures. Many national and international studies have been carried out over time to attempt to explain the mechanisms leading up to such proceedings and to categorise these events.

Explosions are driven by the rate of expansion from reactant to product. This thermal expansion, which may normally be in the order of 1:8, can also produce expansions of 1:40 and may produce near and far field overpressures of up to 50 atmospheres.

For many new sites, including processing plants, refineries, oil and gas platforms etc., a high percentage of the risk regarding events leading up to an explosion can be reduced, simply by following appropriate design criteria. This is reinforced by providing an on-going safety risk management process and procedure, such as Control of Major Accident Hazards Regulations (COMAH) [1], which are statutory and enforceable in the UK.

In most instances there will be an opportunity to improve existing sites by altering site layout and design, or by installing third party mitigation processes, such as water deluge and explosion venting measures. The overall assessment process in determining the suitability of a mitigation system must ensure that the conditions that favour the occurrence of such explosive events are reduced to acceptable levels. Financial budgets must be set to allow for appropriate initial design measures or alterations to existing sites, with an on-going commitment to risk management and a continuous review process.

The use of water sprays in explosion suppression and mitigation research has been previously carried out by many authors including, the American Bureaux of Mines, British Gas, GexCon and the University of Aberystwyth. The focus of the previous work has been the employment of atomisers and sprays and their suitability in producing appropriate spray characteristics, with mean droplet sizes ($D_{32} \geq 100\mu m$) and sufficient liquid volume flux (variable see Chapter 3, Section 3.6.4) required to mitigate or suppress high speed explosions with propagating flame speeds ranging from 100m/s - 2000m/s. The flame speeds used in the previous aforementioned research were generally representative of those associated with high loss incidents caused by flame acceleration and consequential high overpressures.

With accelerated flame speeds the blast wave ahead of the combustion wave can provide the dynamic forces required to break up the water droplets into much smaller diameters. Mitigation of the flame or suppression of combustion activity only occurred in previous work when the dynamic forces created by the blast wave were great enough to overcome the surface tension forces in the water droplets. Fine mists formed by the hydrodynamic breakup of the larger droplets could then progress through the flame. Providing there was adequate liquid volume flux (Q_f) and sufficient ‘residence time’ (t) for droplets in reaction zone of the flame to facilitate suppression or global mitigation of combustion, a high degree of success was reported. These fundamentals, which have been studied qualitatively and quantitatively by many authors, are discussed exclusively in Chapter 3. The previous studies exclusively concluded that water was found to be very effective in the suppression or mitigation of gas and vapour cloud explosions, even at supersonic flame speeds (or detonations) typically 1500m/s – 2000m/s.

In summarising some of the previous studies, Harris and Wickens [2] additionally highlighted significant areas of concern regarding water based mitigation systems:-

i. The turbulence caused by water spray momentum may be transferred into the unburned mixture, or the flame front, thus causing turbulence and an overall increase in local or global flame speeds.
ii. Accidental water ingress into electrical apparatus and switch gear may lead to an electrical spark, which may cause re-ignition of a flammable mixture, or even cause secondary fires.
iii. Water storage volumes need to be large enough to provide uninterrupted sprays for very long periods.

It has become evident that previous water spray mitigation research (see also Chapter 3) exclusively relied on the subsequent break up of water droplets into fine mist. To achieve this break up, the forces contained in the blast wave must be greater than the forces holding the droplets together in the first instance. In many instances, particularly when an explosion occurs in an unconfined area, overpressures may be as little as a few hundred Pascal’s (Pa), whereby water droplets would not initiate further break up, thus retaining their original geometry. The fundamental relationship between critical break up velocity, drop size and resulting break up mechanisms are discussed in Sections 3.5.3.1 and 3.6.3.

This present study provides a unique and novel opportunity, in which very fine water droplets ($D_{32}\leq30\mu m$) will be deployed from a specialist atomising system in an attempt to suppress, or mitigate slow moving propagating flames with speeds of ≤30m/s, with a typical flame front thickness of approximately 1mm, coupled with droplet residence times of about 0.03milliseconds (ms).

It is worth noting that at such low flame speeds the droplet sizes used in previous research of $D_{32}\geq100\mu m$ would simply pass through the flame, thus allowing the flame to continue to propagate at a finite speed or as in some cases may even cause the flame to accelerate further. (see also CFD consideration, Chapter 6)

1.2 Contribution to research

Although there has been significant research in the utilisation of water sprays as an explosion suppressant and mitigation measure, the contributions to the field in these present investigations were:-

i. To design and develop an apparatus that was capable of producing slow and high speed deflagrations (or subsonic flame propagations), utilising homogeneous stoichiometric mixtures and ignitions to produce flame speeds of ≤30m/s under ‘partly confined’ and ‘partly confined/vented’ conditions. This has led to the total extinguishment and mitigation of a propagating flame without relying on further droplet division by dynamic bag type breakup mechanisms (or secondary atomisation).

ii. Utilisation of the existing liquid atomiser known as the Spill Return Atomiser (SRA) was adapted, refined and modified to produce single and multiple poly-dispersed sprays of ideal droplet size ($D_{32}\leq30\mu m$), mean droplet velocity (0m/s - 21.4m/s) and liquid volume flux (approximately 0.047 $cm^3/s/cm^2$) to fully mitigate a range of lean, stoichiometric and rich homogeneous methane-air and propane-air explosions.

1.3 Aims and objectives

1.3.1 Aims

The overall aims of this research are to:-

i. Design and construct unique laboratory scale test equipment (*hot and cold*) to carry out explosion mitigation trials on low speed fuel gas-air deflagrations of $\leq$30m/s.
ii. Characterise the spray dynamics using various laser techniques under ambient conditions (*cold*) and the integration into a simulated flame propagation tube (*hot*).
iii. Use a water based atomising system capable of mitigating a propagating flame in a flammable mixture, utilising droplets of $D_{32} \leq 30\mu m$ and without relying on further hydrodynamic break-up of the droplets within the spray.
iv. Provide a sample knowledge database in attempting to validate a Computational Fluid Dynamics (CFD) software package, which could be used as a future design tool.

1.3.2 Objectives

To achieve the overall aims of this research, the following objectives will be addressed using an analytical, practical and systematic approach:

i. Evaluate the characteristics and performance of several atomiser configurations in atmospheric conditions using various imaging and non-intrusive laser techniques i.e. Phase Doppler Anemometry (PDA) (*cold trial*).
ii. Appraise the individualities and implementation of a number of atomiser arrangements in a simulated tube environment using assorted procedures (*cold trial*).
iii. Create a safe experimental set up as required to fully evaluate a series of counter flow, parallel flow and cross flow sprays in homogeneous combustible fuel gas-air mixtures (*hot trial*).
iv. Determine through experimental means, the critical droplet size (D_{32}), liquid volume flux (Q_f), droplet velocity (d_v), spray cone angle (θ) and spray configuration to affect the complete extinction of a propagating flame (*hot trial*).
v. Verify the effectiveness of several spray configurations and also the relationship between sprays and induced turbulence leading to flame acceleration (*hot trial*).
v. Attempt to model the conditions within the Flame Propagation and Mitigation Rig (FPMR) and to compare a sample of results from the experimental trials using CFD.
vi. Consider the effectiveness of the CFD software as a suitable design tool.

1.4 Summary of Chapters

Chapter 1 includes an overview of the concept of mitigation of explosions by water sprays and a brief description of the current problem.

Literature Surveys I and II : In providing a logical structure for this thesis the literature survey has been sub-divided, thus giving way to *Chapters 2 and 3*.

Chapter 2 Literature Survey I, provides a literature survey incorporating some fundamental concepts relating to combustion, fire, explosions and flame quenching.

Chapter 3 Literature Survey II, considers various fine spray atomisers and also contains an extensive review of previous research, findings and discoveries in the utilisation of sprays used for fire and explosion suppression and mitigation.

Chapter 4 presents the apparatus design and set up, procedures and methods of data processing used in this study. Furthermore, this Chapter also reviews the development of an existing novel Spill Return Atomiser (SRA), previously utilised for decontamination spraying, including the alterations carried out under 'cold trial' conditions, prior to the subsequent explosion and mitigation 'hot trials'.

Chapter 5 includes the experimental findings from the 'cold and hot' trials utilising apparatus and rigs. The FPMR rig was used to conduct over 250 explosion and mitigation trials using various fuel gas-air mixtures and water spray configurations. This Chapter includes a representative sample of selected hot trials, whereas all of the hot trials are provided in *Appendix 9* of the accompanying Appendices CD volume (called here *Volume III*).

The data from all of the hot trial experiments yielded in excess of 8,000,000 data points, all of which have been processed, presented and discussed. Although most of the testing was carried out using high purity methane, a small representative number of trials were also performed using commercial propane. The results from the propane tests were processed and reviewed and have been used to suggest further research in *Chapter 7*.

Chapter 6 considers the application and suitability of a Computational Fluid Dynamics (CFD) software package and suitability as a design tool, leading to making a set of recommendations for future work.

In *Chapter 7* the conclusions and recommendations for the *cold* and *hot* experimental trials and *CFD consideration attempt* are revealed. Additionally, proposals and potential markets for two new product developments are discussed. Recommendations and suggestions for realistic full scale trials are also offered. There are also suggestions for further usages for the SRA, such as mitigation of jet fires involving gas and liquid fuel.

CHAPTER 2

LITERATURE REVIEW : I

GAS AND VAPOUR CLOUD EXPLOSIONS AND MITIGATION

2.1 Overview

This Chapter contains an underlying review of past works which will lead to further justification in carrying out this present study and thus the corresponding ‘hot trials’, with their results and discussions in Chapter 5. Additionally, fundamental theory is also discussed, together with explanations of the elemental principles of combustion, explosions and flame quenching.

Moreover, in Chapter 3 sufficient background information relating to previous studies has been presented which in turn complements the reasoning behind the ‘cold trials’ of this present investigation. These were conducted with regards to atomiser selection and imaging techniques in support of the hot trials.

The benefits, properties and characteristics of flammable gases and vapours are well documented and equally the potential for uncontrolled combustion events involving fire and explosions are also common knowledge. Throughout modern history there have been numerous pioneering individuals and institutions that have provided a vast wealth of background knowledge in explosion and mitigation research.

The following Sections briefly introduce some of the individuals and institutions that will be referenced throughout this current study.

Some of the earliest research carried out in the field of gas and vapour cloud explosions was conducted by Sir Humphrey Davy (1778 – 1829). This British chemist and inventor became interested and involved in the improvement of lighting in underground coalmines. During the early eighteen hundreds, there had been many unfortunate fatal events involving the accidental ignition of methane gas, or coal dust clouds [3].

In one such event in 1812 at the Felling Colliery in Tyne and Wear, England, 92 men and children, the youngest being eight years old lost their lives. The event occurred in a shaft around 180 metres deep. Lighting in those days was poor and normally provided by open flame oil lamps carried by the minors. A ‘sacrificial minor’ wearing a wet blanket as thermal protection, sometimes referred to as a ‘monk’, would often enter areas of the mine holding an open flame on a long pole. This was to ignite any minor pockets of gas accumulations before allowing others to enter.

Davy devised the minor's safety lamp, often referred to as the 'Davy Lamp' shown in Figure 2.1, which consisted of a flame produced by a wick burning 'lamp oil' surrounded by an iron gauze. Davy's work helped him to determine the gauge of the gauze which surrounded the flame and its ability to prevent flame propagation from one side of the gauze to the other.

Figure 2.1 : Minors Safety Lamp or 'Davy Lamp' [3]

Davy produced some of the early pioneering work [4] in the subject of flame quenching. The lamp could be taken into areas of known gas accumulations without fear of accidental ignition. Another useful attribute was that the length of the flame within the lamp, whereby the flame length would vary with respect to gas concentration and burning velocity and was represented by a scale on the side of the lamp.

In 1910, the American Bureaux of Mines, under the U.S. Department of the Interior was established and began to operate a new research centre in Pittsburgh, PA, in response to the alarming number of explosions, fires and fatalities in underground coalmines. The original key objectives for the Bureaux of Mines was to investigate the safety of blasting techniques used in potentially flammable atmospheres containing methane and coal dust.

The test facilities shown in Figure 2.2 included, laboratories, a 30 metre long test passage / galley constructed to simulate an underground mine entry and a 38 acre tract of land, leased from the Pittsburgh Coal Company [5].

Figure 2.2 : Planned coal-mine explosion at the Bureau of Mine's first research site [5]

Some of the projects and research carried out at the Bureaux of Mines [5] were:-

- Ventilation requirements for coal mines with respect to methane gas occurrence
- Testing and certification of electrical apparatus, such as lighting and methane detectors
- Coal dust explosion quenching with 'rock dust'
- Mitigation and inerting of methane explosions with water sprays
- Risk of explosions in hospital operating rooms due to ignition of aesthetic gases
- Characterising of flames, burning velocities, flame speeds, propagation and quenching
- Safe methods for ejecting fuel from a space capsule at 30,000 metres, for the National Aeronautics and Space Administration (NASA)

Under the new leadership of Dr. Bernard Lewis, the division was renamed the Explosives and Physical Science Division in 1946. Dr Lewis is acclaimed to be one of the world's most influential scientists in the field of combustion, flames and explosions. In 1951 Dr. Lewis and another of his co-workers, Guenther von Elbe published the formative book *'Combustion, Flames and Explosions of Gases' (Lewis and von Elbe 1951)* [6]. The publication has been revised twice to date and is used worldwide in combustion science and engineering academia. In 1954 Lewis was influential and dominant in the forming the *Combustion Institute,* in Pittsburgh. The institute hosts the International Combustion Symposium every two years and produces the journal *Combustion and Flame* [7].

British Gas (BG) have always played a major role in combustion and explosion research. In addition to the supply of natural gas to millions of homes and businesses in the UK, British Gas operates, or has an interest in, many oil and gas platforms and sites throughout the world.

BG previously operated three research stations in the UK. These were, the Midlands Research Station, Solihull, The Engineering Research Station, Newcastle and also Watson House, London. Midlands Research Station (MRS) soon became a leading institution for combustion and explosion research, with laboratories and full scale test facilities. These facilities were later moved to Loughborough and managed by Advantica Technologies (a division of British Gas) with the full scale research facilities relocated to Spadeadem, Cumbria, UK, as shown in Figure 2.3.

Figure 2.3 : GL Noble Denton's World Leading Test Centre : Flame acceleration tests

The Spadeadem Test Site is now operated by G.L. Noble Denton and offers a unique testing facility for petroleum and gas, process and energy industries, also construction industries and other work for government agencies.

Some of the testing carried out at Spadeadem includes:-

- Blast and High Explosive Testing
- Fire Testing - Jet fire, pool fire
- Explosion Testing - confined and unconfined gas & vapour cloud explosions
- Pipeline Counter Terrorism Measures
- Flame Acceleration and DDT
- Flame Arresting Equipment
- Explosion Mitigation Measures - water sprays, aqueous foam, halons
- Water Deluge System Testing

For over 35 years, Christian Michelsen Research (CMR) has focused on research and consultancy in the field of gas explosion and dispersion modelling. GexCon was established as a new brand name in 1987, but the gas explosion consultancy activity was formally separated from CMR in 1998. In 2000 GexCon took over all explosion safety activities from CMR. With similar full scale explosion test facilities to G.L. Noble Denton, the GexCon test site is situated on the Island of Sotra, just outside Bergen, Norway as illustrated in Figure 2.4.

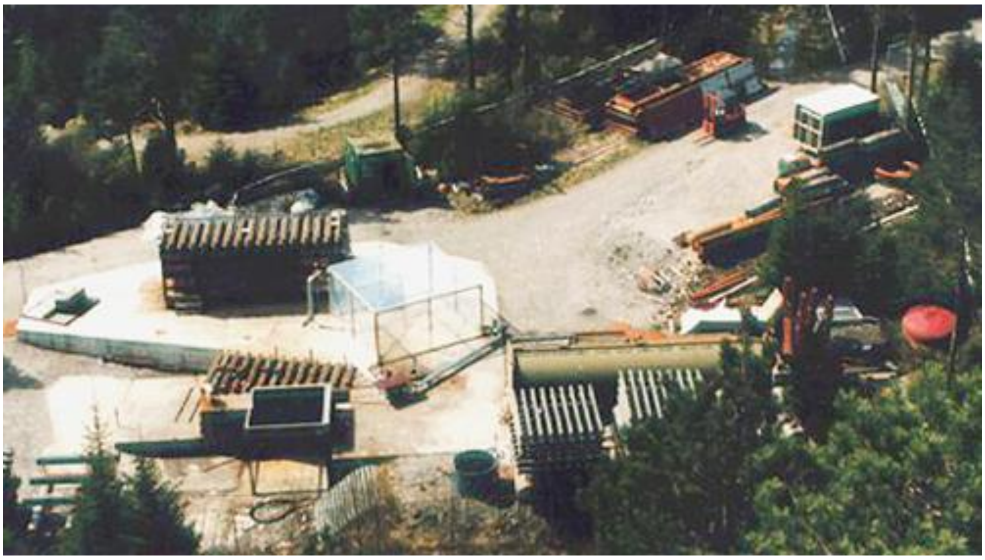

Figure 2.4 : GexCon's full scale test site on the Island of Sotra, Norway [11]

GexCon are also renowned for their explosion simulator software, known as FLACS. FLACS is a computation fluid dynamics (CFD) package, used widely for gas dispersion and explosion modelling. FLACS has become an industry standard, used by oil and gas platform, storage depots operators and industry to assist with site design and explosion hazard risk assessments.

The effects of environmental geometry and location of obstacles can be modelled with respect to fuel type, fuel-air percentages, flame speeds and predicted overpressures. Mitigation measures, such as explosion relief and venting can also be reproduced to assess their effectiveness. In Chapter 6 consideration will be given to the suitability of a CFD software package will be considered as a future design tool.

The University of Aberystwyth, Wales has long since been involved in combustion and explosion research, as displayed in Figure 2.5 and is recognised for knowledge and experience in the relevance of water sprays employed in explosion suppression.

Thomas and Brenton of University of Aberystwyth carried out a study on behalf of the Health and Safety Executive (HSE) [39] to investigate the relevance of factors during explosion suppression by water sprays. In this study they reviewed much of the previous work, which exclusively dealt with high speed flame propagations and even detonations, leading to hydrodynamic droplet break up. This study [39] is referred to and summarised in Chapter 3.

Figure 2.5 : End of line detonation arrestor testing , under supervision from Thomas [39]

The above research institutions have been included in this Section as a means of introduction and acknowledgement of their previous contributions to research. Although their research was entirely related to large water droplets (≥100μm) and high speed flame propagations (≥100m/s), a number of their investigations will be reviewed with relevance to this current study in Chapter 3.

2.2 Explosion environments

The resulting consequences following the accidental ignition and subsequent 'explosion' of a flammable mixture are largely affected by the environment in which the event takes place. Nasr, G.G. *et al* [8] discuss extensively the safety challenges involved with respect to explosions in flammable mixtures. Explosion occurrences may be categorised with respect to the degree of confinement in which they ensue. The three principle categories are:-

i. Confined explosion
ii. Partly confined explosion
iii. Unconfined 'explosion'

It is worth noting that in the current study the apparatus was systematically designed to simulate partly confined and unconfined conditions. In the following Sections, attempts have been made to describe each of the explosion environment classifications in order to give a better understanding of the subject area in the subsequent Chapters.

2.2.1 Confined explosion

Confined explosions have the potential to cause rapid pressure increases with catastrophic consequential outcomes. These explosions may occur in storage vessels or tanks, process pipework, furnaces and other closed areas. In the petrochemical and gas industry, confined areas such as modules are often fitted with explosion relief openings to limit overpressure and to reduce the magnitude of the event, thus creating 'partly confined explosion' conditions as discussed in Section 2.2.2.

Storage vessels are often equipped with a relief valve, however the relief valve in this case is only provided to facilitate operational pressure relief due to the transient thermal expansion of the contained product. Figure 2.6 illustrates a confined explosion in a storage vessel.

In some processes, the resulting pressures associated with confined explosions are exploited, such as the reciprocating internal combustion engine and weapons of war, e.g. artillery shells. In the former, the expanding gases are used to induce momentum into a piston. In the later, the expansion is momentarily contained thus allowing the pressure to increase within the shell. The resulting explosion generated pressures being many orders of magnitude ($1kPa \leq P \leq 5MPa$) greater than if the explosive or fuel had been ignited in open or unconfined conditions.

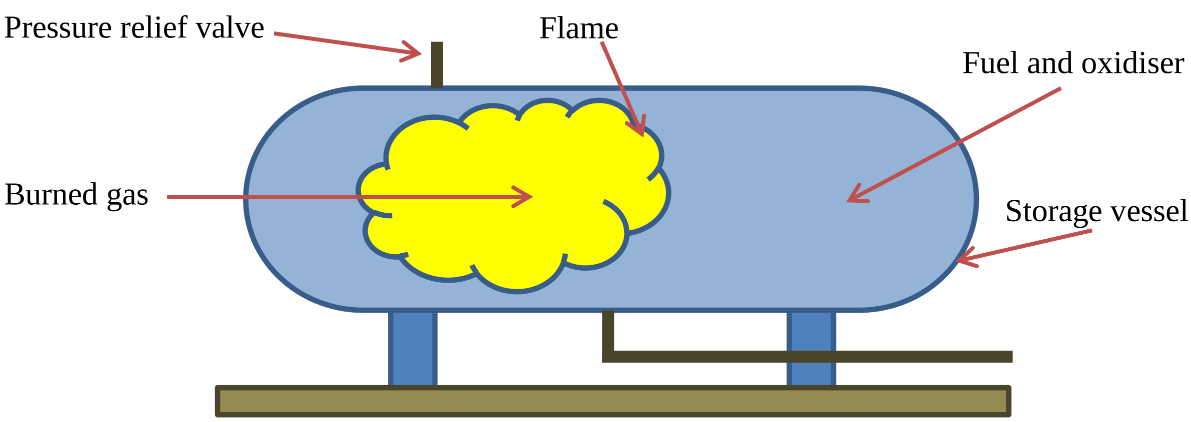

Figure 2.6 : Confined explosion within a storage vessel

Explosion tubes, vessels and enclosures have been used to study confined explosions, with particular interest in the effects of geometry and propagation into adjoining vessels, pipework and enclosures. Although confined explosions generate high explosion pressures, the flame propagation rates and flame speeds are relatively slow. These relatively slow flame speeds are not generally suited to the application of conventional water sprays (typically containing drop sizes of D_{32} 200 - 500µm), as droplets in this size range require high speed impact forces to break up and be effective as a mitigation measure. Droplet break up and the conditions required to initiate this phenomenon are discussed exclusively in Chapter 3.

2.2.2 Partly confined explosion

A partly confined explosion may occur in area of containment, such as a plant room which may be equipped with an explosion relief vent or panel, or may include light weight construction materials such as windows or doors as shown in Figure 2.7.

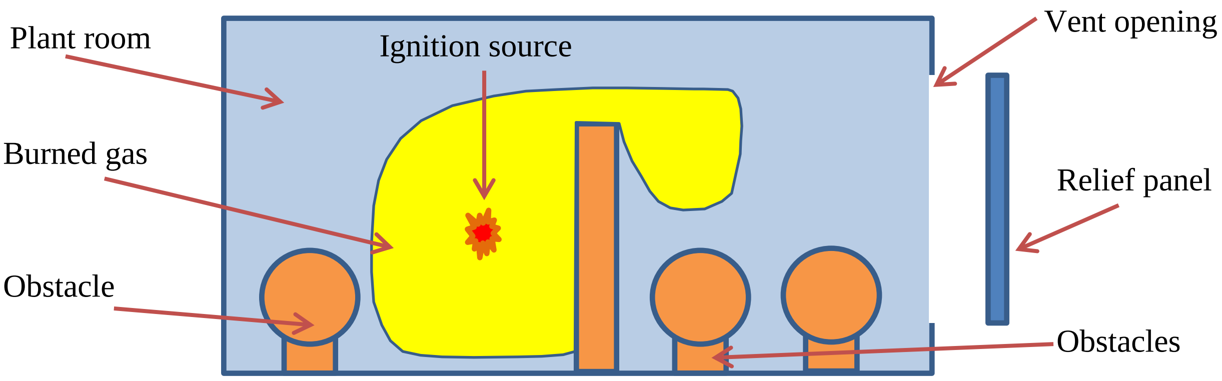

Figure 2.7 : Partly confined gas explosion in a plant room

In Figure 2.7 above, in which an ignition source is central to the 'burned gas' area, a flame kernel will develop initially and begin to propagate in a divergent manner, typically at laminar flame speeds. Due to the thermal expansion of the hot combustion gases pressure will begin to build up. At a pre-determined pressure, the explosion relief vent/panel will operate. As the explosion relief operates some of the unburned gas from the plant room will be forced out through the opening. In this scenario the flow field will encounter obstacles in the form of plant and equipment. The obstacles will induce turbulence in the flow field and this is likely to result in flame acceleration. In many cases flame speeds will become turbulent and will result in high overpressures.

The above scenario highlights the importance of the positioning of the relief vent, relative to potential ignition sources i.e. pumps, motors etc.

Harrison and Eyre [9] and Patel, *et al* [10] carried out work is relation to obstacles placed in the exiting flow fields and concluded that turbulent stretch dominated the regions upstream of obstacles and that flamelet stretch dominated in the flow fields around the obstacles. The results from both of these works have been used to produce and modify existing CFD codes such as FLACS [11]. In this present study, CFD has also been considered and attempts were made to examine the sensitivity of the simulation in summary by the hot trial and cold trial experimental findings. (See Chapter 6)

2.2.3 Unconfined explosion

An unconfined explosion is used to describe ignition of a combustible cloud where thermal expansion is truly unobstructed. Minor overpressures will be produced during the 'burn' period, which will reduce rapidly back to the original conditions almost immediately after the burn period.

Where an unconfined explosion propagates into an area of partial confinement, such as the conditions associated with a gas or petroleum site as illustrated in Figure 2.8, the outcome is likely to be more severe. These events are often called Vapour Cloud Explosions (VCE).

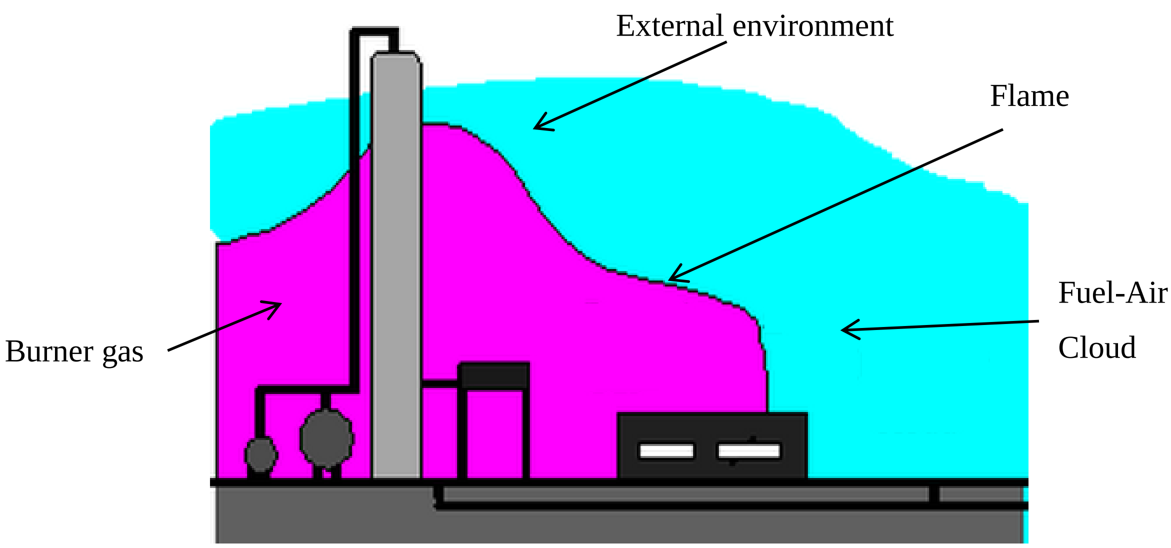

Figure 2.8 : Unconfined gas explosion and plant layout [11]

Previous water spray studies [2] have all concentrated on the conditions required to mitigate high speed explosions, in which the flow field is capable of shattering large water droplets into fine mist. (See also Chapter 3, Fundamentals and utilisation of fine sprays in explosion mitigation : Literature review II)

Unconfined explosions where little or no obstructions are present are of particular interest to this current work, as the relatively slow associated flame speeds (≤30m/s) are incapable of breaking up water droplets any further. To supress or mitigate a slow moving flame front, water droplets must initially be small enough (≤30 μm) to directly absorb heat from the flame.

In previous studies, arrays of atomisers were placed within or beyond areas of repeated obstacles in which the flame had been encouraged to accelerate, prior to attempting to suppress or mitigate its propagation. These studies are extensively discussed in Chapter 3.

This present research however, is focussed on mitigation of the flame prior to the acceleration phase (described above), thus potentially limiting any consequential overpressure damage caused by the explosion. Due to the parametric safety issues surrounding explosion research, an apparatus was designed for this current study (see also Chapter 4) that was 'partly confined', with immediate venting upstream of the propagating flame and is therefore described as *'partly confined / vented'* in the subsequent Sections and Chapters.

The rationale for this *'partly confined / vented'* scenario is that it closely represents 'unconfined conditions', whereby the only confinement limiting the direction of travel of the flame is the walls of the propagation tube arrangement, used to facilitate these trials. The unique apparatus design, set up, procedures and methods of data processing used in this study are exclusively discussed in Chapter 4.

2.2.4 Blast waves

The term blast wave can be used in conjunction with sonic compression waves and supersonic shock waves. A blast wave is an area of pressure expanding outwards resulting from the release of a large amount of energy from a relatively small volume.

Blast waves cause damage by compressing the air ahead on them, often forming a shock wave. This is because blast waves obey the same physical laws as any other type of wave forms in a free unrestricted air. In addition to the positive pressure phase, a blast wave also produces a negative phase and the resultant winds that follow. Friedlander [11] described the waveform associated with the blast wave as a function of pressure and time, as shown in Figure 2.9.

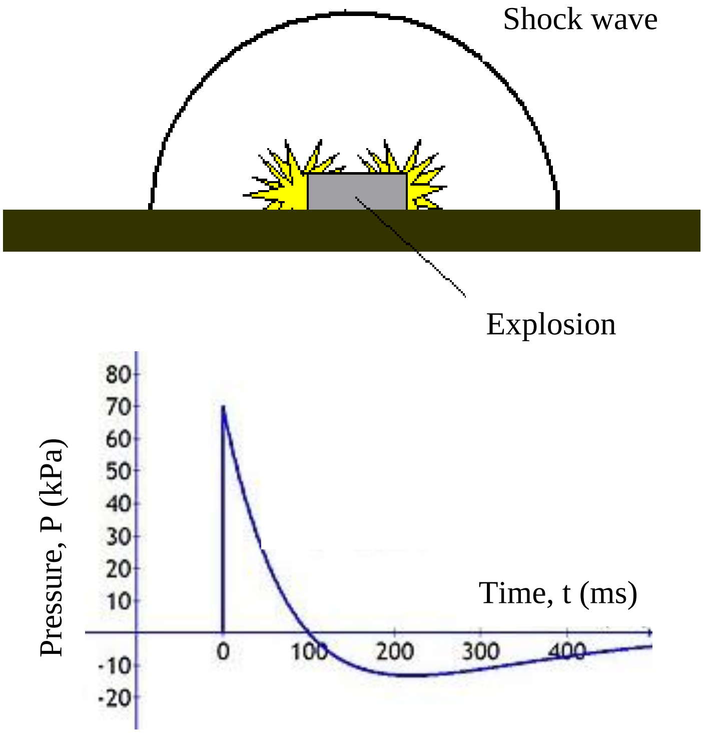

Figure 2.9 : Blast wave and single peak pressure-time profile (Friedlander waveform) [11]

It is important to understand the relationship between explosions and their resulting blast waves, as all previous research has relied on this blast energy to shatter water droplets into fine mist. In the graphical illustration shown above in Figure 2.9, the explosion pressure rises to 70kPa and falls rapidly to zero within 100ms. Any droplets not shattered by this finitely short burst of energy, will remain too large (≥30µm) to effectively extract heat from the combustion reaction.

Figure 2.10 illustrates in principle different types of blast waves as a function of pressure and time:-

(a) Illustrates a shock wave followed by a rarefaction wave. In terms of explosion strength, this is the strongest of the three.
(b) Illustrates a shock wave, followed by a sonic compression wave and then a rarefaction wave
(c) Illustrates a sonic compression wave and a rarefaction wave. This type of blast wave depends on how and when the energy is released in the explosion and the distance from the explosion area. In terms of explosion strength this is the weakest of the three.

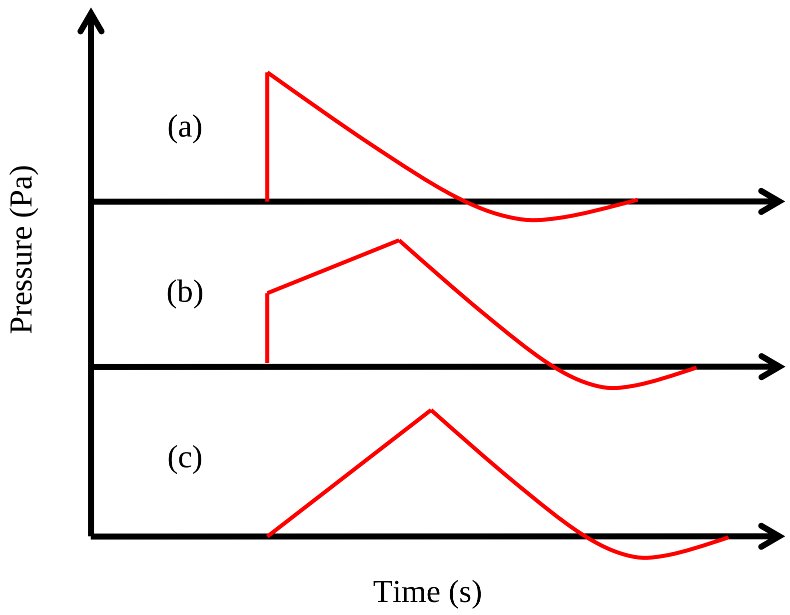

Figure 2.10 : Types of blast waves

These three different types of blast waves have been included to reinforce and underpin the reliance and their critical presence in other previous water spray studies.

In the following Section the effects of these explosion overpressures are discussed in relation to everyday objects.

2.2.5 Overpressure development

Clancey [12] reported the resulting overpressure indicators associated with thermal explosions and the damaging effects of particular overpressures to everyday materials, such as glass, brickwork and metal objects as listed in Table 2.1

Material / Structure	Pressure
Typical pressure for glass failure	1 kPa (10 millibar)
Minor damage to house structures	4.8 kPa (48 millibar)
50% destruction of brickwork of a house	17 kPa (170 millibar)
Rupture of oil storage tanks	27 kPa (270 millibar)
Severe crushing of cars	34kPa (340millibar)
Loaded train box cars completely demolished	62kPa (620millibar)
Probable total destruction of buildings	69kPa (690millibar)

Table 2.1 : Pressure indicators for everyday materials [12]

In an explosion there are essentially two forces to consider, the blast wave extending outwards in the direction of flame propagation and the impulse created by the hot expanding gases in the opposite direction. Deflagrations and detonations both produce a backwards impulse. This backwards impulse is far greater if a detonation has occurred.

The resulting net drag damage and subsequent indicators following an explosion can assist investigators to determine the energy contained in the blast and whether a deflagration or a detonation had occurred. In a detonation (or supersonic wave), the net drag will be backwards towards the point of ignition as shown in Figure 2.11, whereas the damage caused by a deflagration (or subsonic propagation) will be predominantly outwards from the source of ignition.

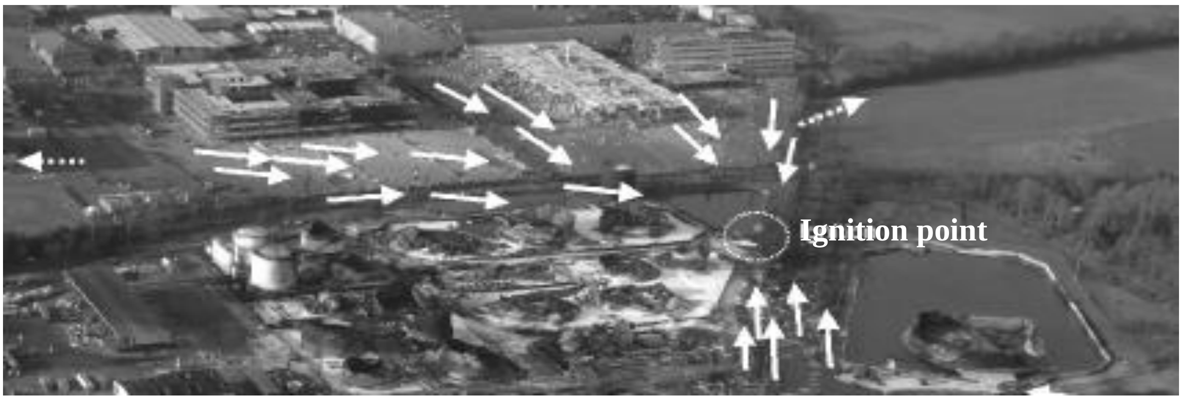

Figure 2.11 : Explosion indicators showing net drag towards ignition [16]

Within this present study the later will prevail and overpressures will be negligible due to the specific design considerations included in the Flame Propagation and Mitigation Rig (FPMR), whereby the flame speed generated will only be in the order of ≤30m/s.

2.3 Gas and vapour cloud explosion : Events

The accidental release and subsequent ignition of flammable gas and vapour clouds has led to a great number of incidents with catastrophic consequences. There have been many unfortunate *events* in recent history involving energy releases from pipework, fittings and vessels. The accidental release of flammable gas or vapour may occur due to a single, or multiple factors that lead to a number of scenarios and thus the circumstances surrounding such events may include:-

i. Operational error – e.g. overfill, drain valves left open or similar
ii. Equipment failure – e.g. relief valve failure, inoperable valve or similar
iii. Natural disaster – e.g. earth quake, hurricane or similar
iv. Maintenance error – e.g. incorrect safe isolation procedure or similar
v. Poor design – e.g. specification of inferior materials or similar
vi. Terrorism – e.g. sabotage using plastic explosives, perlite or similar
vii. Arson – e.g. similar to terrorism for non-political reasons

Harris and Wickens [2] produced a report communicated and published by the Institution of Gas Engineers and Managers (IGEM), in which they reviewed the general understanding of vapour cloud explosions. Some historical occurrences and events and also the level of Vapour Cloud Explosion (VCE) research being conducted by British Gas and other organisations worldwide are presented in the report, which refers to explosion research in Unconfined Vapour Cloud Explosions (UVCE) and incidents involving vapours clouds entering areas of congestion and repeated obstacles.

There have been many experimental programs involving unconfined vapour clouds and all are in agreement that unconfined vapour clouds are incapable of producing explosion overpressures of damaging magnitudes beyond their cloud boundary. This is predominantly due to the divergent manner in which the combustion wave propagates, with resultant flame stretch and wrinkling of the flame. Flame propagation is discussed in more detail in Section 2.4.5. This current study has a fundamental aim to mitigate slow moving flames (≤30m/s) with similar characteristics to those associated with UVCE.

A full scale experiment carried out in 1983 was the world's largest hydrogen-air deflagration tests in atmosphere. The tests were performed at the Fraunhofer Institute for Propellants and Explosives, Germany by Pfortner and Schneider *et al* [13] utilising a 20m diameter by 10m high hydrogen-air filled hemispherical polyethylene (PE) enclosure, as revealed in Figure 2.12. These series of tests where simply known as GHT 34.

The report [13] also refers to flame acceleration experiments where high overpressures were recreated in long polyethylene covered enclosures containing areas of severe congestion and repeated obstacles. Under certain conditions involving repeated obstacles and congestion, low speed laminar flames accelerated to high speeds. In some cases the flame became highly turbulent and then detonated. This phenomenon is known as *Deflagration to Detonation Transition* (DDT) and is discussed in Section 2.4.5.8. Cronin and Wickens [14] of the British Gas Midland Research Station, carried out some large scale experimental work in this field. Additionally, the same realistic scale rigs and apparatus used for the above flame acceleration studies were subsequently utilised to assess the effectiveness of water sprays. (See also Chapter 3)

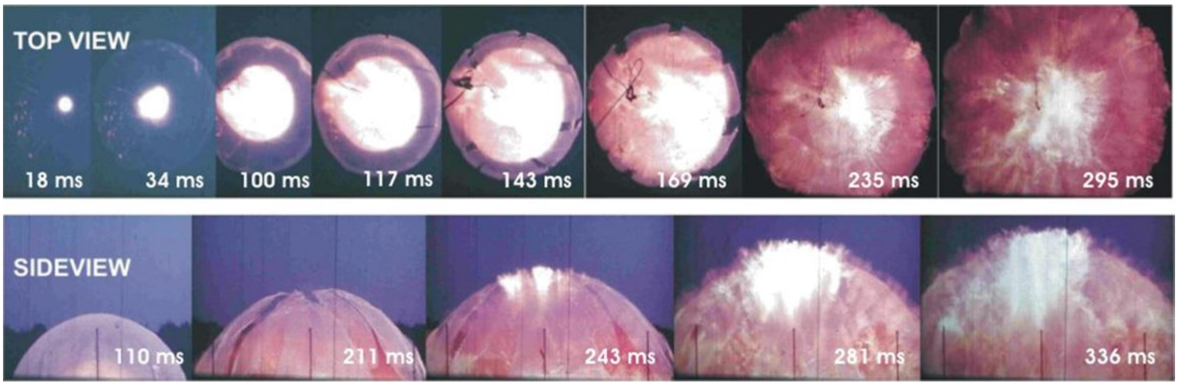

Figure 2.12 : High speed photography and still images from GHT 34 tests [13]

Explosion consequences and calculated magnitudes are often stated using TNT equivalences, where the explosion potential is modelled against an equivalent mass of TNT explosive.

A number of common factors occur in many of the occurrences, many of which are due to poor site layout and design. Harris and Wickens [2] also discuss guidelines for new plant design aimed to reduce the risk of vapour cloud releases coming into contact with areas of congestion. These include the separation of large pipe arrays and process areas, with recommendations relating to further research into passive or triggered mitigation measures.

One *triggered system* normally found installed on platforms, processing or storage depots, is the *general area deluge systems* designed to control or extinguish fires. Many studies have been conducted to assess the effectiveness of existing fire deluge systems when deployed in the event of a VCE. In these studies various existing atomiser systems that had been specifically designed for the control and extinguishment of fire, were evaluated to ascertain the mechanisms and conditions required for suppression of mitigation of high speed flames ($\geq$100m/s). Some of these previous studies and their relevance to this current work are reviewed in Chapter 3.

2.3.1 Fuel type, properties and methods of storage

Other factors that are likely to influence the consequences and event outcomes are the fuel type, exothermicity and the method of storage i.e. storage pressure, phase (gas, liquid or solid) and method of containment. The above factors will influence the effectiveness of the various explosion control and mitigation measures currently available, whereas a *multi-use mitigation system* would prove to be highly beneficial in many different event scenarios. This current study focuses on the mitigation of methane-air explosions and also provides recommendations for future advancement in Chapter 7.

2.3.1.1 Fuel type and properties

Although there have been many damaging explosion incidents involving natural gas, they have all occurred due to the presence of a *degree of confinement*. Due to the relative density of natural gas (being lighter than air), releases in outdoor unconfined areas tend to disperse rapidly and ignition of such unconfined releases are rare. The ignition of such releases would probably only result in a ‘flash fire’, rather than an ‘explosion’, with accompanying minimal overpressures.

Gases and vapours with densities similar to or heavier than air are more likely to be involved in and associated with unconfined vapour cloud explosions (UVCE). Natural gas is also considered to have a lower level of reactivity due to the single bonds in the molecule, compared to the some of the other fuels listed in Table 2.2, with respect to fundamental properties such as burning velocity, flame speed, ignition temperature and minimum ignition energy. An effort to describe these terms is provided in the subsequent Sections.

Material released		**Number of documented incidents**
Natural Gas		0
Ethylene		13
LPG	Propane	3
	Butane	8
	Propylene	4
	Butadiene	2
	Not Specified	4
Cyclohexane		2
Others		12

Table 2.2 : Recorded vapour cloud explosion events [2]

2.3.1.2 Method of storage

Where a product is stored at atmospheric pressure i.e. liquefied natural gas in cryogenic storage at -162˚C, there have been no recorded explosions [2] following the uncontrolled release of the product. Whereas, products stored under pressure will tend to mix readily with the surrounding air when released, as the turbulent discharging jet will promote air entrainment and mixing, however, a vapour cloud will almost certainly form in the latter. The level of engulfment of the surrounding area will normally be determined by site attributes, such as location and concentration of surrounding buildings, obstacles and the general terrain of the land.

2.3.2 Environmental implications and past events

The post event analysis of all previous vapour cloud explosions has indicated that a third party phenomenon rigorously contributed towards the generation of high overpressures. For damaging overpressures to develop, the explosion front must travel at speeds greater than those found in a totally unconfined situation. Areas of confinement or repeated areas of congestion such as pipe arrays, open sided buildings and even densely packed areas of woodland have all proven to have a dramatic effect on flame acceleration and resultant overpressures. (See also Nasr, G.G. *et al* [8])

There is currently new research being considered by GL Noble Denton into the effects of woodland areas and the contribution to flame propagation speeds and even DDT.

In the following Section some high loss and high profile events have been highlighted. These provide more supportive evidence to justify the scale and impact of gas and vapour cloud explosions and the need for further research to reduce their future numbers. Taken from 'The 100 Largest Losses 1972 – 2001': Marsh Risk Consulting [15], Tables 2.3 and 2.4 provide an indication of the scale of loss for both onshore and offshore events.

Date	Location	Plant Type	Event Type	PD Loss ($MM)
23-10-89	Texas	Petrochemical	VCE	839
01-09-01	France	Chemical	Explosion	750
24-06-00	Kuwait	Refinery	Explosion	412
04-05-88	Nevada	Chemical	Explosion	383
05-05-88	Louisiana	Refinery	VCE	368
27-09-98	Mississippi	Refinery	Hurricane	340
14-11-87	Texas	Petrochemical	VCE	285
25-12-97	Malaysia	Gas Plant	Explosion	282
23-07-84	Illinois	Refinery	VCE	268
09-11-92	France	Refinery	VCE	262
13-12-94	Iowa	Chemical	Explosion	224
18-09-89	Virgin Islands	Refinery	Hurricane	207
17-08-99	Turkey	Refinery	Earthquake	200
27-05-94	Ohio	Chemical	Explosion	200
25-09-98	Australia	Gas Plant	Explosion	200
23-07-84	Illinois	Refinery	Explosion	191
16-10-92	Japan	Refinery	Explosion	187
04-03-77	Qatar	Gas Plant	VCE	174

Table 2.3 : Largest onshore property damage loss (1972 - 2001) [15]
(Property damage in excess of $150,000,000)

Newark, New Jersey, 1983

This event occurred in 1983 when the overfilling of a storage tank caused a spillage of up to 265 tonnes of gasoline into a bund. A vapour cloud approximately 450m to 600m long and 60m to 90m wide was formed. The explosion caused significant damage on site, including damage to storage tanks hundreds of metres from the point of release, and glass breakage out to a distance of 3.5 miles (5.6km).

A full account of the findings of the investigation can be found in Bouchard J.K. Gasoline Storage Tank Explosion and Fire: Newark NJ January 7, 1983. National Fire Protection Association (NFPA) Summary Investigation Report (in cooperation with Federal Emergency

Management Agency/United States Fire Administration and National Bureau of Standards/Centre for Fire Research) (referenced in BMIIB Initial report). [16]

Naples, Italy, 1985

This event occurred in 1985 when the overfilling of a gasoline storage tank resulted in spillage of about 700 tonnes into a bunded area. The explosion resulted in serious damage to structures within 100m and glass breakage out to 0.62 miles (1km). A full account of the findings of the investigation can be found in Maremonti M, Russo G, Salzano E *et al* 'Post accident Analysis of Vapour Cloud Explosions in Fuel Storage Areas'. [17]

Saint Herblain, France, 1991

This event occurred in 1991, in which a release of gasoline from a section of pipe inside a bund produced a vapour cloud. Ignition of the vapour cloud produced extensive damage.

A full account of the findings of the investigation can be found in Lechaudel JF and Mouilleau Y 'Assessment of an accidental vapour cloud explosion. A case study: Saint Herblain, October the 7th 1991, FRANCE' Loss Prevention and Safety Promotion in the Process Industries 1995 1 377388 [18]

Date	Location	Facility Type	Event Type	PD Loss ($MM)
07-07-88	North Sea	Platform	Explosion	1085
26-08-92	Gulf of Mexico	Platforms	Hurricane	931
15-03-01	Brazil	Platform	Explosion/Fire	500
23-08-91	North Sea	Concrete Jacket	Mech Damage	474
24-04-92	Brazil	Platform	Blowout	421
01-11-92	Australia	Jacket	Mech Damage	314
20-01-89	North Sea	Drilling	Blowout	273
02-11-99	Indonesia	Process Deck	Mech Damage	210
01-07-75	Dubai	Platform	Blowout	204
04-11-87	Gulf of Mexico	Platform	Blowout	200
01-10-74	North Sea	Platform	Mech Damage	196

Table 2.4 : Largest offshore property damage loss (1972 - 2001) [15]
(Property damage in excess of $150,000,000)

Sri Racha, Laem Chabang, Thailand, 1999

This event occurred on 2nd December 1999, in which overfilling of a gasoline storage tank resulted in a fire and explosion causing damage to nearby buildings. Five gasoline storage tanks were destroyed and fires burned for some 35 hours. Eight people died and 13 were seriously injured as a result of the incident. The event occurred at 23:30 and had the explosion occurred earlier, the loss of life may have been much higher.

This potential for a spillage of 'cold' gasoline to lead to a vapour cloud explosion was also recognized by Kletz in 'Will cold petrol explode in the open air', (The Chemical Engineer, June 1986, IChemE) [19]. A full account of the findings of the investigation can be found in the 100 Largest Losses 1972-2001[15].

Port Hudson, Missouri, 1970

This event occurred on 9th December 1970 when liquid propane was released from a pipeline owned by Phillips Pipeline Company. A large vapour cloud engulfed the valley as shown in Figure 2.13 and was ignited in a rural area, generating severe explosion damage and high overpressures.

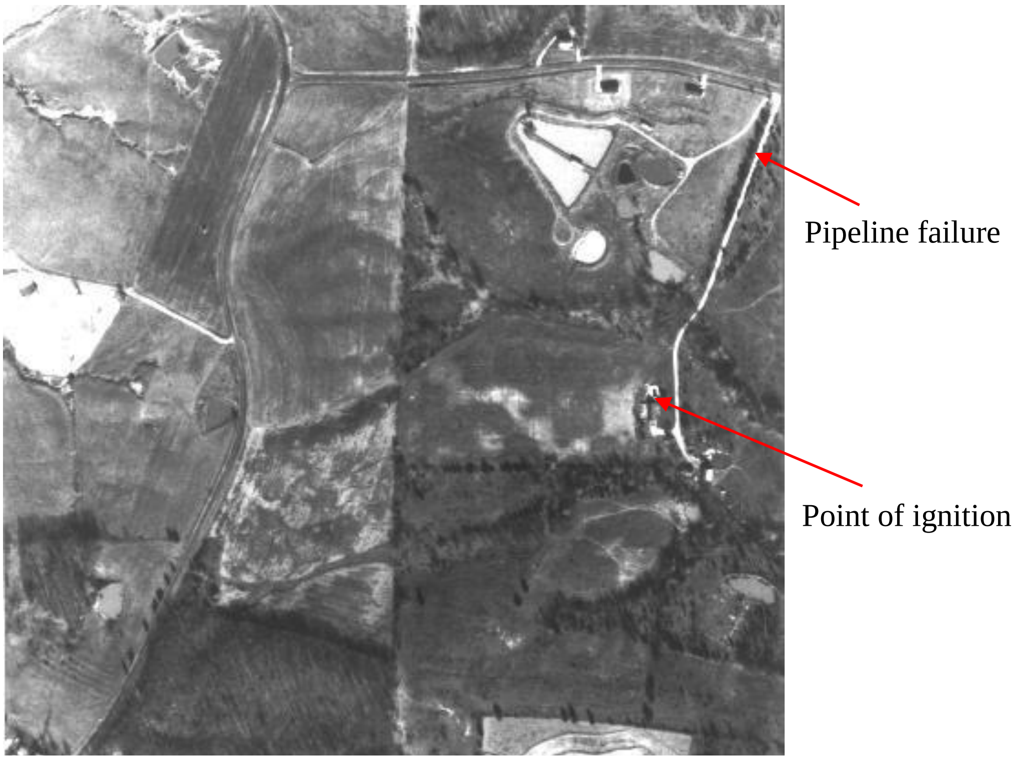

Figure 2.13 : Port Hudson - pipeline failure and point of ignition [15]

There was no pipework congestion present, however the conditions were calm and the vapour cloud dispersed throughout the valley, engulfing buildings and wooded areas.

It is believed that the explosion started in a pump house, which triggered a detonation in the vapour cloud. As such the accident is widely quoted as one of the first, if not the first, confirmed cases of Deflagration to Detonation Transition (DDT). See also Section 2.4.5.8.

Flixborough, UK, 1974

The chemical plant at Flixborough, UK was owned by Nypro UK and had been in operation since 1967. On 1st June 1974 a temporary bypass pipe carrying cyclohexane (C_6H_{12}) at 1MPa and 150^{o}c ruptured. Within one minute 40 tonnes of cyclohexane escaped forming a vapour cloud in the region of 100-200 metres in diameter. The cloud subsequently ignited and exploded, completely destroying the plant as shown below in Figure 2.14.

Figure 2.14 : Aerial photo of the remains of the Flixborough plant [16]

The explosion was estimated to be equivalent to 15 tonnes of TNT, 28 people were killed and another 36 were injured. At the time this was Great Britain's largest peacetime explosion. There were 1821 houses and 167 shops damaged by the blast within one mile radius of the plant site. In addition to localised damage, substantial structural damage affected areas of the nearby town of Scunthorpe, approximately 3 miles away and the blast was heard over 30 miles away in Grimsby.

The inquiry findings [20] concluded that failure of the 8 inch (200mm) diameter temporary bypass pipe occurred due to it being inadequately installed and poorly supported on scaffolding with flexible bellows at the ends. The pipework had not been designed for the purpose, nor had it been strength tested prior to use. Additionally, there were no active or triggered VCE mitigation measures in place at the plant.

Ufa, Russia, 1989

One of the most dominant catastrophic events involving a VCE occurred at Ufa in the Ural Mountains in Russia, on 4th June 1989. The explosion happened in a valley with dense forest area after an LPG pipeline ruptured. The ignition occurred when two passenger trains travelling in opposite directions on the Kuybyshev Railway entered the flammable cloud. The explosion killed 575 people and injured around 800. Figure 2.15 displays the tragic aftermath of this terrible event.

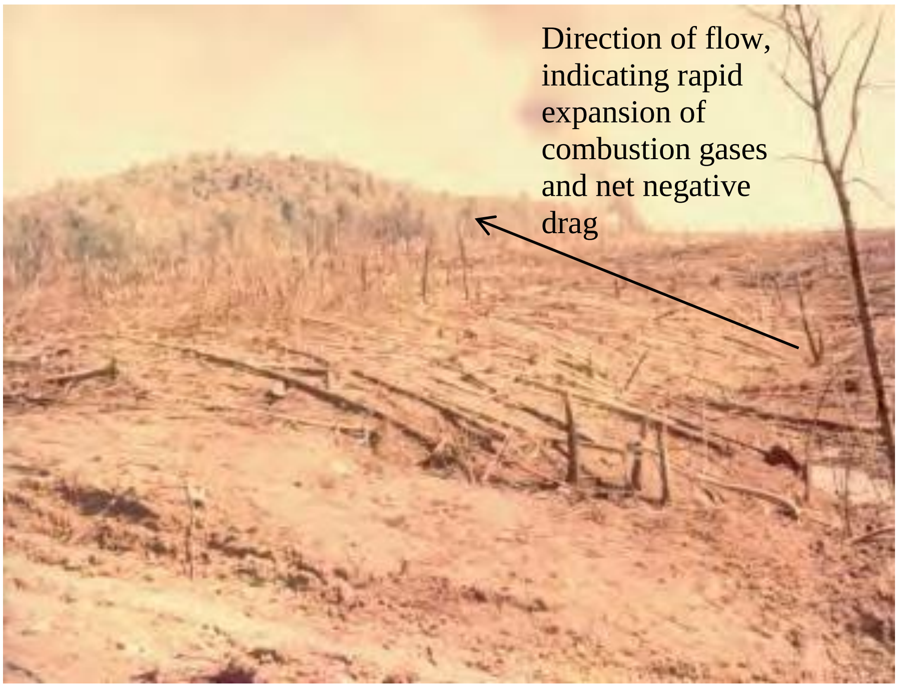

Figure 2.15 : Ufa, Russia, 1989 - Explosion indicators [17]

This was the most lethal railway accident in Soviet history. The explosion occurred when a LPG pipeline leak created a highly flammable cloud that was ignited by sparks created by two passenger trains passing each other nearby. Both trains were carrying many children.

The estimated scale of the blast would have been in the region between 250 to 10,000 tons of TNT equivalent. Three hours before the explosion local pipeline engineers noticed a dramatic drop in pressure. A decision was made to increase the pressure in the main, instead of identifying the cause. Figure 2.15, shown previously, illustrates that many of the trees fell towards the point of ignition, indicating that rapid flame acceleration, coupled with high speed venting of combustion products had occurred. This phenomenon in discussed further in Sections 2.4.5.7 and 2.4.5.8.

Piper Alpha, North Sea, 1998

This event occurred on 6th July 1998 on a large fixed platform situated 120 miles (193km) northeast of Aberdeen, Scotland, UK. The platform was equipped with two condensate pumps (pumps A & B) which were routinely maintained every two weeks. On 6th July pump A's safety valve was removed for routine maintenance and the open end was sealed off with a blind flange. As the duty engineer could not complete the maintenance by 18:00 a document was completed stating that the pump 'shall not be used under any circumstances'.

In addition to the on-going maintenance, the diesel pumps used for the platforms automatic fire fighting and deluge system had been placed in manual mode, as divers had been carrying out routine operations in the water. This was common practice, as there are large intakes underwater for the fire fighting system, which pose a significant risk to divers.

At 21:45 condensate pump B stopped suddenly and would not re-start. The duty manager was unaware of the previous aborted maintenance visit and accompanying documentation. Coincidently another permit had been issued to overhaul pump A and with this he assumed that pump A was good to start. At 21:55 pump A was switched on and the temporary seal used to cap off the safety valve connection was unable to withstand the pressure.

High pressure gas escaped rapidly and audibly from the opening and within a very short time ignited and exploded. Piper Alpha was also being fed by other gas lines (1400mm diameter) from Tartan another nearby platform. The gas pipes subsequently melted and ruptured during the fire, releasing 15-30 tonnes of gas per second and producing a 150m fireball. At around 22:50 the MCP-01 gas riser failed resulting in a third major explosion.

The fire fighting equipment was never started, although two men lost their lives attempting to reinstate it. In total 167 men lost their lives on Piper Alpha. The Piper Alpha Memorial Statue, as shown in Figure 2.16 was erected in 1991 and unveiled by the Queen Mother, in Hazlehead Park Aberdeen, in memory of the victims of the 1988 disaster.

Figure 2.16 : Piper Alpha Memorial Statue [17]

La Mede, France 1992

This event arose 9th November 1992 at a refinery and gas plant. The gas detection system alarmed at 05.17 indicating a major gas escape. The first vapour cloud explosion occurred at 05:20 while the unit operator was still in the process of warning the security service. The inquiry concluded that the gas release occurred when a pipe used to recover propane and butane ruptured.

Brenham, Texas, 1992

This incident occurred on 7th April 1992, in which the ignition of a vapour cloud comprising a mixture of hydrocarbons in a rural area resulted in significant damage to nearby buildings. No pipework congestion was present but the cloud engulfed wooded areas.

A salt dome cavern used to store LPG and similar products was overfilled, leading to an uncontrolled release of Highly Volatile Liquids (HVL's). A large vapour cloud formed that later exploded. Three people died from injuries sustained either from the blast or in the following fire. An additional 21 people were treated for injuries at area hospitals. Damage from the accident exceeded $9 million.

Buncefield, UK, 2005

This event occurred on 11th December 2005 at the Buncefield Oil Storage Depot. During a routine filling operation of 'Tank 912' shown in Figure 2.17, 300 tonnes of winter mix gasoline (incorporating approximately 10% butane) had spilled from the storage tank following an over fill. The gasoline spillage occurred for approximately 40 minutes, resulting in a large vapour cloud covering an area in the order of 100,000m^2. The sites CCTV records show the low lying vapour with an estimated minimum height of 2m throughout the area.

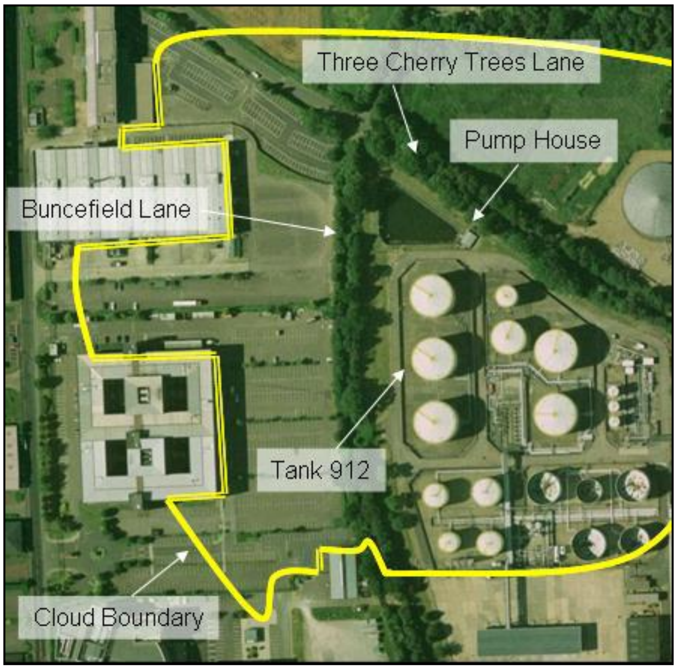

Figure 2.17: Buncefield site prior to explosion showing approximate cloud boundary [16]

Ignition occurred at the pump house, which was subsequently destroyed by the blast causing ignition and deflagration of the main cloud. The site had a number of areas with densely populated trees and undergrowth, which provided the necessary congestion to accelerate the flame to several hundred metres per second. This resulted in a DDT (see also Section 2.4.5.8.) The detonation wave then propagated through the remaining cloud.

Forensic evidence including pressure damage to vehicles and structures indicated overpressures of greater than 200kPa. Directional indicators such as the bending of sign posts and street lighting by the blast, normally associated with the flow field and direction of propagation in a deflagration, were actually bent in the opposite direction. This was caused by the rapid venting and expanding of hot combustion gases and was in the opposite direction to the detonation.

Although there were no fatalities involved, 43 people were injured and significant damage occurred to both commercial and residential properties in the vicinity. There was also damage reported further afield with windows blown out 5 miles (8km) away in St Albans. Total damages were of the order of $1.5 billion. This event was also monitored by British Geological Survey, which measured 2.4 on the Richter scale.

Jaipur, India, 2009

This incident occurred at the Jaipur Oil Depot on 29th October 2009, when 1000 tonnes of gasoline leaked from a storage tank. A large vapour cloud developed and subsequently ignited. Due to the congestion of the site, a DDT explosion occurred. Directional markers and indicators seen in Figure 2.18 were used to assess the direction of the blast wave and the net negative impulse.

Figure 2.18 : Jaipur, India, 2009 - Directional markers and indicators across the site [15]

2.4 Combustion theory

The following Sections have been included to highlight a better fundamental understanding of combustion theory, flame propagation and flame extinguishment. Information has been included with particular relevance to flammable gas and vapour cloud explosions.

Combustion is a self-sustaining exothermic chemical chain reaction, of heat and mass transfer of the chemical species. The chemical reactions between fuel and oxidant are the result of complex chain reactions and chemical kinetics, producing heat and normally light in the form of a flame. The reaction chains in combustion consist of hundreds of transitional stages where hydrogen and oxygen (hydro-peroxides) decompose and break up to form hydroxyl radicals. In turn these *free radical reactions* produce further reactions within the hydrogen and carbon chains, which lead to terminal reactions to complete the hydrogen and carbon chains. (See also Nasr, G.G. *et al* [8])

The combustion science of hydrocarbon fuels (solids, liquids, gases and dusts) has been studied in great detail and the processes are well documented. Zabetakis, of the US Bureaux of Mines [21] dedicated many years of experimental research into the flammability characteristics of combustible gases and vapours. The fundamental findings of this research are still used to this day to tabulate the properties and characteristics of flammable gases and vapours.

In order to suppress, or fully mitigate the chain reactions in the combustion process, the chains must be either broken, thus affecting the further propagation of free radicals and forcing the radical reactions to early termination, or the *activation energy* level required to sustain the reactions must be prevented from occurring in the first instance.

2.4.1 Activation Energy

To initiate and/or to sustain a combustion reaction, there must be sufficiently high enough energy levels to break, or ‘thermally crack’ the bonds within the molecules of the fuel and oxidant, thus allowing reactions to occur and products to form. Many saturated hydrocarbons exhibit very similar burning rates, with exceptions including alkenes such as ethylene which has a higher activation energy and resultant greater exothermicity, due to the presence of a double bond in the molecule. Alkynes such as acetylene contain a triple bond with even greater activation energy and exothermicity.

This energy level, measured in calories (cal) or kilojoules (kJ) per mole, is known as the activation energy [22] and is defined by the Arrhenius function (k), whereby:-

$$k = Ae^{-Ea/RT} \tag{2.1}$$

Where; k = the rate constant of chemical reactions

A = the pre-exponential factor

Ea = the activation energy (kJ)

R = Universal gas constant (J/kg K)

T = Absolute temperature (K)

Activation energy (E_a) in chemistry terms is the minimum energy required in order to commence a chemical reaction. Some elements and compounds will react with each other simply by bringing them into contact and these are known as 'spontaneous chemical reactions'. For others it is necessary to supply an external energy input, in the form of heat, or radiation, or electrical charge in order to initiate the reaction. At Standard Temperature and Pressure (STP) hydrocarbon fuel atoms will not combine with oxygen atoms. This is due to the very strong bonds that hold together their atomic structures.

The point at which the reaction begins is known as the 'energy barrier'. The energy barrier and activation energy of atoms are fixed properties for each atom, depending on the valence and type of chemical bond, i.e. single, covalent or triple bond. The reactivity of elements, in particular hydrocarbon gases and vapours are discussed later in this Section.

The total energy required to break this bond can be reduced by the inclusion of a catalyst. A catalyst is something that contributes to the lowering of the activation energy in a reaction. The lower activation levels in the presence of a catalyst are shown in Figure 2.19.

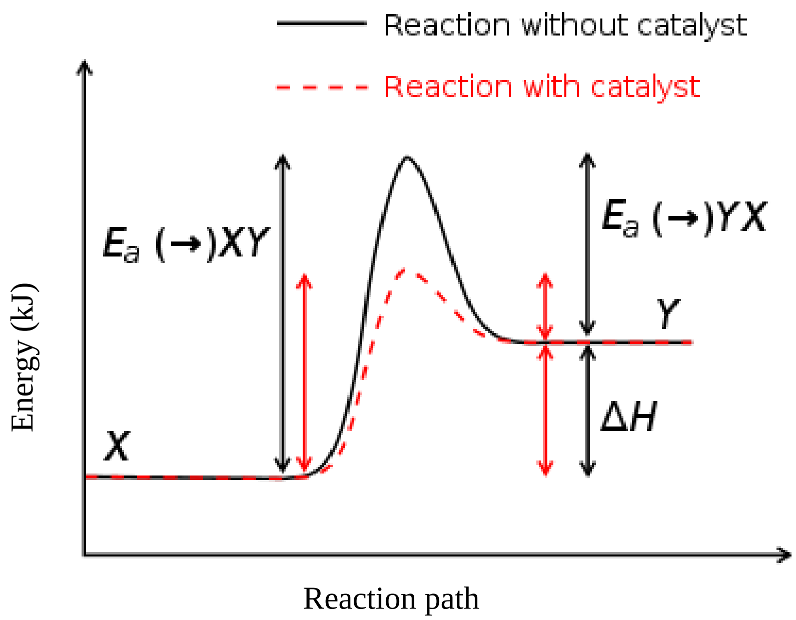

Figure 2.19 : Illustration of a reaction path with/without catalyst [22]

2.4.2 Governing factors

If a closed vessel containing a flammable mixture of fuel and oxygen at standard temperature and pressure is slowly heated at a controlled rate, a steady state may be achieved without ignition or flame. In experiments carried out by Bone and Wheeler [23] it was found that when a flammable mixture of methane and oxygen reached temperatures in the order of 573–673K at pressures of 200-230kPa, both species became sufficiently active to react chemically.

Although an exothermic reaction occurred, the heat produced by the reactions was lost through the vessel walls. To achieve this steady state a continuous controlled amount of energy in the form of heat was transferred into the mixture. Whilst rates of heat transfer are linear, the rates of the collisions and reactions vary exponentially with temperature.

If insulation was applied to the vessel, or if the energy input into the vessel increased, then the temperature of the mixture would begin to rise. This would bring about an increase in the rate of reactions, which would initiate an increase in pressure. The exponential increase in collisions would eventually lead to a critical temperature at which 'ignition' would occur. An explosion would then follow and energy in the form of heat and pressure would be released. Energy released as heat in this manner is known as a 'thermal explosion'.

When a flammable mixture of fuel and oxidant reaches this critical temperature known as the ‘ignition temperature’ a flame will begin to develop, which may then propagate through the remaining unburned mixture. The rate of this propagation is finite, but is also dependent on several governing factors. These include, the:-

i. Reactivity of the fuel
ii. Burning velocity, S_u (m/s) and flame speed, S_f (m/s) of the mixture
iii. Equivalence ratio, Φ (ER) or ratio of fuel and oxidant within the flammable range
iv. Temperature, t of the mixture (K)
v. Static pressure, P of the mixture (Pa)
vi. Geometry of containment
vii. Level of pressure relief during propagation (%)
viii. Positioning, shape, size (m) and concentration of obstacles within the mixture
ix. Level of mixing that has occurred – stratified or homogenous
x. Speed of sound, c (through the mixture) (m/s)

Furthermore, the criteria that is necessary for the extinction of a combustion wave or flame is determined by several other factors. One such factor is a dimensionless parameter known as the Damköhler Number (Da) [22]. The Damköhler number is used to relate fluid turbulence integral timescales and chemical reaction timescales in a system, and measures the importance between turbulence and chemistry.

In combustion, the rate at which reactants are consumed is proportional to the exponential value of the absolute temperature in the system, which may be expressed by the Arrhenius equation. Therefore, for a small reduction in temperature at the flame front, there will be an exponential decrease in the number of moles present in the gas which have energies equal to, or in excess of their activation energy.

Low Damköhler numbers are associated with relatively inert flows, whereas higher values are allied with faster chemical reaction rates. Figure 2.20 illustrates the characteristic ‘S’ shape relationship between Damköhler number and flame temperature.

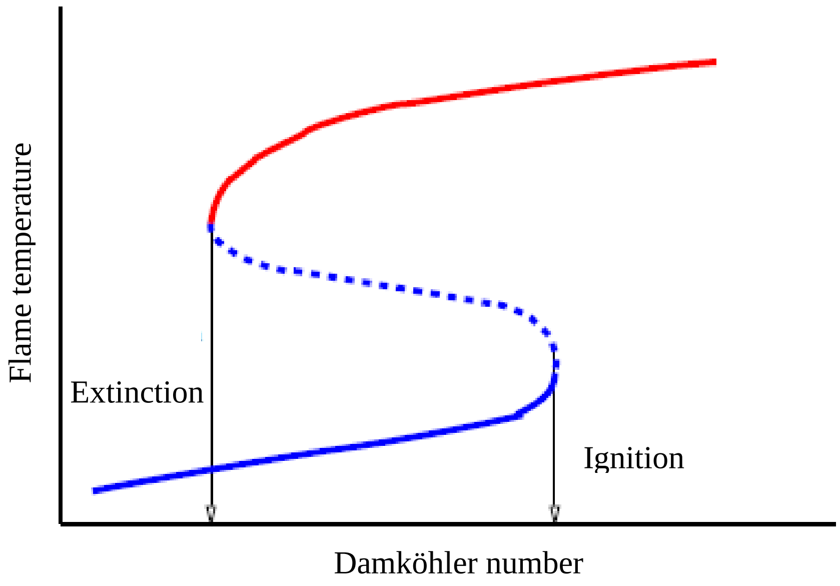

Figure 2.20 : Damköhler number characteristic 'S' shape curve [22]

Thus: $$Da = \tau_{t\,/}\,\tau_c \tag{2.2}$$

Where τ_t is the turbulence time scale and τ_c is the chemical reaction time scale.

The chemical reaction time at which extinction occurs is written as τ_{ext} . This is the defined as point at which combustion occurrence is impossible.

For Da smaller than a critical value combustion will be extinguished.

This is known as the Critical Damköhler number (Da_{crit}).

Therefore, combustion may occur when $$\tau_{t\,/}\,\tau_{ext} > Da_{crit} \tag{2.3}$$

And combustion will not occur when $$\tau_{t/}\,\tau_{ext} < Da_{crit} \tag{2.4}$$

The critical Damköhler number (Da_{crit}) is often considered when solving complex numerical and chemical kinetics solutions and may also be referred to in Computational Fluid Dynamics (CFD) code. However, within this present study, an experimental approach will be dominate proceedings, whereby the aims and objectives are to ascertain the effectiveness of a novel spray system and the unique dynamic spray criteria required to fully extinguish and mitigate a propagating flame.

2.4.3 Combustion waves, mass and heat transfer

If a quiescent mixture of flammable gas and air is ignited in the centre of the volume, a spherical combustion wave will develop. The wave will progress as a finite series of concentric *mass and heat transfer* interactions, as illustrated in Figure 2.21.

The heat transfer in a spherical combustion wave will always flow from the burned to unburned gas in a divergent manner. As the wave moves outward from the ignition source, the non-planer wave, or flame front will become an increasingly larger sphere. The rate of heat transfer from the burned gas to the unburned gas will eventually become insufficient to maintain initial rate of propagation and the combustion wave will begin to slow down, eventually being quenched. This phenomenon is also known a 'flame stretch' and is discussed in Section 2.5.1.

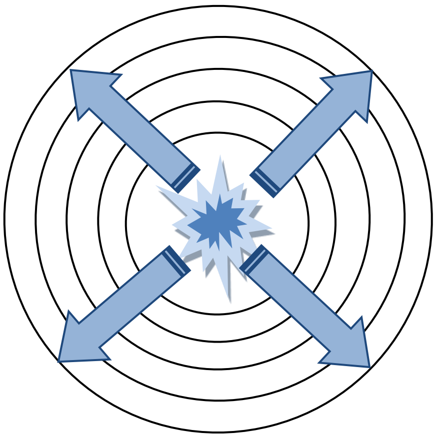

Figure 2.21 : Typical divergent propagation

The species diffusion and thermodynamics of mass and heat transfer occurring within an adiabatic plane combustion wave are best described by the work carried out by Fristrom, R.M. and Westenburg, A.A. [24], as summarised by Lewis and Von Elbe [25].

Fristrom and Westenburg demonstrated the elements of mass diffusion and heat transport in a series of experiments involving Schlieren photography, micro gas sampling, micro thermocouples and resistance wires.

Figure 2.22 shows schematically the following mass and heat transfer mechanisms:-

i. Heat is flowing from right to left, from the boundary on *b* to *u*

ii. Mass is flowing from left to right, from the boundary on *u* to *b*

iii. In the pre-heat zone ($T_u - T_1$) the mass receives heat in the form of thermal conduction

iv. In the reaction zone ($T_1 - T_b$) the mass reaches a critical temperature and then becomes a heat source. Although the mass is still feeding back heat into the pre-heat zone, there is an overall net heat gain from the downstream elements.

v. The temperature continues to increase until all of the chemical energy is depleted at point T_b.

vi. The chemical heat evolution can also be described by changes in heat flow according to the initial convex curve ($T_u - T_1$), followed by the concave nature of the curve ($T_1 - T_b$).

vii. Analogous attentions can be applied to the concentration mass fraction of the reactant molecules as they diffuse through the wave ($T_u - T_b$) and the products diffusing in the opposite direction($T_b - T_u$).

viii. The two opposing curves, of heat and mass elements diffuse in their respective directions, whereas intermediate products formed in the reaction zone will diffuse in both directions.

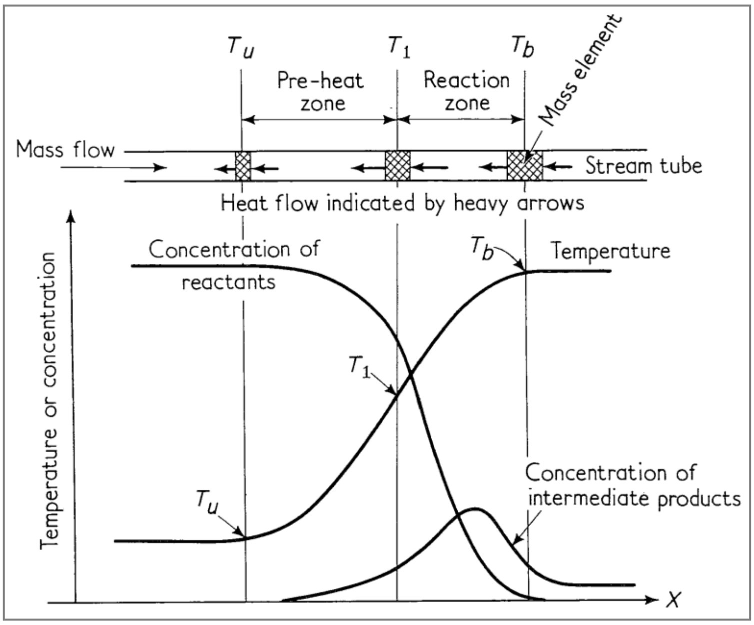

b Burned

u Unburned

Figure 2.22 : Concentration of reactants and temperatures in a plane combustion wave [25]

In the case of laminar combustion flow, adjacent layers of fluid will move smoothly past each other with a high degree of order. Whereas, in turbulent combustion flows (higher Reynolds number) eddies move back and forth across adjacent layers thus dissipating energy. In turbulent combustion waves, the surface area of the flame front will increase with instantaneous changes in reactions rates and thermodynamics with time.

In this present study the water droplets ($D_{32} \leq 30\mu m$) will be deployed into the flame front (pre-heat and reaction zone) in three different configurations. These are counter flow (C/F), parallel flow (P/F) and cross flow (X/F), or perpendicular to the plane of the wave.

Moreover, to ignite a fuel-oxidant mixture a finite quantity within the mixture must first reach a critical temperature. The ignition temperature can be determined by the intersection point of the two symmetrically opposing curves shown previously in Figure 2.22. The intersection occurs just inside the reaction zone, downstream of the pre-heat zone and upstream of the visible flame zone.

In addition, to ignite a combustible gas mixture or vapour cloud a minimum energy source is required; this is known as the *minimum ignition energy*. If a low energy spark occurs in the flammable mixture that is lower than the minimum level required, the spark will simply pass through the mixture without ignition occurring.

Experiments have been carried out by many authors to determine the minimum ignition energy of various fuels using a high tension electrical spark. Zabetakis of the US Bureaux of Mines [21] conducted several years of experiments to establish the minimum ignition energy required for various fuel types and mixture concentrations. The lowest ignition level (spark energy mJ) was found to occur in concentrations slightly lean of stoichiometric. For homogenous methane-air mixtures, the minimum ignition energy of was observed as 0.3mJ as illustrated in Figure 2.23.

For mixtures approaching the upper and lower limits of flammability 3mJ was found to be sufficient to ignite the mixture. The value was shown to be significantly higher at the extremes of the flammability limits. This was in the order of 10mJ.

The level of ignition energy used to ignite a mixture can also have an effect on the rate of propagation and flame speed. Where the ignition energy supplied is of many orders of magnitude higher than the minimum requirement, the additional energy may be transferred into the mixture thus producing an exponential increase in reaction tares. Extremely high energy levels are often used to detonate explosive. Such devices are known as *charges*.

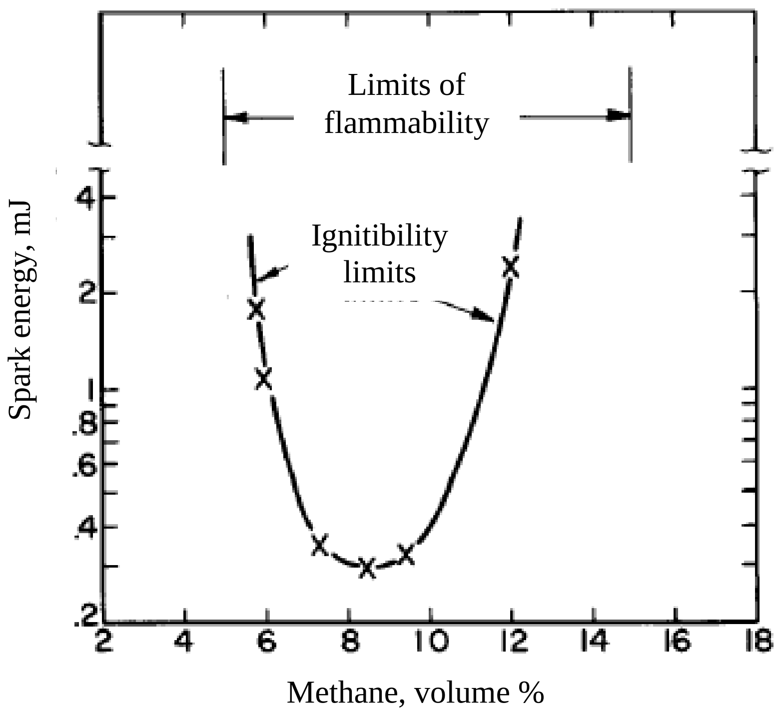

Figure 2.23 : Typical spark energy values (mJ) for methane-air mixtures [21]

When carrying out gas and vapour cloud explosion forensic investigations, the source and intensity of the ignition are often critical to the conclusions of the incident investigator.

The ignition system used for this current investigation will be supplied via a simple high tension spark, produced by an ignition transformer (see Chapter 4, Section 4.5.4.1). The ignition energy produced by the ignition unit was approximately 10mJ and was sufficient for the majority of mixture ranges tested in this present study.

However, during the supplementary trials (see also Chapter 5 and Appendix 9, where fuel rich methane-air mixtures were used between 11% - 14% methane (E.R.(ϕ) 1.18, 1.30, 1.43, 1.65)), an alternative, higher energy ignition source was found to be required. The ignition unit was used was the type normally associated with a fuel oil burner (see also Chapter 4), which had a spark energy of approximately 15-20mJ.

It is also important to note and explain the term Auto-Ignition Temperature (AIT). This is described as the spontaneous ignition temperature of a flammable substance in the absence of an external ignition source, such as a spark. The auto-ignition temperature reflects the general reactivity of a fuel and free radical reaction rate. Auto-ignition temperatures are affected by fuel composition and concentration in air, or oxygen.

In general, the pressure in the system will also have an effect on AIT as an increase in pressure will also promote higher rates of collisions in the species. Le Chatelier (see Section 2.4.5.2) carried out research into determining the auto-ignition temperatures of various gas-air mixtures. This research was performed in a uniformly heated vessel where various gas-air mixture samples were introduced.

Zabetakis [21] summarises many of the previous studies carried out in this field, concluding that the AIT of a hydrocarbon fuel was inversely proportional to the average carbon chain length. .

In designing the Flame Propagation and Mitigation Rig (FPMR) for this present study for methane-air mixtures, the ignition level provided would also be suitable for other longer chain alkanes. Figure 2.24 illustrates relationship between minimum auto-ignition temperature (AIT) and average carbon chain length

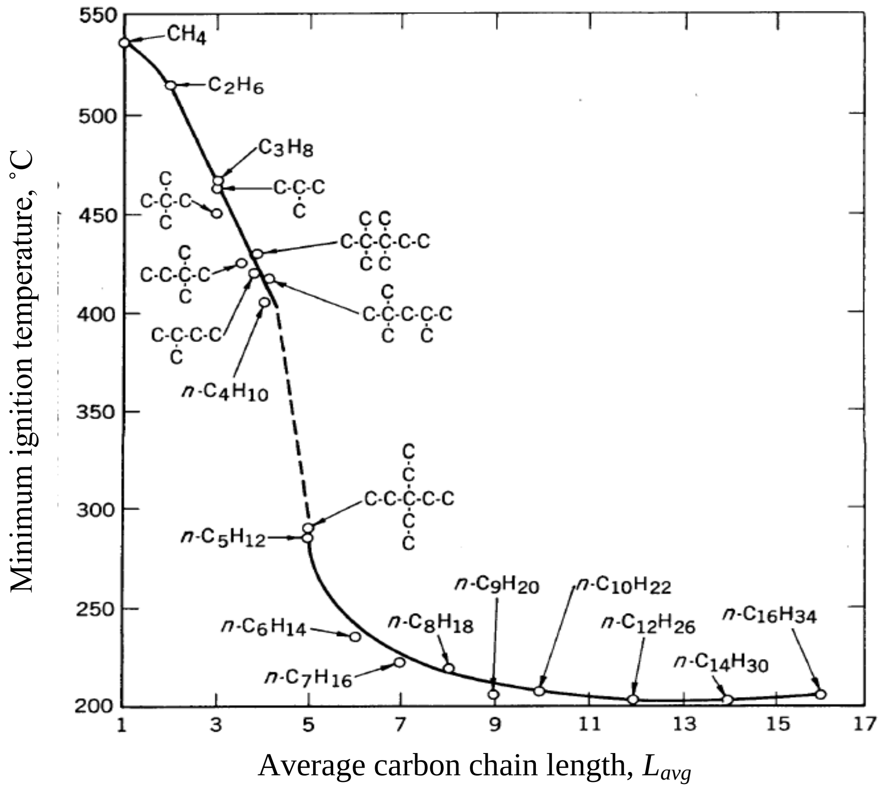

Figure 2.24 : Typical relationship between AIT and average carbon chain length [21]

2.4.4 Limits of Flammability

The terms *limits of flammability*, *explosive limits* and *flammable range* are all generally used as interchangeable terms used to express the volumetric percentages of fuel-air mixtures.

Although the terms are generalised and quite indistinguishable, the quantitative measurement techniques used to verify explosive limits and flammability limits have differed in previous published literature and apparatus [26]. Volumetric percentages are very useful for gaseous mixtures, whereas liquid and solid fuels are usually expressed as mol percentages of fuel-air mixtures.

For the purpose of this current research the terms 'flammable limits / range' will be used, rather than 'explosive limits / range'. Although it is recognised that small traces of gas can be easily oxidised in air beyond the limits of flammability, a combustion wave will only propagate within the defined limits.

In an ideal homogenous mixture, sustained combustion cannot take place above or below the limits of the flammable range. The limits of the range are normally given as the upper limit (fuel rich) and lower limit (fuel lean). This fundamental property of fuel-air mixtures has been studied in detail in the past and there has been a great deal of research conducted in this area. In industry it is often important to have access to specific data when storing or utilising flammable liquids or gases. This data allows for appropriate risk assessments to be carried out and appropriate control measures to be employed.

Although there are some minor variations in published values for limits of flammability, the limits published by Zabetakis [19] are normally accepted as an industry standard and will be used for this current work, as shown in Table 2.5 below.

Gas	Stoichiometric Gas in Air %	Limits of Flammability (volume %)	
		(LFL) Lower flammability limit	(UFL) Upper flammability limit
Methane	9.4	5.0	15.0
Propane	4	2.1	9.5
Butane	3.12	1.8	8.4
Hydrogen	29.5	4.0	75.0

Table 2.5 : Summary of limits of flammability and stoichiometric air requirements [21]

In order to reduce the number of accidental fires, gas and coal dust explosions associated with coal mining, the American Bureaux of Mines for the U.S. Department or the Interior, conducted many years of ground breaking research. Between 1910 and 1924, detailed research into the flammability characteristics of over 200 combustible gases, vapours and also coal dust was carried out [21]. Flammable mixtures fall into one of three categories:-

i. Mist
ii. Saturated vapour-air mixtures
iii. Unsaturated flammable mixtures

N.B. The term mist consists of vaporised fuel droplets suspended in an air-fuel cloud.

Bureaux of Mines research also confirmed the relationship between temperature and pressure, on the limits of flammability and auto-ignition temperature.

Figure 2.25 illustrates the relationship and effect of temperature on limits of flammability. In a fuel-air mixture at an initial temperature at point ‘A’, the mixture may be non-flammable. However, as the limits of flammability tend to widen with respect to an increase in temperature, the mixture would then become flammable at point B.

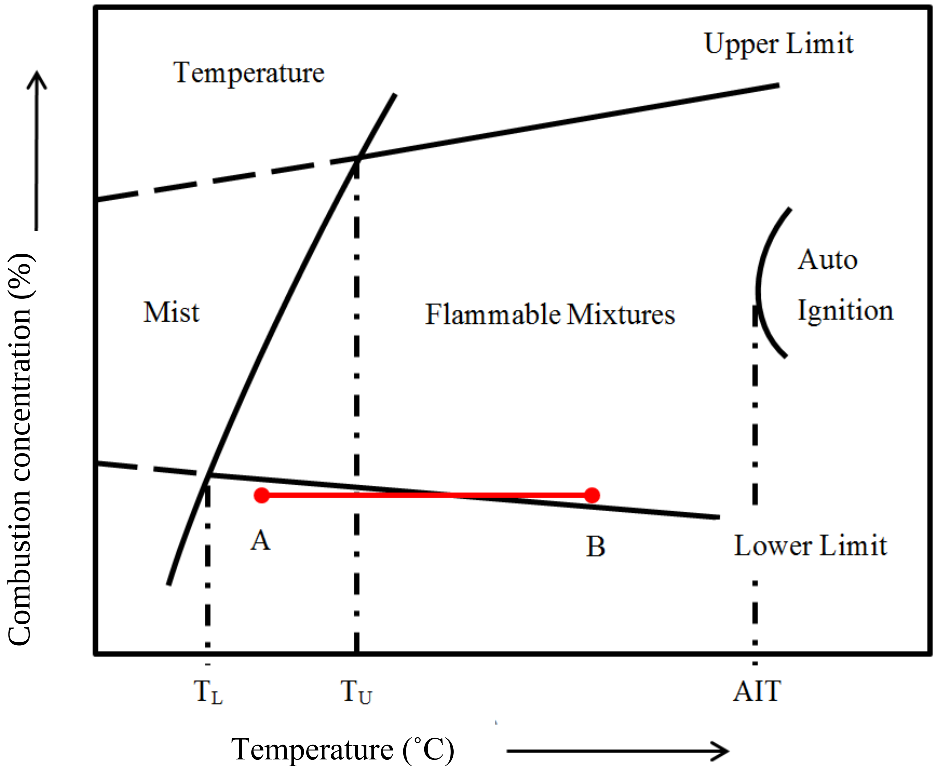

Figure 2.25 : Effect of temperature on limits of flammability [23]

An increase in pressure or temperature will increase the frequency of collisions occurring in the mixture, thus causing the flammability limits to extend.

Within this current study the reference conditions for the flammable mixtures will be taken as room temperature, approximately 20˚C.

Fuel-air mixture concentrations are generally expressed on either a molar basis, percentage volume fuel in air, or by using the 'Equivalence Ratio'. The term Equivalence Ratio, ϕ, (ER) is often used to compare the oxidiser-fuel mixture being used to the stoichiometric oxidiser-fuel value. The equivalence ratio may be used to express the oxidiser-fuel ratio on a mass, molar or volumetric basis.

One of the advantages of using equivalence ratio in this research is to allow comparisons to previous work. A fuel-oxidiser ratio is reliant to the units of measurement being used (mass, molar or volume), whereas the equivalence ratio does not have the same reliance on units.

Considering a mixture of one mole of methane and one mole of oxygen, the E.R. can be expressed as:-

$$\phi = \frac{[\text{fuel-oxidiser ratio}]_{\text{actual}}}{[\text{fuel-oxidiser ratio}]_{\text{stoic}}} \quad \text{or} \quad \frac{[\text{oxidiser-fuel ratio}]_{\text{stoic}}}{[\text{oxidiser-fuel ratio}]_{\text{actual}}}$$

Hence E.R. on a Mass Basis

$$\frac{{}^{m}CH_4}{{}^{m}O_2} = \frac{1\,(1 \cdot 12 + 4 \cdot 1)}{1\,(2 \cdot 16)} = \frac{16}{32} = 0.5 \qquad (2.5)$$

And on Mole basis

$$\frac{{}^{n}CH_4}{{}^{n}O_2} = \frac{1}{1} = 1 \qquad (2.6)$$

Using a mole or mass method will produce different values. Therefore, it is important to quote equivalence ratios in literature to allow others to review and compare the work.

Consider the combustion equation $_{\text{stoic}}$ for methane.

$$CH_4 + 2O_2 \longrightarrow CO_2 + 2H_2O \qquad (2.7)$$

The E.R. of the fuel-oxygen ratio by mass

$$\phi = \frac{{}^{m}CH_4}{{}^{m}O_{2stoic}} = \frac{1\,(1 \cdot 12 + 4 \cdot 1)}{2\,(2 \cdot 16)} = \frac{16}{64} = 0.25 \qquad (2.8)$$

And the fuel-oxygen ratio by mole

$$\phi = \frac{{}^{n}CH_4}{{}^{n}O_{2stoic}} = \frac{1}{2} = 0.5 \qquad (2.9)$$

Therefore if we use the equivalence ratio to determine the mixture used:

By mass

$$\phi = \frac{{}^{m}CH_4 / {}^{m}O_2 = 0.5/0.25}{({}^{m}CH_4 / {}^{m}O_2)_{stoic}} = 2 \qquad (2.10)$$

By mole

$$\phi = \frac{{}^{n}CH_4 / {}^{n}O_2}{({}^{n}CH_4 / {}^{n}O_2)_{stoic}} = 1/0.5 = 2 \qquad (2.11)$$

Where;

$\phi < 1$ the mixture is fuel lean, oxidiser rich

$\phi = 1$ the mixture is stoichiometric

$\phi > 1$ the mixture is a fuel rich mixture, oxidiser lean

For example:- a methane-oxygen mixture with 10% excess oxygen (fuel lean) would be represented as:-

$$\phi = \frac{[\text{1 fuel-2.2 oxygen ratio}]_{\text{actual}}}{[\text{1 fuel-2 oxygen ratio}]_{\text{stoic}}} \quad \text{or} \quad \frac{[\text{2 oxygen ratio-1 fuel}]_{\text{stoic}}}{[\text{2.2 oxygen ratio-1 fuel}]_{\text{actual}}}$$

ϕ = 0.909 **Φ = 0.909**

Both calculations give the E.R. (ϕ) of **0.909** (i.e. fuel lean, oxidiser rich).

In this present study methane-air mixture will be initially quantified by volume percent using a Gascoseeker, as discussed exclusively in Chapter 4, Section 4.7.2. However, to allow analysis and comparison with previous studies, these values will be presented and discussed with reference to their E.R., ϕ in the subsequent Sections and Chapters.

2.4.5 Flame Propagation

Flame propagation is the spread of a flame outwards from the origin of where combustion commences. Previously in Section 2.4.2 the experiments carried out by Bone and Wheeler [23] were considered, where a flammable mixture was heated at a controlled rate, prompting air and fuel to combine chemically without the existence of a flame. In the experiments the energy input to, and heat losses from the vessel were carefully controlled with respect to the temperature rise caused by the exothermic reaction, yet there was no presence of any flame in this balanced state.

Most explosions are initiated by the energy contained in a spark as discussed in Section 2.4.6.1 whether in the form an intentional source such as an ignition electrode, or from an unintentional source such as electrical arcing from a motor etc. When considering the former, for a flame to propagate outwards through a flammable mixture the ignition source must have sufficient energy and the spark gap must be within a tolerable range.

Many of the early flame propagation experiments that were either conducted or summarised by Lewis and von Elbe [25], were carried out with soap bubbles containing an explosive mixture and a pair of ignition electrodes. As soap bubbles pose practically no resistance to thermal expansion, the flame was able to propagate outwards as a spherical divergent non-planer wave at a constant pressure. This work also prompted addition research into the ideal conditions required to develop a 'flame kernel', which in turn contained sufficient energy to propagate beyond the cavity between the ignition electrodes.

The rate of outward propagation from the kernel throughout the flammable mixture is governed by several key factors. The degree of environmental confinement is a principal influential factor relating to the resultant flame speed in which three scenarios, previously described in greater detail in Section 2.2, may ensue. In summary the three main environmental conditions are:-

i. Unconfined explosions
ii. Partly confined explosions
iii. Confined explosions

Mitigation and risk reduction measures will vary depending on the scenario and the flame speeds likely to occur. These are discussed in detail in Chapter 3.

2.4.5.1 Burning Velocity

Burning velocity (S_u), burning rate, mass burning rate and flame speed (S_f) are terms used to describe the rate of a combustion reaction. Although each of the terms describes a very different phenomena, they have all been repeatedly used incorrectly in the past [26] as interchangeable terms. In early combustion research Bunsen [27], Coward and Hartwell [28], Michelson [29], Gouy [30], Stevens [31] and Lewis and Von Elbe [25], employed several methods to attempt to qualify and quantify the rate of combustion.

The methods varied, from igniting a mixture at one end of a tube and timing its propagation rate, to large soap bubbles filled with flammable mixtures, to 'seeded' mixtures containing very fine particles which were 'tracked' through the flame and water cooled heat flux burners that form a hovering disc like flame as, shown in Figure 2.26.

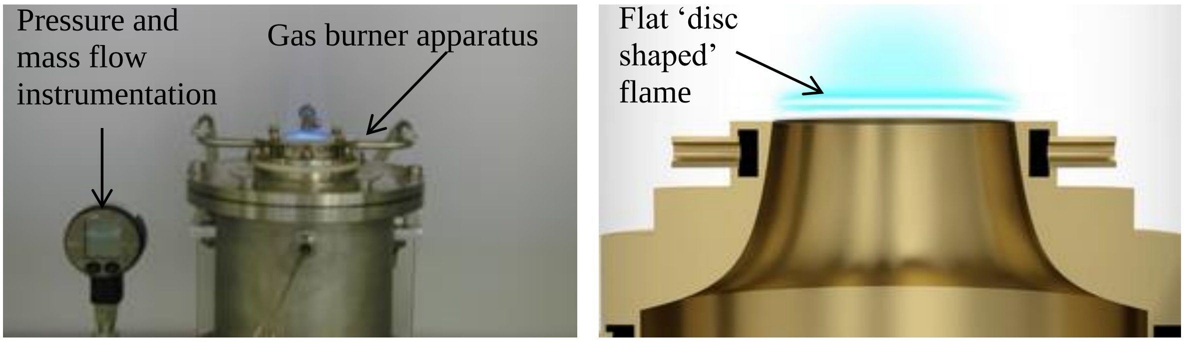

Figure 2.26 : Heat flux burner for measuring adiabatic laminar burning velocity

In the latter method (Figure 2.26 above), a flat flame is assumed to be one-dimensional and essentially adiabatic, meaning that there are no heat losses to the surroundings. Air and gas mass flow controllers calculate the flow rate of the unburned mixture (S_g), which is equilibrium with the burning velocity of the one-dimensional flame. Therefore $S_g = S_u$.

In much of the other earlier work discussed above, the speed of the flame relative to a stationary observer was postulated. These days we refer to this as *flame speed*, as described in the following Section 2.4.5.2. Andrew and Bradley [32] published a review paper relating to burning velocity in 1972, offering the following overt definition of *burning velocity*;

"It is the velocity, relative to the unburned gas, which a plane, one dimensional flame front travels along the normal to its surface".

2.4.5.2 Flame Speed

Flame speed (S_f) can be described as the velocity of a flame relative to a stationary observer, or fixed reference point e.g. thermocouple or photodiode. The flame speed will always be greater than the burning velocity, as the propagating flame front and the unburned gas (u) are driven by the hot expanding products of combustion.

Therefore the relationship between flame speed and burning velocity can be defined as;

$$S_f = S_u + u \qquad (2.12)$$

The volume occupied by the expanded burned gases is significantly greater than that of the unburned gases. This expansion relationship (E) can be expressed using density (ρ) comparisons.

Therefore the expansion factor (E) can be defined as;

$$E = \rho_u / \rho_b \qquad (2.13)$$

Where ρ_u is the density of the unburned gases and ρ_b is the density of the burned gases.

The expansion relationship (E) can also be expressed with respect to temperature (T) and the number of moles (n);

$$E = \left(\frac{Tb}{Tu}\right)\left(\frac{nb}{nu}\right) \qquad (2.14)$$

This expansion relationship between burning velocity and flame speed varies only slightly between flammable gases and vapours, the E values are generally between 7 and 8 as revealed in Table 2.6.

Property	Methane	Propane	Hydrogen
S_u (m/s)	0.45	0.52	3.5
S_f (m/s)	3.5	4.0	28
E	7.4	7.6	8.0

Table 2.6 : Expansion relationship between burning velocity and flame speed [21]

In this present study the effects of thermal expansion on flame speed will be controlled by the unique characteristics of the flame propagation and mitigation rig, whereby flame speeds are limited by design to ≤30m/s. (See also in Chapter 4)

Furthermore, Henry-Louis Le Chatelier carried out some of the earliest acclaimed scientific research [33] in the field of combustion in the late eighteen hundreds and early nineteen hundreds.

Le Chatelier's principle, also known as the equilibrium law can be used to describe the changes in a chemical system such as combustion, when fixed parameters such as air-fuel concentration, temperature, pressure and burning velocity are altered. The principle simply states that any change in the initial reaction conditions will prompt an opposite reaction in the responding system. Figure 2.27 typically represents a forward and reverse reaction, with respect to time.

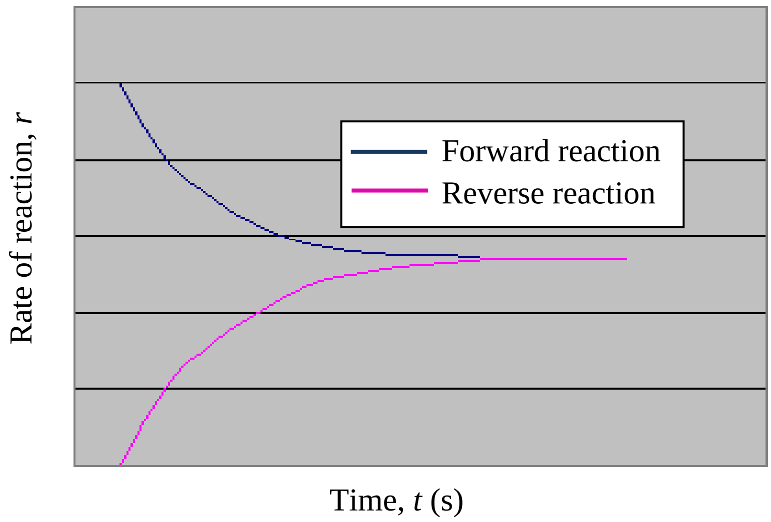

Figure 2.27 : Variation of forward and reverse reactions with respect to time [33]

When considering a flame on a burner, the mixture speed (U_g) is in dynamic equilibrium with the burning velocity (S_u) normal to the flame front. Therefore, the mixture is moving forward at the same rate as the flame is moving backwards.

If this equilibrium state ceases to be in balance, then the flame will either lift away from the burner, or flash back into the burner.

Flame suppression, mitigation or quenching systems must sufficiently affect this equilibrium by either by reducing the temperature of the exothermic reaction, thus causing a reduction in burning velocity, or by breaking down the intermediate chain reactions, also leading to a reduction in burning rate. In the case of the flame on the burner, the flame will begin to lift off as the reduced burning velocity fails to overcome the unchanging mixture speed.

2.4.5.3 Flame Thickness

The thickness of a laminar flame (δ_l) is a predetermined characteristic length at a particular dynamic condition, such as fuel-air mixture ratio (E.R.). Flame thickness is influenced by flame speed and is dependently coupled with temperature, density and pressure.

In previous studies Zeldovich *et al* [34] observed that the laminar flame thickness (δ_l) can be approximated to Δx, as the tangent spanning the Δt between the burned (T_b) and unburned (T_u) gases and illustrated in Figure 2.28.

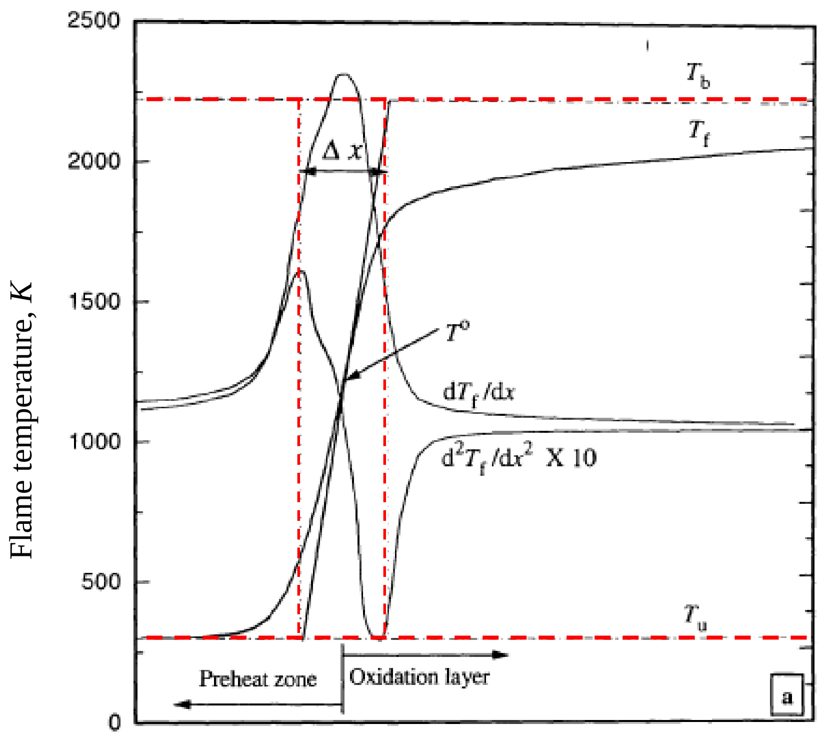

Figure 2.28 : Flame thickness in relation to unburned and burned gas temperature [34]

In experimental studies Andrews and Bradley [35] measured the temperature profile across a premixed ethane-air flame directly using 12.7μm thermocouples and a Schlieren interferometer. The flame thicknesses obtained by Andrews and Bradley are widely accepted and referenced in scientific journals [32] and will also be used in this current study.

Alternative approximations of flame and preheat zone thickness have be calculated using the CHEMKIN Sandia premix code. Various chemical reaction and reduced reaction mechanisms known as GRI-Mech2.11 were used to solve the relationship between flame thickness and equivalence ratio.

Gottgen *et al* [36] calculated flame thickness from burning velocity using 82 specific elementary kinetic reactions for, lean hydrogen, methane, ethylene, acetylene and propane flames. Figure 2.29 reveals the relationship between flame thickness and air-fuel ratio (equivalence ratio ϕ). Although there is some disagreement with the various sources of results, considering the practical, physical and computational difficulties in accurately measuring, or predicting the extreme isothermal gradients associated with combustion, the important factor with respect to *flame quenching, suppression or mitigation*, is the trend and the overall relationship.

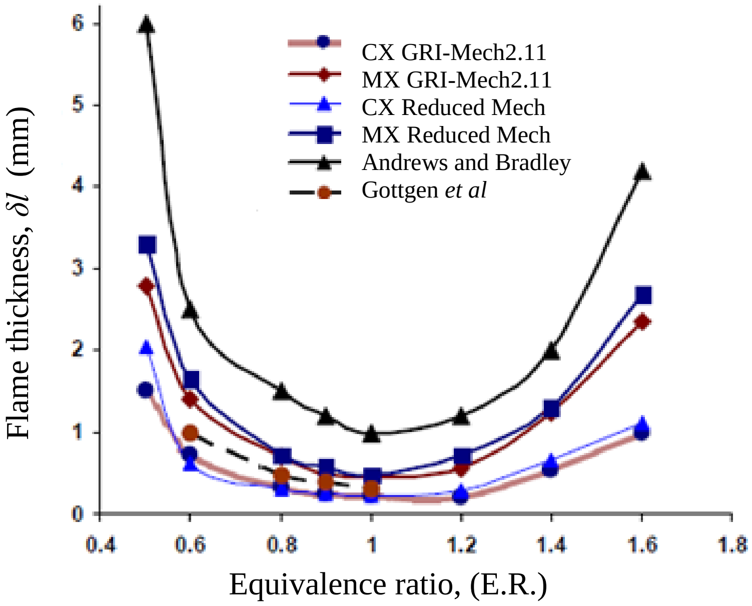

Figure 2.29 : Relationship between flame thickness (δl) and equivalence ratio (ϕ) [35]

The thickness of the flame and preheat zones has a direct influence on the interaction of water sprays and flames. Water droplets are afforded very short 'residence times' for heat transfer, or to even evaporate fully within the reaction zones of the flame.

As the equivalence ratio approaches unity, the flame speed it at its greatest and the flame thickness is at its finest. With this in mind, droplet diameters and their intrinsic heat up and evaporation rates must correspond to this worst case scenario. In this study the methane-air mixture of E.R. (ϕ) 0.95 produced the greatest challenges and was the most difficult to mitigate, as discussed explicitly in Chapter 5, Results and discussions.

2.4.5.4 Laminar and turbulent combustion

Combustion is a complex thermodynamic and fluid dynamic process. In fluid dynamics, flow regimes are segregated into two main areas; laminar and turbulent flow. In laminar flow, the combustion process has a degree of order and predictability with respect to mass and energy transfer mechanisms, burning velocity and flame thickness. The subject of laminar flame propagation was previously approached in Section 2.4.5.1.

In turbulent combustion flows, the flame front is highly irregular and disorganised. The disorder caused by such vortices and eddies, creates a *wrinkled flame front* with a much greater surface area than a corresponding laminar flame. The turbulent disorder also has an amplifying effect on the mass and heat transfer mechanisms occurring in the reaction zones, as illustrated in Figure 2.30. Flame thickness in turbulent flames is highly irregular and complex. Therefore, in line with previous studies [2, 39] reference will be made only to corresponding laminar thicknesses when discussing droplet transition through the flame front.

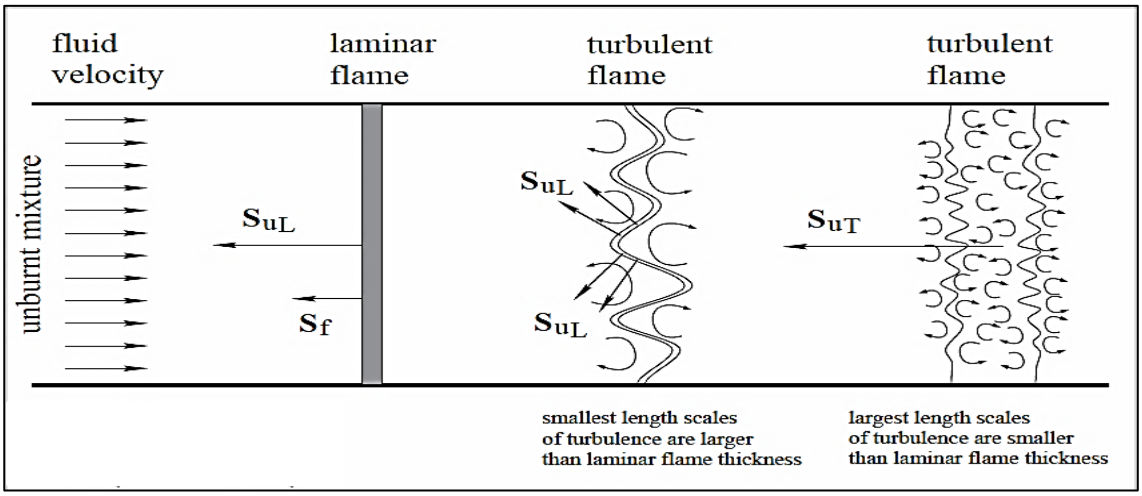

Figure 2.30 : Illustration of laminar and turbulent combustion flame front [24]

In order that turbulent flames could be studied in the past, the concept of the laminar 'flamelet' was introduced and adopted. As previously discussed combustion takes place in asymptotic thin layers. In turbulent combustion, these well-defined asymptotic layers that are embedded in the flow field are well understood and can be predicted. The inner structure of the flamelet is one dimensional and is also time dependent.

Other non-dimensional parameters included in this kinetic modelling process are the Damköhler number and activation energy / Zeldovich number. These were previously discussed in Sections 2.4.1 and 2.4.2. Laminar and turbulent flows regimes are often distinguishable by their resultant Reynolds number. This dimensionless number can be defined as the relationship between *inertia and viscous forces*. In this present study, combustion occurred in homogenous fuel-air mixtures, where still images of the flame propagation qualitatively revealed a typical laminar flow profile in many of the trials. (See also Chapter 5, Results and discussions)

2.4.5.5 Deflagrations

Where a combustion wave propagates at subsonic speeds relative to the speed of sound in the unburned gas mixture, this is referred to as a deflagration. A deflagration may also exist as a ‘stationary’ flame using a device such as a burner e.g. a pre-aerated natural draught burner as found on a gas cooker or gas water heater, or as a combustion wave propagating through a flammable fuel-air cloud.

Ignition of a flammable mixture in a truly unconfined area will generally result in a deflagration, with laminar flame speeds and resulting overpressures of just a few hundred Pascals (Pa). Where an explosion occurs in an area with a degree of confinement, overpressures in the order of several atmospheres have occurred beyond the cloud boundary as shown in the explosion testing scenario in Figure 2.31.

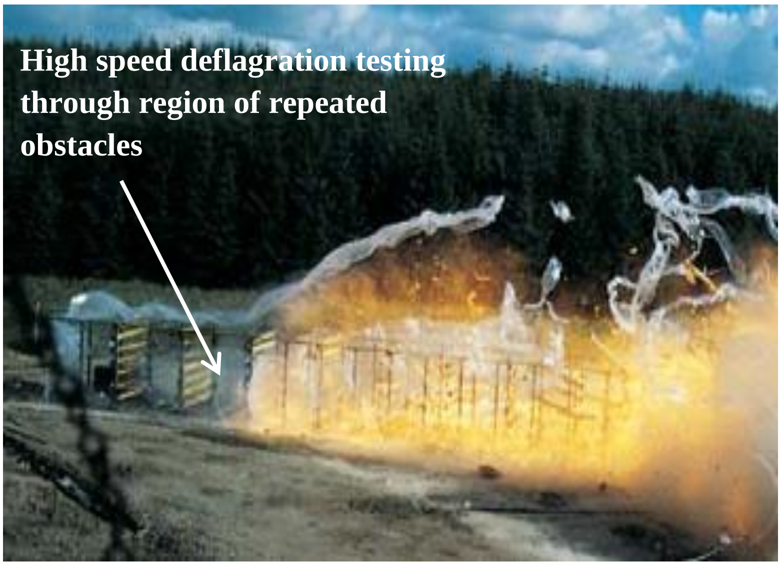

Figure 2.31 : 45m long polythene covered test rig 3m x 3m in cross section [14]

These instantaneous and dynamic flame speeds are governed by several factors, which are discussed further in Section 2.4.5.7.

Cronin and Wickens of British Gas MRS [14] carried out a large scale study of the conditions required for sustained high speed flame propagation in a flammable vapour cloud. These tests were undertaken using a 45m long, polythene covered test rig a shown previously in Figure 2.31, which was 3m x 3m in cross section.

High initial flame speeds were generated by using a 9m long reinforced steel 'driver' section, where the ignition was also generated. Along the test rig at 1.5m intervals, various obstacles in the form of 180mm polyethylene pipes were placed horizontally to simulate pipe racks and arrays. Various configurations were used with an assortment of blockage ratios.

In one test using a stoichiometric natural gas-air mixture, the flame exited the 9m long reinforced steel driver section at just below 500m/s into the combustible vapour cloud and congested area of repeated obstacles. In this test the blockage ratio in the pipe arrays was 40% (vol/vol), as shown below in Figure 2.32 with the pipe arrays were placed at 1.5m intervals along the polythene covered section. The flame decelerated rapidly as it left the congested zone to an almost steady rate of about 40m/s.

Figure 2.32 : Pipe array with 40% blockage ratio [14]

In another test using a stoichiometric natural gas-air mixture, the flame exited the 9m long reinforced steel driver section at slightly greater than 500m/s into the external vapour cloud and congested area of repeated obstacles. The blockage ratio in the pipe arrays was also 40% (vol/vol) at 1.5 m intervals. The flame propagated through the external region of repeated obstacles at a sustained flame speed averaging 500 – 550 m/s.

Repeatable and sustained high speed propagation was achieved in natural gas-air mixture concentrations of 7.8 – 12% (vol/vol). Higher flame speeds in the order of 650 m/s were achieved in the stoichiometric natural gas-air mixture by increasing the number of 40% blockage pipe arrays and by placing them 0.75m apart, instead of 1.5m apart. In this test pressures generated within the cloud were around 0.4 – 0.8MPa (4 – 8bar), with local peak pressures of up to 1.5MPa (15bar). Far field shock wave pressures were recorded at 175m away from the test site, in the region of 2MPa (20bar).

High speed propagation beyond the initial 9m section did not occur:-

i. When the flame in the stoichiometric natural gas-air mixture crossed into a region that was unconfined and unobstructed by pipe arrays.
ii. When the flame in the stoichiometric natural gas-air mixture crossed into a region with half the number of repeated obstacles i.e. 20% blockage ratio at 1.5m intervals, or 40% blockage ratio at 3m intervals.
iii. When the flame in the stoichiometric natural gas-air mixture crossed a single gap of 3m, in the standard 40% blockage, 1.5m interval scenario.

None of the experiments carried out using natural gas-air mixture produced speeds great enough to undergo transition from deflagration to detonation (DDT). However, similar tests using stoichiometric propane-air mixtures did result in deflagration to detonation transition (DDT). This concept is discussed explicitly in Section 2.4.5.8.

It is worth noting that the apparatus used for the above study would be highly suitable to conduct realistic scale mitigation trials, whereby a lattice of suitable atomisers could be placed upstream and downstream of the congested regions to evaluate the suppression and mitigation properties of the atomiser array in both configurations. Suggestions for further studies and full scale realistic trials are discussed in Chapters 5 and 7.

2.4.5.6 Detonations

Where a combustion wave propagates at supersonic speeds relative to the speed of sound in the unburned flammable mixture, this is referred to as a detonation wave. In a detonation the flame is accompanied by a leading 'shock front'.

Heat is generated by the shock compression as it travels though the unburned gas cloud, as illustrated in Figure 2.33. The heat produced is more than sufficient to achieve auto ignition. Once a shock wave is generated, a supersonic combustion wave will propagate through the flammable gas cloud at speeds of up to 2000m/s resulting in extreme overpressures of greater than 20 atmospheres in some cases. These overpressures have the potential to cause far reaching and catastrophic damage.

In basic terms a detonation wave may be described as a shock wave immediately followed by a flame, known as ZND theory. Furthermore, a detonation wave is a three-dimensional shock wave followed by the reaction zone.

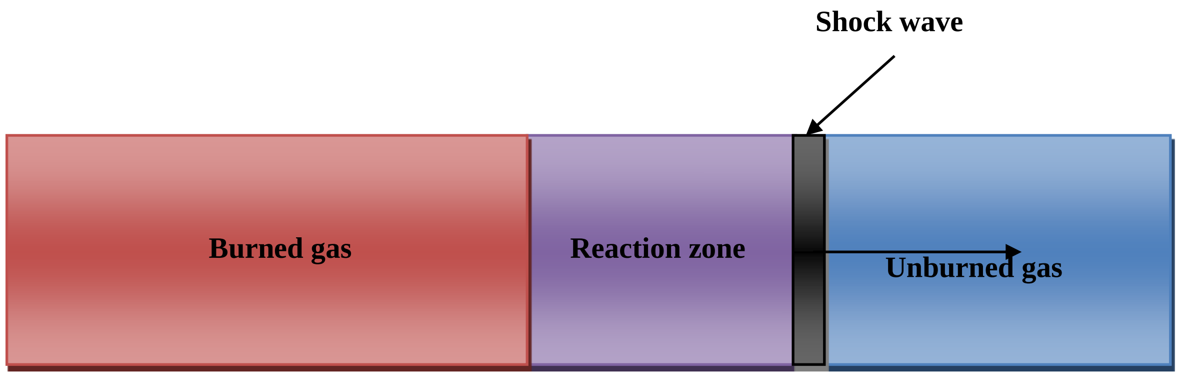

Figure 2.33: Shock wave immediately followed by a flame (ZND theory)

Detonations may occur due to direct or indirect means. Direct means of detonation include high energy ignition charges in the order of thousands of amperes, as with those used to detonate plastic explosives such as Semtex or C-4.

If a detonation charge was triggered within a combustible gas cloud, the shock wave produced would propagate ahead of the flame and continue throughout the mixture indefinitely, provided that the combustible gas cloud mixture is within the 'detonation limits'. Detonation limits are similar to flammability limits, in that a detonation wave will only propagate within the confines of the upper and lower limit.

Detonation limits are normally expressed a percentage of gas in air, (by volume) and are generally narrower in band width than the flammability limits, as shown in Table 2.7.

Fuel	Confined detonation limit O_2		Confined detonation limit air		Unconfined detonation limit O_2		Unconfined detonation limit air		Flammability limit O_2		Flammability limit air	
	lower	upper	lower	upper	lower	upper	lower	upper	lower	upper	lower	upper
H_2	15.0	90.0	18.3	58.9					4.0	95.0	4.0	75.0
CH_4			5.7	14							5.3	15
C_2H_6	3.60	46.4	2.87	12.20	11.0	39.0	4.0	9.2	3.0	66.0	3.0	12.4
C_3H_8	2.50	42.5	2.57	7.37	7.0	31.0	3.0	7.0			2.1	9.5
nC_4H_{10}	2.05	38.0	1.98	6.18			2.5	5.2			1.8	8.4
nC_8H_{18}	1.55	17.3	1.45	2.85							0.95	
C_2H_4	4.10	60.0	3.32	14.70	9.2	51.0			2.9	80.0	2.7	36.0
C_3H_6	2.50	50.0	3.55	10.40	6.7	37.0	3.5	8.5	2.1	53.0	2.4	11.0
C_2H_2	2.90	88.8	4.20	50.0	6.7	68.0			2.5	80.0		
CH_3OH	9.50	64.5									6.7	36.0
C_2H_5OH			5.1	9.8							3.3	19.0
$C_2H_5OC_2H_5$	2.6	>40	2.8	4.5	14.7	29.0			2.0	82.0	1.9	36.0
gasoline			1.1	3.3							1.4	7.6
CO	38.0	90.0							15.5	93.3		
NH_3	25.4	75.0							13.5	79		
C_6H_6	1.55	36.0	1.60	5.55							1.3	7.9
xylene	1.05	26.5									1.1	6.4
CH_3COCH_3	3.3	40.0									2.6	13.0

Table 2.7 : Flammability limits, confined and unconfined detonation limits (vol %) [21]

Indirect means of producing detonations include the flame acceleration of a deflagration wave to a detonation wave (DDT), often caused by turbulent flows instigated by areas of congestion, such as repeated obstacles. The subjects of flame acceleration and DDT are discussed in Sections 2.4.5.7 and 2.4.5.8.

The ZND detonation model is a one-dimensional model originally used to illustrate the process of detonation of an explosive. ZND theory was originally developed during World War II by Y. B. Zeldovich, John von Neumann and Werner Döring (ZND).[37]

The ZND theory assumes a finite rate in the transpiring chemical reactions and thus the process of detonation consists of the following stages.

1. An infinitely thin shock wave compresses the explosive to a high pressure called the von Neumann spike.

2. At the von Neumann spike point, the explosive still remains dormant and has not yet reacted

3. The von Neumann spike marks the onset of the zone of exothermic chemical reactions, which finishes at the Chapman-Jouguet state.

4. The leading shock wave triggers exothermic chemical reactions in the reaction zone which continues until the flow becomes sonic for a C-J detonation (see Figure 2.34)

5. After the Chapman-Jouguet state the detonation products expand rapidly backward.

6. In the reference frame in which the shock is stationary, the flow following the shock is subsonic. Because of this energy release behind the shock, it is able to be transported acoustically to the shock for its support.

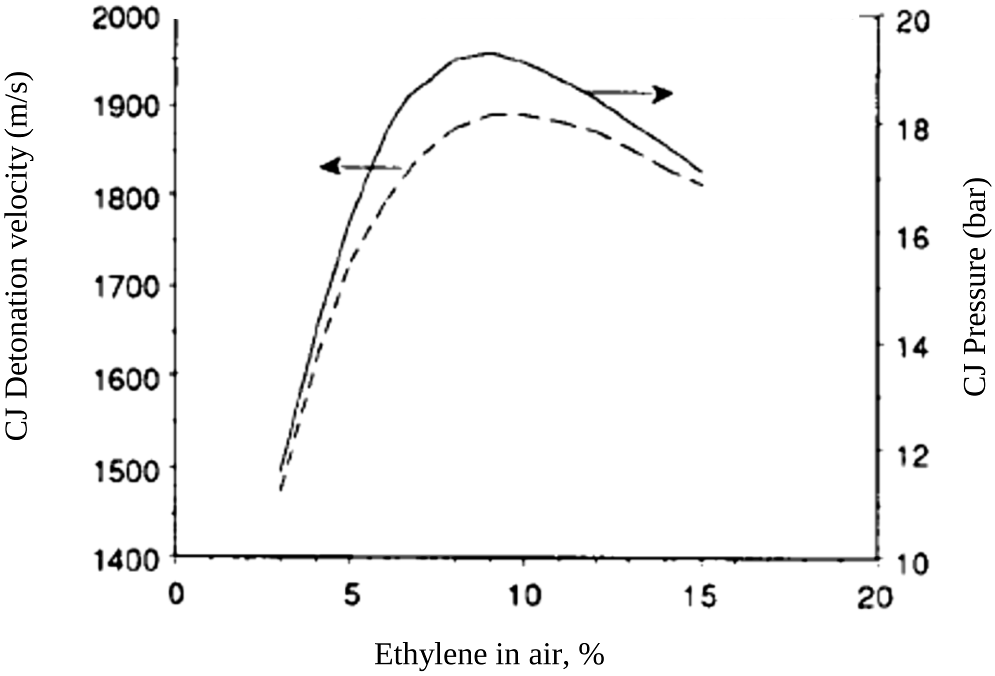

Figure 2.34 : CJ Detonation Velocity and Pressure for Ethylene-Air [37]

7. For a self-propagating detonation, the shock relaxes to a speed given by the Chapman–Jouguet condition, which induces the material at the end of the reaction zone to have a locally sonic speed in the reference frame in which the shock is stationary.

8. Effectively all of the chemical energy is harnessed to propagate the shock wave forward. The reaction rate will control the thickness of this reaction zone.

9. The ZND theory gives the same detonation pressures and velocities as the C-J theory. The difference in the two models is the wave thickness.

Figure 2.35 illustrates the complex multi-dimensional cellular structure of a detonation wave, which consists of a cell, triple points, transvers waves, reaction front and leading shock waves.

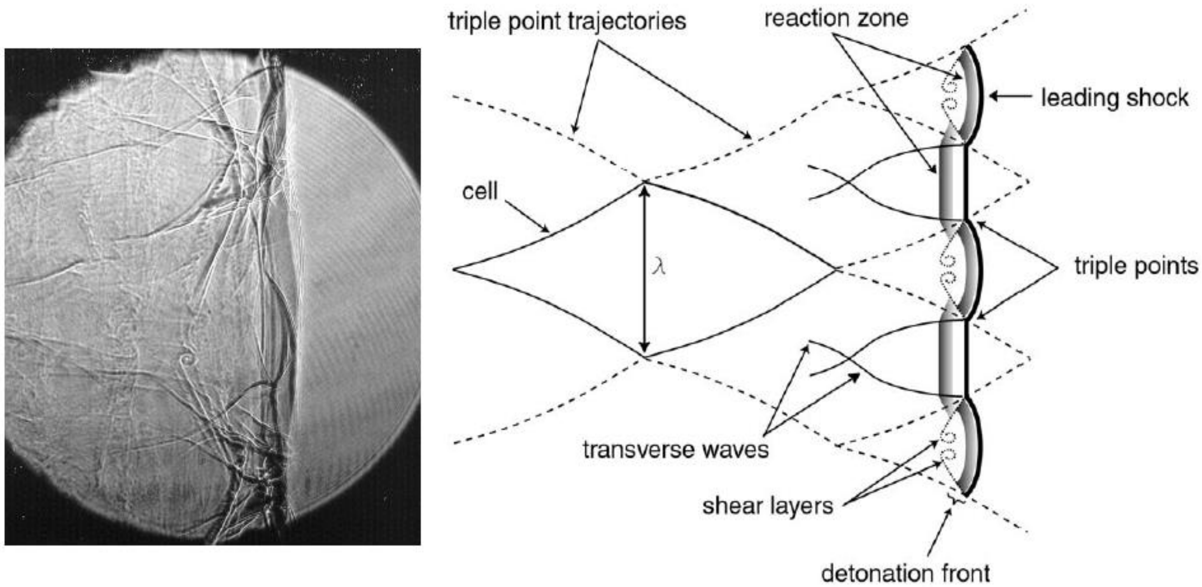

Figure 2.35 : Multi-dimensional shockwave [37]

Although the aims, objectives and scope of this present study are clearly directed towards slow moving deflagrations of ≤30m/s, there should considerations for future studies to assess the suitability of a fine mist mitigation system with respect to detonation flame speeds. Suggestions for additional research outside the scope of this study can be found in Chapter 7.

2.4.5.7 Flame acceleration (FA)

Real life flame acceleration (FA) events and full scale experimental studies [14] as shown in Figure 2.36, have been observed by many authors with particular interest in the resulting combustion mechanisms and consequential overpressures.

In theory a flame will propagate at a finite speed based on the intrinsic properties of the fuel-oxidant mixture. This finite speed is directly proportional to the mass and energy transfer mechanisms occurring between the flame and the unburned gas mixture.

The rate of mass and energy transfer may be influenced by:-

i. the reactivity of the fuel
ii. the burning velocity (S_u) and flame speed (S_f) of the mixture
iii. ratio of fuel and oxidant within the flammable range (Φ E.R.)
iv. temperature of the mixture (t, K)
v. static pressure of the mixture (P Pa)
vi. level of pressure relief during propagation (%)
vii. positioning, shape, size and density of obstacles within the mixture cloud
viii. level of mixing that has occurred – stratified or homogenous
ix. speed of sound (through the mixture) (m/s)

It is also recognised that relative humidity can potentially affect reaction rates and can lead to the shortening and completion of hydrogen chain radical reactions.

A free propagating flame is ‘driven’ by the thermal expansion of hot combustion products. In the absence of confinement the divergent flame will eventually stretch and be quenched. In the presence of obstructions and repeated obstacles as shown in Figure 2.36 (i-viii), turbulence will increase and thus increasing the burning rate. This is due to the localised flame wrinkling and subsequent increase in surface area and mass and energy transfer.

When a flame accelerates through an unburned flammable cloud in an area of congestion and frequent obstacles it will continue to accelerate due to the feedback mechanisms of mass and energy transfer. The flame will either increase to a finite subsonic speed, or detonate as its speed extends to beyond the speed of sound. If the flame speed remains subsonic, then the combustion wave will decelerate immediately as it exits the congested area.

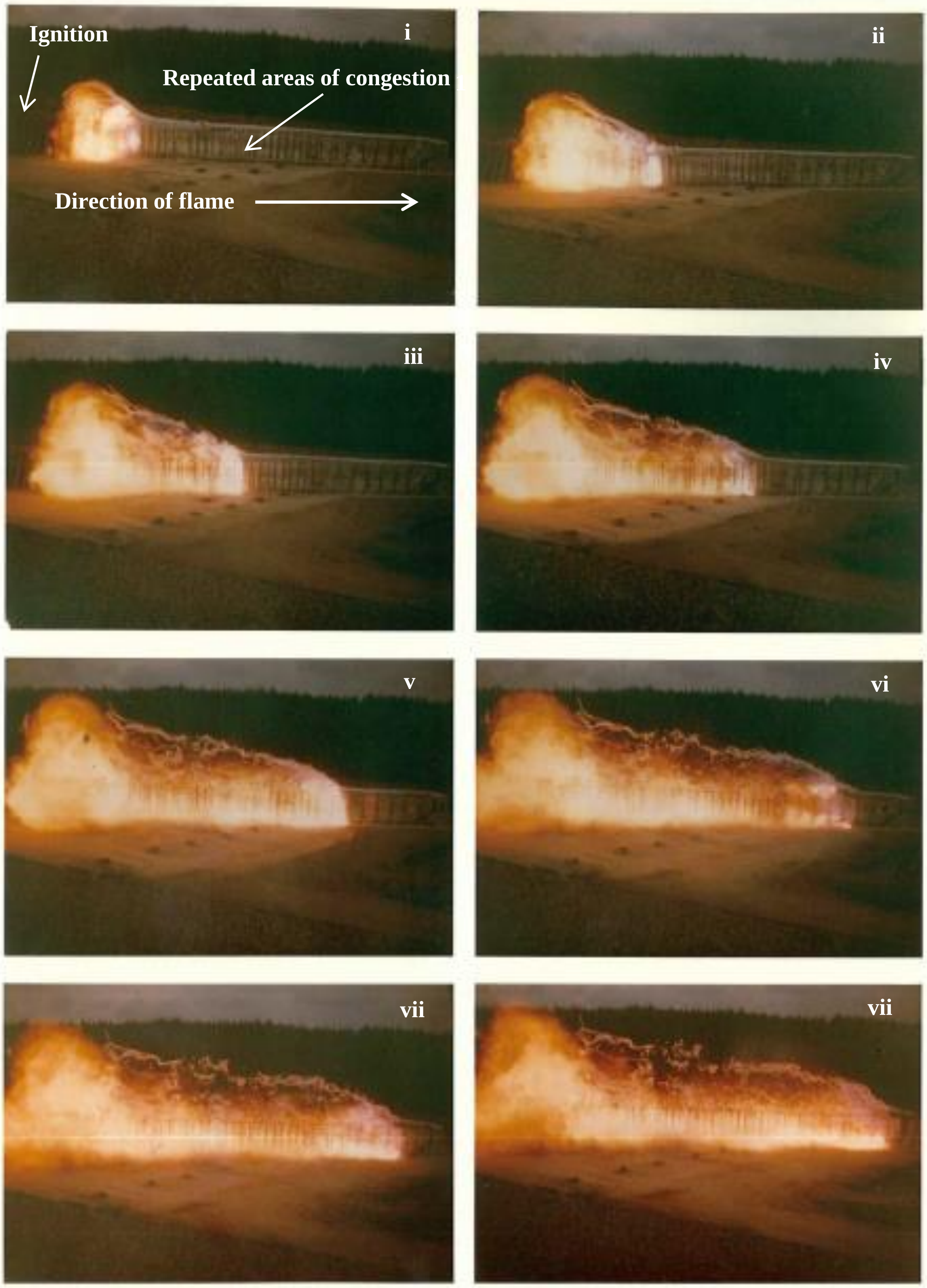

Figure 2.36 : Propagating flame acceleration tests [14]

2.4.5.8 Deflagration to Detonation Transition (DDT)

There have been many worldwide catastrophic explosion events where an unconfined vapour cloud has propagated into an area of congestion and repeated obstacles. Other events have occurred inside pipelines containing flammable mixtures. Conditions that favour low and high speed flame propagation were discussed previously in Sections 2.4.5.5– 2.4.5.7.

Where a flame continues to accelerate though repeated obstacles, around bends or restrictions in pipework, known as the 'run up distance', the flame speed will tend towards the speed of sound. Bollinger *et al* [38] carried out work on 'induction distances' or 'run up distance' and categorised many fuels using the induction distance length to diameter ratio $^{L}/_{D}$. Ratios of 10 – 60 : 1 are usually required for DDT to occur. However, in highly reactive and unstable fuels such as acetylene, the $^{L}/_{D}$ ratio may be as little as 3 : 1.

At a critical velocity, the flame speed will exceed the speed of sound and will become supersonic. A supersonic shock front will then form ahead of the flame, which acts like a porous piston heating and compressing the unburned gas as it propagates at supersonic speeds, detonating the remainder of the unburned gas cloud. This phenomenon is known as Deflagration to Detonation Transition (DDT).

Following the occurrence of DDT, the flame will continue to propagate at supersonic speeds through the unburned cloud, regardless of the inclusion, or absence of repeated obstacles. In some cases that have been investigated post explosion, the DDT occurred in one area of the site and the detonation wave propagated throughout the combustible cloud. Environmental conditions that favour detonation include:-

- the mixture is within the detonable range
- run up distance (fuel dependant, inversely proportional to fuel reactivity)
- elevated mixture temperatures (widens the detonable range)
- Maximum experimental safe gap (MESG) – the lower the MESG the greater the risk of detonation

DDT mitigation in pipework is normally achieved using inline arrestors, or fast acting (20 - 40ms) automatic valves and vents. Thomas *et al* [39] successfully used large droplet (≥100μm) water sprays to mitigate detonation waves, as discussed in Chapter 3.

2.5 The theory of flame extinction

When cogitating the extinguishing of a flame, a number of scenarios must be considered. For the purpose of this work two scenarios are presented:-

a) A stationary flame, or fire formed by the ignition, subsequent heating and organic decomposition of a solid material e.g. wood
b) A stationary flame such as a burner, or a propagating combustion wave in a flammable gas-air or vapour-air mixture

a) Wood is made up of multiple inhomogeneous layers. Due to the fibrous and non-uniform structure of wood, the combustion occurring in small localised regimes may be very different to the global properties of the fire.

Wood contains a mixture of natural polymers, such as cellulose, hemicellulose and lignin. It is the decomposition of these long chain polymers by endothermic pyrolysis that produces the volatile gases and vapours that can be seen burning around and above the wood, as revealed in Figure 2.37.

Volatile vapours burning above solid organic material e.g. wood

Figure 2.37 : Burning wood fire and volatile gases

Approximately 50% of the polymers found in wood are cellulose, which begins to soften at approximately 227˚C and then starts to decompose at approximately 240˚C. Hemicellulose and lignin decompose at 200˚C and 260˚C respectively.

The heat produced by the flames in a fire poses two distinct problems with respect to extinguishment of the fire:-

1. The heat from the flame will raise the temperature of the surrounding fabric, which will also begin to decompose and will eventually combust.
2. The heat from the flames at the base of the fire maintains the high surface temperature on the surface of the fuel, therefore producing further decomposition and combustible volatiles. This energy feedback cycle dominates the progression or deterioration of the fire.

Therefore, if water is used to extinguish a fire the droplets must be large enough and have sufficient momentum to penetrate the thermal up draught created by the fire.

Herterich [40] recommended that free falling droplets of ≤100μm should not be considered for fighting fires, due to their low mass and terminal velocity. Kaleta [41] carried out a theoretical analysis relating to the free fall of droplets from sprinkler systems and he estimated that the optimum droplet size (μm) discharging from a sprinkler should be 300≤μm≤900. He also concluded that the height of the sprinkler above the fire dictated the effectiveness of the free falling droplets.

Smaller diameter sprays such as Marioff Hi-Fog [42], as shown in Figure 2.38 can now also be used for fire fighting, as these systems are pumped through atomising heads at pressures of ≤10 MPa (100bar), thus providing the momentum to penetrate the up draught currents.

Figure 2.38 : Various Marioff Hi-Fog - Spray heads and ceiling mounted head in-situ [42]

When fighting a fire with water there are several scenarios to consider. A specific strategy using one or more of the actions listed in Table 2.8 must be employed, based on the knowledge and loading of the fire type.

Scenario	Action
Does the spray have to cool the product of combustion?	Fine droplets
Does the spray have to cool the fuel?	Large droplets
Does the spray have to cool the flame?	Fine droplets
Does the spray have to provide protection against thermal radiation?	Fine droplets
Does the spray have to wet other combustible items?	Large droplets
Does the spray have to overcome obstacles?	Fine droplets

Table 2.8 : Droplet size consideration scenarios used in fire fighting [41]

b) With stationary flame such as a burner, or a propagating combustion wave in a flammable gas-air or vapour-air mixture, suppression or mitigation utilising water sprays provides very different challenges to those associated with fires involving organic solids.

Organic solids burn at a much slower rate than flammable gas-air or vapour-air mixtures. One of the key factors associated with slower burning velocities, is the increase in flame thickness. The thicker flame front and reaction zones associated with fires involving organic solids, gives way to a greater ‘residence time’ for water droplets to vaporise and consequently produce steam. This change of state gives up the release of latent heat of vaporisation.

In a gas or vapour cloud explosion, flame speeds are generally much greater that those associated with burning solids. In laminar flames, the flame thickness is at its narrowest when conditions are close to stoichiometric and at its thickest close to the upper and lower limit of flammability (see Section 2.4.5.3). As the *residence times* for droplets in a gas explosion fronts are very short (approximately 0.03ms in this current study), droplet diameters need to be in the order of $\leq 30\mu m$. Sprays used for gas explosion suppression must either, deploy large droplets into an accelerated explosion flow field thus relying on further break up by dynamic shattering, or release droplets in the order of $\leq 30\mu m$, that are small enough to absorb heat or even fully vaporise without additional break up.

This current study will exclusively consider latter condition, whereas all previous research has been based on larger droplets in accelerated explosion flow fields.

2.5.1 Flame Quenching and flame stretch

Spalding [43] considered that the isothermal energy transfers occurring in a flame could be readily solved by conveniently assuming an adiabatic system, where no energy is lost from the system, either downstream or from any of the boundaries of the combustion wave.

If a heat sink such as a solid or liquid with sufficient heat capacity is placed in a flame, heat will flow from the flame to the heat sink. Bray [44] demonstrated that a temperature drop equal to 90% of the adiabatic flame temperature will give rise to localised extinction of the flame.

Brenton and Thomas [45] carried out two experimental studies on the effects of solid and liquid heat sinks in a flame. In the first experiment a 1mm diameter water cooled capillary tube was placed in a flame of a slot burner normal to the flame front, as illustrated in Figure 2.39.

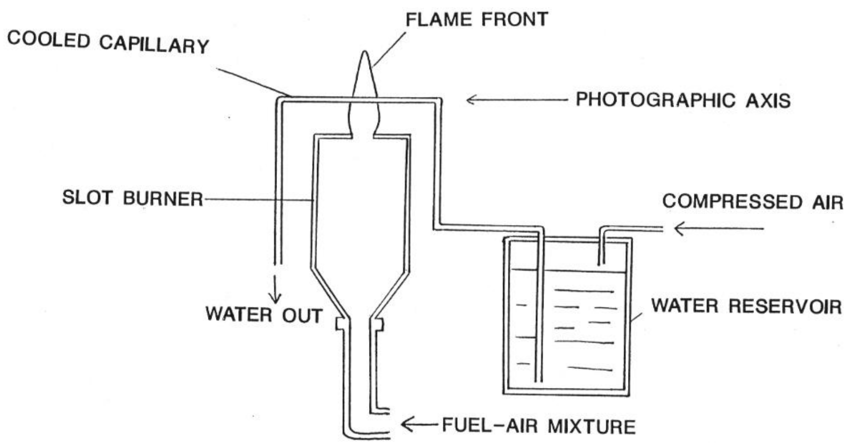

Figure 2.39 : Illustration of water cooled capillary tube experimental set up [45]

High speed photography was used to analyse the axial cooling effects of the 1mm capillary tube, which was perpendicular to the flame front. The images displayed a '*dark region*' around the tube where there was no visible light release. The omission of light from this region showed that combustion had ceased in the local area. Figure 2.40 reveals the existence of the 'dark region' around the water cooled tube.

Reference will be made to the above study and 'dark regions' when qualitatively discussing the results of the mitigation trials in Chapter 5 and Appendix 9.

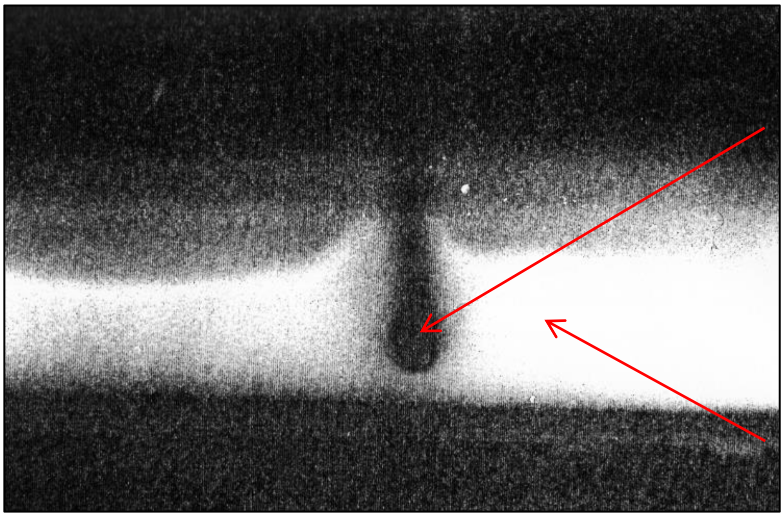

Figure 2.40 : Capillary tube passing through slot burner flame [45]

In the second experiment a droplet generator was used to produce a horizontal train of 85µm monodispersed water droplets. The water droplet train entered the slot burner flame approximately normal to the flame front at velocities from 1m/s– 3.8m/s. These droplets were analysed both upstream and downstream of the flame using laser interferometry. This was to assess the change in size of the droplet, due to level of vaporisation occurring in the flame.

The results of this work demonstrated a reduction in droplet size on exiting the flame, proving that some degree of vaporisation had occurred. Downstream of this point, there was a small increase again which was due to thermal expansion.

High speed photography was used again to show '*dark regions*' around the droplets as they entered and exited the flame as shown in Figure 2.41. Localised extinction appeared to occur in these experiments also.

Brenton and Thomas [45] concluded that at low droplet train velocities, the dominant factor relating to localised flame extinction was the thermal cooling (heat sink) effect. Whereas, when the droplet train velocity was increased, this caused a high level of air entrainment, which then entered the flame resulting in localised flame stretch extinction.

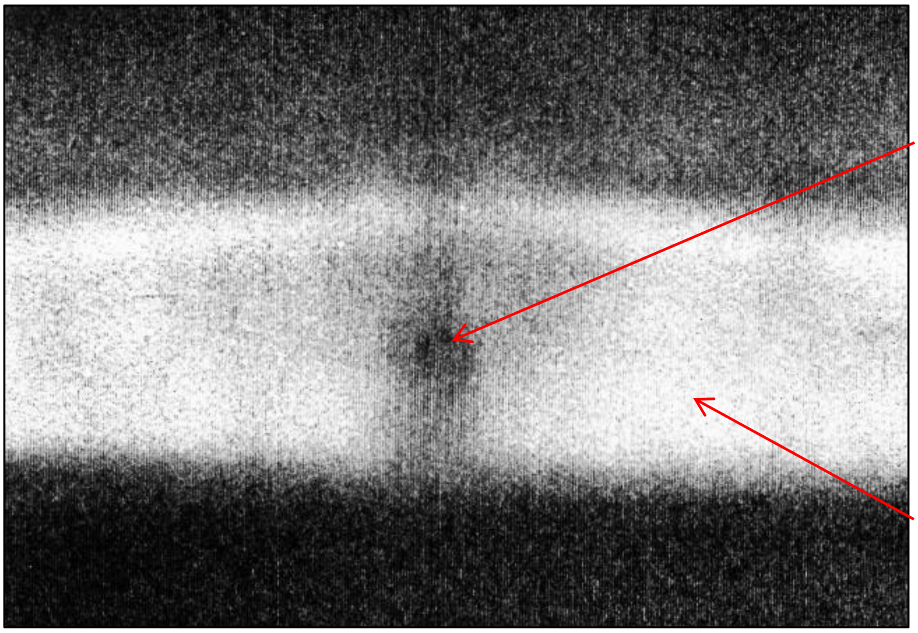

Figure 2.41 : Water droplet penetrating the flame at a velocity of 1m/s [45]

In a polydispersed fine spray system, rather than individual monodispersed droplets, the mode of extinction is likely to be a combination of cooling and stretch. If the spray density, or liquid volume flux (Q_f) was sufficiently concentrated to produce multiple localised extinction events, similar to those in Brenton and Thomas's experiments [45] and the space between the locally occurring extinction events was less that than *quenching distance* for the given fuel, then in theory global extinction would occur.

In the case of extinction by stretch, as the spray volume enters the flame front, the droplets will pass through the flame opening up temporary transient gaps in the flame front. If the sprays are then turned off the transient gaps will close up again as they are filled with new unburned fuel gas-air mixture. In order to close these gaps with respect to time, the flame surface will have to 'stretch'.

Bott [46] proposed that if the gaps were filled too quickly, then the sudden stretch and change in the surface area of the flame may be sufficient to trigger global extinction.

In this present study, high definition (HD) imagery will also be used to qualitatively evaluate flame quenching. These images will be critically analysed with respect to the quenching effects of counter flow (C/F), parallel flow (P/F) and cross flow (X/F) sprays. The images captured during the 'hot trials' are discussed with reference to quenching and the appearance of dark regions in Chapter 5, Results and discussions.

2.6 Chapter summary

This Chapter serves to provide a literature review, together with the essential background information required to progress to the subsequent Chapters. In this Chapter the following areas were presented and discussed with relevance:-

i. A review of some of individual scientists and organisations that had a key role in combustion, explosion and flame quenching research.
ii. Explosion environments and their influence on the dynamics and consequences of resulting explosion event scenarios.
iii. A summary of some of the world's greatest 'high loss' explosion events, in terms of loss of life and financial implications.
iv. Fundamental combustion principles and relevant terminology used.
v. The theory of flame extinction, including flame quenching and flame stretch.

The following Chapter includes a review of typical fine spray atomising systems used in industry and discusses the relevance of one particular atomiser known as a Spill Return Atomiser (SRA). Additionally, previous research in explosion suppression and mitigation in the presence of water sprays is extensively reviewed with significance, as well as other alternative methods.

CHAPTER 3

LITERATURE REVIEW : II

FUNDAMENTALS AND UTILISATION OF FINE SPRAYS IN EXPLOSION MITIGATION

3.1 Introduction

The word “spray” refers to a droplet-laden flow of gas or liquid droplets moving through essentially ambient medium, where a jet-like momentum is assumed for the flow [49]. In other words a spray is defined as a dispersion of droplet**s** in a gaseous atmosphere with sufficient momentum energy to penetrate the surrounding medium. Further explanation of the term may also be defined as “a process which uses an orderly array of droplets or a process whereby suspension of fine droplets, or droplets falling under gravity takes place.”

The word ‘atomisation’ describes physical dispersion of a bulk fluid into small particles in a gaseous medium. In atomisation a liquid jet or sheet is broken down by the in intrinsic kinetic energy of the liquid itself, or by an external energy force such as high pressure gas, vibration or rotary means.

Devices that are designed specifically to atomise bulk liquids are known as ‘atomisers’. Atomisers are often found in the form of nozzles, however, there are a number of different atomisers that are all designed to produce droplets following the same disintegration process of liquid ‘sheet-ligament-droplet’, as shown in Figure 3.1

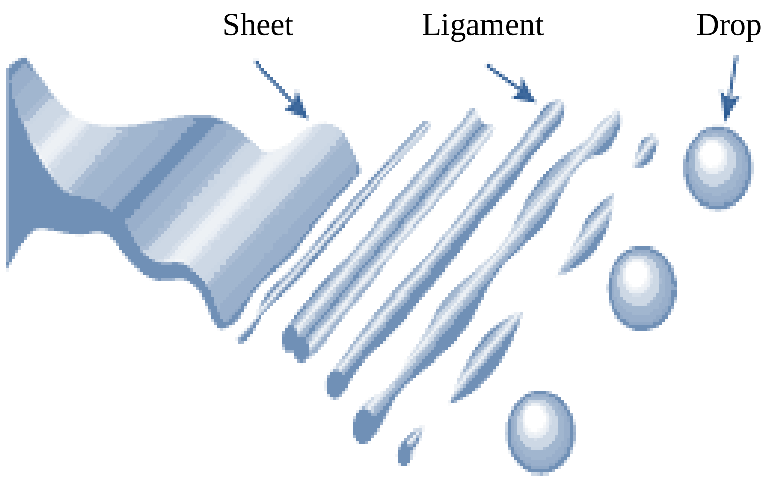

Figure 3.1 : Different stages of liquid sheets [47]

Other droplet disintegration processes will be discussed briefly with respect to various atomiser types in Section 3.3. Another process that will be discussed with relevance to this present study is referred to as ‘*secondary atomisation’* by ‘*inverted bag type breakup’*, in which previously atomised drops are broken down further by other means, into fine mist.

Liquids are often atomised to benefit a process, with the principle advantage being a large increase in surface area. In combustion or explosion mitigation it is this increase in surface area that is fundamental to the solution. Theoretical studies [45] have suggested that droplets in the order of 10–20µm will vaporise during their transit through a flame front of 1mm thickness. Within this range the droplet surface area to volume ratio should provide ideal conditions, thus benefiting from the latent heat transfer within the reaction zone of the flame.

Atomisers are often categorised by their 'energy source' as illustrated in Figure 3.2. The process of atomisation often requires high relative energy input levels and consequently atomisation is a very inefficient process. For example, a liquid pressure atomiser has a typical efficiency of about 2 – 5%.

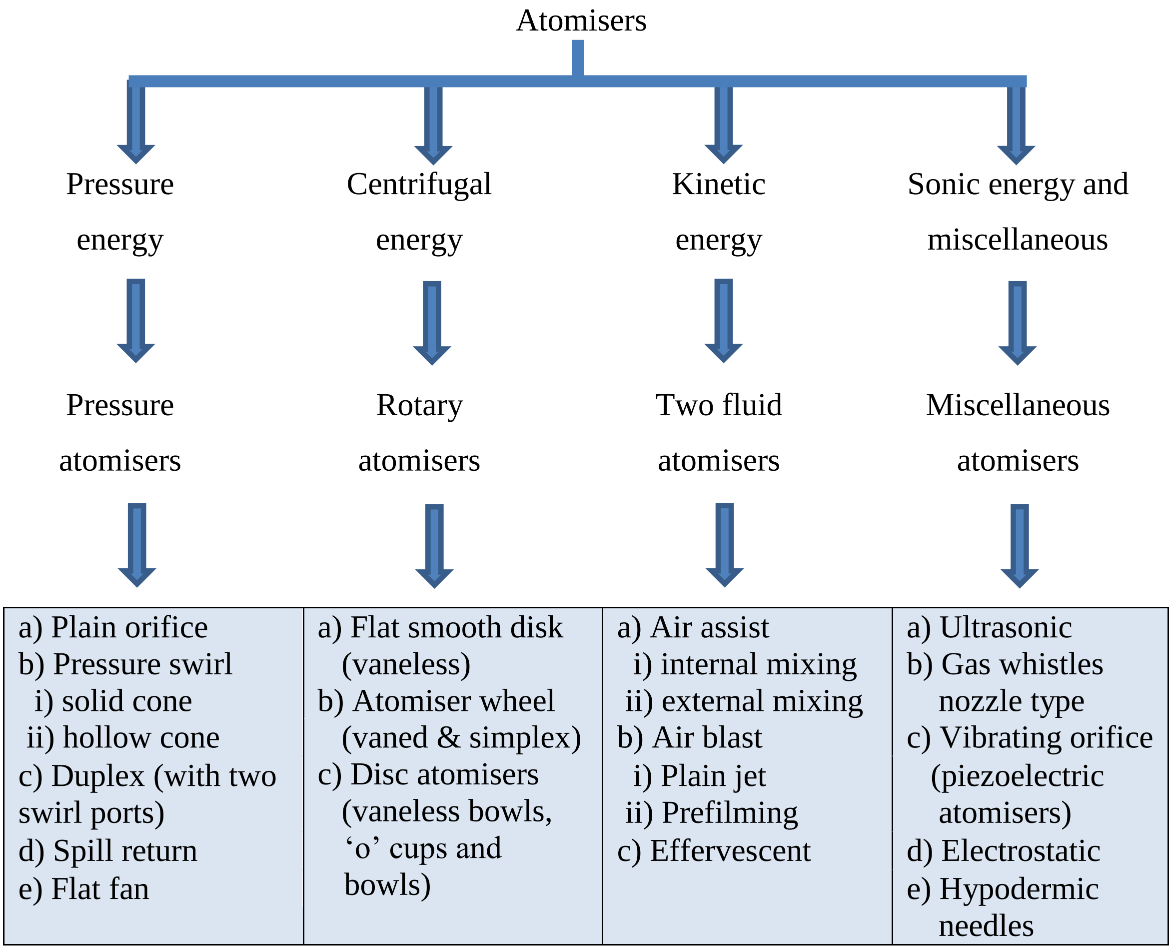

Figure 3.2 : General classification of atomisers

Sprays are normally classified and grouped according to their average droplet size. Although several systems exist, a simple five tier structure is offered below:-

Very fine sprays

These are defined a sprays when the diameter is ≤15µm which have been used in medical, combustion, decontamination and disinfection.

Fine sprays

These are defined a sprays when the diameter is between 15µm and 50µm which have been used in combustion, fire suppression and metal powders.

Medium sprays

These are defined when diameter is between 50µm and 250µm, which have been used in spray drying, cooling of metals, and paint sprays.

Coarse sprays

These contain droplets between range of 250µm and 900µm and have been used for de-scaling and cleaning.

Very coarse sprays

These contain droplets of >900µm and have been used in fire suppression (sprinklers), de-scaling and cleaning.

Usually a spray is one type of two phase flow. It changes a liquid as the discreet phase into the form of droplets and gas as a continuous phase. Usually different types of flow in liquid phase and gas phase can be sprayed.

The density of liquids or gases is a critical factor which may affect droplet motion, kinematic inertia, higher drag force and droplet sizes and diameters.

In the spraying of liquids, the disintegration of liquid sheets is an importance factor which has significant effects on the liquid discharge velocity. The liquid sheet can take the form of a flat sheet created by impingement of two liquids jets, or conical sheets where a tangential velocity component is imparted to the liquid as it leaves the orifice of the atomiser [48].

Fraser and Eisenklam [50] identified three modes of disintegration; the first mode is described as a 'rim disintegration' that occurs at low liquid velocities. The surface tension causes the liquid to contract at the boundary resulting in the formation of a thick rim; this then breaks up under the mechanism of a free jet. This process is prevalent with liquids with low velocity, high viscosity or high surface tension, and droplets formed by this mechanism are typically large [49].

In Figure 3.1 shown previously, illustrates the different stages of liquid sheets. As the liquid exits the atomiser orifice, sheets form due to the effect of high exit velocities reaching a critical value. The sheet then disintegrates into ligaments, which are essentially unstable and then break up into individual droplets.

Several factors may influence the atomisation process. These include the atomiser type, liquid supply pressure, orifice diameter, liquid viscosity, liquid density and the relative velocity of the liquid and air medium. One of the most influential factors in the break-up of liquids is viscosity, which is closely associated with surface tension.

Yule and Dunkley [34] described the effects of relative velocity on liquid jet break up as shown below in Figure 3.3. At a velocity of ≤1 m/s, dilation of the cylindrical jet occurs. By increasing the velocity of liquid, braking up of droplets will begin to occur which extend closer to the atomiser. At velocity >30 m/s graceful distortion of the jet occurs and at very high velocity, >100 m/s the liquid stripping occurs.

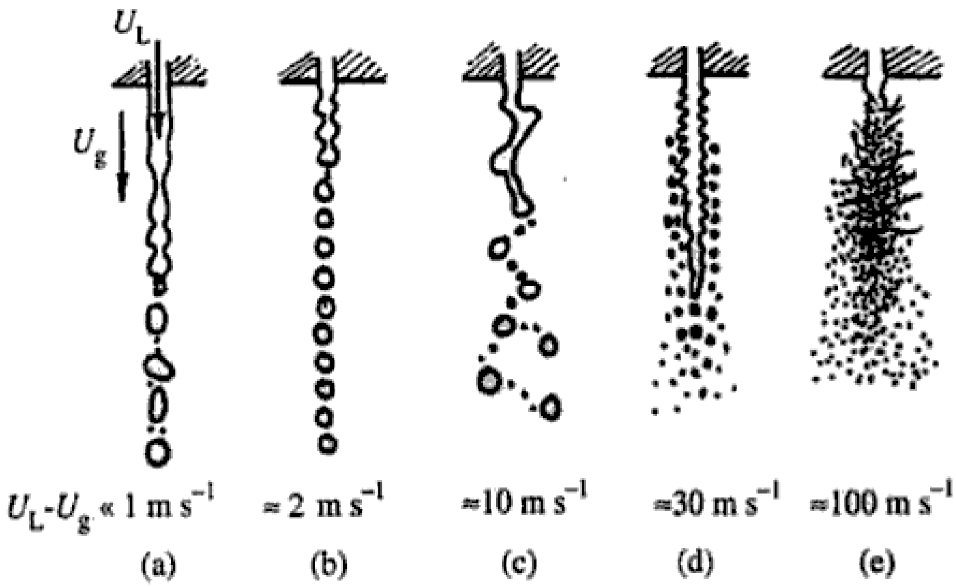

Figure 3.3 : Liquid break up at different velocities [47]

Therefore, to achieve small droplet sizes from a liquid pressure atomiser, the velocity difference between the liquid and surrounding gaseous medium must be as high as possible. Atomiser type, pressure, capacity, liquid properties and spray angle are some of the important factors that have significant effects on the resulting drops size.

3.2 Properties of Sprays

3.2.1 Patternation

The general term used to describe the overall characteristics of a spray is 'patternation'. This includes characteristics such as spray cone angle, shape and mean droplets size. The spray cone angle is measured by taking two straight lines from the origin of the spray i.e. the atomiser exit orifice. Previously this was carried out using developed images (photographs), whereby the lines would be drawn using a pen and measured using a protractor. This method is quite subjective although it is very useful for comparing sprays. These days images are produced digitally and spray cone angles can be measured accurately using software, such as Adobe Photoshop which contains an angle finder tool.

Another suitable method involves measuring the 'width' of the spray at a given distance downstream of the exit orifice. Given the two measurements the spray cone angle can easily be calculated using basic trigonometry. Again this is quite subjective when dealing with fine droplets regarding the visual limits of the spray.

Subsequent to the spray angle being determined by a suitable method, it can be further defined by one of three categories, these are; narrow ($\theta<30^o$), medium ($30^o\leq\theta\leq70^o$) and wide ($\theta>70^o$). The spray cone angle is a very important parameter of the spray pattern created in this current study, since to mitigate a flame propagating through a volume of space, it is important that the volume is enveloped by the spray.

The spatial location of droplets in a spray may also be important in certain applications. A device known as a patternator is sometimes used to measure volumetric flux (Q_f) and the radial distribution of the spray (N). A typical patternator is shown in Figure 3.4.

Generally a patternator consists of a number of individual containment areas, sometimes called 'bins' designed to collect liquid from the spray over a given time period. The liquid can then be quantified, normally by weight and converted into volume flow rate.

Patternators can be very useful when dealing with multiple overlapping sprays, for example impact nozzles used in water deluge systems as illustrated in Figure 3.5.

Figure 3.4 : Single spray directly over patternator [47]

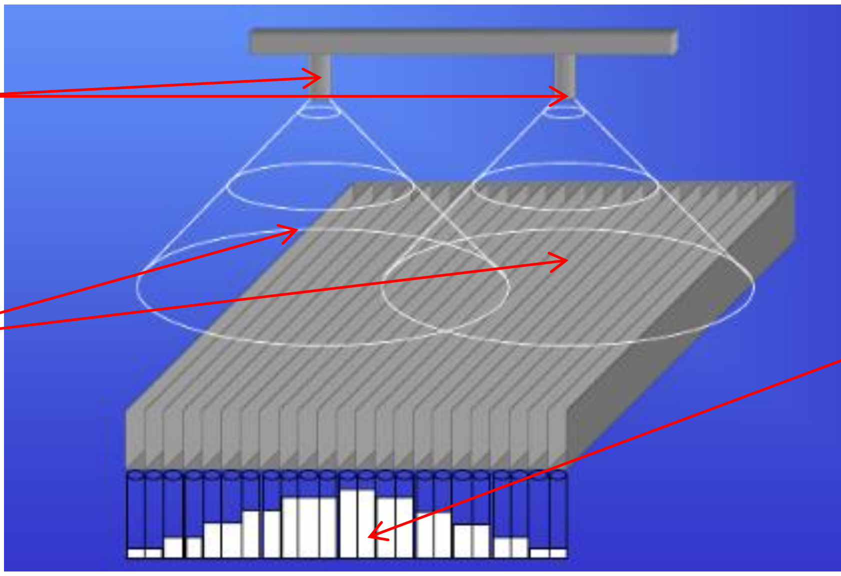

Figure 3.5 : Illustration of patternator used to quantify overlapping sprays [51]

The application and use of a spray will often dictate the shape and symmetry requirement desired from a spray. While some spray applications require flat sprays, most spray patternation is axi-symmetric. Figure 3.6 illustrates various spray formations and provides a visualization of some of the terms commonly used in the industry.

Figure 3.6 : General classification of atomisers [47]

3.2.2 Drop size and mean distribution

In a mono dispersed spray of identical droplets in colloidal suspension, a single number would suffice to describe the droplet diameter. Whereas in a poly dispersed spray, particles or droplets will be many different sizes and even orders of magnitude. During the formation of a spray, liquids are atomised as discussed earlier. From the moment that droplets are formed their pathway within the spray is somewhat unpredictable, as some droplets may remain unchanged and others with lose or gain mass. To solve this problem of the quantification and classification of sprays various 'mean' diameters are used to express the particular aspect of the spray characteristics.

Droplet diameter may be represented in several forms as summarised in Table 3.1 and Figure 3.7. The most commonly used term to express the mean droplet diameter in a spray is referred to as D_{32} or Sauter Mean Diameter (SMD).

Symbol	Term	Description
D_{10}	Arithmetic mean diameter	the average of the diameters of all the droplets in the spray sample.
D_{20}	Surface mean diameter	the diameter of a droplet whose surface area, if multiplied by the total number of droplets, will equal the total surface area of the sample.
D_{30}	Volume mean diameter	the diameter of a droplet whose volume, if multiplied by the total number of droplets, will equal the total volume of the sample.
D_{32}	Sauter mean diameter	the diameter of a droplet whose ratio of volume to surface area is equal to that of the complete spray sample
$DV_{0.1}$	Mass median diameter 10%	drop diameter is such that 10% of total liquid volume is in drops of a smaller diameter
$DV_{0.5}$	Mass median diameter 50%	drop diameter is such that 50% of total liquid volume is in drops of a smaller diameter.
D_{Peak}	Peak diameter	value of D corresponding to the peak of the drop size frequency curve

Table 3.1 : Typical terms used to represent droplet diameters [48]

The D_{32} value featured in Table 3.1 above is usually referred to as the Sauter Mean Diameter (SMD). The D_{32} or SMD was originally developed by German scientist J.Sauter in the late 1920's and can be defined as mean droplet or particle size.

The D_{32} is defined as the diameter of a sphere that has the same volume/surface area ratio as a particle (droplet) of interest. Also the D_{32} is the diameter of the drop whose ratio of the volume to surface area works out to be the same as that of the entire spray.

For most sprays the D_{32} is larger than the D_{10}, D_{20} and D_{30} and is derived by determining the volume mean diameter (D_{30}) which may be described as the diameter of a droplet whose volume, if multiplied by the total number of droplets, will equal the total volume of the sample, and the surface mean diameter (D_{20}) which equates to the diameter of a droplet whose surface area, if multiplied by the total number of droplets, will equal the total volume of the sample. By combining the equations for the volume mean diameter (D_{30}) and surface mean diameter (D_{20}), the D_{32} expression is derived as shown in Table 3.2.

The D_{32} Sauter mean diameter is used widely as an 'industry standard' in fire and explosion suppression, providing an accurate representation for mass and energy transfer applications and will be referred to throughout this study for comparison and clarification.

Symbol	**Name**	**Expression**
D_{20}	Surface mean diameter	$(\Sigma N_iD_i^2 / \Sigma N_i)^{1/2}$
D_{30}	Volume mean diameter	$(\Sigma N_iD_i^3 / \Sigma N_i)^{1/3}$
D_{32}	Sauter mean diameter	$(\Sigma N_iD_i^3 / \Sigma N_iD_i^2)$
Where ; N_i is the number of drops in size range, *i* D_i is the middle diameter in the size range, *i*		

Table 3.2 : Mean diameters and their expressions [48]

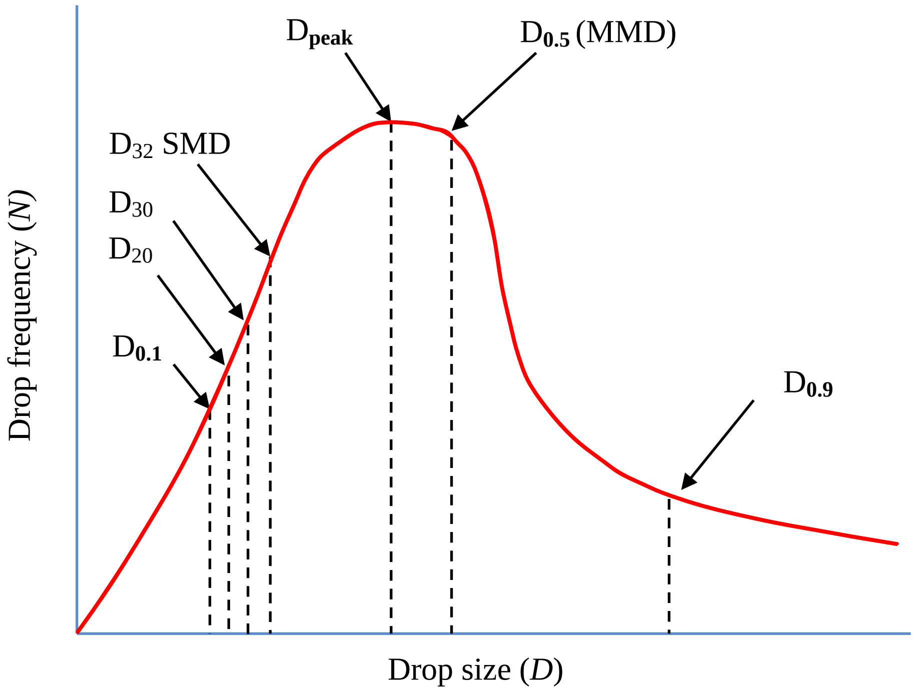

Figure 3.7: Locations of various representative diameters

An intrusive picture of drop size distribution can be obtained by plotting a histogram of drop size. Initially a frequency distribution table must be produced from the data acquired during the non-intrusive laser characterisation of the spray (see also Section 3.4). In this table the drop sizes are sorted into corresponding groups i.e. 5µm to ≤10µm etc. Each coordinate representing the number of drops whose dimension fall between the limits D-ΔD/2 and D+ΔD/2. A typical histogram of this type is shown in Figure 3.8, in which droplets can be studied above and below a particular set value, i.e. the objectives of this current study are with respect to droplets of ≤30µm, as illustrated.

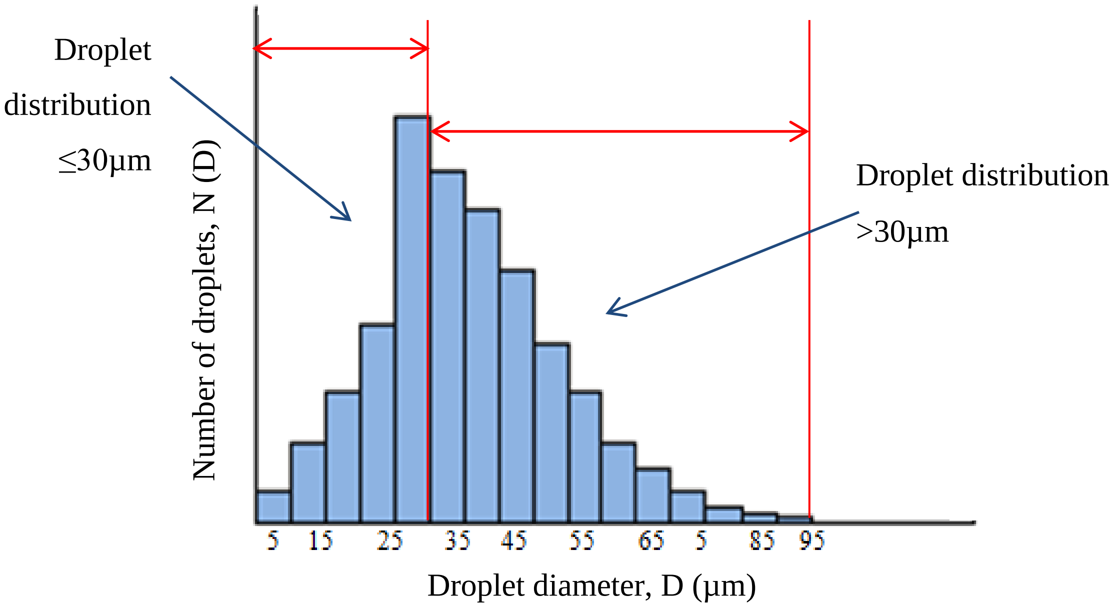

Figure 3.8 : Typical drop size histogram [51]

If the volume corresponding to a range of drop size between D-ΔD/2 and D+ΔD/2 is plotted as histogram instead of plotting the number of drops, the result of distribution is 'skewed' to the right, as shown in Figure 3.9. This is explicitly due to the weighting effect of the larger drops.

As ΔD is made smaller, the histogram may assume the form of a curve, known as a 'frequency distribution curve' shown typically in Figure 3.10, which may be regarded as characteristic of spray, provided it is based on a sufficiently large sample. During this current study Phase Doppler Anemometry (PDA) was used to characterise the spray (see also Section 3.4), in which high sampling rates were maintained within the order of 10,000 – 20,000, thus ensuring a high level of accuracy and dependability, as discussed in Chapter 4.

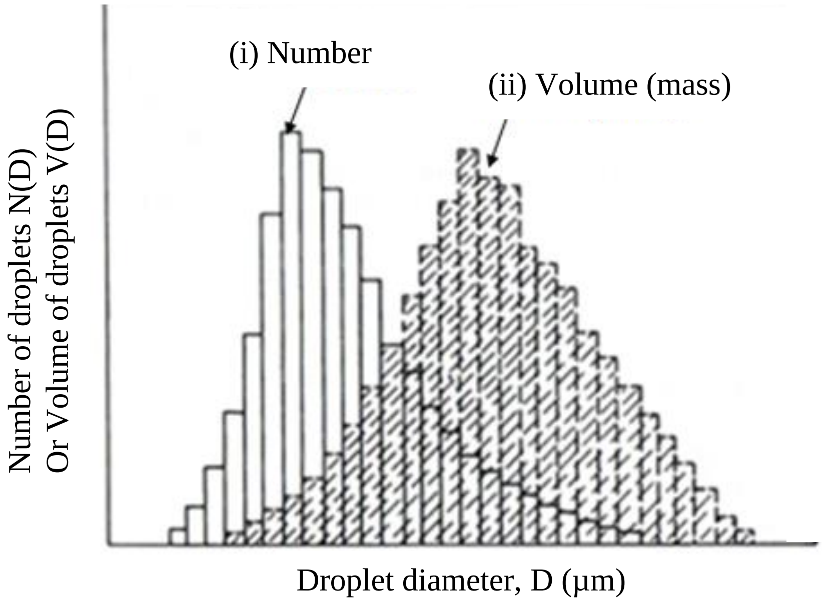

Figure 3.9 : Characteristic drop size histograms based on (i) number and (ii) volume [47]

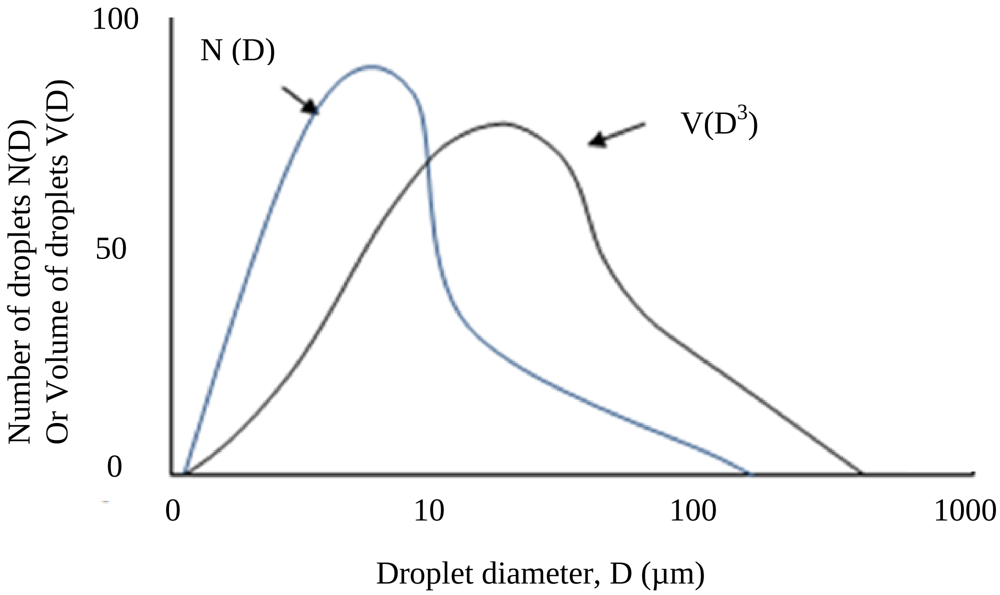

Figure 3.10 : Typical drop size frequency distribution curves (number and volume)

It is worth noting that all of the results plotted in this study are based on the Sauter Mean Diameter (SMD or D_{32}) in line with all previous investigations. Although this 'industry norm' represents the volume distribution and D_{32}, the actual 'number distribution', skewed to the left, contains a greater number of smaller droplets than the value being considered.

3.2.3 Liquid volume flux

Liquid volume flux (Q_f) represents the volume of liquid passing through a unit area of space with respect to time. In addition to drop size and distribution, liquid volume flux will be pertinent to the outcome of this study. These two spray properties are very closely coupled, if not inseparable with respect to mitigation or suppression of a propagating flame.

Section 3.6.4 provides detailed information and discussion relating to the wide range of drop sizes found in previous studies and the corresponding inconsistencies in liquid volume flux values. In a normal solid cone spray liquid volume flux will be greatest at the radial centre of the spray and will tend to reduce towards the radial limits of the spray envelope. Additionally liquid volume flux will decrease with a corresponding increase in axial position downstream of the atomiser exit orifice. Figure 3.11 illustrates a typical graphical representation of liquid volume flux.

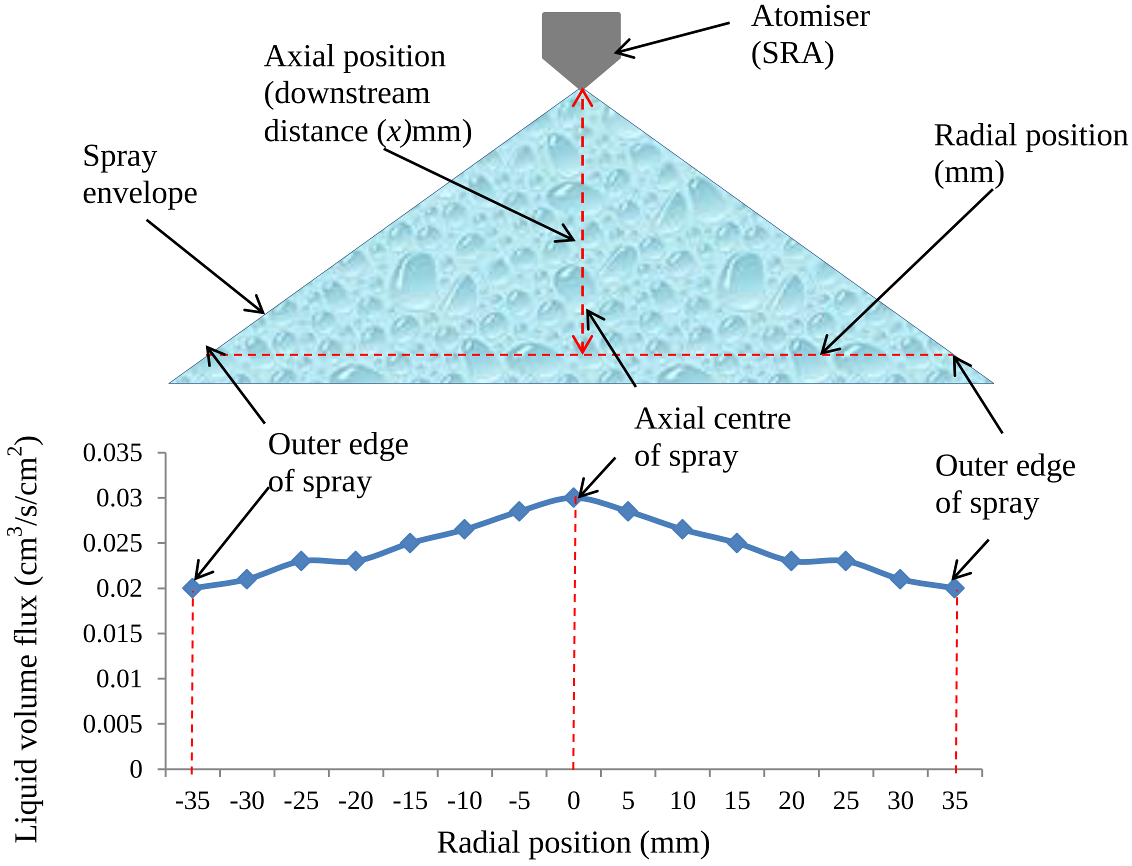

Figure 3.11 : Typical liquid volume flux representation at downstream distance (*x*) mm

3.2.4 Droplet velocity

The relevance of liquid velocity (D_{LV}) in relation to the surrounding gas was previously discussed in Section 3.1, in that the liquid velocity will generally dictate the critical break up regimes and subsequent droplet velocity. Consequently, with traditional pressure jet atomisation the higher the liquid pressure, the smaller the resulting drop size.

When water sprays are used to suppress or mitigate explosions, the momentum of the issuing jet and spray is likely to cause a disturbance throughout the unburned combustible mixture, which may result in an increase in flame speed caused by the resulting induced turbulence. This subject was previously discussed briefly in Chapter 2 and will also be considered in this Chapter.

To limit this effect, an ideal atomiser for suppression and mitigation of slow moving flames in relatively quiescent mixtures would be one that includes the benefits of high pressure turbulent liquid flow, with low flow exit velocities. A novel atomiser will be required to provide these ideal characteristics.

The subsequent Section will discuss a range of atomisers that were considered for this current study, together with their typical applications and characteristics, with additional reasons for their selection and denunciation provided and tabulated in Section 3.3.10.

3.3 Fine spray atomiser systems

3.3.1 Pressure jet

A very simple and common pressure jet atomiser is used to inject atomised diesel into internal combustion engines, as shown in Figure 3.12. Utilising a small exit orifice usually <0.3mm and high liquid pressure of about >100MPa, fine sprays are produced in the order of D_{32} < 20μm. This arrangement provides efficient penetration of the spray within the engine combustion chambers.

There is evidence that cavitation inside these simple orifices is important for increasing turbulence and improving atomisation. There is however a danger of excessive cavitation producing 'hydraulic flip' when the liquid jet separates inside the orifice, resulting in poor atomisation (Nasr, G.G. *et al*. 2002) [47]. Simple orifice injectors such as pressure jets do not atomise well when injected into atmospheric conditions as aerodynamic forces are insufficient.

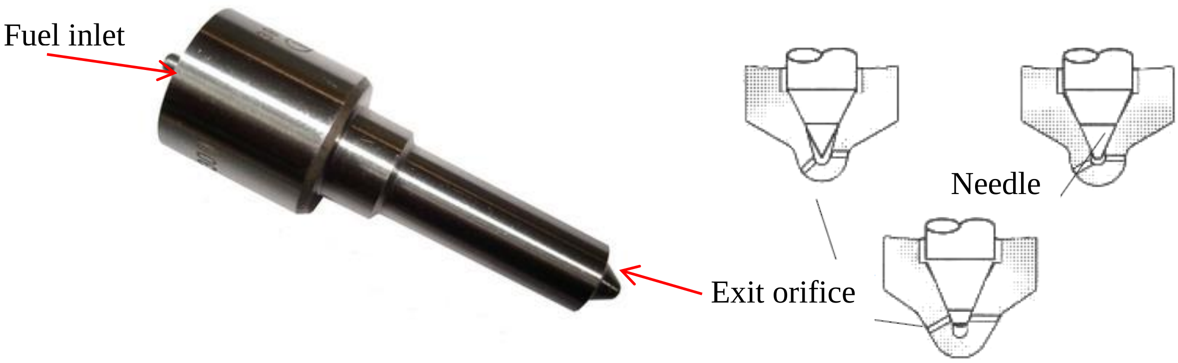

Figure 3.12 : Typical fuel injector for a diesel engine [52]

General characteristics

Simple, good penetration, low entrainment, coarse atomisation (unless gas density high and liquid pressure >100bar), solid cone, poor vaporisation, very high impact momentum, relatively narrow size distribution. Suitability for this current study (see Section 3.3.10)

Typical usage

Industrial cleaning, industrial showers, fire fighting, diesel injection (as shown above in Figure 3.12), localised cooling

3.3.2 Fan jet

A fan jet or ‘v’ jet is a departure from a simple pressure jet orifice in which the liquid flow convergence shape of the orifice is externally grooved, resulting in an elliptically shaped exit hole [49]. The sprays produced are classed as either flat tapered and even or non-tapered. Figure 3.13 shows a typical fan jet atomiser.

Flat sprays produce a triangular liquid sheet, with typical angles of 0˚ - 110˚ of which is determined by the orifice shape and the upstream convergence of the orifice. Non-tapered sprays are flat, with relatively parallel extremities compared to tapered types and are often used when multiple sprays are required without any overlap.

As the supply pressure is increased the spray angle increases up to a point, resulting in more linear spray edges. These edges are where any relatively large droplets are formed.

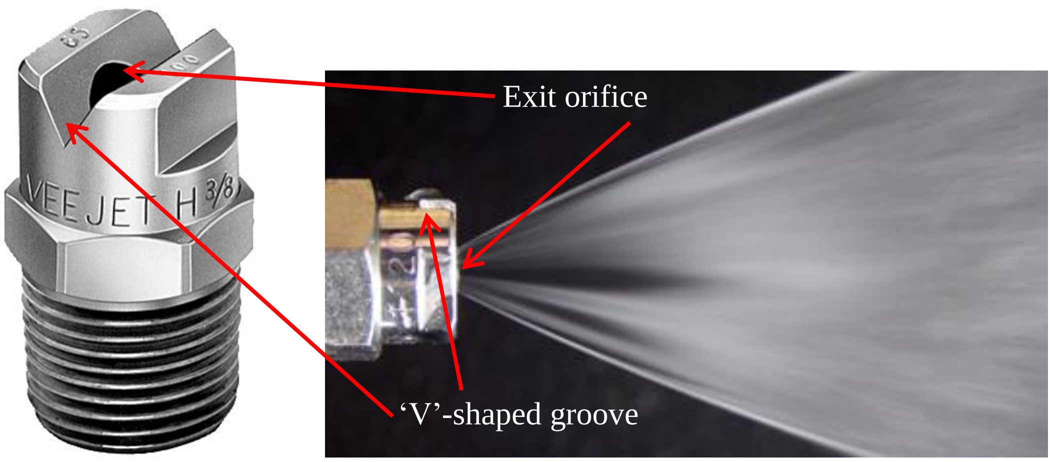

Figure 3.13 : Fan jet atomiser and characteristic flat tapered spray [47]

General characteristics

Good penetration, low entrainment, fairly complex geometry, coarse-medium atomisation, very flexible patternation (solid cone, flat or square sprays), wide range of spray angles, poor vaporisation, fairly high impact momentum, relatively narrow size distribution. For suitability for this current study (see Section 3.3.10)

Typical usage

Industrial cleaning, airless painting, surface cooling and descaling

3.3.3 Pressure swirl atomiser

This type of atomiser is probably the most widely used, both industrially and in devices such as aerosol cans used for deodorants, air-fresheners and paint spraying [47]. The liquid is introduced with a tangential velocity component into the swirl chamber at the core of the atomiser. This stationary core induces a vortex motion which naturally develops a low pressure close to the centre of the swirl chamber.

This motion entrains the surrounding atmosphere (normally air) into the centre of the vortex, which creates an air core which forces the liquid to emerge as a cylindrical sheet from the exit orifice. Finely atomised sprays of ≤20μm can be produced. Another characteristic with the pressure swirl atomiser is that the spray angle reduces with downstream distance. Figure 3.14 features an exploded view of a pressure swirl atomiser. The pressure swirl atomiser is considered to be the more efficient than standard pressure jet atomisation, producing a fine spray using lower liquid pressures.

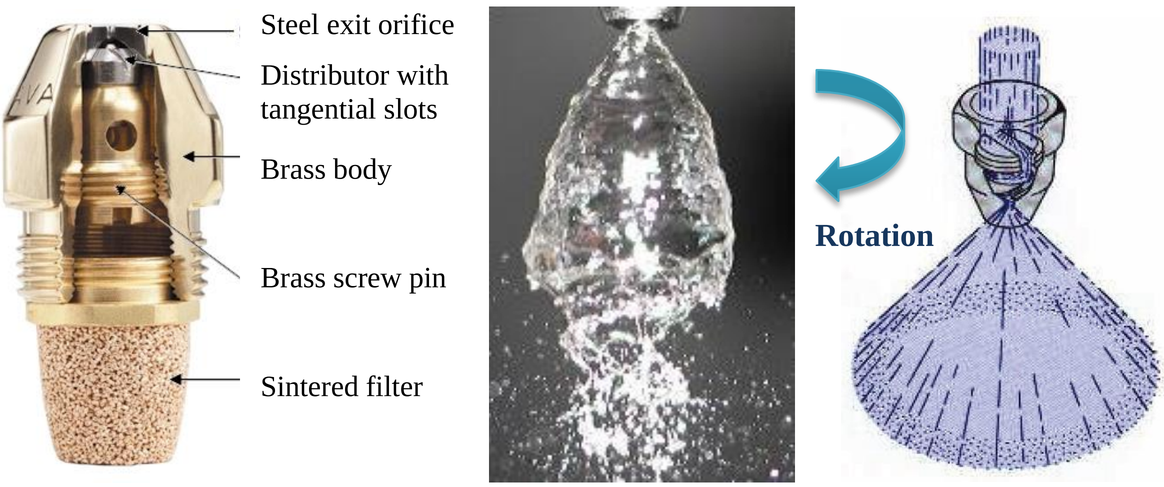

Figure 3.14 : Exploded view of a pressure swirl atomiser and typical spray motion

General characteristics

Moderate penetration, moderate entrainment, complex geometry, medium atomisation, Patternation; wide range of spray angles, moderate vaporisation, moderate impact momentum, relatively narrow size distribution. For suitability for this current study (see Section 3.3.10)

Typical usage

Fuel injection, fire protection, airless painting, cooling, agricultural, fuel oil combustion

3.3.4 Impact type pressure atomiser

Generally the liquid is impacted upon a surface as it emerges from the orifice in a flat spray pattern [47]. These atomisers tend to be used when a flat spray pattern is required, however the orifice size must be relatively large, approximately ≤5mm in order to minimise the chance of blockage.

Water deluge and fire sprinklers systems utilise this type of atomisation as shown in Figure 3.15 as they must provide a reliable spray when a fire occurs. In these atomisers the low pressure liquid jet hits the impact plate, thus disrupting the flow stripping the liquid into sheets and ligaments. In a fire involving burning organic materials, the droplets produced need to be large enough (previously discussed in Chapter 2) and contain sufficient mass to penetrate the up draught from the rising hot gases.

Figure 3.15 : Impact type pressure atomiser [54]

General characteristics

Poor penetration – although this in not essential as gravity provides droplet direction, moderate entrainment, complex geometry, poor atomisation.

Patternation; wide range of spray angles, poor vaporisation, poor impact momentum, relatively narrow size distribution. Suitability for this current study (see Section 3.3.10)

Typical usage

Fire protection, deluge systems, cooling of vessels and transformers

3.3.5 Two-fluid atomiser

These atomisers benefit from the extremely high Weber numbers resulting from the interaction of a fluid with a high velocity gas. These atomisers are often referred to as 'air assist' and can be further sub-divided into two categories:-

3.3.5.1 ***Internal Mixing*** two-fluid atomisers introduce a high pressure / high velocity gaseous supply to the liquid inside the atomiser before forcing the mixture out through one or more orifices. Figure 3.16 shows a typical internal mixing two-fluid atomiser and schematic view of the inside of the atomiser, revealing the air and fluid mixing prior to the exit orifice.

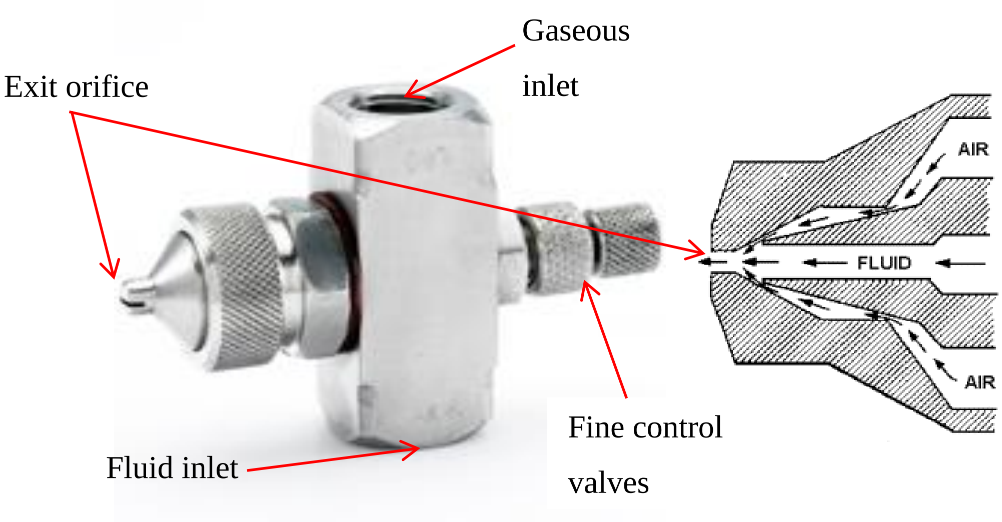

Figure 3.16 : Typical internal mixing two-fluid atomiser and schematic

General characteristics

Moderate penetration, high entrainment, complex geometry, very fine atomisation, Patternation; range of spray shapes according to air cap designs, high vaporisation, low impact momentum, relatively wide size distribution. Suitability for this current study (see Section 3.3.10)

Typical usage

Fuel injection, fire suppression, humidifying, cooling, medical, spray drying

3.3.5.2 ***External Mixing*** atomisers, as shown in Figure 3.17 introduce the liquid and high velocity gas to each other outside the atomiser, inducing highly turbulent activity within the first few millimetres downstream of the liquid exit orifice, giving way to effective atomisation. There are a number of designs available which differ in shape, size, position and orifice diameter. Figure 3.17 shows a typical external mixing two fluid atomiser.

Two-fluid atomisers typically produce a spray angle of between 50^{o}-180^{o}. Standard operating pressures are between ≤0.6MPa (6 bar) air and ≤0.9MPa (9bar) liquid. Flow rates vary depending on nature of application and use.

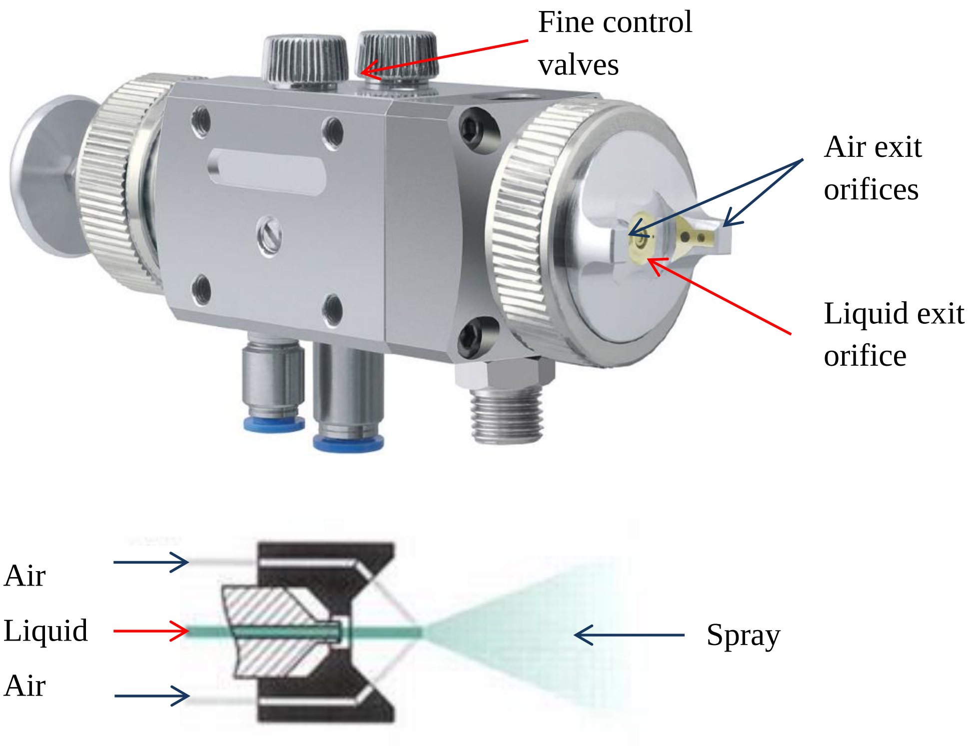

Figure 3.17 : Typical external mixing two-fluid atomiser and schematic

General characteristics

Good penetration, high entrainment, complex geometry, fine/medium atomisation. Patternation; range of spray shapes according to air cap designs, high vaporisation, medium impact momentum, relatively wide size distribution. Suitability for this current study (see Section 3.3.10)

Typical usage

Fuel injection, paint spraying, humidifying, cooling, spray drying

3.3.6 Rotary atomiser

These atomisers use the centrifugal force applied to the liquid to 'throw' a thin film of spray from a rotating cup or disk. The basic spray pattern is thus that of a 360^{o} disk. This spray technique has two potential benefits: (1) the possibility of producing particularly narrow droplet size distributions, and (2) the flexibility of the nozzle whilst in use. Narrow droplet size distributions can only be obtained using relatively low flow rates as it requires the atomiser to operate in the direct droplet or ligament regimes of break-up at the rim of the cup/disk. A variation of the rotary atomisation method uses a rotating porous cylinder. The liquid forms a thin even film on the inner surface of the cylinder and is flung from the pores to form a fine spray. Other variations use 'wheels' containing radial channels and exit orifices along their peripheries. These devices are often used in the atomisation of foodstuffs and chemicals [47]. Figure 3.18 shows a typical rotary atomiser and wheel.

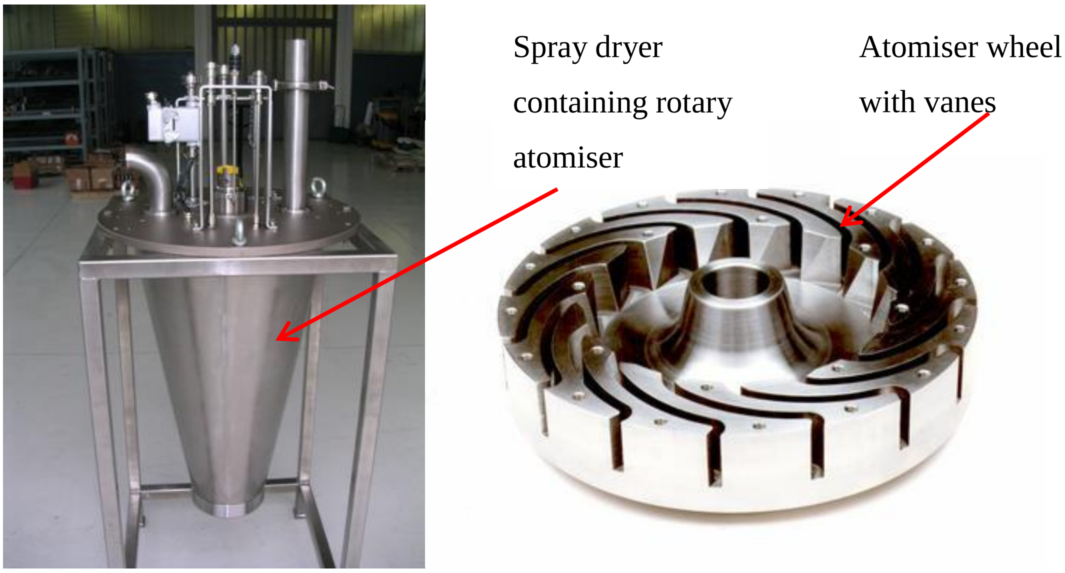

Figure 3.18 : Spray dryer and rotary atomiser wheel [47]

General characteristics

Low/medium penetration, low entrainment, very complex geometry, coarse-medium-fine atomisation, very restricted flat.

Patternation; 180˚ spray angle, moderate vaporisation, fairly low impact momentum, very narrow size distribution. Suitability for this current study (see Section 3.3.10)

Typical usage

Spray drying, agriculture, medical, paint

3.3.7 Ultrasonic Atomiser

Ultrasonic atomisers produce very fine droplets as small as 1 μm in diameter and produce a ‘fog’ like spray which is often used for decontamination, cooling (by evaporation), humidity control and dust suppression. These atomisers have two inlet connections as shown in Figure 3.19, whereby one connection is for the liquid that is to be atomised and the other being for air or gas. The air/gas flow enters the atomiser which then passes through a converging section, thus resulting in very high velocities. At the end of the converging section, the liquid enters the stream immediately prior to the combined flow entering an expanded section, known as the sonic energy core. A shock wave is produced, which reflects back from the resonator chamber cap, thus increasing/amplifying the initial shock wave.

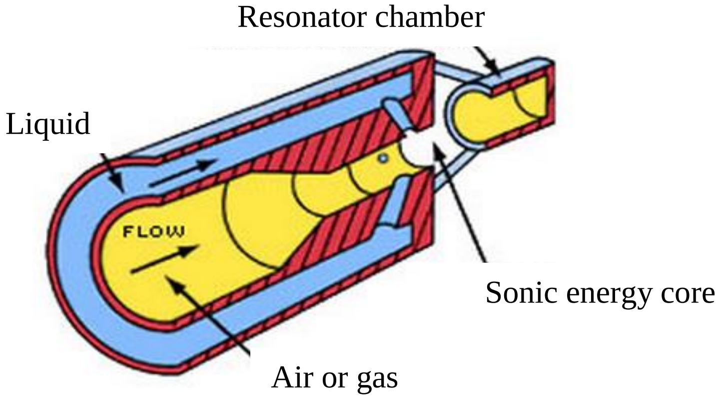

Figure 3.19 : Cross-sectional diagram of ultrasonic atomiser [55]

The resulting shock wave shears the liquid into very fine droplets. These droplets are generally very uniform and have low mass and low velocity, as shown in Figure 3.20. The exit orifice is normally quite large compared to a pressure jet atomiser and therefore nozzle wear and deterioration of spray quality do not present a problem.

General characteristics

Low penetration, low entrainment, complex geometry, fine/medium atomisation. Patternation; controllable by applied field, high vaporization, very low impact momentum, relatively narrow size distribution, low flow rates. Suitability for this current study (see Section 3.3.10)

Typical usage

Medium, humidifying, fine metal powders, agricultural

Figure 3.20 : Ultrasonic atomiser used for disinfection and decontamination [51, 55]

3.3.8 Electrostatic Atomiser

True electrostatic atomisers inject a charge into the liquid so that the charge at the surface of a jet or sheet of liquid acts against surface tension, causing a break-up of the liquid [48]. These atomisers are rarely used in practical devices although its use is being actively explored in several areas, which include fuel atomisation. A typical electrostatic atomiser is shown in Figure 3.21. Potential advantages include the production of relatively narrow drop size distributions, the flexibility of controlling the drop size by varying the charge injection, and the possibility of manipulating the charged droplets. Suitability for this current study (see Section 3.3.10)

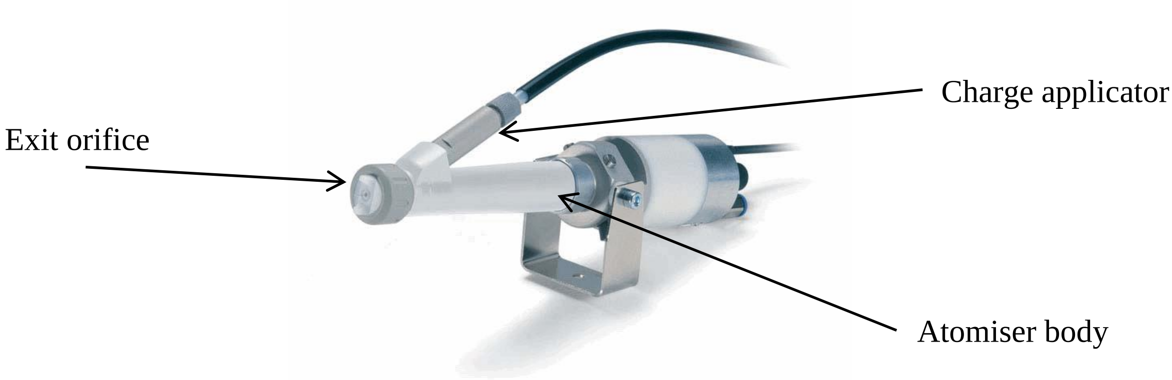

Figure 3.21 : Example of an electrostatic atomiser [51]

Typical usage

Paint spraying, laser printing, photocopying, agriculture

3.3.9 Spillback or spill return atomiser

A spillback, or Spill Return Atomiser (SRA) is an adaptation of the pressure swirl atomiser, over which it holds many advantages. High pressure liquid is normally introduced into a swirl chamber where vortices are formed. The turbulent flow then exits the atomiser via the exit orifice, with a regulated amount 'spilling back' via the spill return as shown in Figure 3.22.

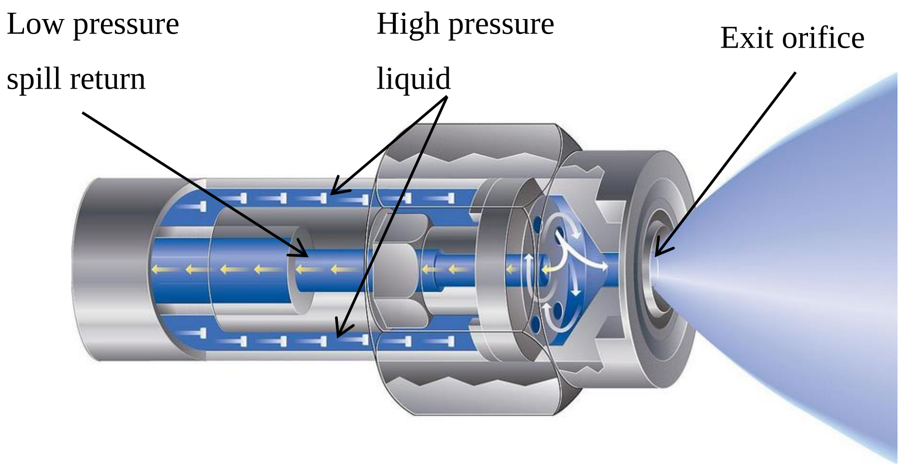

Figure 3.22 : Traditional spill return atomiser [56]

In a novel commercial Spill Return Atomiser (SRA) recently developed for decontamination and disinfection purposes, the high pressure liquid enters with a tangential velocity component into the swirl chamber at the core of the atomiser, as revealed in Figure 3.24. This process creates a vortex which naturally develops a low pressure close to the centre of the swirl chamber.

Once the flow has been triggered, the external gas which in often the ambient air, or in the case of an explosive atmosphere, the fuel gas-air mixture will be drawn into the centre of the vortex. This creates an 'air' core which forces the liquid to emerge as a cylindrical sheet from the exit orifice. In all finely atomised sprays of ≤20µm, the spray angle reduces with increasing downstream distance.

The SRA provides ideal characteristics for decontamination spraying environments as shown in Figure 3.23, producing an ultrafine mist with very small droplets sizes of ≤30µm, with good penetration and a low exit flow rate.

Eight miniature spill return atomisers (SRA) strategically placed within decontamination shower

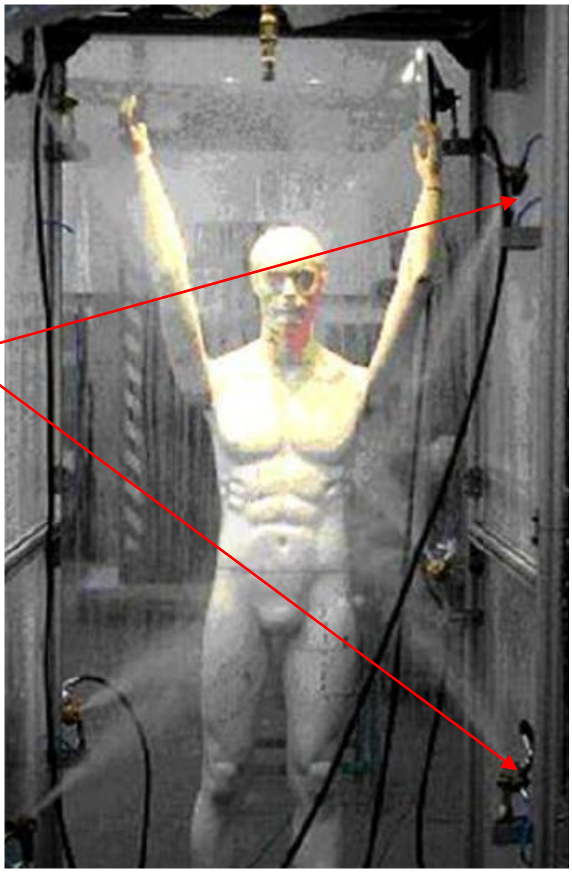

Figure 3.23 : Safety shower prototype incorporating eight miniature SRA's [51]

The spill return function allows the SRA to operate under high liquid pressure, 10 – 15MPa (100 – 150bar) at relatively low exit flow rate conditions. Tests have shown that spill return facilities can return as much as 85% of the total flow rate [51].

SRA's are ideally suited for the purpose of these investigations as they can provide the required drop size $D_{32} \leq 30\mu m$ and can additionally be easily modified with respect to flow rate, volume flux and spray cone angle by reconfiguration of some of the interchangeable components. The interchangeable components of the SRA are described below and are shown in Figures 3.24:-

i. **The spill orifice diameter** : increasing the spill orifice will reduce the flow at the exit orifice and conversely, decreasing the spill orifice will increase flow at the exit orifice.

ii. **The two opposing tangential inlet orifices to the swirl chamber** : reducing the diameter of the tangential inlet orifices to the swirl chamber will increase the flow velocity at a given pressure, thus increasing the turbulence at the exit orifice, resulting in a smaller mean droplet size.

iii. **The exit orifice** : increasing the diameter of the exit orifice will increase flow rate at the exit, causing a reduction in flow at the spill orifice. Another consequence of increasing the exit orifice is an increase in mean droplet size.

iv. **The swirl chamber** : this integral 'machined' component that was developed extensively by Nasr, G.G. *et al* [53] which is supplied by two 0.6mm tangentially opposed inlet orifices. The length and diameter of the swirl chamber were optimised to ensure maximum turbulence within the swirl chamber and at the exit orifice.

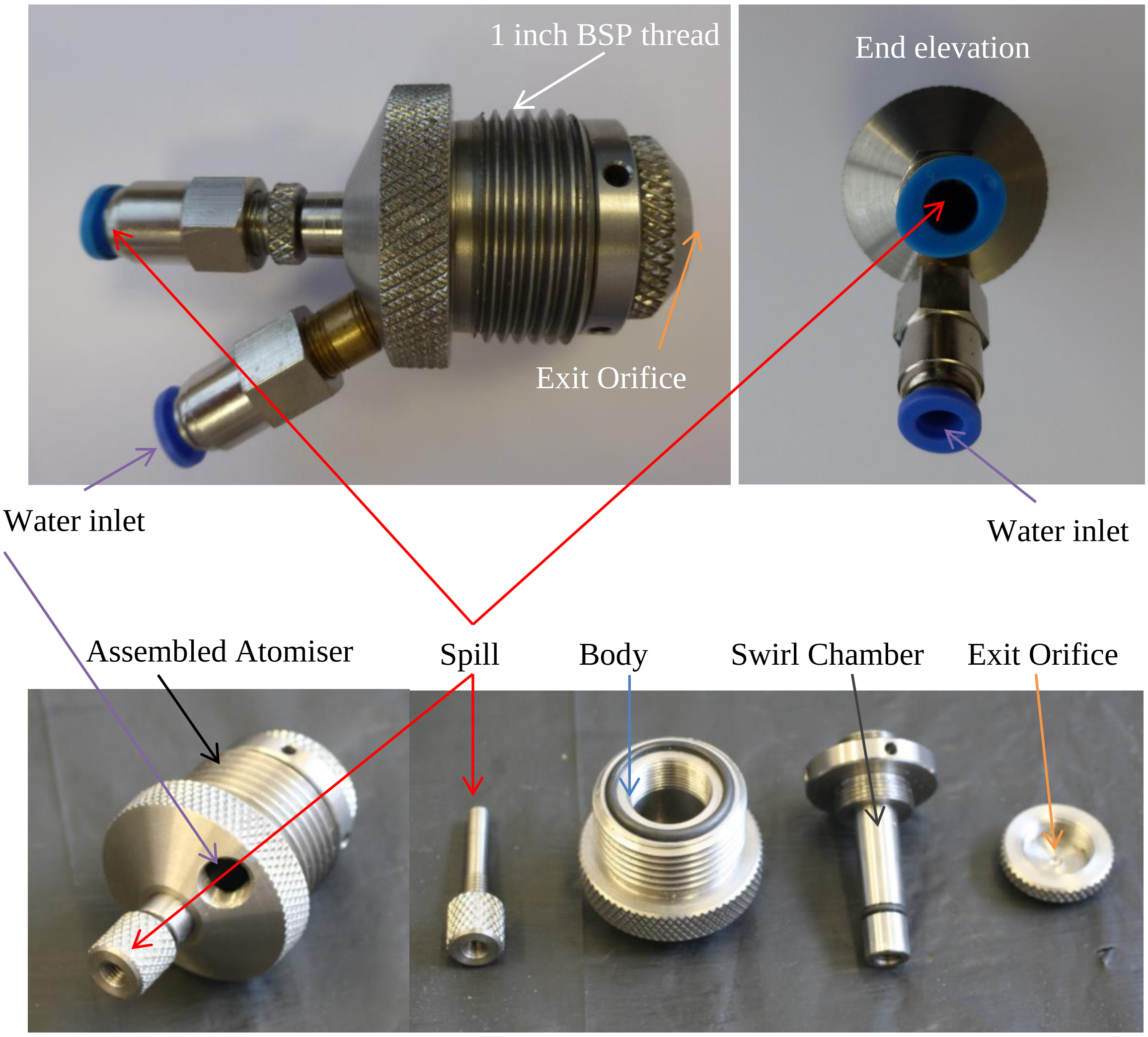

Figure 3.24 : Spill Return Atomiser (SRA) showing connections and component parts

3.3.10 Summary of atomisers and selection process

Based on the above review of fine spray atomising systems, the SRA was selected as the most suitable and versatile option for use and application in this present study. Table 3.3 provides a brief summary of all the atomisers considered in this review, together with reference to their suitability or denunciation.

The next Section will provide various laser measuring apparatus, emphasising the equipment used during this investigation in characterising the corresponding sprays. Moreover, a review of previous fire and explosions studies, particularly involving water sprays will be addressed.

Atomiser type	Spray type	Pressure (MPa)	Typical flow rate (l/m)	Spray angle (^{o})	Typical D_{32} (μm)	Suitable drop size range	Suitability of other characteristics	Overall suitability
Pressure Jet	1.Flat 2.Hollow 3.Full/Solid	1. 12 2. 0.03-2.5 3. 0.4	1. 50 2. 56-119 3. 60	1.15-40 2.50-180 3.Various	40-70	No	High exit flow rate, potential flame acceleration	No
Fan Jet	Flat fan	0.03-3.5	0.22-270	0-110 at 3 bar	25-45	Yes	High exit flow rate, potential flame acceleration	No
Pressure Swirl	Full/Solid	L: 1.4 A: 0 -0.7	L:19-56 A:99-4.5	Various	15-30	Yes	High exit flow rate, potential flame acceleration	No
Solid Cone	Full/Solid	4	191	30-100	20-35	Yes	High exit flow rate, potential flame acceleration	No
Impact-type	Hollow	1.3-1.7	48	50-130	2500-5000	No	Droplets would not break up in slow explosion field	No
Two-fluid	Flat or round	L: 0.3 A: 0 -0.7	L:19-56 A:99-4.5	50-100	20-40	Yes	Air stream would interfere with mixture homogeneity	No
Rotary	Full/Solid	0.04-0.06	0.365-0.6	Various	4-10	Yes	Equipment too large	No
Ultrasonic	Full/Solid	0.05-0.3	0 - 0.35	0-170	7-15	Yes	Insufficient flow rates	No
Electrostatic	Full/Solid	0.01-0.03	0.04-0.1	60-140	10-40	Yes	Insufficient flow rates	No
Spill Return	Full/Solid	10 -15	0.341	35-70	17-30	Yes	Potentially ideal velocity and liquid volume flux	Yes

Table 3.3 : Summary of atomisers and selection and denunciation rationale

3.4 Measuring Sprays

3.4.1 Laser Diffraction Anemometry (LDA)

This non-intrusive dynamic particle measurement technique was originally developed based on the principle of diffraction of a parallel beam of monochromic light by a moving drop. The laser diffraction method uses the theory that as a laser light (helium-neon, He-Ne, laser providing a monochromatic, coherent light) is passed through a spray, the light is scattered by the particles in the droplets in different directions. In the case of a large droplet the light is diffracted through a small angle and vice versa. Laser diffraction relies on the Mie theory [48] of scattering of light to determine drop size and distribution. An example of typical LDA equipment is shown in Figure 3.25.

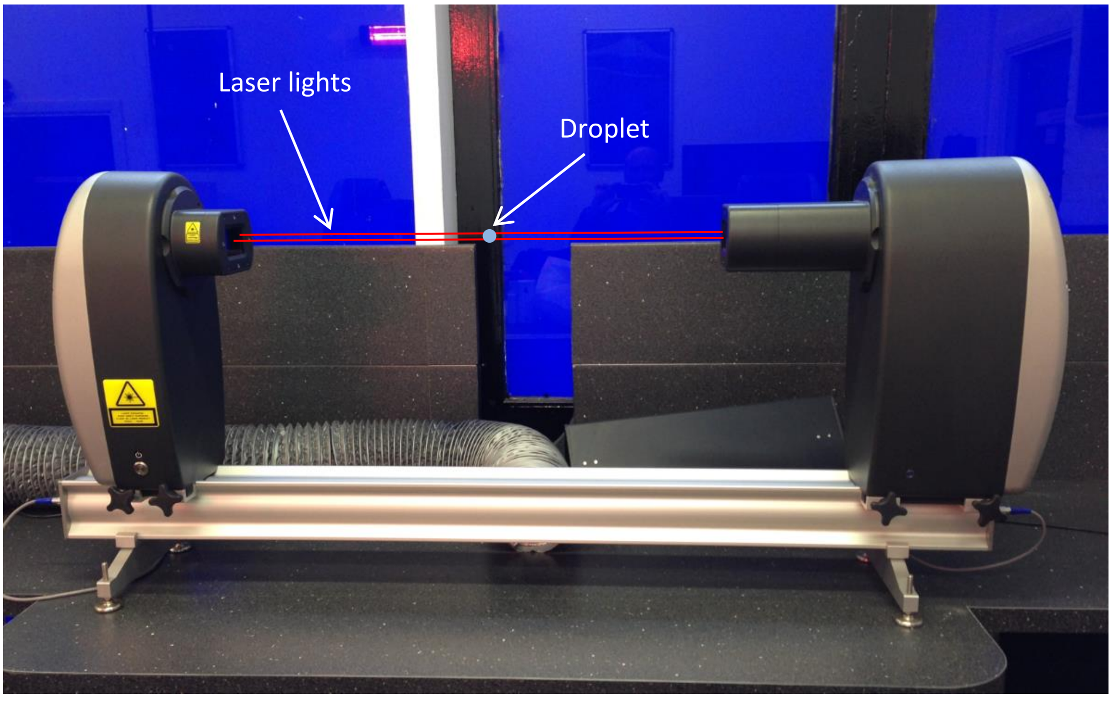

Figure 3.25 : Laser Diffraction equipment

Wide dynamic range from submicron to the millimetre size range (0.02 - 2000µm).
Rapid production of measurements, with results being generated in less than a minute.
Repeatability of results with large numbers of particles are sampled in each measurement.
Instant feedback to monitor and control the particle dispersion process.

Accuracy	Better than 1%
Reproducibility	1% variation

3.4.2 Phase Doppler Anemometry (PDA)

Phase Doppler Anemometry (PDA) is a non-intrusive method used to quantify and measure the size, concentration and velocity of droplets and bubbles in liquid or gaseous flow fields. PDA is used commonly in the characterisation of sprays produced by liquid atomisers and is sometimes referred to as Particle Dynamics Analysis.

In simple terms, the basic principles of PDA are that the light generated by a continuous wave laser is split into two beams by a Bragg cell. The two parallel beams then exit the transmitting optics via a lens which focuses them to converge in a special area, forming the *measurement volume* as shown in Figures 3.26 and 3.27. Droplets that are passing through the measurement volume will refract the laser light in both forward and backwards direction, following one internal surface refraction. Receiving optics (photo detectors) then convert the optical signal into a Doppler burst.

The intensity of the incident ray is partly reflected and refracted. The intensity ratio is given by the Fresnel coefficients and depends on the incident angle, polarization and relative refractive index. The scattering angle is given by Snell's law, which is used to describe the relationship between the incident rays and the refracted light. Most of the intensity is contained in the first three scattering modes as shown in Figure 3.26.

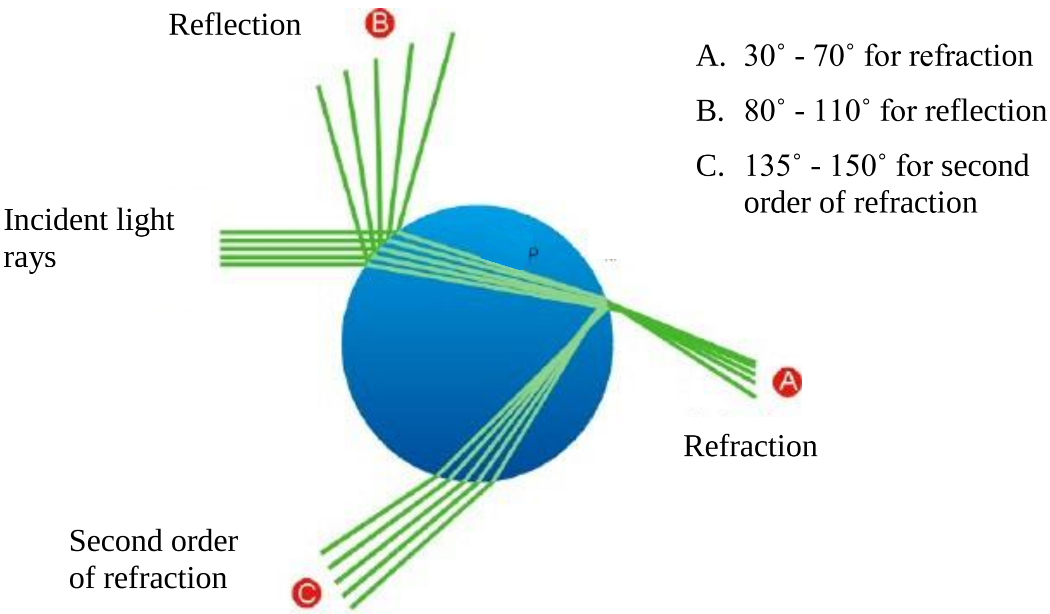

Figure 3.26 : Angles of incidence, reflection and refraction in a droplet [57]

Figure 3.27 illustrates the main components and some of the terms used with PDA equipment, in which a laser beam passes through a Bragg Cell. A Bragg Cell, or acousto-optic modulator is a device with consists of a piezoelectric transducer that produces sound waves designed to vary the phase and amplitude of the laser light beam.

The PDA equipment used for this current study including set up procedures, operating principles and potential sources of error is given in Chapter 4.

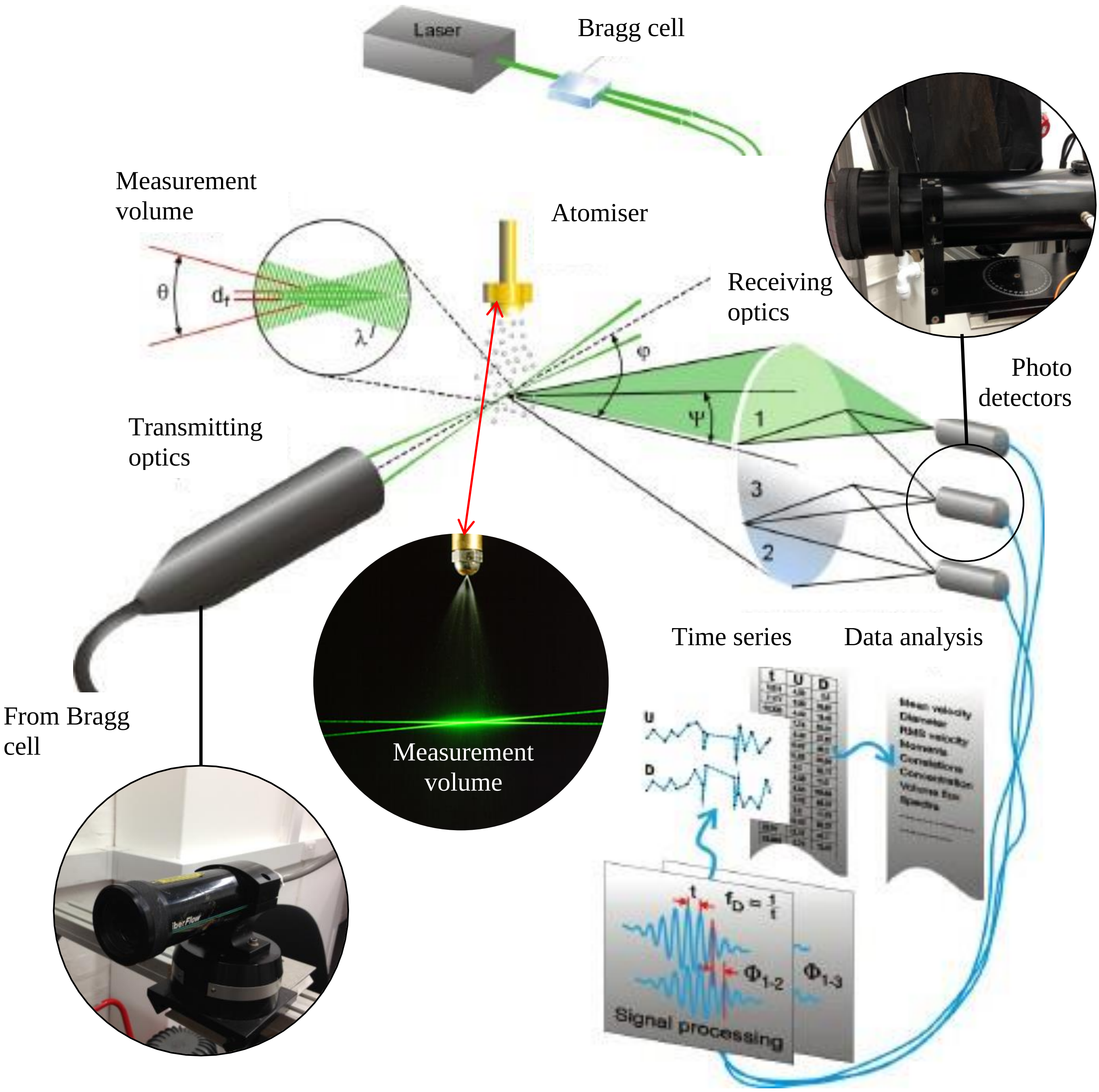

Figure 3.27 : PDA equipment - laser, transmitting and receiving optics

The preceding Sections in this Chapter have provided useful background information, including fundamental atomiser and spray technology and also a rationale for atomiser selection in this present study. The subsequent Sections will discuss some of the previous water spray explosion mitigation investigations, with relevance to this current study.

3.5 Review of previous fire and explosions studies involving water sprays

This section includes a review of previous work by several authors. Due to the sheer volume of published and unpublished work available, it has been impractical to review all of the available literature. This Section of the literature review discusses some of the previous published work carried out by highly respected scientists and organisations.

It is important to note that **all** of the previous studies were designed to consider the effects and suitability of water sprays in explosion suppression and mitigation, where the flow field ahead of the flame front has the necessary characteristics to break up large water droplets into smaller ones. This mechanism, known as hydrodynamic droplet break up results in the production of fine droplets which are small enough to act as a heat sink in the propagating flame. Further information is provided in Sections 3.5.1.4 and 3.5.3.1.

Although the scope, aims and objectives of this present study differ completely to the previous work, the general principles and apparatus used have been considered with respect to the design of the flame propagation and mitigation rig (FPMR) in Chapter 4 and will be used to postulate further realistic scale trials in Chapter 7. The subsequent Sections in this Chapter include a review which includes research from all over the world.

3.5.1 United Kingdom

3.5.1.1 British Gas – Midlands Research Station

3.5.1.2 HSE – Health and Safety Laboratory (HSL), Buxton, England

3.5.1.3 University of Aberystwyth, Wales

3.5.2 USA

3.5.2.1 US Bureaux of Mines, Pittsburgh, PA

3.5.2.2 US Naval Surface Warfare Centre, Potomac, Maryland

3.5.2.3 NFPA, Massachusetts

3.5.3 Norway

3.5.3.1 Christian Michelsen Institute, Bergen

3.5.3.2 CMR Gexcon, Bergen

3.5.1 United Kingdom

3.5.1.1 British Gas – Midlands Research Station

This project [58] includes a full literature survey and full scale investigation into the performance of various passive barriers and water sprays. A number of designs, including existing mitigation methods and some novel designs were tested and reviewed.

British Gas have carried out many years of full scale experimental research into the causes, outcomes and consequences of gas and vapour cloud explosions. Much of this work was focused on situations where a vapour/gas leakage had occurred in an outside atmosphere and where ignition had been delayed for a finite period.

Due to this delay in ignition gas/vapour is allowed to travel and spread over the site, often engulfing areas of closely packed, repeated obstacles such as pipe arrays. Under unconfined conditions following ignition, a combustion wave will proceed to propagate though the unconfined cloud at relatively low speed, producing very low overpressures. In many cases this incident may be categorised as a ‘flash fire’.

However, where the propagating wave comes in contact with areas of confinement, pipe arrays and other such areas of closely packed, repeated obstacles, this may lead to a high level of turbulence in the flame front. In turn, this produces an increase in flame area due to wrinkling, coupled with an increase in heat and mass transfer of the species. There will also be an instantaneous increase in flame speed, causing yet more turbulent action, hence causing a further increase in flame speed. A consequence of this increase in flame speed is the formation of a blast wave ahead of the flame, resulting in high overpressures, in the order of 10 atmospheres for natural gas and even greater for higher hydrocarbons.

The tests carried out at MRS in this report were designed to evaluate and test devices with relevance to flame deceleration and/or global mitigation. The test rig that was used is shown in Figure 3.28 and is similar to that used in MRS 4348 for the study of conditions required for sustained high speed propagation. This full scale testing rig consisted of a 46.5m long enclosure, complete with 3m x 3m steel arches positioned at 1.5 m intervals. The ignition end consisted of a 12m semi enclosed ‘driver’ section.

The remainder of the rig was covered with 500 gauge (125 μm) polythene sheet which was fixed and sealed to the concrete pad using ‘polygrasp’ strip. When the enclosure was filled with fuel-air mixture, the polythene covered section inflated to approximately 5m x 4m in cross section.

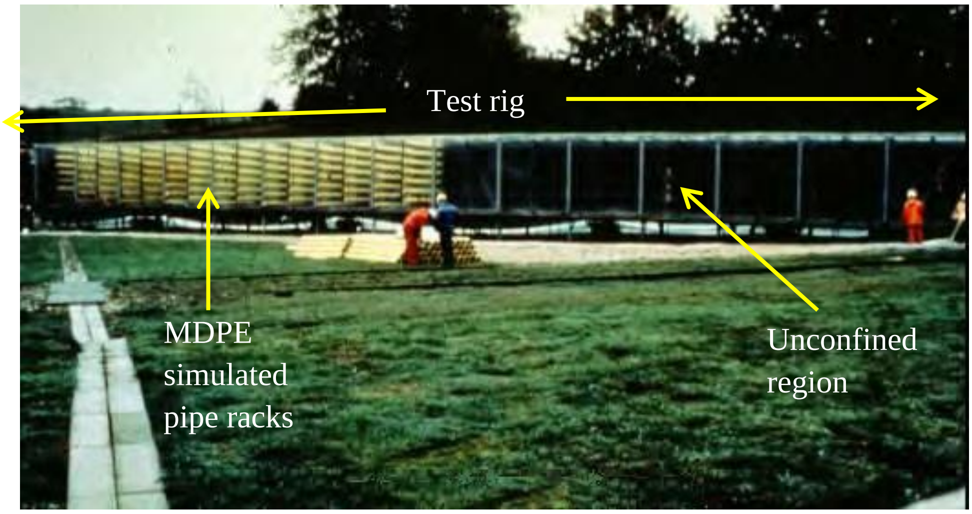

Figure 3.28 : Large scale flame acceleration test rig [58]

The 3m x 3m arches were used to support various pipe arrays, made from 3m lengths of 0.180m diameter M.D.P.E. pipe with two different configurations of congestion (array A & B), each array providing a 42% blockage ratio. In the mitigation tests, these arches and pipe arrays were either adapted to hold water bags or powder containers, or completely replaced with flame suppression equipment.

Initially three potential ‘passive’ methods of flame suppression and mitigation were tested using the rig as follows:-

i. Flame arrestors
ii. Distributed ammonium phosphate dust barrier
iii. Distributed water barrier

i) **Flame arrestors**

Two flame arrestors were manufactured to assess their mitigation ability. The arrestors were 3.5m x 3.5m x 0.5m in size and packed with approximately 250 kg of steel wool. One arrestor was packed with traditional fine wire wool and the other with the steel ribbon type. The flame arrestors were positioned at 26m and 36.5m from the spark as shown in Figure 3.29.

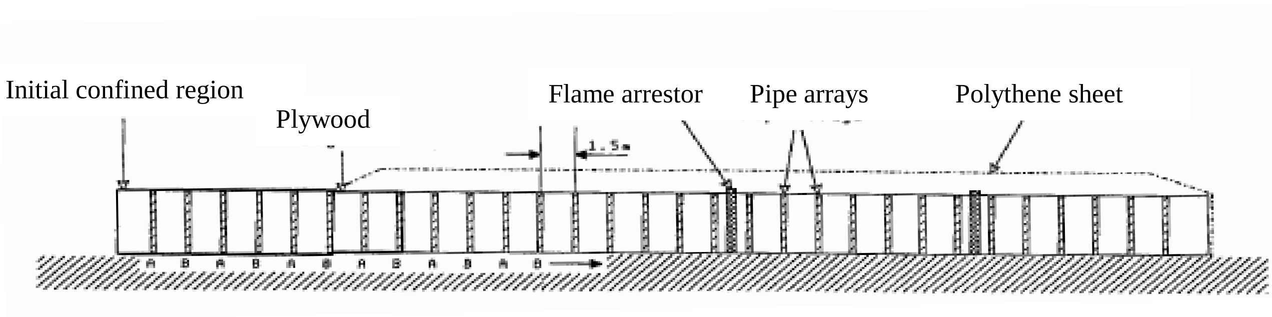

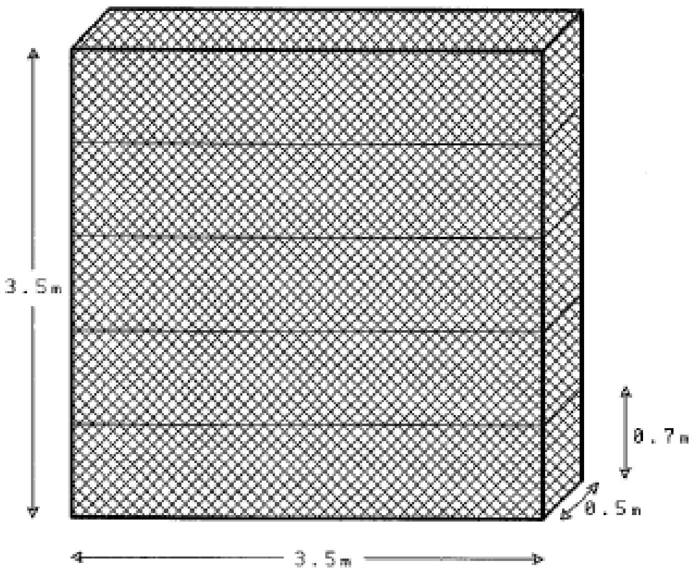

Figure 3.29 : Rig configuration and flame arrestor [58]

The review of the high speed cine camera film and pressure transducer data showed that the flame arrestors had little or no effect on flame speed. The flame propagated at an average speed of 500 m/s and even ignited the steel wool as it passed through the arrestors.

Many small scale flame arrestors work on the principle of a quenching distance, or quenching diameter. Some do contain stainless steel wire mesh, but others have multiple smaller diameter passageways of diameters less than the critical quenching diameter. It is clear that there was an insufficient density, depth and quantity of material to extract sufficient heat from the flame and hence quench the propagating combustion wave. However, some heat must have been extracted from the flame to ignite the steel wool.

ii) **Distributed ammonium phosphate dust barrier**

Small plastic bags were filled with approximately 0.5kg of ammonium phosphate fire retardant dust. In total there were 53 pairs of bags evenly distributed on one of the 3m x 3m pipe arrays containing a total of 53kg of dust. The single pipe array and bags were situated 21m from the spark, as revealed in Figure 3.30.

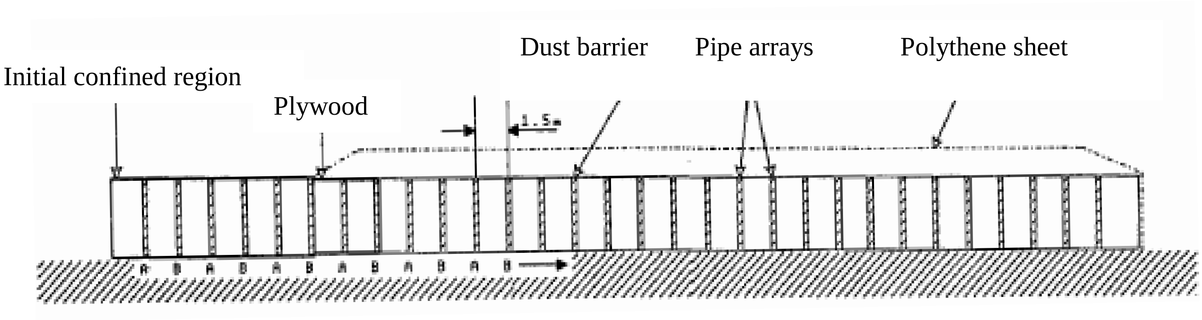

Figure 3.30 : Positions of distributed ammonium phosphate dust barriers [58]

In this test the flame emerged at an average speed of 500 m/s and appeared to decelerate briefly as it passed through the dust barrier, before returning to high speed. This pulsing could have been as a coincidence of the constricted openings in the pipe arrays due to the addition of the bags of ammonium phosphate dust prior to rupture.

Ammonium phosphate dust has proven to be a very successful ‘triggered’ barrier/suppressant, having been also tested and implemented by the American Bureaux of Mines. However in mines and other scenarios, systems are used to deploy the dust, rather than relying on the blast wave to shatter the bags evenly, thus distributing the powder thus allowing for sufficient transit time in the reaction zone.

iii) **Distributed water barrier**

Plastic bags containing approximately 2.5 litres of water were tied to three pipe arrays. These were positioned at 22.5m, 24m and 25.5m from the spark. On each array a total of 39 pairs of bags were evenly positioned, thus providing approximately 200 litres of suspended water per array and a total of approximately 600 litres distributed throughout a 3m x 3m x 3m cube section of the rig as illustrated in Figure 3.31 below.

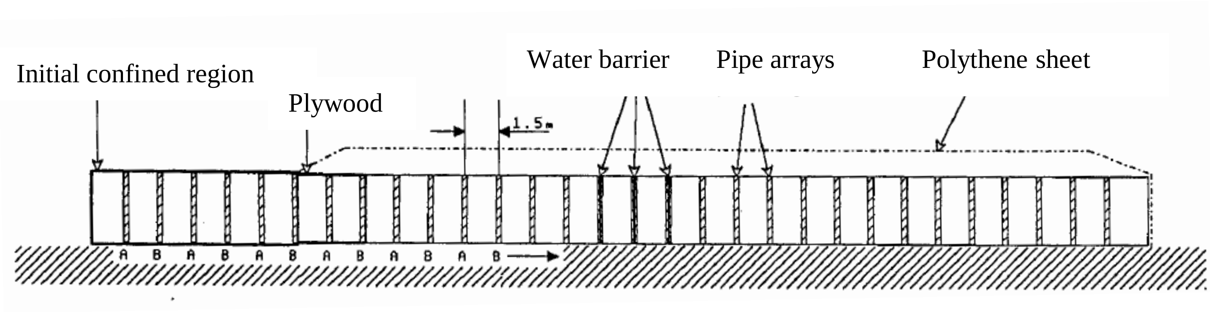

Figure 3.31 : Positions of distributed water barrier [58]

As with the previous test the flame emerged at an average speed of 500 m/s and appeared to decelerate briefly as it passed through the distributed water barrier, before returning to high speed. This pulsing could also have been as a coincidence of the constricted openings in the pipe arrays, due to the addition of the bags of water prior to rupture.

Water sprays containing droplets in the order of 100 – 1000μm have proven very effective in causing rapid flame deceleration in similar tests. Droplets are known to be shattered by the blast wave in an inverted bag type break up. In the distributed water barrier case, the water was contained in 2.5kg volumes and contained in plastic bags. The energy and time required to rupture the bags and to disperse the water into small enough droplets or sheets, would be insufficient in slow flow fields. This argument was confirmed by the fact that in similar tests using water sprays, the estimated amount of 'suspended' water at any given time was approximately 600 litres, being the same volume as the 39 pairs of bags.

Other experiments were also carried out using water sprays in a 1/5 scale replica pipe rack structure. To replicate speeds that may be achieved in the full scale rig, in some of the tests carried out on the 1/5 scale rig the mixture was enriched with oxygen i.e. for flame speeds up to 250m/s an enrichment of 25% gave conservative estimates and 26.5% enrichment reproduced flame speeds in the order of 500 – 600m/s.

Scaled atomisers were placed in rows 0.5m apart, with the atomisers in each row also 0.5m apart. The objective of this scaled experiment was to ascertain the number of atomisers required to dissociate the flame from the leading shock wave, in high speed propagation. To account for the thinner flame produced in an oxygen enriched mixture, droplet size was also scaled.

In the full scale tests using water sprays the rig was 30m long x 4.7m wide x 2.5m high. Three atomising nozzle types had been carefully selected to assess their high speed flame suppression characteristics:

i. 120˚ full cone, droplet sizes D_{32} 480µm. Operating at 0.3MPa (3bar) with a water flow rate of 12 l/m, as shown in Figure 3.32.

ii. 120˚ flat jet, with similar droplet sizes, operating pressure and flow rates to the above full cone atomisers.

iii. Two fluid atomising nozzles (air and water), with a supply pressure of 0.25MPa (2.5bar) for both water and air, with respective flow rates of 5 litres per minute and 20 m^3/h

The sprays were turned on several minutes prior to ignition to allow the spray to develop. However, the air stream on the two fluid atomisers was only turned on 30 seconds before ignition, to avoid dilution of the mixture.

Two rows of three full cone atomisers (see Figure 3.32) were required to dissociate the leading shock wave from the flame, whereas a single row of three full cone nozzles had some effect on the reduction of flame speed, although the flame did not fully dissociate the flame from the shock and would have re-accelerated to high speed if distance permitted.

Two rows of three flat or fan jet nozzles were required to dissociate the leading shock wave from the flame, whereas a single row of three flat jet nozzles had no significant effect.

The most effective atomiser was the two fluid type, which successfully dissociated the leading shock wave with a single row of three nozzles, resulting in rapid deceleration.

All three atomiser types were also assessed with respect to turbulence created by the sprays and the effect of this turbulence on flame speed.

Figure 3.32 : Typical 120˚ full cone atomiser droplet sizes (D_{32} 480μm) [58]

Although turbulence was clearly apparent and may well have led to localised flame acceleration, the overall suppression and mitigation effects of water sprays was proven.

This research program examined the effects of three passive barriers and three different water sprays. Some of the key issues raised are important and are dealt with within in this current study:

i. The above research relies solely on the hydrodynamic break up of water droplets by inverted bag type break up mechanisms into fine sprays that will heat up / vaporise in the flame and relies on all explosions generating the necessary forces to perform this type of break up.
ii. Where a vapour cloud is ignited in an unconfined region there will generally be insufficient energy to induce the break up mechanisms discussed above.
iii. The atomising nozzles used in the research were of the type found to be employed on many existing gas and petrochemical sites/platforms. This research was valid with respect to testing the explosion mitigation effectiveness and performance of existing fire deluge systems.
iv. The atomisers did have a degree of mitigation success when used in conjunction with an established high speed propagating combustion wave. The success rate depended

on their spray pattern, liquid volume flux, relative positioning and number of atomisers used. This information will be considered in the design of apparatus for these present studies, as discussed in Chapter 4.

v. Many external explosion events commence with a slow moving propagation (≤30m/s) through the gas/vapour cloud. To quench this type of event, a much finer spray (≤30μm) is required that will readily extract heat from the propagating flame.

3.5.1.2 HSE – Health and Safety Laboratory (HSL), Buxton, England

In 2005 the Health and Safety Executive (HSE) carried out extensive large scale testing [59] at its Health & Safety Laboratory (HSL), Buxton, England. The objectives of this testing was to demonstrate the effectiveness of 18 overlapping atomising nozzles forming a spray barrier as shown in Figure 3.33.

This type of barrier is recommended for use when employing a tunnel boring machine. HSE currently recommends one of these spray barriers at the end of the tunnel and subsequently at 500m intervals.

Figure 3.33 : HSL 18 atomiser, tunnel spray barrier [59]

Spray barriers of this nature are not designed to mitigate explosions, but are used as a fire and smoke barrier.

The important results from this work have helped to understand the interaction of overlapping spray patterns. As a result of this, one of the configurations developed for this present study involves the utilisation of ‘overlapping sprays’. Further information and rationales relating to the atomiser configuration used in this study are given extensively in Chapter 4, Section 4.5.5.

3.5.1.3 University of Aberystwyth, Wales

Thomas and Brenton [60] of University of Aberystwyth, Wales, carried out many years of research and produced countless papers and reports in the field of explosion mitigation by water sprays and the interaction mechanisms associated with extinction.

Thomas and Brenton mitigated high speed accelerated flame using a 76mm diameter, 5 m long pipe, as illustrated in Figure 3.34. The length to diameter ratio ($^L/_D$) was 65.7 with an internal volume of $0.023m^3$. The ignition and driver section contained corrugated liners to promote turbulence and flame acceleration.

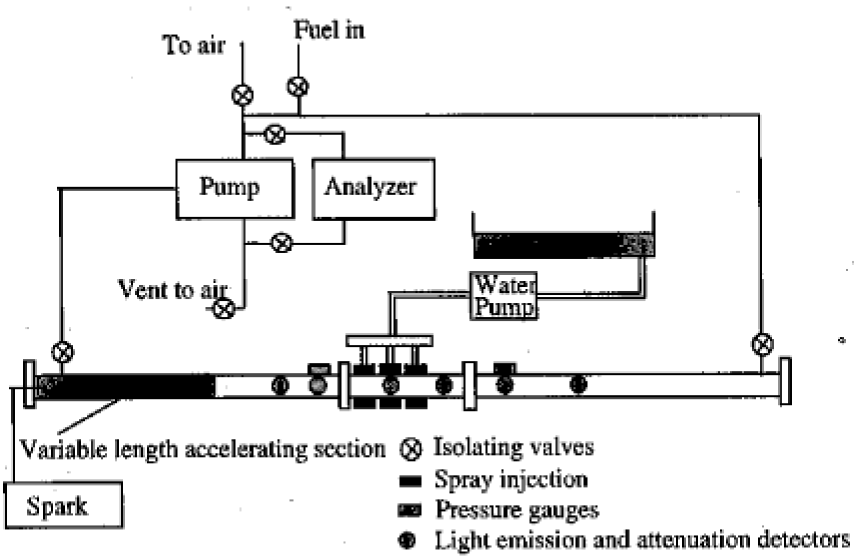

Figure 3.34 : Typical 76mm diameter by 5m long apparatus [60]

The rig contained three pairs of diametrically opposing atomisers. Pressurised water was fed from a pump at 0.7MPa (7bar). Three different atomisers were tested, (i) Woolworth D_{32} 52µm, (ii) Luxmark D_{32} 87.6µm and (iii) Delevan D_{32} 142.7µm. The Woolworth atomisers mitigated the flame in 28% of the tests, the Luxmark atomisers mitigated the flame in 32% of the tests and Delevan atomisers mitigated the flame in 58% of the tests.

Thomas and Brenton concluded that water sprays were capable of extinguishing a propagating flame. Also droplets with a Weber number of greater than 12 gave a higher mitigation success rate. Additionally Thomas and Brenton stated that smaller droplets would carried by accelerated flow field, therefore hydrodynamic shattering and inverted bag breakup would be less likely to occur.

The objectives for this current study are very different, as the sprays utilised will consist of droplets in the order of D_{32} 17 - 30μm and flame speeds will be much slower (≤30m/s). At such slow impact speeds hydrodynamic break up will not occur (see also Section 3.63), thus the mitigation of combustion activity in these circumstances will be reliant on droplet sizes being small enough to readily extract heat from the flame front.

3.5.2 Previous studies in the USA

3.5.2.1 US Bureaux of Mines, Pittsburgh, PA

Sapko *et al* [61] carried out some of the earliest published work into quenching methane-air ignitions with water sprays. Two experiments were carried out:-

i. To produce an atmosphere / mixture that would inert an explosion in a methane-air mixture using water sprays
ii. To quench a propagating explosion front using water sprays

Two different types of apparatus were used each made from 155mm (I.D.) plexiglass (PMMA) tube of 1m length in a vertical plane, as shown in Figure 3.35. Ignition was provided by a 15,000v spark via a 6mm spark gap for 200ms. A two fluid Sonicore 035H atomising nozzle, using water and steam from an electric boiler was used in the inerting experiments, whereby the condensate was collected and weighed to calibrate the atomiser. For the spray quenching, various ‘Spray Systems Co.’ hydraulic atomisers were used at differing pressures and flow rates.

The results of the quenching experiments are shown in Figure 3.36. Three different water temperatures were chosen to assess the effects of initial water temperature on droplet vaporisation. According to Kumm [62] a decrease in droplet size or an increase in initial water temperature would positively contribute to the effectiveness of a quenching system. This is predominantly due to the increase in latent heat of vaporisation as the droplet reaches boiling point during its transitional passage through the flame front.

Figure 3.36 will be analysed in Chapter 5 to compare the liquid volume flux and mean droplets sizes obtained. The straight lines plotted by Sapko *et al* have been extended into the ≤30μm droplet region (red dashed line) to provide initial guidance for atomiser characteristics and water pump requirements. This information will be considered as part of the design process for rigs and equipment used in this current study.

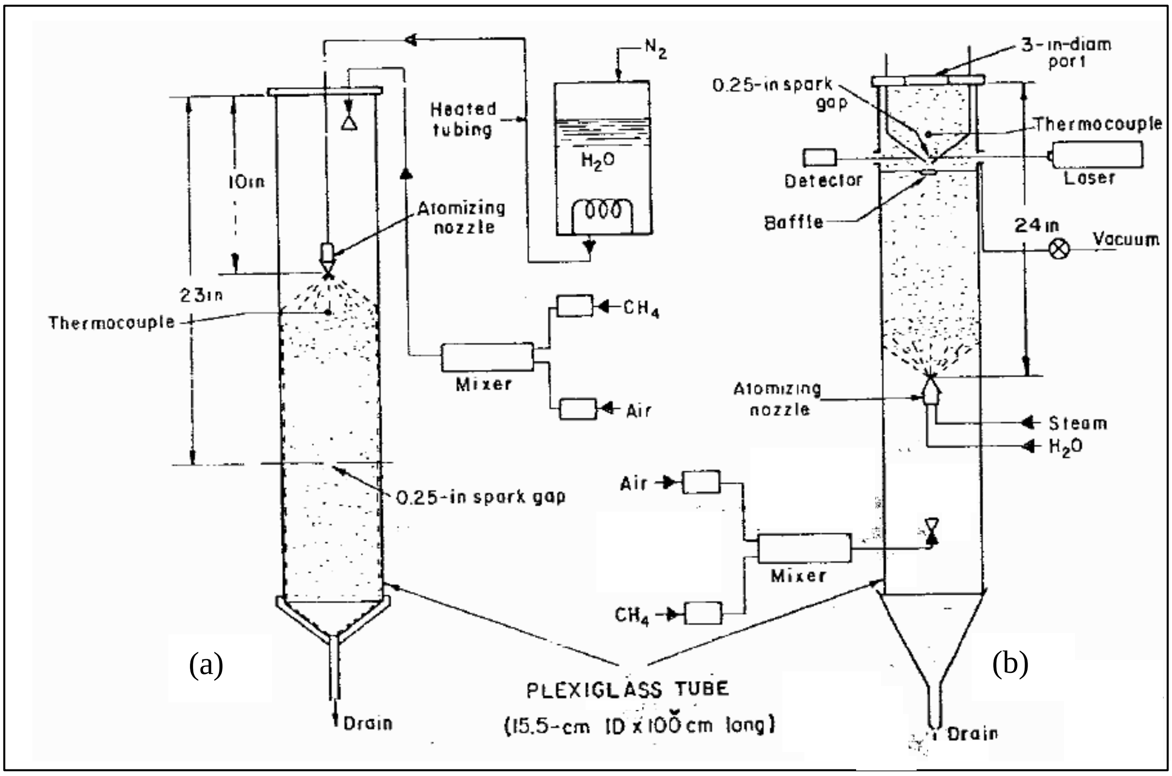

Figure 3.35 : Experimental apparatus for; (a) spray quenching and (b) inerting [61]

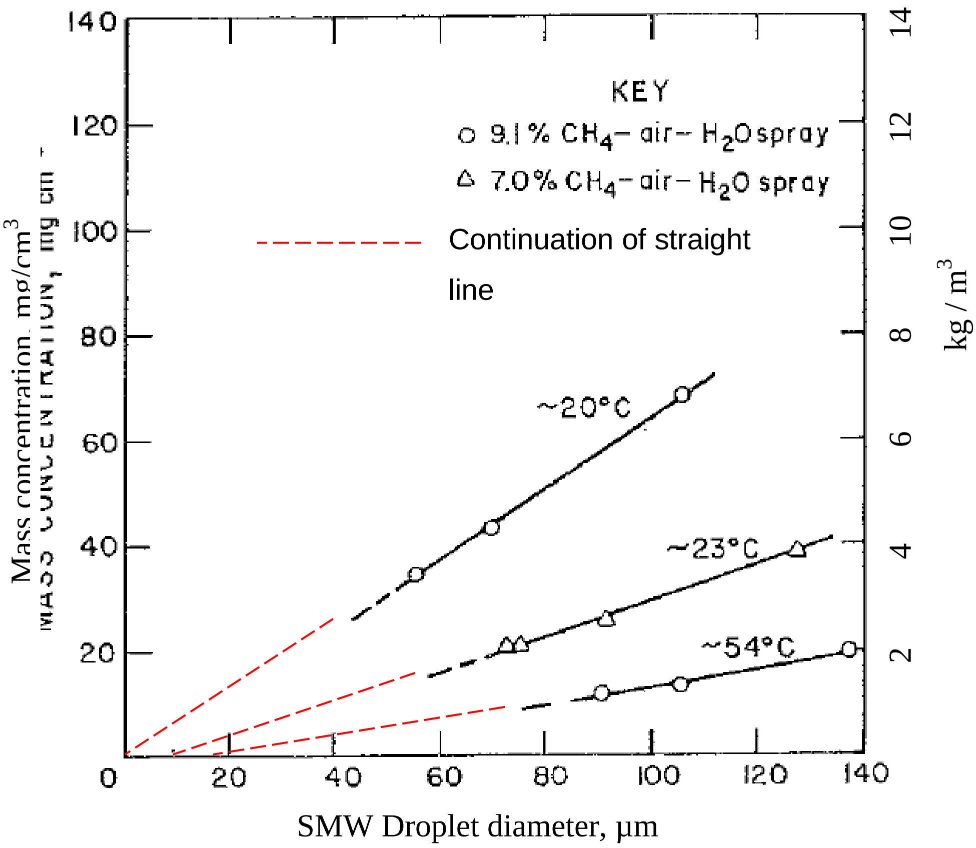

Figure 3.36 : Minimum water spray mass concentrations (SWM) for quenching methane-air flames [61]

- From previous work by Zabetakis, M.G. [21] approximately 26% v/v water vapour was required to render a stoichiometric methane-air mixture inert
- The water requirements for inerting a methane-air mixture were much less than that required to quench a sustained propagating flame
- According to Kumm, E.L.[62] calculations relating to the heat up and evaporation rate of sprays in a 9% methane air-mixture, an 18µm droplet will just about heat to boiling point in a flame propagating at 2.3m/s.
- This report includes variations of droplet size and temperatures, together with mixture percentage composition
- The conditions required for inerting were not as severe as in the methane flame propagating into the counter flow water spray
- Droplet size distributions were determined in some experiments using magnesium oxide impact methods, laser light transition and in conjunction with a microscope and calibrated eyepiece
- Lowering the methane concentration, or increasing the spray temperature reduced burning velocity and increased the thickness of the flame front, thus increasing residence time of the droplet in the reaction zone.
- The smallest droplets used in the spray quenching tests were 56µm SWM (surface weighted mean) with a water temperature of 20˚C. The atomiser had a flow rate of 0.775 l/m with a droplet quenching concentration of 34.6 mg/cm^3.
- The smallest droplets used in the inerting were 27µm SWM (surface weighted mean) using the laser method
- A moderate increase in water temperature greatly increased ability to quench the flame.

In Sapko's discussions [61] there was no reference made to hydrodynamic breakup of droplets, or detail relating the actual flame speed calculations during the experiments. Additionally, manufacturer's data was used to quote mean droplet sizes, or the sprays were characterised using magnesium oxide impact methods, which has since been superseded by more accurate non-intrusive methods such as Phase Doppler Anemometry (PDA) and Particle Image Velocimetry (PIV). Laser measurement techniques were used to characterise sprays in this present study and were discussed briefly in Section 3.4.

3.5.2.2 US Naval Surface Warfare Centre, Potomac, Maryland

This test facility was previously known as the David Taylor Naval Ship Research and Development Centre, which was renamed the David Taylor Research Centre (DTRC) in 1987, later becoming the Carderock Division of the Naval Surface Warfare Centre (NSWC) in 1992.

In 1990 Keenan and Wager [63] carried out explosion mitigation testing to assess to effects of placing large quantities of water in close proximity to explosives. A cylindrical charge of 2.12kg of TNT was placed inside a closed explosion chamber and detonated.

'Dry' explosion testing was initially conducted to establish the overpressures generated by the explosives within the confines of the explosion chamber. The charge was then surrounded on three sides by water filled containers, as shown in Figure 3.37.

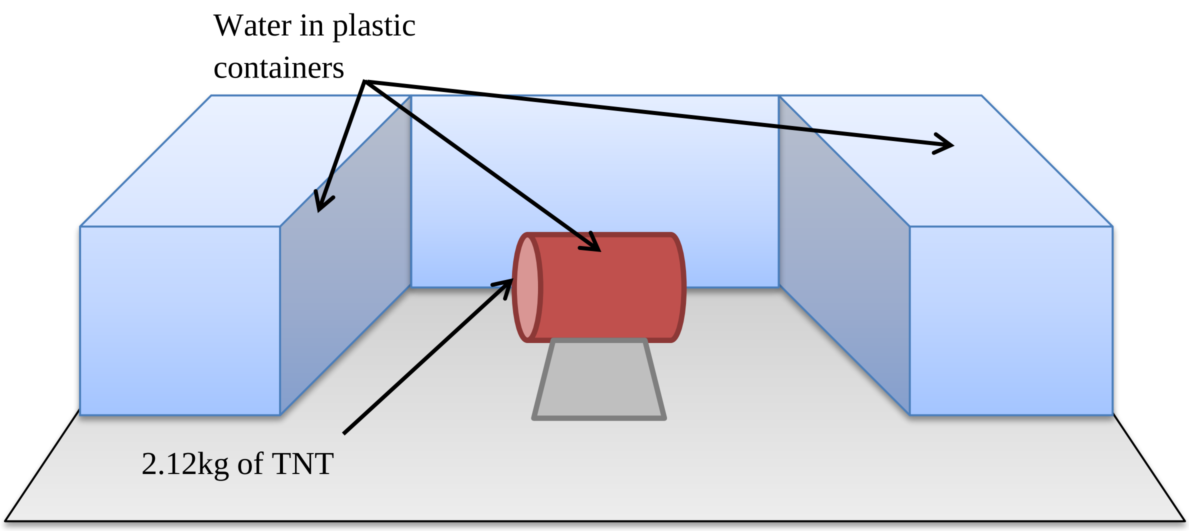

Figure 3.37 : Illustration of TNT charge surrounded on three sides by water containers

It was found that the overpressure was reduced by up to 89% when surrounded on three sides by water filled containers.

During the summer of 2005 the Naval Surface Warfare Centre (NSWC) was used to conduct a series of experiments to assess the mitigation ability of water mist when applied to confined space explosions using TNT [63].

These experiments were conducted in three phases:-

i. The atomisers were installed and their sprays were characterised in situ.
ii. The mitigation effects of the sprays were assessed using different high explosive detonations
iii. The explosives were then detonated in dry conditions, without water sprays being present to gather unmitigated reference data e.g. high speed imaging, flame speeds, temperature and overpressure.

Three atomising nozzle sets were used for the experiments, consisting of various pressure jet and two fluid Marrioff atomisers. The sprays were categorised and resulting mean diameters between D_{32} 27µm and 116µm were tabulated, with droplet concentrations between 36g/m^3 and 70g/m^3. Image analysis was carried out using a Vision Phantom 4s camera capable of capturing 3100 frames per second.

The time-pressure data shown in Figure 3.38 was gathered from the experiments and demonstrates a reduction in overpressure of 35% - 40% with water mist concentrations of 70g/m^3 and droplet sizes of D_{32} 54µm.

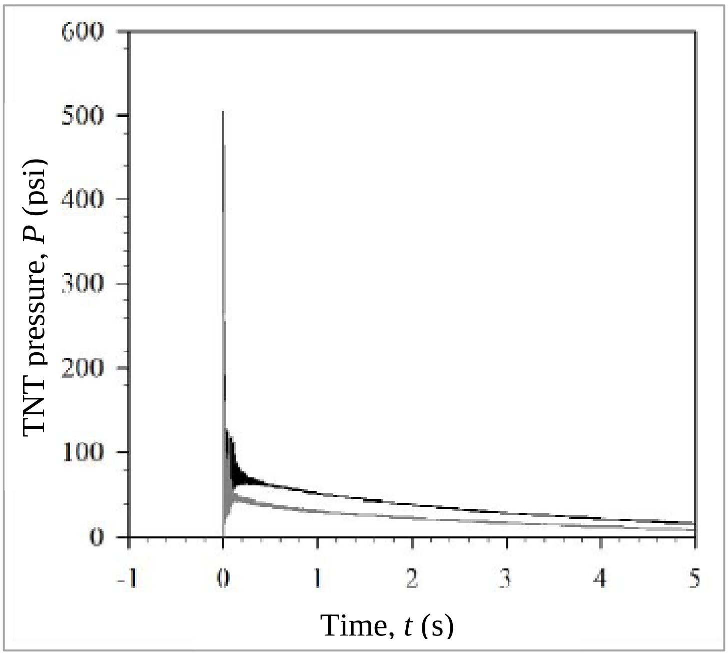

Figure 3.38 : 50 lbs TNT Pressure Trace with and without water mist Black (baseline), Grey (with sprays) [63]

The water mist concentrations used in this work are in general agreement with those presented by Thomas *et al* [39] and suggest that the latent heat absorbed by evaporation was the primary quenching mechanism occurring in droplets that had been shattered into fine mists by dynamic explosion forces, which would be in the order of 10μm. A 200μm droplet shattering into a 10μm fine mist would reduce its vaporisation time from approximately 0.78 seconds to 0.002 seconds to evaporate. As discussed in the previous Sections, this current study will not rely on secondary atomisation processes.

2.7.2.3 NFPA, Massachusetts

In 1993 representatives from water mist manufacturers, insurance companies, industrial users and enforcement authorities met to form the NFPA Technical Committee on 'Water Mist Suppression Systems'. Their main objective was to produce a code of practice, now known and VFPA 750, covering the design, installation, use and maintenance of water mist fire protection systems.

Since the 1940's when the first water mist systems were introduced, there has been a steady interest in water spray applications. However, following the introduction of the Montreal Protocol [64] and the phasing out of halons, a renewed interest in mist systems, together with the new technologies now available are included in the code.

The NFPA 750 code addresses and formalises several key issues, including:-

- components and hardware
- system types
- installation requirements
- design objectives
- hazard classifications
- calculations, water supplies
- atomising media
- plans and documentation
- acceptance criteria
- maintenance considerations
- additional Chapter specific to marine systems

3.5.3 Norway

3.5.3.1 Christian Michelsen Institute and GexCon, Bergen

Van Wingerden and various co-workers have carried out many analytical and experimental investigations into the mitigation of gas explosions using water sprays. Van Wingerden *et al* [65] carried out a study using a 1.5m^3 explosion box containing various different types of atomising nozzles. The atomisers that were tested produced water sprays with relatively large droplets of D_{32} 500 - 1000µm. In addition, fogging atomisers were also tested with droplet mean diameters of D_{32} 50 - 100µm.

An *increase in burning rate* of approximately 1.5 – 2.0 times was reported in the presence of water sprays in experiments using propane as the fuel gas and 1.4 – 2.3 times for similar trials using methane. This reported increase in flame speed is illustrated in Figure 3.39.

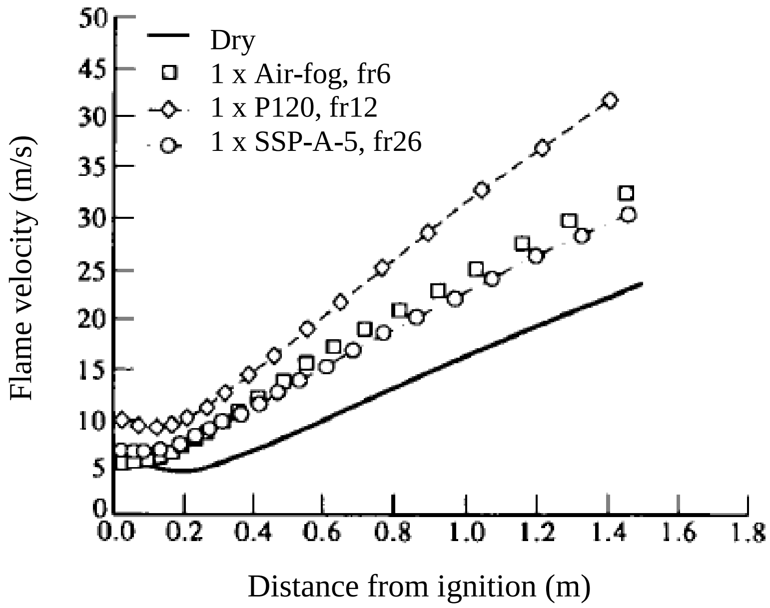

Figure 3.39 : The influence of various atomisers on flame speed [65]

From the above experiments Van Wingerden concluded that the induced turbulence from the bulk flow of water was present throughout the whole of the mixture and not just in the areas where the atomisers were positioned.

Van Wingerden *et al* [65] suggest that droplet sized between 20µm - 200µm are least effective, since they accelerate and readily adopt to the flow generated by the explosion.

Van Wingerden and Linga [66] carried out investigations into droplet break up in accelerated gas explosion flows. Figure 3.40 shows images from high speed photography of the secondary break up mechanisms associated with water droplets in high speed explosion flows. This type of secondary atomisation is known as 'inverted bag type break up' and occurs when an explosion front contains forces higher than the forces holding the droplets together, i.e. their surface tension forces.

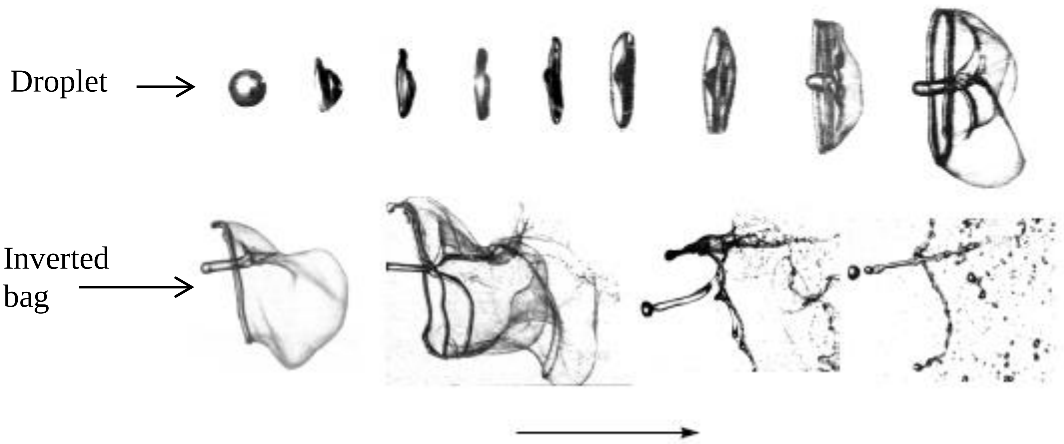

Figure 3.40: High speed images of 'inverted bag break-up' [66]

A dimensionless number known as the *Weber number* is used to quantify the relationship between a two corresponding fluids and is a ratio between the inertia and surface tension effects.

The Weber number is expressed as follows:-

$$We = \rho v^2 d/\sigma \tag{3.1}$$

Where ρ = density of the gas mixture stream (kg/m^3)

v = velocity of the gas mixture stream relative to the velocity of the droplet (m/s)

d = diameter of the droplet (m)

σ = surface tension (N/m)

Figure 3.41 illustrates two examples with different Weber numbers. Figure 3.41(a) shows a water fountain on a still day which is producing steady stream of water held together by surface tension, whereas Figure 3.41(a) shows another fountain on a windy day where the stream is being broken up into mist by the movement of air. Under still conditions the Weber number will be very low, compared to higher values on the windy day.

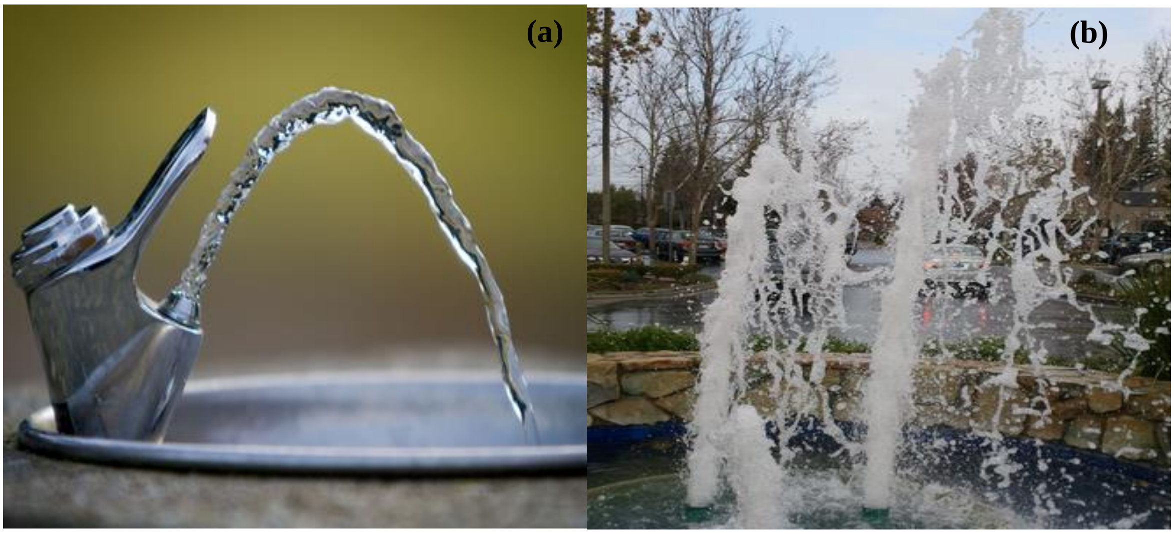

Figure 3.41 : (a) Fountain on a still day (b) fountain on a windy day

Surface tension is an intrinsic property of a fluid, however, the addition of a surfactant such as soap or other hydrophobic organic compound will reduce the surface tension, thus increasing the Weber number. Several authors [39, 58, 60, 65, 66] have examined the effects of surfactants used in water sprays in explosion mitigation trials and have all reported a positive contribution to droplet break up.

Van Wingerden and Linga estimated that only approximately 30% of the original droplet would break up into fine mist, whereas the other 70% would coalesce to form larger droplets.

Van Wingerden also stated that the droplets in the order of 10µm will behave the same as water vapour and that the water vapour concentration required to initiate mitigation of a methane-air mixture (ER = 1) is 31.5% vol/vol. This equates to a concentration by mass of 234g/m^3.

Although it is important to understand the relationship between droplet break up and Weber number, the sprays used in these current trials will not require any further, secondary break up and will therefore not be reliant on a finite range of flame speeds.

Additionally, because the droplets in this study will not be required to break up further, the use of surfactants will also not be necessary.

3.5.4 Alternative suppression and mitigation systems

The ATEX hot water advanced inerting system (HWAIT) [67] is a ‘triggered’ hygienic explosion suppression system designed for use in the dairy food industry. The system comprises of a large pressure vessel as shown in Figure 3.42, containing superheated pressured hot water stored at 1 MPa (10bar).

Figure 3.42 : ATEX Hot water advanced inerting system (HWAIT) [67]

The water is heated by electrical elements and the system is triggered by ambient pressure sensors. If the system receives a triggered response, then actuators are fired which in turn open a rapidly opening valve(s). This immediate loss of pressure in the vessel causes the superheated water to ‘flash off’ to vapour. This rapid expansion and change of state produces fine water droplets of about 50µm, without the need for nozzles or atomisers.

Advantages (as supplied by the manufacturer) [67]

- No nozzles or atomisers required
- Self-contained ‘package’ unit
- After deployment there is no cleaning or decontamination required, as with the major clear up required after using a powder system
- Easily refilled with water after deployment
- Highly effective

Disadvantages

- Must ***always*** be active i.e. full of water and heated to appropriate temperature
- Limited ***only*** to contained areas which do not have access to personnel, due to risk of severe scalding or even death

Whilst the above system is suitable for the purpose for which it was intended, it is highly unsuitable for this present laboratory scale study, or for any further consideration for full scale realistic trials, due to safety reasons and the mean droplet sizes being too large.

3.6 Effectiveness of sprays and criteria for extinction

3.6.1 Transit time of a water droplet in a flame

For the effective spray quenching or mitigation of a flame using water droplets, a number of the water droplets within the spray must fully vaporise. The basic problem is the very short residence times encountered by droplets as they traverse through a propagating flame front. In line with previous studies [39, 61], droplet transition through a flame is best described for laminar flame fronts [62, 68]. As turbulent flows are highly complex and irregular, a concept known as the 'laminar flamelet' is often used, whereby small iterations are used to describe and calculate localised flow properties.

For a flame travelling at 1.0m/s a water droplet will pass through a typical 1mm thick reaction zone in 1.0 millisecond (ms). Table 3.4 presents the droplet residence times afforded in a 1mm reaction zone with flame speeds from ≤30m/s.

Flame speed (m/s)	Droplet residence time (ms)
1	1.000
5	0.200
10	0.100
20	0.050
25	0.040
30	0.033

Table 3.4: Theoretical droplet residence times in a 1mm thick reaction zone

The above residence times will be additionally affected by spray orientation and fuel gas-air mixtures. Droplets may enter the propagating flame front in either counter flow, parallel flow or cross flow conformation. Residence time will vary each of these configurations, whereby, if the flame and spray are in counter flow the resulting ‘impact velocity’ will approximate the sum of the flame speed and the droplet velocity.

Conversely, if the flame and spray are in parallel flow, the resulting ‘impact velocity’ will be the difference between the flame speed and the droplet velocity, whereas in cross flow the droplets will be entering the flame perpendicular to the propagating direction and will be approximately stationary at the impact plane.

Therefore, the importance and relevance of spray configuration will be studied extensively as part of this program, with the inclusion of novel spray conformations in counter, parallel and cross flow formation. The consideration, comparison and subsequent testing of these three potential spray regimes has not been included in any previous literature and is therefore unrivalled.

3.6.2 Vaporisation of a water droplet

As previously mentioned in 3.5.2.1, Sapko *et al* [61] analysed the steady state expression given by Kumm [62] with respect to his work on droplet heat up and vaporisation.

$$R_o^2 = \left(\frac{2\, t_o\, K_a\, Ln\, (1 + c_p\,(T_a - T_b))}{\Delta H_v} \right) \Big/ \rho_\iota\ c_p \tag{3.2}$$

where, R_o = initial droplet radius (cm)
t_o = total droplet evaporation time (second)
K_a = average thermal conductivity of vapour between the surface and the flame
T_a = adiabatic flame temperature (K)
T_b = liquid boiling point
ΔH_v = latent heat of vaporisation at T_b (cal/g)
c_p = average heat capacity vapour at $(T_a - T_b) / 2$ (cal/g K)
ρ_ι = droplet density (g/cm^3)

When applying Kumm’s expression for example to a flame speed of 2.3m/s, a 1mm thick reaction zone and adiabatic flame temperature of 2185 K, then a water droplet of ≤8µm would be completely vaporised in a flame of a 9% methane-air mixture (E.R. 0.95). Williams [68] estimated that a minimum of ~20% of the evaporation time could be attributed to the sensible heat exchange period.

Sapko *et al* [61] also applied Williams [68] estimation of ~20% in conjunction with Kumm's formula to calculate that an 18µm droplet would just reach its boiling point in the same 9% methane-air mixture (E.R. 0.95) in 0.43 milliseconds (ms).

To fully vaporise the 18µm droplet, a much longer evaporation time of 2.2ms would be required. The droplet radius square was then plotted against the evaporation times (t_o) to produce Figure 3.43.

As the average droplet sizes used by Sapko *et al* were much greater than 18µm, they would not have fully vaporised in the flame or even reach their boiling point. Sapko *et al* attributed the quenching that they witnessed to the sensible heat transfer between the "unusually high water mass concentration" of initial droplet sizes and the flame.

It is also worth noting that there is no discussion or consideration in their work [61] regarding secondary atomisation or further droplet break up.

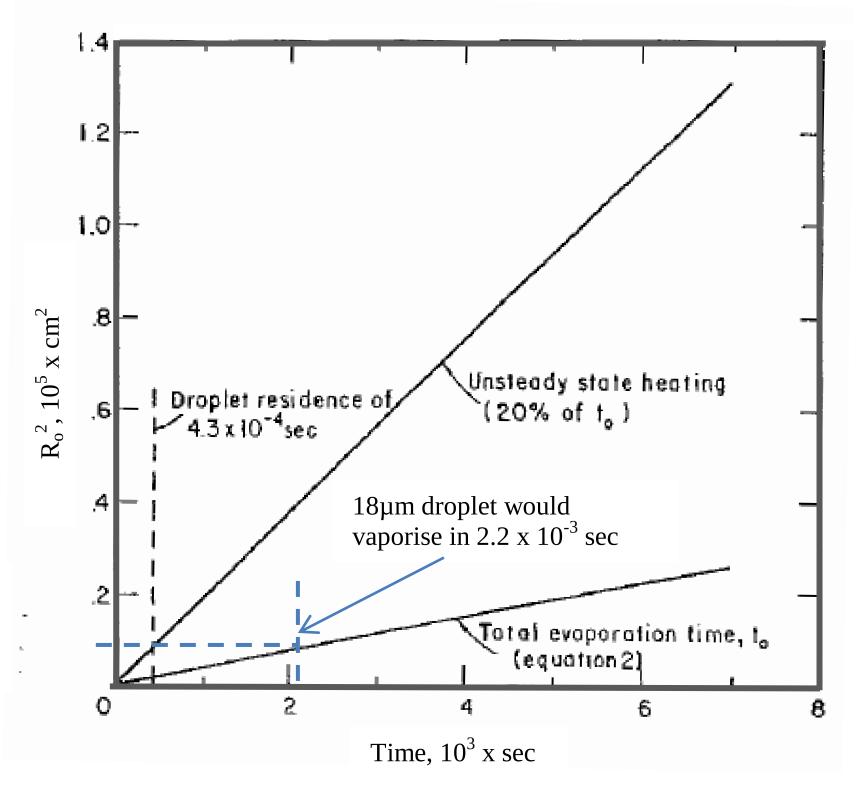

Figure 3.43 : Droplet radius square verses evaporation time (t_o) and unsteady heat up time to boiling [61]

Bjorkhaug *et al* [69] calculated evaporation times using a model offered by Kuo [70] in which the flame thickness and flame speed were assumed to be 1mm and 0.41m/s respectively. In this work [69] the authors are in agreement with Sapko *et al* [61], concluding that only droplets smaller than 10μm would vaporise fully in a flame.

Complete vaporisation of the water droplets will release the efficient abstraction potential of the latent heat of vaporisation. However, in reality the relative velocities between propagating flames and water droplets will be much higher than 0.41m/s, thus resulting in extremely short residence times. Flame speeds used in this current study will be ≤30m/s.

3.6.3 Ideal droplet size

The ‘ideal’ droplet size for water sprays used for explosion suppression or mitigation depends on several governing factors. These include:-

i. The anticipated flame speed likely to occur
ii. The geometry of the area : unconfined, partly confined or confined etc.
iii. The potential for flame acceleration (in the case of repeated obstacles)
iv. Whether the droplets are expected to break up further into ultrafine mist in the flow field, or without further break up in the flow field.

Van Wingerden *et al* [65] and Thomas and Brenton [39] carried out detailed studies into droplet dynamics and hydrodynamic break up. Both studies express the great relevance of the Weber number and present high speed photography of the inverted bag type break up mechanisms that occur in explosion flow fields. (see Section 3.5.3.1 shown previously)

Lane [71] presented the following relationship between droplet diameter and the critical velocity needed to overcome the intrinsic forces i.e. surface tension, which hold droplets together.

$$v_c^2\, d = 0.612\ \mathrm{m^3 s^{-2}} \qquad (3.3)$$

where v_c = the critical relative gas stream velocity for droplet break up (m/s)
d = the droplet diameter (μm)

Whereby, the surface tension of water is taken to be 73.10mN/m and the gas mixture density is assumed to be 1.2 kg/m^3. Lane’s formula is consistent with a critical Weber number stated by many authors of 10 – 12 required for droplet break up.

Table 3.5 demonstrates the critical break up velocities required, according to Lane [71], for a range of droplet sizes from 5µm - 1000µm.

Droplet diameter (µm)	**Critical break up velocity (m/s)**
5	349.86
10	247.39
20	174.93
50	110.63
100	78.23
200	55.32
500	34.99
1000	24.74

Table 3.5 : Critical break up velocities for various sized droplets

In this current study one of the key objectives is to quench or mitigate a propagating flame using water droplets, without further droplet break up mechanism occurring. The flame propagation and mitigation rig (FPMR) has been designed to facilitate a wide range of flame speeds.

The maximum flame speed likely to occur in the experimental trials of this study is approximately 30m/s, with mean water droplet sizes of $D_{32} \leq 30$µm. Given that the critical break up velocity of a 30µm water droplet would be approximately 142.8m/s, it may be assumed that the droplets will *not undergo any secondary atomisation* and are therefore highly likely enter the reaction zone of the flame maintaining their original form and size.

Given previous studies, the transitional residence times, boiling and vaporisation times of water droplets presented in 2.7.2 and 2.7.3, it is unlikely that sprays with mean droplets in the order of 30µm will fully vaporise in the flame. Moreover, as poly-dispersed sprays consist of droplet sizes above and below the Sauter Mean Diameter (SMD) or D_{32}, there will however be a number of droplets smaller than the actual D_{32}. Therefore, droplet distribution either side of the D_{32} value will play an important role in the mitigation qualities of the spray. With this in mind droplet distribution histograms are included and discussed with relevance in the results found in Chapter 5.

From the previous research discussed in this Chapter, droplets between 20µm – 200µm were least effective when used with high speed explosions. This is because they are likely to accelerate in the flow field due to their relatively low mass. Whereas droplets between 200µm – 800µm were found to be more effective when deployed in association with high speed explosions, in which conditions favoured the critical Weber numbers ideal for hydrodynamic bag type break up.

Lentati and Chelliah [72] carried out a *theoretical study* of water droplet dynamics in counter flow flames, in which the authors concluded that droplets of 15µm would be the most effective, with the maximum rate of vaporisation occurring at the *plane where radical formation is at its greatest.*

3.6.4 Droplet density to initiate flame extinction

There is a great deal of conflicting information relating to the droplet density, or liquid volume flux associated with suppression, extinction and mitigation of flames. The basic problem relates to the authors' initial objectives. For example, in many of the reported full scale trials, existing water deluge systems and atomisers were tested to assess the behaviour of sprays when propagating accelerated flames passed through the region of the sprays. These tests were carried out using the same atomising nozzles, spacing distances and supply pressures associated with realistic site deluge systems, such as those found at gas and petrochemical storage depots and offshore modules.

Whereas, many of the experimental laboratory scale trials have adopted the use of various types of atomisers, configurations, geometries and supply pressures. In addition to the above inconsistencies, the flame speeds and mean droplet sizes and droplet distribution differ in almost every case.

Other variables include the terminology used to describe, and methods used to report the droplet density. In some experiments atomiser manufacturer's data was used, whereas in others the atomisers were characterised using PDA, PIV, Laser Doppler Anemometry (LDA) or other dynamic particle measuring techniques.

Table 3.6 demonstrates the inconsistency problem and includes examples of the wide variation in reported droplet density data, which is variable in some cases by several orders of magnitude.

Author(s)	**Mean droplet size (µm)**	**Droplet density (various)**
Sapko *et al*	56, 70 and 106	34.6, 43.3 and 68.8 kg/m^3
Van Wingerden *et al*	10	234g/m^3 or 31.5% vol/vol
Cronin and Johnson	600 – 800	Fw 0.02 and 0.005%
US Navy Research	27 and 116	36 and 70 g/m^3
Catlin *et al*	600 – 800	Fw 0.02 and 0.005%
Zalosh and Bajpai	20 - 100	0.1to 1.0 kg/m^3
Thomas and Brenton	See table 15	See table 15

Table 3.6 : Typical representation of droplet densities reported in previous studies

In a theoretical study, on behalf of the Health and Safety Executive (HSE) Thomas and Brenton [39] calculated spray densities (liquid flux) and water volume fractions (Fw) for mono-dispersed sprays of 10µm - 100µm, as presented in Table 3.7. They concluded that droplets of ≤20µm, with spray loading densities of 0.03kg/m^3 were required for extinction. For larger droplets, much higher loading densities were needed.

As previously discussed and with the exception of theoretical studies, there have been *no reported experimental investigations* to corroborate the extinction flux required using fine spray atomisers and systems producing droplets of D_{32}≤30µm.

Sprays containing small droplets have much greater surface areas than those with larger droplets and therefore the results presented in this study are highly relevant and novel in the field of explosion suppression and mitigation.

Droplet diameter (µm)	**Number density (m^{-3})**	**Volume fraction x 10^3**	**Loading density kg/m^3**
10	6.0e + 10	0.031	3.1e - 02
15	2.0e + 10	0.035	3.5e – 02
20	8.0e + 09	0.034	3.3e – 02
30	3.6e + 09	0.051	5.1e – 02
50	1.1e + 09	0.072	7.2e – 02
100	7.0e + 08	0.37	3.6e - 01

Table 3.7 : Calculated mass loading densities and water volume fraction for mono-dispersed sprays [39]

3.7 Concerns : Utilisation of water sprays

There are two principle concerns surrounding the use of water sprays for explosion mitigation:-

i. Risk of ignition due to electrical sparks or arcing
ii. Generation of induced turbulence

3.7.1 Risk of ignition due to electrical sparks or arcing

Where water sprays are used in the vicinity of electrical items such as transformers or switch gear, there is an obvious risk of electrical sparks or arcing where sprays impinge on electrical connections. Transformer connections are normally separated by dielectric materials, such as ceramic insulators. Depending on the potential current and gap between these insulators, a water spray may provide a pathway for electrical discharge.

Water ingress into electrical equipment is another potential risk that may result in a spark. The *IP* code or *International Protection* code shown in Figure 3.44 specifies the degree of intrusion that electrical apparatus will withstand from water, dust and even human body parts, such as fingers and hands. The IP system is referenced in most water deluge installation codes and is recognised worldwide. The IP code is sometimes referred to as ‘Ingress Protection’.

It is worth noting that some spray systems are often deployed in the event of equipment failure, such as transformers as shown in Figure 3.45. NFPA 15 provides guidance relating to atomiser positioning in the proximity of electrical equipment. Prior to discharging, the atomising nozzles electricity should be isolated where possible.

Another potential source of ignition that has raised concerns in the past is electrostatic discharge. The UK offshore operators association (UKOOA) have issued guidance [73] which includes reference to ignition sources associated with water deluge systems.

Previous studies [74] have demonstrated that the potential static discharge from deluge systems is negligible when compared to the ignition energy required to ignite a vapour cloud. Van Wingerden *et al* [65] also concluded that during all of the CMR and British Gas research, there was no reported accidental ignition due to static or electrical discharge.

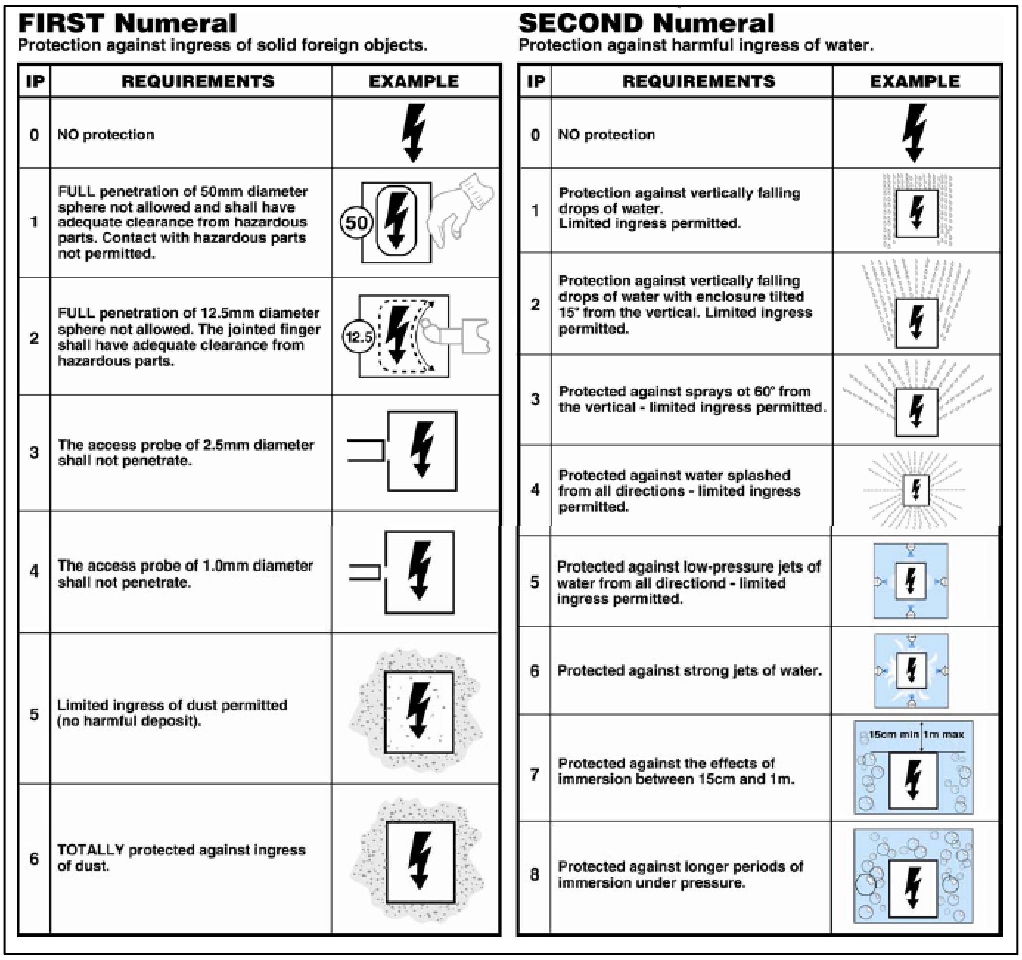

FIRST Numeral
Protection against ingress of solid foreign objects.

IP	REQUIREMENTS	EXAMPLE
0	NO protection	
1	FULL penetration of 50mm diameter sphere not allowed and shall have adequate clearance from hazardous parts. Contact with hazardous parts not permitted.	50
2	FULL penetration of 12.5mm diameter sphere not allowed. The jointed finger shall have adequate clearance from hazardous parts.	12.5
3	The access probe of 2.5mm diameter shall not penetrate.	
4	The access probe of 1.0mm diameter shall not penetrate.	
5	Limited ingress of dust permitted (no harmful deposit).	
6	TOTALLY protected against ingress of dust.	

SECOND Numeral
Protection against harmful ingress of water.

IP	REQUIREMENTS	EXAMPLE
0	NO protection	
1	Protection against vertically falling drops of water. Limited ingress permitted.	
2	Protection against vertically falling drops of water with enclosure tilted 15° from the vertical. Limited ingress permitted.	
3	Protected against sprays ot 60° from the vertical - limited ingress permitted.	
4	Protected against water splashed from all directions - limited ingress permitted.	
5	Protected against low-pressure jets of water from all directional - limited ingress permitted.	
6	Protected against strong jets of water.	
7	Protected against the effects of immersion between 15cm and 1m.	15cm min 1m max
8	Protected against longer periods of immersion under pressure.	

Figure 3.44 : IP codes and index system

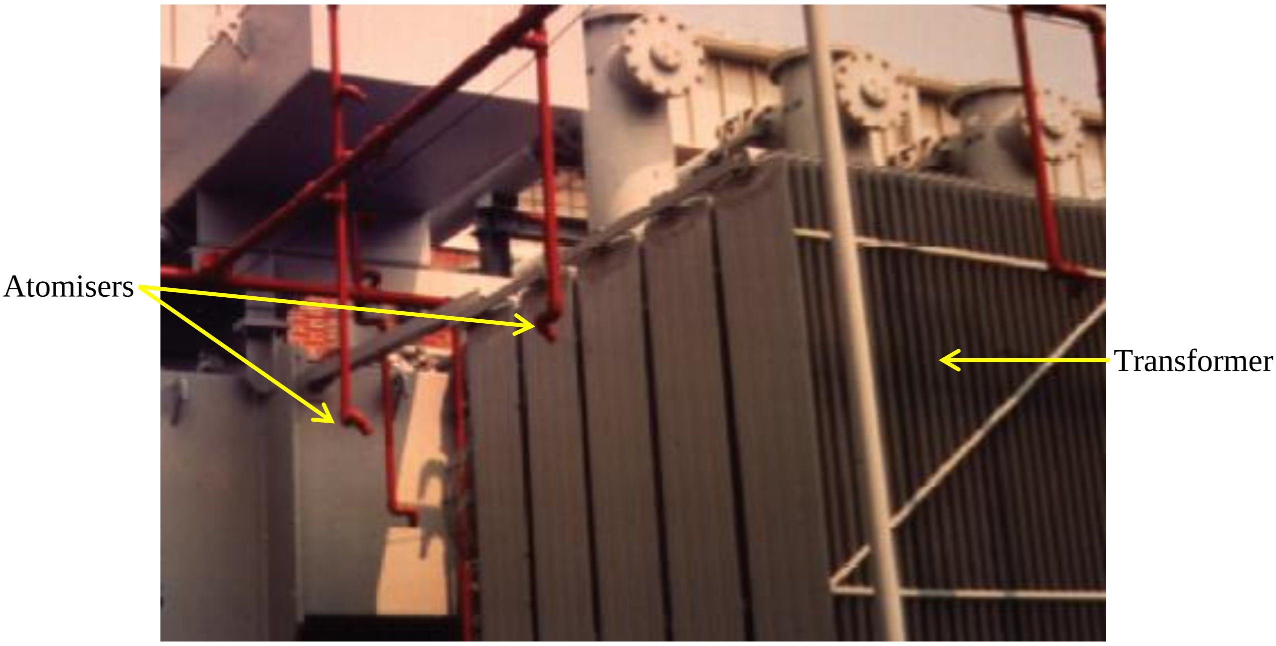

Figure 3.45 : Complete water impingement system for oil filled electrical transformer [74]

During this present study, in excess of 250 'hot trials' were performed with water sprays in counter flow (C/F), parallel flow (P/F) and cross flow (X/F) conformation to the propagating flame. Throughout the trials there was *no evidence* of any electrostatic discharge involving the various spray configurations ($D_{32} \leq 30\mu m$).

3.6.2 Generation of induced turbulence

Although water sprays have been proven to be an effective flame suppressant, several authors have reported an initial increase in flame speed in the presence of sprays. In previous experiments into explosion mitigation by water sprays, there have been number of reported cases where the bulk flow of water from the sprays has contributed to turbulence generation in the vapour cloud.

Van Wingerden and Wilkins [75] reported an increase in flame speed which in the vicinity of sprays of 500µm - 1000µm using fogging nozzles with droplets in the order of 50µm – 100µm, compared to the same mixture without sprays (dry). The increased flame speeds appeared to be equally distributed throughout the mixture, not only in the presence of the sprays. This would indicate that the increase was due to a disturbance of the mixture, rather than the direct contact between the sprays and the mixture.

Thomas and Brenton [39, 60] conducted experiments using a vessel 2.4m high, 0.3m wide and 0.21m deep and various Luxmark nozzles, using droplets diameters (D_{10}) in the order of 100 – 350µm, which were characterised using various laser diffraction techniques. They also report similar findings in methane-air explosions, concluding that large scale eddies were the overriding factor. The authors also reported that even after the sprays were shut down for a few seconds prior to ignition, there was still an increase in flame speed due to the imposed disorder, rather than direct droplet interaction.

Thomas and Brenton [39, 60] and Van Wingerden [65, 66] carried out many tests in the absence of sprays to establish baseline conditions, followed by further trials with water sprays, whereby high speed imaging and temperature and pressure data was gathered and subsequently processed. In both cases the authors concluded that although there was a significant overall reduction in pressures in the presence of water sprays, an initial increase in flame speed was observed and attributed to *induced turbulence*.

The potential turbulent effects of water sprays have been 'coded' by GexCon [10] into their commercial CFD explosion modelling software tool FLACS, which can be used to predict and model the turbulence generation effects of various atomisers (≥100μm).

In the many experiments carried out by British Gas, the authors concluded that although in all cases there was an increase in flame speed upstream of the water sprays, there was a was global reduction in flame speed and overpressures immediately downstream of the sprays.

In addition to establishing the accumulative effects of spray orientation i.e. counter, parallel and cross flow configuration, with respect to explosion droplet residence times and mitigation as discussed earlier, the spray conformations used in these studies will also be appraised with regard to the general disturbance of the fuel gas-air mixture and the resulting consequential flame speeds.

Due to the variation in spray configurations and total number of trials conducted in this program, the resulting effects caused by induced turbulence will be compared for single and multiple counter flow, parallel flow and cross flow atomiser configurations. The results from this unique research are discussed with relevance in Chapter 5.

3.8 Chapter Summary

- This Chapter provides a basic understanding of spray fundamentals and atomisation techniques. Additionally some of the terminology associated with spray utilisation and research has been described.
- An overview of various atomisers was also discussed and presented, with a tabulated rationale for the selection and denunciation process in respect to finding a suitable atomiser for this current study.
- A Section was also included to provide background information for some of the spray measurement equipment used in this study.
- Previous experimental and theoretical studies in the field of mitigation by water sprays are also presented and analysed. Comparisons are made between the results and conclusions presented in previous work, together with discussion relating to some of the agreements and disagreements.

- Although previous experimental studies have concentrated on high speed propagations (≥100m/s), coupled with dynamic bag type break up of relatively large droplets (D_{32}≥100μm) into fine mist (D_{32}≤30μm), the mathematical predictions relating to the subsequent vaporisation of finer droplets has been proven to be very useful.
- Droplet transit and residence times within the flame front, together will flux density comparisons from previous work has also assisted with the selection and evolution of the atomising systems employed in this current research.
- The SRA provides the ideal characteristics required for this present study, with the additional benefits of the ease of interchangeabilty of various components, resulting in drop sizes of D_{32}≤30μm, liquid volume flux Q_f ≤0.047$cm^3/s/cm^2$ and droplet velocities V_d≤21.4m/s.
- Further reference will be made to these highly relevant aforementioned investigations throughout the experimental phase, results and conclusions of this present study.

The following Chapter examines and reviews the experimental apparatus, procedures and methods of data processing used in the ‘cold’ and ‘hot’ trials of this present study.

CHAPTER 4

APPARATUS, PROCEDURES AND METHOD OF DATA PROCESSING

4.1 Introduction

This Chapter discusses the experimental challenges and achievements, qualitative and quantitative collection procedures and methods of data and imagery processing within these investigations. Due to the significant wealth of experimental research carried out in this study, as summarised in the flow diagram shown in Figure 4.1, this Chapter has also been separated into two distinct groups in line with other Chapters. These are:-

i. ***'Cold trials'***
ii. ***'Hot trials'***

The ***'cold trials'*** were experimental assessments, observations and tests conducted in the absence of a fuel-air mixture or propagating flame. Included in the cold trials were a series of dynamic non-intrusive laser assessments using Phase Doppler Anemometry (PDA), which were all performed in the Spray Research Group (SRG) laboratory and will be discussed in detail in the following Section. The results of the cold trials can be found in Chapter 5.

All of the ***'hot trials'*** were carried out within the Petroleum Technology Research Group (PTRG) laboratory using the purpose built 'Flame Propagation and Mitigation Rig' (FPMR), which will be discussed, explained and rationalised extensively in this Chapter.

The creations of numerous combustible mixtures, together with ignition activities were conducted within the FPMR. A selection of commercial atomiser configurations, called here SRA's (Spill Return Atomisers), were examined to appraise their explosion mitigation capabilities. The results of the series of experimental trials carried out in the hot trials are discussed and summarised in Chapter 5 and Appendix 9.

As discussed previously in Chapter 1, the aims and objectives of this research are quite different to previous studies, with the emphasis being to mitigate relatively slow moving propagating flames of ≤30m/s. The cold trials were designed to explore and develop an existing SRA and to provide a selection of suitable configurations that would be assessed in the hot trials in the FPMR. Also, as previously reported in Chapters 1, 2 and 3, earlier studies [2, 39, 45, 58, 61, 65] concentrated on the effects of the hydrodynamic breakup of large water droplets in the order of ≥100μm, with respect to explosion mitigation by water sprays. Whereas this present research is focused on the development of a fine spray system, consisting of average droplets of D_{32}≤30μm, capable of producing a spray that will readily absorb heat in the flame, without relying on further droplet breakup (secondary atomisation).

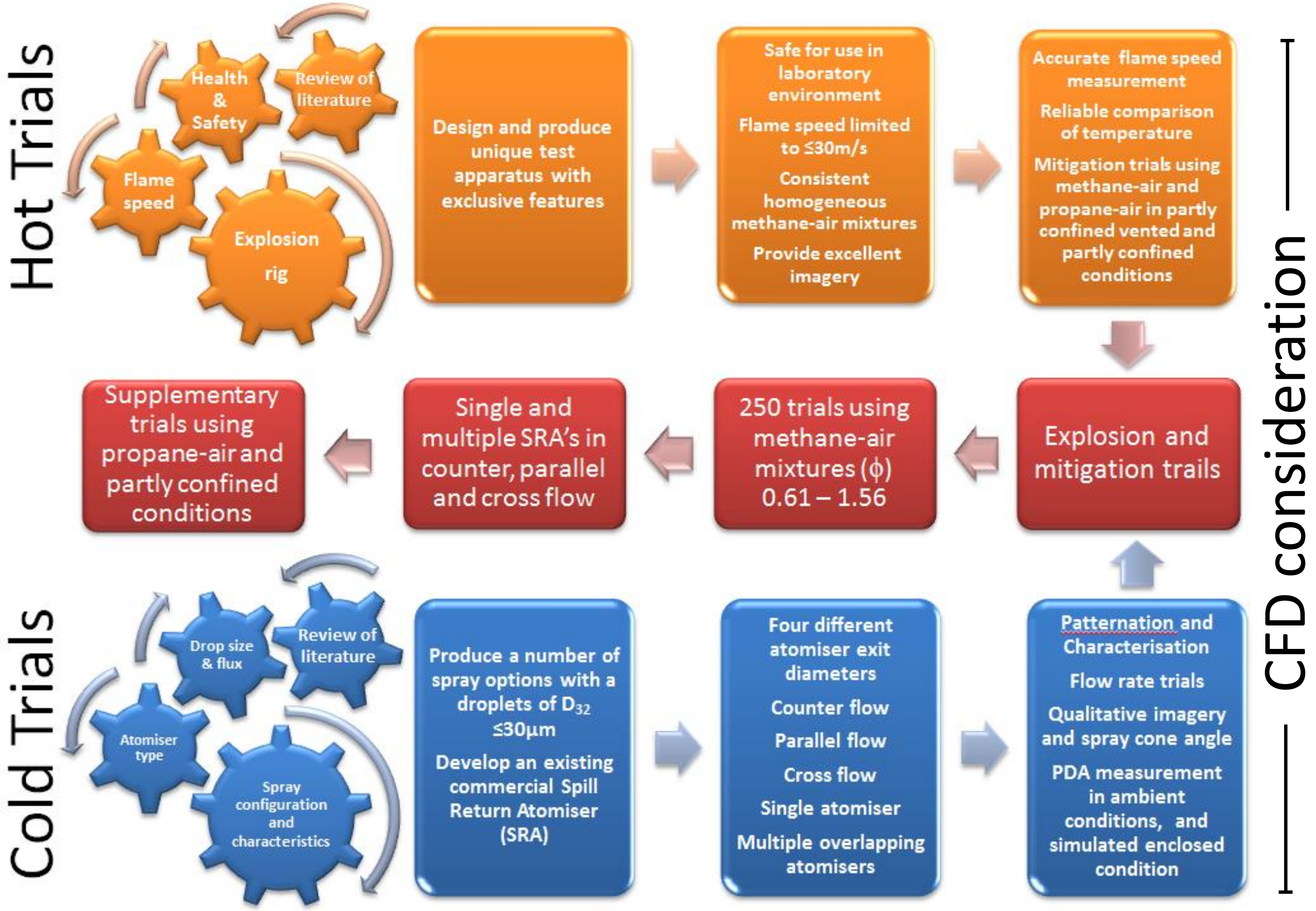

Figure 4.1 : Experimental and simulation validation stages

4.2 Apparatus, procedures and data processing : Cold trials

The following Section discusses the apparatus, design, set up and methods of data processing used during these cold trials.

4.2.1 Experimental apparatus and set up

Figure 4.2 shows the general experimental arrangement and set up that was used throughout the cold trial study. As it can be seen in Figure 4.2 water was supplied using a pump with supply pressures ranging from 5 – 15MPa. The pump apparatus was used to supply two different arrangements:

(i) A simulated Polymethyl-Methacrylate (PMMA) tube *(also see Section 4.3.2.1)*

(ii) A volumetric flow rate trials rig *(also see Section 4.2.1.3)*

The simulated PMMA tube apparatus used in the cold trials and shown here in Figure 4.2 was constructed to emulate the spray conditions within the clear section of the FPMR used for the subsequent series of hot trials.

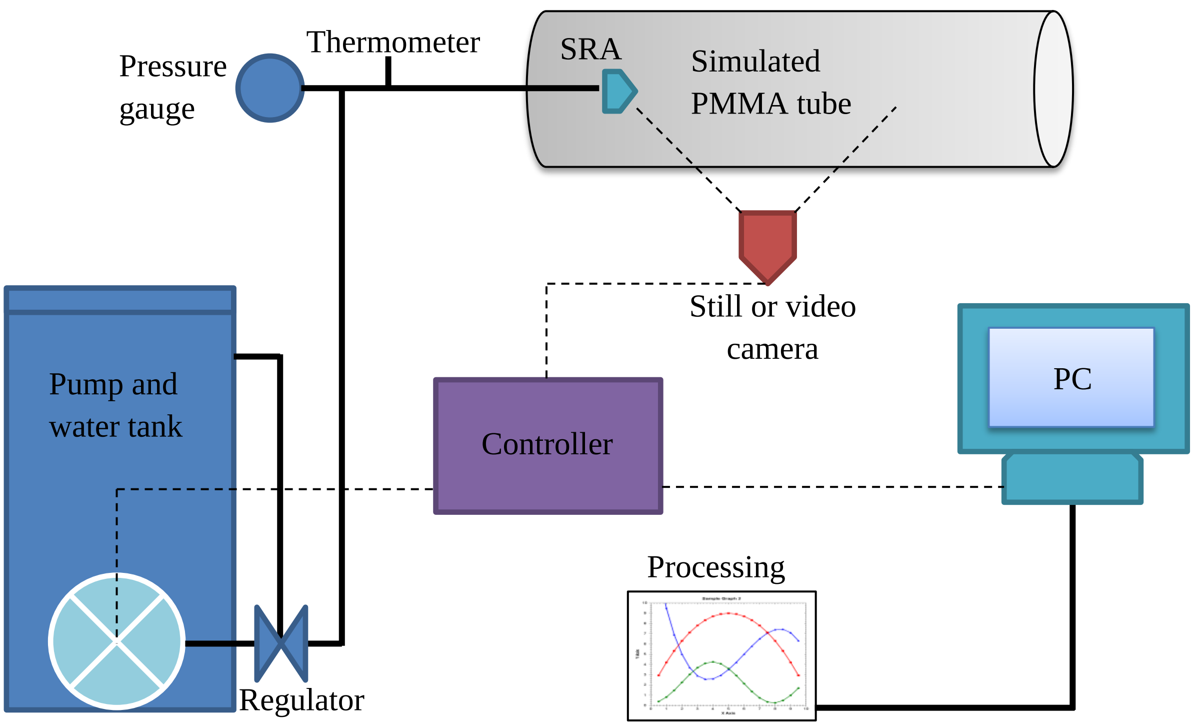

Figure 4.2 : Diagram of cold trials apparatus and set up including simulated PMMA tube

As previously mentioned, the aim of these ‘cold trials’ was to produce and characterise a novel system, proficient in the delivery of ideal spray conditions required to mitigate a slow propagating flame.

Although the SRA had been successfully developed for disinfection and decontamination activities, the existing spray characteristics were not however suitable for use in the explosion mitigation trials. The following objectives describe the challenges and advances required to progress the existing SRA technology and thus to be aligned to the present application.

i. To study the development of the existing SRA and to understand the fundamental concepts of operation.
ii. To characterise the sprays in open ambient conditions and within the simulated Polymethyl-Methacrylate (PMMA) tube (drop size, droplet velocity and mass flux) using non-intrusive laser techniques.
iii. To increase the flux density and water volume fraction, without compromising the mean droplet sizes produced by the SRA.
iv. To produce a spray envelope containing a sufficient quantity of droplets that are small enough to reach boiling point and begin to vaporise within the flame.
v. To increase droplet ‘residence time’ in the flame front, thus permitting greater heat transfer.
vi. To produce suitable quality imaging i.e. still, HD video and high speed video within the confines of the explosion and mitigation tube

Moreover, to suppress or mitigate a slow speed deflagration requires fine water sprays with drop sizes of $D_{32} \leq 30\mu m$. This innovative study is novel for two main reasons:-

i. The relatively slow speed deflagrations that will be generated in the Flame Propagation and Mitigation Rig (FPMR) will be of ≤30m/s. Whereas previous authors have used highly turbulent explosions in the order of 100m/s to in excess of 2000m/s.
ii. Such low flame speeds (≤30m/s) do not possess the inertia necessary to instigate dynamic bag type droplet break up, which was discussed in detail in Chapters 2 and 3. Therefore the droplet sizes required for this research would have to be small enough ($D_{32} \leq 30\mu m$) to extract sufficient heat from a propagating flame, during the very short droplet residence times afforded within the flame front.

In previous theoretical research, Sapko *et al* [61] suggested that droplets of 18μm will just about heat up to boiling point within the flame front of a stoichiometric methane-air mixture travelling at a flame speed of 2.3m/s. In addition Van Wingerden *et al* [65] stated that the droplets in the order of 10μm, with a concentration of 31.5% vol/vol would initiate mitigation in a methane-air mixture. This equates to a concentration by mass of 234g/m^3.

To produce very fine sprays in the order of ≤30μm a number of commercial atomisers are available, which were previously discussed exclusively in Chapter 3. In general, as discussed in earlier Chapters the SRA comprises of several engineered components as depicted in Figure 4.3, with the option to replace some of the component parts to produce a range of different spray formations and characteristics.

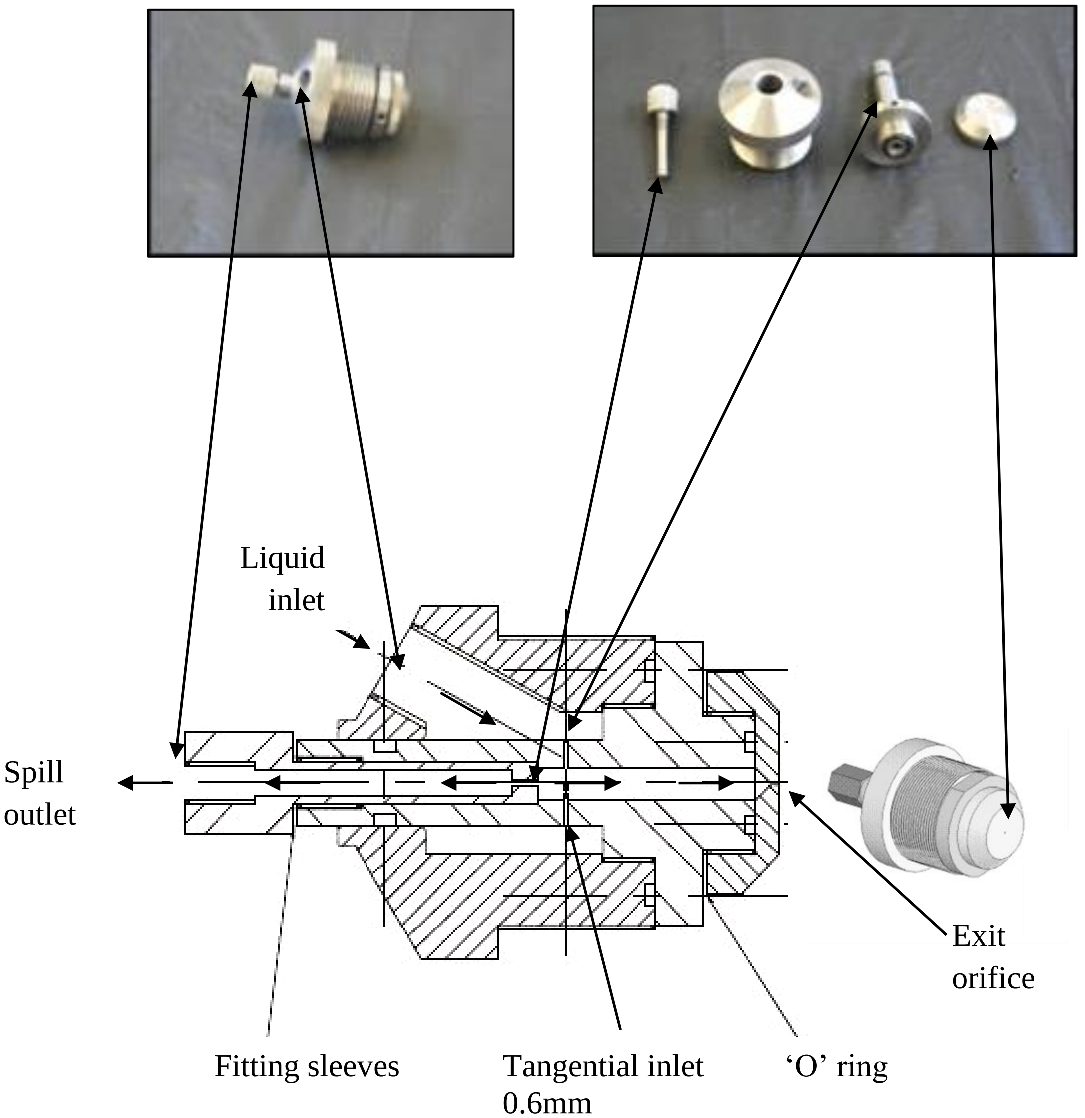

Figure 4.3 : (a) Illustration of SRA with (b) detail design [51]

The production of ultrafine droplets ($D_{32} \leq 30\mu m$) without the need for a gaseous stream, are pertinent requirements in this study as compared with two fluid and ultrasonic atomisers. The spray characteristics and results from the previous study by Nasr, G.G. *et al* [53] have been included, together with the additional characteristics from new SRA configurations from this work, for comparison and confirmation purposes in Chapter 5. In the following however, various design configurations using SRA's have been assembled which are examined conceptually and verified via the cold trials prior to the hot trials.

4.2.1.1 Evaluation of water supply, storage and pumping systems

To carry out the cold and hot trials, an effective and reliable water storage and pumping system was required.

The performance criteria set for the storage and pumping system was:-

i. Output pressure : to supply a range of 5 – 15 MPa (50 – 150bar)
ii. Output flow rate : to supply single and multiple SRA's
iii. Suitable for hot and cold water
iv. Reliability and consistency of pressure/flow and good turn down ratio
v. Water storage capacity
vi. Time taken to achieve desired pressure from start up
vii. Contamination of water during 'down time'
viii. Maintenance requirements
ix. Compatibility with control rig control system
x. Ease of installation and connection

Two existing and one new custom built pump and water storage systems were evaluated against the set criteria using the experimental set up previously shown in Figure 4.2, to assess their performance and suitability for this current study.

The three systems evaluated were:-

(i) Decontamination and disinfection pump and water storage system (used in previous study [51]
(ii) Pneumatic pump and water storage system (supplied by HSS [51])
(iii) Custom built pump and water storage system (designed for this present study)

(i) Decontamination and disinfection pump and water storage system

The apparatus shown in Figure 4.4 was originally constructed and used by Stewart, J. [51] using a Spill Return Atomiser (SRA).

The equipment comprised of a SRA attached to an aluminium pole, which in turn is fixed to a portable trolley. On the trolley is mounted a 10 litre tank acting as a reservoir for the liquid and a Feiya BJZ100 pressure washer pump was used to provide the liquid at high pressure 9 – 12MPa to the atomiser.

A pressure gauge and distribution block were included and a high pressure hose to deliver the liquid from the pump to the atomiser. There was also a spill return pipe that returns the liquid to the tank via the swirl chamber. The SRA is mounted on an adjustable bracket attached to the pole to allow for height and angle alterations.

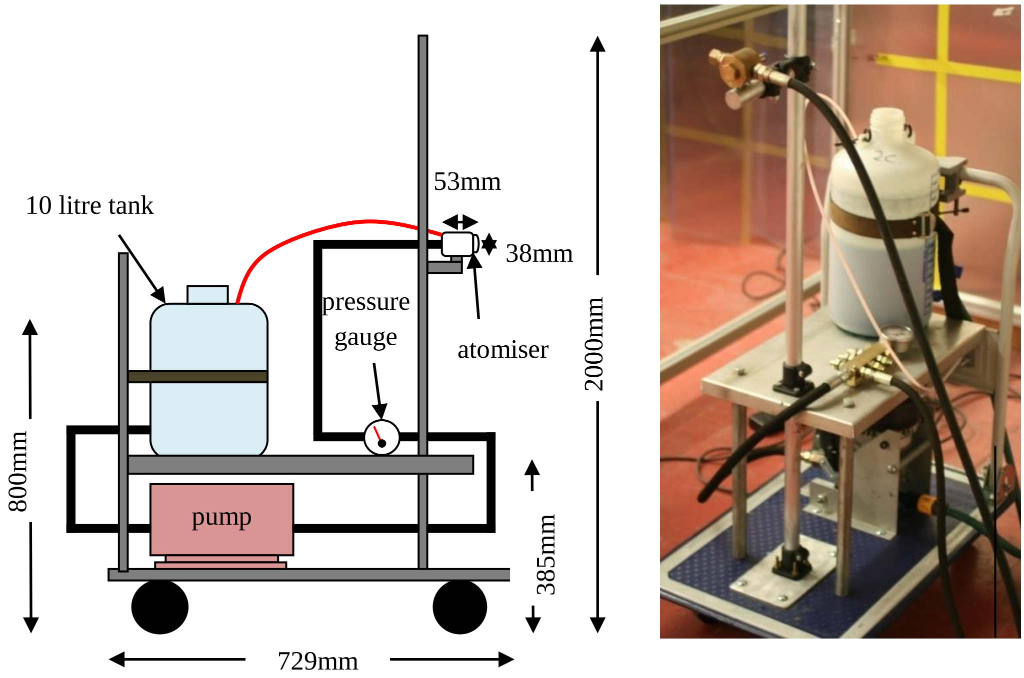

Figure 4.4 : Pump and water storage rig [51]

The pump apparatus was adapted and connected to the ‘cold trials’ test rig. A number of evaluation tests were carried out, whereby the evaluation outputs are presented in Table 4.1.

Evaluation test criteria	Evaluation test output
Output pressure – to supply a range of 5 – 15 MPa (50 – 150bar)	9 – 12MPa (90 – 120bar)
Output flow rate – to supply single and multiple atomisers	3 L/min @ 12MPa (120bar)
Good turn down ratio	Limited turn down controllability
Reliability and consistency of pressure/flow throughout range	Reliable throughout the range of 9 – 12MPa (90 – 120bar)
Water storage capacity	10 litres
Time taken to achieve desired pressure from start up	≤ 2 seconds
Contamination of water during 'down time'	Standing water became contaminated after 7 day 'down time' period. Contaminant particles large enough to block SRA outlet orifice
Maintenance requirements	Lubrication oil periodically and full high pressure flush before every new day of testing

Table 4.1 : Evaluation tests and output : Decontamination and disinfection pump and water storage rig

Following the evaluation of the output data summarised in Table 4.1 above, the decontamination and disinfection pump and water storage system failed to meet all of the performance criteria and was therefore not selected for further use in these trials. The main reasons were:-

i. Although the flow rate was suitable for some individual SRA's, it was insufficient for multiple SRA's.
ii. The output pressure was insufficient for individual and multiple SRA's.
iii. The water storage tank was limited to a 10 litre capacity, which was not convenient for the current study.
iv. Water left 'standing' in the equipment became contaminated after a short period, which caused unacceptable blockages in the SRA orifices.
v. The flow adjustment regulator was also limited and did not produce reliable flow rates at reduced pressures.

(ii) Pneumatic pump and water storage system

The air driven or pneumatic pump (supplied by HSS [51]) shown in Figure 4.5 was relatively quiet in operation and when used to deliver pressurised water to the SRA system should eliminate the build-up of metallic fragments and heat during operation. The reasons for this are:-

i. As the pump is powered by compressed air and not an electric motor, there will be no heat build-up in the liquid
ii. The Hughes positive power air pump makes minimal noise during operation (≤34.2dB)
iii. The stainless steel pump and components will stop any build-up of metallic fragments within the system.

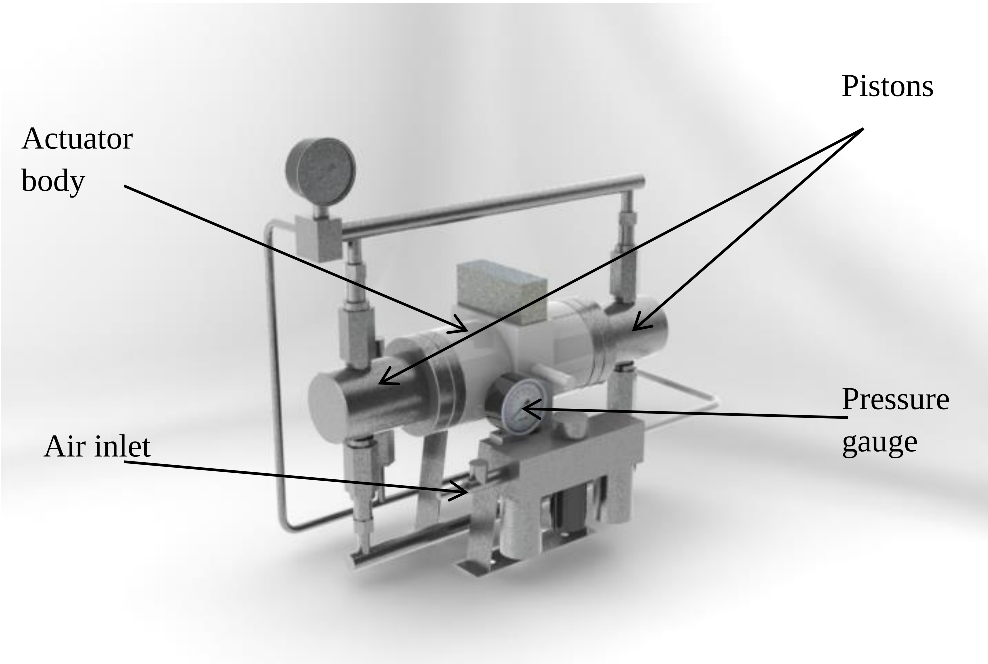

Figure 4.5 : HSS pneumatic pump [51]

The pump apparatus was adapted and connected to the ‘cold trials’ test rig. The evaluation tests and outputs are shown in Table 4.2.

Evaluation test criteria	**Evaluation test output**
Output pressure – to supply a range of 5 – 15 MPa (50 – 150bar)	4 – 9MPa (40 – 90bar) using standard air compressor with 0.8MPa(8 bar) air pressure
Output flow rate – to supply single and multiple atomisers	0.5 L/min @ 9MPa (90bar)
Good turn down ratio	Limited turn down controllability
Reliability and consistency of pressure/flow throughout range	Reliable throughout the range of 9 – 12MPa (90 – 120bar)
Water storage capacity	10 litres
Time taken to achieve desired pressure from start up	≤ 5 seconds
Contamination of water during ‘down time’	Standing water was uncontaminated after 7 day ‘down time’ period
Maintenance requirements	Lubrication oil periodically

Table 4.2 : Evaluation tests and output : HSS pneumatic pump

Further to the evaluation of the output data shown in Table 4.2 above, the HSS pneumatic pump and water storage system failed to meet all of the performance criteria and was also not selected for further use in these trials. The main reasons were:-

i. The flow rate was only suitable for the low flow rate individual SRA and was insufficient for other high flow rate single SRA’s and all multiple SRA’s.
ii. The output pressure was insufficient for individual and multiple SRA’s.
iii. The water storage tank was limited to a 10 litre capacity, which was not convenient for the current study.
iv. The flow adjustment regulator was also limited and did not produce reliable flow rates at reduced pressures.
v. The pump could not operate using compressed air from a standard compressor. A dedicated high pressure compressed air cylinder was required to operate the pump, which would have also needed a high pressure solenoid valve for integration with the FPMR control system.

(iii) Custom built pump and water storage system

From the evaluation of the commercial pumps and water storage systems described above, and other available systems, it became evident that there was no commercial package available to fully meet all of the design criteria for the present study. Therefore, individual components were sourced and a pump and storage system was assembled and tested, as detailed in Figure 4.6.

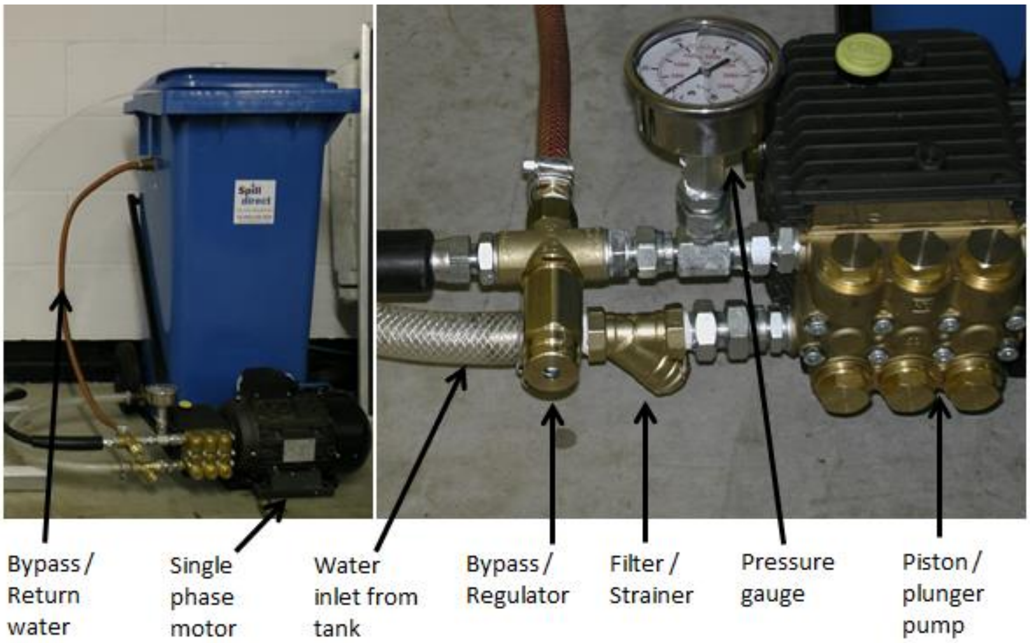

Figure 4.6 : Custom built pump and water storage apparatus

Table 4.3 also shows a tabulated format of evaluation test criteria with corresponding test output which fully meets the required performance criteria for the present investigations.

Evaluation test criteria	Evaluation test output
Output pressure – to supply a range of 50 – 140 bar (5 – 14 MPa)	5 – 17MPa (50 – 170 bar) via single phase electric driven piston pump
Output flow rate – to supply single and multiple atomisers	9 L/min @ 17MPa (170 bar)
Good turn down ratio	Suitable turn down controllability
Reliability and consistency of pressure/flow throughout range	Reliable throughout the range of 5 – 17MPa (50 – 170 bar)
Water storage capacity	120 litres
Time taken to achieve desired pressure from start up	≤ 2 seconds
Contamination of water during ‘down time’	Standing water was uncontaminated after 7 day ‘down time’ period
Maintenance requirements	Lubrication oil periodically

Table 4.3 : Evaluation tests and output : customer built pump

4.2.1.2 SRA configurations

As discussed the purpose of these cold trials was to assist with the selection process relating to this study, since the parametric effect of spray properties, with regards to drop size, droplet velocity, flow rate and penetration are directly related to the suppression and mitigation of gas and vapour cloud explosions. The Spill Return Atomiser (SRA) was developed further in these 'cold trials' to produce higher liquid flow rates, drop velocities and liquid volume flux and wider spray cone angles, while maintaining the drop size as low as possible ($D_{32} \leq 30\mu m$).

Furthermore, there was a need to assess and characterise the selected sprays within the confinement of the enclosed PMMA tube section of the flame propagation and mitigation rig. PMMA is similar in appearance to Polycarbonate and will be discussed in detail in Section 4.4.1. For convenience short sections of PMMA tube were used to simulate conditions expected within the flame propagation and mitigation tube. Various rigs and apparatus produced for the 'cold trials' are discussed in the following Sections.

Four SRA configurations were developed by replacing or modifying the exit orifice diameters. For clarity and ease of further reference, the atomiser arrangements were given the designated terms of Type A, B, C and D for identification throughout this study and are shown in Table 4.4 below with corresponding colour coded index.

SRA designation	Exit orifice diameter (mm)	Spill orifice diameter (mm)	Tangential inlet orifice diameter (mm)
Type A	0.3	0.5	0.6 x 2
Type B	0.5	0.5	0.6 x 2
Type C	0.8	0.5	0.6 x 2
Type D	1.0	0.5	0.6 x 2

Table 4.4 : Summary of orifice dimensions for SRA configuration types A, B, C and D

The four SRA configurations (Type A, B, C and D) were initially chosen to be assessed with respect to their suitability for selection and further use in the 'hot trials' part of this study.

For convenience, Table 4.5 lists the spray evaluation trials conducted in the following Sections, with references to their location in this Chapter and the corresponding 'Results and Discussions' Chapter 5.

Atomiser type	Apparatus set up	Atomiser configuration	Chapter 4 Section Reference	Results Chapter 5 Reference
Spill return atomiser (SRA)	Volumetric flow rate (L/min)	SRA Type A	4.2.1.3	5.2.2
		SRA Type B	4.2.1.3	5.2.2
		SRA Type C	4.2.1.3	5.2.2
		SRA Type D	4.2.1.3	5.2.2
	Cone angle (degree)	SRA Type A	4.2.1.4	5.2.3
		SRA Type B	4.2.1.4	5.2.3
		SRA Type C	4.2.1.4	5.2.3
		SRA Type D	4.2.1.4	5.2.3
	Droplet diameter D_{32} (µm), velocity of droplets (m/s) and liquid volume flux ($cm^3/s/cm^2$) in **ambient conditions**	SRA Type A	4.3.1	5.3.1.1
		SRA Type B	4.3.1	5.3.1.2
		SRA Type C	4.3.1	5.3.1.3
		Multiple overlap SRA Type B	4.3.1	5.3.1.4
	Droplet diameter D_{32} (µm), velocity of droplets (m/s) and liquid volume flux ($cm^3/s/cm^2$) in **enclosed conditions**	SRA Type B	4.3.2	5.3.2.1
		SRA Type C	4.3.2	5.3.2.2

Table 4.5 : Summary and reference for spray characterisation ‘cold trials’

4.2.1.3 Volumetric flow rate

A series of volumetric flow rate trials were conducted to provide systematic flow rate data for the four single atomiser configurations, Type A, B, C and D, as well as comparing related previous data with present atomiser configurations.

Each of the atomisers were evaluated by subjecting them to a range of pressures from 5MPa – 14MPa (50bar – 140bar). A test rig was designed and constructed to carry out the flow rate trials. The apparatus shown in Figure 4.7 consisted of a mounting frame, calibrated pressure gauge, atomiser mounting connections and spray convergence passage.

Due to the fine droplets and aerosols corresponding to the SRA spray, the SRA was connected to a convoluted conical tube, referred to here as the 'spray convergence passage'. This device conveniently allowed the droplets and mist to coalesce, thus producing a reliable flow of water from its exit.

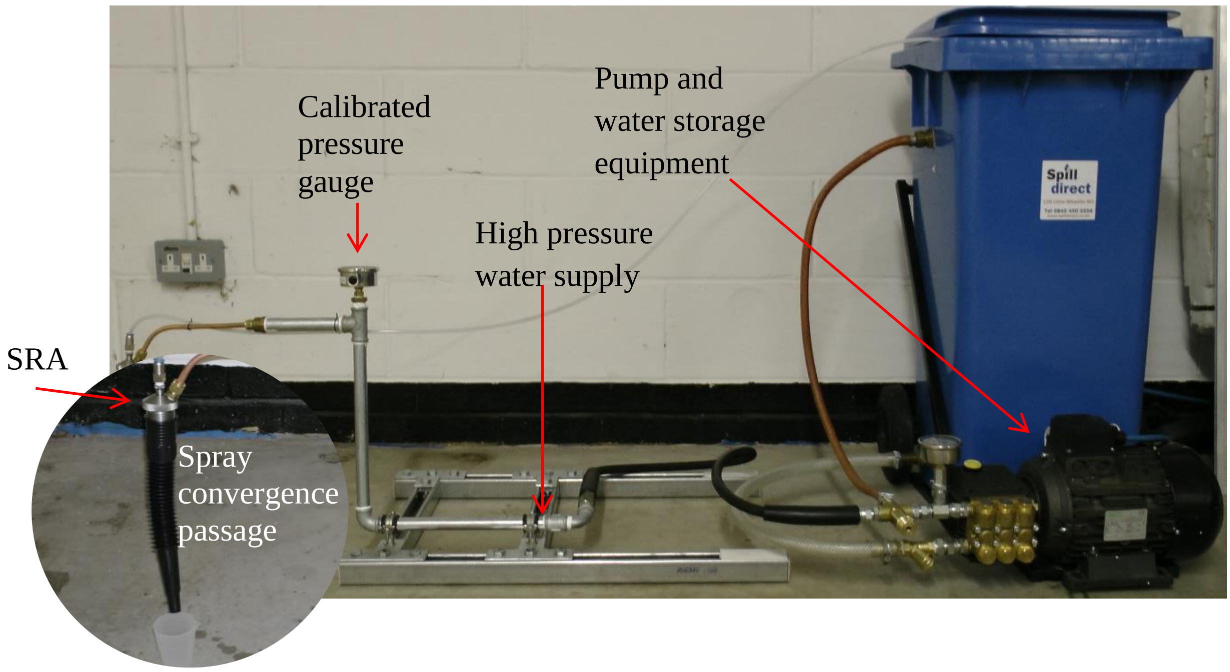

Figure 4.7 : Volumetric flow rate test rig

To ensure validity, reliability and consistency of results all of the tests were carried out on the same day and under the same conditions. In all tests the water pump was permitted time to reach optimum output pressure and for the feed pipework to be purged of air. Additionally an allowance was made to guarantee a uniform flow from the spray convergence passage.

Since the spray convergence passage was convoluted, the water was allowed to run freely from its outlet for about 20 seconds prior to collecting and timing the measurement volume.

Following this 20 second stabilisation period, a water volume was collected and timed using a stopwatch. Two methods of water measurement were considered. Initially the digital scales, accurate to ± 0.1g were set to zero and a dry measuring beaker was placed centrally on the scales. Using the 'tare' function as shown in Figure 4.8, the scales were then zeroed. The water could then be collected and its net weight recorded.

Figure 4.8 : Typical digital scales used for weighing water collections

In a second method which was subsequently adopted, a spread sheet was used to subtract the weight of the beaker prior to converting the volume into litres. This procedure was repeated with water pressures between 5MPa – 14MPa (50bar – 140bar) in 1MPa (10bar) increments. On completion of the exit orifice measurements, a similar process was repeated to collect and measure water volumes from the spill orifice.

The results were processed using Microsoft Excel and corresponding graphical representations were produced for comment and discussion. The results of these flow rate trials are discussed in Chapter 5. Accuracy and potential sources of error resulting from this trial are presented in Section 4.4.

4.2.1.4 SRA spray cone angle measurement : configuration Type A, B, C, D

In this series of trials individual atomiser configurations were installed in the test rig shown in Figure 4.9 and were supplied with deionised water at a pressure of 13MPa. The spray images were captured using a high resolution Canon EOS digital SLR camera. An 18-55mm 1:3.5-5.6 IS zoom lens was used to take close-up images with a resolution of 3456 x 2304. Images taken during the cold and hot trials were all recorded from consistent distances to ensure reliability.

Figure 4.9 : Canon EOS digital SLR camera [76]

Although several acceptable methods of spray cone angle measurement practiced, the method chosen for this current study was used recently in work published by Nourian, A [85] to measure the spray cone angles produced by household aerosol cans. Images were processed using Adobe Photoshop, whereby the cone angles were measured using the Adobe 'angle finder tool' shown in Figure 4.10. (see also Section 4.2.4.2 for data processing).

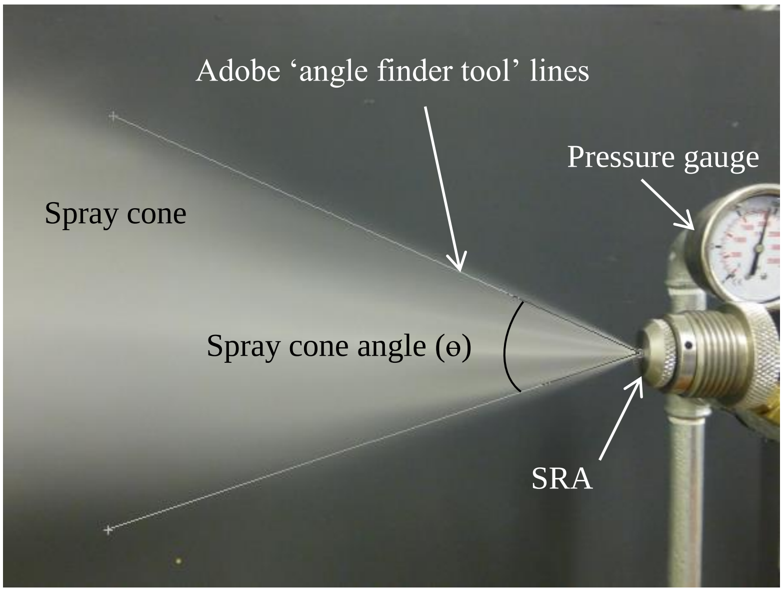

Figure 4.10 : Typical spray cone angle measurement

4.2.1.5 Imaging and photography techniques

Although some previous data and photography existed for the SRA sprays used in the previous study [51], new characteristics such as mean droplet size, velocity and liquid volume flux were required to assess the behaviour of the spray within the confines of the FPMR. Other features of the spray likely to differ within a tube, such as cone angle and penetration were also considered.

To establish the spray characteristics of the single atomisers chosen for this research within the confines of an explosion and mitigation tube environment, a cold trials test rig previously revealed in Figure 4.1 was assembled in a separate part of the laboratory. The cold trials test rig comprised of:-

i. 1m sections of 190mm (I.D.) PMMA
ii. A mounting frame for the 200mm (O/D) PMMA
iii. A water induction / atomiser mounting pipe
iv. Waste water collection and quantifying containers
v. Scales (accurate to 0.1g) for flow rate measurement calculation
vi. High pressure water pump and delivery system (9 L/min @ 170bar max)
vii. Digital thermometer
viii. Digital still camera

As the sprays used in this research were operating inside a 190mm internal diameter clear PMMA tube, several challenges were encountered when trying to obtain good quality photography and video images. The challenges were:-

i. Light reflection from the outside of the PMMA tube
ii. Misting of the inside of the PMMA tube
iii. Illuminating of the sprays within the PMMA tube

i) Light reflection from the outside of the PMMA tube

The laboratory had various light sources, both natural and artificial such as natural daylight, fluorescent lighting and spot lighting. All of the light sources were found to be challenging with respect to the polished surfaces (external and internal) of the PMMA tube.

One method of overcoming the interference from the various lighting inputs, was to isolate the PMMA tube from all laboratory lighting by means of a 'black-out' cone. Figure 4.11 shows the original design concept and Figure 4.12 displays the actual set up used in this work.

The black-out cone was made from 270gms A1 black sheets, covering the whole length of the 1m PMMA tube, before reducing to a 50mm diameter entry hole for the camera optics.

The black-out cone was very successful and could easily be applied to these cold trials, comprising of a short 1m length of PMMA tube. However, this method could not be utilised for the hot trials research as the whole tube needed to be observed during explosion and mitigation test runs.

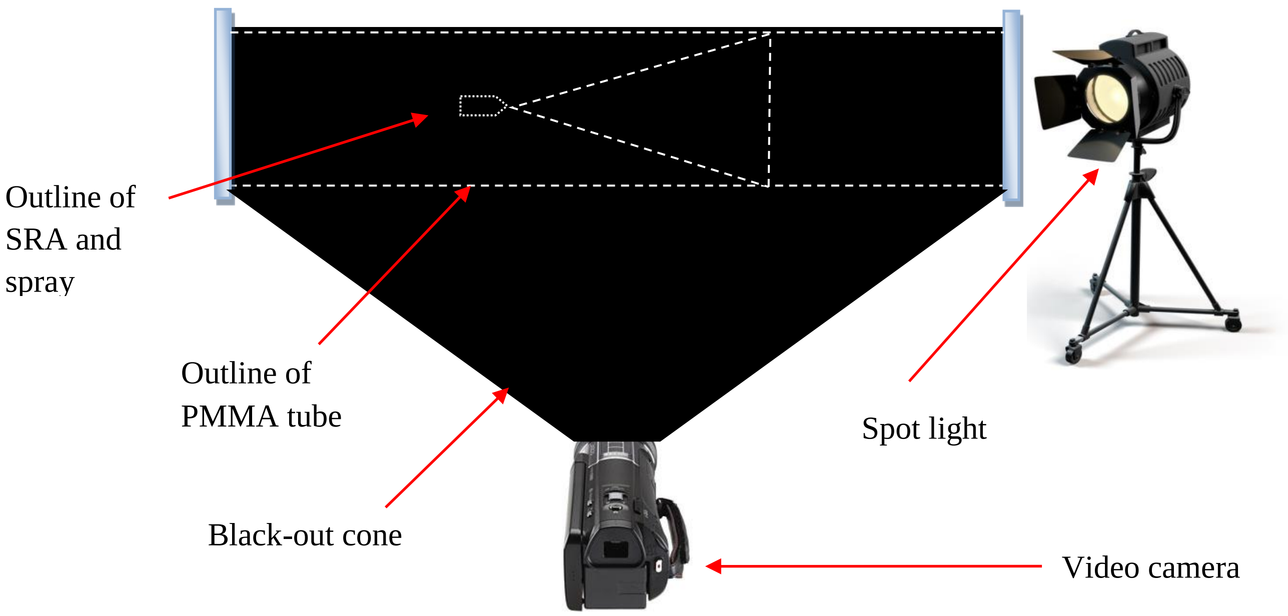

Figure 4.11 : Black-out cone (concept)

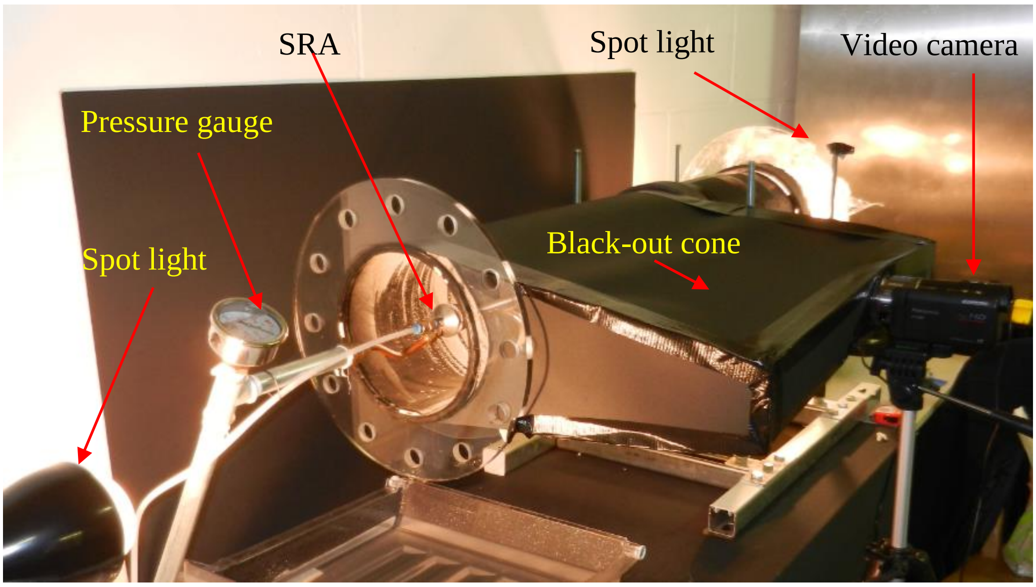

Figure 4.12 : Black-out cone (assembled)

An alternative approach to reduce the glare of lighting, but permit full view of the PMMA tube had to be considered for the hot trials imagery. Following a search and consultation with a number of professional photographers, the outer surface of the tube was coated with an anti-reflection matt spray.

Following several trials with various manufacturers' products, Kenro Kenair KENR07 anti-reflection matt spray, as presented in Figure 4.13 was preferred. This product is used by photographers on shiny surfaces such as glass, plastic and silver, to enhance image quality.

Figure 4.13 : Kenro Kenair KENR07 is an anti-reflection matt spray [77]

ii) Misting of the inside of the PMMA tube

The sprays produced by the four variations in SRA configuration all resulted in water droplets of $D_{32} \leq 30\mu m$. Additionally, within all of the sprays there was also a percentage of ultra-fine aerosol sized droplets. Although these were ideal theoretical droplet sizes for explosion mitigation, the resulting mist very quickly coalesced on the inner wall of the tube, thus obscuring the view for photography.

Three methods were tested to reduce this problem:-

i. Coating the inner surface of the tube with a fine layer of bees wax furniture polish
ii. Coating the inners surface of the tube with a surfactant
iii. Coating the inside of the tube with hydrophobic spray ('CarPro Reload Professional')

All three methods produced some degree of success. However, the water repelling hydrophobic spray, gave the best overall results. Figures 4.14(i) and (ii) demonstrate the highly successful effectiveness of the hydrophobic spray, whereby the spray is seen to coalesce and form an obscure coating on the inner surface of the PMMA tube in Figure 4.14(i), whereas Figure 4.14(ii) shows the resulting substantial improvement in image quality.

Each single coating permitted approximately 10 trials, after which the inner surface of the tube was fully cleaned and dried prior to the re-application of the water repelling spray.

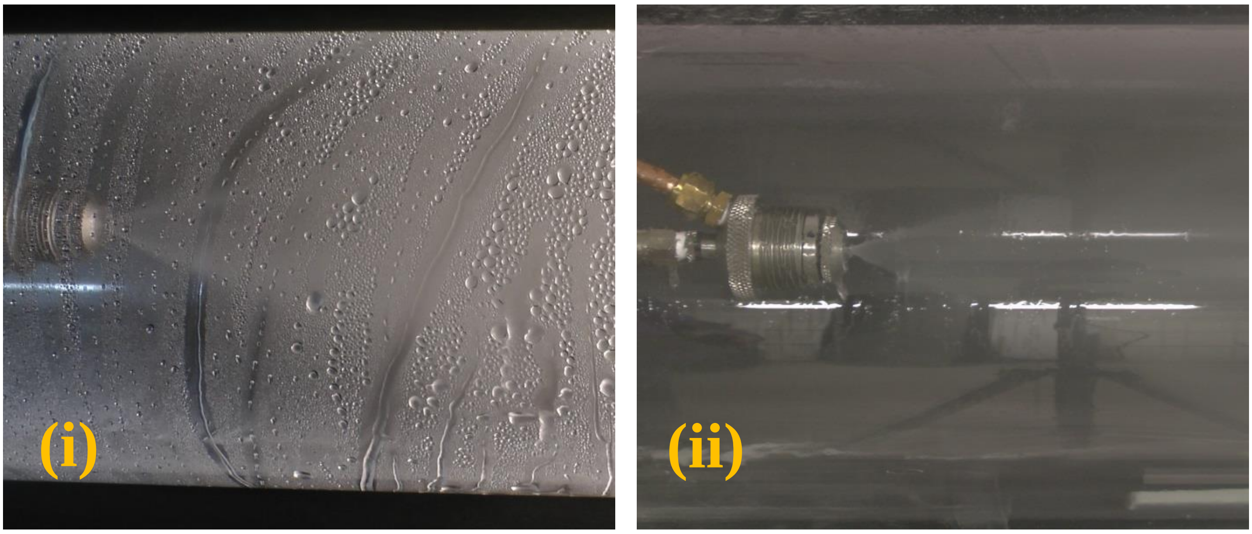

Figure 4.14 : Typical effectiveness (i) without hydrophobic spray (ii) with hydrophobic spray

iii) Illuminating the spray within the PMMA tube

With all of the natural and artificial light being omitted from the tube perimeter and length by the black-out cone, light could only enter the tube from one, or both of the open ends.

Three methods were attempted to establish the optimum lighting of the spray, thus to enable the best quality of imaging:-

i. Lighting from the left hand side (upstream of the spray)
ii. Lighting from the right hand side (downstream of the spray)
iii. Lighting from the left and right hand sides (upstream & downstream of the spray)

When using the blackout cone, lighting method (iii) produced the best imagery, for both still and video photography.

After completing the above comprehensive testing, the following configuration was adopted for all of the cold trial experiments.

i. Outer tube surface coated with anti-reflection matt spray
ii. Inner tube surface coated with water repelling hydrophobic spray
iii. Lighting from the left and right hand sides (upstream & downstream of the spray)

It was also found that if the tube was heated with warm air from a fan heater for approximately one minute between tests, better images were obtained as the ultrafine water droplets were less inclined to coalesce on the inner surface of the PMMA tube.

4.2.2 Experimental procedures and data processing : Cold trials

Using the experimental set up illustrated previously in Figure 4.2 and shown here in Figure 4.15 the cold trials were conducted according to the following procedures.

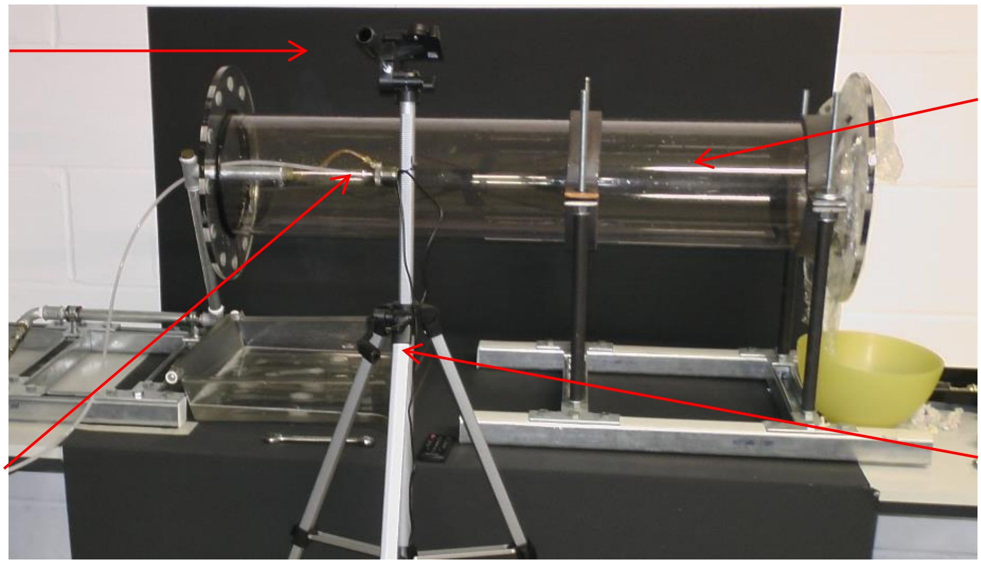

Figure 4.15 : Cold trials apparatus and set up including simulated PMMA tube

4.2.3 Volume flow rate

4.2.3.1 Experimental procedure

i. The equipment previously shown in Figure 4.1 was connected and commissioned using approximately 5 litres of water, whilst also checking for water leakage.

ii. The water tank was then filled with deionised water at room temperature (approximately 20˚C).

iii. The water pump regulator was tested for adjustment operation and corresponding values were observed on the calibrated pressure gauge.

iv. The digital scales were placed on a level surface and checked for accuracy using a 250g slug weight.

v. The SRA configuration was placed in the apparatus with the spray convergence passage connected to gather the exiting spray.

vi. The pump was activated and the pressure was set to the desired value, which was subsequently recorded on the trial record template, shown in Table 4.6. The flow was then allowed to stabilise. A measuring beaker was then placed beneath the flow whilst simultaneously commencing the timing of the event using a stop watch.

vii. The beaker was allowed to fill to approximately 75% of its capacity then removed from the flow, where the stop watch was immediately stopped. The time was then recorded on the trial record template shown in Table 4.6.

viii. The collected water and container were weighed and their combined weight recorded on the trial record template shown in Table 4.6.

ix. The process was repeated for all four SRA configurations.

Water pressure *P* (MPa)	**Water collection time from exit orifice** ***t*** **(s)**	**Water collected from exit + container** ***W*** **(g)**	**Exit orifice volume flow rate** ***Q*** (L/min)	**Water collection time from spill orifice** ***t*** **(s)**	**Water collected from spill + container** ***W*** **(g)**	**Spill orifice volume flow rate** ***Q*** (L/min)
5						
6						
7						
8						
9						
10						
11						
12						
13	13.37	499.00	*Excel calculation*	17.09	138.40	*Excel calculation*
14						

Table 4.6 : Typical trial record template for volume flow rate

4.2.3.2 Data processing

The data from the trial record template was transferred to an Excel spread sheet, which was used to calculate the volume flow rate by comparing the sample collection time with the weight of the water (minus the weight of the container). The density of water used for the calculation was $1g/cm^3$. Graphical illustrations were also plotted using Excel, which are presented and discussed in Chapter 5.

Accuracy and potential sources of error resulting from this trial are presented in Section 4.4.

4.2.4 Spray cone angle measurement

4.2.4.1 Experimental procedure

i. The equipment previously shown in Figure 4.10 was connected, then commissioned using approximately 5 litres of water and checked for signs of water leakage.
ii. The water tank was then filled with deionised water at room temperature (approximately 20˚C).
iii. The water pump regulator was tested for adjustment operation and corresponding values were observed on the calibrated pressure gauge.
iv. The SRA configuration was placed in the apparatus and the camera was switched on.
v. Photographic ‘test shots’ were taken to ensure that light conditions and image quality were satisfactory.
vi. The pump was activated and the pressure was set to the desired value (13MPa). The flow was then allowed to stabilise.
vii. Several still images were taken of the resulting spray against the matt black background. Image file names were immediately changed to represent the spray configuration i.e. ‘TypeB.001’ and recorded on the cone angle trials template shown in Table 4.7.
viii. This process was repeated for all four SRA configurations.

Atomiser configuration type (SRA)	**Image file name *n* (name)**	**Cone angle θ (degree)**	**Cone radius C_r (mm)**	**Cone diameter C_d (mm)**	**Penetration d_p (mm)**
A					
B	TypeB.001	42.7	*Excel calculation*	*Excel calculation*	*Excel calculation*
C					
D					

Table 4.7 : Typical template for cone angle and estimated penetration within PMMA tube

4.2.4.2 Data processing

The images for each of the spray configurations were assessed qualitatively, whereby one suitable image for each SRA type was selected. The selected images were 'opened' using Adobe Photoshop where the 'angle finder tool' was selected. Using the angle finder process, the spray cone angles were determined and subsequently recorded on the cone angle trials template shown above in Table 4.7.

The spray cone angles were then entered on a spread sheet, in which spray penetration was determined using basic trigonometry. The results of the spray cone angle and penetrations distances are provided and discussed in Chapter 5. (See also Section 4.4 sources of error)

4.3 Phase Doppler Anemometry (PDA)

There are numerous invasive and non-invasive methods for measuring the fundamental characteristics of sprays such as diameter, D_{32} (µm), droplet velocity, D_v (m/s) and liquid volume flux, Q_f ($cm^3/s/cm^2$). These methods include:-

i. Mechanical methods – where the droplets are collected in a frozen state and analysed
ii. Electronic methods – where an electronic pulse that is created by the droplets in a specific measurement volume is detected
iii. Acoustical methods – this is where the acoustic signature produced by the droplets is measured and the measurement determined.
iv. Optical methods – by passing a light beam through the spray the deflections of light can be measured and therefore the droplet size determined by the refraction index produced by the incidence of the light beam on the droplets.
v. Laser methods – this is where a laser is passed through the spray and the variations in the beam as it is penetrated is measured by a high speed processor which can then determine the droplet sizes and velocities.

To evaluate the characteristics and to consider the explosion mitigation attributes of the new and existing SRA atomiser arrangements, non-invasive dynamic particle analysis was carried out using Phase Doppler Anemometry (PDA) throughout this work. The next Section will provide the set up arrangement, procedures and method of data processing using PDA for:-

(i) PDA : Ambient conditions (4.3.1)
(ii) PDA : Simulated PMMA tube (4.3.2)

4.3.1 PDA : Ambient conditions

4.3.1.1 Experimental apparatus and set up

The basic operating principles of PDA were previously discussed in Chapter 3. The PDA apparatus used in this work was a Dantec Particle Analyser, which consisted of the following:-

i. Laser (Argon ion (Ar ++) laser (100mW). This produces a green beam of coherent light (514.5μm)
ii. Transmitting Optics
iii. Receiving Optics or photo-detectors
iv. Signal Processor
v. Software package

Since the transmitting and receiving optics are in fixed and calibrated positions, to obtain the spray characteristics at various radial and downstream positions the atomiser was mounted in a traversing frame system, as shown in Figure 4.16.

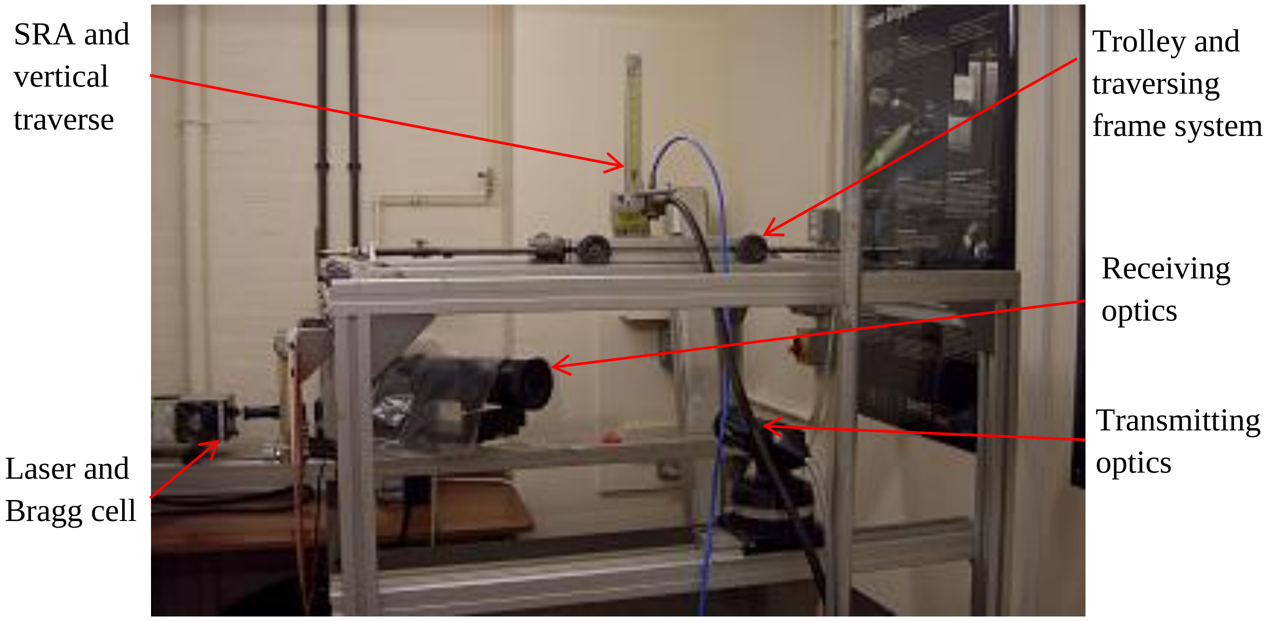

Figure 4.16 : Atomiser mounting and traversing frame system

During the experimental set-up, both the transmitting and receiving optics were optimised for data acquisition. The only setting that can be adjusted on the transmitting optics is the power level of the laser. For the duration of all the tests carried out, the maximum power setting was used. This is known to have the effect of increasing the measuring volume.

The receiving optics were set to receive first order refraction from the particles, with the scattering angle being 72° which is the optimum forward refraction mode with reduced bias in the results due to the reflected light, thus ensuring good scattering light intensity levels (high signal to noise). In this mode the first order refraction has intensity levels twenty times greater than that due to reflected light, thus making it suitable for measuring small particles.

The focal length of the receiver was 310mm. Decreasing the focal length of the receiver increases the sensitivity of the optics allowing the receiver to measure smaller particles. However there are trade-offs with reducing the focal length such as, reducing the size of the measurement volume and reducing the maximum droplet diameter that can be measured. The set focal length of 310mm was suitable for measuring the range of particles in the experiments.

The PDA system was set up to acquire and measure between 10,000 - 20,000 samples for each radial and downstream position for all three experimental arrangements. The transmitting and receiving optics were set up in accordance with the values shown in Table 4.8.

	Description	**Symbol**	**Value**	**Units**
Transmitting optics	Laser power	P	100	mW
	Wavelength	λ	514.5	µm
	Beam Separation	df	38	mm
	Focal length	f_{tr}	400	mm
	Beam diameter	d_b	1.35	mm
	Fringe Spacing	s	5.42	µm
	Number of fringes	N_f	37	-
Receiving optics	Focal length	f_{rc}	310	mm
	Scattering Angle	θ	72	degrees
	Aperture setting	-	0.5	mm

Table 4.8 : PDA Transmitting and receiving optics set up data [51]

4.3.1.2 Experimental procedure

To obtain radial positions throughout the flow, the atomiser mounting trolley was traversed horizontally relative to the beams with the transmission optics fixed. The radial positions were situated at 5 or 10mm intervals from the centre of the atomiser orifice. A vertical traverse was constructed in order to record radial plots with each atomiser configuration at various downstream distances.

In previous studies Stewart [51] considered measurements at various axial intervals downstream (DS) of the SRA up to and including 700mm. However, for this study there was a need to capture data axially from downstream position of 95mm, as illustrated in Figure 4.17. This data point and spatial position was considered to be approximately the centre of the spray when enclosed within a 190mm PMMA tube of the FPMR.

Figure 4.17 shows schematically typical radial positions used for measuring the velocity, drop size (D_{32}) and liquid volume flux of the droplets using PDA in this present study. To ensure clarity readings taken to the left of centre were given a minus (-) prefix as shown.

Following each of the PDA data measurements, the corresponding data file was re-named to identify the SRA type, axial and radial position i.e. *File name: TypeC.95mmDS.-30mm.*

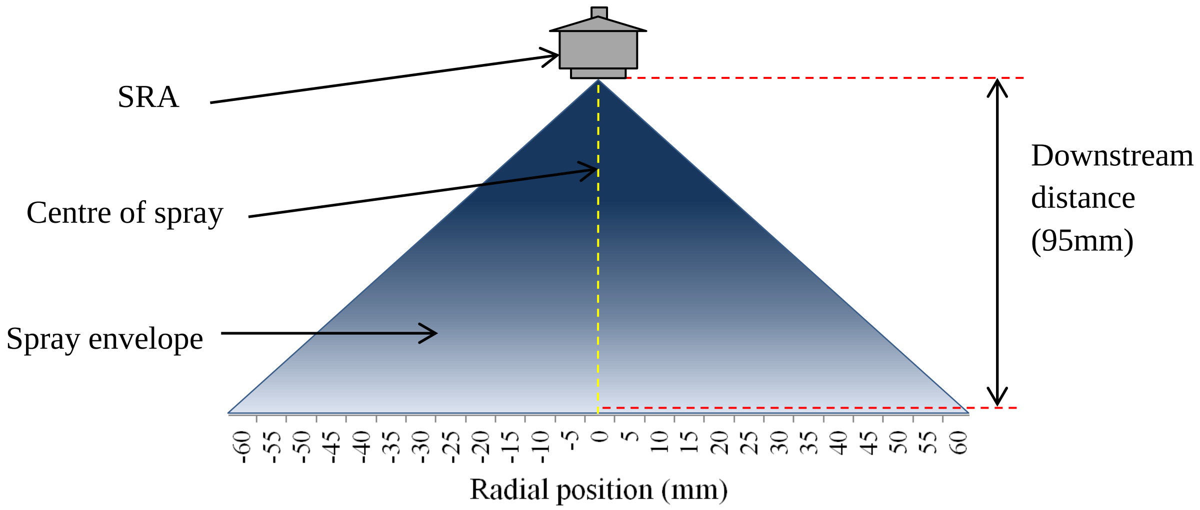

Figure 4.17 : Axial and radial sampling positions

A data sheet was used to systematically compile the PDA sample positions against the output data file as shown in Table 4.9. Each data file was checked for content i.e. 20,000 counts containing appropriate data columns, before commencing the next compilation.

Test #	Axial position (mm)	Radial position (mm)	PDA output file, given file name	Data checked
1				
2				
3	95	35	TypeC.95mmDS.35mm	Yes
4				
5				
6				

Figure 4.9 : PDA data collection and file allocation sheet

4.3.1.3 Data processing

The PDA output data file was opened and processed using MS Excel, whereby various graphical representations were formed for droplet diameter, D_{32} (µm), droplet velocity, D_v (m/s) and liquid volume flux Q_f ($cm^3/s/cm^2$), which are presented and discussed in Chapter 5.

Accuracy and potential sources of error resulting from this trial are presented in Section 4.4.

4.3.2 PDA : Simulated PMMA tube conditions

4.3.2.1 Experimental apparatus and set up

To ensure that valid and reliable conclusions could be derived from the hot trials, additional tests were carried out to characterise and assess the behaviour of the sprays within the simulated conditions of the FPMR.

A new test rig was constructed within the existing PDA and traversing system as shown in Figure 4.18, which facilitated the mounting of a short section of 190mm (I.D) PMMA tube.

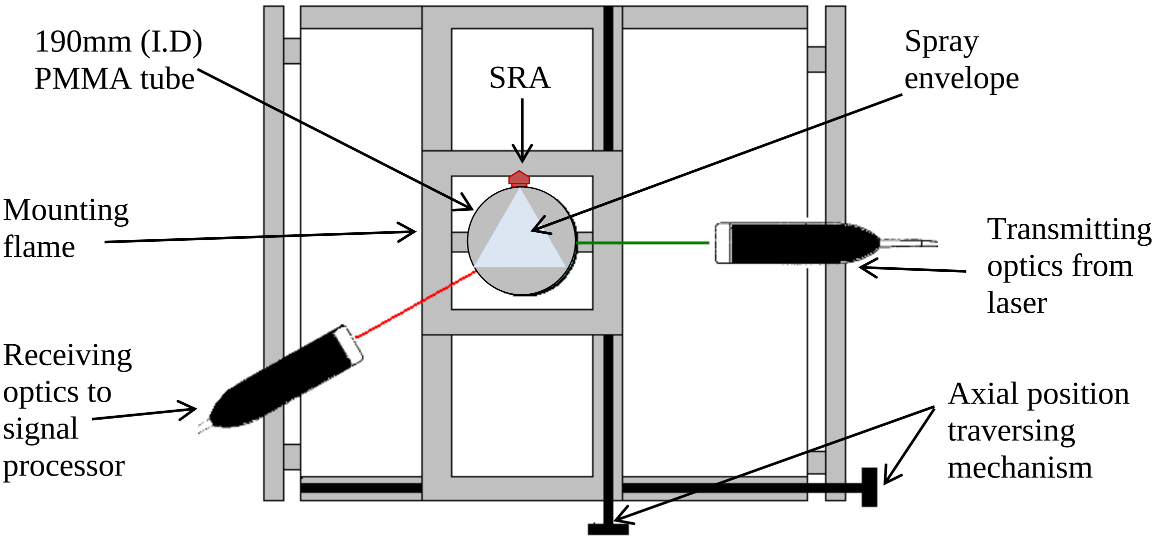

Figure 4.18 : Plan view of the mounting arrangement for the PMMA tube, SRA position (cross flow)and PDA optics

Although the PMMA tube was coated liberally with hydrophobic spray, the main challenge in obtaining data was the build-up of water droplets on the inside surface of the tube. Initial trials produced highly irregular results whereby many cases resulted in trials being aborted, due to the receiving optics not being able detect droplets in the measuring volume.

A consequence of the deposition and coalescence of water droplets on the inner surface of the PMMA tube resulted in the laser beams exiting the transmitting optics being refracted and diverted. Additionally, although the outer surface of the PMMA tube was coated with anti-reflective matt spray, the shiny surface was also detrimental to data acquisition.

Figure 4.19 illustrates the problem showing the laser light ‘bending’ around the circumference of the PMMA tube. An alternative method was required to capture the droplets within the tube, which would provide clear 'line of sight' for the lasers and the transmitting and receiving optics.

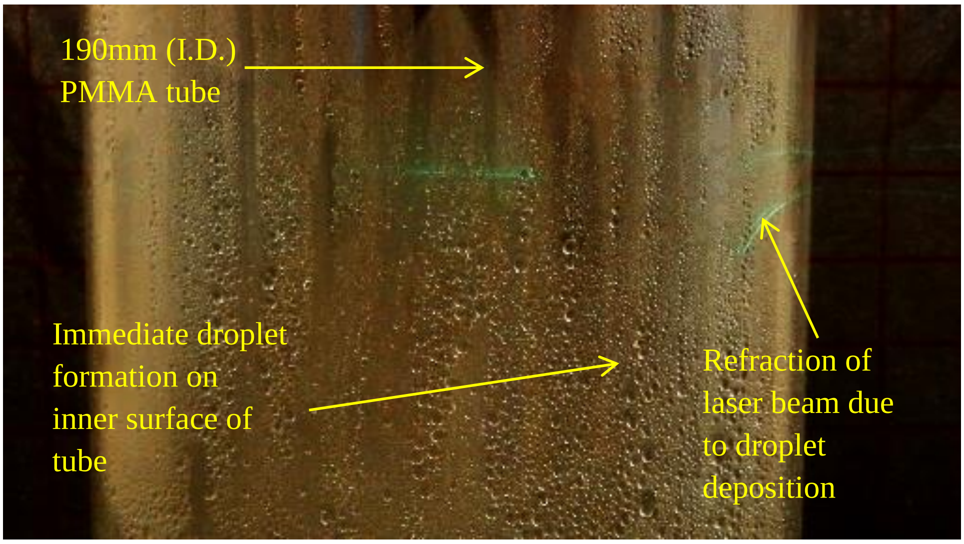

Figure 4.19 : Droplet deposition and refraction of laser beams in simulated PMMA tube

The equipment shown in Figure 4.20 was refined through experimental trials and eventually a successive series of tests were performed with a consistent level of success. Two slots were cut on opposite sides of the PMMA tube to provide line of site for the transmitting and receiving optics. Additionally a wet and dry vacuum was placed near to the receiving optics slot to reduce the misting of the lens caused by the aerosols in the spray.

Other than the introduction of the section of PMMA tube, the set up criteria and collection methods were identical to the ambient PDA trials discussed previously in Section 4.3.1.1. The atomiser arrangements selected for the enclosed 'cross tube' characterisation trials were:-

i. SRA arrangement type B (0.5mm exit orifice and 0.5mm spill diameter)
ii. SRA arrangement type C (0.8mm exit orifice and 0.5mm spill diameter)

Although all of the results and data gathered from this series of trials were consistently repeatable, it is likely that some droplets might not be captured in the measuring volume. This could be due to the high degree of misting and pluming caused by the ultrafine aerosols and mist within the tube. These droplets could have been as small as $D_{32} \leq 10\mu m$, which normally rapidly vaporise in ambient conditions.

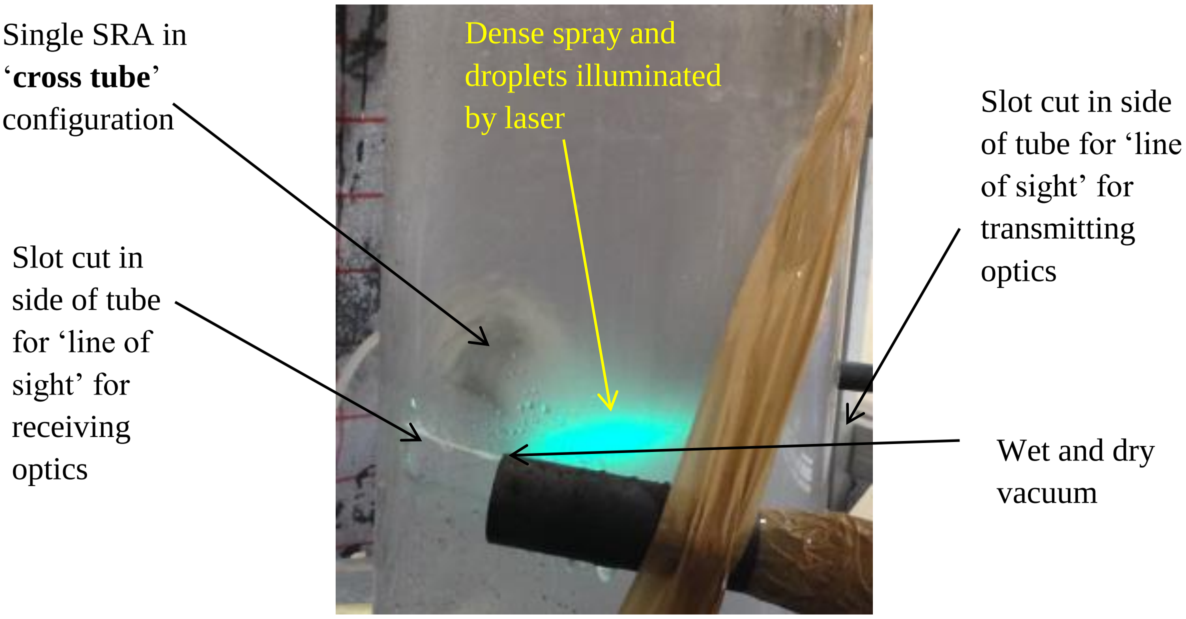

Figure 4.20 : Set up to acquire data for enclosed single SRA cross spray conditions

4.3.2.2 Experimental procedure

This series of PDA trials were conducted using the PMMA simulated tube and were carried out using the same experimental procedures as the ambient PDA tests, previously discussed in Section 4.3.1.2.

4.3.2.3 Data processing

This series of PDA trials were conducted using the PMMA simulated tube and were carried out using the same data processing techniques as the ambient PDA tests, previously discussed in Section 4.3.1.3. The results from this trial series are presented and discussed in Chapter 5.

Accuracy and potential sources of error resulting from this trial are presented in Section 4.4.

4.4 Accuracy and sources of error : Cold trials

4.4.1 Volumetric flow rate

During the volumetric flow rate trial, the results produced were highly consistent. This was reinforced by the SRA Type B configuration, whereby the exit orifice and spill diameter were both 0.5mm. The resulting water collection volumes and subsequent calculated flow rates from the SRA Type B configuration were found to be within ± 1%. (See also Section 5.2.2, Figure 5.4 and Appendix 8)

Table 4.10 provides information and data with respect to the accuracy and potential sources of error relating to this experimental task.

Digital scale	
Scale range	0 – 1000g
Accuracy	± 0.1g (manufacturers data)
Resolution	0.1g
Certificate of calibration	Yes
Measuring beaker	
Tare weight	67.5g (± 0.1g)
Accuracy	± 0.1g (manufacturers data)
Water weight to volume	
Molar mass of deionised water	18.01528 g/mol
Density of deionised water	999.972kg/m^3 (~1000 kg/m^3)
Pressure gauge	
Scale range	0 – 20MPa
Accuracy	± 1.6% (manufacturers data)
Pump	
Scale range	5 – 17MPa
Accuracy	± 2% (manufacturers data)

Table 4.10 : Flow rate trials sources of error and accuracy information

4.4.2 Spray cone angle

The spray cone angle produced by an atomiser is a consequence of the liquid pressure, exit orifice diameter, exit orifice coefficient of discharge and in this case, the unique swirl chamber properties of the SRA. Therefore, although it was important to measure the spray cone angle of the spray, the resulting angles were only used to compare the four sprays and to approximate the penetration within the 190mm (I.D.) PMMA tube using trigonometry.

Table 4.11 provides an indicative estimate of the accuracy of this method of measurement.

Adobe Photoshop	
Angle finder tool	Approximately ± 1.0%
Human error / subjectivity	Approximately ± 1.0%

Table 4.11 : Cone angle measurement sources of error and accuracy information

4.4.3 Phase Doppler Anemometry (PDA)

The main systematic errors for the PDA system are due to measuring volume positioning, velocity bias and Doppler frequency broadening. The random encounters are due to the statistical sampling uncertainty. Throughout the PDA experiments, endeavours have been made to keep these to a minimum.

Statistical sampling uncertainty was kept to a minimum by using a sufficiently large sample range of 10,000 – 20,000 'counts'. Statistical sampling uncertainty was reduced to a minimum level, due to the highest sample rate adopted. From previous studies and published journal papers [51, 53] where this equipment was used, the following accuracy and sources of error information were stated, as shown in Figure 4.12.

Dantec Particle Analyser	
Traversing error (X and Y) of the SRA	Approximately ± 0.25mm
Traversing errors (Z direction) downstream	Approximately ± 1mm
Water flow rate through SRA	Approximately ± 1.0%
Typical nominal errors for diameter	4% on diameter (manufacturers data)

Table 4.12 : PDA and sources of error and accuracy information

The next Section will provide detailed description with regards to apparatus, procedures and method of data processing relevant to the ***hot trials.***

4.5 Apparatus, procedures and data processing : Hot trials

The apparatus that was required for these investigations needed to be innovative and purpose built to safely facilitate the assessment of a selected number of SRA atomiser configurations with respect to their explosion suppression / mitigation capabilities.

The design configurations and orientations of the SRA's together with the respective sprays and their subsequent interaction with the incoming flame within the PMMA tube are profoundly crucial, since the overall aim of this study (highlighted previously in Chapter 1), is to 'fully' mitigate a propagating flame with complete combustion extinguishment in a homogeneous fuel gas : air mixture.

A suitable ***hot trials*** test rig was thus designed and commissioned, complete with selected hardware, data acquisition and processing capabilities. It is also worth noting that due to the specific intentions and requirements of this study, rig designs used in other investigations [39] would be ineffective if emulated in this present research.

The following Sections therefore describe the:-

i. Apparatus design and set up used for the hot trials (Section 4.5.1)
ii. Atomiser configuration designs, including methodology and rationale for use (Section 4.5.5)
iii. Imaging techniques (Section 4.6)
iv. Procedures and data processing (Section 4.7)

4.5.1 Apparatus design and set up

There were two main factors governing the design of the rig apparatus, these were:-

i. Health and safety considerations
ii. The scope of engineering and design considerations

Due to the risk and consequences of explosion research, safety could not be compromised. Although all explosion research carries an obvious level of risk, all of the 'hot trials' in this study would be carried out inside the laboratory. The consequences of an accident or error in one of the experimental trials could potentially be catastrophic.

Following an extensive design review, as summarised in Chapters 2 and 3, there was a need to formulate a creative design capable of producing slow moving explosions in a combustible methane-air mixture, with resulting flames propagating in the order of ≤30m/s.

Prior to the commissioning and subsequent hot trials, a thorough risk assessment was carried out, which included the use of computational fluid dynamics (CFD) modelling to predict potential likelihoods and consequences of several event scenarios.

The resulting CFD predictions and risk assessments from this exercise can be found in Appendix 1 on the accompanying CD of Appendices (Volume III).

Although there has been wealth of previous research (see Chapter 3) in the suppression and mitigation of explosions using water sprays, all of the past work has dealt with larger droplets (≥100μm) and/or faster flame speeds (≥100m/s) than this present program. With the objectives of this study being to design and construct a unique piece of laboratory scale test equipment to carry out water spray mitigation trials on low speed gas-air deflagrations of ≤30m/s, the following criteria was applied to the design of the **Flame Propagation and Mitigation Rig (FPMR)** to ensure:-

i. Safe operation for use in an indoor environment, complete with procedures and checklists.
ii. A control system that would facilitate the safe filling, recirculating and subsequent ignition of various homogeneous methane-air mixtures.
iii. Hardware and software capabilities to record relevant quantitative information
iv. A clear mid-section to permit qualitative analysis of flame progression and mitigation and to allow the measurement of average flame speeds.
v. Variable mounting positions for single and multiple atomiser configurations including counter flow (C/F), parallel flow(P/F) and cross flow (X/F) arrangement with respect to the propagating flame front.
vi. Controllable flame speeds with the facility to vary the environmental conditions in which the explosion event occurred i.e. confined, partly confined, partly confined vented. These terms were explicitly discussed in Chapter 2.
vii. Flexibility in the design to afford continued use of the equipment for future studies.

Furthermore, a number of features were built into the rig design to permit various permutations, such as overall length to diameter ratio and the accommodation a range of single and multiple atomisers. These design **features** and their **benefits** are highlighted in Table 4.13, which also includes reference to further descriptive Sections in this Chapter.

Feature	Benefit	Section
The rig is sectional	As the rig was sectional it can be easily moved or transported. The 1m and 2m long polycarbonate sections can be added or removed using flanged joints to allow for increase or decrease in length to diameter ratio (l/d).	**4.5.2**
Multi use test points	'Pete's Plug' multi use, self-sealing test points have been fitted to the rig at 600mm intervals. These allow a 4mm test probe to be inserted for, temperature, pressure, gas-air mixture composition etc.	**4.5.3**
Magnetic hinged panel	All 'hot trials' were carried out with the flame propagating towards an open end. This was achieved by employing a magnetic hinge. The magnetic hinge was fully interlocked with the ignition system to prevent ignition occurring with the end closed.	**4.5.4.5**
Atomiser mounting positions	A water induction pipe/manifold is situated concentrically within the polycarbonate section. The position of the atomiser could be moved by the addition or removal of stainless steel extension pieces and placed in counter and parallel flow configuration. Additional external mounting connections were included to accommodate cross flow conformation.	**4.5.4.6 / 4.5.5**
Control system	The control system was designed to allow full control of all functioning components in a systematic and safe manner. The ignition circuit remained inactive until a push button is pressed and the hinged panel opens.	**4.5.4.11**
Recirculation system	When the rig was initially filled with gas and air the mixture was stratified and non-uniform. The gas booster pump and turbine flow meter facilitate the recirculation and homogenous mixing of the gas and air.	**4.5.4.2**
Exhaust gas outlets	The rig is equipped with 6 x 80mm outlets to allow the products stream (exhaust) to discharge. These outlets can be open or closed, thus allowing variety of flame speeds and conditions.	**4.5.4.4**
Rig legacy	The rig has been designed to allow for future research in the field of explosions, flame speeds and suppression/mitigation. The rig has been designed to withstand much higher pressures and temperatures than those expected in this current study.	**All**

Tables 4.13 : Summary of test rig 'features and benefits'

4.5.2 Design and construction concepts

The explosion propagation and mitigation tube was designed to withstand the pressures and temperatures normally associated with propagating deflagrations in unconfined and partly confined situations.

All pipework, fittings and components associated with the fabrication of the rig conform fully with appropriate standards, such as ANSI, BSI or European (CE) standards.

The principle criteria for the rig was to provide a representative small scale testing facility to assess the performance of a range atomisers and configurations, with the primary objective of mitigating a slow moving methane-air deflagration. Previous studies [39] in this field focused on high speed flames and accelerated combustion waves, which have the capability of shattering and breaking up water droplets into very fine mist that is readily vaporised in the flame.

This current research is focused on the design and validation of a novel atomising system capable of producing a fine spray system consisting of water droplet of $D_{32} \leq 30\mu m$, which may be scaled in future large scale realistic trials (see Chapter 7, Conclusions and recommendations), to provide an effective explosion mitigation measure for new and existing gas, oil or petrochemical sites. The aim of the novel full scale spray system would be to mitigate slow moving deflagrations before flame acceleration conditions prevail.

As summarised previously in Table 4.13, the main rationale and design concepts associated with the laboratory scale rig are as follows:-

i. The length of the rig : the 1m or 2m long polycarbonate sections can be added or removed using flanged joints to allow for increase, or decrease in length to diameter ratio (l/d). This will have an overall effect on the limiting flame speed as it reaches the atomiser. This flexibility also allows sections to be pre-assembled with additional components i.e. an array of atomisers can be installed in a section, tested and characterised, then simply bolted in position.

ii. Exhaust gas outlets : the 6 x 80mm exhaust gas outlets will allow seven options for explosion trials, either all exhaust outlets closed, or one to six outlets open during the test. As flame speed is a function of the pressure resulting from the rapid expansion of gases upstream of the flame, a number of scenarios could be created and tested.

iii. Test points : as the rig can be extended or shortened, several test point and drain point connections have been added. In some cases the test points will be plugged off and in others they will be fitted with optional third party devices for temperature and pressure measurement and gas-air concentration.

iv. Due to the high pressures and flow rates required for atomiser operation, a water storage, pumping and delivery system was produced for counter flow (C/F), parallel flow (P/F) and cross flow (X/F) configurations.

4.5.3 Initial conceptual designs

A series of initial design concepts were considered with respect to the aims and objectives and additional requirements and conditions. Whilst a small number of examples are included in this Section, additional designs are provided in Appendix 2 of the accompanying Appendices CD (Volume III).

Figure 4.21 shows an original conceptual design sketch, giving some approximate dimensions and consideration for upstream venting via the 6 x 80mm exhaust outlets.

Figure 4.22 displays an example of an early design which again incorporates the 6 x exhaust outlets, equipped for fast acting solenoids or bursting membranes. At the opposite and exit end of the rig there is a membrane that would be punctured by a pointed electro-magnetic reamer, prior to ignition. This concept was later superseded by the magnetic hinged panel, which is discussed in Section 4.5.4.5.

Figure 4.23 illustrates the initial laboratory bench set up, including extract ventilation and the matt black boards fitted behind the rig for imaging purposes.

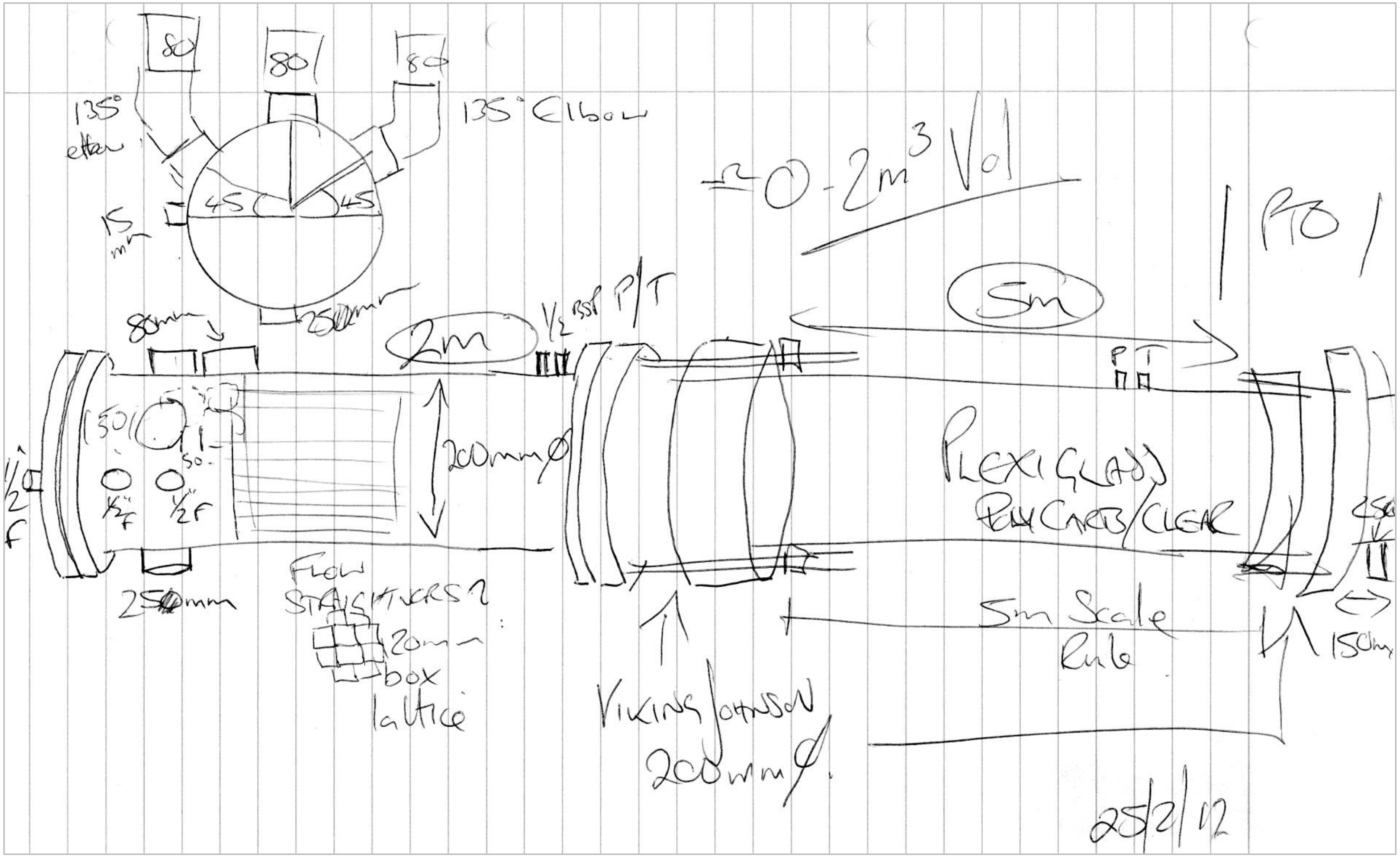

Figure 4.21 : Initial concept sketch of FPMR (25-02-12)

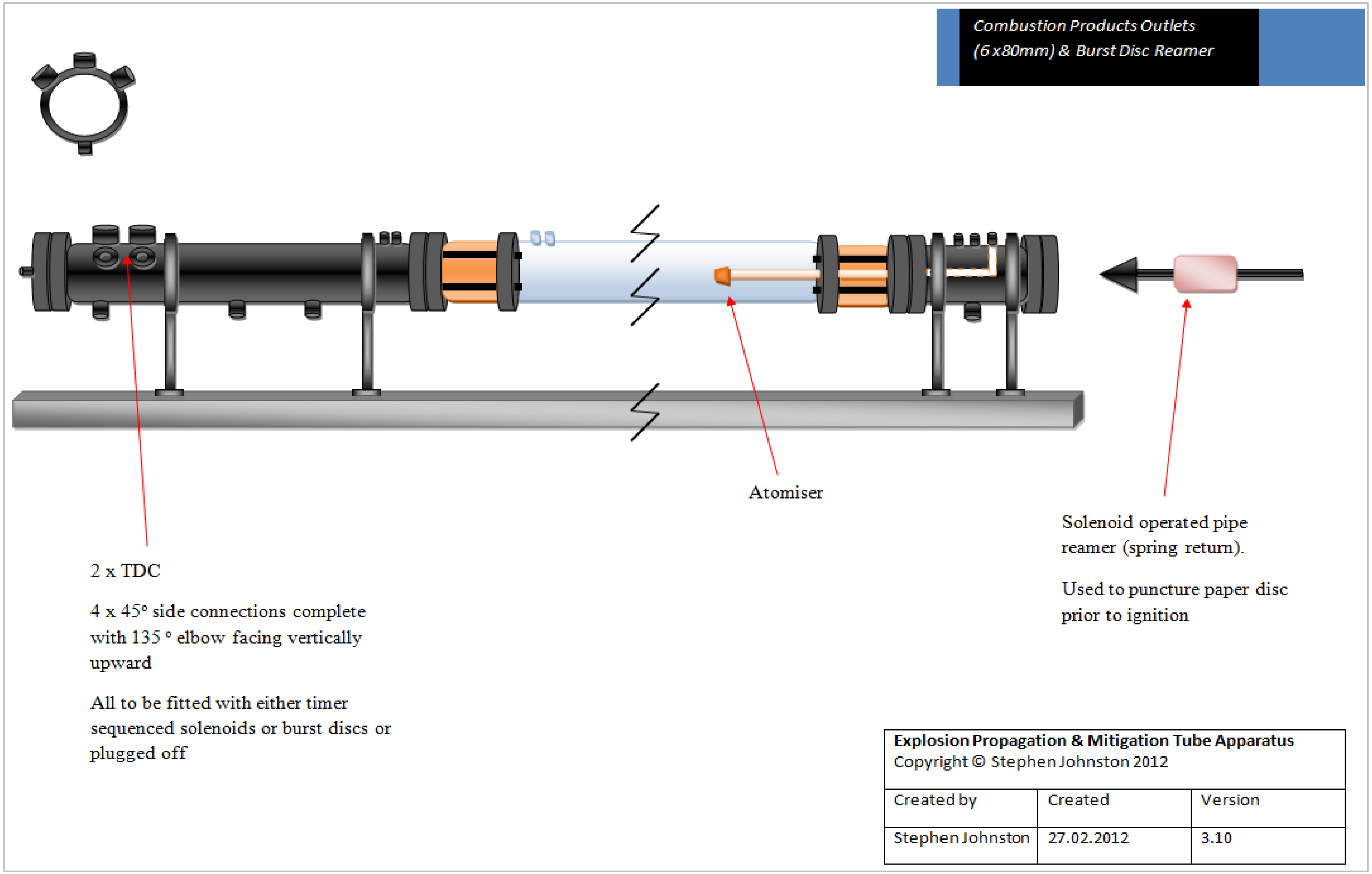

Figure 4.22 : Initial design drawing of FPMR

Rig Support Bench and Supplementary Requirements

N.B. The cupboards must be fixed to the floor and the bench top must to be fixed to the units.

The explosion and mitigation rig must be fixed to the bench top.

The cupboards must be parallel with the side wall and at least 1.5m from the side wall.

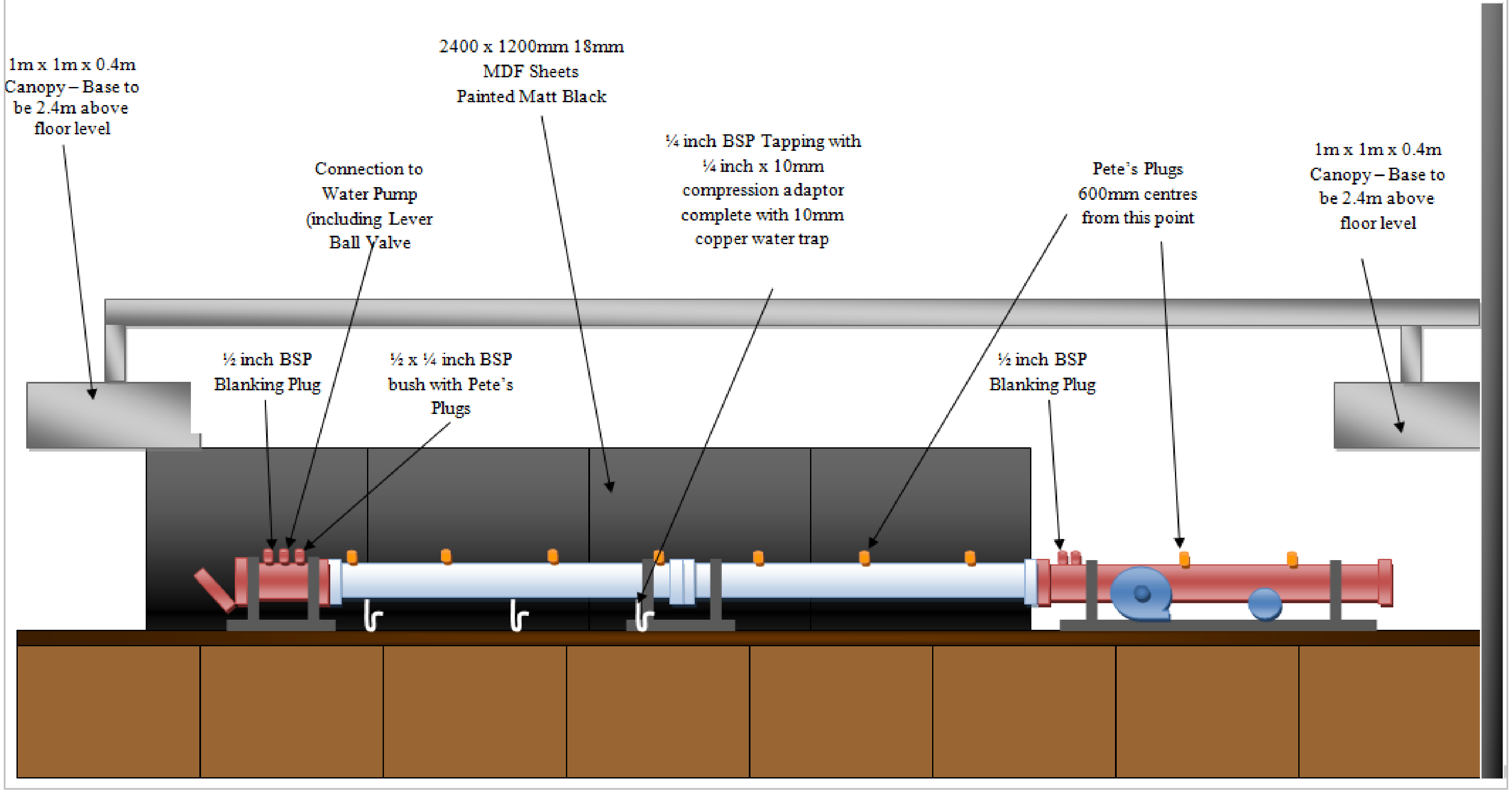

Figure 4.23 : Initial design drawing laboratory set up (29-03-12)

4.5.4 Final design : components and assembly

Subsequent to the initial conceptual designs and iterations, the final design was constructed which also meets the overall aims and objectives required in this study. (See also Chapter 1)

To comply with the safety requirements and to facilitate the fabrication of a robust design, both of the ends of the rig were constructed using 8 inch (200mm) diameter mild steel to ANSI schedule 40 [78] with fully welded connections and flanges. The 8 inch (200mm) pipe had an internal diameter of 7.981 inches (202.7mm) and a wall thickness of 0.322 inches (8.4mm) as shown in Table 4.14.

Pipe Size *(in)*	Diameter *(in)*		Nominal Thickness *(in)*	Transverse Areas *(in^2)*			Length of Pipe *(per sq. foot of)*		Volume *(ft^3/ft)*	Weight		Number of Threads per inch of Screw
	External	Internal		External	Internal	Steel	External Surface *(ft)*	Internal Surface *(ft)*		*lb/ft*	*kg/m*	
1/8	0.41	0.27	0.07	0.13	0.06	0.07	9.43	14.20	0.0004	0.24	0.36	27
¼	0.54	0.36	0.09	0.23	0.10	0.13	7.07	10.49	0.0007	0.42	0.63	18
3/8	0.68	0.49	0.09	0.36	0.19	0.17	5.66	7.75	0.0013	0.57	0.84	18
½	0.84	0.62	0.11	0.55	0.30	0.25	4.55	6.14	0.0021	0.85	1.26	14
¾	1.05	0.82	0.11	0.87	0.53	0.33	3.64	4.64	0.0037	1.13	1.68	14
1	1.32	1.05	0.13	1.36	0.86	0.49	2.90	3.64	0.0060	1.68	2.50	11 ½
1 ¼	1.66	1.38	0.14	2.16	1.50	0.67	2.30	2.77	0.0104	2.27	3.38	11 ½
1 ½	1.90	1.61	0.15	2.84	2.04	0.80	2.01	2.37	0.0141	2.72	4.04	11 ½
2	2.38	2.07	0.15	4.43	3.36	1.08	1.61	1.85	0.0233	3.65	5.43	11 ½
2 ½	2.88	2.47	0.20	6.49	4.79	1.70	1.33	1.55	0.0333	5.79	8.62	8
3	3.50	3.07	0.22	9.62	7.39	2.23	1.09	1.25	0.0513	7.58	11.27	8
3 ½	4.00	3.55	0.23	12.56	9.89	2.68	0.95	1.08	0.0687	9.11	13.56	8
4	4.50	4.03	0.24	15.90	12.73	3.17	0.85	0.95	0.0884	10.79	16.06	8
5	5.56	5.05	0.26	24.30	20.00	4.30	0.69	0.76	0.1389	14.61	21.74	8
6	6.63	6.07	0.28	34.47	28.89	5.58	0.58	0.63	0.2006	18.97	28.23	8
8	8.63	7.98	0.32	58.42	50.02	8.40	0.44	0.48	0.3552	28.55	42.49	8
10	10.75	10.02	0.37	90.76	78.85	11.90	0.36	0.38	0.5476	40.48	60.24	8

Table 4.14 : ANSI schedule 40 pipe table [78]

With the exception of instrumentation tubes and conduits, all of the other joints i.e. recirculation system, were made with threaded joints (BSP) using jointing compounds or PTFE tape to EN751-2 and EN751-3, or with flanges and appropriate gaskets.

It was obligatory that the middle section of the rig be clear to permit qualitative observations and recording of the flame propagation and successive mitigation. The material chosen for the middle section was a Polymethyl-methacrylate (PMMA) tube.

PMMA is an economical alternative to Polycarbonate (PC) when extreme strength is not necessary. Also PMMA does not contain the potentially harmful bisphenol-A sub-units found in Polycarbonate. It is often used because of its moderate properties, easy handling and processing, however the material is more prone to scratching than conventional inorganic glass.

Polymethyl-Methacrylate (PMMA) is often referred to as ‘Acrylic’. PMMA/Acrylic is sold by many trade names including Acrylex, Acrylic Glass, Acrylite, Acrylplast, Altuglas, Limacryl, Lucite, Oroglass, Per-Clax, Perspex, Plazcryl, Plexiglass, Polycast, and R-Cast. Plexiglass tube was previously used successfully and proven to be a suitable material for explosion suppression research and was successfully used in early experiments by Sapko *et al* [61]. PMMA is often used as an alternative to glass and some of its properties are summarised in Table 4.15.

Property / Characteristic	**Formula / Value**
Chemical formula	$(C_5O_2H_8)_n$
Density	1.18 g/cm^3
Melting point	160˚C (320˚F)
Boiling point	200˚C(392 ˚F)

Table 4.15 : Properties of Polymethyl methacrylate (PMMA).

PMMA is often preferred because of its higher impact strength, easy handling and processing. Scratches may easily be removed by polishing. PMMA has excellent environmental stability compared to other plastics such as polycarbonate and is therefore often the material of choice for outdoor applications

Figures 4.24 and 4.25 reveal some images taken during the construction and fabrication processes, which are further described with accompanying photographs in Appendix 2. Figure 4.24 shows the fabrication and construction of the steel driver and related sections, together with Figure 4.25 showing the clear mid-section of the rig.

The steel and plastic sections of the rig were fabricated and mounted on a heavy duty 40mm steel sub-frame, which was bolted to the laboratory bench for safety and security and is shown in Figure 4.26. Additionally and for convenience, Figure 4.26 is also presented to provide a comprehensive visual representation of the completed rig and some of the terminology used in this Section.

(i) Two of the 6 x 80mm sockets welded onto one end of ignition driver section

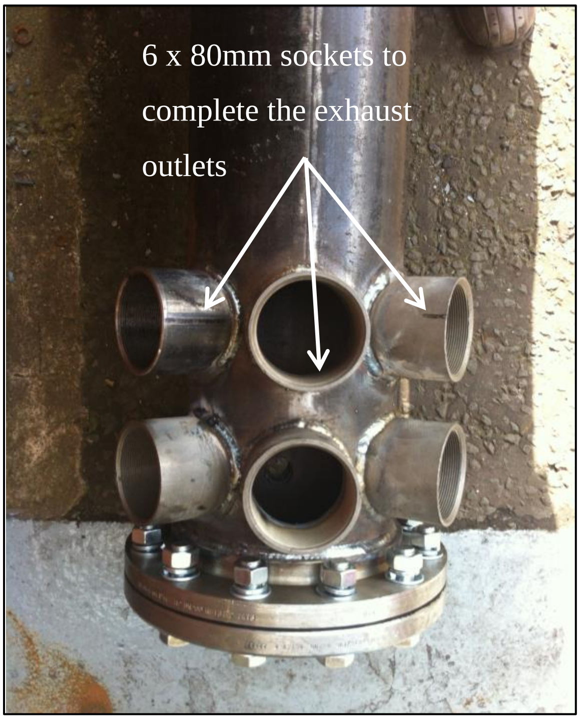

(ii) Six exhausts and view of the ignition end of explosion driver section

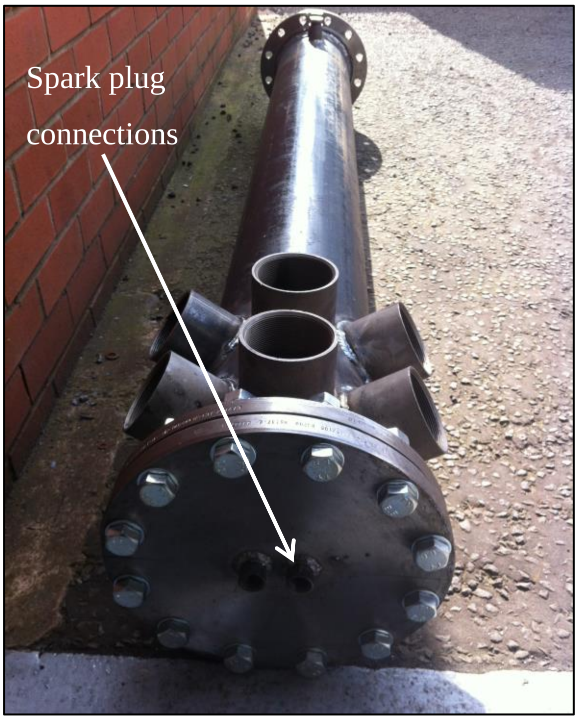

(iii) Completed explosion driver section revealing spark plug connection

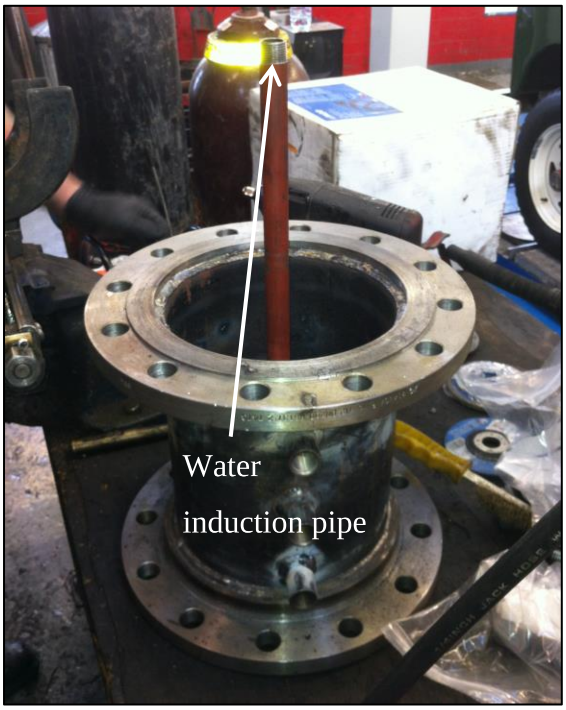

(iv) Outlet end of the rig, revealing atomiser water induction and mounting pipe

Figure 4.24 : Fabrication and construction of steel driver and end sections

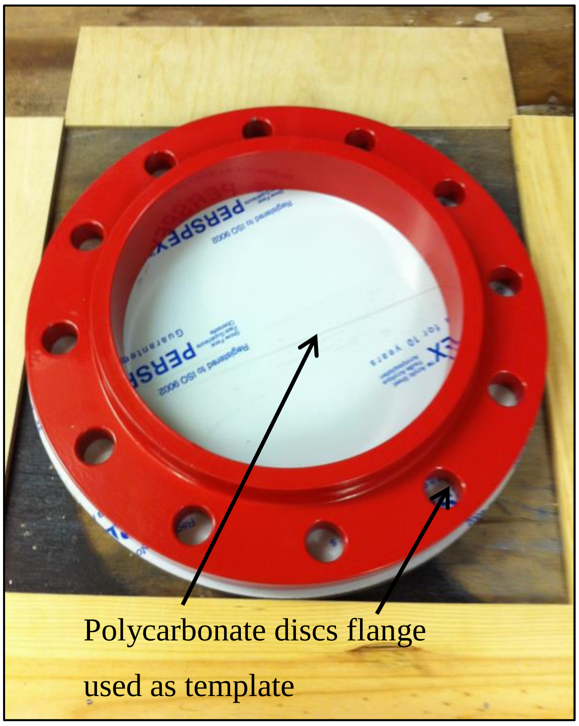

(i) Polycarbonate discs (350mm diameter x 10mm thick) and flange used as template

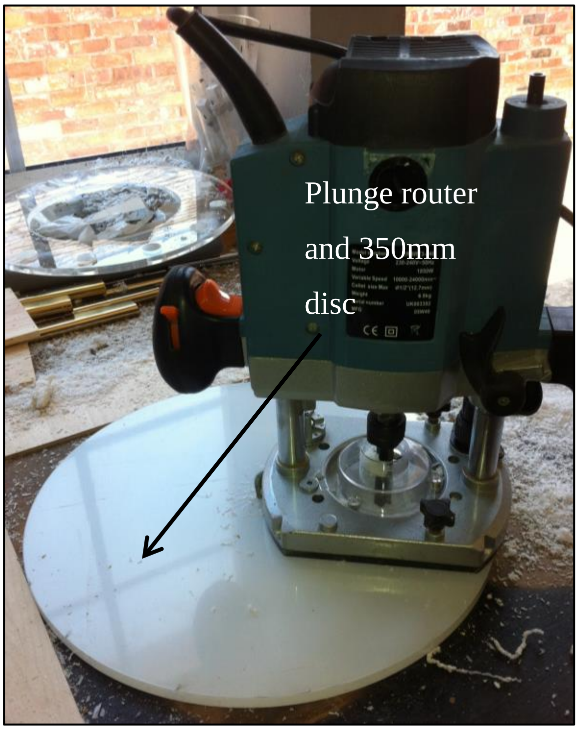

(ii) Plunge router used to cut out the centre of the flanges

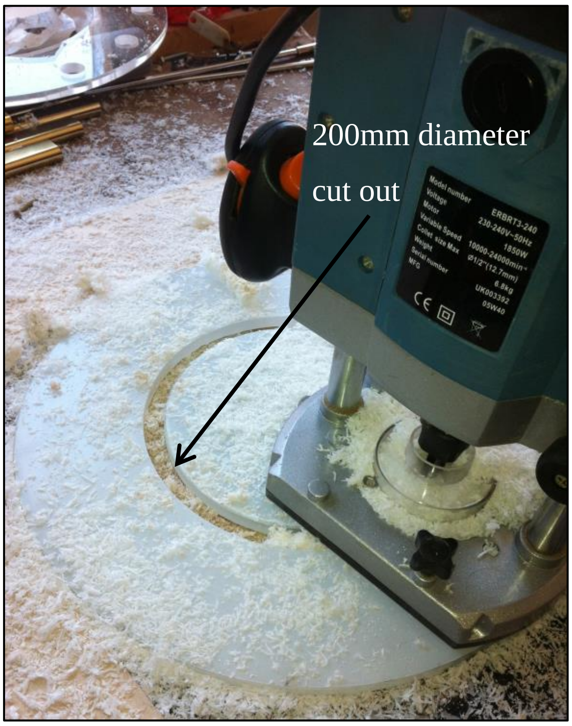

(iii) Plunge router used to cut out the centre of the flanges revealing a 200mm cut out

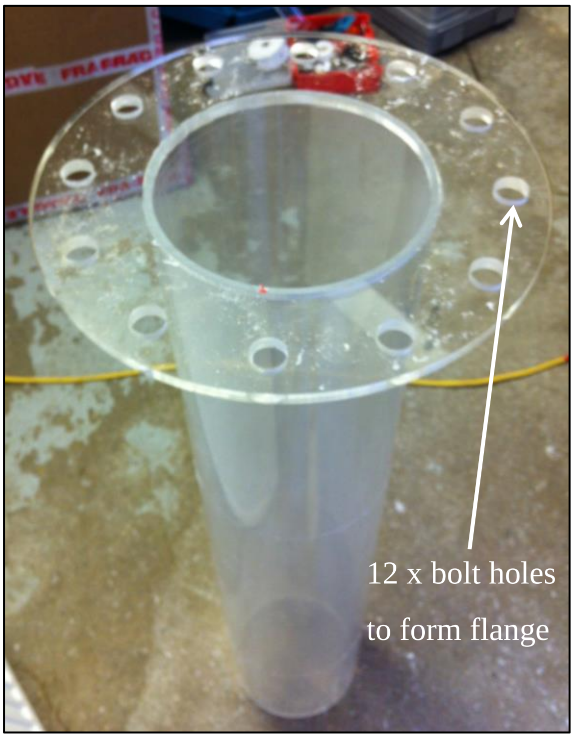

(iv) completed flange with 200mm diameter centre hole and 12 x 20mm bolts holes

Figure 4.25 : Fabrication and construction of PMMA clear mid-sections

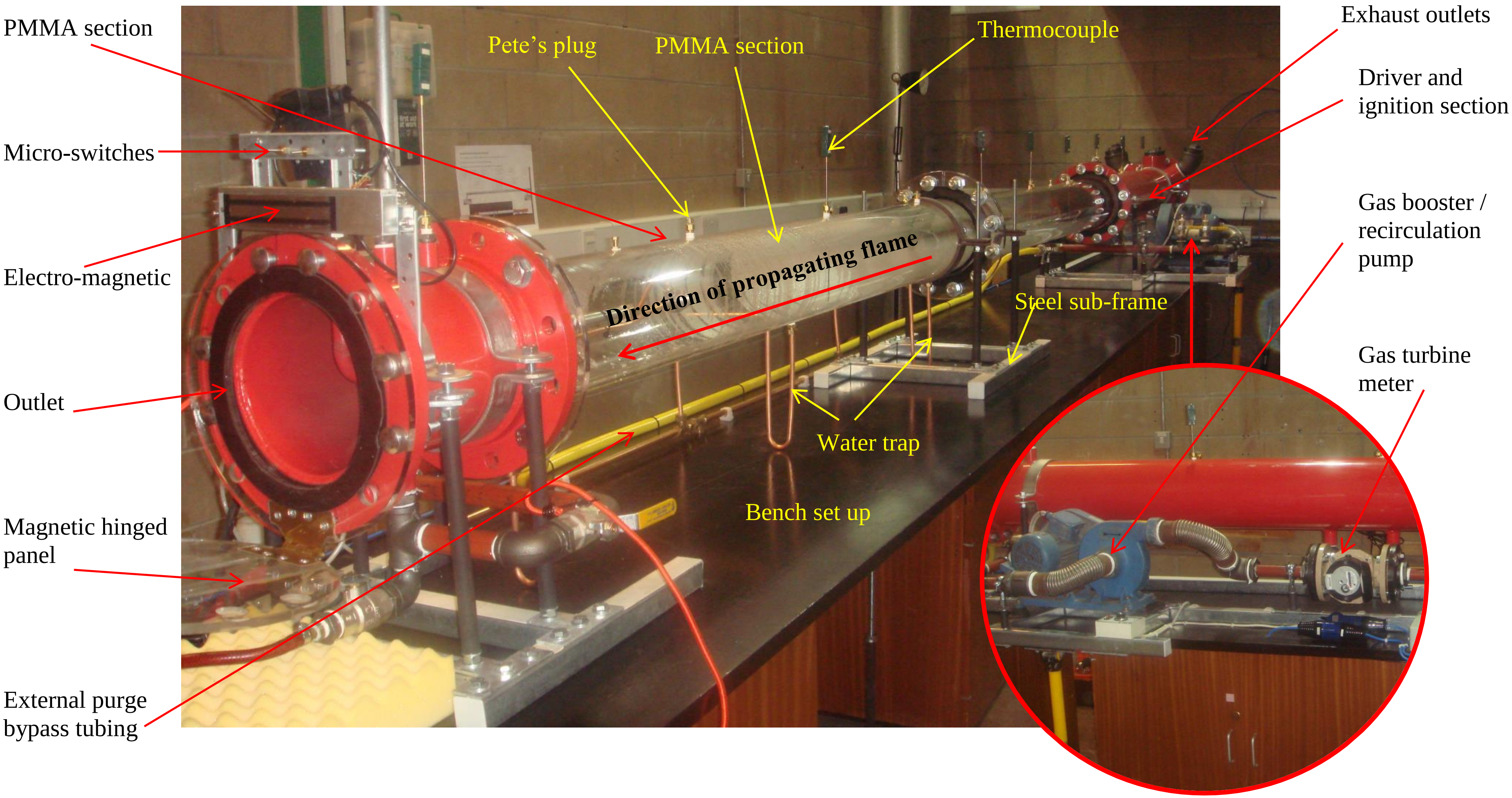

Figure 4.26 : Completed assembly of Flame Propagation and Mitigation Rig (FPMR) including principle component parts

In the following, attempts are made to provide rationalised and detailed descriptions of each of the components used in the building of the rig.

4.5.4.1 Ignition system

The ignition system, which was positioned at the right hand side of the FPMR (see also Figure 4.26) comprised of three main components:

i. Ignition electrode/spark plug
ii. Ignition spark generator
iii. Double insulated HT cables

To prevent inadvertent and premature ignition of the mixture, the ignition circuitry was fully interlocked. In addition to this, a series of manual safety checks where performed and recorded before each experimental run. (See also Figure 4.7.1)

i. Ignition electrode/spark plug

The ignition spark was provided by one of the two standard ‘long reach’ combustion engine spark plugs as presented in Figure 4.27. The spark plugs were fitted in the end flange plate of the driver section, as can be seen in Figure 4.28.

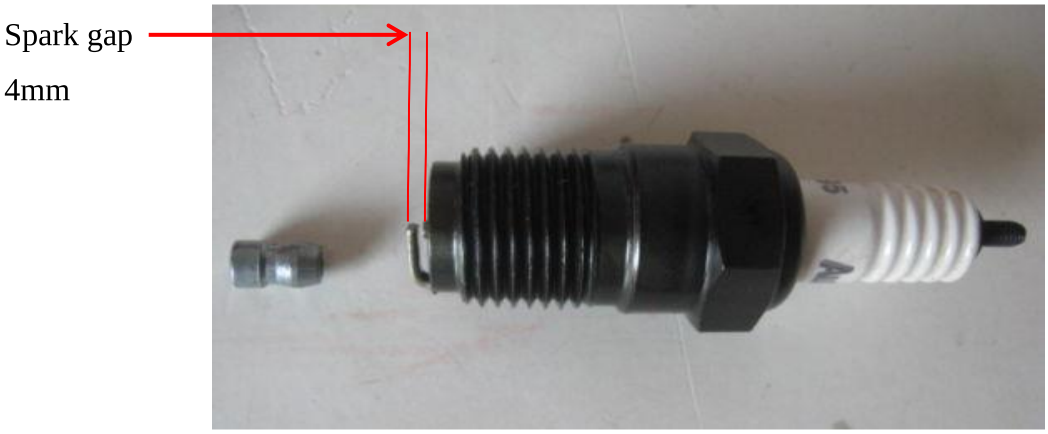

Figure 4.27 : Typical of primary and auxiliary ignition spark plugs [79]

Although two spark plugs were installed in the rig, only one was used during each test run to create the spark. The other spark plug was to be used as an auxiliary backup, should the primary spark fail to ignite the mixture. This prevented any unnecessary purging and emptying of the mixture volume due to a faulty spark plug, or other ignition/misfire problem, such as moisture from the sprays affecting the quality of the spark.

Each spark plug ‘gap’ was adjusted and set to 4mm and was also cleaned, rechecked and adjusted where necessary after every ten successive ignitions.

ii. Ignition transformer and spark generator

Following a review of previous explosion research, the ignition energy of approximately 10mJ was adopted throughout the flammability range in these experiments. This was sufficient to ignite all of the methane-air mixtures of E.R. (ϕ) 0.61 – 1.06. A 10,000v ignition transformer and spark generator was used to supply the required high tension (HT) spark.

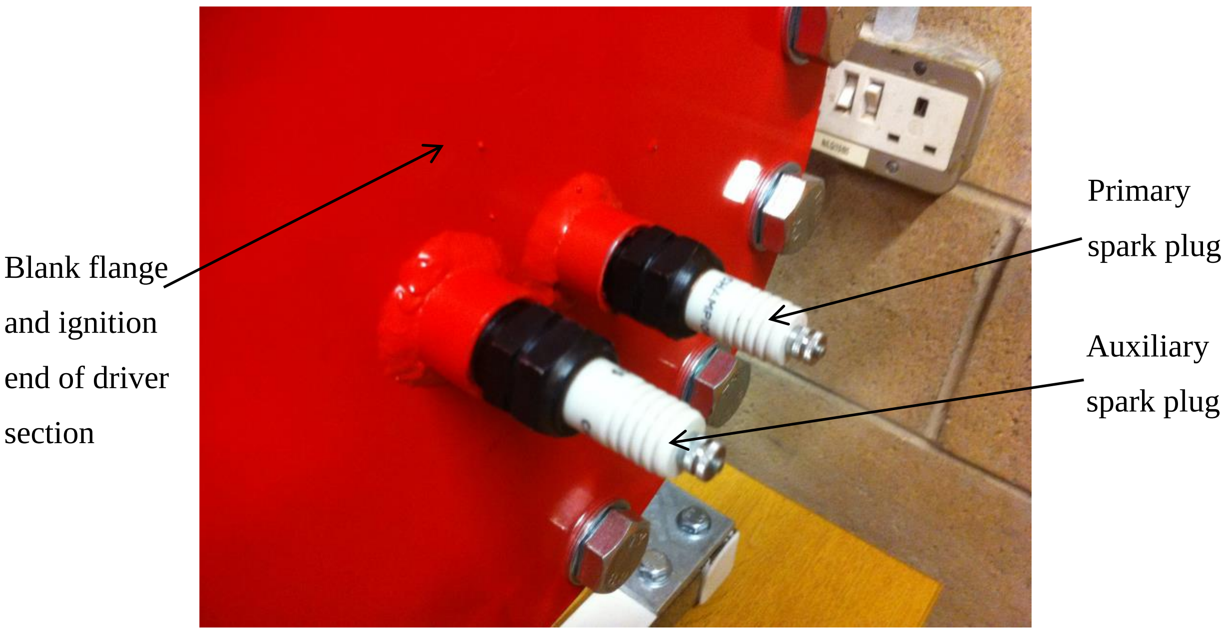

Figure 4.28 : Primary and auxiliary spark plug

iii. Double insulated HT cables

Two Universal Durite 19/0.30mm double insulated copper core high tension (HT) leads were used to connect the ignition transformer and spark generator to the ignition electrodes/spark plugs. The cables were checked for wear and tear periodically and replaced where necessary.

4.5.4.2 Gas recirculation system

To ensure mixture homogeneity within the FPMR prior to ignition, several methods have been adopted by previous authors [58, 60, 61]. These include:-

i. Purge filling
ii. Premix
iii. Gas Recirculation

i. Purge filling

In a purge filling system, the fuel gas and air streams are fed directly, or indirectly via a mixing tee into one end of the explosion propagation tube via calibrated rotameters. The mixture is then released from the opposite end of the rig for a finite time period until the desired concentration is achieved, based on the length, cross section and volume of the rig. This method has an unacceptable high level of risk when used within the confines of a laboratory and is more suited to outdoor testing, where large volumes of potentially flammable fuel gas-air mixture may be released.

As the laboratories at the University of Salford are used for many other areas of research, potential sources of ignition were unavoidable. In addition to the obvious risks in conducting explosion research, there was also a statutory need to satisfy the Universities Health and Safety Department. Therefore, because of the unfavourable risks involved, the utilisation of a purge filling system was discounted from this current research.

ii. Pre-mix

In a pre-mix system, fuel gas and air (or oxygen) is supplied separately to a mixing machine. These machines vary from simple mechanical devices, to complex computer controlled systems. Pre-mix machines are normally designed to supply closely controlled fuel air-gas ratios to industrial process plant burner systems e.g. oxygas burners used in glass shaping and manipulation.

Although previous authors [61] have used this method successfully, mixture homogeneity can only be achieved if several volumes are purged through the rig to atmosphere. This system also has an unwelcomed risk in a laboratory environment.

iii. Gas recirculation

In the gas recirculation system, the fuel gas and air streams are supplied into one end of the sealed FPMR via calibrated rotameters. At each end of the rig a connection was made to re-circulate the fuel gas-air mixture through an external parallel stream, as shown in Figure 4.31.

In this present study, a gas booster pump as displayed in Figure 4.29 was installed in a parallel recirculation stream to create a pressure differential through the main explosion tube and recirculation bypass circuit and thus induce flow.

Figure 4.29 : Gas booster pump

The gas recirculation system was adopted predominantly for safety reasons, however in practical terms it consistently produced homogeneous mixtures. The pipe diameter chosen for the recirculation system was 25mm in diameter, being much smaller than the main explosion tube. This was to promote high velocity turbulent mixing in the bypass and ensure homogeneity throughout the main tube. A turbine gas meter was also installed in the bypass circuit to quantify recirculation volumes, which is presented in Figure 4.30.

Based on laboratory trials and previous literature [65], a recirculation volume of ten volumes of the apparatus was applied to every experimental trial to ensure consistency and reliability. The bypass booster pump was then switched off and allowed to stabilise for one minute until the mixture became quiescent.

The mixture concentration was then measured, verified and recorded at three points (both ends and centre of the main tube). The bypass recirculation circuit was then isolated using two quarter turn isolation valves, one at each end. In line flame arrestors were also installed in the recirculation circuit as secondary safety devices to mitigate the risk of an explosion from the main propagation tube into the recirculation circuit.

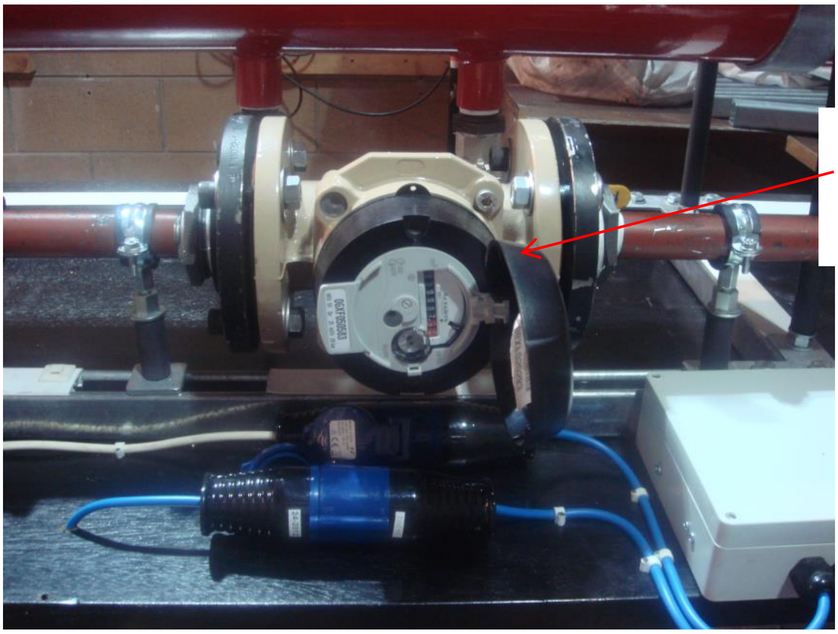

Figure 4.30 : Turbine gas meter

Although the majority of the recirculation pipework was constructed using 25mm ridged steel pipe, a section of reinforced hose was used to connect the two ends of the recirculation system.

This design concept addresses two key issues:-

i. As the recirculation system would almost certainly contain a flammable gas-air mixture during fillings times, the recirculation bypass hose shown in Figure 4.31 would provide a point of ‘pressure relief’ in the rig. Should accidental ignition occur within the recirculation system, this would prevent over pressurisation and possible fracturing of metallic pipework, booster fan and gas meter.

ii. The flexible connection would facilitate the addition or removal of lengths of Polymethyl-methacrylate (PMMA) tubing without disturbing the recirculation system.

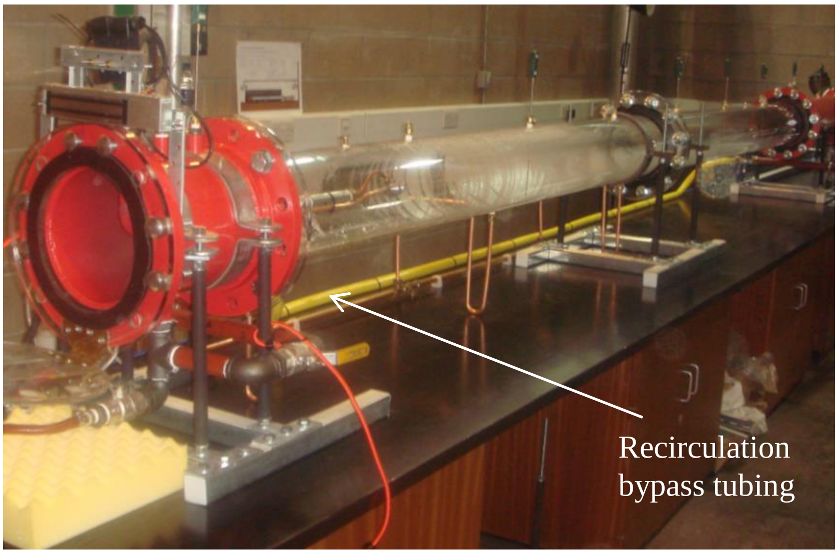

Figure 4.31 : Recirculation bypass tubing

4.5.4.3 Post explosion purge process

To ensure that the apparatus was fully purged and ready to receive a new fuel gas-air concentration, the following procedure was adopted after each experimental trial:

i. The main explosion propagation tube was allowed to stand for 15 minutes between experiments, whilst open at both ends. Due to the relative positioning and orientation of the exhaust outlets and the temperature differential between the ends of the main explosion propagation tube, laboratory air was allowed to diffuse throughout the tube.

ii. The gas recirculation system was purged by introducing air from a cylinder and regulator at one end, then expelled via a temporary connection at the other end direct to outside atmosphere through an appropriate purge hose.

iii. Both the main explosion propagation tube and gas recirculation system were then tested for gas concentrations. A value of ≤5% LFL was deemed to be satisfactory.

4.5.4.4 Exhaust solenoids / bursting membranes

At the ignition end of the FPMR there are six exhaust outlets. These outlets consist of an 88mm hole cut through the pipe wall and an 80mm (3 inch) BSP socket welded in position over the hole, shown previously in Figure 4.24. The rationale for the outlets is as follows:-

The combined cross sectional area of the six outlets is approximately greater than or equal to the cross sectional area of the main propagation tube driver section.

Cross Sectional Area (CSA) of exhaust outlets (Area = πr^2) (4.1)

Area of 88.90mm diameter connection = π 44.45mm^2

Area of 88.90mm diameter connection = 6209.67mm^2

Area of 6 x 80mm diameter connections = 37257.99mm^2

Cross Sectional Area of explosion tube (Area = πr^2)

Area of the 202.7mm (ID) main pipe = π 101.35mm^2

Area of the 202.7mm (ID) main pipe = 32282.87mm^2

The exhaust outlets were designed to control the ‘blockage ratio’ of the burnt gases exiting the rig and those driving the flame. By controlling the blockage ratio (see Table 4.16) of the burnt gases, the rig was capable of producing a variety of explosion conditions.

Variable degrees of venting and resulting flame speeds were achievable by simply blocking off one, or several of the exhaust outlets. However, the ‘solid’ blocking of exhausts openings was not utilised during the main body of this work.

Number of exhaust outlet(s) open	Total area of opening(s) (mm^2)	Propagation tube area (mm^2)	Total openings ratio (%)	Total blockage ratio (%)
0	0.00	32282.87	0.00	100
1	6209.67	32282.87	19.24	80.76
2	12419.33	32282.87	38.47	61.53
3	18628.99	32282.87	57.71	42.29
4	24838.66	32282.87	76.94	23.06
5	31048.33	32282.87	96.18	3.82
6	37257.99	32282.87	115.41	0.00

Table 4.16 : Areas and percentages of exhaust outlet openings

Two methods of controlling the exhaust gas outlets were originally conceived and considered:-

i. The use of rapid acting, high temperature solenoid operated gate valves.
ii. The use of a bursting disc or membrane.

i) Rapid acting, high temperature solenoid operated gate valves

The first option was to install 6 x rapid acting, high temperature rated solenoid operated gate valves, as exhibited in Figure 4.32 in the six exhaust outlets. The solenoids would be controlled and sequenced automatically via six channels in the main control box. One or a number of solenoids would then open just a few milliseconds after the spark was supplied, via a time delay relay. Hot burnt gases would then be vented upstream of the flame front, providing a degree of control over flame speed and downstream overpressure.

The risk of solenoid malfunction was deemed to be unacceptable, as potentially dangerous flame speeds and overpressures could have resulted with catastrophic outcomes. Also the high capital expenditure relating to the six solenoids and additional control circuitry needed to operate the valves, together with pre planned maintenance costs, resulted in this option being dismissed.

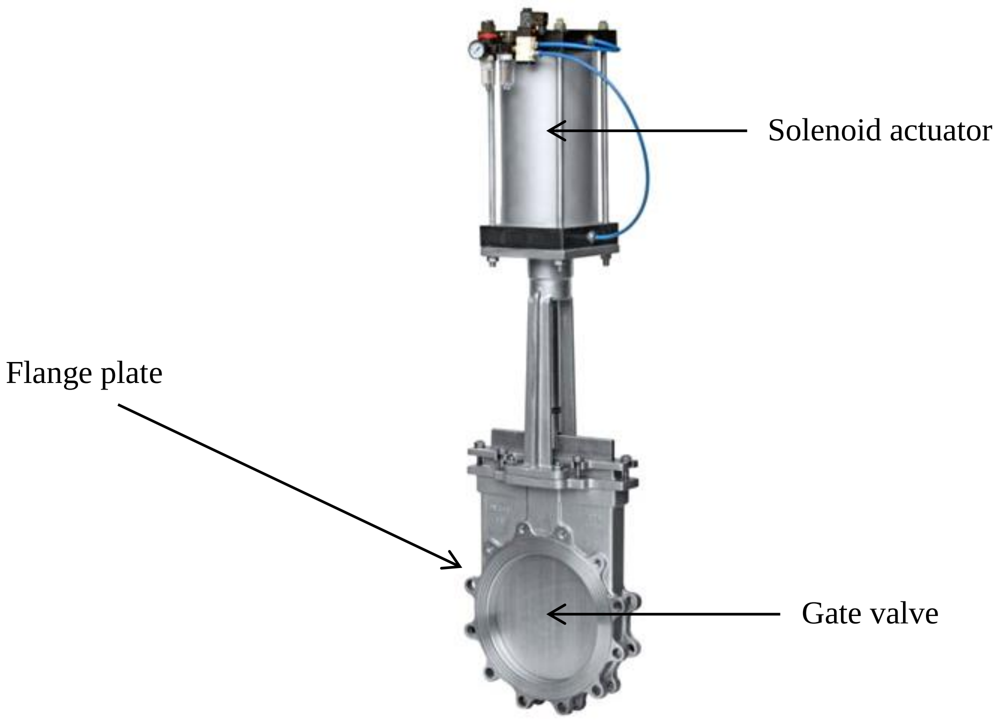

Figure 4.32 : 80mm, rapid acting, high temperature, solenoid operated gate valve [80]

ii) Bursting disc or membrane

The second option was to employ bursting discs/membranes in one, or a number of the six exhaust outlets. Whereby, shortly after ignition the disc or membrane would burst/rupture due to the pressure differential between the inside and outside of the tube. Hot burnt gases would then be vented upstream of the flame front, thus giving a similar degree of control as the above method (i) over flame speed and overpressure.

The exhaust outlets were all fitted with bursting discs membranes, or were sealed off with 80mm BSP threaded plugs to prevent the discharge of flammable air-gas mixtures during the filling process.

Low density polyethylene sheet ‘cling film’ was chosen to act as a bursting disc membrane. This was applied to the relevant exhaust outlets prior to commencing the next experimental run. The low density polyethylene sheet was secured in place by adjustable Velcro straps as shown in Figure 4.33, which sealed the ‘cling film’ against a foam strip, forming a temporary gas tight seal.

The low density polyethylene ‘cling film’ sheet was found to rupture when subjected to an instantaneous pressure rise of approximately 1.6 - 2kPa (16 - 20mb). This method was chosen primarily for safety reasons; however, it also produced highly consistent results and was not reliant on additional electrical or mechanical systems.

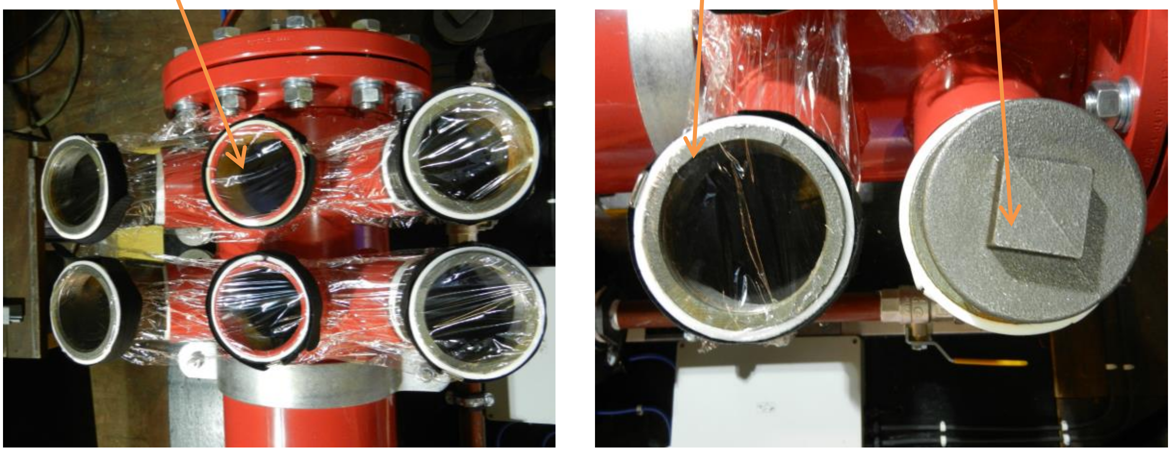

Figure 4.33 : Examples of exhaust outlets being sealed prior to ignition and explosion

4.5.4.5 Magnetic hinged outlet

Whilst the above system allows for the pressure relief and control of exhaust gases upstream of the flame front, another system was required to control the opposite end of the rig. Previous workers [39] have used flame propagation tubes with sealed ends to carry out similar experiments, however their work has focused on high speed flame propagation and the effects of hydrodynamic inverted bag type break-up of the water droplets in the spray.

For this current study a relatively slow moving flame of ≤30 m/s was required, whereby potential flame acceleration caused by compression of gases upstream or downstream of the flame was to be avoided. Additionally the rig needed to be gas tight at the point of filling with fuel gas-air, during the recirculation and mixing period and for an additional minute to allow the homogeneous mixture to become quiescent.

Figure 4.34 presents the original concept diagram for the magnetic hinged panel, complete with ignition interlock micro switch.

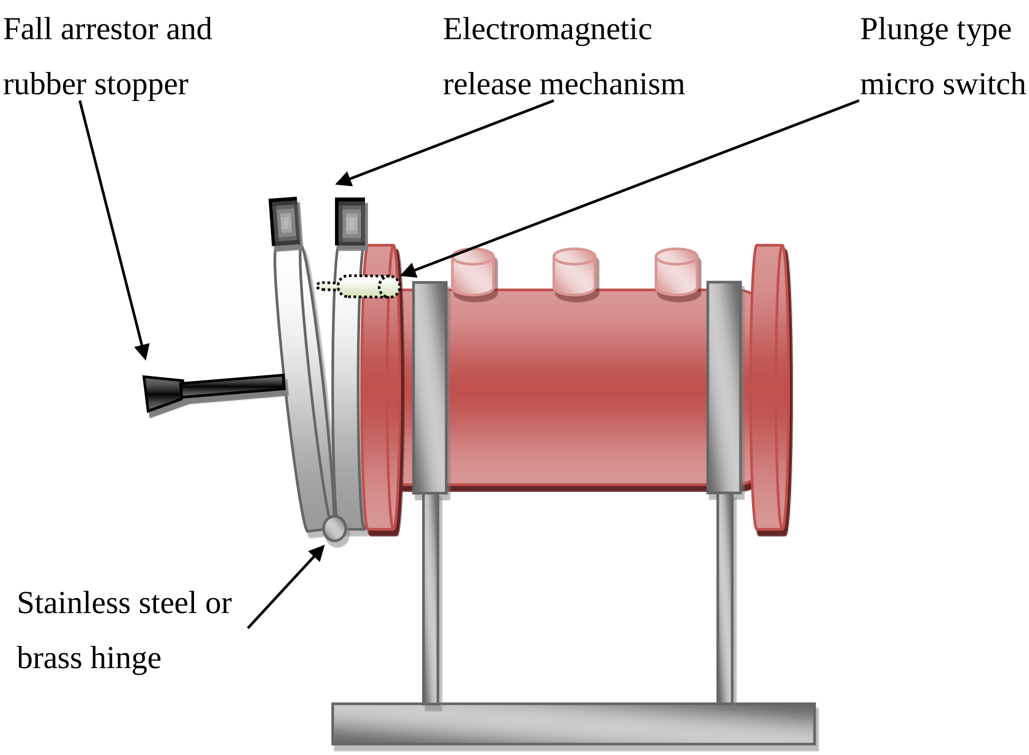

Figure 4.34 : Original design concept for magnetic hinged panel

A system was required that would open fully at the flame exit end of the rig, thus ensuring that the flame would be allowed to propagate from the ignition end, without any confinement ahead of the flame front.

The magnetic hinged outlet design concept previously shown in Figure 4.40 was adopted and fabricated, consisting of a ‘full bore’ hinged end plate controlled by an electromagnetic latching system, as pictured in Figure 4.35. The electromagnetic latching system was of the type normally associated with an automatic door entry system. The strength of the DC electromagnetic field, together with the area of the latching plates was sufficient to hold the end panel closed and gas tight.

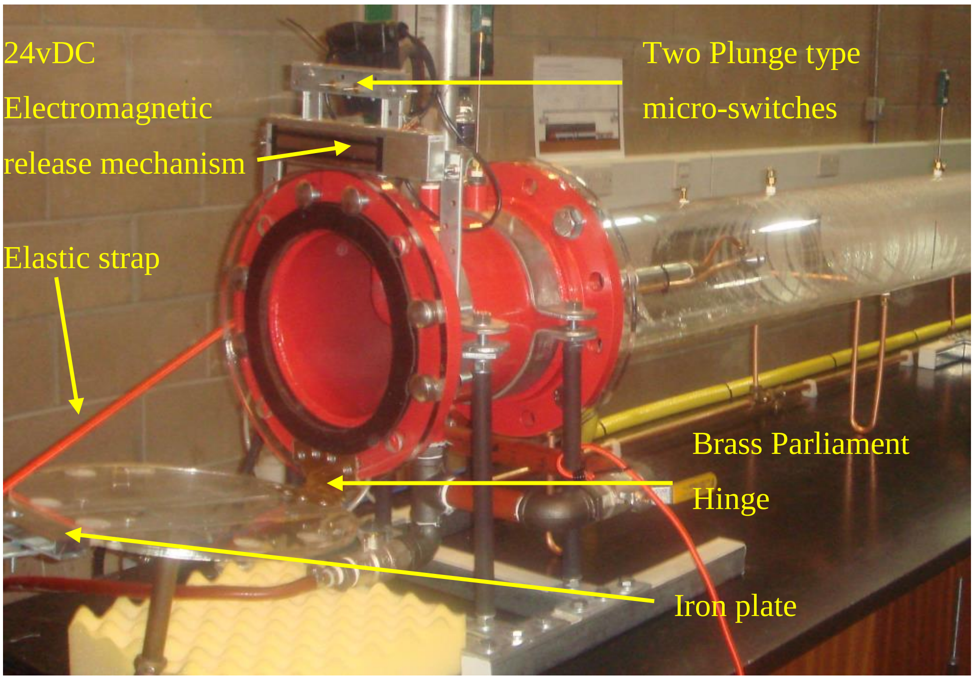

Figure 4.35 : Electromagnetic hinged panel and component parts

The magnetic latch was controlled by a 24v DC supply via a ‘time delay’ relay in the control panel. The hinged plate was ‘weighted’ by the mass of the iron plate that formed the other part of the latching system. The mass of the iron plate provided a controlled and consistent opening speed for the end plate. This action was dampened by an elastic strap, designed to prevent the panel from jerking the hinge and fixings each time it opened.

At the beginning of the filling period the latch was closed manually and energised by operating the primary key switch on the controller. The seal was checked for gas tightness with a Gascoseeker and leak detection spray as the rig was being filled.

To avoid ignition within the closed tube, the magnetic hinged panel was equipped with two ‘plunge type’ micro-switches. As the end plate is manually closed, the two micro-switches wired in series, switched over from their normally closed (NC) to their normally open position (NO). These switches formed part of the ignition system and spark generator interlock circuit. When the magnetic hinged panel was ‘de-latched’ by the timer relay, the panel began to open, assisted by the mass of the iron core counter weight. The two micro switches shown in Figure 4.36 were adjusted to operate only when the magnet had de-energised and the panel had begun to fall.

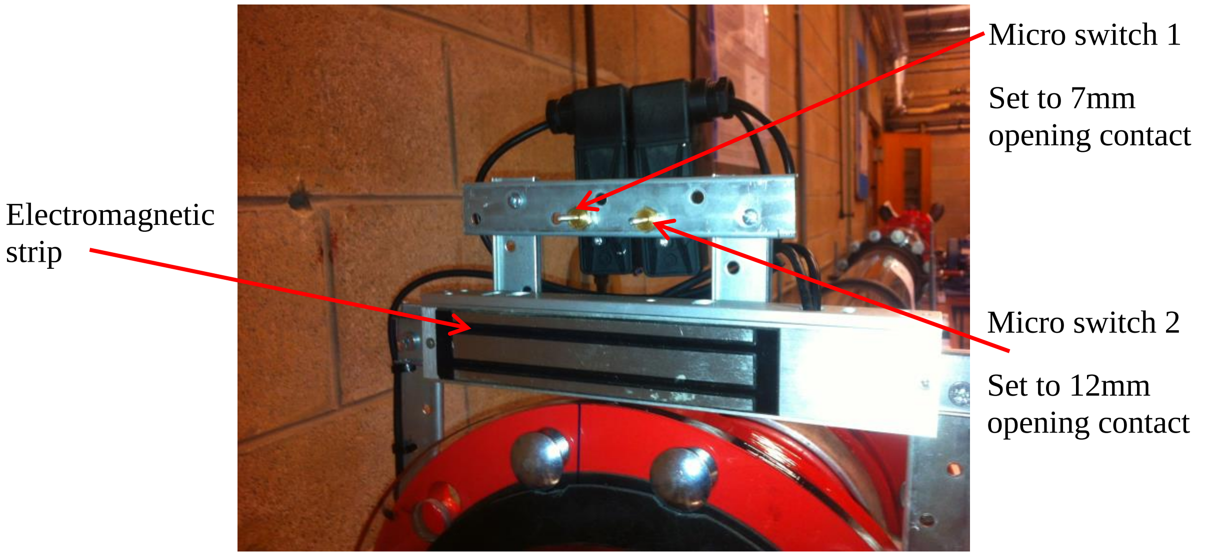

Figure 4.36 : End view of electromagnet and micro switches

The first micro-switch was designed to operate as the panel opened by approximately 7mm and second micro-switch then operated moments later, as the panel moved a further 5mm, simultaneously activating the ignition system. This original system, which successfully provides safe reliable opening of the exit end of the rig, has not been considered or utilised in any other water spray mitigation studies.

4.5.4.6 Atomiser induction pipe and manifold

To allow for a series of suitable atomisers to be enclosed and operated within the FPMR, a pressurised water induction pipe was included in the design as presented in Figure 4.37. This pipe allowed for Spill Return Atomisers (SRA) to be fixed securely and coaxially within the cross section of the gas stream.

Either single or multiple atomisers could be tested using a manifold arrangement. The atomiser injection pipe could also be extended or shortened with a series of stainless steel extension pieces.

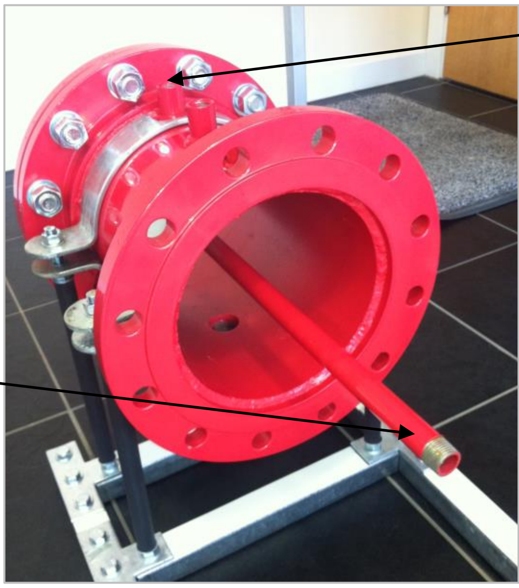

Figure 4.37 : Atomiser induction pipe

The steel atomiser induction pipe was initially made from 15mm (½ inch) galvanised mild steel pipe. From time to time the inner wall of this pipe would suffer from mild corrosion, particularly if left to stand for a week or so. This was due to the small amount of surplus water remaining in the pipe. The rig would then have to be flushed thoroughly for 10 minutes to ensure that there were no rust deposits in the system, as even minor particulates caused full or partial blockages in the outlet orifices of some of the SRA's.

To prevent this occurrence, the 15mm (½ inch) galvanised mild steel pipe was replaced with 15mm 316 stainless steel tube and fittings, which was pressure rated to 25MPa (250bar). Further information relating to the stainless steel tube arrangement, configuration and design are discussed in Section 4.5.5.

4.5.4.7 Pressurised water supply system

During the ‘cold trials’ phase of this work, three pumping systems were tested (see previous Section 4.2.1.1) and evaluated to ascertain their performance and characteristics and suitability for the ‘cold and hot trials’ work. The performance criteria set for the pumping system was tabulated previously in Section 4.2.1.1 and is listed below as a reminder:-

i. Output pressure – to supply a range of 50 – 150 bar (5 – 15 MPa)
ii. Output flow rate – to supply single and multiple SRA’s
iii. Suitable for hot and cold water
iv. Reliability and consistency of pressure/flow and good turndown ratio
v. Water storage capacity
vi. Time taken to achieve desired pressure from start up
vii. Contamination of water during ‘down time’
viii. Maintenance requirements
ix. Compatibility with control rig control system
x. Ease of installation and connection

Referring to Table 4.17, the custom built pump and storage system was adopted for all of the cold and hot trials in this program. It is worth noting that in order to provide the desired water pressures and flow rates required for this study, the individual components that made up this ‘custom built pump and storage system’ were sourced and assembled to produce an exclusive piece of equipment for this work.

Details	Specification
Manufacturer	Interpump
Model	W1208
Type	Ceramic plunger pump, oil bath crankcase lubrication
Flow rate	9 L/min
Rotation speed	1450 rpm
Outlet pressure	17MPa (140 bar) @ 9 L/min

Table 4.17 : Water pump specifications

Water storage was solved by adapting a 120 litre wheelie bin, which also provided portability of the pumping system. The motor and pump assembly was obtained from an industrial pressure washer supplies company and is shown in Figure 4.38.

The suitable general applications for the pressure washer pump were for hot and cold pressure washers, engine driven pressure washers, forecourt pressure washers, pressure test equipment, industrial cleaning products and special duty applications.

The excellent turndown ratio was achieved by the introduction of a bypass regulator. A bypass regulator maintains a high flow rate through the pump, whilst returning a low pressure flow back to the storage vessel.

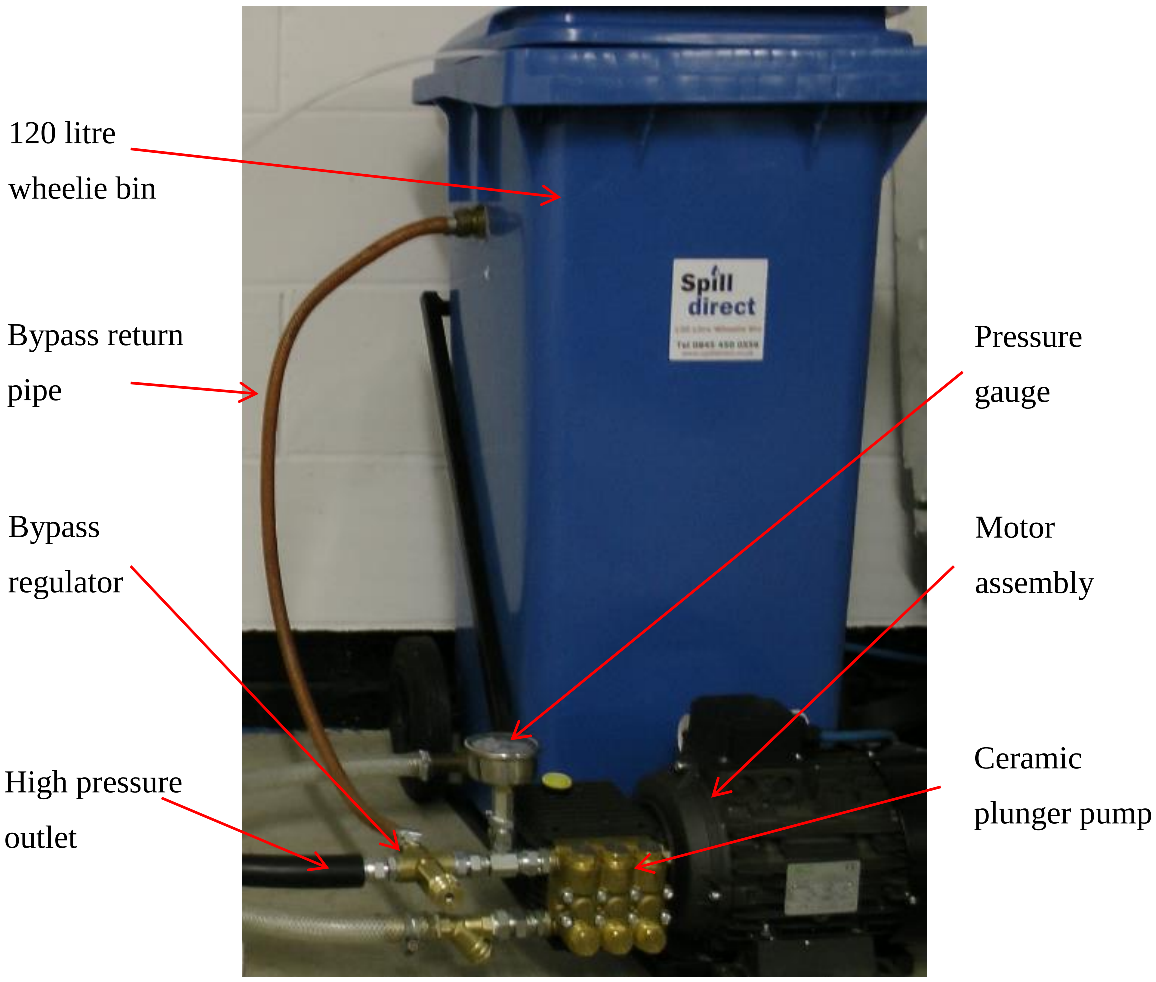

Figure 4.38 : Custom built water pump and storage system

4.5.4.8 Water drain and collection

The rig was fitted with three 10mm diameter drain connections complete with water traps in the clear PMMA section of the rig, as illustrated in Figure 4.39 and with a larger 22mm diameter drain and water trap in the steel driver section.

The drains were positioned to ensure that spray water was removed quickly and efficiently from inside of the rig. Collected water was then conveyed via drainage pipework and collected in a storage vessel below the rig.

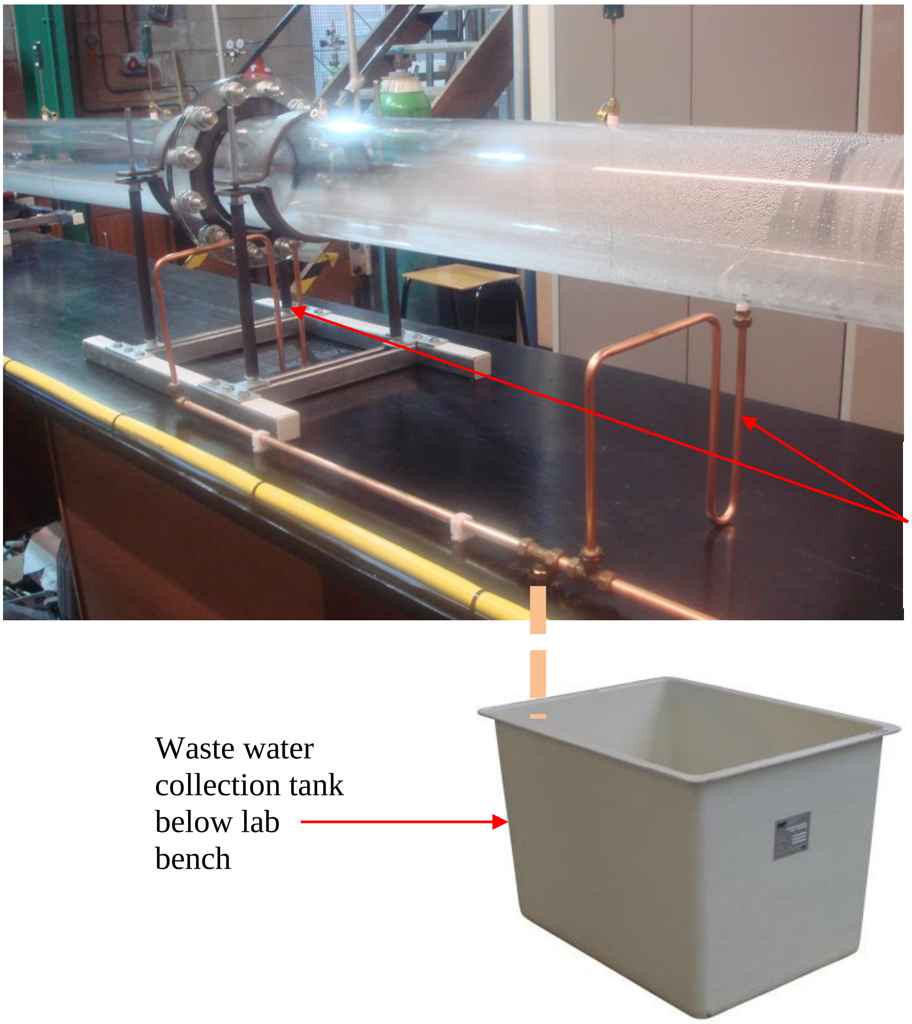

Figure 4.39 : The drainage piping system

4.5.4.9 Fuel gas-air supply system

The fuel gas-air supply system comprised of two 50 litre cylinders, one containing laboratory grade methane - N4.5 (see following Section) and the other containing industrial grade compressed air. Both cylinders were equipped with suitable connections, regulators and additional downstream isolation valves.

The fuel gas and air supplies were connected via two rotameters to the inlet connections in the driver section of the rig, each with additional isolation valves.

The rotameters were used in conjunction with a stopwatch to quantify the gases flowing into the rig. Following several 'filling' trials where a number of flow rates were tested, a convenient flow rate of 200 L/min which provided consistency and reliability was set.

Table 4.18 details an indicative list of rig 'fill' times. This was used primarily as a guide, whereby the final concentration was quantified following the recirculation cycle by direct measurement using calibrated GMI Gascoseeker, as discussed in Section 4.6.2.

Methane-air (%)	Flow rate (L/min)	Duration (min:sec)
6	200	02:25
7	200	02:45
8	200	03:00
9	200	03:25
10	200	03:40
11	200	04:05

Table 4.18 : Approximate fill times and 'gas in air' percentages (Gascoseeker)

The gas cylinders and regulators were supplied and certificated by BOC (see also next Section). Methane cylinders were stored externally and only brought into the laboratory during the trials.

Valves and regulators were visually inspected prior to connection and then tested using leak detection spray.

4.5.4.10 Gas composition and quality

For the main part of this program standard industrial grade compressed air was used as the oxidant and high purity methane was selected as the fuel gas, for convenient comparison and reference with past studies. High purity methane was also chosen for the main part of these trials because of its relatively low exothermicity. Although a handful of supplementary propane trials were also carried out, the confinement of the laboratory limited the use of other gases. Chapter 7 provides recommendations for further research with other alkane gases and also alkenes and alkynes.

Pure gases are classified by grade using the following system:

Example 1 N3.0

The first digit of the classification indicates the number of ‘nines purity’ (for example, N3.0 = 99.9% purity)

Example 2 N4.6

The second digit is the number following the last nine (for example N4.6 has a guaranteed minimum purity of 99.996% and a corresponding maximum impurity level of 0.004% or 40ppm).

The methane used in these experiments was classified as ‘Laboratory Grade Methane’ with a purity of N4.5. Therefore, this gas has minimum purity value of 99.995% and a maximum impurity value of 0.005% or 50ppm.

The standard industrial grade compressed air (non-medical grade) using in these trials is generally used in industry for the following applications:

i. Brazing and hard soldering
ii. Applications such as plasma-cutting
iii. Metallurgical processes such as die-casting and blast furnaces
iv. As an alternative to an air compressor e.g. to drive pneumatic drills etc.

The methane and air data sheets, together with certificates of purity can be found in Appendix 3 and 4 on the accompanying CD of Appendices (Volume III).

4.5.4.11 Electrical sequence controller system

To carry out these explosion mitigation trials, a complex and systematic control system was required in conjunction with a suitable procedure and sequence of operations. To control the systematic sequence of operations and to ensure safety, a unique control system, shown in Figure 4.48 was also designed and built to manage the essential automated operations relating to the FPMR. Safety interlocks were also included in the design to prevent the rig from being 'fired' prematurely or accidentally.

As the laboratory was occasionally used by other students, a bolt lock and micro-switch was fitted to the laboratory door. The micro-switch was connected in series with the 'primary key switch', thus preventing any operations with the lab door open. If the door was opened during testing, the hinged panel would de-magnetise and open, thus leaving ignition circuits without power. The sequence controller wiring diagram is illustrated in Appendix 7.

Primary key
All 230V and 24V circuits are controlled by this key. The laboratory door switch is also in series with this.

Booster key
This key controls the booster pump via a relay. This key must be turned off, to allow power to the ignition key

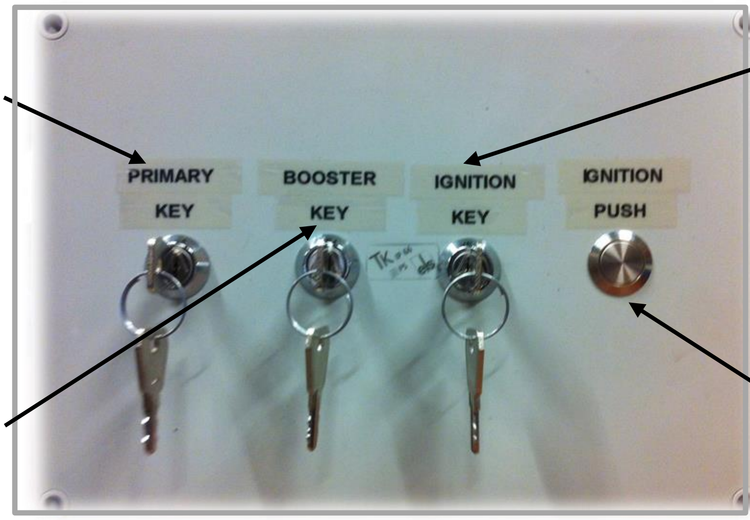

Ignition key
This key supplies power to the ignition relay switches and ignition push button

Ignition push
This button is depressed for a moment, operating the ignition relay coil and timer relay coil

Figure 4.40: Sequence controller illustrating operator keys and ignition button

The electrical sequence controller was used to interlock all of the essential electrical devices on the rig. A number of manual sequential actions were also devised to operate the rig safely, whereby a *'safe system of operations'* was provided (see Section 4.7.1).

The next Section provides the design, methodology and rationale for various SRA configurations and arrangements used in the hot trials.

4.5.5 Atomiser configuration : Design, methodology and rationale

To maximise the quantity and variation of experimental hot trials, a number of single and multiple atomiser configurations were chosen. The following Section deals with the equipment specification, methodology and the rational for choosing each of the arrangements. The atomiser provisions were:-

i. Single SRA in counter flow (C/F) with the flame direction
ii. Single SRA in parallel flow (P/F) with the flame direction
iii. Overlapping SRA's in parallel flow (P/F) with the flame direction
iv. Multiple SRA's in cross flow (X/F) with the flame direction

As discussed previously, the original water induction tube in the rig was made from galvanised mild steel pipe, complete with 150mm extension pieces to vary the atomiser position. The galvanised mild steel pipe was proven to be very problematic, as mild corrosion occurred within the pipe during dormant periods, even during periods as short as 24 hours. As trials were resumed, the iron oxide particles were scrubbed from the inner pipe wall by the high pressure water supply, resulting in nuisance blockage of the exit and spill orifices. To overcome this, high pressure 316 stainless steel tube and fittings were used to fabricate the various configurations.

4.5.5.1 Single SRA in counter flow (C/F) with the flame

The equipment and position within the FPMR comprised of:

- Single SRA in counter flow configuration
- 15mm 316 stainless steel tube and fittings
- 8mm 316 stainless steel tube and fittings
- Length of tube from water inlet to SRA exit orifice : 1475mm
- Distance from SRA exit orifice to ignition electrodes : 4675mm

Methodology

The counter flow configuration was set up with the SRA mounted at the end of the stainless water feed tube, which was adjusted and secured centrally in the FPMR at a distance of 4675mm from the ignition electrodes. This set up, which is shown in Figure 4.41 was installed within the FPMR and was rigorously tested using a range of water pressures prior to any hot trials.

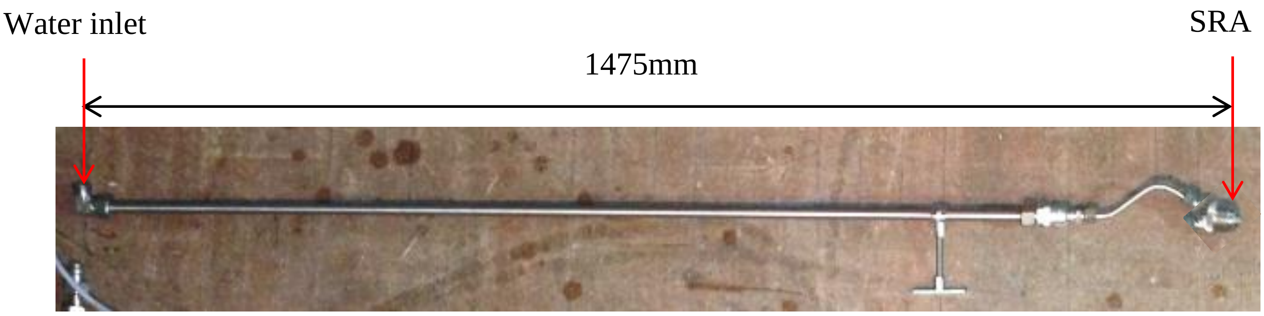

Figure 4.41 : Single SRA in counter flow (C/F) configuration

During the hot trials, SRA configurations A, B, and C (see previous Table 4.4) were supplied with deionised water at an operating pressure of 13MPa (130bar). Each of the SRA configurations were subjected to explosion mitigation trials in methane-air mixtures of E.R. (ϕ) 0.61, 0.72, 0.95, 1.06. The results of all of the hot trials can found in Chapter 5 and Appendix 9.

Rationale

The use of atomisers in counter flow (C/F) configuration with respect to the propagating flame was chosen because:-

a) The momentum from the spray was expected to cause a disturbance in the unburned mixture, which in turn may produce an increase in flame speed.
b) The impact velocity of the spray and flame in counter flow will be approximately the sum of the spray velocity and flame speed (see also Chapter 5, Results and discussions). This will have an overwhelming effect on the residence times of the droplets within the reaction zone of the flame. Residence times in counter flow will be substantially reduced, when compared to a static droplet entering the flame and therefore heat transfer will also be minimised.

4.5.5.2 Single SRA in parallel flow (P/F) with the flame

The equipment and position within the FPMR comprised of:

- Figure 4.42 : Single SRA in parallel flow (P/F) with flame
- 15mm 316 stainless steel tube and fittings
- 8mm 316 stainless steel tube and fittings
- Length of tube from water inlet to SRA exit orifice : 1900mm
- Distance from SRA exit orifice to ignition electrodes : 4250mm

Methodology

The parallel flow configuration was set up with the SRA mounted at the end of the stainless water feed tube, which was adjusted and secured centrally in the explosion and mitigation tube at a distance of 4250mm from the ignition electrodes. This set up, as shown in Figure 4.42 was installed within the FPMR and was subsequently thoroughly tested through a range of pressures prior the hot trials.

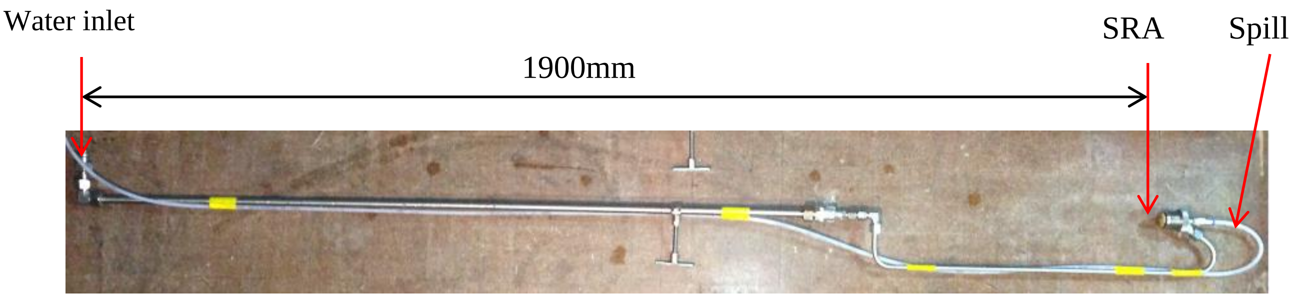

Figure 4.42 : Single SRA in parallel flow (P/F) with flame

In the ‘hot trials’, SRA configurations A, B, and C were supplied with deionised water at an operating pressure of 13MPa (130bar). Each of the SRA configurations were subjected to explosion mitigation trials in methane-air mixtures of E.R. (ϕ) 0.61, 0.72, 0.95, 1.06). The results of all of the ‘hot trials’ can found in Chapter 5 and Appendix 9.

Rationale

The use of SRA’s in parallel flow configuration with respect to the propagating flame appears to be unique and was not reported in any of the literature reviewed in Chapter 3. Parallel flow sprays are more likely to produce a higher mitigation success rate when compared to the corresponding counter flow sprays.

The reasons for this are twofold:-

a) As with the C/F configuration, the momentum from the spray is expected to cause a disturbance in the unburned mixture, which in turn may produce an increase in flame speed. However, the percentage increase across the sprays is anticipated to be less than that resulting from the C/F configuration.
b) The impact velocity of the spray and flame in parallel flow will be approximately the difference between spray velocity and flame speed. This would have a positive effect on the residence times of the droplets within the reaction zone of the flame. Residence times will be significantly increased when compared to static or counter flow droplets entering the flame and therefore heat transfer will be maximised, as opposed to configurations with C/F single SRA's.

4.5.5.3 Overlapping SRA's in parallel flow (P/F) with the flame

The equipment and position within the FPMR comprised of:

- Figure 4.43 : Parallel flow multiple overlapping SRA manifold configuration
- 15mm 316 stainless steel tube and fittings
- 8mm 316 stainless radial steel tube and fittings
- Distance from water inlet to SRA exit orifice : 3150mm
- Distance from ignition to SRA outlet : 3000mm

Methodology

The parallel flow multiple overlapping SRA manifold shown in Figure 4.43, was fabricated to permit the simultaneous operation of two SRA's. The radial manifold was designed to fit centrally within the explosion and mitigation tube at a distance of 3000mm from the ignition electrodes.

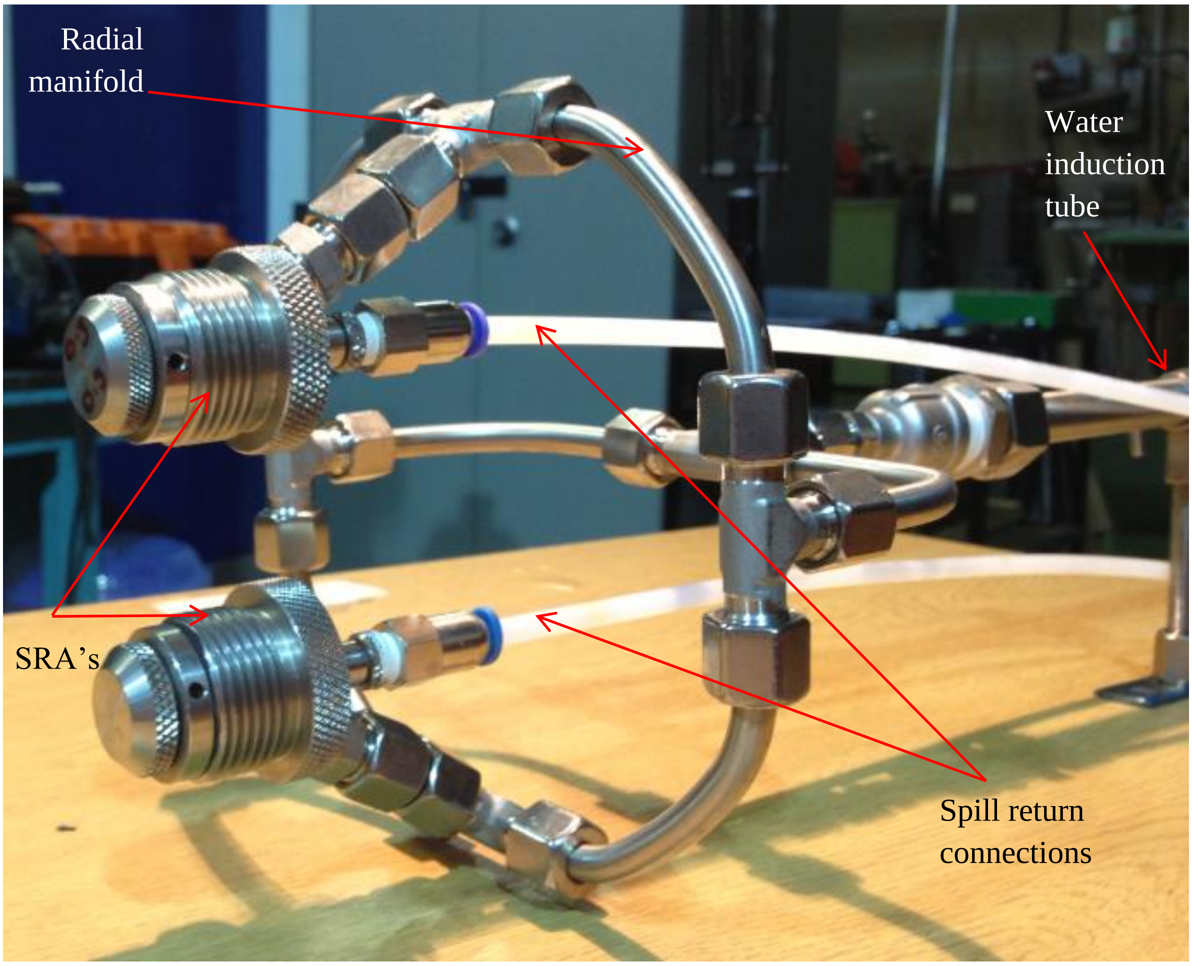

Figure 4.43 : Parallel flow multiple overlapping SRA manifold configuration

The parallel flow multiple overlapping SRA manifold configuration was set up with the SRA's mounted on the stainless steel radial manifold, which was adjusted and secured centrally in the explosion and mitigation tube at a distance of 3000mm from the ignition electrodes, as illustrated below in Figure 4.44.

This set up was installed within the FPMR and was systematically assessed with a range of water pressures, prior to the hot trials.

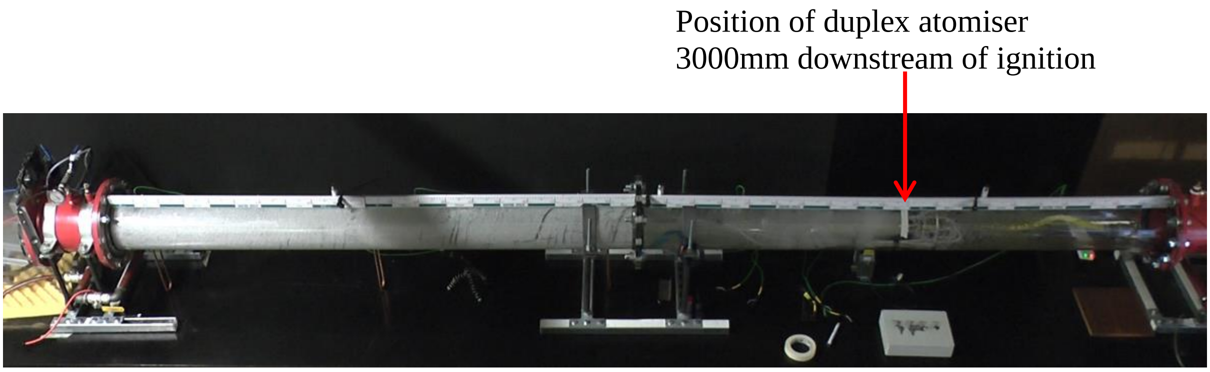

Figure 4.44 : Position of multiple overlapping SRA's in explosion and mitigation tube

During the hot trials SRA configurations Type B and C (shown previously in Table 4.4) were supplied with deionised water at an operating pressure of 13MPa (130bar). Each of the SRA configurations were subjected to explosion mitigation trials in methane-air mixtures of E.R. (ϕ) 0.61, 0.72, 0.95, 1.06). The results of all of the 'hot trials' can found in Chapter 5 and Appendix 9.

Rationale

By increasing the number of atomisers, there will be a global increase in liquid volume flux. Studies by previous authors (see previous Table 3.6) demonstrate total disagreement relating to the minimum volume flux required to instigate mitigation. One of the main reasons for this is that previous authors have used a variety of different droplet sizes, as revealed previously in Table 3.6, giving rise to differences in reported results of at least one order of magnitude.

The multiple overlapping SRA manifold configurations will only be tested in parallel flow with the flame, as it was felt that the potential level of disturbance resulting from the motion of the sprays would almost certainly translate into a dramatic increase in flame speed.

4.5.5.4 Multiple SRA's in cross flow (X/F) with the flame

The equipment and position within FPMR tube consisted of:

- Atomiser 'boss' manufacture and installation
- Four atomiser 'boss' connections printer on a 3D printer
- Tapped out with 1 inch BSP parallel thread
- Secured and sealed to the main tube with 'o' rings, nuts and bolts
- Distance from water inlet to centre of sprays : 3150mm
- Distance from ignition to centre of sprays : 3000mm

Methodology

The previous SRA arrangements discussed in this Chapter were all classified as 'in-tube' applications, in which single or multiple SRA configurations are installed centrally within the explosion and mitigation tube, in either counter, or parallel flow with the propagating flame.

To assess the mitigation success of cross flow atomisers, the SRA's had to be mounted externally. This was due to the physical size of the SRA's and the need to supply them with a water feed and a spill exit tube.

To mount the atomisers externally, a unique connection system was required that would facilitate the installation of up to four atomisers, whereby several options were considered and tested. The method adopted in this case was an interface component between the external pipe wall and the atomiser body, known as a 'boss'.

To create a gas and water tight interface component Solid Works software was used to design and scale the 'boss' fitting, which was then printed using a 3D printer and tapped out with a BSP thread, as shown in Figures 4.45 and 4.46. Additionally the water feed and spill return connections had to be adapted via an external modular manifold array, complete with individual isolation valves.

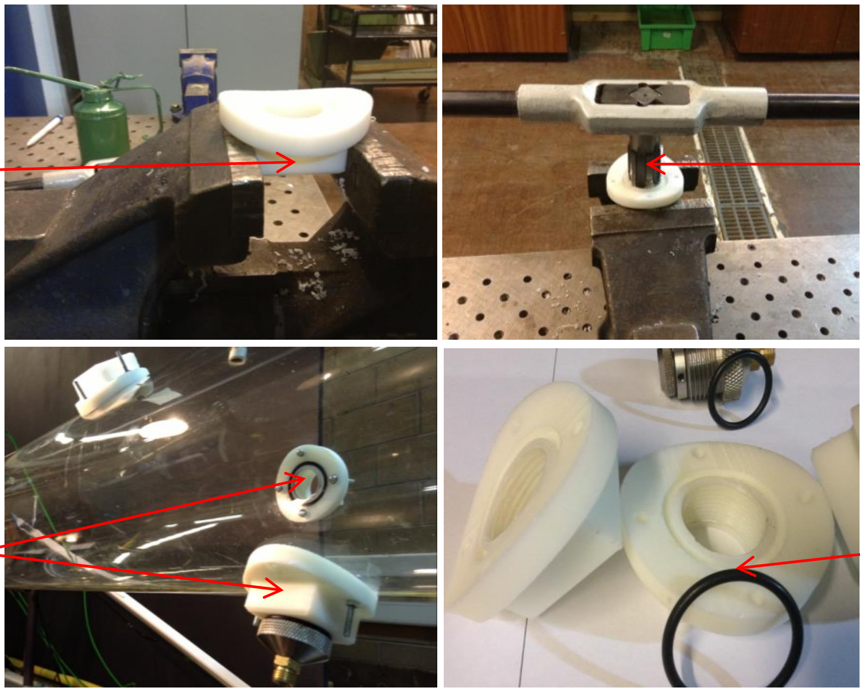

Figure 4.45 : Atomiser 'boss' manufacture and installation

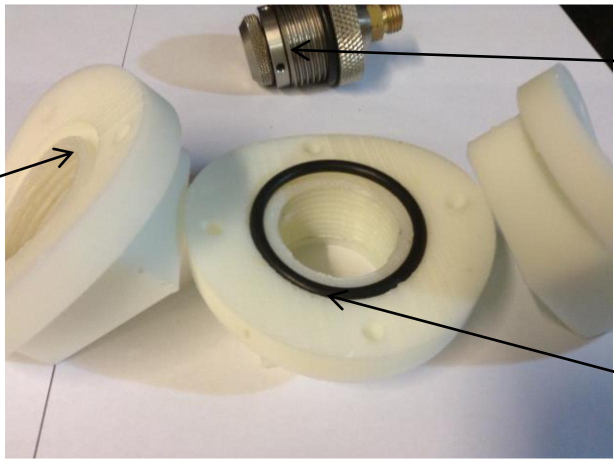

Figure 4.46 : Atomiser 'bosses' made on 3D printer

The bosses were separated by a linear distance of 105mm and circumferentially by 120°. This arrangement was initially modelled using 3D graphics software, presented in Figure 4.47 to ensure that the sprays were not overlapping or impinging on each other.

Figure 4.48 shows the final set up of the externally mounted cross flow SRA's and the water supply manifold, including pressure gauge and spill return connections.

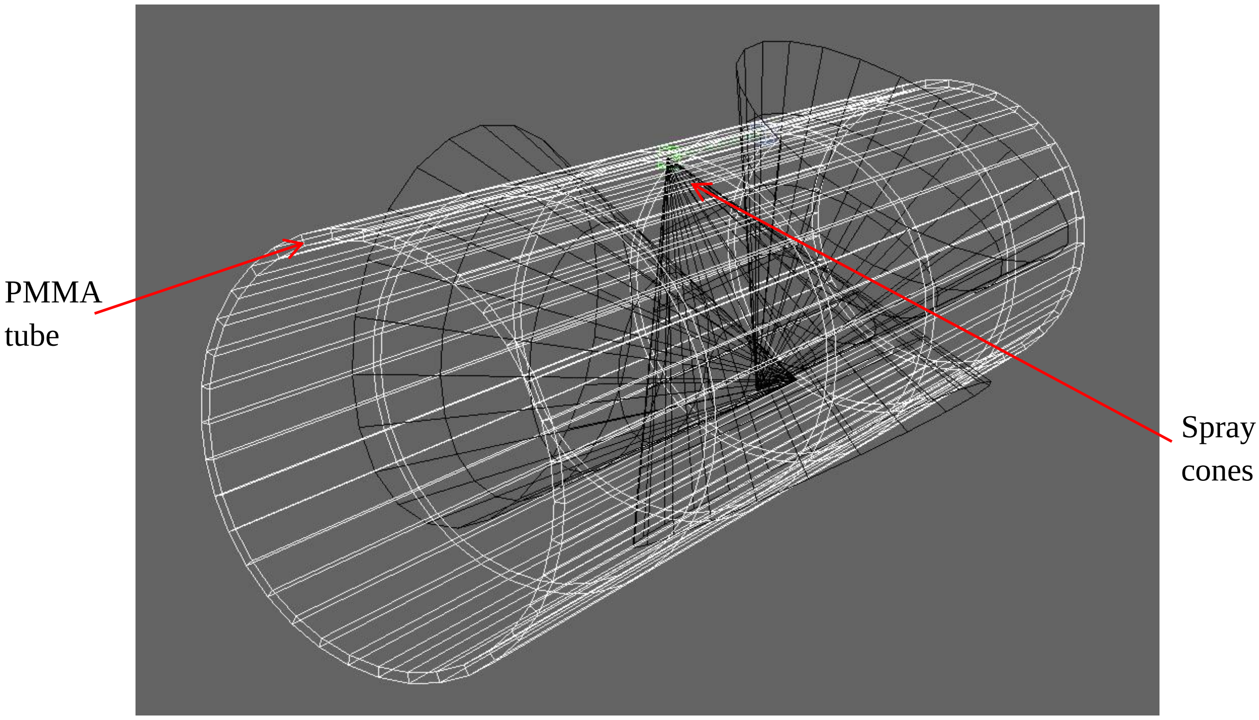

Figure 4.47 : 3D graphic of sprays within tube

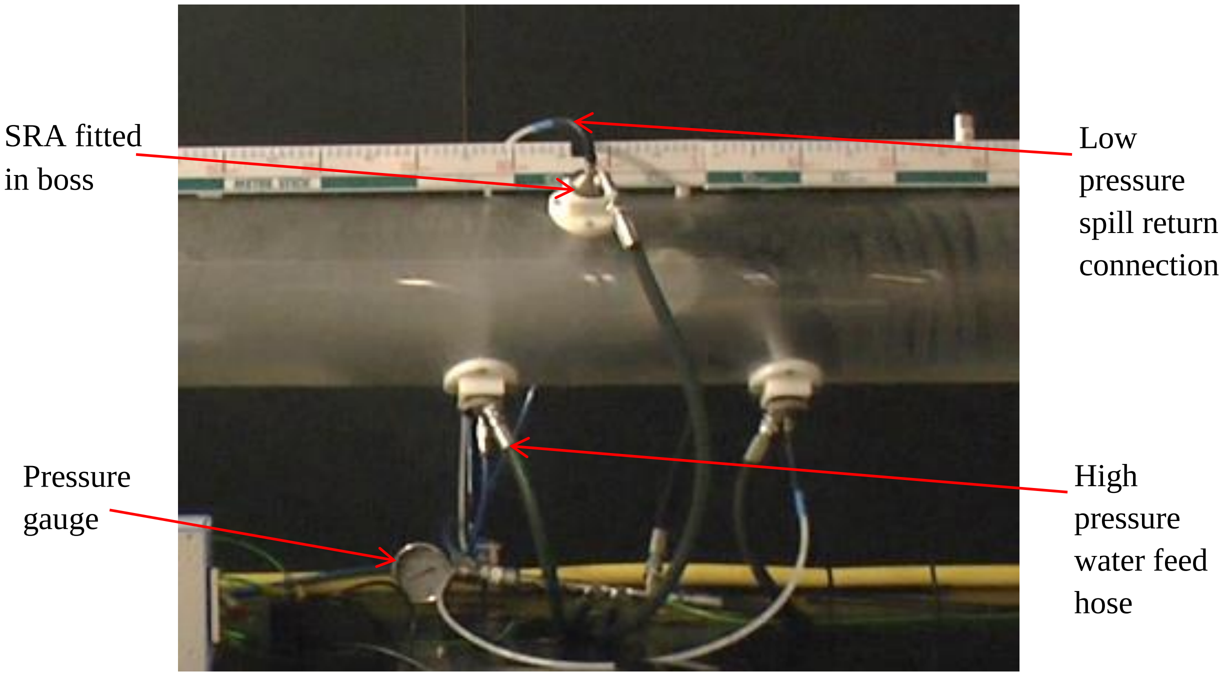

Figure 4.48 : External atomisers and water supply manifold

The next Section will provide the imaging techniques that were adopted for qualitative analysis during the hot trial investigations.

4.6 Imaging techniques

The qualitative analysis of images obtained during the hot trials was of great significance. Supported by corresponding quantitative data, this enables the gaining of a full understanding of the mitigation process, in terms of:-

i. No mitigation
ii. Partial mitigation
iii. Full mitigation

The subsequent representations show typical processed images from the hot trials whereby the flame is initially shown upstream of the sprays, followed by three additional images taken at 20ms intervals.

In Figure 4.49 the flame is shown passing through the region of the sprays and continuing to propagate downstream (no mitigation). In Figure 4.50 the flame area is shown to reduce through the region of the sprays, but continues to propagate downstream (partial mitigation). Additionally, Figure 4.51 shows that the flame has been completely extinguished in the spray region (full mitigation). Further details, together with all of the results are discussed in Chapter 5 and Appendix 9.

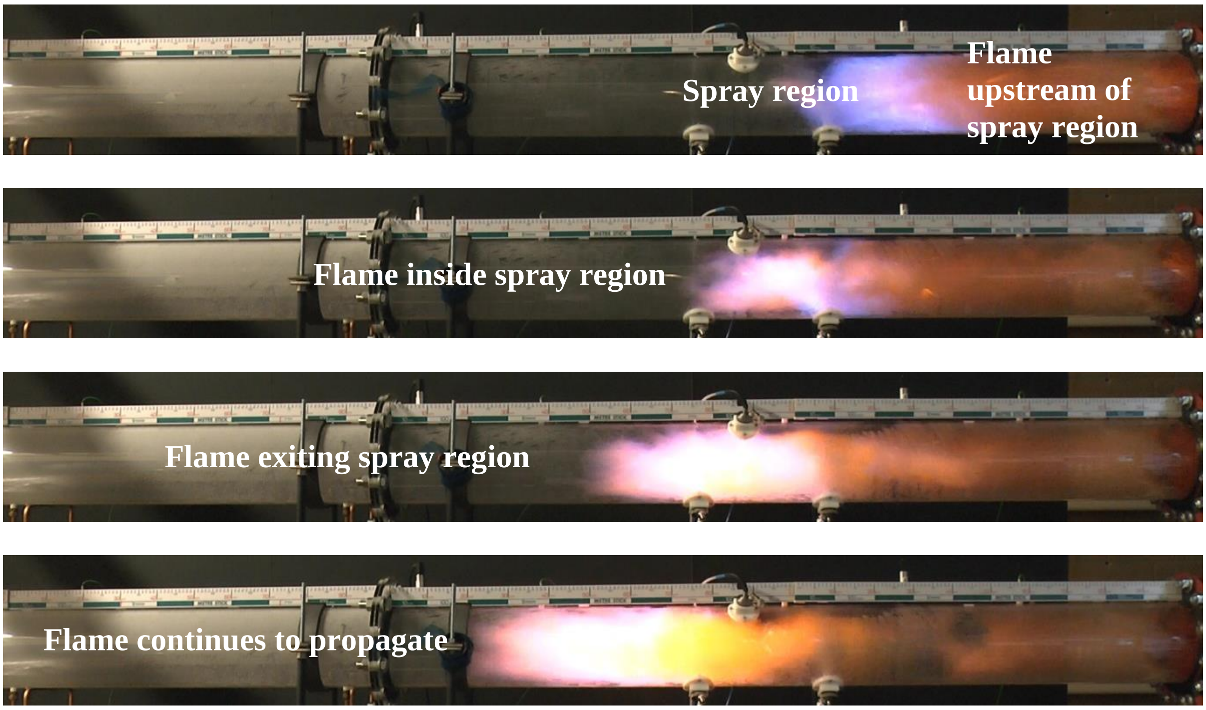

Figure 4.49 : Characteristic images showing ‘no mitigation’

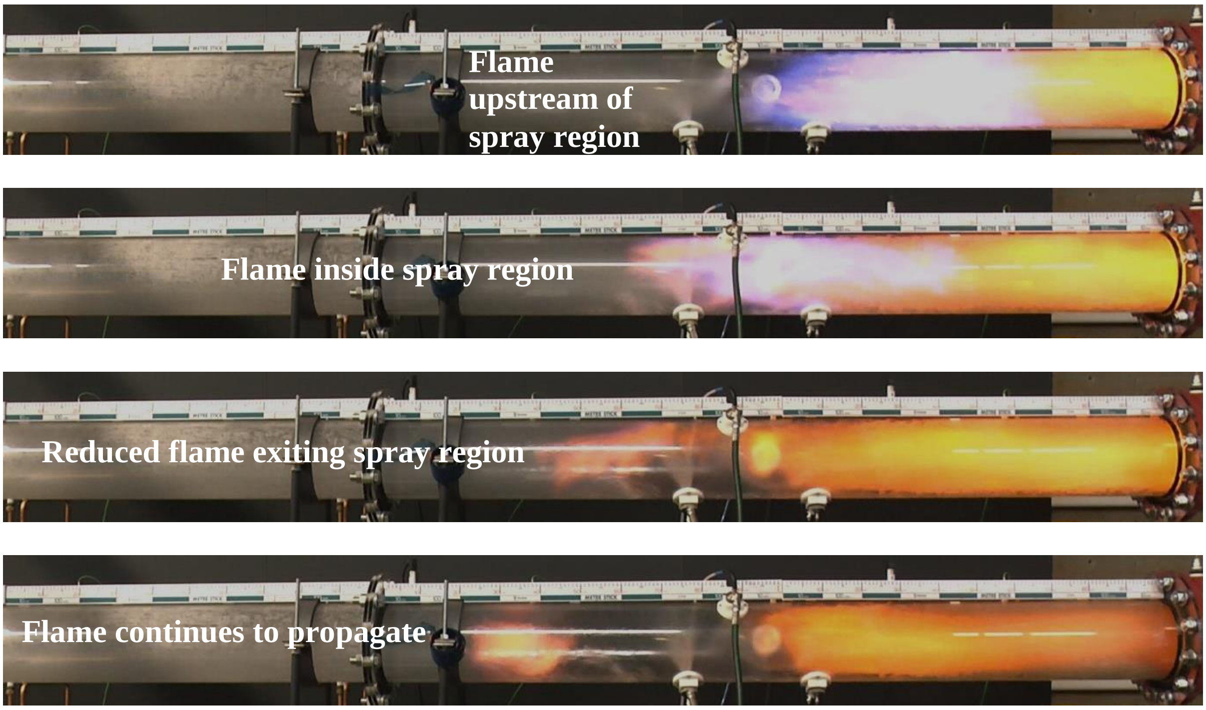

Figure 4.50 : Distinctive images showing ‘partial mitigation’

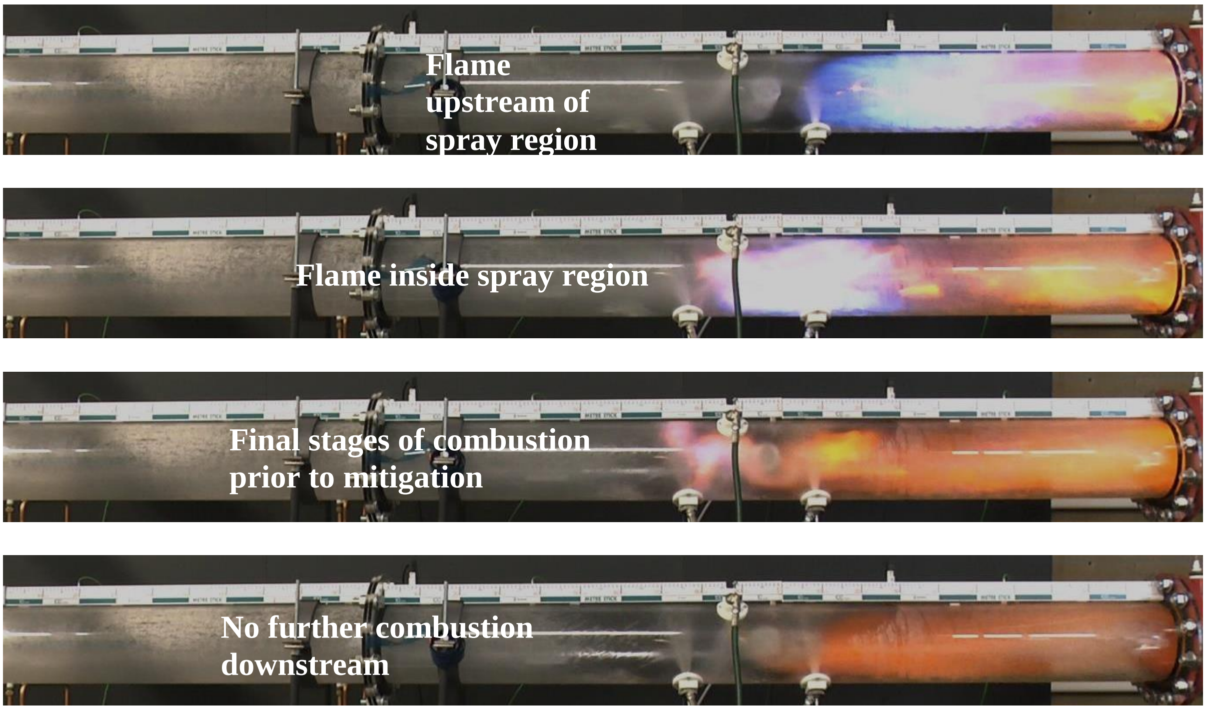

Figure 4.51 : Typical images depicting ‘full mitigation’

4.6.1 Still camera

A Canon EOS digital high resolution (HR) SLR camera used for still image photography during the cold trials, was also used here in the hot trials in capturing ‘still’ HR images for qualitative analysis. This was previously discussed and illustrated in in Section 4.2.1.4.

4.6.2 High definition (HD) video camera

A high definition (HD) Panasonic HDC-TM900 Camcorder, as shown in Figure 4.52 was used to capture all of the ‘hot trials’. The 50 frames per second (fps) HD video was then reviewed to assess flame behaviour and also to determine the average flame speed throughout the clear section of the FPMR.

Figure 4.52 : Panasonic HDC-TM900 Camcorder [81]

The camcorder has an optical image stabilisation system which further improves image clarity and all of the images are shot in full-HD (1920 x 1080) for either wide or zoom shots. Images were recorded from equal distances to ensure constancy and reliability.

All of the HD video images were time-code edited using Adobe Premiere Pro CS6. This software was essential to permit ‘joggling’ between frames to assess the average flame speeds. A Griffin PowerMate USB Controller, as revealed in Figure 4.53 was used to control the frame by frame analysis. Using still images of the flame from Adobe Premiere Pro CS6 and Adobe Photoshop CS4, the images were scaled using the pixel measurement tool. The Adobe pixel measurement tool provided consistent measurements for determining average flame speeds.

Figure 4.53 : The Griffin PowerMate USB Controller [82]

4.6.8 Image analysis by high speed video camera

A Redlake Motion Pro HS-3, presented in Figure 4.54 was used to record high-speed imagery of the sprays interacting with the propagating flame. A 14mm lens was used to record the high speed imagery with the frame rate set to 3000 fps and the resolution set to 1280 x 1024 during all tests.

Figure 4.54 : Redlake Motion Pro HS-3/3000 fps / resolution 1280 x 1024 [51]

All imagery was obtained from equal distances for each series of trials to ensure constancy and reliability, which was then stored for post processing (see following Section 4.7.1).

4.7 Procedures and data processing : Hot trials

4.7.1 Procedures

Figure 4.55 shows a flow diagram of the Flame Propagation and Mitigation Rig (FPMR) and experimental set up used throughout the hot trials.

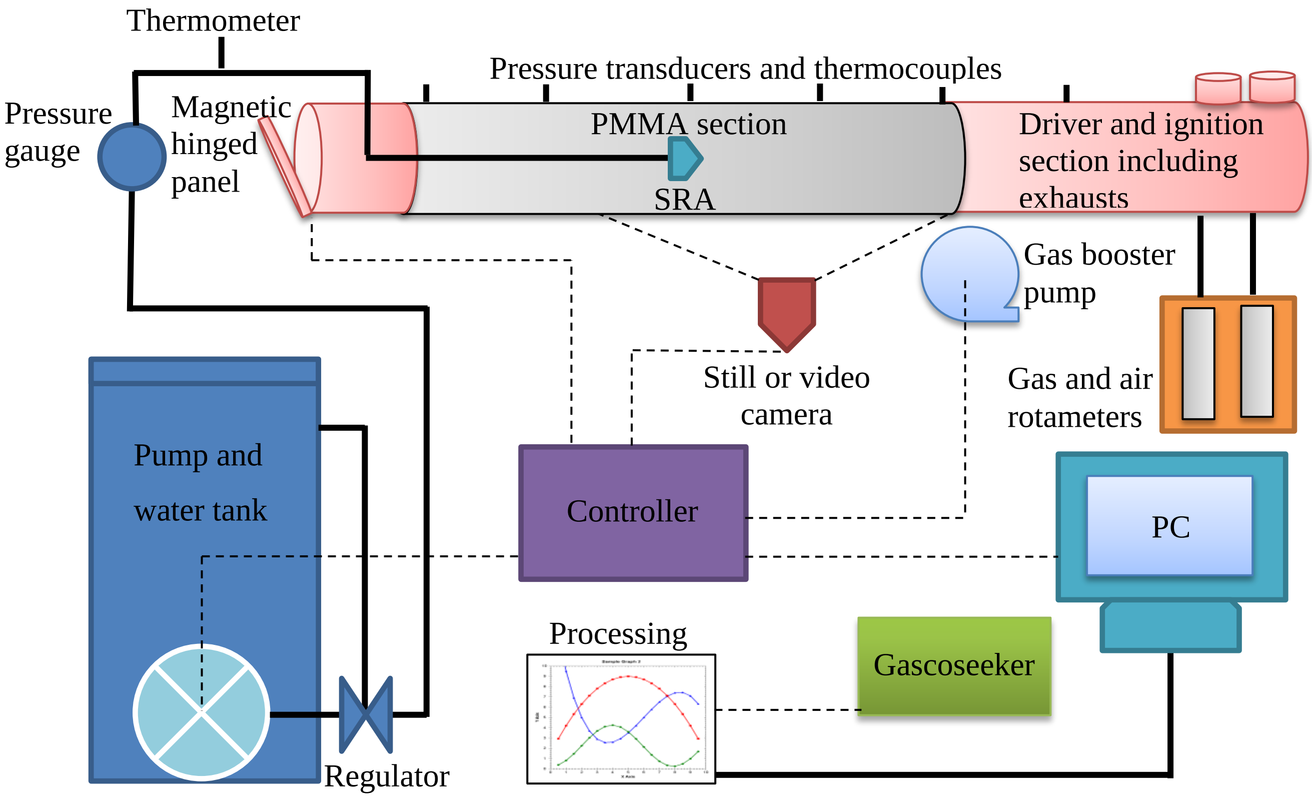

Figure 4.55 : Illustrated flow diagram for hot trials

During this research program, in excess of 250 'hot trials' were conducted utilising the numerous manifestations of unique features of the explosion and mitigation rig. To ensure that consistent quantitative and qualitative data and imagery were acquired from each experimental trial, the following procedure was adopted throughout.

i. One of the first considerations was the laboratory lighting, as it was important to eliminate as much reflection from the clear PMMA section as possible. This was achieved by turning off non-essential lighting and ensuring that the whole of the 4m PMMA section was treated internally with hydrophobic spray and externally with anti-reflecting matt spray. On a small number of occasions natural light did cause a reflective nuisance on the outlet end of the rig, however this was during the cross flow trials, whereby all of the imagery was being gathered towards the ignition end of the PMMA section.

ii. Following the setting up of the ideal lighting conditions, the laboratory and whole of rig was visually checked for safety, which included a periodic pressure test to ensure gas tightness of the fuel gas carrying components, as part of the risk assessment control measures. Any defects were identified and repaired where necessary.

iii. To ensure safety, other than the author and the Laboratory Technician, there were no other personnel permitted in the laboratory for the subsequent operations. To ensure this, the laboratory door was equipped with a micro switch which formed part of the interlock circuit for the controller. Additionally the door was 'bolted' on the inside and signs placed outside the laboratory warning that explosion events were being conducted within. An additional emergency exit door was situated in the laboratory, which led directly to outside.

iv. Where services were not already connected to the rig, fuel gas, air, water and electricity were connected and verified for leakage and safety. Before any further preparations the control system was checked for operation. This involved testing the operation of the magnetic hinged panel, booster pump and gas meter.

v. Additionally all data and imagery acquisition hardware and software, as discussed in Section 4.6 was checked for operation in accordance with manufacturer's instructions, this included the Gascoseeker, thermocouples, pressure transducers, iNet data acquisition system and accompanying PC, the high definition (HD) still image camera and the HD video camera.

vi. Following all successive safety checks and equipment verification checks, the FPMR was prepared for the subsequent trial. Initially the 'primary key' was operated on the sequence controller and the magnetic hinged panel was manually closed, which was held in place by the electromagnet. At the opposite end of the rig the exhaust outlets were sealed using 'cling film' and Velcro straps. Although the exhaust outlets would also accommodate a fixed permanent 'plug', this configuration was not desirable for the main Section of this study.

vii. With the ends of the rig now sealed, the methane and air could be introduced via the respectful rotameters for the appropriate time period to achieve the desired mixture. Following the introduction of the methane and air, the 'booster' key was operated and the mixture was circulated through the rig and parallel bypass stream. The gas meter was observed until approximately 10 volumes of the rig had been passed, this was estimated to be $2.2m^3$. The 'booster' key was then switched off and the methane and air supplies were isolated.

viii. All of the data and imagery acquisition hardware and software were then activated and the homogeneous mixture was allowed to stabilise for one minute to ensure it became quiescent. The Gascoseeker was then used to verify the methane-air percentages, which were recorded on the checklist shown later in Table 4.21.

ix. Prior to operation of the 'ignition' key and subsequent depression of the ignition button, a verbal description of the configuration was relayed to the video camera, this included:

a) Methane-air percentage
b) SRA configuration i.e. counter, parallel or cross flow
c) Water pump operating pressure
d) Water temperature

This audible description was used to catalogue video imagery, whereby each file could then be renamed with confidence.

x. When the ignition push button was depressed the water pump was immediately powered and began to supply water to the atomiser(s). The ignition spark generator transformer was not energised for a further seven seconds. Following several earlier commissioning trials, seven seconds was found to be the optimum time to allow the sprays to fully develop, prior to the activation of the ignition spark.

xi. Following the ignition of the combustible mixture and subsequent explosion / mitigation event, all services were isolated and the rig was allowed to vent naturally for 15 minutes. During this period all electronic data and imagery files were checked for content and renamed with respect to:-

- Methane-air percentage
- SRA configuration i.e. counter, parallel or cross flow
- Water pump operating pressure
- Water temperature
- Date of test

xii. The gas recirculation system was then purged by introducing air from a cylinder and regulator at one end then expelled via a temporary connection at the other end, direct to outside atmosphere through an appropriate purge hose. Both the main explosion propagation tube and gas recirculation system where then tested for methane-air concentrations. A value of ≤5% LFL was deemed to be satisfactory.

The 'safe operations' flow diagram shown in Figure 4.56 provides a summary of the procedures listed above, which were carried out throughout the hot trials.

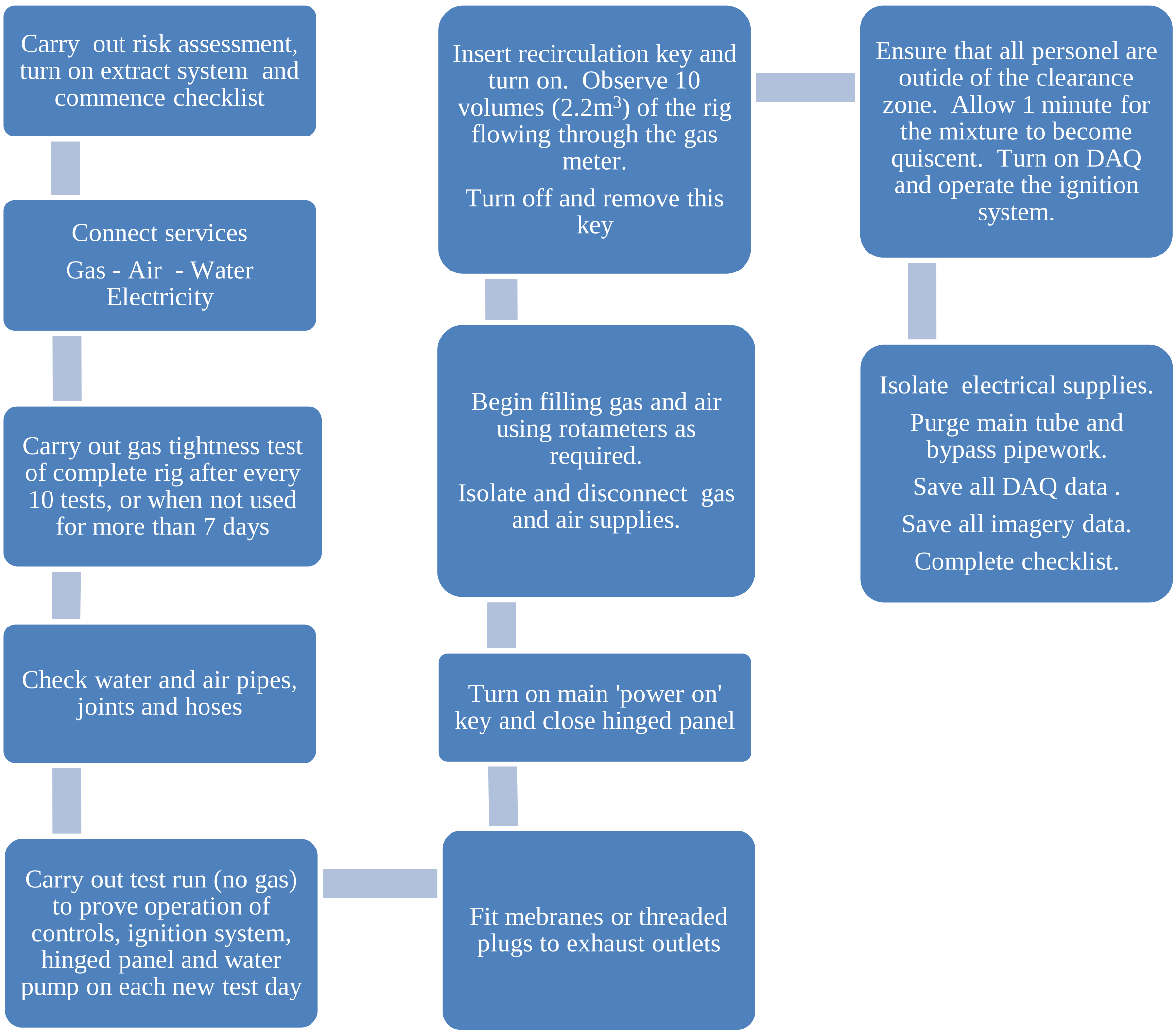

Figure 4.56 : 'Safe Operations' flow chart

Due to the sheer number of hot trials conducted in this study, a series of checklists and forms were developed to ensure safety and consistency. Examples of these checklists and forms are shown in Tables 4.19, 4.20 and 4.21.

Table 4.19 illustrates the manual and automatic sequence required to safely operate the FPMR. When carrying out explosion and mitigation ‘hot trials’, two persons competent in applying this procedure were always present. Normally this was the Research Assistant (R.A.) and the Laboratory Technician.

Table 4.20 shows a typical hot trial matrix which was used to confirm various key stages involved in the hot trials, including the naming of data and imagery files, as previously discussed above.

Table 4.21 displays the ‘hot trials data recording sheet and smart table’ created in MS Excel, which was used to record critical data and to auto-calculate various outcomes such as flame speed and flame speed reduction percentage across the sprays. Graphical illustrations were also populated from the data and are included in Chapter 5, Results and discussions.

Sequence order	Action	Manual / Automated	Checked (insert √)
1.	Close laboratory door and lock the bolt	Manual	
2.	Visually check rig for obvious defects	Manual	
3.	Check gas and air cylinder gauges	Manual	
4.	Connect gas and air to rig isolation valves	Manual	
5.	Visually check water pump rig	Manual	
6.	Fill or top-up water tank	Manual	
7.	Check or connect water hose to rig isolation valve	Manual	
8.	Check or connect water pump rig electrics to control box	Manual	
9.	Connect and turn on main rig power supply	Manual	
10.	Operate 'primary' key switch	Manual	
11.	Raise hinged end panel to closed position	Manual	
12.	24v DC magnet on hinged end plate is energised	Automated	
13.	Fill rig with desired concentration of gas and air, using rotameters and stopwatch to measure flow & volumes	Manual	
14.	Operate 'recirculation booster' key switch	Manual	
15.	Observe x10 volumes of the rig volume passing through turbine meter	Manual	
16.	Switch off 'recirculation booster' key switch	Manual	
17.	Allow 1 minute for mixture to become quiescent	Manual	
18.	Turn on data recorder and energise thermocouples and pressure transducers. Set up camera(s)	Manual	
19.	Check and verify air:gas concentration at 3 test points	Manual	
20.	Isolate gas and air supplies	Manual	
21.	Ensure that any personnel or visitors are outside the exclusion zone	Manual	
22.	Operate 'ignition' key switch and final safety check	Manual	
23.	Operate 'ignition' push button	Manual	
24.	Water pump is activated and starts	Automated	
25.	Water pump operates and develops steady spray	Automated	
26.	After 7 seconds 24v DC magnet on hinged end plate is energised	Automated	
27.	Hinged panel begins to fall open	Automated	
28.	Hinged panel opens >6mm and 2 micro-switches operate	Automated	
29.	Spark deployed at primary spark plug	Automated	
30.	Mixture ignites and propagates along tube	Automated	
31.	Primary key switch turned off	Manual	
32.	Waste water quantified and rig purged with air (direct to outside)	Manual	
33.	Data records named, copied and saved	Manual	
34.	Photographic records named, copied and saved	Manual	
35.	Video records named, copied and saved	Manual	

Table 4.19 : Manual and automated control sequence and check list

No.	Test Title	Configuration	Experiment complete	Imagery labelled	Data Log labelled	Imagery processed	Data processed & graphed
1-3	6% Dry - No atomiser in place	Without water sprays	√	√	√	√	√
4-6	7% Dry - No atomiser in place		√	√	√	√	√
7-9	9% Dry - No atomiser in place		√	√	√	√	√
10-12	10% Dry - No atomiser in place		√	√	√	√	√
13-15	6% Dry - With atomiser in place		√	√	√	√	√
16-18	7% Dry - With atomiser in place		√	√	√	√	√
19-21	9% Dry - With atomiser in place		√	√	√	√	√
22-24	10% Dry - With atomiser in place		√	√	√	√	√
25-27	6% Wet - 0.3mm Tip 130bar - CF	Counter flow water spray	√	√	√	√	√
38-30	7% Wet - 0.3mm Tip 130bar - CF		√	√	√	√	√
31-33	9% Wet - 0.3mm Tip 130bar - CF		√	√	√	√	√
34-36	10% Wet - 0.3mm Tip 130bar - CF		√	√	√	√	√
37-39	6% Wet - 0.5mm Tip 130bar - CF		√	√	√	√	√
40-42	7% Wet - 0.5mm Tip 130bar - CF		√	√	√	√	√
43-45	9% Wet - 0.5mm Tip 130bar - CF		√	√	√	√	√
46-48	10% Wet - 0.5mm Tip 130bar - CF		√	√	√	√	√
49-51	6% Wet - 0.8mm Tip 130bar - CF		√	√	√	√	√
52-54	7% Wet - 0.8mm Tip 130bar - CF		√	√	√	√	√
55-57	9% Wet - 0.8mm Tip 130bar - CF		√	√	√	√	√
58-60	10% Wet - 0.8mm Tip 130bar - CF		√	√	√	√	√
61-63	6% Wet - 0.3mm Tip 130bar - PF	Parallel flow water spray	√	√	√	√	√
64-66	7% Wet - 0.3mm Tip 130bar - PF		√	√	√	√	√
67-69	9% Wet - 0.3mm Tip 130bar - PF		√	√	√	√	√
70-72	10% Wet - 0.3mm Tip 130bar - PF		√	√	√	√	√
73-75	6% Wet - 0.5mm Tip 130bar - PF		√	√	√	√	√
76-78	7% Wet - 0.5mm Tip 130bar - PF		√	√	√	√	√
79-81	9% Wet - 0.5mm Tip 130bar - PF		√	√	√	√	√
82-84	10% Wet - 0.5mm Tip 130bar - PF		√	√	√	√	√
85-87	6% Wet - 0.8mm Tip 130bar - PF		√	√	√	√	√
88-90	7% Wet - 0.8mm Tip 130bar - PF		√	√	√	√	√
91-93	9% Wet - 0.8mm Tip 130bar - PF		√	√	√	√	√
94-96	10% Wet - 0.8mm Tip 130bar - PF		√	√	√	√	√

Table 4.20 : Typical hot trials matrix checklist

Series 4 Test No.	Atomiser position (downstream of ignition) m	Counter Flow (C/F) Parallel Flow (P/F) Cross Flow (X/F)	Number of atomisers	Spill orifice diameter mm	Outlet orifice diameter mm	SMD of Spray µm	Cone Angle degrees°	Spray Flux ($cm^3/s/cm^2$)	Water Pressure (MPA)	Water Volume Flow Rate (L/min)	Water Temperature °c	Gas Type	Gas in Air % within tube	Equivalence Ratio (φ) within tube	Number of exhaust vents plugged	Number of exhaust vents with burst discs	% of exhaust openings to main tube CSA	Ignition delay time after water pump (sec)	Upstream distance of travel	Duration of travel (ms)	Average upstream flame speed	Downstream distance of travel in 50ms	Duration of travel (ms)	Average downstream flame speed	% Reduction in flame speed
1																									
2																									
3																									
4																									
5																									
6																									
7																									
8																									
9																									
10																									
11																									
12																									
13																									
14	3	X/F	3	0.5	0.5	29	42.7	0.024	13	2.2	20	Methane	6	0.61	0	6	115.41	7	650	60	10.83	Mitigation			100.00
15																									
16																									
17																									
18																									

Table 4.21 : Representative hot trials data recording sheet and smart table

4.7.2 Data processing : Hot trials

The hot trials data recording sheet and smart table shown above in Table 4.21 was used to record data from each of the test run conditions.

As previously discussed in Section 4.5.4.9, Solartron Mobrey rotameters were placed in the gas and air pipework between the supply cylinders and the FPMR. The Rotameters were used in conjunction with the gas filling and blending process. The flow rate and filling times for the fuel gas and air were recorded for subsequent processing.

A GMI Gascoseeker Mk2-500, also discussed previously in Section 4.5.4.9 and shown here in Figure 4.57, was used to verify the percentage 'gas in air' concentrations within the FPMR. Samples were taken from three points along the length of the rig to ensure the uniformity of the methane-air mixture immediately prior to ignition. This was recorded for further data analysis with regards to equivalence ratios (ϕ).

Figure 4.57 : GMI Gascoseeker Mk2-500 [83]

The temperature measurement was carried out using mineral insulated, exposed junction, type K thermocouples. The mineral insulated section of the thermocouple was 50mm in length and has an external diameter of 3mm. The exposed junction was 0.6mm in diameter and is revealed in Figure 4.58. These thermocouples are manufactured, certified and supplied by TC Ltd, Uxbridge, UK and the calibration certificates can be found in Appendix 6.

The thermocouples complete with 4m (manufacturer supplied and certified) extension cables were individually connected to separate channels in the iNet Expandable Modular Data Acquisition System, which is shown in Figure 4.59.

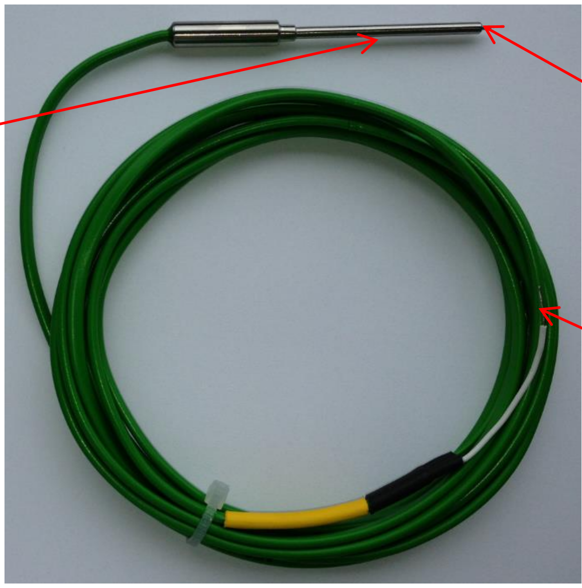

Figure 4.58 : Mineral insulated, exposed junction, type K thermocouple (TC Ltd, UK)

Figure 4.59 : iNet Expandable Modular Data Acquisition (DAQ) System [84]

The exposed junction, type K thermocouples were placed along the length of the flame propagation and mitigation rig at 600mm intervals and held in place using 'Pete's Plug' adapters, as shown previously in Figure 4.26. Due to lag time associated with thermocouples as shown in Table 4.22, the data measurements offered during the hot trials are not intended to represent the actual flame temperatures within the flame propagation and mitigation tube. The use of these exposed junction thermocouples has been demonstrated to be an acceptable method for comparing flame propagation within 'confined', 'partly confined' and 'unconfined' explosion testing in confined and partly confined vessels and pipework. These were extensively described in numerous previously published works [87,88,89].

Thermocouple 'junction' diameter (mm)	Response times (s)
0.25	0.015
0.5	0.03
1.0	0.15
1.5	0.3
2.0	0.4
3.0	0.8

Table 4.22 : Typical thermocouple response times (source data : TC Ltd)

The thermocouple temperatures were simultaneously recorded by the DAQ system, whereby each data file was systematically 'named' and sorted for further processing.

To obtain dynamic pressure data from within the explosion propagation and mitigation tube, several pressure transducers (PD) were strategically placed along the length of the tube. Additional information relating to the use of the PD's can be found in Chapter 5 (Results and discussions).

Initial explosion trials were conducted using a calibrated digital manometer with data lock facility, to assist with specifying the pressure range of the transducers. In all of the initial trials the maximum pressure peak was about ≤2kPa (20 mbar).

Omega MM PX409 pressure transducers, shown in Figure 4.60 were selected for these trials, with a pressure range of 0 – 2.5kPa (0 – 25mbar).

Figure 4.60 : Omega MM PX409 pressure transducers [86]

These transducers contain a Wheatstone bridge that has been diffused into a silicon wafer and then micro-machined to exacting standards to produce a silicon sensor that has excellent stability, linearity, long term stability and are certified as providing an accuracy of ±0.20% [86].

The silicon sensors are then mounted into the PX409 core module, with a thin layer of oil and a stainless steel diaphragm isolating the silicon from the process media. The transducers are supplied with NIST traceable certificates of calibration, which can be found in Appendix 5. The linear transducer signal voltage output was in a range of 0 – 5Vdc representing the pressure values of 0 – 2.5kPa (0 – 25mbar). An Excel spread sheet was used to convert this linear relationship during the post processing.

4.7.3 Data acquisition (DAQ)

A data acquisition (DAQ) system was required to gather data from the pressure transducers and thermocouples situated along the length of the FPMR. Due to the relatively short data acquisition time of ≤1.5 seconds available for each experimental trial, a system was required that was capable of sampling multiple channels at a rate of 400 - 1000 samples per second.

The iNet Expandable Modular Data Acquisition System manufactured by Instrunet and presented previously in Figure 4.59, was chosen because of its compact, but expandable size and moderately simple connectivity to a Windows based computer. External measurement devices, such as thermocouples, resistance temperature detectors (RTD's), thermistors, strain gauges, load cells, voltage, current, resistance and accelerometer inputs can be connected to the iNet510 Wiring Box. [84]

The iNet software supplied had a real time data acquisition display and was fully compatible with MS Excel. The software also facilitated manual or triggered start for data acquisition and processing. The triggered start was used in all of this work to ensure consistency and reliability of results. The thermocouple nearest to the ignition end of the driver section was used to trigger the data collection. A trigger value of 5˚C temperature rise above ambient, was programmed into the software. This ensured that all trials were measured from the same datum point, thus allowing acquired data to be analysed and compared with a high level of dependability.

4.8 Accuracy and sources of error : Hot trials

It is recognised that although every attempt has been made to ensure that the results presented are consistent and accurate, this work may be subject to measurement errors due to instrumentation exactitude. In some cases, where several measurement instruments were used simultaneously, a compound effect may have occurred thus affecting the overall resulting outcomes. However, every qualitative and quantitative submission within the study was obtained by the author in a highly organised, systematic and disciplined manner.

The following information is a summary of accuracy and tolerances, including declared manufacturers values and resolution.

4.8.1 Methane-air mixture verification

Throughout this study hundreds of methane-air mixtures were formulated and mixed prior to explosion and mitigation testing. Although the Gascoseeker 500 was used to verify the final mixture percentages, the methane-air mixture were initially blended using calibrated rotameters as previously described in Section 4.5.4.9.

Following the introduction of methane-air and subsequent mixing, the Gascoseeker was used as a verification check. On every occasion the methane-air percentage was as expected. Therefore, the methane-air mixture used in every trial can be said to be consistent, with a maximum error of ± 2%. e.g. for a methane-air mixture of 10% methane in air, the actual value would fall between 9.8 – 10.2% methane in air. The manufacturer’s data is summarised and given in Table 4.23.

GMI Gascoseeker 500	
Manufacturer	GMI
Model	Gascoseeker 500
Serial number	GD542109
Current certificate of calibration	Yes
Accuracy data / information	Resolution 1% / Accuracy ± 2%
Comments	For the purpose of this work, consistency of measurement was important. The GMI Gascoseeker is used globally for gas percentage measurement.

Tables 4.23 : GMI Gascoseeker certification and accuracy information

4.8.2 Flame temperature measurement

The Type K thermocouples used in this study were previously described in Section 4.7.2. Precise flame temperatures for methane-air mixtures are tabulated in many publications, whereas in this current study, a consistent and reliable means was required to compare various methane-air mixtures in a number of potential mitigation scenarios. The exposed junction thermocouples provided reliable results within the scope of this study, whereby exactitude of temperature measurement was not required. Moreover, this device has been used for qualitative comparison in many other published works and been deemed suitable by peer review. The manufacturer's data is shown in Table 4.24 with additional pertinent comments.

Exposed junction, type K thermocouples	
Manufacturer	TC Ltd
Model	Mineral insulated, 0.6mm exposed junction, type K thermocouple
Serial number(s)	D/42965P (4), D/439660P (4)
Current certificate of calibration	Yes
Accuracy data / information	Response time < 0.15 and >0.03 seconds
Comments	For the purpose of this work, consistency of measurement was important. Although the temperatures stated may not be accurate, the same margin of error may be applied to all of the experiments. This type of thermocouple has also been used and endorsed by Prof. G.E. Andrews, University of Leeds. [87,88,89]

Table 4.24 : Mineral insulated, exposed junction, Type K thermocouple information

4.8.3 Volume flow rate : Fuel gas and air

Solartron Mobrey rotameters were used to assist with the ‘filling’ of the FPMR with fuel gas and air where required. Each of the rotameters were certificated for purpose i.e. flow rate range and individual fluid characteristics. As previously discussed in Section 4.5.4.9 the rotameters were used in conjunction with the Gascoseeker to facilitate reliable and consistent gas and air charging of the rig. The manufacturer’s data and accuracy are summarised in Table 4.25.

Rotameters	
Manufacturer	Solartron Mobrey
Model	KDG 1100
Serial number(s)	SM-041115-B / SM-041121-B
Current certificate of calibration	Yes
Accuracy data / information	±1.2% measured value + 0.4% full scale value
Comments	The rotameters were highly suitable for the purpose of this work and provided consistent measurements.

Table 4.25 : Solartron Mobrey rotameter accuracy information

4.8.4 Overpressure measurement

The Omega pressure transducers used within this study were previously described in Section 4.7.2. The linear relationship provided by the output transducer produce accuracies of ±0.2%. The manufacturer’s data is summarised and shown in Table 4.26.

Omega pressure transducers	
Manufacturer	Omega
Model	MM PX409
Serial number(s)	430015 / 427001 / 435214
Current certificate of calibration	Yes
Accuracy data / information	Measurement range 0 – 5Vdc : 0 – 25mb Accuracy ±0.2%
Comments	For the purpose of this work, consistency of measurement was important.

Table 4.26 : Omega pressure transducer measurement information

4.8.5 Flame speed calculations

The flame speeds offered in this work are attributed to the manifestation of the unique design characteristics of the FPMR, whereby a partly confined explosion was simultaneously vented. During the hundreds of trials, flame speeds were compared for various methane-air mixtures and a number of spray configurations, where the resulting flame would either, be unaffected, accelerate, decelerate or be mitigated. Table 4.27 offers an indicative summary of the calculated average flame speed accuracy.

In each of the individual trials series, the HD video camera was placed in the same position and still images from the 50fps video (20ms between frames) were used to determine the average flame speed between two fixed points over single or multiple 20ms periods. Pixel measurement using Adobe PS CS4 was estimated to have an accuracy of ±0.5%.

Flame speed calculations	
Manufacturer	Adobe
Model	Premier Pro CS6
Serial number(s)	N/A
Current certificate of calibration	N/A
Accuracy data / information	Flame speeds were calculated using 50fps video and time coding in the software in association with pixel measurement in Adobe PS CS4. Accuracy ±0.5%.
Comments	For the purpose of this work, consistency of measurement was important. All measurements were taken by and processed by the author.
50fps HD camcorder	
Manufacturer	Panasonic
Frame rate	50fps
Frame rate accuracy	Estimated from survey : >99.999% accuracy

Tables 4.27 : Flame speed calculations using image analysis

4.8.6 Water supply : water quality, pump, gauges and temperature

Table 4.28 provides accuracy and error information relating to the high pressure (HP) water delivery system which was previously illustrated and discussed in Section 4.2.1.1.

Pressure gauge	
Manufacturer	Hydraulic megastore
Scale range	0 – 20MPa
Accuracy	± 1.6% (manufacturers data)
Pump	
Manufacturer	Interpump W1208
Scale range	5 – 17MPa
Accuracy	± 2% (manufacturers data)
Thermometer and probe	
Manufacturer	RS RSCAL / Type K 342-8956
Scale range	-50 – 250 ˚C
Accuracy	± 0.75% : Resolution 0.1˚C / ±0.25% (manufacturers data)
Water deionizer	
Manufacturer	Purite electrode deionisation
Purity / conductivity	1-10µS/cm
Accuracy	Within declared range

Table 4.28 : HP water delivery system sources of error and accuracy evidence

4.9 Chapter review

This Chapter has discussed the challenges and achievements in the development of the Flame Propagation and Mitigation Rig (FPMR). Due to the novelty of this current study there was no suitable test apparatus to emulate or adapt.

In summary, this Chapter is subdivided into **cold trials** and **hot trials** and describes the following in terms of apparatus set up, procedures and data processing.

Cold trials

i. Apparatus and set up including simulated PMMA tube
ii. Custom built water pump and storage system
iii. Volumetric flow rate trial
iv. Spray cone angle
v. Imaging techniques applied
vi. PDA spray characterisation : ambient and simulated PMMA tube conditions
vii. Accuracy and sources of error

Hot trials

i. Apparatus design and set up including FPMR development
ii. Initial design concepts
iii. Final rig design including components and assembly
iv. Atomiser configurations for C/F, P/F and X/F utilisation
v. Imaging techniques applied
vi. Explosion and mitigation experimental trials
vii. Accuracy and sources of error

The following Chapter presents and discusses the results from the cold and hot trials that were exclusively carried out using the apparatus described and reviewed in this Chapter.

Mitigation of Gas and Vapour Cloud Explosions using Fine Water Sprays

Volume II of III

By

Stephen Andrew Johnston, M.Sc. MIGEM

Submitted in accordance with the requirements for the degree of Doctor of Philosophy

Department of Gas and Petroleum Engineering
School of Computing, Science and Engineering
University of Salford

February 2015

CHAPTER 5

RESULTS AND DISCUSSIONS

5.1 Overview

This chapter presents the results and discussions of the investigations in to the mitigation of propagating flames in flammable homogeneous gas-air mixtures, using high pressure water sprays with mean droplet sizes of $D_{32} \leq 30\mu m$. Several rigs, apparatus and laboratories have been used to carry out various tests in collating this exclusive data.

In line with previous Chapters, the results have separated into two main groups:-

i. ‘Cold trials’
ii. ‘Hot trials’

The ‘cold trials’ were conducted in the absence of a fuel-air mixture or propagating flame. All of the cold trials were performed in the Spray Research Group (SRG) laboratory as explained and discussed in detail in Chapter 4 and summarised in 5.1.1 and Table 5.2.

All of the ‘hot trials’ were carried out under stringent controlled conditions in the Petroleum Research (PR) laboratory using the purpose built ‘Flame Propagation and Mitigation Rig’ (FPMF) previously explained and rationalised in Chapter 4. Combustible mixtures were formed and ignited within the FPMR and a selection of commercial Spill Return Atomiser (SRA) configurations were assessed with respect to their explosion mitigation capabilities. The series of experiments carried out in the hot trials are summarised in Section 5.1.2 and Table 5.3.

The need to ensure reliability and repeatability of experimental trials has been maintained throughout this work, which is reflected in the results presented herewith. Whilst every attempt has been made to collect valid and dependable data, it is recognised that accuracy and reliability is reliant on the exactitude of the equipment used in this work and the consistency of the operation.

The rigorous procedures that were applied, together with the potential sources of error relating to the equipment used in this study were previously reviewed in Chapter 4.

5.1.1 Definition of Cold trials

The purpose of these cold trials was to assist with the selection process relating to this study, since the parametric effect of spray properties with regard to drop size, droplet velocity, flow rate and penetration are directly related to the suppression and mitigation of gas and vapour cloud explosions. Thus a commercial atomiser known as the Spill Return Atomiser (SRA), which had been previously developed for disinfection and decontamination work [51, 53] was found to possess some of the vital characteristics required.

During this work the SRA was developed further to produce higher liquid flow rates, velocities and liquid volume flux and wider spray cone angles.

Additionally there was a requirement to assess and characterise the selected sprays within the confinement of the enclosed PMMA tube section of the FPMF. For convenience a short section of PMMA tube was used, as previously described in 4.3.2, to simulate conditions expected within the flame propagation and mitigation tube.

The cold trials conducted in this study were:-

i. Volumetric flow rate trials for a number of selected SRA configurations, supplied with a range of water pressures.
ii. Characterisation and analysis of chosen SRA configurations in open ambient conditions using non-intrusive laser techniques (Phase Doppler Anemometry - PDA).
iii. Classification and evaluation of elected configurations within the confinement of an enclosed PMMA tube using PDA.

Full details regarding the SRA configurations used in the study were detailed explicitly in Chapter 4. For clarity and ease of reference, the atomisers were designated as Type A, B, C and D and colour coded, which are shown here again for convenience in Tables 5.1 and 5.2.

SRA designation	Exit orifice diameter (mm)	Spill orifice diameter (mm)	Tangential inlet orifice diameter (mm)
Type A	0.3	0.5	0.6 x 2
Type B	0.5	0.5	0.6 x 2
Type C	0.8	0.5	0.6 x 2
Type D	1.0	0.5	0.6 x 2

Table 5.1 : Summary of orifice dimensions for SRA configuration types A, B, C and D

5.1.1.1 Summary of cold trials matrix and results at a glance

Atomiser type	Tests conducted	Atomiser configuration	Section	Result
Spill return atomiser (SRA)	Volumetric flow rate (L/min)	SRA Type A	5.2.2	Suitable for hot trial
		SRA Type B	5.2.2	Suitable for hot trial
		SRA Type C	5.2.2	Suitable for hot trial
		SRA Type D	5.2.2	Not suitable for hot trial
	Spray cone angle (degree)	SRA Type A	5.2.3	Suitable for hot trial
		SRA Type B	5.2.3	Suitable for hot trial
		SRA Type C	5.2.3	Suitable for hot trial
		SRA Type D	5.2.3	Suitable for hot trial
	Droplet diameter D_{32} (µm), velocity of droplets (m/s) and liquid volume flux ($cm^3/s/cm^2$) in **ambient conditions**	SRA Type A	5.3.1.1	Suitable for hot trial
		SRA Type B	5.3.1.2	Suitable for hot trial
		SRA Type C	5.3.1.3	Suitable for hot trial
		Multiple overlap SRA Type B	5.3.1.4	Suitable for hot trial
	Droplet diameter D_{32} (µm), velocity of droplets (m/s) and liquid volume flux ($cm^3/s/cm^2$) in **enclosed conditions**	SRA Type B	5.3.2.1	Suitable for hot trial
		SRA Type C	5.3.2.2	Suitable for hot trial

Table 5.2 : Summary of cold trials matrix and results at a glance

5.1.2 Definition of Hot trials

The purpose of the hot trials was to assess the mitigation capabilities of the Spill Return Atomisers (SRA) selected from the cold trial process. Previous authors [14, 39, 45, 61] had used various apparatus and rigs, ranging from small one metre long explosions tubes in laboratories, to full scale modules and pipe arrays at open air specialist research centres as described in Chapters 2 and 3.

The objectives of this current work are unique, in that the selected atomisers would be assessed with respect to their explosion mitigation capabilities in the presence of slow moving explosions of ≤30m/s. This makes the previous rig designs ineffective to be emulated in this present study.

The FPMF and supplementary apparatus used throughout these hot trials was conceived, designed and constructed by the author. The design concepts and rationale supporting the FPMF are detailed in Chapter 4.

The hot trials conducted for this study were:-

i. single SRA configurations in counter flow (C/F) with a propagating methane-air flame.
ii. single SRA configurations in parallel flow (P/F) with a propagating methane-air flame.
iii. multiple overlapping SRA configurations in parallel flow (P/F) with a propagating methane-air flame.
iv. Single and multiple SRA configurations in cross flow (X/F) with a propagating methane-air flame.
v. multiple SRA configurations in cross flow (X/F) with a propagating methane-air flame front using heated water at various temperatures .
vi. multiple SRA configurations in cross flow (X/F) with a propagating propane-air flame.
vii. multiple SRA configurations in cross flow (X/F) with a propagating methane-air flame front under partly confined explosion conditions.

The local geometry within which an explosion occurs can profoundly affect the severity of the ‘**outcome of the event**’. Three principle environmental explosions conditions known as ‘confined’, ‘partly confined’ and ‘unconfined’ were previously described in detail in Chapter 2, including the implications with respect to resulting overpressures (P_{max}) and pressure rise and decay within the cloud (*dP/dt*).

Throughout these experimental explosion mitigation trials, the conditions are described as '**partly confined / vented'**. This is due to the initial design concepts of the FPMR as previously detailed in Chapter 4, whereby the rig conditions were initially confined and gas tight during the filling stage for safety reasons.

However, at the time of ignition both ends of the rig became open ended and 'unconfined', almost immediately. The resultant propagating flame was then allowed to travel, unconfined by the upstream and downstream ends of the rig, with the only confinement being imposed by the internal surface of the propagation tube.

5.1.2.1 Summary of hot trials and results at a glance.

During this research program approximately 250 mitigation trials were conducted using various spray configurations and fuel-air mixtures. Following a careful selection process the results of 101 hot trials are discussed herewith.

Within this current Chapter a small representative selection of results are offered and discussed. Table 5.3 provides a summary matrix of hot trials and results at a glance; including a colour coded '**event outcome'** for each of the explosion trials events listed. An additional column has also been provided to facilitate easy reference in relation to the location of the results in either, Chapter 5, Appendix 9, or both.

For convenience all 101 hot trials are presented in Appendix 9, together with all of the additional Appendices that are supplied as an additional electronic volume on the accompanying CD (Volume III).

Trial	Configuration	E.R. (ϕ)	General event outcome	Section / Appendix
Mitigation trials for a single water spray in **counter flow** (C/F) with a methane-air flame	SRA configuration type A Water pressure : 13MPa Water temperature : 20°C	0.61	NMFA	5.5.1/A9.1.1
		0.72	NMFA	A9.1.1
		0.95	NMFA	A9.1.1
		1.06	NMFA	A9.1.1
	SRA configuration type B Water pressure : 13MPa Water temperature : 20°C	0.61	NMFA	A9.1.2
		0.72	NMFA	A9.1.2
		0.95	NMFA	A9.1.2
		1.06	NMFA	A9.1.2
	SRA configuration type C Water pressure : 13MPa Water temperature : 20°C	0.61	FMFE	A9.1.3
		0.72	NMFA	A9.1.3
		0.95	NMFA	A9.1.3
		1.06	NMFA	A9.1.3
Mitigation trials for a single water spray in **parallel flow** (P/F) with a methane-air flame	SRA configuration type A Water pressure : 13MPa Water temperature : 20°C	0.61	NMFA	5.5.2/A9.2.1
		0.72	NMFA	A9.2.1
		0.95	NMFA	A9.2.1
		1.06	NMFA	A9.2.1
	SRA configuration type B Water pressure : 13MPa Water temperature : 20°C	0.61	NMFA	A9.2.2
		0.72	NMFA	A9.2.2
		0.95	NMFA	A9.2.2
		1.06	NMFA	A9.2.2
	SRA configuration type C Water pressure : 13MPa Water temperature : 20°C	0.61	FMFE	5.5.3/A9.2.3
		0.72	NMFA	A9.2.3
		0.95	NMFA	A9.2.3
		1.06	NMFA	A9.2.3
Mitigation trials for two water sprays in **parallel flow** (P/F) with a methane-air flame	2 x Overlapping Type B SRA's Water pressure : 13MPa Water temperature : 20°C	0.61	FMFE	5.5.4/A9.3.1
		0.72	NMFA	A9.3.1
		0.95	NMFA	A9.3.1
		1.06	NMFA	A9.3.1
	2 x Overlapping Type C SRA's Water pressure : 13MPa Water temperature : 20°C	0.95	FMFE	A9.3.2
		0.95	FMFE	A9.3.2
		1.06	FMFE	A9.3.2
Mitigation trials for water sprays in **cross flow** (X/F) with the methane-air flames	Single SRA type B Water pressure : 13MPa Water temperature : 20°C	0.61	NMFA	A9.4.1
		0.72	NMFA	A9.4.1
		0.95	NMFA	A9.4.1
		1.06	NMFD	A9.4.1
	Two SRA type B Water pressure : 13MPa Water temperature : 20°C	0.61	NMFD	A9.4.2
		0.72	NMFD	A9.4.2
		0.95	NMFD	A9.4.2
		1.06	NMFD	A9.4.2

General event outcome	Code
No Mitigation with resulting Flame Acceleration	NMFA
No Mitigation with resulting Flame Deceleration	NMFD
No Mitigation with resulting Unaffected Flame	NMUF
Partial Mitigation with resulting Flame Propagation	PMFP
Full Mitigation resulting in Flame Extinguishment	FMFE

Table 5.3 : Summary of hot trials matrix and results at a glance

Trial	Configuration	E.R. (ϕ)	General event outcome	Section / Appendix
Mitigation trials for water sprays in **cross flow** (X/F) with the methane-air flames	Three SRA type B Water pressure : 13MPa Water temperature : 20°C	0.61	FMFE	A9.4.3
		0.72	NMFD	A9.4.3
		0.95	NMFD	A9.4.3
		1.06	NMFD	A9.4.3
	Four SRA type B Water pressure : 13MPa Water temperature : 20°C	0.61	FMFE	A9.4.4
		0.72	FMFE	5.5.5/A9.4.4
		0.95	NMFA	A9.4.4
		1.06	NMFD	A9.4.4
Mitigation trials for water sprays in **cross flow** (X/F) with the methane-air flames	Single SRA type C Water pressure : 13MPa Water temperature : 20°C	0.61	NMFD	A9.4.5
		0.72	NMFD	A9.4.5
		0.95	NMFA	A9.4.5
		1.06	NMFD	A9.4.5
	Two SRA type C Water pressure : 13MPa Water temperature : 20°C	0.61	NMFD	A9.4.6
		0.72	NMFD	A9.4.6
		0.95	NMFA	A9.4.6
		1.06	NMFD	A9.4.6
	Three SRA type C Water pressure : 13MPa Water temperature : 20°C	0.61	FMFE	A9.4.7
		0.72	NMFD	A9.4.7
		0.95	NMFD	A9.4.7
		1.06	NMFD	A9.4.7
	Four SRA type C Water pressure : 13MPa Water temperature : 20°C	0.61	FMFE	A9.4.8
		0.72	FMFE	A9.4.8
		0.95	FMFE	5.5.6/A9.4.8
		1.06	FMFE	A9.4.8
(X/F) Type B and C SRA's using variable supply pressures and water temperature : 20°C	3 type C and 1 type B:13MPa	0.95	NMFD	A9.5.1
	2 type C and 2 type B:13MPa	0.95	NMFA	A9.5.1
	1 type C and 3 type B:13MPa	0.95	NMFD	A9.5.1
	1 type C and 3 type B:15MPa	0.95	NMFA	A9.5.1
Varying number of **(X/F)**Type C SRA's using variable supply pressures and water temperature : 20°C	3 type C only:14MPa	0.95	NMFD	A9.5.2
	3 type C only:15MPa	0.95	NMFD	A9.5.2
	3 type C only:15MPa	0.95	FMFE	A9.5.2
	3 type C only:16MPa	0.95	NMFD	A9.5.2
	3 type C only:17MPa	0.95	NMFA	A9.5.2
	3 type C only:18MPa	0.95	NMFD	A9.5.2
Varying number of **(X/F)**Type B SRA's using variable supply pressures and water temperature : 20°C	4 type B only:14MPa	0.95	NMFD	A9.5.3
	4 type B only:15MPa	0.95	FMFE	A9.5.3
	4 type B only:16MPa	0.95	NMFD	A9.5.3
	4 type B only:17MPa	0.95	NMFD	A9.5.3
	4 type B only:18MPa	0.95	NMFA	A9.5.3

General event outcome	Code
No Mitigation with resulting Flame Acceleration	NMFA
No Mitigation with resulting Flame Deceleration	NMFD
No Mitigation with resulting Unaffected Flame	NMUF
Partial Mitigation with resulting Flame Propagation	PMFP
Full Mitigation resulting in Flame Extinguishment	FMFE

Table 5.3 : Summary of hot trials matrix and results at a glance

Trial	Configuration	E.R. (ϕ)	General event outcome	Section / Appendix
Three **(X/F)**Type C SRA's using variable supply pressures and water temperatures	3 type C only:13MPa : 30°C	0.95	FMFE	A9.5.4
	3 type C only:15MPa : 35°C	0.95	NMFD	A9.5.4
	3 type C only:15MPa : 40°C	0.95	NMFD	A9.5.4
	3 type C only:16MPa : 45°C	0.95	NMFD	A9.5.4
	3 type C only:15MPa : 50°C	0.95	NMFD	A9.5.4
Three **(X/F)**Type C SRA's using variable supply pressures and water temperatures	4 type C only:13MPa : 25°C	0.95	FMFE	A9.5.5
	4 type C only:13MPa : 25°C	0.95	FMFE	A9.5.5
	4 type C only:13MPa : 30°C	0.95	FMFE	A9.5.5
	4 type C only:13MPa : 30°C	0.95	FMFE	A9.5.5
	4 type C only:13MPa : 40°C	0.95	FMFE	A9.5.5
	4 type C only:13MPa : 40°C	0.95	FMFE	A9.5.5
	4 type C only:13MPa : 50°C	0.95	FMFE	A9.5.5
	4 type C only:13MPa : 50°C	0.95	FMFE	5.5.7/A9.5.5
Supplementary trials				
Four **(X/F)**Type C SRA's trials with methane rich, methane-air flames	4 type C only:13MPa : 20°C	1.18	FMFE	A9.6.1
	4 type C only:13MPa : 20°C	1.30	FMFE	A9.6.1
	4 type C only:13MPa : 20°C	1.43	FMFE	A9.6.1
	4 type C only:13MPa : 20°C	1.56	FMFE	5.5.8/A9.6.1
Four **(X/F)**Type C SRA's trials with propane-air flames	4 type C only:13MPa : 20°C	0.49	FMFE	A9.6.2
	4 type C only:13MPa : 20°C	0.74	FMFE	A9.6.2
	4 type C only:13MPa : 20°C	1.00	FMFE	5.5.9/A9.6.2
Four **(X/F)**Type C SRA's trials with methane-air flames, with partial blockage of exhaust outlets	One exhaust outlet blocked	0.95	FMFE	A9.6.3
	Two exhaust outlets blocked	0.95	FMFE	A9.6.3
	Three exhaust outlets blocked	0.95	FMFE	5.5.10/ A9.6.3

General event outcome	Code
No Mitigation with resulting Flame Acceleration	NMFA
No Mitigation with resulting Flame Deceleration	NMFD
No Mitigation with resulting Unaffected Flame	NMUF
Partial Mitigation with resulting Flame Propagation	PMFP
Full Mitigation resulting in Flame Extinguishment	FMFE

Table 5.3 : Summary of hot trials matrix and results at a glance

5.2 Introduction to cold trial results and discussions

As discussed in Chapter 2 the aim of this work is to suppress, quench or mitigate a gas explosion with fine water sprays. In the previous studies reviewed in Chapter 3, three types of atomiser have been largely used:-

i. Liquid pressure (pressure jet)
ii. Impact-type pressure atomiser (fire sprinkler)
iii. Two-fluid (external mixing)

From the atomisers listed above, the only atomiser capable of producing the fine sprays required for this work of ≤30μm is the two-fluid type. This type of atomiser, which was previously described in detailed in Chapter 3 is supplied with a liquid stream (e.g. water) and gaseous stream (e.g. air). An everyday example of the application of a two fluid atomiser is a paint spray gun. The gaseous stream is used to atomise the liquid stream, either internally before exiting the atomiser, or externally as shown below in Figure 5.1.

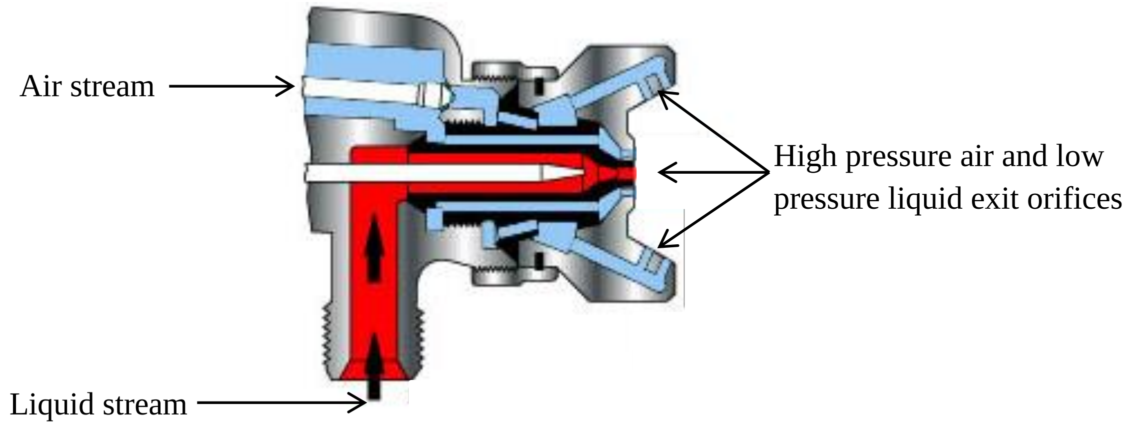

Figure 5.1 : Typical two-fluid (external mixing) atomiser [47]

Although two-fluid atomisers are capable of producing the typical drop sizes of ≤30μm needed for this study, the air stream would be detrimental due to:-

i. The introduction of air into the FMPR would undoubtedly disturb the quiescent homogeneous gas-air mixture around the area of the atomiser, which could even render the mixture non-flammable.
ii. The introduction of the turbulent air stream could cause a disturbance in the unburned mixture, thus promoting an increase in flame speed.

iii. The physical size and contouring of the external mixing two-fluid atomiser may promote flame acceleration as the flame passes over the surfaces of the atomiser.

Individual or accumulative combinations of the above scenarios would give rise to unacceptable errors and inconsistency of results. Therefore for this reason an alternative commercial atomiser, known as a Spill Return Atomiser (SRA) was sourced. The SRA was explicitly discussed previously in Chapters 3 and 4.

5.2.1 Atomiser selection overview

Chapter 4 presents the challenges, developments and achievements in the field of spray research relating to this current work. Previous authors have studied the effects of the hydrodynamic breakup of large water droplets in the order of ≥100μm, with respect to explosion mitigation capabilities, as described in Chapter 3. Whereas, this present work is focused on the development of a fine spray system with average droplets of D_{32} ≤30μm, capable of producing a spray that will readily heat up, or even vaporise in the flame. The droplets will then extract heat from a flame propagating in the partly confined / vented conditions of the FPMR, *without relying on further droplet breakup*.

An existing atomiser known as a Spill Return Atomiser (SRA) was recently developed for disinfection and decontamination applications [51, 53]. The SRA has a novel swirl chamber that promotes turbulent flow at the exit orifice, thus giving way to very efficient atomisation. Figure 5.2 illustrates the main components of the SRA. The full description of the SRA, including technical data was discussed previously in Chapters 3 and 4.

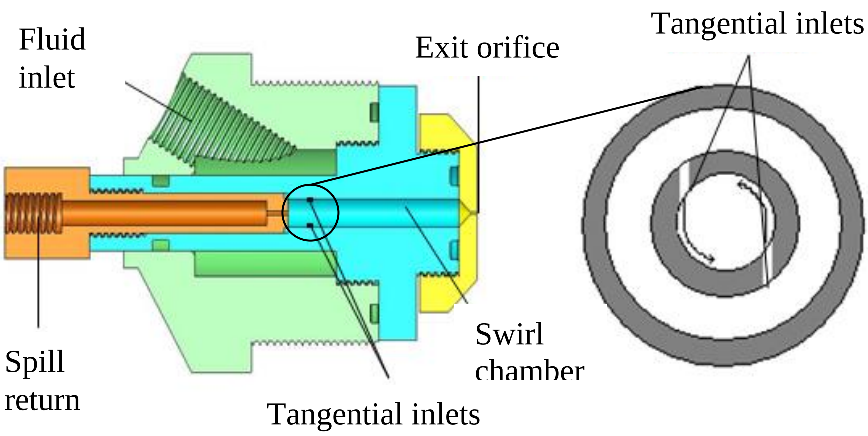

Figure 5.2 : Spill Return Atomiser (SRA) [51]

In previous work by Nasr, G.G. et al [53] the SRA was used for spraying decontamination agents, where the outcomes favoured the use of the 0.3mm exit orifice, with a 0.5mm spill return (referred to in this current work as SRA configuration 'Type A'). Although there was sufficient published data available for the SRA configuration Type A, there was only limited data for the SRA configuration Type B and therefore further characterisation was required to enhance the data from the previous work.

Chapter 4 discusses the rationale behind the new development of two additional SRA configurations for this work known as the Type C and Type D atomiser. These atomisers were also tested and characterised as part of these cold trials.

Supplementary experiments were conducted to assess the spray characteristics of SRA configuration Types B and C within the enclosed environment of a 190mm (I.D.) PMMA tube. This was to ascertain whether there were any significant changes in spray characteristics compared to those found in ambient open air conditions, prior to the hot trials. Details of the experimental apparatus used to carry out this work were previously provided Chapter 4.

5.2.2 Volumetric flow rate trials using spill return atomisers (SRA)

A series of volumetric flow rate trials were conducted to provide systematic flow rate data for the four single atomiser configuration Types A, B, C and D, as well as comparing related previous data with present atomiser configurations.

Each of the atomisers were tested and evaluated by subjecting them to a range of pressures from 5MPa – 14MPa (50bar – 140bar). A test rig was designed and constructed to carry out the flow rate trials. The apparatus shown in Figure 5.3 consisted of a mounting frame, calibrated pressure gauge, atomiser mounting connections and spray convergence passage.

Due to the fine droplets and aerosols associated with the spray, the SRA was connected to a convoluted conical tube, shown in Figure 5.3 and referred to as the 'spray convergence passage'. This conveniently caused the droplets and mist to coalesce, thus producing a reliable flow of water from its exit. Full details of the apparatus set up and test procedures were provided Chapter 4.

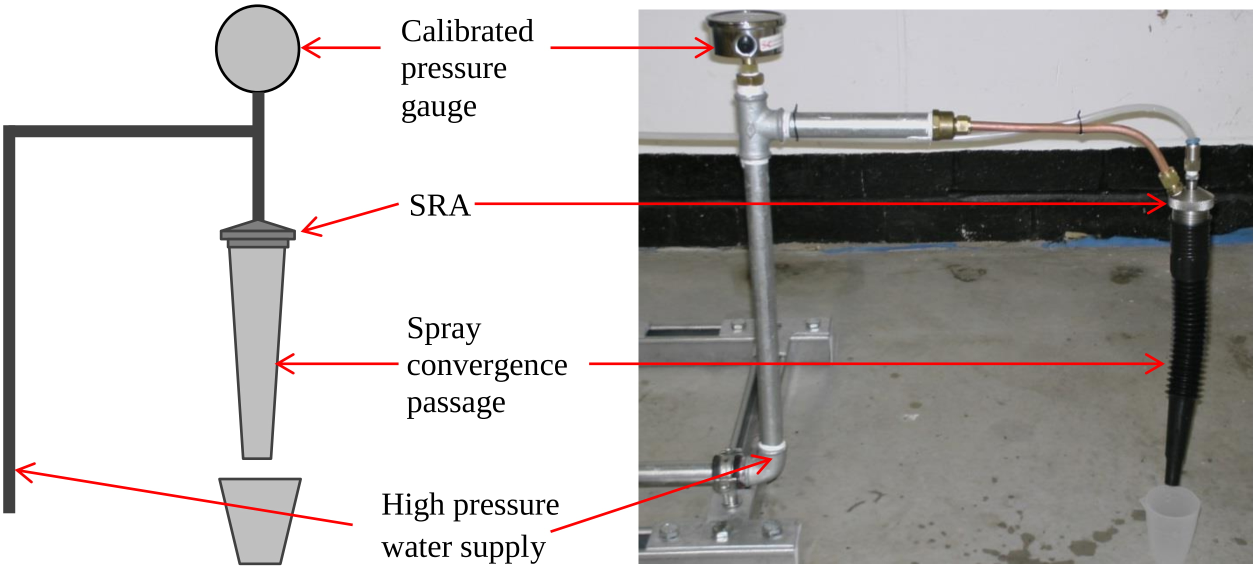

Figure 5.3 : Volumetric flow rate test rig (schematic and photograph)

The tabulated data obtained from the flow rate trials can be found in Appendix 8. Additionally, Figure 5.4 was produced from the data and was used to assess the throughput consistency of each of the atomisers over a range of typical operating pressures. The SRA configurations Type A, B and C can be seen to exhibit typical linear relationships between pressure and flow in both the exit and spill diameters. Whereas, the Type D SRA only produced consistent linear results at the exit orifice. The spill diameter flow rates were found to be non-uniform and this was coupled with an erratic, spluttering stream from the spill tube. A second series of tests were conducted using the Type D SRA to validate the apparent inconsistency, whereby the results were found to be in agreement with the original data that has been presented.

The inconsistencies found in the spill flow rates of configuration Type D have been attributed to the flow rate limitations in the swirl chamber of original design of the SRA. To achieve the demanding increased flow rates, modifications would be required to increase the tangential inlets which would also necessitate the re-designing of the swirl chamber. This extensive additional level of research was deemed to be outside the scope of this current work and has been recommended for further work in Chapter 7.

The above irregularities associated with the SRA Type D configuration subsequently resulted in it to be removed and discounted from the selection list of potential atomiser configurations.

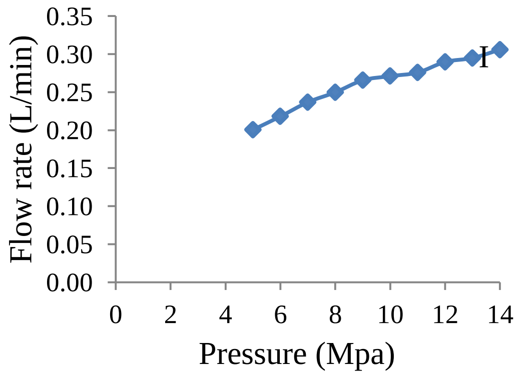

SRA Type A – Exit orifice

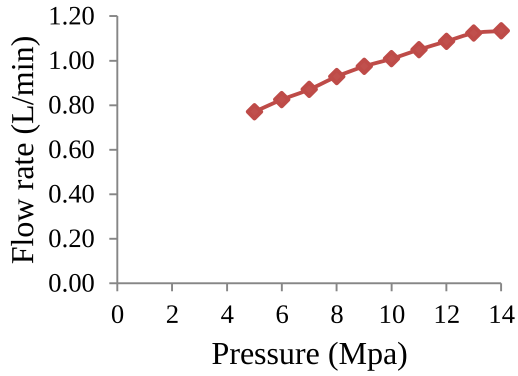

SRA Type A – Spill return orifice

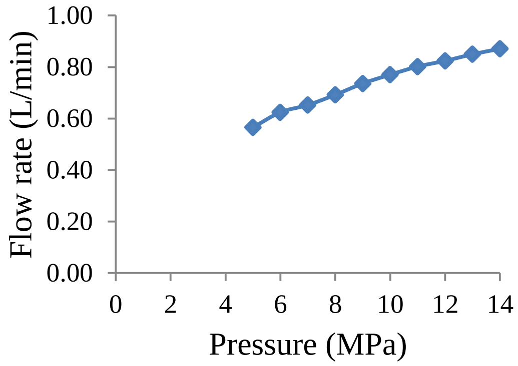

SRA Type B – Exit orifice

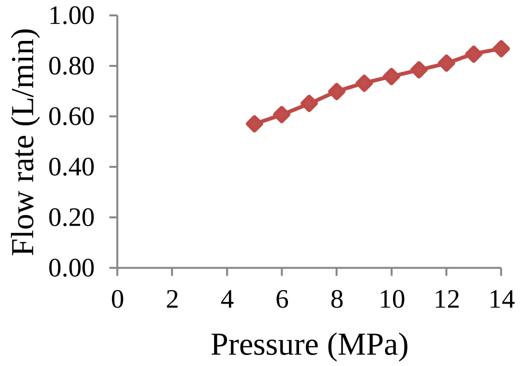

SRA Type B – Spill return orifice

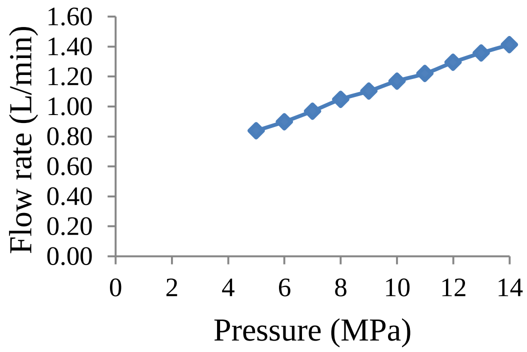

SRA Type C – Exit orifice

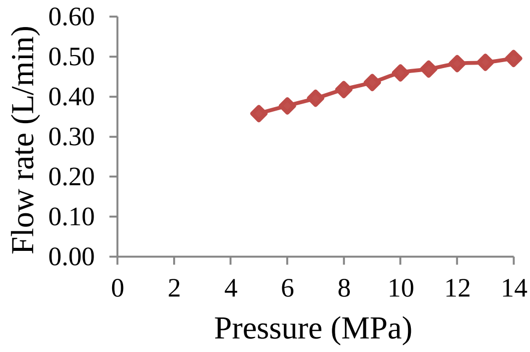

SRA Type C – Spill return orifice

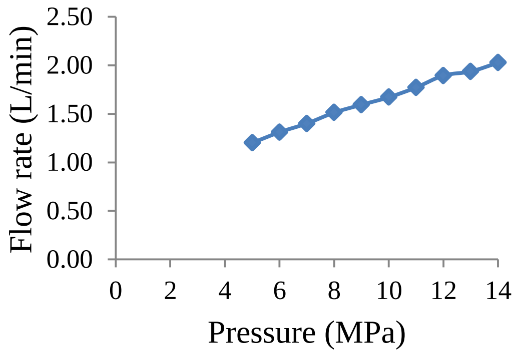

SRA Type D – Exit orifice

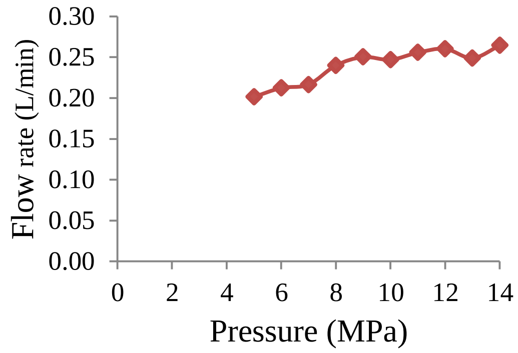

SRA Type D – Spill return orifice

Figure 5.4 : Typical flow rates (L/min) for SRA Types A, B, C and D from 5 – 14MPa

5.2.3 SRA spray cone angle

To measure the spray cone angle of various atomiser configurations in free air, a small rig was assembled, which was discussed previously in Chapter 4 and can be seen in Figure 5.5. Although atomiser configuration D had already been discounted in the previous Section 5.2.2, all four SRA configurations (A, B, C and D) were subject to the cone angle measurement process. The reason for further assessment of the SRA Type D was to provide a comparison with the other atomisers and an approximation of the cone angle.

The importance of the spray cone angle varies with different studies and applications. In this present study it was important that the spray envelope completely filled the internal cross section of the 190mm PMMA tube of the FPMR, as discussed in 5.2.3.1 and previously in Chapter 4.

5.2.3.1 SRA spray cone angle : configuration type A, B, C, D

The individual atomiser configurations were installed in the test rig shown in Figure 5.5 and were supplied with de-ionised water at a pressure of 13MPa. The spray images were captured using a high resolution Canon EOS digital SLR camera, which were then processed using Adobe Photoshop where the cone angles were measured using the Adobe angle finder tool. Additional information relating to methods used for spray cone angle measurement and sources of error were also discussed beforehand in Chapter 4.

The images and measured spray cone angles are presented in Figure 5.5 and summarised below:-

i. SRA configuration type A – **angle 34.7°**
ii. SRA configuration type B – **angle 42.7°**
iii. SRA configuration type C – **angle 49.2°**
iv. SRA configuration type D – **angle 54.2°**

Although all of the atomisers were capable of producing a spray that would fill the cross Section of the 190mm I.D. tube, the spray penetration (d_p) was significantly longer for the narrower cone angles. Table 5.4 provides the calculated penetration value for each of the measured angles.

A consequence of increasing the penetration (d_p) of a spray is the reduction in liquid volume flux (Q_f). This fundamental property of sprays was discussed extensively in Chapter 3.

Atomiser configuration type	Exit orifice diameter d_o (mm)	Cone angle θ (degree)	Cone radius C_r (mm)	Cone diameter C_d (mm)	Penetration d_p (mm)
A	0.3	34.7	95	190	304
B	0.5	42.7	95	190	243
C	0.8	49.2	95	190	207
D	1.0	54.2	95	190	186

Table 5.4 : Cone angle and calculated penetration within 190mm (I.D.) tube

Previous studies [39, 58, 65, 66] described in Chapter 3, found droplet diameter, D_{32} (μm) and liquid volume flux ($cm^3/s/cm^2$) to be the principle influencing characteristics of the spray, with respect to mitigation of high speed flames. The order of the concentration of droplets was approximately proportional to the reduction in flame speed. The spray characteristics of SRA configuration Type A, B and C were measured by non-intrusive laser techniques i.e. Phase Doppler anemometry (PDA) and these results are presented in the next Section.

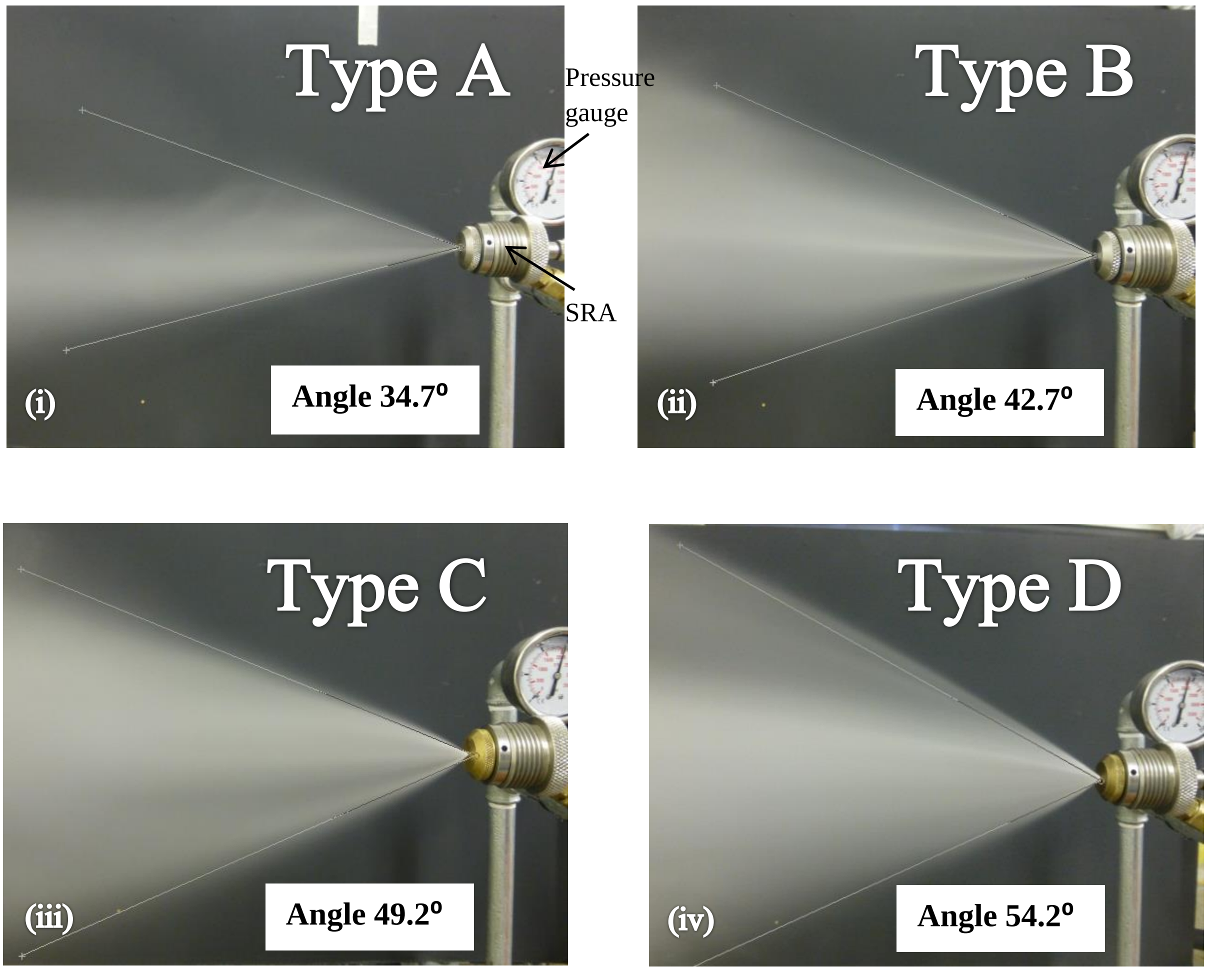

Figure 5.5 : Spray angles for (i) Type A (ii) Type B (iii) Type C (iv) Type D – SRA's

5.3 Spray characterisation : Droplet size, droplet velocity and liquid volume flux

A critical factor in the assessment of atomiser suitability is the dynamic measurement of droplet diameter, D_{32} (µm), droplet velocity, D_v (m/s) and liquid volume flux, Q_f ($cm^3/s/cm^2$). Phase Doppler Anemometry (PDA) was used to characterise the sprays of the different SRA configurations under this cold trial study.

The arrangement of the atomisers in the cold trials replicated those that were subsequently used in the hot trials. Sprays were characterised under ambient conditions in the surrounding atmosphere, as well as in the simulated tube. The conditions and the test apparatus used were explicitly discussed in Chapter 4, whereby the liquid supply pressure was 13MPa.

In the following, the results of the study are discussed according to:-

i. Spray characterisation of SRA configurations in ambient conditions using PDA.
ii. Spray characterisation of SRA configurations in the simulated PMMA tube conditions using PDA.

5.3.1 Ambient conditions

5.3.1.1 Single SRA configuration : Type A

A previous publication by Nasr, G.G. et al [53] produced data for a single SRA spray in ambient conditions with a 0.3mm exit orifice (tip) and 0.5mm spill return orifice, known as the SRA 'Type A' in this present study. These results were obtained using the same PDA apparatus and traversing frame system as used by the author in these current trials (see also Chapter 4). It may be assumed that the accuracy and sources of error in the previous reported work approximates those encountered in this current study. Accuracy and sources of error were previously discussed and tabulated in Chapter 4.

The results presented in the following are discussed with relevance to this current study and are used, where appropriate, from the previous decontamination study by Nasr, G.G. et al [53], mostly for comparative analysis.

The atomiser selection process within this study requires that a spray is formed which contains a suitable number of droplets, of a small enough diameter ($D_{32} \leq 30\mu m$) to extract heat from the flame front, within the finitely short time ($\leq 0.03ms$) afforded as the droplets traverse the flame front and reaction zone (~1mm thickness).

To achieve this, previous studies [61] have postulated that water droplets of 18μm would just reach boiling point within a 1mm thick flame front, in a stoichiometric methane-air mixture travelling at 2.3m/s. Recent mathematical [65] and CFD studies [88] are in agreement with these original claims [61]. Moreover, the higher the frequency of droplets, that are small enough to vaporise in the spray, the greater the heat transfer from flame to droplet owing to the release of the latent heat of vaporisation. From the previous study by Sapko et al [61], the ratio of droplets from ≤18μm : >18μm may be considered as an estimate of the ratio of heat transfer by latent heat : sensible heat. These droplet vaporisation and heat transfer mechanisms were discussed extensively in Chapter 3.

In the previous study by Nasr, G.G. et al [53] single SRA sprays were characterised at various downstream distances across the radial axis of the spray using PDA. This is shown in Figure 5.6.

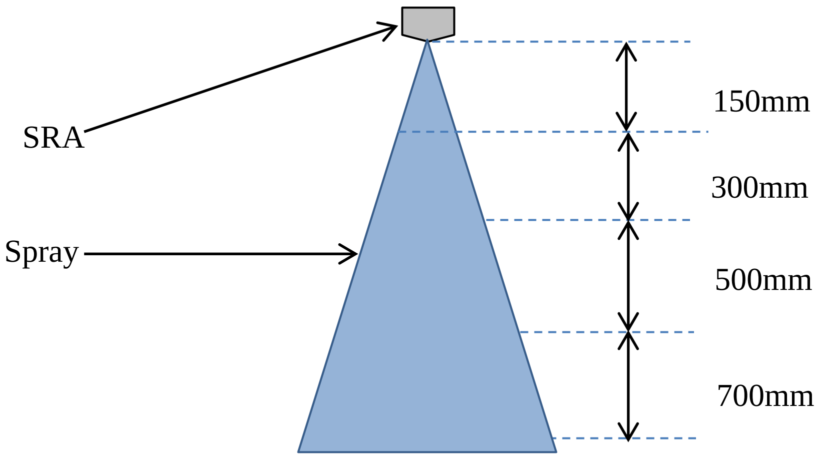

Figure 5.6 : Downstream distance sampling positions across the radial axis of the spray [53]

It is worth noting that in the previous study the measurements were taken at downstream distances ranging of 150mm, 300mm, 500mm and 700mm across the radial axis of the spray. Figure 5.7 shows the D_{32} for the SRA with 0.3mm exit orifice and 0.5mm spill diameter, known in this study as Type A configuration, as previously shown in Table 5.1, provided a D_{32} of about 17μm when characterised using PDA.

From Figure 5.8 [51], the D_{32} increases downstream of the spray, as the downstream distance increases. Acknowledging the two examples included in Figure 5.7 it is noted that at a distance of 100mm downstream, the D_{32} is typically 14μm, whereas at 200mm downstream the D_{32} has increased to approximately 20µm. The conceivable reasons for this increase include:-

i. Preferred vaporisation of the smaller drops.
ii. Coalescence occurring downstream.
iii. Because the larger drops tend to concentrate towards the centre of the spray, the laser beam measures proportionally more than for the wider spray further downstream.
iv. Velocity biasing effects change with distance downstream as the larger drops adapt more slowly to the local gas velocity.

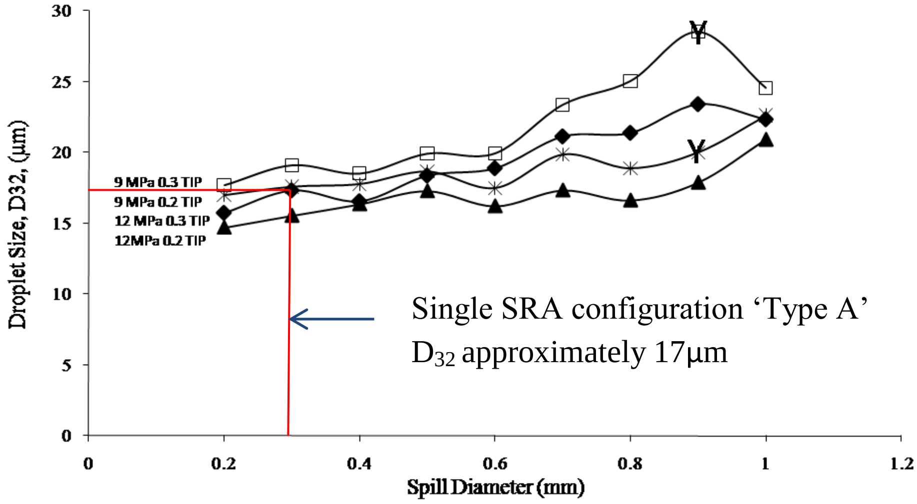

Figure 5.7 : Variation in D_{32} (µm) for various SRA configurations [51]

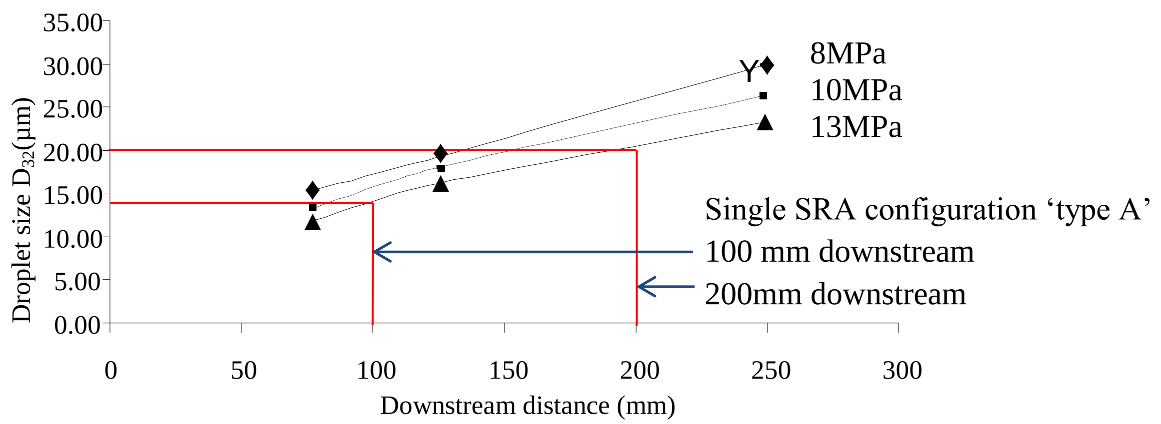

Figure 5.8 : Effect of downstream distance on droplet size, D_{32} (µm) [51]

In addition to the traditional histogram representations as shown in Figures 5.9 and 5.10, other methods commonly used to represent spray distribution include drop size frequency distribution curves, radial plots and iso-contour plots. By employing a combination of all these graphical accounts, a comprehensive picture of the spray can be efficiently depicted.

As previously discussed, droplet diameters tend to increase the further downstream they travel. This phenomenon is represented below in Figure 5.9 taken 150mm downstream and in Figure 5.10, taken at 700mm downstream where a 17μm droplet line has been added in order to consider the droplets of ≤17μm. Within the partly confined / vented conditions of the FPMR, consideration of downstream distribution was governed by the internal dimensions of the tube and the orientation of the spray i.e. counter / parallel flow or cross flow as discussed previously in Chapter 4. The importance of droplet distribution in these cold trials is paramount, as the percentage of droplets in the spray of D_{32} ≤30μm will have profound effects on the findings from the hot trials.

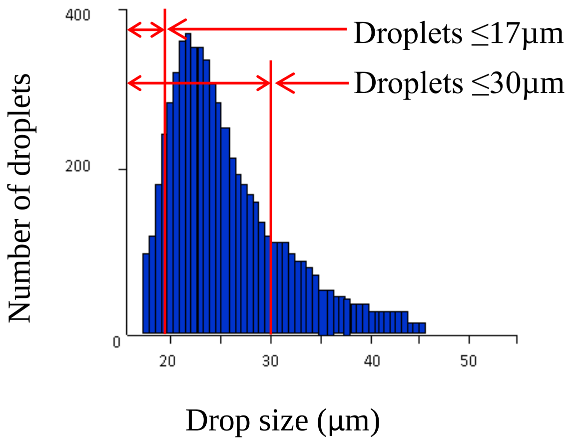

Figure 5.9 : Drop size distribution histogram for atomiser type A – 150mm downstream [51]

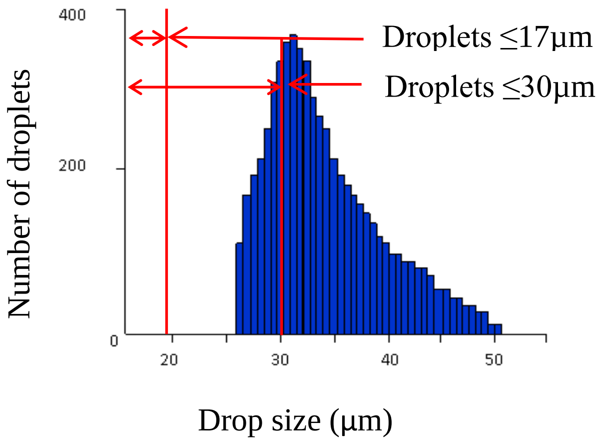

Figure 5.10 : Drop size distribution histogram for atomiser type A – 700mm downstream [51]

Droplet velocity and liquid volume flux are found to be at their greatest in the centre of a spray and decrease with radial position and with downstream location. This is due to the axisymmetric entrainment of the surrounding gaseous stream component i.e. ambient air, or in the case of the FPMR, this would be the homogeneous combustible gas-air mixture.

From the previous study [51], Figure 5.11 illustrates mean axial droplet velocity and Figure 5.12 represents the liquid volume flux at various radial and downstream intervals.

For example, in the centre of the spray at a downstream position of 190mm, the mean droplet velocity is typically 13.5m/s, whereas the liquid volume flux is $\geq 0.011 cm^3/s/cm^2$. Although the data from the previous studies [51, 53] was satisfactory for some of the hot trials, it was also necessary to obtain spray characteristics including drop size, droplet velocity and liquid volume flux for downstream distances of approximately 95mm for SRA configuration Types B and C, which are discussed in the next Section.

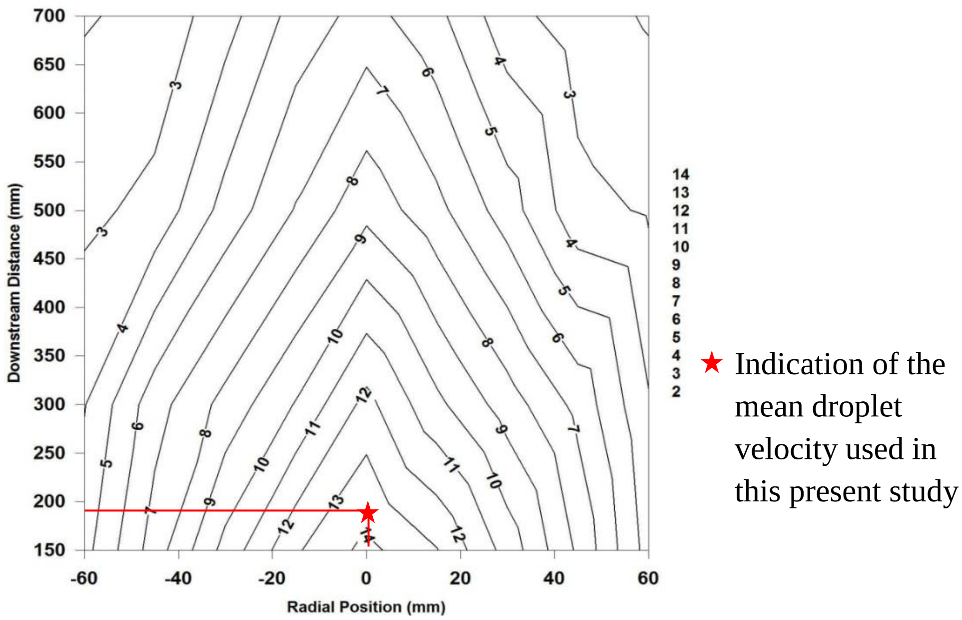

Figure 5.11 : Mean axial drop velocity (m/s) contours for single SRA Type A [51]

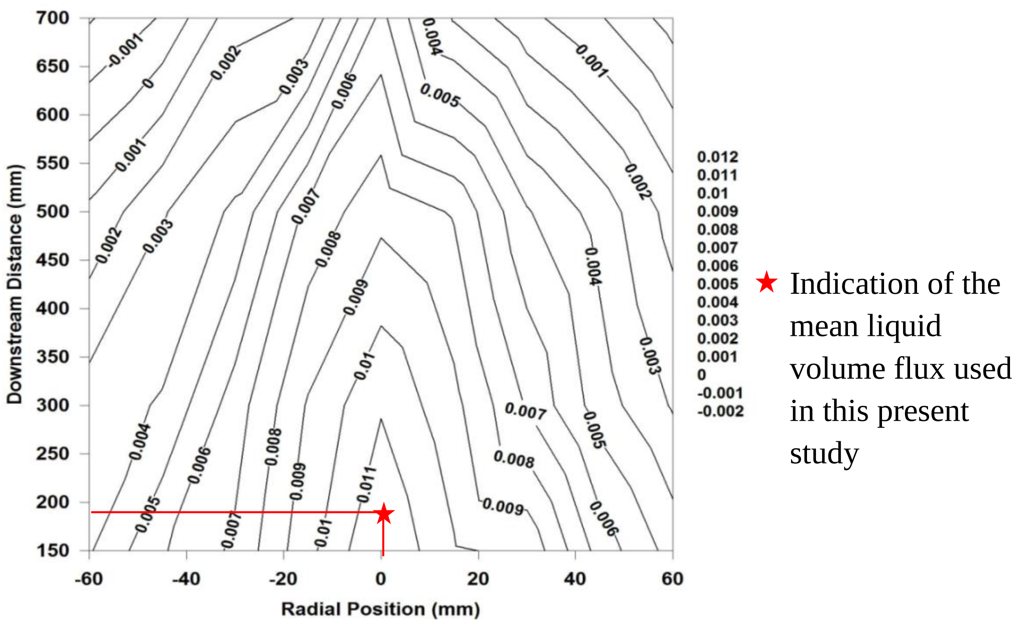

Figure 5.12 : Liquid volume flux ($cm^3/s/cm^2$) contours for single SRA Type A [51]

5.3.1.2 Single SRA configuration : Type B

As mentioned above, although some data was available for the SRA with 0.5mm exit orifice and 0.5mm spill diameter from previous work [51, 53], known as the SRA Type B in this present study, there was a need to capture further data axially from downstream position of 95mm, as illustrated in Figure 5.13. This data could then be analysed and compared to the same spatial position, approximately the centre of the spray when the spray was enclosed within a 190mm PMMA tube.

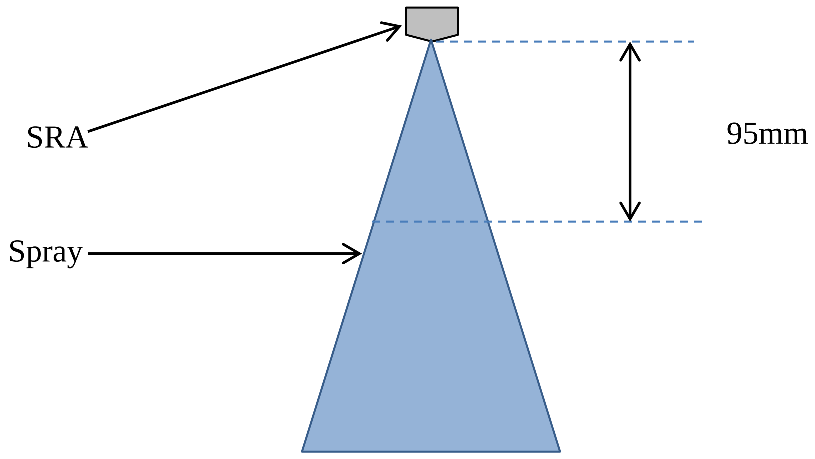

Figure 5.13 : Downstream distance sampling position across the radial axis of the spray

Figure 5.14 has been produced using the data acquisition from the new characterisation of the Type B SRA in ambient conditions at a downstream position of 95mm. Figure 5.14 illustrates the D_{32} of the spray at various radial positions. The mean diameter of the spray was found to have a D_{32} of 26µm, which is consistent with the previous study. The D_{32} (µm) values from the previous study are represented in Figure 5.15.

Although this mean diameter is slightly larger than the ≤18µm suggested by Sapko et al [61] for a 1mm thick flame front, the droplet distribution indicates a large percentage of droplets that are ≤30µm, in line with the principle objectives of this current study.

Figure 5.16 represents the distribution of D_{32} droplets within the spray and may be used to approximate the typical percentage of D_{32} droplets that are ≤26µm. The percentage of D_{32} droplets in the spray of ≤30µm has also been highlighted in Figure 5.16 and is discussed in the hot trials results Section, with relevance to partly confined / vented explosion mitigation.

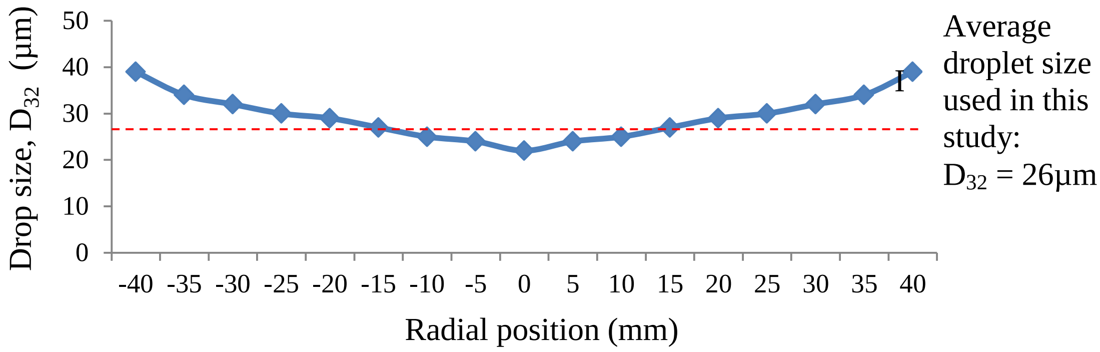

Figure 5.14 : D_{32} (μm) at 95mm downstream at various radial positions for SRA Type B

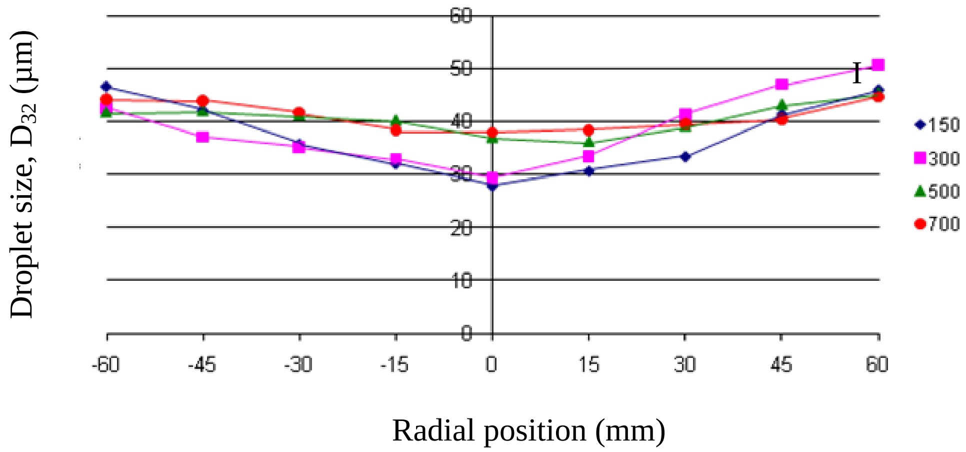

Figure 5.15 : D_{32} (μm) at various radial positions for SRA Type B (previous study [51])

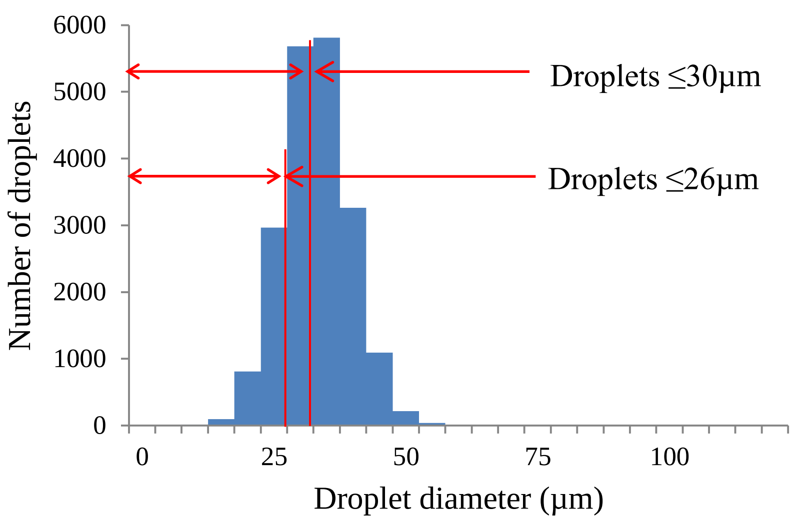

Figure 5.16 : Droplet distribution histogram at 95mm downstream for SRA Type B

The droplet velocity profile offered in Figure 5.17 is consistent with the velocity profile from the previous research (51) shown in Figure 5.18. The mean radial droplet velocity was estimated to be 21.41m/s and will be used for analysis and conclusions in the hot trials results and discussions.

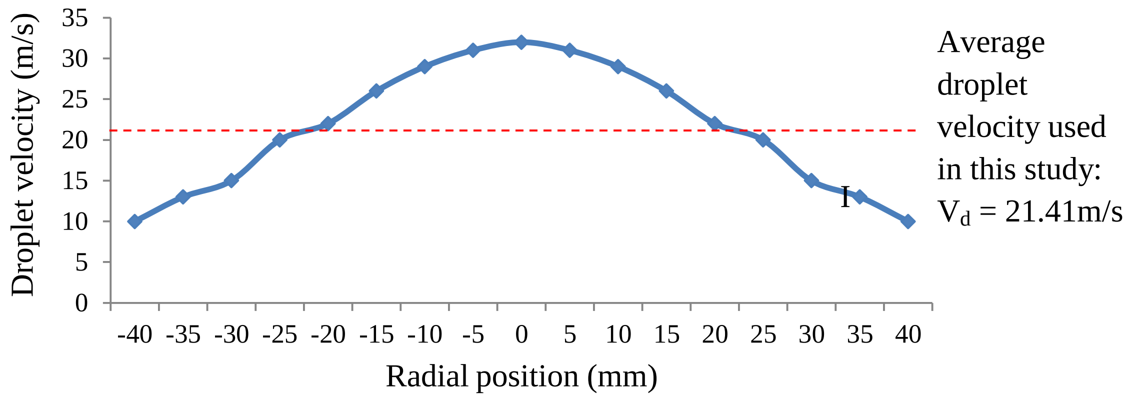

Figure 5.17 : Droplet velocity (m/s) at 95mm downstream for various radial positions for SRA Type B

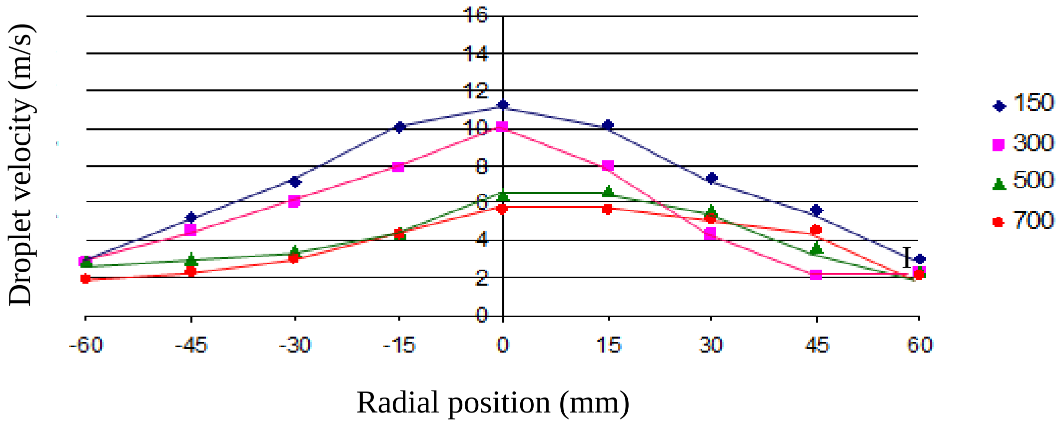

Figure 5.18 : Droplet velocity (m/s) at various downstream and radial positions for SRA Type B (previous study [51])

The liquid volume flux profile shown in Figure 5.19 is comparable with the velocity profile from the previous research [51] revealed in Figure 5.20. The mean radial liquid volume flux was estimated to be 0.024cm³/s/cm² and will be used for analysis and conclusions in the hot trials results and discussion.

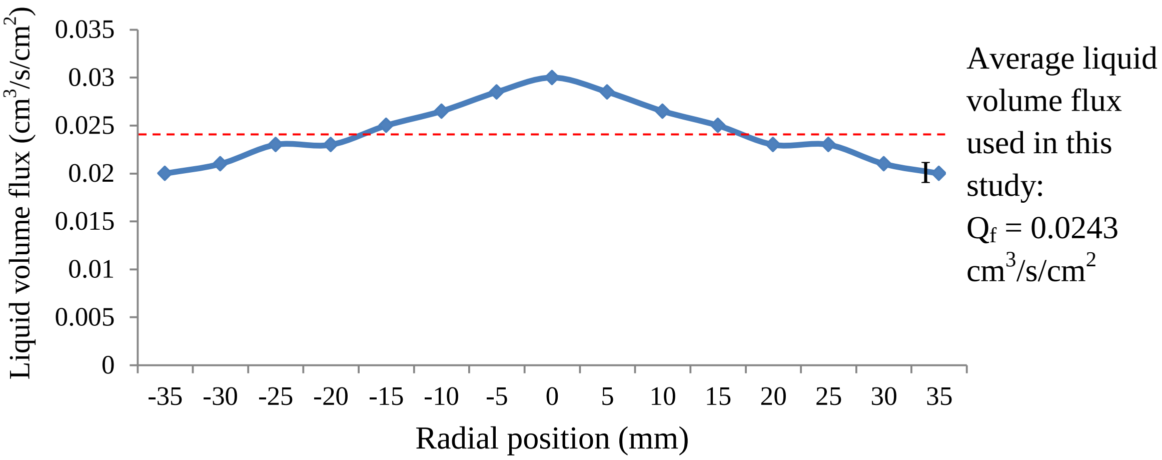

Figure 5.19 : Liquid volume flux (cm^3/s/cm^2) for SRA Type B

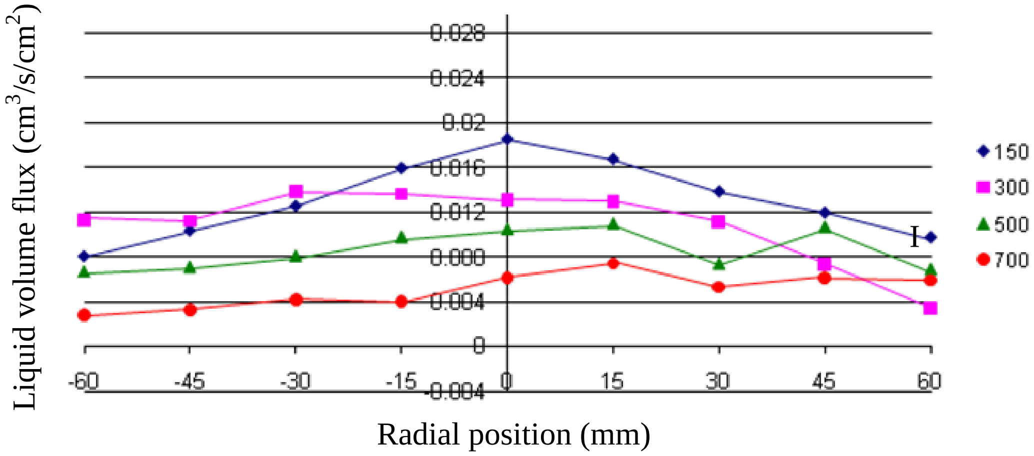

Figure 5.20 : Liquid volume flux (cm^3/s/cm^2) for SRA Type B (previous study [51])

The results presented in this Section are in agreement with the previous study [51] and demonstrate a high level of repeatability and therefore confirm the reliability of the set up used in these present investigations.

5.3.1.3 Single SRA configuration : Type C

The single SRA configuration Type C was developed by the author for this current study to provide a larger spray cone angle with resulting spray envelope, to be used within the enclosed conditions of the FPMR, as previously discussed in Chapter 4. As no existing data was available to be utilised, the SRA Type C was characterised using the same PDA equipment and arrangement as before.

Figures 5.21 - 5.24 have been produced using the data obtained from the new characterisation of the SRA type C in ambient conditions, at a downstream position of 95mm, as previously shown in Figure 5.13. The SRA Type C exhibits an exit diameter of 0.8mm and a spill return diameter of 0.5mm (see also Table 5.1)

Figure 5.21 illustrates the D_{32} of the spray at various radial positions, with the average radial D_{32} droplet size was estimated to be 29µm. This coincides with the principle objective of this current work, in the use of sprays with $D_{32} \leq 30$µm.

Figure 5.22 represents the distribution of D_{32} droplets within the spray and may be used to approximate the typical percentage of D_{32} droplets that are ≤29µm. The percentage of D_{32} droplets in the spray of ≤30µm has been highlighted in Figure 5.22 and is discussed in the hot trials Section with significance to partly confined and vented explosion mitigation.

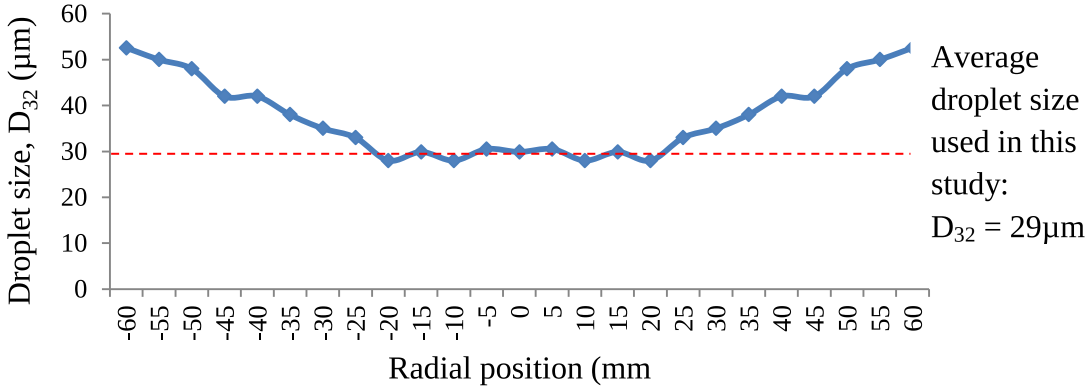

Figure 5.21 : D_{32} (µm) at 95mm downstream for various radial positions for SRA Type C

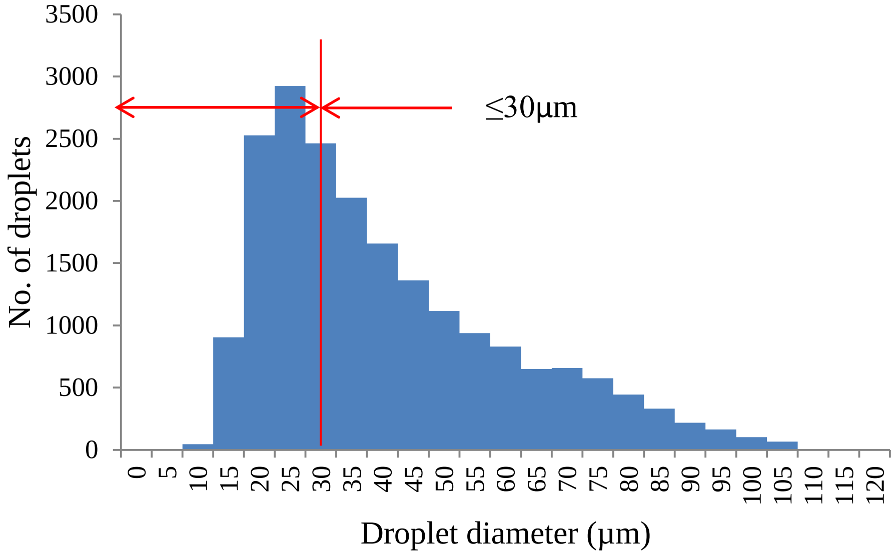

Figure 5.22 : Droplet distribution histogram at 95mm downstream for SRA Type C

The droplet velocity profile for the spray is illustrated in Figure 5.23. The velocity at the axial centre of the spray was found to be 22m/s, with an average across the full axis of the spray of 13.5m/s. Droplet velocity will influence the transit time in the flame front, which will differ when applied to counter flow, cross flow and parallel flow spray configuration. This will be discussed in the relevant Sections of the hot trial experimental results.

Liquid volume flux has been plotted in Figure 5.24, where the values ranged from 0.02 – 0.061cm^3/s/cm^2, with an average across the full axis of the spray of 0.039cm^3/s/cm^2. The effect of this on mitigation will also be discussed in the hot trials results.

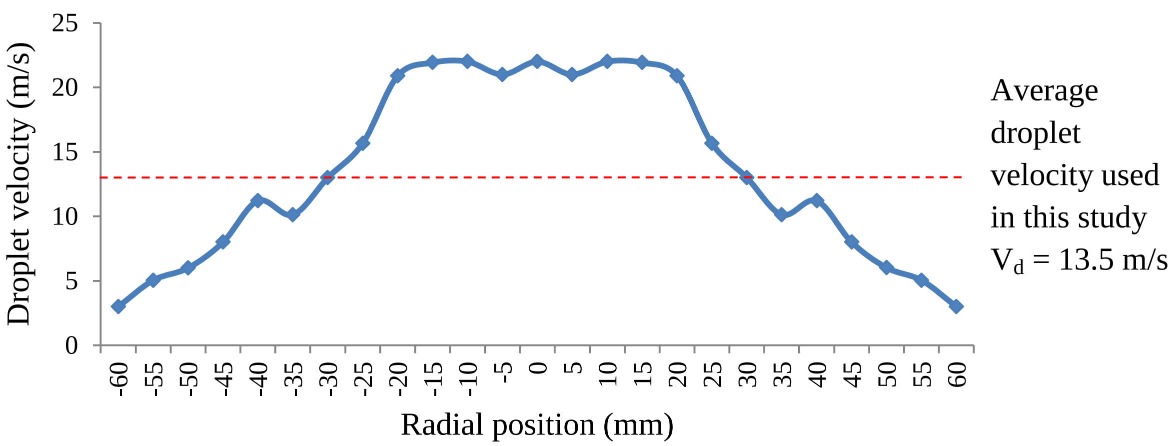

Figure 5.23 : Droplet velocity (m/s) at 95mm downstream SRA configuration Type C

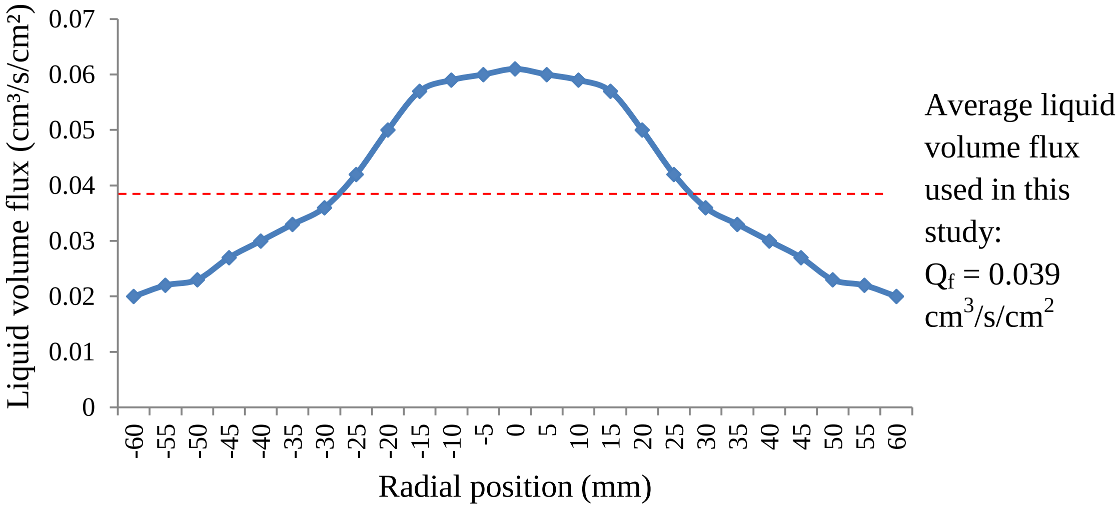

Figure 5.24 : Liquid volume flux ($cm^3/s/cm^2$) at 95mm downstream SRA Type C

To increase the volume of spray and subsequent liquid volume flux in the path of the propagating flame within the FPMR, a unique manifold arrangement was devised and fabricated which comprised of two overlapping sprays. This equipment was extensively discussed in Chapter 4.

The next Section will discuss the results of the spray characterisation of the multiple overlap SRA configurations using the same PDA equipment and arrangement as before. This configuration used two of the Type B SRA's with 0.5mm exit orifices diameter and 0.5mm spill diameters.

5.3.1.4 'Multiple overlap' spray configuration : Type B

In addition to the use of single SRA configurations, an 'in-tube' manifold array was developed whereby two SRA's with 0.5mm exit orifice and 0.5mm spill diameter could be securely mounted and operated in counter or parallel flow, within the FPMR. The manifold was fabricated using 316 stainless steel tube and is referred to as the 'multiple overlap' atomiser manifold. Figure 5.25 illustrates the main components of the 'multiple overlap' SRA. Full details relating to the concept and design of this equipment can be found in Chapter 4.

Subsequent to the completion of individual spray characteristics in ambient conditions, the sprays from the multiple overlap atomisers also needed to be appraised using PDA, prior to hot trial testing in the FPMR to assess to potential effects of spray overlap.

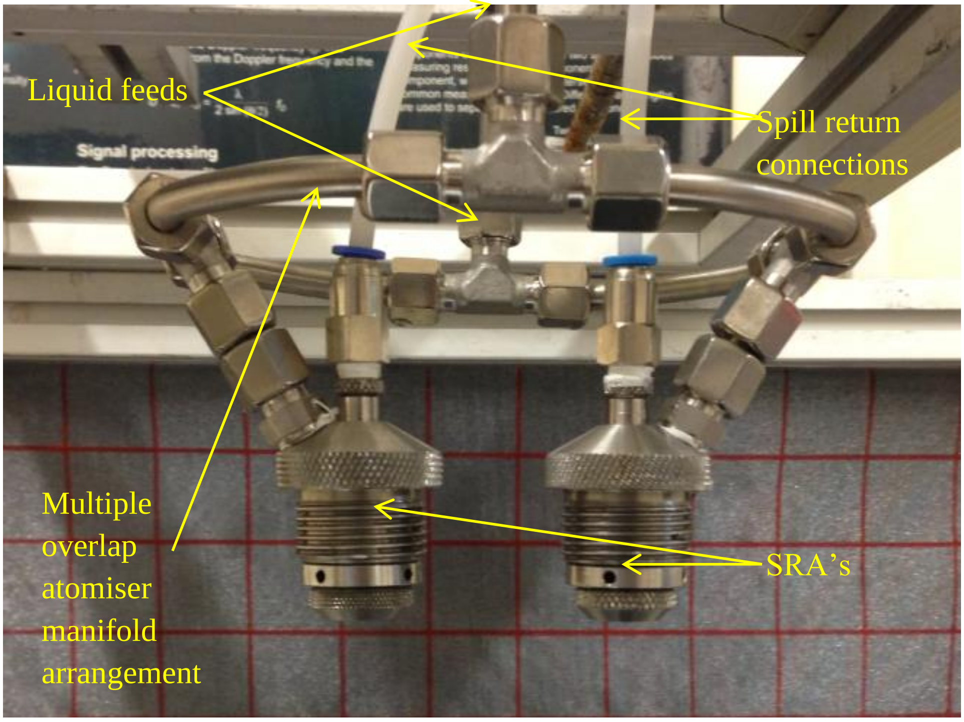

Figure 5.25 : 'Multiple overlap' atomiser manifold with two Type B SRA's

The multiple overlap atomiser manifold was attached to the traversing frame system and the PDA was set up as described in Chapter 4. The atomisers were supplied with de-ionised water at a pressure of 13MPa and were adjusted to deliver overlapping sprays that intersected 95mm downstream of the exit orifices. This intersection point is defined as the radial position '0.0' in Figures 5.26, 5.27, 5.29 and 5.30.

The distance of 95mm has been applied in this trial and is consistent with all of the other PDA cold trials carried out in the study, thus approximating the central position of the spray within the confines of the PMMA tube.

Figure 5.26 shows qualitatively the spray image of the multiple overlap atomiser arrangement. It is worth noting that a significant amount of entrainment was occurring, this was instigated by the interaction of the sprays and also subsequent coalescence of droplets at the point of intersection and immediately downstream of the sample axis. This is reinforced and discussed in the following corresponding data.

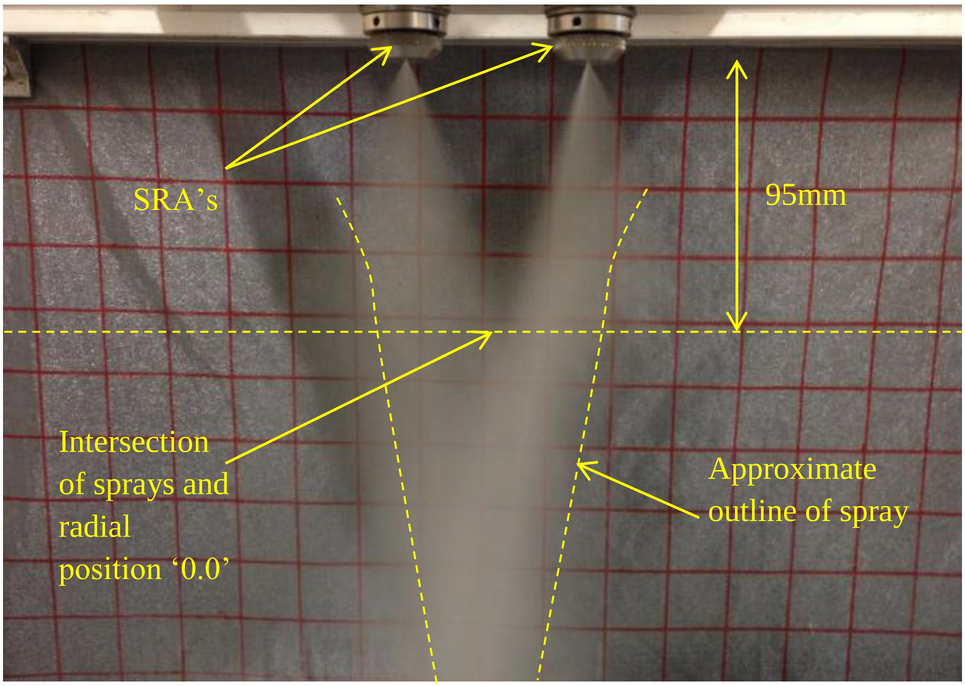

Figure 5.26 : Multiple SRA Type B spray

The subject of overlapping sprays has been examined and modelled by several authors. Kaesemann and Fahlenkamp [90] derived a computational model for sprays used in a flue gas scrubber. In all cases there was a higher droplet concentration reported in the overlapping region, coupled with an increase in D_{32} due to the collision and coalescence of droplets.

In certain fire suppression or explosion mitigation situations overlapping sprays will provide an advantage, such as:-

i. in a fire curtain or deluge system consisting of multiple sprays, the larger droplets resulting from overlapping sprays will have a greater mass, thus increasing the likelihood of the droplets overcoming thermal up draught currents from the fire and therefore allowing the water droplets to reach the seat of the fire and to cool the solid fuel material.

ii. in high speed flame propagation and mitigation experiments, larger droplets are used because of their ideal Weber number and hydrodynamic instability. Many of the studies discussed in Chapter 3 utilised overlapping sprays.

However, the consequential increase in D_{32} from overlapping sprays is unlikely to be an advantage in this current work, as droplet heating and vaporisation within the flame front is the principle mechanism of heat transfer. Whereas in previous studies using accelerated flames, droplets were broken up by the force of the blast into ultrafine mist.

The D_{32} of the multiple overlapping Type B atomisers was found to range from approximately 35 - 45μm in the centre of the spray, rising to 54μm at a radial position of 50mm, as shown in Figure 5.27. A significant increase in drop size was also observed towards the extreme limits of the spray. These were probably droplets that had gained sufficient mass, so as not to be entrained with the smaller droplets. This is reinforced in Figure 5.27, where only a very small number of droplets were found between 70 - 80μm.

For explosion mitigation, droplet distribution is equally as important as the D_{32}. With smaller drop sizes providing a greater chance of achieving boiling point and the subsequent release of latent heat, it is important to consider the percentage of droplets in the spray below a certain value. Figure 5.27 illustrates the percentage of droplets in the sample that are, D_{32}, ≤30μm, in line with the objectives of this thesis and also for droplets of D_{32}≤26μm, for comparison with the single SRA Type B spray which had a D_{32} of approximately 26μm.

Sapko et al [61] originally postulated a relationship between droplet diameter and heat up times presented by Kumm [62]. Kumm's formula was discussed explicitly in Chapter 3. This formula has been adapted for these trials, with the additional consideration of the unique low flame speeds and thicker flame fronts produced in the FPMR.

As anticipated, droplet velocity and liquid volume flux are highly irregular across the sample and this is reinforced by the representations in Figures 5.29 and 5.30. In the Figure 5.29 the velocity is initially slow in the centre of the sprays at the point of overlap. Equally, this is at the same point that the liquid volume flux is at its greatest, as shown in Figure 5.30.

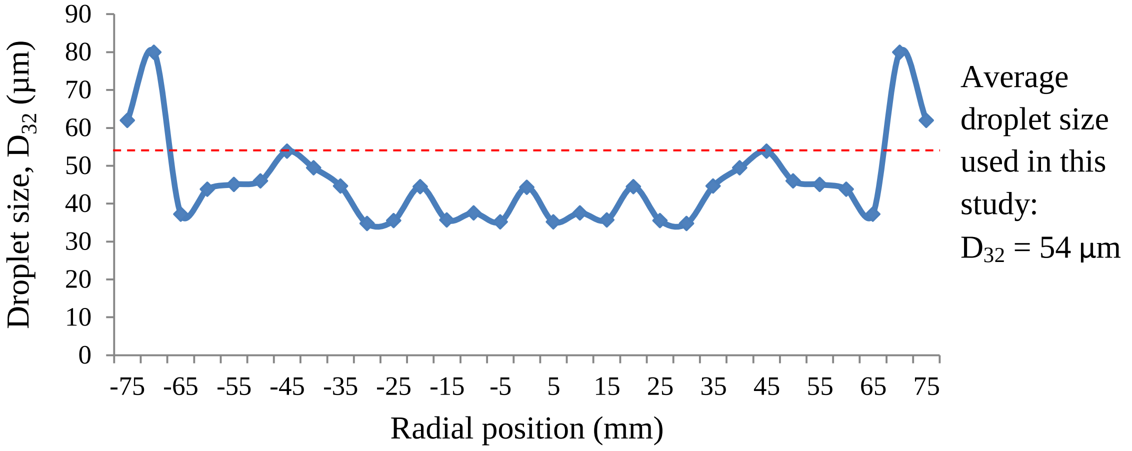

Figure 5.27 : D_{32} at 95mm downstream for overlapping SRA Type B spray arrangement

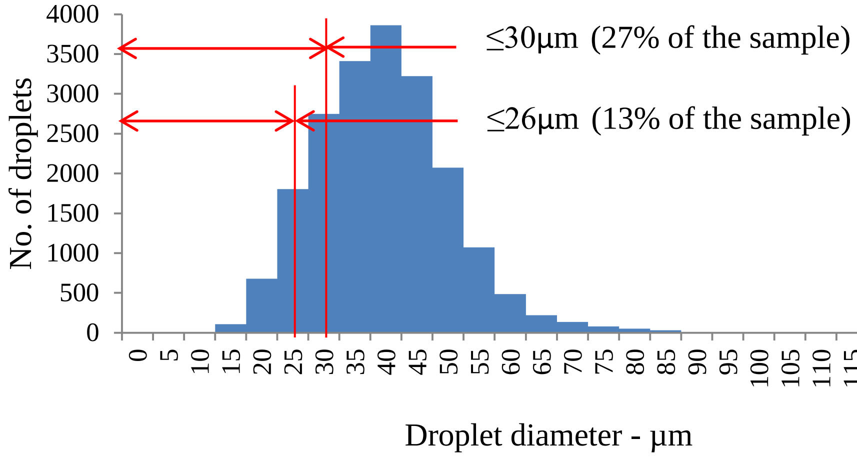

Figure 5.28 : Droplet distribution at 95mm downstream for multiple overlapping SRA Type B spray arrangement

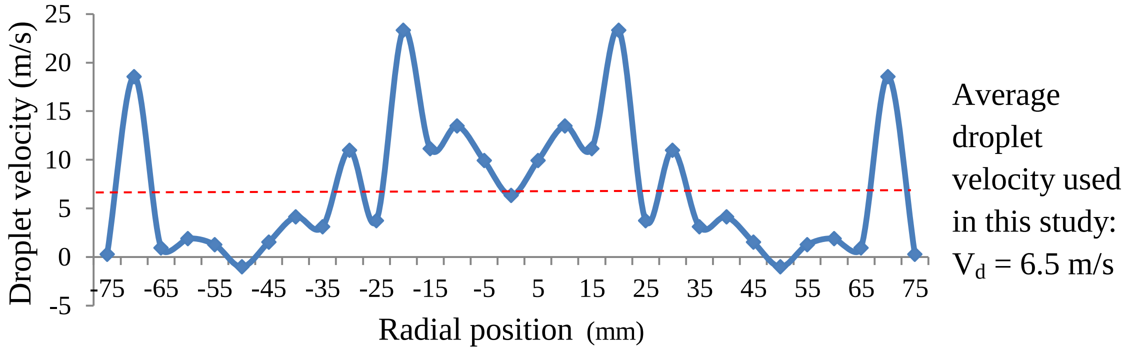

Figure 5.29 : Droplet velocity (m/s) at 95mm downstream for multiple overlapping SRA Type B spray arrangement

Entrainment resulting from the interaction of the liquid stream with the atmospheric air stream is also apparent with a reduction of droplet velocity to zero and even slightly negative at the radial position of 50 – 55mm, as previously shown in Figure 5.29.

This negative droplet velocity is an indication that droplets were travelling in the opposing direction and may be attributed to the recirculating eddies in the extremities of the spray caused by the air entrainment. This is not apparent in Figure 5.30, as droplet direction or trajectory will not affect liquid volume flux.

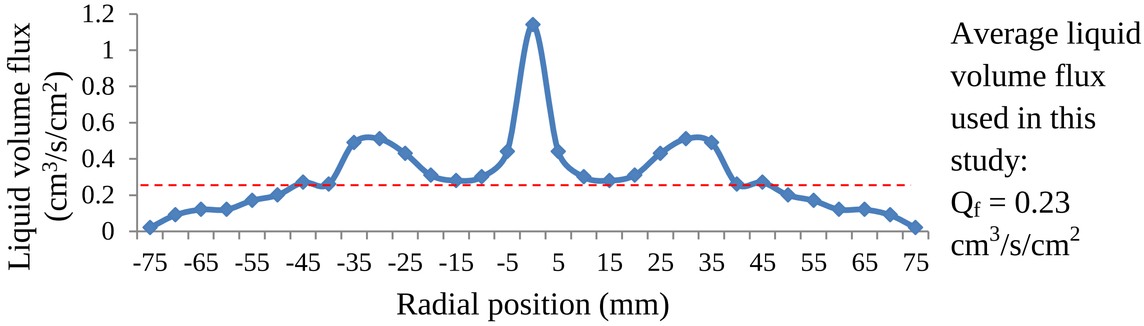

Figure 5.30 : Liquid volume flux ($cm^3/s/cm^2$) at 95mm downstream for multiple overlapping SRA Type B spray arrangement

In this series of spray characterisation trials the sprays were all mounted in a vertical plane in the surrounding atmosphere. In the subsequent Section, single SRA's were characterised in a segment of PMMA tube to simulate the conditions within the FPMR. Single SRA configurations Type B and C were appraised using PDA techniques in cross tube conformation and in a horizontal plane, prior to the hot trials.

5.3.2 SRA spray within simulated PMMA tube

To ensure that valid and reliable conclusions could be derived from the hot trials, additional spray characterisation was necessary to assess the behaviour of the sprays within the FPMR. Throughout the literature survey discussed previously in Chapter 3, there was no evidence that this was either carried out, or considered in any of the previous work. Consequently the inclusion of this additional testing will reinforce the reliability of the reported evidence in the hot trials. Conversely, the omission of such information in previous studies casts some doubt into the accuracy and degree of error in their reported findings.

A new test rig was constructed within the existing PDA and traversing system which facilitated the mounting of a short section of 190mm (I.D.) PMMA tube. The concept, design challenges and set up processes for this apparatus were provided formally in Chapter 4.

Initial trials produced highly irregular results, including many cases in which the experiment was aborted as the receiving optics could not detect the droplets in the measuring volume. The main challenge was the build-up of fine water droplets and aerosols on the inside surface of the tube.

Figure 5.31 shows the laser beam from the transmitting optics being refracted by the external surface of the tube and by the droplet deposition on the inside of the tube. An alternative method was required to capture the droplets within the tube, with a clear ‘line of sight’ for the transmitting and receiving optics.

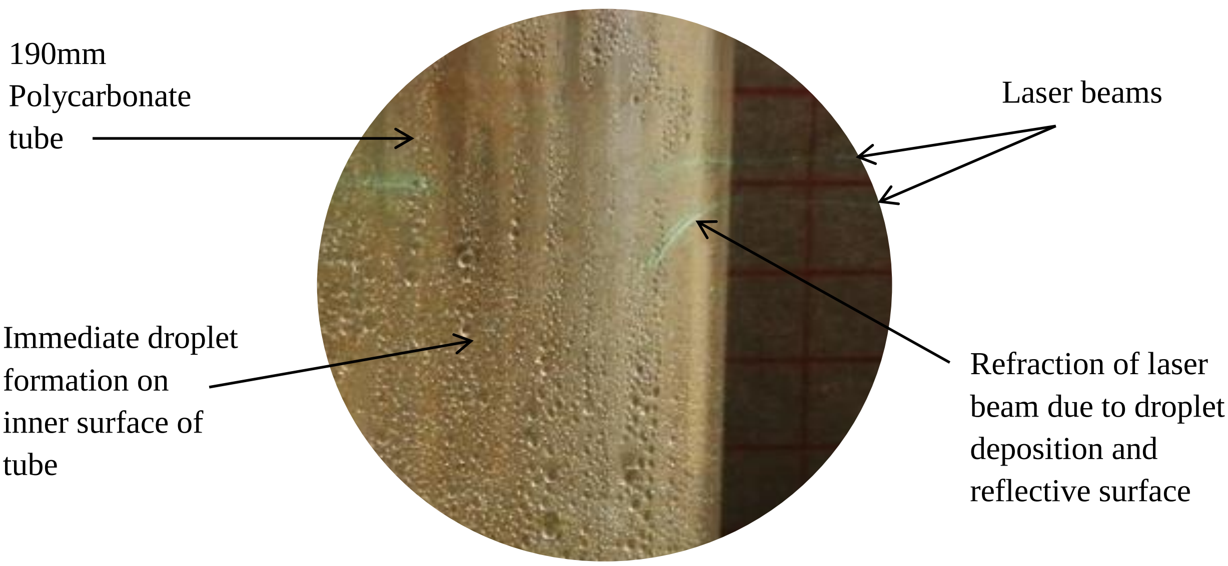

Figure 5.31 : Droplet deposition and refraction of laser beams in simulated tube

The equipment shown in Figure 5.32 was refined through experimental trials and eventually an uninterrupted series of tests were performed with a consistent level of success. The atomiser arrangements selected for the enclosed ‘cross tube’ characterisation trials were:-

i. SRA arrangement Type B (0.5mm exit orifice and 0.5mm spill diameter)
ii. SRA arrangement Type C (0.8mm exit orifice and 0.5mm spill diameter)

Although not all of the droplets in the spray were enabled to be captured, the results presented were all repeatable. This was due to the high degree of misting and pluming caused by aerosols within the tube, with the atomisers being in cross tube conformation. It is conceivable that limited secondary atomisation would have been occurring, as the spray droplets impacted against the opposing internal surface of the tube. (See also CFD consideration, Chapter 6)

While deemed to be outside of the scope of this current study, additional spray research to attempt to quantify the aerosol sized droplets (≤10μm) would be beneficial for future work. Methods including, Particle Image Velocimetry (PIV), ultra high resolution photography and supercooled droplet analysis should be considered within the scope of future studies.

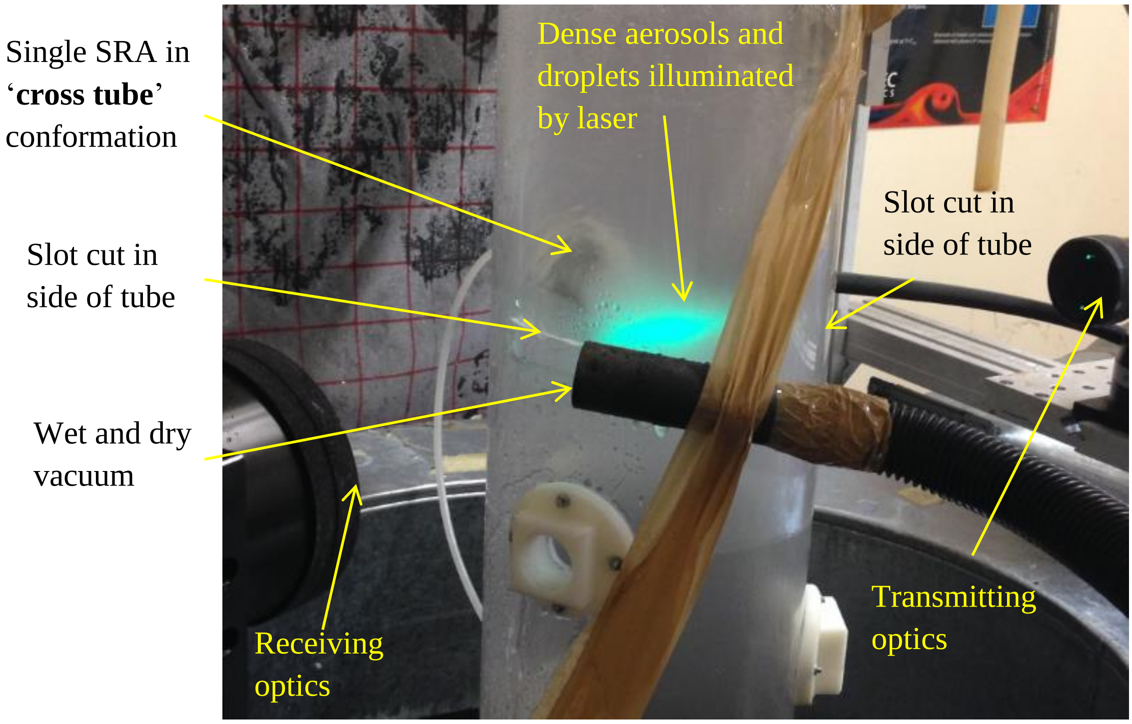

Figure 5.32 : Set up to acquire data for enclosed single SRA cross spray conditions

5.3.2.1 Single SRA configuration : Type B

The single SRA Type B configuration was characterised in **'cross tube'** spray confirmation using the additional set up shown previously in Figure 5.32. The D_{32} of the spray was found to range between 30 - 46µm across the radial axis, 95mm downstream of the SRA exit orifice. This range was narrower than that found with the corresponding atomiser in ambient air, as illustrated previously in Section 5.3.1.2. In addition, the D_{32} measured at the axial centre of the spray was found to be 30µm in this enclosed trial as shown in Figure 5.33, compared to 25µm in the ambient sample, as shown previously in Figure 5.15.

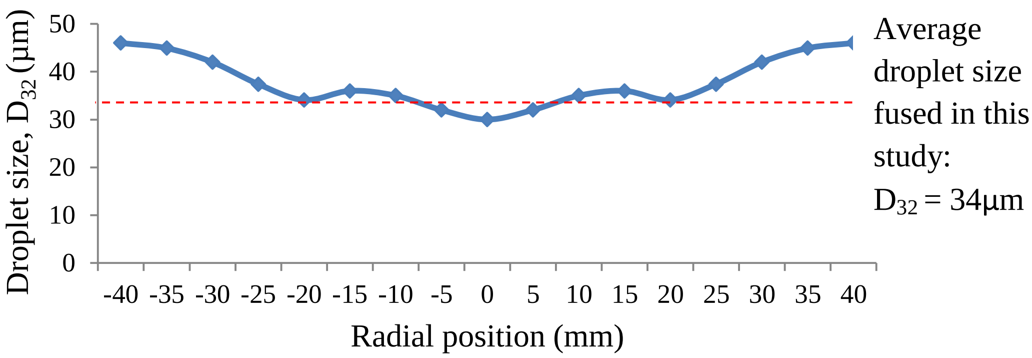

Figure 5.33 : D_{32} (µm) at 95mm downstream for enclosed SRA type B

The most likely reason for this increase, is that the droplets in the region of the sampling volume were gathering some mass from the droplets and mist returning in the opposite direction, resulting from the impact from the opposing internal surface of the tube. This postulation is supported by the velocity profile presented in Figure 5.35, which demonstrates a high level of disorder across the spray. Additionally the area of the graph below the x axis in Figure 5.35 is approximately equal to the area above the x axis, which represents an average velocity of approximately ≤0 m/s. This 'mean suspension' of radial droplet activity provides for ideal conditions for droplet interaction with the approaching flame front.

In Figure 5.34 it is noted that 48.5% of droplets in the sample were of D_{32} ≤30µm and 19.7% were of D_{32} ≤25µm. Droplet residence times and heat transfer in the flame were discussed formally in Chapter 3 and will be also consider in the following Sections.

The liquid volume flux profile for this spray configuration is revealed in Figure 5.36, where values range from 0.02 – 0.8cm^3/s/cm^2, with a sample average of 0.044cm^3/s/cm^2.

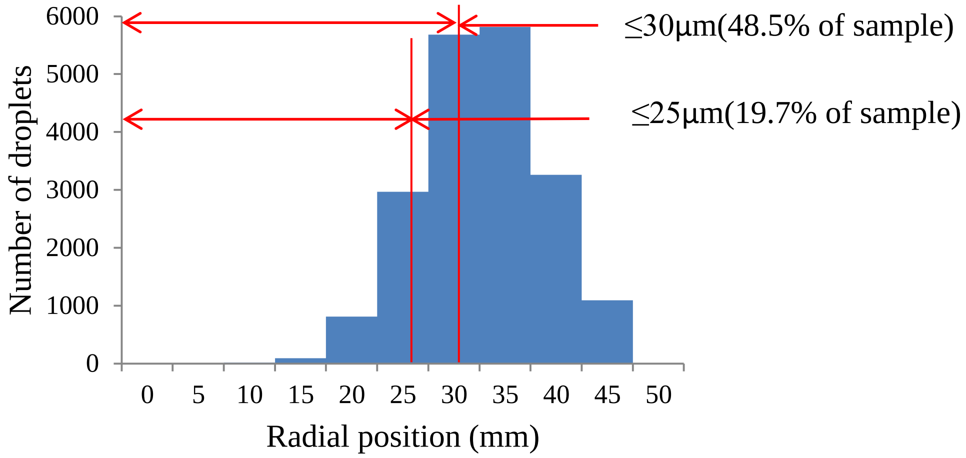

Figure 5.34 : Droplet distribution at 95mm downstream for enclosed SRA type B

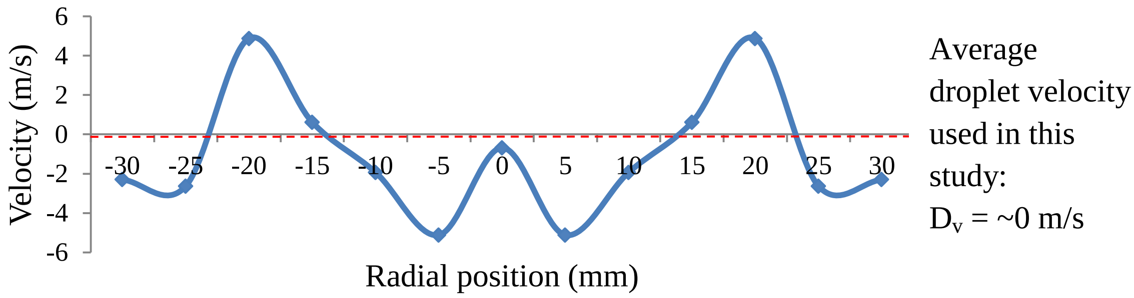

Figure 5.35 : Droplet velocity (m/s) at 95mm downstream for enclosed SRA type B

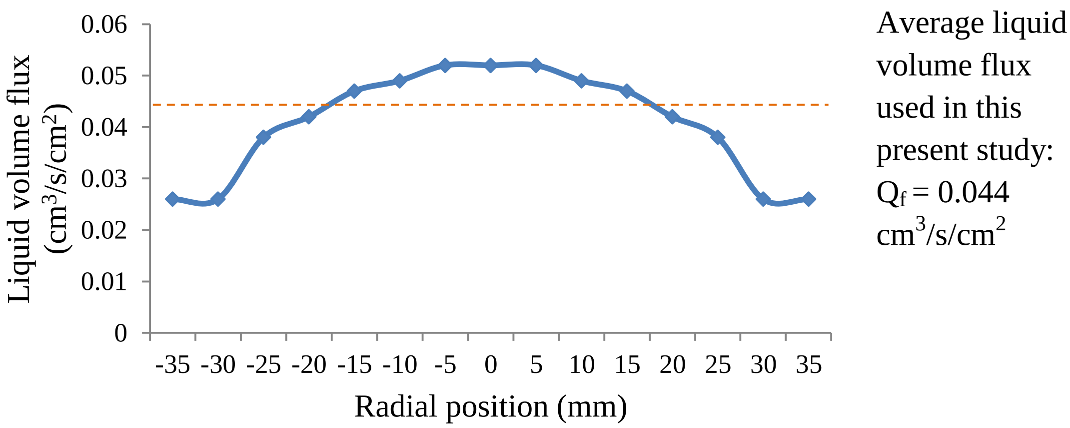

Figure 5.36 : Liquid volume flux ($cm^3/s/cm^2$) at 95mm downstream for enclosed SRA type B

5.3.2.2 Single SRA configuration : Type C

In agreement with the results obtained from the enclosed condition trials for the SRA Type B, the enclosed SRA Type C also displayed an increase in droplet size and a dramatic reduction in velocity, when compared to ambient results previously presented in Section 5.3.1.3. Figure 5.37 shows the D_{32} profile of the spray with drop sizes ranging from D_{32} 34.14 – 51.05µm and resulting average value of D_{32} 39µm as shown.

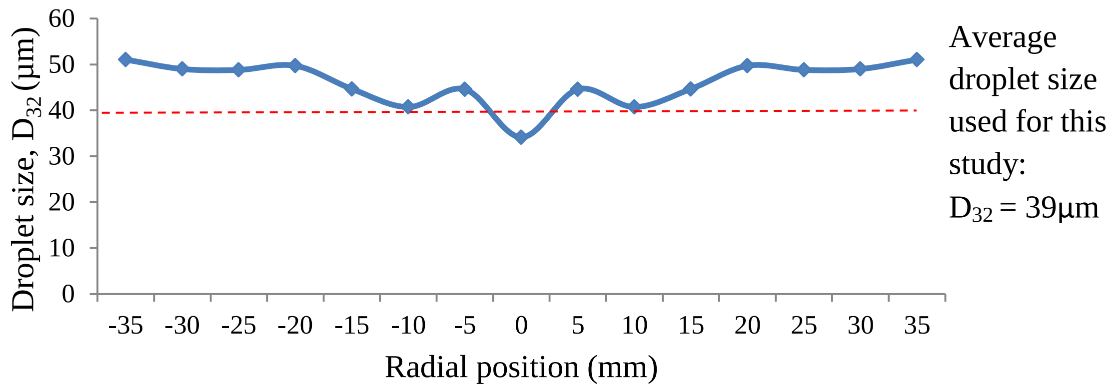

Figure 5.37: D_{32} (µm) at 95mm downstream for enclosed SRA Type C

In Figure 5.38 it is noted that 28% of droplets in the sample were of ≤30µm and 8.1% were of ≤25µm. Droplet transit times and heat transfer in the flame were discussed explicitly in Chapter 2 and will also be considered later in the discussions of the hot trials results.

The liquid volume flux profile for this spray configuration is exhibited in Figure 5.39, which ranged from 0.06 – 0.82cm^3/s/cm^2, with a radial sample average of 0.045cm^3/s/cm^2.

As with the observations concerning the enclosed conditions for the SRA Type B, the droplet velocity shown in Figure 5.40 is highly disorganised across the sample. This is due to droplet collision and consequential break up on the opposite internal tube surface.

As discussed earlier in this Section, not all of the droplets in the spray were enabled to be captured, although the results presented were all repeatable. This was due to the high degree of misting and pluming caused by aerosols within the tube. This field of further research activity was deemed to be outside of the scope of this current study.

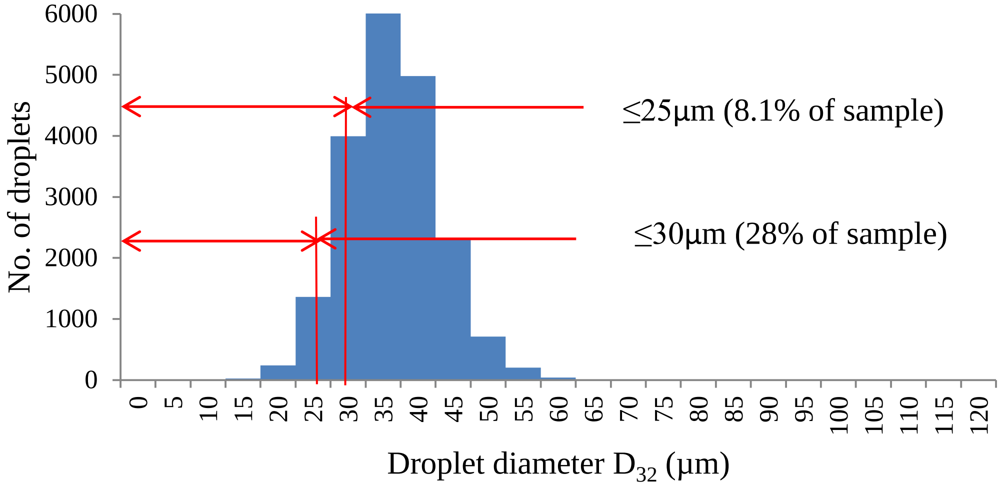

Figure 5.38 : Droplet distribution at 95mm downstream for enclosed SRA type C

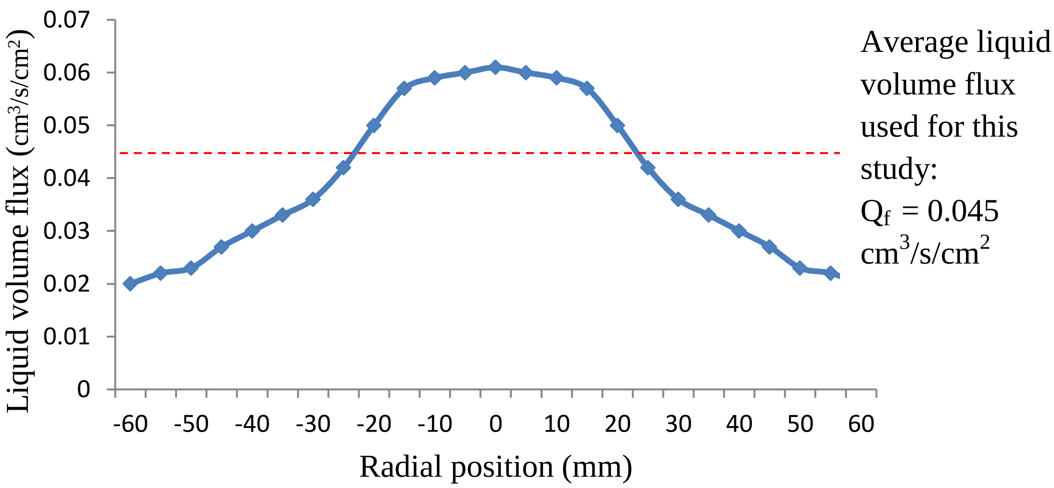

Figure 5.39 : Liquid volume flux ($cm^3/s/cm^2$) at 95mm downstream for enclosed SRA type C

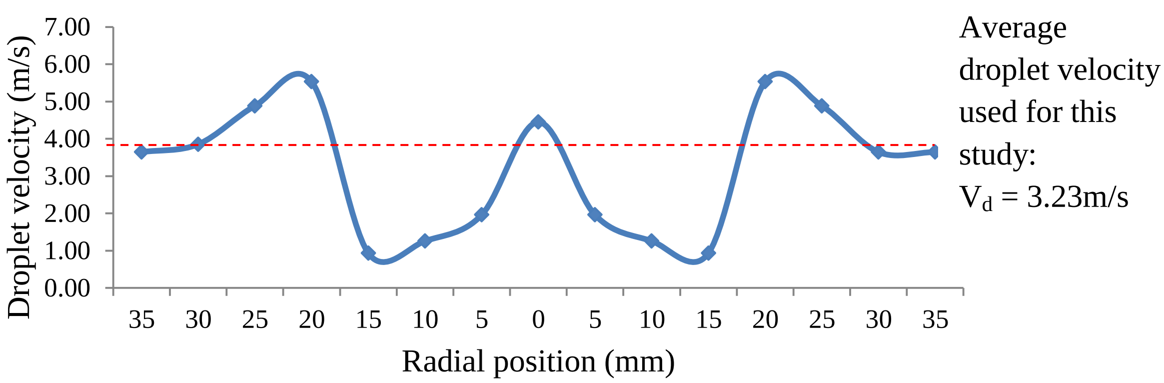

Figure 5.40 : Droplet velocity (m/s) at 95mm downstream for enclosed SRA type C

5.3.3 Summary of Cold trials

The principle objectives of these cold trials were to characterise a series of Spill Return Atomiser (SRA) configurations and to assess their potential suitability for selection for the hot trial series of this study. Throughout the hot trials, various SRA configurations will be placed within the FPMR to permit a study of the mitigation of **partly confined / vented explosions**.

Table 5.5 is presented here again for convenience, provides a reminder of the critical orifice dimensions for SRA configuration types A, B and C.

SRA designation	Exit orifice diameter (mm)	Spill orifice diameter (mm)	Tangential inlet orifice diameter (mm)
Type A	0.3	0.5	0.6 x 2
Type B	0.5	0.5	0.6 x 2
Type C	0.8	0.5	0.6 x 2

Table 5.5 : Summary of orifice dimensions for SRA configuration types A, B and C

As a consequence of the flow rate trials described in Section 5.22, the SRA Type D configuration was eliminated from the selection process due to flow irregularities. Further studies have been recommended in Chapter 7 relating to the utilisation and development of the SRA and its suitability for future larger realistic scale trials.

Following this series of dynamic spray and droplet measurements including exit and spill orifice flow rates, Q (L/min), spray cone angle (θ) of droplet diameter, D_{32} (µm), velocity, D_v (m/s) and liquid volume flux, Q_f ($cm^3/s/cm^2$), Table 5.6 was produced in summary.

The main objective of these cold trials was to characterise a number of SRA configurations and conformations as part of a selection and elimination process prior to the subsequent hot trials phase of this study. Six of the seven SRA's included in these cold trials were deemed suitable for use in the succeeding hot trials, with the SRA Type D being dismissed from further use, due to flow irregularities in the spill return orifice.

In the following *hot trials*, the SRA's were placed within the FPMR in the path of a propagating flame front. The corresponding hot trial experiments were each designed to assess and appraise the ability of a number of the SRA configurations with relevance to the successful mitigation of partly confined / vented gas explosions.

Atomiser configuration type and conformation	Cone angle θ (degree)	Penetration d_p (mm)	Exit orifice flow rate Q (L/min)	Spill orifice flow rate Q (L/min)	Average droplet diameter D_{32} (μm)	Average droplet velocity V_d (m/s)	Average liquid volume flux, Q_f ($cm^3/s/cm^2$)	Percentage of D_{32} droplets ≤30μm (%)
SRA Type A in ambient conditions	34.7	304	0.295	1.120	17 [53]	13.50 [53]	0.011 [53]	58 [53]
SRA Type B in ambient conditions	42.7	243	0.850	0.850	26	21.41	0.024	48
SRA Type C in ambient conditions	49.2	207	1.360	0.490	29	13.50	0.039	46
SRA Type D in ambient conditions	54.2	186	1.940	0.250	N/A	N/A	N/A	N/A
SRA Type B in overlapping ambient conditions	N/A	300	1.700	1.700	54	6.50	0.038	27
SRA Type B in simulated tube	42.7	190	0.850	0.850	34	~ 0.0	0.044	48.5
SRA Type C in simulated tube	49.2	190	1.360	0.490	39	3.23	0.047	28

Table 5.6 : Summary of dynamic spray and droplet measurements using a water pressure of 13MPa

5.4 Hot trials : Results and discussions

Further to the completion of a successful series of safety and commissioning trials, the following *explosion and mitigatation* testing was performed under controlled laboratory conditions using the calibrated and certificated equipment as described in Chapter 4.

Prior to the corresponding assessment of atomiser performance in the FPMR, a series of conditioning trials where carried out to establish initial explosion conditions within the FPMR, including imagery of the propagating flame front, determination of flame speeds, together with pressure and temperature profiles. Initially these explosion tests were performed without the atomisers in position, followed by tests with the atomiser in position, but without high pressure water being supplied. These will be refered to as 'dry' conditions and were conducted to establish any affects that the atomiser and water supply pipework might have on flame speeds, pressures and temperature profiles within the confines of the FPMR.

A large percentage of these hot trials were performed using the four designated methane-air mixtures as shown in table 5.7. For convenience some of the cross flow trials were only carried out using a single *methane-air mixture of E.R. (ϕ) 0.95*, since this mixture presented the *greatest mitigation challenges* in all of the other tests. Eqivalence ratios, E.R. (ϕ) have been stated to allow for comparison with other studies. This method is widely used to compare the actual fuel-air mixture with the equivalent stoichiometric fuel-air mixture. This relationship was discussed previously in Chapter 4.

Gas type	Gas in air volume percentage (%) within tube	Equivalence ratio (ϕ) within tube
Methane	6	0.61
Methane	7	0.72
Methane	9	0.95
Methane	10	1.06

Table 5.7 : Methane-air volume percentage (%) and Equivalence ratio (ϕ)

Following the 'dry' explosion trials all of the remaining tests were carried out using either single, or multiple SRA configuration Types A, B, and C, in counterflow (C/F), parallel flow (P/F) and (X/F) cross flow with the propagating flame. These terms are described and illustrated in the subsequent Section.

5.4.1 Water sprays in counter flow, parallel flow and cross flow with a propagating methane-air flame

This novel series of explosion mitigation trials were devised by the author and subdivided into three principle categories, with the main objectives being the acquisition of unique, valid and reliable research data and imagery. The three categories were:-

i. water sprays in counter flow configuration with a methane-air flame (Figure 5.41 (i))
ii. water sprays in parallel flow configuration with a methane-air flame (Figure 5.41 (ii))
iii. water sprays in cross flow configuration with a methane-air flame (Figure 5.41 (iii))

Additional information relating to the construction of the apparatus, operational procedures, arrangement and position of hardware and sources of error can be found in Chapter 4.

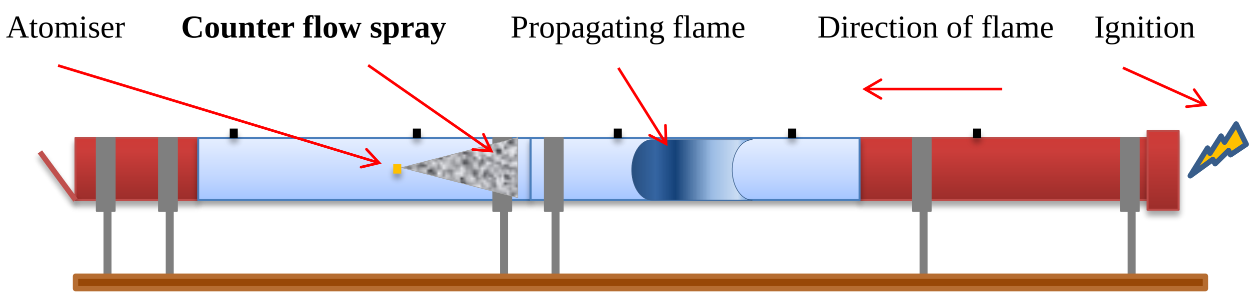

(i) water sprays in counter flow configuration with a methane-air flame

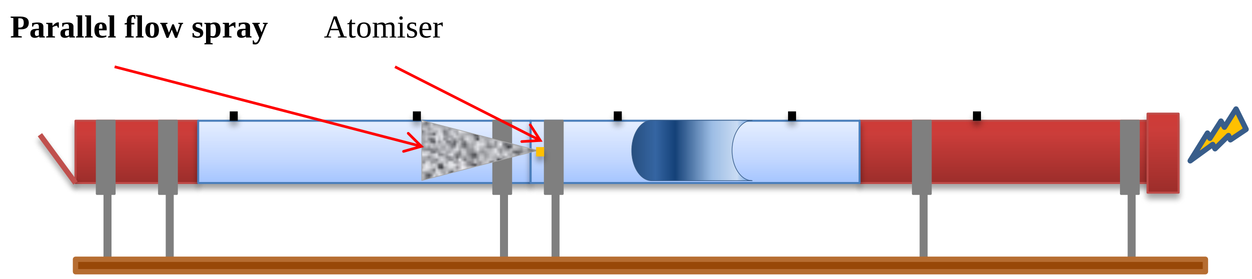

(ii) water sprays in parallel flow configuration with a methane-air flame

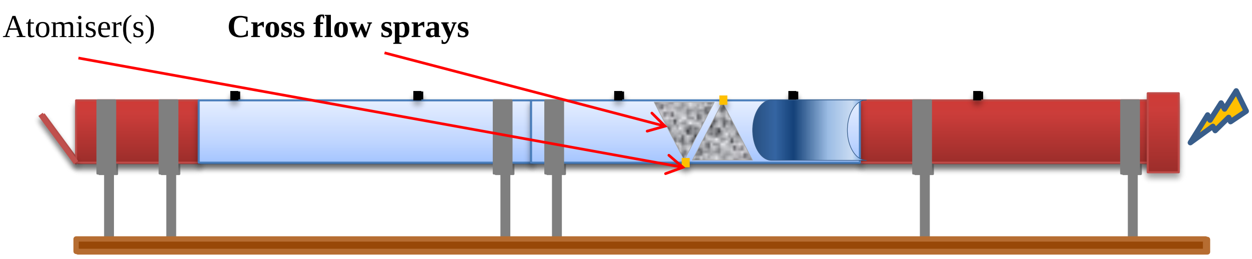

(iii) water sprays in cross flow configuration with a methane-air flame

Figure 5.41 : Illustration of flame propagation direction and water spray configuration

5.4.2 Commissioning and conditioning trials

The commissioning and conditioning trials took place subsequent to the cold trials and were devised to achieve the following objectives:-

i. Verify the safe, reliable and consistent operation of the FPMR
ii. Prove the reliability of the safety, process flow and operating procedures
iii. Check the reliability and validity of data acquisition hardware and software
iv. Test the photographic and video equipment and ensure adequacy of output imagery

To ensure that consistent methane-air mixtures were present in the FPMR, a volume of methane was introduced into the rig via a rotameter, circulated around an external bypass as shown previously in Chapter 4 and then measured using a calibrated GMI Gascoseeker. Since the rig length volume would be unchanged for all of these trials, several tests were carried out to assess the reliability of filling the rig at a given flow rate over a measured time period. Following a number of trials, a convenient flow rate of 200 L/min was adopted. Table 5.8 was produced to simplify the rig filling process, although the methane-air mixture was additionally verified following the recirculation of the mixture around the external bypass circuit and prior to ignition. Methane-air sampling was carried out approximately one minute after the mixing, at three points along the length of the rig. Information relating to the suitability and accuracy of the GMI Gascoseeker can also be found in Chapter 4.

Methane-air (%)	Flow rate (L/min)	Duration (min:sec)
6	200	02:25
7	200	02:45
8	200	03:00
9	200	03:25
10	200	03:40
11	200	04:05

Table 5.8 : Typical filling times for various methane-air mixtures

During the commissioning trials, an important discovery was made with respect to the water supply induction tube on which the atomisers were mounted and supplied with a high pressure water supply. The original water induction tube shown in Figure 5.42 was fabricated using galvanised steel pipe. Whilst commissioning, minor oxidation was found to be occurring in the pipe overnight, resulting in partial or complete blockage of the SRA with ultrafine rust particles. Prior to the main trials, the induction tube was modified and replaced with 316 stainless steel. It is recommended that any further work following on from this current study shall only use stainless steel or plastic water supply systems.

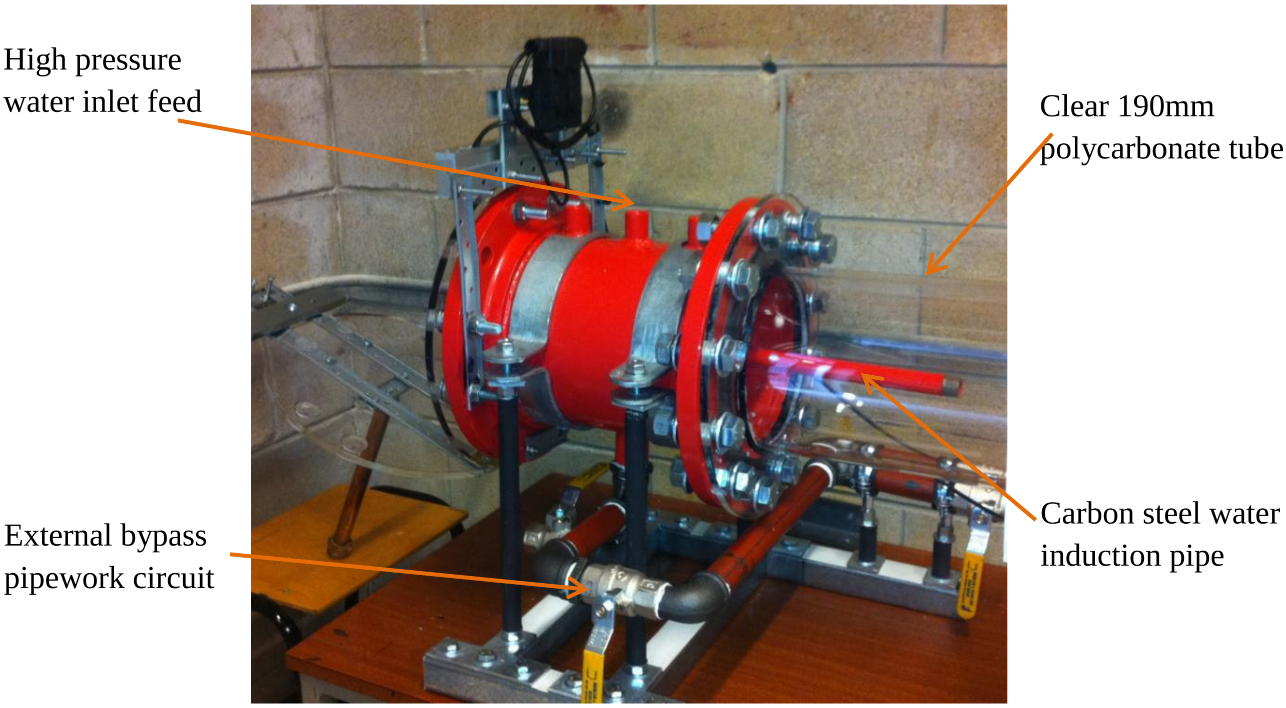

Figure 5.42 : Original high pressure water connections and induction pipework

Photography and video imagery taken during the commissioning trials were edited and processed to ensure satisfactory quality and definition for the remaining trials.

Data acquisition hardware and software were also tested to ensure their correct performance and reliability. The exposed junction, type K thermocouples were placed at intervals along the length of the flame propagation and mitigation rig in accordance with Figure 4.44.

Due to lag time associated with thermocouples as previously discussed in Chapter 4, the data measurements offered during the hot trials are not intended to represent the actual flame temperatures within the FPMR. The use of these exposed junction thermocouples has been demonstrated to be an acceptable method for comparing flame propagation within ‘confined’, ‘partly confined’ and ‘unconfined’ explosion testing in vessels and pipework. These were extensively described in numerous previously published works [87,88,89]. (See also Chapters 3 and 4)

The time-temperature data acquired throughout these hot trials will be used to compare temperature profiles for unmitigated and mitigated experiments. All of the time-temperature results have been illustrated over a two second period. The two second period was extracted from the unprocessed data commencing at a point where a 5˚C temperature rise occurred at TC1 (thermocouple no.1). This point will be used to indicate the onset of flame propagation and will be referred to as the 'trigger point'. Although the time-temperature curve for TC1 has been included in each case, data will not be considered in post processing or discussions.

Pressure transducers had been used by previous authors when examining the relationship with flame speed and over pressure. As a flame propagates through a combustible mixture it acts as a porous piston partly consuming flammable mixture, whilst also pushing unburned mixture forwards. Inertia resistance to the forward flow results in a pressure wave. In these previous experiments flame speeds were significantly higher, often by several orders of magnitude than those employed in this current study. The relevance of peak over pressures and subsequent reductions in pressures was highly important to the previous studies.

In this current study the rig was filled with a methane-air mixture, which was vented immediately upon ignition, with an initial pressure rise of only ≤2KPa. This small pressure rise was dispersed immediately and was only detectable in the first 2m section of the rig.

During the commissioning trials several tests were performed using a range of methane-air mixtures (ϕ) 0.5≤1.0≤1.69 (5 - 15%), in the presence of water sprays and also without the inclusion of water sprays. The pressure data acquisition equipment was in unison with the thermocouple data and was also triggered by the 5˚C temperature rise at TC1. Figure 5.43 illustrates the time-pressure relationship from four of the commissioning trials.

Figure 5.43(i) methane-air mixture E.R. (ϕ) 0.61 with **no sprays** activated (*dry*). The initial peak pressure was 1.7KPa, which decayed to approximately 0.3KPa.

Figure 5.43(ii) methane-air mixture E.R. (ϕ) 0.95 with **no sprays** activated (*dry*). The initial peak pressure was 1.9KPa, which decayed to approximately 0.4KPa.

Figure 5.43(iii) methane-air mixture E.R. (ϕ) 0.61 and **with sprays** activated. The initial peak pressure was 1.8KPa, which decayed to approximately 0.33KPa.

Figure 5.43(iv) methane-air mixture E.R. (ϕ) 0.95 and **with sprays** activated. The initial peak pressure was 1.9KPa, which decayed to approximately 0.34KPa.

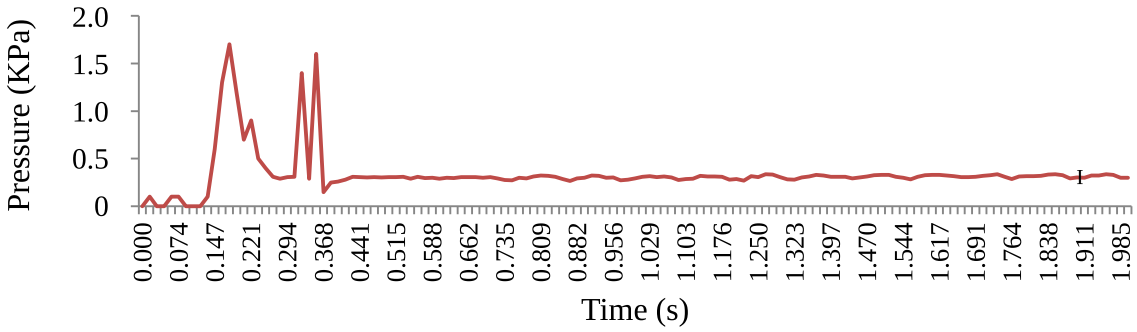

(i) Typical time-pressure profile for ER (ϕ) 0.61 – **no spray (*Dry*)**

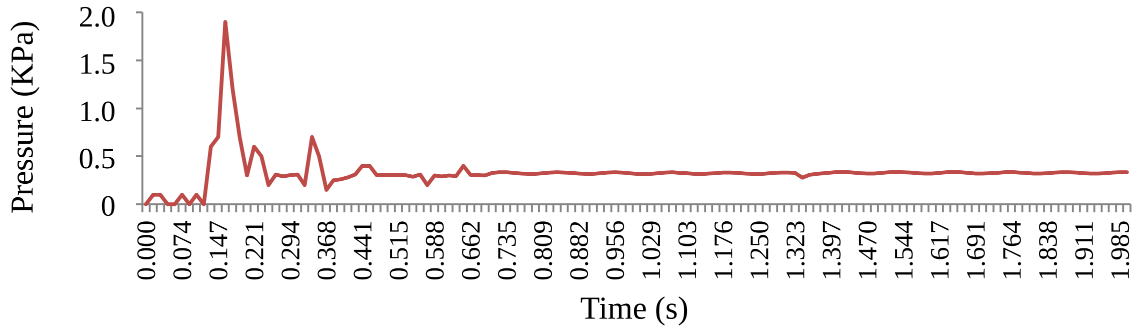

(ii) Typical time-pressure profile for ER (ϕ) 0.95 – **no spray (*Dry*)**

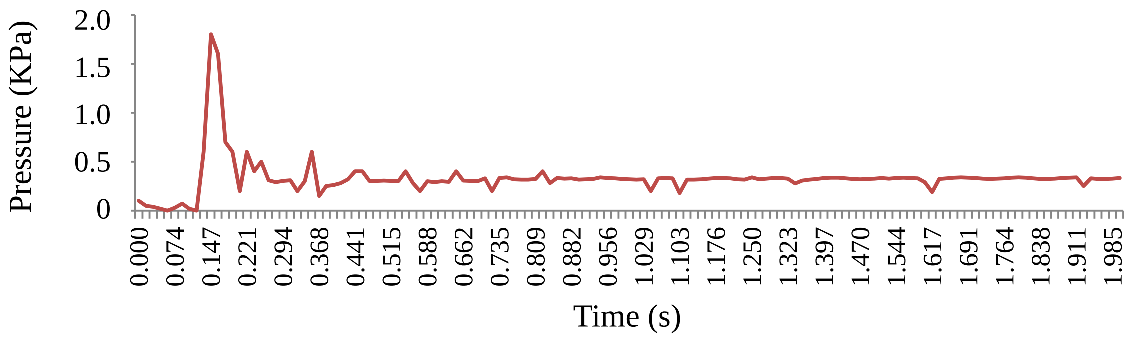

(iii) Typical time-pressure profile for ER (ϕ) 0.61 – **with sprays**

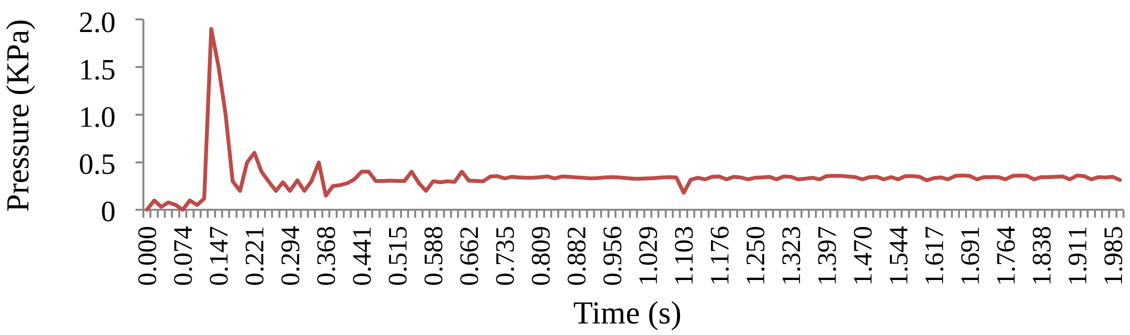

(iv) Typical time-pressure profile for ER (ϕ) 0.95 – **with sprays**

Figure 5.43 : Time-pressure profiles for different (ϕ) 0.95 for tests **with and without sprays**

The time-pressure profiles presented above in Figure 5.43 illustrate how the FPMR immediately and consistently vented the majority of the explosion overpressure to the surrounding atmosphere of the laboratory. This *reflects the aims and objectives* and the original apparatus concept as described in Chapter 4, whereby the propagating flame speeds are *limited to ≤30m/s by design*.

Because of this design feature and the unique characteristics of the rig, there were no significant differences between any of the examples presented in figure 5.43, regardless of mixture E.R., or whether sprays were operating or not. For this reason, the remaining unprocessed pressure data will not be included in the subsequent hot trials results.

5.4.3 Preliminary flame speed : No atomiser (dry)

The following flame speed test results were obtained by assembling the FPMR without any atomisers, or in other words ‘**dry**’ conditions without the presence of water sprays or SRA’s. This provided a series of data, imagery and results relating to the performance characteristics of the rig prior to the series of atomiser performance hot trials. These conditions permitted the free propagation of the flame along the length of the rig from right to left, undisturbed by any third party interference.

Figure 5.44 provides further clarification regarding the apparatus and direction of travel of the flame. Thermocouples (TC) locations are also shown in figure 5.44, with their precise positions given in Table 5.9.

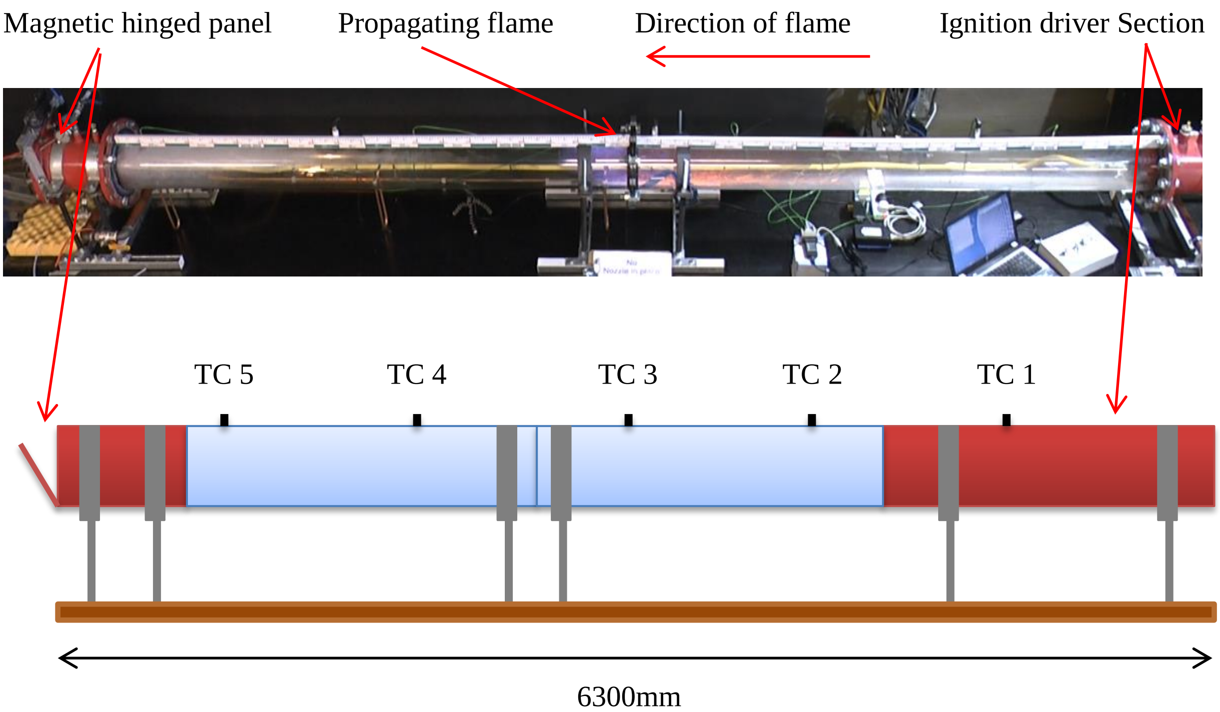

Figure 5.44 : Position of thermocouples (relative to right hand ignition end)

Component	TC position (measured from right hand end)
Thermocouple (TC1)	1200mm
Thermocouple (TC2)	2400mm
Thermocouple (TC3)	3600mm
Thermocouple (TC4)	4800mm
Thermocouple (TC5)	6000mm
Atomiser outlet orifice	Not installed

Table 5.9 : Measured position of thermocouples

This series of experimental tests were carried out using four different methane-air mixtures as shown previously in Table 5.7. Figures 5.46, 5.47, 5.48 and 5.49 are still images that have been selected and processed from the high definition (HD) video. In the first image from each series the flame has become visible as it emerges from the steel driver section, into the clear PMMA portion of the rig travelling from right to left.

In the three remaining images in each series the flame propagation can be observed. Each of the images has been referenced to the previous with respect to time (ms). The high quality still images have thus been used to estimate the average flame speeds along the length of the clear PMMA section. All of the HD video images were edited and time-coded using Adobe Premiere Pro CS6. Using these still images of the flame in conjunction with Adobe Photoshop CS4, the image was scaled using the pixel measurement tool. This method of flame speed measurement and level of accuracy was applied throughout this study.

Table 5.10 displays the resulting average flame speeds for each of the methane-air concentrations. Additionally the flame speeds have been graphically represented in Figure 5.45, which will be compared to other flame speeds in Section 5.44.

E.R. (ϕ)	Distance travelled by flame (mm)	Time period (ms)	Average flame speed (m/s)
0.61	3400	160	21.50
0.72	3250	140	23.21
0.95	3150	120	26.25
1.06	3000	120	25.00

Table 5.10 : Average flame speed for various methane-air mixtures E.R. (ϕ)

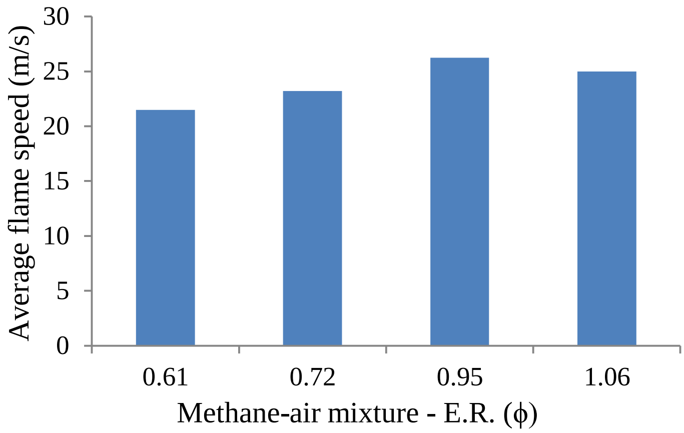

Figure 5.45 : Average flame speed for various methane-air mixtures E.R. (ϕ)

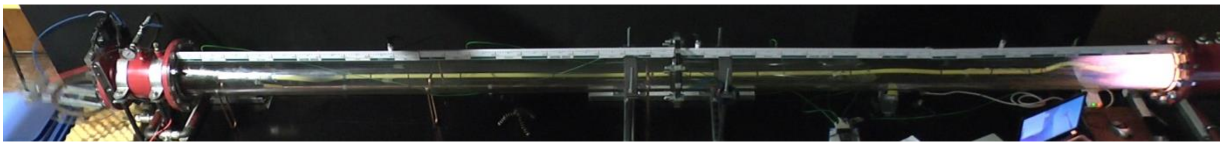

(i) Methane-air mixture - E.R. (ϕ) 0.61 : flame emerging from driver section

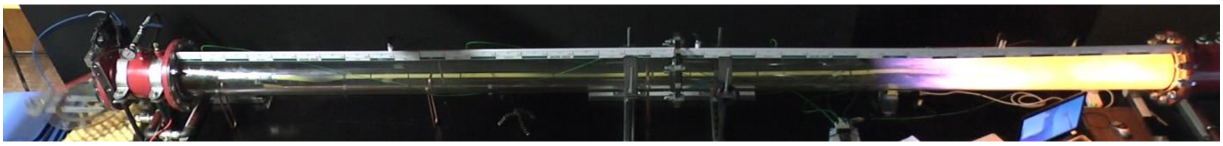

(ii) Methane-air mixture - E.R. (ϕ) 0.61 : flame 40ms downstream of (i)

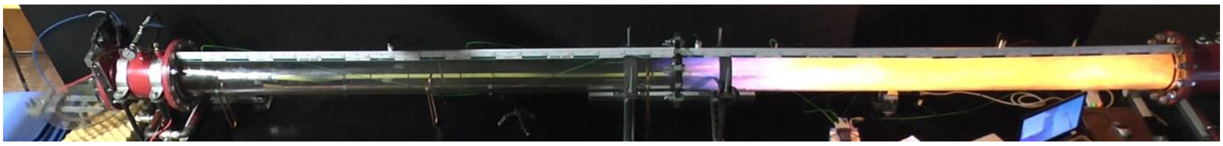

(iii) Methane-air mixture - E.R. (ϕ) 0.61 : flame 40ms downstream of (ii)

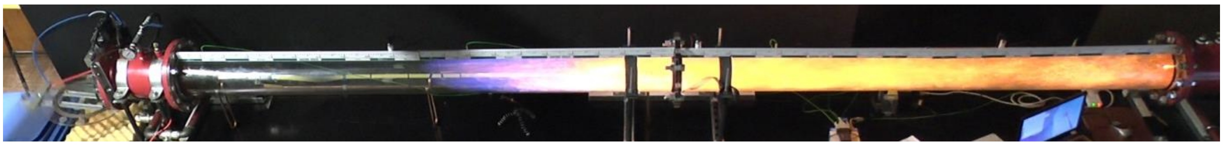

(iv) Methane-air mixture - E.R. (ϕ) 0.61 : flame 40ms downstream of (iii)

Figure 5.46 : Flame speed trial E.R. **(ϕ) 0.61** (***dry***) with **no atomisers** or spray present

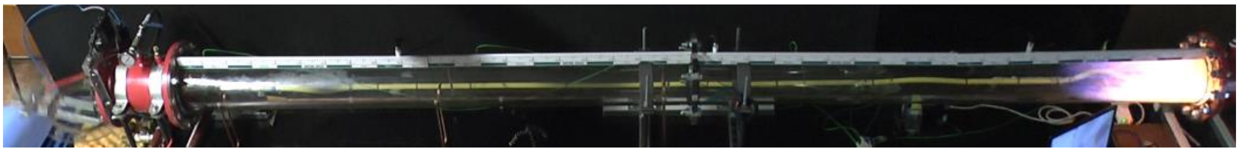

(i) Methane-air mixture - E.R. (ϕ) 0.72 : flame emerging from driver section

(ii) Methane-air mixture - E.R. (ϕ) 0.72 : flame 40 ms downstream of (i)

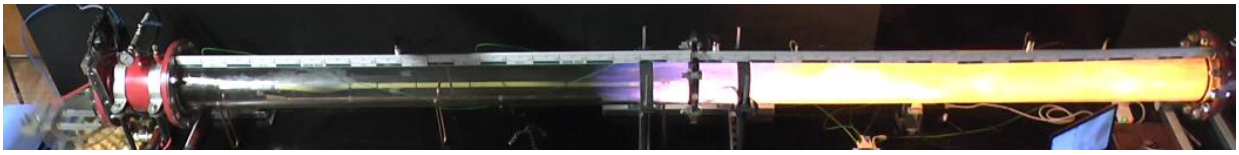

(iii) Methane-air mixture - E.R. (ϕ) 0.72 : flame 40 ms downstream of (ii)

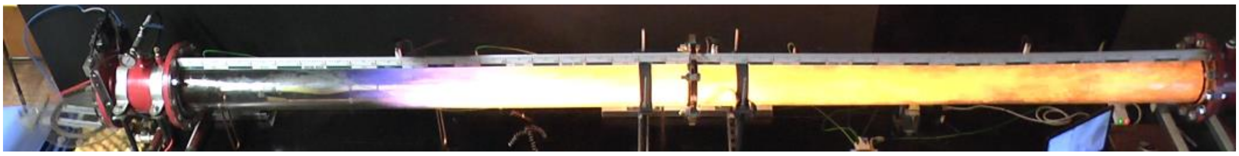

(iv) Methane-air mixture - E.R. (ϕ) 0.72 : flame 40 ms downstream of (iii)

Figure 5.47 : Flame speed trial E.R. **(ϕ) 0.72** (***dry***) with **no atomisers** or spray present

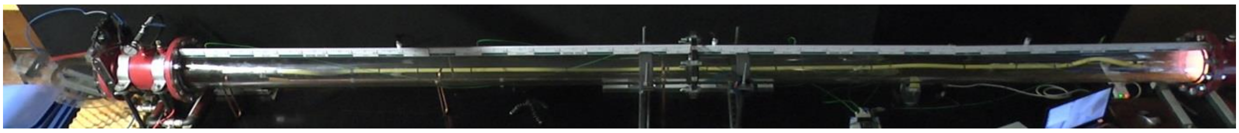
(i) Methane-air mixture - E.R. (ϕ) 0.95 : flame emerging from driver section

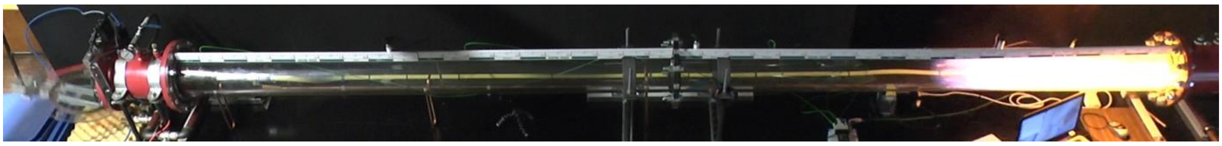
(ii) Methane-air mixture - E.R. (ϕ) 0.95 : flame 20 ms downstream of (i)

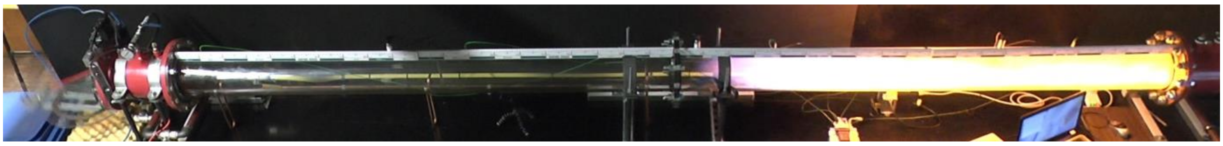
(iii) Methane-air mixture - E.R. (ϕ) 0.95 : flame 20 ms downstream of (ii)

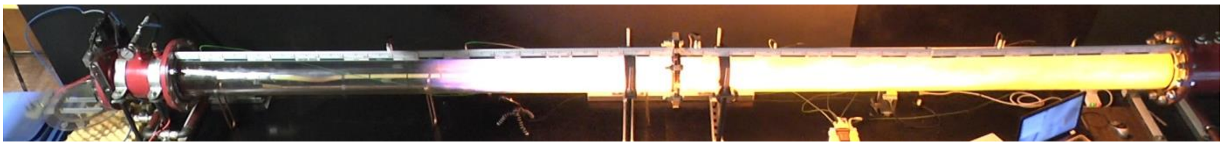
(iv) Methane-air mixture - E.R. (ϕ) 0.95 : flame 20 ms downstream of (iii)

Figure 5.48 : Flame speed trial E.R. **(ϕ) 0.95** (***dry***) with **no atomisers** or spray present

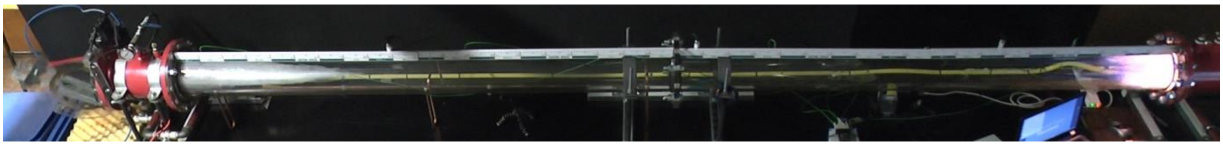
(i) Methane-air mixture - E.R. (ϕ) 1.06 : flame emerging from driver section

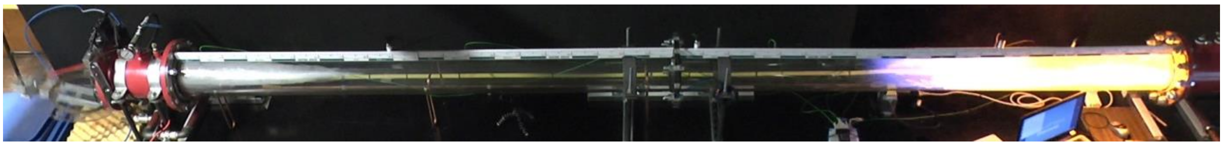
(ii) Methane-air mixture - E.R. (ϕ) 1.06 : flame 40 ms downstream of (i)

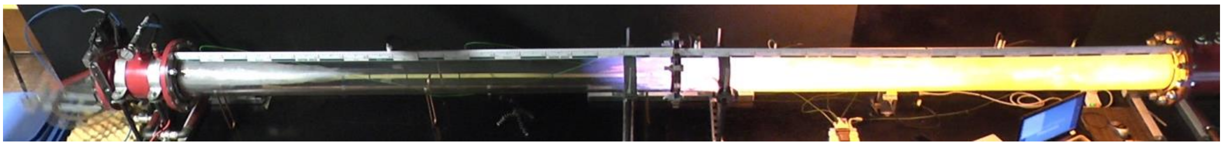
(iii) Methane-air mixture - E.R. (ϕ) 1.06 : flame 40 ms downstream of (ii)

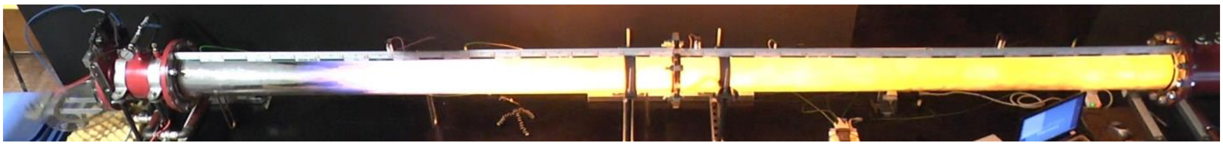
(iv) Methane-air mixture - E.R. (ϕ) 1.06 : flame 40 ms downstream of (iii)

Figure 5.49 : Flame speed trial E.R. **(ϕ) 1.06** (***dry***) with **no atomisers** or spray present

Figure 5.50 represents the thermocouple output data for each of the four methane-air mixtures. As anticipated the time-temperature profile for various E.R. (ϕ) tends to be in agreement with the flame speeds measurements and calculations previously shown in Table 5.10 and Figure 5.50. This relationship is apparent by observing each of the representations in Figure 5.50 and comparing the base line temperature (ambient room temperature typically 20˚C) and the duration between the onset of temperature rise.

For example in Figure 5.50(i) with a methane-air mixture of E.R. (ϕ) 0.61, TC5 began to rise in temperature 0.428 seconds after the TC1 trigger point. Whereas in Figure 5.50(iii) with a methane-air mixture of E.R. (ϕ) 0.95, TC5 began to rise in temperature 0.192 seconds after the TC1 trigger point. This transitional reduction between TC1 and TC5 is partly due to the increase in flame speed and partly due to the increase in flame temperature.

The data and results presented in this preliminary trial will be used for comparison only with subsequent trials which include another ‘dry’ condition. The following Section will show the set up with SRA’s in position, but with no sprays active.

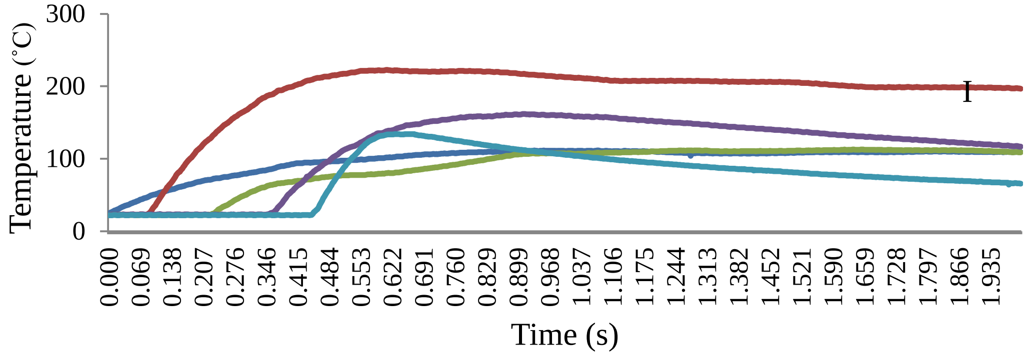

(i) Methane-air mixture of E.R. (ϕ) 0.61

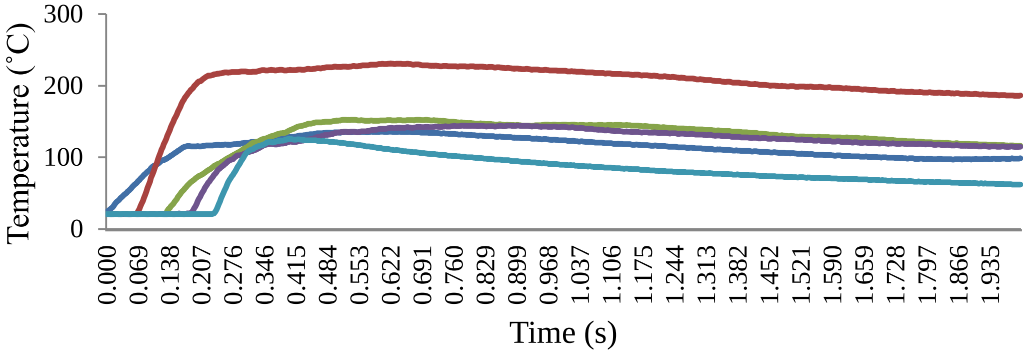

(ii) Methane-air mixture of E.R. (ϕ) 0.72

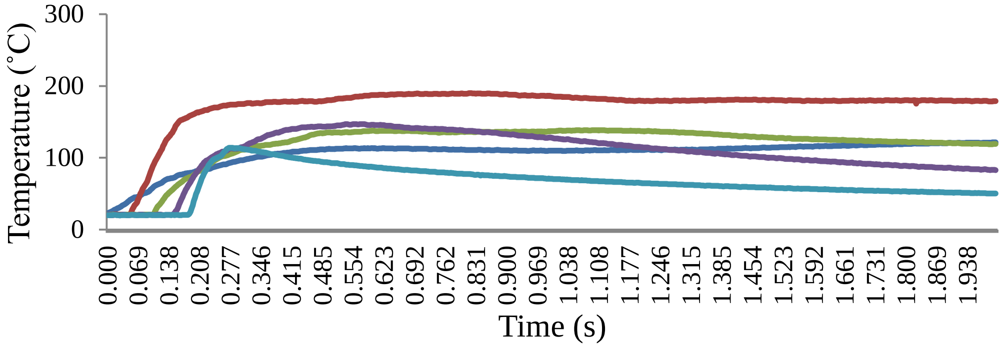

(iii) Methane-air mixture of E.R. (ϕ) 0.95

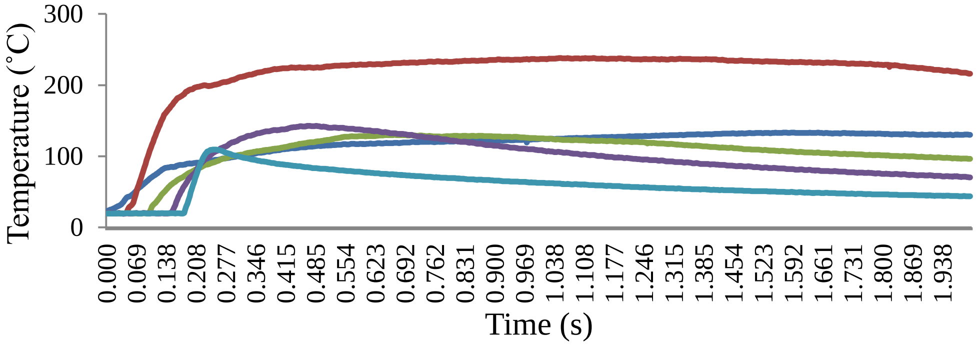

(iv) Methane-air mixture of E.R. (ϕ) 1.06

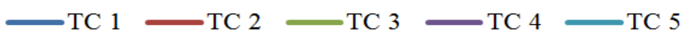

Figure 5.50 : Time-temperature profile for various E.R. (ϕ) : **no SRA (dry)**

5.4.4 Preliminary flame speed : atomiser in position (dry)

The following flame speed test results were obtained by assembling the FPMR with the inclusion of a single SRA and water supply pipework, but under ‘dry’ conditions with no spray. This provided a series of data, imagery and results relating to the performance characteristics of the rig, under this configuration. This test was conducted to conclude whether there was any interference with the flame attributed to the relative positioning of the atomiser.

Figure 5.51 illustrates the experimental rig and direction of travel of the flame. Thermocouple (TC) locations are also shown in Figure 5.51, with their precise positions given in Table 5.11.

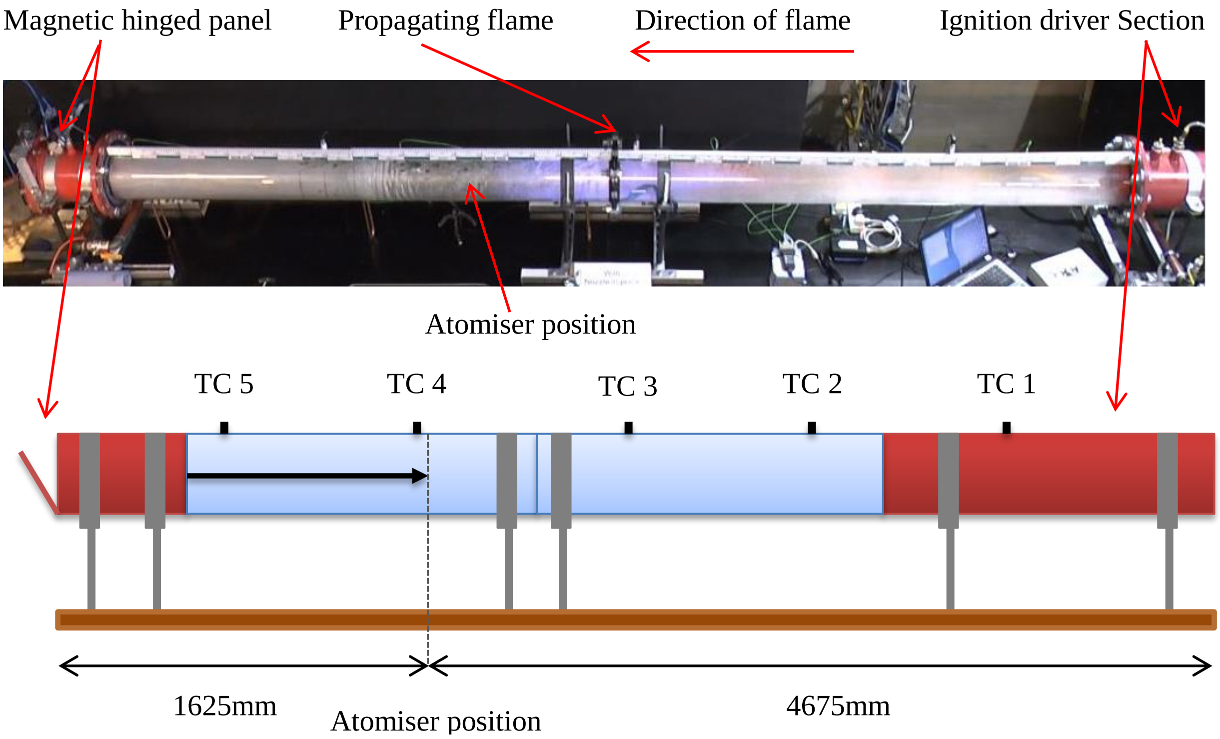

Figure 5.51 : Position of thermocouples and SRA (relative to right hand ignition end)

Component	Position (measured from right hand end)
Thermocouple (TC1)	1200mm
Thermocouple (TC2)	2400mm
Thermocouple (TC3)	3600mm
Thermocouple (TC4)	4800mm
Thermocouple (TC5)	6000mm
Atomiser outlet orifice (counter flow)	4675mm

Table 5.11 – Measured position of thermocouples (TC)

In this series of experimental trials, tests were carried out using four different methane-air mixtures as shown in Table 5.7 and with the SRA mounted on the induction tube as show in Figure 5.51. Figures 5.52, 5.53, 5.54 and 5.55 are still images that have been selected and processed from the high definition (HD) video. In the first image from each series, the flame can be seen as it emerges from the steel driver section on the right hand side of the rig, into the clear PMMA section of the rig travelling from right to left.

In the three remaining images the flame propagation may be observed. Each of the images has been referenced to the previous with respect to time in milliseconds (ms). The original high quality stills have been used to estimate the average flame speeds along the length of the clear PMMA section.

Table 5.12 displays the resulting average flame speeds for each of the methane-air concentrations. The flame speeds have been graphically represented in Figure 5.57, which have been compared to flame speeds from Section 5.43 in Figure 5.63.

Figure 5.57 displays the average flame speed with various E.R. (ϕ), with and without the SRA installed. Using the same technique for measurement and calculation of flame speed as described in 5.4.3, it is apparent that the placement of the atomiser produced an overall decrease in flame speed, when compared to the corresponding tests without the SRA in position. This may be attributed to the cooling effect on the flame by the stainless steel atomiser and induction pipework. A ‘bluff body’ placed in the path a flame is known to reduce burning velocity. This fundamental combustion concept was considered in Chapter 2.

This reduction in flame temperature and consequential reduction in flame speed can also be observed when comparing TC5 temperatures in Figures 5.50 and 5.56. For example, when comparing diagram (iv) in each case, Figure 5.50 (iv) shown previously has a peak TC5 temperature of 109˚C compared to a peak TC5 temperature of 79˚C in Figure 5.55 (iv). However, when comparing the TC2 and TC3 temperatures the introduction of the atomiser body and pipework appears to cause an initial increase in flame temperature. This increase in flame temperature may be attributed to the partial restriction in the path of the exiting pressure front caused by the body of the atomiser. (See also Chapter 2).

Therefore, although there was in initial increase in flame temperature, the combined effects of the inclusion of the atomiser body and pipework are credited to causing a minor reduction in flame speed along the full length of the 4m clear section of the rig.

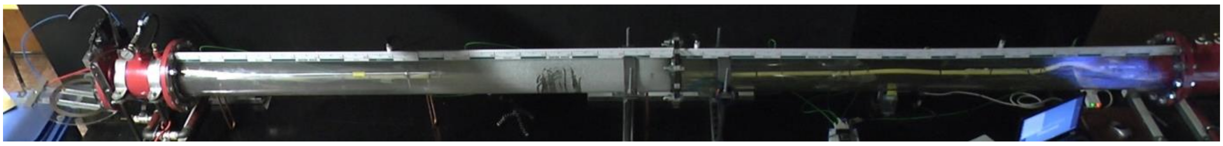

(i) Methane-air mixture - E.R. (ϕ) 0.61 : flame emerging from driver section

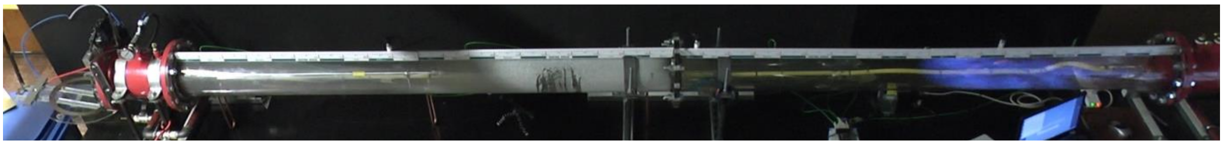

(ii) Methane-air mixture - E.R. (ϕ) 0.61 : flame 60 ms downstream of (i)

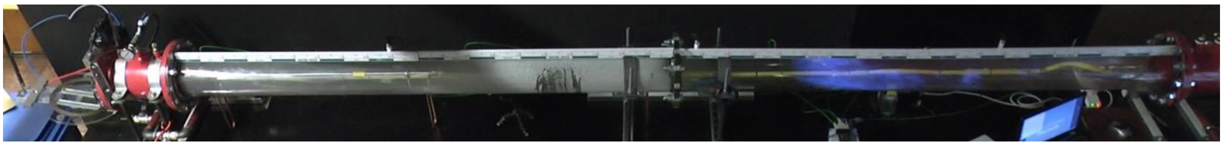

(iii) Methane-air mixture - E.R. (ϕ) 0.61 : flame 60 ms downstream of (ii)

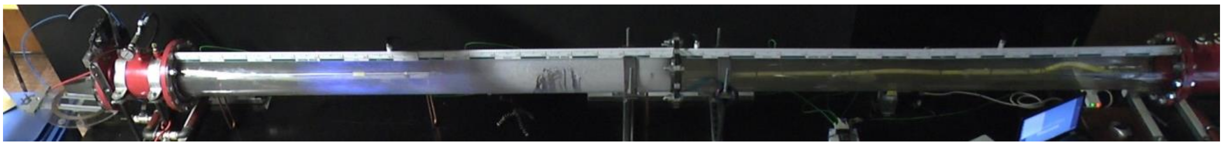

(iv) Methane-air mixture - E.R. (ϕ) 0.61 : flame 120 ms downstream of (iii)

Figure 5.52 : Flame speed trial E.R. **(ϕ) 0.61** (***dry***) with **SRA in position**

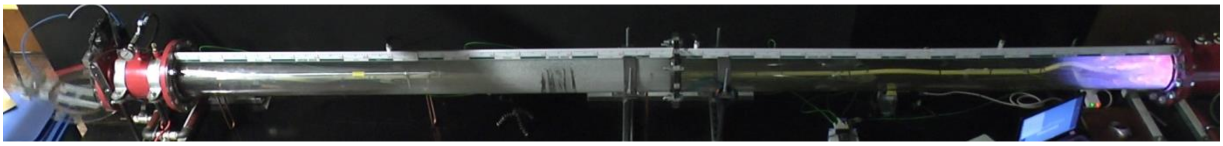

(i) Methane-air mixture - E.R. (ϕ) 0.72 : flame emerging from driver section

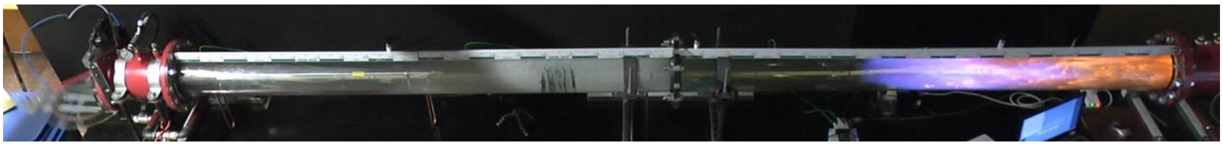

(ii) Methane-air mixture - E.R. (ϕ) 0.72 : flame 40ms downstream of (i)

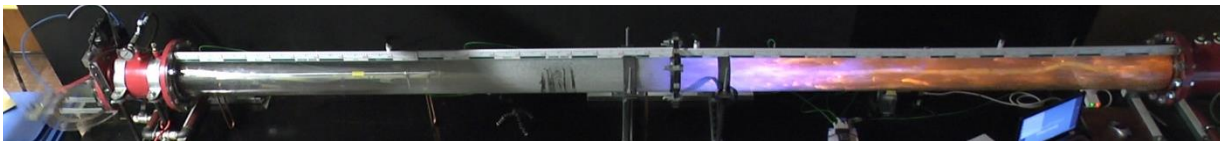

(iii) Methane-air mixture - E.R. (ϕ) 0.72 : flame 40ms downstream of (ii)

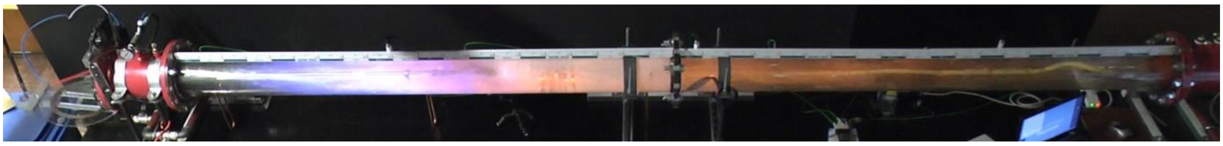

(iv) Methane-air mixture - E.R. (ϕ) 0.72 : flame 60ms downstream of (iii)

Figure 5.53 : Flame speed trial E.R. **(ϕ) 0.72** (***dry***) with **SRA in position**

(i) Methane-air mixture - E.R. (ϕ) 0.95 : flame emerging from driver section

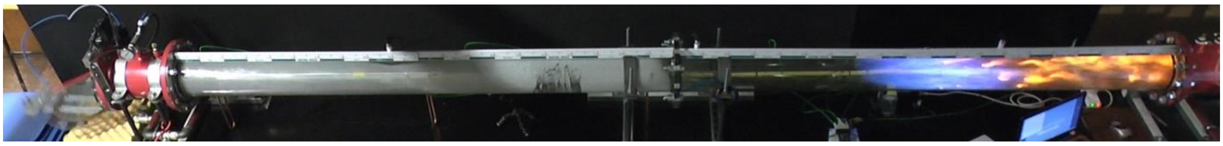

(ii) Methane-air mixture - E.R. (ϕ) 0.95 : flame 40ms downstream of (i)

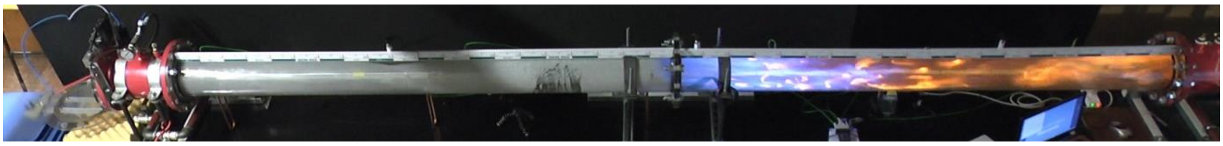

(iii) Methane-air mixture - E.R. (ϕ) 0.95 : flame 40ms downstream of (ii)

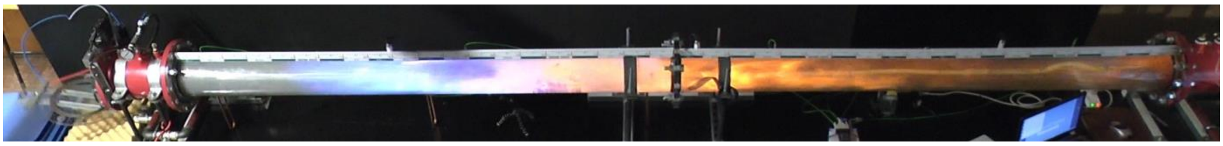

(iv) Methane-air mixture - E.R. (ϕ) 0.95 : flame 60ms downstream of (iii)

Figure 5.54 : Flame speed trial E.R. **(ϕ) 0.95** (***dry)*** with **SRA in position**

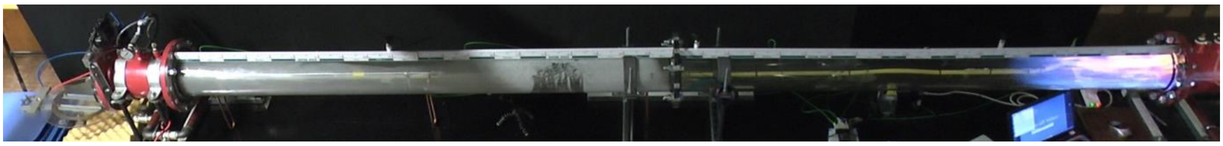

(i) Methane-air mixture - E.R. (ϕ) 1.06 : flame emerging from driver section

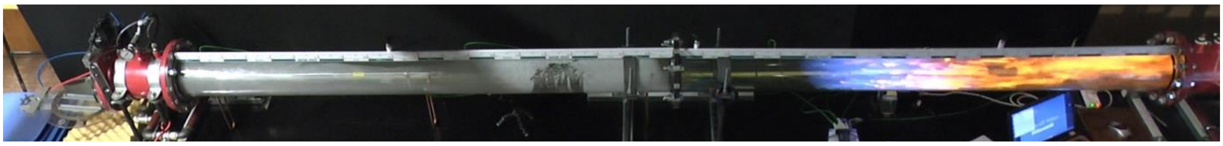

(ii) Methane-air mixture - E.R. (ϕ) 1.06 : flame 40ms downstream of (i)

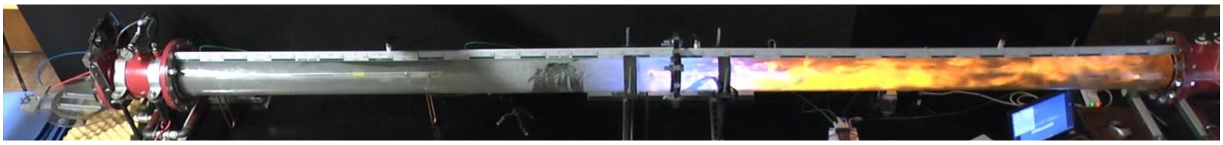

(iii) Methane-air mixture - E.R. (ϕ) 1.06 : flame 40ms downstream of (ii)

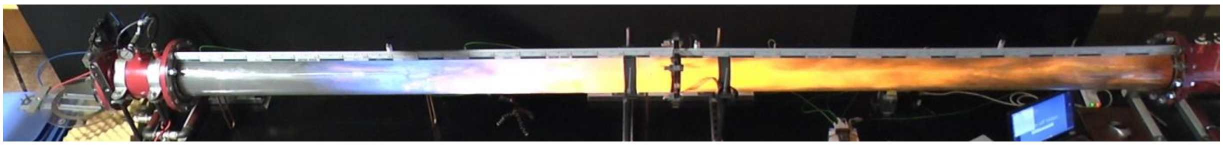

(iv) Methane-air mixture - E.R. (ϕ) 1.06 : flame 40ms downstream of (iii)

Figure 5.55 : Flame speed trial E.R. **(ϕ) 1.06** (***dry)*** with **SRA in position**

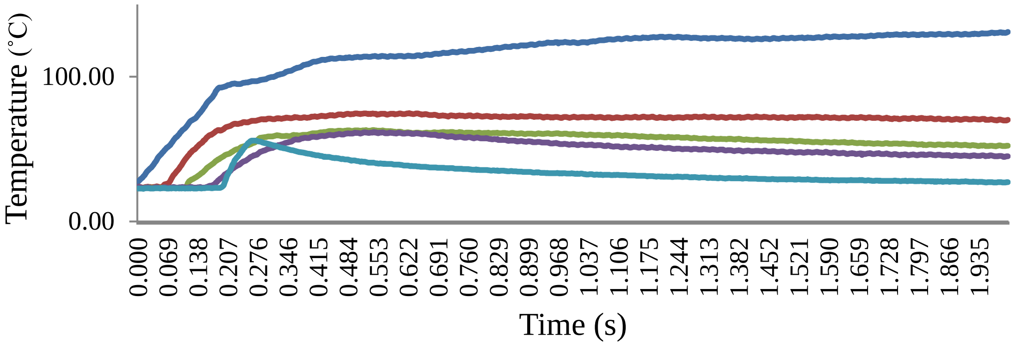

(i) Methane-air mixture of E.R. (ϕ) 0.61

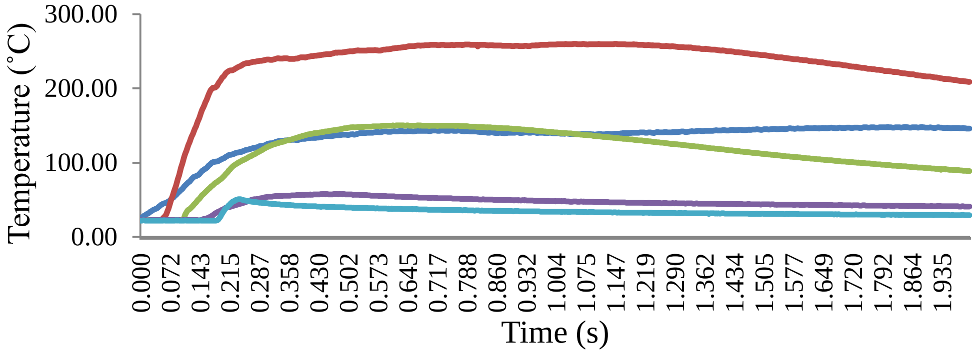

(ii) Methane-air mixture of E.R. (ϕ) 0.72

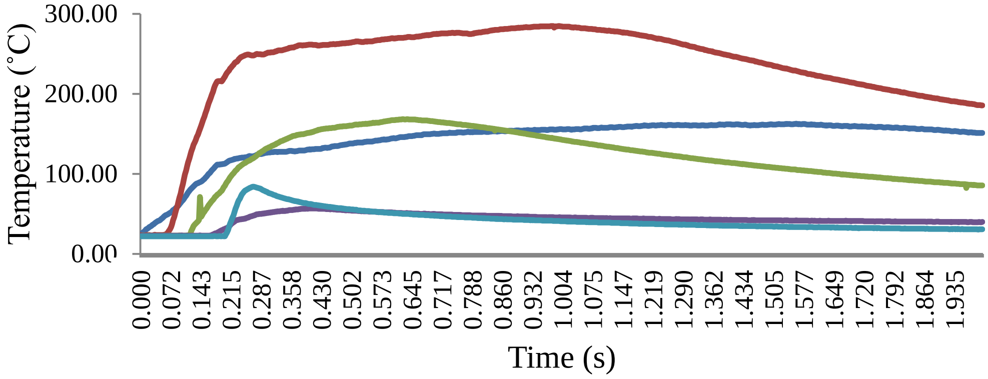

(iii) Methane-air mixture of E.R. (ϕ) 0.95

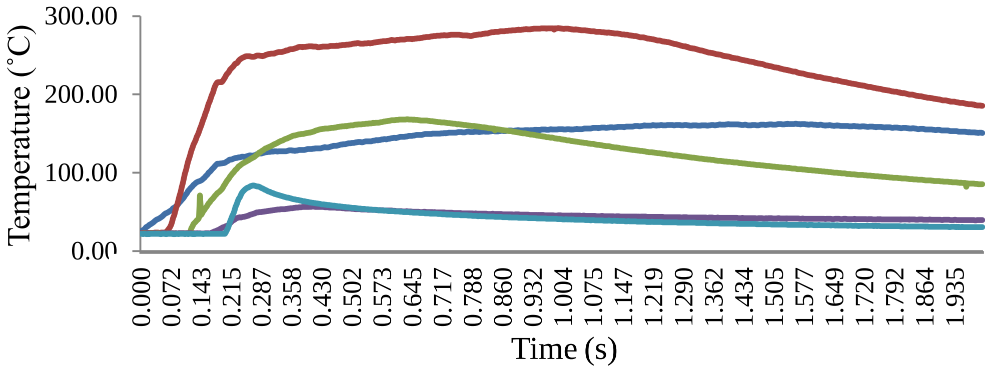

(iv) Methane-air mixture of E.R. (ϕ) 1.06

TC 1 TC 2 TC 3 TC 4 TC 5

Figure 5.56 : Time-temperature profile for various E.R. (ϕ) : **(dry) with SRA installed**

E.R. (ϕ)	Distance travelled (mm)	Time period (ms)	Average flame speed (m/s)
0.61	3500	160	21.88
0.72	3100	140	22.14
0.95	3450	140	24.64
1.06	2700	120	22.50

Table 5.12 : Average flame speed for various E.R. (ϕ) with SRA in position (dry)

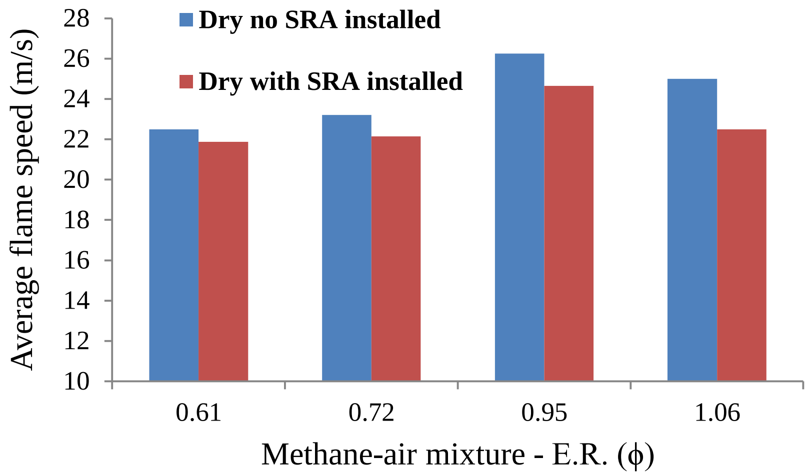

Figure 5.57 : Average flame speed for various E.R.(ϕ) with and without SRA installed (dry)

E.R. (ϕ)	Average flame speed (dry) no SRA (m/s)	Average flame speed (dry) with SRA (m/s)	Percentage flame speed reduction (%)
0.61	22.5	21.88	2.78
0.72	23.21	22.14	4.60
0.95	26.25	24.64	6.12
1.06	25	22.50	10.00

Table 5.13 : Flame speed reductions – with and without SRA installed (dry)

5.5 Mitigation hot trials for various spray configurations

To ensure reliability and consistency of data and imagery, all of the hot trials were validated a minimum of three times. Due to the sheer number of ***hot trials*** conducted within this research it has not been practical to present all of results with the same degree of detail.

For convenience and ease of reference the results and discussions for **all** of the hot trials are presented in **Appendix 9** on the accompanying **CD of Appendices** (called here : Volume III)

To categorise the outcome of each trial, five **general event outcome** consequences were developed, whereby each of the experimental hot trials will be classified as follows:-

i. No Mitigation with resulting Flame Acceleration (NMFA)
ii. No Mitigation with resulting Flame Deceleration (NMFD)
iii. No Mitigation with resulting Unaffected Flame (NMUF)
iv. Partial Mitigation with resulting Flame Propagation (PMFP)
v. Full Mitigation resulting in Flame Extinguishment (FMFE)

Table 5.14 is shown again here for convenience and provides a colour coded matrix of the *general event outcome* categories for all *101 selected hot trials*, using the above *five classifications* and also contains the location of the results and discussions for each individual experimental trial.

In the following Sections 5.5.1 – 5.5.10, selected results for representative trial arrangements have been discussed with relevance. The results presented are:-

5.5.1 Single (C/F) SRA Type A : E.R. (ϕ) 0.61
5.5.2 Single (P/F) SRA Type A : E.R. (ϕ) 0.61
5.5.3 Single (P/F) SRA Type C : E.R. (ϕ) 0.61
5.5.4 Two Type B overlapping SRA's : E.R. (ϕ) 0.61
5.5.5 Four (X/F) Type B SRA's : E.R. (ϕ) 0.72
5.5.6 Four (X/F) Type C SRA's : E.R. (ϕ) 0.95
5.5.7 Four (X/F) Type C SRA's : Water temperature 50°C and E.R. (ϕ) 0.95
5.5.8 Four (X/F) Type C SRA's in a methane-air E.R. (ϕ) 1.65
5.5.9 Four (X/F) Type C SRA's in a propane-air E.R. (ϕ) 1.00
5.5.10 Four (X/F) Type C SRA's with three exhaust outlets blocked

Trial	**Configuration**	**E.R. (ϕ)**	**General event outcome**	**Section / Appendix**
Mitigation trials for a single water spray in **counter flow** (C/F) with a methane-air flame	SRA configuration type A Water pressure : 13MPa Water temperature : 20°C	0.61	NMFA	5.5.1/A9.1.1
		0.72	NMFA	A9.1.1
		0.95	NMFA	A9.1.1
		1.06	NMFA	A9.1.1
	SRA configuration type B Water pressure : 13MPa Water temperature : 20°C	0.61	NMFA	A9.1.2
		0.72	NMFA	A9.1.2
		0.95	NMFA	A9.1.2
		1.06	NMFA	A9.1.2
	SRA configuration type C Water pressure : 13MPa Water temperature : 20°C	0.61	FMFE	A9.1.3
		0.72	NMFA	A9.1.3
		0.95	NMFA	A9.1.3
		1.06	NMFA	A9.1.3
Mitigation trials for a single water spray in **parallel flow** (P/F) with a methane-air flame	SRA configuration type A Water pressure : 13MPa Water temperature : 20°C	0.61	NMFA	5.5.2/A9.2.1
		0.72	NMFA	A9.2.1
		0.95	NMFA	A9.2.1
		1.06	NMFA	A9.2.1
	SRA configuration type B Water pressure : 13MPa Water temperature : 20°C	0.61	NMFA	A9.2.2
		0.72	NMFA	A9.2.2
		0.95	NMFA	A9.2.2
		1.06	NMFA	A9.2.2
	SRA configuration type C Water pressure : 13MPa Water temperature : 20°C	0.61	FMFE	5.5.3/A9.2.3
		0.72	NMFA	A9.2.3
		0.95	NMFA	A9.2.3
		1.06	NMFA	A9.2.3
Mitigation trials for a two water sprays in **parallel flow** (P/F) with a methane-air flame	2 x Overlapping Type B SRA's Water pressure : 13MPa Water temperature : 20°C	0.61	FMFE	5.5.4/A9.3.1
		0.72	NMFA	A9.3.1
		0.95	NMFA	A9.3.1
		1.06	NMFA	A9.3.1
	2 x Overlapping Type C SRA's Water pressure : 13MPa Water temperature : 20°C	0.95	FMFE	A9.3.2
		0.95	FMFE	A9.3.2
		1.06	FMFE	A9.3.2
Mitigation trials for water sprays in **cross flow** (X/F) with the methane-air flames	Single SRA type B Water pressure : 13MPa Water temperature : 20°C	0.61	NMFA	A9.4.1
		0.72	NMFA	A9.4.1
		0.95	NMFA	A9.4.1
		1.06	NMFD	A9.4.1
	Two SRA type B Water pressure : 13MPa Water temperature : 20°C	0.61	NMFD	A9.4.2
		0.72	NMFD	A9.4.2
		0.95	NMFD	A9.4.2
		1.06	NMFD	A9.4.2

General event outcome	Code
No Mitigation with resulting Flame Acceleration	NMFA
No Mitigation with resulting Flame Deceleration	NMFD
No Mitigation with resulting Unaffected Flame	NMUF
Partial Mitigation with resulting Flame Propagation	PMFP
Full Mitigation resulting in Flame Extinguishment	FMFE

Table 5.14 : Trial results location matrix and general event outcome

Trial	**Configuration**	**E.R. (ϕ)**	**General event outcome**	**Section / Appendix**
Mitigation trials for water sprays in **cross flow** (X/F) with the methane-air flames	Three SRA type B Water pressure : 13MPa Water temperature : 20°C	0.61	FMFE	A9.4.3
		0.72	NMFD	A9.4.3
		0.95	NMFD	A9.4.3
		1.06	NMFD	A9.4.3
	Four SRA type B Water pressure : 13MPa Water temperature : 20°C	0.61	FMFE	A9.4.4
		0.72	FMFE	5.5.5/A9.4.4
		0.95	NMFA	A9.4.4
		1.06	NMFD	A9.4.4
Mitigation trials for water sprays in **cross flow** (X/F) with the methane-air flames	Single SRA type C Water pressure : 13MPa Water temperature : 20°C	0.61	NMFD	A9.4.5
		0.72	NMFD	A9.4.5
		0.95	NMFA	A9.4.5
		1.06	NMFD	A9.4.5
	Two SRA type C Water pressure : 13MPa Water temperature : 20°C	0.61	NMFD	A9.4.6
		0.72	NMFD	A9.4.6
		0.95	NMFA	A9.4.6
		1.06	NMFD	A9.4.6
	Three SRA type C Water pressure : 13MPa Water temperature : 20°C	0.61	FMFE	A9.4.7
		0.72	NMFD	A9.4.7
		0.95	NMFD	A9.4.7
		1.06	NMFD	A9.4.7
	Four SRA type C Water pressure : 13MPa Water temperature : 20°C	0.61	FMFE	A9.4.8
		0.72	FMFE	A9.4.8
		0.95	FMFE	5.5.6/A9.4.8
		1.06	FMFE	A9.4.8
(X/F) Type B and C SRA's using variable supply pressures and water temperature : 20°C	3 type C and 1 type B:13MPa	0.95	NMFD	A9.5.1
	2 type C and 2 type B:13MPa	0.95	NMFA	A9.5.1
	1 type C and 3 type B:13MPa	0.95	NMFD	A9.5.1
	1 type C and 3 type B:15MPa	0.95	NMFA	A9.5.1
Varying number of **(X/F)**Type C SRA's using variable supply pressures and water temperature : 20°C	3 type C only:14MPa	0.95	NMFD	A9.5.2
	3 type C only:15MPa	0.95	NMFD	A9.5.2
	3 type C only:15MPa	0.95	FMFE	A9.5.2
	3 type C only:16MPa	0.95	NMFD	A9.5.2
	3 type C only:17MPa	0.95	NMFA	A9.5.2
	3 type C only:18MPa	0.95	NMFD	A9.5.2
Varying number of **(X/F)**Type B SRA's using variable supply pressures and water temperature : 20°C	4 type B only:14MPa	0.95	NMFD	A9.5.3
	4 type B only:15MPa	0.95	FMFE	A9.5.3
	4 type B only:16MPa	0.95	NMFD	A9.5.3
	4 type B only:17MPa	0.95	NMFD	A9.5.3
	4 type B only:18MPa	0.95	NMFA	A9.5.3

General event outcome	Code
No Mitigation with resulting Flame Acceleration	NMFA
No Mitigation with resulting Flame Deceleration	NMFD
No Mitigation with resulting Unaffected Flame	NMUF
Partial Mitigation with resulting Flame Propagation	PMFP
Full Mitigation resulting in Flame Extinguishment	FMFE

Table 5.14 : Trial results location matrix and general event outcome

Trial	**Configuration**	**E.R. (ϕ)**	**General event outcome**	**Section / Appendix**
Three **(X/F)**Type C SRA's using variable supply pressures and water temperatures	3 type C only:13MPa : 30°C	0.95	FMFE	A9.5.4
	3 type C only:15MPa : 35°C	0.95	NMFD	A9.5.4
	3 type C only:15MPa : 40°C	0.95	NMFD	A9.5.4
	3 type C only:16MPa : 45°C	0.95	NMFD	A9.5.4
	3 type C only:15MPa : 50°C	0.95	NMFD	A9.5.4
Three **(X/F)**Type C SRA's using variable supply pressures and water temperatures	4 type C only:13MPa : 25°C	0.95	FMFE	A9.5.5
	4 type C only:13MPa : 25°C	0.95	FMFE	A9.5.5
	4 type C only:13MPa : 30°C	0.95	FMFE	A9.5.5
	4 type C only:13MPa : 30°C	0.95	FMFE	A9.5.5
	4 type C only:13MPa : 40°C	0.95	FMFE	A9.5.5
	4 type C only:13MPa : 40°C	0.95	FMFE	A9.5.5
	4 type C only:13MPa : 50°C	0.95	FMFE	A9.5.5
	4 type C only:13MPa : 50°C	0.95	FMFE	5.5.7/A9.5.5
Supplementary trials				
Four **(X/F)**Type C SRA's trials with methane rich, methane-air flames	4 type C only:13MPa : 20°C	1.18	FMFE	A9.6.1
	4 type C only:13MPa : 20°C	1.30	FMFE	A9.6.1
	4 type C only:13MPa : 20°C	1.43	FMFE	A9.6.1
	4 type C only:13MPa : 20°C	1.65	FMFE	5.5.8/A9.6.1
Four **(X/F)**Type C SRA's trials with propane-air flames	4 type C only:13MPa : 20°C	0.49	FMFE	A9.6.2
	4 type C only:13MPa : 20°C	0.74	FMFE	A9.6.2
	4 type C only:13MPa : 20°C	1.00	FMFE	5.5.9/A9.6.2
Four **(X/F)**Type C SRA's trials with methane-air flames, with partial blockage of exhaust outlets	One exhaust outlet blocked	0.95	FMFE	A9.6.3
	Two exhaust outlets blocked	0.95	FMFE	A9.6.3
	Three exhaust outlets blocked	0.95	FMFE	5.5.10/ A9.6.3

General event outcome	**Code**
No Mitigation with resulting Flame Acceleration	NMFA
No Mitigation with resulting Flame Deceleration	NMFD
No Mitigation with resulting Unaffected Flame	NMUF
Partial Mitigation with resulting Flame Propagation	PMFP
Full Mitigation resulting in Flame Extinguishment	FMFE

Table 5.14 : Trial results location matrix and general event outcome

5.5.1 Single (C/F) SRA Type A : E.R. (ϕ) 0.61

5.5.1.1 Trial set up

The pre-assembled Spill Return Atomiser (SRA), thermocouples (TC) and water feed pipework were installed within the FPMR in accordance with Figure 5.58 and Table 5.15. Water was supplied at 20˚C and at a pressure of 13MPa (130bar).

In this arrangement a single Type A SRA, previously tested under the cold trials was placed in counter flow (C/F) arrangement with the propagating flame. The Type A SRA consisted of a 0.3mm diameter exit orifice and 0.5mm spill diameter, as previously described in Section 5.1.1, Table 5.1, Chapter 4 and is also summarised in Table 5.16.

The explosion and mitigation apparatus (FPMR) was prepared for use in accordance with the all relevant health and safety requirements, risk assessments and the process flow diagram shown previously in Chapter 4. Due to laboratory layout and for convenience, ignition was delivered at the right hand end of the FPMR as shown in Figure 5.58. Ignition was provided by a single spark via an individual spark electrode with 4mm spark gap, as discussed beforehand in Chapter 4.

Following the introduction and subsequent mixing of the methane-air mixture E.R. (ϕ) 0.61, the homogeneous sample was allowed to stabilise for one minute to allow it to become still and quiescent.

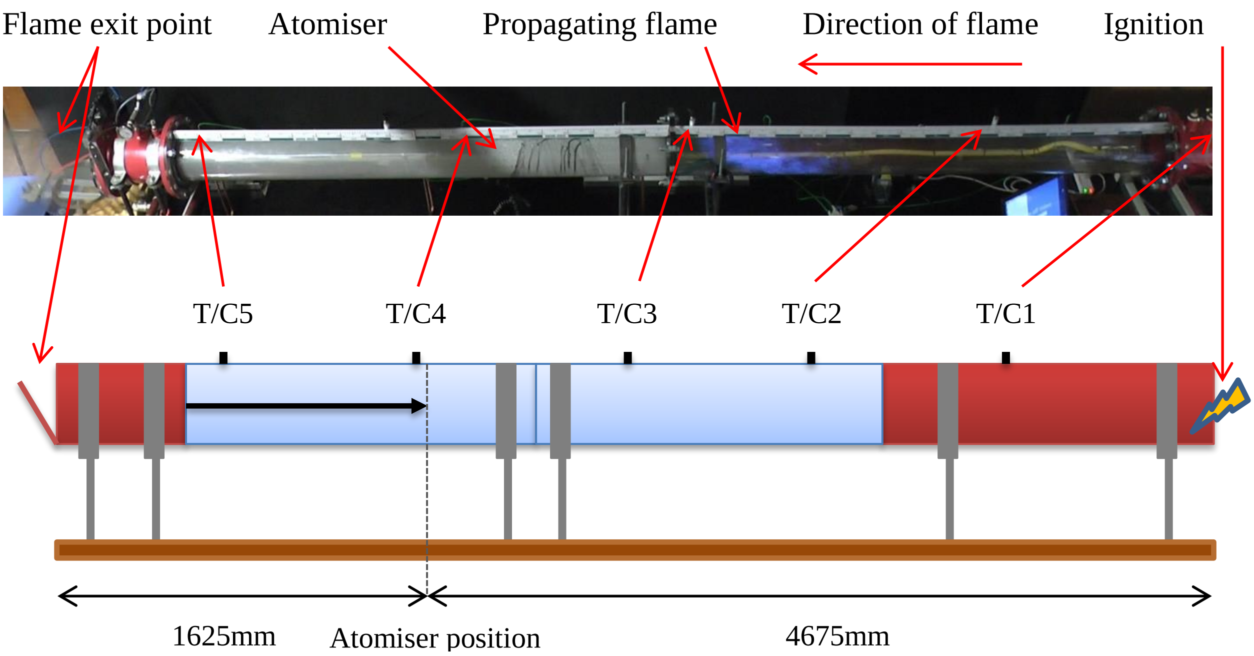

Figure 5.58 : Position of atomiser and thermocouples (relative to right hand ignition end)

Component	Position (measured from right hand end)
Thermocouple (T/C1)	1200mm
Thermocouple (T/C2)	2400mm
Thermocouple (T/C3)	3600mm
Thermocouple (T/C4)	4800mm
Thermocouple (T/C5)	6000mm
Atomiser outlet orifice (counter flow)	4675mm

Table 5.15 : Measured positions of SRA and thermocouples

The full atomiser characteristics relating to the SRA Type A configuration were revealed previously in the cold trials Section 5.3 and are summarised in Table 5.16 below.

Mean D_{32} (μm)	Mean liquid volume flux ($cm^3/s/cm^2$)	Mean droplet velocity (m/s)
17	0.011	13.5

Table 5.16 : Typical characteristics for SRA type A 150mm downstream of exit orifice

5.5.1.2 Flame speed

In this present investigation the flame was required to propagate relatively slowly, at speeds of approximately ≤30m/s. This was achieved in the design of the FPMR by the author, which included a magnetic hinged panel at the flame exit point and a series of rupturing membranes at the ignition end of the tube, as previously described in full in Chapter 4. Additionally, with the exception of the SRA and its supply pipework, there were no other obstructions or obstacles within the FPMR, or in the path of the flame.

These features in the design by the author are used throughout this study, thus the manifestation of the unique attributes of the FPMR apparatus that were included. The rig design, features and rationale are described earlier in Chapter 4. These pertinent qualities where included in the design criteria to ensure that laminar flow profiles, with flame speeds of ≤30m/s were produced under all of the testing conditions. This being contrary to previous studies [9, 14, 65, 66], where flames were intentionally accelerated using turbulators and other means to disturb the unburned fuel-air mixture.

Following the successful ignition of the (ϕ) 0.61 mixture, the flame initially exited the steel driver section of the FPMR. The average flame speed was recorded and calculated to be approximately 5.33m/s immediately upstream of the counter flow spray. In this instance the flame propagated directly through the region of the spray and began to accelerate to about

27.5m/s. This consequential increase in flame speed of 22.17m/s is represented in Figure 5.59 as negative value with respect to 'flame speed reduction %', therefore representing an increase flame speed of approximately 415%.

In this series of tests the flame speeds for (ϕ) 0.61, 0.72, 0.95 and 1.06 were all measured upstream and downstream of the counter flow spray. Figure 5.59 illustrates the percentage flame speed reductions observed. The percentage reductions in this series all exhibit negative values, which shows that all four methane-air mixtures resulted in a global increase in average flame speed across the sprays. The additional results for the (ϕ) 0.72, 0.95 and 1.06 trials can be found in Appendix 9 on the separate CD volume (Volume III).

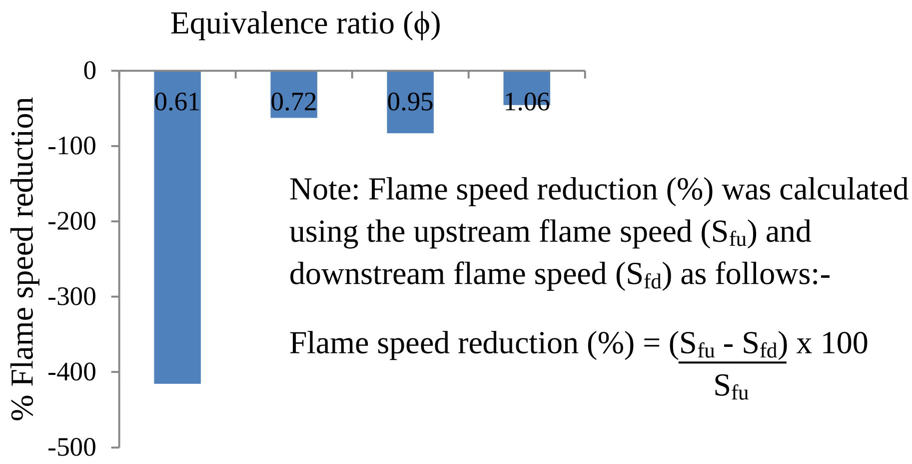

Figure 5.59 : Average flame speed reduction percentage (%) from upstream to downstream of SRA in various methane-air mixtures

This increase in flame speed, which was coupled with a temperature rise across the atomiser and spray is consistent with previous author's [39, 65, 66] observations in similar experimental conditions, although their studies involved much higher initial flame speeds in the order of ≥100m/s and larger water droplets of ≥100μm. This phenomenon was discussed earlier in Chapter 3 and is particularly noticeable in this instance due to the gas mixture employed here, being towards the lower explosive limit (LEL) and also with respect to the slow flame speeds initially produced, due to the unique characteristics of the FPMR.

The flame immediately upstream of the counter flow SRA would have had a typical flame thickness of approximately 2.4mm by extrapolation from previous studies by Andrews and Bradley [35], as shown in Figures 5.60.

This relationship was previously discussed explicitly in Chapter 2, Section 2.4.5.3 and is also referred to in relevant Sections of these results and discussions.

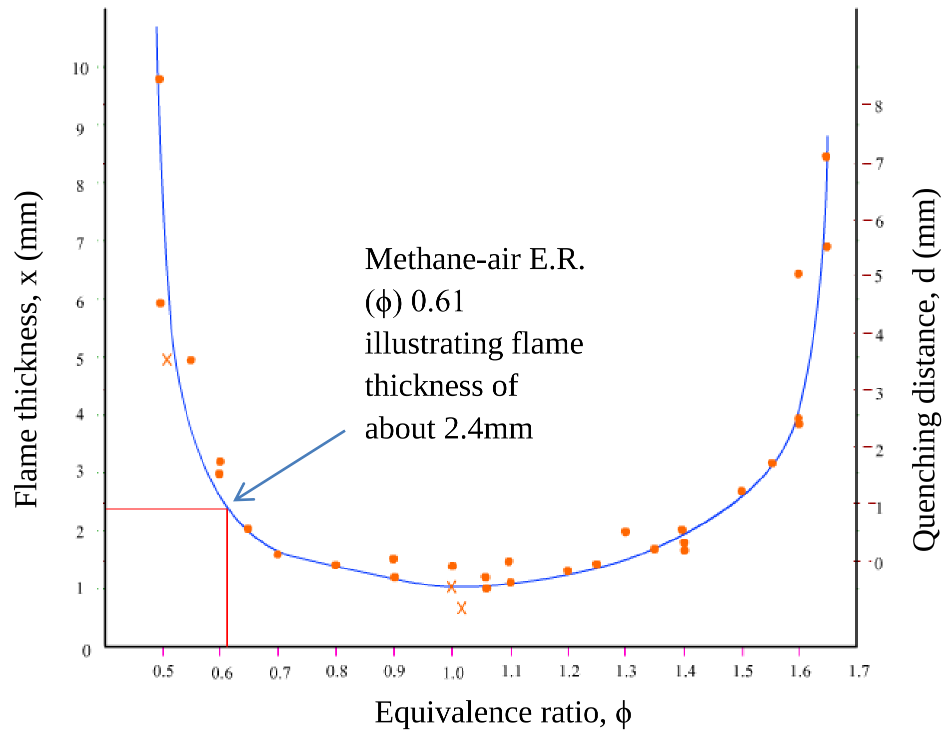

Figure 5.60 : Methane-air E.R. (ϕ) 0.61- illustrating flame thickness of 2.4mm [35]

An important factor relating to flame extinction and mitigation by water sprays, is the *transit time* that the droplet is afforded as it passes through the flame front (reaction and preheat zone) as illustrated in Figure 5.61. This transition through the flame front, or *residence time* within the flame, is where energy is transferred from the flame to the water droplet. Therefore, greater residence times lead to higher heat transfer rates and thus resulting temperature rise in the water droplets. Water droplets entering the flame will initially absorb sensible heat, expanding immediately upstream due to heat transfer and reducing downstream of the flame due to surface vaporisation, as observed by Thomas and Brenton [45].

Sapko et al [61] stated that water sprays with droplet diameters of ≤18μm will just about reach boiling point in a 9% methane-air flame travelling at 2.3m/s by sensible heat transfer. This was based on droplet vaporisation work previously carried out by Kumm [62]. With smaller droplets or greater residence times, droplets will potentially begin to vaporise thus giving up their latent heat of vaporisation. The subject of laminar flame thickness, droplet heat up and vaporisation was discussed explicitly in Chapter 3, Section 3.6.2.

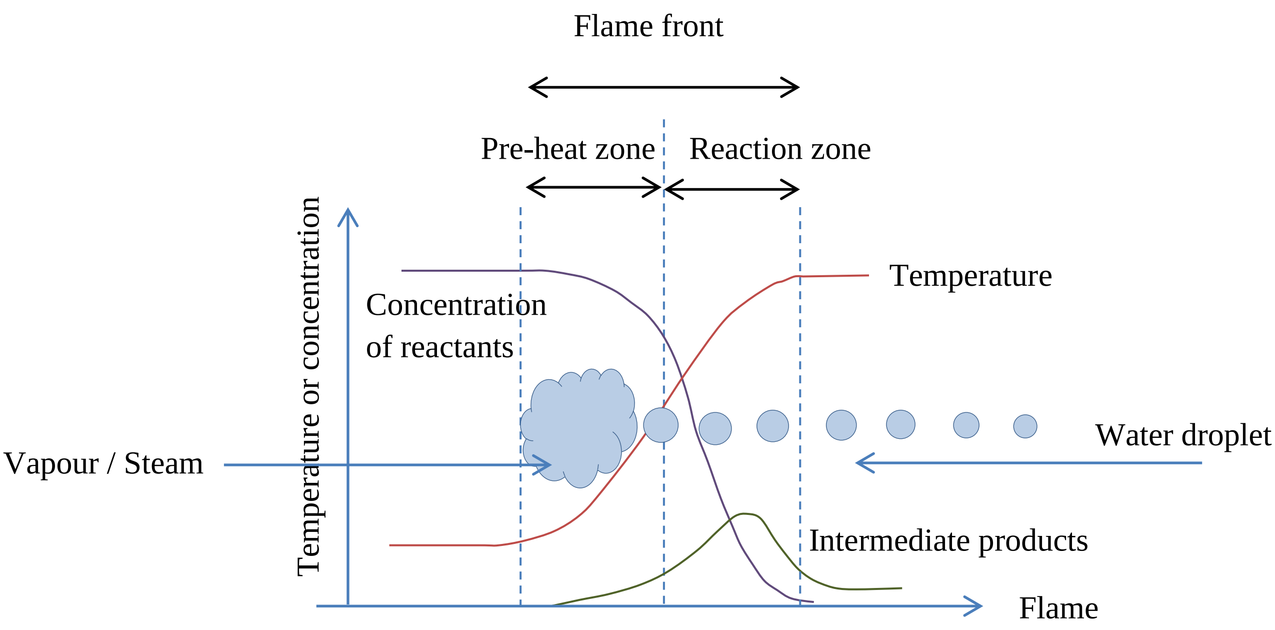

Figure 5.61 : Schematic of water droplet passing through a flame front and vaporising

One of the key objectives of this present study was to ensure that droplets did not undergo break up prior to entering the flame. This was achieved in this investigation due to the slow flame speeds employed (≤30m/s) and by the drop sizes (D_{32}≤30µm) utilised.

Lane [71] also presented a relationship between droplet diameter and the critical velocity needed to overcome the intrinsic hydrodynamic forces (or surface tension), which essentially holds the droplets together. Lane's [71] expression was discussed beforehand in Chapter 3 and is shown again here for convenience:-

$$v_c^2\, d = 0.612\ (m^3/s^2) \qquad \text{Equation 5.1}$$

where v_c = the critical relative gas stream velocity for droplet break up (m/s)

d = the droplet diameter (µm)

Figure 5.62 illustrates Lane's relationship and reveals that a 17µm droplet would still remain hydrodynamically stable with impact velocities in excess of 100m/s. Using Lane's relationship, an impact velocity of ≥189.74m/s would be required to instigate 'bag type' break up. The approximate impact velocity in this counter flow arrangement may be determined by the sum of the average flame speed and the mean droplet velocity. The impact velocity in this trial was therefore estimated to be approximately 34m/s and is highlighted on Figure 5.62.

As the impact velocity was significantly less than the critical droplet break up velocity, this demonstrates that the droplets will not have undergone any form of secondary atomisation by hydrodynamic break up.

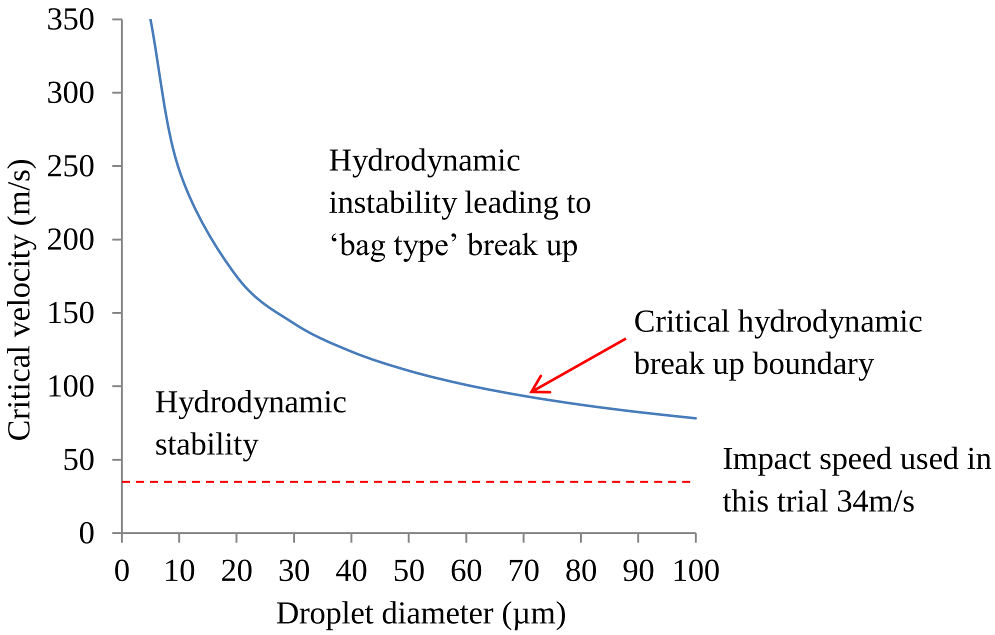

Figure 5.62 : Distinctive critical droplet break up velocity (m/s) with respect to droplet diameter (µm).[Lane 71]

5.5.1.3 Time-temperature response

As previously discussed in 5.4.2 the lag time associated with thermocouples, limits the accuracy of the temperature measurements provided in these results. The exposed junction thermocouples used in this current study have been used extensively and are described in numerous previous published works [71, 72, 73] and have been demonstrated to be a highly acceptable method for comparing flame propagation within confined and partly confined explosion testing in vessels and pipework.

The time-temperature response shown in Figure 5.63 displays the temperatures recorded over a two second period. In harmony with the flame speed trials in Sections 5.4.3 and 5.4.4, a two second period was extracted from the unprocessed data, commencing at a point where a 5˚C temperature rise at measured at TC1. This point indicates the onset of combustion and is referred to as the trigger point. Although the time-temperature curve for TC1 is also displayed in Figure 5.63, the data plotted for TC1 will not be included in the corresponding post processing discussions.

In Figure 5.63 the temperature can be seen to decay with respect to propagation distance. This has been attributed to heat losses to the walls of the FPMR, as shown in studies by Lewis and von Elbe [6].

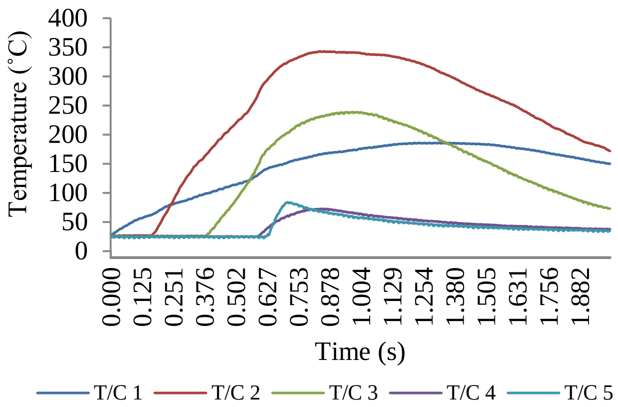

Figure 5.63 : Typical time-temperature profile for SRA type A in C/F arrangement with methane-air mixture of E.R. (ϕ) 0.61

5.5.1.4 Qualitative analysis

Qualitatively, the resulting flame propagation and subsequent degree of flame speed reduction (where applicable) or mitigation were captured with a high definition (HD) video camera, as previously discussed in Chapter 4. Utilisation of the frame by frame still images that were extracted and processed from the HD video, thus enabled the production of flame propagation images upstream and downstream of the atomiser.

Figure 5.64(i) shows the flame propagating from the ignition region on the right hand side (RHS) of the image. In this frame the flame is approaching the region of the spray.

Figure 5.64(ii) depicts the flame a further 20ms downstream. In this frame the flame is engaging with the extreme droplets in the spray.

In Figure 5.64(iii) the flame has travelled another 20ms and is fully engaged with the droplets as it passes through the region of counter flow water droplets of D_{32} 17μm, where it is seen to accelerate.

Figure 5.65 magnifies the zone in Figure 5.64(iii), where combustion is visible as a continuous flame, with no obvious signs of local extinction in the form of 'dark regions', or global flame quenching or mitigation.

Note: 'Dark regions' in water-flame interaction photographs were observed and discussed in monodispersed droplet experiments by Thomas and Brenton [45]. This was previously discussed in Chapter 2, Section 2.5.1.

Figure 5.64(iv) confirms the flame position, in which it is accelerating towards the exit end of the FPMR at the left hand side (LHS) of the image.

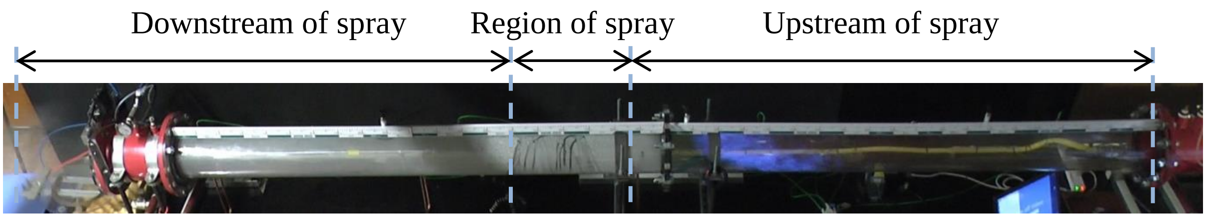

i. Flame propagating in methane-air mixture of E.R. (ϕ) 0.61 upstream of SRA

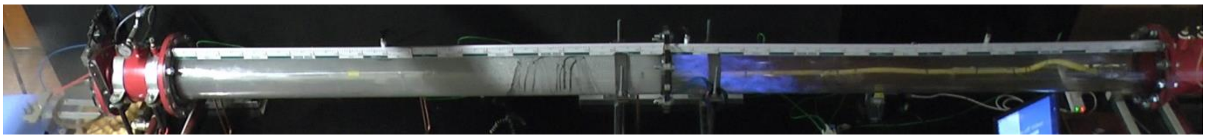

ii. Flame propagating in methane-air mixture of E.R. (ϕ) 0.61 upstream of SRA

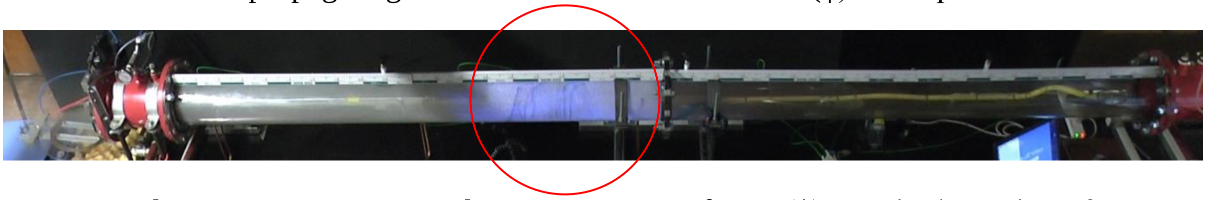

iii. Flame propagating in methane-air mixture of E.R. (ϕ) 0.61 in the region of spray

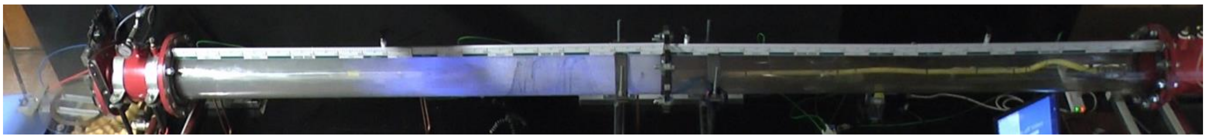

iv. Flame propagating in methane-air mixture of E.R. (ϕ) 0.61 downstream of SRA

Figure 5.64 : Flame propagating upstream and downstream of C/F SRA type A for a methane-air mixture (ϕ) 0.61

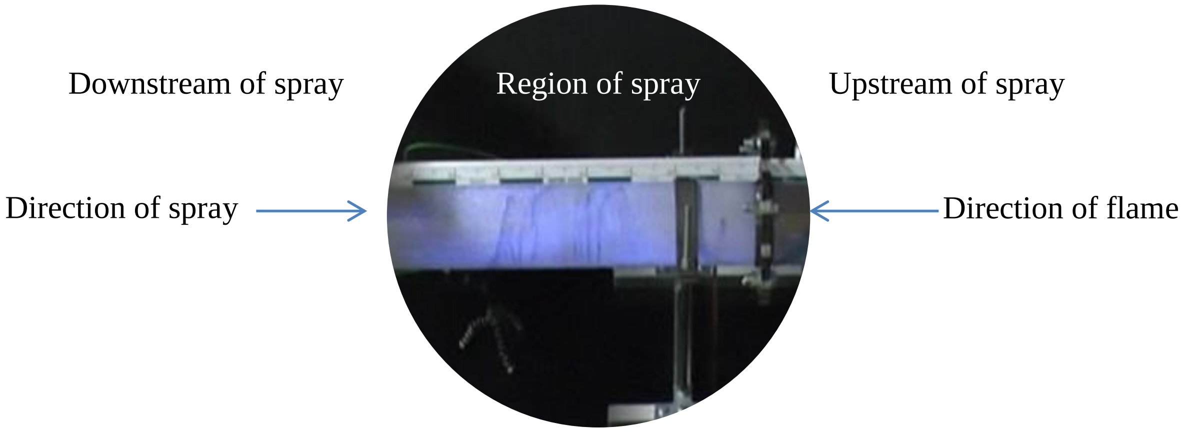

Figure 5.65 : Expanded view of region of spray highlighted in Figure 5.64(iii) with **no mitigation**

5.5.1.5 General event outcome

Table 5.17 provides a summary of the 'general event outcome' for this trial using the five potential 'outcome' categories offered in Section 5.5. The results of all hot trials were previously provided in Table 5.14.

Trial configuration	General event outcome	Code
Single C/F SRA : (ϕ) 0.61	No Mitigation with resulting Flame Acceleration	NMFA

Table 5.17 : General event outcome (trial series 5.5.1)

In this experimental trial using a single SRA Type A in counter flow arrangement with a propagating methane-air flame E.R ϕ 0.61, the spray was found to be ineffective in causing any positive quenching, or mitigation results. In fact, in this instance the resulting outcome produced a net increase in flame speed across the spray. The reasons for this outcome are justified below:-

i. The counter flow spray arrangement induced turbulent disorder into the otherwise quiescent unburned methane-air mixture ahead of the flame.
ii. The resulting increase in flame speed caused by the disturbance from the spray gave way to a reduction in droplet residence time potential.
iii. Although the droplets of D_{32} 17μm in the spray were of the order suggested by Sapko et al [61] for flame speeds of 2.3m/s, the droplet concentration/liquid volume flux of 0.011cm³/s/cm² were clearly insufficient to cause a positive quenching, or mitigation result.

5.5.2 Single (P/F) SRA Type A : E.R. (ϕ) 0.61

5.5.2.1 Trial set up

The pre-assembled Spill Return Atomiser (SRA), thermocouples (TC) and water feed pipework were installed within the FPMR in accordance with Figure 5.66 and Table 5.18. Water was supplied at 20˚C and at a pressure of 13MPa (130bar).

In this arrangement a single Type A SRA, previously tested in the cold trials was placed in parallel flow (P/F) arrangement with the propagating flame. The Type A SRA consisted of a 0.3mm diameter exit orifice and 0.5mm spill diameter, as previously described in Section 5.1.1, Table 5.1 and Chapter 4 and is summarised in Table 5.16.

The FPMR apparatus was again prepared for use in accordance with the all relevant health and safety requirements, risk assessments and the process flow diagram shown previously in Chapter 4. Again, due to laboratory layout and for convenience, ignition was delivered at the right hand end of the explosion and mitigation test rig as shown in Figure 5.66. Ignition was provided by a single spark via a single spark electrode with 4mm spark gap as discussed in Chapter 4.

Following the introduction and subsequent mixing of the methane-air mixture E.R. (ϕ) 0.61, the resulting homogeneous mixture was permitted to settle for one minute to allow it to become motionless.

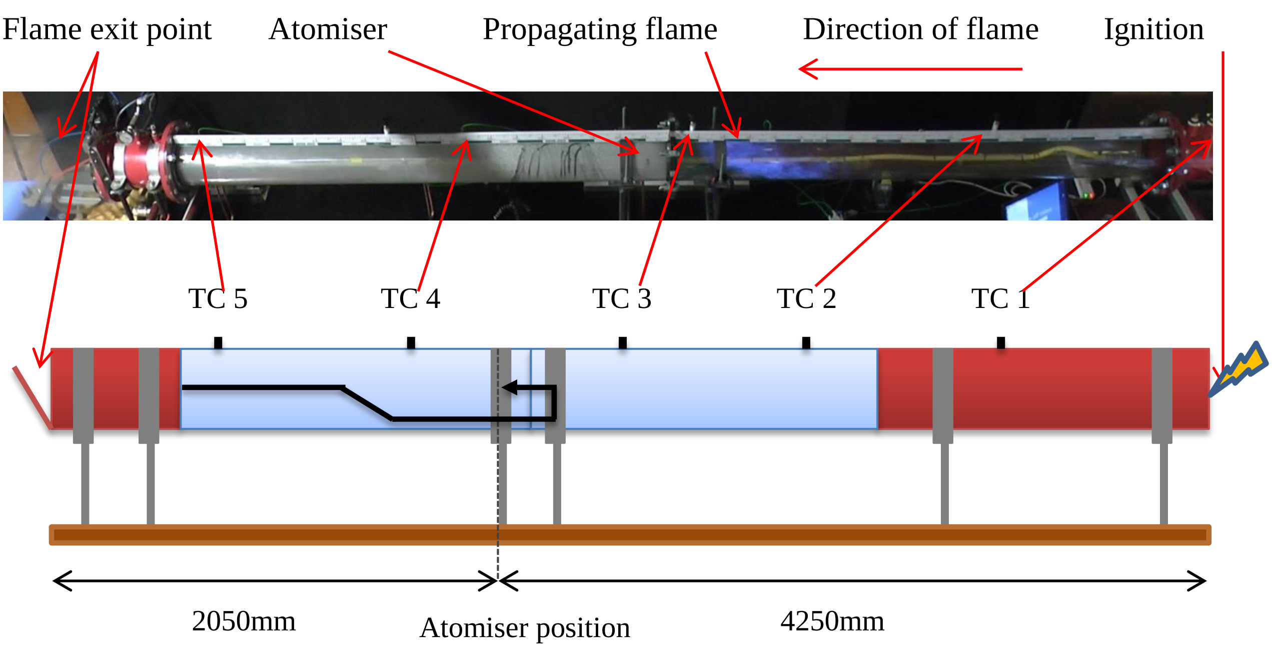

Figure 5.66 : Position of atomiser and thermocouples (relative to right hand ignition end)

Component	Position (measured from right hand end)
Thermocouple no.1 (T/C1)	1200mm
Thermocouple no.1 (T/C2)	2400mm
Thermocouple no.1 (T/C3)	3600mm
Thermocouple no.1 (T/C4)	4800mm
Thermocouple no.1 (T/C5)	6000mm
Atomiser outlet orifice (parallel flow)	4250mm

Table 5.18 : Measured position of thermocouples and SRA

The full atomiser characteristics relating to the SRA type A configuration were detailed formally in the cold trials Section 5.3 and are summarised for convenience in Table 5.16 below.

Mean D_{32} (μm)	Mean liquid volume flux ($cm^3/s/cm^2$)	Mean droplet velocity (m/s)
17	0.011	13.5

Table 5.19 : Typical characteristics for SRA type A 150mm downstream of exit orifice

5.5.2.2 Flame speed

In this series of tests the flame speeds for (ϕ) 0.61, 0.72, 0.95 and 1.06 were all measured upstream and downstream of the parallel flow spray. Figure 5.67 illustrates the percentage flame speed reductions observed. As the percentage reductions in this series all exhibit negative values, this confirms that all four methane-air mixtures tested resulted in a global increase in average flame speed across the sprays. The additional results for the (ϕ) 0.72, 0.95 and 1.06 trials can be found in Appendix 9 on the accompanying CD volume.

Following the successful ignition of the (ϕ) 0.61 mixture, the flame exited the steel driver section of the FPMR. The average flame speed was recorded as approximately 14m/s immediately upstream of the parallel flow spray. On this occasion the flame propagated directly through the region of the spray, followed by acceleration to about 37.5m/s. This consequential increase in flame speed of 23.5m/s is represented in Figure 6.67 as negative value, therefore characterising an increase flame speed of approximately 168%.

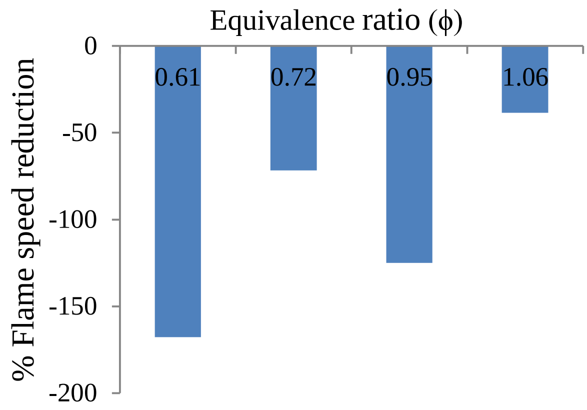

Figure 5.67 : Average flame speed reduction percentage (%) from upstream to downstream of parallel flow SRA in various methane-air mixtures

With counter flow sprays the approximate impact velocity was calculated by the sum of the average droplet velocity and the average flame speed. However, with parallel flow sprays approximate impact velocity is determined by the average flame speed, minus the average droplet velocity. Consequently, parallel flow sprays should therefore afford greater droplet residence times within the flame front.

Although there was still an overall increase in flame speed across this parallel flow spray, the increase in this instance was significantly less than the corresponding equivalent counter flow experiment, described previously in Section 5.5.1. The reduced increase in flame speed in this methane-air mixture of (ϕ) 0.61 may be attributed to:-

i. The increased droplet residence times afforded by this parallel flow conformation
ii. The reduction in disturbance in the unburned mixture ahead of the flame

From the literature reviewed in Chapters 2 and 3, there have been no other reported results or observations comparing the effects of counter flow, parallel flow and cross flow spray configurations.

5.5.2.3 Time-temperature response

The time-temperature profile for this trial is shown in Figure 5.68. The thermocouples downstream of the sprays exhibit consistent trends with respect to an increase in flame speed. The abrupt gradient found in TC5 is consistent with the disturbance of the downstream unburned mixture. It is highly likely that the flame would have continued to accelerate to a finite speed, if the flame propagation tube could have extended beyond its current length.

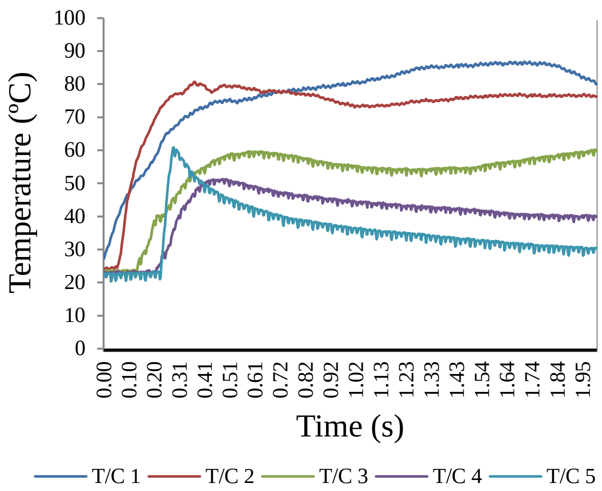

Figure 5.68 : Typical time-temperature profile for SRA Type A in P/F arrangement with methane-air mixture of E.R. (ϕ) 0.61

To provide a representative comparison for this single parallel flow SRA arrangement, the other methane-air trials in this series of (ϕ) 0.72, 0.95 and 1.06 were performed using the same conditions.

Rather than extending the length of the flame propagation and mitigation tube, it was decided to move the position of the spray(s) for the multiple parallel overlapping and cross flow trials. The position is shown briefly in Figure 5.69 below and is discussed in Section 5.5.4.

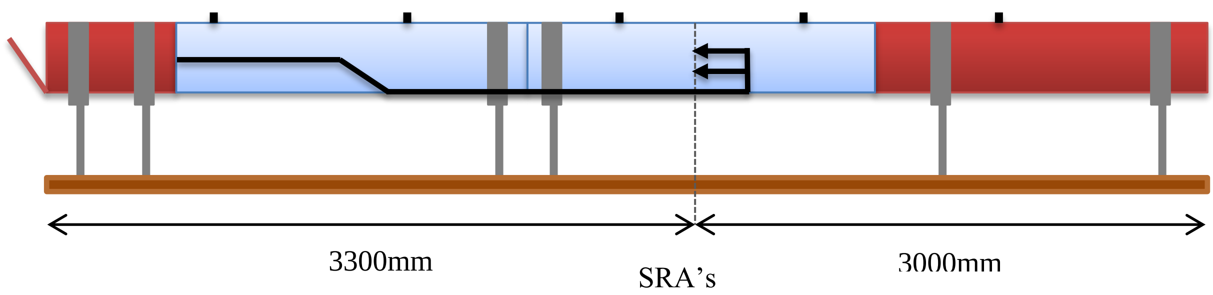

Figure 5.69 : Position of twin overlapping SRA manifold

5.5.2.4 Qualitative analysis

Figure 5.70 shows still images taken from the high definition video for the methane-air mixture E.R. (ϕ) 0.61 experimental trial. The flame can be observed upstream of the parallel flow Type A SRA spray and can also be seen to enter the P/F spray, this image has also been expanded to provide a close up image offered in Figure 5.71. In this experimental test the flame passed through the spray region and immediately accelerated by about 168%. This acceleration was significantly less than that observed in the corresponding counter flow trial utilising the same SRA, which was approximately 416% as shown previously.

Figure 5.71 offers no visible ‘dark regions’ in the flames, thus indicating an absence of areas of a localised suspension of combustion activity.

Equivalence ratio (ϕ) 0.61

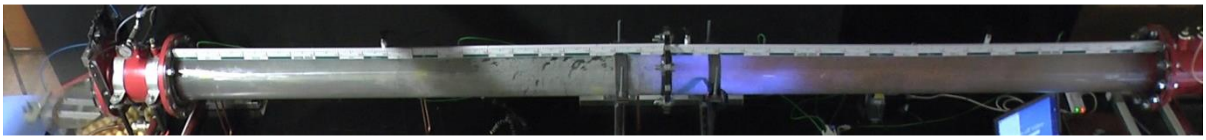

i. Flame propagating in methane-air mixture of E.R. (ϕ) 0.61 upstream of SRA

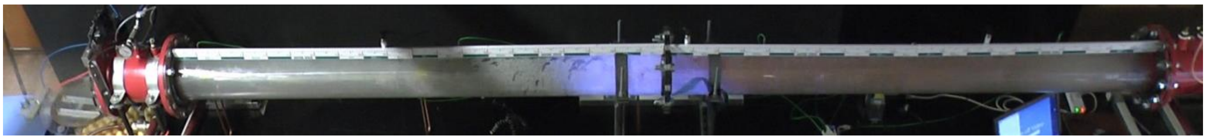

ii. Flame propagating in methane-air mixture of E.R. (ϕ) 0.61 upstream of SRA

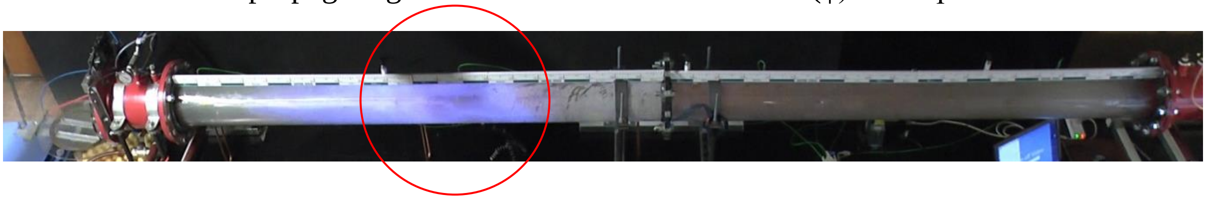

iii. Flame propagating in methane-air mixture of E.R. (ϕ) 0.61 in the region of spray

iv. Flame propagating in methane-air mixture of E.R. (ϕ) 0.61 downstream of SRA

Figure 5.70 : Flame propagating upstream and downstream of P/F SRA Type A for a methane-air mixture (ϕ) 0.61

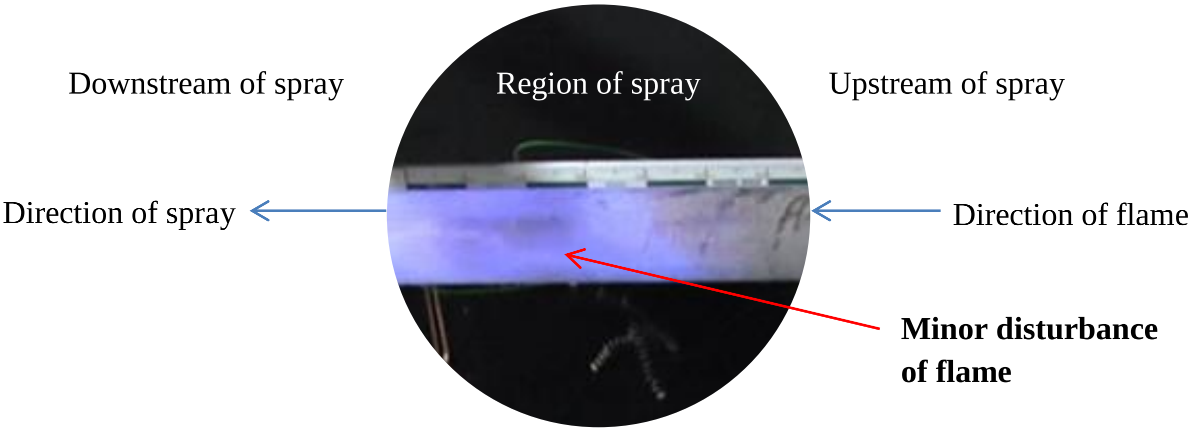

Figure 5.71 : Close up view of region of spray highlighted in Figure 5.70(iii) with **no mitigation**

5.5.2.5 General event outcome

Table 5.20 provides a summary of the 'general event outcome' for this trial, using the five potential 'event outcome' categories offered in Section 5.5. The results of all hot trials were previously given in Table 5.14.

Trial configuration	General event outcome	Code
Single P/F SRA (ϕ) 0.61	No Mitigation with resulting Flame Acceleration	NMFA

Table 5.20 : General event outcome (trial series 5.5.2)

It is worth noting that when comparing the results of this parallel flow trial to those of the corresponding counter flow trial, it may be concluded that under the current conformation and relative positioning of the SRA's, that the parallel flow configuration contributed significantly less towards flame acceleration, than in the correspondent counter flow trial.

5.5.3 Single (P/F) SRA Type C : E.R. (ϕ) 0.61

5.5.3.1 Trial set up

In this series of hot trials a single Type C SRA was assembled and installed in parallel flow (P/F) conformation in the FPMR, as previously shown in Figure 5.64 and Table 5.18. The full atomiser spray characteristics relating to the Type C SRA configuration were previously detailed in the cold trials Section 5.3 and are summarised in Table 5.21 below.

Mean SMD (µm)	Mean liquid volume flux ($cm^3/s/cm^2$)	Mean droplet velocity (m/s)
29	0.039	13.5

Table 5.21 : Typical characteristics for SRA Type C 95mm downstream of exit orifice

5.5.3.2 Flame speed

In these tests the flame speeds were all measured upstream and downstream of the parallel flow spray region. Figure 5.72 indicates the percentage flame speed reductions observed. The upstream flame speed in this methane-air mixture (ϕ) E.R. 0.61 was estimated to be 9.38m/s, whereby 100% mitigation was achieved in the spray region. In the other three mixtures in this series an increase in average flame speed was observed across the sprays.

When comparing the results shown in Figure 5.72 with the results for the corresponding counter flow trials illustrated in Figure 5.73 and Appendix A9.1.3.2, the methane-air mixture (ϕ) E.R. 0.61 was mitigated in both cases, whereas flame acceleration occurred in the other methane-air mixtures.

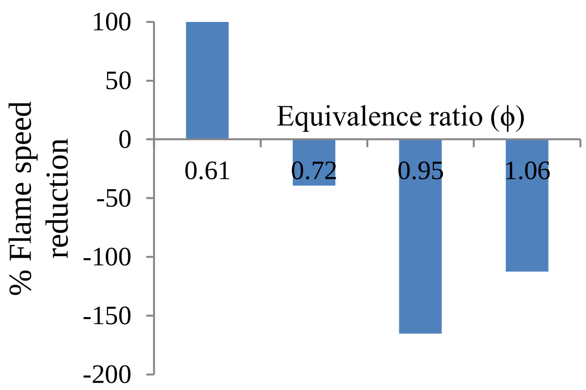

Figure 5.72 : Average flame speed reduction percentage (%) from upstream to downstream of Type C parallel flow SRA in various methane-air mixtures

Interestingly, the methane-air mixtures E.R. (ϕ) 0.72 and 1.06 in this parallel flow series produced smaller flame speed increases than their C/F equivalents shown in Figure 5.73.

Whereas, the methane-air mixtures (ϕ) E.R. 0.95 produced very similar outcomes in both C/F and P/F trials, resulting in an increase in flame speed of about 164% in both cases.

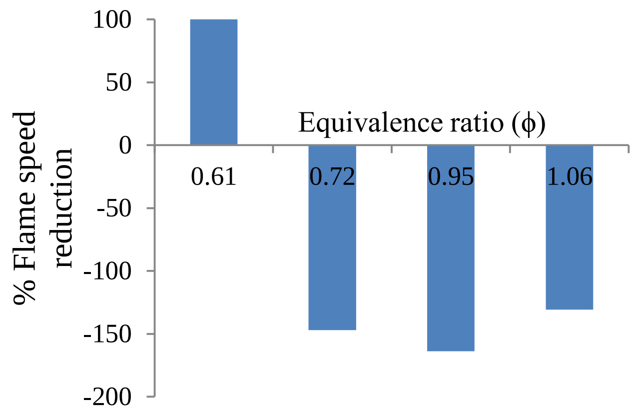

Figure 5.73 : Average flame speed reduction percentage (%) from upstream to downstream of Type C counter flow SRA in various methane-air mixtures

5.5.3.3 Time-temperature response

The time-temperature profiles produced from this trial are shown in Figure 5.74, whereby the profiles of thermocouples TC4 and TC5, downstream of the sprays exhibit consistent trends with respect combustion mitigation. The maximum temperature rise in TC5 was about 8˚C.

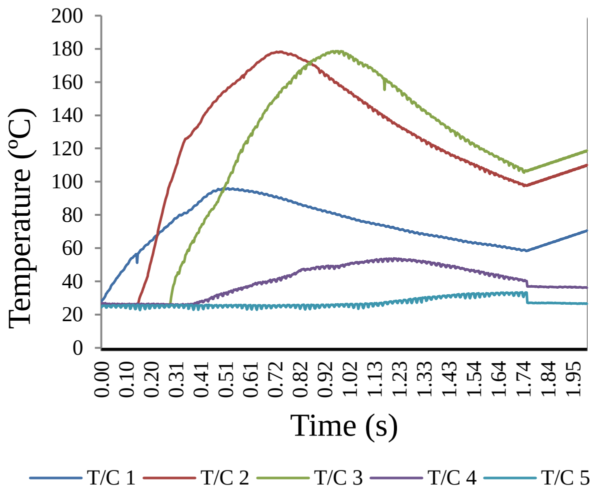

Figure 5.74 : Typical time-temperature profile for SRA Type C in P/F arrangement with methane-air mixture of E.R. (ϕ) 0.61

5.5.3.4 Qualitative analysis

Figure 5.75 shows the propagation and subsequent mitigation of a methane-air mixture of E.R. (ϕ) 0.61.

In Figure 5.75(i) the developed flame is seen to propagate through the unburned mixture, upstream of the spray region.

Figure 5.75(ii) shows a reduction in flame length and volume as the flame approaches the spray region.

Figure 5.75(iii) shows a further reduction in flame length and volume as the flame encounters the spray. Figure 5.76 shows an expanded view of the final stages of combustion, as the flame reaches the widest part of the spray. At this point the whole cross section of the flame propagation and mitigation tube was enveloped by the spray.

Finally, in Figure 5.75(iv) the flame has been completely mitigated by the single parallel flow Type C SRA.

Equivalence ratio (ϕ) 0.61

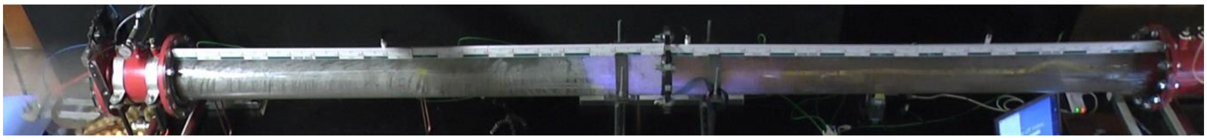

i. Flame propagating in methane-air mixture of E.R. (ϕ) 0.61 upstream of SRA

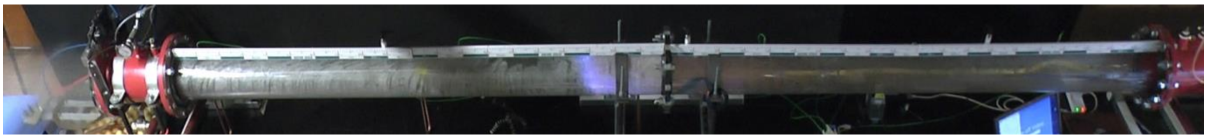

ii. Flame propagating in methane-air mixture of E.R. (ϕ) 0.61 upstream of SRA

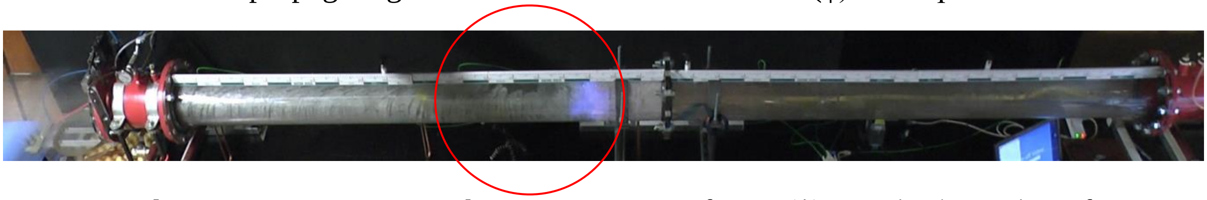

iii. Flame propagating in methane-air mixture of E.R. (ϕ) 0.61 in the region of spray

iv. **Mitigation** of methane-air mixture of E.R. (ϕ) 0.61 downstream of SRA

Figure 5.75 : Flame propagating upstream and mitigation of combustion using a Type C P/F SRA in a methane-air mixture (ϕ) 0.61

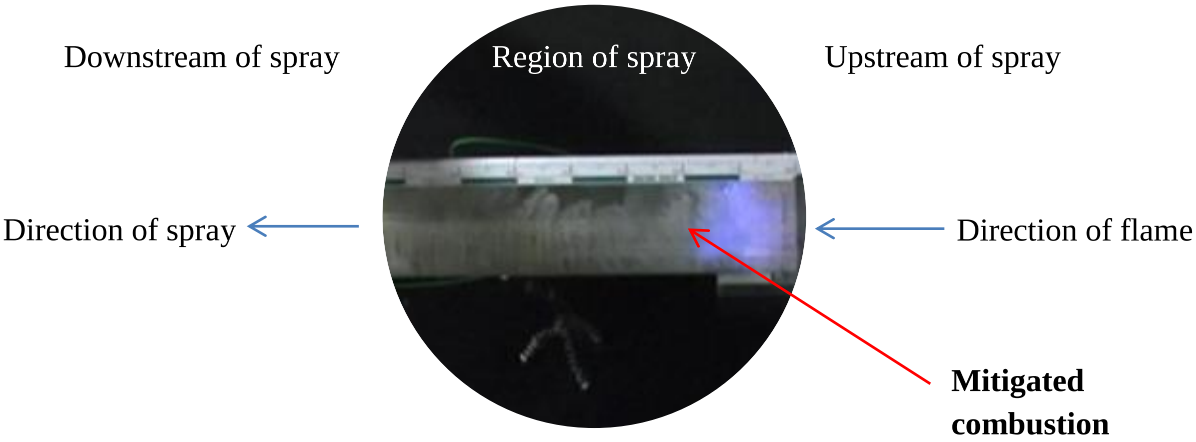

Figure 5.76 : Expanded view of region of spray highlighted in Figure 5.75(iii)

5.5.3.5 General event outcome

Table 5.22 provides a summary of the 'general event outcome' for this trial using the five potential 'event outcome' categories. The results of all hot trials were previously given in Table 5.14.

Trial configuration	General event outcome	Code
Single P/F SRA (ϕ) 0.61	Full Mitigation resulting in Flame Extinguishment	FMFE

Table 5.22 : General event outcome (trial series 5.5.3)

In this trial a single Type C parallel flow SRA configuration resulted in ***global mitigation*** of a propagating flame in a methane-air mixture of (ϕ) 0.61. Following the initial observations from this trial, the results would appear to suggest that a spray containing droplets of (D_{32}) 29 µm, with a mean liquid volume flux of 0.039cm^3/s/cm^2 exhibit the appropriate physical attributes and characteristics required to mitigate a slow moving explosion of 9.38m/s, thus accomplishing one of the principle objectives of this present study into the mitigating of explosions with flame speeds of ≤30m/s.

However, as this configuration was only capable of successive mitigation of a methane-air mixture of E.R. (ϕ) 0.61, further developments were necessary to mitigate the other corresponding methane-air mixtures of (ϕ) 0.72, 0.95 and 1.06.

5.5.4 Two Type B overlapping SRA's : E.R. (ϕ) 0.61

5.5.4.1 Trial set up

A unique manifold arrangement comprising of multiple overlapping SRA's was designed and developed for these trials, which was discussed previously in detail in Chapter 4 and is shown again in Figure 5.78. The manifold (see also Figure 5.78) was installed in the FPMR in parallel flow conformation with the propagation flame direction, as illustrated in Figure 5.77 and in accordance with the dimensions in Table 5.23

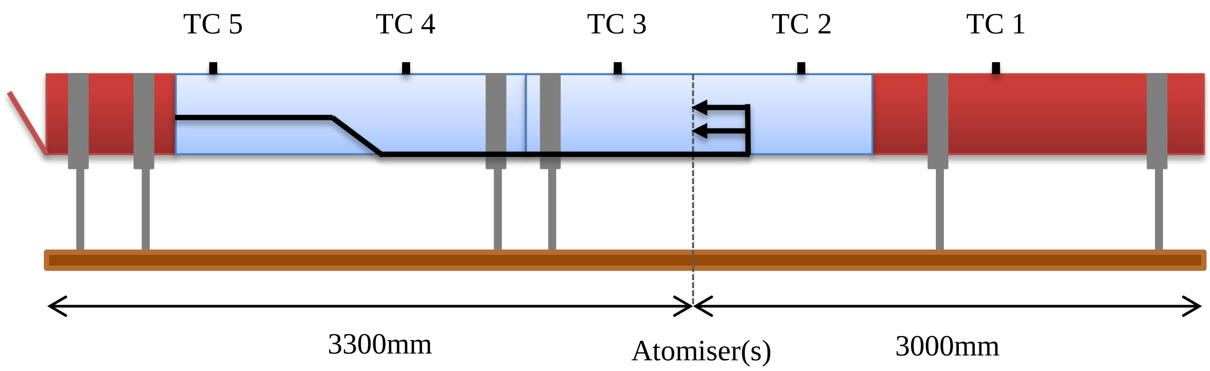

Figure 5.77 : Position of atomisers and thermocouples (relative to right hand ignition point)

Component	Position (measured from right hand end)
Thermocouple (TC1)	1200mm
Thermocouple (TC2)	2400mm
Thermocouple (TC3)	3600mm
Thermocouple (TC4)	4800mm
Thermocouple (TC5)	6000mm
Atomiser outlet orifices (parallel flow)	3000mm

Table 5.23: Measured position of thermocouples and SRA

In this trial series a twin parallel flow Type B (0.5mm exit orifice and 0.5mm spill diameter) overlapping SRA manifold was developed to deliver higher liquid volume flux sprays, than their single spray counterpart. This arrangement was previously developed and tested during the cold trials period of this study and was previously described in Chapter 4 and Section 5.3.5. The manifold was supplied with deionised water at 20˚C and at a pressure of 13MPa.

Table 5.24 provides a summary of the spray characteristics for this twin overlapping Type B SRA arrangement.

Mean SMD (µm)	**Mean liquid volume flux ($cm^3/s/cm^2$)**	**Mean droplet velocity (m/s)**
54	0.038	27

Table 5.24 : Typical characteristics for 2 x Overlapping Type B SRA's

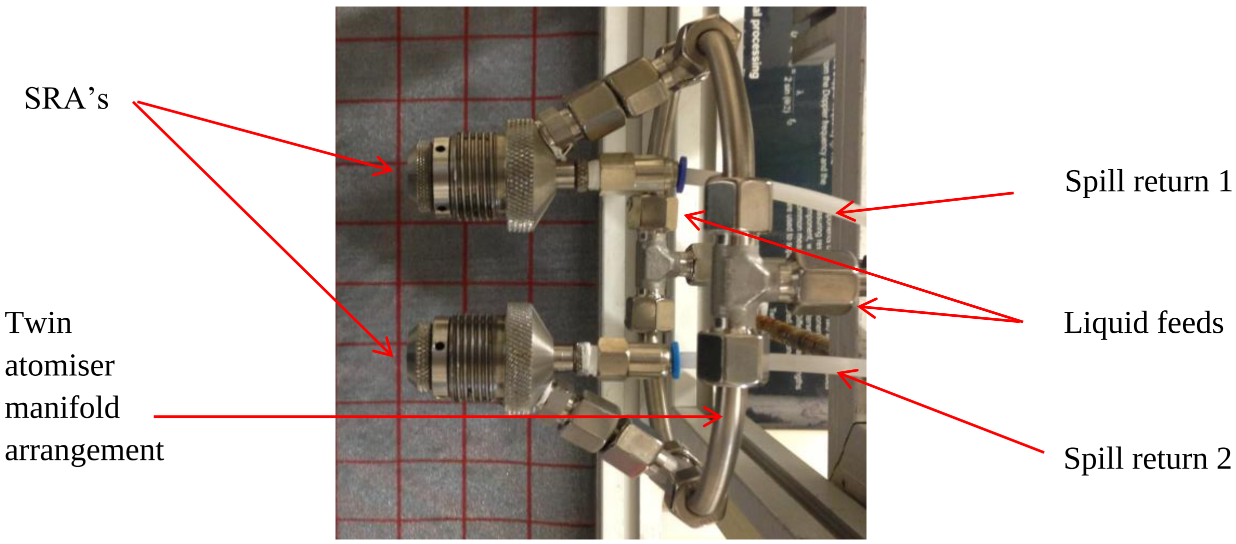

Figure 5.78 : Multiple overlapping spray manifold incorporating 2 x Type B SRA's

5.5.4.2 Flame speed

In this series of tests the flame speeds were all measured upstream and downstream of the twin parallel flow sprays. The upstream flame speed in this methane-air mixture of E.R. (ϕ) 0.61 was approximately 16.7m/s. Figure 5.79 illustrates the percentage flame speed reductions observed in the four trials in this series for the methane-air mixtures of E.R. (ϕ) 0.61, 0.72, 0.95 and 1.06

In the methane-air mixture of E.R. (ϕ) 0.61, the flame was *completely mitigated* and *did not continue to propagate* downstream. However, the other methane-air mixtures of E.R. (ϕ) 0.72, 0.95 and 1.06 all resulted in an increase in average flame speed across the sprays. However, when these results are compared to the corresponding single parallel flow trials previously reported, the resulting flame acceleration was significantly less. This would indicate that the increase in liquid volume flux (Q_f) from 0.024 to 0.038$cm^3/s/cm^2$ had positively affected the outcome with respect to *flame suppression*.

Full details of the other trials in this series can be found in Appendix 9, on the accompanying CD volume.

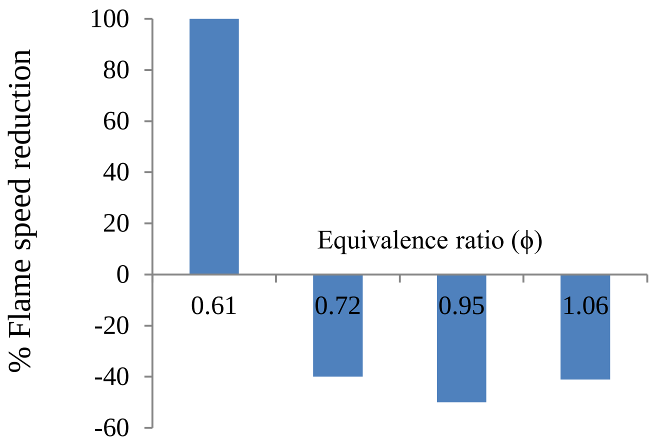

Figure 5.79 : Average flame speed reduction percentage (%) from upstream to downstream of overlapping parallel flow SRA's in various methane-air mixtures

5.5.4.3 Time-temperature response

The time-temperature profile produced for this trial is shown in Figure 5.80, where the profiles for thermocouples TC3, TC4 and TC5, which were downstream of the sprays, are consistent with combustion mitigation, without further ignition of the downstream mixture.

In this series of trials, thermocouple TC2 was situated downstream of TC1 and upstream of the sprays. In all cases a noteworthy temperature rise was detected between TC1 and TC2, indicating that an upstream disturbance had been transferred into the methane-air mixture, which may have been be due to the high level of entrainment upstream of the twin SRA arrangement. The temperature rise noted in these twin overlapping spray trials was not observed in any of the single atomiser trials.

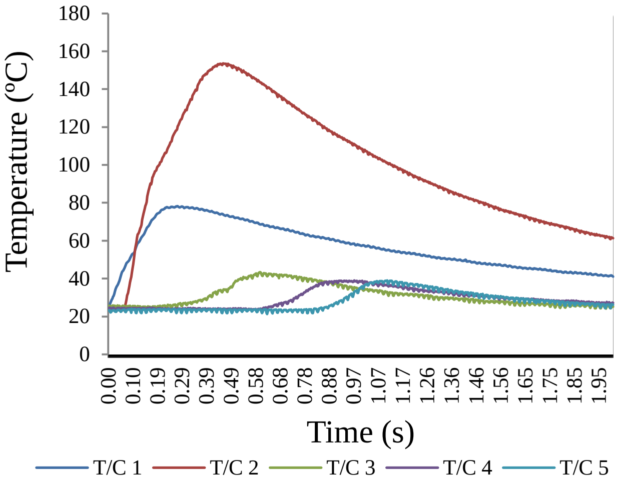

Figure 5.80 : Typical time-temperature profile for two overlapping Type B SRA's in P/F arrangement with methane-air mixture of E.R. (ϕ) 0.61

5.5.4.4 Qualitative analysis

The related images for this series of trials are presented in Figures 5.81and 5.82 for methane-air mixture of E.R. (ϕ) 0.61.

The flame can be observed in Figure 5.81(i) initially upstream of the sprays.

In Figure 5.81(ii) the flame can be seen to be in contact with the sprays and exhibits a concave shape in appearance.

In Figure 5.81(iii) the flame has been quenched and virtually extinguished by the sprays. The quenching is captured and has been enlarged in Figure 5.82.

Finally in Figure 5.82(iv) there is no further presence of combustion.

Equivalence ratio (ϕ) 0.61

i. Flame propagating in methane-air mixture of E.R. (ϕ) 0.61 upstream of SRA

ii. Flame propagating in methane-air mixture of E.R. (ϕ) 0.61 upstream of SRA

iii. Flame propagating in methane-air mixture of E.R. (ϕ) 0.61 in the region of spray

iv. Mitigation of methane-air mixture of E.R. (ϕ) 0.61 downstream of SRA

Figure 5.81 : Flame propagating upstream and downstream of two overlapping parallel flow Type B SRA's for a methane-air mixture (ϕ) 0.61

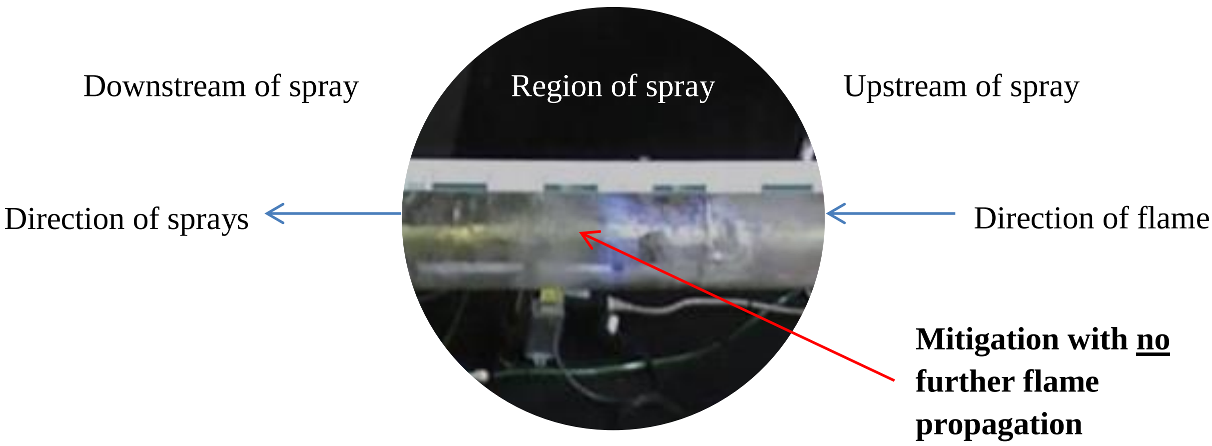

Figure 5.82 : Expanded view of region of spray highlighted in Figure 5.81(iii)

Due to the re-positioning of the atomiser location for this series, additional observations could be made of downstream activities. As the flame was totally mitigated in this event, there was no evidence of flame emerging from the outlet end of the FPMR tube. However, Figure 5.83 reveals a large 'plume' of water vapour (steam) being emitted from the exit, immediately following the mitigation event.

This water vapour is indicative of *droplet vaporisation* and provides evidence that a percentage of the spray must have been *small enough to vaporise*. This would have resulted in a degree of *latent heat transfer* within the flame front, in addition to the sensible heat transfer from droplets that were not sufficiently heated to phase transition.

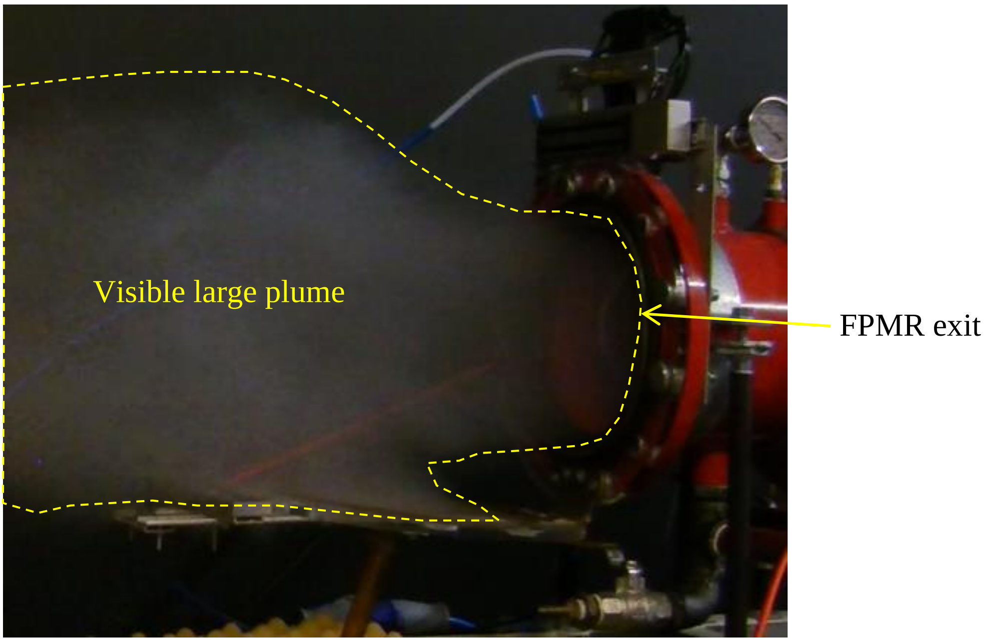

Figure 5.83 : Visible large plume of water vapour at exit end of apparatus

This phenomenon has only been studied previously by CFD analysis and mathematical modelling [65, 66], whereby the assumptions were made that droplets of, $D_{32} \leq 10\mu m$ would vaporise in a flame front.

While the D_{32} of the spray used in this trial was 54μm, the spray *must have* contained a significant amount of fine aerosols (≤10μm) that were too small to be detected by the PDA in the corresponding cold trials. Although the quantifying of aerosol sized droplets would have provided useful data, this requires specialist equipment and techniques and was considered to be outside of the scope of this current study.

5.5.4.5 General event outcome

Table 5.25 provides a summary of the ‘general event outcome’ for this trial using the five potential ‘event outcome’ categories. The results of all hot trials were previously given in Table 5.14.

Trial configuration	General event outcome	Code
Two P/F SRA : (ϕ) 0.61	Full Mitigation resulting in Flame Extinguishment	FMFE

Table 5.25 : General event outcome (trial series 5.5.4)

5.5.5 Four (X/F) Type B SRA's : E.R. (ϕ) 0.72

5.5.5.1 Trial set up

In this series of trials, four cross flow (X/F) Type B SRA's were assembled and installed in positions #1, #2, #3 and #4 as shown in Figures 5.84 and 5.85 and Table 5.26. This atomiser configuration was subjected to four trials with different methane-air mixtures of (ϕ) 0.61, 0.72, 0.95 and 1.06.

In this experimental trial, four cross flow (X/F) Type B SRA's were supplied with water at 20˚C and a pressure of 13MPa. The FPMR was filled with a methane-air mixture of (ϕ) 0.72 and allowed to become still for a further minute. The additional related results for the methane-air mixtures of (ϕ) 0.61, 0.95 and 1.06 can be found in Appendix 9.

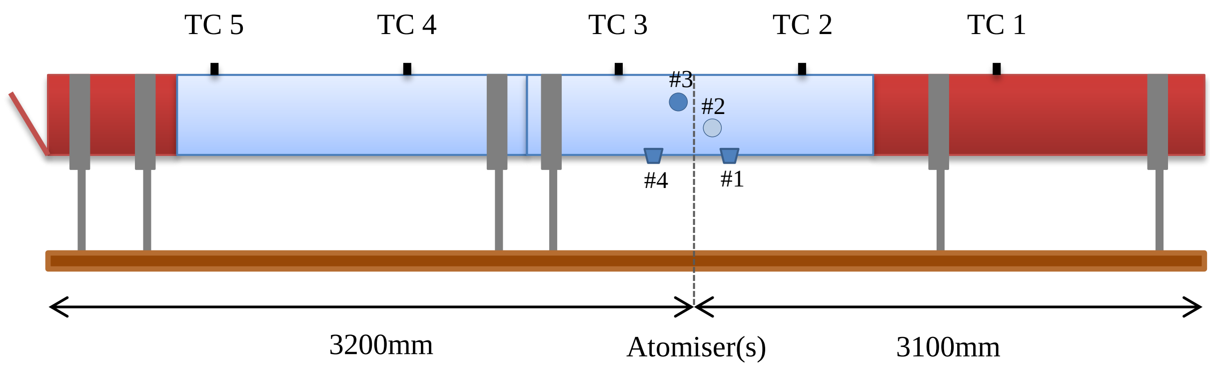

Figure 5.84 : Position of atomiser and thermocouples (relative to right hand ignition)

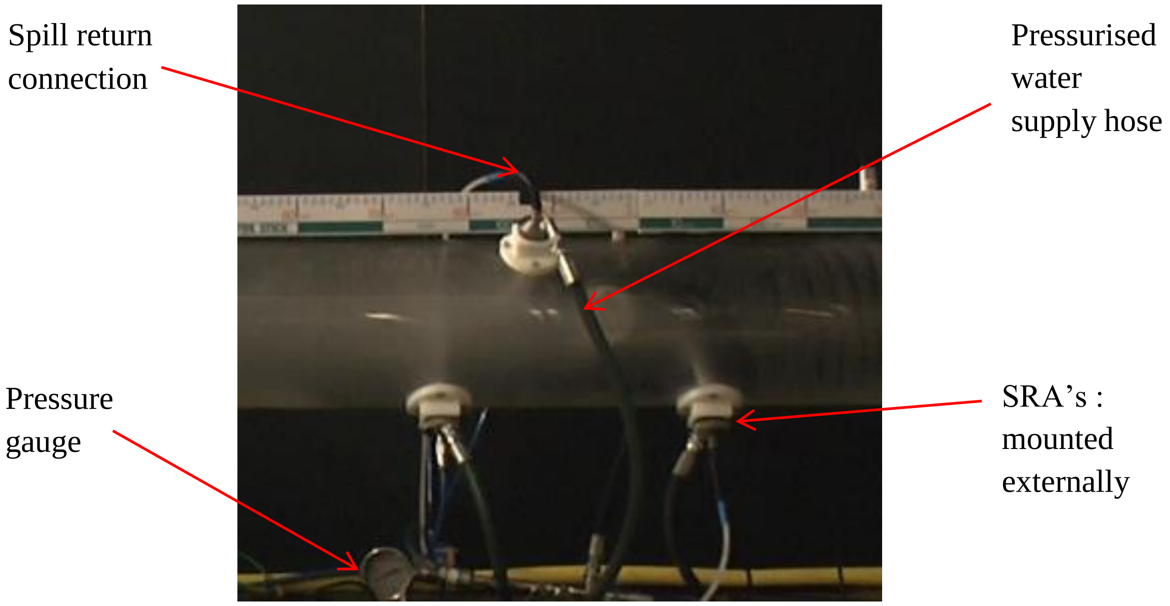

Figure 5.85 : Cross flow SRA arrangement and ancillary connections

Component	Position (measured from right hand end)
Thermocouple (TC1)	1200mm
Thermocouple (TC2)	2400mm
Thermocouple (TC3)	3600mm
Thermocouple (TC4)	4800mm
Thermocouple (TC5)	6000mm
Atomiser outlet orifice (cross flow)	3100mm (centre of sprays)

Table 5.26 : Measured position of thermocouples and SRA's

The full atomiser spray characteristics relating to the Type B SRA configuration were previously detailed in the cold trials Section 5.3 and are summarised in Table 5.27 below.

Mean D32 (µm)	Mean liquid volume flux ($cm^3/s/cm^2$)	Mean droplet velocity (m/s)
26	0.024	21.4

Table 5.27 : Typical characteristics for SRA Type B 95mm downstream of exit orifice

5.5.5.2 Flame speed

Average flame speeds were measured both upstream and downstream of the spray region, which are illustrated in Figure 5.86 as flame speed reduction values.

In the methane-air mixture (ϕ) 0.72 the upstream flame speed was estimated to be 11m/s. In this atomiser configuration the flames in the methane-air mixtures of (ϕ) 0.61 and 0.72 were *fully mitigated, with no evidence of further downstream propagation*. This is shown in the Figure 5.86 below as a 100% flame speed reduction.

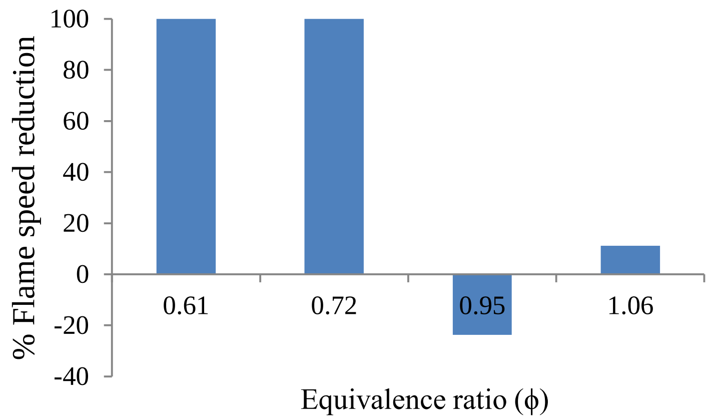

Figure 5.86 : Average flame speed reduction percentage (%) from upstream to downstream of four X/F Type B SRA's in various methane-air mixtures

5.5.5.3 Time-temperature response

The typical time-temperature profiles are presented in Figure 5.87 and reinforce the two mitigation events in the (ϕ) 0.61 and 0.72 mixtures, with TC3, TC4 and TC5 only indicating a slight increase of $\leq 5^{\circ}C$, thus indicating suspension of the combustion process.

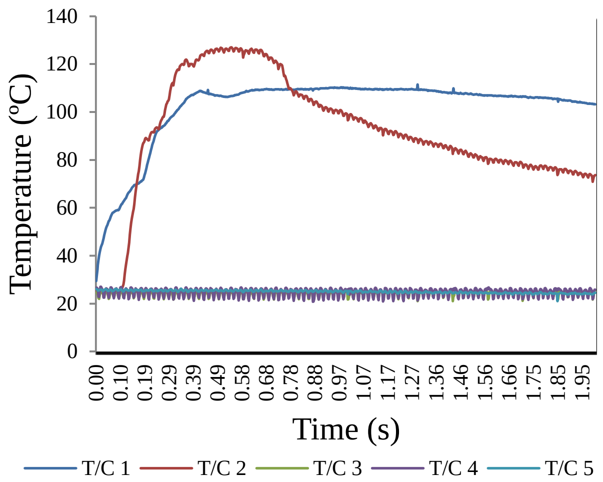

Figure 5.87 : Characteristic time-temperature profile for four SRA Type B in X/F arrangement with methane-air mixture of E.R. (ϕ) 0.72

5.5.5.4 Qualitative analysis

In Figure 5.88(i) the upstream progression of the flame can be observed.

Figure 5.88(ii) reveals the flame passing through spray #1, however '*dark regions'* are visible in the flame profile.

In Figure 5.88(iii) the flame has been *partially quenched* and flame area has been reduced significantly.

Figure 5.88(iv) shows traces of combustion between SRA's #1 and #2. In this case the flame was completely mitigated by SRA #3.

Figure 5.89 offers an expanded view of the final traces of combustion SRA's #1 and #2, prior to a *total mitigation event*.

Equivalence ratio (ϕ) 0.72

i. Flame propagating in methane-air mixture of E.R. (ϕ) 0.72 upstream of SRA

ii. Flame propagating in methane-air mixture of E.R. (ϕ) 0.72 upstream of SRA

iii. Flame propagating in methane-air mixture of E.R. (ϕ) 0.72 in the region of spray

iv. **Mitigation** in methane-air mixture of E.R. (ϕ) 0.72 downstream of SRA

Figure 5.88 : Flame propagating upstream and downstream of four X/F SRA Type B for a methane-air mixture (ϕ) 0.72

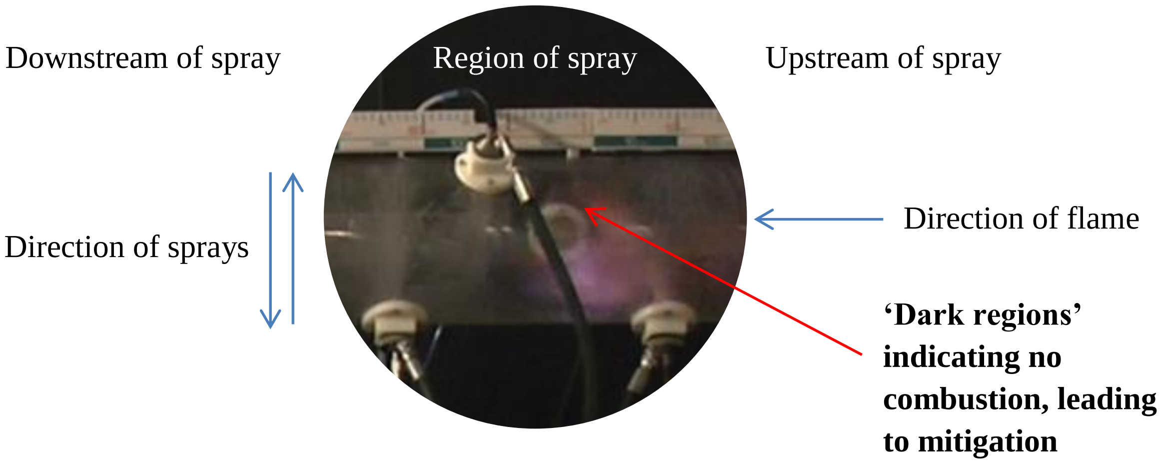

Figure 5.89 : Enlarged view of region of spray highlighted in Figure 5.88(iii)

5.5.5.5 General event outcome

Table 5.28 provides a summary of the 'general event outcome' for this trial using the five potential 'event outcome' categories. The results of all hot trials were previously given in Table 5.14.

Trial configuration	General event outcome	Code
Four X/F SRA : (ϕ) 0.72	Full Mitigation resulting in Flame Extinguishment	FMFE

Table 5.28 : General event outcome (trial series 5.5.5)

This configuration of four Type B (X/F) SRA's produced the *first mitigation event* in a methane-air mixture of *E.R. (ϕ) 0.72*. This event was significant in this research, as previous mitigation events had only occurred in 'lean' methane-air mixture of E.R. (ϕ) 0.61.

The reasons for this connotation are:-

i. A laminar flame propagating in a methane-air mixture of (ϕ) 0.61 will have a relative flame front of approximately 2.4mm thick, whereas the flame front in a methane-air mixture of (ϕ) 0.72 is about 1.65mm thick, as shown on Figure 5.90.
ii. The flame speed in a (ϕ) 0.72 mixture is generally faster than in a (ϕ) 0.61 mixture.
iii. This reduced flame thickness and greater flame speed would lead to a reduced droplet residence time in the flame, thus increasing the difficulty to mitigate combustion.

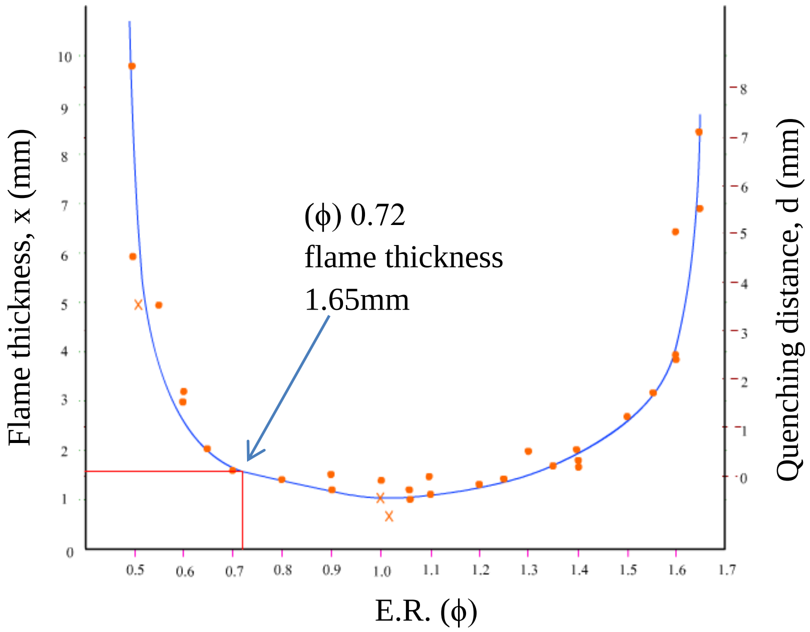

Figure 5.90 : Typical equivalence ratio : flame thickness relationship for methane-air [35]

5.5.6 Four (X/F) Type C SRA's : E.R. (ϕ) 0.95

5.5.6.1 Trial set up

In this series of trials four Type C SRA's were assembled and installed in positions #1, #2, #3 and #4 as previously shown in Figures 5.84 and 5.85 and Table 5.26. The atomisers were supplied with deionised water at 20˚C, at an operating pressure of 13MPa and were subjected to four trials with different methane-air mixtures of (ϕ) 0.61, 0.72, 0.95 and 1.06.

5.5.6.2 Flame speed

Average flame speeds were measured both upstream and downstream of the spray region, which are illustrated in Figure 5.91 as flame speed reduction values. In this SRA configuration the methane-air mixture E.R. (ϕ) 0.95 was completely mitigated, as were all of the other methane-air mixtures in the corresponding series. The additional discussion relating to the methane-air mixtures of (ϕ) 0.61, 0.72 and 1.06 can be found in Appendix 9 on the accompanying CD, Volume III.

The mitigation event in the methane-air mixture E.R. (ϕ) 0.95 is shown in the diagram as a 100% flame speed reduction, with the initial upstream flame speed being about 23.5m/s and no downstream combustion activity. This noteworthy event was the *first SRA configuration with resulting successful mitigation in all four methane-air mixtures*. (See also Appendix 9)

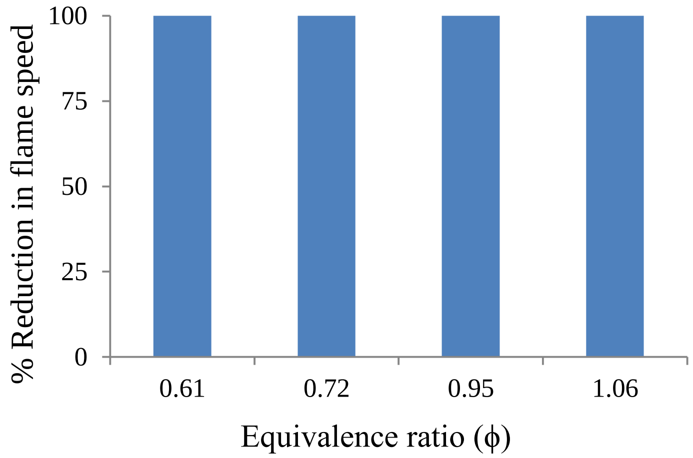

Figure 5.91 : Average flame speed reduction percentage (%) from upstream to downstream of four X/F SRA's in a various methane-air mixtures

5.5.6.3 Time-temperature response

The typical time-temperature profiles presented in Figure 5.92 reinforce the mitigation event in the (ϕ) 0.95 methane-air mixture, with TC5 only indicating a slight increase of $\leq 5^{\circ}$C, thus indicating global cessation of the combustion process.

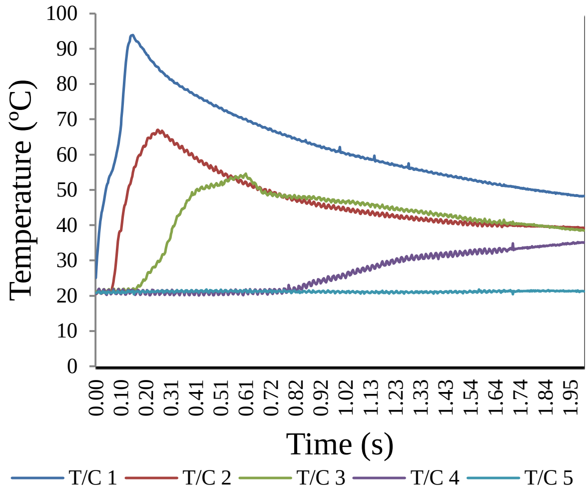

Figure 5.92 : Typical time-temperature profile for four SRA Type C in X/F arrangement with methane-air mixture of E.R. (ϕ) 0.95

5.5.6.4 Qualitative analysis

In Figure 5.93(i) the propagating flame can be seen immediately upstream of SRA #1.

Figure 5.93(ii) shows the flame within the spray region, with reveals some disturbance and also a large area of ‘dark region’ where combustion is not occurring.

In Figure 5.93(iii) the flame is finally mitigated by SRA spray #4. This event has been magnified for convenience and is displayed in Figure 5.94.

In Figure 5.93(iv) shows some trailing intermediate reactions in their final stages

Equivalence ratio (ϕ) 0.95

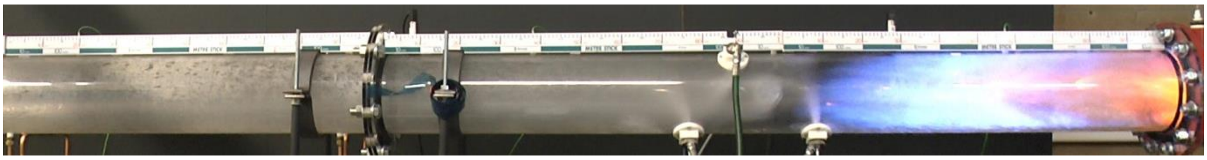

i. Flame propagating in methane-air mixture of E.R. (ϕ) 0.95 upstream of SRA

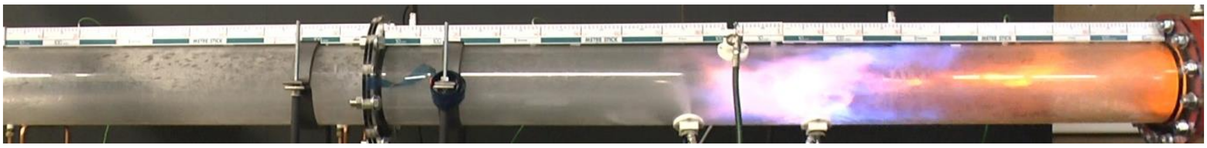

ii. Flame propagating in methane-air mixture of E.R. (ϕ) 0.95 upstream of SRA

iii. Flame propagating in methane-air mixture of E.R. (ϕ) 0.95 in the region of spray

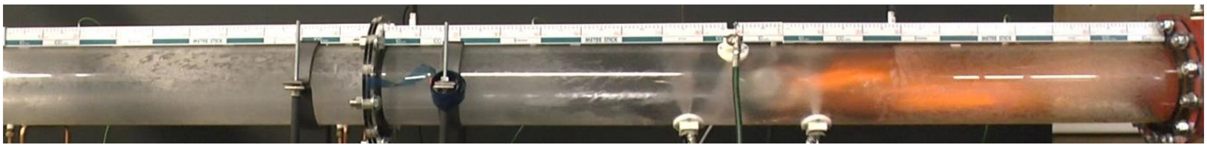

iv. **Mitigation** in methane-air mixture of E.R. (ϕ) 0.95 downstream of SRA

Figure 5.93 : Flame propagating upstream of four X/F SRA Type C, with no combustion activity downstream for a methane-air mixture (ϕ) 0.95

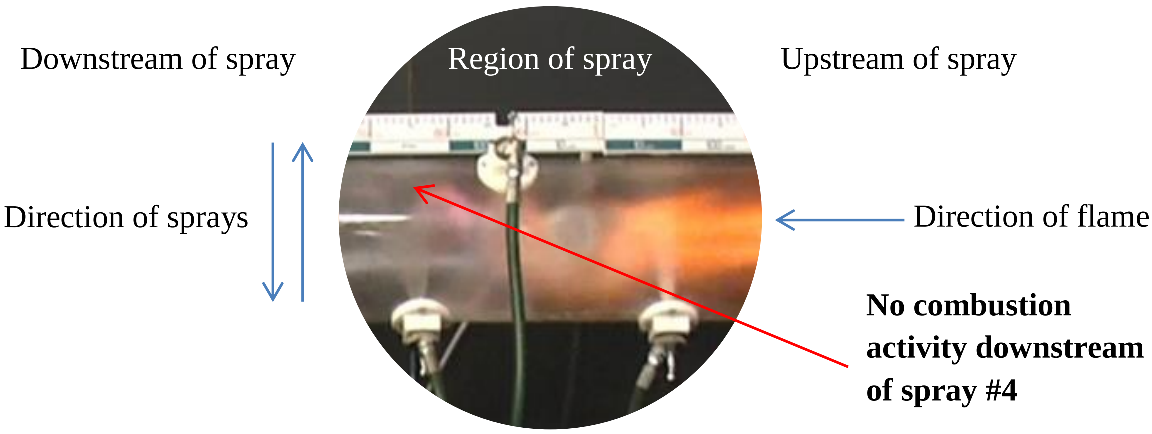

Figure 5.94 : Close up view of region of spray highlighted in Figure 5.93(iii)

5.5.6.5 General event outcome

Table 5.29 provides a summary of the 'general event outcome' for each trial in this current series, using the five potential 'event outcome' categories. The results of all hot trials were previously given in Table 5.14.

Trial configuration	General event outcome	Code
Four X/F SRA's (ϕ) 0.95	Full Mitigation resulting in Flame Extinguishment	FMFE

Table 5.29 : General event outcome (trial series 5.5.6)

This configuration of four Type C (X/F) SRA's produced the *first mitigation event in a methane-air mixture of E.R. (ϕ) 0.95*. This was a *momentous event* in the current study, as no other atomiser configuration had been successful, due to the challenges presented by this *near stoichiometric methane-air mixture* of E.R. (ϕ) 0.95.

The reasons for this significance are:-

i. Combustion in a (ϕ) 0.95 mixture is highly exothermic, consequently a significant heat transfer is required between droplet and flame to cause a mitigation event.
ii. A flame propagating in a methane-air mixture of (ϕ) 0.61 will have a relative flame front of approximately 2.4mm thick, whereas flame front in a methane-air mixture of (ϕ) 0.95 is about 1.05mm thick, as shown previously in Figure 5.90.
iii. The flame speed in a (ϕ) 0.95 mixture was generally fastest of all the mixtures used
iv. This reduced comparative flame thickness and greater flame speed would lead to a reduced droplet residence time in the flame, thus increasing the difficulty to mitigate combustion.

5.5.7 Four (X/F) Type C SRA's : Water temperature 50°C, E.R. (ϕ) 0.95

5.5.7.1 Trial set up

In this series of experimental trials four cross flow (X/F) Type C SRA's were supplied with de-ionised water at a pressure of 13MPa and at a variety of water temperatures from 25°C to 50°C. The aim of this series of tests was to establish the effects of an increase in water temperature supplied to the sprays. The positions of thermocouples and atomisers are illustrated in Figure 5.95 and Table 5.30.

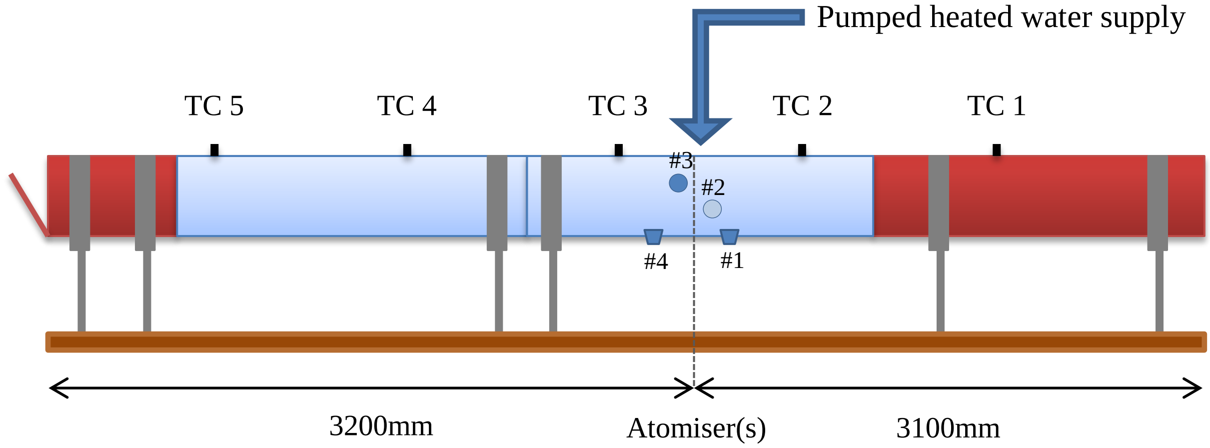

Figure 5.95 : Position of atomisers, thermocouples and heated water supply (relative to right hand ignition)

Component	Position (measured from right hand end)
Thermocouple (TC1)	1200mm
Thermocouple (TC2)	2400mm
Thermocouple (TC3)	3600mm
Thermocouple (TC4)	4800mm
Thermocouple (TC5)	6000mm
Atomiser outlet orifice (cross flow)	3100mm (centre of sprays)

Table 5.30 : Measured position of thermocouples and SRA's

In ensure the validity and reliability of the results in this series, two tests were performed at each of the selected temperatures and are presented as follows:-

a. Water supply temperature 25°C : Test (i) and (ii) : see Appendix 9
b. Water supply temperature 30°C : Test (i) and (ii) : see Appendix 9
c. Water supply temperature 40°C : Test (i) and (ii) : see Appendix 9
d. Water supply temperature 50°C : Test (i) and (ii) : see also Appendix 9

In previous studies Sapko *et al* [61] carried out a small scale trial with a respect to water droplet heat transfer, whereby reference was made to Kumm's [62] droplet heat up and vaporisation expression. Sapko's work [61] was extensively discussed in Chapter 2 and 3.

Table 5.31 has been produced to demonstrate the conditions and temperatures considered in this series of trials. In Table 5.31 column two, the flame speed values are listed for upstream of the spray. Notably the upstream flame speed is shown to reduce with the increase in spray temperature. This relationship has not been observed in any of the previous studies offered as reference throughout this current work. The likely cause of this upstream reduction in flame speed is the interaction of droplets in the preheat zone of the flame front.

Column three of Table 5.31 shows the estimated droplet residence times for each of the tests, based on the upstream flame speed and a comparative flame thickness of 1.05mm for the methane-air mixture E.R. (ϕ) 0.95. Columns four, five and six reveal the calculated residence times required to bring water droplets of various diameters to their boiling point, using Kumm's relationship [62].

It is clear that in each of the scenarios offered for 10, 20 and 30μm droplets, that the actual residence time for each case is at least one or two orders of magnitude less than that required to bring all the droplets to boiling point. Based on the information presented in Table 5.31 and for the Type C spray being in the order of D_{32} = 25 - 30μm, the principle mode of heat transfer would favour sensible heat exchange.

Water temperature (˚C)	Upstream flame average speed (m/s)	Calculated droplet residence time (sec)	Calculated unsteady heat up time to bring droplet to boiling point (sec) Kumm [62]		
			10μm	20μm	30μm
25	27.5	3.7e-5	2.29e-4	9.14e-4	2.05e-3
25	27	3.7e-5	2.29e-4	9.14e-4	2.05e-3
30	27.5	3.7e-5	2.28e-4	9.12e-4	2.05e-3
30	26.5	3.6e-5	2.28e-4	9.12e-4	2.05e-3
40	23.75	4.2e-5	2.27e-4	9.07e-4	2.04e-3
40	23.5	4.2e-5	2.27e-4	9.07e-4	2.04e-3
50	21.25	4.7e-5	2.26e-4	9.02e-4	2.03e-3
50	17.75	5.6e-5	2.26e-4	9.02e-4	2.03e-3

Table 5.31 : Flame speeds (m/s), droplet residence times (s) and unsteady heat up time (s) to bring droplet to boiling point

From an observational perspective, all of the experimental trials in this series produced a large plume of water vapour (steam) from the exit end of the FPMR as shown in Figure 5.96, thus indicating that the spray *must have contained a number of aerosol sized droplets, in the order of* D_{32}*, 10µm* that were vaporising. Droplet vaporisation releases the additional benefits of *latent heat transfer*.

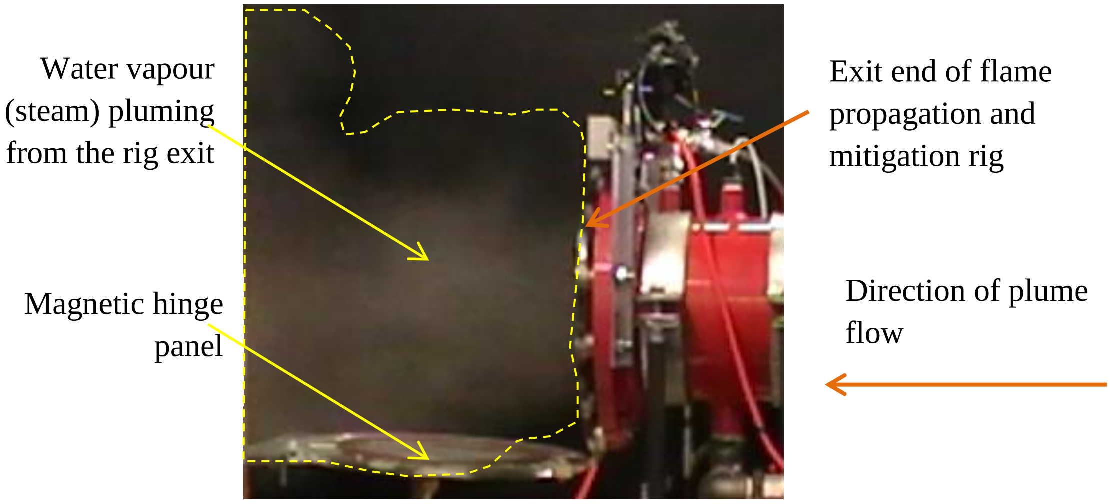

Figure 5.96 : Example of water vapour pluming from the rig exit following mitigation

5.5.7.2 Flame speed

Figure 5.97 shows the typical flame speed reduction (%) resulting from the eight trials in this series, whereby it is clear that all of the tests resulted in complete mitigation of the propagating methane-air flame (E.R.(ϕ) 0.95). Upstream flame speeds were given previously in Table 5.31.

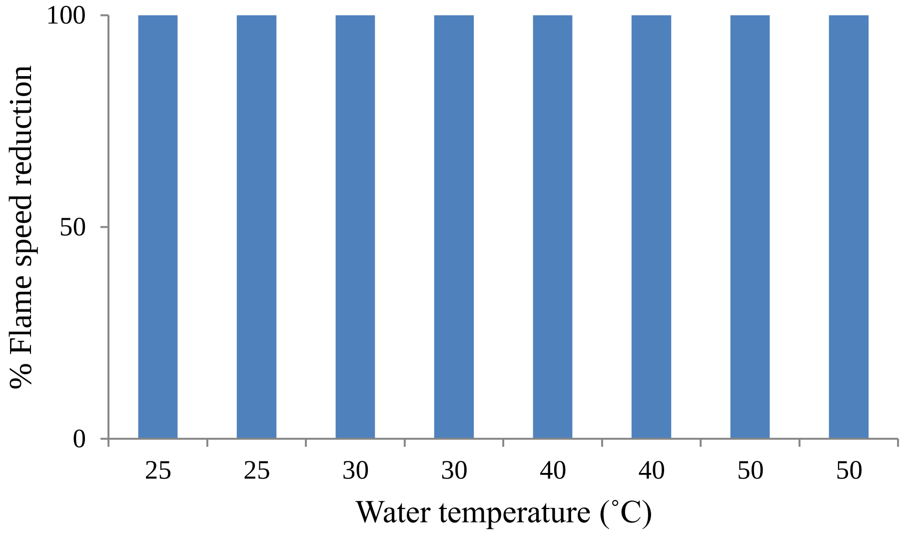

Figure 5.97 : Typical flame speed reductions for four Type C SRA's at 13MPa

5.5.7.3 Time-temperature response

Water supply pressure 13MPa and temperature 50˚C : Test (i) and (ii)

In Figures 5.98 and 5.99 the water supply temperature was 50˚C. Both of the time-temperature profiles exhibit similar appearances. In this case thermocouple TC5 shows a much higher increase over the two seconds of data than any of the other trials in this series (see Appendix 9).

Although mitigation occurred in both of the 50˚C trials, TC3 and TC4 indicate an increase in temperature representing a value of about 20 - 30˚C. This is consistent with the observation that was previously discussed and shown in Figure 5.96, whereby a plume of water vapour appeared from the exit point of the apparatus. The resulting plume from these 50˚C trials appeared to be larger (visually) than in any other reported findings in these investigations.

(i) Water supply pressure 13MPa and temperature 50 °C

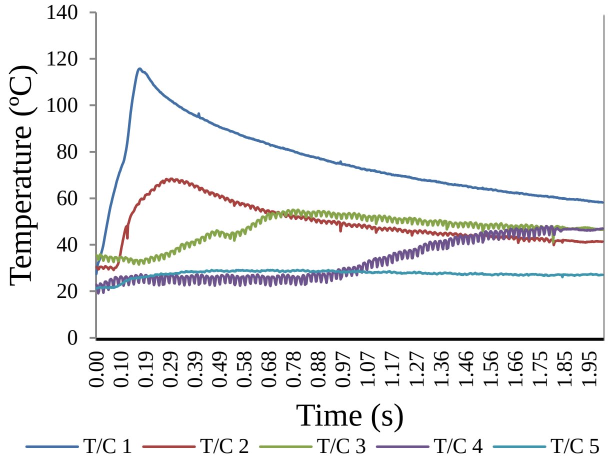

Figure 5.98 : Characteristic time-temperature profile for four Type C SRA's operating at 13MPa and water temperature 50 °C – E.R.(ϕ) 0.95

(ii) Water supply pressure 13MPa and temperature 50 °C

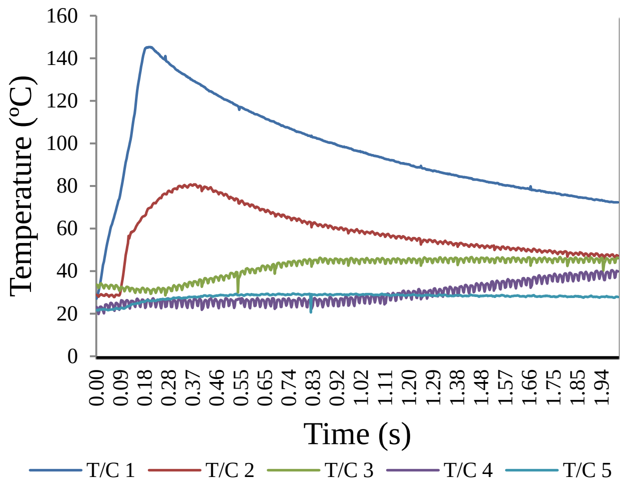

Figure 5.99 : Distinctive time-temperature profile for four Type C SRA's operating at 13MPa and water temperature 50 °C – E.R.(ϕ) 0.95

5.5.7.4 Qualitative analysis

Water supply pressure 13MPa and temperature 50°C : Tests (i) and (ii)

In Figure 5.100 the still photographs show the initial propagation of the flame and its passage through the sprays. In this test the flame did not propagate beyond spray #3. Figure 5.101 offers a magnified image of the flame being mitigated at spray #3.

The same experimental conditions were repeated and the relevant still photographs are revealed in Figure 5.102. In this trial the flame did not propagate after spray #3. Figure 5.103 reveals an expanded image of the flame being mitigated by spray #3.

Water supply pressure 13MPa and temperature 50°C (i)

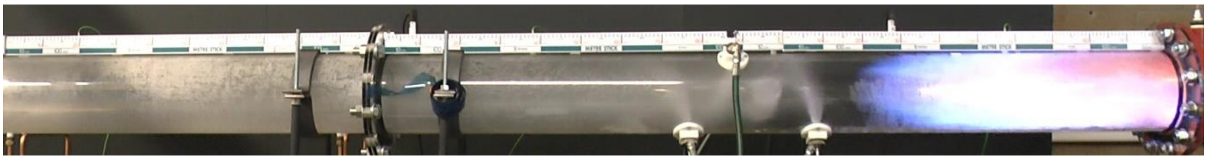

i. Flame propagating in methane-air mixture of E.R. (ϕ) 0.95upstream of SRA

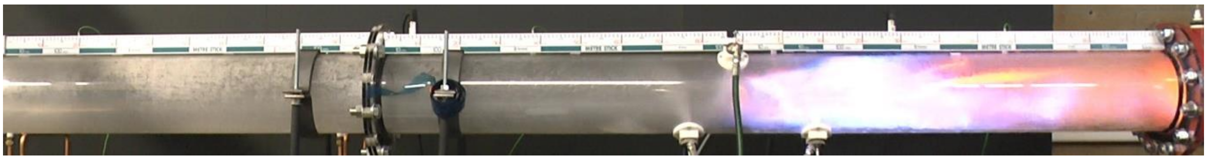

ii. Flame propagating in methane-air mixture of E.R. (ϕ) 0.95 upstream of SRA

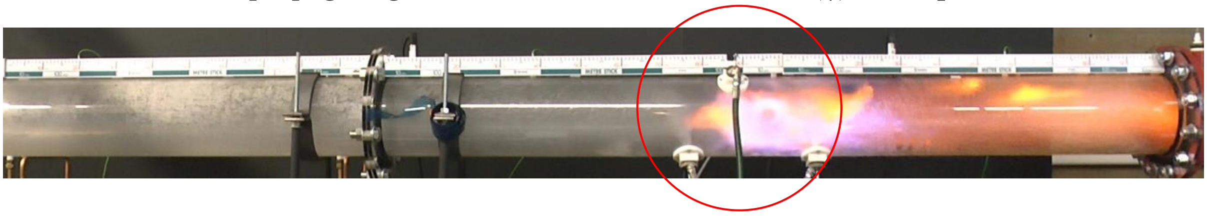

iii. **Mitigated** flame in methane-air mixture of E.R. (ϕ) 0.95in the region of spray

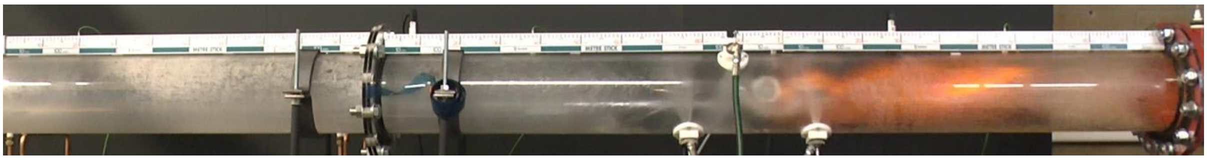

iv. Final stages of combustion occurrence

Figure 5.100 : Flame propagating upstream and downstream of four X/F Type C SRA's with water temperature of 50°C in a methane-air mixture (ϕ) 0.95

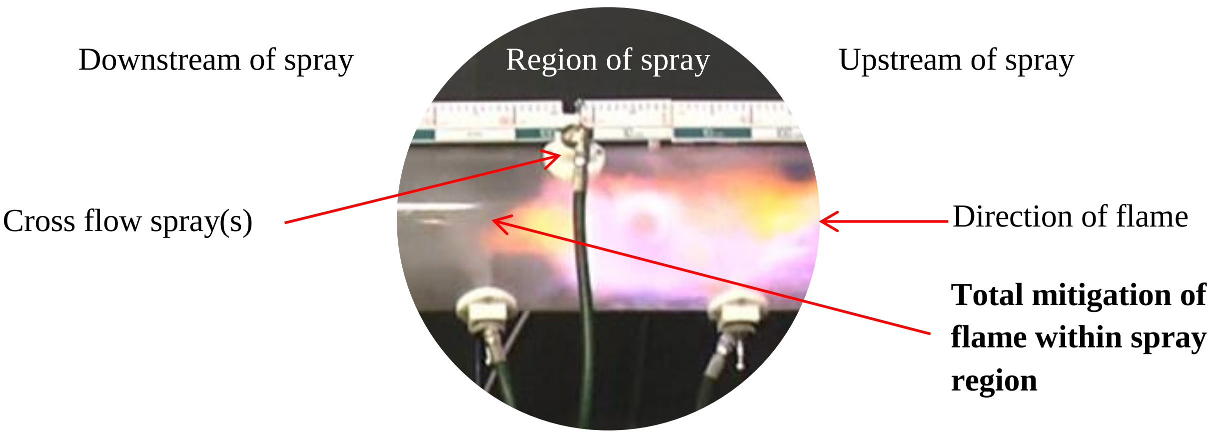

Figure 5.101: Enlarged view of region of spray highlighted in Figure 5.100(iii)

Water supply pressure 13MPa and temperature 50°C (ii)

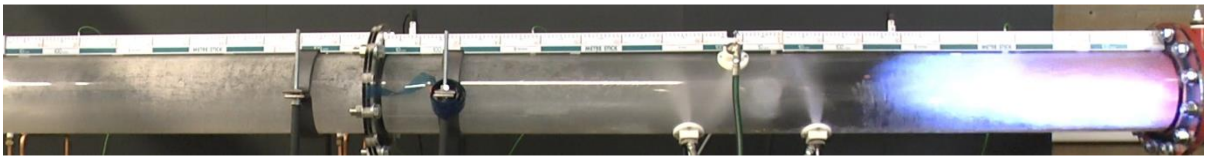

i. Flame propagating in methane-air mixture of E.R. (ϕ) 0.95upstream of SRA

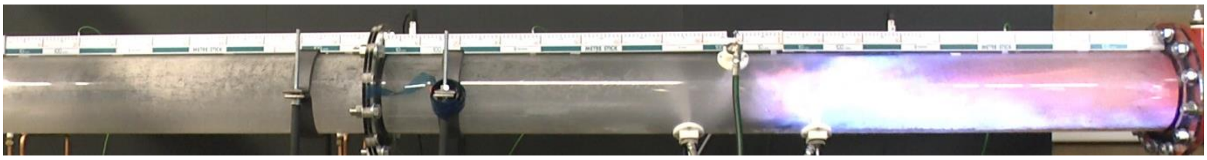

ii. Flame propagating in methane-air mixture of E.R. (ϕ) 0.95 upstream of SRA

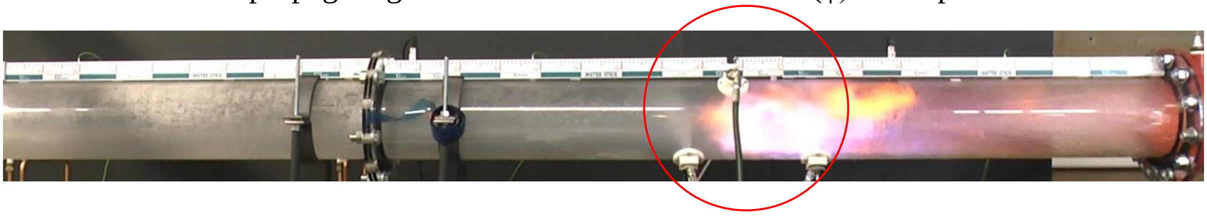

iii. **Mitigation** in methane-air mixture of E.R. (ϕ) 0.95in the region of spray

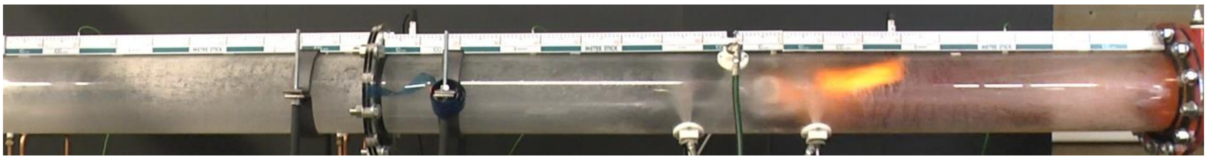

iv. Small trace of luminous flame which did not propagate any further

Figure 5.102 : Flame propagating upstream and downstream of four X/F Type C SRA's with water temperature of 50°C in a methane-air mixture (ϕ) 0.95

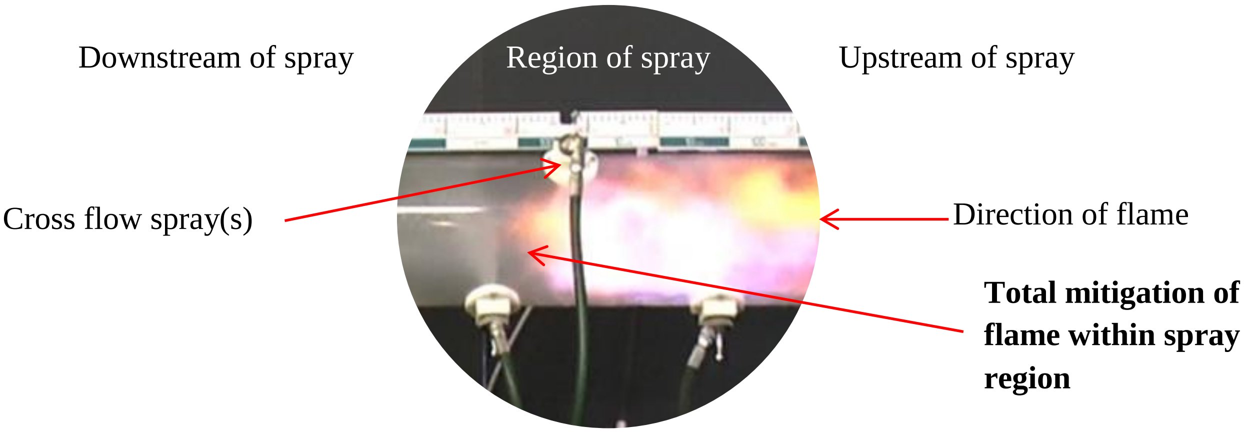

Figure 5.103 : Close up view of region of spray highlighted in Figure 5.102(iii)

5.5.7.5 General event outcome

Table 5.32 provides a summary of the 'general event outcome' for this trial using the five potential 'outcome' categories. The results of all hot trials were previously given in Table 5.14.

Trial configuration	General event outcome	Code
4 X/F Type C : 50°C (i)	Full Mitigation resulting in Flame Extinguishment	FMFE
4 X/F Type C : 50°C (ii)	Full Mitigation resulting in Flame Extinguishment	FMFE

Table 5.32 : General event outcome (trial series 5.5.7)

In these elevated water temperature trials it is important to note that the flame was mitigated in spray #3, whereas in the 20°C equivalent trials mitigation normally occurred at spray #4.

When considering a realistic full scale triggered explosion mitigation system; environmental, economic and practical challenges must be considered, these include:-

i. The cost of heating and maintaining the water at the desired temperature
ii. Bacterial implications such as Legionella, which has a high risk factor in water storage systems at temperatures ranging from 25 – 50°C.
iii. The capital expenditure benefits gained by the reduction in atomisers required, versus the capital costs of the water heating and storage equipment
iv. The increased risk of scale formation in pipework, exit orifices and spill diameters (as scale deposition tends to increase with temperature rise).

One of the significant differences between the extinguishment of a fire and explosion mitigation is, that during a fire involving burning organic material such as wood, the principle objective it to lower the temperature of the organic material to prevent further endothermic pyrolysis occurring (see Chapters 2 and 3). Consequently, the colder the water spray temperature, the more effective the system.

Whereas, based on the results from this and previous other studies [61], cooler water temperatures are less effective in explosion mitigation due to the short droplet residence times and heat transfer with the flame front, as discussed previously in Chapter 2 and 3.

Chapter 7 offers some suggestions and recommendations for further research in full scale and realistic environments utilising water storage at ambient temperature.

5.5.8 Four (X/F) Type C SRA's in a methane-air E.R. (ϕ) 1.65

5.5.8.1 Trial set up

For this series of experimental trials, four alternative 'methane rich' methane-air mixtures of E.R. (ϕ) 1.18, 1.30, 1.43, 1.65 (11%, 12%, 13%, 14% methane in air) were used to evaluate the operation of the four cross flow (X/F) Type C SRA arrangement, previously used in Section 5.5.5.1 for methane-air mixtures of E.R. (ϕ) 0.61, 0.72, 0.95, 1.06 (6%, 7%, 9%, 10% methane in air).

The relationship between equivalence ratio (ϕ) and comparative laminar flame thickness was previously discussed in Chapter 2. The typical flame thickness for the methane-air mixtures used in these trials are summarised in Figure 5.104 and Table 5.33.

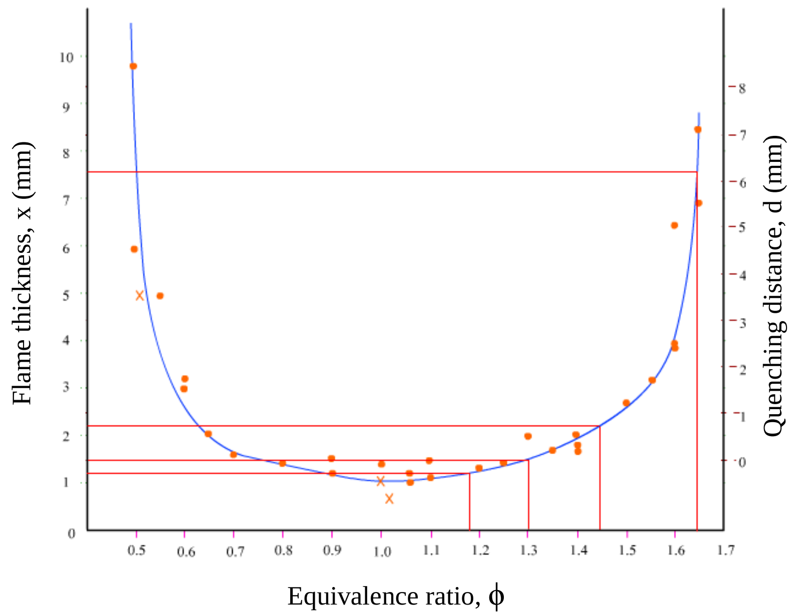

Figure 5.104 : Typical equivalence ratio-flame thickness for methane-air mixtures of E.R. (ϕ) 1.18, 1.30, 1.43, 1.65 [32]

One of the challenges encountered when igniting gas-air mixtures above stoichiometric (or E.R. (ϕ) >1), particularly in mixtures tending towards the upper explosive limit (UEL), is the requirement for a higher level ignition energy. This phenomenon was previously discussed in Chapter 2. In order to overcome the increased ignition difficulties several options were considered. To ensure reliability of ignition *two spark plugs* were used simultaneously via a high powered ignition transformer, normally associated with a heavy fuel oil burner system. The ignition transformer output was approximately 20,000v and produced a repetitive spark which was activated by the same safety interlock system used for all other trials in this study.

5.5.8.2 Flame speed

All four of the methane-air mixtures tested in this series were completely mitigated by the spray. Flame speed reduction percentages are illustrated in Figure 5.105. The additional results and discussions relating to this trials series can be found in Appendix 9 (Volume II).

The flame speeds produced in this series were predictably slower than those found in the previous trials. The combination of these slower flame speeds, together with the increased flame thickness resulting from higher equivalence ratios, provided greater residence time for the droplets to extract heat from the flame. This is also evident in the photographs shown in 5.5.8.4 with respect to the position in the spray region at which the flame was extinguished. Average flame speeds measured upstream of the SRA position can be found in Table 5.33.

Equivalence ratio (ϕ)	Approximate flame thickness (mm) [32]	Average upstream flame speed (m/s)
1.18	1.2	24.50
1.30	1.5	22.25
1.43	2.2	20.75
1.65	7.5	19.75

Table 5.33 : Approximate flame thickness and flame speeds

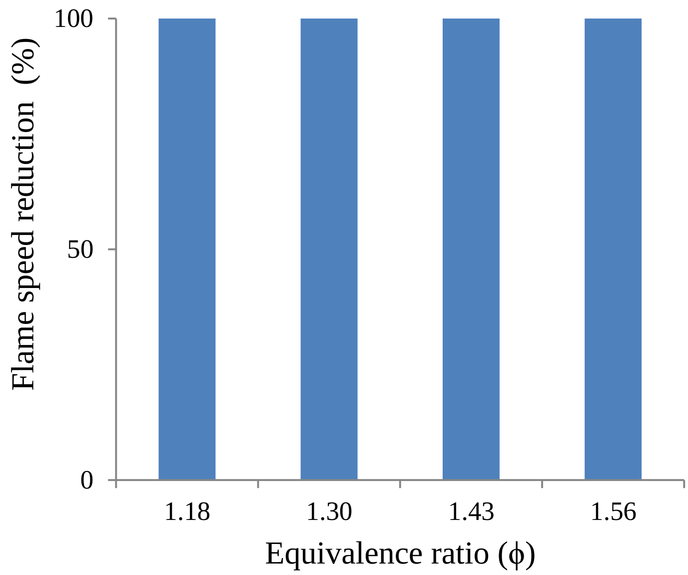

Figure 5.105 : Typical flame speed reductions (%) for four Type C SRA's at 13MPa and E.R.(ϕ)1.18, 1.30, 1.43, 1.65

5.5.8.3 Time-temperature response

Methane-air mixture of E.R. (ϕ) 1.65

Figure 5.106 shows the typical time-temperature profiles resulting from the methane-air mixture E.R. (ϕ) 1.65. The profiles for TC4 and TC5 exhibit typical trends relating to a successful mitigation event, with little or no temperature rise occurring. The rise in TC3 is ascribed to the rapid heating and vaporisation of droplets in the sprays.

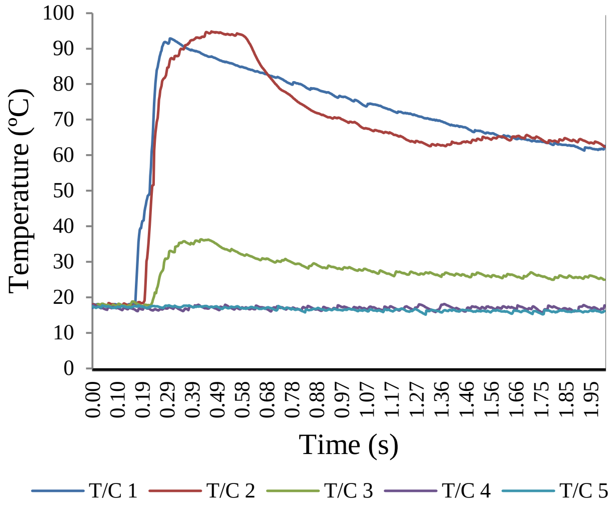

Figure 5.106 : Representative time-temperature profile for four SRA Type C in X/F arrangement with methane-air mixture of E.R. (ϕ) 1.65

5.5.8.4 Qualitative analysis

Methane-air mixture of E.R. (ϕ) 1.65

Figure 5.107(i) reveals the flame upstream of the first spray prior to any interaction.

In Figure 5.107(ii) displays dark regions with no flame progression beyond spray #3 which is magnified and shown in Figure 5.108.

Figure 5.107(iii) was captured 20ms after Figure 5.107(ii) and confirms that the flame did not re-establish or continue to propagate.

Figure 5.107(iv) was captured 40ms after Figure 5.107(ii) and confirms the retraction of the trailing intermediate reactants

Methane-air mixture of E.R. (ϕ) 1.65

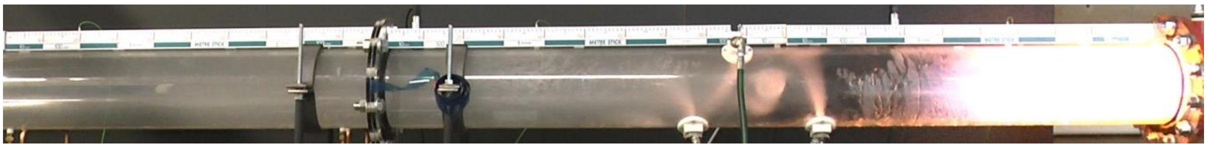

i. Flame propagating in methane-air mixture of E.R. (ϕ) 1.65 upstream of SRA

ii. **Mitigation** of methane-air mixture of E.R. (ϕ) 1.65 upstream of SRA

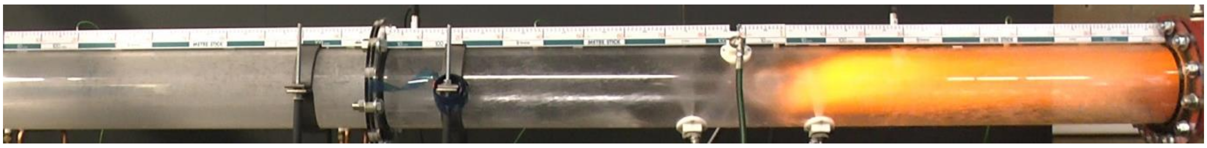

iii. 20ms after mitigation of methane-air mixture of E.R. (ϕ) 1.65

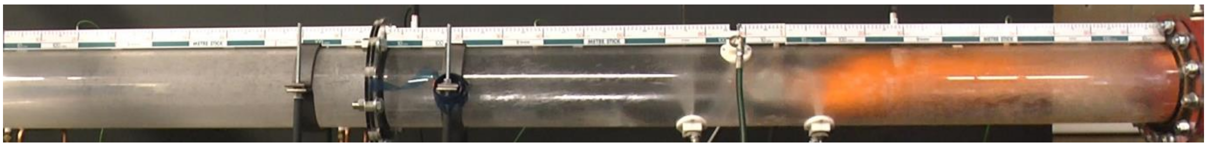

iv. 40ms after mitigation of methane-air mixture of E.R. (ϕ) 1.65

Figure 5.107: Flame propagating upstream and mitigation using four Type C cross flow (X/F) SRA's in a methane-air mixture (ϕ) 1.65

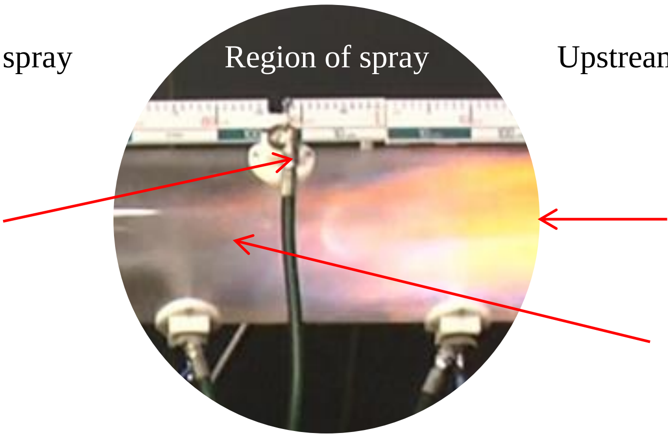

Figure 5.108: Enlarged view of region of spray highlighted in Figure 5.107(ii)

5.5.8.5 General event outcome

Table 5.34 provides a summary of the 'general event outcome' for this trial using the five potential 'outcome' categories. The results of all hot trials were previously given in Table 5.14.

Trial configuration	General event outcome	Code
4 X/F Type C : (ϕ) 1.65	Full Mitigation resulting in Flame Extinguishment	FMFE

Table 5.34 : General event outcome (trial series 5.5.8)

The results gained from this trial series were somewhat predictable, based on the theory of combustion, quenching and mitigation that were formally discussed extensively in Chapter 2. Gas-air mixtures tending towards their *UEL exhibit less exothermicity* than those closer to their stoichiometric mixtures.

The same can also be said for gas, liquid or solid fuels with greater carbon to hydrogen ratios than methane, whereby the cessation of carbon chain progression, through the quenching intermediate reactants and ending free radical production, results in early termination of combustion and consequential extinguishment.

Although the mitigation suitability of the Spill Return Atomiser (SRA) has only been confirmed with respect to propagating methane-air and propane-air flames (see subsequent Section) in this current study, there is good reason to suggest the potential for use in *fixed and portable fire mitigation equipment.*

Suggestions for further research activities in *'jet fire' suppression and mitigation* are presented and discussed in Chapter 7.

5.5.9 Four (X/F) Type C SRA's in a propane-air

5.5.9.1 Trial set up

A large number of explosive events have involved heavier than air flammable vapours, many of which are petroleum based derivatives. With the exception of this current series which utilises commercial propane-air mixtures, all of the experimental trials and results offered in this current study were conducted using high purity methane-air, as previously discussed in Chapter 4.

For convenience of availability, commercial propane, rather that high purity laboratory propane was used in this series of tests. Three different commercial propane-air mixtures of E.R. (ϕ) 0.49, 0.74, 1.00 (2%, 3%, 4% commercial propane in air) were used to evaluate the operation of the four cross flow (X/F) Type C SRA arrangement.

Although commercial propane liberates approximately 2.5 times the amount of energy by volume than methane during combustion, the lower limit of flammability is significantly less than methane. Additionally, the Theoretical Air Requirement (TAR) for methane is approximately 9.6:1, whereas the TAR for commercial propane is about 24:1. With these properties in mind, the commercial propane-air mixture volumes used in this series were considered to contain similar energy content to those used in earlier methane-air trials.

Other than the fuel supply, the equipment used in this series was set up as previously shown in Section 5.5.5.1 and Figures 5.84 and 5.85.

5.5.9.2 Flame speed

The average upstream flame speeds recorded in these commercial propane-air trials were very similar to the methane-air tests. Many saturated hydrocarbons containing single covalent bonds exhibit very similar burning velocities.

Alkenes such as ethylene have a higher flame temperature and burning velocity as a result of their greater exothermicity, due to the presence of a double bond in the molecule. Alkynes such as acetylene contain a triple bond with even greater exothermicity and resultant higher flame temperatures and burning rates.

The average flame speeds achieved upstream of the SRA position, together with approximate flame thickness can be found in Table 5.35 for each of the mixtures tested in this series.

Equivalence ratio (ϕ)	Approximate flame thickness (mm)	Average upstream flame speed (m/s)
0.49	1.8	7.5
0.74	1.3	14.5
1.00	1.00	22.25

Table 5.35 : Approximate flame thickness and flame speeds

In this approximately stoichiometric (E.R. (ϕ) 1) commercial propane-air mixture, complete global mitigation was achieved by the spray configuration. Flame speed reduction percentages are illustrated in Figure 5.109. Additional information regarding propane-air mixtures of E.R. (ϕ) 0.49, 0.74 can be found in Appendix 9, in the accompanying Appendices CD (Volume III)

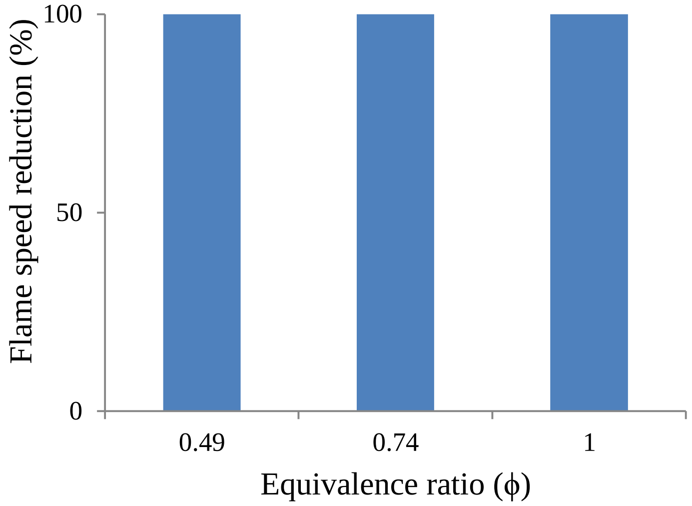

Figure 5.109: Typical flame speed reductions for four Type C SRA's at 13MPa and propane-air mixture E.R. ϕ 0.49, 0.74, 1.00

5.5.9.3 Time-temperature response

Figure 5.105 shows the distinctive time-temperature profiles resulting from the propane-air mixture E.R. (ϕ) 1.00. The profiles for TC3, TC4 and TC5 are in agreement with those presented for other mitigation events observed in this study, which are all approximately parallel to each other, indicating that the flame did not continue to propagate. Consequently the very small rise in TC3 is again attributed to the rapid vaporisation of droplets.

This is a characteristic of the very early mitigation between spray #1 and #2 as revealed in Figure 5.106 and where less water vapour would have been produced.

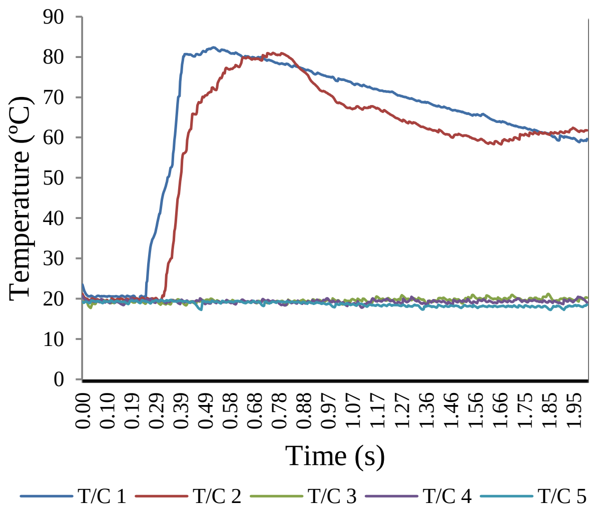

Figure 5.110 : Distinctive time-temperature profile for four SRA Type C in X/F arrangement with propane-air mixture of E.R. (ϕ) 1.00

5.5.9.4 Qualitative analysis

In Figure 5.111(i) the flame is shown upstream of the first spray prior to any interaction.

Figure 5.111(ii) displays the suppression of the flame and interaction with spray #1

In Figure 5.111(iii) the flame length began to shorten during its transit through spray #1 and #2. An expanded view of this moment is shown in Figure 5.112.

Figure 5.111(iv) captures the final milliseconds of the flames existence in the lower part of the propagation tube. This is due to the density of propane being greater than that of air.

Propane-air mixture of E.R. ϕ 1.00

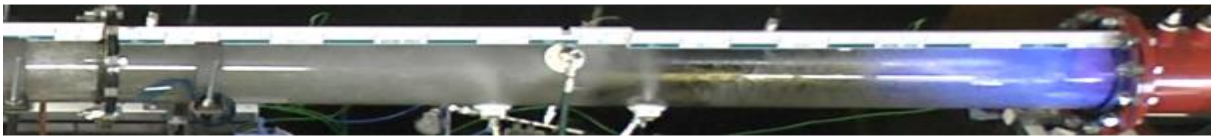

i. Flame propagating in propane-air mixture of E.R. (ϕ) 1.00 upstream of SRA

ii. Flame approaching sprays in propane-air mixture of E.R. (ϕ) 1.00 upstream of SRA

iii. Shortened flame due to interaction with spray in propane-air mixture of E.R. (ϕ) 1.00

iv. Flame almost *completely extinguished in* propane-air mixture of E.R. (ϕ) 1.00

Figure 5.111: Flame propagating upstream and subsequent mitigation using four Type C cross flow SRA's in a propane-air mixture (ϕ) 1.00

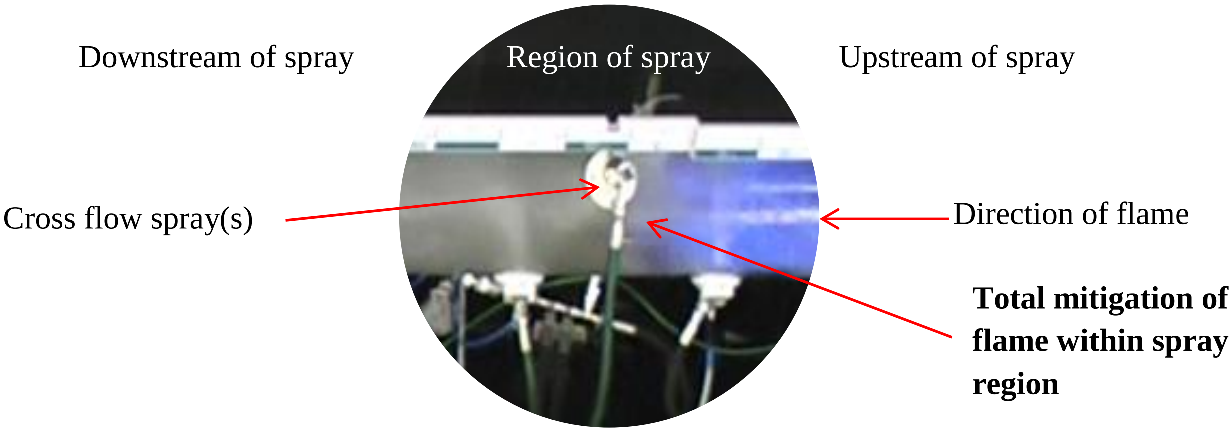

Figure 5.112 : Expanded view of region of spray highlighted in Figure 5.111(iii)

5.5.9.5 General event outcome

Table 5.36 provides a summary of the ‘general event outcome’ for this trial using the five potential ‘event outcome’ categories. The results of all hot trials were previously given in Table 5.14.

Trial configuration	General event outcome	Code
4 X/F Type C : (ϕ) 1.00	Full Mitigation resulting in Flame Extinguishment	FMFE

Table 5.36 : General event outcome (trial series 5.5.9)

Although the majority of this current research program has been conducted using laboratory grade methane-air mixtures, the inclusion of this small number of commercial propane-air (heavy than air vapour) trials has highlighted the opportunity to expand the research to include other alkanes and also alkenes and alkynes.

Considerations and suggestions for further research are proposed in Chapter 7.

5.5.10 Four (X/F) Type C SRA's with three exhaust outlets blocked

5.5.10.1 Trial set up

With the exception of this final series of tests, all of the previous methane-air and propane-air trials were conducted in the **partly confined / vented** conditions provided by the design characteristics of the FPMR. At the point of ignition, the flame exit was fully opened by the magnetic hinge panel and the exhausts were all vented with the rupturing of the membranes covering each of the six outlets.

The purpose of the six 80mm diameter exhaust vents was to provide a cross sectional area (CSA) of greater than or equal to the diameter of the main driver section, as extensively described in Chapter 4. The temporary blockage of one or more of the six exhaust outlets will affect the explosion conditions, with the principle outcome being an increase in flame speed due to the partial retardation of escaping, hot expanding products of combustion. As the exhaust outlets were originally designed and manufactured with BSP threads, they were readily sealable with a standard 'BSP plug' as illustrated in Figure 5.113

Three tests were carried out using methane-air mixtures of E.R. (ϕ) 0.95 using the following exhaust blockages:-

i. One exhaust outlet blocked (providing relief openings of 96% of main tube CSA)
ii. Two exhaust outlets blocked (providing relief openings of 77% of main tube CSA)
iii. Three exhaust outlets blocked (providing relief openings of 58% of main tube CSA)

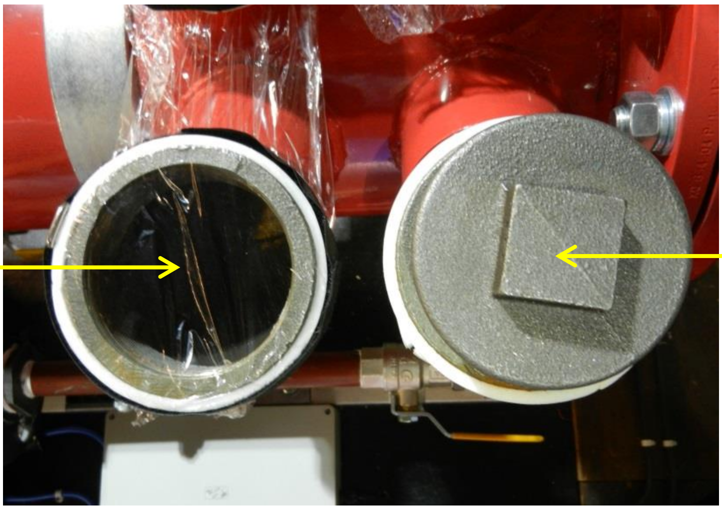

Figure 5.113 : Example of exhaust outlet preparation prior to testing

5.5.10.2 Flame speed

The flame speeds produced in this series were predictably faster than those found in the previous trials, as indicated in Table 5.37. The combination of these greater flame speeds in conjunction with the narrow band of comparative flame thickness of 1.05mm associated with the methane-air mixture E.R. (ϕ) 0.95 would have had a negative effect on the residence time for the droplets to extract heat from the flame.

Although the resulting *flame speeds were faster* than the previous trials, the propagating flame was *completely extinguished and mitigated* by the spray configuration. Flame speed reduction percentages (%) are given in Figure 5.114. Additional results and information relating to the one and two blocked exhaust trials can be found in Appendix 9, found on the accompanying Appendices CD (Volume III).

Number of blocked exhaust ports	Equivalence ratio (ϕ)	Approximate flame thickness (mm)	Average upstream flame speed (m/s)
1	0.95	1.05	25
2	0.95	1.05	29.5
3	0.95	1.05	34.5

Table 5.37 : Approximate flame thickness and flame speeds

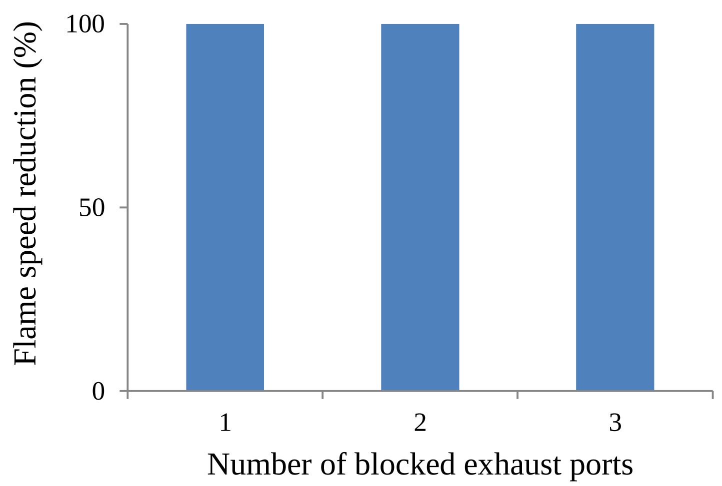

Figure 5.114 : Typical flame speed reductions for four Type C SRA's at 13MPa and methane-air flame E.R. ϕ 0.95 with various blocked exhaust ports

5.5.10.3 Time-temperature response

Three exhaust outlets blocked.

In this trial three of the exhaust outlets were blocked, with the other three openings sealed and prepared with low density polyethylene sheet ‘cling film’ bursting membranes. The blockage of the outlets resulted in exhaust relief openings of about 58% of the main tube cross sectional area (CSA). (See also Chapter 4)

Figure 5.115 shows the characteristic time-temperature profile for four X/F Type C SRA’s with three exhaust outlets blocked in a methane-air mixture of E.R. (ϕ) 0.95. In this instance the flame propagated into the sprays and was severely retarded.

Although a small region of flame passed directly through the sprays, the severely suppressed flame failed to propagate in the remaining downstream unburned mixture. This can be seen as small a rise in the temperature of the unburned mixture, which is manifested in the temperature profiles for TC3, TC4 and TC5.

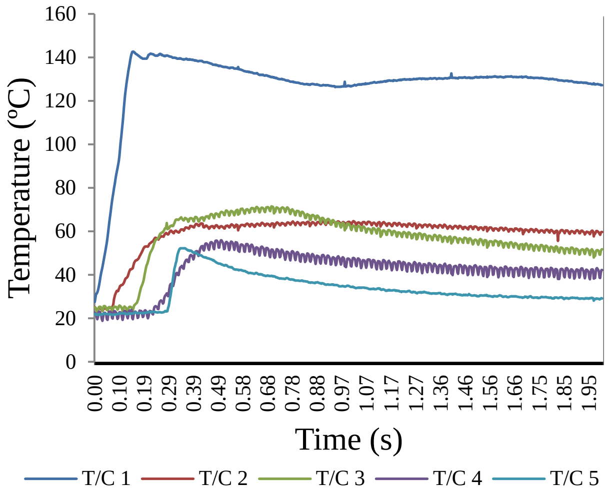

Figure 5.115 : Characteristic time-temperature profile for four X/F Type C SRA’s with three exhaust outlets blocked methane-air mixture of E.R. (ϕ) 0.95

5.5.10.4 Qualitative analysis

Three exhaust outlets blocked.

In Figure 5.116(i) the flame is shown upstream of the first spray prior to any interaction.

In Figure 5.116(ii) the flame is approaching the final spray and exhibits dark regions and a shortening of the flame length.

Figure 5.116(iii) reveals a small luminous area of flame which has propagated beyond the sprays

Figure 5.116(iv) shows the resulting flame 20ms after the previous frame, where the flame is retreating. Flame was not present in any further video frames. Figure 5.117 shows an enlarged section of the spray region.

Three exhaust outlets blocked

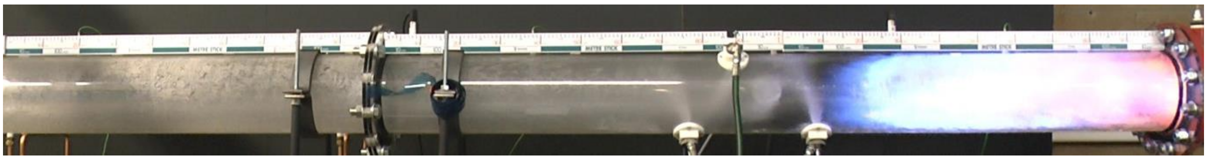

i. Flame propagating in methane-air mixture of E.R. (ϕ) 0.95 upstream of SRA

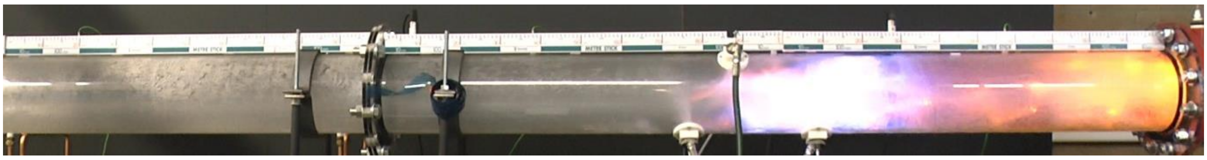

ii. Flame propagating in methane-air mixture of E.R. (ϕ) 0.95 in the region of spray

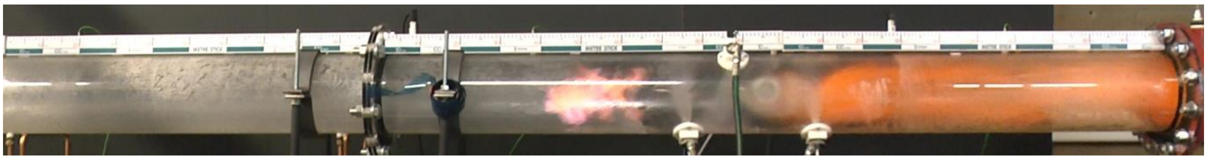

iii. A degree of combustion still occiring downstream of the sprays E.R. (ϕ) 0.95

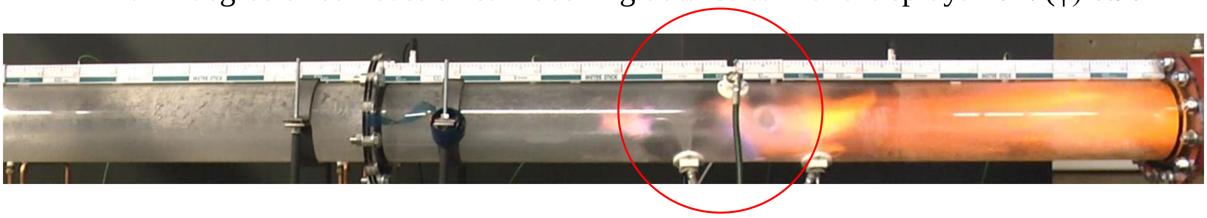

iv. Insufficient energy for propagation through the remaining combustible mixture of E.R. (ϕ) 0.95 downstream of SRA

Figure 5.116 : Flame propagating upstream and subsequent mitigation using four X/F Type C SRA's with three exhaust outlet blocked methane-air mixture of E.R. (ϕ) 0.95

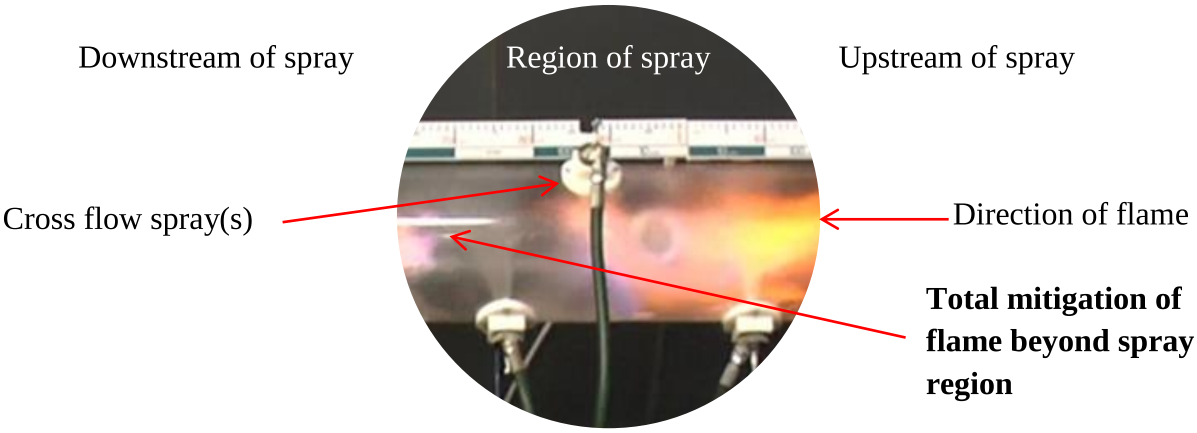

Figure 5.117 : Expanded view of region of spray highlighted in Figure 5.116(iv)

5.5.10.5 General event outcome

Table 5.38 provides a summary of the 'general event outcome' for this trial using the five potential 'outcome' categories. The results of all hot trials were previously given in Table 5.14.

Trial configuration Four (X/F) SRA's	General event outcome	Code
3 blocked exhausts	Full Mitigation resulting in Flame Extinguishment	FMFE

Table 5.38 : General event outcome (trial series 5.5.10)

This series of trials have been included to provide an initial assessment of the effectiveness of the four (X/F) Type C SRA's configuration in *partly confined conditions* (see also Chapter 2). The four (X/F) Type C SRA's configuration has proven to be highly effective in the presence of low speed methane-air and propane-air flames, throughout the flammable range, with flame speeds of ≤30m/s.

Although the flame speed produced in this trial was 34.5m/s and total mitigation was successfully achieved, further trials in utilising greater confinement were deemed to be outside of the scope and objectives of this current work. The consideration of SRA's in higher flame speed (>30m/s) situations is another area recommended for further research.

Chapter 7 offers several proposals for additional research and development.

5.6 Chapter summary

The numerous and exclusive experimental trials conducted during this present study into the *mitigation of slow moving propagating flames of* $\leq 30m/s$ using fine water sprays containing droplets of $D_{32} \leq 30\mu m$, with mean velocities, D_v, *of* $\leq 21.4m/$s and liquid volume flux, Q_f, *0.011 - 0.047*$cm^3/s/cm^2$ have produced a unique series results, requirements and findings.

From the accomplishments of the cold trials, to the completion of over 250 hot trials, a wealth of quantitative and qualitative information has been collected.

Due to the total number of hot trials completed in this study, it was not practicable to appraise all of them, however, 101 experimental trials were nominated to be analysed and evaluated. The results and discussions of all of the 101 hot trials are discussed and have been included in Appendix 9, which is provided on the accompanying CD of Appendices (called here : Volume III). The hot trials results were all previously summarised at a glance in Table 5.14.

Various experimental trials using the ***4 x Type C SRA's in Cross Flow (X/F)*** configuration were successfully conducted, whereby homogeneous methane-air mixtures throughout the whole flammable range E.R. $0.5 \leq (\phi) 1.0 \leq 1.69$ (5 - 15%), with flame speeds (S_f) ranging from 5 - 30m/s, where completely extinguished and thus mitigated.

In addition to all of the methane-air hot trials carried out in this study, a small sample of commercial propane-air explosion mitigation trials were also conducted, whereby the 4 x Type C SRA's in Cross Flow (X/F) arrangement effectively fully mitigated a range of combustible mixtures. The results of this preliminary investigation may benefit future laboratory and full scale research.

Additionally, there has also been sufficient knowledge gained from this work to suggest several other future studies, including the production of a *full scale realistic* experimental test rig that may give way to a significant *new product development* for use in *petrochemical, oil and gas production and on storage sites*. Recommendations and concepts for further research are offered in Chapter 7

The next Chapter discusses the set up conditions, modelling practices, sensitivity studies and results relating a preliminary consideration attempt using a commercial Computation Fluid Dynamics (CFD) software package, as a future design tool for explosion mitigation apparatus.

CHAPTER 6

CONSIDERATION OF CFD (COMPUTATIONAL FLUID DYNAMICS)

6.1 Introduction

Computational fluid dynamics (CFD) is a numerical technique that allows for the analysis of fluid flows using a computer based program. CFD can be used to understand fluid flow in a number of applications including aerodynamic flows over vehicles, chemical mixing, metrological predictions and numerous other areas of fluid flow. CFD has also been used previously in the areas of sprays and combustion such as, propulsion, fire suppression [91], [92] and the spread of fires in buildings.

A preliminary evaluation attempt has been undertaken to model single and multiple cross flow (X/F) SRA spray configurations, using a sample of the methane-air mixtures and flame propagation events. Throughout the experimental stages of this research, there were two distinctive studies conducted, known as the cold trials and the hot trials. The cold trials included the development of a novel spray system and subsequent characterisation of the spray properties and the hot trials involved assessment of the suppression and mitigation qualities of a range of sprays systems developed during the cold trials. The collaborative experimental data and results collected from the cold and hot trials have been used collectively for this CFD consideration.

In this Chapter attempts have been made to model spray configurations which include single and multiple cross flow (X/F) Type B SRA's in methane-air mixtures, E.R. ϕ 0.72 and 0.95 (7% and 9% FAR). Also, as a result of the experimental trials, a recommendation has been made to further develop the potential of the SRA in realistic full scale trials. The further advancement of this initial CFD evaluation should be included in future 'scale up' predictions in the development of practical applications of the findings (See also Chapter 7, Section 7.2).

6.2 Set up and conditions

6.2.1 CFD modelling practices adopted

Commercial CFD packages such as *Ansys CFX*, as used in this study, utilise four user interfaces which involve building the geometry, meshing the geometry, setting the physics, solving the setup and post processing the results.

Within the *pre-processor* the geometry that the fluid will come in contact with is defined, this becomes known as the *computational domain*. A mesh of the domain is then created; the subsequent accuracy of solution is dependent upon the fineness of this mesh. There is a trade off with mesh density in terms of computational time and expense. Boundary conditions are then selected on the domain to define the characteristics of the flow, whereby the physical properties of fluid are also defined before the problem can be solved.

The fluid problem is then solved by a separate package known as *the solver*. The solver uses the finite volume technique in which the computational fluid domain is divided into a finite number of volumes. For greater volumes, the discretised governing equations that describe the fluid flow are solved for using an iterative method.

After the model definition has been solved, the solution can be analysed in the final interface, the *post-processor*. The post-processor allows for the visualisation of the results, producing for example vector and contour plots.

To have confidence in the solutions provided by CFD, good modelling practices should be adopted. Such practices have been taken from the CFX user manual and Rayer [93]. It is essential that all CFD analyses are treated with caution and should be validated before placing great reliance in the results. Validation can be undertaken on a simulation by considering the following:

- Sensible pressure drops.
- Representative velocities.
- Characteristic mass flows and mass conservation.
- Conventional temperatures and energy conservation.
- That the y+ values are sufficient for resolution of the boundary layer.

During any CFD process there are four critical phases:-

i. Setting out the objectives of the study
ii. Pre-processing phase
iii. Processing and simulation phase
iv. Post processing phase

These phases are also summarised and illustrated as a process flow in Figure 1.

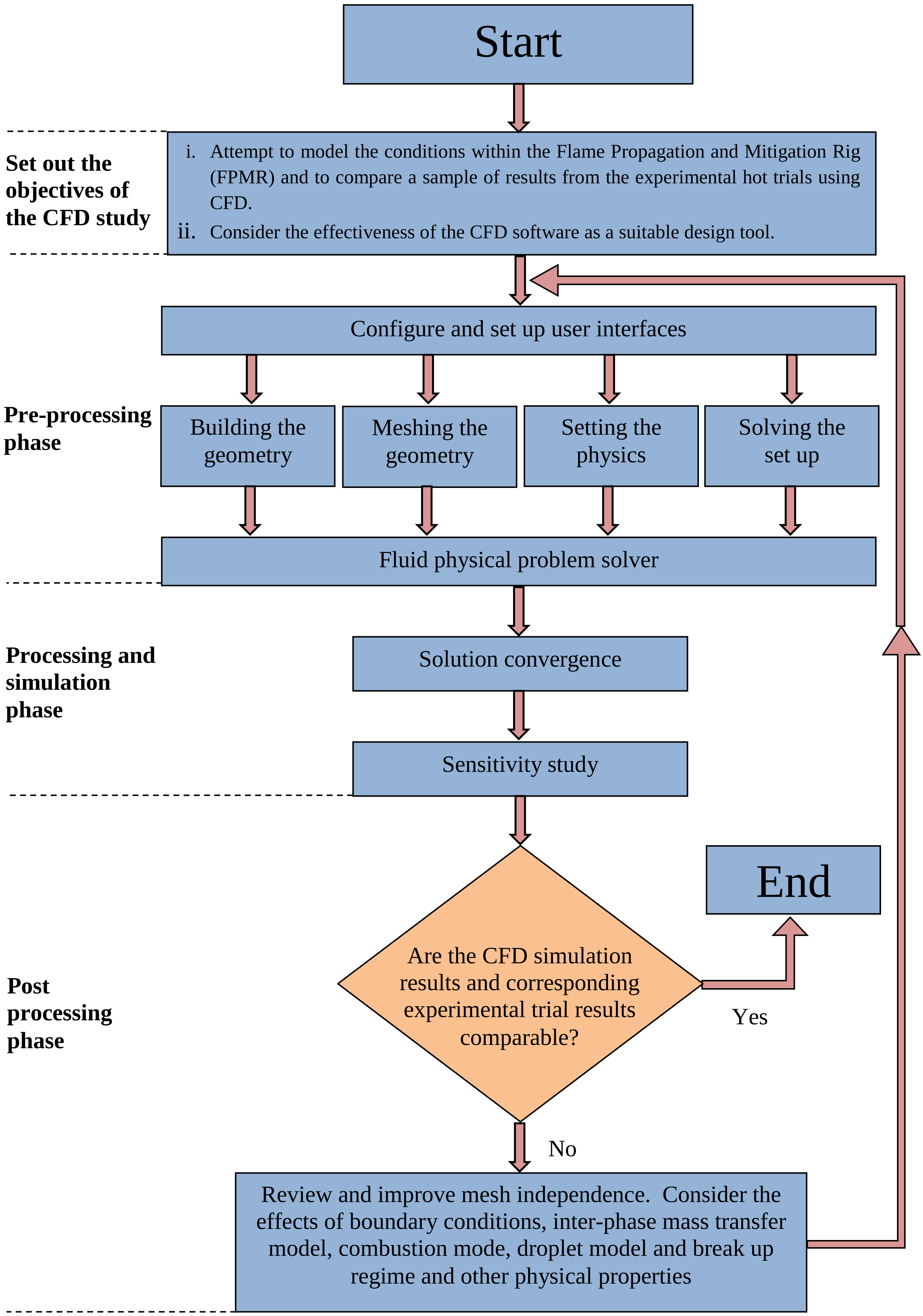

Figure 6.1 : Critical CFD implementation phases and process flow

6.2.2 Model definition

The experimental setup was modelled in 3D (see also Appendix 10) based on the precise dimensions of the Flame Propagation and Mitigation Rig (FPMR), as shown in Figure 6.2. The model consisted of a mass flow inlet for methane and air mixture, with the values inputted to give the required equivalence ratios of E.R. (ϕ) 0.72 and 0.95 (referred to in other studies as Fuel-Air Ratio (FAR) of 7% and 9%). The sprays were modeled as a number of point sources that were injected into the domain from the side walls of the pipe, consistent with the trial setup, previously shown in Section 4.5.5.4. An opening was also specified as the outlet to the pipe.

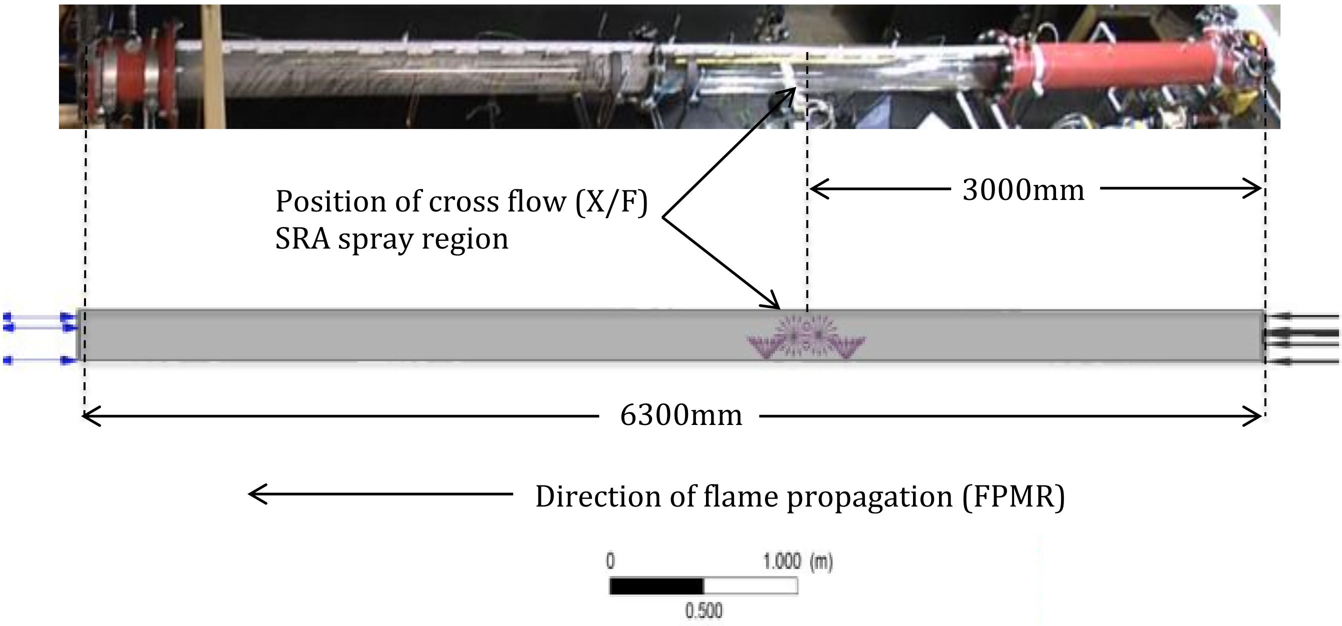

Figure 6.2: FPMR and typical model configuration

Although in excess of 250 experimental hot trials were conducted to fulfil the principle aims and objectives of the research program, this CFD consideration will only relate to a sample number of trials, consisting of the following:-

i. Methane-air mixtures of E.R. (ϕ) 0.72 and 0.95 (actual conditions from hot trials)
ii. Type SRA in cross flow (X/F) configuration (actual conditions from cold / hot trials)
iii. Spray region consisting of 1, 2, 3 and 4 SRA's (actual conditions from cold / hot trials)
iv. Mean droplet diameter of D32, 26μm (actual conditions from cold trials)
v. Mean droplet diameter of D32, 80μm (simulated conditions in the CFD simulation)

6.2.3 Setting of conditions

6.2.3.1 Inlet /outlet boundary

The inlet and outlet boundary conditions that can be specified in CFX are shown in Table 6.1. The most stable inlet and outlet boundary conditions were applied to the models to provide a converged solution that was a velocity or a mass flow for the inlet and a P_{static} for the outlet.

Inlet	Outlet	Stability
Mass flow / Velocity	P_{static}	Most stable, inlet total pressure result of prediction
P_{total}	Velocity / Mass flow	Stable, static pressure at outlet and inlet velocity part of the solution.
P_{total}	P_{static}	Sensitive to initial guess, mass flow part of solution

Table 6.1: Recommended boundary specifications

6.2.3.2 Wall boundary

The wall boundary used in the models was a non-slip, with the fluid at the wall boundary having zero velocity. The boundary layers in the models were resolved using a scalable wall function and is reviewed later in the Chapter. The wall was treated as adiabatic thus allowing no heat transfer across the wall boundary, $q_w = 0$.

To aid in simplifying the simulation, the droplets impacting upon the wall boundary were given a restitution wall coefficient of zero, so there would be no elastic collision with the surface of the wall. This is not necessarily what would occur experimentally, as there would be a number of complex mechanisms taking place, such as droplet bouncing off the wall resulting in further secondary atomisation and droplets adhering to the surface of the wall, coalescing and producing films/ streams of water on the internal surface of the pipe.

6.2.3.3 Droplet model

The spray was modelled as a point source and injected into the domain as a cone shaped pattern providing a mass flow, cone angle and a droplet distribution based upon the experimental data.

The droplet was given a Rosin-Rammler distribution. This is a continuous probability distribution which describes the size distribution of particles and was first formulated for

(6.1)

powders. It is frequently used to illustrate the droplet size distribution by mean diameter, and is expressed as,

$$1 - Q = \exp - (D / X)^q$$

where, Q is the fraction of the total volume contained in droplet diameter less than D and X (representative diameter) and q (measure of the drop size spread) are constant for the spray. The spray input conditions used in the simulation are shown in Table 6.2.

SRA Type	Cone Angle	Water Flow Rate	Droplet Size
B	42°	0.014 kg/s	Rosin Rammler 26µm, q=1.8

Table 6.2 : Characteristic SRA conditions used in the simulation

The injected particles were introduced normal to the pipe wall and corresponded to the same locations downstream as in the experimental setup. (See also Chapter 4)

The trajectories of the droplets were considered using the Eulerian-Lagrangian approach, which considers the gas phase as a continuum and the liquid droplet phase being tracked individually by the Lagrangian method. The equations of motion for the droplet is described by Newton's second law,

$$m_d \frac{dU_d}{dt} = F_D + F_B + F_R + F_{VM} + F_P + F_{BA} \tag{6.2}$$

Where the terms on the right hand side of the equation relate respectively as,

FD, Drag force on the droplet
FB, Buoyancy force due to gravity
FR, forces due to domain rotation, centripetal and coriolis forces
FVM, Force to accelerate the virtual mass of the fluid in the volume occupied by the particle (as in the motion of bubbles)
FP, pressure gradient force applied on a particle due to the pressure gradient in the fluid (significant when the fluid density is comparable to, or greater than the particle density).
FBA, Basset force which accounts for deviation in flow pattern around the droplet from steady state.

For the modelling of the droplet in this exercise, only drag and buoyancy forces on the droplet are to be included,

$$m_d \frac{dU_d}{dt} = \frac{1}{2} C_D \rho_F A_F |U_s| U_s + \frac{\pi}{6} d_p^3 (\rho_d - \rho_F) g \tag{6.3}$$

where,

U_s is the slip velocity
C_D is the drag coefficient
A_F is the particle cross section

The Schiller Naumann drag model [94] was used to calculate the drag coefficient C_D of the droplet, given by.

$$C_D = \frac{24}{\text{Re}}\left(1 + 0.15\,\text{Re}^{0.687}\right), \text{Re} > 1000 \tag{6.4}$$
$$0.44\,\text{Re} > 1000$$

The Reynolds number of the droplet is given by,

$$R_e = \frac{d_p |U_{slip}|}{\mu} \tag{6.5}$$

where dp is the droplet diameter and U_{slip} is the slip velocity given by,

$$|U_{slip}| = \left[(u_1 - u_2)^2 + (v_1 - v_2)^2 + (w_1 - w_2)^2\right]^{1/2} \tag{6.6}$$

To account for the turbulent dispersion of droplets in the flow field due to the fluctuating velocity component, with the instantaneous fluid velocity composed of a mean velocity $\bar{v}_{f'}$, and a fluctuating velocity $v_{f'}$. The dispersion model assumes that the particle is always within a single eddy. Each eddy has a characteristic fluctuating velocity $v_{f'}$ lifetime τ_e, and length scale le.

When a droplet enters the eddy, the fluctuating velocity for that eddy is added to the local mean fluid velocity to obtain the instantaneous fluid velocity. The turbulent fluid velocity is then assumed to prevail as long as the particle/eddy interaction time is less than the eddy lifetime and the displacement of the particle relative to the eddy is less than the eddy length.

Respectively, the turbulent velocity, eddy and length scale and lifetime are calculated from,

$$v_{f'} = \Gamma(2k/3)^{0.5} \tag{6.7}$$

$$l_e = \frac{C_\mu^{3/4} k^{3/2}}{\varepsilon} \tag{6.8}$$

$$\tau = \frac{l_e}{(2k/3)^{1/2}} \tag{6.9}$$

where k and ε are the local and turbulent kinetic energy and dissipation and C_μ is the turbulence constant. Also included in the equation is as a normally distributed random number Γ which is used to account for the randomness of turbulence in the flow. For anisotropic flow the fluctuating components of velocity, $u', v' w'$ may each have different variables.

The droplets were fully coupled to the continuous phase, which enables the continuous flow to affect the particles, and the particles to affect the continuous flow

6.2.3.4 Inter-phase mass transfer

Since the droplets would be introduced into a combusting flow, heat transfer has to be considered between the droplets and the hot gases. The convective heat transfer *Qc*, is calculated by,

$$Q_C = \pi d \lambda Nu(T_G - T) \tag{6.10}$$

Where, λ is the thermal conductivity of the fluid, T_G and T are the temperatures of the fluid and Nu is the Nusselt number given by,

$$Nu = 2 + 0.6\mathrm{Re}^{0.5}\left(\mu \frac{C_p}{\lambda}\right)^{1/3} \tag{6.11}$$

Where, *Cp* is the specific heat of the fluid. The mass transfer between the gas and the droplets is given by the relationship,

$$Q_M = \sum \frac{dm}{dt} L \tag{6.12}$$

Where, the sum is taken overall all components of the particle for which heat transfer is taking place. The latent heat of vaporisation L, is temperature dependent and is specified by the user in the materials form.

The radiative heat transfer Q_R for a particle with a droplet diameter of d_d and uniform temperature T_d and emissivity, ε_d is shown by,

$$Q_R = \frac{1}{4}\varepsilon_d \pi d_d (I - \sigma n T_p^4) \tag{6.13}$$

where, *I* is the irradiation flux on the particle surface at the particle location, *n* is the refractive index of the fluid and σ is the Stefan-Boltzmann constant.

Each component of mass transferred between the continuous and particle phase satisfies the equation,

$$\frac{dm}{dt} = bA(m_{v,s} - m_{v,g}) \tag{6.14}$$

$$\dot{m} = bA(Y_{v,s} - Y_{v,g}) \tag{6.15}$$

where,

mv,s, mass fraction of the water vapour at the droplet interface

mv,g, mass fraction of the gas at the droplet interface

b, mass transfer coefficient

A, area

With the mass fractions given as,

$$Y_{v,s} = \frac{M_w p_{sat}}{RT_s} \tag{6.16}$$

$$Y_{v,g} = \frac{M_g H p_{sat}}{RT_g} \tag{6.17}$$

where,

Mw, *Mg* Molecular weight of water and gas respectively

Psat, Saturation pressure

R, universal gas constant

Ts,Tg, temperature of surface, gas respectively

H, enthalpy

The mass transfer number is a function of the Sherwood number *Sh*.

$$Sh = \frac{bd_p}{D} \tag{6.18}$$

where,

b mass transfer number,

dp, droplet diameter

D, diffusivity

To calculate the Sherwood number the Ranz Marshall correlation was used. This correlation is based upon the forced convection heat transfer coefficient for a single sphere [95, 96] $(1<Re<10^5, 0.6<Pr<380)$

$$\boldsymbol{Nu} = \mathbf{2 + 0.6 Re^{0.5} Pr^{0.33}} \tag{6.19}$$

where,

Pr, Prandtl number

Re, Reynolds number

Nu, Nusselt number

The model assumes that mass transfer is driven by concentration differences and does not adequately account for the vapour pressure dependence on particle temperature, which is a factor in evaporating liquids. To account for this the liquid evaporation model, using the Antoine equation,

$$P_{vap} = P_{sat} \exp\left(A - \frac{B}{T + C} \right) \tag{6.20}$$

Where, *A*, *B* and *C* are coefficients supplied by the user

It accounts for the heat and mass transfer of droplets in a high temperature gas phase. The model uses two mass transfer correlations depending whether the droplet is above or below the boiling point. The droplet is considered to be boiling if the vapour pressure is greater than the gaseous pressure.

Above the boiling point the mass transfer is determined by the convective heat transfer.

$$\frac{dm}{dt} = -\frac{Q_c}{L} \tag{6.21}$$

Below the boiling point, the mass transfer is determined by,

$$\frac{dm}{dt} = \pi d D Sh \frac{W_c}{W_g} \log\left(\frac{1 - X}{1 - X_G} \right) \tag{6.22}$$

where, Wc and W_G are the molecular weights of the vapour and the mixture in the continuous phase and X and X_g are the molar fractions in the drop and in the gas phase.

To determine the heat exchange between the droplets and the gas, the temperature between the two phases, T_s is used,

$$q_{g\rightarrow s} = h_g A(T_s - T_g) \tag{6.23}$$

$$q_{s\rightarrow l} = h_l A(T_s - T_l) \tag{6.24}$$

where,

$q_{g\text{-}s}$, heat transfer from gas to the interface

$q_{s\text{-}l}$,, heat transfer from the interface to the liquid

h_g and h_l are the heat transfer coefficients respectively

A is the interface area

Ts, T_g and T_l, are the interface temperature, gas temperature and liquid temperature respectively.

The heat transfer coefficients are calculated from,

$$h_g = \frac{Nuk_g}{d_p} \tag{6.25}$$

$$h_l = \frac{3k_l}{(d_p/2)} \tag{6.26}$$

where N_u is the Nusselt number, k_g and k_l, heat transfer coefficients for gas and liquid respectively and dp the droplet diameter. From this the heat transfer from the gas to the surface of the droplet is given by,

$$q_{g-s} = \dot{m}\left[C_{p,g}(T_s - T_g) + L\right] \tag{6.27}$$

where, Cp,g is the specific heat capacity and L is the latent heat.

6.2.3.5 Droplet breakup

There are a number of droplet breakup models available in CFX that cover both primary and secondary atomisation. These are based upon the Weber number, We,

$$W_e = \frac{\rho_f V_{slip}^2 D}{\sigma} \tag{6.28}$$

and the Ohnesorge number Oh,

$$O_h = \frac{\mu}{\sqrt{\rho_d \sigma D_d}} \tag{6.28}$$

From experimental observation, a number of breakup regimes [97] have been identified based upon the Weber number, as shown in Table 6.3.

Droplet breakup type	Weber number
Vibrational breakup	We<12
Bag breakup	12<We<50
Bag and stamen breakup	50<We<100
Sheet stripping	100<We<350
Catastrophic breakup	350<We

Table 6.3 : Typical droplet break up regimes

For the majority of the simulation cases, no secondary breakup model was used as the droplets being introduced had a Weber number of less than 12, thus there will be limited aerodynamic shattering of the droplet. The Taylor Analogy Breakup (TAB) model [98] was used for the four SRA's case to investigate the sensitivity of the CFD analysis to droplet size.

The TAB model assumes that the breakup of the droplet can be treated as a spring, mass damper, with forced, damped and harmonic oscillation. A droplet of spherical radius *a*, is cased to oscillate either from an initial disturbance or by aerodynamic forces which continues after time zero. The perturbation of the radius is called *x*, and if it exceeds *a*, the droplet will break apart.

The model is given by:

$$\rho_l a^3 \frac{d^2x}{dt^2} = \frac{2}{3}\rho_g a^2 V_r^{\,2} - 8\sigma x - 5\mu_l a \frac{dx}{dt} \tag{6.30}$$

for the droplet, μ_l, is the viscosity, ρ_l is the density, σ is the surface tension and V_r is the relative velocity of the ambient gas and the droplet.

After breakup, the Sauter mean radius of the 'child' droplets is calculated from,

$$\frac{r_{P,Parent}}{r_{P,Child}} = \left[1 + 0.4K + \frac{\rho_P r_{P,Parent}^3}{\sigma}\frac{d^2x}{dt^2}\left(\frac{6K-5}{120}\right)\right] \tag{6.31}$$

The equation is based on the conservation of surface energy bound in the distortion and oscillation of the *parent* droplet, $r_{P,Parent}$ and the surface energy and kinetic of the *child* droplets, $r_{P,Child}$. The normal velocity of the child droplet after breakup is taken as the velocity normal to the equator of the parent droplet normal to the parent path.

The default TAB model constants used are shown in Table 6.4.

Name	Value
Critical amplitude coefficient, C_b	0.5
Damping coefficient, C_d	5.0
External force coefficient, C_f	1/3
Restoring force coefficient, C_k	8.0
New droplet velocity factor, C_v	1.0
Energy ratio factor, K	10/3

Table 6.4 : Typical TAB model constants

6.2.3.6 Combustion model

The model used in the simulations was the Eddy Dissipation Model (EDM) [99,100] that can be used for premixed and diffusion flame in turbulent reacting flows. The EDM is based on a one step reaction and fast chemistry assumption. In a turbulent flow, which would be experienced in the region of the SRA's, the mixing time is dominated by the eddy properties, thus giving the rate proportional to a mixing time defined by the turbulent kinetic energy, k and the dissipation, ε.

$$rate = \frac{\varepsilon}{k} \tag{6.32}$$

The main idea of the model is to replace the chemical time scale of an assumed one-step reaction by the turbulent time scale. The rate of progression of the elementary reaction, k is determined by the smallest of the reactants and the products. The turbulent dissipation rate of the fuel (R_{fu}), oxygen (R_{ox}) and products (R_{pr}) can be expressed as,

$$R_{fu} = -A\rho m_{fu}\frac{\varepsilon}{k} \tag{6.33}$$

$$R_{ox} = -A\rho\frac{m_{ox}}{s}\frac{\varepsilon}{k} \tag{6.34}$$

$$R_{pr} = -B\rho\frac{m_{pr}}{(1+s)}\frac{\varepsilon}{k} \tag{6.35}$$

Where, A and B are model constants and s is the stoichiometric oxygen to fuel mass ratio. A transport equation for the mass fraction of the fuel is solved,

$$S_{fu} = -\rho\frac{\varepsilon}{k}\min\left[Am_{fu}, A\frac{m_{ox}}{s}, B\frac{m_{pr}}{1+s}\right] \tag{6.36}$$

CFX has other combustion models, such as Finite Rate Chemistry (FRC), Probability Density Function Flamelet (PDF Flamelet), Burning Velocity Model (BVM) (partially pre-mixed), Extended Coherent Flame Model (ECFM) and the Fluid Dependent Model (FDM). It should be noted that the results presented in this Section only used the EDM model, as the model yielded good results. Additionally it is important to note that this CFD modelling Chapter was only performed to carry out a preliminary evaluation of convenient CFD program, as a suitable design tool for future work in the design of flame mitigation equipment.

The EDM is robust, but it neglects the effects of chemical kinetics and can over predict the reaction rate in regions with a highly strained flow field. The effectiveness of the model is also dependent upon the model constants that are used. Therefore in future analysis other combustion models should be explored, such as the flamelet combustion model. This model would provide information on minor species and radicals such as CO and OH, and accounts for turbulent fluctuations in temperature and local extinction at high scalar dissipation rates. The model obtains the mass fraction of each species through the use of flamelet tables.

The Burning Velocity Model (BVM) and the Extended Coherent Flame Model (ECFM) can also be used on premixed or partially premixed flame by solving a scalar transport equation for the reaction progress. The BVM uses an algebraic correlation for modelling the propagation speed of the flame in a turbulent flow. Both the BVM and ECFM are combined with the flamelet model in order to describe the composition and properties of the burned mixture.

6.2.3.7 Meshing

The *mesher* uses triangular/ tetrahedral meshing elements, with the meshing operation split into two parts: the generation of the surface mesh and the generation of the volume mesh. The surface mesh generator allows the user to vary the density of the surface mesh and the rate at which the mesh expands along the surface.

The second part of the meshing is the volume mesher. This is not interactive and is performed by the computer acting upon the input from the surface mesh. The surface mesh is created using a Delaunay method that is set as a default. The volume mesh is created using Advancing Front and Inflation (AFI). The AFI volume mesher allows for element inflation, this is used to grow a series of prismatic volume elements from triangular elements created from the surface mesh.

Numerical diffusion is a numerical error caused by the truncation of the higher order terms in the discretisation of the fluid flow equations. The effect can be similar to flow diffusion. Numerical diffusion is also a function of the mesh alignment with the streamlines of the flow with the diffusion being inversely related to mesh resolution.

In the case of unstructured meshes, which use tetrahedral volumes (6 edges and 4 nodes), numerical diffusion will affect the solution more than if a structured mesh of hexahedrals (102 edges and 8 nodes) had been used. This effect can be reduced significantly if the discretisation is made second order accurate and that a mesh independent solution is obtained.

The quality of the mesh was determined from the mesh statistics produced after the volume meshing. The quality of the mesh is determined by the number of properties, mesh orthogonality, expansion and aspect ratio. Mesh orthogonality (or skewness) relates to how close the angles between adjacent faces or adjacent edges are to some optimal angle (for example 90° for quadrilateral elements and 60° for triangular faced elements). The minimum orthogonality angle should be greater than 10°. The skewness of 0.80 was calculated for the mesh, which is less than 0.85 for an acceptable mesh. Mesh expansion, relates to the smoothness of change of the adjacent element areas or volumes. Elements, such as any issues with regard to large jumps in cell size, typically the mesh expansion factor should be less than 20. The mesh aspect ratio was also considered, which relates to the degree that mesh elements are stretched. For an acceptable range, the aspect ratio should be less than 100, although other aspect ratios were also considered.

To obtain a mesh independent solution the mesh was refined until the solution no longer varied with additional mesh refinement. Three mesh sizes were used to investigate the effect of mesh refinement: 100k, 200k and 400k elements. Monitoring points were used throughout the domain to see how the velocity varied with mesh refinement. It was found that there was a change in the solution between the 100k and 200k element mesh and the 400k element mesh. Between the 200k and 400k element mesh the velocity profiles were very similar throughout the domain, therefore mesh sizes of approximately 200k elements were used for all the models.

To ensure adequate accuracy and numerical stability the discretisation scheme used throughout the models was the 2nd order High Resolution Scheme (HRS), which has the desirable property of giving 2nd order accurate gradient resolution while keeping solution variables physically bounded.

6.2.3.8 Turbulence models

All turbulence models simplify the complex phenomena of turbulence; some turbulence models are better than others in the assumptions that are used to model the equations. The Reynolds averaged Navier-Stokes equations are generated from the instantaneous Navier-Stokes equations using the following transformations,

$$u_i = \bar{u}_i + u_i', \quad \rho = \bar{\rho} + \rho' \text{ and } p = \bar{p} + p' \tag{6.37}$$

The overbar and prime indicate the time-averaged quantity and an instantaneous fluctuation respectively (velocity, density and pressure).

The momentum equation in Cartesian form is given by,

$$\frac{\partial}{\partial t}(\rho u_i) + \frac{\partial}{\partial x_j}(\rho u_i u_j) = -\frac{\partial p}{\partial x_i} + \frac{\partial}{\partial x_j}\left[\mu\left(\frac{\partial u_i}{\partial x_j} + \frac{\partial u_j}{\partial x_i}\right) - \frac{2}{3}\mu\frac{\partial u_k}{\partial x_k}\delta_{ij}\right] + F_i + \frac{\partial}{\partial x_j}(-\rho\overline{u_i' u_j'}) \tag{6.38}$$

The Reynolds stresses as shown by the last term in Equation 38 is calculated using the Boussinesq hypothesis [101],

$$-\rho\overline{u_i u_j} = \mu_t\left(\frac{\partial u_i}{\partial x_j}+\frac{\partial u_j}{\partial x_i}\right)-\frac{2}{3}\left(\rho k+\mu_t\frac{\partial u_i}{\partial u_i}\right)\delta_{ij} \tag{6.39}$$

Where, μ_t is the eddy viscosity computed from,

$$\mu_t = \rho C_\mu \frac{k^2}{\varepsilon} \tag{6.40}$$

Where, k is the turbulent kinetic energy and ε is the dissipation rate of turbulent kinetic energy.

Two turbulence models were used in the CFD simulations, the k-ε and the Reynolds Stress Model in order to determine which turbulence model best captured the turbulence in the region near the SRA's.

i) k-ε model

Launder and Spalding [12] developed the standard k-ε two equation turbulence model. This models the Reynolds stress as a function of the turbulent viscosity μ_t, which is the product of a turbulent velocity, and a length scale. Known deficiencies with this model are:

i. Poor sensitivity to adverse pressure gradients
ii. Poor sensitivity to streamline curvature
iii. Assumes turbulence is isotropic

For the standard k-ε model the scalar quantities for the turbulent kinetic energy k and the dissipation rate of turbulent kinetic energy ε are calculated from the following equations;

$$\frac{\partial}{\partial t}(\rho k)+\frac{\partial}{\partial x_i}(\rho u_i k)=\frac{\partial}{\partial x_i}\left[\left(\mu+\frac{\mu_t}{\sigma_k}\right)\frac{\partial k}{\partial x_i}\right]+G_k-\rho\varepsilon \tag{6.41}$$

$$\frac{\partial}{\partial t}(\rho\varepsilon)+\frac{\partial}{\partial x_i}(\rho u_i\varepsilon)=\frac{\partial}{\partial x_i}\left[\left(\mu+\frac{\mu_t}{\sigma_\varepsilon}\right)\frac{\partial \varepsilon}{\partial x_i}\right]+C_{1\varepsilon}\frac{\varepsilon}{k}G_k-C_{2\varepsilon}\rho\frac{\varepsilon^2}{k} \tag{6.42}$$

The generation of k due to turbulent stresses, Gk is given by

$$Gk = -\rho \overline{u_i u_j} \frac{\partial u_j}{\partial x_i} \tag{6.43}$$

The constants used have been determined experimentally (Launder and Spalding [12]) to be: $C_{1\varepsilon}$=1.44, $C_{2\varepsilon}$=1.92, C_{μ}=0.09, σ_k=1.0 and σ_{ε}=1.3.

ii) k-ε Renormalised group (RNG) model

The k-ε (RNG) model as proposed by Yakhot *et al.* [103], [104] and [105] was an attempt to modify the standard k-ε model to become more sensitive in regions of strong streamline curvature such as in the case of swirl and flow impingement. The transport equations for the turbulence generation and dissipation are the same as for the standard k-ε model but the model constants differ. The model constants are derived from renormalisation group theory, which are based upon statistical techniques.

The transport equations for the turbulence generation and dissipation are the same as the k-ε model, but the model constants are replaced by the function $C_{\varepsilon 1RNG}$.

The transport equation for the dissipation of turbulent kinetic energy becomes:

$$\frac{\partial}{\partial t}(\rho\varepsilon) + \frac{\partial}{\partial x_i}(\rho u_i \varepsilon) = \frac{\partial}{\partial x_i}\left[\left(\mu + \frac{\mu_t}{\sigma_{\varepsilon RNG}}\right)\frac{\partial \varepsilon}{\partial x_i}\right] + C_{\varepsilon 1RNG}\frac{\varepsilon}{k}G_k - C_{\varepsilon 2RNG}\rho\frac{\varepsilon^2}{k} \tag{6.44}$$

The constants used have been determined experimentally [15] to be:
$C_{\varepsilon 1RNG}$=1.063, $C_{\varepsilon 2RNG}$=1.92, $C_{\mu}=0.084$, σ_k=1.0 and σ_{ε}=1.3

6.2.3.9 Reynolds stress model (RSM)

The RSM for 3D flow introduces six additional transport equations into the model as well as the equations for the mean flow. This models the transport of the Reynolds stresses (turbulent shear and normal stress) in each direction, thus treating the flow as anisotropic, i.e. the turbulence varies in intensity and direction. This provides a better representation of flows with complex strain fields. The use of the RSM does increase the computational time and processing power compared to the aforementioned turbulence models.

The Reynolds stress model (RSM) of Speziale, Sarkar and Gatski [106] does not use the eddy viscosity hypothesis as used in the k-ε and k-ε (RNG) models but solves differential transport equations for the individual Reynolds stresses. With the exact production term and the modelling of the anisotropies, this theoretically makes the RSM more suited to swirling flow. Since the turbulence dissipation appears in the individual stress equations, an equation for ε is still required, in the form of:

$$\frac{\partial}{\partial t}(\rho\varepsilon)+\frac{\partial}{\partial x_i}(\rho u_i \varepsilon)=\frac{\partial}{\partial x_i}\left[\left(\mu+\frac{\mu_t}{\sigma_\varepsilon}\right)\frac{\partial \varepsilon}{\partial x_i}\right]+C_{\varepsilon 1}\frac{\varepsilon}{k}G_k-C_{\varepsilon 2}\rho\frac{\varepsilon^2}{k} \tag{6.45}$$

The constants used in the CFX package are: $C_{\varepsilon 1}$=1.45, $C_{\varepsilon 2}$=1.83.

6.2.3.10 Treatment of the boundary layer

Wall functions are used to resolve the boundary layer without the need to use a large number of nodes, which would be computationally expensive. Figure 6.3 highlights the near wall region.

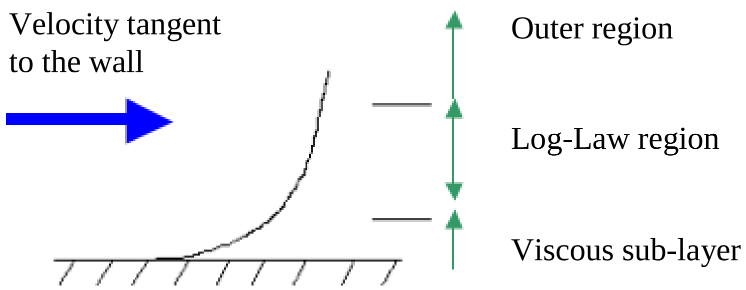

Figure 6.3: Near wall region

Close to the wall in the laminar sub-layer (y^+<5) viscous forces dominate the flow. Outside of the laminar sub layer there is a region known as the Log-law region (30<y^+<500) where both turbulent and viscous forces dominate. In the outer region the flow is free from viscous effects and turbulence forces dominate.

On coarse grids where the boundary layer (BL) is not resolved by the nodes near the wall, a wall function models the BL by an assumed functional shape (logarithmic profile) of the velocity profile. On very fine grids where there are sufficient nodes to resolve the BL the wall function model will turn itself off.

The best resolution of the BL is achieved when sufficient nodes are placed near the walls in order to resolve the BL. It is recommended that a minimum of 5 nodes should be located in the BL and if possible more should be used. If the grid is too coarse the solver assumes the wall function profile shape to resolve the BL.

One indicator of the closeness of the first node to the wall is the y^+ value. At the lower limit a value of y^+ of less than or equal to 11 indicates that the first node is in the laminar sub-layer of the boundary flow. Values larger than this indicate that the assumed log shape of the velocity profile is being used.

From plots of y^+ for the models it can be seen that the wall function is being used to model the BL. To totally resolve the BL for the models it would require a larger amount of computing power than that currently unavailable.

6.2.3.11 Solution convergence

When the *solver* is run, a convergence history of the discretised equations is plotted, each iteration relates to a residual (an error), which is a measure of the satisfaction of overall conservation of the flow. A solution is said to have converged when the normalised residuals have dropped to 0.0004. For the CFD models, a converged solution was usually achieved within 100 and 150 iterations.

The residual history was used to give an indication as to how the solution was progressing. If the residuals histories were not settling down into a steady convergence, it could be an indication that the mesh was not sufficiently fine in a particular region. This region could be obtained by looking at where the value of the maximum residual was located. Local mesh refinement in that particular region would then be carried out. It was also possible to make the solution scheme more stable by adjusting the *relaxation factor*; however changing this causes the solution to converge at a slower rate.

6.2.3.12 Sensitivity studies

Various *sensitivity studies* were carried out to check for a unique solution. One such check was *mesh independence*; this was to ensure that the solution was independent of mesh size. This was carried out by doubling the mesh size by reducing the global edge length in the preprocessor, re-meshing the model and then solving. If the solution had not changed with regard to flow structure and velocity profiles, a mesh independent solution would have been achieved.

Different turbulence models were also used during the analyses to decide upon which turbulence model would be the most suitable to resolving the nature of the flow. As mentioned earlier in the Chapter, some turbulence models are better at capturing complex flow structures than others.

It is worth noting that during the experimental 'hot trials', thermocouple output temperatures were only evaluated for comparative purposes to ascertain the flame progression within the tube and were not representative of the actual flame temperatures. This was previously justified and rationalised in Chapter 4, Section 4.7.2 and therefore a comparison will not be made between the simulation flame temperatures and the correspondent experimental results.

Other potential sources of error that have been considered during the evaluation of the CFD simulation data are:-

i. SRA volumetric flow rate : Accuracy ±1% (See also Chapter 4, Section 4.4.1)
ii. SRA spray cone angle : Measured using Adobe angle finder tool, accuracy ±1% and human error / subjectivity ±1%. (See also Chapter 4, Section 4.4.2)
iii. SRA volumetric flow rate : Accuracy ±1% (See also Chapter 4, Section 4.4.1) SRA droplet D_{32} mean diameter : Characterised using Phase Doppler Anemometry (PDA). Typical nominal errors for diameter : 4% on diameter (manufacturer's data). (See also Chapter 4, Section 4.4.3) Methane-air mixture verification : Resolution 1% / Accuracy ± 2%. (See also Chapter 4, Section 4.8.1)
iv. Flame speed calculations : Camera frame rate accuracy >99.999% accuracy and Adobe Pixel measurement accuracy approximately ±0.5%. (See also Chapter 4, Section 4.8.5)

6.3 Results and discussion : CFD simulation

For convenience, the quantitative results for each simulation will be initially discussed, followed by qualitative illustrations shown subsequently. The results shown in Figures 6.4 to 6.21 are for the four spray cases using the Type B SRA. The contour plots presented show the temperature and velocity upstream and downstream of the SRA's. Half way down the pipe there are streamlines showing the trajectory and lifetime of the droplets. The fuel air ratio (FAR) for the one, two and three SRA cases were at 7% methane-air by volume (E.R.Φ 0.72) and 9% methane-air by volume (E.R. Φ 0.95) for one case using the four SRA's.

During the hot trials, temperature data was acquired and processed methodically in accordance with the procedures previously described in Chapter 4, Sections 4.7 and 4.8. Due to lag time associated with thermocouples, the data measurements offered during the hot trials were not intended to characterise the actual flame temperatures. The use of exposed junction thermocouples is however, a proven and conventional method for comparing flame propagation in 'confined', 'partly confined' and 'unconfined' explosion testing and in confined and partly confined vessels and pipework. Several published journal papers [87,88,89] have extensively described the use of such devices. Therefore, there will be no comparisons made between the flame temperature data from the FPMR in the hot trails and those from the corresponding simulations.

Additionally, throughout the hot trials average flame speeds were measured and calculated by qualitative analysis of the HD video and still imagery, in conjunction with the pixel measurement tool found in Adobe Photoshop (see also Chapter 4, Sections 4.7 and 4.8). Hence, flame speeds from the hot trials, as shown in Table 6.5, will be considered and discussed with relevance to the equivalent CFD simulations where appropriate.

Number of Type B SRA's the spray region	Methane-air E.R. Φ 0.72 Flame speeds (m/s)		Methane-air E.R. Φ 0.95 Flame speeds (m/s)	
	Upstream of spray(s)	Downstream of spray(s)	Upstream of spray(s)	Downstream of spray(s)
1	21	27.5	25	26
2	17.5	16	22	18
3	20	20	23	27
4	18	0	19	23.5

Table 6.5 : Average flame speeds recorded in experimental hot trials

As shown in Figure 6.4 and 6.5, using the RSM turbulence model for the one SRA case, the flame has a temperature of around 2400K and a mean velocity of 23m/s prior to the SRA. In the localised region of the SRA the spray does reduce the temperature to around 500K, but soon recovers to around 1500K, which is well above the ignition temperature of a pre-mixed methane mixture.

Due to the small droplet size, the majority of the droplets only penetrate half way across the pipe section and are taken down stream and are vaporised within three pipe diameters.

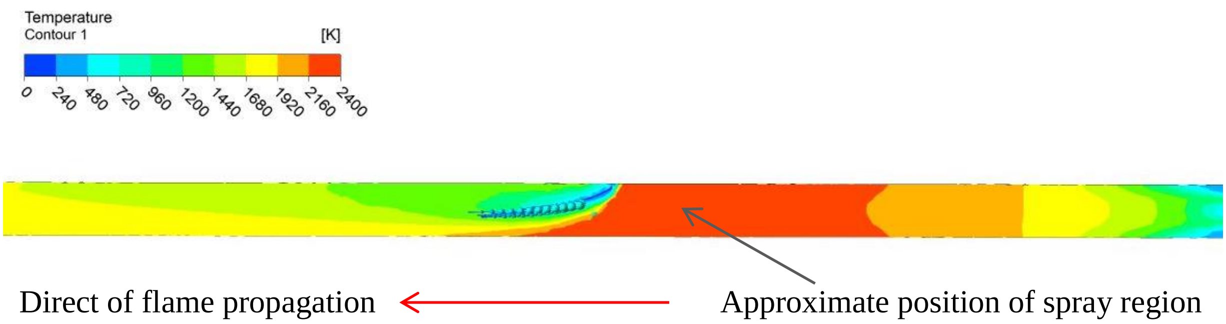

Figure 6.4 : Temperature contour for Single X/F Type B SRA at E.R. (Φ) 0.95

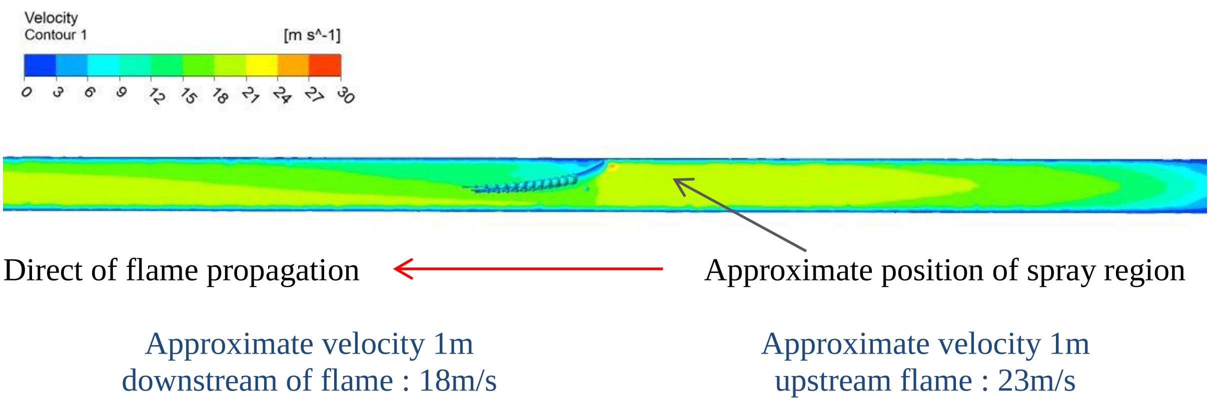

Figure 6.5 : Velocity contour for Single X/F Type B SRA at E.R. (Φ) 0.95

A similar profile of temperature and velocity are also predicted for the two SRA's case, as shown in Figures 6.6 and 6.7 at 9% methane-air by volume (E.R. Φ 0.95) and using the RSM model. For both cases there is **no flame mitigation** downstream of the SRA.

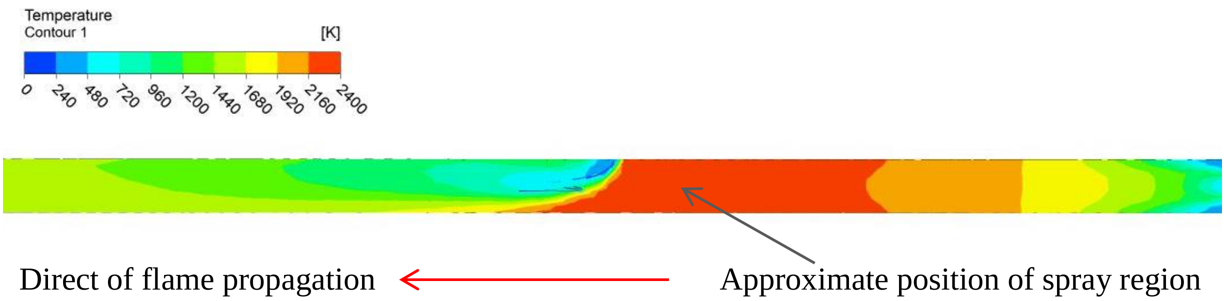

Figure 6.6 : Temperature contour for two X/F Type B SRA's at E.R. (Φ) 0.95, RSM

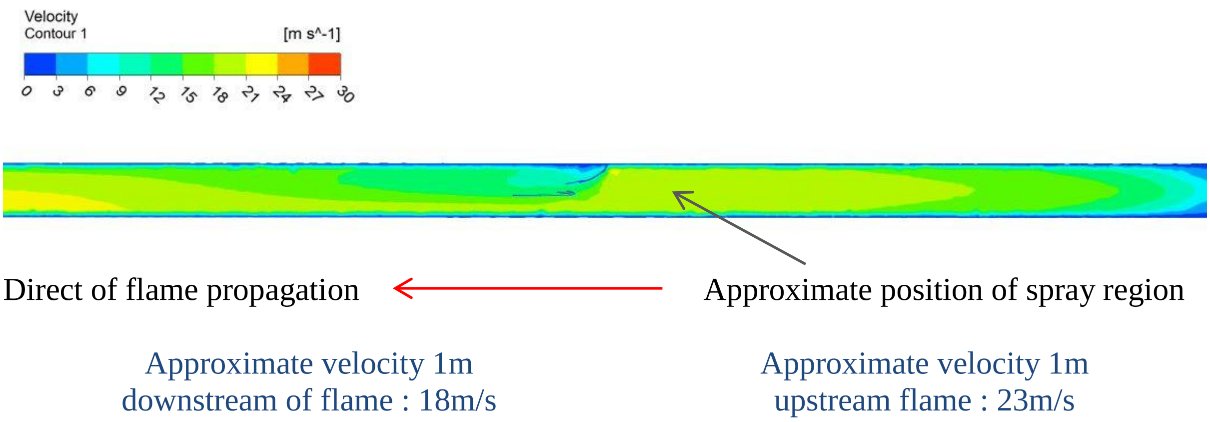

Figure 6.7 : Velocity contour for two X/F Type B SRA's at E.R. (Φ) 0.95, RSM

Figures 6.8 to 6.11 are for the three SRA's case at 9% methane-air by volume (E.R. Φ 0.95). Figures 6.8 and 6.9 show the temperature contour using the k-ε and RSM model respectively. When comparing the k-ε model (Figure 6.8) with the RSM model (Figure 6.9), the k-ε profile shows that the mixing of the fuel-air to a stoichiometric mixture is completed nearer to the fuel air inlet.

The temperature profile through the spray region is also more defined, especially around the centerline of the pipe.   There is also a greater drop in temperature at the end of the pipe for the RSM case. For both turbulence models, the temperature profile immediately downstream of the sprays have been vaporised within four pipe diameters and the downstream temperature (around 1200K) is above the ignition temperature for methane resulting in flame propagation.

The velocity contours shown in Figure 6.10 for the k-ε at 9% methane-air by volume (E.R. Φ 0.95) show a greater velocity 22m/s upstream of the SRA's than for the RSM model, as shown in Figure 6.11. The greater reduction in flame temperature downstream of the SRA's produces a lower velocity for the RSM model.

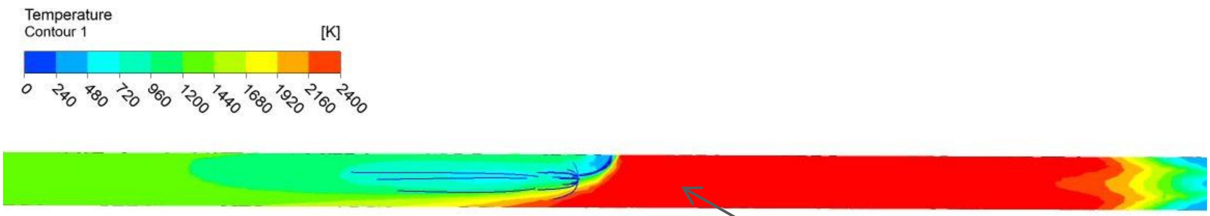

Direct of flame propagation ← Approximate position of spray region

Figure 6.8: Temperature contour for three X/F Type B SRA's at E.R. (Φ) 0.95, $\boldsymbol{k-\varepsilon}$.

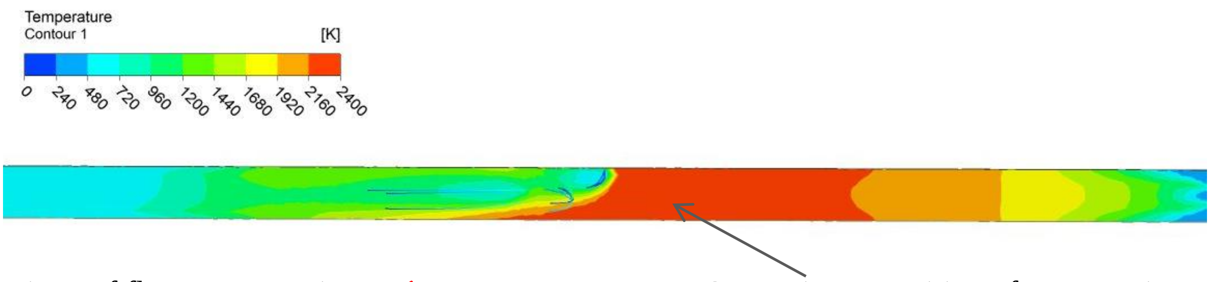

Direct of flame propagation ← Approximate position of spray region

Figure 6.9 : Temperature contour for three X/F Type B SRA's at E.R. (Φ) 0.95, RSM.

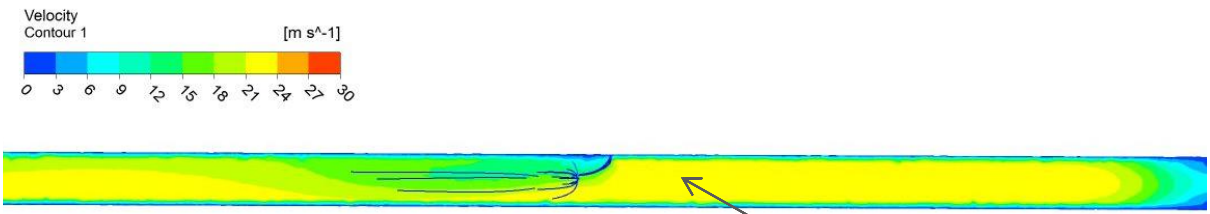

Direct of flame propagation Approximate position of spray region

Approximate velocity 1m downstream of flame : 16m/s

Approximate velocity 1m upstream flame : 22m/s

Figure 6.10 : Velocity contour for three X/F Type B SRA's at E.R. (Φ) 0.95, $\boldsymbol{k-\varepsilon}$.

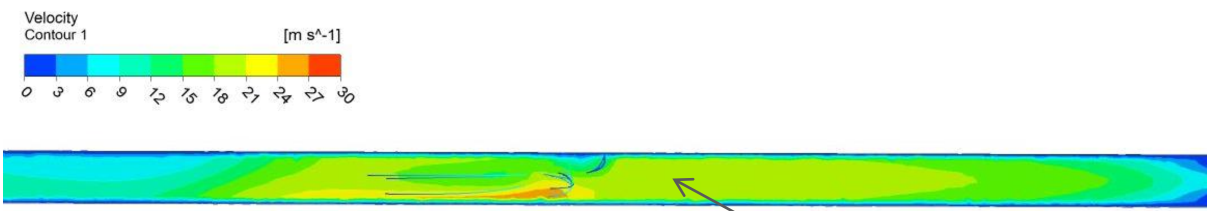

Direct of flame propagation Approximate position of spray region

Approximate velocity 1m downstream of flame : 14m/s

Approximate velocity 1m upstream flame : 20m/s

Figure 6.11 : Velocity contour for three X/F Type B SRA's at E.R. (Φ) 0.95, RSM.

Figures 6.12 to 6.19 show the temperature and velocity contours for the four SRA's case. Figures 6.12 and 6.13 show the temperature contour for the k-ε and RSM turbulent models for 9% methane-air by volume (E.R. Φ 0.95). For both turbulent models the temperature downstream of the spray has been lowered below the ignition point and the flame has been quenched. The velocity contours shown in Figures 6.14 and 6.15 also illustrate that the flame has been quenched and the velocity being reduced to around 2 m/s at the outlet.

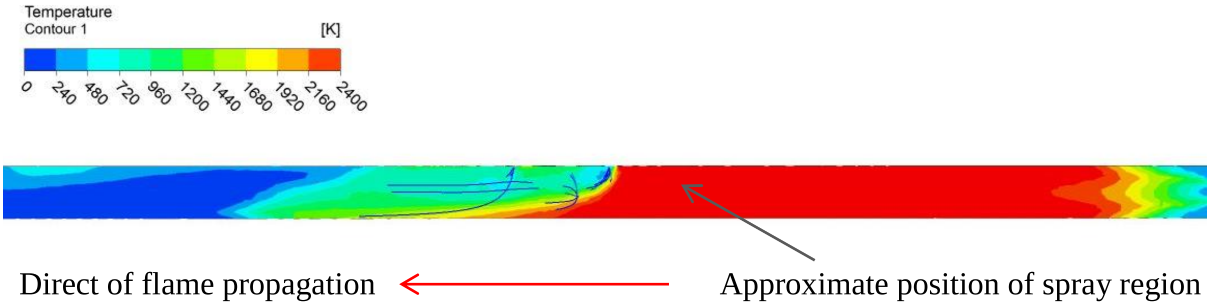

Figure 6.12 : Temperature contour for four X/F SRA's Type B at E.R. (Φ) 0.95, $\boldsymbol{k-\varepsilon}$.

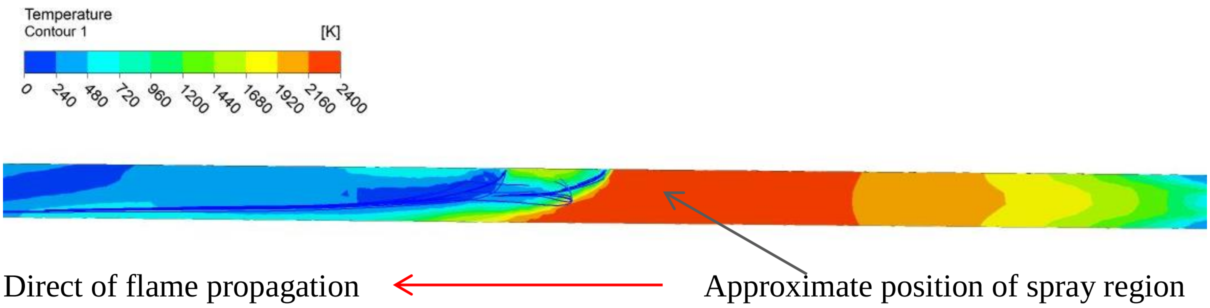

Figure 6.13 : Temperature contour for four X/F Type B SRA's at E.R. (Φ) 0.95, RSM.

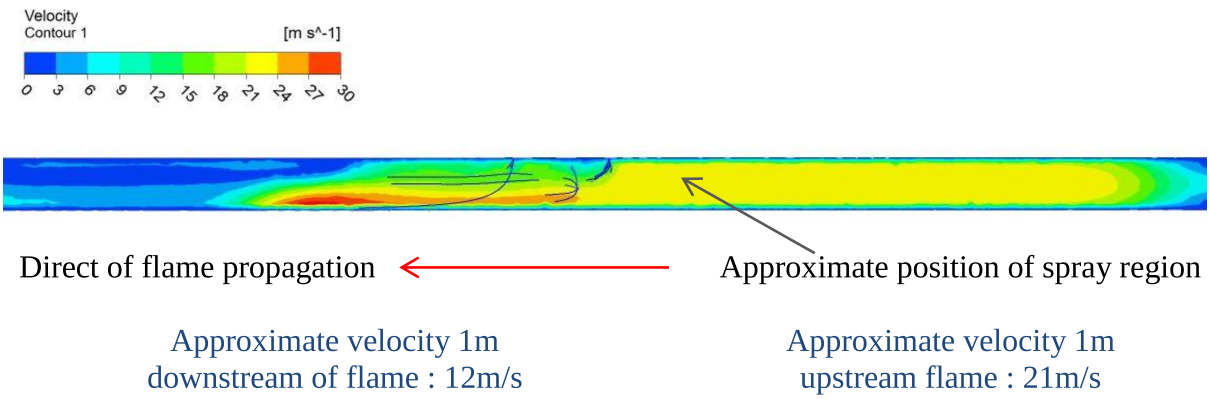

Figure 6.14 : Velocity contour for four X/F Type B SRA's at E.R. (Φ) 0.95, $\boldsymbol{k-\varepsilon}$.

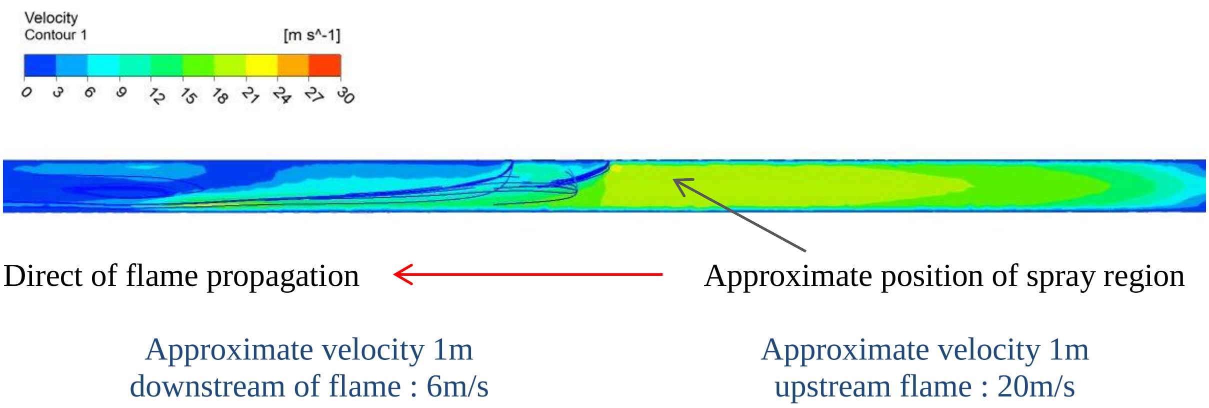

Figure 6.15 : Velocity contour for four X/F Type B SRA's at E.R. (Φ) 0.95, RSM.

It is worth noting that in the experimental trial at this condition (E.R. Φ 0.95), the spray did *not mitigate the flame*, whereby mitigation only occurred only at the leaner mixtures of E.R. Φ 0.61 and 0.72 (6% and 7% methane-air). This is illustrated by the CFD in Figures 6.16 and 6.17 at E.R. Φ 0.72 (7% methane-air) and using the RSM turbulence model. Figure 6.16 also shows the still image taken from the mitigation event in the equivalent experimental trial. (See also Chapter 5, Section 5.5.5)

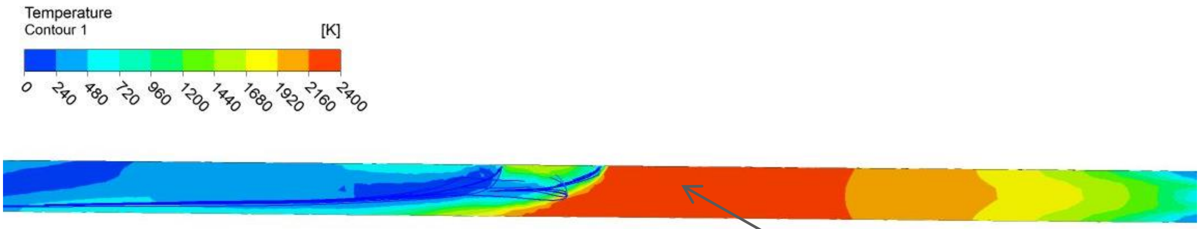

Direct of flame propagation

Approximate position of spray region

Corresponding experimental trial image (Chapter 5, Section 5.5.5)

Figure 6.16 : Temperature contour for four X/F Type B SRA's at E.R. (Φ) 0.72, RSM

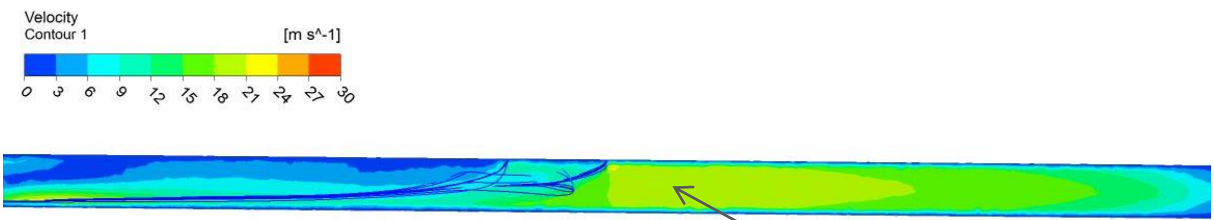

Direct of flame propagation

Approximate position of spray region

Approximate velocity 1m downstream of flame : 5m/s

Approximate velocity 1m upstream flame : 19m/s

Figure 6.17 : Velocity contour for four X/F Type B SRA's at E.R. (Φ) 0.72, RSM

To see whether the model was resolving the effect of droplet size and the latent heat transfer of the droplets and to assess the use of the TAB breakup model, droplets were introduced into the domain at the same mass flow rates as the D_{32} 26µm representative size droplet, but in this case giving a Rosin Rammler distribution of 80µm representative droplet diameter and a spread of 1.8. Figures 6.18 and 6.19 at E.R. Φ 0.95 (9% methane-air) show the case when the droplets were introduced, but without the breakup model. As can be seen, the droplets are *not vaporised due to their initial size* and are not significant in number to lower the temperature downstream of the SRA's to quench the flame.

When the droplet breakup model is used, as shown in Figures 6.20 and 6.21, the droplets are vaporised in around 4 pipe diameters downstream. The release of the latent heat is probably not localised enough to adequately quench / mitigate the flame, thus the flame continues to propagate through the mixture.

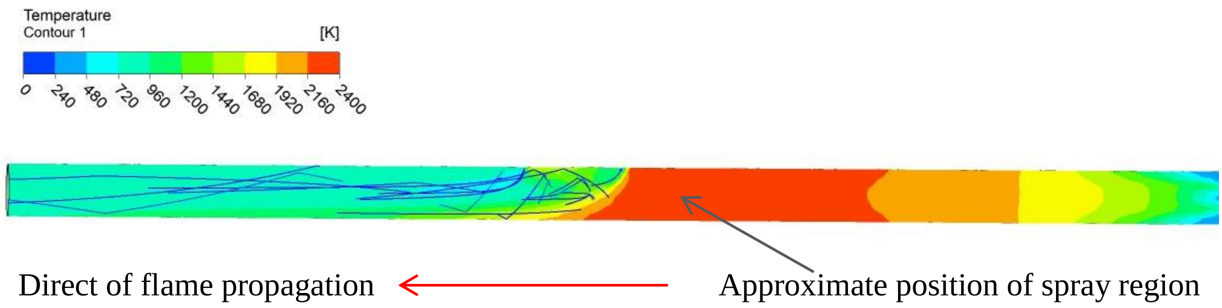

Figure 6.18 : Temperature contour for four X/F Type B SRA's
E.R. (Φ) 0.95, D_{32} 80µm, RSM.

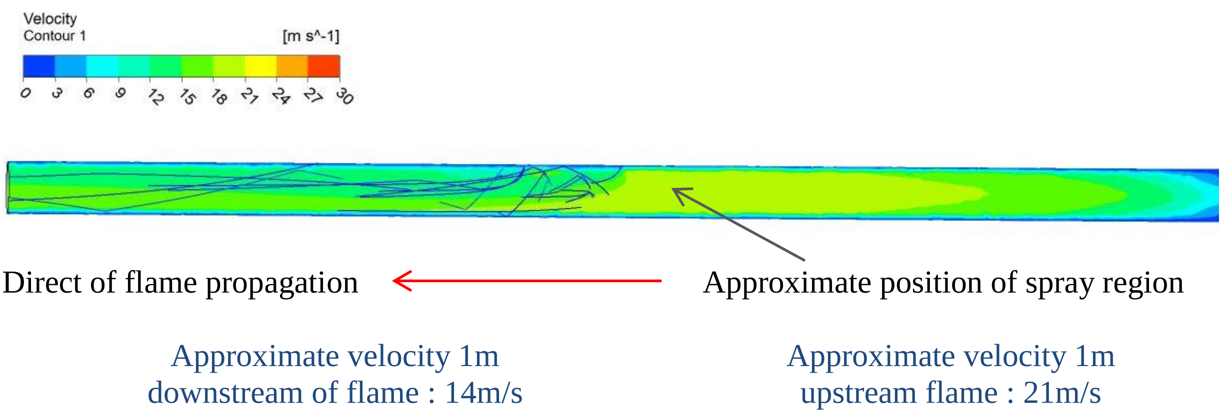

Figure 6.19 : Velocity contour for four X/F Type B SRA's
E.R. (Φ) 0.95, D_{32} 80µm, RSM.

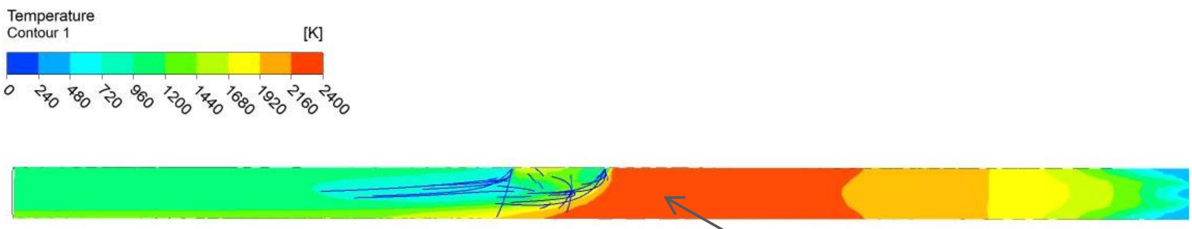

Direct of flame propagation ⟵ Approximate position of spray region

Figure 6.20 : Temperature contour for four X/F Type B SRA's :
E.R. (Φ) 0.95, D_{32} 80μm, RSM, with breakup.

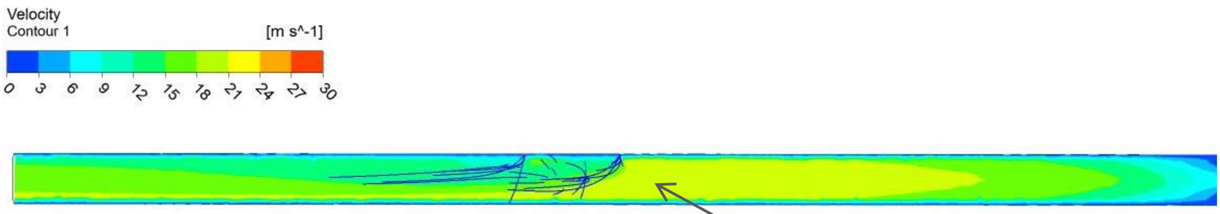

Direct of flame propagation ⟵ Approximate position of spray region

Approximate velocity 1m downstream of flame : 14m/s

Approximate velocity 1m upstream flame : 22m/s

Figure 6.21 : Velocity contour for four X/F Type B SRA's
E.R. (Φ) 0.95, D_{32} 80μm, RSM, with breakup.

6.4 Chapter summary

This Chapter has considered the use of Computational Fluid Dynamics (CFD) as a design tool and how it may also be used to complement the design process. The aim of this CFD attempt has been for preliminary evaluation purposes of the software program, rather than the development of CFD code.

Additionally, there has been a review of CFD terminology and the methodology used in creating the CFD models, including a rationale for the various modelling practices that have been considered within this Chapter.

The results have shown that CFD does approximate the physics of the flow, with respect to flame speed and has also predicted the number of SRA's required to mitigate / quench the flame using fine sprays. However, the results from the sample appraisal were not consistent with respect to all of the methane-air mixtures (E.R.) witnessed in the corresponding experimental hot trials. In particular, the simulation indicated a mitigation event in a methane-air mixture (ϕ) 0.95, when in fact a rise in flame speed occurred during the resulting experimental hot trials.

Further investigations into the suitability of the CFD program, together with the effects of droplet size on flame quenching / mitigation and the consideration of other combustion models, are recommended for future work in Chapter 7.

CHAPTER 7

CONCLUSIONS AND RECOMMENDATIONS

7.1 Conclusions

Within this study there were two separate fundamental areas of research, these were the *cold trials* and *hot trials*. The selected results from the cold and hot trials were comprehensively discussed in Chapter 5 and also in Appendix 9, which is supplied on a separate CD (called here, Volume III).

Additionally, attempts were considered with respect to modelling the complex *hot trial* conditions within the Flame Propagation and Mitigation Rig (FPMR) using a Computational Fluid Dynamics (CFD) software package, whereby the effectiveness of the program as a suitable future design tool was reviewed.

7.1.1 Cold trials

The purpose of the cold trials was to further develop an existing single atomiser, known as the Spill Return Atomiser (SRA) and to produce a number of single and multiple SRA arrangements and configurations containing drop sizes of $D_{32} \leq 30\mu m$, which would subsequently be suitable for placement and assessment in the hot trials apparatus (or FPMR). The summary conclusions from the cold trials are given below:-

- The cold trials results were discussed explicitly in Chapter 5 and were successful in the further advancement of an existing commercial Spill Return Atomiser (SRA) in demonstrating the potential suitability of each of the resulting configurations for the subsequent hot trials.
- Four manifestations of the SRA (Type A, B, C and D) were derived and successively characterised using the various dynamic measurement methods. These characteristics were previously tabulated, summarised and discussed in Section 5.33, Table 5.6.
- Throughout the cold trials the ideal liquid pressure was found to be 13MPa. This infers that the tangentially supplied swirl chamber within the SRA, produced the optimum turbulence for atomisation at 13MPa.
- The four SRA's were evaluated and their volumetric flow rates were tabulated (see also Table 5.6), with additional attention paid to the consistency of the exit to spill ratio. Exit flow rates at 13MPa were found to be 0.295, 0.85, 1.36 and 1.94 L/min , with spill flow rates being 1.12, 0.85, 0.49 and 0.25 L/min respectively. The flow rate in the Type D SRA spill was very erratic and non-linear. This indicated the boundary of the limits of the

present SRA swirl chamber and thus the SRA Type D was de-selected from any further consideration.

- Spray cone angles (ɵ) were measured for the SRA's (Type A, B, C and D) during the trials using 13MPa liquid pressure, which were found to be 37.4˚, 42.7˚, 49.2˚ and 54.2˚respectively. The spray cone angles were also considered with respect to spray penetration (d_p), whereby the penetration was calculated to be 304, 243, 207 and 186mm respectively. Of the four SRA configurations, the optimum spray cone angle for use in the 190mm (I.D.) PMMA tube of the flame propagation and mitigation rig (FPMR) was the Type C SRA (ɵ 49.2˚ and d_p, of 207mm)
- Four unique spray arrangements were developed during the cold trials, with each adaptation facilitating combinations of the three selected SRA's (Type A, B and C). These were:-
  - i. a single SRA in counter flow with the incoming propagating flame
  - ii. a single SRA in parallel flow with the incoming propagating flame
  - iii. multiple SRA's in parallel flow with the incoming propagating flame
  - iv. multiple SRA's in cross flow with the incoming propagating flame
- Phase Doppler Anemometry (PDA) was used to characterise the sprays above, whereby dynamic measurements of droplet diameter, D_{32}, were found between 17 - 29µm, droplet velocities, D_v, of ≤21.4m/s and liquid volume flux, Q_f, 0.011 - 0.047cm^3/s/cm^2. The sprays were measured radially at a downstream distance of 95mm, this being the approximate centre of the spray within the tube conditions. PDA analysis was carried out in ambient conditions and also in a simulated PMMA tube environment.
- All three selected SRA's (Type A, B and C) produced ambient drop sizes within the scope and aims of this study of $D_{32} \leq 30$µm.
- Cross flow sprays (X/F) were also characterised in the simulated PMMA tube, whereby the D_{32} values were found to be slightly higher, as shown in Table 7.2. However, 48.5% of the droplets in the Type B SRA and 28% for the Type C SRA spray were of ≤30µm. This was also coupled with a significant increase in liquid volume flux (Q_f) within the simulated tube, which was approximately 83% for the Type B and 21% for the Type C.
- In the simulated PMMA tube, cross flow characteristics varied also with respect to velocity, in which a noteworthy reduction in average velocity resulted in values of ~0.0m/s for the Type B SRA configuration and ≤3.23m/s for the Type C SRA configuration.

7.1.2 Hot trials

The hot trials apparatus, known as the Flame Propagation and Mitigation Rig (FPMR) was conceived, designed and built by the author specifically for this program of study and will hopefully be used by other R.A.'s in many future studies. The FPMR was constructed with the fundamental aim of producing slow, low speed gas-air deflagrations of ≤30m/s, contrary to all previous research which only focused on high speed deflagrations (≥100m/s) and detonations (up to 2000m/s). The summary conclusions from the hot trials are given below:-

- Spray orientation with respect to the propagating flame, coupled with droplet velocity was found to have a significant effect on the level of flame acceleration in the flammable mixture, particularly in the SRA Type A case where the liquid volume flux (Q_f) was clearly insufficient to initiate mitigation.
- The single Type B SRA (0.5mm exit orifice and 0.5mm spill diameter) parallel flow trials produced more instances of flame acceleration than their counter flow equivalents. The average droplet velocity in the Type B spray was 21.41m/s compared to 13.5m/s for the Type B spray. This relationship between counter and parallel flow sprays has **not** been reported in any of the previous published literature. The fundamental spray properties of these configurations were previously provided and examined with significance in Section 5.33, Table 5.6.
- With a single SRA Type C (0.8mm exit orifice and 0.5mm spill diameter) spray, it was possible to mitigate a methane-air mixture of E.R. (ϕ) 0.61, utilising *counter flow* and *parallel flow* configurations. The Type C SRA produced a spray containing droplets of $D_{32} \leq 29\mu m$, with a liquid volume flux being approximately $0.04 cm^3/s/cm^2$ and average velocity of 13.5m/s in ambient conditions.
- In the single SRA Type C spray, the flame acceleration in the counter flow arrangements was found to be approximately *four times greater* than the parallel flow equivalent configuration and was particularly prevalent in the methane-air mixture of E.R. (ϕ) 0.72, but less so in the (ϕ) 0.95 and 1.06 mixtures, due to their high exothermicity. This was contrary to the SRA Type B, as reported above in the second bullet point. These two conflicting outcomes demonstrate the critical importance of drop size (μm), volume flux ($cm^3/s/cm^2$) and velocity (m/s).
- Single Type B and C SRA sprays configurations were ineffective when used in *cross flow* due to the limitations of the spray cone angle and corresponding spray envelope, thus not

being sufficient to completely engulf the cross sectional area of the FPMR mitigation tube and permitting flame propagation through the spray free space.

- The twin overlapping parallel flow Type B SRA's produced a mitigation event in the methane-air mixture of E.R. (ϕ) 0.61. In the other three mixtures (ϕ) 0.72, 0.95 and 1.06, there was a degree of flame acceleration caused by the disturbance of the sprays however, this was significantly less than in the corresponding single parallel flow trials.
- The twin overlapping parallel flow (P/F) Type C SRA's produced the first instance of mitigation in a methane-air mixture of E.R. (ϕ) 0.95. In the graphical illustrations shown previously in Chapter 5, there was a small temperature rise of approximately 25˚C, which is attributed to the flash vaporisation and subsequent cooling that was also observed both visually and audibly at the point of mitigation.
- In the twin overlapping parallel flow Type C SRA trials there was a noticeable increase in flame speed upstream of the sprays, which has been accredited to the entrainment in the overlapping configuration.
- The various multiple cross flow (X/F) SRA configurations proved to be the most successful conformation, whereby four Type B X/F SRA's caused a mitigation event in a methane-air mixture of E.R. (ϕ) 0.72.
- A multiple cross flow (X/F) configuration utilising four Type C X/F SRA's, each exhibiting individual ambient spray characteristics of $D_{32} \leq 29\mu m$ and liquid volume flux (Q_f) of approximately $0.044 cm^3/s/cm^2$, proved to be highly effective in *total flame extinguishment* and *complete mitigation in all fuel-air mixture scenario*. The *flame speeds produced were all ≤30m/s*, with resulting *flame thickness* of approximately *1mm for E.R. ~1.0*. The manifestation of the configuration and marginal separation distance between each of the sprays in the 'spray region' consisted of four sprays, each 105mm apart with individual SRA's each opposed by 120˚ (*spray region of 315mm* spray centre to centre).
- In the heated water supply trials the flame was shown to be mitigated at an earlier point, during its transition through the spray region, indicating that a greater percentage of the spray must have been reaching boiling temperature and vaporising, thus giving way to latent heat transfer. Additionally there was a large visible plume of water vapour at exit end of apparatus which was shown previously in Chapter 5.
- In the supplementary trials using propane-air, the flame was mitigated at an earlier position during its passage through the sprays. This may be credited to the greater atomic ratio of carbon : hydrogen associated with propane, when compared to that of methane.

7.1.3 CFD consideration

An attempt was made to model single and multiple cross flow sprays, in a representative sample of methane-air mixtures, whereby the overall outcome of the CFD simulation is summarised below:-

- During the experimental phase of this present study, there were two distinct areas of research. These were previously described throughout this thesis as the cold trials and the hot trials. The data and results from the experimental trials were conveniently combined for the CFD attempt.
- Although the CFD simulation effort did not consider all of the fuel-air mixtures and atomiser configurations utilised in the 250 corresponding hot trials, attempts were made to model the methane-air mixtures, E.R. ϕ 0.72 and 0.95 (7% and 9% FAR) and a spray configuration which included single and multiple cross flow (X/F) Type B SRA's.
- The flame speeds that were predicted in the simulation for the methane-air mixture E.R. Φ 0.95 (9% by volume) were approximately 21 – 25m/s, compared to about 19 – 26m/s found in the corresponding experimental trials.
- In the CFD simulation the flame was completely quenched and mitigated in the methane-air mixture E.R. ϕ 0.72 and 0.95 (7% and 9% FAR). Although the flame in the E.R. ϕ 0.72 (7%) equivalent experimental trial was completely extinguished, the flame in the methane-air mixture E.R. ϕ 0.95 (9%) passed directly through the spray region, coupled with an increase in flame speed of about 20%. The subsequent increase in flame speed observed in the hot trial, was attributed to the induced turbulence caused in the spray region.
- To assess the heat transfer and latent heat model within the simulation, the drop sizes were increased from D_{32} 26µm to D_{32} 80µm. This action resulted in the flame passing directly through the spray region, thus confirming that heat transfer in the sprays consisting of D_{32} 80µm droplets was predominantly by means of sensible heat and that there were not significant droplets to lower the temperature downstream of the SRA's to quench the flame. Whereas, the D_{32} 26µm sprays completely quenched and mitigated the flame, thus benefitting from the release of latent heat within the flame front.

7.2 Recommendations and further work

It is anticipated that the developments and findings within the present study will give way to a renewed interest in explosion mitigation research using fine water sprays. As discussed, previous studies concentrated on the use of larger droplets of ≥100μm and faster flame speeds in the order of ≥100m/s to approximately 2000m/s. In the aforementioned research, droplets were hydrodynamically shattered by inverted bag type break, thus giving way to finer droplets that were then small enough to absorb heat from the flame front.

With recent advances in spray research and the development of the Spill Return Atomiser (SRA), this current study has shown the effectiveness of fine sprays (D_{32}≤30μm) in completely mitigating slow moving methane-air and propane-air deflagrations of ≤30m/s, without the reliance of hydrodynamic inverted bag type break up.

In the next Section recommendations are presented for further research that will provide an excellent platform to enrich the knowledge acquired as a result of this present study. Such investigations will further evaluate the capabilities and achievements of the SRA in realistic, full scale conditions. The author also wishes to pledge his enthusiasm, support and assistance in any future proceedings.

7.2.1 CFD modelling

Whilst this present study has focused exclusively on experimental trials and subsequent findings, a CFD validation attempt was also performed (discussed previously in Chapter 6) which has proven to be a worthwhile consideration exercise, with the sample experimental physical flow conditions being closely approximated by the software predictions.

Future realistic full scale experimental studies (see also next Section) may also benefit by adopting this initial CFD modelling practices set out in Chapter 6, in developing further iterations. Considerations for further CFD studies may include:-

i. Variable attempts with other types of combustion model used i.e. Finite Rate Chemistry (FRC), Probability Density Function Flamelet (PDF Flamelet), Burning Velocity Model (BVM) (partially pre-mixed), Extended Coherent Flame Model (ECFM) and the Fluid Dependent Model (FDM)
ii. Turbulence models with respect to 'dry' conditions without the operation of sprays and the subsequent effect of sprays on the quiescent fuel-air mixture.

7.2.2 Full scale realistic explosion mitigation conditions

- The concept of fine spray applications has far reaching safety implications for oil and gas refineries, platforms and other industries where there is the potential for explosive gas and/or flammable vapour mixtures. If the technology can be proven in realistic scale tests, such a system may in the future become mandatory for all these types of installations.
- By understanding the effects of droplet interaction with propagating flames and the conditions needed for flame quenching and mitigation, a suitable spray system may be designed to mitigate flame propagation and explosions in partly confined scenarios.
- The work can also be further extended to develop a protective explosive mitigation system for unconfined areas, to prevent entry of the flame into areas that promote turbulence and flame acceleration, such as pipe arrays etc. as shown in Figure 7.1.

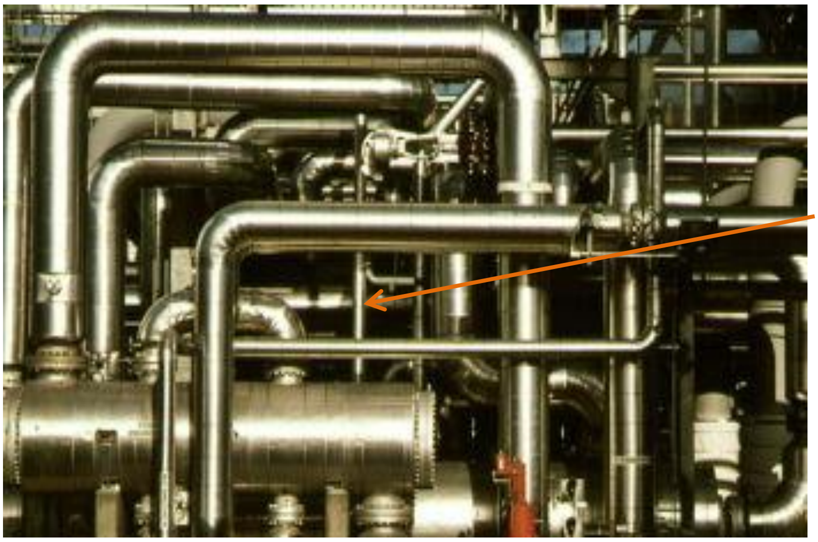

Pipe Array consisting of complex interwoven pipework geometries

Figure 7.1 : Representative severely congested pipework array

- The test centre at GL Noble Denton, Spadeadam, offers unique testing facilities for further work. Some of the testing carried out at Spadeadam includes: blast and high explosive testing, fire testing - jet fire, pool fire, explosion testing confined and unconfined gas and vapour cloud explosion, pipeline counter terrorism measures, flame acceleration and DDT, Flame arresting equipment, explosion mitigation measures - water sprays, aqueous foam, halons and water deluge system testing.

- Figure 7.2 offers a conceptual image of a *Mitigation Curtain Module (MCM).* The concept behind the MCM is that it will be suitable for fitting to new installations, or retro-fitted to existing pipe arrays. The MCM could be installed along the sides or the top and even below the congested pipe array, where necessary.

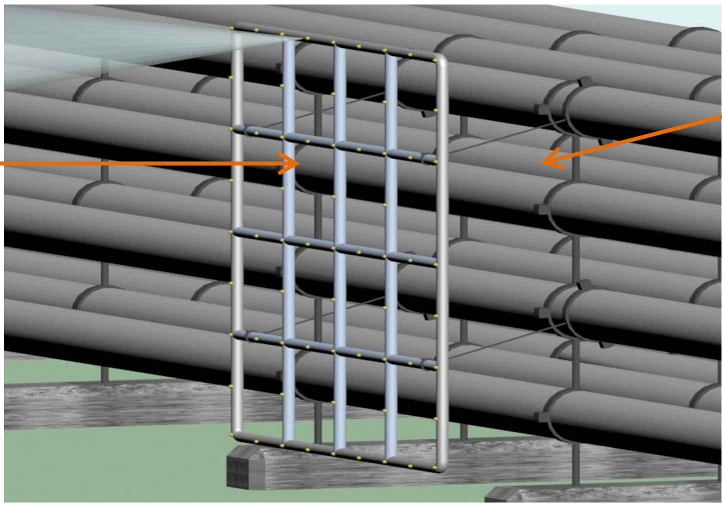

Figure 7.2 : Concept for the SRA ‘Mitigation Curtain Module’ (MCM)

- To achieve the required drop size, liquid volume flux and other parametric spray properties needed for future realistic scaled conditions, it may also be worth considering further development of the SRA in order to permit greater flow rates and wider spray cone angles, without compromising the mean drop size ($D_{32} \leq 30\mu m$).
- Alternatively, other commercial atomisers may also be available to consider, adapt, modify and improve to achieve the desired spray characteristics that favour future full scale applications.

7.2.3 Jet fire mitigation

- Finally, another potential purpose and new product development for the SRA is in *fire suppression*, in particular involving *jet fires*. These fires are frequently the result of a high velocity jet release of gaseous or liquid fuel and subsequent ignition, as shown in Figure 7.3 and are often the outcome of a ruptured pipeline or sheered fitting, normally associated with pipework operations on petrochemical, oil or gas sites. Impingement of the resulting jet flame on other materials may even lead to secondary fires, or a dangerous temperature rise in other contained products i.e. a pipe or vessel as illustrated below.

Figure 7.3 : Typical jet fire resulting from leaking pipe

- The study would involve the design and construction of test apparatus, followed by a series of cold and hot trials to evaluate the suppression and mitigation performance of a string of *multiple SRA's* incorporated within a *tubular stainless steel helicoil arrangement.*
- It is envisaged that the *Helicoil Mitigation Apparatus (HMA)* could be lowered over a jet fire by a robotic device, such as a land based remotely operated vehicle (ROV) with self-contained water supply as depicted in Figure 7.4 (a).
- An initial design concept for the HMA is offered in Figure 7.4 (b). The HMA trials should initially commence with laboratory scale (cold and hot) studies, followed by full scale realistic trials using a 500mm - 1000mm diameter helicoil.

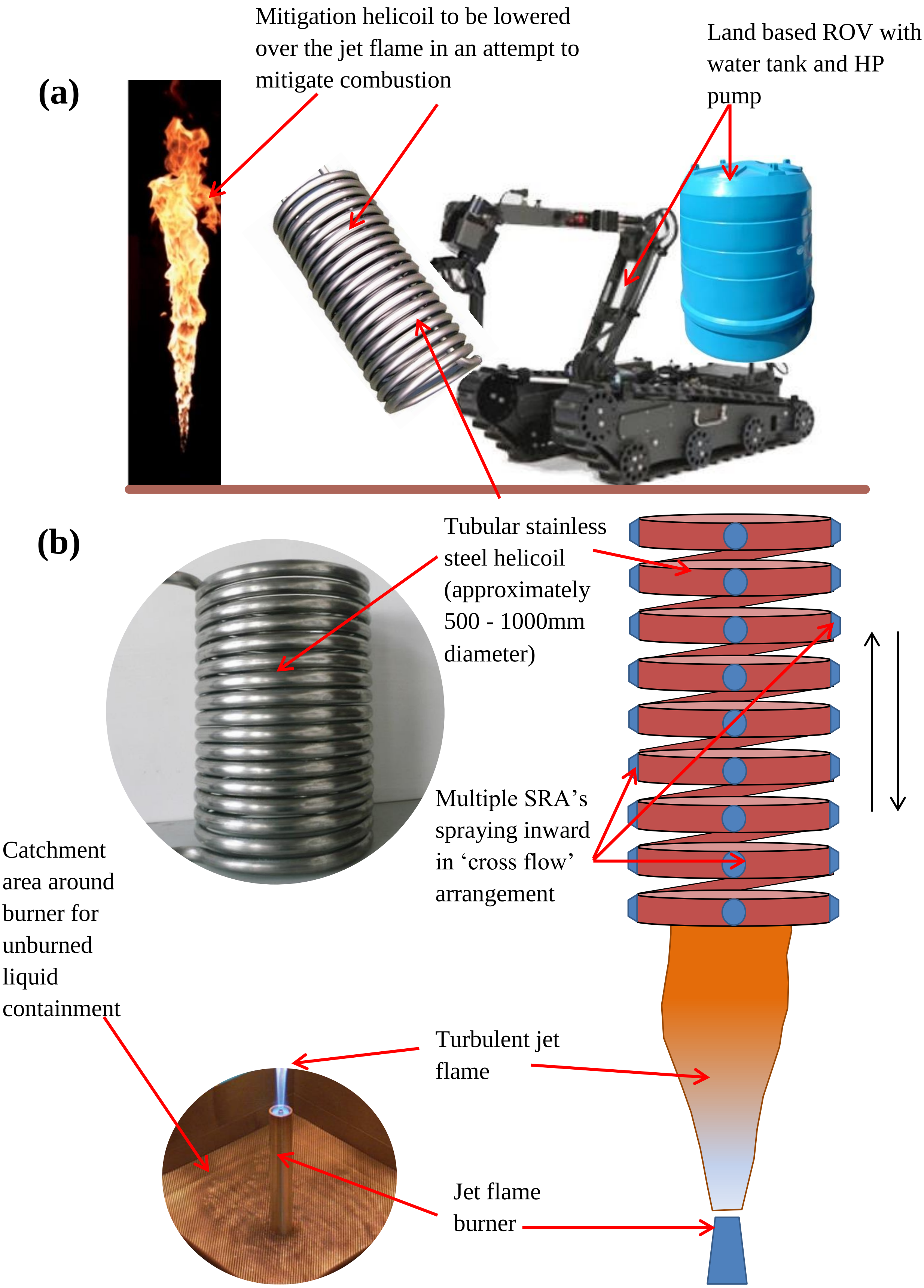

Figure 7.4 : (a) Concept for turbulent jet flame 'Helicoil Mitigation Apparatus' (HMA) with ROV vehicle and (b) proposed experimental set up.

REFERENCES

[1] Health and Safety Executive. *'A guide to the Control of Major Accident Hazards Regulations 1999 (as amended)'.*ISBN 978071766175X, HES Books. 2006

[2] Harris, R.J. and Wickens, M.J. *Understanding vapour cloud explosions – an experimental study*. The Institution of Gas Engineers, Communication 1408. 1989

[3] BBC Website. Retrieved 13th September 2012 from http:// www. bbc.co.uk /history/historic_figures/davy_humphrey.shtml

[4] ENARDO Flame Arrestor Technology. Retrieved 18th July 3013from www.enardo.com

[5] Smith, A.C. & Thimons, E.D. '*A Summary of U. S. Mine Fire Research'*. National Institute for Occupational Safety and Health (NIOSH), Pittsburgh, PA, USA

[6] Lewis, B & Von Elbe, G. *'Combustion, flames and explosion of gases'*. Academic Press, 1st Edition. 1951

[7] Kohse-Höinghaus, K., President of the Combustion institute. Retrieved from https://www.combustioninstitute.org/pages/page166.php on 14th February 2012

[8] Nasr, G.G. et al. *Natural Gas Engineering and Safety Challenges*. Springer (2014)

[9] Harrison, A.J. and Eyre, J.A., (1987) Combustion Science Technology 52, 91-106

[10] Patel, S., Ibrahim, S.S., Yahia, M.A. & Hargrave , G.K. *Investigation of premixed turbulent combustion in a semi-confined explosion chamber* Experimental Thermal and Fluid Science – 27 – 2003 (355-361)

[11] Internet research. GexCON. Accessed 11th December 2013. http://www.gexcon.com

[12] Clancey, V.J., 1972, *Diagnostic features of explosion damage*. 6th International Meeting of Forensic Sciences, Edinburgh.

[13] Fraunhofer-institut fur treib-und explosivstoffe 1983.ICT-Projektforschung 1983. Forschungsprogramm*"Prozeßgasfreisetzung - Explosion in der Gasfabrik und Auswirkungen von Druckwellen auf das Containment".*Ballonversuchezur Untersuchung der Deflagration von Wasserstoff / Luft-Gemischen (Abschlußbericht).Projektleiter: H.Pf¨ortner, Bearbeiter: H.Schneider, Dezember 1983

[14] Cronin, P., & Wickens, M. J. (1986).*A large scale experimental study of the conditions required to sustain high speed flame propagation in a flammable vapour cloud.* Solihull, UK:British Gas - Midland Research Station

[15] Coco, J.C., Editor *The 100 Largest Losses 1972 – 2001* : 20th*Edition – Large Property Damage Losses in the Hydrocarbon-Chemical Industries*. Marsh Risk Consulting Practice 2003

[16] Johnson, DM. *'The Potential for Vapour Cloud Explosions - Lessons from Buncefield'*. Loughborough, UK, GL Noble Denton

[17] Maremonti M, Russo G, Salzano E et al '*Post accident Analysis of Vapour Cloud Explosions In Fuel Storage Areas'* Trans IChemE 1999 77 (B) 360365

[18] Lechaudel JF and Mouilleau Y *'Assessment of an accidental vapour cloud explosion. A case study: Saint Herblain*, October the 7th 1991, FRANCE' Loss Prevention and Safety Promotion in the Process Industries 1995 1 377388

[19] Kletz in *'Will cold petrol explode in the open air'*, (The Chemical Engineer, June 1986, IChemE)

[20] Department for Employment (UK) *Official report and inquiry – The Flixborough Disaster, Report of the Court of Inquiry* – ISBN 011 361075 0. 1975

[21] Zabetakis, M. G., *Flammability characteristics of combustible gases and vapors*. US Bureau of Mines Bulletin 627. United States Bureau of the Interior, Washington, 1965

[22] The Arrhenius Equation. Retrieved 13th September 2012 https://www.boundless.com/chemistry/chemical-kinetics/activation-energy-and-temperature-dependence/the-arrhenius-equation/

[23] Bone and Wheeler. *The combination of hydrogen and oxygen in contact with hot surfaces*, Phil. Trans. A206, 1 (1906)

[24] Fristrom, R.M. and Westenberg, A.A. *Flame structure* McGraw-Hill, New York, 1965. xiv + 424 pp.

[25] Lewis, B & Von Elbe, G. *'Combustion, flames and explosion of gases'*. Academic Press, 3rd Edition. 3rd Edition. 1987

[26] Combustion terminology a disaster area" is the title of a paper by Bradley and Weinberg (1991)

[27] Michelson, W.: Annalen der Physik und Chemie, Volume XXXVII, 1 (1889).

[28] Coward, H.F. and Hartwell, F.J.: Journal of the Chemical Society (London), p. 2676, (1932).

[29] Michelson, W.: Annalen der Physik und Chemie, Volume XXXVII, 1 (1889).

[30] Gouy, G.L.: Annales de Chimie et de Physique, 5th Series, Volume XVII, 27 (1879)

[31] Stevens, F.W.: Journal of the American Chemical Society. 50, 3244 (1928).

[32] Andrews, G.E. and Bradley, D, The burning velocity of methane-air mixtures, Combustion and flame, 19, 275. 1972

[33] M. E and L. Chatelier, “No Titl,” *Ann. Mines*, vol. 4, pp. 379–568, 1883

[34] Zeldovich number. Internet research. Retrieved 13th September 2012 http://www.encyclopediaofmath.org/index.php/Activation_energy

[35] Andrews, G.E. and Bradley, D. The burning velocity of methane-air mixtures, Combustion and flame, 19, 275. (1972)

[36] Gottgen, J. et al. Approximations of burning velocities and flame thickness of lean hydrogen, methane, ethylene, acetylene and propane flames 24th symposium on combustion, 129. 1992

[37] ZND theory : Internet research. Accessed 9th December 2013. http://en.wikipedia.org/wiki/ZND_detonation_model

[38] Bollinger, L.E. et al *Experimental measurements and theoretical analysis of detonation induction distances*, ARS Journal, May 1961, pp 588-595.

[39] HSE-OTH 94 463. Prepared by the University College of Wales. *An investigation of factors of relevance during explosion suppression by water sprays.* HMSC 1996 ISBN 0-7176-1118-3

[40] Herterich, A.O. *Library of the science of fire protection and related issues*. Huthig Publishing. Heidleberg 1960.

[41] Keleta, A. *The effect of drop size on extinguishing effectiveness of a water spray*. Archiwum Combustion V6 #34. 1986

[42] Marioff Hi-Fog. Internet research. Accessed 11th December 2013. http://www.marioff.com/fire-protection/hi-fogr-system-components/spray-heads

[43] Spalding, D.B. *A theory of inflammability limits and flame quenching*. Communicated by Linnett, J.W., FRS – Received 31st October 1956

[44] Bray, K.N.C., *Suspension of explosions by water sprays*. Presentation at the 12th UKELG at MRS 1991

[45] Brenton, J.R. and Thomas, G.O. (1992) *Investigations into factors controlling the local extinction of flames by water droplets*. ICHEME Research event 1992.

[46] Bott, D.M., *The effect of water addition on stretch extinction of turbulent flames*, *Thesis*. Institute of Mechanical Engineering, University of Cambridge, 1991

[47] Nasr, G.G. et al. *Industrial Sprays and Atomisation Course notes.* Spray Research Group (SRG). 2012.

[48] Nasr, G.G.et al. *Industrial Sprays and Atomisation: Design, Analysis and Application.* ISBN 10: 1849968756 ISBN 13: 9781849968751. Springer 2010

[49] Lefebvre, A.H. *Atomization and Sprays.* CRC Press 1988

[50] Fraser and Eisenklam. Internet research. *http://onlinelibrary.wiley.com/* Accessed 15th December 2013

[51] Stewart, J.A. *Design and development of a novel spill return atomiser (SRA) disinfection system for healthcare environments.* PhD thesis, University of Salford 2011.

[52] Internet search. *http://www.lulusoso.com/products/Diesel-Engine-Fuel-Injector.html.* Accessed 28th June 2012.

[53] Nasr, G.G. et al. *A new fine spray, low flow rate, spill return swirl atomiser.* IMechE, Vol. 255 Part C;J. Mechanical Engineering Science. 24th August 2010.

[54] Internet search. *http://www.slcfd.com/sprinklerfacts.htm*. 24th August 2011.

[55] Internet search. *http://www.jdultrasonics.co.uk/.* 24th August 2011.

[56] Internet search. *http://www.lechler.de/Products/Environmental-Technologies/Gas-Conditioning/Overview-Nozzles/Spillback-Nozzles/cbbnd_AAABwCMAAAEy.t0N2ABm-en_US*

[57] Internet search. *http://www.dantecdynamics.com/.* Accessed 24th August 2011.

[58] British Gas | MRS | 5325 | *Preliminary investigations of methods of mitigating gas explosion overpressures*. July 1990 | Project M08411

[59] Grant, S.E. Health and Safety Laboratory (HSL), Buxton, England. *CFD modelling of water spray barriers.* HSL/2006/79. (2006)

[60] Thomas, G.O. *On the conditions required for explosion mitigation by water sprays.* Trans I Chem:Part B – Process Safety and Environmental Protection Vol. 78p.p. 339 – 354 (2000)

[61] Sapko, M., Furno, A., and Kuchta, J.M., *Quenching Methane-Air Ignitions with Water Sprays* U.S. Bureau of Mines, R.I. 8214, 1977.

[62] Kumm, E.L. *Calculations on the evaporation rate of sprays in rapidly moving gases.* Report AL916 (1949), North American Aviation Inc Aerophysics Laboratory, Project MX-770

[63] Keenan, W.A. and Wager, P.C., *Mitigation of Confined Explosion Effects by Placing Water in Proximity of Explosives*, 25th DoD Explosives Safety Seminar, Anaheim, CA, Aug. 18-20, 1992.

[64] United Nations Environment Programme (2000) *The Montreal protocol on substances that deplete the ozone layer*. ISBN: 92-807-1888-6 (2000)

[65] Van Wingerden, K., et al. *The influence of water sprays on gas explosions.* 27th October 1995. J. Loss Prevention. Process Industries, 1995, Volume 8, No.2.

[66] Van Wingerden, K and Langa, H. (1997) *New Aspects of the effect of water sprays on gas explosions in offshore rigs*, Paper presented at ERA conference Fire & Blast Engineering, 19th November, London

[67] ATEX Hot water advanced inerting system (HWAIT). Accessed on 8th January 2014. http://www.explosionhazards.co.uk.

[68] Williams, F.A. *On the assumptions underlying droplet vaporisation and combustion theories*. Journal of Chem. Physics, vol 33, no. 1, July 1960

[69] Bjorkhaug et al. *Experimental investigation of the effect of water deluge on gas explosions in a 10 metre radial vessel*. Christian Michelsen Institute Report. CMI-90-F25072 (company confidential) 1990

[70] Kuo, K. *Principles of combustion*, Wiley, New York, 1986

[71] Lane, W.R. Industrial Engineering and Chem. 1951, 43(6), 1312 – 1317

[72] Lentati A. M. and Chelliah, K. H., 1999, *Dynamics of water droplets in counter flow field and their effect on flame extinction,* Combustion and Flame 155:158-179

[73] UKOOA and HSE (2003) *Fire and explosion guidance, part 1: Avoidance and mitigation of explosions,* Issue 1, October 2003

[74] Health and Safety Executive. (1995) *Electrostatic hazards associated with water deluge and explosion suppression systems offshore.* HSE books, OTO 95 026, 1995.

[75] Van Wingerden, K. and Wilkins, B.A. (1995), *The influence of water spray on gas explosions, Part 1* : Water spray generated turbulence, J.Loss prev. Process Ind.

[76] Internet search. http://www.canon.co.uk/For_Home/Product_Finder/ Cameras/Digital_SLR/. Accessed 11th July 2014

[77] Internet search. http://kenro.co.uk/products/kenro-anti-reflect-spray-full-matt/. Accessed 11th July 2014

[78] Internet search. *http://www.engineeringtoolbox.com/ansi-steel-pipes-d_305.html.* 11th July 2014

[79] Internet search. *http://www.ebay.co.uk/itm/Champion-25-1-2-inch-NPT-Spark-Plug-Hit-Miss-Maytag-/110653147946. 11th July 2014*

[80] Internet search. *https://www.google.co.uk/search?q=80mm,+rapid+acting,+high+temperature+rated,+solenoid+valve&espv*. Accessed 19th July 2014

[81] Internet search. *http://shop.panasonic.com/shop/model/HDC-TM900K*. Accessed 19th July 2014

[82] Internet search. *http://store.griffintechnology.com/powermate*. Accessed 19th July 2014

[83] Internet search. *http://www.gmiuk.com/product/gascoseeker-2-500/*. Accessed 19th September 2014

[84] Internet search. *http://www.omega.com/pptst/iNET-400_Series.html*. Accessed 19th September 2014

[85] Nourian, A. *Next generation of consumer aerosol valve design using inert gases.* Proceedings of the Institution of Mechanical Engineers, Part C: Journal of Mechanical Engineering Science 0954406214559998, first published on November 17, 2014

[86] Internet search. *http://www.omega.com/pptst/MM-PX409_Series.html*. Accessed 19th September 2014

[87] Ferrara, G.,et al. *Venting of premixed gas explosions with a relief pipe of the same area as the vent.* ' Proceedings of the European Combustion Meeting ECM2005 (CD format), Louvain-la-Neuve, Belgium. Paper #213, April 2005.

[88] Kasmani, R. M, et al. *Self Accelerating Gas Flames in Large Vented Explosion Volumes That are Not Accounted for in Current Vent Design Correlations.* Proceedings of the 2ndInternational Conference on Safety & Environment in Process Industry, Naples,Italy, May 2006.

[89] Willacy, S. K., et al. *Ignition of Stratified Propane-Air Explosions in a Duct Vented Geometry: Effect of Concentration, Ignition and Injection Position* IChemE B: Process Safety and Environmental Protection, 2007,85(B2), pp153-161

[90] Kaesemann and Fahlenkamp. *The Meaning of Droplet-Droplet Interaction for the Wet Flue-Gas Cleaning Process.* Chemical Engineering and Technology. Volume 25, Issue 7, pages 739–742, 9 July 2002

[91] Rasbash, D.J., 1962, *The Extinction of Fires by Water Sprays*, Fire Research Abstract Review, Vol. 4, No. 1, pp. 28-52.

[92] Mawhinney J.R and Back, G.G., 2000 *Water Mist Fire Suppression Systems*, SFPE handbook, 3rd edition, pp. 4-311.

[93] Rayer, Q.G., 2001, *Computational Fluid Dynamics Guidelines for Best Working Practice*, NAFEMS international Journal of CFD case studies, vol 3, July.

[94] Schiller, L and Naumann, A., 1933. *Uber die grundlegenden berechnungen bei der schwerkraftaufbereitung*. Zeitung des vereins deutscher ingenieure, 77- 318.

[95] Ranz, W, E ad Marshall W,R., 1952, Chem. Eng. Prog 48, pp. 141.

[96] Ranz, W, E ad Marshall W,R., 1952, Chem. Eng. Prog 48, pp. 173.

[97] Pilch, M and Erdman, C.A., 1987, *Use of Breakup Time Data and Velocity History Data to Predict the Maximum Size of Stable Fragments for Acceleration-Induced Breakup of a Liquid Drop,* Int. J. Multiphase Flow, Vol. 13, No. 6, pp. 741-757.

[98] O'Rourke, P.J and Amsden, A.A., 1987, *The TAB Method for Numerical Calculation of Spray Droplet Breakup*, SAE Technical Paper 872089, 1987.

[99] Magnussen, B., 1981, *On the Structure of Turbulence and a Generalized Eddy Dissipation Concept for Chemical Reaction in Turbulent Flow*. 19th AIAA Aerospace Science Meeting. St Louis, Missouri, USA.

[100] Magnussen, B. F., B. H. Hjertager, J. G. Olsen and D. Bhaduri (1979). *Effects of Turbulent Structure and Local Concentrations on Soot Formation and Combustion in C2H2 Diffusion Flames*, Symposium (International) on Combustion 17(1): pp1383 - 1393.

[101] Hinze, J. O., 1975, T*urbulence*, McGraw-Hill Publishing Co., New York.

[102] Launder, B.E and Spalding, D.B., 1974, *The Numerical Computation of Turbulent Flows*, Comp Meth Appl Mech Eng, vol. 3, pp. 269-289.

[103] Yakhot, V and Orzag, S. A., 1986, *Renormalization Group Analysis of Turbulence. I. Basic Theory*, J. Science and Computing, 1, 3.

[104] Yakhot, V and Smith, L. M., 1992, *The Renormalization Group the Epsilon-Expansion and Derivation of Turbulence Models*, J. Science and Computing, 7,35.

[105] Yakhot, V., Orszag, S.A., Tangham, S., Gatski, T. B and Speciale, C.G., 1992, *Development of Turbulence Models for Shear Flows by a Double Expansion Technique*, Phys. Fluids, vol. 7, pp. 1510-1520

[106] Speziale, C.G., Sarkar, S and Gatski, T.B., 1991, *Modelling the Pressure- Strain Correlation of Turbulence*, J. Fluid Mech., 227, pp. 245-272.

LIST OF APPENDICES

Accompanying CD (VOLUME III)

Accompanying CD (VOLUME III)

Mitigation of Gas and Vapour Cloud Explosions using Fine Water Sprays

Volume III of III

By

Stephen Andrew Johnston, M.Sc. MIGEM

Submitted in accordance with the requirements for the degree of Doctor of Philosophy

Department of Gas and Petroleum Engineering
School of Computing, Science and Engineering
University of Salford

February 2015

APPENDIX 1

JOURNAL PAPER

A1.1 Moratorium and journal paper options

Due to the confidential sensitivity and novelty of some of the results and findings contained within this thesis, a decision has been made by the University of Salford to embargo the entire content of this study for the reasons listed, whereby this research:-

i. is highly commercially sensitive
ii. contains several other ideas for progressive study and commercial development

A moratorium has therefore been imposed on the content of this thesis for an initial period of two years, with an option to extend for additional single years, up to a maximum of five years. In view of the above restrictions, the author has not had the opportunity to publish any journal papers or extracts from this study. However, a journal paper has been produced in **draft form** in readiness for submission, following authorisation from the University. For convenience, some of the Figures and Tables have been copied directly from the main thesis and will be re-sized and re-formatted prior to final submission of the final journal paper.

An initial survey was conducted to ascertain an appropriate publication platform, with attention given to the readership audience and journal impact factor. Three publications were considered, each with a suitable distribution in combustion science, fire control and process engineering. The publications and impact their factors are summarised below:-

Progress in Energy and Combustion Science

Source Normalized Impact per Paper (SNIP):	12.573
SCImago Journal Rank (SJR):	8.490
Impact Factor:	16.909
5-Year Impact Factor:	20.320

Fire Safety Journal

Source Normalized Impact per Paper (SNIP):	2.869
SCImago Journal Rank (SJR):	0.937
Impact Factor:	1.063
5-Year Impact Factor:	1.751

Process Safety and Environmental Protection

Source Normalized Impact per Paper (SNIP):	1.838
SCImago Journal Rank (SJR):	0.957
Impact Factor:	1.829
5-Year Impact Factor:	1.912

Due to the high level impact factor associated with the publication, **Process in Energy and Combustion Science**, the attached draft journal paper (see PDF copy in Appendix 10 folder) was produced in line with the author information pack (see also PDF copy in Appendix 10 folder).

PROGRESS IN ENERGY AND COMBUSTION SCIENCE

An International Review Journal

AUTHOR INFORMATION PACK

TABLE OF CONTENTS

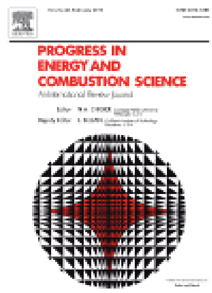

ISSN: 0360-1285

DESCRIPTION

Conservation of energy requires an efficient combustion of fossil fuels, and the protection of the environment demands a limitation of the pollutants emitted from combustion systems. *Progress in Energy and Combustion Science* contains articles by internationally recognized authors in the fields of **combustion**, **flames**, **fuel science** and **technology** and **energy studies**.

Each volume contains a number of specially commissioned review articles on a specific topic, which provides the reader with an orderly and concise survey of a particular aspect of combustion and energy. The length of the articles allows authors to discuss their subjects more fully and comprehensively than can be undertaken in papers reporting original work. These review articles provide an opportunity for research workers to become usefully informed in fields other than their own. They are of use to students seeking a review of a particular subject, together with a comprehensive bibliography. Certain volumes are also aimed at engineers working in government and industrial research establishments, seeking practical solutions to problems in the fields of energy and pollution.

Benefits to authors

We also provide many author benefits, such as free PDFs, a liberal copyright policy, special discounts on Elsevier publications and much more. Please click here for more information on our author services.

Please see our Guide for Authors for information on article submission. If you require any further information or help, please visit our support pages: http://support.elsevier.com

AUDIENCE

Energy and Combustion Libraries, University Libraries for energy, chemistry, engineering, fuel science, Industry involved in aeroengines, boilers, automobile engines, processing, fire control.

IMPACT FACTOR

2013: 16.909 © Thomson Reuters Journal Citation Reports 2014

ABSTRACTING AND INDEXING

APILIT
Aerospace Database
American Petroleum Institute Abstracts
Applied Mechanics Reviews
Compendex
Current Contents
EI Compendex Plus
Ei Engineering
Energy Science and Technology
Environmental Periodicals Bibliography
Fuel and Energy Abstracts
GeoRef
OCLC Contents Alert
PASCAL/CNRS
Referativnyi Zhurnal VINTI-RAN (Russian Academy of Sciences)
Science Citation Index
Scisearch
Web of Science
Engineering Information Database EnCompass LIT (Elsevier)
Scopus
Academic Search (EBSCO)

EDITORIAL BOARD

GUIDE FOR AUTHORS

Introduction

Conservation of energy requires an efficient combustion of fossil fuels, and the protection of the environment demands a limitation of the pollutants emitted from combustion systems. *Progress in Energy and Combustion Science* contains articles by internationally recognized authors in the fields of combustion, flames, fuel science and technology and energy studies. Each volume contains a number of specially commissioned review articles on a specific topic, which provides the reader with an orderly and concise survey of a particular aspect of combustion and energy. The length of the articles allows authors to discuss their subjects more fully and comprehensively than can be undertaken in papers reporting original work. These review articles provide an opportunity for research workers to become usefully informed in fields other than their own. They are of use to students seeking a review of a particular subject, together with a comprehensive bibliography. Certain volumes are also aimed at engineers working in government and industrial research establishments, seeking practical solutions to problems in the fields of energy and pollution.

Types of Contributions

Full-length review articles by internationally recognised authorities in the fields of combustion, flames, fuel science and technology, and energy studies. The majority of articles are commissioned by the Editor; direct submissions may be considered but the Editor should be contacted prior to submission.

Page charges

This journal has no page charges.

BEFORE YOU BEGIN

Ethics in publishing

For information on Ethics in publishing and Ethical guidelines for journal publication see http://www.elsevier.com/publishingethics and http://www.elsevier.com/journal-authors/ethics.

Conflict of interest

All authors are requested to disclose any actual or potential conflict of interest including any financial, personal or other relationships with other people or organizations within three years of beginning the submitted work that could inappropriately influence, or be perceived to influence, their work. See also http://www.elsevier.com/conflictsofinterest. Further information and an example of a Conflict of Interest form can be found at: http://help.elsevier.com/app/answers/detail/a_id/286/p/7923.

Submission declaration and verification

Submission of an article implies that the work described has not been published previously (except in the form of an abstract or as part of a published lecture or academic thesis or as an electronic preprint, see http://www.elsevier.com/postingpolicy), that it is not under consideration for publication elsewhere, that its publication is approved by all authors and tacitly or explicitly by the responsible authorities where the work was carried out, and that, if accepted, it will not be published elsewhere in the same form, in English or in any other language, including electronically without the written consent of the copyright-holder. To verify originality, your article may be checked by the originality detection service CrossCheck http://www.elsevier.com/editors/plagdetect.

Changes to authorship

This policy concerns the addition, deletion, or rearrangement of author names in the authorship of accepted manuscripts:

Before the accepted manuscript is published in an online issue: Requests to add or remove an author, or to rearrange the author names, must be sent to the Journal Manager from the corresponding author of the accepted manuscript and must include: (a) the reason the name should be added or removed, or the author names rearranged and (b) written confirmation (e-mail, fax, letter) from all authors that they agree with the addition, removal or rearrangement. In the case of addition or removal of authors, this includes confirmation from the author being added or removed. Requests that are not sent by the corresponding author will be forwarded by the Journal Manager to the corresponding author, who must follow the procedure as described above. Note that: (1) Journal Managers will inform the Journal Editors of any such requests and (2) publication of the accepted manuscript in an online issue is suspended until authorship has been agreed.

After the accepted manuscript is published in an online issue: Any requests to add, delete, or rearrange author names in an article published in an online issue will follow the same policies as noted above and result in a corrigendum.

Article transfer service

This journal is part of our Article Transfer Service. This means that if the Editor feels your article is more suitable in one of our other participating journals, then you may be asked to consider transferring the article to one of those. If you agree, your article will be transferred automatically on your behalf with no need to reformat. Please note that your article will be reviewed again by the new journal. More information about this can be found here: http://www.elsevier.com/authors/article-transfer-service.

Copyright

This journal offers authors a choice in publishing their research: Open access and Subscription.

For subscription articles

Upon acceptance of an article, authors will be asked to complete a 'Journal Publishing Agreement' (for more information on this and copyright, see http://www.elsevier.com/copyright). An e-mail will be sent to the corresponding author confirming receipt of the manuscript together with a 'Journal Publishing Agreement' form or a link to the online version of this agreement.

Subscribers may reproduce tables of contents or prepare lists of articles including abstracts for internal circulation within their institutions. Permission of the Publisher is required for resale or distribution outside the institution and for all other derivative works, including compilations and translations (please consult http://www.elsevier.com/permissions). If excerpts from other copyrighted works are included, the author(s) must obtain written permission from the copyright owners and credit the source(s) in the article. Elsevier has preprinted forms for use by authors in these cases: please consult http://www.elsevier.com/permissions.

For open access articles

Upon acceptance of an article, authors will be asked to complete an 'Exclusive License Agreement' (for more information see http://www.elsevier.com/OAauthoragreement). Permitted reuse of open access articles is determined by the author's choice of user license (see http://www.elsevier.com/openaccesslicenses).

Retained author rights

As an author you (or your employer or institution) retain certain rights. For more information on author rights for:

Subscription articles please see http://www.elsevier.com/journal-authors/author-rights-and-responsibilities.

Open access articles please see http://www.elsevier.com/OAauthoragreement.

Role of the funding source

You are requested to identify who provided financial support for the conduct of the research and/or preparation of the article and to briefly describe the role of the sponsor(s), if any, in study design; in the collection, analysis and interpretation of data; in the writing of the report; and in the decision to submit the article for publication. If the funding source(s) had no such involvement then this should be stated.

Funding body agreements and policies

Elsevier has established agreements and developed policies to allow authors whose articles appear in journals published by Elsevier, to comply with potential manuscript archiving requirements as specified as conditions of their grant awards. To learn more about existing agreements and policies please visit http://www.elsevier.com/fundingbodies.

Open access

This journal offers authors a choice in publishing their research:

Open access

• Articles are freely available to both subscribers and the wider public with permitted reuse
• An open access publication fee is payable by authors or their research funder

Subscription

• Articles are made available to subscribers as well as developing countries and patient groups through our access programs (http://www.elsevier.com/access)
• No open access publication fee

All articles published open access will be immediately and permanently free for everyone to read and download. Permitted reuse is defined by your choice of one of the following Creative Commons user licenses:
Creative Commons Attribution (CC BY): lets others distribute and copy the article, to create extracts, abstracts, and other revised versions, adaptations or derivative works of or from an article (such as a translation), to include in a collective work (such as an anthology), to text or data mine the article, even for commercial purposes, as long as they credit the author(s), do not represent the author as endorsing their adaptation of the article, and do not modify the article in such a way as to damage the author's honor or reputation.
Creative Commons Attribution-NonCommercial-ShareAlike (CC BY-NC-SA): for non-commercial purposes, lets others distribute and copy the article, to create extracts, abstracts and other revised versions, adaptations or derivative works of or from an article (such as a translation), to include in a collective work (such as an anthology), to text and data mine the article, as long as they credit the author(s), do not represent the author as endorsing their adaptation of the article, do not modify the article in such a way as to damage the author's honor or reputation, and license their new adaptations or creations under identical terms (CC BY-NC-SA).
Creative Commons Attribution-NonCommercial-NoDerivs (CC BY-NC-ND): for non-commercial purposes, lets others distribute and copy the article, and to include in a collective work (such as an anthology), as long as they credit the author(s) and provided they do not alter or modify the article.

To provide open access, this journal has a publication fee which needs to be met by the authors or their research funders for each article published open access.
Your publication choice will have no effect on the peer review process or acceptance of submitted articles.

The open access publication fee for this journal is **$3,300**, excluding taxes. Learn more about Elsevier's pricing policy: http://www.elsevier.com/openaccesspricing.

Language (usage and editing services)
Please write your text in good English (American or British usage is accepted, but not a mixture of these). Authors who feel their English language manuscript may require editing to eliminate possible grammatical or spelling errors and to conform to correct scientific English may wish to use the English Language Editing service available from Elsevier's WebShop (http://webshop.elsevier.com/languageediting/) or visit our customer support site (http://support.elsevier.com) for more information.

Submission
Our online submission system guides you stepwise through the process of entering your article details and uploading your files. The system converts your article files to a single PDF file used in the peer-review process. Editable files (e.g., Word, LaTeX) are required to typeset your article for final publication. All correspondence, including notification of the Editor's decision and requests for revision, is sent by e-mail.

Submission Address
Please submit your article via http://ees.elsevier.com/pecs

Referees
Please submit the names and institutional e-mail addresses of several potential referees. For more details, visit our Support site. Note that the editor retains the sole right to decide whether or not the suggested reviewers are used.

PREPARATION

LaTeX
You are recommended to use the Elsevier article class *elsarticle.cls* (http://www.ctan.org/tex-archive/macros/latex/contrib/elsarticle) to prepare your manuscript and BibTeX (http://www.bibtex.org) to generate your bibliography.
For detailed submission instructions, templates and other information on LaTeX, see http://www.elsevier.com/latex.

Article structure

Subdivision - numbered sections
Divide your article into clearly defined and numbered sections. Subsections should be numbered 1.1 (then 1.1.1, 1.1.2, ...), 1.2, etc. (the abstract is not included in section numbering). Use this numbering also for internal cross-referencing: do not just refer to 'the text'. Any subsection may be given a brief heading. Each heading should appear on its own separate line.

Introduction
State the objectives of the work and provide an adequate background, avoiding a detailed literature survey or a summary of the results.

Theory/calculation
A Theory section should extend, not repeat, the background to the article already dealt with in the Introduction and lay the foundation for further work. In contrast, a Calculation section represents a practical development from a theoretical basis.

Conclusions
The main conclusions of the study may be presented in a short Conclusions section, which may stand alone or form a subsection of a Discussion or Results and Discussion section.

Essential title page information
• ***Title.*** Concise and informative. Titles are often used in information-retrieval systems. Avoid abbreviations and formulae where possible.
• ***Author names and affiliations.*** Where the family name may be ambiguous (e.g., a double name), please indicate this clearly. Present the authors' affiliation addresses (where the actual work was done) below the names. Indicate all affiliations with a lower-case superscript letter immediately after the author's name and in front of the appropriate address. Provide the full postal address of each affiliation, including the country name and, if available, the e-mail address of each author.
• ***Corresponding author.*** Clearly indicate who will handle correspondence at all stages of refereeing and publication, also post-publication. **Ensure that phone numbers (with country and area code) are provided in addition to the e-mail address and the complete postal address. Contact details must be kept up to date by the corresponding author.**
• ***Present/permanent address.*** If an author has moved since the work described in the article was done, or was visiting at the time, a 'Present address' (or 'Permanent address') may be indicated as a footnote to that author's name. The address at which the author actually did the work must be retained as the main, affiliation address. Superscript Arabic numerals are used for such footnotes.

Abstract
A concise and factual abstract is required. The abstract should state briefly the purpose of the research, the principal results and major conclusions. An abstract is often presented separately from the article, so it must be able to stand alone. For this reason, References should be avoided, but if essential, then cite the author(s) and year(s). Also, non-standard or uncommon abbreviations should be avoided, but if essential they must be defined at their first mention in the abstract itself.

Keywords
Immediately after the abstract, provide a maximum of 6 keywords, using American spelling and avoiding general and plural terms and multiple concepts (avoid, for example, 'and', 'of'). Be sparing with abbreviations: only abbreviations firmly established in the field may be eligible. These keywords will be used for indexing purposes.

Immediately after the abstract, provide a maximum of 6 keywords, using American spelling and avoiding general and plural terms and multiple concepts (avoid, for example, "and", "of"). Be sparing with abbreviations: only abbreviations firmly established in the field may be eligible. These keywords will be used for indexing purposes.

Abbreviations
Define abbreviations that are not standard in this field in a footnote to be placed on the first page of the article. Such abbreviations that are unavoidable in the abstract must be defined at their first mention there, as well as in the footnote. Ensure consistency of abbreviations throughout the article.

Acknowledgements
Collate acknowledgements in a separate section at the end of the article before the references and do not, therefore, include them on the title page, as a footnote to the title or otherwise. List here those individuals who provided help during the research (e.g., providing language help, writing assistance or proof reading the article, etc.).

Units
Follow internationally accepted rules and conventions: use the international system of units (SI). If other units are mentioned, please give their equivalent in SI.

Math formulae
Please submit math equations as editable text and not as images. Present simple formulae in line with normal text where possible and use the solidus (/) instead of a horizontal line for small fractional terms, e.g., X/Y. In principle, variables are to be presented in italics. Powers of e are often more conveniently denoted by exp. Number consecutively any equations that have to be displayed separately from the text (if referred to explicitly in the text).

Footnotes
Footnotes should be used sparingly. Number them consecutively throughout the article. Many word processors can build footnotes into the text, and this feature may be used. Otherwise, please indicate the position of footnotes in the text and list the footnotes themselves separately at the end of the article. Do not include footnotes in the Reference list.

Artwork
Electronic artwork
General points
• Make sure you use uniform lettering and sizing of your original artwork.
• Embed the used fonts if the application provides that option.
• Aim to use the following fonts in your illustrations: Arial, Courier, Times New Roman, Symbol, or use fonts that look similar.
• Number the illustrations according to their sequence in the text.
• Use a logical naming convention for your artwork files.
• Provide captions to illustrations separately.
• Size the illustrations close to the desired dimensions of the printed version.
• Submit each illustration as a separate file.
A detailed guide on electronic artwork is available on our website:
http://www.elsevier.com/artworkinstructions
You are urged to visit this site; some excerpts from the detailed information are given here.
Formats
If your electronic artwork is created in a Microsoft Office application (Word, PowerPoint, Excel) then please supply 'as is' in the native document format.
Regardless of the application used other than Microsoft Office, when your electronic artwork is finalized, please 'Save as' or convert the images to one of the following formats (note the resolution requirements for line drawings, halftones, and line/halftone combinations given below):
EPS (or PDF): Vector drawings, embed all used fonts.
TIFF (or JPEG): Color or grayscale photographs (halftones), keep to a minimum of 300 dpi.
TIFF (or JPEG): Bitmapped (pure black & white pixels) line drawings, keep to a minimum of 1000 dpi.
TIFF (or JPEG): Combinations bitmapped line/half-tone (color or grayscale), keep to a minimum of 500 dpi.
Please do not:
• Supply files that are optimized for screen use (e.g., GIF, BMP, PICT, WPG); these typically have a low number of pixels and limited set of colors;
• Supply files that are too low in resolution;
• Submit graphics that are disproportionately large for the content.

Color artwork
Please make sure that artwork files are in an acceptable format (TIFF (or JPEG), EPS (or PDF), or MS Office files) and with the correct resolution. If, together with your accepted article, you submit usable color figures then Elsevier will ensure, at no additional charge, that these figures will appear in color online (e.g., ScienceDirect and other sites) regardless of whether or not these illustrations are reproduced in color in the printed version. **For color reproduction in print, you will receive information regarding the costs from Elsevier after receipt of your accepted article**. Please indicate your preference for color: in print or online only. For further information on the preparation of electronic artwork, please see http://www.elsevier.com/artworkinstructions.
Please note: Because of technical complications that can arise by converting color figures to 'gray scale' (for the printed version should you not opt for color in print) please submit in addition usable black and white versions of all the color illustrations.

Figure captions
Ensure that each illustration has a caption. Supply captions separately, not attached to the figure. A caption should comprise a brief title (**not** on the figure itself) and a description of the illustration. Keep text in the illustrations themselves to a minimum but explain all symbols and abbreviations used.

Tables
Please submit tables as editable text and not as images. Tables can be placed either next to the relevant text in the article, or on separate page(s) at the end. Number tables consecutively in accordance with their appearance in the text and place any table notes below the table body. Be sparing in the use of tables and ensure that the data presented in them do not duplicate results described elsewhere in the article. Please avoid using vertical rules.

References
Citation in text
Please ensure that every reference cited in the text is also present in the reference list (and vice versa). Any references cited in the abstract must be given in full. Unpublished results and personal communications are not recommended in the reference list, but may be mentioned in the text. If these references are included in the reference list they should follow the standard reference style of the journal and should include a substitution of the publication date with either 'Unpublished results' or 'Personal communication'. Citation of a reference as 'in press' implies that the item has been accepted for publication.

References in a special issue
Please ensure that the words 'this issue' are added to any references in the list (and any citations in the text) to other articles in the same Special Issue.

Reference style
Text: Indicate references by number(s) in square brackets in line with the text. The actual authors can be referred to, but the reference number(s) must always be given.
List: Number the references (numbers in square brackets) in the list in the order in which they appear in the text.
Examples:
Reference to a journal publication:
[1] Van der Geer J, Hanraads JAJ, Lupton RA. The art of writing a scientific article. J Sci Commun 2010;163:51–9.
Reference to a book:
[2] Strunk Jr W, White EB. The elements of style. 4th ed. New York: Longman; 2000.
Reference to a chapter in an edited book:
[3] Mettam GR, Adams LB. How to prepare an electronic version of your article. In: Jones BS, Smith RZ, editors. Introduction to the electronic age, New York: E-Publishing Inc; 2009, p. 281–304.
Note shortened form for last page number. e.g., 51–9, and that for more than 6 authors the first 6 should be listed followed by 'et al.' For further details you are referred to 'Uniform Requirements for Manuscripts submitted to Biomedical Journals' (J Am Med Assoc 1997;277:927–34) (see also http://www.nlm.nih.gov/bsd/uniform_requirements.html).

AudioSlides
The journal encourages authors to create an AudioSlides presentation with their published article. AudioSlides are brief, webinar-style presentations that are shown next to the online article on ScienceDirect. This gives authors the opportunity to summarize their research in their own words and to help readers understand what the paper is about. More information and examples are available at http://www.elsevier.com/audioslides. Authors of this journal will automatically receive an invitation e-mail to create an AudioSlides presentation after acceptance of their paper.

Supplementary data
Elsevier accepts electronic supplementary material to support and enhance your scientific research. Supplementary files offer the author additional possibilities to publish supporting applications, high-resolution images, background datasets, sound clips and more. Supplementary files supplied will be published online alongside the electronic version of your article in Elsevier Web products, including ScienceDirect: http://www.sciencedirect.com. In order to ensure that your submitted material is directly usable, please provide the data in one of our recommended file formats. Authors should submit the material in electronic format together with the article and supply a concise and descriptive caption for each file. For more detailed instructions please visit our artwork instruction pages at http://www.elsevier.com/artworkinstructions.

Interactive plots

This journal encourages you to include data and quantitative results as interactive plots with your publication. To make use of this feature, please include your data as a CSV (comma-separated values) file when you submit your manuscript. Please refer to http://www.elsevier.com/interactiveplots for further details and formatting instructions.

Submission checklist

The following list will be useful during the final checking of an article prior to sending it to the journal for review. Please consult this Guide for Authors for further details of any item.

Ensure that the following items are present:

One author has been designated as the corresponding author with contact details:

• E-mail address
• Full postal address
• Phone numbers

All necessary files have been uploaded, and contain:

• Keywords
• All figure captions
• All tables (including title, description, footnotes)

Further considerations

• Manuscript has been 'spell-checked' and 'grammar-checked'
• References are in the correct format for this journal
• All references mentioned in the Reference list are cited in the text, and vice versa
• Permission has been obtained for use of copyrighted material from other sources (including the Web)
• Color figures are clearly marked as being intended for color reproduction on the Web (free of charge) and in print, or to be reproduced in color on the Web (free of charge) and in black-and-white in print
• If only color on the Web is required, black-and-white versions of the figures are also supplied for printing purposes

For any further information please visit our customer support site at http://support.elsevier.com.

AFTER ACCEPTANCE

Use of the Digital Object Identifier

The Digital Object Identifier (DOI) may be used to cite and link to electronic documents. The DOI consists of a unique alpha-numeric character string which is assigned to a document by the publisher upon the initial electronic publication. The assigned DOI never changes. Therefore, it is an ideal medium for citing a document, particularly 'Articles in press' because they have not yet received their full bibliographic information. Example of a correctly given DOI (in URL format; here an article in the journal *Physics Letters B*):

http://dx.doi.org/10.1016/j.physletb.2010.09.059

When you use a DOI to create links to documents on the web, the DOIs are guaranteed never to change.

Online proof correction

Corresponding authors will receive an e-mail with a link to our online proofing system, allowing annotation and correction of proofs online. The environment is similar to MS Word: in addition to editing text, you can also comment on figures/tables and answer questions from the Copy Editor. Web-based proofing provides a faster and less error-prone process by allowing you to directly type your corrections, eliminating the potential introduction of errors.

If preferred, you can still choose to annotate and upload your edits on the PDF version. All instructions for proofing will be given in the e-mail we send to authors, including alternative methods to the online version and PDF.

We will do everything possible to get your article published quickly and accurately. Please use this proof only for checking the typesetting, editing, completeness and correctness of the text, tables and figures. Significant changes to the article as accepted for publication will only be considered at this stage with permission from the Editor.It is important to ensure that all corrections are sent back to us in one communication. Please check carefully before replying, as inclusion of any subsequent corrections cannot be guaranteed. Proofreading is solely your responsibility.

Offprints

The corresponding author, at no cost, will be provided with a personalized link providing 50 days free access to the final published version of the article on ScienceDirect. This link can also be used for sharing via email and social networks. For an extra charge, paper offprints can be ordered via the offprint order form which is sent once the article is accepted for publication. Both corresponding and co-authors may order offprints at any time via Elsevier's WebShop (http://webshop.elsevier.com/myarticleservices/offprints). Authors requiring printed copies of multiple articles may use Elsevier WebShop's 'Create Your Own Book' service to collate multiple articles within a single cover (http://webshop.elsevier.com/myarticleservices/booklets).

AUTHOR INQUIRIES

You can track your submitted article at http://help.elsevier.com/app/answers/detail/a_id/89/p/8045/. You can track your accepted article at http://www.elsevier.com/trackarticle. You are also welcome to contact Customer Support via http://support.elsevier.com.

Contents lists available at ScienceDirect

Progress in Energy and Combustion Science

journal homepage: www.elsevier.com/locate/pecs

Mitigation of gas and vapour cloud explosions using fine water droplets

S A Johnston[1]

[1] Department of Gas and Petroleum Engineering, School of Computing, Science and Engineering, University of Salford, Manchester, UK.

Abstract

For the past fifty years or so there has been a great deal of interest in the use of water based explosion suppression systems, designed to mitigate or reduce the impact of thermal explosions and their consequential overpressures. Previous research has focused on the suppression and mitigation proficiency of existing or new water deluge systems, which deploy sprays containing droplets $200 \leq D_{32} \leq 1000\mu m$. Where a high speed flame propagates through a region of spray containing such droplets, the flow ahead of the flame will hydrodynamically break up the droplets into fine mist, which in turn will act as a heat sink in the flame, with resulting suppression. These previous studies concluded that in most cases existing deluge systems contributed to a global reduction in flame speed and subsequent damaging overpressures. This present study is focused on the mitigation of slow deflagrations with resulting speeds of ≤30m/s. A flame travelling at such low relative speeds will not possess the inertia to inflict secondary atomisation by hydrodynamic break up. An innovative high pressure atomiser known as a Spill Return Atomiser (SRA) was selected, which contained a unique swirl chamber and was originally developed for decontamination and disinfection. The efficient atomisation of the SRA produced fine sprays containing droplets, D_{32}, 15µm - 29µm. With droplets D_{32}, ≤30µm requiring impact velocities of approximately ≥142.83m/s to break up further, the flame speeds experienced in these trials of ≤30m/s would <u>not</u> have caused hydrodynamic break up of the droplets in the sprays. Therefore, due to the flame speeds and drop sizes utilised in this study, the droplets entering the flame front would have been in their original form. A configuration consisting of 4 x SRA's in cross flow (X/F) configuration, successfully and repeatedly, completely mitigated homogeneous methane-air mixtures throughout the whole flammable range E.R. $0.5 \leq \phi 1.0 \leq 1.69$ (5 - 15%), with flame speeds ranging from 5 - 30m/s.

Key words

Explosion mitigation, water spray nozzles, combustion suppression, water mist, fire and explosion, spill return atomiser (SRA)

Contents

1. Introduction

Regrettably gas and vapour cloud explosions will always occur. This is partly due to the reactivity and flammability of the species and the increased risk of likelihood caused by contributing several factors, including engineering and human failures. Many national and international studies have been carried out over time to attempt to explain the mechanisms leading up to such proceedings and to categorise these events.

Explosions are driven by the rate of expansion from reactant to product. This thermal expansion, which may normally be in the order of 1:8, can also produce expansions of 1:40 and may produce near and far field overpressures of up to 50 atmospheres, Nasr, G.G. *et al* [1].

For many new sites, including processing plants, refineries, oil and gas platforms etc., a high percentage of the risk regarding events leading up to an explosion can be reduced, simply by following appropriate design criteria. This is reinforced by providing an on-going safety risk management process and procedure, such as Control of Major Accident Hazards Regulations (COMAH) [2], which are statutory and enforceable in the UK.

In most instances there will be an opportunity to improve existing sites by altering site layout and design, or by installing third party mitigation processes, such as water deluge and explosion venting measures. The overall assessment process in determining the suitability of a mitigation system must ensure that the conditions that favour the occurrence of such explosive events are reduced to acceptable levels. Financial budgets must be set to allow for appropriate initial design measures or alterations to existing sites, with an on-going commitment to risk management and a continuous review process.

1.1 Previous studies

The use of water sprays in explosion suppression and mitigation research has been previously carried out by many authors including, the American Bureaux of Mines, British Gas, GexCon and the University of Aberystwyth. The focus of the previous work has been the employment of atomisers and sprays and their suitability in producing appropriate spray characteristics, with mean droplet sizes ($D_{32}\geq100\mu m$) and sufficient liquid volume flux (Table 1) required to mitigate or suppress high speed explosions with propagating flame speeds ranging from 100m/s - 2000m/s. The flame speeds used in the previous aforementioned research were generally representative of those associated with high loss incidents caused by flame acceleration and consequential high overpressures.

With accelerated flame speeds the blast wave ahead of the combustion wave can provide the dynamic forces required to break up the water droplets into much smaller diameters. Mitigation of the flame or suppression of combustion activity only occurred in previous work when the dynamic forces created by the blast wave were great enough to overcome the surface tension forces in the water droplets. Fine mists formed by the hydrodynamic breakup of the larger droplets could then progress through the flame.

Author(s)	Mean droplet size (μm)	Droplet density (various)
Sapko *et al*	56, 70 and 106	34.6, 43.3 and 68.8 kg/m^3
Van Wingerden *et al*	10	$234 g/m^3$ or 31.5% vol/vol
Cronin and Johnson	600 – 800	Fw 0.02 and 0.005%
US Navy Research	27 and 116	36 and 70 g/m^3
Catlin *et al*	600 – 800	Fw 0.02 and 0.005%
Zalosh and Bajpai	20 - 100	0.1to 1.0 kg/m^3

Table 1 : Typical representation of droplet densities reported in previous studies

Providing that there was adequate liquid volume flux (Q_f) and sufficient ‘residence time’ (t) for droplets in reaction zone of the flame to facilitate suppression or global mitigation of combustion, a high degree of success was reported. The previous studies exclusively concluded that water was found to be very effective in the suppression or mitigation of gas and vapour cloud explosions, even at supersonic flame speeds (or detonations) typically 1500m/s – 2000m/s.

In summarising some of the previous studies, Harris and Wickens [3] additionally highlighted significant areas of concern regarding water based mitigation systems:-

i. The turbulence caused by water spray momentum may be transferred into the unburned mixture, or the flame front, thus causing turbulence and an overall increase in local or global flame speeds.
ii. Accidental water ingress into electrical apparatus and switch gear may lead to an electrical spark, which may cause re-ignition of a flammable mixture, or even cause secondary fires.
iii. Water storage volumes need to be large enough to provide uninterrupted sprays for very long periods.

It has become evident that previous water spray mitigation research exclusively relied on the subsequent break up of water droplets into fine mist. To achieve this break up, the forces contained in the blast wave must be greater than the forces holding the droplets together in the first instance. In many instances, particularly when an explosion occurs in an unconfined area, overpressures may be as little as a few hundred Pascals (Pa), whereby water droplets would not initiate further break up, thus retaining their original geometry. Lane [4] presented the following relationship between droplet diameter and the critical velocity needed to overcome the intrinsic forces i.e. surface tension, which hold droplets together.

$$v_c^2\, d = 0.612\ m^3 s^{-2}$$

where v_c = the critical relative gas stream velocity for droplet break up ($m\ s^{-1}$)
d = the droplet diameter (µm)

Whereby, the surface tension of water is taken to be 73.10mN/m and the gas mixture density is assumed to be 1.2 kg/m^3. Lane's formula is consistent with a critical Weber number stated by many authors of 10 – 12 required for droplet break up.

This present study provides a unique and novel opportunity, in which very fine water droplets (D_{32}≤30µm) will be deployed from a specialist atomising system in an attempt to suppress, or mitigate slow moving propagating flames with speeds of ≤30m/s, with a typical representative flame front thickness of approximately 1mm, coupled with droplet residence times of about 0.03milliseconds (ms).

It is worth noting that at such low flame speeds the droplet sizes used in previous research of D_{32}≥100µm would simply pass through the flame, thus allowing the flame to continue to propagate at a finite speed or as in some cases may even cause the flame to accelerate further.

2. Apparatus, procedures and method of data processing

Within these investigations there were several experimental challenges and achievements, including the design and fabrication of new apparatus and rigs, qualitative and quantitative collection procedures and methods of data and imagery processing. It is worth noting that due to the specific intentions and requirements of this study, rig designs used in other investigations [3,5,6,7,8,9,10] would be ineffective if emulated in this present research. Additionally, due to the significant wealth of experimental research carried out in this study, the trials were subdivided into two distinct groups. These are the '*Cold trials' and the 'Hot trials'*

The 'Cold trials' were experimental assessments, observations and tests conducted in the absence of a fuel-air mixture or propagating flame. Included in the cold trials were a series of dynamic non-intrusive laser assessments using Phase Doppler Anemometry (PDA), which were all performed in the Spray Research Group (SRG) laboratory.

All of the 'hot trials' were carried out within the Petroleum Technology Research Group (PTRG) laboratory using the purpose built 'Flame Propagation and Mitigation Rig' (FPMR).

The creations of numerous combustible mixtures, together with ignition activities were conducted within the FPMR. A selection of commercial atomiser configurations, called here SRA's (Spill Return Atomisers), were examined to appraise their explosion mitigation capabilities.

As discussed previously in Section 1, the aims and objectives of this research are quite different to previous studies, with the emphasis being to mitigate relatively slow moving propagating flames of ≤30m/s. The cold trials were designed to explore and develop an existing SRA and to provide a selection of suitable configurations that would be assessed in the hot trials in the FPMR. Also, as previously discussed in Section 1.1, earlier studies [3,5,6,7,8,9,10] concentrated on the effects of the hydrodynamic breakup of large water droplets in the order of ≥100µm, with respect to explosion mitigation by water sprays. Whereas this present research is focused on the development of a fine spray system, consisting of average droplets of D_{32}≤30µm, capable of producing a spray that will readily absorb heat in the flame, without relying on further droplet breakup (or secondary atomisation).

2.1 Cold trials

The SRA previously designed by Nasr, G.G. *et al* [11] was ideally suited for the purpose of these investigations as the atomiser was capable of providing the required drop size D_{32}≤30µm and was additionally easily modified with respect to flow rate, liquid volume flux and spray cone angle by reconfiguration of some of the interchangeable components, as shown below in Figure 1.

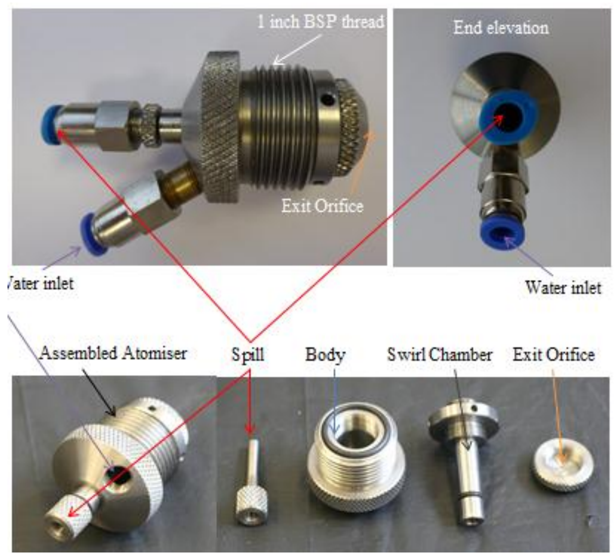

Figure 1 : Assembled and SRA and component parts

Four SRA configurations were developed by replacing or modifying the exit orifice diameters. For clarity and ease of further reference, the atomiser arrangements were designated as Type A, B, C and D for identification throughout this study and are shown in Table 2 below.

SRA designation	Exit orifice diameter (mm)	Spill orifice diameter (mm)	Tangential inlet orifice diameter (mm)
Type A	0.3	0.5	0.6 x 2
Type B	0.5	0.5	0.6 x 2
Type C	0.8	0.5	0.6 x 2
Type D	1.0	0.5	0.6 x 2

Table 2 : SRA critical orifice diameters

The following objectives describe the challenges and advances required to progress the existing SRA technology and thus to be aligned to the present application.

i. To study the development of the existing SRA and to understand the fundamental concepts of operation.
ii. To characterise the sprays in open ambient conditions and within the simulated Polymethyl-Methacrylate (PMMA) tube (drop size, droplet velocity and mass flux) using non-intrusive laser techniques.
iii. To increase the flux density and water volume fraction, without compromising the mean droplet sizes produced by the SRA.
iv. To produce a spray envelope containing a sufficient quantity of droplets that are small enough to reach boiling point and begin to vaporise within the flame
v. To increase droplet 'residence time' in the flame front, thus permitting greater heat transfer.
vi. To produce suitable quality imaging i.e. still, HD video and high speed video within the confines of the explosion and mitigation tube (see cold trial apparatus in Figure 2).

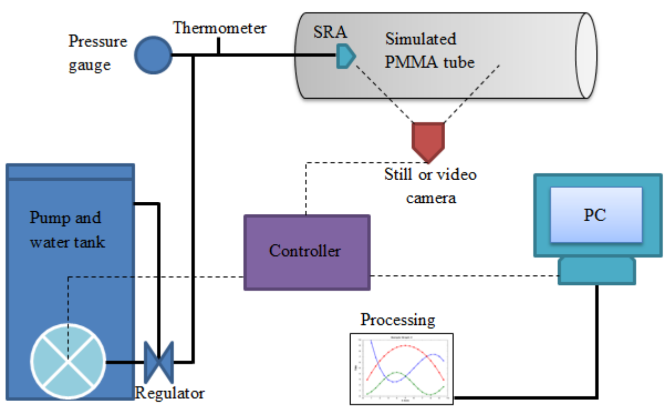

Figure 2 : Diagram of cold trials apparatus and set up including simulated PMMA tube

To achieve the objectives described above, a series of non-intrusive evaluation techniques were applied to characterise the four SRA configurations, previously detailed in Table 2. They were:

i. Volumetric flow rate.
ii. SRA spray cone angle.
iii. Spray characterisation in ambient conditions using Phase Doppler Anemometry (PDA).
iv. Spray characterisation within the simulated conditions of the PMMA tube using PDA.

i) Volumetric flow rate

A series of volumetric flow rate trials were conducted to provide systematic flow rate data for the four single atomiser configurations, Type A, B, C and D, as well as comparing related previous data with present atomiser configurations. Each of the atomisers were evaluated by subjecting them to a range of pressures from 5MPa – 14MPa (50bar – 140bar). A test rig was designed and constructed to carry out the flow rate trials. The apparatus shown in Figure 3 consisted of a mounting frame, calibrated pressure gauge, atomiser mounting connections and spray convergence passage.

Due to the fine droplets and aerosols corresponding to the SRA spray, the SRA was connected to a convoluted conical tube, referred to here as the 'spray convergence passage'. This device conveniently allowed the droplets and mist to coalesce, thus producing a reliable flow of water from its exit.

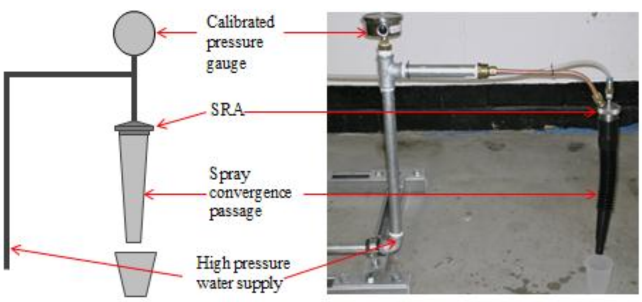

Figure 3 : Volumetric flow rate test rig

ii) Spray cone angle

The importance of the spray cone angle varies with different studies and applications. In this present study it was important that the spray envelope completely filled the internal cross section of the 190mm PMMA tube of the FPMR. The individual atomiser configurations were installed in the test rig shown in Figure 4 and were supplied with de-ionised water at a pressure of 13MPa. The spray images were captured using a high resolution Canon EOS digital SLR camera, which were then processed using

Adobe Photoshop, where the cone angles were measured using the Adobe angle finder tool.

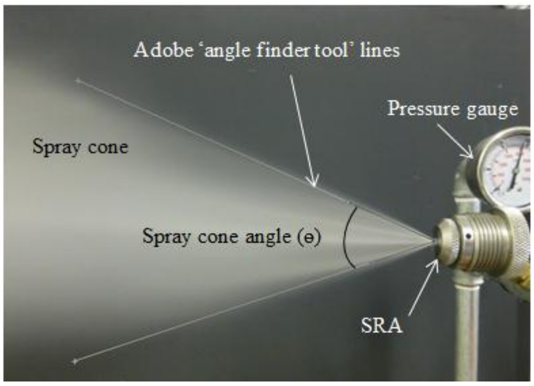

Figure 4 : Typical spray cone angle measurement

iii) Spray characterisation in ambient conditions using Phase Doppler Anemometry (PDA)

To obtain radial positions throughout the flow, the atomiser was traversed horizontally using a mounting trolley relative to the beams with the transmission optics fixed, as shown in Figure 5. The radial positions were situated at 5 or 10mm intervals from the centre of the atomiser orifice. A vertical traverse was constructed in order to record radial plots with each atomiser configuration at various downstream distances.

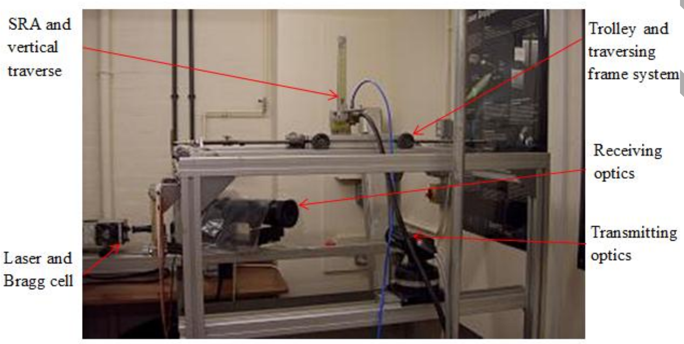

Figure 5 : Atomiser mounting and traversing frame system

Previous studies by Nasr, G.G. *et al* [11] considered measurements at various axial intervals downstream (DS) of the SRA up to and including 700mm. However, for this study there was a need to capture data axially from downstream position of 95mm, as illustrated in Figure 6. This data point and spatial position was considered to be approximately the centre of the spray when enclosed within a 190mm PMMA tube of the FPMR.

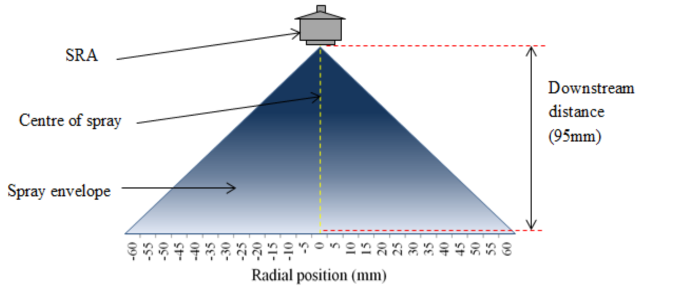

Figure 6 : Axial and radial sampling positions

iv) Spray characterisation within the simulated conditions of the PMMA tube using PDA

A new test rig was constructed within the existing PDA and traversing system as shown in Figure 7, which facilitated the mounting of a short section of 190mm (I.D) PMMA tube.

Although the PMMA tube was coated liberally with hydrophobic spray, the main challenge in obtaining data was the build-up of water droplets on the inside surface of the tube. Initial trials produced highly irregular results whereby many cases resulted in trials being aborted due to the receiving optics not being able detect droplets in the measuring volume.

A consequence of the deposition and coalescence of water droplets on the inner surface of the PMMA tube resulted in the laser beams exiting the transmitting optics being refracted and diverted. Additionally, although the outer surface of the PMMA tube was coated with anti-reflective matte spray, the shiny surface was also detrimental to data acquisition.

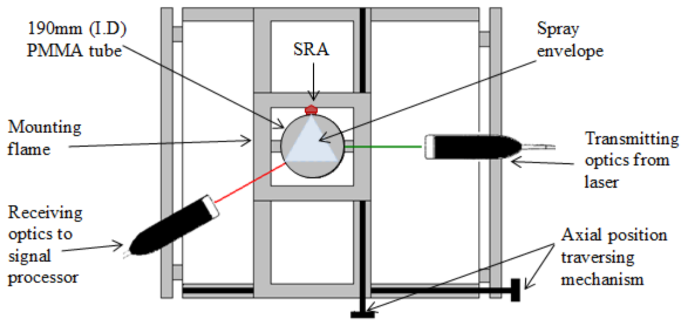

Figure 7 : Plan view of the mounting arrangement for the PMMA tube, SRA position (cross flow) and PDA optics

The equipment shown in Figure 7 was refined through experimental trials and eventually a successive series of tests were performed with a consistent level of success. Two slots were cut on opposite sides of the PMMA tube to provide line of site for the transmitting and receiving optics. Additionally a wet and dry vacuum was placed near to the receiving optics slot to reduce the misting of the lens caused by the aerosols in the spray.

2.2 Hot trials

The apparatus that was required for these investigations needed to be innovative and purpose built to safely facilitate the assessment of a selected number of SRA atomiser configurations with respect to their explosion suppression / mitigation capabilities.

The design configurations and orientations of the SRA's together with the respective sprays and their subsequent interaction with the incoming flame within the PMMA tube are profoundly crucial, since the overall aim of this study, was to 'fully' mitigate a propagating flame with complete combustion extinguishment in a homogeneous fuel gas : air mixture.

A suitable hot trials test rig was thus designed and commissioned, complete with selected hardware, data acquisition and processing capabilities. It is worth noting that due to the specific intentions and requirements of this study, rig designs used in other investigations [3,5,6,7,8,9,10] would be ineffective if imitated in this present research.

The manifestation of the apparatus conceived for these investigations is shown in Figure 8 and is known in this study as the Flame Propagation and Mitigation Rig (FPMR). The FPMR specification was designed to ensure:-

i. Safe operation for use in an indoor environment, complete with procedures and checklists.
ii. A control system that would facilitate the safe filling, recirculating and subsequent ignition of various homogeneous methane-air mixtures.
iii. Hardware and software capabilities to record relevant quantitative information.
iv. A clear mid-section to permit qualitative analysis of flame progression and mitigation and to allow the measurement of average flame speeds.
v. Variable mounting positions for single and multiple atomiser configurations including counter flow (C/F), parallel flow (P/F) and cross flow (X/F) arrangement with respect to the propagating flame front. (See also Figure 8.)
vi. Controllable flame speeds with the facility to vary the environmental conditions in which the explosion event occurred i.e. confined, partly confined, partly confined vented.
vii. Flexibility in the design to afford continued use of the equipment for future studies.

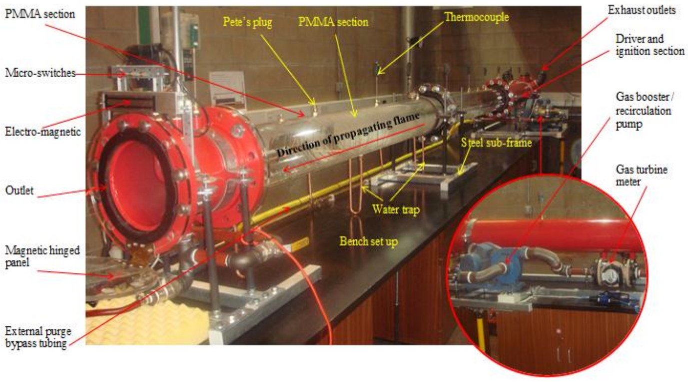

Figure 8 : Schematic of Flame Propagation and Mitigation Rig (FPMR)

The main rationale and design concepts associated with the laboratory scale rig were as follows:-

i. The length of the rig: the 1m or 2m long polycarbonate sections can be added or removed using flanged joints to allow for increase, or decrease in length to diameter ratio (l/d). This will have an overall effect on the limiting flame speed as it reaches the atomiser. This flexibility also allows sections to be pre-assembled with additional components i.e. an array of atomisers can be installed in a section, tested and characterised, then simply bolted in position.
ii. Exhaust gas outlets: the 6 x 80mm exhaust gas outlets will allow seven options for explosion trials, either all exhaust outlets closed, or one to six outlets open during the test. As flame speed is a function of the pressure resulting from the rapid expansion of gases upstream of the flame, a number of scenarios could be created and tested.
iii. Due to the high pressures and flow rates required for atomiser operation, a water storage, pumping and delivery system was produced for counter flow (C/F), parallel flow (P/F) and cross flow (X/F) configurations.

This novel series of explosion mitigation trials were devised by the author and subdivided into three principle categories, with the main objectives being the acquisition of unique, valid and reliable research data and imagery. The three categories were:-

i. water sprays in counter flow configuration with a methane-air flame (Figure 9 (i))
ii. water sprays in parallel flow configuration with a methane-air flame (Figure 9 (ii))
iii. water sprays in cross flow configuration with a methane-air flame (Figure 9 (iii))

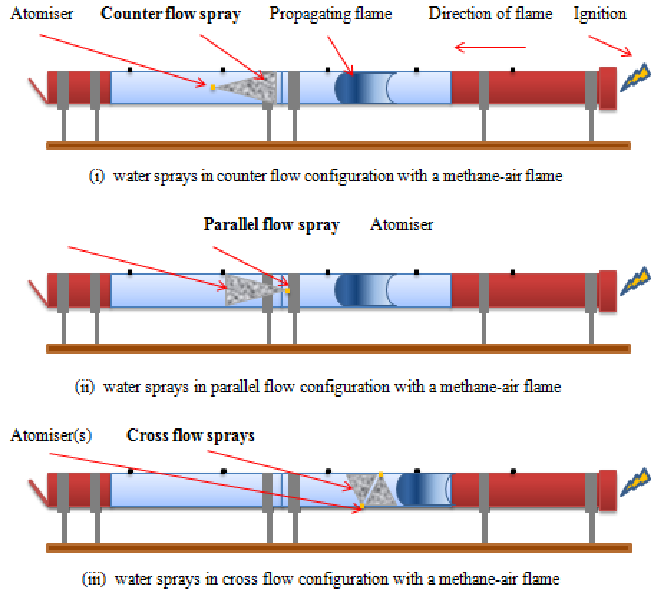

Figure 9 : Illustration of flame propagation direction and water spray configuration

For this current study a relatively slow moving flame of ≤30 m/s was required, whereby potential flame acceleration caused by compression of gases upstream or downstream of the flame was to be avoided. A magnetic hinged outlet design was adopted and fabricated, consisting of a 'full bore' hinged end plate controlled by an electromagnetic latching system, as pictured in Figure 10. The electromagnetic latching system was of the type normally associated with an automatic door entry system. The strength of the DC electromagnetic field, together with the area of the latching plates was sufficient to hold the end panel closed and gas tight.

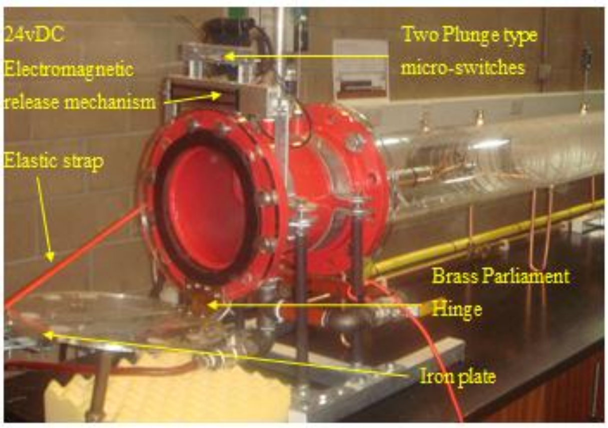

Figure 10 : Electromagnetic hinged panel and component parts

To control and vary the types of explosion produced, six exhaust outlets were positioned at the ignition end of the FPMR. Variable degrees of venting and resulting flame speeds were achievable by simply blocking off one, or several of the exhaust outlets. However, the 'solid' blocking of exhausts openings was not utilised during the main body of this work.

Number of exhaust outlet(s) open	Total area of opening(s) (mm^2)	Propagation tube area (mm^2)	Total opening ratio (%)	Total blockage ratio (%)
0	0.00	32282.87	0.00	100
1	6209.67	32282.87	19.24	80.76
2	12419.33	32282.87	38.47	61.53
3	18628.99	32282.87	57.71	42.29
4	24838.66	32282.87	76.94	23.06
5	31048.33	32282.87	96.18	3.82
6	37257.99	32282.87	115.41	0.00

Table 3 : Areas and percentages of exhaust outlet openings

Bursting discs/membranes were utilised in one, or a number of the six exhaust outlets. Whereby, shortly after ignition the disc or membrane would burst/rupture due to the pressure differential between the inside and outside of the tube. Hot burnt gases would then be vented upstream of the flame front, thus giving a similar degree of control as the above method (i) over flame speed and overpressure.

Low density polyethylene sheet 'cling film' was chosen to act as a bursting disc membrane. This was applied to the relevant exhaust outlets prior to commencing the next experimental run. The low density polyethylene sheet was secured in place by adjustable Velcro straps as shown in Figure 11, which sealed the 'cling film' against a foam strip, forming a temporary gas tight seal.

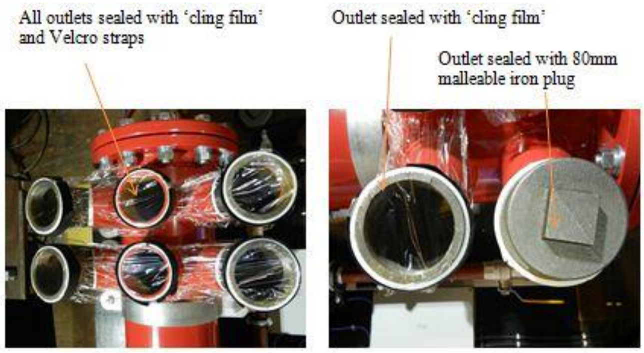

Figure 11 : Examples of exhaust outlets being sealed prior to ignition and explosion

To maximise the quantity and variation of experimental hot trials, a number of single and multiple atomiser configurations and arrangements were designed, manufactured and tested/evaluated thoroughly under cold trial conditions, prior to the subsequent hot trials.

The following Section deals with the equipment specification, methodology and the rational for choosing each of the arrangements.

The atomiser provisions were:-

i. Single SRA in counter flow (C/F) with the flame direction.
ii. Single SRA in parallel flow (P/F) with the flame direction.
iii. Overlapping SRA's in parallel flow (P/F) with the flame direction.
iv. Multiple SRA's in cross flow (X/F) with the flame direction.

The single SRA's were mounted on a stainless steel supply system, centrally within the FPMR, in counter and parallel flow with the propagating flame.

To increase liquid volume flux, a parallel flow multiple overlapping SRA manifold, shown in Figure 12, was fabricated to permit the simultaneous operation of two SRA's. The radial manifold was designed to fit centrally within the explosion and mitigation tube at a distance of 3000mm from the ignition electrodes.

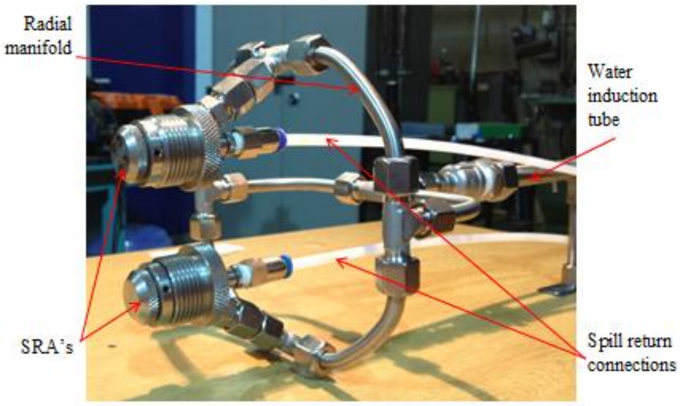

Figure 12 : Parallel flow multiple overlapping SRA manifold configuration

To assess the mitigation success of cross flow atomisers, the SRA's had to be mounted externally. This was due to the physical size of the SRA's and the need to supply them with a water feed and a spill exit tube.

To mount the atomisers externally, a unique connection system was required that would facilitate the installation of up to four atomisers, whereby several options were considered and tested. The method adopted in this case was an interface component between the external pipe wall and the atomiser body, known as a 'boss'.

To create a gas and water tight interface component Solid Works software was used to design and scale the 'boss' fitting, which was then printed using a 3D printer and tapped out with a BSP thread, as shown in Figures 13..

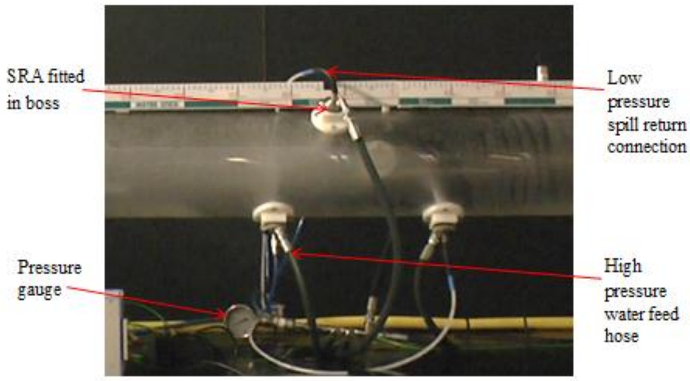

Figure 13 : External atomisers and water supply manifold

Figure 14 shows a flow diagram of the Flame Propagation and Mitigation Rig (FPMR) and experimental set up used throughout the hot trials.

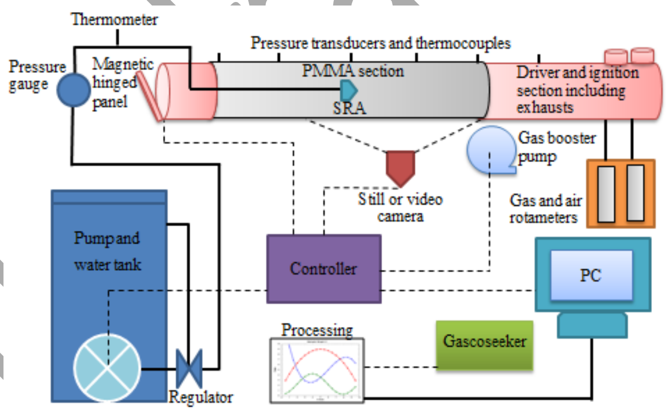

Figure 14 : Illustrated flow diagram for hot trials

The temperature measurement was carried out using mineral insulated, exposed junction, type K thermocouples. The mineral insulated section of the thermocouple was 50mm in length and has an external diameter of 3mm. The exposed junction was 0.6mm in diameter. These thermocouples are manufactured, certified and supplied by TC Ltd, Uxbridge, UK.

The thermocouples complete with 4m (manufacturer supplied and certified) extension cables were individually connected to separate channels in the iNet Expandable Modular Data Acquisition System.

The exposed junction, type K thermocouples were placed along the length of the flame propagation and mitigation rig at 600mm intervals and held in place using 'Pete's Plug' adapters. Due to lag time associated with thermocouples, the data measurements offered during the hot trials are not intended to represent the actual flame temperatures within the flame propagation and mitigation tube. The use of these exposed junction thermocouples has been demonstrated to be an acceptable method for comparing flame propagation within 'confined', 'partly confined' and 'unconfined' explosion testing in confined and partly confined vessels and pipework. These were extensively described in numerous previously published works [12,13,14].

3. Results and discussions

3.1 Cold trials

Four manifestations of the SRA (Type A, B, C and D) were derived and successively characterised using the various dynamic measurement methods. Throughout the cold trials the ideal liquid pressure was found to be 13MPa. This infers that the tangentially supplied swirl chamber within the SRA, produced the optimum turbulence for atomisation at 13MPa.

The four SRA's were evaluated and their volumetric flow rates were recorded, with additional attention paid to the consistency of the exit : spill ratio. Exit flow rates at 13MPa were found to be 0.295, 0.85, 1.36 and 1.94 l/m , with spill flow rates being 1.12, 0.85, 0.49 and 0.25 l/m respectively. The flow rate in the Type D SRA spill was very erratic and non-linear. This indicated the boundary of the limits of the present SRA swirl chamber and thus the SRA Type D was de-selected from any further consideration.

Spray cone angles (ɵ) were measured for the SRA's (Type A, B, C and D) during the trials using 13MPa liquid pressure, which were found to be 37.4˚, 42.7˚, 49.2˚ and 54.2˚respectively. The spray cone angles were also considered with respect to spray penetration (d_p), whereby the penetration was calculated to be 304, 243, 207 and 186mm respectively. Of the four SRA configurations, the optimum spray cone angle for use in the 190mm (I.D.) PMMA tube of the flame propagation and mitigation rig (FPMR) was the Type C SRA (ɵ 49.2˚ and d_p, of 207mm)

Four unique spray arrangements were developed during the cold trials, with each adaptation facilitating combinations of the three selected SRA's (Type A, B and C). These were:-

- Single SRA in counter flow with the incoming propagating flame
- Single SRA in parallel flow with the incoming propagating flame
- Multiple SRA's in parallel flow with the incoming propagating flame
- Multiple SRA's in cross flow with the incoming propagating flame

Phase Doppler Anemometry (PDA) was used to characterise the sprays above, whereby dynamic measurements of droplet diameter, D_{32}, were found between 17 - 29µm, droplet velocities, D_v, of ≤21.4m/s and liquid volume flux, Q_f, 0.011 - 0.047cm^3/s/cm^2. The sprays were measured radially at a downstream distance of 95mm, this being the approximate centre of the spray within the tube conditions. PDA analysis was carried out in ambient conditions and also in a simulated PMMA tube environment.

All three selected SRA's (Type A, B and C) produced ambient drop sizes within the scope and aims of this study of D_{32}≤30µm.

Cross flow sprays (X/F) were also characterised in the simulated PMMA tube, whereby the D_{32} values were found to be slightly higher, as shown in Table 7.2. However, 48.5% of the droplets in the Type B SRA and 28% for the Type C SRA spray were of ≤30µm. This was also coupled with a significant increase in liquid volume flux (Q_f) within the simulated tube, which was approximately 83% for the Type B and 21% for the Type C.

In the simulated PMMA tube, cross flow characteristics varied also with respect to velocity, in which a noteworthy reduction in average velocity resulted in values of ~0.0m/s for the Type B SRA configuration ≤3.23m/s for the Type C SRA configuration.

3.2 Hot trials

Spray orientation with respect to the propagating flame, coupled with droplet velocity was found to have a significant effect on the level of flame acceleration in the flammable mixture, particularly in the SRA Type A case where the liquid volume flux (Q_f) was clearly insufficient to initiate mitigation.

The single Type B SRA (0.5mm exit orifice and 0.5mm spill diameter) parallel flow trials produced more instances of flame acceleration than their counter flow equivalents. The average droplet velocity in the Type B spray was 21.41m/s compared to 13.5m/s for the Type B spray. This relationship between counter and parallel flow sprays has not been reported in any of the previous published literature.

With a single SRA Type C (0.8mm exit orifice and 0.5mm spill diameter) spray, it was possible to mitigate a methane-air mixture of E.R. (ϕ) 0.61, utilising counter flow and parallel flow configurations. The Type C SRA produced a spray containing droplets of D_{32}≤29µm, with a liquid volume flux being approximately 0.04cm^3/s/cm^2 and average velocity of 13.5m/s in ambient conditions.

In the single SRA Type C spray, the flame acceleration in the counter flow arrangements was found to be approximately four times greater than the parallel flow equivalent configuration and was particularly prevalent in the methane-air mixture of E.R. (ϕ) 0.72, but less so in the (ϕ) 0.95 and 1.06 mixtures, due to their high exothermicity. These two conflicting outcomes demonstrate the critical importance of drop size (µm), volume flux (cm^3/s/cm^2) and velocity (m/s).

Single Type B and C SRA sprays configurations were ineffective when used in cross flow due to the limitations of the spray cone angle and corresponding spray envelope, thus not being sufficient to completely engulf the cross sectional area of the FPMR mitigation tube and permitting flame propagation through the spray free space.

The twin overlapping parallel flow Type B SRA's produced a mitigation event in the methane-air mixture of E.R. (ϕ) 0.61. In the other three mixtures (ϕ) 0.72, 0.95 and 1.06, there was a degree of flame acceleration caused by the disturbance of the sprays however, this was significantly less than in the corresponding single parallel flow trials.

The twin overlapping parallel flow (P/F) Type C SRA's produced the first instance of mitigation in a methane-air mixture of E.R. (ϕ) 0.95. There was a small temperature rise of approximately 25˚C, which is attributed to the flash vaporisation and subsequent cooling that was also observed both visually and audibly at the point of mitigation.

In the twin overlapping parallel flow Type C SRA trials there was a noticeable increase in flame speed upstream of the sprays, which has been accredited to the entrainment in the overlapping configuration.

The various multiple cross flow (X/F) SRA configurations proved to be the most successful conformation, whereby four Type B X/F SRA's caused a mitigation event in a methane-air mixture of E.R. (ϕ) 0.72. (See Figure 15)

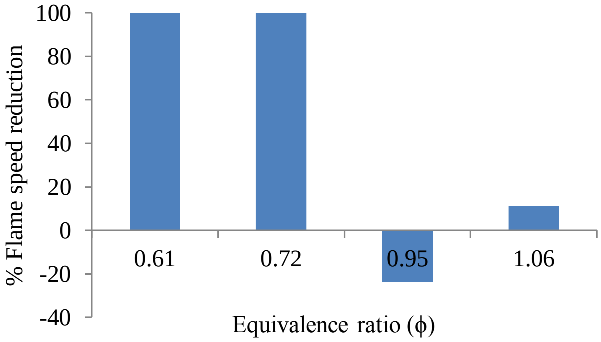

Figure 15 : Average flame speed reduction percentage (%) from upstream to downstream of four X/F SRA's in various methane-air mixtures

Figure 16 shows the flame propagation and subsequent suppression and total mitigation of the flame, in the methane-air mixture of E.R. (ϕ) 0.72.

A multiple cross flow (X/F) configuration utilising four Type C X/F SRA's, each exhibiting individual ambient spray characteristics of $D_{32} \leq 29\mu m$ and liquid volume flux (Q_f) of approximately $0.044 cm^3/s/cm^2$, proved to be highly effective in total flame extinguishment and complete mitigation in all fuel-air mixture scenario. The flame speeds produced were all ≤30m/s, with resulting flame thickness of approximately 1mm for E.R. ~1.0 [8,9,].

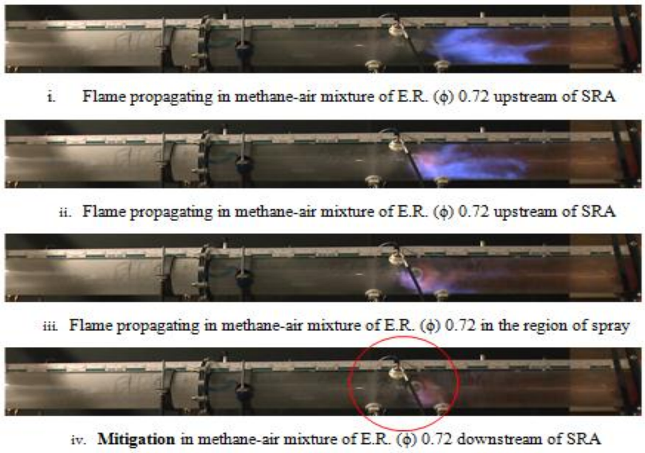

Figure 16 : Flame propagating upstream and downstream of four X/F SRA Type B for a methane-air mixture (ϕ) 0.72

The manifestation of the configuration and marginal separation distance between each of the sprays in the 'spray region' consisted of four sprays, each 105mm apart with individual SRA's each opposed by 120˚ (spray region of 315mm spray centre to centre). Figure 17 shows 100% that mitigation occurred when utilising four Type C X/F SRA's, with cessation of flame propagation.

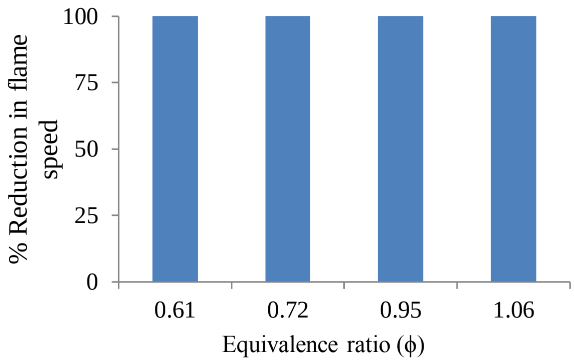

Figure 17: Average flame speed reduction percentage (%) from upstream to downstream of four X/F SRA's in a various methane-air mixtures

In the heated water supply trials the flame was shown to be mitigated at an earlier point, during its transition through the spray region, indicating that a greater percentage of the spray must have been reaching boiling temperature and vaporising, thus giving way to latent heat transfer. Additionally there was a large visible plume of water vapour at exit end of apparatus which was shown in Figure 18.

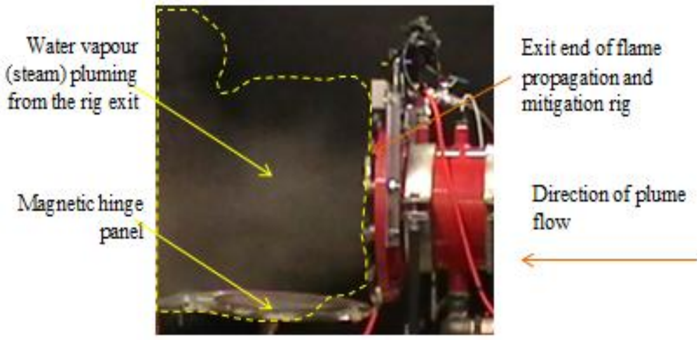

Figure 18 : Example of water vapour pluming from the rig exit following mitigation

In the supplementary trials using propane-air, the flame was mitigated at an earlier position during its passage through the sprays. This may be credited to the greater atomic ratio of carbon : hydrogen associated with propane, when compared to that of methane. Figure 19 shows the propagation and mitigation of a stoichiometric propane-air flame.

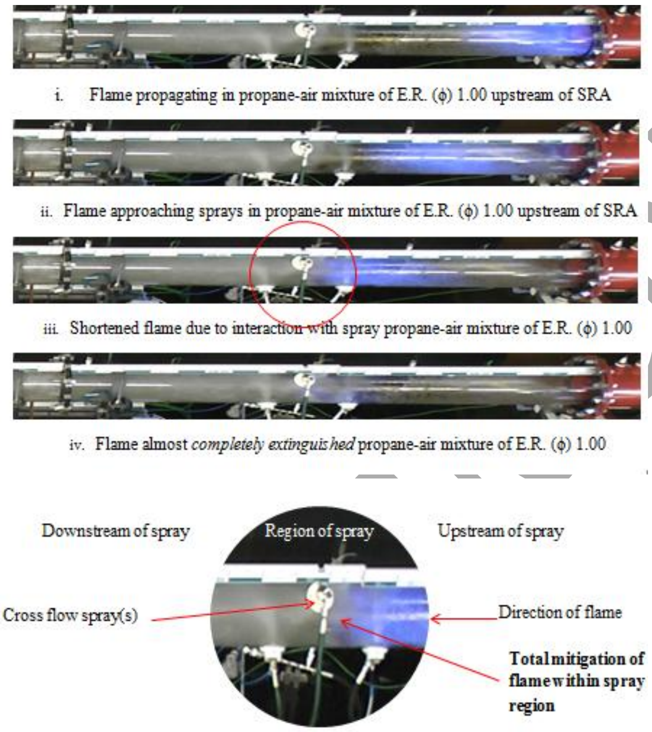

Figure 19 : Flame propagating upstream and subsequent mitigation using four Type C cross flow SRA's in a propane-air mixture (ϕ) 1.00

4 Recommendations and further work

It is anticipated that the developments and findings within the present study will give way to a renewed interest in explosion mitigation research using fine water sprays. As discussed, all previous studies concentrated on the use of larger droplets of ≥100µm and faster flame speeds in the order of ≤100m/s to 2000m/s. Whereby droplets were hydrodynamically shattered by inverted bag type break, thus giving way to finer droplets that were then small enough to absorb heat from the flame front.

With recent advances in spray research and the development of the Spill Return Atomiser (SRA), this current study has shown the effectiveness of fine sprays (D_{32}≤30µm) in completely mitigating slow moving methane-air and propane-air deflagrations of ≤30m/s, without the reliance of hydrodynamic inverted bag type break up.

In the next Section recommendations are presented for further research that will provide an excellent platform to enrich the knowledge acquired as a result of this present study. Such investigations will further evaluate the capabilities and achievements of the SRA in realistic, full scale conditions.

The concept of fine spray applications has far reaching safety implications for oil and gas refineries, platforms and other industries where there is the potential for explosive gas and/or flammable vapour mixtures. If the technology can be proven in realistic scale tests, such a system may in the future become mandatory for all these types of installations.

By understanding the effects of droplet interaction with propagating flames and the conditions needed for flame quenching and mitigation, a suitable spray system may be designed to mitigate flame propagation and explosions in partly confined scenarios.

The work can also be further extended to develop a protective explosive mitigation system for unconfined areas, to prevent entry of the flame into areas that promote turbulence and flame acceleration, such as pipe arrays etc. as shown in Figure 7.1.

Figure 7.2 offers a conceptual image of a Mitigation Curtain Module (MCM). The concept behind the MCM is that it will be suitable for fitting to new installations, or retro-fitted to existing pipe arrays. The MCM could be installed along the sides or the top and even below the congested pipe array, where necessary.

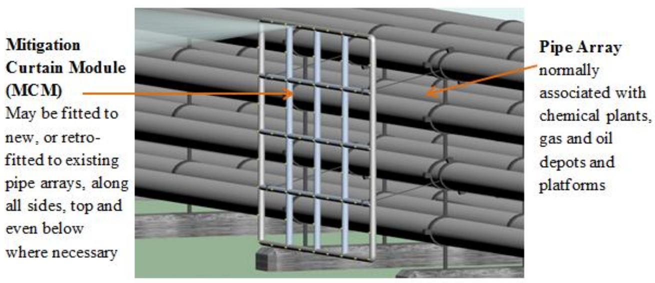

Figure 20 : Concept for the SRA 'Mitigation Curtain Module' (MCM)

Finally, another potential purpose and new product development for the SRA is in fire suppression, in particular involving jet fires. These fires are frequently the result of a high velocity jet release of gaseous or liquid fuel and subsequent ignition, as shown in Figure 21and are often the outcome of a ruptured pipeline or sheered fitting normally associated with pipework operations on petrochemical, or oil and gas sites.

Figure 21 : Typical jet fire resulting from leaking pipe

The study would involve the design and construction of test apparatus, followed by a series of cold and hot trials to evaluate the suppression and mitigation performance of a string of multiple SRA's incorporated within a tubular stainless steel helicoil arrangement.

It is envisaged that the Helicoil Mitigation Apparatus (HMA) could be lowered over a jet fire by a robotic device, such as a land based remotely operated vehicle (ROV) with self-contained water supply as depicted in Figure 22 (a).

An initial design concept for the HMA is offered in Figure 22 (b). The HMA trials should initially commence with laboratory scale (cold and hot) studies, followed by full scale realistic trials using a 500mm - 1000mm diameter helicoil.

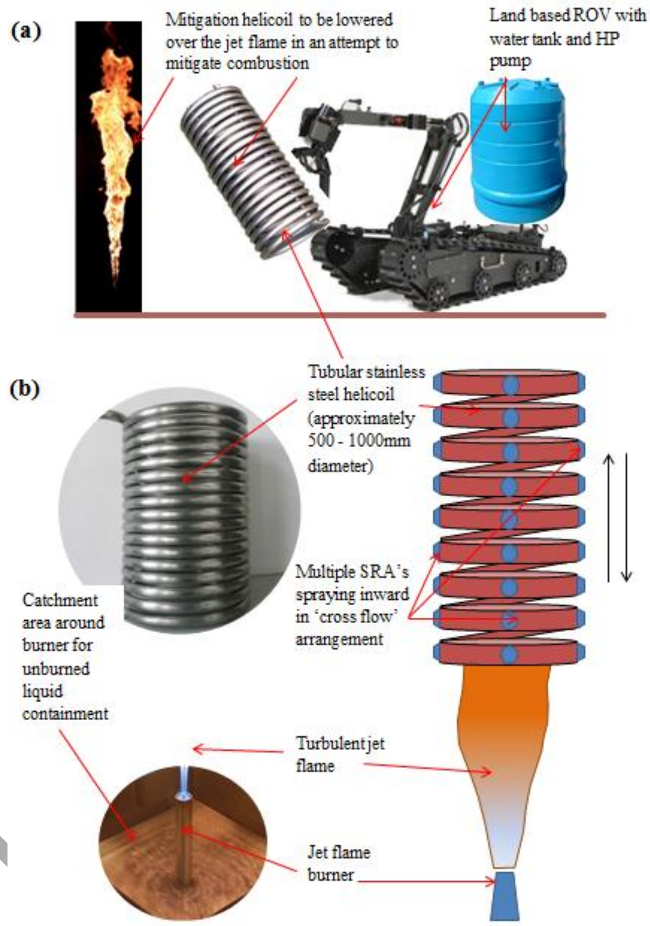

Figure 22 : (a) Concept for turbulent jet flame 'Helicoil Mitigation Apparatus' (HMA) with ROV vehicle and (b) proposed experimental set up.

References

[1] Nasr, G.G. et al. *Natural Gas Engineering and Safety Challenges*. Springer (2014)

[2] Health and Safety Executive. *'A guide to the Control of Major Accident Hazards Regulations 1999 (as amended)'*.ISBN 978071766175X, HES Books. 2006

[3] Harris, R.J. and Wickens, M.J. *Understanding vapour cloud explosions – an experimental study*. The Institution of Gas Engineers, Communication 1408. 1989

[4] Lane, W.R. Industrial Engineering and Chem. 1951, 43(6), 1312 – 1317

[5] HSE-OTH 94 463. Prepared by the University College of Wales. *An investigation of factors of relevance during explosion suppression by water sprays*. HMSC 1996 ISBN 0-7176-1118-3

[6] Brenton, J.R. and Thomas, G.O. (1992) *Investigations into factors controlling the local extinction of flames by water droplets*. ICHEME Research event 1992.

[7] Thomas, G.O. *On the conditions required for explosion mitigation by water sprays*. Trans IChem:Part B–Process Safety and Environmental Protection Vol. 78p.p. 339 – 354 (2000)

[8] Sapko, M., Furno, A., and Kuchta, J.M., *Quenching Methane-Air Ignitions with Water Sprays* U.S. Bureau of Mines, R.I. 8214, 1977.

[9] British Gas | MRS | 5325 | *Preliminary investigations of methods of mitigating gas explosion overpressures*. July 1990 | Project M08411

[10] Van Wingerden, K., et al. *The influence of water sprays on gas explosions.* 27th October 1995. J. Loss Prevention. Process Industries, 1995, Volume 8, No.2

[11] Nasr, G.G. et al. *A new fine spray, low flow rate, spill return swirl atomiser.* IMechE, Vol. 255 Part C;J. Mechanical Engineering Science. 24th August 2010.

[12] Ferrara, G.,et al. *Venting of premixed gas explosions with a relief pipe of the same area as the vent.*' Proceedings of the European Combustion Meeting ECM2005(CDformat), Louvain-la-Neuve, Belgium. P #213, April 2005.

[13] Kasmani, R. M, et al. *Self Accelerating Gas Flames in Large Vented Explosion Volumes That are Not Accounted for in Current Vent Design Correlations.* Proceedings of the 2nd International Conference on Safety & Environment in Process Industry, Naples,Italy, May 2006.

[14] Willacy, S. K., et al. *Ignition of Stratified Propane-Air Explosions in a Duct Vented Geometry: Effect of Concentration, Ignition and Injection Position* IChemE B: Process Safety and Environmental Protection, 2007,85(B2), pp153-161

APPENDIX 2

SAFETY AND RISK ASSESSMENT

A2.1 Safety and risk assessment

Risk management is the identification, assessment, and prioritisation of risks is defined in ISO31000 [1] as 'the effect of uncertainty on objectives, whether positive or negative' followed by coordinated and economical application of resources to minimise, monitor, and control the probability and/or impact of unfortunate events.

The risk assessment process comprises of five steps:

i. Identify the hazards.
ii. Decide who may be harmed and how.
iii. Assess the risk and the adequacy of existing control measures and decide what more should be done to control the risk to an acceptable level.
iv. Record the significant findings.
v. Review and revise the assessment.

To comply with the University rules and regulations a full risk assessment was required, complete with mitigation and control measures.

There were three significant risks relating to the operation of the test rig, which were compounded by the fact that the experiments would all be conducted within an internal environment. The three significant risks were:-

1. Leakage of gas during the filling and priming stages of each experimental test from the rig itself, or any of the auxiliary pipework.
2. The overpressure within the laboratory caused by the controlled explosion in each of the experimental trials.
3. The flame exiting from the rig at the exit point and the exhausts

To control and manage the above risks, a 'Safe operations' flow chart shown Section A2.3, Figure A2.12 was produced, together with a 'manual and automated control sequence and check list' as revealed in A2.13.

The following risk assessments were conducted using current IGEM codes of practice and FLACS CFD software.

A2.1.1 Risk Assessment : Leakage of fuel gas during 'hot trials'

To mitigate the risk of an uncontrolled release of fuel gas within the confines of the laboratory, several control measures were adopted. The obvious potentially catastrophic risk was allowing the fuel gas to build up within the laboratory to greater than, or equal to its lower explosive limit (LEL). The safety data sheet for methane can be found in Appendices 3 and 4.

The risk assessments produced in A2.1.4 and A2.2.4 were adopted for use in the laboratory were designed to meet the requirements of ISO 31000, HSE and IGEM guidelines. In addition to the risk assessment flow diagrams and checklist, 'Stop Work' procedure and 'Emergency Response Plan' was also put in place, which was designed ensure effective evacuation of the area, followed by a full investigation should there be any incidents relating to safety.

A2.1.2 Stop work system

HSE document HSG 250 [2] states, that wherever a permit is given to carry out work, there should also be a system in place to stop, or suspend an activity whilst an investigation takes place. In this instance the 'Stop Work' procedure is as follows:-

1. Ensure that the research assistant (R.A.) and all other personnel are safely removed from the affected area.
2. Where safe to do so, isolate fuel supplies.
3. Where required contact the emergency services
4. Contact the head of division and the University health & safety department
5. University health and safety department will issue 'Stop Work' instruction
6. Give a statement to head of division and the University health and safety department within 24 hours
7. University health and safety department to investigate and provide report of findings, together with any improvements required to commence work again.
8. University health and safety to issue new permit to continue with work

A2.1.3 Emergency response plan

When faced with an emergency situation, it is imperative to adopt the correct approach, that is, not to place yourself or anybody else at additional risk and that the emergency services are called, where it is felt their involvement will be required.

Follow the steps laid out below (S.C.E.N.E.):-

S = Stop (Give yourself time to think, call for the assistance of the emergency services where required)

C = Check for danger (Do not put yourself at risk and remove other persons from the area where there is an inherent risk)

E = Exposure Protection (Are there any specific hazards, which will need to be removed or isolated such as fuel, substance flow, energy such as electricity or the venting of gases)

N = No obvious risk (Is it safe to intervene?)

E = Establish Priorities (Only if you are competent to do so should you administer first aid to an injured person. Do not move an injured person where it is not necessary and there is risk of worsening the injuries)

A2.1.4 Risk Assessment Report

COMPANY	DEPARTMENT	AREA	DATE
University of Salford	Gas and Petroleum Engineering	Petroleum Lab	13th Dec 2012

Please identify in box 1 the type of Risk identified giving as much detail as possible. Indicate by a tick in the appropriate box the current level of Risk posed without any control measures being applied.

RISK IDENTIFIED 1

LEVEL OF RISK		
HIGH	MED	LOW
		√

Gas leakage into internal environment (laboratory).
Gas leakage may reach LEL levels

RISK TO 2 Please state who or what is at Risk & the likely cause of injury: e.g. fire, impact etc

Competent Research Student and Technician.
Laboratory area.

In box 3 please state the appropriate action required to reduce/control the Risk detailed in box 1 above. Indicate by a tick in the appropriate box the level of Risk now perceivedNote control measures should reduce level of risk rating from that identified in box 1

ACTION 3

LEVEL OF RISK		
HIGH	MED	LOW
		√

1. Research Student is Qualified Gas Engineer
2. No other unauthorised person to operate rig
3. Method statement in place
4. Operation flow diagram in place
5. Checklist in place
6. Control box and safety interlocks in place
7. On-going maintenance & testing of rig and pipework
8. Monitoring of lag gas levels with Gascoseeker
9. Calculation of potential gas / energy release:-

IGE/UP/1 [3] – Maximum continuous energy release into an internal space $0.054MJh^{-1}$.
Therefore for Methane with a CV of $39.9MJ/m^3$, maximum permitted permanent leakage rate is $0.0014\ m^3h^{-1}$.

Volume of the rig = approx. $0.227m^3$
Volume of Laboratory = 10m x 6m x 10m = $600m^3$
$0.227m^3$ / $600m^3$ x 100 = 0.04% Gas in Air (V/V)

Therefore it would require 26 consecutive failed tests each with 100% gas, all leaking uncontrollable into the lab, without any ventilation to reach a level of 1% gas in air (V/V) or 20% LEL.
In reality the rig will only be filled with 10% gas, therefore it would require 264 consecutive failed tests all leaking uncontrollable into the lab, without any ventilation to reach a level of 1% gas in air (V/V) or 20% LEL

RISK ASSESSMENT CONDUCTED BY:	SIGNATURE:	DATE:
Steve Johnston	S A Johnston	13thDec 2012
ACTION CONFIRMED/IMPLEMENTED BY:	SIGNATURE:	DATE:
Steve Johnston	S A Johnston	13th Dec 2012

RISK ASSESSMENT REVIEW DATE (NOT TO EXCEED 24 MONTHS)	12th Dec 2014

Figure A2.1 : Gas escape risk assessment

A2.2 Overpressure within the laboratory during 'hot trials'

To satisfy the health and safety requirements of the University it was necessary to estimate the potential overpressures likely to occur during the explosion and mitigation 'hot trials'.

A computational fluid dynamics (CFD) software package, known as FLACS was used to evaluate and predict the consequential outcomes of several test scenarios.

Four initial scenarios were investigates for the following configurations:-

1. Closed tube – 9.9% Gas in Air (ϕ E.R. 1.05) – Worst case scenario
2. Two vents open – 9.9% Gas in Air (ϕ E.R. 1.05)
3. Six vents open – 9.9% Gas in Air (ϕ E.R. 1.05)
4. Closed tube – 7.5% Gas in Air (ϕ E.R. 0.775) – Lean mixture

Geometry and grid size as shown in Figure A2.2

- 6.5m of pipe
- internal diameters 202.7mm (first 2m and last 0.5m) and 190mm (from 2-6m)
- 2cm Grid

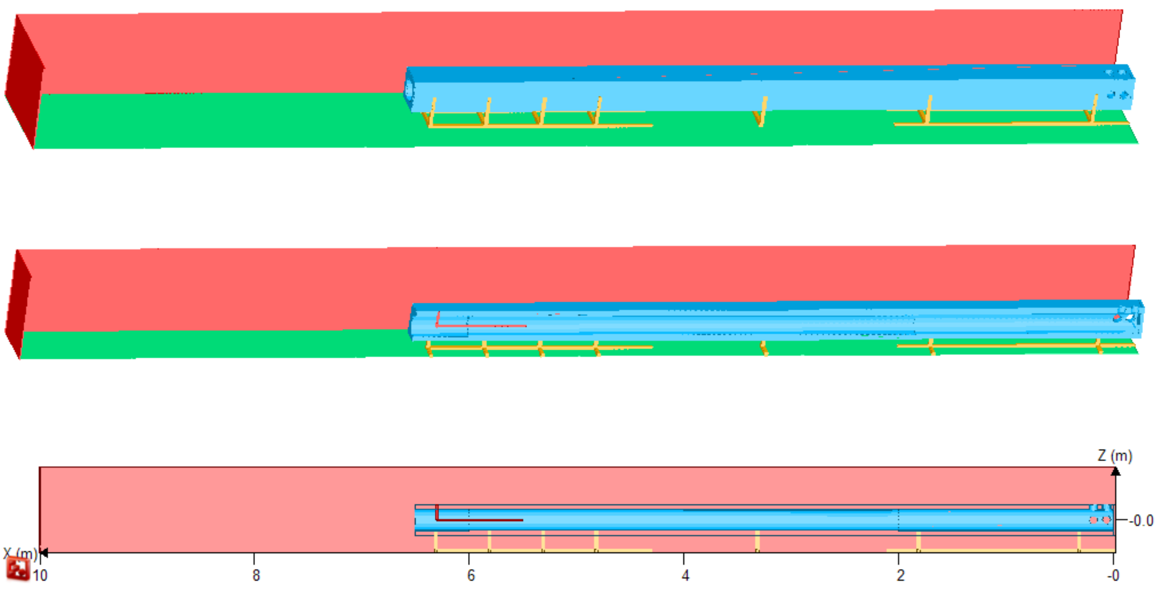

Figure A2.2 : FLACS geometry and grid

A.1.2.1 Scenario 1 : Closed tube (E.R. (ϕ) 1.05) – Worst case scenario

In this worst case scenario the methane-air mixture was E.R. ϕ 1.05 and is shown in Figure A2.3, whereby all of the exhaust outlets have been blanked off, therefore all of the explosion energy and thermal expansion generated by the explosion is contained upstream of the flame, within the explosion propagation tube.

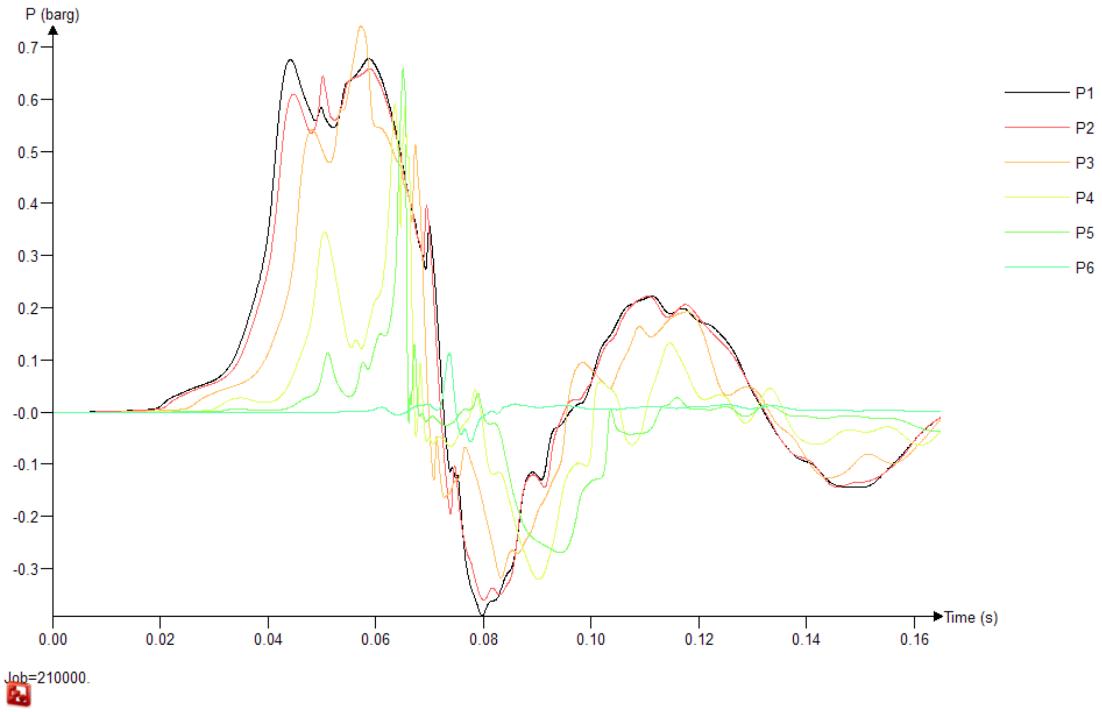

Figure A2.3 : Expected pressures for 'closed tube' scenario (ϕ E.R. 1.05)

<u>Pressure Sensor Positions</u>

P1 1.9m downstream of ignition (within the tube)
P2 2.3m downstream of ignition (within the tube)
P3 4.0m downstream of ignition (within the tube)
P4 5.6m downstream of ignition (within the tube)
P5 6.4m downstream of ignition (within the tube)
P6 10m downstream of ignition (on the far wall of the laboratory)

These conditions would generate the highest potential overpressure and flame speeds. The maximum flame speed in this simulation was 133.3m/s, with the average flame speed being 79.02m/s as shown in Table A2.1. As the main emphasis of this current study focuses on slow laminar flame speeds, these are undesirable conditions for this research and consequently will not be used for this work.

The explosion and mitigation rig was designed, certified and strength tested to 0.1MPa (1 bar) and is therefore adequately strong enough to withstand this worst case scenario and transitional pressures. The highest pressure predicted within the tube was recorded at pressure sensor P3 and was approximately 0.073MPA (0.73 bar) after 0.058 seconds post ignition and the localised ambient exit pressures were ≤0.03MPA (0.3 bar) as shown in Figure A2.4.

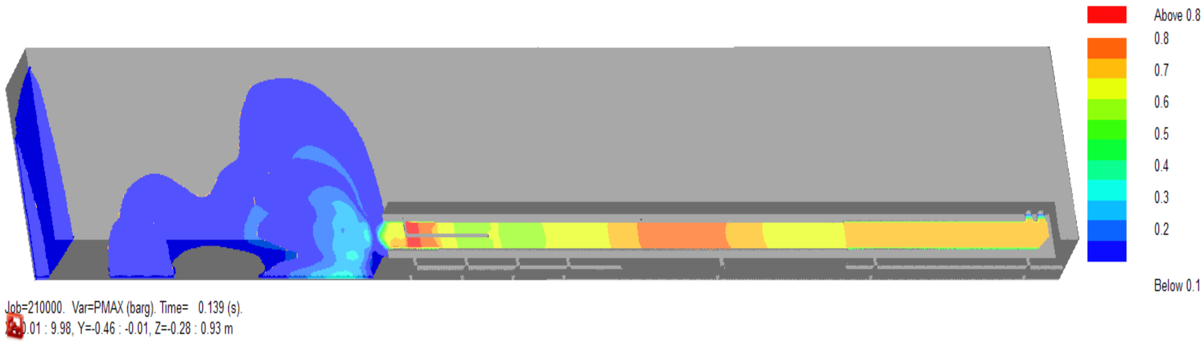

Figure A2.4 : Pressure profile associated with 'closed tube' scenario (ϕ E.R. 1.05)

Sensor	Time to achieve peak pressure (s)	Sensor position (m) (downstream of ignition)	Flame Speed (m/s)
P1	0.045	1.9	42.22
P2	0.048	2.3	47.92
P3	0.058	4.0	68.97
P4	0.065	5.6	86.15
P5	0.067	6.4	95.52
P6	0.075	10.0	133.33
		Average flame speed	79.02

Table A2.1 : Average and maximum flame speed associated with 'closed tube' (ϕ E.R. 1.05)

Conclusions:-

Maximum pressure within explosion tube	0.073MPa (0.73bar)
Maximum pressure outside the tube	0.03MPa (0.3bar)
Maximum flame speed	133.3m/s
Average flame speed	79.02m/s

A.1.2.2 Scenario 2 - Two vents open (E.R. ϕ 1.05)

In this scenario the methane-air mixture was E.R. ϕ 1.05 and is illustrated in Figure A2.5, whereby four of the exhaust outlets have been blanked off and two of the vents are open, to provide initial relief from the explosion energy and thermal expansion generated is contained within the explosion propagation tube. Further information relating to the exhaust vent blockage ratios and percentages can be found in Chapter 4.

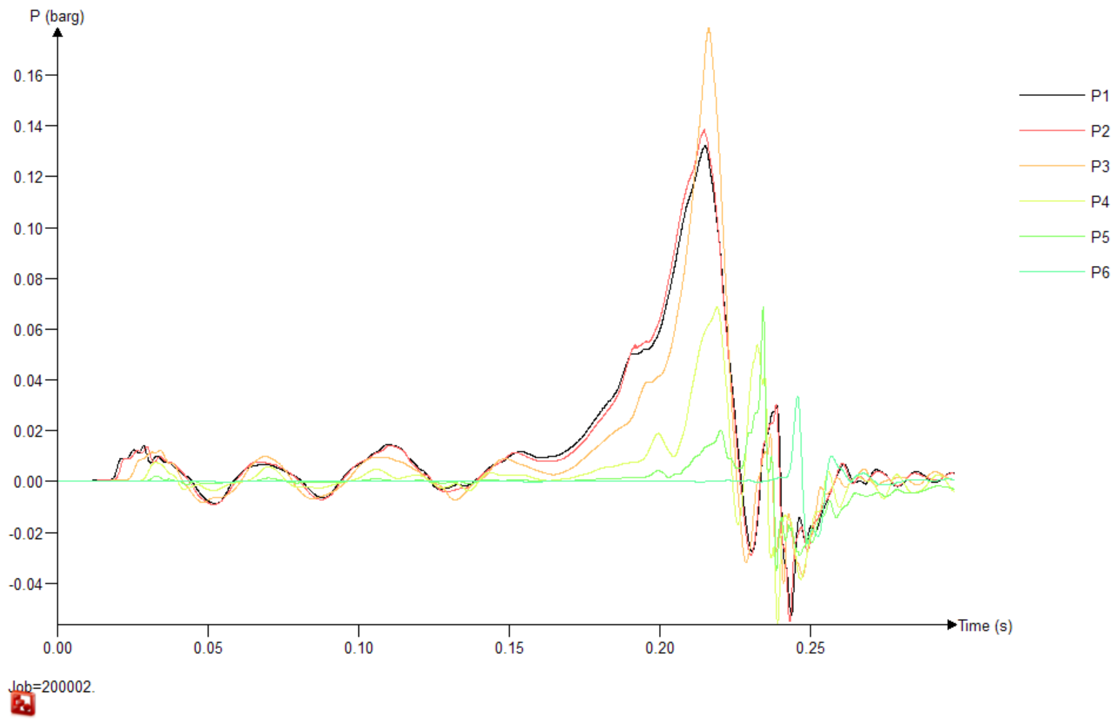

Figure A2.5 : Expected pressures for 'two vents open' scenario (ϕ E.R. 1.05)

<u>Pressure Sensor Positions</u>

P1 1.9m downstream of ignition (within the tube)
P2 2.3m downstream of ignition (within the tube)
P3 4.0m downstream of ignition (within the tube)
P4 5.6m downstream of ignition (within the tube)
P5 6.4m downstream of ignition (within the tube)
P6 10m downstream of ignition (on the far wall of the laboratory)

The maximum flame speed in this simulation was 40.82m/s, with the average flame speed being 21.81m/s as revealed in Table A2.2. As the main emphasis of this work focuses on slow laminar flame speeds, these conditions are unfavourable for any of this research and subsequently will not be used for this work.

As previously stated, the apparatus itself was designed, certified and strength tested to 0.1MPa (1 bar) and is therefore adequately strong enough to withstand this scenario and transitional pressures. Figure A2.6 shows the highest pressure predicted within the tube was recorded at pressure sensor P3 and was approximately 0.018MPa (0.18 bar) after 0.22 seconds post ignition and the localised ambient exit pressures were ≤0.006MPa (0.06 bar).

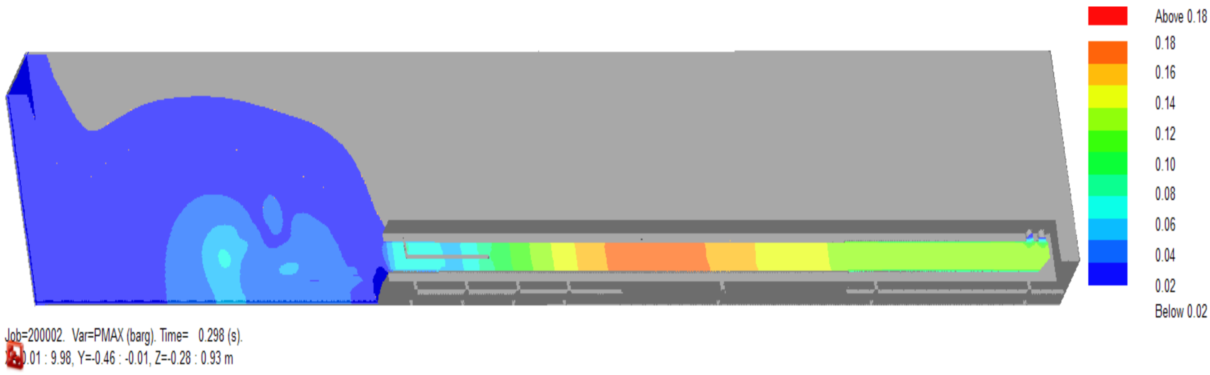

Figure A2.6 : Pressure profile associated with 'two vents open' scenario (ϕ E.R. 1.05)

Sensor	Time to achieve peak pressure (s)	Sensor position (m) (downstream of ignition)	Flame Speed (m/s)
P1	0.215	1.9	8.84
P2	0.218	2.3	10.55
P3	0.220	4.0	18.18
P4	0.222	5.6	25.23
P5	0.235	6.4	27.23
P6	0.245	10.0	40.82
		Average flame speed	21.81

Table A2.2 : Average and maximum flame speed associated with 'two vents open' scenario (ϕ E.R. 1.05)

Conclusions:-

Maximum pressure within explosion tube	0.018MPa (0.18bar)
Maximum pressure outside the tube	0.006MPa (0.06bar)
Maximum flame speed	40.82m/s
Average flame speed	21.81m/s

A2.2.3 Scenario 3 - Six vents open (E.R. ϕ 1.05)

In this scenario the methane-air mixture was E.R. ϕ 1.05 and is illustrated in Figure A2.7, whereby none of the exhaust outlets have been blanked off and all six of the exhaust vents were open to provide maximum initial relief from the explosion energy and thermal expansion generated by the explosion. Further information relating to the exhaust vent blockage ratios and percentages can be found in Chapter 4.

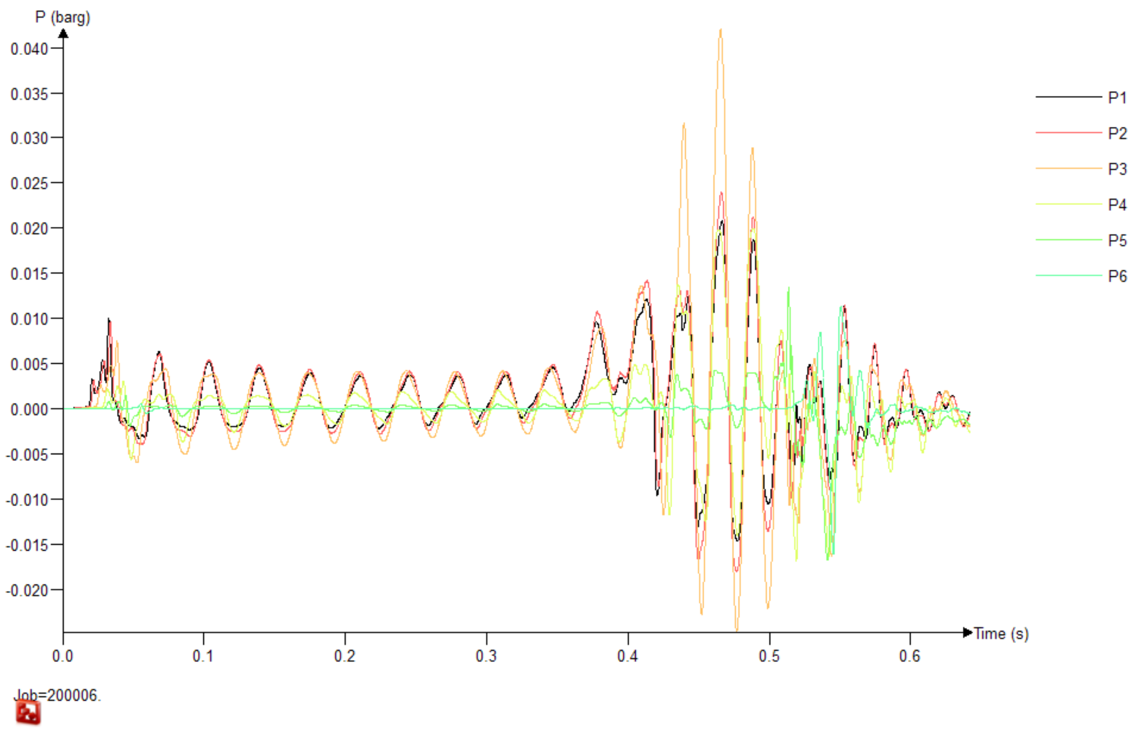

Figure A2.7 : Expected pressures for 'six vents open' scenario (ϕ E.R. 1.05)

<u>Pressure Sensor Positions</u>

P1 1.9m downstream of ignition (within the tube)
P2 2.3m downstream of ignition (within the tube)
P3 4.0m downstream of ignition (within the tube)
P4 5.6m downstream of ignition (within the tube)
P5 6.4m downstream of ignition (within the tube)
P6 10m downstream of ignition (on the far wall of the laboratory)

The maximum flame speed in this simulation was 18.12m/s, with the average flame speed being 9.75m/s as revealed in Table A2.3.

The 'hot trials' rig was originally designed to produce flame speeds of ≤30 m/s, whereby six exhaust vents would be open. This condition was been adopted for the main 'hot trials'.

The highest predicted pressure within the tube was recorded at pressure sensor P3 as shown in Figure A2.8 and was approximately 4.2KPa (0.042 bar) after 0.47 seconds post ignition and the localised ambient exit pressures were ≤2KPa (0.02 bar).

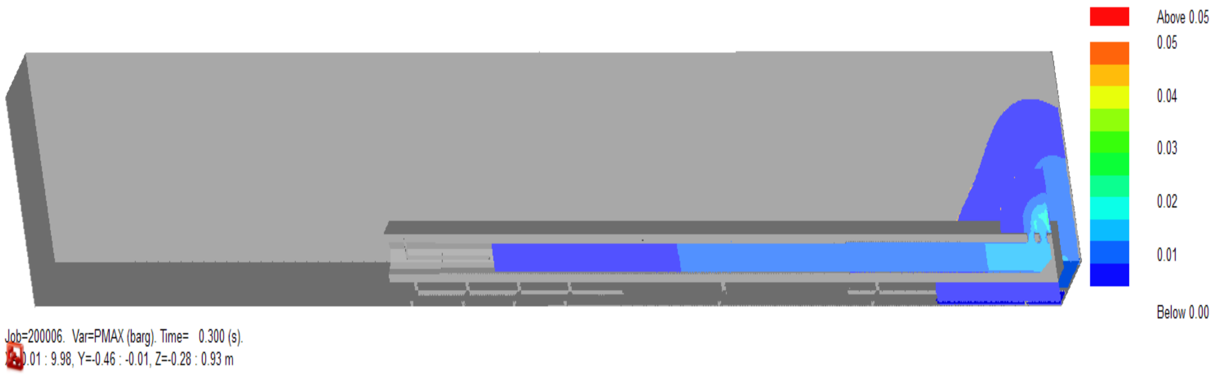

Figure A2.8 : Pressure profile associated with 'six vents open' scenario (ϕ E.R. 1.05)

Sensor	**Time to achieve peak pressure (s)**	**Sensor position (m) (downstream of ignition)**	**Flame Speed (m/s)**
P1	0.475	1.9	4.00
P2	0.480	2.3	4.79
P3	0.482	4.0	8.30
P4	0.510	5.6	10.98
P5	0.520	6.4	12.31
P6	0.552	10.0	18.12
		Average flame speed	9.75

Table A.1.3 : Average and maximum flame speed associated with 'six vents open' scenario (ϕ E.R. 1.05)

Conclusions:-

Maximum pressure within explosion tube	4.2KPa (0.042 bar)
Maximum pressure outside the tube	2KPa (0.02 bar)
Maximum flame speed	18.12 m/s
Average flame speed	9.75m/s

A2.2.4 Scenario 4 : Closed tube (E.R. ϕ 0.775) – Lean mixture

In this scenario the same blockage ratio conditions were the same scenario A2.2.1, however this time the mixture was 'lean' of stoichiometric. The methane-air content was 7.5% by volume (ϕ E.R. 0.775) and is shown in Figure A2.9. All of the exhaust outlets have been blanked off to ensure that the maximum explosion energy and thermal expansion is generated and contained within the explosion propagation tube. Further information relating to the exhaust vent blockage ratios and percentages can be found in Chapter 4.

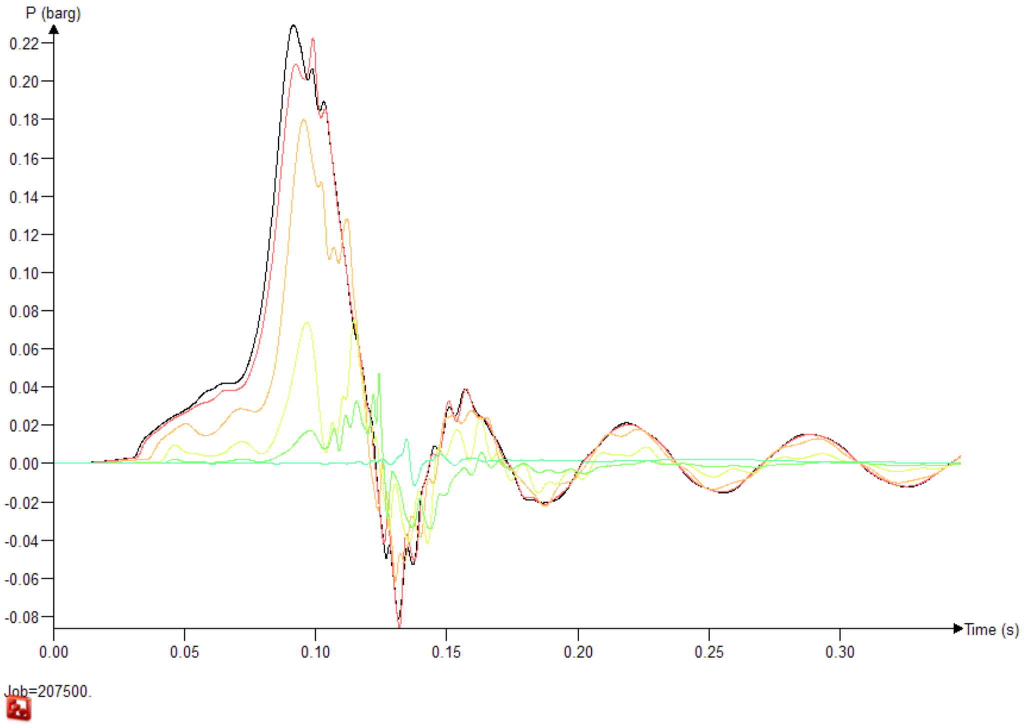

Figure A2.9 : Expected pressures for 'closed tube' scenario (ϕ E.R. 0.775)

<u>Pressure Sensor Positions</u>

P1 1.9m downstream of ignition (within the tube)
P2 2.3m downstream of ignition (within the tube)
P3 4.0m downstream of ignition (within the tube)
P4 5.6m downstream of ignition (within the tube)
P5 6.4m downstream of ignition (within the tube)
P6 10m downstream of ignition (on the far wall of the laboratory)

The maximum flame speed in this simulation was 74.07 m/s, with the average flame speed being 41.98m/s as revealed in Table A2.4. These speeds are also in excess of 30m/s and those required for this research and therefore these conditions will not be applied during these hot trials.

The highest pressure predicted within the tube was recorded at pressure sensor P1 and was approximately 23KPa (0.23 bar) after 0.095 seconds post ignition and the localised ambient exit pressures were ≤4KPa (0.04 bar) as shown in Figure A2.10.

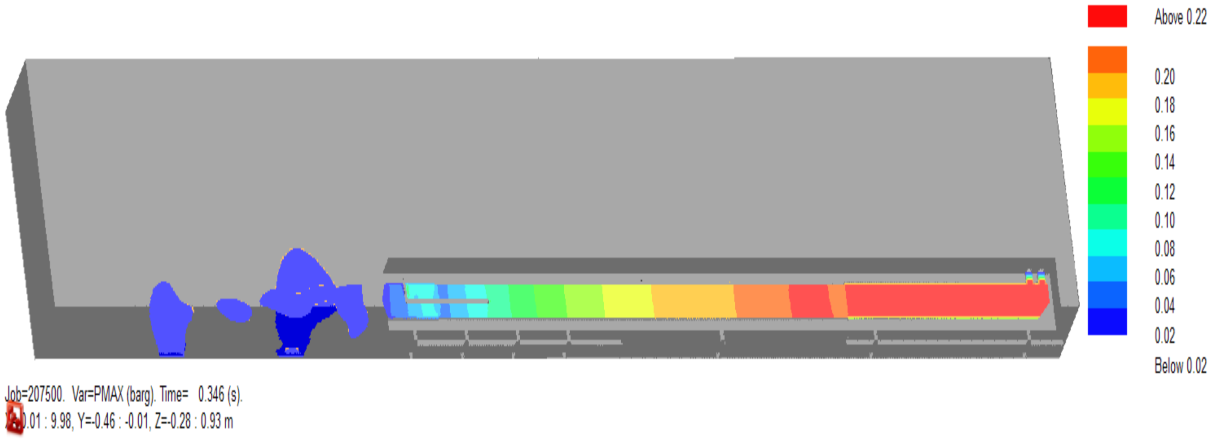

Figure A2.10: Pressure profile associated with 'closed tube' scenario (ϕ E.R. 0.775)

Sensor	Time to achieve peak pressure (s)	Sensor position (m) (downstream of ignition)	Flame Speed (m/s)
P1	0.095	1.9	20.00
P2	0.105	2.3	21.90
P3	0.100	4.0	40.00
P4	0.120	5.6	46.67
P5	0.130	6.4	49.23
P6	0.135	10.0	74.07
		Average flame speed	41.98

Table A2.4 : Average and maximum flame speed associated with 'closed tube (ϕ E.R. 0.775)

Conclusions:-

Maximum pressure within explosion tube	23KPa (0.23 bar)
Maximum pressure outside the tube	4KPA (0.04 bar)
Maximum flame speed	74.07 m/s
Average flame speed	41.98m/s

A2.2.5 Risk assessment report

Based on the finding previously discussed in A2.2.1 – A2.2.4 the risk assessment shown in Figure A2.11 was produced.

COMPANY	DEPARTMENT	AREA	DATE
University of Salford	Gas & Oil Engineering	Petroleum Lab	13th Dec 2012

Please identify in box 1 the type of Risk identified giving as much detail as possible. Indicate by a tick in the appropriate box the current level of Risk posed without any control measures being applied.

RISK IDENTIFIED | 1

LEVEL OF RISK		
HIGH	MED	LOW
		√

Explosion Overpressure
Potential Health & Safety Risk
Potential Risk to Building / Fabric

RISK TO | 2 | Please state who or what is at Risk & the likely cause of injury: e.g. fire, impact etc

Competent Research Student and Technician.
Laboratory area.

In box 3 please state the appropriate action required to reduce/control the Risk detailed in box 1 above. Indicate by a tick in the appropriate box the level of Risk now perceived. Note control measures should reduce level of risk rating from that identified in box 1

ACTION | 3

LEVEL OF RISK		
HIGH	MED	LOW
		√

FLACS CFD simulation for four scenarios:-

1. Closed tube – 9.9% Gas in Air (ϕ E.R. 1.05) – Worst case scenario
2. Two vents open – 9.9% Gas in Air (ϕ E.R. 1.05)
3. Six vents open – 9.9% Gas in Air (ϕ E.R. 1.05)
4. Closed tube – 7.5% Gas in Air (ϕ E.R. 0.775) – Lean mixture

Scenario no. 3 (Six vents open) will be adopted for all of the main hot trials and the methane-air mixtures will vary between 5% to 10% gas in air (by volume).

Therefore the worst case conditions for the hot trials testing will be:-

Maximum pressure within explosion tube	0.042 bar(g)
Maximum pressure outside the tube	0.02 bar(g)& typically ≤ 0.01 bar(g)
Maximum flame speed	18.12 m/s
Average flame speed	9.75 m/s

RISK ASSESSMENT CONDUCTED BY:	SIGNATURE:	DATE:
Steve Johnston	S A Johnston	13th Dec 2012
ACTION CONFIRMED/IMPLEMENTED BY:	SIGNATURE:	DATE:
Steve Johnston	S A Johnston	13th Dec 2012

RISK ASSESSMENT REVIEW DATE (NOT TO EXCEED 24 MONTHS)	12th Dec 2014

Figure A2.11 : Overpressure risk assessment using FLACS CFD software

A2.3 Additional safety precautions and procedures

A2.3.1 Flow diagram and checklist

The flow diagram and manual and automated sequence checklist shown in Figures A2.12 and A2.13 illustrate the manual and automatic sequence required to safely operate the flame propagation and mitigation rig. When carrying out 'hot trials' two persons, competent in applying this procedure, must always be present. Normally this will be the research assistant R.A. and the laboratory technician. The manual and automated control sequence and check list shown in Figure A2.13 shall be completed and accompany each of the 'hot trials'.

Figure A2.12 : 'Safe Operations' flow chart

A2.3.2 Manual and automated sequence checklist

Sequence order	Action	Manual / Automated	Checked (insert √)
1.	Close laboratory door and lock the bolt	Manual	
2.	Visually check rig for obvious defects	Manual	
3.	Check gas and air cylinder gauges	Manual	
4.	Connect gas and air to rig isolation valves	Manual	
5.	Visually check water pump rig	Manual	
6.	Fill or top-up water tank	Manual	
7.	Check or connect water hose to rig isolation valve	Manual	
8.	Check or connect water pump rig electrics to control box	Manual	
9.	Connect and turn on main rig power supply	Manual	
10.	Operate ‘primary’ key switch	Manual	
11.	Raise hinged end panel to closed position	Manual	
12.	24v DC magnet on hinged end plate is energised	Automated	
13.	Fill rig with desired concentration of gas and air, using rotameters and stopwatch to measure flow & volumes	Manual	
14.	Operate ‘recirculation booster’ key switch	Manual	
15.	Observe x10 volumes of the rig volume passing through turbine meter	Manual	
16.	Switch off ‘recirculation booster’ key switch	Manual	
17.	Allow 1 minute for mixture to become quiescent	Manual	
18.	Turn on data recorder and energise thermocouples and pressure transducers. Set up camera(s)	Manual	
19.	Check and verify air:gas concentration at 3 test points	Manual	
20.	Isolate gas and air supplies	Manual	
21.	Ensure that any personnel or visitors are outside the exclusion zone	Manual	
22.	Operate ‘ignition’ key switch and final safety check	Manual	
23.	Operate ‘ignition’ push button	Manual	
24.	Water pump is activated and starts	Automated	
25.	Water pump operates and develops steady spray	Automated	
26.	After 7 seconds 24v DC magnet on hinged end plate is energised	Automated	
27.	Hinged panel begins to fall open	Automated	
28.	Hinged panel opens >6mm and 2 micro-switches operate	Automated	
29.	Spark deployed at primary spark plug	Automated	
30.	Mixture ignites and propagates along tube	Automated	
31.	Primary key switch turned off	Manual	
32.	Waste water quantified and rig purged with air (direct to outside)	Manual	
33.	Data records named, copied and saved	Manual	
34.	Photographic records named, copied and saved	Manual	
35.	Video records named, copied and saved	Manual	

Figure A2.13 : Manual and automated control sequence and check list

A2.3.3 Personal protective equipment (PPE)

The following PPE was worn during every ‘hot trial’ to reduce the overall risk of danger:-

i. Ear plugs
ii. Safety shoes / boots
iii. Safety goggles
iv. Lab coat

A2.3.4 Supervision and support

The risk assessment, previously shown in Figure A2.1 states that a minimum of two persons must be present at all times during the hot trials. Lone working shall not be permitted.

A2.3.5 First aid

University health and safety procedures ensure that all laboratories are equipped with a suitably worded notice providing emergency contact details, including designated first aiders.

A2.3.6 Fire fighting equipment

University health and safety procedures ensure that all laboratories are suitably equipped with appropriate fire extinguishers and fire blankets where applicable. A suitably worded notice providing fire marshal contact details is also available.

A2.3.7 Evacuation and roll call

The personnel/visitors log shall used to identify all persons entering and leaving the laboratory. University health and safety procedures ensure that all laboratories have a suitably worded notice stating the designated assembly area for the zone being occupied. The laboratory visitors log must be used at roll call to account for personnel and visitors.

List of Figures

List of Tables

References

1 AIRMIC, Alarm. IRM : 2010. *A structured approach to Enterprise Risk Management (ERM) and the requirements of ISO 31000*

2 Health and Safety Executive : 2005. *Guidance on permit-to-work systems. A guide for the petroleum, chemical and allied industries.* ISBN 978 0 7176 2943 5

3 IGEM : August 2005. *IGE/UP/1 – Edition 2 – Strength testing, tightness testing and direct purging of industrial and commercial gas installations*. ISBN 978 0 7177 0145 2

APPENDIX 3

FLAME PROPAGATION AND MITIGATION RIG FABRICATION

A3.1 Metallic sections

Figure A3.1 shows the initial stages of the fabrication process. In this photo the ignition and explosion development section or 'driver section' can be seen. This consists of a 2 metre length of 8 inch / 219.2mm diameter mild steel pipe (ANSI schedule 40) with fully welded connections, complete with BSP threaded outlets and welded flanges to PN16 (12 x bolt holes). The pipe has an internal diameter of 7.981 inches / 202.7mm and a wall thickness of 0.322 inches / 8.4mm.

Figure A3.1: Ignition and explosion development section (pre drilling or welding)

Figure A3.2 reveals the next stage in the fabrication process. Two 80mm holes were drilled using a hole saw in the 8 inch / 202.7mm diameter mild steel pipe, in readiness to accept two 80mmBSP sockets. All rough edges were then removed and the sockets were placed in position in a vertical plane.

Figure A3.2 : 2 x 80mm holes in readiness to accept 2 x 80mm welded BSP sockets

Figure A3.3 shows the next stage in the fabrication process. Another four 80mm holes were drilled using a hole saw in the 8 inch / 202.7mm diameter mild steel pipe, in readiness to accept a further four 80mm BSP sockets. All rough edges were then removed and the sockets were placed in position at an angle of 45° to the vertical plane

Figure A3.3 : 6 x 80mm holes in readiness to accept 6 x 80mm welded BSP sockets

Two 80mm sockets were then welded in a vertical plane, perpendicularly to the axis, as shown in Figure A3.4 at the top, ignition end, of the ignition and explosion development section. These will form two of six exhaust outlets.

Figure A3.4 : Two 80mm BSP sockets, these will form two of six exhaust outlets

Figure A3.5 bares two 25mm sockets that have been welded in a vertical plane, perpendicularly to the axis, at the top, outlet end, of the ignition and explosion development section. These will be 'bushed' down to appropriate diameters, in readiness to accept a pressure transducer and thermocouple. The flange has also now been weleded in position, both internaily and externally, to provide greater mechanical strength.

Figure A3.5 : Outlet end of ignition and explosion driver section

Figure A3.6 reveals a plan view of the ignition end, of the ignition and explosion development section. The flange has also now been weleded in position, both internaily and externally, to provide greater mechanical strength.A blanking flange has been bolted in position to close this end of the section. The blank flange also has also been prepared to accept the primary and auxiliary ignition electrodes / spark plugs. Also see Figure.

Figure A3.6 : Plan view of exhaust outlets in the ignition and explosion driver section

Figure A3.7 displays a view from the ignition end, of the ignition and explosion development section. In this photo the blank flange has also been prepared to accept the primary and secondary ignition electrodes / spark plugs.

Figure A3.7 : Top side end view of ignition and explosion driver section

Figure A3.8 uncovers a view of underside of the ignition and explosion development section, taken from the ignition end. Three other connections are now exposed. The two 25mm BSP sockets welded to the pipe in the centre of the photo are to facilitate the gas and air filling valves. Whilst the third connection, also 25mm BSP (at the ignition end), has been provided to accommodate the valve and flame arrestor for the recirculation pipework.

Figure A3.8 : Underside end view of ignition and explosion development section

Figure A3.9 shows the terminal section of the rig. This 300mm section is also fabricated from 8 inch / 202.7mm diameter mild steel pipe (ANSI schedule 40) with fully welded connections, complete with BSP threaded outlets and welded flanges to PN16. There are three 15mm BSP connections and one 25mm BSP connection. Two of these connections are provided to accommodate a pressure transducer and a thermocouple.

Figure A3.9 : Terminal section of the rig, complete with four connections

Figure A3.10 shows the terminal section of the rig, complete with 15mm extended atomiser injection pipe. This pipe is connected via a welded sweep elbow to the lower connection, as seen on the photo. This configuration is to facilitate the introduction of water to supply the atomiser coaxially in the gaseous phase. The outlet end of the 15mm pipe has been threaded to permit the addition of additional pipe or a manifold arrangement.

Figure A3.10 : Terminal section of the rig, complete water induction tube

Figure A3.11 shows the terminal section of the rig, complete with four connections. The three connections on the right hand side are described above. The fourth connection is a 25mm BSP socket provided to accommodate the valve and flame arrestor for the recirculation pipework. The recirculation pipework will be connected between this connection and the similar connection, provided at the ignition end.

Figure A3.11 : Terminal section of the rig complete with four connections

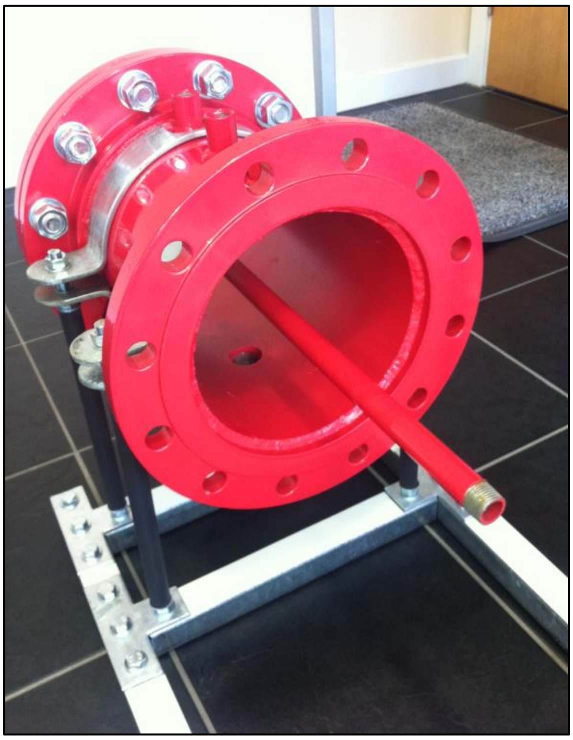

The terminal section of the rig shown in Figure A3.11 was cleaned by sand blasting and then hydrostatically strength tested to 0.1MPa (1 bar) prior to being sent for powder coating.

The rig was then assembled and mounted in the steel sub-frame as shown in Figure A3.12.

Figure A3.12 : Terminal section of rig - Powder coated and mounted

The ignition and explosion development section, or driver section shown below in Figure A3.13, was cleaned by sand blasting and then hydrostatically strength tested to 0.1MPa (I bar) prior to being sent for powder coating.

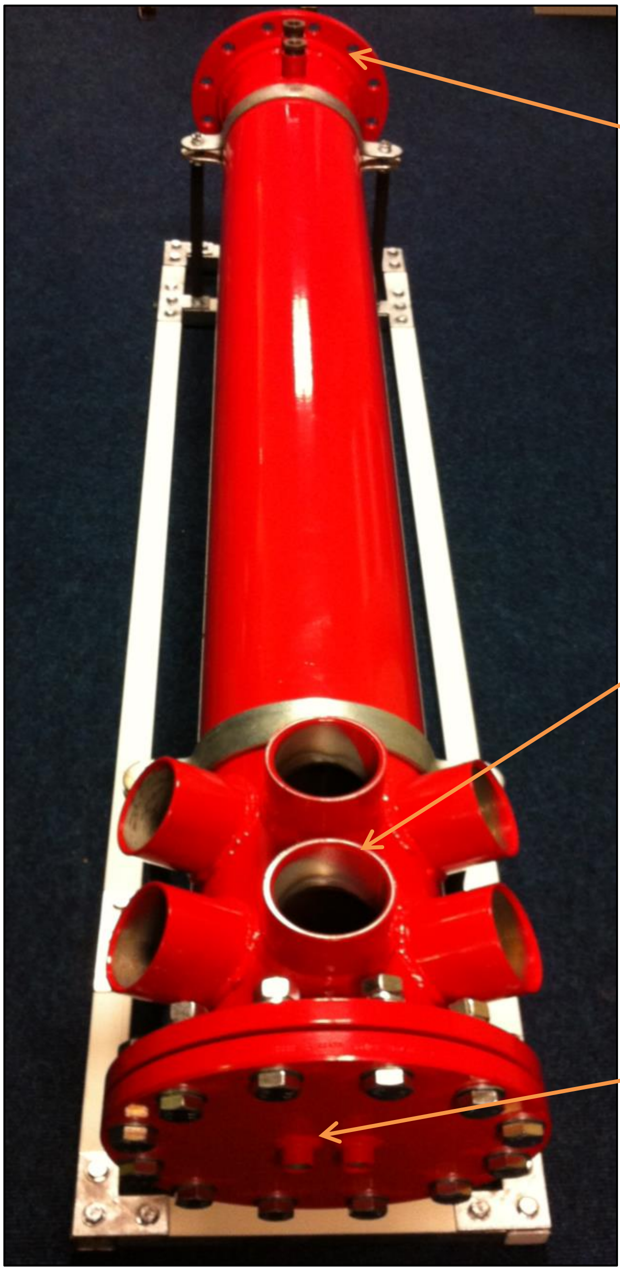

Two connections at the outlet end of the ignition and explosion development section for a thermocouple and a pressure transducer.

6 x 80mm connections at the ignition end of the ignition and explosion development section for varying flame speed and degree of explosion confinement

Two connections for the primary and auxiliary spark plugs at the closed end of the ignition and explosion development section.

Figure A3.13 : Ignition and explosion development section (driver section)

The rig was then assembled and mounted in the steel sub-frame. The steel sub-frame will also be used to facilitate the fixing of additional pipework, such as the re-circulation pipework, gas pump, meter and sample points.

A3.2 Poly(methyl-methacrylate) (PMMA) & Polycarbonate sections

Standard components were not available for the clear polycarbonate sections of the rig. Therefore materials had to be sourced / designed to enable the clear tubular section to be built. Polished polycarbonate discs (350mm diameter x 10mm thick) revealed in Figure A3.14 was used to form the flanges. The centre was found by using a compass and scribing three arcs. A 6mm hole was drilled to provide a rotation point for the plunge router.

A3.14 : Polished polycarbonate disc - 350mm diameter x 10mm thick

An 8 inch x PN16 flange of the same type used in the metallic sections of the rig, shown in Figure A3.15 being used as a template to mark the centres for the 22mm diameter bolt holes.

The bolt holes were formed using a high speed, 22mm diameter hole saw, complete with 6mm pilot drill.

A3.15 : 8 inch x PN16 flange used as template

Figure A3.16 shows a plunge router used to cut out the centre of the flanges.

A plunge router is a cutting, or milling machine designed to be ‘plunged’ into, or through the material and then moved laterally, cutting through the material. Many modern routers allow the speed of the bit's rotation to be varied. A slower rotation allows bits of larger cutting diameter to be used safely. Typical speeds range from 8,000 to 30,000 rpm

A3.16 : Plunge router in position to cut out centre of flange

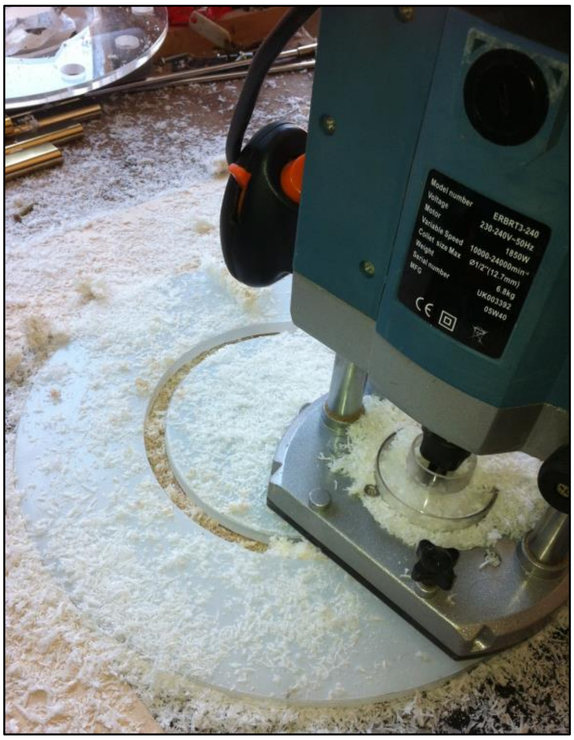

The router speed was carefully selected and controlled to ensure that the router bit cleared the cutting debris (swarf), whilst maintaining a smooth cutting operation. The time taken to complete the orbital cut was approximately three minutes (see Figure A3.17). This slow lateral movement was needed to ensure that the finished surfaces were even and uniform, to allow a good bond to the 200mm diameter PMMA tube.

Figure A3.17 : Plunge router used to cut out inner edge of flange

Figure A3.18 reveals a completed flange, with 200mm diameter centre hole and 12 x 22mm diameter bolts holes.

In this photo the polycarbonate flange has been positioned to check the tolerances of the orbital cutting, prior to polycarbonate bonding adhesive being applied.

Figure A3.18 : Bolt holes cut with 22mm hole saw and positioned on pipe for bonding

The assembled rig was pressure tested for leakage with air at a pressure of 0.1mpA (1bar)for a period of 30 minutes. The rig was retested for leakage after every 10 experiments, or if not used for more than a 24 hour period. A further test was also conducted when new components were added or removed.

The following designs shown in Figures A3.19 – A3.22 were some of the original design concepts for the Flame Propagation and Mitigation Rig (FPMR).

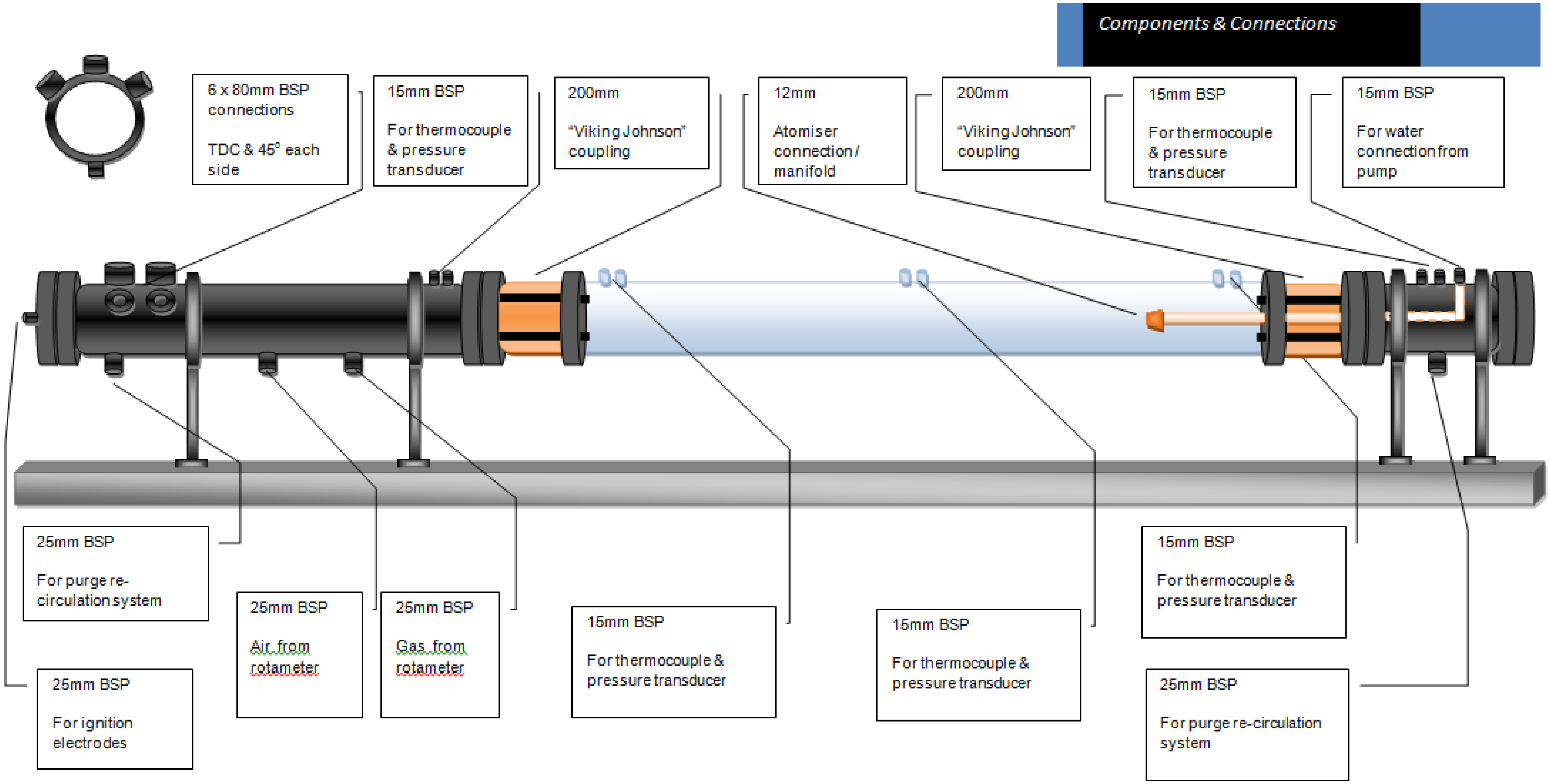

Explosion Propagation & Mitigation Tube Apparatus Copyright © Stephen Johnston 2012		
Created by	Created	Version
Stephen Johnston	27.02.2012	3.10

Figure A3.19 : Original design : example 1

Dimensions & Materials

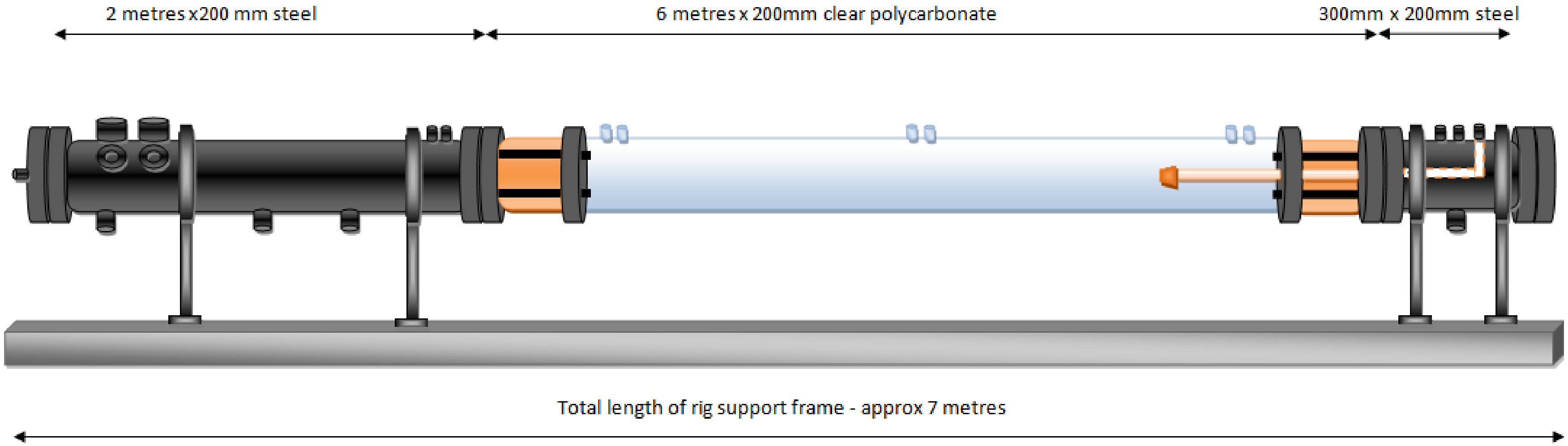

Explosion Propagation & Mitigation Tube Apparatus Copyright © Stephen Johnston 2012		
Created by	Created	Version
Stephen Johnston	27.02.2012	3.10

Figure A3.20 : Original design : example 2

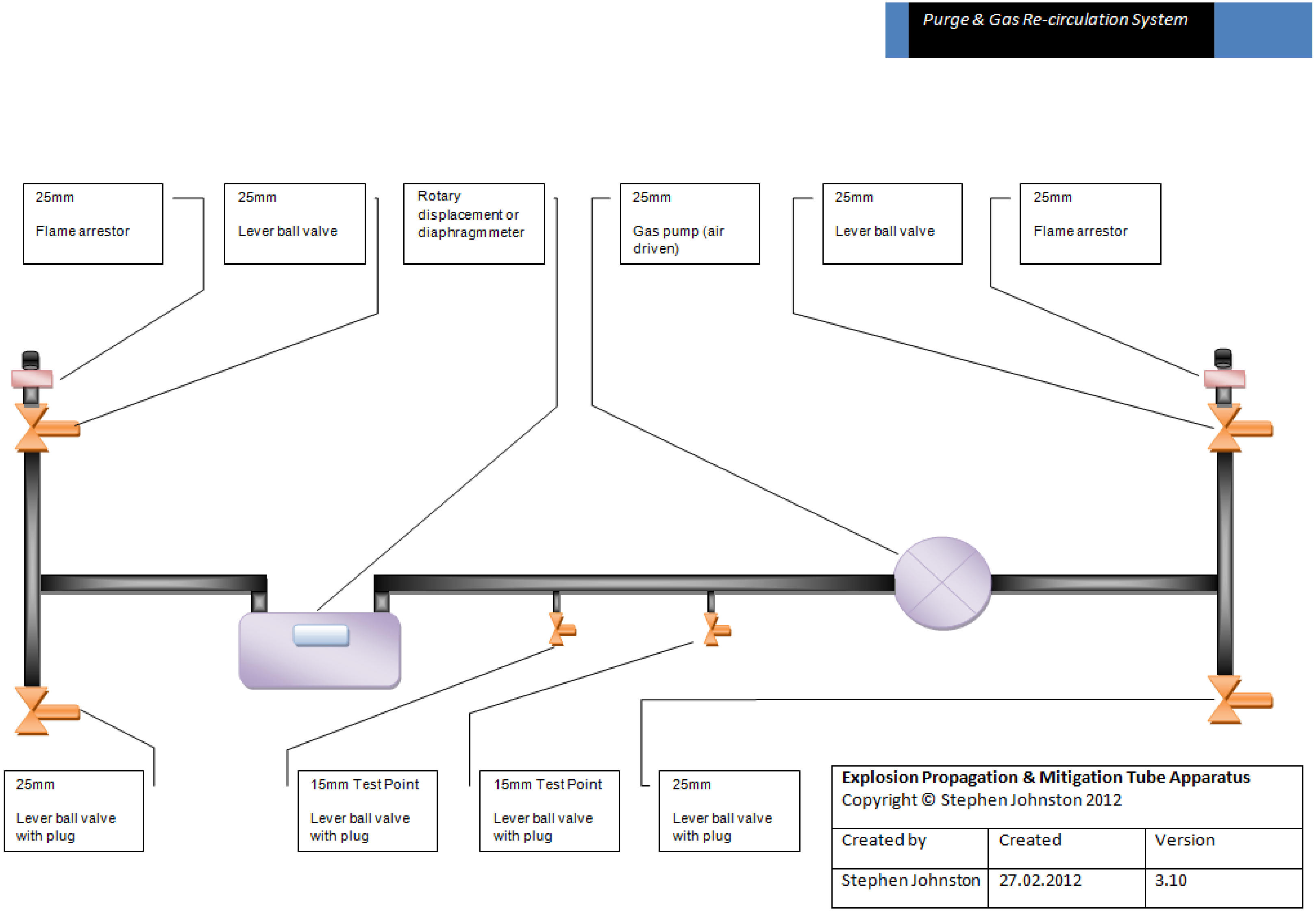

Figure A3.21 : Original design : example 3

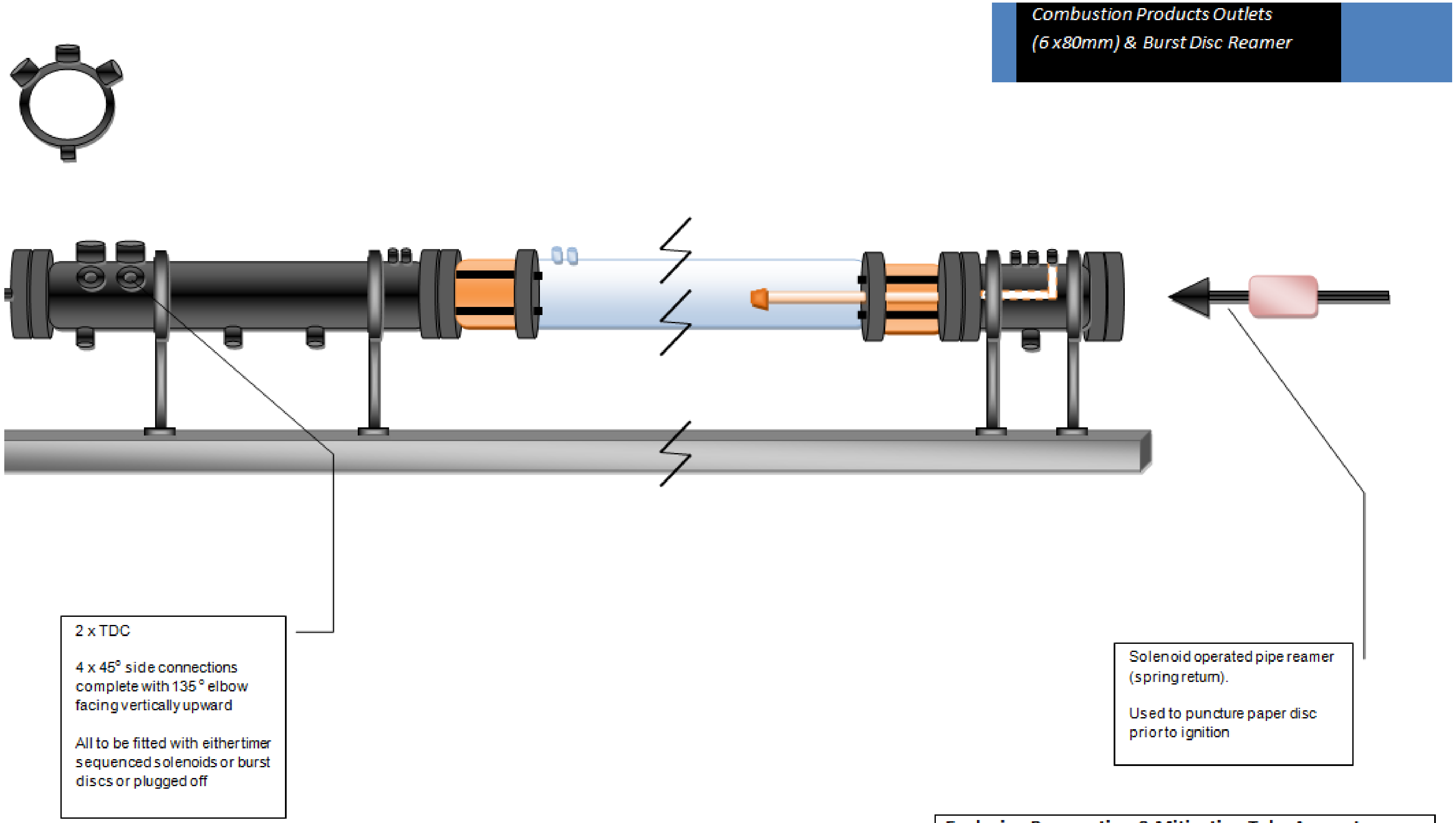

Explosion Propagation & Mitigation Tube Apparatus Copyright © Stephen Johnston 2012		
Created by	Created	Version
Stephen Johnston	27.02.2012	3.10

Figure A3.22 : Original design : example 4

List of figures

APPENDIX 4

METAHNE AND AIR DATA AND CERTIFICATION SHEETS

A4.1 Methane certification of purity

BOC
A Member of The Linde Group

Certificate

Technical and other enquiries:
The Priestley Centre, 10 Priestley Road
The Surrey Research Park
Guildford GU2 7XY, UK
Tel: 01483 244067 Fax: 01483 532115

UK gas and equipment orders:
Tel: 0800 02 0800
Fax: 0800 136 601

Export gas and equipment orders:
Tel: +44 1483 244067
Fax: +44 1483 532115

COMPONENT	NOMINAL CONCENTRATION			CERTIFIED VALUES
METHANE RESEARCH GRADE	100	%	>	99.995%

Certificate Date: 02.10.2012 Use By: 01.10.2017

APPROVED SIGNATORY Adam Martin

PROD ORDER	CYLINDER NO.	PRODUCT CODE	PAGE
2479569	S1079828	157682-L-C	1 of 2

FORM 5390

BOC
A Member of The Linde Group

Certificate

Technical and other enquiries:
The Priestley Centre, 10 Priestley Road
The Surrey Research Park
Guildford GU2 7XY, UK
Tel: 01483 244067 Fax: 01483 532115

UK gas and equipment orders:
Tel: 0800 02 0800
Fax: 0800 136 601

Export gas and equipment orders:
Tel: +44 1483 244067
Fax: +44 1483 532115

To reorder, please quote 157682 L CERTIFIED

CYLINDER DETAILS :

Cylinder Size: L	50.00Litres	Valve Outlet : BS4
Nominal Pressure:	200.0	Bar(g) at 15°C

This product conforms to the following specification:

N4.5
SG = 0.5543 @15°C, 1013.25mbar (ISO 6976)

BOC supplies a full range of gas control equipment to suit all applications.

PROD ORDER	CYLINDER NO.	PRODUCT CODE	PAGE
2479569	S1079828	157682-L-C	2 of 2

A4.2 Methane safety data sheet

BOC
A Member of The Linde Group

Safety data sheet
Methane, compressed.

Creation date :	27.01.2005	Version : 1.4	GB / E	SDS No. : 8321
Revision date :	30.04.2012			page 1 / 5

SECTION 1: Identification of the substance/mixture and of the company/undertaking

1.1. Product identifier
Product name
Methane, compressed.

EC No (from EINECS): 200-812-7
CAS No: 74-82-8
Index-Nr. 601-001-00-4
Chemical formula CH_4
REACH Registration number:
Not available.

1.2. Relevant identified uses of the substance or mixture and uses advised against
Relevant identified uses
Industrial and professional. Perform risk assessment prior to use.
Uses advised against
Consumer use.

1.3. Details of the supplier of the safety data sheet
Company identification
BOC, Priestley Road, Worsley, Manchester M28 2UT
E-Mail Address ReachSDS@boc.com

1.4. Emergency telephone number
Emergency phone numbers (24h): 0800 111 333

SECTION 2: Hazards identification

2.1. Classification of the substance or mixture

Classification acc. to Regulation (EC) No 1272/2008/EC (CLP/GHS)
Press. Gas (Compressed gas) - Contains gas under pressure; may explode if heated.
Flam. Gas 1 - Extremely flammable gas.

Classification acc. to Directive 67/548/EEC & 1999/45/EC
F+; R12
Extremely flammable.
Risk advice to man and the environment
In high concentrations may cause asphyxiation.
Compressed gas.

2.2. Label elements
- Labelling Pictograms

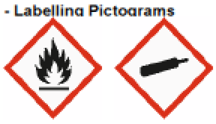

- Signal word
Danger

- Hazard Statements

H280	Contains gas under pressure; may explode if heated.
H220	Extremely flammable gas.

- Precautionary Statements

Precautionary Statement Prevention

P210	Keep away from heat/sparks/open flames/hot surfaces. - No smoking.

Precautionary Statement Response

P377	Leaking gas fire: Do not extinguish, unless leak can be stopped safely.
P381	Eliminate all ignition sources if safe to do so.

Precautionary Statement Storage

P403	Store in a well-ventilated place.

Precautionary Statement Disposal
None.

2.3. Other hazards
None.

SECTION 3: Composition/information on ingredients

Substance / Mixture: Substance.

3.1. Substances
Methane, compressed.
CAS No: 74-82-8
Index-Nr.: 601-001-00-4
EC No (from EINECS): 200-812-7
REACH Registration number:
Not available.
Contains no other components or impurities which will influence the classification of the product.

3.2. Mixtures
Not applicable.

SECTION 4: First aid measures

4.1. Description of first aid measures
First Aid General Information:
Remove victim to uncontaminated area wearing self contained breathing apparatus. Keep victim warm and rested. Call a doctor. Apply artificial respiration if breathing stopped.
First Aid Inhalation:
Remove victim to uncontaminated area wearing self contained breathing apparatus. Keep victim warm and rested. Call a doctor. Apply artificial respiration if breathing stopped.
First Aid Skin / Eye:
Adverse effects not expected from this product.
First Aid Ingestion:
Ingestion is not considered a potential route of exposure.

4.2. Most important symptoms and effects, both acute and delayed
In high concentrations may cause asphyxiation. Symptoms may include loss of mobility/consciousness. Victim may not be aware of asphyxiation. In low concentrations may cause narcotic effects. Symptoms may include dizziness, headache, nausea and loss of co-ordination.

4.3. Indication of any immediate medical attention and special treatment needed
None.

SECTION 5: Fire fighting measures

5.1. Extinguishing media
Suitable extinguishing media
Dry powder. Carbon dioxide. Use water spray or fog to control fire fumes.

Unsuitable extinguishing media
Do not use a solid water stream.

5.2. Special hazards arising from the substance or mixture
Specific hazards
Exposure to fire may cause containers to rupture/explode.
Hazardous combustion products
Incomplete combustion may form carbon monoxide.

5.3. Advice for fire-fighters
Specific methods
If possible, stop flow of product. Move container away or cool with water from a protected position. Do not extinguish a leaking gas flame unless absolutely necessary. Spontaneous/explosive re-ignition may occur. Extinguish any other fire.
Special protective equipment for fire-fighters
Normal firefighters' equipment consists of an appropriate SCBA (open-circuit positive pressure compressed air type) in combination with fire kit. Equipment and clothing to the following standards will provide a suitable level of protection for firefighters.
Guideline:
EN 469:2005: Protective clothing for firefighters. Performance requirements for protective clothing for firefighting., EN 137 Respiratory protective devices — Self-contained open-circuit compressed air breathing apparatus with full face mask — Requirements, testing, marking., EN 15090 Footwear for firefighters., EN 443 Helmets for fire fighting in buildings and other structures., EN 659 Protective gloves for firefighters.

SECTION 6: Accidental release measures

6.1. Personal precautions, protective equipment and emergency procedures
Wear self-contained breathing apparatus when entering area unless atmosphere is proved to be safe. Ensure adequate air ventilation. Eliminate ignition sources. Consider the risk of potentially explosive atmospheres. Evacuate area.

6.2. Environmental precautions
Try to stop release.

6.3. Methods and material for containment and cleaning up
Ventilate area.

6.4. Reference to other sections
See also sections 8 and 13.

SECTION 7: Handling and storage

7.1. Precautions for safe handling
Ensure equipment is adequately earthed. Suck back of water into the container must be prevented. Purge air from system before introducing gas. Use only properly specified equipment which is suitable for this product, its supply pressure and temperature. Contact your gas supplier if in doubt. Keep away from ignition sources (including static discharges). Refer to supplier's handling instructions. The substance must be handled in accordance with good industrial hygiene and safety procedures. Do not allow backfeed into the container. Purge system with dry inert gas (e.g. helium or nitrogen) before gas is introduced and when system is placed out of service. Assess the risk of a potentially explosive atmosphere and the need for explosion-proof equipment. Consider the use of only non-sparking tools. Do not smoke while handling product. Only experienced and properly instructed persons should handle gases under pressure. Protect containers from physical damage; do not drag, roll, slide or drop. Never use direct flame or electrical heating devices to raise the pressure of a container. Do not remove or deface labels provided by the supplier for the identification of the container contents. When moving containers, even for short distances, use appropriate equipment eg. trolley, hand truck, fork truck etc. Replace valve outlet caps or plugs and container caps where supplied as soon as container is disconnected from equipment. Ensure the complete gas system has been (or is regularly) checked for leaks before use. If user experiences any difficulty operating container valve discontinue use and contact supplier. Close container valve after each use and when empty, even if still connected to equipment. Never attempt to repair or modify container valves or safety relief devices. Damaged valves should be reported immediately to the supplier. Keep container valve outlets clean and free from contaminates particularly oil and water. Never attempt to transfer gases from one container to another.

7.2. Conditions for safe storage, including any incompatibilities
Observe all regulations and local requirements regarding storage of containers. Containers should not be stored in conditions likely to encourage corrosion. Cylinders should be stored in the vertical position and properly secured to prevent falling over. Stored containers should be periodically checked for general conditions and leakage. Container valve guards or caps should be in place. Store containers in location free from fire risk and away from sources of heat and ignition. Keep away from combustible materials. All electrical equipment in the storage areas should be compatible with the risk of potentially explosive atmosphere. Keep container below 50°C in a well ventilated place. Segregate from oxidant gases and other oxidants in store.

7.3. Specific end use(s)
None.

SECTION 8: Exposure controls/personal protection

8.1. Control parameters
No occupational exposure limit.
DNEL not available
PNEC not available.

8.2. Exposure controls
Appropriate engineering controls
A risk assessment should be conducted and documented in each work area to assess the risks related to the use of the product and to select the PPE that matches the relevant risk. The following recommendations should be considered. Product to be handled in a closed system. Gas detectors should be used when quantities of flammable gases/vapours may be released. Keep concentrations well below lower explosion limits. Consider work permit system e.g. for maintenance activities. Systems under pressure should be regularly checked for leakages. Provide adequate general or local ventilation. The substance is not classified for human health hazards or for environment effects and it is not PBT or vPvB so that no exposure assessment or risk characterisation is required. For tasks where the intervention of workers is required, the substance must be handled in accordance with good industrial hygiene and safety procedures.
Personal protective equipment
Eye and face protection
Wear eye protection to EN 166 when using gases.
Guideline:
EN 166 Personal Eye Protection
Skin protection
Hand protection
Advice: Wear working gloves and safety shoes while handling containers.
Guideline: EN 388 Protective gloves

Body protection

Personal protective equipment for the body should be selected based on the task being performed and the risks involved.
Other protection
Wear flame resistant/retardant clothing. Take precautionary measures against static discharges. Wear working gloves and safety shoes while handling containers. ISO/TR 2801:2007 Clothing for protection against heat and flame -- General recommendations for selection, care and use of protective clothing. EN ISO 20345 Personal protective equipment - Safety footwear.
Respiratory protection
Not required
Thermal hazards
Not required
Environmental Exposure Controls
Specific risk management measures are not required beyond good industrial hygiene and safety procedures. Refer to local regulations for restriction of emissions to the atmosphere. See section 13 for specific methods for waste gas treatment.

SECTION 9: Physical and chemical properties

9.1. Information on basic physical and chemical properties
General information
Appearance/Colour: Colourless gas.
Odour: None.
Melting point: -182 °C
Boiling point: -161 °C
Flash point: Not applicable for gases and gas mixtures.
Flammability range: 4,4 %(V) - 15 %(V)
Vapour Pressure 20 °C: Not applicable.
Relative density, gas (Air=1): 0,6
Solubility in water: 26 mg/l
Partition coefficient: n-octanol/water: 1,09 logPow
Autoignition temperature: 595 °C
Explosive properties:
Explosive acc. EU legislation: Not explosive.
Explosive acc. transp. reg.: Not explosive.
Oxidising properties: Not applicable.
Molecular weight: 16 g/mol
Critical temperature: -82 °C
Relative density, liquid (Water=1): 0,42

9.2. Other information
None.

SECTION 10: Stability and reactivity

10.1. Reactivity
Unreactive under normal conditions.

10.2. Chemical stability
Stable under normal conditions.

10.3. Possibility of hazardous reactions
Can form potentially explosive atmosphere in air., May react violently with oxidants.

10.4. Conditions to avoid
Keep away from heat/sparks/open flames/hot surfaces. - No smoking.

10.5. Incompatible materials
Oxidising agents. Air, Oxidiser. For material compatibility see latest version of ISO-11114.

10.6. Hazardous decomposition products
Under normal conditions of storage and use, hazardous decomposition products should not be produced.

SECTION 11: Toxicological information

11.1. Information on toxicological effects
Acute inhalation toxicity
Value: LC50
Species: Mouse
Exposure time: 2 h
Value in non-standard unit: 539600 ppm
Read across
Skin irritation
No data available.
Eye irritation
No data available.
Repeated dose toxicity
Species: Rat
Route of application: Inhalation
Value type: NOAEC
Value: 4000 ppm

Value type: LOAEC
Value: 12000 ppm
Genetic toxicity in vitro
Test type: Chromosome abberration
Result: Negative.
Method: OECD Test Guideline 473 (In vitro Mammalian Chromosome Aberration Test)
Read across
Genetic toxicity in vivo
Test type: Drosophila Sex-Linked Recessive Lethal Assay (SLRL) test
Negative.
Toxicity to reproduction/fertility
Species: Rat
Route of application: Inhalation
Value type: NOAEC
Value:

Value type: Gestation
Value: 9.000 ppm
Value type: Fertility
Value: 3.000 ppm
Method: OECD Guideline 422 (Combined Repeated Dose Toxicity Study with the Reproduction / Developmental Toxicity Screening Test)
Developmental toxicity/teratogenicity
Species: Rat
Route of application: Inhalation
Value type: NOAEC
Value: 9.000 ppm
Method: OECD Guideline 422 (Combined Repeated Dose Toxicity Study with the Reproduction / Developmental Toxicity Screening Test)

SECTION 12: Ecological information

12.1. Toxicity
When discharged in large quantities may contribute to the greenhouse effect.
Acute and prolonged toxicity fish
Species: Various (Freshwater)
Exposure time: 96 h
Value type: LC50
Value in standard unit mg/l: 49,9 mg/l

Method: Calculated

Species: Various (Freshwater)
Exposure time: 96 h
Value type: LC50
Value in standard unit mg/l: 27,98 mg/l
Method: Calculated
Acute toxicity aquatic invertebrates
Species: Water flea (Daphnia magna)
Exposure time: 48 h
Value type: LC50
Value in standard unit mg/l: 27,14 mg/l
Method: Calculated
Not harmful to invertebrates

Species: Water flea (Daphnia magna)
Exposure time: 48 h
Value type: LC50
Value in standard unit mg/l: 46,6 mg/l
Method: Calculated
Not harmful to invertebrates
Toxicity microorganisms
Species: Algae
Exposure time: 96 h
Value type: EC50
Value in standard unit mg/l: 19,37 mg/l
Not harmful to microorganisms

12.2. Persistence and degradability

Biodegradation
Test type: Aquatic.
Biodegradation: 100 %
Exposure time: 16,06 d
Readily biodegradable

12.3. Bioaccumulative potential
Not applicable.

12.4. Mobility in soil
The substance is a gas, not applicable.

12.5. Results of PBT and vPvB assessment
Not classified as PBT or vPvB.

12.6. Other adverse effects
Global Warming Potential GWP
25

SECTION 13: Disposal considerations

13.1. Waste treatment methods
Do not discharge into areas where there is a risk of forming an explosive mixture with air. Waste gas should be flared through a suitable burner with flash back arrestor. Do not discharge into any place where its accumulation could be dangerous. Contact supplier if guidance is required. Refer to the EIGA code of practice (Doc.30 "Disposal of Gases", downloadable at http://www.eiga.org) for more guidance on suitable disposal methods.
Gases in pressure containers (including halons) containing dangerous substances
EWC Nr. 16 05 04*

SECTION 14: Transport information

ADR/RID

14.1. UN number
1971

14.2. UN proper shipping name
Methane, compressed

14.3. Transport hazard class(es)
Class: 2
Classification Code: 1F
Labels: 2.1
Hazard number: 23
Tunnel restriction code: (B/D)
Emergency Action Code: 2SE

14.4. Packing group (Packing instruction)
P200

14.5. Environmental hazards
None.

14.6. Special precautions for user
None.

IMDG

14.1. UN number
1971

14.2. UN proper shipping name
Methane, compressed

14.3. Transport hazard class(es)
Class: 2.1
Labels: 2.1
EmS: FD, SU,

14.4. Packing group (Packing instruction)
P200

14.5. Environmental hazards
None.

14.6. Special precautions for user
None.

14.7. Transport in bulk according to Annex II of MARPOL73/78 and the IBC Code
Not applicable.

IATA

14.1. UN number
1971

14.2. UN proper shipping name
Methane, compressed

14.3. Transport hazard class(es)
Class: 2.1
Labels: 2.1

14.4. Packing group (Packing instruction)
P200

14.5. Environmental hazards
None.

14.6. Special precautions for user
None.

BOC
A Member of The Linde Group

Safety data sheet
Methane, compressed.

Creation date :	27.01.2005	Version : 1.4	GB / E	SDS No. : 8321
Revision date :	30.04.2012			page 5 / 5

Other transport information
Avoid transport on vehicles where the load space is not separated from the driver's compartment. Ensure vehicle driver is aware of the potential hazards of the load and knows what to do in the event of an accident or an emergency. Before transporting product containers ensure that they are firmly secured. Ensure that the container valve is closed and not leaking. Ensure that the valve outlet cap nut or plug (where provided) is correctly fitted. Ensure that the valve protection device (where provided) is correctly fitted. Ensure adequate ventilation. Ensure compliance with applicable regulations.

SECTION 15: Regulatory information

15.1. Safety, health and environmental regulations/legislation specific for the substance or mixture
Seveso Directive 96/82/EC: Listed

Other regulations
Dangerous Substances and Explosive Atmospheres Regulations (DSEAR 2002 No. 2776)
Management of Health and Safety at Work Regulations (1999 No. 3242)
The Regulatory Reform (Fire Safety) Order 2005 (2005 No. 1541)
Control of Substances Hazardous to Health Regulations (COSHH, 2002 No. 2677)
Equipment and Protective Systems Intended for Use in Potentially Explosive Atmospheres Regulations (EPS, 1996 No. 192)
Provision and Use of Work Equipment Regulations (PUWER, 1998 No. 2306)
Personal Protective Equipment Regulations (1992 No. 2966)
Control of Major Accident Hazards Regulations (COMAH, 1999 No. 743)
Chemical Hazards Information and Packaging for Supply (CHIP, 1994 No. 3247)
Pressure Systems Safety Regulations (PER, 2000 No. 128)
This Safety Data Sheet has been produced to comply with Regulation (EU) 453/2010.

15.2. Chemical safety assessment
CSA has not been carried out.

SECTION 16: Other information

Ensure all national/local regulations are observed. Ensure operators understand the flammability hazard. The hazard of asphyxiation is often overlooked and must be stressed during operator training. Before using this product in any new process or experiment, a thorough material compatibility and safety study should be carried out.

Advice
Whilst proper care has been taken in the preparation of this document, no liability for injury or damage resulting from its use can be accepted. Details given in this document are believed to be correct at the time of going to press.

Further information
Note:
When using this document care should be taken, as the decimal sign and its position complies with rules for the structure and drafting of international standards, and is a comma on the line.
As an example 2,000 is two (to three decimal places) and not two thousand, whilst 1.000 is one thousand and not one (to three decimal places).

References
Various sources of data have been used in the compilation of this SDS, they include but are not exclusive to:

Agency for Toxic Substances and Diseases Registry (ATSDR) (http://www.atsdr.cdc.gov/)
European Chemical Agency: Guidance on the Compilation of Safety Data Sheets.
European Chemical Agency: Information on Registered Substances http://apps.echa.europa.eu/registered/registered-sub.aspx#search
European Industrial Gases Association (EIGA) Doc. 169/11 Classification and Labelling guide.
ISO 10156:2010 Gases and gas mixtures – Determination of fire potential and oxidizing ability for the selection of cylinder valve outlets.
International Programme on Chemical Safety (http://www.inchem.org/)
Matheson Gas Data Book, 7th Edition.
National Institute for Standards and Technology (NIST) Standard Reference Database Number 69
The ESIS (European chemical Substances 5 Information System) platform of the former European Chemicals Bureau (ECB) ESIS (http://ecb.jrc.ec.europa.eu/esis/).
The European Chemical Industry Council (CEFIC) ERICards.
Threshold Limit Values (TLV) from the American Conference of Governmental Industrial Hygienists (ACGIH).
United States of America's National Library of Medicine's toxicology data network TOXNET (http://toxnet.nlm.nih.gov/index.html)
Substance specific information from suppliers.
EH40 (as ammended) Workplace exposure limits.

End of document

A4.3 Air safety data sheet

BOC
A Member of The Linde Group

Safety data sheet
Air, compressed.

Creation date : 27.01.2005 Version : 1.2 GB / E SDS No. : 8309
Revision date : 15.12.2011 page 1 / 4

SECTION 1: Identification of the substance/mixture and of the company/undertaking

1.1. Product identifier
Product name
Air, compressed.
Trade name
Compressed air

EC No (from EINECS): Mixture not applicable
CAS No: 132259-10-0
Index-Nr. Mixture not applicable
Chemical formula Mixture of N2 and O2
REACH Registration number: Not applicable, both substances are exempt from registration.

1.2. Relevant identified uses of the substance or mixture and uses advised against.
Industrial / technical grade unsuitable for medical application / inhalation

1.3. Details of the supplier of the safety data sheet
Company identification
BOC, Priestley Road, Worsley, Manchester M28 2UT
E-Mail Address ReachSDS@boc.com

1.4. Emergency telephone number
Emergency phone numbers (24h): 0800 111 333

SECTION 2: Hazards identification

2.1. Classification of the substance or mixture

Classification acc. to Regulation (EC) No 1272/2008/EC (CLP/GHS)
Press. Gas (Compressed gas) - Contains gas under pressure; may explode if heated.

Classification acc. to Directive 67/548/EEC & 1999/45/EC
Not classified as hazardous to health.
Risk advice to man and the environment
Compressed gas.

2.2. Label elements
- Labelling Pictograms

- Signal word
Warning

- Hazard Statements
H280 Contains gas under pressure; may explode if heated.

- Precautionary Statements

Precautionary Statement Prevention
None.

Precautionary Statement Response
None.

Precautionary Statement Storage

P403 Store in a well-ventilated place.

Precautionary Statement Disposal
None.

2.3. Other hazards
None.

SECTION 3: Composition/information on ingredients

Substance / Mixture: Mixture.

3.1. Substances
Not applicable.

3.2. Mixtures

	Contents	CAS No.	EC No.	Reg.No.	Classification
Oxygen	<= 20 %	7782-44-7	231-956-9	*1	O; R8
					Ox. Gas 1 (H270) Press. Gas (H280)
Nitrogen	>= 80 %	7727-37-9	231-783-9	*1	Not classified as hazardous to health
					Press. Gas (H280)

*1 Listed in Annex IV/V of Regulation (EC) No 1907/2006 (REACH), exempted from registration.

SECTION 4: First aid measures

4.1. Description of first aid measures
First Aid General Information:
Adverse effects not expected from this product.
First Aid Inhalation:
Adverse effects not expected from this product.
First Aid Skin / Eye:
Adverse effects not expected from this product.
First Aid Ingestion:
Ingestion is not considered a potential route of exposure.

4.2. Most important symptoms and effects, both acute and delayed
Adverse effects not expected from this product.

4.3. Indication of any immediate medical attention and special treatment needed
None.

SECTION 5: Fire fighting measures

5.1. Extinguishing media
Suitable extinguishing media
All known extinguishants can be used.

5.2. Special hazards arising from the substance or mixture
Specific hazards
Exposure to fire may cause containers to rupture/explode. Supports combustion.
Hazardous combustion products
None.

BOC
A Member of The Linde Group

Safety data sheet
Air, compressed.

Creation date : 27.01.2005		Version : 1.2	GB / E	SDS No. : 8309
Revision date : 15.12.2011				page 2 / 4

5.3. Advice for fire-fighters
Specific methods
Move container away or cool with water from a protected position.
Special protective equipment for fire-fighters
Normal firefighters' equipment consists of an appropriate SCBA (open-circuit positive pressure compressed air type) in combination with fire kit. Equipment and clothing to the following standards will provide a suitable level of protection for firefighters.
Guideline:
EN 469:2005: Protective clothing for firefighters. Performance requirements for protective clothing for firefighting., EN 137 Respiratory protective devices — Self-contained open-circuit compressed air breathing apparatus with full face mask — Requirements, testing, marking., EN 15090 Footwear for firefighters., EN 443 Helmets for fire fighting in buildings and other structures., EN 659 Protective gloves for firefighters.

SECTION 6: Accidental release measures

6.1. Personal precautions, protective equipment and emergency procedures
None

6.2. Environmental precautions
None

6.3. Methods and material for containment and cleaning up
None

6.4. Reference to other sections
See also sections 8 and 13.

SECTION 7: Handling and storage

7.1. Precautions for safe handling
Only experienced and properly instructed persons should handle gases under pressure. The product must be handled in accordance with good industrial hygiene and safety procedures. Use only properly specified equipment which is suitable for this product, its supply pressure and temperature. Contact your gas supplier if in doubt. Ensure the complete gas system has been (or is regularly) checked for leaks before use. Refer to supplier's handling instructions. Suck back of water into the container must be prevented. Do not allow backfeed into the container. Protect containers from physical damage; do not drag, roll, slide or drop. When moving containers, even for short distances, use appropriate equipment eg. trolley, hand truck, fork truck etc. Leave valve protection caps in place until the container has been secured against either a wall or bench or placed in a container stand and is ready for use. If user experiences any difficulty operating container valve discontinue use and contact supplier. Never attempt to repair or modify container valves or safety relief devices. Damaged valves should be reported immediately to the supplier. Keep container valve outlets clean and free from contaminates particularly oil and water. Replace valve outlet caps or plugs and container caps where supplied as soon as container is disconnected from equipment. Close container valve after each use and when empty, even if still connected to equipment. Never attempt to transfer gases from one container to another. Never use direct flame or electrical heating devices to raise the pressure of a container. Do not remove or deface labels provided by the supplier for the identification of the container contents.

7.2. Conditions for safe storage, including any incompatibilities
Keep container below 50°C in a well ventilated place. Secure cylinders to prevent them from falling. Observe all regulations and local requirements regarding storage of containers. Stored containers should be periodically checked for general conditions and leakage. Container valve guards or caps should be in place. Store containers in location free from fire risk and away from sources of heat and ignition. Keep away from combustible materials. Cylinders should be stored in the vertical position and properly secured to prevent falling over. Containers should not be stored in conditions likely to encourage corrosion.

7.3. Specific end use(s)
None.

SECTION 8: Exposure controls/personal protection

8.1. Control parameters

No occupational exposure limit.

DNEL not available
PNEC not available.

8.2. Exposure controls
Appropriate engineering controls
A risk assessment should be conducted and documented in each work area to assess the risks related to the use of the product and to select the PPE that matches the relevant risk. The following recommendations should be considered. Consider work permit system e.g. for maintenance activities. Systems under pressure should be regularly checked for leakages. The product is not classified for human health hazards or for environment effects and it is not PBT or vPvB so that no exposure assessment or risk characterisation is required. For tasks where the intervention of workers is required, the product must be handled in accordance with good industrial hygiene and safety procedures.
Personal protective equipment
Eye and face protection
Wear eye protection to EN 166 when using gases.
Guideline:
EN 166 Personal Eye Protection
Skin protection
Hand protection
Advice: Wear working gloves and safety shoes while handling containers.
Guideline: EN 388 Protective gloves

Body protection
No precautionary measures are necessary.
Other protection
Wear working gloves and safety shoes while handling containers.
EN ISO 20345 Personal protective equipment - Safety footwear.
Respiratory protection
No precautionary measures are necessary.
Thermal hazards
No precautionary measures are necessary.
Environmental Exposure Controls
Specific risk management measures are not required beyond good industrial hygiene and safety procedures. Refer to local regulations for restriction of emissions to the atmosphere. See section 13 for specific methods for waste gas treatment.

SECTION 9: Physical and chemical properties

9.1. Information on basic physical and chemical properties
General Information
Appearance/Colour: Colourless gas.
Odour: None.
Odour threshold:
Mixture not applicable

BOC
A Member of The Linde Group

Safety data sheet
Air, compressed.

Creation date :	27.01.2005	Version : 1.2	GB / E	SDS No. : 8309
Revision date :	15.12.2011			page 3 / 4

Melting point: Mixture not applicable
Boiling point: -194.3°C
Flash point: Not applicable for gases and gas mixtures.
Flammability range: Mixture not applicable
Vapour Pressure 20 °C: Mixture not applicable
Solubility in water: Mixture not applicable
Partition coefficient: n-octanol/water: Mixture not applicable
Autoignition temperature: Mixture not applicable
Explosive properties:
Explosive acc. EU legislation: Not explosive.
Explosive acc. transp. reg.: Not explosive.
Oxidising properties: Not applicable.
Molecular weight: 28.96 g/mol
Critical temperature: Mixture not applicable
Relative density, liquid (Water=1): Mixture not applicable
Relative density, gas (Air=1): 1

9.2. Other information
Not applicable.

SECTION 10: Stability and reactivity

10.1. Reactivity
Unreactive under normal conditions.

10.2. Chemical stability
Stable under normal conditions.

10.3. Possibility of hazardous reactions
None.

10.4. Conditions to avoid
None.

10.5. Incompatible materials
No reaction with any common materials in dry or wet conditions.

10.6. Hazardous decomposition products
None.

SECTION 11: Toxicological information

11.1. Information on toxicological effects
General
No known toxicological effects from this product.

SECTION 12: Ecological information

12.1. Toxicity
No known ecological damage caused by this product.

12.2. Persistence and degradability
No assessment required.

12.3. Bioaccumulative potential
No assessment required.

12.4. Mobility in soil
No assessment required.

12.5. Results of PBT and vPvB assessment
Not classified as PBT or vPvB.

12.6. Other adverse effects
None.

SECTION 13: Disposal considerations

13.1. Waste treatment methods
Vent to atmosphere in a well ventilated place.

EWC Nr. 16 05 05

SECTION 14: Transport information

ADR/RID

14.1. UN number
1002

14.2. UN proper shipping name
Air, compressed

14.3. Transport hazard class(es)
Class: 2
Classification Code: 1A
Labels: 2.2
Hazard number: 20
Tunnel restriction code: (E)
Emergency Action Code: 2T

14.4. Packing group (Packing instruction)
P200

14.5. Environmental hazards
None.

14.6. Special precautions for user
None.

IMDG

14.1. UN number
1002

14.2. UN proper shipping name
Air, compressed

14.3. Transport hazard class(es)
Class: 2.2
Labels: 2.2
EmS: F-C, S-V

14.4. Packing group (Packing instruction)
P200

14.5. Environmental hazards
None.

14.6. Special precautions for user
None.

14.7. Transport in bulk according to Annex II of MARPOL73/78 and the IBC Code
Not applicable.

IATA

14.1. UN number
1002

Safety data sheet
Air, compressed.

14.2. UN proper shipping name
Air, compressed

14.3. Transport hazard class(es)
Class: 2.2
Labels: 2.2

14.4. Packing group (Packing instruction)
P200

14.5. Environmental hazards
None.

14.6. Special precautions for user
None.

SECTION 15: Regulatory information

15.1. Safety, health and environmental regulations/legislation specific for the substance or mixture

Other regulations
Management of Health and Safety at Work Regulations (1999 No. 3242)
The Regulatory Reform (Fire Safety) Order 2005 (2005 No. 1541)
Control of Substances Hazardous to Health Regulations (COSHH, 2002 No. 2677)
Provision and Use of Work Equipment Regulations (PUWER, 1998 No. 2306)
Personal Protective Equipment Regulations (1992 No. 2966)
Control of Major Accident Hazards Regulations (COMAH, 1999 No. 743)
Chemical Hazards Information and Packaging for Supply (CHIP, 1994 No. 3247)
Pressure Systems Safety Regulations (PER, 2000 No. 128)

This Safety Data Sheet has been produced to comply with Regulation (EU) 453/2010.

15.2. Chemical safety assessment
This product is either exempt from REACH, does not meet the minimum volume threshold for a CSR or the CSA has not yet been carried out.

SECTION 16: Other information

Ensure all national/local regulations are observed. Before using this product in any new process or experiment, a thorough material compatibility and safety study should be carried out.
Advice
Whilst proper care has been taken in the preparation of this document, no liability for injury or damage resulting from its use can be accepted. Details given in this document are believed to be correct at the time of going to press.
Further information
Note:
When using this document care should be taken, as the decimal sign and its position complies with rules for the structure and drafting of international standards, and is a comma on the line.
As an example 2,000 is two (to three decimal places) and not two thousand, whilst 1.000 is one thousand and not one (to three decimal places).
References
Various sources of data have been used in the compilation of this SDS, they include but are not exclusive to:

Agency for Toxic Substances and Diseases Registry (ATSDR) (http://www.atsdr.cdc.gov/)
European Chemical Agency: Guidance on the Compilation of Safety Data Sheets.
European Chemical Agency: Information on Registered Substances http://apps.echa.europa.eu/registered/registered-sub.aspx#search
European Industrial Gases Association (EIGA) Doc. 169/11 Classification and Labelling guide.
ISO 10156:2010 Gases and gas mixtures – Determination of fire potential and oxidizing ability for the selection of cylinder valve outlets.
International Programme on Chemical Safety (http://www.inchem.org/)
Matheson Gas Data Book, 7th Edition.
National Institute for Standards and Technology (NIST) Standard Reference Database Number 69
The ESIS (European chemical Substances 5 Information System) platform of the former European Chemicals Bureau (ECB) ESIS (http://ecb.jrc.ec.europa.eu/esis/).
The European Chemical Industry Council (CEFIC) ERICards.
United States of America's National Library of Medicine's toxicology data network TOXNET (http://toxnet.nlm.nih.gov/index.html)
Substance specific information from suppliers.
EH40 (as ammended) Workplace exposure limits.

End of document

APPENDIX 5

PRESSURE TRANSDUCER CALIBRATION

OMEGADYNE INC.
An Affiliate of Omega Engineering, Inc.
CERTIFICATE OF CALIBRATION

Model Number: MMG10WV5H4MC6T2A1CE

Capacity: 25.00 mbar G
Excitation: 24.00 Vdc
Technician: BNU

Serial Number: 430015
Date: 3/5/2013
Job: R6275

Pressure Connection: G 1/4B-M

WIRING CODE

Electrical Connection:
Pin 1: + EXCITATION
Pin 2: - EXCITATION
Pin 3: + OUTPUT
Pin 4: N/C

CALIBRATION WORKSHEET

Pressure mbar G	OUTPUT Vdc
0.00	0.018
12.50	2.523
25.00	5.023
12.50	2.522
0.00	0.017

NOTES

NIST Traceable Number(s): C-1954, C-1310

Omegadyne Inc., certifies that the above instrumentation has been calibrated and tested to meet or to exceed the published specifications. This calibration was performed using instrumentation and standards that are traceable to the National Institute of Standards and Technology. This document also ensures that all testing performed complies with MIL-STD 45662-A, ISO 10012-1, and ANSI/NCSL Z540-1-1994 requirements. After Final Calibration our products are stored in an environmentally controlled stock room and are considered in bonded storage. Depending on environmental conditions and severity of use, factory calibration is recommended every one to three years after the initial service installation date.

Bruce Lott
Accepted and Certified By

3/5/2013
Date

Omegadyne Inc., 149 Stelzer Court, Sunbury, OH 43074 (740) 965-9340
http://www.omegadyne.com email: info@omegadyne.com (800) USA-DYNE

OMEGADYNE INC.
An Affiliate of Omega Engineering, Inc.
CERTIFICATE OF CALIBRATION

Model Number: MMG10WV5H4MC6T2A1CE

Capacity: 25.00 mbar G
Excitation: 24.00 Vdc
Technician: BNU

Serial Number: 427001
Date: 3/5/2013
Job: R6275

Pressure Connection: G 1/4B-M

WIRING CODE

Electrical Connection:
Pin 1: + EXCITATION
Pin 2: - EXCITATION
Pin 3: + OUTPUT
Pin 4: N/C

CALIBRATION WORKSHEET

Pressure mbar G	OUTPUT Vdc
0.00	0.001
12.50	2.504
25.00	5.004
12.50	2.504
0.00	0.001

NOTES

NIST Traceable Number(s): C-1954, C-1310

Omegadyne Inc., certifies that the above instrumentation has been calibrated and tested to meet or to exceed the published specifications. This calibration was performed using instrumentation and standards that are traceable to the National Institute of Standards and Technology. This document also ensures that all testing performed complies with MIL-STD 45662-A, ISO 10012-1, and ANSI/NCSL Z540-1-1994 requirements. After Final Calibration our products are stored in an environmentally controlled stock room and are considered in bonded storage. Depending on environmental conditions and severity of use, factory calibration is recommended every one to three years after the initial service installation date.

Bruce Lott

Accepted and Certified By

3/5/2013
Date

Omegadyne Inc., 149 Stelzer Court, Sunbury, OH 43074 (740) 965-9340
http://www.omegadyne.com email: info@omegadyne.com (800) USA-DYNE

OMEGADYNE INC.
An Affiliate of Omega Engineering, Inc.
CERTIFICATE OF CALIBRATION

Model Number: MMG10WV5H4MC6T2A1CE

Capacity: 25.00 mbar G
Excitation: 24.00 Vdc
Technician: BNU

Serial Number: 435214
Date: 3/5/2013
Job: R6275

Pressure Connection: G 1/4B-M

WIRING CODE

Electrical Connection: Pin 1: + EXCITATION
Pin 2: - EXCITATION
Pin 3: + OUTPUT
Pin 4: N/C

CALIBRATION WORKSHEET

Pressure mbar G	OUTPUT Vdc
0.00	- 0.002
12.50	2.502
25.00	5.005
12.50	2.503
0.00	0.001

NOTES

NIST Traceable Number(s): C-1954, C-1310

Omegadyne Inc., certifies that the above instrumentation has been calibrated and tested to meet or to exceed the published specifications. This calibration was performed using instrumentation and standards that are traceable to the National Institute of Standards and Technology. This document also ensures that all testing performed complies with MIL-STD 45662-A, ISO 10012-1, and ANSI/NCSL Z540-1-1994 requirements. After Final Calibration our products are stored in an environmentally controlled stock room and are considered in bonded storage. Depending on environmental conditions and severity of use, factory calibration is recommended every one to three years after the initial service installation date.

Bruce Lott

Accepted and Certified By

3/5/2013
Date

Omegadyne Inc., 149 Stelzer Court, Sunbury, OH 43074 (740) 965-9340
http://www.omegadyne.com email: info@omegadyne.com (800) USA-DYNE

APPENDIX 6

THERMOCOUPLE CALIBRATION

CERTIFICATE OF CONFORMANCE

SHIPPED FROM : TC LTD
UNITS 1-6 BIRMINGTON ROAD NORTH
WHITTINGTON MOOR, CHESTERFIELD
DERBYSHIRE, S41 9BE, UNITED KINGDOM

SALES OFFICE: TC LTD, PO BOX 130, UXBRIDGE, UB8 2YS, UNITED KINGDOM
FAX: 01895 273540 TELEPHONE: 01895 252222
E MAIL: sales@tc.co.uk WEB SITE: www.tc.co.uk
Registered in England No. 1125377 VAT No. GB 223 7880 55

DELIVER TO:

SPECIALIST GAS ASSESSMENT
SERVICES LTD - GOODS INWARDS
UNIT 8 BROUGHTON WAY, OFF
THOMPSON RD, WHITEHILLS BUS. PRK
BLACKPOOL, LANCASHIRE, FY4 5QN

OUR REFERENCE
42965P

YOUR ORDER NUMBER
C/CARD

ACCOUNT NUMBER	DESPATCH NUMBER	DESPATCH DATE
/S297-01	D/ 42965P	

DATE ORDER RECEIVED	ESTIMATED SHIP DATE	ORDER ANALYSIS DATA
30/07/13	12/08/13	08/08

PRODUCT	DESCRIPTION	QUANTITY	UNITS	REMARKS
12	THERMOCOUPLE ASSEMBLY TYPE 12 12-K-50-118-3.0-2X-3P2L-3 MTRS A30KX . HSBC CARD PAYMENT TO THE AMOUNT OF 107.64 RECEIVED WITH THANKS . CUSTOMER CONTACT IS STEVE JOHNSTON YOUR CONTACT AT TC IS PAUL SMITH .	4.00	EACH	We certify that the goods supplied against this certificate of conformance have been inspected and tested in accordance with our normal test procedures and fully comply with the description shown, our published specification and the relevant British Standards, details of which are avaliable on Request. Customer Agreed Concession Reference(if applicable) ______
AH	PACKING,CARRIAGE & INSURANCE	1.00	LOT	Inspector's Signature G Date 09 08 13

Any damage or shortage must be reported in writing, or by fax within 7 days of receipt of goods. Customers intending to return goods to us (for any reason what-so-ever) must first obtain our written agreement with instructions as to which factory site the goods are to be returned to. We accept no liability for shortage, damage or non-receipt, in any way, for goods being returned.

CERTIFICATE OF CONFORMANCE

SHIPPED FROM : TC LTD
UNITS 1-6 BIRMINGTON ROAD NORTH
WHITTINGTON MOOR, CHESTERFIELD
DERBYSHIRE, S41 9BE, UNITED KINGDOM

SALES OFFICE: TC LTD, PO BOX 130, UXBRIDGE, UB8 2YS, UNITED KINGDOM
FAX: 01895 273540 TELEPHONE: 01895 252222
E MAIL: sales@tc.co.uk WEB SITE: www.tc.co.uk
Registered in England No. 1125377 VAT No. GB 223 7880 55

DELIVER TO:

SPECIALIST GAS ASSESSMENT
SERVICES LTD - GOODS INWARDS
UNIT 8 BROUGHTON WAY, OFF
THOMPSON RD, WHITEHILLS BUS. PRK
BLACKPOOL, LANCASHIRE, FY4 5QN

OUR REFERENCE
43660P

YOUR ORDER NUMBER
C/CARD

ACCOUNT NUMBER	DESPATCH NUMBER	DESPATCH DATE
/S297-01	D/ 43660P	

DATE ORDER RECEIVED	ESTIMATED SHIP DATE	ORDER ANALYSIS DATA
30/08/13	09/09/13	04/09

PRODUCT	DESCRIPTION	QUANTITY	UNITS	REMARKS
12	THERMOCOUPLE ASSEMBLY TYPE 12 12-K-50-118-3.0-2X-3P2L-3 MTRS A30KX . HSBC CARD PAYMENT TO THE AMOUNT OF 107.64 RECEIVED WITH THANKS . CUSTOMER CONTACT IS STEVE JOHNSTON YOUR CONTACT AT TC IS DEAN TUVEY .	4.00	EACH	We certify that the goods supplied against this certificate of conformance have been inspected and tested in accordance with our normal test procedures and fully comply with the description shown, our published specification and the relevant British Standards, details of which are avaliable on Request. Customer Agreed Concession Reference(if applicable) ______
AH	PACKING,CARRIAGE & INSURANCE	1.00	LOT	Inspector's Signature ______ Date 04-09-13

Any damage or shortage must be reported in writing, or by fax within 7 days of receipt of goods. Customers intending to return goods to us (for any reason what-so-ever) must first *obtain our written agreement with instructions* as to which factory site the goods are to be returned to. We accept no liability for shortage, damage or non-receipt, in any way, for goods being returned.

APPENDIX 7

CONTROLLER WIRING DIAGRAM

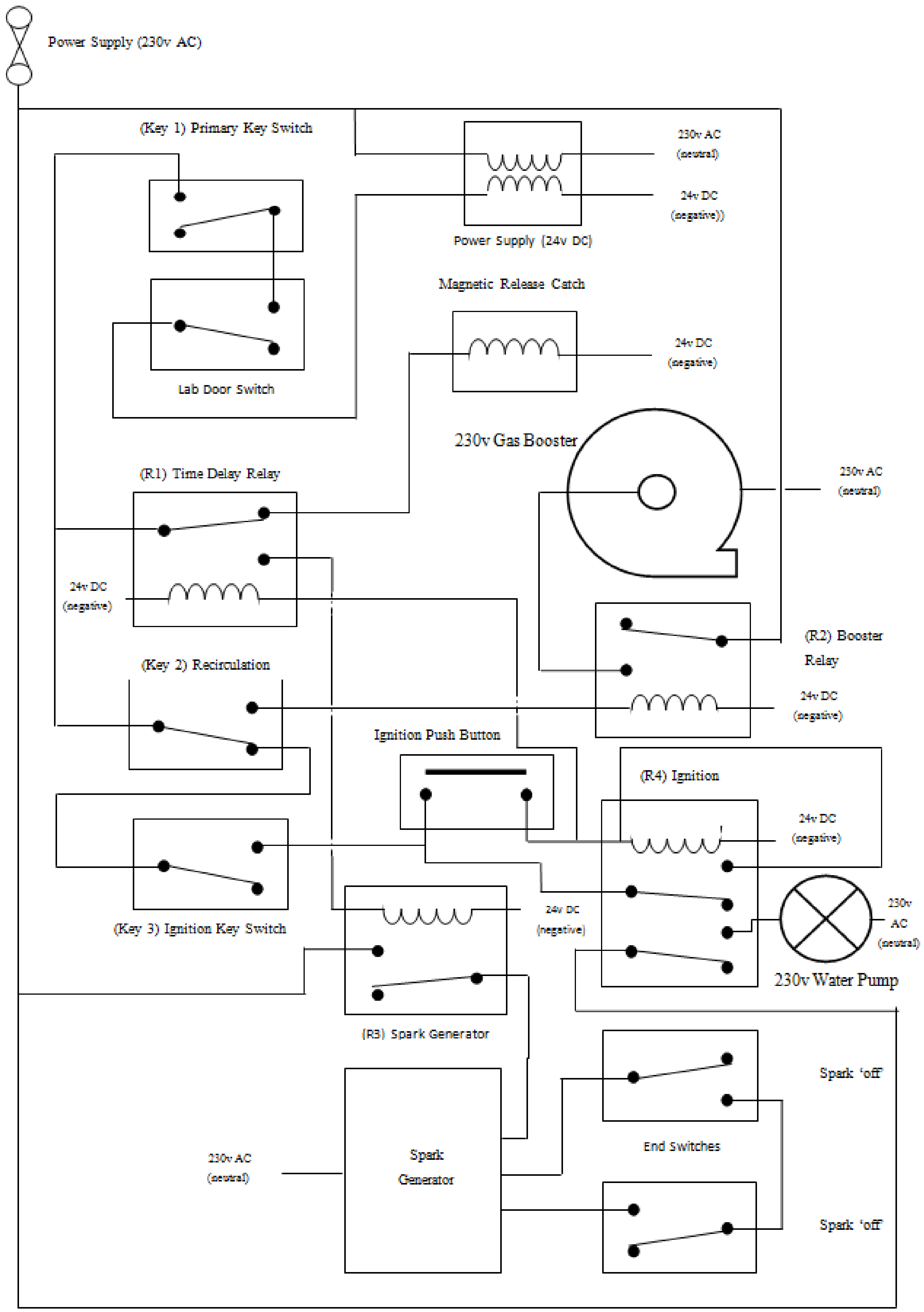

Figure A7.1 : Sequence controller wiring diagram

APPENDIX 8

SPILL RETURN ATOMISER (SRA) FLOW RATE DATA

Atomiser - Inlet & Outlet Orifices			Data Collected									
Tip Orifice Diameter (mm)	Spill Orifice Diameter (mm)	Tangental Orifice Diameter (mm)	P Water Supply Pressure (bar)	Duration of Water Collection from Exit Orifice (seconds)	Container + Water Collected from Exit Orifice (gramms)	Q - Exit Orifice Volume Flow Rate (litres / min)	Duration of Water Collection from Spill Orifice (seconds)	Container + Water Collected from Spill Orifice (gramms)	Q - Spill Orifice Volume Flow Rate (litres / min)	Exit : Spill Flow Rate Ratio	K - Factor (Q / √ P)
0.3	0.5	2 x 0.6	5	15.53	119.40	0.201	10.56	203.10	0.77	0.260	0.090
[redacted]			6	13.29	115.80	0.218	12.11	234.00	0.82	0.264	0.089
			7	13.91	122.40	0.237	13.46	262.80	0.87	0.272	0.090
			8	15.06	130.20	0.250	12.45	260.20	0.93	0.269	0.088
			9	12.22	121.60	0.266	13.55	287.50	0.97	0.273	0.089
			10	16.18	140.60	0.271	11.94	268.20	1.01	0.269	0.086
			11	13.40	129.10	0.276	13.00	294.90	1.05	0.263	0.083
			12	13.75	133.90	0.290	14.53	330.70	1.09	0.267	0.084
			13	12.47	128.80	0.295	11.25	278.20	1.12	0.262	0.082
			14	17.10	154.70	0.306	13.91	330.30	1.13	0.270	0.082

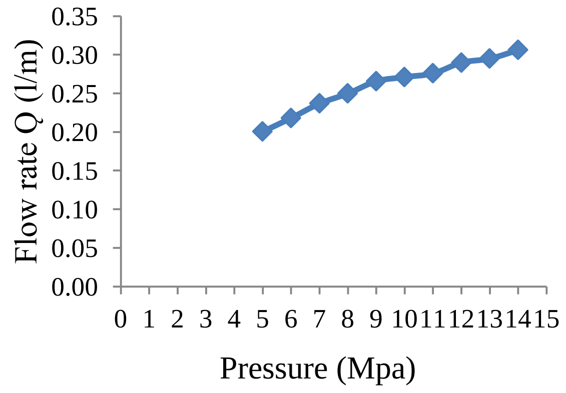

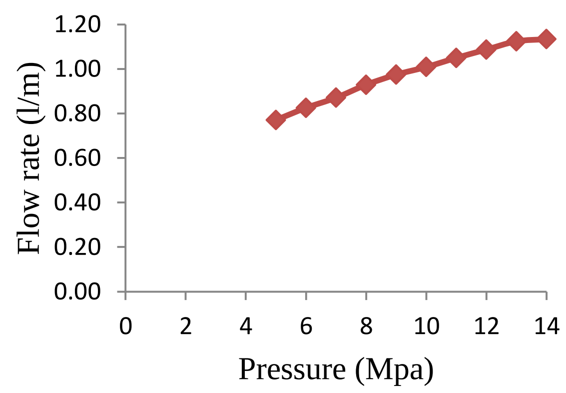

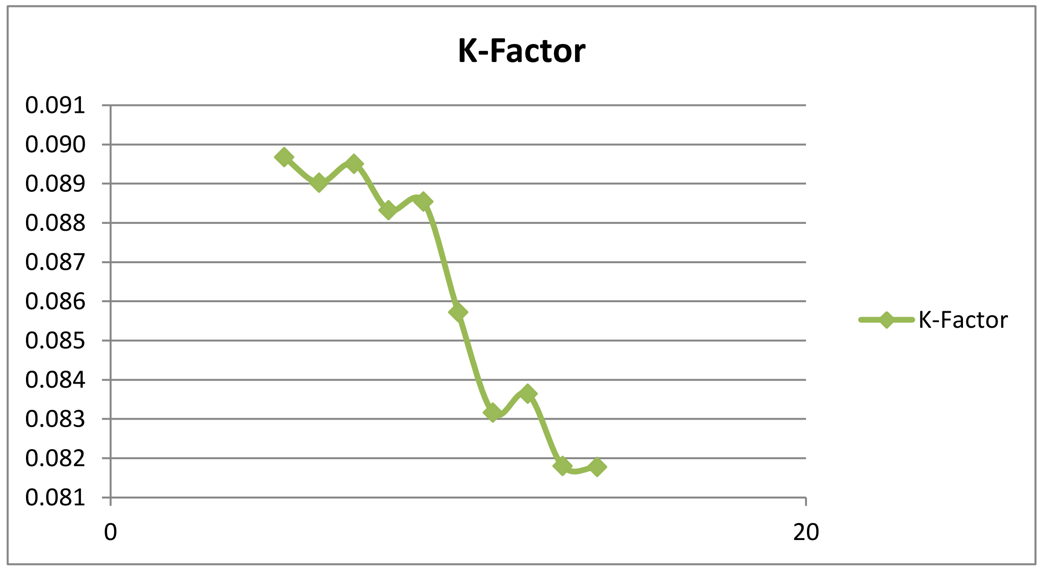

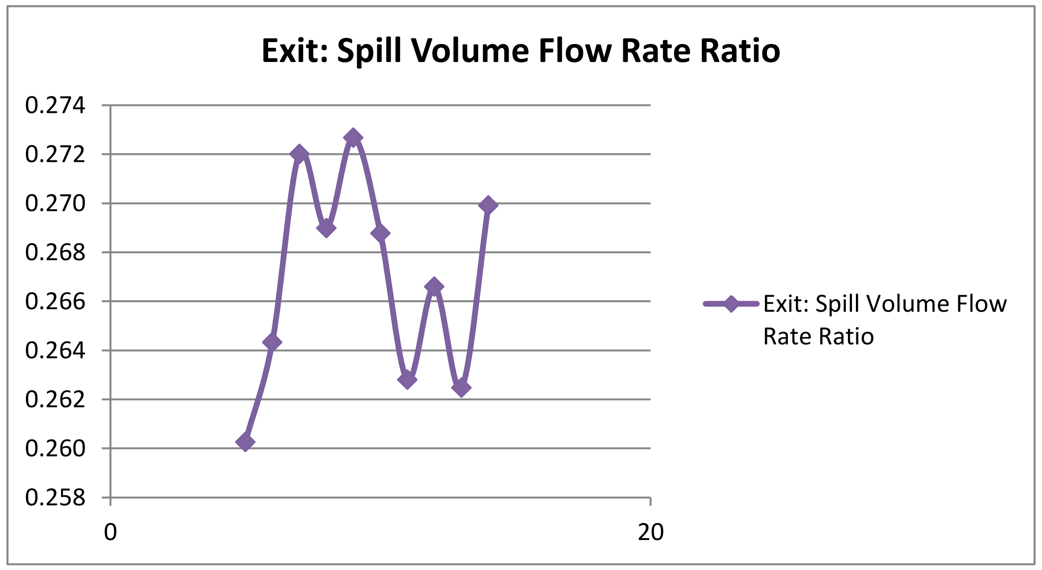

Atomiser - Inlet & Outlet Orifices			Data Collected								
Tip Orifice Diameter (mm)	Spill Orifice Diameter (mm)	Tangental Orifice Diameter (mm)	P Water Supply Pressure (bar)	Duration of Water Collection from Exit Orifice (seconds)	Container + Water Collected from Exit Orifice (gramms)	Q - Exit Orifice Volume Flow Rate (litres / min)	Duration of Water Collection from Spill Orifice (seconds)	Container + Water Collected from Spill Orifice (gramms)	Q - Spill Orifice Volume Flow Rate (litres / min)	Exit : Spill Flow Rate Ratio	K - Factor (Q / √ P)
0.5	0.5	2 x 0.6	5	12.25	183.00	0.57	12.57	187.00	0.57	0.992	0.253
[redacted]			6	12.31	195.60	0.62	13.00	199.20	0.61	1.027	0.255
			7	13.56	215.00	0.65	14.03	219.80	0.65	1.002	0.247
			8	9.69	179.30	0.69	11.28	198.80	0.70	0.991	0.245
			9	11.32	206.40	0.74	12.13	215.50	0.73	1.006	0.245
			10	12.50	228.00	0.77	13.53	238.60	0.76	1.015	0.244
			11	12.75	237.90	0.80	13.66	246.10	0.78	1.022	0.242
			12	13.85	257.70	0.82	15.91	282.70	0.81	1.015	0.238
			13	13.34	256.40	0.85	15.57	287.40	0.85	1.003	0.236
			14	13.31	260.70	0.87	12.56	249.40	0.87	1.002	0.233

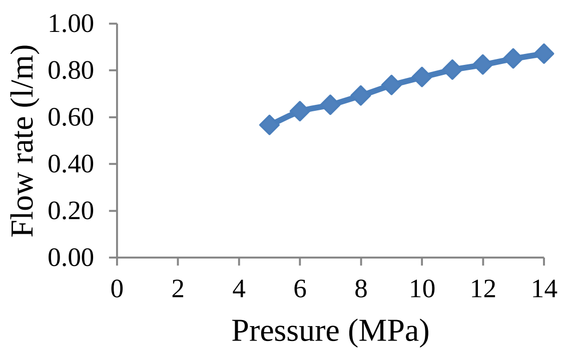

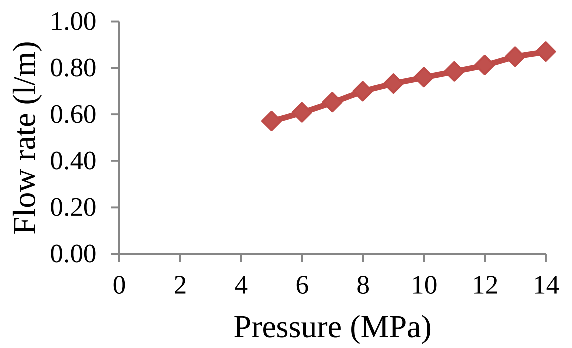

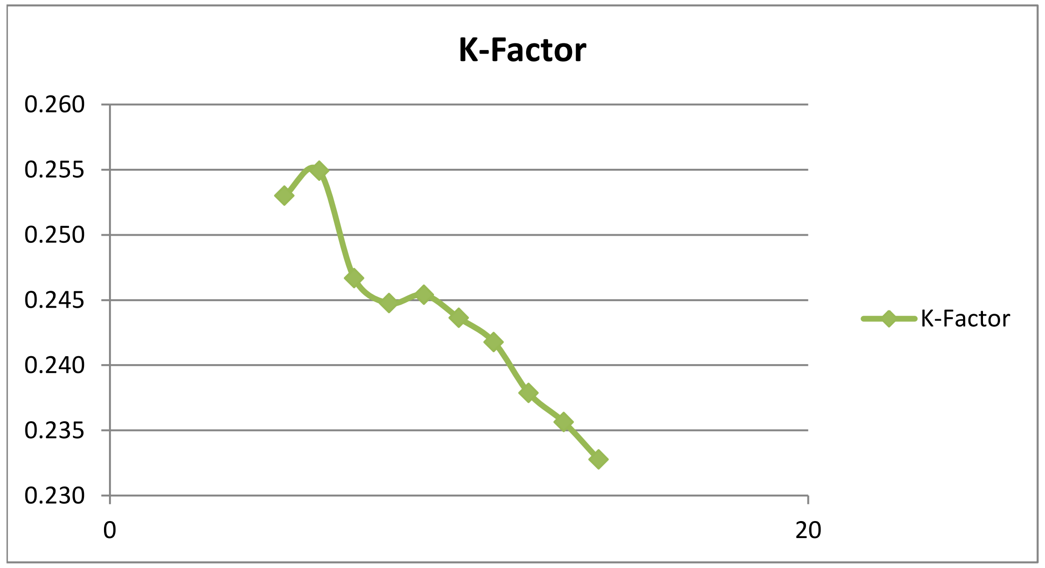

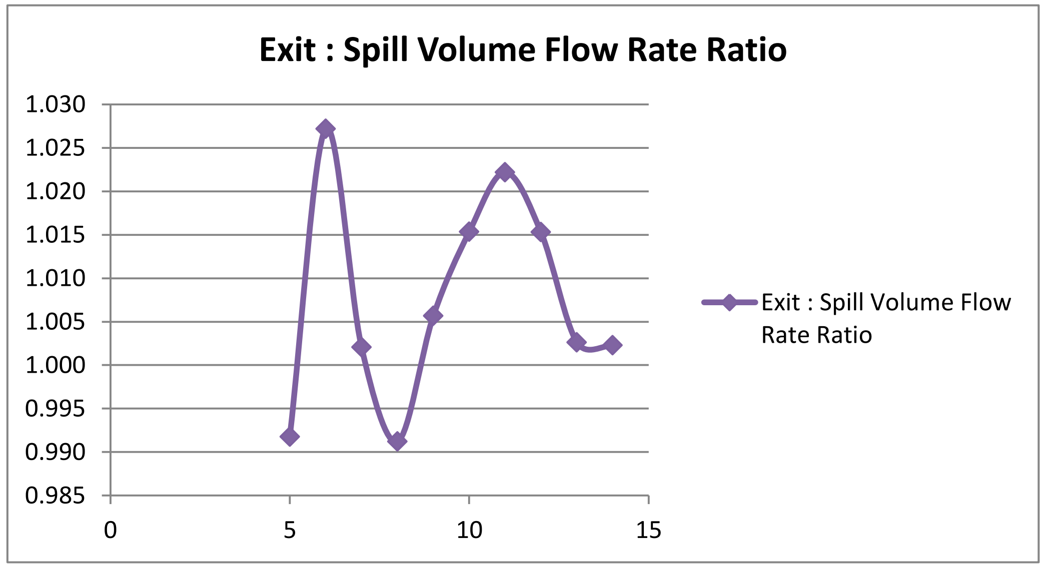

Atomiser - Inlet & Outlet Orifices					
Tip Orifice Diameter (mm)	Spill Orifice Diameter (mm)	Tangental Orifice Diameter (mm)	Water supply pressure (bar)	Water supply pressure (MPa)	Duration of water collection from exit orifice (sec)
0.8	0.5	2 x 0.6	5	0.5	12.31
[redacted]			6	0.6	12.25
			7	0.7	10.50
			8	0.8	12.88
			9	0.9	13.47
			10	1	13.47
			11	1.1	13.50
			12	1.2	14.06
			13	1.3	13.78
			14	1.4	14.50

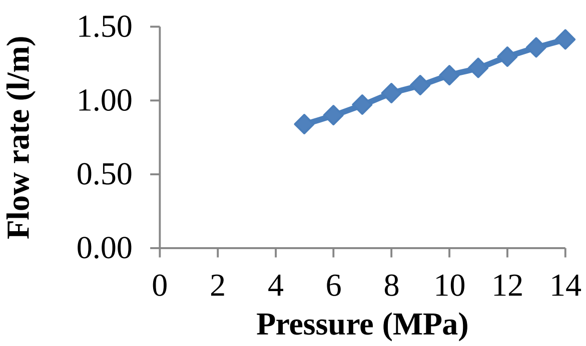

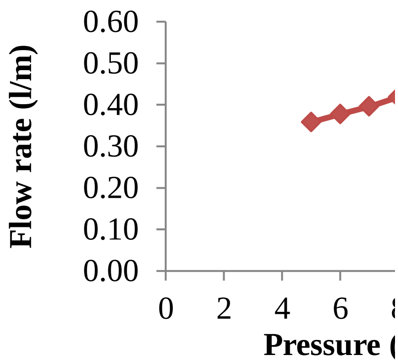

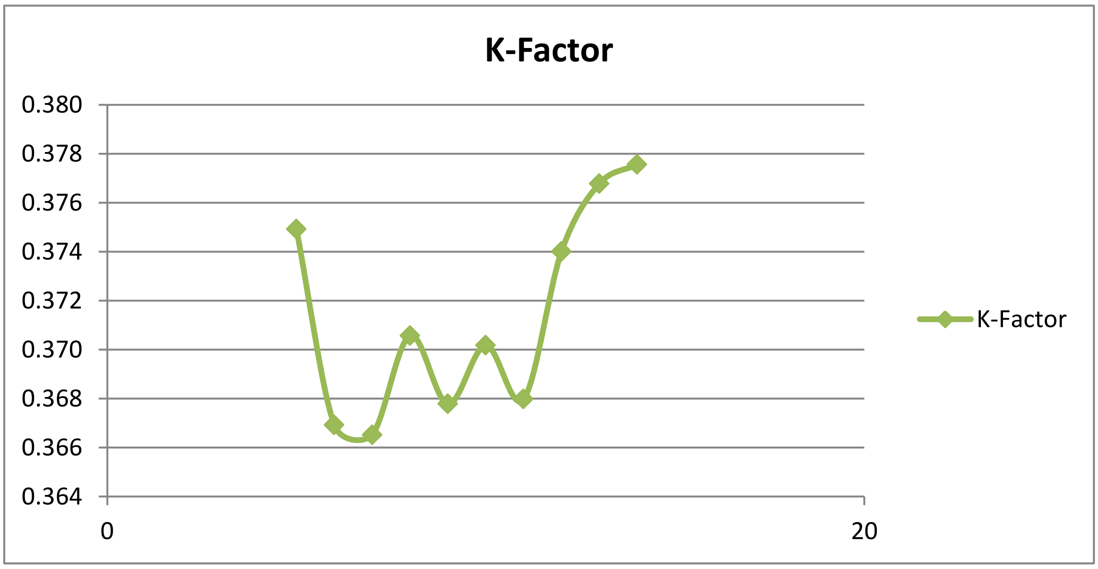

Data Collected

Container + Water Collected from Exit Orifice (g)	Q - Exit Orifice Volume Flow Rate (l/m)	Duration of Water Collection from Spill Orifice (sec)	Container + Water Collected from Spill Orifice (g)	Q - Spill Orifice Volume Flow Rate (l/m)	Exit : Spill Flow Rate Ratio	K - Factor (Q / √ P)
239.50	0.84	12.53	142.30	0.36	2.341	0.375
251.00	0.90	12.75	147.70	0.38	2.381	0.367
237.20	0.97	12.91	152.70	0.40	2.449	0.367
292.50	1.05	12.74	156.30	0.42	2.506	0.371
315.20	1.10	13.09	162.60	0.44	2.531	0.368
330.30	1.17	13.67	172.30	0.46	2.545	0.370
342.10	1.22	13.68	174.50	0.47	2.601	0.368
371.10	1.30	11.81	162.50	0.48	2.684	0.374
379.50	1.36	13.40	176.00	0.49	2.796	0.377
408.90	1.41	13.47	178.80	0.50	2.849	0.378

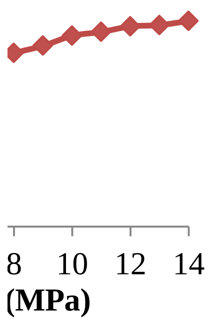

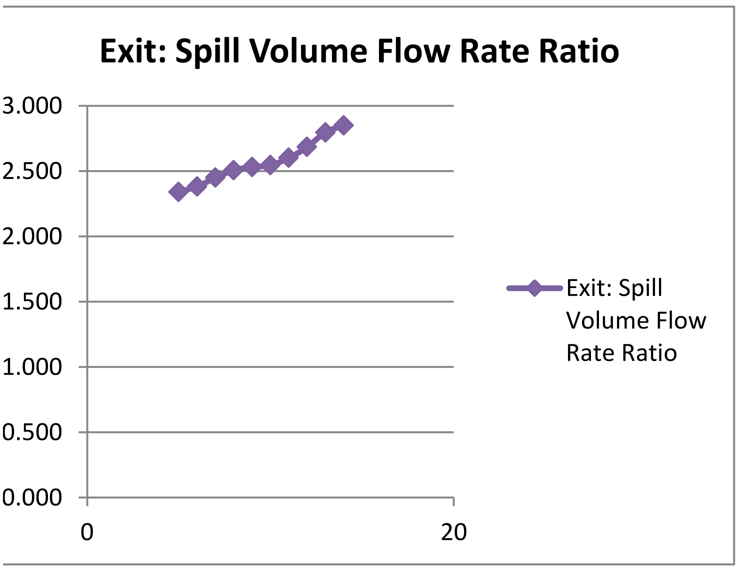

Atomiser - Inlet & Outlet Orifices				
Tip Orifice Diameter (mm)	Spill Orifice Diameter (mm)	Tangental Orifice Diameter (mm)	P Water Supply Pressure (bar)	Duration of Water Collection from Exit Orifice (seconds)
1	0.5	2 x 0.6	5	12.91
[redacted]			6	13.10
			7	12.72
			8	12.78
			9	13.31
			10	17.65
			11	14.68
			12	11.47
			13	13.37
			14	13.75

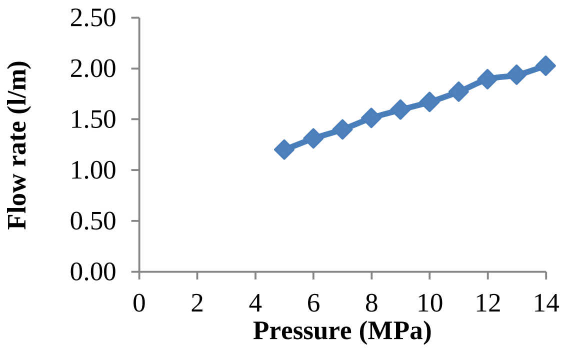

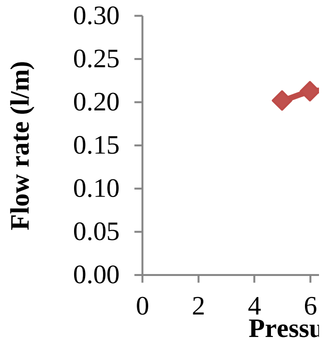

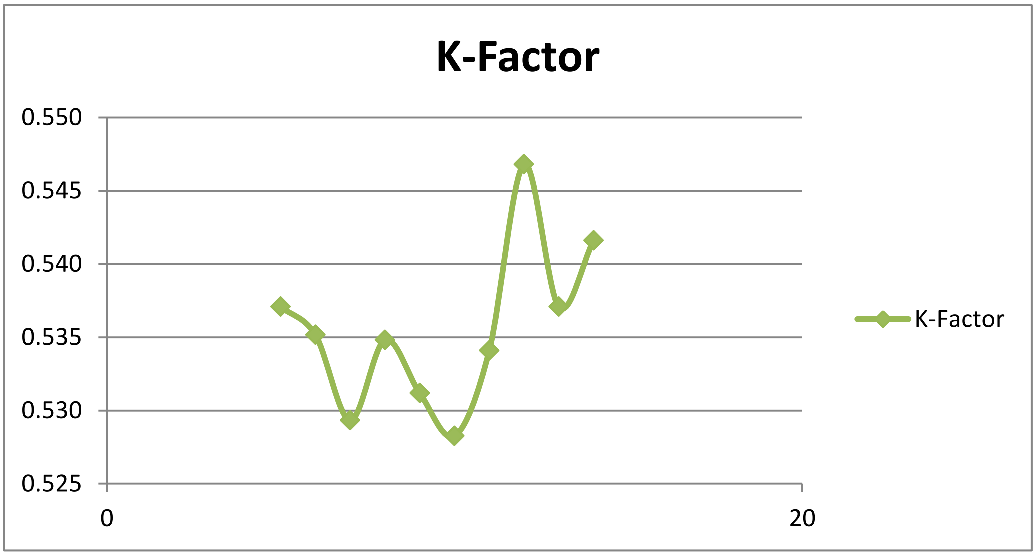

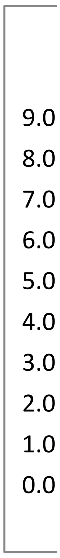

Data Collected

Container + Water Collected from Exit Orifice (gramms)	Q - Exit Orifice Volume Flow Rate (litres / min)	Duration of Water Collection from Spill Orifice (seconds)	Container + Water Collected from Spill Orifice (gramms)	Q - Spill Orifice Volume Flow Rate (litres / min)
325.90	1.20	16.56	123.10	0.20
353.70	1.31	14.28	118.04	0.21
364.40	1.40	18.91	135.71	0.22
389.70	1.51	14.38	125.00	0.24
421.00	1.59	14.03	126.00	0.25
558.90	1.67	16.40	135.00	0.25
500.90	1.77	17.25	141.00	0.26
429.60	1.89	18.12	146.10	0.26
499.00	1.94	17.09	138.40	0.25
531.90	2.03	20.00	155.60	0.26

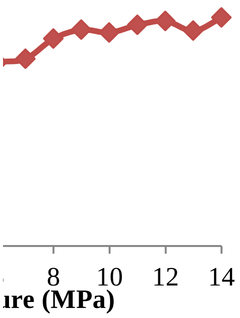

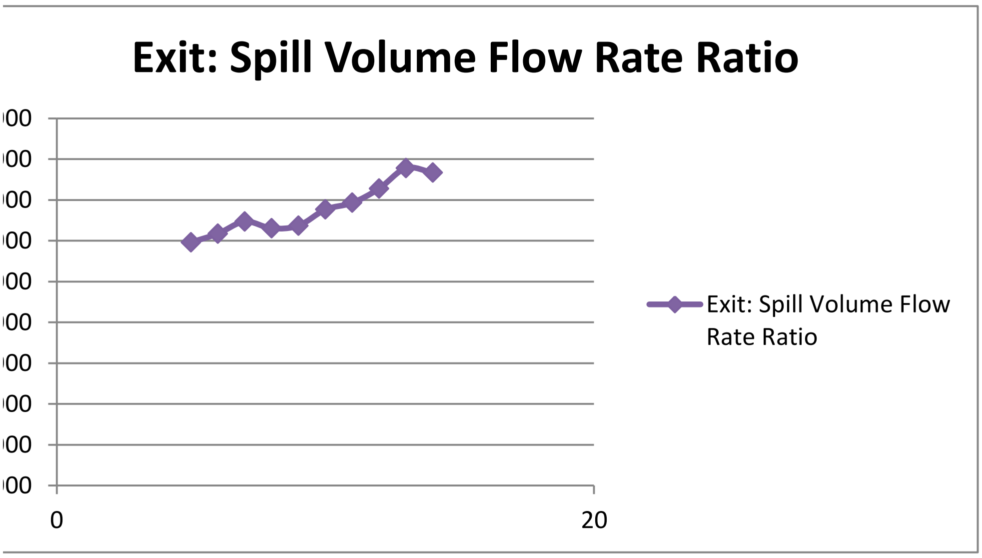

Exit : Spill Flow Rate Ratio	K - Factor (Q / √ P)
5.961	0.537
6.173	0.535
6.471	0.529
6.305	0.535
6.370	0.531
6.764	0.528
6.929	0.534
7.278	0.547
7.779	0.537
7.667	0.542

APPENDIX 9

Results and Discussions

A9.1 Mitigation trials for a single SRA in counter flow (C/F) with a methane-air flame

The pre-assembled Spill Return Atomiser (SRA) and water feed pipework was installed within the Flame Propagation and Mitigation Rig (FPMR) in accordance with Figure A9.1 and Table A9.1. The water pump was adjusted to deliver a supply pressure of 13MPa (130bar) at a temperature of 20˚C. Thermocouples (TC) were positioned in accordance with A9.1 and Table A9.1.

In this series of trials, the SRA spray and propagating flame were in a counter flow arrangement. The three atomisers tested in this series, known as SRA Type A, B and C were previously discussed in Chapter 4. Their configurations were also described in Table 5.1.

Individual SRA configurations were subject to four different methane-air explosion mixtures and previously shown in Table 5.13. Although mixtures were verified by percentage analysis, mixtures are referenced by their equivalence ratio (E.R. or ϕ).

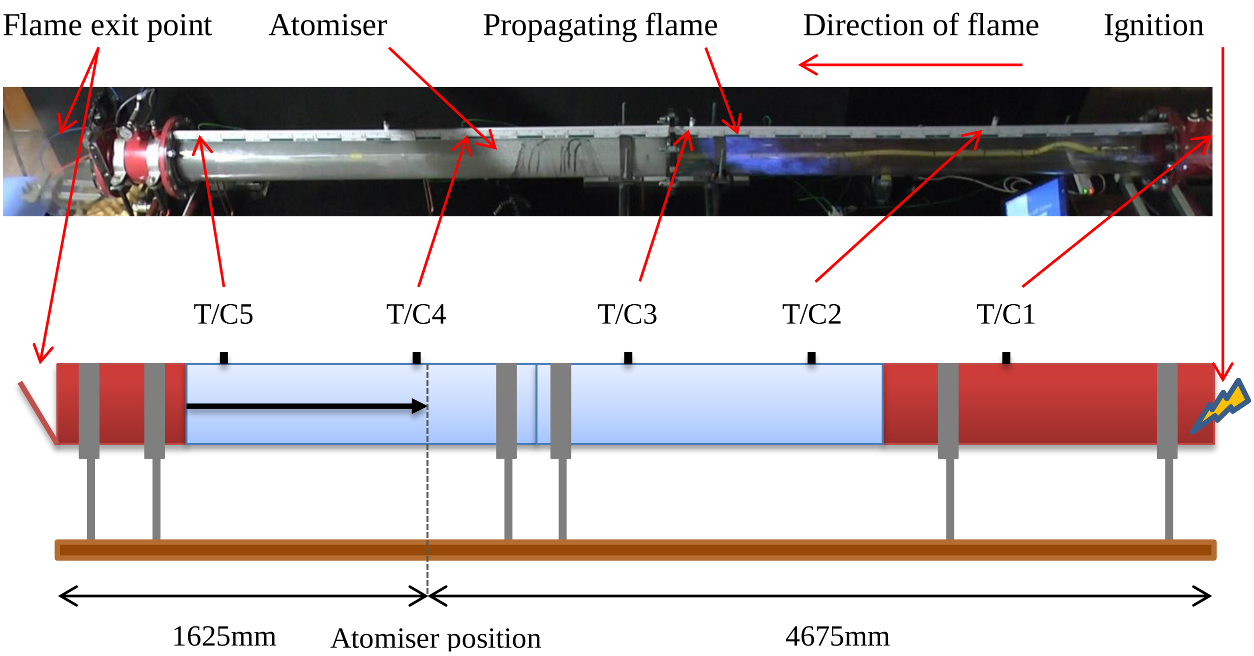

Figure A9.1 : Position of atomiser and thermocouples (relative to right hand ignition end)

Component	Position (measured from right hand end)
Thermocouple (T/C1)	1200mm
Thermocouple (T/C2)	2400mm
Thermocouple (T/C3)	3600mm
Thermocouple (T/C4)	4800mm
Thermocouple (T/C5)	6000mm
Atomiser outlet orifice (counter flow)	4675mm

Table A9.1 : Measured position of thermocouples and SRA

A9.1.1 Single (C/F) SRA Type A

A9.1.1.1 Trial set up

In this series of tests, a single Type A SRA was assembled and installed within the FPMR as previously discussed in accordance with Chapter 4 and positioned as detailed in Figure A9.1 and Table A9.1.

The full atomiser characteristics relating to the SRA Type A configuration were detailed in Section 7.3.8 and are summarised in Table A9.2 below.

Mean D_{32} (µm)	**Mean liquid volume flux ($cm^3/cm^2/s$)**	**Mean droplet velocity (m/s)**
17	0.011	13.5

Table A9.2 : Typical characteristics for SRA Type B 95mm downstream of exit orifice

A9.1.1.2 Flame speed

In the (ϕ) 0.61 mixture the flame initially exited the steel driver section of the FPMR, where the average flame speed was recorded as approximately 5.3m/s immediately upstream of the counter flow spray. In this instance the flame propagated directly through the region of the spray and began to accelerate to about 32.5m/s. The consequential increase in flame speed is represented in Figure A9.1 as negative value with respect to flame speed reduction.

In the (ϕ) 0.72 mixture the flame initially exited the steel driver section of the FPMR, where the average flame speed was recorded as approximately 20m/s immediately upstream of the counter flow spray. In this instance the flame propagated directly through the region of the spray and began to accelerate to approximately 32.5m/s. The consequential increase in flame speed is represented in Figure A9.1 as negative value with respect to flame speed reduction.

The (ϕ) 0.95 mixture the flame again exited the steel driver section of the FPMR, where the average flame speed was recorded as approximately 21.88m/s immediately upstream of the counter flow spray. In this instance the flame propagated straight through the region of the spray and began to accelerate to about 40.00m/s, which is represented in Figure A9.1 as negative value with respect to flame speed reduction of approximately 82.86%.

In the (ϕ) 1.06 mixture the flame again exited the steel driver section of the FPMR, where the average flame speed was recorded as approximately 21.00m/s immediately upstream of the counter flow spray. In this test the flame propagated directly through the region of the spray and began to accelerate to about 30.00m/s, which is represented in Figure A9.1 as negative value, with a resulting increase in flame speed of about 45%.

In this series of tests the flame speeds were all measured upstream and downstream of the counter flow spray. Figure A9.1 illustrates the percentage flame speed reductions observed. As the percentage reductions in this series all exhibit negative values, this shows that all four methane-air mixtures tested resulted in a global increase in average flame speed across the sprays.

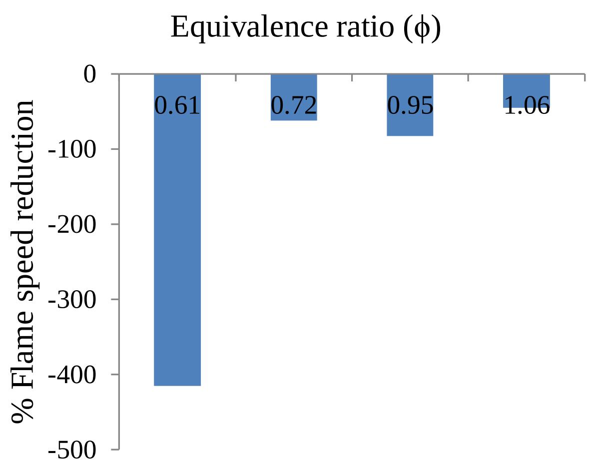

Figure A9.1 : Average flame speed reduction percentage (%) from upstream to downstream of SRA in various methane-air mixtures

A9.1.1.3 Time-temperature response

The time-temperature profiles produced for each of the trials in this series are shown in Figure A9.3 – Figure A9.6. In all of the profiles the thermocouples downstream of the sprays exhibit consistent trends with respect to an increase in flame speed. The steep gradient found with TC5 can be seen in each of the methane-air mixtures.

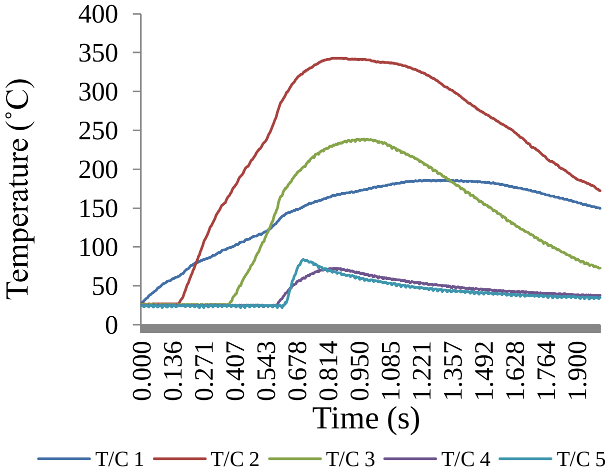

Figure A9.3 : Typical time-temperature profile for SRA Type A in C/F arrangement with methane-air mixture of E.R. (ϕ) 0.61

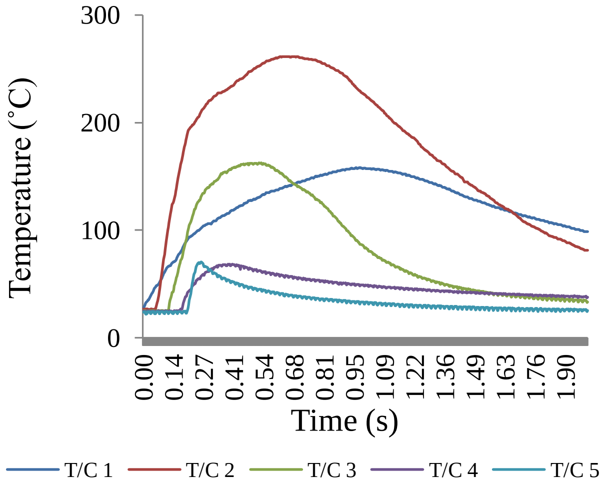

Figure A9.4 : Characteristic time-temperature profile for SRA Type A in C/F arrangement with methane-air mixture of E.R. (ϕ) 0.72

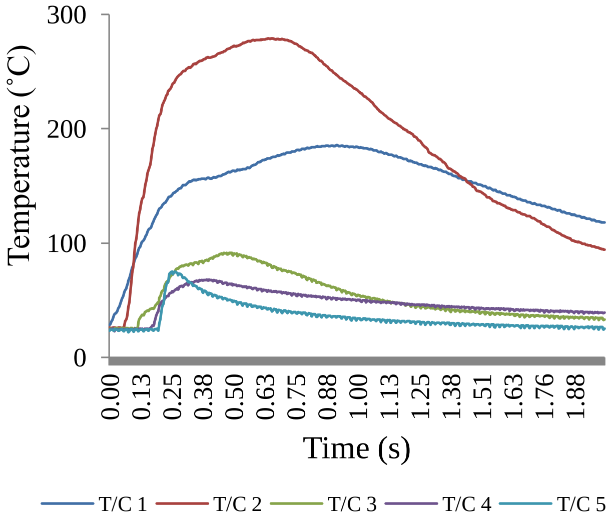

Figure A9.5 : Distinctive time-temperature profile for SRA Type A in C/F arrangement with methane-air mixture of E.R. (ϕ) 0.95

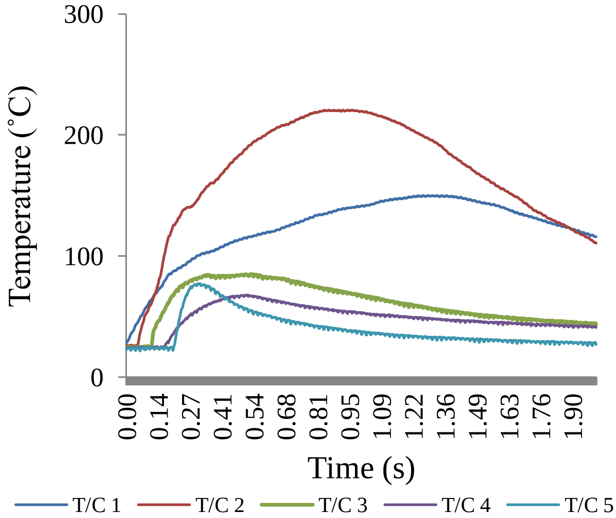

Figure A9.6 : Individual time-temperature profile for SRA Type A in C/F arrangement with methane-air mixture of E.R. (ϕ) 1.06

A9.1.1.4 Qualitative analysis

In the ‘hot trials’ results presented in these Appendices four still photographs have been displayed for each SRA and E.R. (ϕ) configuration to reveal the propagation of the flame upstream and downstream of the spray region. In the cases where successful mitigation occurred, the following frames are included to capture any post mitigation activity. The high definition (HD) video was recorded at 50 frames per second (FPS) with resulting still frames being 20milliseconds (ms) apart.

i) Equivalence ratio (ϕ) 0.61

Figure A9.7(i) shows the flame propagating from the ignition region on the right hand side (RHS) of the photograph. It can be seen in this frame the flame is approaching the region of the spray.

Figure A9.7(ii) depicts the flame a further 20ms downstream. In this frame the flame is engaging with the extreme droplets in the spray.

In Figure A9.7(iii) the flame has travelled another 20ms and is fully engaged with the droplets as it passes through the region of D_{32} 17μm counter flow water droplets, where it is seen to accelerate. Figure A9.8 magnifies this zone where combustion is visible as a continuous flame, with no obvious signs of local of global flame quenching of mitigation.

Figure A9.7(iv) confirms the flame position following a further 20ms, in which it is accelerating towards the exit end of the explosion and mitigation tube, at the left hand side (LHS) of the photograph.

ii) Equivalence ratio (ϕ) 0.72

Figure A9.9(i – iv) shows the flame propagating from right to left. In Figure A9.7 (iii) the flame is passing through the spray region with no obvious tendencies towards suppression or mitigation. Figure A9.10 offers an expanded view of the spray region highlighted in Figure A9.7 (iii).

This view confirms that there were not visual breaks, dark regions or colour changes in the flame, thus confirming that this particular configuration was unsuccessful as a means of explosion suppression or mitigation.

(iii) Equivalence ratio (ϕ) 0.95

Figure A9.11 reveals the flame exiting the steel driver section and propagating towards the counter flow spray. There appears to be evidence of a disturbance in the flame in the region of the spray, as highlighted in Figure A9.12. In this instance the flame accelerated when exiting the spray.

(iv) Equivalence ratio (ϕ) 1.06

Figure A9.13 shows the flame exiting the steel driver section and propagating towards the counter flow spray. There was a visual disturbance in the flame in the region of the spray, which is expanded in Figure A9.14. In this trial the flame accelerated on exiting the spray region.

(i) Equivalence ratio (ϕ) 0.61

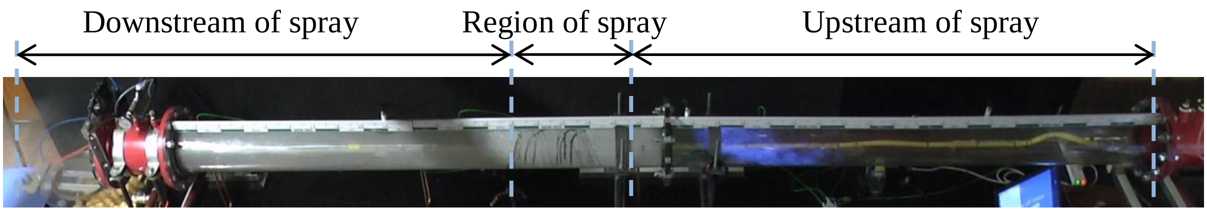

i. Flame propagating in methane-air mixture of E.R. (ϕ) 0.61 upstream of SRA

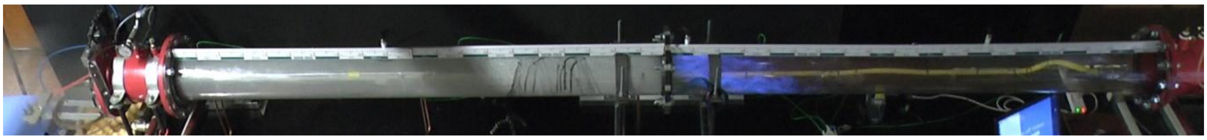

ii. Flame propagating in methane-air mixture of E.R. (ϕ) 0.61 upstream of SRA

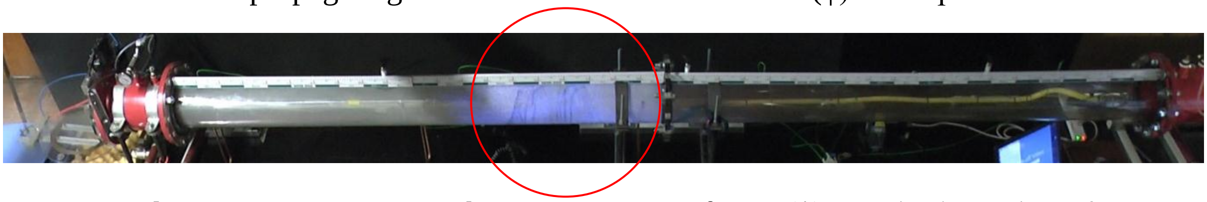

iii. Flame propagating in methane-air mixture of E.R. (ϕ) 0.61 in the region of spray

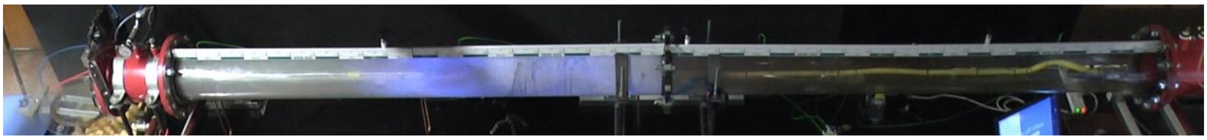

iv. Flame propagating in methane-air mixture of E.R. (ϕ) 0.61 downstream of SRA

Figure A9.7 : Flame propagating upstream and downstream of C/F SRA Type A for a methane-air mixture (ϕ) 0.61

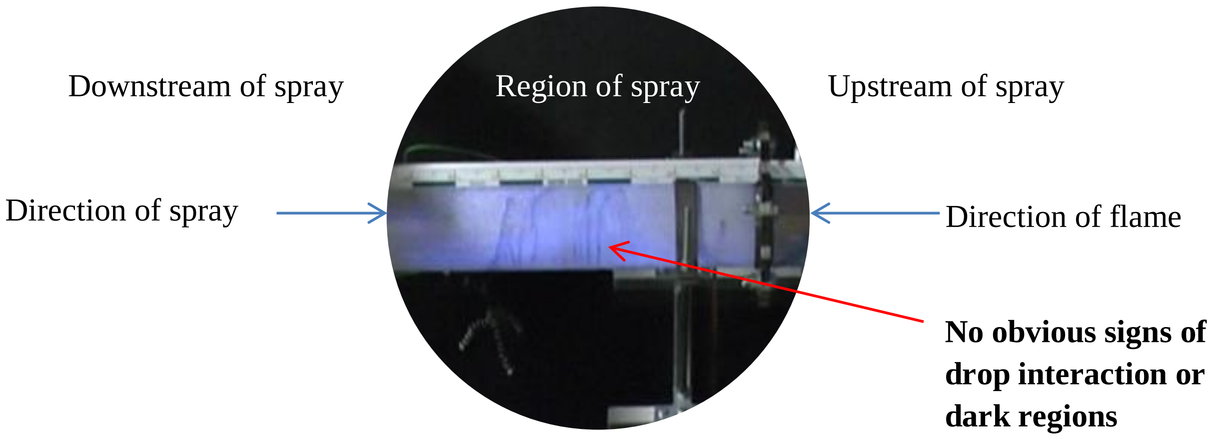

Figure A9.8: Expanded view of region of spray highlighted in Figure A9.7 (iii)

(ii) Equivalence ratio (ϕ) 0.72

i. Flame propagating in methane-air mixture of E.R. (ϕ) 0.72 upstream of SRA

ii. Flame propagating in methane-air mixture of E.R. (ϕ) 0.72 upstream of SRA

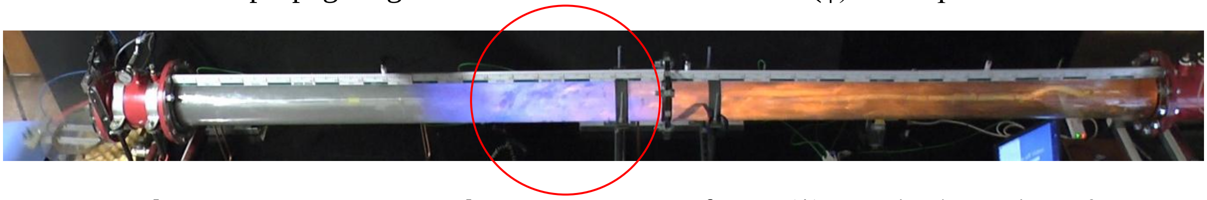

iii. Flame propagating in methane-air mixture of E.R. (ϕ) 0.72 in the region of spray

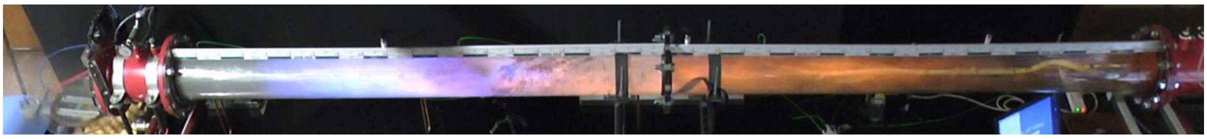

iv. Flame propagating in methane-air mixture of E.R. (ϕ) 0.72 downstream of SRA

Figure A9.9 : Flame propagating upstream and downstream of C/F SRA Type A for a methane-air mixture (ϕ) 0.72

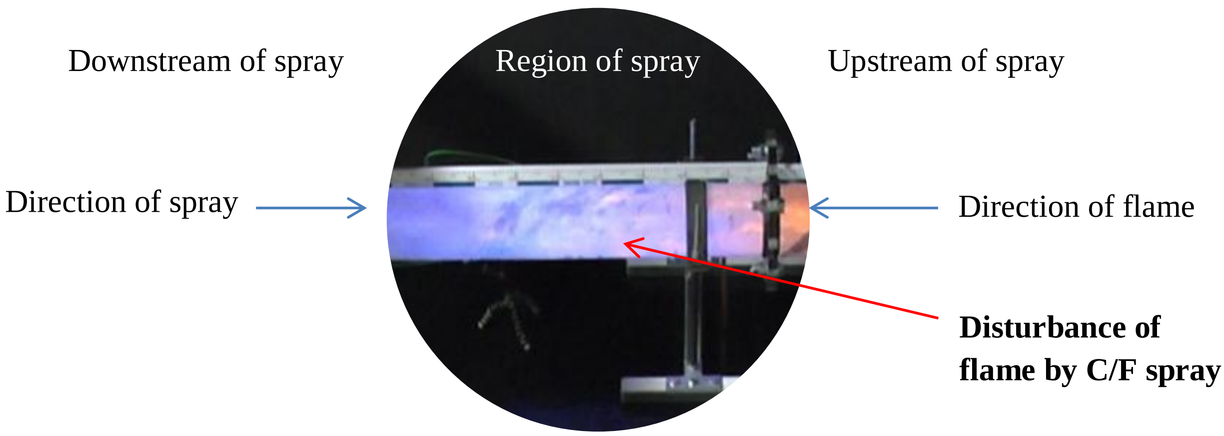

Figure A9.10 : Enlarged view of region of spray highlighted in Figure A9.9(iii)

(iii) Equivalence ratio (ϕ) 0.95

i. Flame propagating in methane-air mixture of E.R. (ϕ) 0.95upstream of SRA

ii. Flame propagating in methane-air mixture of E.R. (ϕ) 0.95 upstream of SRA

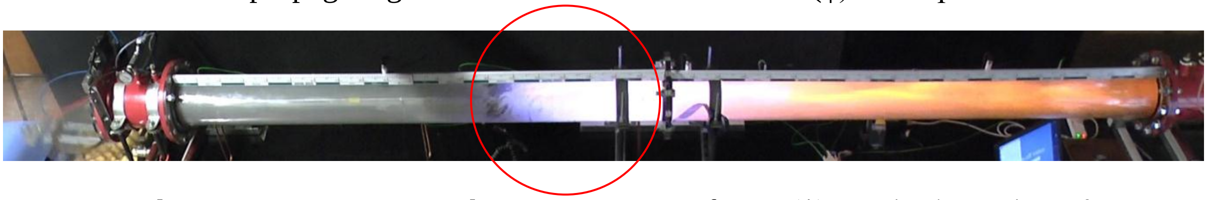

iii. Flame propagating in methane-air mixture of E.R. (ϕ) 0.95in the region of spray

iv. Flame propagating in methane-air mixture of E.R. (ϕ) 0.95 downstream of SRA

Figure A9.11 : Flame propagating upstream and downstream of C/F SRA Type A for a methane-air mixture (ϕ) 0.95

Figure 9.12: Magnified view of region of spray highlighted in Figure A9.11(iii)

(iv) Equivalence ratio (ϕ) 1.06

v. Flame propagating in methane-air mixture of E.R. (ϕ) 1.06 upstream of SRA

vi. Flame propagating in methane-air mixture of E.R. (ϕ) 1.06 upstream of SRA

vii. Flame propagating in methane-air mixture of E.R. (ϕ) 1.06 in the region of spray

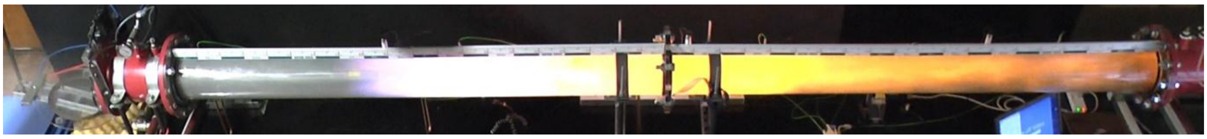

viii. Flame propagating in methane-air mixture of E.R. (ϕ) 1.06 downstream of SRA

Figure A9.13 : Flame propagating upstream and downstream of C/F SRA Type A for a methane-air mixture (ϕ) 1.06

Figure A9.14: Expanded view of region of spray highlighted in Figure A9.13(iii)

A9.1.1.5 General event outcome

Table A9.3 provides a summary of the **'general event outcome'** for each trial in this current series, using the five potential 'outcome' categories offered in Chapter 5. The results of all 'hot trials' were previously given in Table 5.14 and are also shown in Table A9.45.

Trial configuration	General event outcome	Code
Single C/F SRA : (ϕ) 0.61	No Mitigation with resulting Flame Acceleration	NMFA
Single C/F SRA : (ϕ) 0.72	No Mitigation with resulting Flame Acceleration	NMFA
Single C/F SRA : (ϕ) 0.95	No Mitigation with resulting Flame Acceleration	NMFA
Single C/F SRA : (ϕ) 1.06	No Mitigation with resulting Flame Acceleration	NMFA

Table A9.3 : General event outcome (trial series A9.4.1)

A9.1.2 Single (C/F) SRA Type B

A9.1.2.1 Trial set up

In this series of tests a single Type B SRA was assembled and installed in as previously discussed in accordance with Table 5.1 and positioned as detailed in Figure A9.1 and Table A9.4.

The full atomiser characteristics relating to the SRA Type B configuration were detailed in Section 7.3 and are summarised in Table A9.4 below.

Mean D32 (μm)	Mean liquid volume flux ($cm^3/cm^2/s$)	Mean droplet velocity (m/s)
26	0.024	21.41

Table A9.4 : Typical characteristics for SRA Type B 95mm downstream of exit orifice

A9.1.2.1 Flame speed

In these trials flame speeds were all measured upstream and downstream of the counter flow spray. Figure A9.15 illustrates the percentage flame speed reductions observed. As the percentage reductions in this series all exhibit negative values, this shows that all four methane-air mixtures tested resulted in a global increase in average flame speed across the sprays.

The higher droplet velocities produced by the Type B SRA would have resulted greater impact velocities and shorter residence times than those reported in the Type A SRA trials discussed previously in Section A9.1.1.

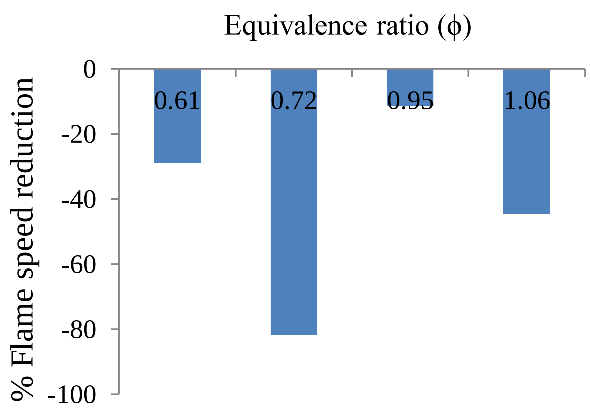

Figure A9.15 : Average flame speed reduction percentage (%) from upstream to downstream of SRA in various methane-air mixtures

A9.1.2.3 Time-temperature response

The time-temperature profiles produced for each of the trials in this series are shown in Figure A9.16 – Figure A9.19. In all of the profiles the thermocouples downstream of the sprays exhibit consistent trends with respect to an increase in flame speed. The steep gradient found with TC5 can be seen in each of the methane-air mixtures.

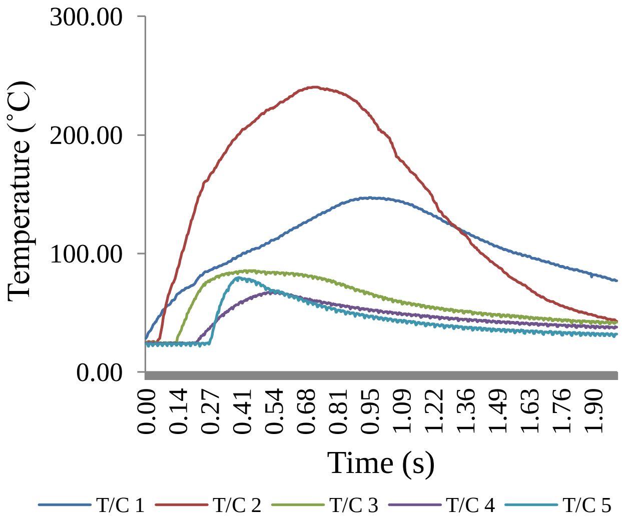

Figure A9.16 : Typical time-temperature profile for SRA Type B in C/F arrangement with methane-air mixture of E.R. (ϕ) 0.61

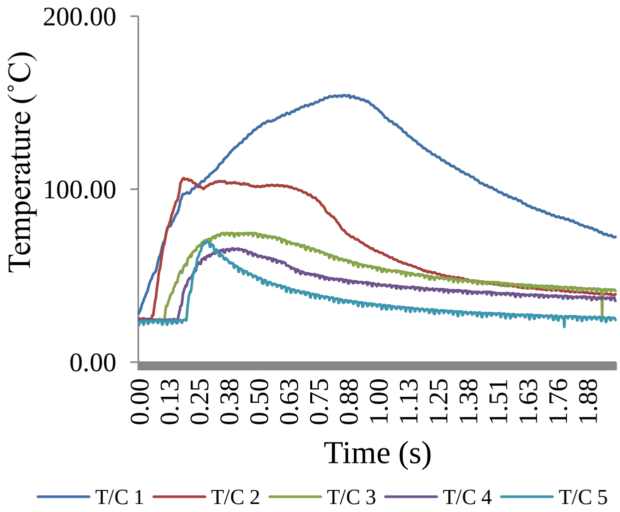

Figure A9.17 : Characteristic time-temperature profile for SRA Type B in C/F arrangement with methane-air mixture of E.R. (ϕ) 0.72

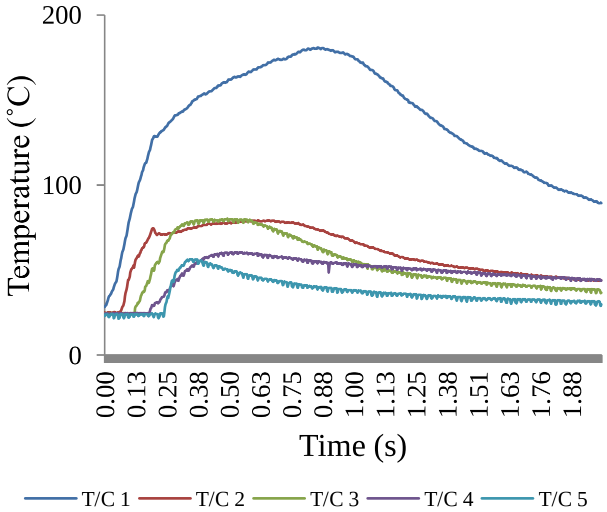

Figure A9.18 : Distinctive time-temperature profile for SRA Type B in C/F arrangement with methane-air mixture of E.R. (ϕ) 0.95

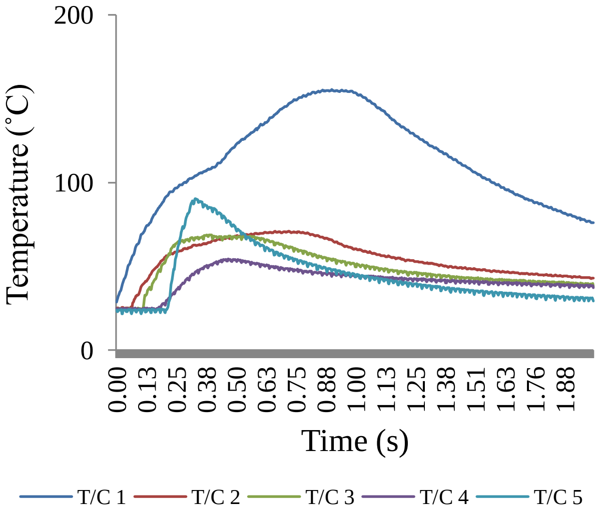

Figure A9.19 : Individual time-temperature profile for SRA Type B in C/F arrangement with methane-air mixture of E.R. (ϕ) 1.06

A9.1.2.4 Qualitative analysis

Figure A9.20 reveals still images extracted from the high definition video footage for the methane-air mixture E.R. (ϕ) 0.61 trial. The flame can be seen upstream and downstream of the counter flow Type B SRA spray. In this experimental test the flame passes through the spray region. Figure A9.21 shows a dark region in the trailing combustion zone, indicating a degree of localised suspension of combustion activity.

Figures A9.22 – A9.27 display the images relating to the additional methane-air mixtures in this series of E.R. (ϕ) 0.72, 0.95 and 1.06. In each case the leading flame passed directly though the spray, followed by a degree of acceleration as previously shown in Figure A9.15. Additionally dark regions displaying signs of a localised cessation of combustion are evident in all cases.

(i) Equivalence ratio (ϕ) 0.61

i. Flame propagating in methane-air mixture of E.R. (ϕ) 0.61 upstream of SRA

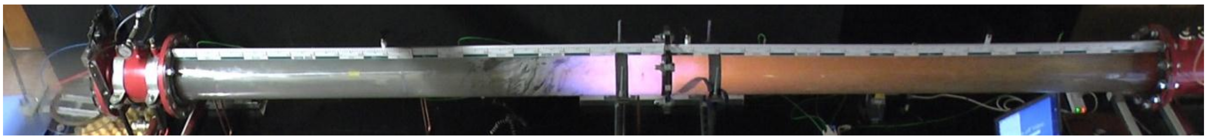

ii. Flame propagating in methane-air mixture of E.R. (ϕ) 0.61 upstream of SRA

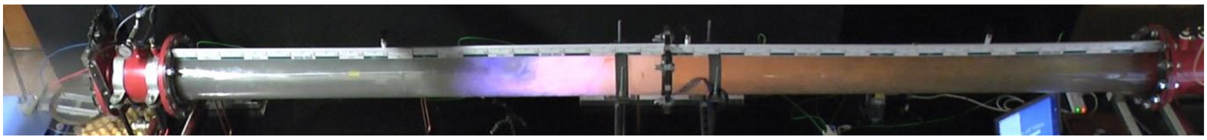

iii. Flame propagating in methane-air mixture of E.R. (ϕ) 0.61 in the region of spray

iv. Flame propagating in methane-air mixture of E.R. (ϕ) 0.61 downstream of SRA

Figure A9.20 : Flame propagating upstream and downstream of C/F SRA Type B for a methane-air mixture (ϕ) 0.61

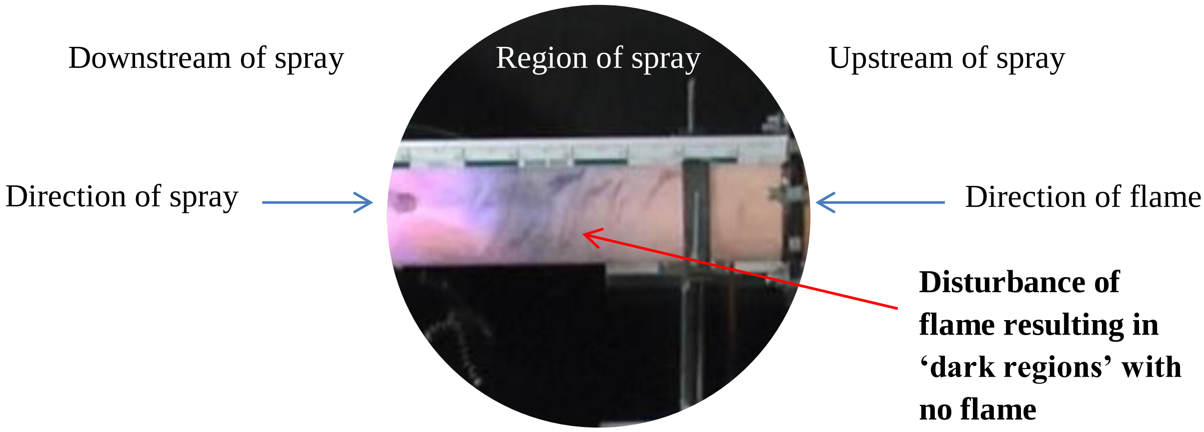

Figure A9.21 : Expanded view of region of spray highlighted in Figure A9.20(iv)

(ii) Equivalence ratio (ϕ) 0.72

v. Flame propagating in methane-air mixture of E.R. (ϕ) 0.72 upstream of SRA

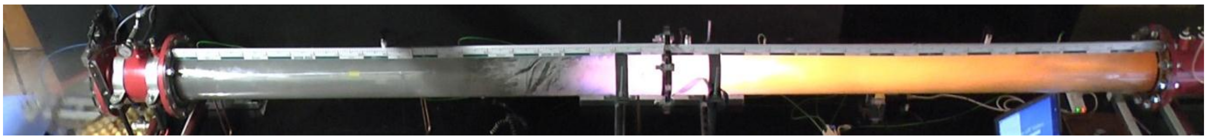

vi. Flame propagating in methane-air mixture of E.R. (ϕ) 0.72 upstream of SRA

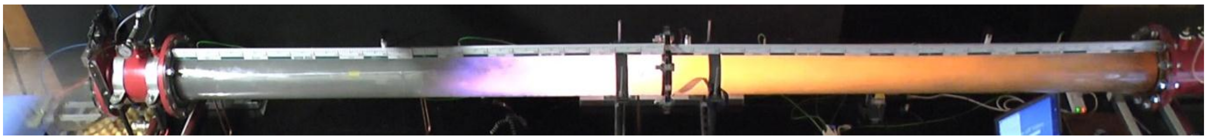

vii. Flame propagating in methane-air mixture of E.R. (ϕ) 0.72 in the region of spray

viii. Flame propagating in methane-air mixture of E.R. (ϕ) 0.72 downstream of SRA

Figure A9.22 : Flame propagating upstream and downstream of C/F SRA Type B for a methane-air mixture (ϕ) 0.72

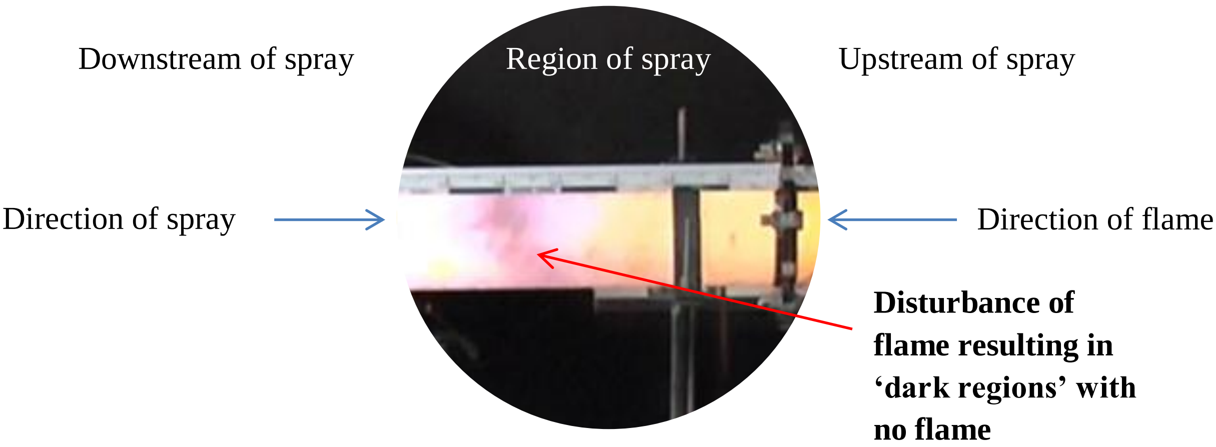

Figure A9.23 : Magnified view of region of spray highlighted in Figure A9.22(iv)

9.1.2.1 (iii) Equivalence ratio (ϕ) 0.95

i. Flame propagating in methane-air mixture of E.R. (ϕ) 0.95 upstream of SRA

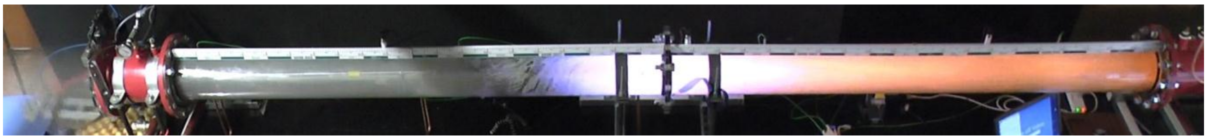

ii. Flame propagating in methane-air mixture of E.R. (ϕ) 0.95 upstream of SRA

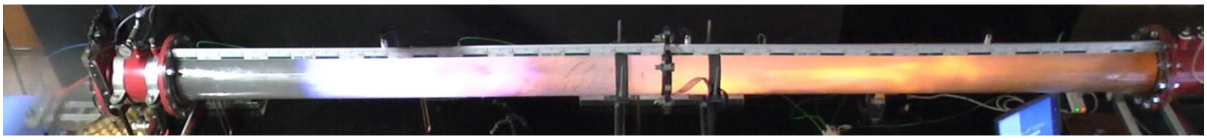

iii. Flame propagating in methane-air mixture of E.R. (ϕ) 0.95 in the region of spray

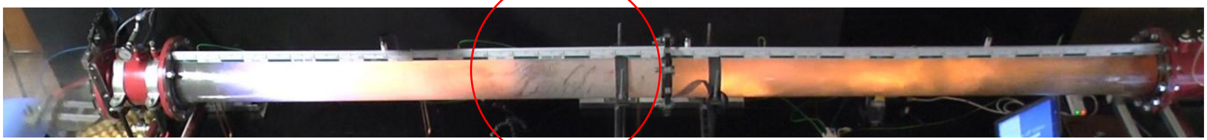

iv. Flame propagating in methane-air mixture of E.R. (ϕ) 0.95 downstream of SRA

Figure A9.24 : Flame propagating upstream and downstream of C/F SRA Type B for a methane-air mixture (ϕ) 0.95

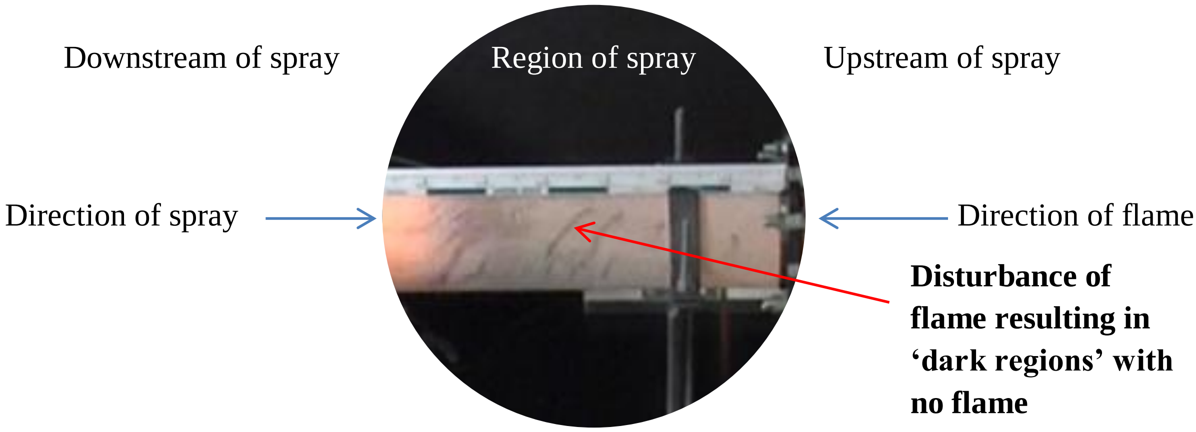

Figure A9.25 : Enlarged view of region of spray highlighted in Figure A9.24(iv)

(iv) Equivalence ratio (ϕ) 1.06

ix. Flame propagating in methane-air mixture of E.R. (ϕ) 1.06 upstream of SRA

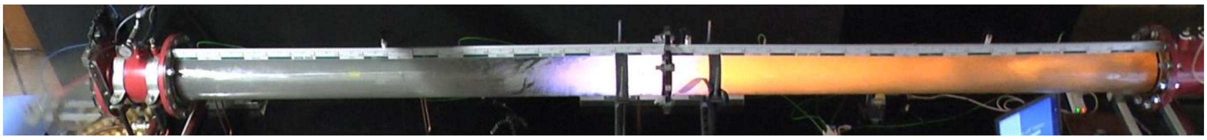

x. Flame propagating in methane-air mixture of E.R. (ϕ) 1.06 upstream of SRA

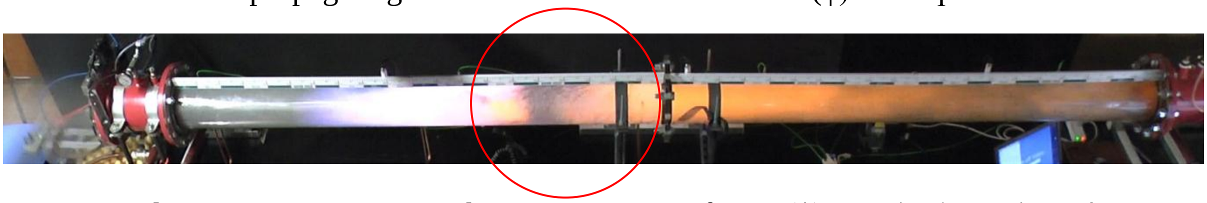

xi. Flame propagating in methane-air mixture of E.R. (ϕ) 1.06 in the region of spray

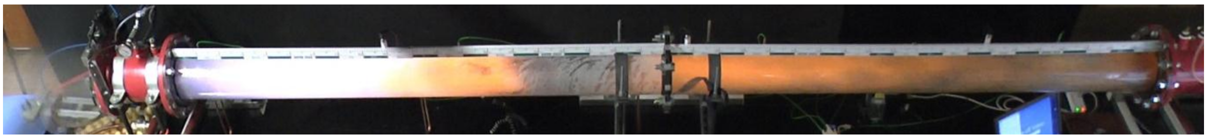

xii. Flame propagating in methane-air mixture of E.R. (ϕ) 1.06 downstream of SRA

Figure A9.26 : Flame propagating upstream and downstream of C/F SRA Type B for a methane-air mixture (ϕ) 1.06

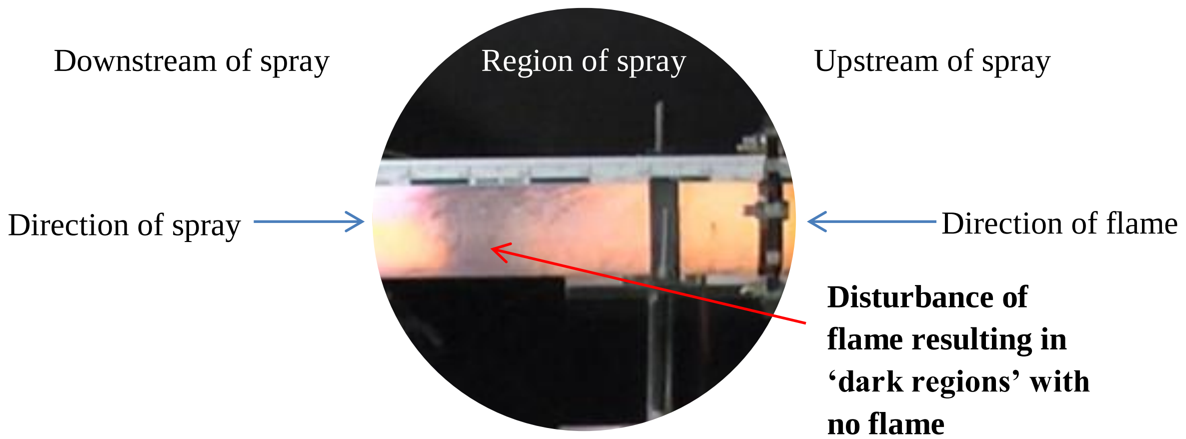

Figure A9.27: Expanded view of region of spray highlighted in Figure A9.26(iii)

A9.1.2.5 General event outcome

Table A9.5 provides a summary of the **'general event outcome'** for each trial in this current series, using the five potential 'outcome' categories offered in Chapter 5. The results of all 'hot trials' were previously given in Table 5.14 and are also shown in Table A9.45.

Trial configuration	General event outcome	Code
Single C/F SRA : (ϕ) 0.61	No Mitigation with resulting Flame Acceleration	NMFA
Single C/F SRA : (ϕ) 0.72	No Mitigation with resulting Flame Acceleration	NMFA
Single C/F SRA : (ϕ) 0.95	No Mitigation with resulting Flame Acceleration	NMFA
Single C/F SRA : (ϕ) 1.06	No Mitigation with resulting Flame Deceleration	NMFA

Table A9.5 : General event outcome (trial series A9.1.2)

A9.1.3 Single (C/F) Type C SRA

A9.1.3.1 Trial set up

In this series of tests, a single SRA Type C was assembled and installed in as previously discussed in accordance with Table 5.1 and positioned as detailed in Figure A9.1 and Table A9.1.

The full atomiser characteristics relating to the SRA Type C configuration were detailed in Section 7.3 and are summarised in Table A9.4below.

Mean D32 (μm)	Mean liquid volume flux ($cm^3/cm^2/$	Mean droplet velocity (m/s)
29	0.039	13.5m/s

Table A9.6 : Typical characteristics for SRA Type C 95mm downstream of exit orifice

A9.1.3.2 Flame speed

In this series of tests the flame speeds were all measured upstream and downstream of the counter flow spray. Figure A9.28 indicates the percentage flame speed reductions observed. With the exception of the methane-air mixture (ϕ) E.R. 0.61 whereby 100% mitigation was achieved, a global increase in average flame speed was observed across the sprays.

The droplet velocities produced by the Type C atomiser were greater than the Type A SRA, but were significantly less than those produced by the Type B SRA. With the application larger mean droplet size and increased spray angle associated with the Type C SRA, a high degree of disturbance would have been transferred into the unburned methane-air mixture. This is evident in the mixtures of (ϕ) E.R. 0.72, 0.95 and 1.06 with the resulting flame acceleration.

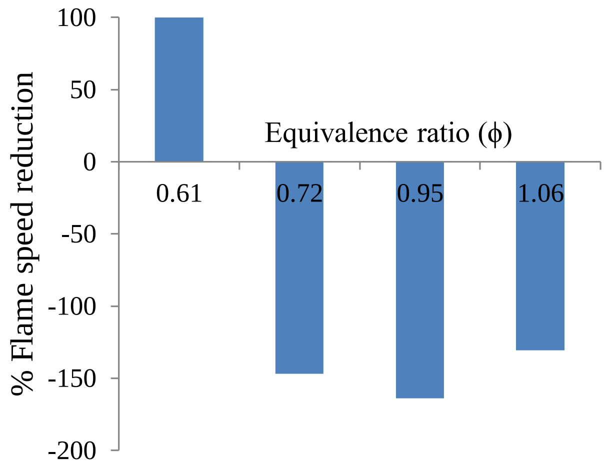

Figure A9.28 : Average flame speed reduction percentage (%) from upstream to downstream of Type C counter flow SRA in various methane-air mixtures

A9.1.3.3 Time-temperature response

The time-temperature profiles produced for each of the trials in this series are shown in Figure A9.29 – Figure A9.32. Figure A9.29 indicates that combustion mitigation has occurred. This is clearly shown by the parallel lines for TC4 and TC5 which are more or less the same as the initial ambient conditions.

In all of the other profiles the thermocouples downstream of the sprays exhibit consistent trends with respect to an increase in flame speed. The steep gradient found with TC5 can be seen in the methane-air mixtures E.R. (ϕ) 0.72, 0.95 and 1.06.

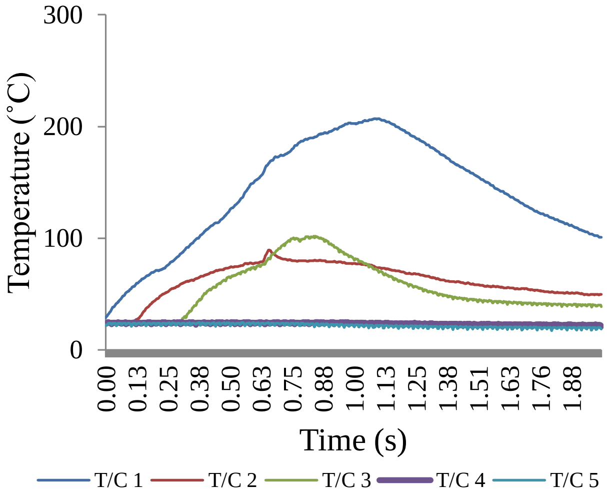

Figure A9.29 : Typical time-temperature profile for SRA Type C in C/F arrangement with methane-air mixture of E.R. (ϕ) 0.61

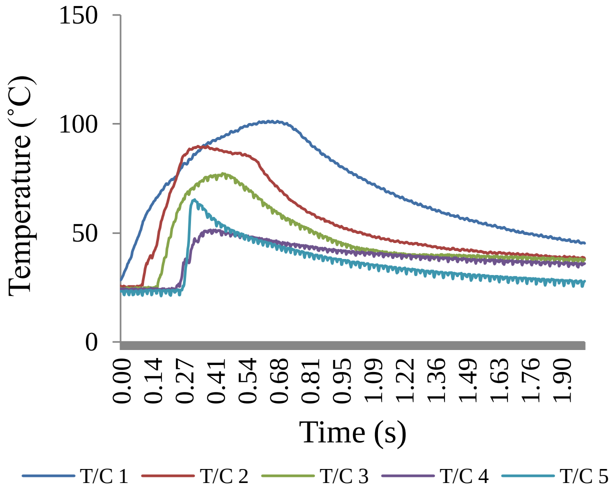

Figure A9.30 : Characteristic time-temperature profile for SRA Type C in C/F arrangement with methane-air mixture of E.R. (ϕ) 0.72

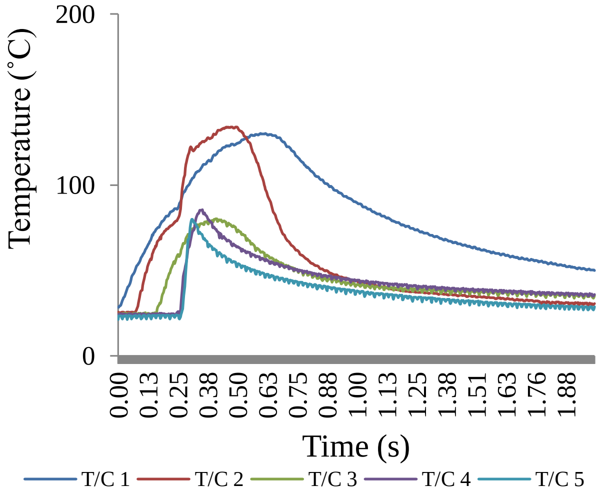

Figure A9.31 : Distinctive time-temperature profile for SRA Type C in C/F arrangement with methane-air mixture of E.R. (ϕ) 0.95

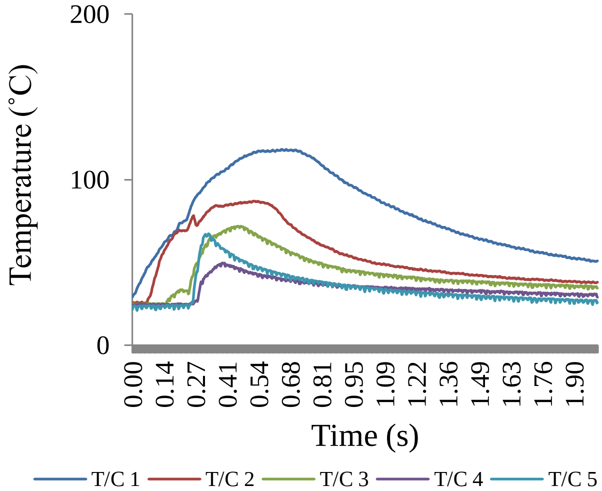

Figure A9.32 : Individual time-temperature profile for SRA Type C in C/F arrangement with methane-air mixture of E.R. (ϕ) 1.06

A9.1.3.4 Qualitative analysis

Figure A9.33 exposes still images taken from the high definition video footage for the methane-air mixture E.R. (ϕ) 0.61 experimental trial. The flame can be observed upstream the counter flow Type C SRA spray and can also be seen to enter the C/F spray, this image has also been expanded and is offered in Figure A9.34. In this experimental test the flame did not pass through the spray region. Subsequent ignition of the downstream flammable mixture did not occur and the propagating flame was mitigated.

Figures A9.35 and A9.39 display the images relating to the methane-air mixtures in this series of E.R. (ϕ) 0.72 and 0.95. In each case the leading flame passed directly though the spray, followed by a degree of acceleration as previously shown in Figure A9.28. Dark regions in the flame indicate areas of a localised suspension of combustion activity.

Figures A9.39 – A9.40 relate to the methane-air mixture of E.R. (ϕ) 1.06. Although the flame passed through the spray, all trailing combustion activity was immediately supressed by the spray.

(i) Equivalence ratio (ϕ) 0.61

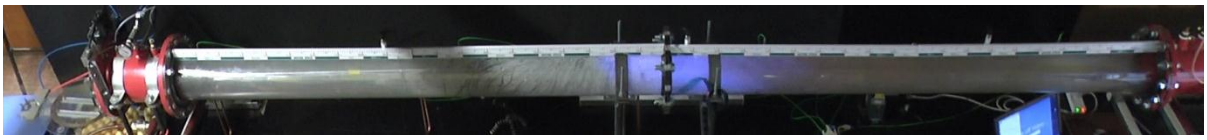

i. Flame propagating in methane-air mixture of E.R. (ϕ) 0.61 upstream of SRA

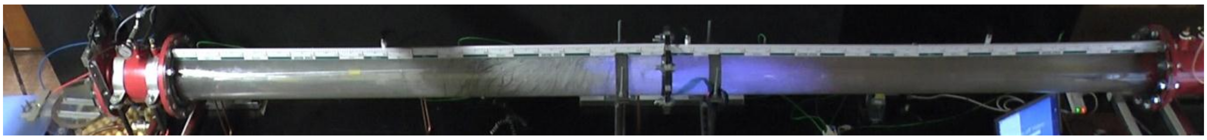

ii. Flame propagating in methane-air mixture of E.R. (ϕ) 0.61 upstream of SRA

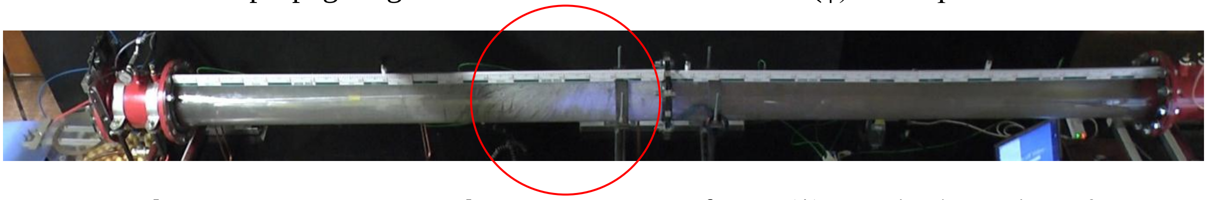

iii. Flame propagating in methane-air mixture of E.R. (ϕ) 0.61 in the region of spray

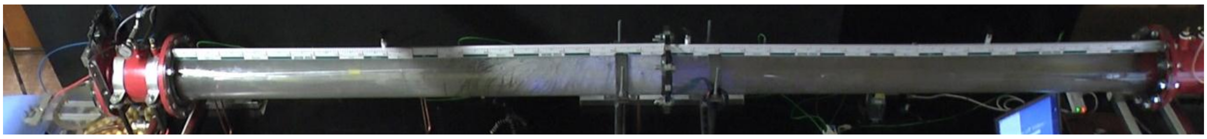

iv. **Mitigation** of flame in methane-air mixture of E.R. (ϕ) 0.61 downstream of SRA

Figure A9.33 : Flame propagating upstream and downstream of C/F SRA Type C for a methane-air mixture (ϕ) 0.61

Figure 9.34 : Expanded view of region of spray highlighted in Figure A9.33(iii)

(ii) Equivalence ratio (ϕ) 0.72

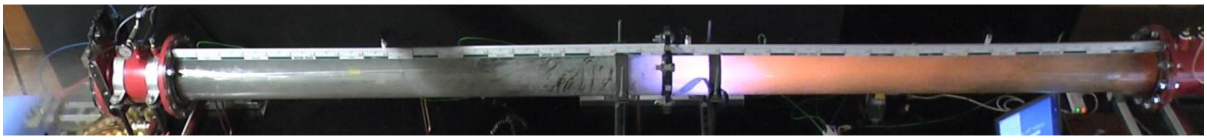

i. Flame propagating in methane-air mixture of E.R. (ϕ) 0.72 upstream of SRA

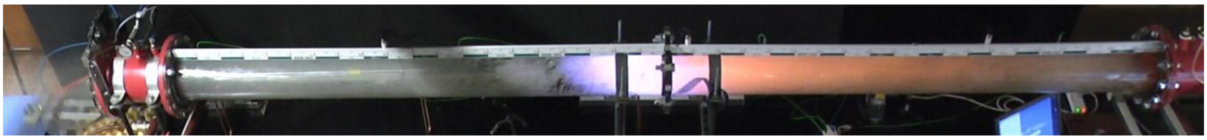

ii. Flame propagating in methane-air mixture of E.R. (ϕ) 0.72 upstream of SRA

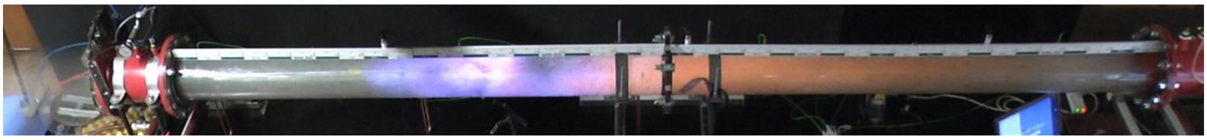

iii. Flame propagating in methane-air mixture of E.R. (ϕ) 0.72 in the region of spray

iv. Flame propagating in methane-air mixture of E.R. (ϕ) 0.72 downstream of SRA

Figure A9.35: Flame propagating upstream and downstream of C/F SRA Type C for a methane-air mixture (ϕ) 0.72

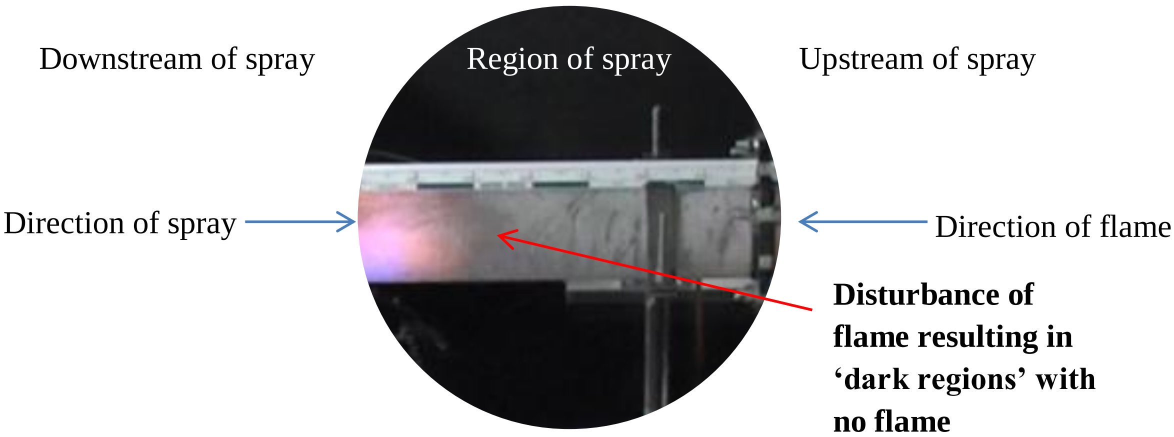

Figure A9.36 : Magnified view of region of spray highlighted in Figure A9.35(iv)

(iii) Equivalence ratio (ϕ) 0.95

i. Flame propagating in methane-air mixture of E.R. (ϕ) 0.95 upstream of SRA

ii. Flame propagating in methane-air mixture of E.R. (ϕ) 0.95 upstream of SRA

iii. Flame propagating in methane-air mixture of E.R. (ϕ) 0.95 in the region of spray

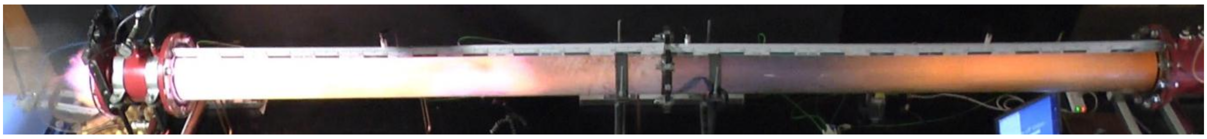

iv. Flame propagating in methane-air mixture of E.R. (ϕ) 0.95 downstream of SRA

Figure A9.37 : Flame propagating upstream and downstream of C/F SRA Type C for a methane-air mixture (ϕ) 0.95

Figure A9.38 : Enlarged view of region of spray highlighted in Figure A9.37(iii)

(iv) Equivalence ratio (ϕ) 1.06

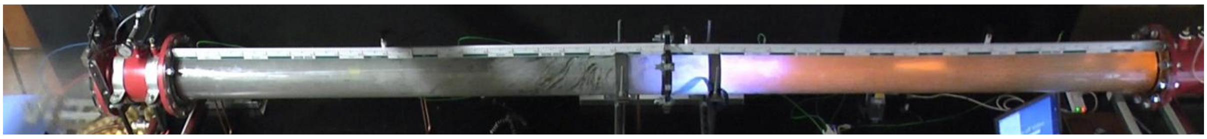

xiii. Flame propagating in methane-air mixture of E.R. (ϕ) 1.06 upstream of SRA

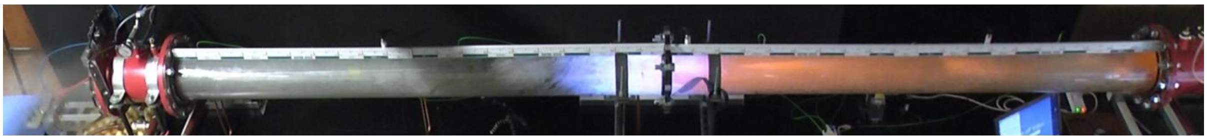

xiv. Flame propagating in methane-air mixture of E.R. (ϕ) 1.06 upstream of SRA

xv. Flame propagating in methane-air mixture of E.R. (ϕ) 1.06 in the region of spray

xvi. Flame propagating in methane-air mixture of E.R. (ϕ) 1.06 downstream of SRA

Figure A9.39 : Flame propagating upstream and downstream of C/F SRA Type C for a methane-air mixture (ϕ) 1.06

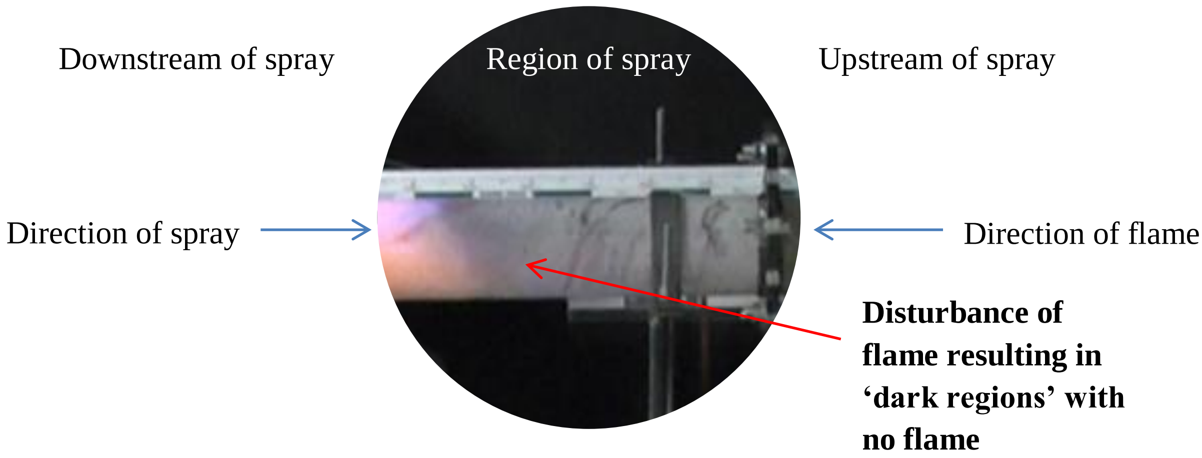

Figure A9.40 : Expanded view of region of spray highlighted in Figure A9.39(iii)

A9.1.3.5 General event outcome

Table A9.7 provides a summary of the **'general event outcome'** for each trial in this current series, using the five potential 'outcome' categories offered in Chapter 5. The results of all 'hot trials' were previously given in Table 5.14 and are also shown in Table A9.45.

Trial configuration	General event outcome	Code
Single C/F SRA : (ϕ) 0.61	Full Mitigation resulting in Flame Extinguishment	FMFE
Single C/F SRA : (ϕ) 0.72	No Mitigation with resulting Flame Acceleration	NMFA
Single C/F SRA : (ϕ) 0.95	No Mitigation with resulting Flame Acceleration	NMFA
Single C/F SRA : (ϕ) 1.06	No Mitigation with resulting Flame Acceleration	NMFA

Table A9.7 : General event outcome (trial series A9.1.3)

A9.2 Mitigation trials for a single SRA in parallel flow (P/F) with a methane-air flame

The pre-assembled spill return atomiser and water feed pipework was installed within the explosion and mitigation tube in accordance with Figure A9.41 and Table A9.5. The water pump was adjusted to deliver a supply pressure of 13MPa at a temperature of 20˚C. Thermocouples (TC) were positioned in accordance with A9.41 and Table A9.5.

In this series of trials, the SRA spray and propagating flame were in a parallel flow arrangement. The three atomisers tested in this series were known as SRA Type A, B and C and have been previously discussed. Their configurations were described in Table 5.1.

Individual SRA configurations were subject to four different methane-air explosion mixtures and previously shown in Table 5.13. Although mixtures were verified by percentage analysis, mixtures are referenced by their equivalence ratio (E.R. or ϕ).

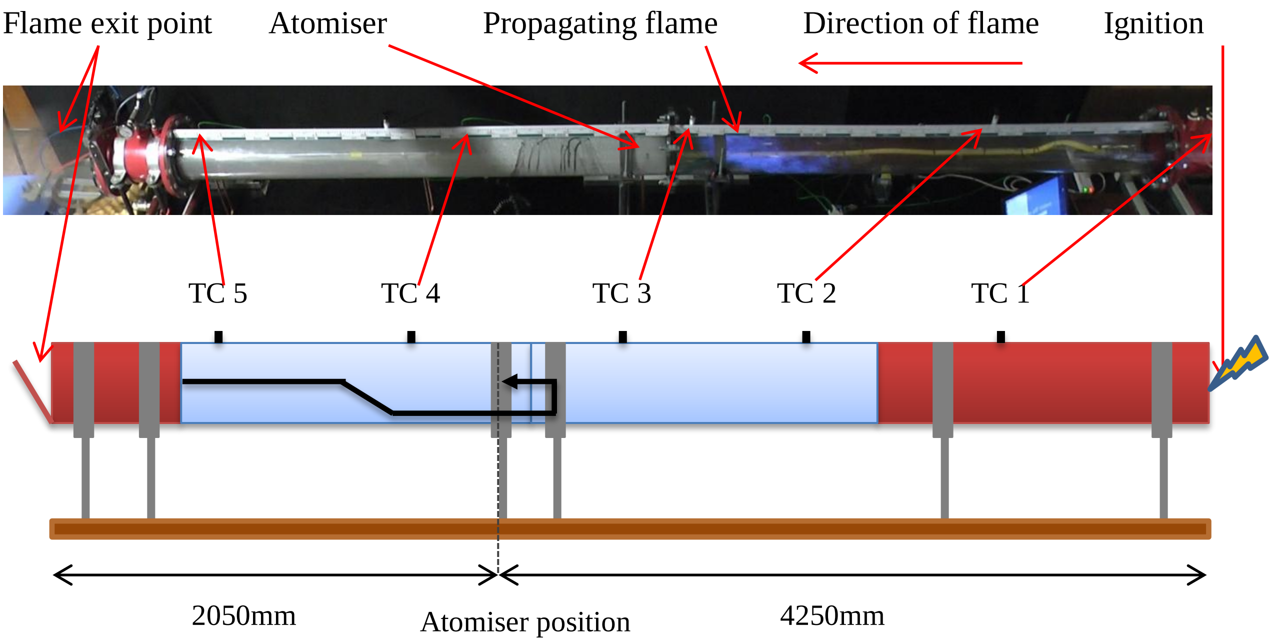

Figure A9.41 : Position of atomiser and thermocouples (relative to right hand ignition point)

Component	Position (measured from right hand end)
Thermocouple (T/C1)	1200mm
Thermocouple (T/C2)	2400mm
Thermocouple (T/C3)	3600mm
Thermocouple (T/C4)	4800mm
Thermocouple (T/C5)	6000mm
Atomiser outlet orifice (parallel flow)	4250mm

Table A9.8 : Measured position of thermocouples and SRA

A9.2.1 Single (P/F) Type A SRA

A9.2.1.1 Trial set up

The following results and discussions relate to a single SRA configuration Type A in parallel flow with a propagating methane-air flame. The full atomiser characteristics relating to the SRA Type A configuration were detailed in Section 7.3 and are summarised in Table A9.2 below.

Mean D32 (μm)	**Mean liquid volume flux ($cm^3/cm^2/s$)**	**Mean droplet velocity (m/s)**
17	0.011	6.5

Table A9.2 : Typical characteristics for SRA Type A 95mm downstream of exit orifice

A9.2.1.2 Flame speed

In this series of tests the flame speeds were all measured upstream and downstream of the parallel flow spray. Figure A9.42 illustrates the percentage flame speed reductions observed. As the percentage reductions in this series all exhibit negative values, this shows that all four methane-air mixtures tested resulted in a global increase in average flame speed across the sprays.

With counter flow sprays the approximate impact velocity was calculated by the sum of the average droplet velocity and the average flame speed. With parallel flow sprays approximate impact velocity is determined by the average flame speed, minus the average droplet velocity. Consequently parallel flow sprays should therefore afford greater droplet residence times within the flame front.

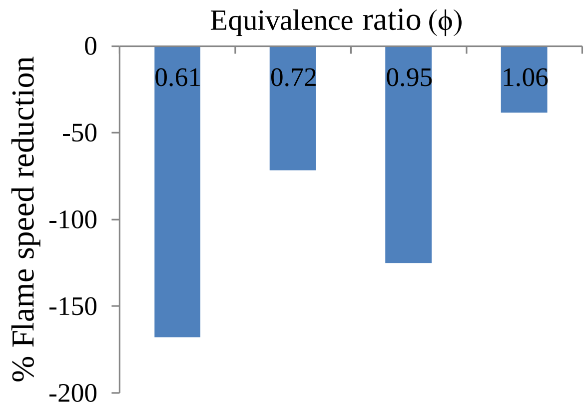

Figure A9.42 : Average flame speed reduction percentage (%) from upstream to downstream of parallel flow SRA in various methane-air mixtures

A9.2.1.3 Time-temperature response

The time-temperature profiles produced for each of the trials in this series are shown in Figure A9.43 – Figure A9.46. In all of the profiles the thermocouples downstream of the sprays exhibit consistent trends with respect to an increase in flame speed. The abrupt gradient found in the TC5 profile is apparent in each of the methane-air mixtures.

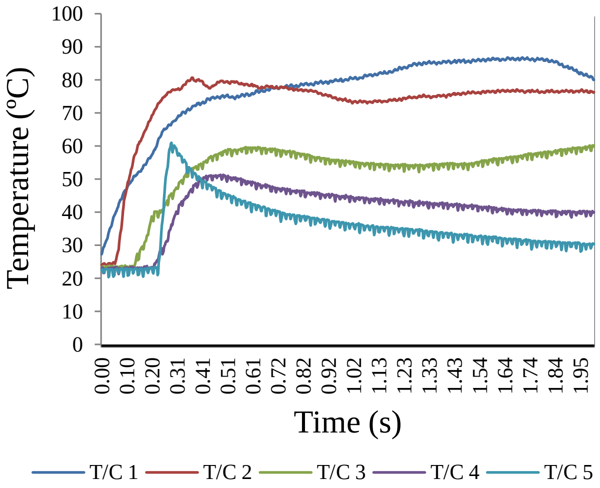

Figure A9.43 : Typical time-temperature profile for SRA Type A in P/F arrangement with methane-air mixture of E.R. (ϕ) 0.61

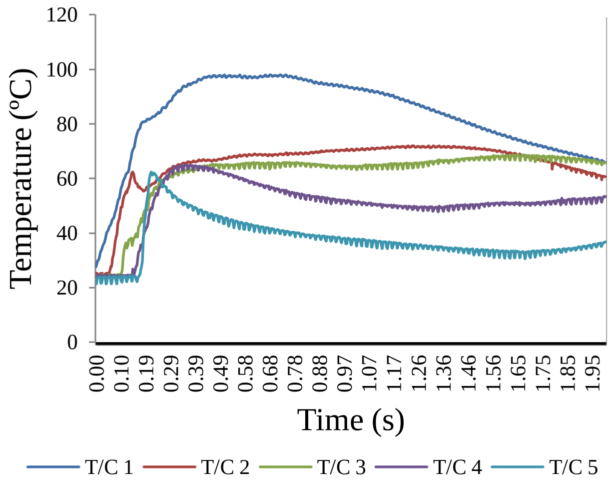

Figure A.44 : Characteristic time-temperature profile for SRA Type A in P/F with methane-air mixture of E.R. (ϕ) 0.72

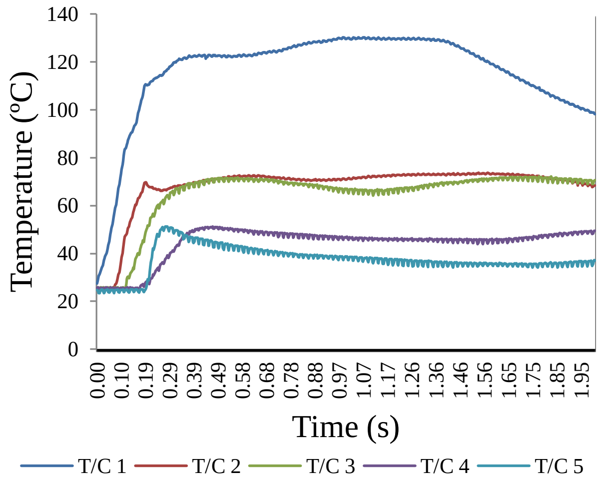

Figure A9.45 : Distinctive time-temperature profile for SRA Type A in P/F with methane-air mixture of E.R. (ϕ) 0.95

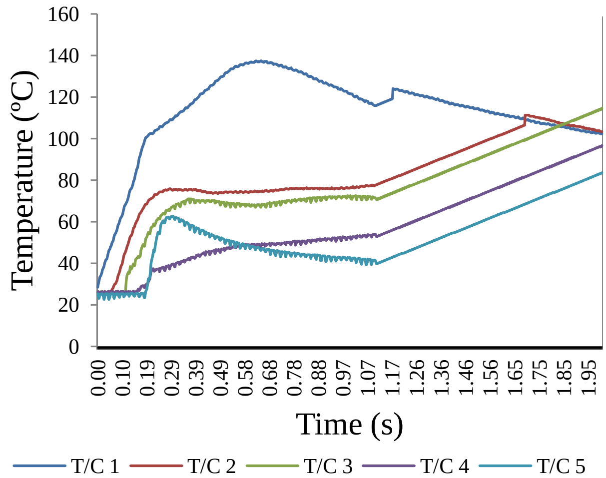

Figure A9.46 : Individual time-temperature profile for SRA Type A in P/F with methane-air mixture of E.R. (ϕ) 1.06

A9.2.1.4 Qualitative analysis

Figure A9.47 shows still images taken from the high definition video for the methane-air mixture E.R. (ϕ) 0.61 experimental trial. The flame can be observed upstream the parallel flow Type A SRA spray and can also be seen to enter the P/F spray, this image has also been expanded and a close up image is offered in Figure A9.58. In this experimental test the flame passed through the spray region and immediately accelerated by about 168%. This was significantly less than the acceleration observed in the counter flow trial utilising the same SRA, which was approximately 416% as shown previously.

Figures A9.49 – A9.54 display the images relating to the additional methane-air mixtures in this series of E.R. (ϕ) 0.72, 0.95 and 1.06. In each case the leading flame passed directly though the spray, followed by a degree of acceleration as previously shown in Figure A9.42. There were no dark regions in the flames, thus indicating an absence of areas of a localised suspension of combustion activity.

In the methane-air mixtures of E.R. (ϕ) 0.72, 0.95 and 1.06 the flames all accelerated greater than that witnessed in the counter flow trial utilising the same SRA, as discussed previously in Figure A9.1.

Comparing the trials carried out in A9.1.1 and those in this current series, the parallel flow arrangement caused significantly higher increases in flame speed form upstream to downstream of the spray. From this information it is reasonable to conclude that the disturbance in the unburned mixture downstream of the spray in the P/F tests would have been similar to the disturbance between the spray and the propagating flame in the C/F tests.

Therefore it may also be assumed that disturbance and subsequent increase in flame speed interposed by the sprays was retarded effectively in the C/F configuration. The reduction in speed increase observed in the C/F trials compared to the P/F trials, offers some initial evidence of the SRA’s suitability for mitigation operations.

(i) Equivalence ratio (ϕ) 0.61

i. Flame propagating in methane-air mixture of E.R. (ϕ) 0.61 upstream of SRA

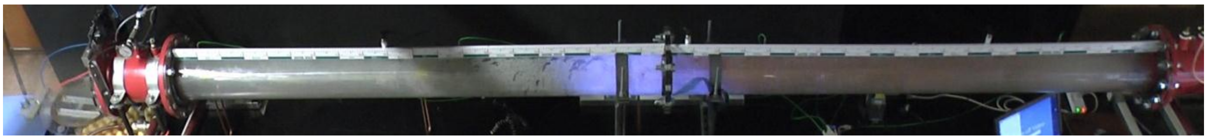

ii. Flame propagating in methane-air mixture of E.R. (ϕ) 0.61 upstream of SRA

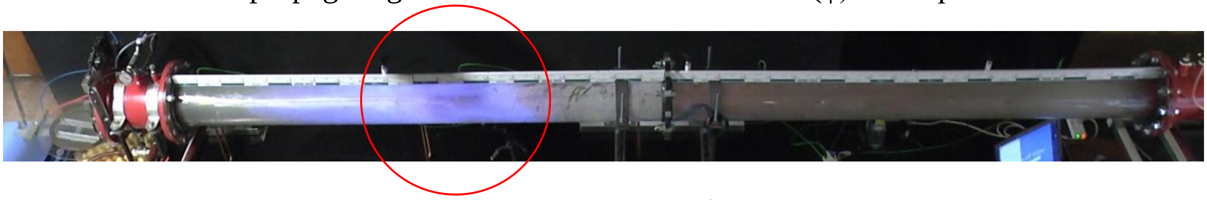

iii. Flame propagating in methane-air mixture of E.R. (ϕ) 0.61 in the region of spray

iv. Flame propagating in methane-air mixture of E.R. (ϕ) 0.61 downstream of SRA

Figure A9.47 : Flame propagating upstream and downstream of P/F SRA Type A for a methane-air mixture (ϕ) 0.61

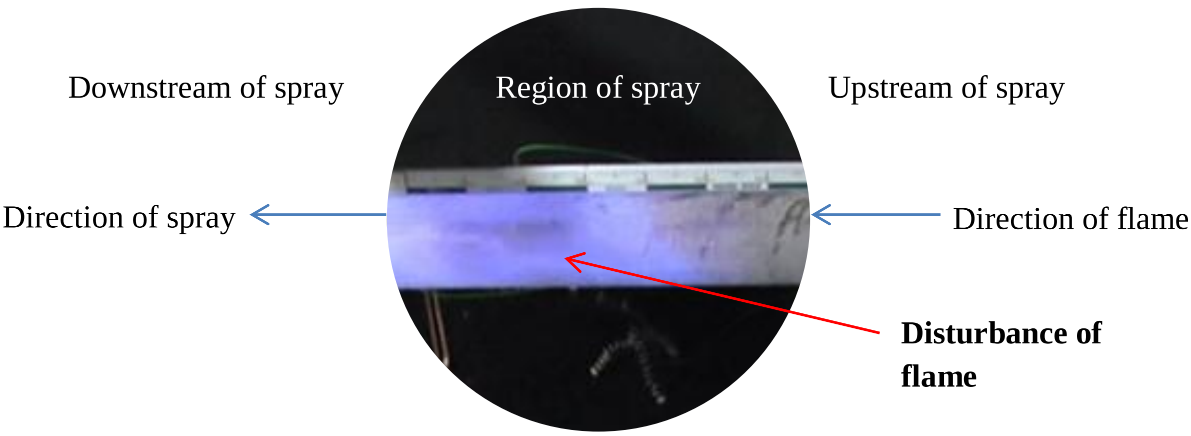

Figure A9.48 : Close up view of region of spray highlighted in Figure A9.47(iii)

(ii) Equivalence ratio (ϕ) 0.72

i. Flame propagating in methane-air mixture of E.R. (ϕ) 0.72 upstream of SRA

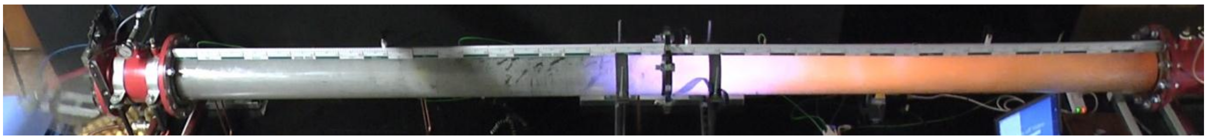

ii. Flame propagating in methane-air mixture of E.R. (ϕ) 0.72 upstream of SRA

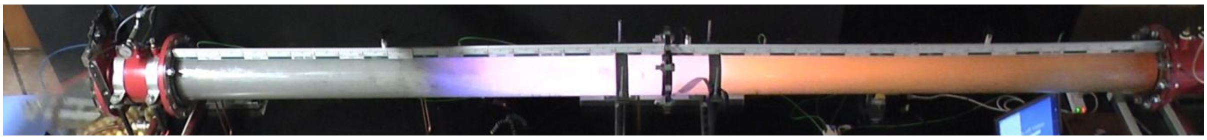

iii. Flame propagating in methane-air mixture of E.R. (ϕ) 0.72 in the region of spray

iv. Flame propagating in methane-air mixture of E.R. (ϕ) 0.72 downstream of SRA

Figure A9.49 : Flame propagating upstream and downstream of P/F SRA Type A for a methane-air mixture (ϕ) 0.72

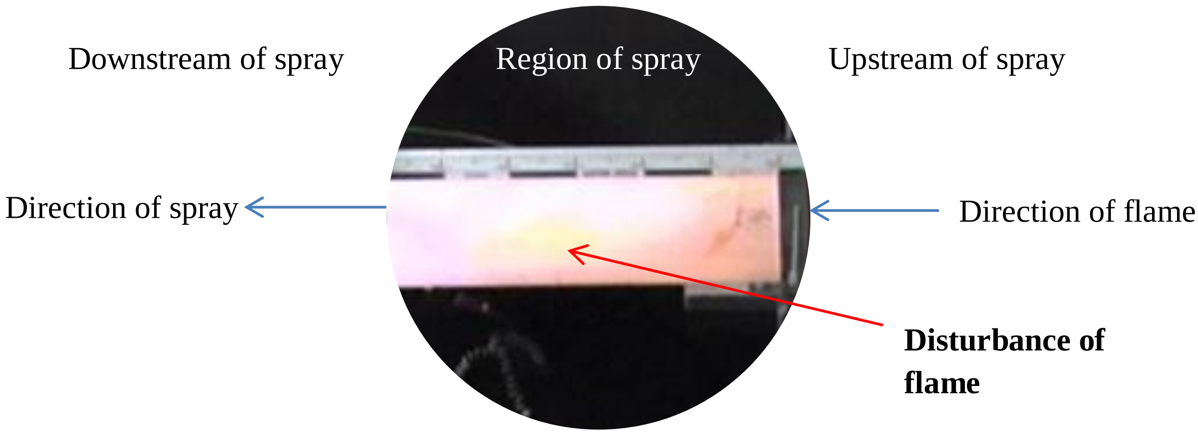

Figure A9.50 : Magnified view of region of spray highlighted in Figure A9.49(iv)

(iii) Equivalence ratio (ϕ) 0.95

i. Flame propagating in methane-air mixture of E.R. (ϕ) 0.95upstream of SRA

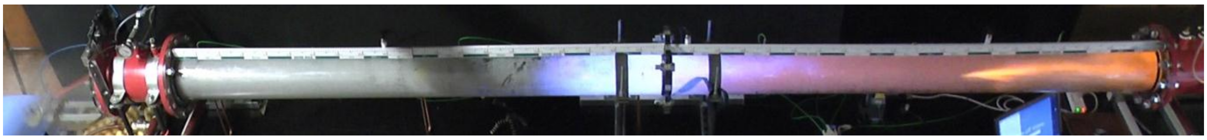

ii. Flame propagating in methane-air mixture of E.R. (ϕ) 0.95 upstream of SRA

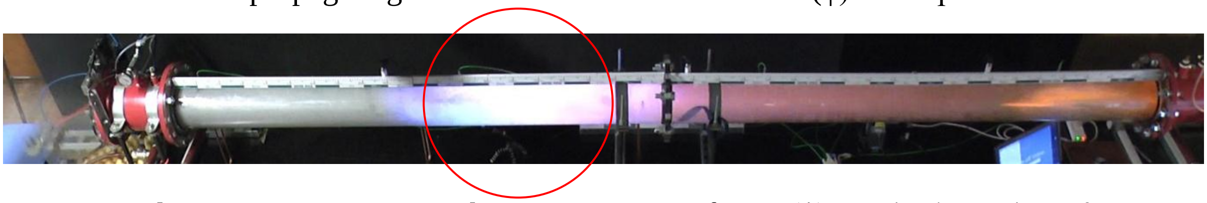

iii. Flame propagating in methane-air mixture of E.R. (ϕ) 0.95in the region of spray

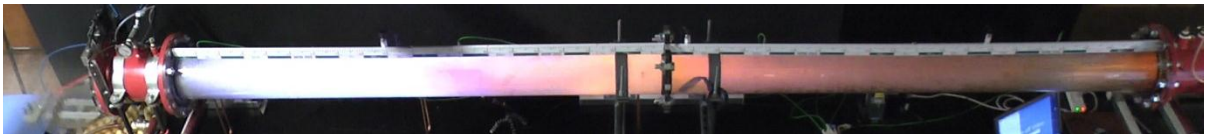

iv. Flame propagating in methane-air mixture of E.R. (ϕ) 0.95 downstream of SRA

Figure A9.51 : Flame propagating upstream and downstream of P/F SRA Type A for a methane-air mixture (ϕ) 0.95

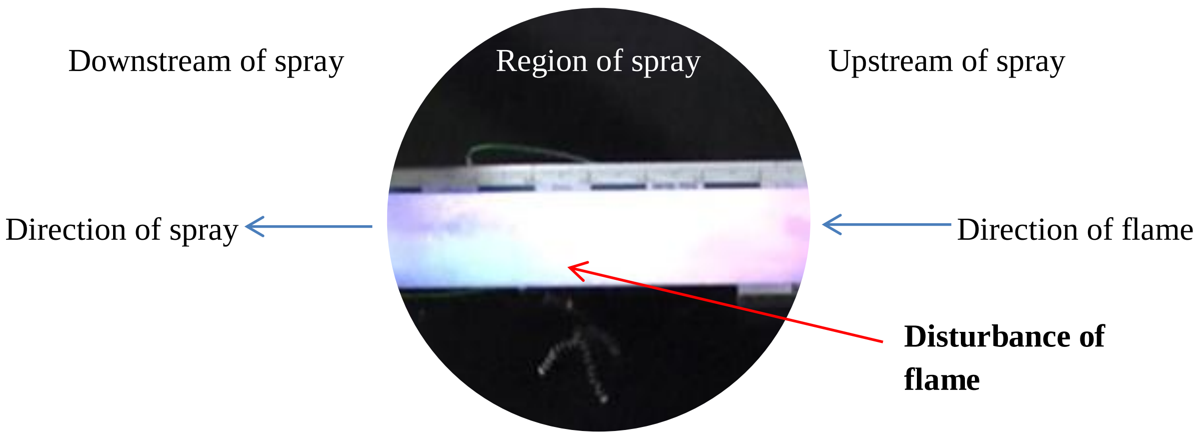

Figure 9.52 : Expanded view of region of spray highlighted in Figure A9.51(iii)

(iv) Equivalence ratio (ϕ) 1.06

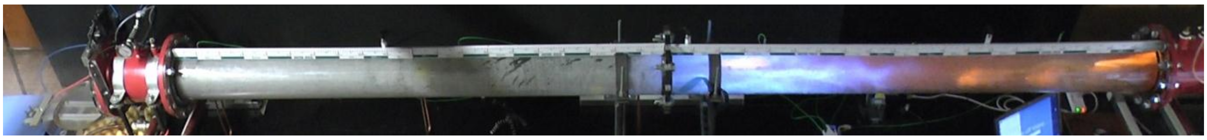

i. Flame propagating in methane-air mixture of E.R. (ϕ) 1.06 upstream of SRA

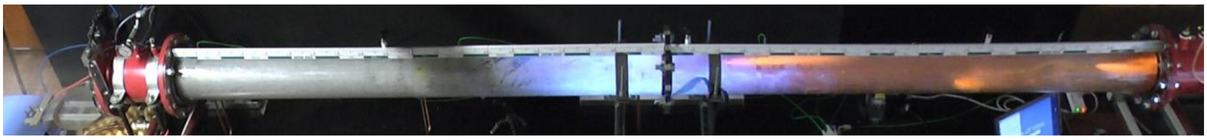

ii. Flame propagating in methane-air mixture of E.R. (ϕ) 1.06 upstream of SRA

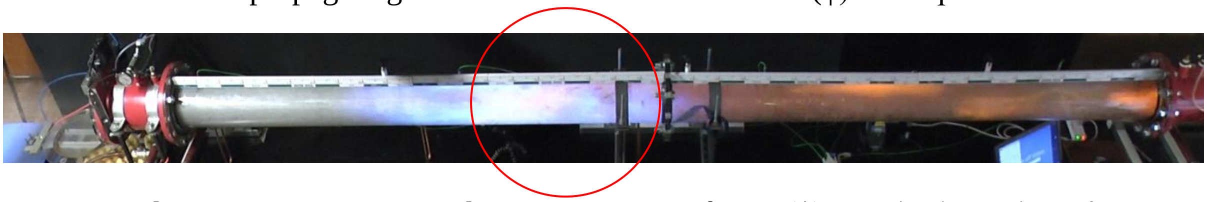

iii. Flame propagating in methane-air mixture of E.R. (ϕ) 1.06 in the region of spray

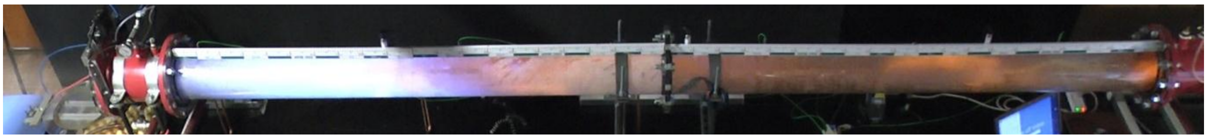

iv. Flame propagating in methane-air mixture of E.R. (ϕ) 1.06 downstream of SRA

Figure A9.53 : Flame propagating upstream and downstream of P/F SRA Type A for a methane-air mixture (ϕ) 1.06

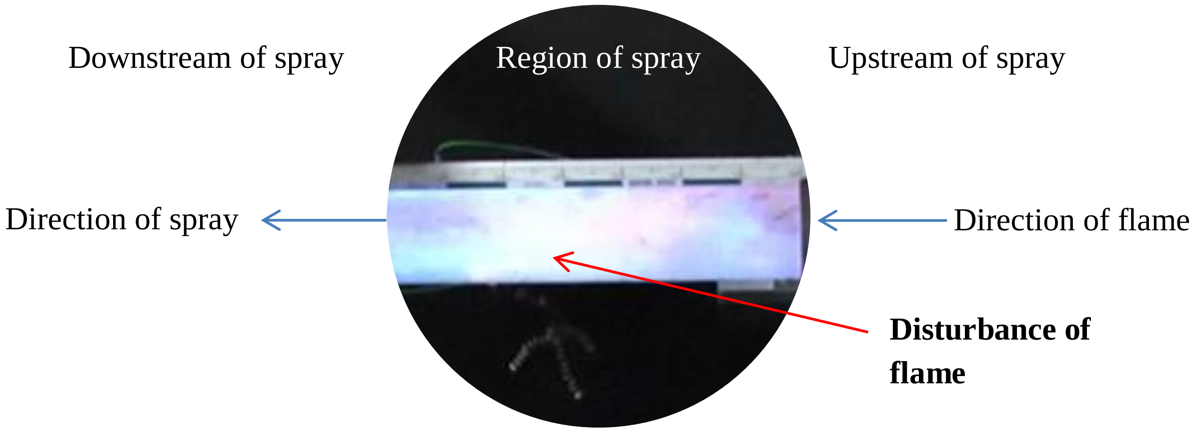

Figure A9.54: Enlarged view of region of spray highlighted in Figure A9.53(iii)

A9.2.1.5 General event outcome

Table A9.10 provides a summary of the **'general event outcome'** for each trial in this current series, using the five potential 'outcome' categories offered in Chapter 5. The results of all 'hot trials' were previously given in Table 5.14 and are also shown in Table A9.45.

Trial configuration	General event outcome	Code
Single P/F SRA : (ϕ) 0.61	No Mitigation with resulting Flame Acceleration	NMFA
Single P/F SRA : (ϕ) 0.72	No Mitigation with resulting Flame Acceleration	NMFA
Single P/F SRA : (ϕ) 0.95	No Mitigation with resulting Flame Acceleration	NMFA
Single P/F SRA : (ϕ) 1.06	No Mitigation with resulting Flame Acceleration	NMFA

Table A9.10 : General event outcome (trial series A9.2.1)

A9.2.2 Single (P/F) Type B SRA

A9.2.2.1 Trial set up

In this series of tests, a single atomiser known as SRA Type B was assembled and installed in as previously discussed in accordance with Table 5.1 and positioned as detailed in Figure A9.1 and Table A9.1. The full atomiser characteristics relating to the SRA Type B configuration were detailed in Section 7.3 and are summarised in Table A9.11 below.

Mean D32 (µm)	Mean liquid volume flux ($cm^3/cm^2/s$)	Mean droplet velocity (m/s)
26	0.024	21.41

Table A9.11 : Typical characteristics for P/F SRA Type B 95mm downstream of exit orifice

A9.2.2.2 Flame speed

In this series of tests the flame speeds were all measured upstream and downstream of the parallel flow spray. Figure A9.55 illustrates the percentage flame speed reductions observed. With the percentage reductions in this series all exhibiting negative values, this shows that all four methane-air mixtures tested resulted in a significant increase in average flame speed across the sprays.

The flame acceleration resulting from this P/F trial was found to being substantially greater that the observed in the C/F atomiser configuration. The average increase in flame speed in the P/F trials was found to be approximately three times greater than the increase observed in the C/F trials.

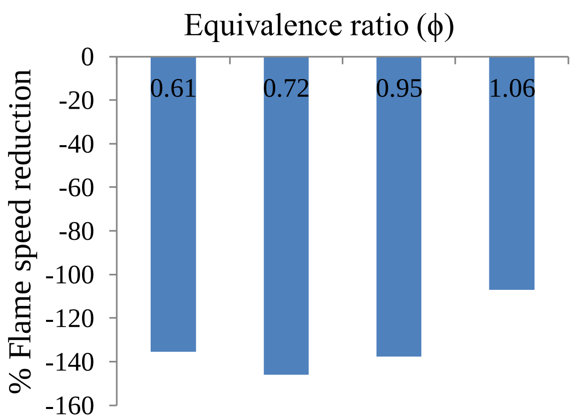

Figure A9.55 : Average flame speed reduction percentage (%) from upstream to downstream of P/F SRA in various methane-air mixtures

A9.2.2.3 Time-temperature response

The time-temperature profiles produced for each of the trials in this series are shown in Figure A9.56 – Figure A9.59. In all of the profiles the thermocouples downstream of the sprays exhibit consistent trends with respect to an increase in flame speed. The sharp gradient found with TC5 can be seen in each of the methane-air mixtures. Additional the peak temperatures observed in the TC5 thermocouples are all higher than the temperatures at TC4, at the same point in time. This indicates an increase in combustion activity as a result of the induced turbulence from the spray.

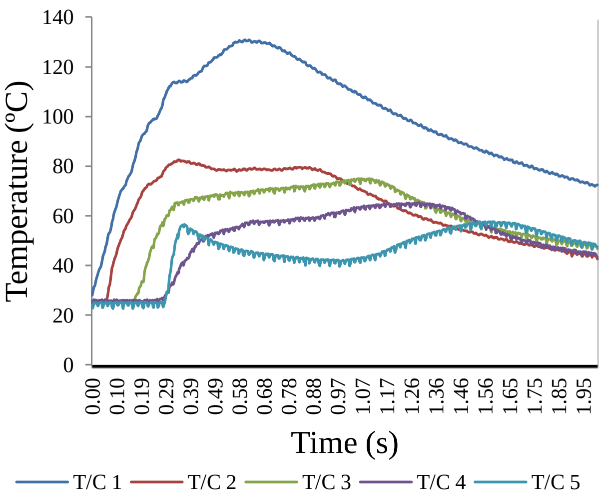

Figure A9.56 : Typical time-temperature profile for SRA Type B in P/F arrangement with methane-air mixture of E.R. (ϕ) 0.61

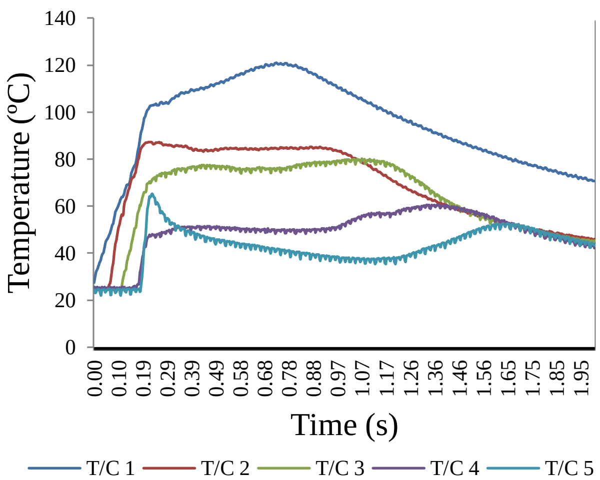

Figure A9.57 : Characteristic time-temperature profile for SRA Type B in P/F with methane-air mixture of E.R. (ϕ) 0.72

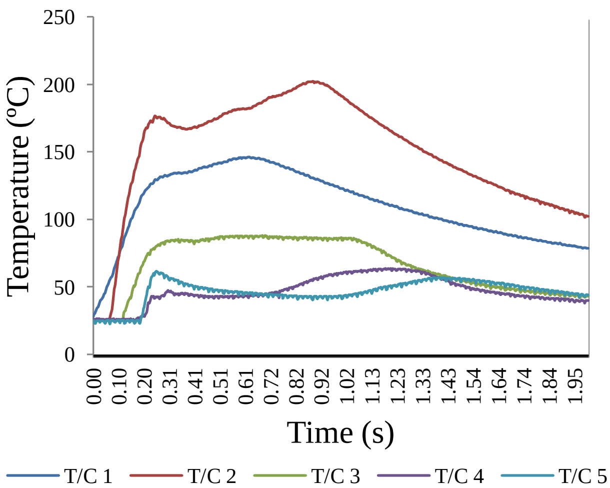

Figure A9.58 : Distinctive time-temperature profile for SRA Type B in P/F with methane-air mixture of E.R. (ϕ) 0.95

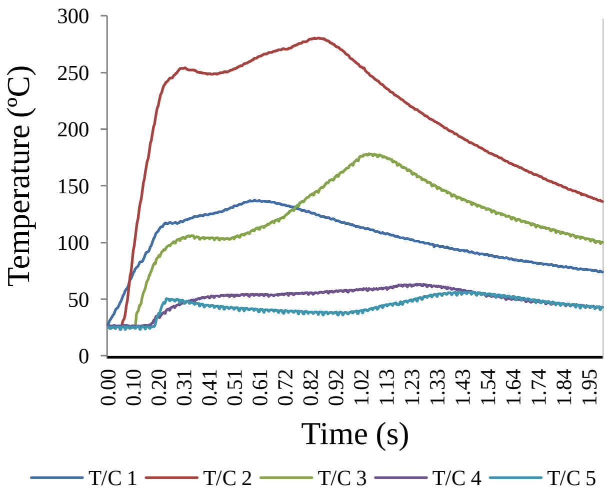

Figure A9.59 : Individual time-temperature profile for SRA Type B in P/F with methane-air mixture of E.R. (ϕ) 1.06

A9.2.2.4 Qualitative analysis

Figures A9.60 – A9.67 display the images relating to the additional methane-air mixtures in this series of E.R. (ϕ) 0.61, 0.72, 0.95 and 1.06. In each case the leading flame passes directly though the spray, followed by an increase in the flame length and flame speed.

Comparing the trials carried out in A9.1.2 with this current series, the parallel flow assembly instigated a threefold increase in flame speed from upstream to downstream of the spray.

This is consistent with the conclusion previously offered in A9.2.1 in that the disturbance in the unburned mixture downstream of the spray in the P/F tests would have been similar to the disturbance between the spray and the propagating flame in the C/F tests, consequently it may also be assumed that disturbance and subsequent increase in flame speed interposed by the sprays was retarded effectively in the C/F configuration.

In agreement with the summary statement made in A9.2.1, the reduction in speed increase observed in the C/F trials compared to the P/F trials, offers more evidence of the SRA’s suitability for mitigation operations.

(i) Equivalence ratio (ϕ) 0.61

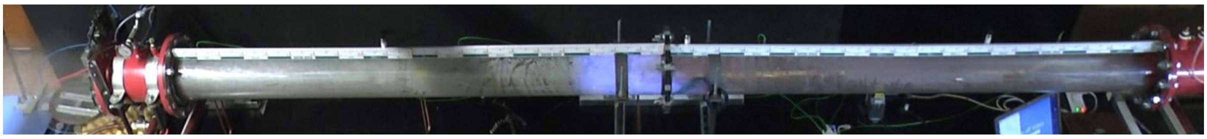

i. Flame propagating in methane-air mixture of E.R. (ϕ) 0.61 upstream of SRA

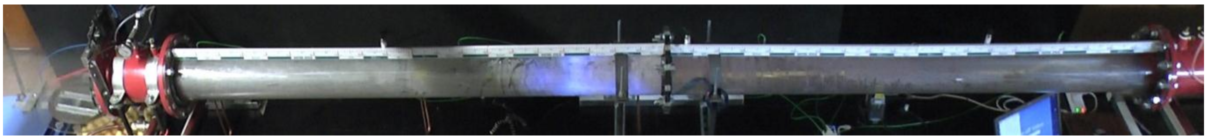

ii. Flame propagating in methane-air mixture of E.R. (ϕ) 0.61 upstream of SRA

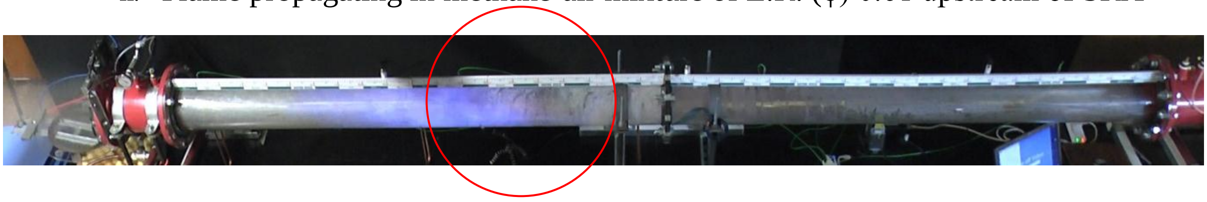

iii. Flame propagating in methane-air mixture of E.R. (ϕ) 0.61 in the region of spray

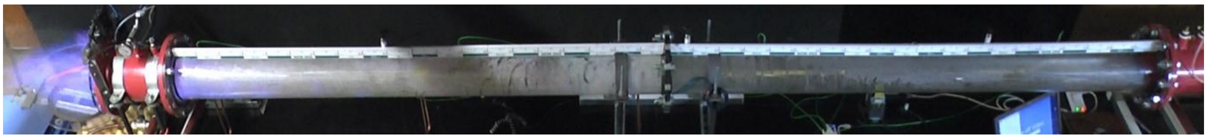

iv. Flame propagating in methane-air mixture of E.R. (ϕ) 0.61 downstream of SRA

Figure A9.60 : Flame propagating upstream and downstream of P/F SRA Type B for a methane-air mixture (ϕ) 0.61

Downstream of spray

Upstream of spray

Direction of spray

Direction of flame

Figure A9.61: Expanded view of region of spray highlighted in Figure A9.60(iii)

(ii) Equivalence ratio (ϕ) 0.72

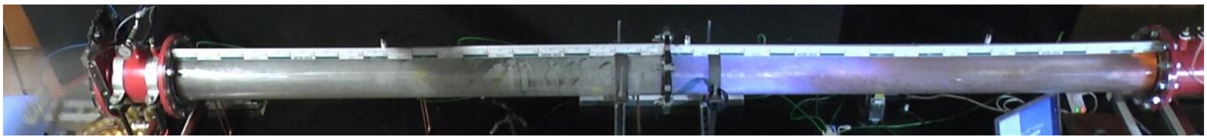

i. Flame propagating in methane-air mixture of E.R. (ϕ) 0.72 upstream of SRA

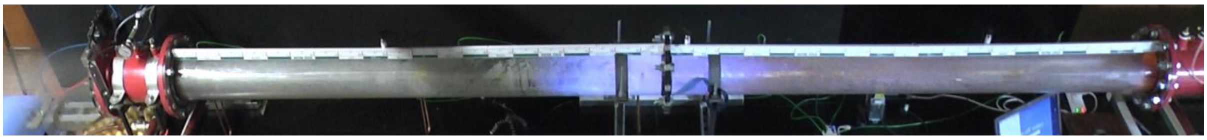

ii. Flame propagating in methane-air mixture of E.R. (ϕ) 0.72 upstream of SRA

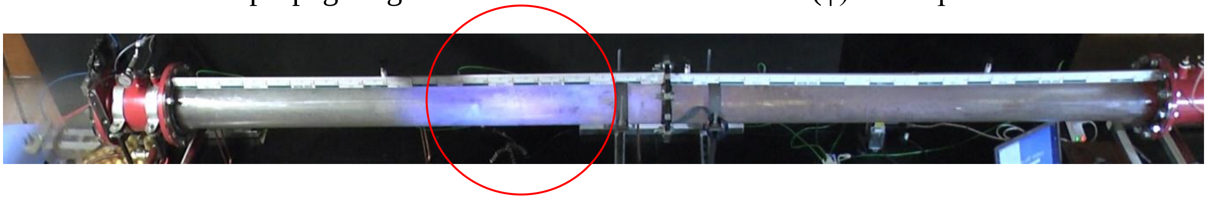

iii. Flame propagating in methane-air mixture of E.R. (ϕ) 0.72 in the region of spray

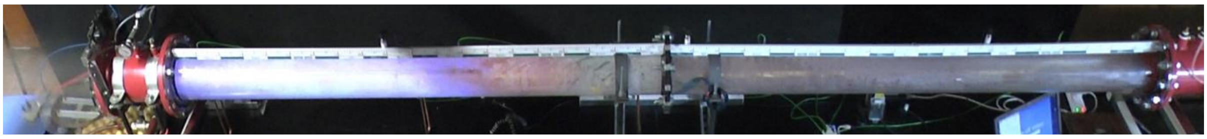

iv. Flame propagating in methane-air mixture of E.R. (ϕ) 0.72 downstream of SRA

Figure A9.62 : Flame propagating upstream and downstream of P/F SRA Type B for a methane-air mixture (ϕ) 0.72

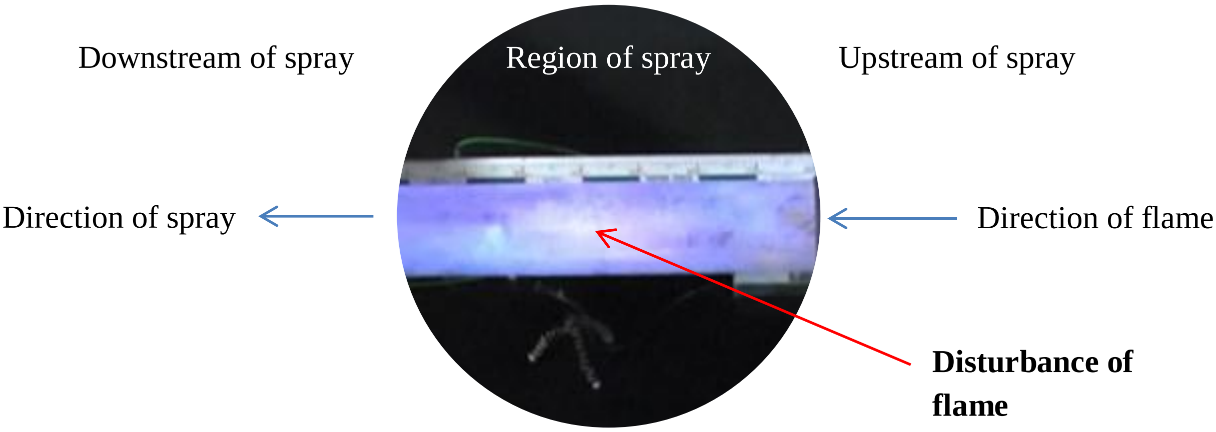

Figure A9.63 : Magnified view of region of spray highlighted in Figure A9.61(iii)

(iii) Equivalence ratio (ϕ) 0.95

i. Flame propagating in methane-air mixture of E.R. (ϕ) 0.95 upstream of SRA

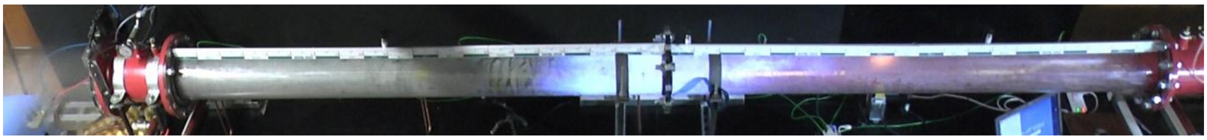

ii. Flame propagating in methane-air mixture of E.R. (ϕ) 0.95 upstream of SRA

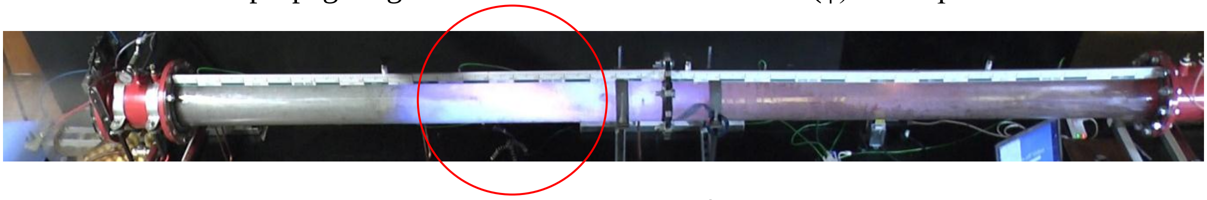

iii. Flame propagating in methane-air mixture of E.R. (ϕ) 0.95 in the region of spray

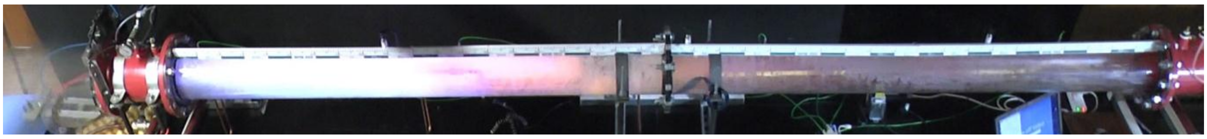

iv. Flame propagating in methane-air mixture of E.R. (ϕ) 0.95 downstream of SRA

Figure A9.64 : Flame propagating upstream and downstream of P/F SRA Type B for a methane-air mixture (ϕ) 0.95

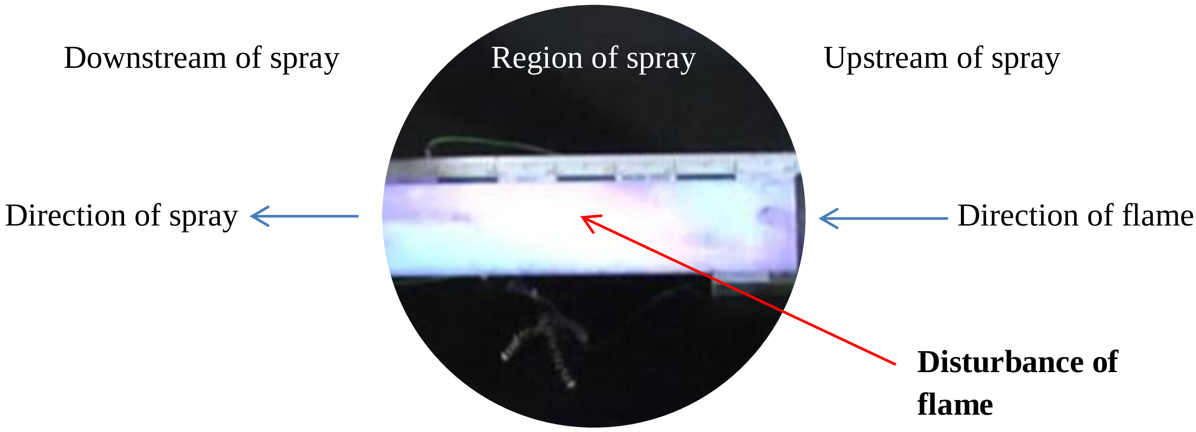

Figure A9.65 : Exploded view of region of spray highlighted in Figure A9.64(iii)

(iv) Equivalence ratio (ϕ) 1.06

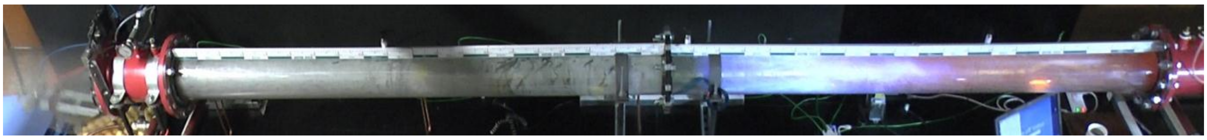

i. Flame propagating in methane-air mixture of E.R. (ϕ) 1.06 upstream of SRA

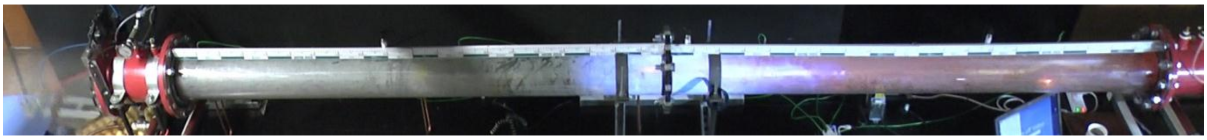

ii. Flame propagating in methane-air mixture of E.R. (ϕ) 1.06 upstream of SRA

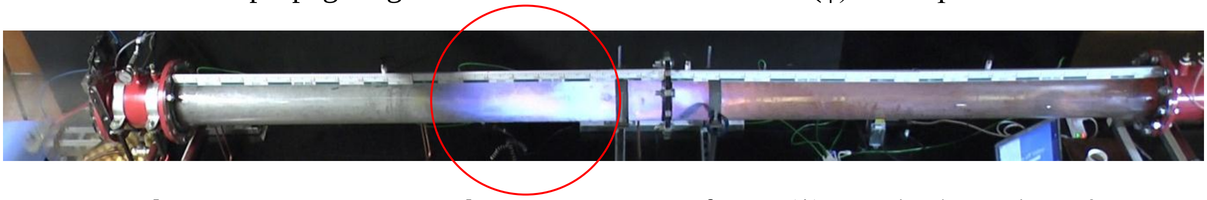

iii. Flame propagating in methane-air mixture of E.R. (ϕ) 1.06 in the region of spray

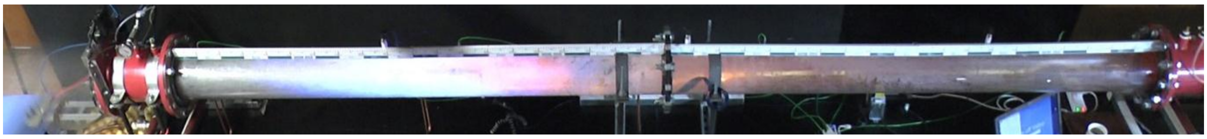

iv. Flame propagating in methane-air mixture of E.R. (ϕ) 1.06 downstream of SRA

Figure A9.66 : Flame propagating upstream and downstream of P/F SRA Type B for a methane-air mixture (ϕ) 1.06

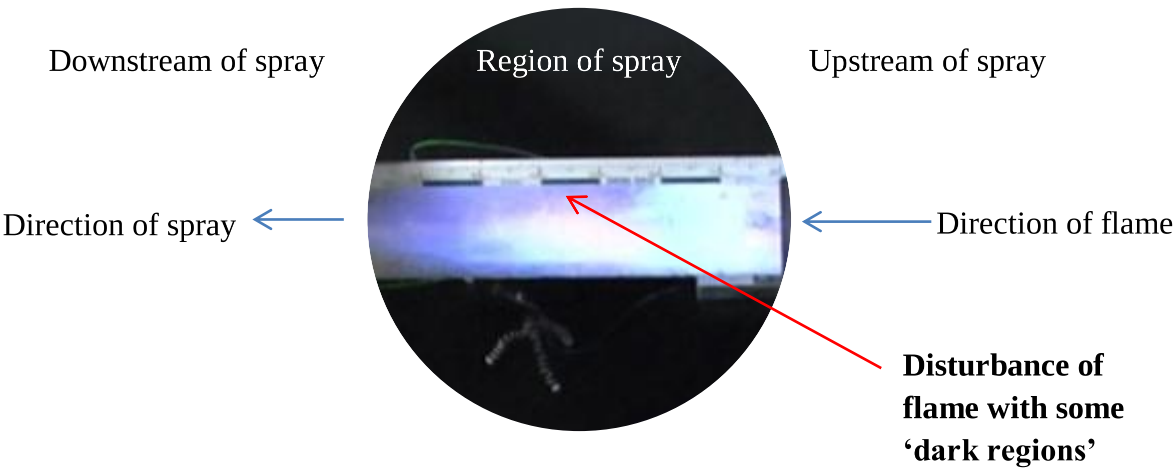

Figure A9.67: Close up view of region of spray highlighted in Figure A9.66(iii)

A9.2.2.5 General event outcome

Table A9.12 provides a summary of the **'general event outcome'** for each trial in this current series, using the five potential 'outcome' categories offered in Chapter 5. The results of all 'hot trials' were previously given in Table 5.14 and are also shown in Table A9.45.

Trial configuration	General event outcome	Code
Single P/F SRA : (ϕ) 0.61	No Mitigation with resulting Flame Acceleration	NMFA
Single P/F SRA : (ϕ) 0.72	No Mitigation with resulting Flame Acceleration	NMFA
Single P/F SRA : (ϕ) 0.95	No Mitigation with resulting Flame Acceleration	NMFA
Single P/F SRA : (ϕ) 1.06	No Mitigation with resulting Flame Acceleration	NMFA

Table A9.12 : General event outcome (trial series A9.2.2)

A9.1.3 Single (P/F) Type C SRA

A9.2.3.1 Trial set up

In this series of tests, a single atomiser known as SRA Type C was assembled and installed in as previously discussed in accordance with Table 5.1 and positioned as detailed in Figure A9.1 and Table A9.1. The full atomiser characteristics relating to the SRA Type C configuration were detailed in Section 7.3 and are summarised in Table A9.8 below.

Mean D32 (µm)	Mean liquid volume flux ($cm^3/cm^2/s$)	Mean droplet velocity (m/s)
29	0.039	13.5

Table A9.13 : Typical characteristics for SRA Type C 95mm downstream of exit orifice

A9.2.3.2 Flame speed

In this series of tests the flame speeds were all measured upstream and downstream of the parallel flow spray. Figure A9.68 indicates the percentage flame speed reductions observed. With the exception of the methane-air mixture (ϕ) E.R. 0.61 whereby 100% mitigation was achieved, a global increase in average flame speed across the sprays was observed.

When comparing the results shown in Figure A9.68 with the results for the corresponding C/F trials illustrated previously in Figure A9.28, the methane-air mixture (ϕ) E.R. 0.61 was mitigated in both cases, whereas flame acceleration occurred in the other mixtures. Interestingly the methane-air mixtures (ϕ) E.R. 0.72 and 1.06 in this P/F series produced smaller flame speed increases than their C/F equivalents.

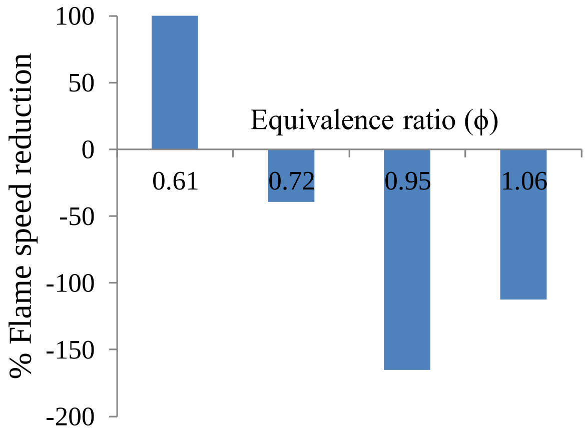

Figure A9.68 : Average flame speed reduction percentage (%) from upstream to downstream of Type C parallel flow SRA in various methane-air mixtures

A9.2.3.3 Time-temperature response

The time-temperature profiles produced for each of the trials in this series are shown in Figure A9.69 – Figure A9.72. In Figure A9.67 the profiles of thermocouples TC4 and TC5, downstream of the sprays, exhibit consistent trends with respect combustion mitigation.

The gradient associated with TC5 in Figures A9.70 – A9.72 indicates an increase in flame temperature at the exit end of the flame propagation and mitigation which is consistent with the results shown in Figure A9.66 and discussed previously in A9.2.3.

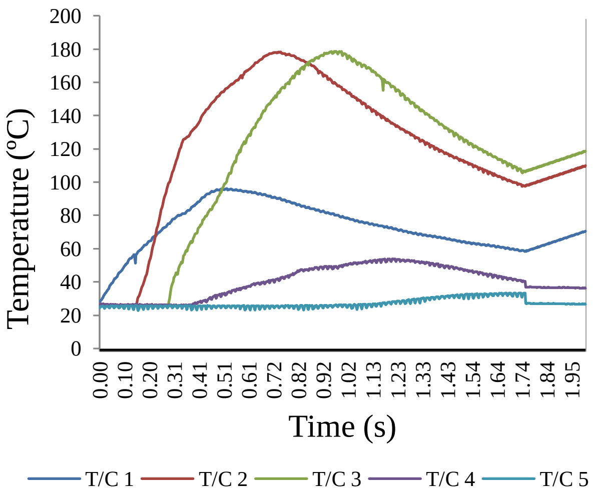

Figure A9.69 : Typical time-temperature profile for SRA Type C in P/F arrangement with methane-air mixture of E.R. (ϕ) 0.61

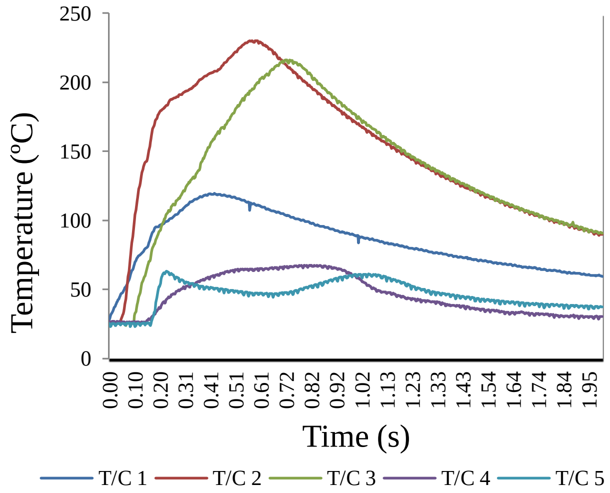

Figure A9.70 : Characteristic time-temperature profile for SRA Type C in P/F with methane-air mixture of E.R. (ϕ) 0.72

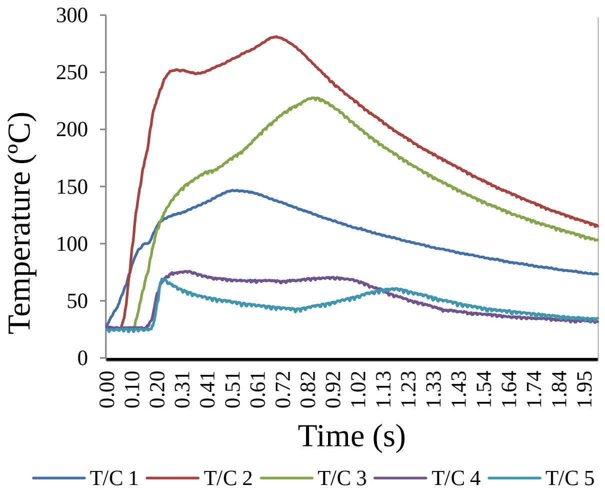

Figure A9.71 : Distinctive time-temperature profile for SRA Type C in P/F with methane-air mixture of E.R. (ϕ) 0.95

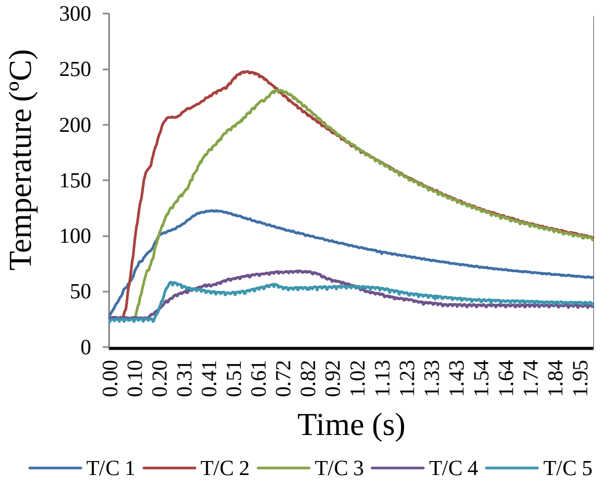

Figure A9.72 Individual time-temperature profile for SRA Type C in P/F with methane-air mixture of E.R. (ϕ) 0.95

A9.2.3.4 Qualitative analysis

Figure A9.73 shows the propagation and subsequent mitigation of a methane-air mixture of E.R. (ϕ) 0.61. Figure A9.74 shows an expanded view of the final stages of combustion, as the flame reaches the widest part of the spray. At this point the whole cross section of the flame propagation and mitigation tube was enveloped by the spray.

In Figure A9.75 the flame in seen to pass through the spray region. However in Figure A9.76 an enlarged view of Figure A.97(iii) displays dark regions where combustion may be assumed to have ceased.

In Figure A.77 the leading profile of the flame front is clearly affected by the spray. This can be seen in the exploded view in Figure A9.78 where a concave region can be seen in the flame at the flame / spray interface.

In Figure A.79 the flame again passes through the spray. Figure A9.80 shows a magnified view of the flame in the spray region, where the disturbance in visible together will the lengthening and subsequent acceleration of the flame.

The combustion mitigation potential of all three SRA's has been clearly demonstrated in these single 'in flow' experimental trials. However, neither of the SRA configurations or flow arrangements were successful in mitigating a propagating flame greater than E.R. (ϕ) 0.61.

To mitigate a flame of E.R. (ϕ) >0.61 the droplet density and spray volume in the path of the flame needs to be increased. A twin 'in flow' atomiser arrangement was developed to assess the performance of two overlapping parallel flow sprays. The results of the twin parallel flow overlapping sprays are presented and discussed in Section A9.3.

(i) Equivalence ratio (ϕ) 0.61

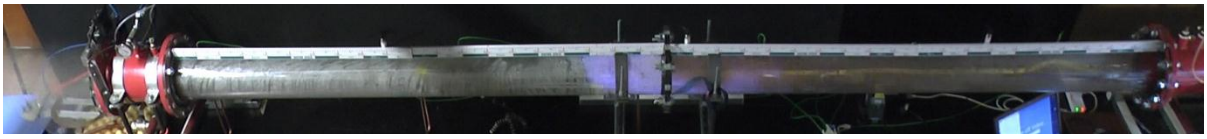

i. Flame propagating in methane-air mixture of E.R. (ϕ) 0.61 upstream of SRA

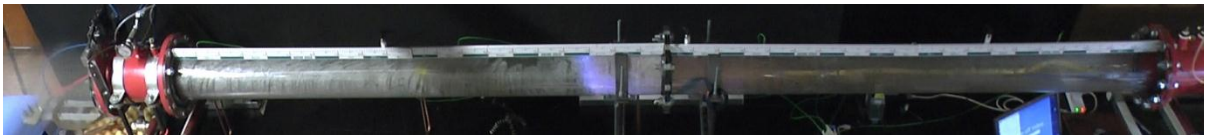

ii. Flame propagating in methane-air mixture of E.R. (ϕ) 0.61 upstream of SRA

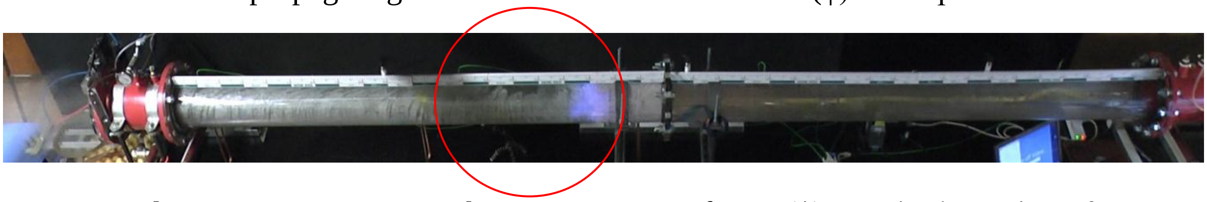

iii. Flame propagating in methane-air mixture of E.R. (ϕ) 0.61 in the region of spray

iv. **Mitigation** of methane-air mixture of E.R. (ϕ) 0.61 downstream of SRA

Figure A9.73 : Flame propagating upstream and downstream of P/F SRA Type C for a methane-air mixture (ϕ) 0.61

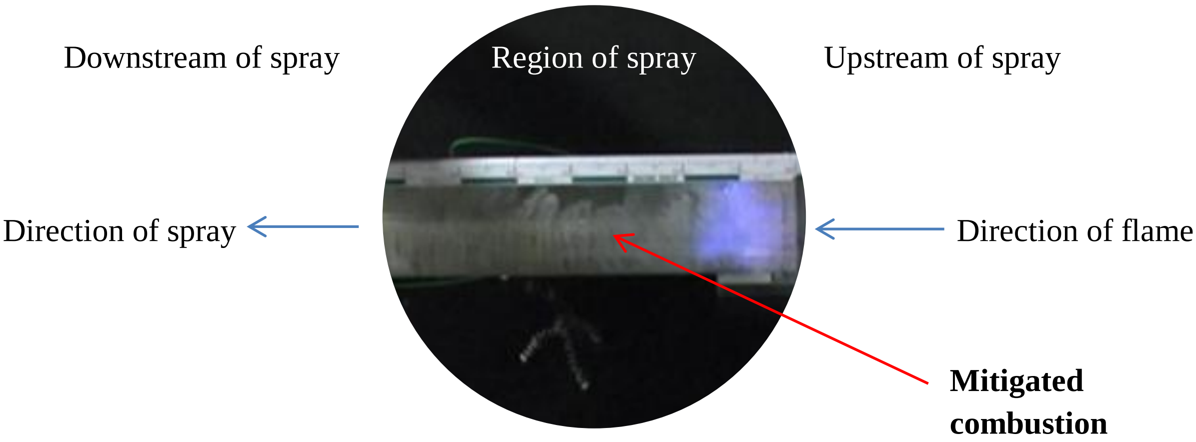

Figure 9.74 : Expanded view of region of spray highlighted in Figure A9.73(iii)

(ii) Equivalence ratio (ϕ) 0.72

i. Flame propagating in methane-air mixture of E.R. (ϕ) 0.72 upstream of SRA

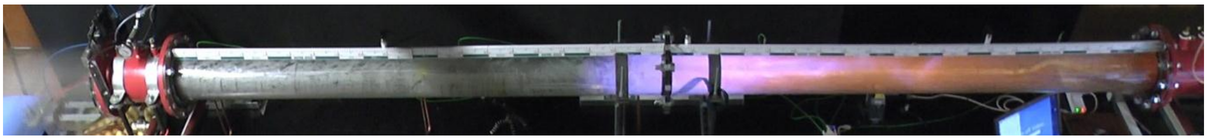

ii. Flame propagating in methane-air mixture of E.R. (ϕ) 0.72 upstream of SRA

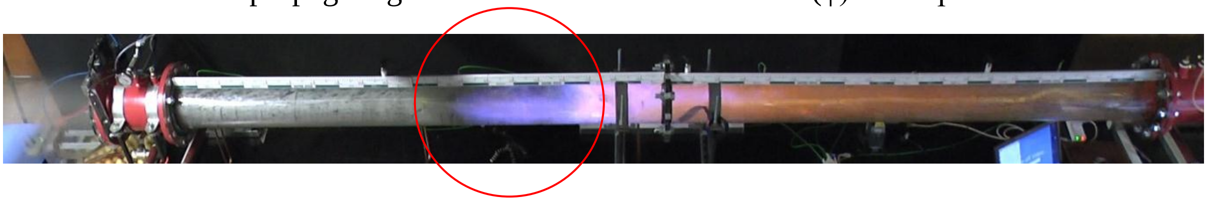

iii. Flame propagating in methane-air mixture of E.R. (ϕ) 0.72 in the region of spray

iv. Flame propagating in methane-air mixture of E.R. (ϕ) 0.72 downstream of SRA

Figure A9.75: Flame propagating upstream and downstream of P/F SRA Type C for a methane-air mixture (ϕ) 0.72

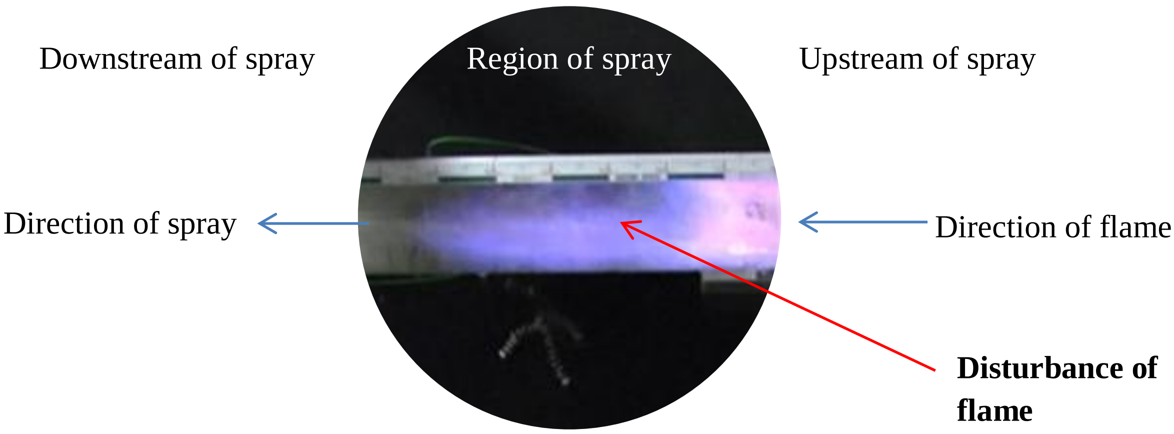

Figure A9.76 : Enlarged view of region of spray highlighted in Figure A9.75(iii)

(iii) Equivalence ratio (ϕ) 0.95

i. Flame propagating in methane-air mixture of E.R. (ϕ) 0.95 upstream of SRA

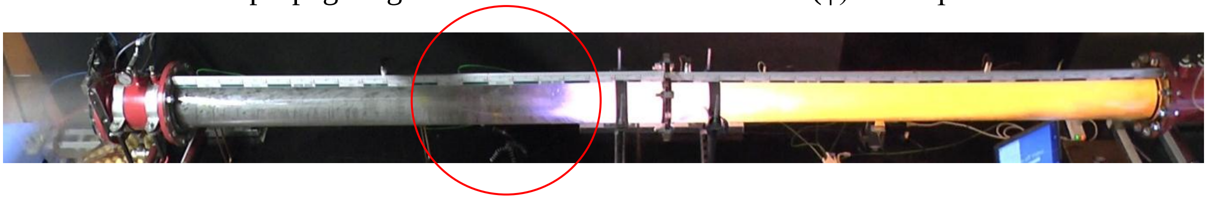

ii. Flame propagating in methane-air mixture of E.R. (ϕ) 0.95 upstream of SRA

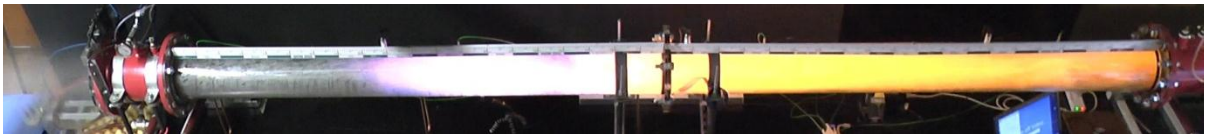

iii. Flame propagating in methane-air mixture of E.R. (ϕ) 0.95 in the region of spray

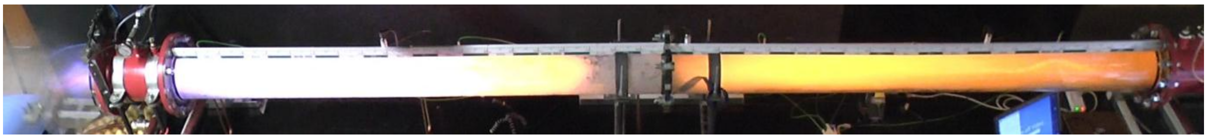

iv. Flame propagating in methane-air mixture of E.R. (ϕ) 0.95 downstream of SRA

Figure A9.77: Flame propagating upstream and downstream of P/F SRA Type C for a methane-air mixture (ϕ) 0.95

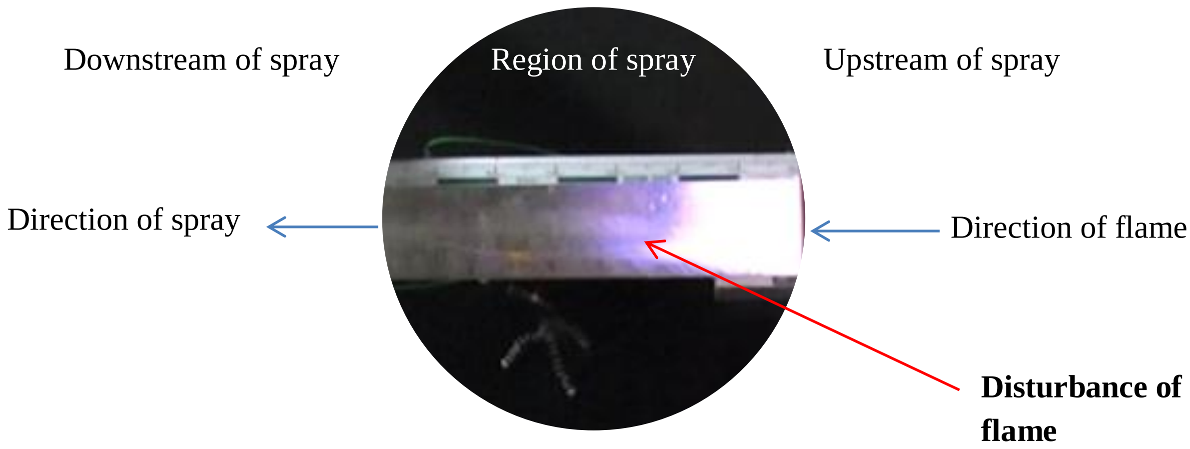

Figure A9.78 : Exploded view of region of spray highlighted in Figure A9.77(ii)

(iv) Equivalence ratio (ϕ) 1.06

i. Flame propagating in methane-air mixture of E.R. (ϕ) 1.06 upstream of SRA

ii. Flame propagating in methane-air mixture of E.R. (ϕ) 1.06 upstream of SRA

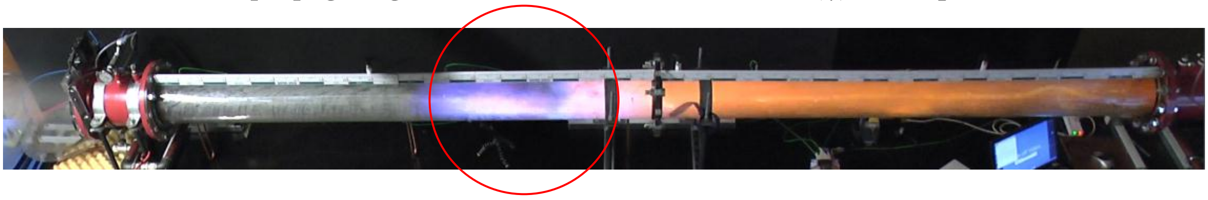

iii. Flame propagating in methane-air mixture of E.R. (ϕ) 1.06 in the region of spray

iv. Flame propagating in methane-air mixture of E.R. (ϕ) 1.06 downstream of SRA

Figure A9.79 : Flame propagating upstream and downstream of P/F SRA Type C for a methane-air mixture (ϕ) 1.06

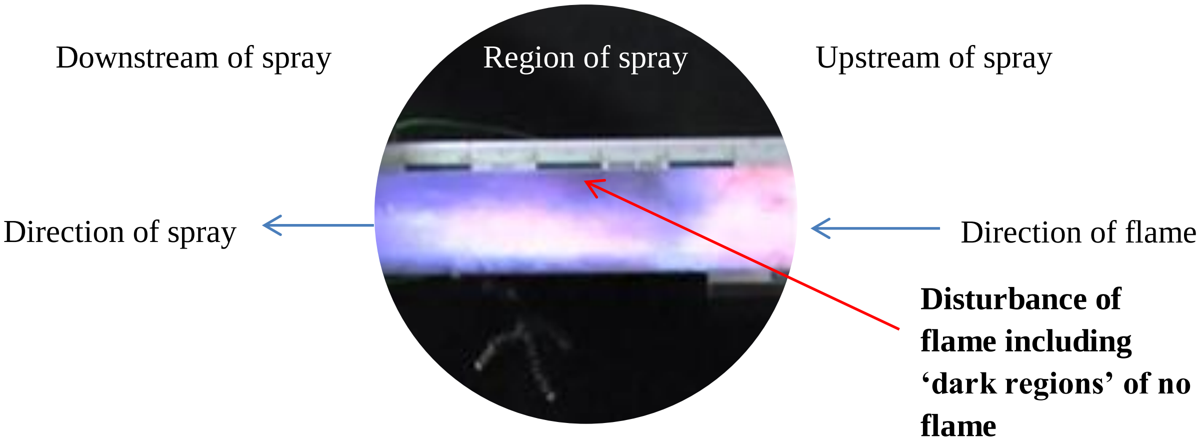

Figure A9.80 : Magnified view of region of spray highlighted in Figure A9.79(iii)

A9.2.3.5 General event outcome

Table A9.14 provides a summary of the **'general event outcome'** for each trial in this current series, using the five potential 'outcome' categories offered in Chapter 5. The results of all 'hot trials' were previously given in Table 5.14 and are also shown in Table A9.45.

Trial configuration	General event outcome	Code
Single P/F SRA : (ϕ) 0.61	Full Mitigation resulting in Flame Extinguishment	FMFE
Single P/F SRA : (ϕ) 0.72	No Mitigation with resulting Flame Acceleration	NMFA
Single P/F SRA : (ϕ) 0.95	No Mitigation with resulting Flame Acceleration	NMFA
Single P/F SRA : (ϕ) 1.06	No Mitigation with resulting Flame Acceleration	NMFA

Table A9.14 : General event outcome (trial series A9.2.3)

A9.3 Mitigation trials for a two water sprays in parallel flow with a methane-air flame

A unique manifold arrangement of multiple overlapping SRA's as shown in Figure A9.82 was designed and developed by the author for these trials and was discussed previously in detail in Chapter 4. The manifold was installed in the FPMR in parallel flow conformation with the propagation flame direction, as illustrated in Figure A9.81 and in accordance with the dimension in Table A9.15

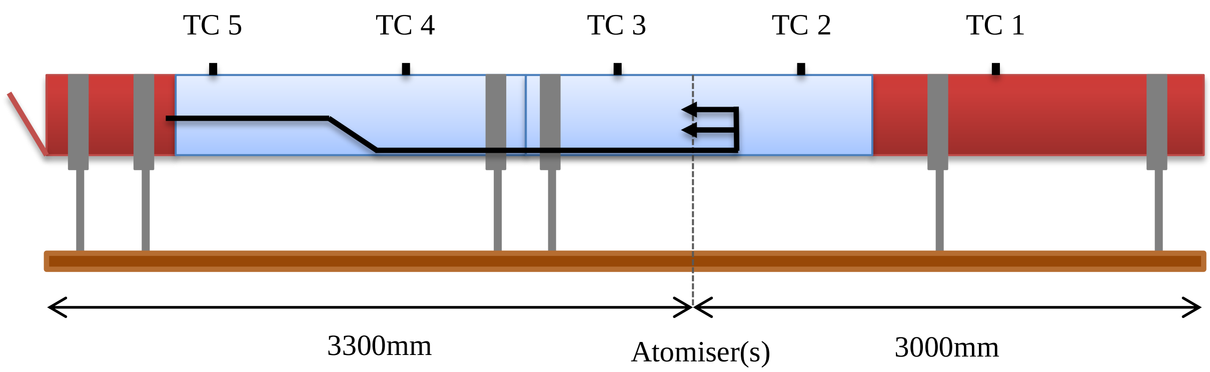

Figure A9.81 : Position of atomisers and thermocouples (relative to right hand ignition point)

Component	Position (measured from right hand end)
Thermocouple (T/C1)	1200mm
Thermocouple (T/C2)	2400mm
Thermocouple (T/C3)	3600mm
Thermocouple (T/C4)	4800mm
Thermocouple (T/C5)	6000mm
Atomiser outlet orifices (parallel flow)	3000mm

Table A9.15 : Measured position of thermocouples and SRA

A9.3.1 Two Type B overlapping SRA's

A9.3.1.1 Trial set up

In the following section the trial results for two parallel flow, Type B overlapping SRA's are presented and discussed. The SRA manifold was installed as illustrated in Figure A9.81 and in accordance with the dimension in Table A9.15. Table A9.16 provides a summary of the spray characteristics for this overlapping Type B SRA arrangement.

Mean D32 (µm)	Mean liquid volume flux ($cm^3/ cm^2/s$)	Mean droplet velocity (m/s)
54	0.038	27

Table A9.16 : Typical characteristics for 2 x Overlapping Type B SRA's

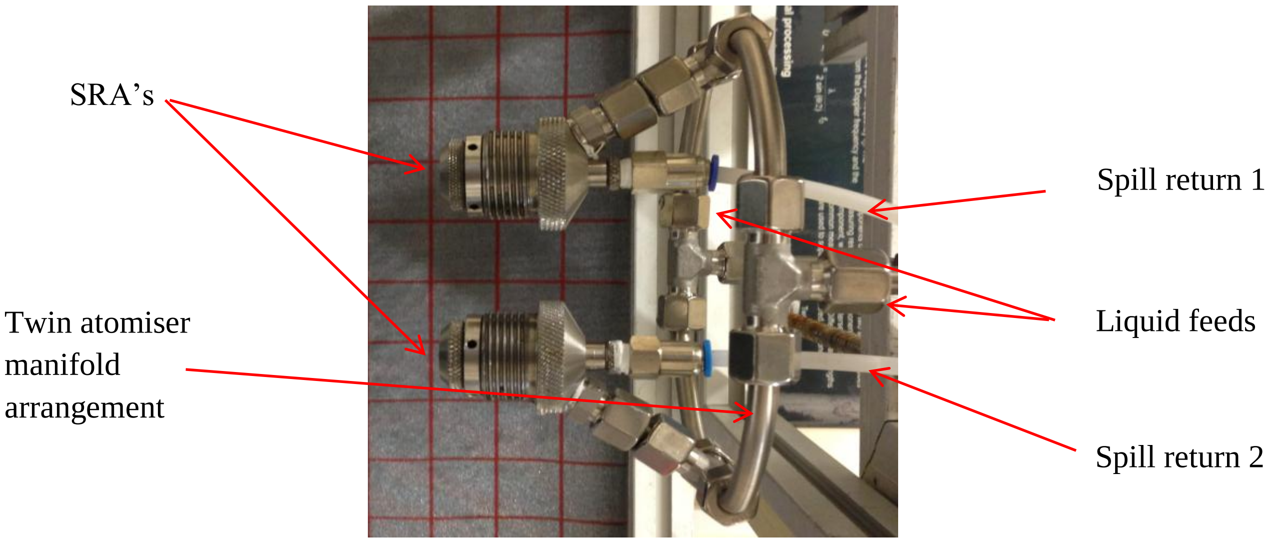

Figure A9.82 : Multiple overlapping spray manifold incorporating 2 x Type B SRA's

A9.3.1.2 Flame speed

In this series of tests the flame speeds were all measured upstream and downstream of the twin parallel flow sprays. Figure A9.83 illustrates the percentage flame speed reductions observed in the four trials in this series. In the methane-air mixture of E.R. (ϕ) 0.61 the flame was completely mitigated and did not continue to propagate downstream. However, the other methane-air mixtures of E.R. (ϕ) 0.72, 0.95 and 1.06 all resulted in an increase in average flame speed across the sprays. However, when these results are compared to the single parallel flow trials in Section A9.2, the resulting flame acceleration was significantly less. This would indicate that the increase in liquid volume flux had a positive outcome with respect to flame suppression.

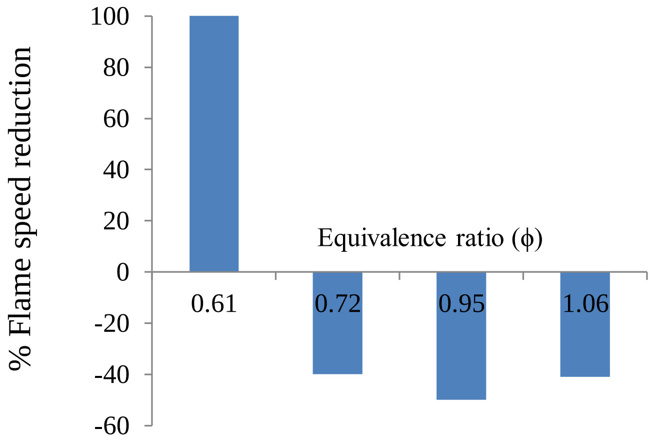

Figure A9.83 : Average flame speed reduction percentage (%) from upstream to downstream of overlapping parallel flow SRA's in various methane-air mixtures

A9.3.1.3 Time-temperature response

The time-temperature profiles produced for each of the trials in this series are shown in Figure A9.84 – Figure A9.87. In Figure A9.84 the profiles for thermocouples TC3, TC4 and TC5 which were downstream of the sprays are consistent with combustion mitigation.

In this series of trials thermocouple TC2 was situated downstream of TC1 and upstream of the sprays. In all cases a noteworthy temperature rise was detected between TC1 and TC2, indicating that an upstream disturbance had been transferred into the methane-air mixture, which may have been be due to the high level of entrainment upstream of the twin SRA arrangement. The temperature rise noted in these twin overlapping trials was not observed in any of the single atomiser trials.

Figures A9.85 – A9.87 all exhibit similar temperature profiles consistent with a degree of flame acceleration consistent with the values reported in Figure A9.83.

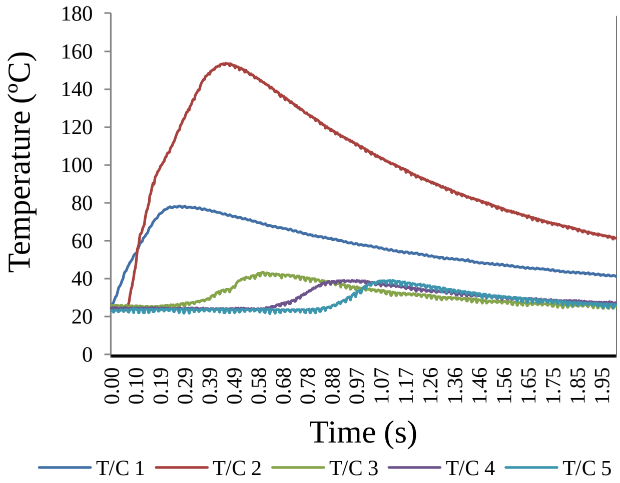

Figure A9.84 : Typical time-temperature profile for two overlapping Type B SRA's in P/F arrangement with methane-air mixture of E.R. (ϕ) 0.61

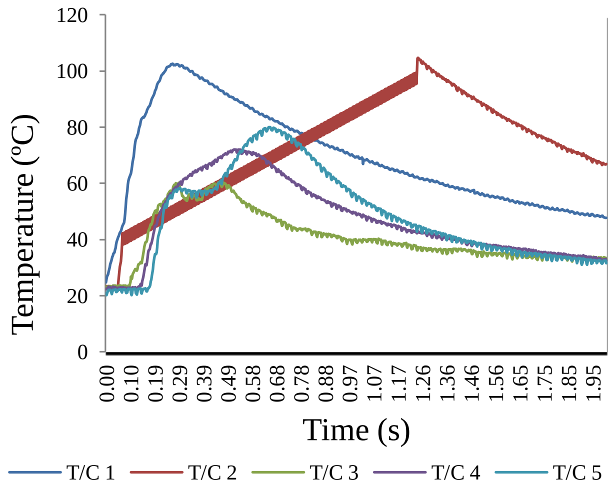

Figure A9.85 : Characteristic time-temperature profile for two overlapping Type B SRA's in P/F arrangement with methane-air mixture of E.R. (ϕ) 0.72

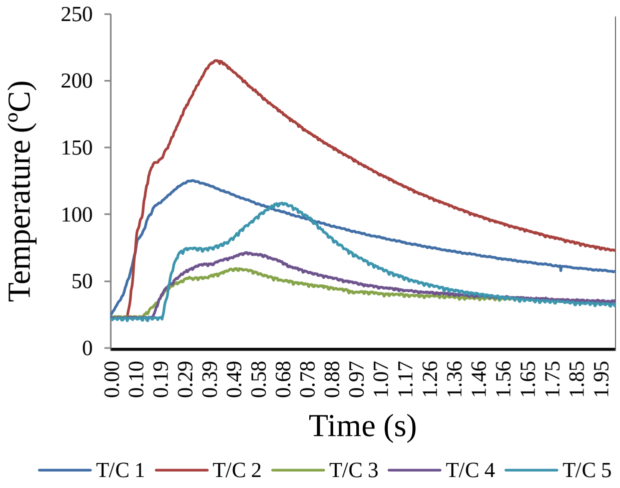

Figure A9.86 : Distinctive time-temperature profile for two overlapping Type B SRA's in P/F arrangement with methane-air mixture of E.R. (ϕ) 0.95

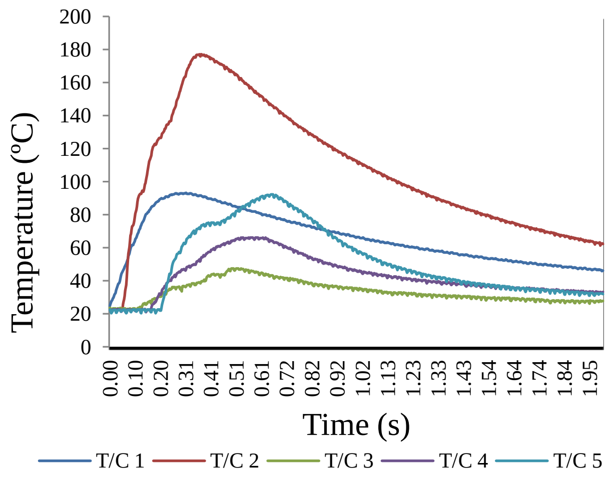

Figure A9.87 : Individual time-temperature profile for two overlapping Type B SRA's in P/F arrangement with methane-air mixture of E.R. (ϕ) 1.06

A9.3.1.4 Qualitative analysis

The related images for this series of trials are presented in Figures A9.88 – A9.95 for methane-air mixtures of E.R. (ϕ) 0.61, 0.72, 0.95 and 1.06. For the methane-air mixture of E.R. (ϕ) 0.61 the flame can be observed in Figure A9.88(i) initially upstream of the sprays.

In Figure A9.88(ii) the flame can be seen to be in contact with the sprays and exhibits a concave appearance in shape. In Figure A9.86(iii) the flame has been quenched and virtually extinguished by the sprays. Finally in Figure A9.86(iv) there is no further presence of combustion.

In the remaining three methane-air mixtures of E.R. (ϕ) 0.72, 0.95 and 1.06, the flame propagated through the sprays and began to accelerate. As previously documented, this acceleration was notably less than that observed in the single parallel atomiser trials.

(i) Equivalence ratio (ϕ) 0.61

i. Flame propagating in methane-air mixture of E.R. (ϕ) 0.61 upstream of SRA

ii. Flame propagating in methane-air mixture of E.R. (ϕ) 0.61 upstream of SRA

iii. Flame propagating in methane-air mixture of E.R. (ϕ) 0.61 in the region of spray

iv. **Mitigation** of methane-air mixture of E.R. (ϕ) 0.61 downstream of SRA

Figure A9.88 : Flame propagating upstream and downstream of two overlapping parallel flow Type B SRA's for a methane-air mixture (ϕ) 0.61

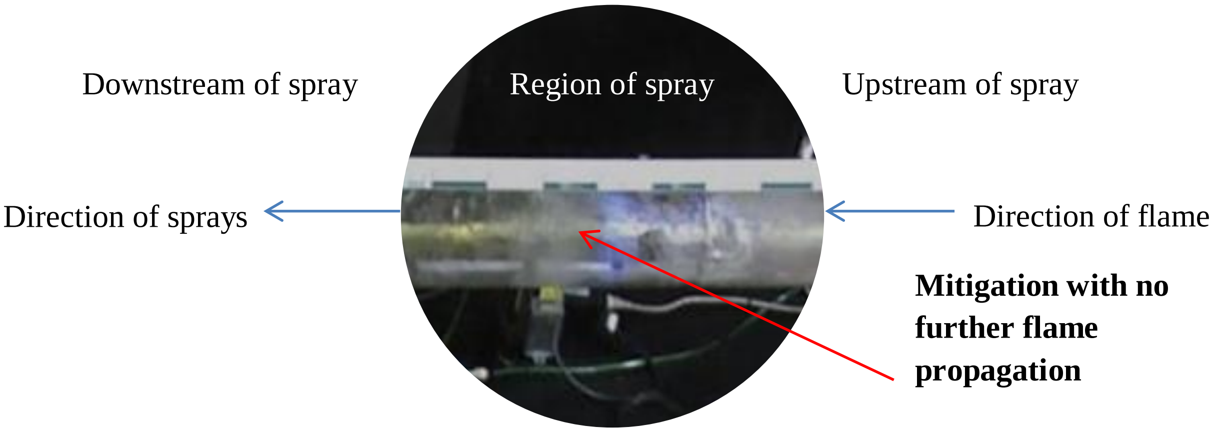

Figure A9.89 : Expanded view of region of spray highlighted in Figure A9.88(iii)

(ii) Equivalence ratio (ϕ) 0.72

i. Flame propagating in methane-air mixture of E.R. (ϕ) 0.72 upstream of SRA

ii. Flame propagating in methane-air mixture of E.R. (ϕ) 0.72 upstream of SRA

iii. Flame propagating in methane-air mixture of E.R. (ϕ) 0.72 in the region of spray

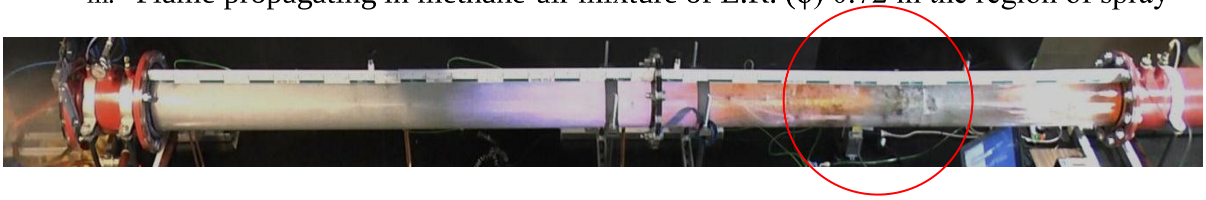

iv. Flame propagating in methane-air mixture of E.R. (ϕ) 0.72 downstream of SRA

Figure A9.90 : Flame propagating upstream and downstream of two overlapping parallel flow Type B SRA's for a methane-air mixture (ϕ) 0.72

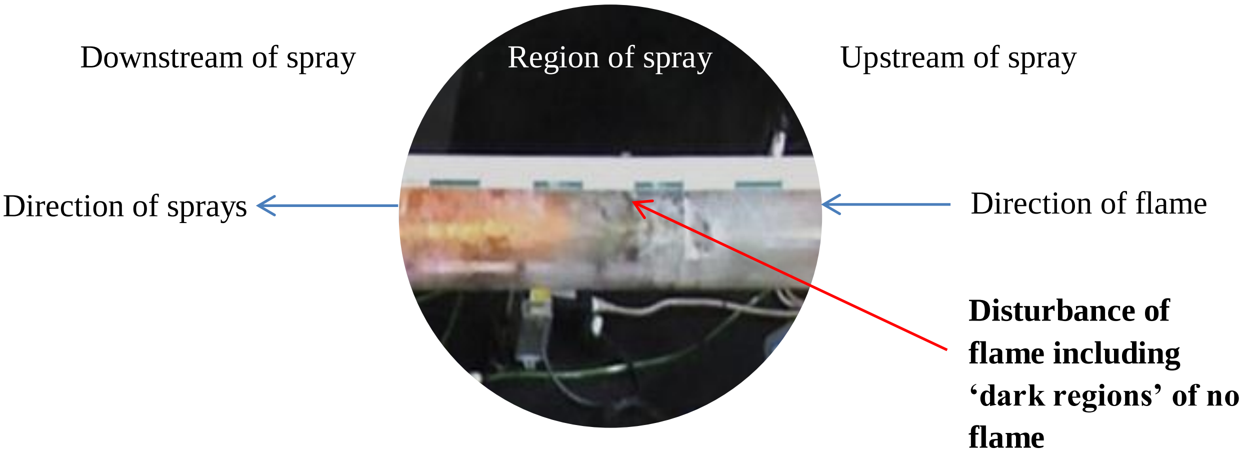

Figure A9.91 : Magnified view of region of spray highlighted in Figure A9.90(iv)

(iii) Equivalence ratio (ϕ) 0.95

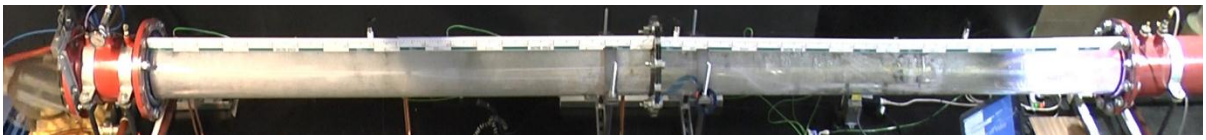

i. Flame propagating in methane-air mixture of E.R. (ϕ) 0.95upstream of SRA

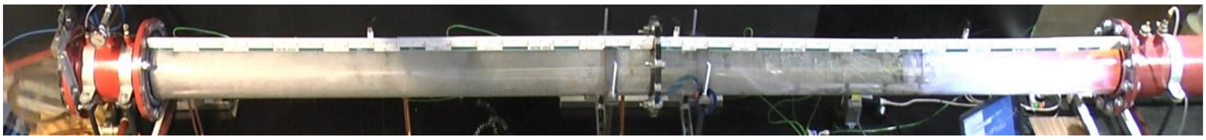

ii. Flame propagating in methane-air mixture of E.R. (ϕ) 0.95 upstream of SRA

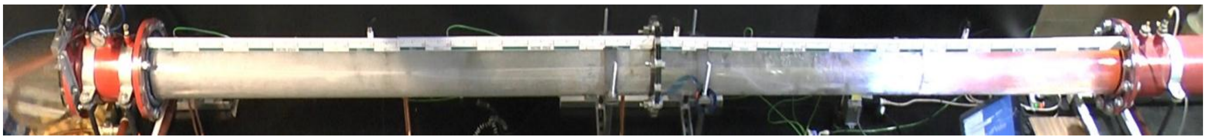

iii. Flame propagating in methane-air mixture of E.R. (ϕ) 0.95in the region of spray

iv. Flame propagating in methane-air mixture of E.R. (ϕ) 0.95 downstream of SRA

Figure A9.92 : Flame propagating upstream and downstream of two overlapping parallel flow Type B SRA's for a methane-air mixture (ϕ) 0.95

Figure 9.93: Expanded view of region of spray highlighted in Figure A9.92(iv)

(iv) Equivalence ratio (ϕ) 1.06

i. Flame propagating in methane-air mixture of E.R. (ϕ) 1.06 upstream of SRA

ii. Flame propagating in methane-air mixture of E.R. (ϕ) 1.06 upstream of SRA

iii. Flame propagating in methane-air mixture of E.R. (ϕ) 1.06 in the region of spray

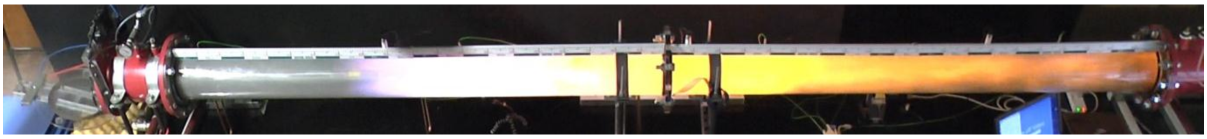

iv. Flame propagating in methane-air mixture of E.R. (ϕ) 1.06 downstream of SRA

Figure A9.94 : Flame propagating upstream and downstream of two overlapping parallel flow Type B SRA's for a methane-air mixture (ϕ) (ϕ) 1.06

Figure A9.95: Close up view of region of spray highlighted in Figure A9.94(iii)

A9.3.1.5 General event outcome

Table A9.17 provides a summary of the **'general event outcome'** for each trial in this current series, using the five potential 'outcome' categories offered in Chapter 5. The results of all 'hot trials' were previously given in Table 5.14 and are also shown in Table A9.45.

Trial configuration	General event outcome	Code
Two P/F SRA : (ϕ) 0.61	Full Mitigation resulting in Flame Extinguishment	FMFE
Two P/F SRA: (ϕ) 0.72	No Mitigation with resulting Flame Acceleration	NMFA
Two P/F SRA: (ϕ) 0.95	No Mitigation with resulting Flame Acceleration	NMFA
Two P/F SRA: (ϕ) 1.06	No Mitigation with resulting Flame Acceleration	NMFA

Table A9.17 : General event outcome (trial series A9.3.1)

A9.3.2 Two Type C overlapping SRA's

A9.1.3.1 Trial set up

In the following results two Type C overlapping SRA's in parallel flow with a propagating flame in a methane-air mixture of E.R. (ϕ) 0.95 are discussed. The SRA's were assembled and mounted on the manifold array and installed in the 'hot trial' rig illustrated in Figure A9.79 and in accordance with the dimension in Table A9.15.

A9.1.3.2 Flame speed

In this series of tests the flame speeds were all measured upstream and downstream of the twin parallel flow sprays. The upstream flame speeds in this series were all in the range of 20m/s – 22m/s. Figure A9.96 illustrates the percentage flame speed reductions observed in the three trials.

In this series a methane-air mixture of E.R. (ϕ) 0.95 was applied to each experimental test, where the flame was completely mitigated on each occasion and did not continue or re-establish further downstream.

The increase in volume flux afforded by the twin SRA arrangement compared to a single atomiser, was consistently adequate to mitigate a near stoichiometric methane-air mixture.

Lane's [1] relationship between droplet instability, droplet diameter and critical break up velocities was presented previously reviewed in Chapter 3. By applying Lane's relationship it may be stated that during these three successful mitigation events that the droplets in the spray would have remained their original size, prior to their passage through the flame front.

The unique nature of the circumstances created in this current series of tests has not been reported in any of the literature reviewed in Chapters 2 and 3.

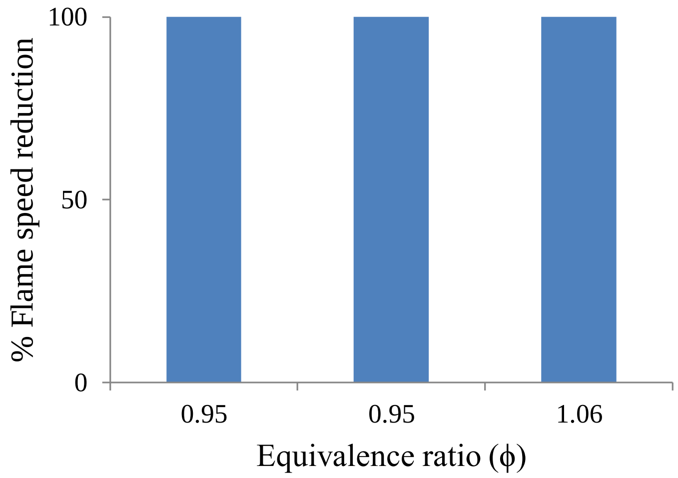

Figure A9.96 : Average flame speed reduction percentage (%) from upstream to downstream of two overlapping parallel flow Type C SRA's in a various methane-air mixtures

A9.3.2.3 Time-temperature response

The time-temperature profiles produced for each of the trials in this series are shown in Figure A9.98 – Figure A9.100. In all of the profiles the thermocouples downstream of the sprays exhibit consistent trends. The temperature downstream of the sprays is indicated by TC3 and in all cases this appears much higher than the initial ambient temperature, albeit mitigation occurred upstream of TC3 in each test. The temperature detected at TC3 may be attributed to the flash vaporisation of the smaller droplets in the spray. Droplets sizes, residence times, boiling and evaporation rates were discussed extensively in Chapter 3.

During each of the trials in this series, a noticeable audible 'hiss' accompanied the moment of mitigation, believed to be the sound of the flash vaporisation of water droplets to steam.

Additionally, following the mitigation of the flame and accompanying 'hissing', a large plume of water vapour was observed exiting the flame propagation and mitigation apparatus, as illustrated in Figure A9.97.

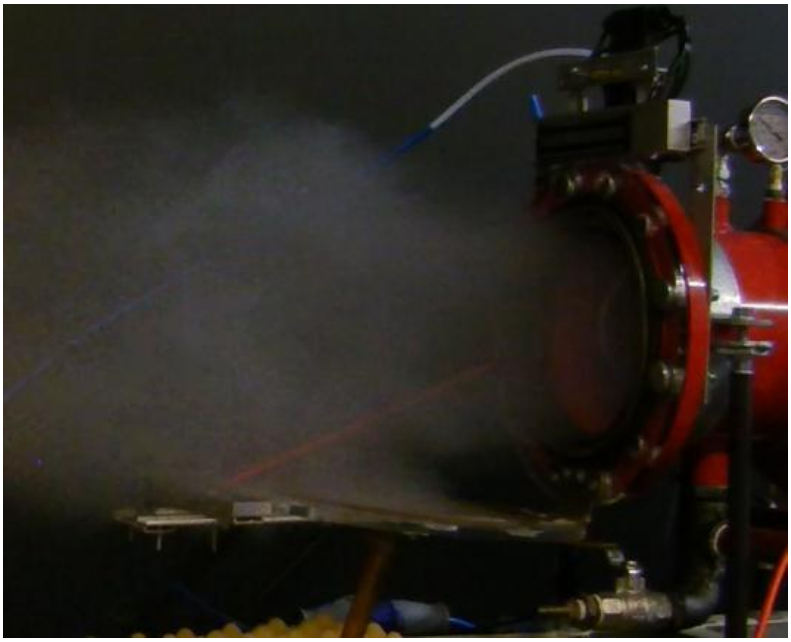

Figure A9.97 : Visible large plume of water vapour at exit end of apparatus

In all cases TC4 demonstrates the cooling and condensing of the water vapour, which finally exited the flame propagation and mitigation apparatus at approximately ambient temperature, which would account for the clear visibility of the condensing water vapour shown in Figure A9.97.

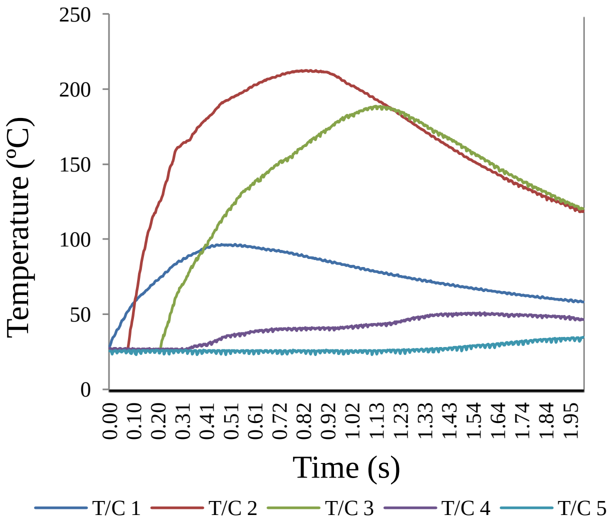

Figure A9.98 : Typical time-temperature profile for two overlapping Type C SRA's in P/F arrangement with methane-air mixture of E.R. (ϕ) 0.95

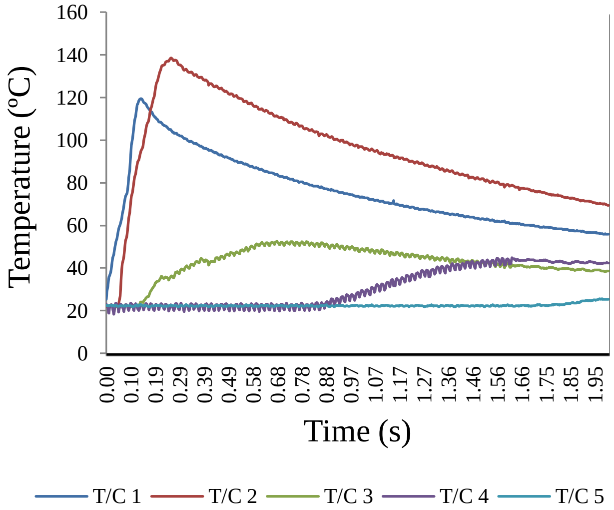

Figure A9.99 : Characteristic time-temperature two overlapping Type C SRA's in P/F arrangement with methane-air mixture of E.R. (ϕ) 0.95

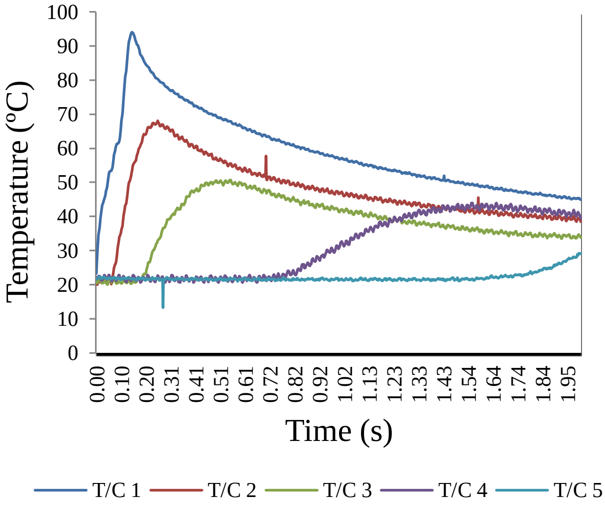

Figure A9.100 : Distinctive time-temperature two overlapping Type C SRA's in P/F arrangement with methane-air mixture of E.R. (ϕ) 1.06

A9.3.2.4 Qualitative analysis

Figures A9.101 – A9.106 reveal the still images extracted from the high definition video taken during each event. The initial flame propagation and subsequent mitigation is clearly illustrated in all three experimental trials.

(i) Equivalence ratio (ϕ) 0.95

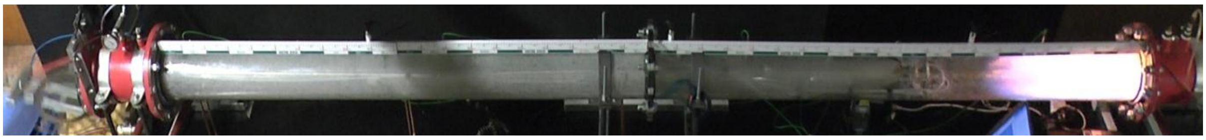

i. Flame propagating in methane-air mixture of E.R. (ϕ) 0.95 upstream of SRA

ii. Flame propagating in methane-air mixture of E.R. (ϕ) 0.95 upstream of SRA

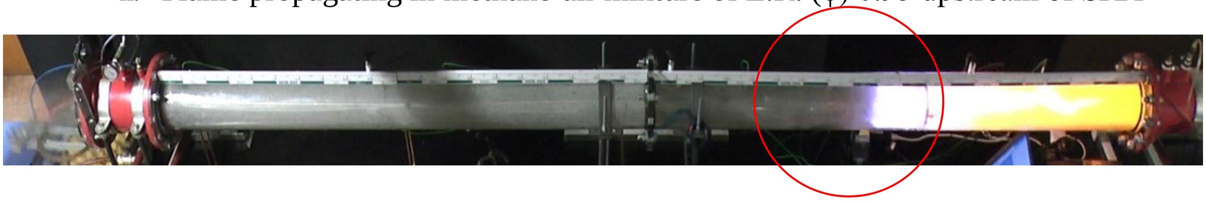

iii. **Mitigation** of methane-air mixture of E.R. (ϕ) 0.95 in the region of spray

iv. Final stages of combustion of methane-air mixture E.R. (ϕ) 0.95 downstream of SRA

Figure A9.101 : Flame propagating upstream and downstream of two overlapping parallel flow Type C SRA's for a methane-air mixture (ϕ) 0.95

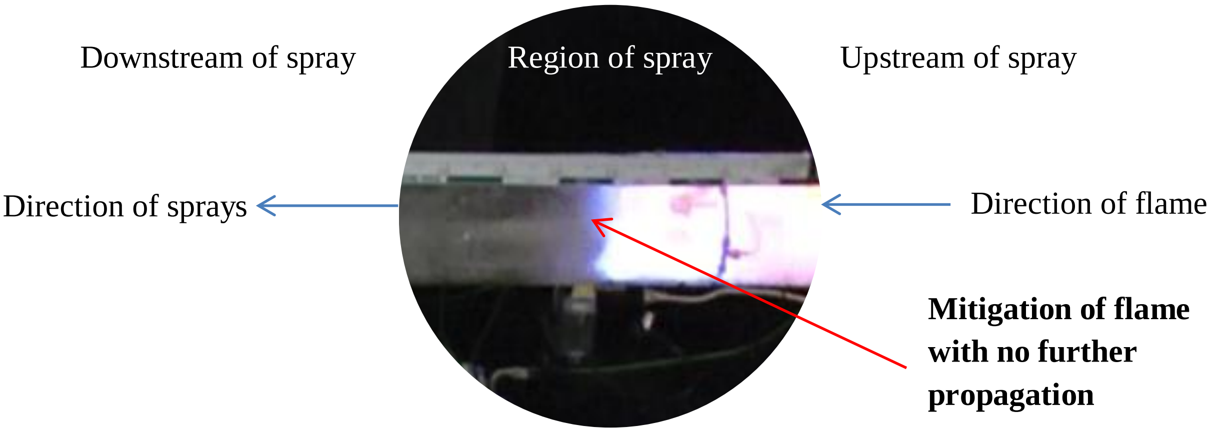

Figure A9.102 : Expanded view of region of spray highlighted in Figure A9.101(iii)

(ii) Equivalence ratio (ϕ) 0.95

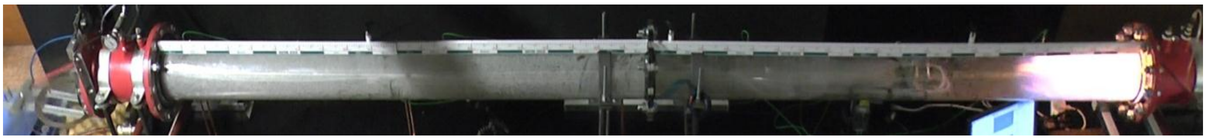

i. Flame propagating in methane-air mixture of E.R. (ϕ) 0.95 upstream of SRA

ii. Flame propagating in methane-air mixture of E.R. (ϕ) 0.95 upstream of SRA

iii. **Mitigation** of methane-air mixture of E.R. (ϕ) 0.95 in the region of spray

iv. Final stages of combustion of methane-air mixture E.R. (ϕ) 0.95 downstream of SRA

Figure A9.103 : Flame propagating upstream and downstream of two overlapping parallel flow Type C SRA's for a methane-air mixture (ϕ) 0.95

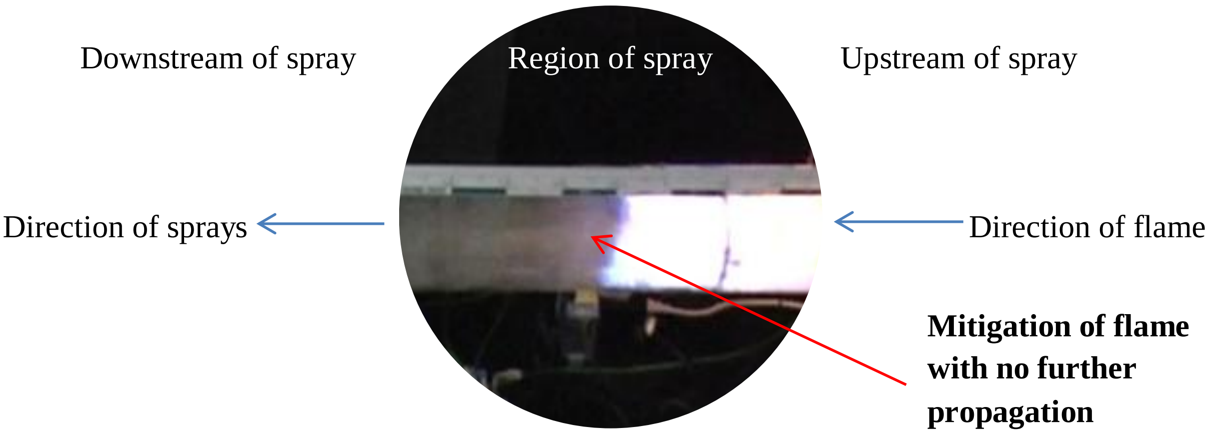

Figure 9.104: Enlarged view of region of spray highlighted in Figure A9.103(iii)

(iii) Equivalence ratio (ϕ) 1.06

i. Flame propagating in methane-air mixture of E.R. (ϕ) 1.06 upstream of SRA

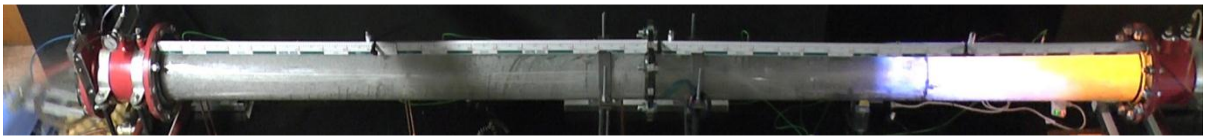

ii. Flame propagating in methane-air mixture of E.R. (ϕ) 1.06 upstream of SRA

iii. **Mitigation** of methane-air mixture of E.R. (ϕ) 1.06 in the region of spray

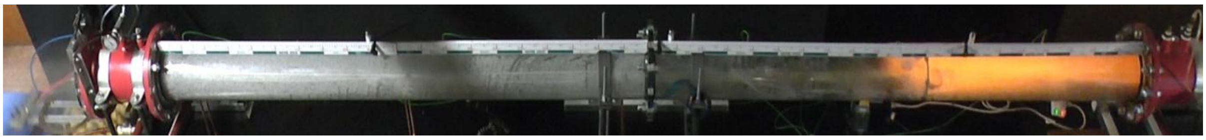

iv. Flame propagating in methane-air mixture of E.R. (ϕ) 1.06 downstream of SRA

Figure A9.105 : Flame propagating upstream and downstream of two overlapping parallel flow Type C SRA's for a methane-air mixture (ϕ) 1.06

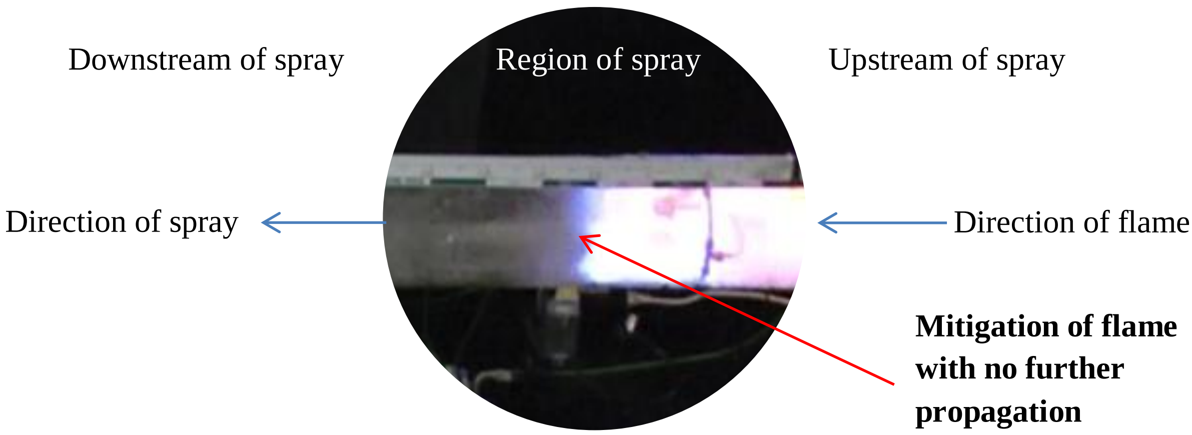

Figure A9.106 : Magnified view of region of spray highlighted in Figure A9.105(iii)

A9.3.2.5 General event outcome

Table A9.18 provides a summary of the **'general event outcome'** for each trial in this current series, using the five potential 'outcome' categories offered in Chapter 5. The results of all 'hot trials' were previously given in Table 5.14 and are also shown in Table A9.45.

Trial configuration	General event outcome	Code
Two P/F SRA : (ϕ) 0.95	Full Mitigation resulting in Flame Extinguishment	FMFE
Two P/F SRA : (ϕ) 0.95	Full Mitigation resulting in Flame Extinguishment	FMFE
Two P/F SRA : (ϕ) 1.06	Full Mitigation resulting in Flame Extinguishment	FMFE

Table A9.18 : General event outcome (trial series A9.3.2)

A9.4 Cross Flow (X/F) Trials

In this series of experimental trials the pre-assembled SRA, complete with external water feed pipework and hoses were installed in the explosion and mitigation tube, in accordance with figure A9.107 and Table A9.19. The water pump was adjusted to deliver a pressure of 13MPa and the water in the storage vessel was maintained at approximately 20˚C. Thermocouples were positioned in accordance with figure A9.107 and Table 9.10.

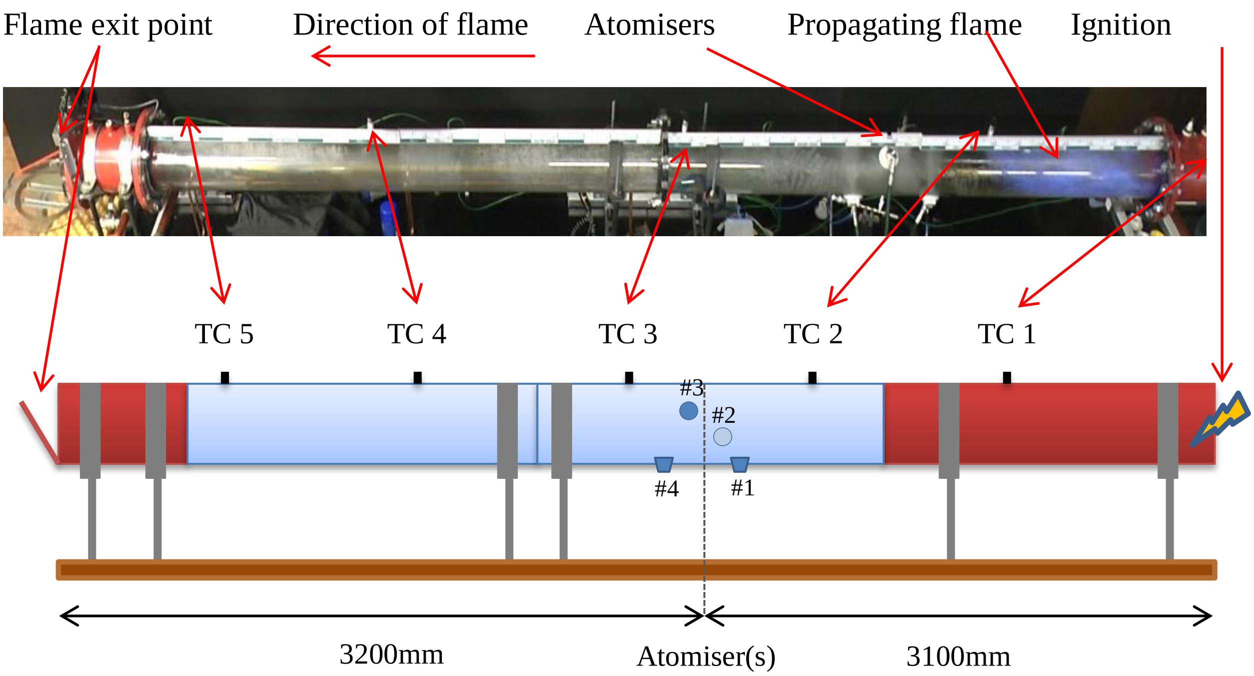

Figure A9.107 : Position of atomisers and thermocouples (right hand ignition point)

Component	Position (measured from right hand end)
Thermocouple (TC1)	1200mm
Thermocouple (TC2)	2400mm
Thermocouple (TC3)	3600mm
Thermocouple (TC4)	4800mm
Thermocouple (TC5)	6000mm
Atomiser outlet orifice (cross flow)	3100mm (centre of sprays)

Table A9.19 : Measured position of thermocouples and SRA's

A9.4.1 Single (X/F) Type B SRA

A9.4.1.1 Trial set up

In this series of trials a single SRA Type B was assembled and installed in position #1 as previously shown in Figure A9.107 and Table A9.19. The single (X/F) SRA was subjected to four trials with different methane-air mixtures of E.R. (ϕ) 0.61, 0.72, 0.95 and 1.06.

A9.4.1.2 Flame speed

Average flame speeds were measured both upstream and downstream of the spray region, which are illustrated in Figure A9.108 as flame speed reduction values. The methane-air mixture (ϕ) 0.61 resulted in an increase in flame speed, with is consistent throughout the trials for mixture towards the lower explosive limit (LEL) and is the result of the localised disturbance of the flammable mixture in the spray region. The methane-air mixture (ϕ) 0.72 appears to be less effected by the disturbance, however, an increase in flame speed of approximately 31% was observed. During the (ϕ) 0.95 trial the flame speed only increased marginally by 5% and in the (ϕ) 1.06 test the flame exhibited a reduction in flame speed of about 9%.

The data and results in this case demonstrate that sub-stoichiometric mixtures exhibit an increase in flame speed, whereas the mixture that is greater than stoichiometric resulted in a flame speed reduction.

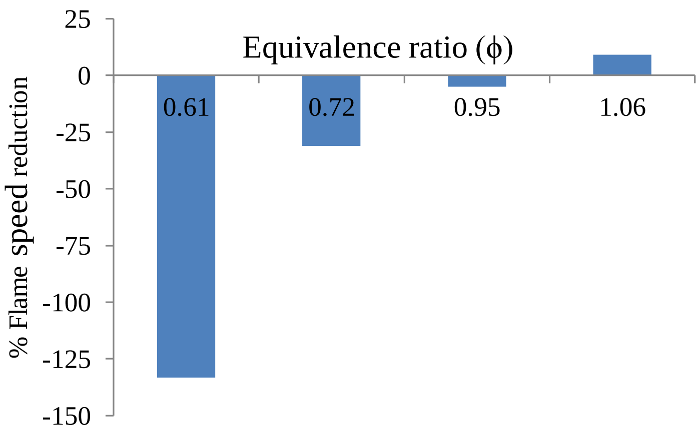

Figure A9.108 : Average flame speed reduction percentage (%) from upstream to downstream of single X/F SRA in various methane-air mixtures

The disturbance caused by the spray in the flammable mixture would also be transferred into the reaction and pre-heat zones of the flame. In this configuration the flame speed exhibited an inverse relationship with flame thickness.

A9.4.1.2 Time-temperature response

Time-temperature profiles have been plotted for each of the scenarios and are presented in Figures A9.109 - A9.112. In these illustrations the trend between TC3 (immediately downstream of the spray) and TC5 (immediately upstream of the flame exit point of the rig) is significant and is in agreement with the flame speed reduction previously shown in Figure A.9.108.

Methane-air mixture concentration affects upstream flame speeds and flame thickness which also dictates droplet residence times. This critical area has been previously emphasised in Chapter 3, with heat transfer from the flame front to the water droplet being paramount to initiate flame suppression of mitigation. In this series, the methane-air mixture of E.R.(ϕ)1.06 clearly displayed a flame speed reduction which demonstrates a degree of flame suppression.

9.4.1.1 (i) Equivalence ratio (ϕ) 0.61

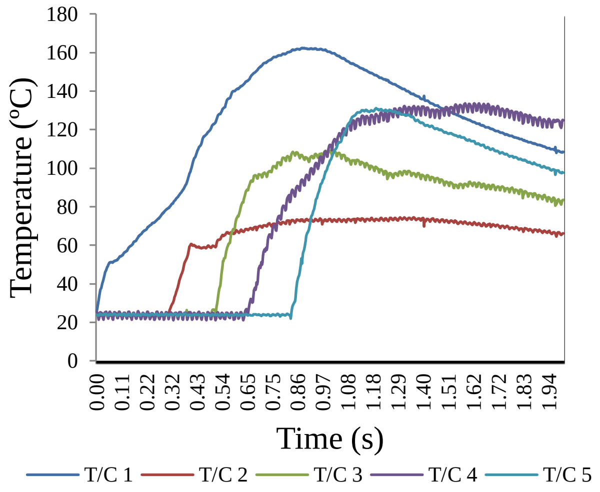

Figure A9.109 : Typical time-temperature profile for single SRA Type B in X/F arrangement with methane-air mixture of E.R. (ϕ) 0.61

(ii) Equivalence ratio (ϕ) 0.72

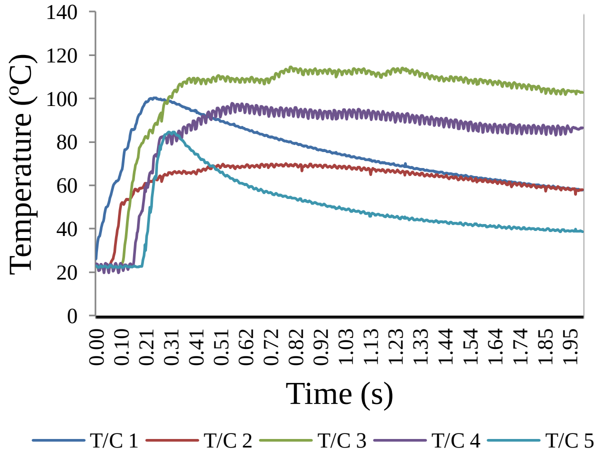

Figure A9.110 : Distinctive time-temperature profile for single SRA Type B in X/F arrangement with methane-air mixture of E.R. (ϕ) 0.72

(iii) Equivalence ratio (ϕ) 0.95

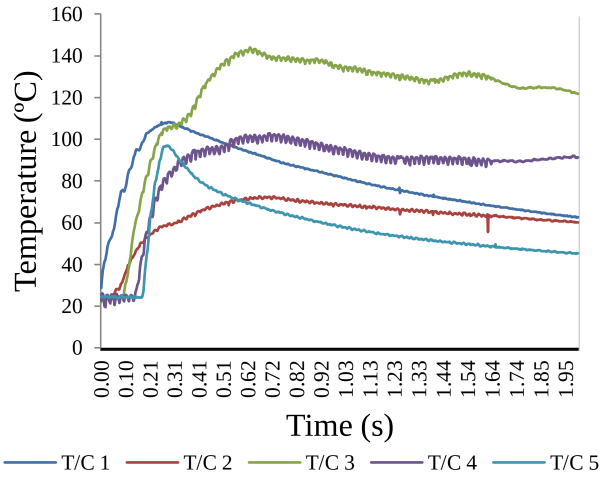

Figure A9.111 : Typical time-temperature profile for single SRA Type B in X/F arrangement with methane-air mixture of E.R. (ϕ) 0.95

(iv) Equivalence ratio (ϕ) 1.06

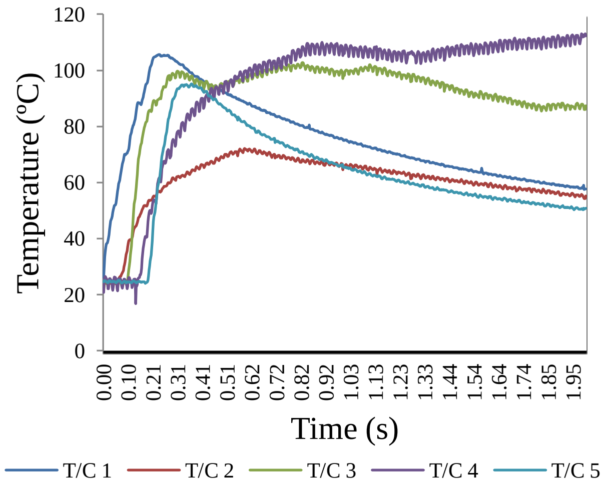

Figure A9.112 : Distinctive time-temperature profile for single SRA Type B in X/F arrangement with methane-air mixture of E.R. (ϕ) 1.06

A9.4.1.4 Qualitative analysis

In Figure A9.113 the methane-air mixture was (ϕ) 0.61. The flame speed upstream of the spray was approximately 3.75m/s. The flame can be seen to pass directly through the single spray as highlighted in Figure A9.112, at which point flame disturbance is apparent, resulting in flame acceleration along the remaining 3.2m of tube with an average downstream speed of 8.75m/s.

In Figure A9.115 the methane-air mixture was (ϕ) 0.72. Figure A9.163 (iii) reveals a disturbance in the flame which has been highlighted and magnified and is visible in Figure A9.116.

In Figure A9.117 the methane-air mixture was (ϕ) 0.95. Figure A9.116 (ii) shows no obvious disturbance of the flame, which is in agreement with the very small increase in flame speed shown previously in Figure A9.108.

In Figure A9.119 the methane-air mixture was (ϕ) 1.06. Figure A9.119 (ii) shows no obvious disorder to the flame, however, a ‘dark region’ is visible at the flame/spray interface, as magnified in Figure A9.120 indicating localised suppression of the combustion process which resulted in an overall flame speed reduction.

(i) Equivalence ratio (ϕ) 0.61

i. Flame propagating in methane-air mixture of E.R. (ϕ) 0.61 upstream of SRA

ii. Flame propagating in methane-air mixture of E.R. (ϕ) 0.61 upstream of SRA

iii. Flame propagating in methane-air mixture of E.R. (ϕ) 0.61 in the region of spray

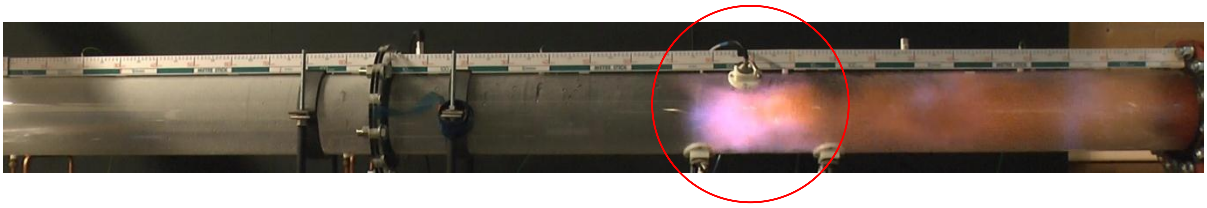

iv. Flame propagating in methane-air mixture of E.R. (ϕ) 0.61 downstream of SRA

Figure A9.113 : Flame propagating upstream and downstream of single X/F SRA Type B for a methane-air mixture (ϕ) 0.61

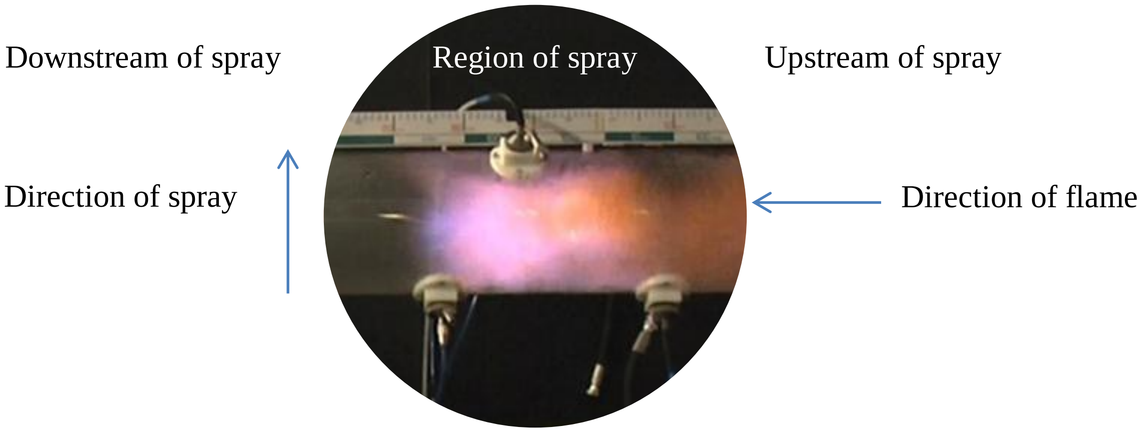

Figure A9.114: Expanded view of region of spray highlighted in Figure A9.113(iv)

(ii) Equivalence ratio (ϕ) 0.72

i. Flame propagating in methane-air mixture of E.R. (ϕ) 0.72 upstream of SRA

ii. Flame propagating in methane-air mixture of E.R. (ϕ) 0.72 upstream of SRA

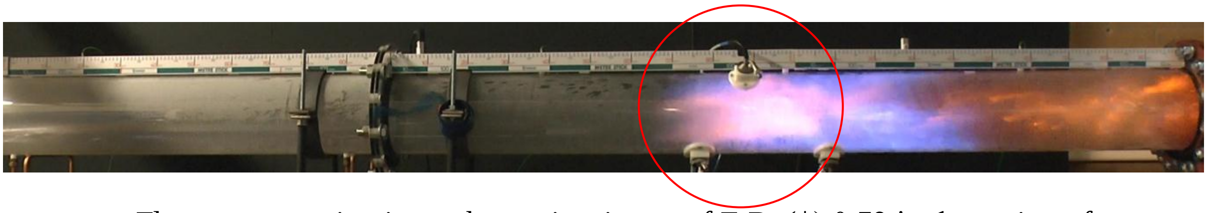

iii. Flame propagating in methane-air mixture of E.R. (ϕ) 0.72 in the region of spray

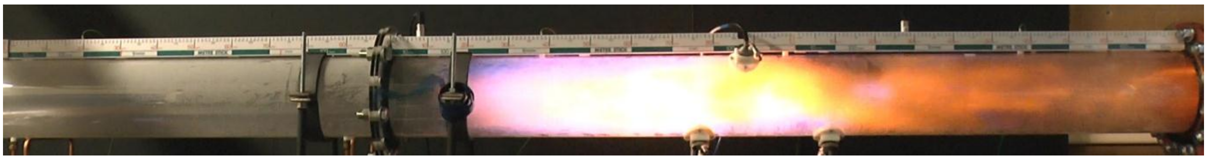

iv. Flame propagating in methane-air mixture of E.R. (ϕ) 0.72 downstream of SRA

Figure A9.115 : Flame propagating upstream and downstream of single X/F SRA Type B for a methane-air mixture (ϕ) 0.72

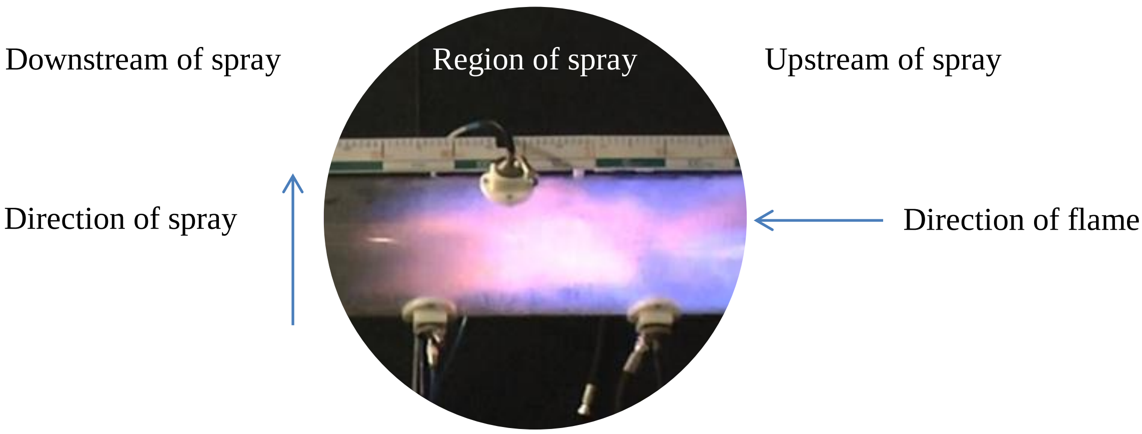

Figure A9.116 : Enlarged view of region of spray highlighted in Figure A9.115(iii)

(iii) Equivalence ratio (ϕ) 0.95

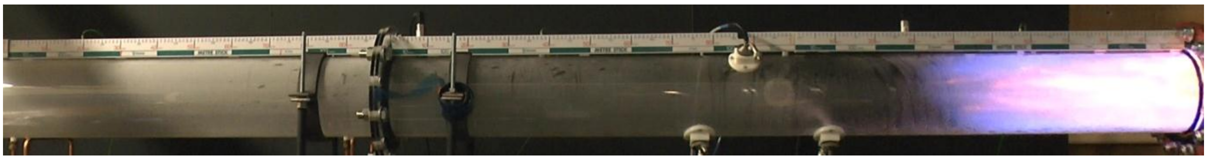

i. Flame propagating in methane-air mixture of E.R. (ϕ) 0.95upstream of SRA

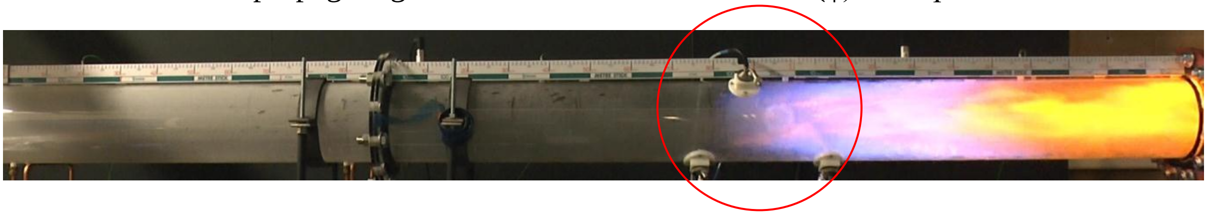

ii. Flame propagating in methane-air mixture of E.R. (ϕ) 0.95 upstream of SRA

iii. Flame propagating in methane-air mixture of E.R. (ϕ) 0.95in the region of spray

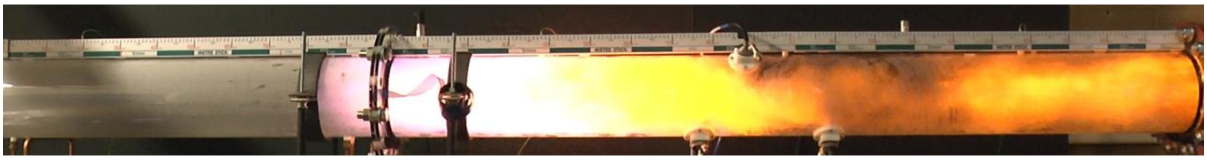

iv. Flame propagating in methane-air mixture of E.R. (ϕ) 0.95 downstream of SRA

Figure A9.117 : Flame propagating upstream and downstream of single X/F SRA Type B for a methane-air mixture (ϕ) 0.95

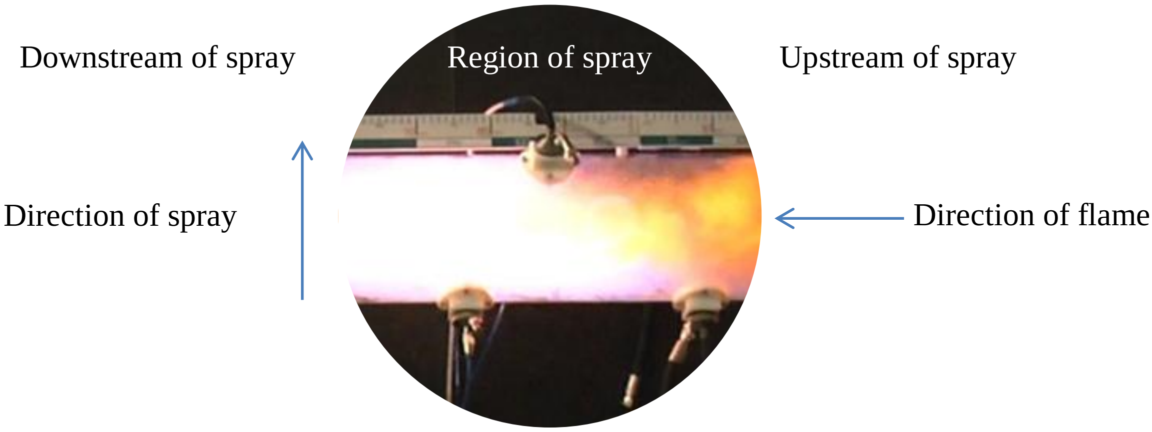

Figure A9.118 : Expanded view of region of spray highlighted in Figure A9.117(ii)

(iv) Equivalence ratio (ϕ) 1.06

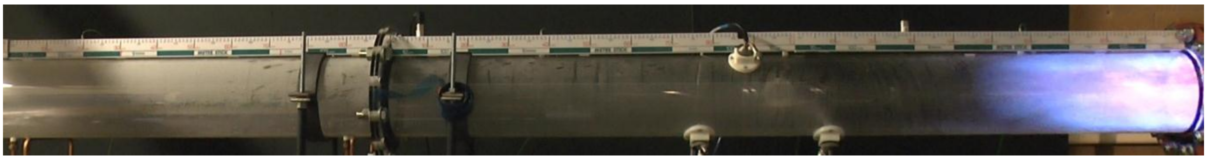

i. Flame propagating in methane-air mixture of E.R. (ϕ) 1.06 upstream of SRA

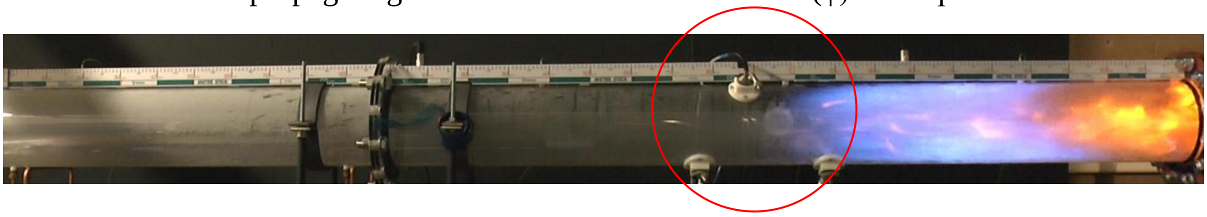

ii. Flame propagating in methane-air mixture of E.R. (ϕ) 1.06 upstream of SRA

iii. Flame propagating in methane-air mixture of E.R. (ϕ) 1.06 in the region of spray

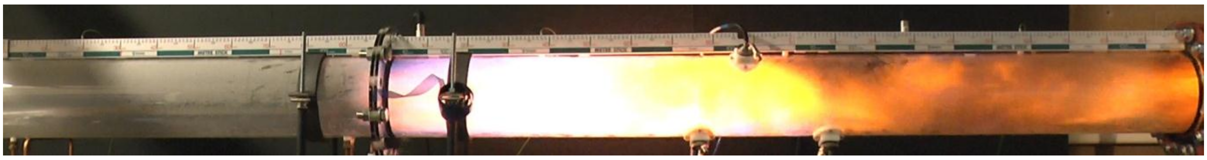

iv. Flame propagating in methane-air mixture of E.R. (ϕ) 1.06 downstream of SRA

Figure A9.119 : Flame propagating upstream and downstream of single X/F SRA Type B for a methane-air mixture (ϕ) 1.06

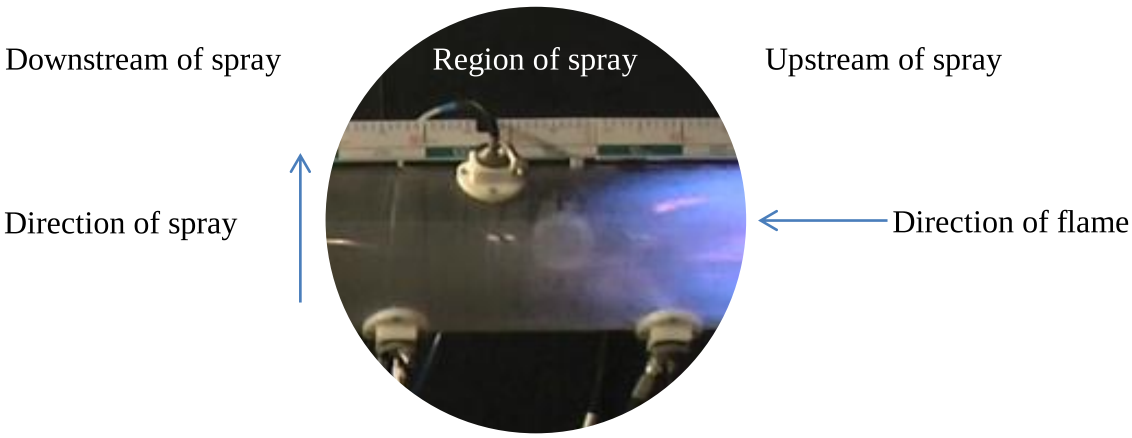

Figure A9.120 : Magnified view of region of spray highlighted in Figure A9.117(ii)

A9.4.1.5 General event outcome

Table A9.20 provides a summary of the 'general event outcome' for each trial in this current series, using the five potential outcome categories discussed in Chapter 5. The results of all 'hot trials' were previously given in Table 5.14 and are also shown in Table A9.45.

Trial configuration	General event outcome	Code
Single X/F SRA : (ϕ) 0.61	No Mitigation with resulting Flame Acceleration	NMFA
Single X/F SRA : (ϕ) 0.72	No Mitigation with resulting Flame Acceleration	NMFA
Single X/F SRA : (ϕ) 0.95	No Mitigation with resulting Flame Acceleration	NMFA
Single X/F SRA : (ϕ) 1.06	No Mitigation with resulting Flame Deceleration	NMFD

Table A9.20 : General event outcome (trial series A9.4.1)

A9.4.2 Two (X/F) Type B SRA's

A9.4.2.1 Trial set up

In this series of trials, two Type B SRA's were assembled and installed in position #1 and#2 as previously shown in Figure A9.107 and Table A9.19. The atomisers were subjected to four trials with different methane-air mixtures, of (ϕ) 0.61, 0.72, 0.95 and 1.06.

A9.4.2.2 Flame speed

Average flame speeds were measured both upstream and downstream of the spray region, which are illustrated in Figure A9.121 as flame speed reduction values. In this atomiser configuration all of the methane-air mixtures tested exhibited a positive outcome, with flame speed reduction occurring in each case. Figure A9.121 displays the percentage values for each of the methane-air mixtures. With there being no atomisers present within the tube of the cross flow trials, due to the external mounting facility as discussed earlier in Chapter 4, the results may be compared to the 'dry' trials previously discussed in Chapter 5, which are shown in Figure A9.122.

The four methane-air mixtures displayed in Figure A9.122 show an increase in flame speed along the clear section of the flame propagation and mitigation tube. In contrast, Figure A9.121 illustrates flame speed reductions ranging from approximately 11% – 19% for all concentrations. Based on this evidence, this is a clear indication that the flame decelerated in the presence of the two Type B X/F SRA's.

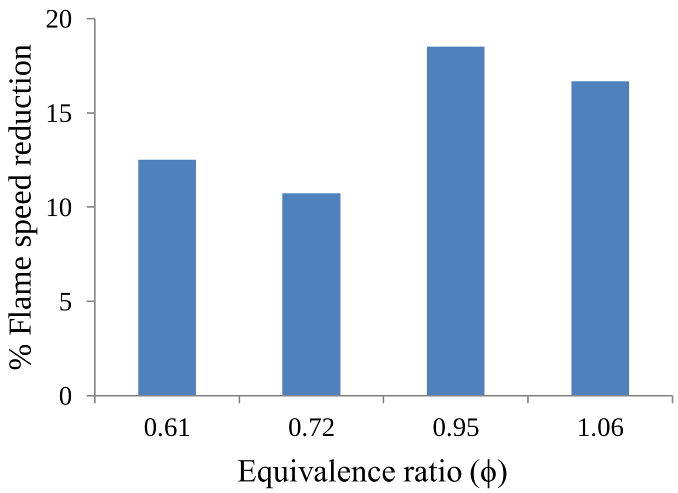

Figure A9.121 : Average flame speed reduction percentage (%) from upstream to downstream of two X/F SRA's in a various methane-air mixtures

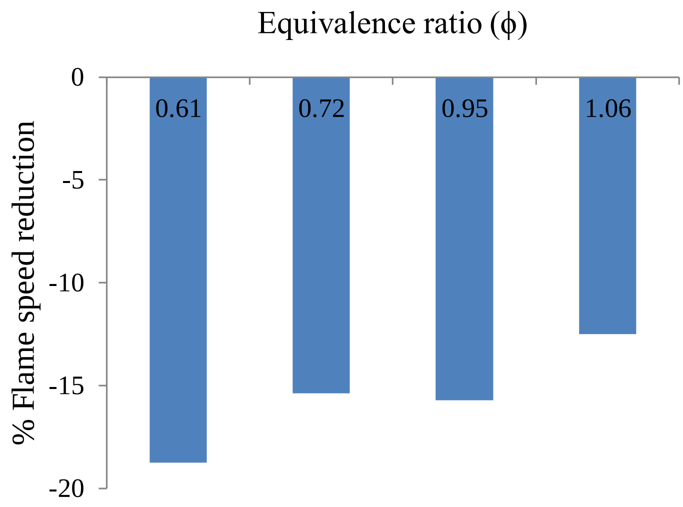

Figure A9.122 : Average flame speed reduction percentage (%) from upstream to downstream single X/F SRA position (dry) in a various methane-air mixtures

A9.4.2.3 Time-temperature response

The typical time-temperature profiles presented in Figures A9.123 – A9.126 reinforce these flame speed reductions. In each of the methane-air mixtures there was an initial increase in temperature immediately downstream of the atomisers shown in the TC3 data, followed by a temperature reduction at TC4 and further reduction at TC5.

9.4.2.1 (i) Equivalence ratio (ϕ) 0.61

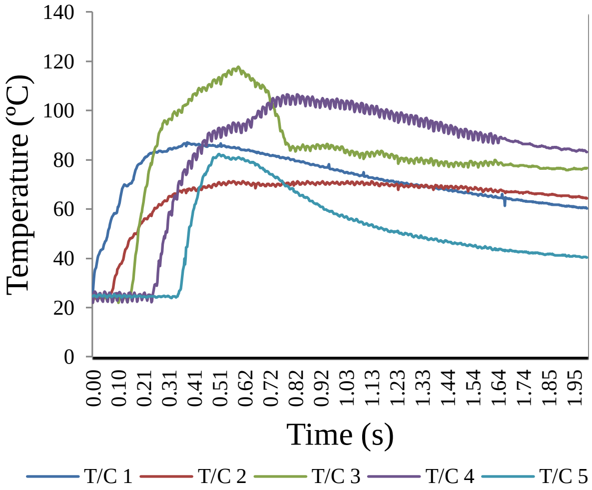

Figure A9.123 : Typical time-temperature profile for two SRA Type B in X/F arrangement with methane-air mixture of E.R. (ϕ) 0.61

(ii) Equivalence ratio (ϕ) 0.72

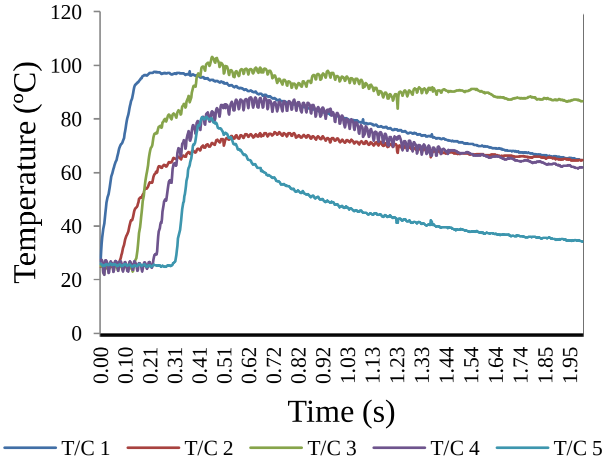

Figure A9.124 : Characteristic time-temperature profile for two SRA Type B in X/F arrangement with methane-air mixture of E.R. (ϕ) 0.72

(iii) Equivalence ratio (ϕ) 0.95

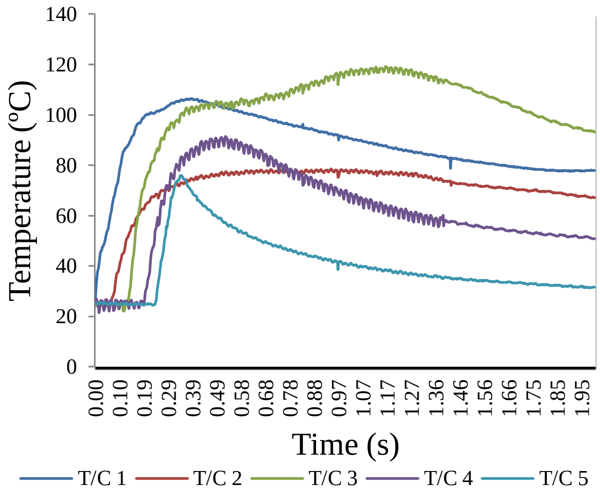

Figure A9.125 : Distinctive time-temperature profile for two SRA Type B in X/F arrangement with methane-air mixture of E.R. (ϕ) 0.95

(iv) Equivalence ratio (ϕ) 1.06

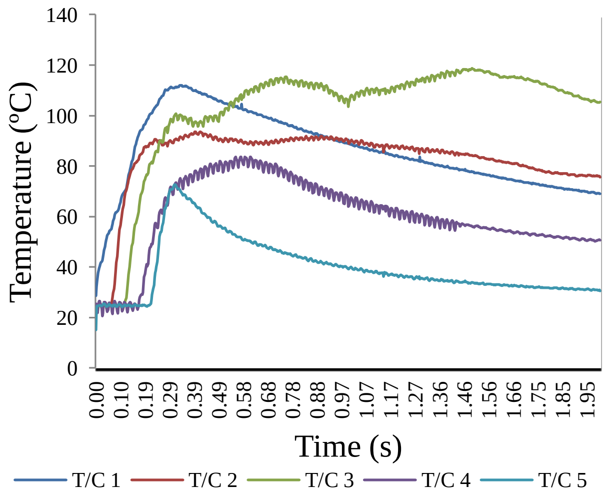

Figure A9.126 : Regular time-temperature profile for two SRA Type B in X/F arrangement with methane-air mixture of E.R. (ϕ) 1.06

A9.4.2.4 Qualitative analysis

In Figure A9.127 the methane-air mixture was (ϕ) 0.61. The progress of the flame can be observed in each of the frames (i – iv). Figure A9.127 (iii) has been highlighted and magnified to reveal the interaction and reduction in flame area. There is also a significant 'dark' area when combustion has clearly ceased.

In Figure A9.129 the methane-air mixture was (ϕ) 0.72. Figure A9.129 (iv) shows 'dark' areas in the combustion signifying that combustion has been stopped locally.

In Figure A9.131 the methane-air mixture was (ϕ) 0.95. Figure A9.131 (iii) displays very similar behaviour to Figure A9.129, with dark areas visible in Figure A9.31 (iii)

In Figure A9.133 the methane-air mixture was (ϕ) 1.06. Figure A9.133 (iii) indicates localised suppression of the combustion process which resulted in a global flame speed reduction.

(i) Equivalence ratio (ϕ) 0.61

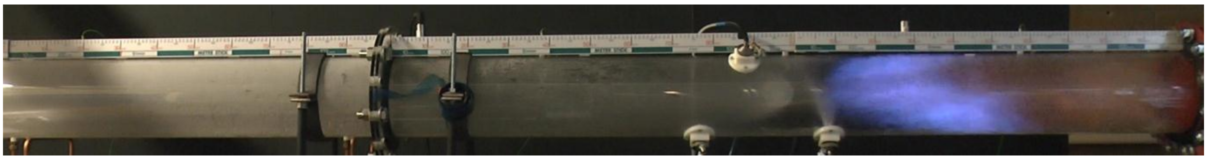

i. Flame propagating in methane-air mixture of E.R. (ϕ) 0.61 upstream of SRA

ii. Flame propagating in methane-air mixture of E.R. (ϕ) 0.61 upstream of SRA

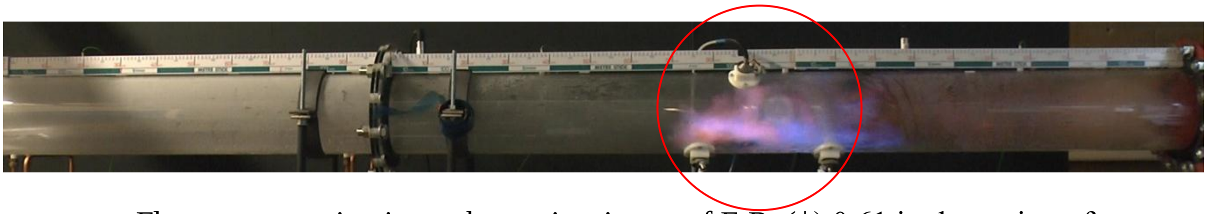

iii. Flame propagating in methane-air mixture of E.R. (ϕ) 0.61 in the region of spray

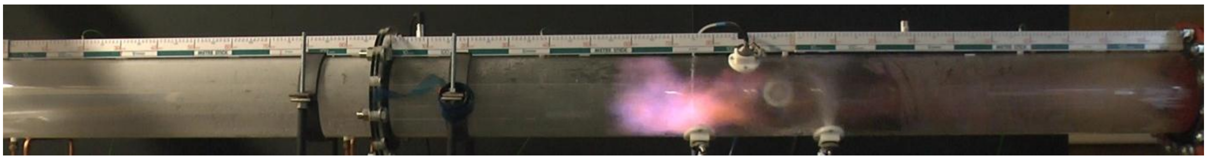

iv. Flame propagating in methane-air mixture of E.R. (ϕ) 0.61 downstream of SRA

Figure A9.127 : Flame propagating upstream and downstream of two X/F SRA Type B for a methane-air mixture (ϕ) 0.61

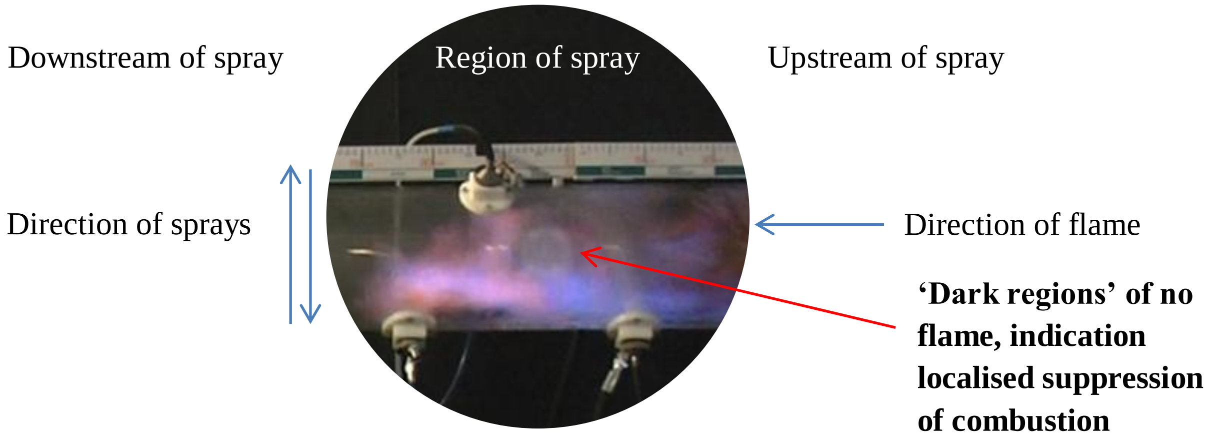

Figure A9.128: Expanded view of region of spray highlighted in Figure A9.127(iii)

(ii) Equivalence ratio (ϕ) 0.72

i. Flame propagating in methane-air mixture of E.R. (ϕ) 0.72 upstream of SRA

ii. Flame propagating in methane-air mixture of E.R. (ϕ) 0.72 upstream of SRA

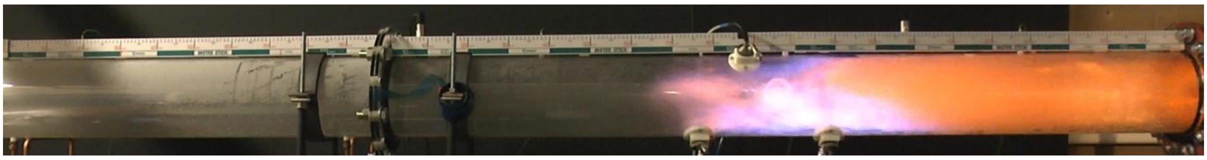

iii. Flame propagating in methane-air mixture of E.R. (ϕ) 0.72 in the region of spray

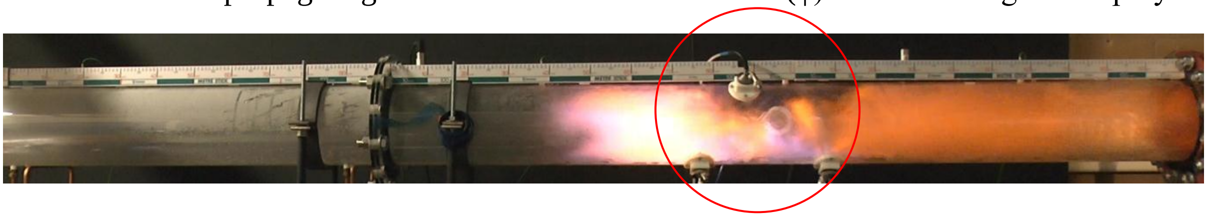

iv. Flame propagating in methane-air mixture of E.R. (ϕ) 0.72 downstream of SRA

Figure A9.129: Flame propagating upstream and downstream of two X/F SRA Type B for a methane-air mixture (ϕ) 0.72

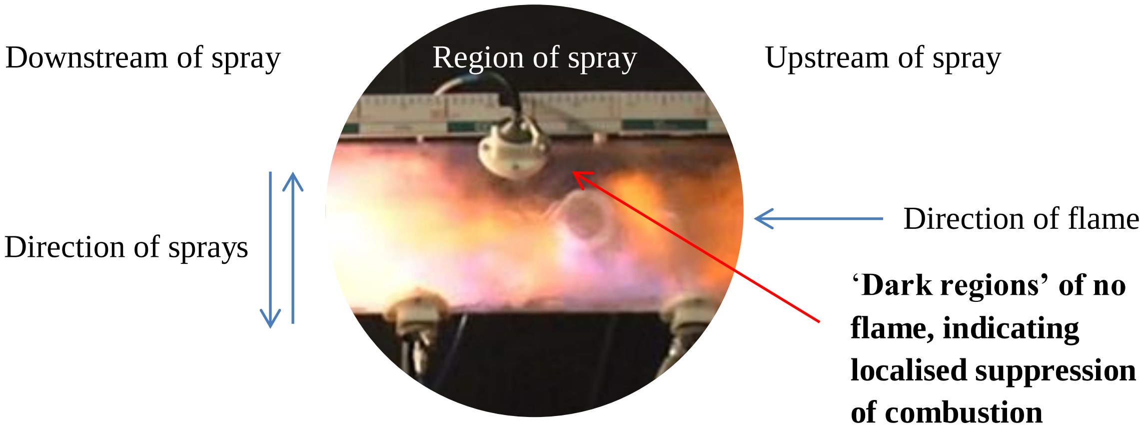

Figure A9.130 : Close up view of region of spray highlighted in Figure A9.129(iv)

(iii) Equivalence ratio (ϕ) 0.95

i. Flame propagating in methane-air mixture of E.R. (ϕ) 0.95 upstream of SRA

ii. Flame propagating in methane-air mixture of E.R. (ϕ) 0.95 upstream of SRA

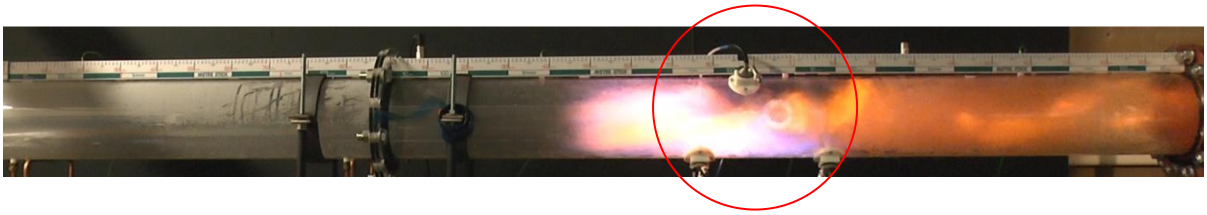

iii. Flame propagating in methane-air mixture of E.R. (ϕ) 0.95 in the region of spray

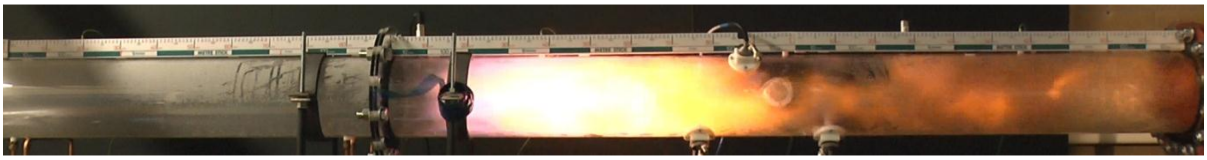

iv. Flame propagating in methane-air mixture of E.R. (ϕ) 0.95 downstream of SRA

Figure A9.31 : Flame propagating upstream and downstream of two X/F SRA Type B for a methane-air mixture (ϕ) 0.95

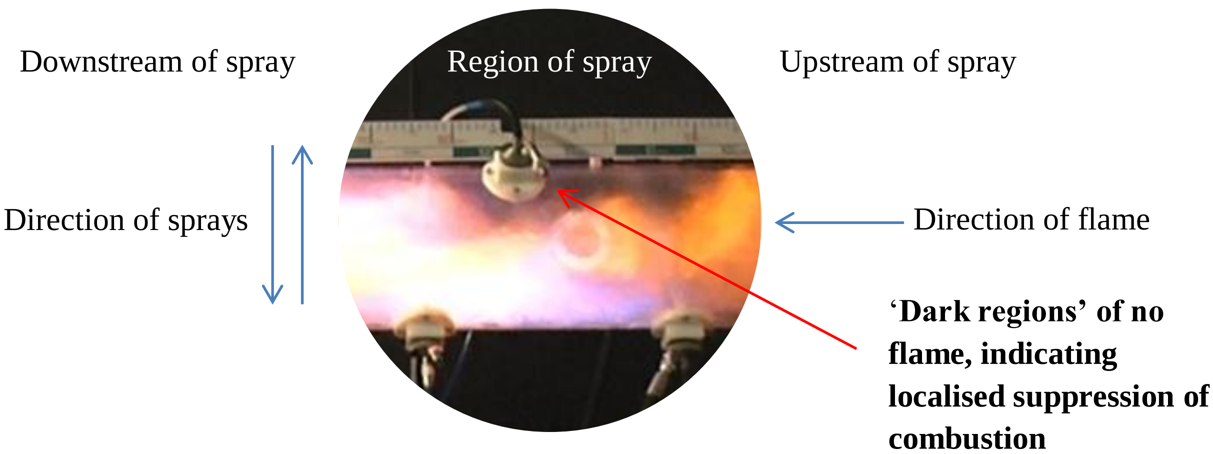

Figure A9.132 : Exploded view of region of spray highlighted in Figure A9.131(iii)

(iv) Equivalence ratio (ϕ) 1.06

i. Flame propagating in methane-air mixture of E.R. (ϕ) 1.06 upstream of SRA

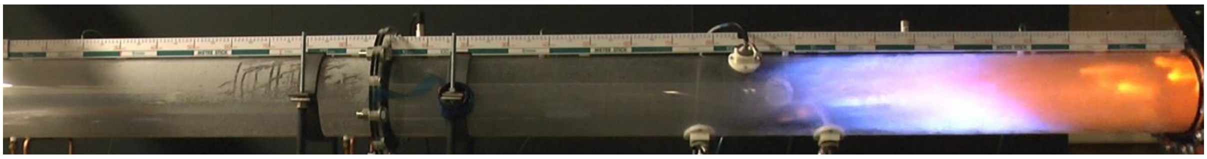

ii. Flame propagating in methane-air mixture of E.R. (ϕ) 1.06 upstream of SRA

iii. Flame propagating in methane-air mixture of E.R. (ϕ) 1.06 in the region of spray

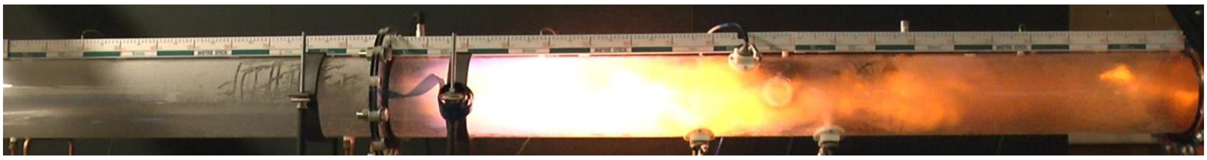

iv. Flame propagating in methane-air mixture of E.R. (ϕ) 1.06 downstream of SRA

Figure A9.133 : Flame propagating upstream and downstream of two X/F SRA Type B for a methane-air mixture (ϕ) 1.06

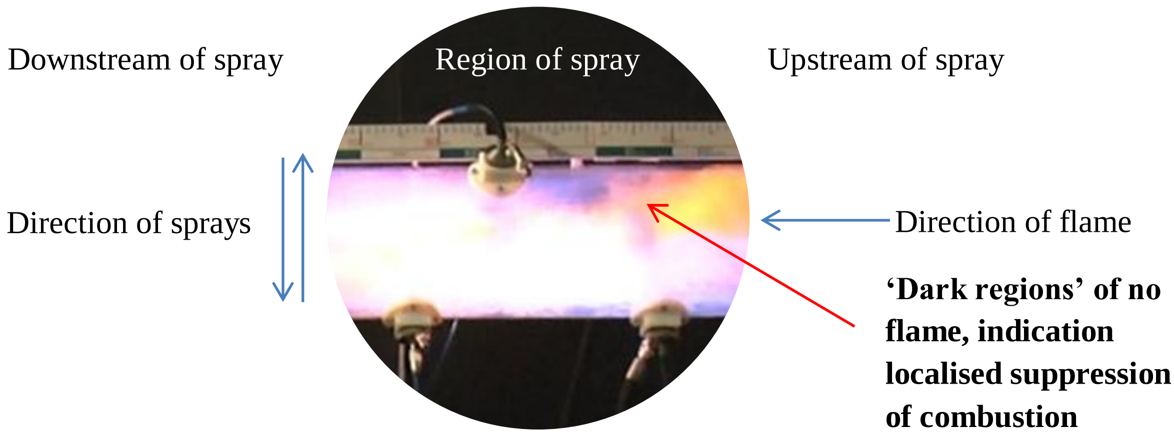

Figure A9.134: Magnified view of region of spray highlighted in Figure A9.131(iii)

A9.4.2.5 General event outcome

Table A9.21 provides a summary of the 'general event outcome' for each trial in this current series, using the five potential 'outcome' categories offered in Chapter 5. The results of all 'hot trials' were previously given in Table 5.14 and are also shown in Table A9.45.

Trial configuration	General event outcome	Code
Two X/F SRA : (ϕ) 0.61	No Mitigation with resulting Flame Deceleration	NMFD
Two X/F SRA : (ϕ) 0.72	No Mitigation with resulting Flame Deceleration	NMFD
Two X/F SRA : (ϕ) 0.95	No Mitigation with resulting Flame Deceleration	NMFD
Two X/F SRA : (ϕ) 1.06	No Mitigation with resulting Flame Deceleration	NMFD

Table A9.21 : General event outcome (trial series A9.4.2)

A9.4.3 Three (X/F) Type B SRA's

A9.4.3.1 Trial set up

In this series of trials, three Type B SRA's were assembled and installed in position #1, #2 and #3 as previously shown in Figure A9.107 and Table A9.19. The atomisers were subjected to four trials with different methane-air mixtures, of (ϕ) 0.61, 0.72, 0.95 and 1.06.

A9.4.3.2 Flame speed

Average flame speeds were measured both upstream and downstream of the spray region, which are illustrated in Figure A9.135 as flame speed reduction values. In this atomiser configuration, the propagating flame was extinguished and mitigated. This is shown in the diagram as a 100% flame speed reduction.

In the remaining three methane-mixtures displayed a slight flame speed reduction from upstream and downstream of the spray region. Although these reductions were not as significant and those offered in A9.4.2, when compared to the 'dry' trial they all resulted in a noteworthy positive outcome. The inclusion of a third spray and resultant induced disturbance of the mixture may have caused the local increase in rate of combustion, leading to an increase of flame speed across the spray region.

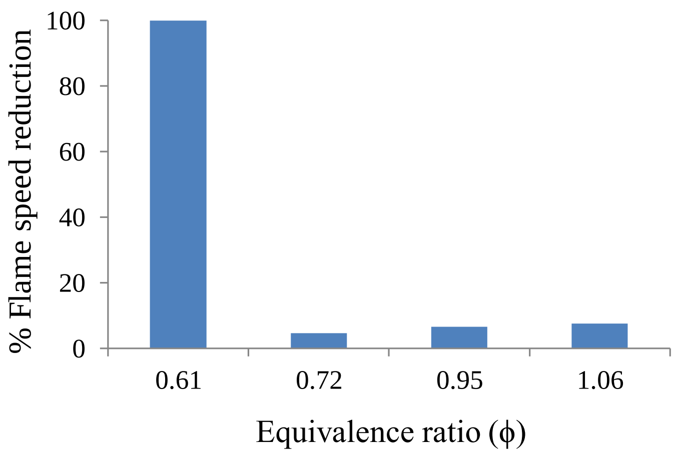

Figure A9.135 : Average flame speed reduction percentage (%) from upstream to downstream of three X/F SRA's in various methane-air mixtures

A9.4.3.3 Time-temperature response

The representative time-temperature profiles presented in Figure A9.136 - A9.139 reinforce these flame speed reductions. In Figure A9.136, TC3, TC4 andTC5 display only display a marginal increase of ≤5˚C which indicates suspension of the combustion process. Each of the remaining time-temperature profiles reveal an initial decrease in temperature immediately downstream of the atomisers shown in the TC3 data, followed by a temperature increase at TC4 and further reduction at TC5.

9.4.3.1 (i) Equivalence ratio (ϕ) 0.61

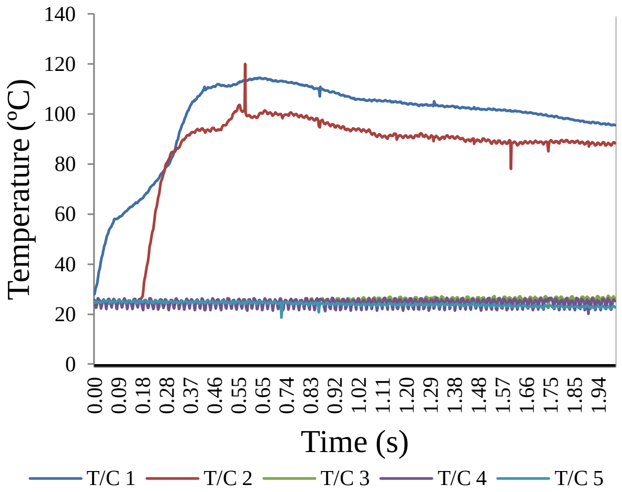

Figure A9.136: Typical time-temperature profile for three SRA Type B in X/F arrangement with methane-air mixture of E.R. (ϕ) 0.61

(ii) Equivalence ratio (ϕ) 0.72

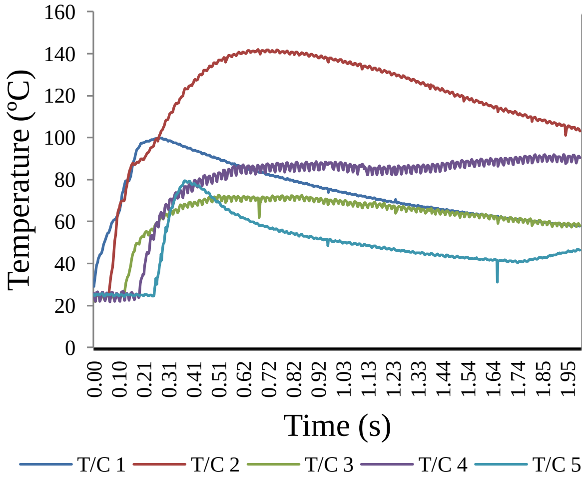

Figure A9.137 : Characteristic time-temperature profile for three SRA Type B in X/F arrangement with methane-air mixture of E.R. (ϕ) 0.72

(iii) Equivalence ratio (ϕ) 0.95

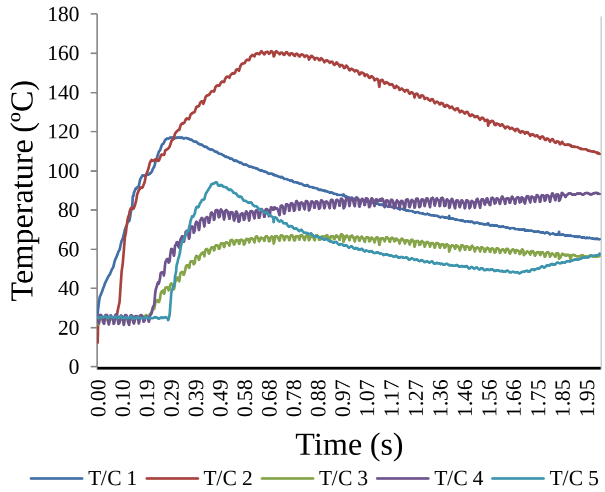

Figure A9.138 : Typical time-temperature profile for three SRA Type B in X/F arrangement with methane-air mixture of E.R. (ϕ) 0.95

(iv) Equivalence ratio (ϕ) 1.06

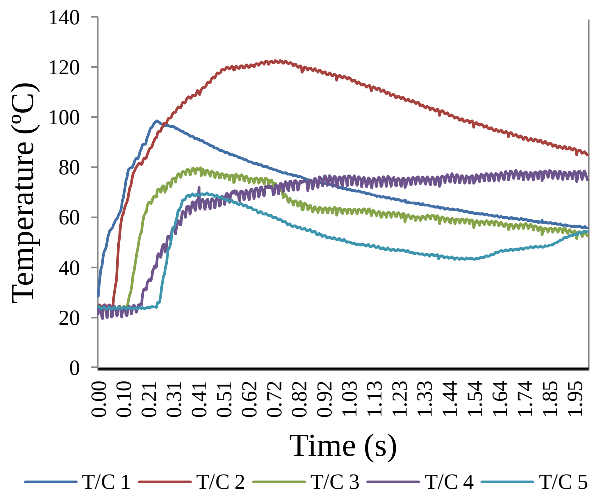

Figure A9.139 : Distinctive time-temperature profile for three SRA Type B in X/F arrangement with methane-air mixture of E.R. (ϕ) 1.06

A9.4.3.4 Qualitative analysis

In Figure A9.140 the methane-air mixture was (ϕ) 0.61. The progress of the flame can be observed in each of the frames i – iii, with no flame visible in (iv). Figure A9.140 (iii) has been highlighted and magnified to emphasise the interaction the reduction in flame area. There is clearly no indication of combustion beyond spray #3. The image presented in Figure A9.140 (iv) was taken 20ms after #3 revealing the absence of any flame and global suspension of combustion.

In Figure A9.142 the methane-air mixture was (ϕ) 0.72. Figure A9.142 (iv) shows 'dark' regions in the flame signifying that combustion has been impeded locally.

In Figure A9.144 the methane-air mixture was (ϕ) 0.95. Figure A9.144 (iii) displays very similar behaviour to Figure A9.142, with dark areas visible in Figure A9.145.

In Figure A9.146 the methane-air mixture was (ϕ) 1.06. Figure A9.147 also confirms localised suppression of the combustion

(i) Equivalence ratio (ϕ) 0.61

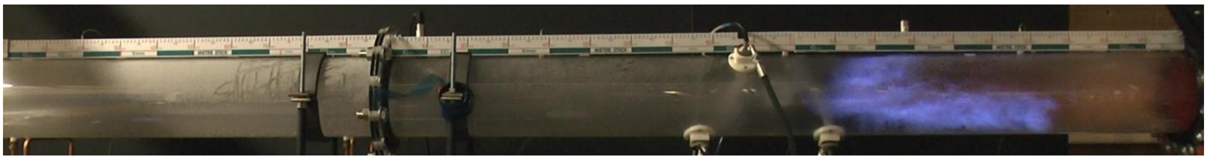

i. Flame propagating in methane-air mixture of E.R. (ϕ) 0.61 upstream of SRA

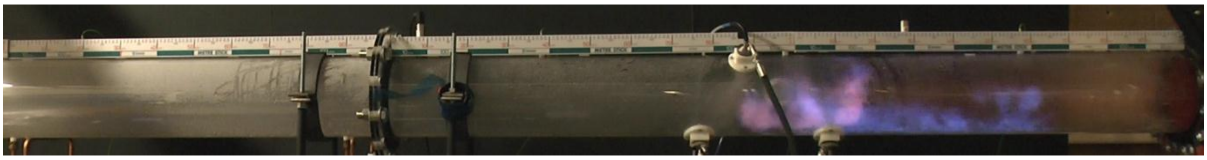

ii. Flame propagating in methane-air mixture of E.R. (ϕ) 0.61 upstream of SRA

iii. Flame propagating in methane-air mixture of E.R. (ϕ) 0.61 in the region of spray

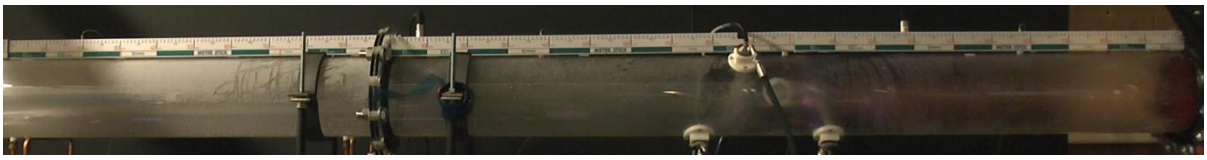

iv. **Mitigation** of methane-air mixture of E.R. (ϕ) 0.61 downstream of SRA

Figure A9.140 : Flame propagating upstream and downstream of three X/F SRA Type B for a methane-air mixture (ϕ) 0.61

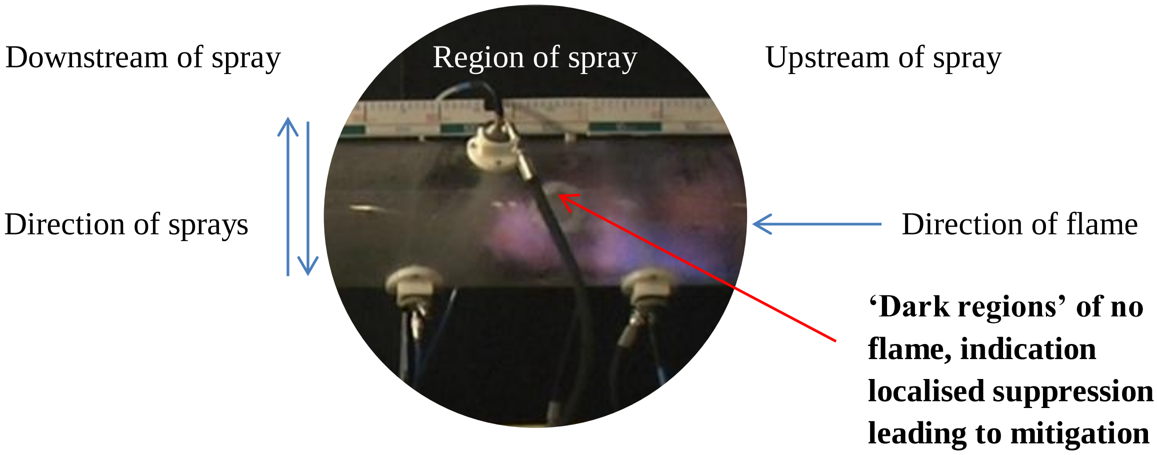

Figure A9.141: Expanded view of region of spray highlighted in Figure A9.140(iii)

(ii) Equivalence ratio (ϕ) 0.72

i. Flame propagating in methane-air mixture of E.R. (ϕ) 0.72 upstream of SRA

ii. Flame propagating in methane-air mixture of E.R. (ϕ) 0.72 upstream of SRA

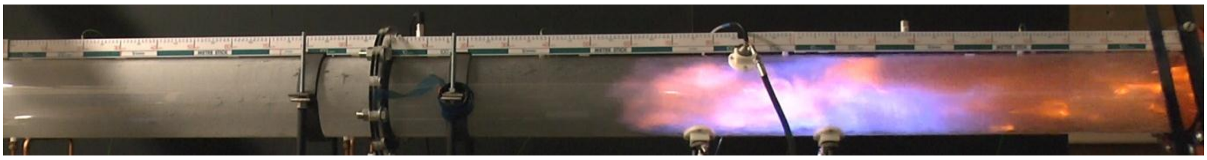

iii. Flame propagating in methane-air mixture of E.R. (ϕ) 0.72 in the region of spray

iv. Flame propagating in methane-air mixture of E.R. (ϕ) 0.72 downstream of SRA

Figure A9.142 : Flame propagating upstream and downstream of three X/F SRA Type B for a methane-air mixture (ϕ) 0.72

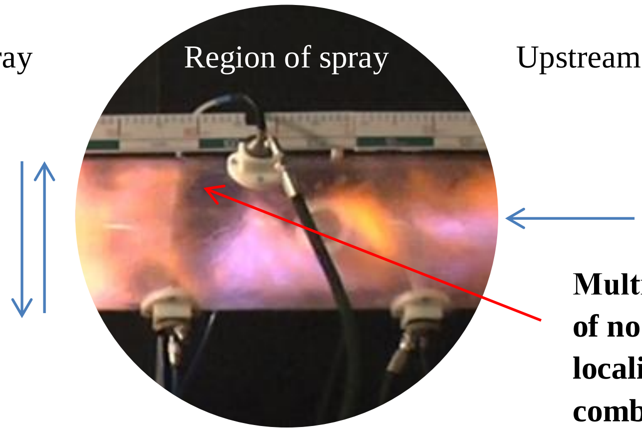

Figure A9.143 : Magnified view of region of spray highlighted in Figure A9.140(iv)

(iii) Equivalence ratio (ϕ) 0.95

i. Flame propagating in methane-air mixture of E.R. (ϕ) 0.95 upstream of SRA

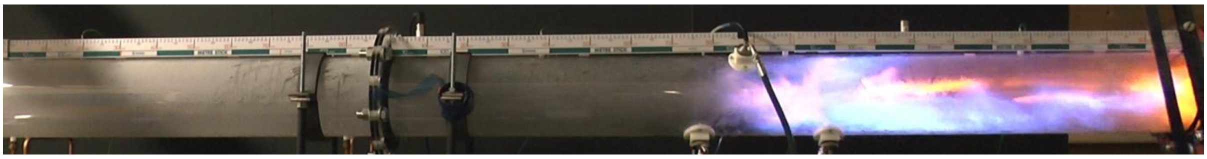

ii. Flame propagating in methane-air mixture of E.R. (ϕ) 0.95 upstream of SRA

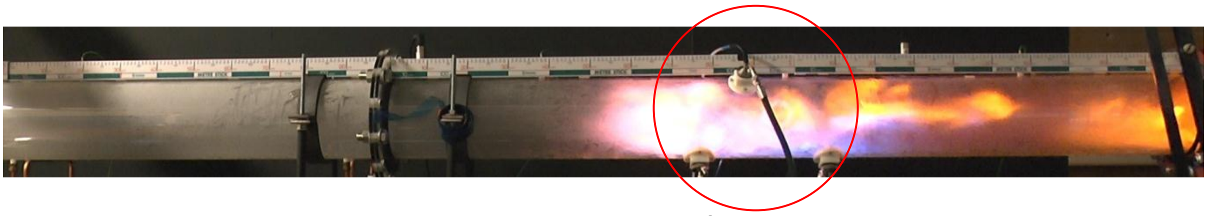

iii. Flame propagating in methane-air mixture of E.R. (ϕ) 0.95 in the region of spray

iv. Flame propagating in methane-air mixture of E.R. (ϕ) 0.95 downstream of SRA

Figure A9.144 : Flame propagating upstream and downstream of three X/F SRA Type B for a methane-air mixture (ϕ) 0.95

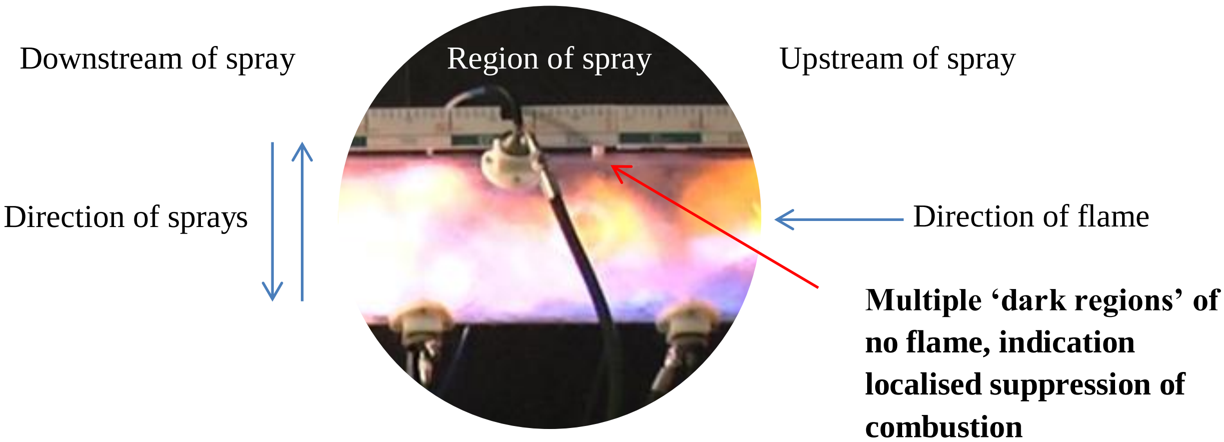

Figure A9.145 : Enlarged view of region of spray highlighted in Figure A9.143(iii)

(iv) Equivalence ratio (ϕ) 1.06

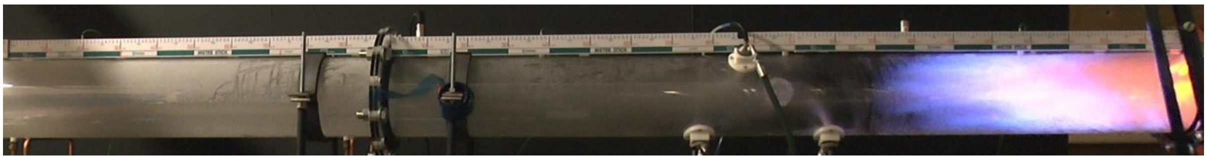

i. Flame propagating in methane-air mixture of E.R. (ϕ) 1.06 upstream of SRA

ii. Flame propagating in methane-air mixture of E.R. (ϕ) 1.06 upstream of SRA

iii. Flame propagating in methane-air mixture of E.R. (ϕ) 1.06 in the region of spray

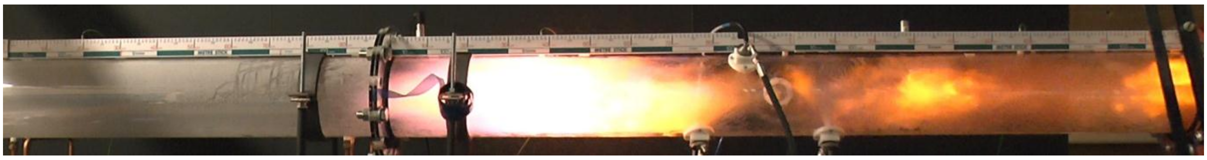

iv. Flame propagating in methane-air mixture of E.R. (ϕ) 1.06 downstream of SRA

Figure A9.146 : Flame propagating upstream and downstream of three X/F SRA Type B for a methane-air mixture (ϕ) 1.06

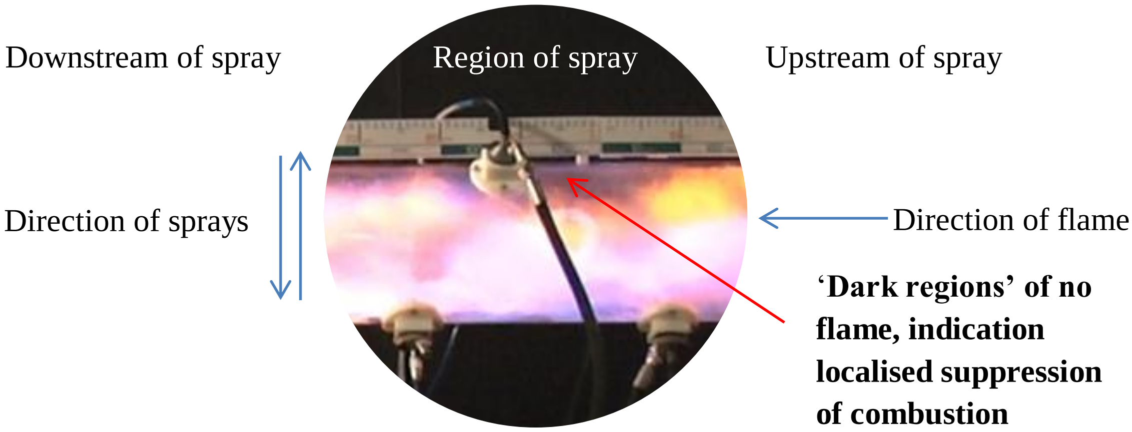

Figure A9.147 : Close up view of region of spray highlighted in Figure A9.144(iii)

A9.4.3.5 General event outcome

Table A9.22 provides a summary of the 'general event outcome' for each trial in this current series, using the five potential 'outcome' categories offered in Chapter 5. The results of all 'hot trials' were previously given in Table 5.14 and are also shown in Table A9.45.

Trial configuration	General event outcome	Code
Three X/F SRA (ϕ) 0.61	Full Mitigation resulting in Flame Extinguishment	FMFE
Three X/F SRA (ϕ) 0.72	No Mitigation with resulting Flame Deceleration	NMFD
Three X/F SRA (ϕ) 0.95	No Mitigation with resulting Flame Deceleration	NMFD
Three X/F SRA (ϕ) 1.06	No Mitigation with resulting Flame Deceleration	NMFD

Table A9.22 : General event outcome (trial series A9.4.3)

A9.4.4 Four (X/F) SRA : configuration Type B

A9.4.4.1 Trial set up

In this series of trials four Type B SRA's were assembled and installed in position #1, #2, #3 and #4 as previously shown in Figure A9.107 and Table A9.19. The atomisers were subjected to four trials with different methane-air mixtures, of (ϕ) 0.61, 0.72, 0.95 and 1.06.

A9.4.4.2 Flame speed

Average flame speeds were measured both upstream and downstream of the spray region, which are illustrated in Figure A9.148 as flame speed reduction values. In this atomiser configuration the methane-air mixtures of (ϕ) 0.61 and 0.72 were fully mitigated. This is shown in the diagram as a 100% flame speed reduction.

The methane-air mixture of (ϕ) 1.06 exhibited a flame speed reduction across the sprays of approximately 11%, whereas the mixture of (ϕ) 0.95 showed an increase of about 23%. Although the mixture of (ϕ) 0.95 presented an increase in flame speed across the sprays, this was less than the increase shown in the 'dry' scenario. Therefore a degree of flame suppression can be inferred.

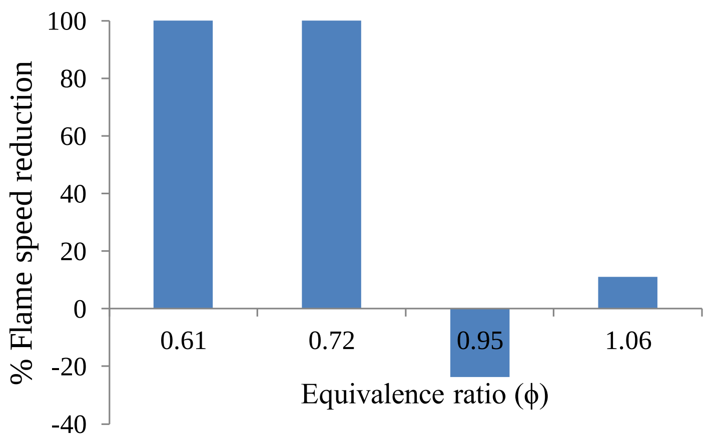

Figure A9.148 : Average flame speed reduction percentage (%) from upstream to downstream of four X/F SRA's in various methane-air mixtures

A9.4.4.3 Time-temperature response

The typical time-temperature profiles presented in Figure A9.149 and A9.150 reinforce the two mitigation events, with TC3, TC4 andTC5 displaying only indicating a slight increase of ≤5˚C, thus indicating suspension of the combustion process. In Figures A9.151 and A9.152 there is a notable reduction in temperature across the spray region, which can been observed by comparing the thermocouple data from TC2 and TC3.

(i) Equivalence ratio (ϕ) 0.61

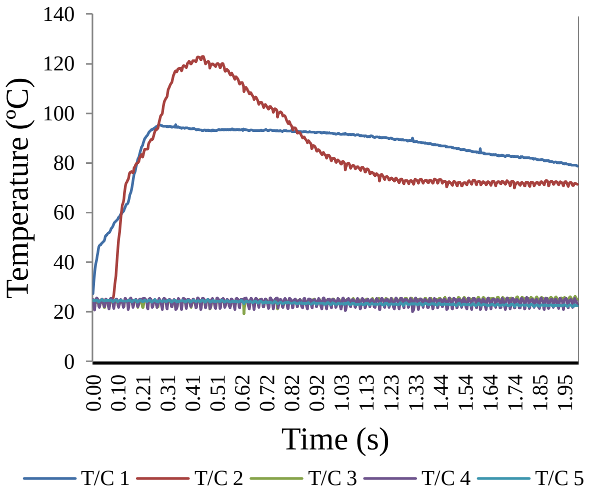

Figure A9.149 : Typical time-temperature profile for four SRA Type B in X/F arrangement with methane-air mixture of E.R. (ϕ) 0.61

(ii) Equivalence ratio (ϕ) 0.72

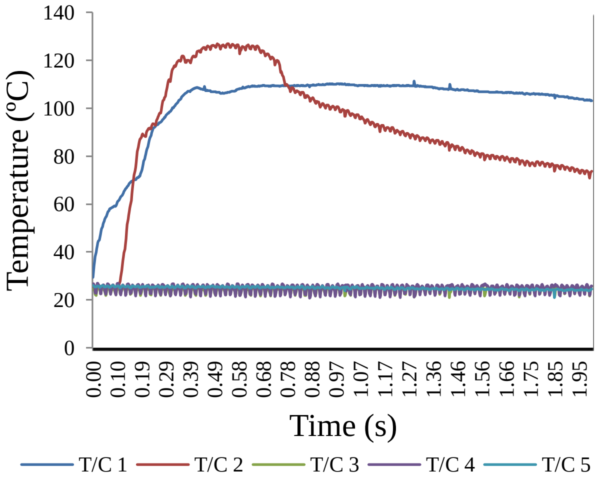

Figure A9.150 : Characteristic time-temperature profile for four SRA Type B in X/F arrangement with methane-air mixture of E.R. (ϕ) 0.72

(iii) Equivalence ratio (ϕ) 0.95

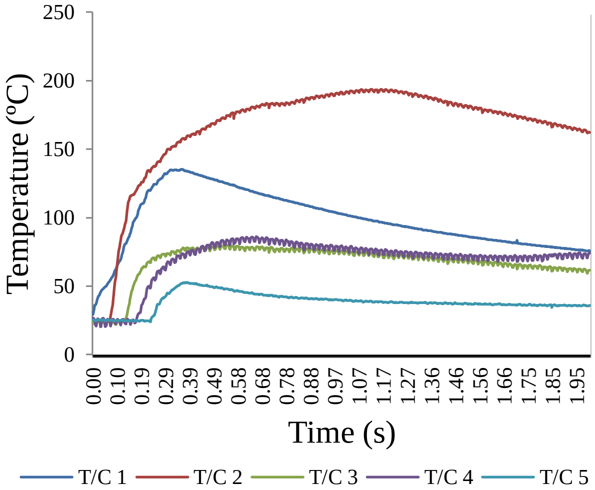

Figure A9.151 : Typical time-temperature profile for four SRA Type B in X/F arrangement with methane-air mixture of E.R. (ϕ) 0.95

(iv) Equivalence ratio (ϕ) 1.06

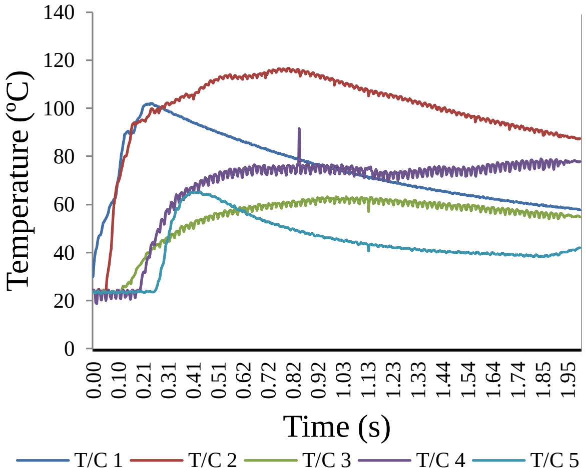

Figure A9.152 : Distinctive time-temperature profile for four SRA Type B in X/F arrangement with methane-air mixture of E.R. (ϕ) 1.06

A9.4.4.4 Qualitative analysis

In Figure A9.151 the methane-air mixture was (ϕ) 0.61. The progress of the flame can be observed in each of the frames i – iii, with no flame visible in (iv). Figure A9.151(iii) has been highlighted and magnified to accentuate the interaction the reduction in flame area. There is clearly no indication of combustion beyond spray #3. The image presented in Figure A9.151(iv) was taken 20ms after Figure A9.151(iii) revealing the absence of any flame, resulting in mitigation of the combustion process.

In Figure A9.153 the methane-air mixture was (ϕ) 0.72. Figure A9.153 (iv) shows traces of combustion between SRA's #1 and #2. In this case the flame was completely mitigated by SRA #3.

In Figure A9.155 the methane-air mixture was (ϕ) 0.95. Figure A9.155 displays dark visible areas in the flame, indicating local flame suppression.

In Figure A9.157 the methane-air mixture was (ϕ) 1.06. Figure A9.158 again verifies localised suppression of combustion.

(i) Equivalence ratio (ϕ) 0.61

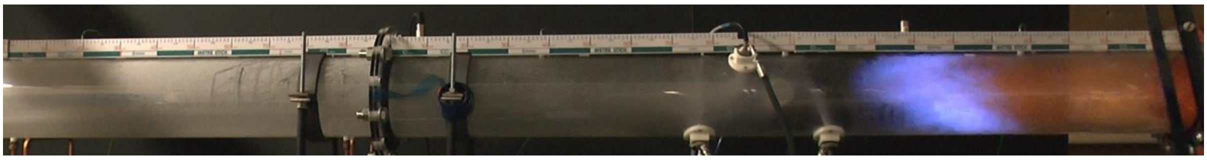

i. Flame propagating in methane-air mixture of E.R. (ϕ) 0.61 upstream of SRA

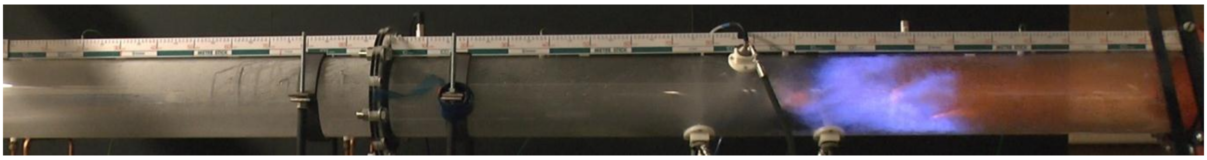

ii. Flame propagating in methane-air mixture of E.R. (ϕ) 0.61 upstream of SRA

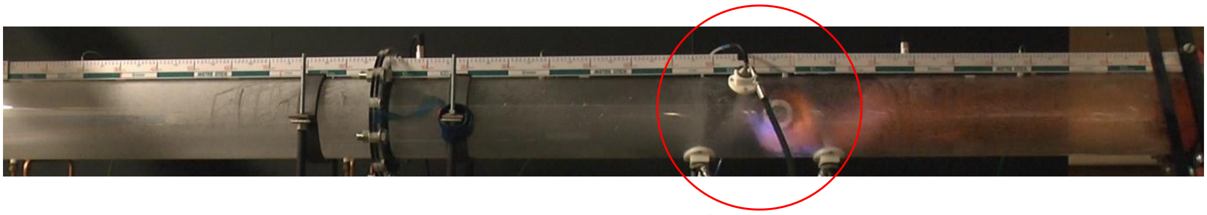

iii. Flame propagating in methane-air mixture of E.R. (ϕ) 0.61 in the region of spray

iv. Mitigation in methane-air mixture of E.R. (ϕ) 0.61 downstream of SRA

Figure A9.153 : Flame propagating upstream and downstream of four X/F SRA Type B for a methane-air mixture (ϕ) 0.61

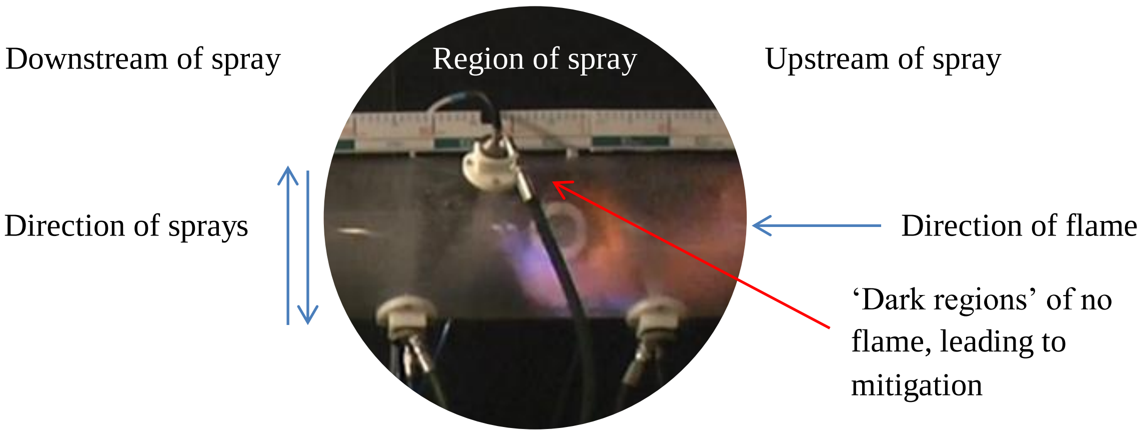

Figure A9.154: Expanded view of region of spray highlighted in Figure A9.153(iii)

(ii) Equivalence ratio (ϕ) 0.72

i. Flame propagating in methane-air mixture of E.R. (ϕ) 0.72 upstream of SRA

ii. Flame propagating in methane-air mixture of E.R. (ϕ) 0.72 upstream of SRA

iii. Flame propagating in methane-air mixture of E.R. (ϕ) 0.72 in the region of spray

iv. Mitigation in methane-air mixture of E.R. (ϕ) 0.72 downstream of SRA

Figure A9.155 : Flame propagating upstream and downstream of four X/F SRA Type B for a methane-air mixture (ϕ) 0.72

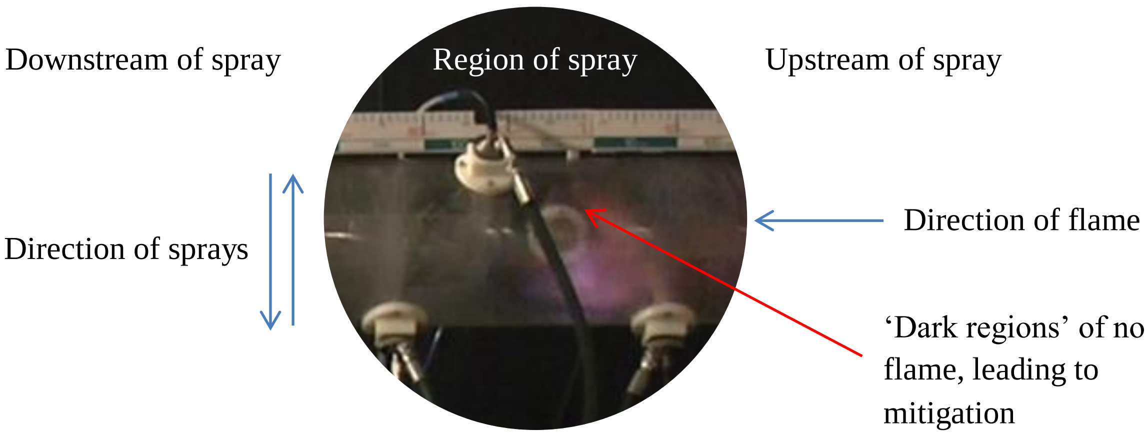

Figure A9.156 : Enlarged view of region of spray highlighted in Figure A9.155(iii)

(iii) Equivalence ratio (ϕ) 0.95

i. Flame propagating in methane-air mixture of E.R. (ϕ) 0.95 upstream of SRA

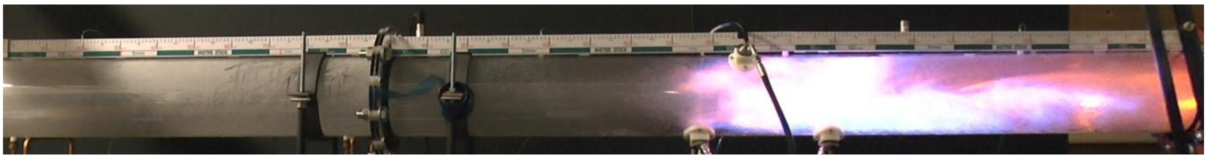

ii. Flame propagating in methane-air mixture of E.R. (ϕ) 0.95 upstream of SRA

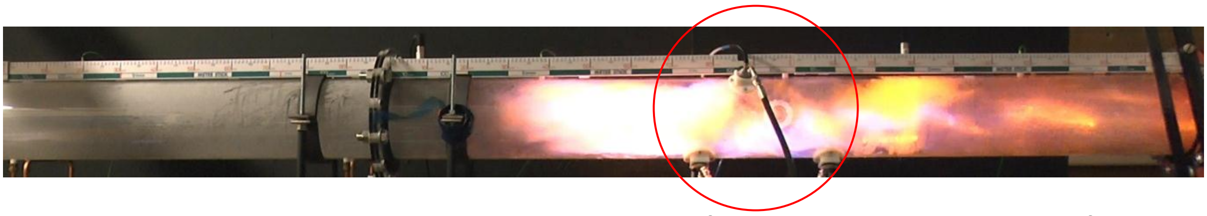

iii. Flame propagating in methane-air mixture of E.R. (ϕ) 0.95 in the region of spray

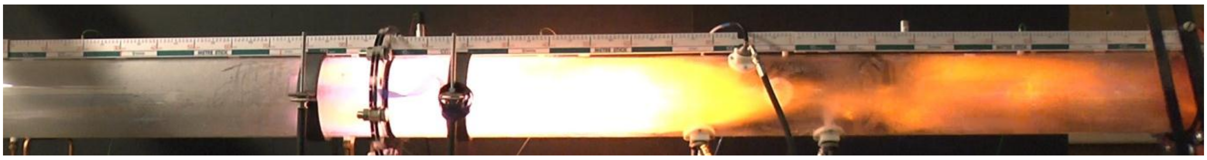

iv. Flame propagating in methane-air mixture of E.R. (ϕ) 0.95 downstream of SRA

Figure A9.157 : Flame propagating upstream and downstream of four X/F SRA Type B for a methane-air mixture (ϕ) 0.95

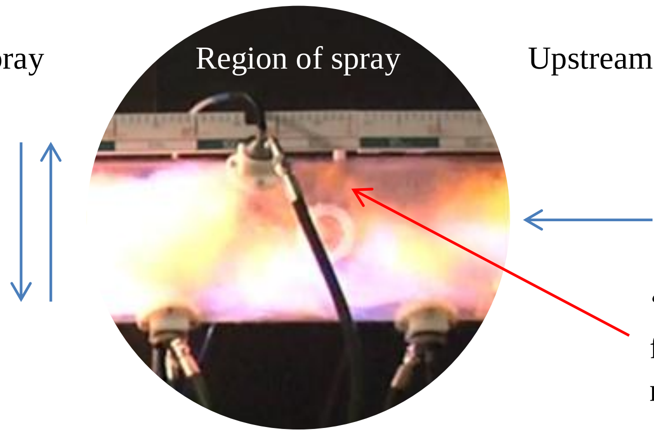

Figure A9.158 : Close up view of region of spray highlighted in Figure A9.157(iii)

(iv) Equivalence ratio (ϕ) 1.06

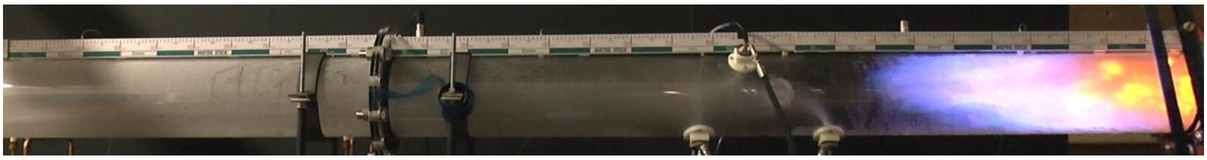

i. Flame propagating in methane-air mixture of E.R. (ϕ) 1.06 upstream of SRA

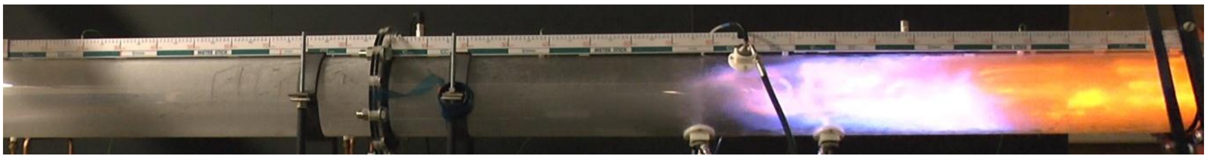

ii. Flame propagating in methane-air mixture of E.R. (ϕ) 1.06 upstream of SRA

iii. Flame propagating in methane-air mixture of E.R. (ϕ) 1.06 in the region of spray

iv. Flame propagating in methane-air mixture of E.R. (ϕ) 1.06 downstream of SRA

Figure A9.159 : Flame propagating upstream and downstream of four X/F SRA Type B for a methane-air mixture (ϕ) 1.06

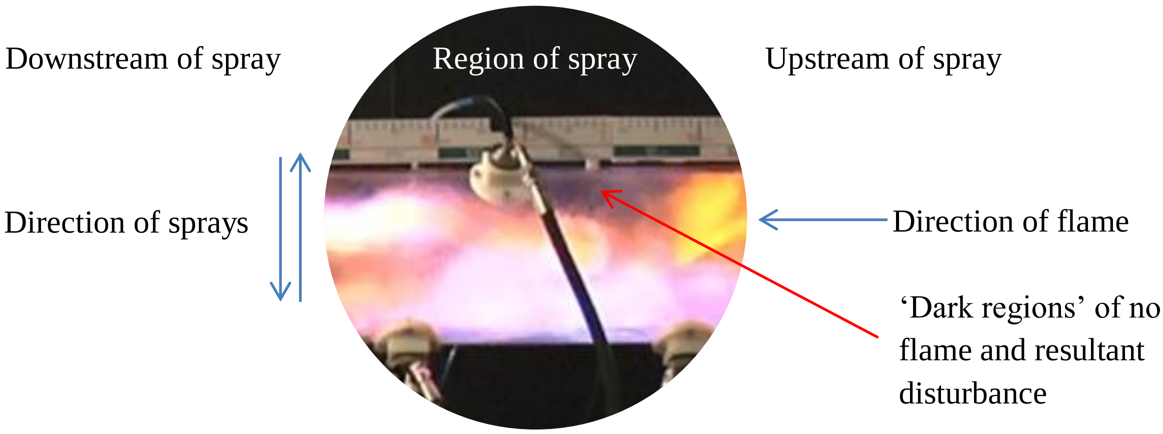

Figure A9.160 : Expanded view of region of spray highlighted in Figure A9.159(iii)

A9.4.4.5 General event outcome

Table A9.23 provides a summary of the 'general event outcome' for each trial in this current series, using the five potential 'outcome' categories offered in Chapter 5. The results of all 'hot trials' were previously given in Table 5.14 and are also shown in Table A9.45.

Trial configuration	General event outcome	Code
Four X/F SRA : (ϕ) 0.61	Full Mitigation resulting in Flame Extinguishment	FMFE
Four X/F SRA : (ϕ) 0.72	Full Mitigation resulting in Flame Extinguishment	FMFE
Four X/F SRA : (ϕ) 0.95	No Mitigation with resulting Flame Acceleration	NMFA
Four X/F SRA : (ϕ) 1.06	No Mitigation with resulting Flame Deceleration	NMFD

Table A9.23 : General event outcome (trial series A9.4.4)

A9.4.5 Single (X/F) Type C SRA

A9.4.5.1 Trial set up

In this series of trials a single Type C SRA was assembled and installed in position #1 as previously shown in Figure A9.107 and Table A9.19. The single atomiser was subjected to four trials with different methane-air mixtures of (ϕ) 0.61, 0.72, 0.95 and 1.06.

A9.4.5.2 Flame speed

Average flame speeds were measured both upstream and downstream of the spray region, which are illustrated in Figure A9.161 as flame speed reduction values. The methane-air mixture (ϕ) 0.61 resulted in marginal decrease in flame speed; whist is likely to be the result of the localised disturbance of the flammable mixture ahead of the flame, coupled with the suppression effects of the spray.

The methane-air mixture (ϕ) 0.72 appears to be less effected by the disturbance, resulting in a flame speed reduction of approximately 28%. During the (ϕ) 0.95 trial, the flame speed increased by a margin of about 10%, although this may be chassed as a reduction when compared to the 'dry' trials. In the (ϕ) 1.06 experimental trial the flame exhibited a reduction in flame speed of approximately 17%

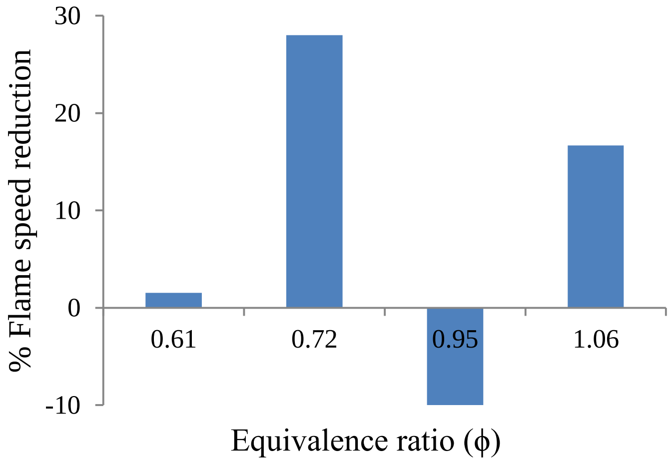

Figure A9.161 : Average flame speed reduction percentage (%) from upstream to downstream of single X/F SRA in various methane-air mixtures

.

A9.4.5.3 Time-temperature response

Time-temperature profiles have been plotted for each of the scenarios and are presented in Figures A9.162 - A9.165. In Figure A9.163 the temperature decrease between TC3 and TC5 is consistent with a reduction in flame speed.

Conversely Figures A9.162 and A9.165 do not exhibit typical profiles associated with an overall flame speed reduction. This is probably due to a deceleration immediately downstream of the spray followed by an increase in burning rate as the flame continued to propagate. Figures A9.164 illustrates similar temperatures at TC 3 and TC5, with a temperature increase across the sprays.

.

(i) Equivalence ratio (ϕ) 0.61

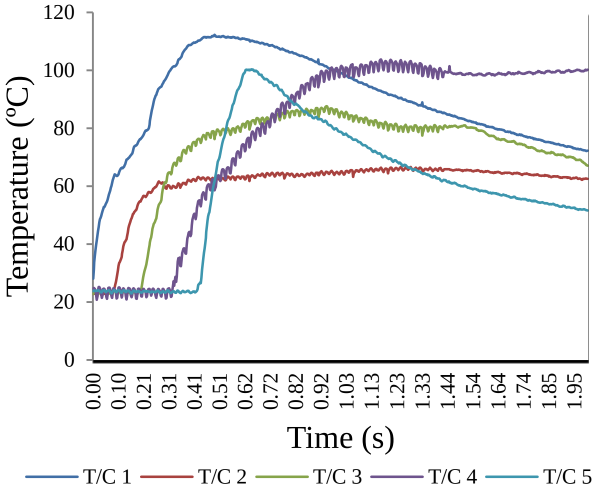

Figure A9.162 : Characteristic time-temperature profile for single SRA Type C in X/F arrangement with methane-air mixture of E.R. (ϕ) 0.61

(ii) Equivalence ratio (ϕ) 0.72

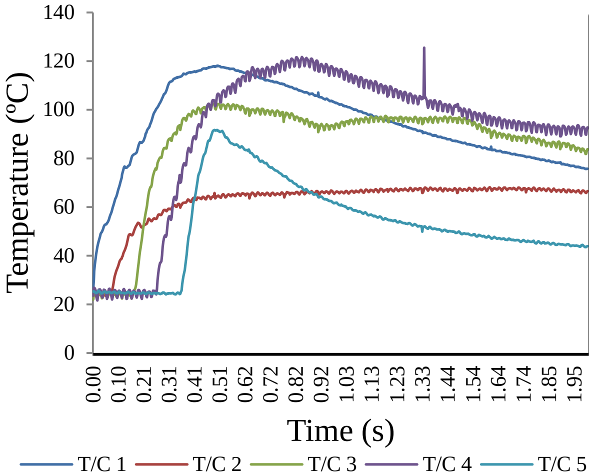

Figure A9.163 : Typical time-temperature profile for single SRA Type C in X/F arrangement with methane-air mixture of E.R. (ϕ) 0.72

(iii) Equivalence ratio (ϕ) 0.95

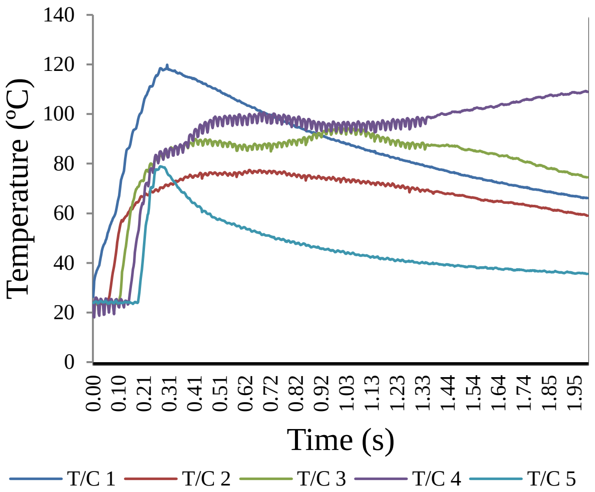

Figure A9.164 : Typical time-temperature profile for single SRA Type C in X/F arrangement with methane-air mixture of E.R. (ϕ) 0.95

(iv) Equivalence ratio (ϕ) 1.06

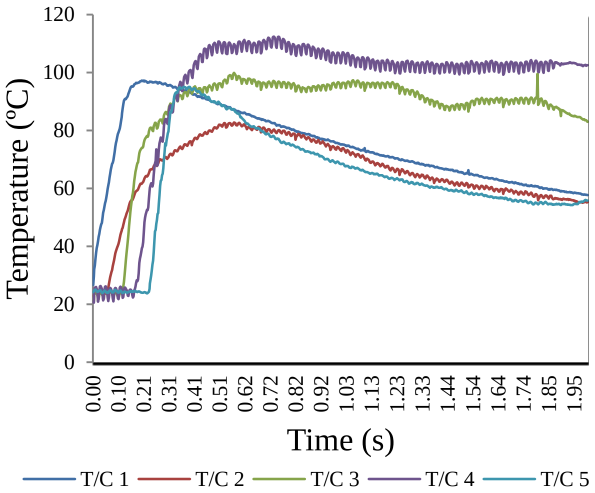

Figure A9.165 : Average time-temperature profile for single SRA Type C in X/F arrangement with methane-air mixture of E.R. (ϕ) 1.06

A9.4.5.4 Qualitative analysis

In Figure A9.166 the methane-air mixture was (ϕ) 0.61. In Figures A9.166(iii) the flame is passing through the single spray in position #1 and is seen to lengthen.

In Figure A9.168 the methane-air mixture was (ϕ) 0.72. In Figures A9.168(ii) and A9.168(iii) dark regions are again visible, indicating that combustion has ceased in those particular areas.

In Figure A9.170 the methane-air mixture was (ϕ) 0.95. Figure A9.170 (ii) shows no obvious dark regions in the flame. Considering this and the disturbance caused by the single spray, the very small increase in flame speed of approximately 10% followed.

In Figure A9.172 the methane-air mixture was (ϕ) 1.06. Figure A9.172 (ii) shows no obvious disorder to the flame, however, a ‘dark region’ is visible at the flame/spray interface, indicating localised suppression of the combustion process which resulted in a global flame speed reduction

(i) Equivalence ratio (ϕ) 0.61

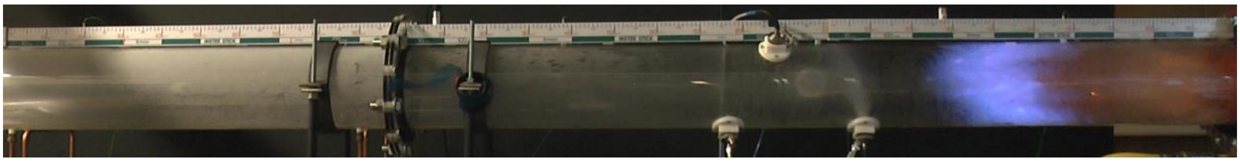

i. Flame propagating in methane-air mixture of E.R. (ϕ) 0.61 upstream of SRA

ii. Flame propagating in methane-air mixture of E.R. (ϕ) 0.61 upstream of SRA

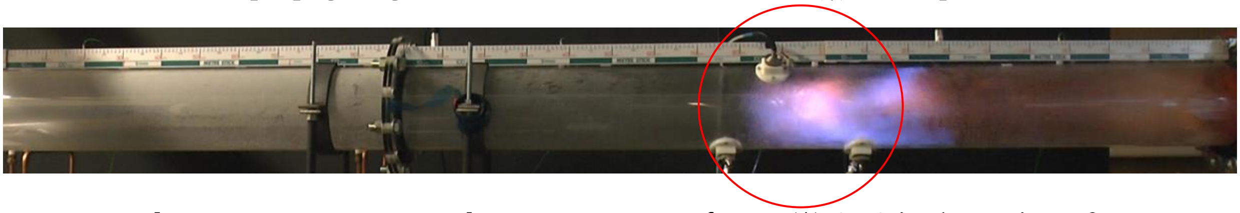

iii. Flame propagating in methane-air mixture of E.R. (ϕ) 0.72 in the region of spray

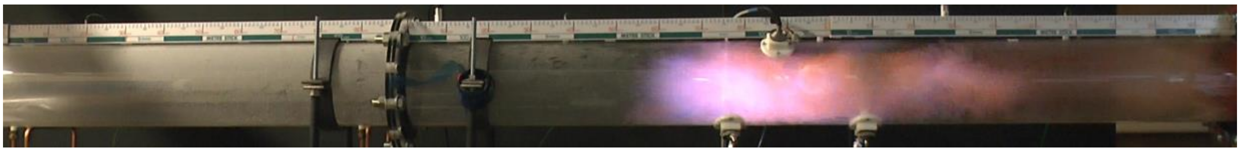

iv. Flame propagating in methane-air mixture of E.R. (ϕ) 0.61 downstream of SRA

Figure A9.166 : Flame propagating upstream and downstream of single X/F SRA Type C for a methane-air mixture (ϕ) 0.61

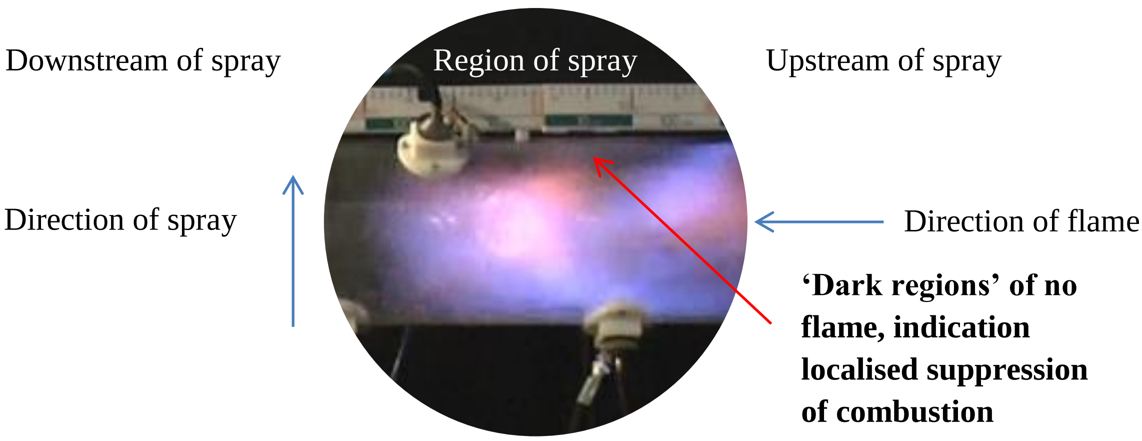

Figure A9.167 : Expanded view of region of spray highlighted in Figure A9.166(iii)

(ii) Equivalence ratio (ϕ) 0.72

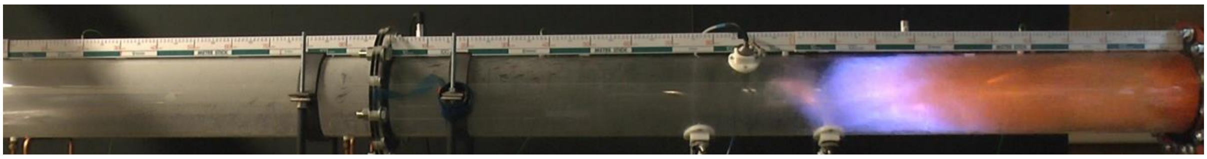

v. Flame propagating in methane-air mixture of E.R. (ϕ) 0.72 upstream of SRA

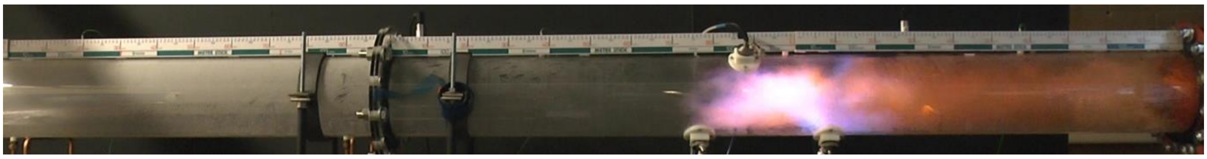

vi. Flame propagating in methane-air mixture of E.R. (ϕ) 0.72 upstream of SRA

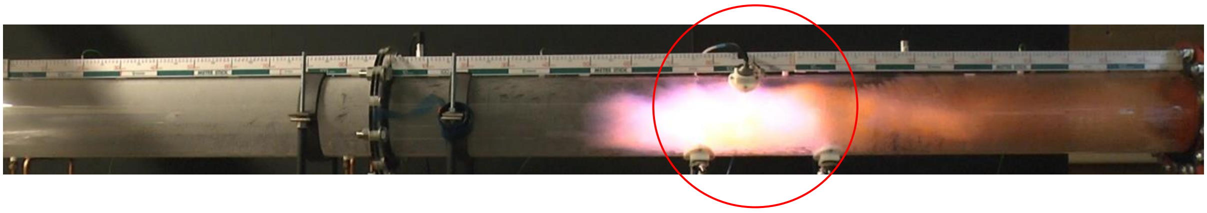

vii. Flame propagating in methane-air mixture of E.R. (ϕ) 0.72 in the region of spray

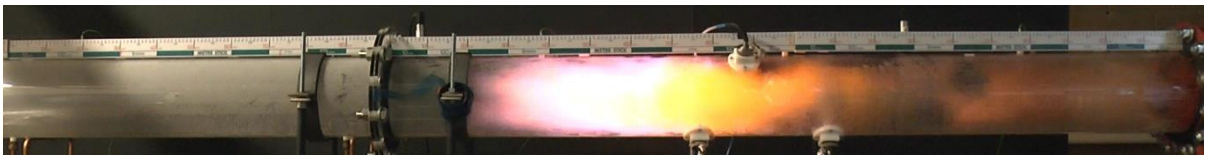

viii. Flame propagating in methane-air mixture of E.R. (ϕ) 0.72 downstream of SRA

Figure A9.168 : Flame propagating upstream and downstream of single X/F SRA Type C for a methane-air mixture (ϕ) 0.72

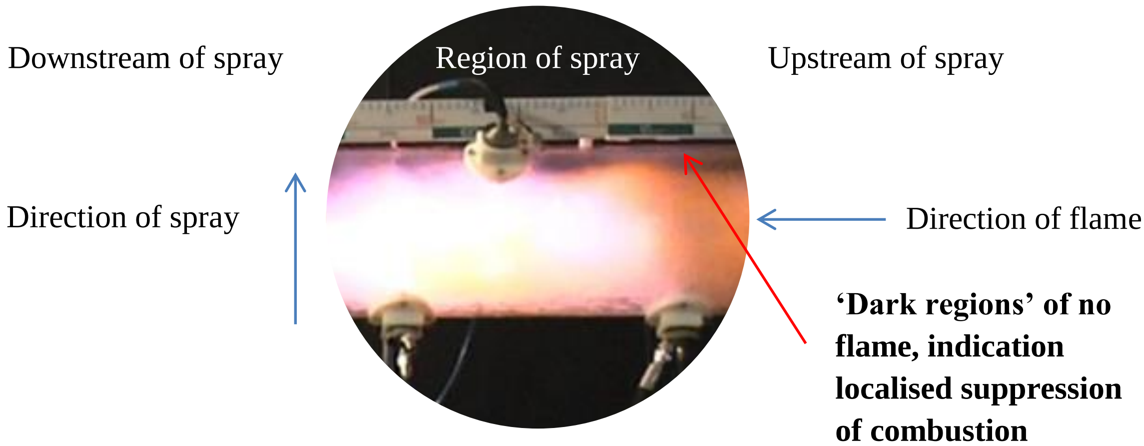

Figure A9.169 : Expanded view of region of spray highlighted in Figure A9.168(iii)

(iii) Equivalence ratio (ϕ) 0.95

i. Flame propagating in methane-air mixture of E.R. (ϕ) 0.95upstream of SRA

ii. Flame propagating in methane-air mixture of E.R. (ϕ) 0.95 upstream of SRA

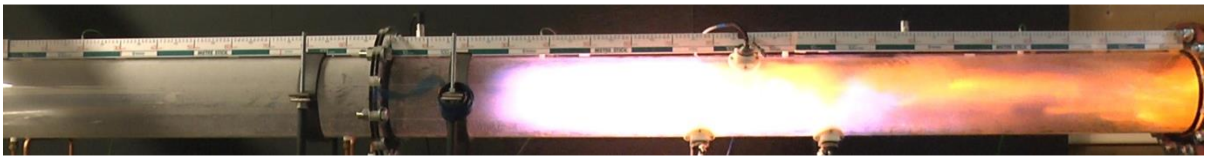

iii. Flame propagating in methane-air mixture of E.R. (ϕ) 0.95in the region of spray

iv. Flame propagating in methane-air mixture of E.R. (ϕ) 0.95 downstream of SRA

Figure A9.170 : Flame propagating upstream and downstream of single X/F SRA Type C for a methane-air mixture (ϕ) 0.95

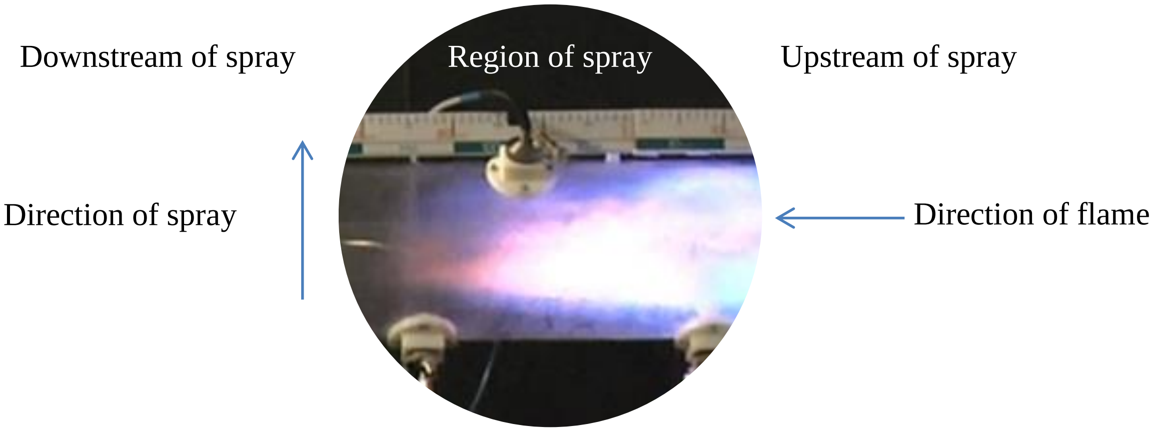

Figure A9.171 : Close up view of region of spray highlighted in Figure A9.170(ii)

(iv) Equivalence ratio (ϕ) 1.06

i. Flame propagating in methane-air mixture of E.R. (ϕ) 1.06 upstream of SRA

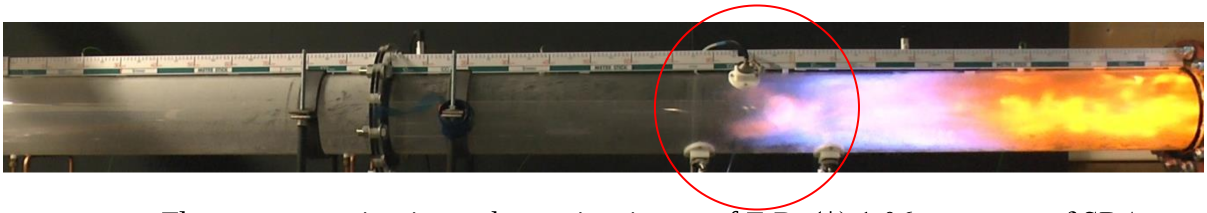

ii. Flame propagating in methane-air mixture of E.R. (ϕ) 1.06 upstream of SRA

iii. Flame propagating in methane-air mixture of E.R. (ϕ) 1.06 in the region of spray

iv. Flame propagating in methane-air mixture of E.R. (ϕ) 1.06 downstream of SRA

Figure A9.172 : Flame propagating upstream and downstream of single X/F SRA Type C for a methane-air mixture (ϕ) 1.06

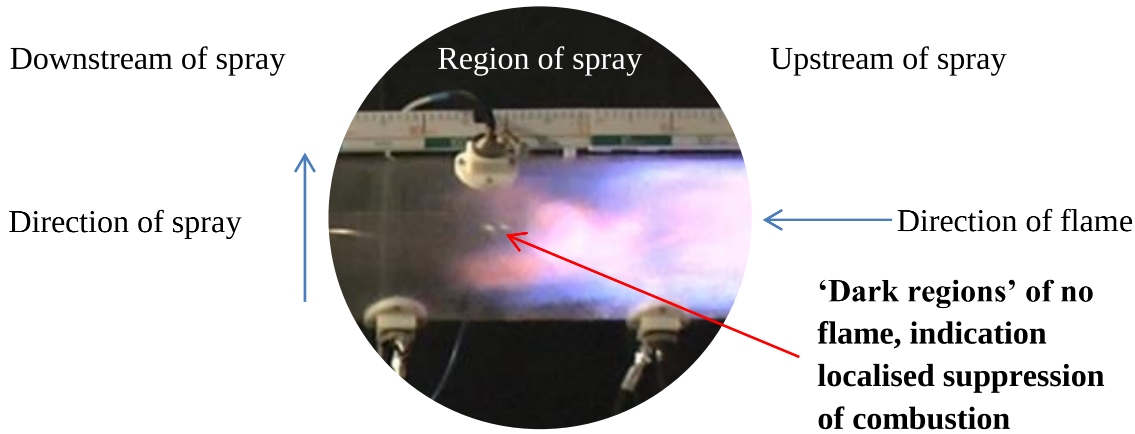

Figure A9.173: Magnified view of region of spray highlighted in Figure A9.172 (ii)

A9.4.5.5 General event outcome

Table A9.24 provides a summary of the **'general event outcome'** for each trial in this current series, using the five potential 'outcome' categories offered in Chapter 5. The results of all 'hot trials' were previously given in Table 5.14 and are also shown in Table A9.45.

Trial configuration	General event outcome	Code
Single X/F SRA : (ϕ) 0.61	No Mitigation with resulting Flame Deceleration	NMFD
Single X/F SRA : (ϕ) 0.72	No Mitigation with resulting Flame Deceleration	NMFD
Single X/F SRA : (ϕ) 0.95	No Mitigation with resulting Flame Acceleration	NMFA
Single X/F SRA : (ϕ) 1.06	No Mitigation with resulting Flame Deceleration	NMFD

Table A9.24 : General event outcome (trial series A9.4.5)

A9.4.6 Two (X/F) Type C SRA's

A9.4.6.1 Trial set up

In this series of trials, two Type C SRA's were assembled and installed in position #1 and#2 as previously shown in Figure A9.107 and Table A9.19. The atomisers were subjected to four trials with different methane-air mixtures, of (ϕ) 0.61, 0.72, 0.95 and 1.06.

A9.4.6.2 Flame speed

Average flame speeds were measured both upstream and downstream of the spray region, which are illustrated in Figure A9.174 as flame speed reduction values. In this atomiser configuration the methane-air mixtures (ϕ) 0.61, 0.72 and 1.06 all exhibited a positive outcome, with flame speed reduction occurring in each case. Figure A9.174 displays an increase in average flame speed for the methane-air mixture (ϕ) 0.95. The methane-air mixture (ϕ) 0.95 consistently presents the greatest challenge in this current research.

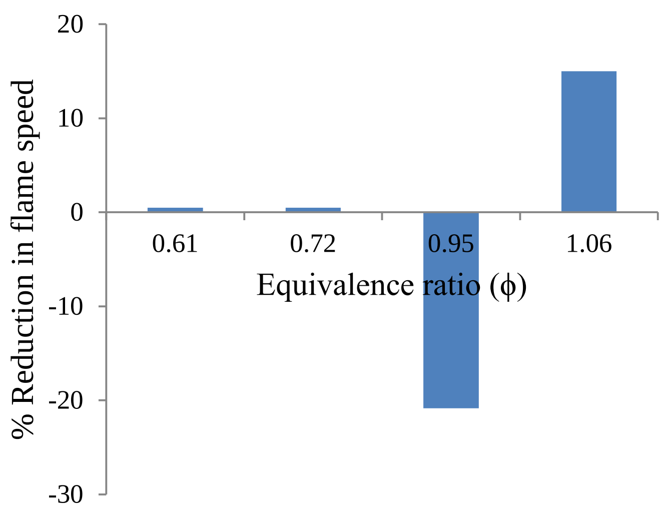

Figure A9.174 : Average flame speed reduction percentage (%) from upstream to downstream of two X/F SRA's in a various methane-air mixtures

A9.4.6.3 Time-temperature response

The typical time-temperature profiles presented in Figures A9.175 – A9.178 reinforce the flame speed reductions shown in FiguresA9.174.

In Figures A9.175, A9.176 and A9.178 there is an increase in temperature between TC3 and TC5 indicating an increase in flame temperature. As the average flame speed actually reduced in these three scenarios, if may be assumed that the sprays initially retarded the flame propagation, although speeds began to increase afterwards.

In Figure A9.177 there in an increase in temperature between TC4 and TC5 indicating and increase in combustion activity and flame speed.

(i) Equivalence ratio (ϕ) 0.61

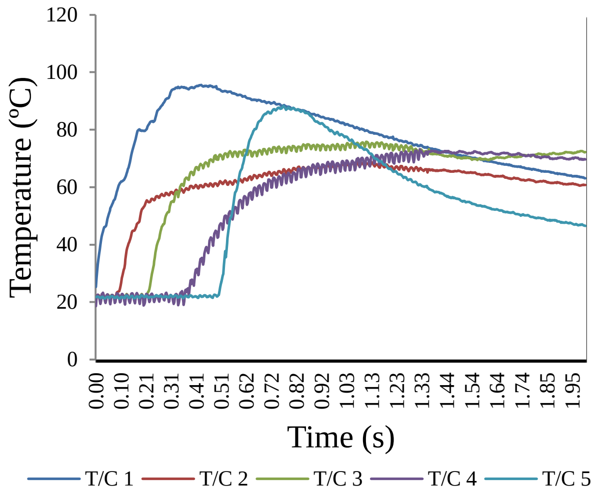

Figure A9.175 : Typical time-temperature profile for two SRA Type C in X/F arrangement with methane-air mixture of E.R. (ϕ) 0.61

(ii) Equivalence ratio (ϕ) 0.72

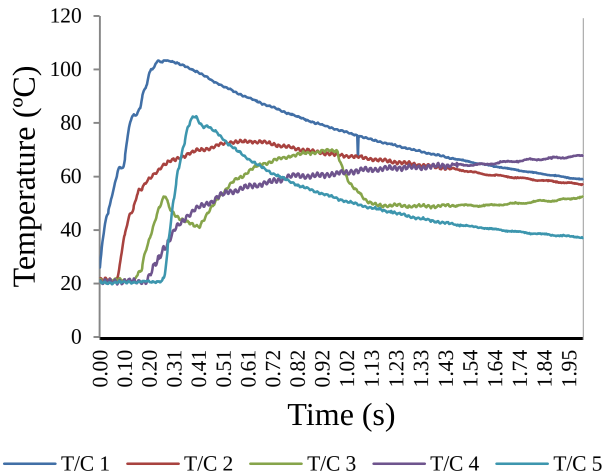

Figure A9.176 : Characteristic time-temperature profile for two SRA Type C in X/F arrangement with methane-air mixture of E.R. (ϕ) 0.72

(iii) Equivalence ratio (ϕ) 0.95

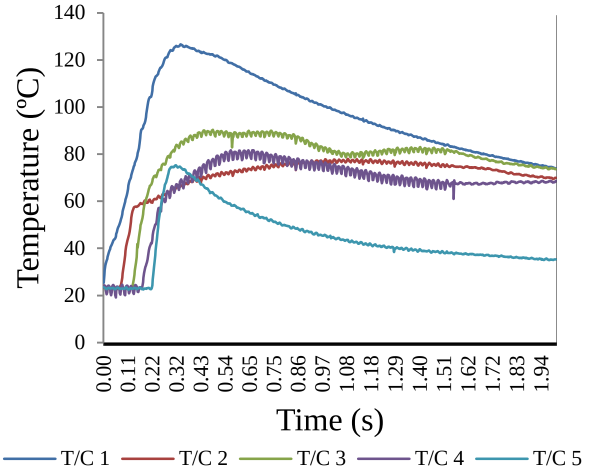

Figure A9.177 : Typical time-temperature profile for two SRA Type C in X/F arrangement with methane-air mixture of E.R. (ϕ) 0.95

(iv) Equivalence ratio (ϕ) 1.06

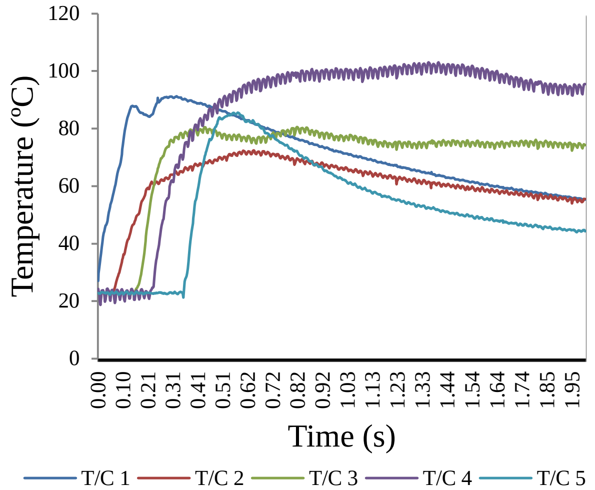

Figure A9.178 : Characteristic time-temperature profile for two SRA Type C in X/F arrangement with methane-air mixture of E.R. (ϕ) 1.06

A9.4.6.4 Qualitative analysis

In Figure A9.179 the methane-air mixture was (ϕ) 0.61. As the flame passes through the spray region there is an obvious reduction in flame volume, whereby localised flame suppression has occurred, which is magnified in Figure A9.180. The flame is seen to exit the sprays and continue to propagate along the tube.

Figure A9.181 exhibits similar qualities to Figure A9.179, although the methane-air mixture was (ϕ) 0.72. The flame progression appears to be highly influenced by the sprays and is magnified for clarity in Figure A9.182. The flame then exits the spray and begins to propagate in the downstream mixture.

In Figure A9.183 the methane-air mixture was (ϕ) 0.95. There appears to be a high degree of disturbance in the spray region, resulting in flame acceleration along the rest of the clear tube section.

Figure A9.185 the methane-air mixture was (ϕ) 1.06 and offers similar results to the methane-air mixtures (ϕ) 0.61 and 0.72, whereby the flame is clearly suppressed by the sprays but continues to re-propagate in the downstream unburned mixture. A close up view is provided in Figure A9.186.

(i) Equivalence ratio (ϕ) 0.61

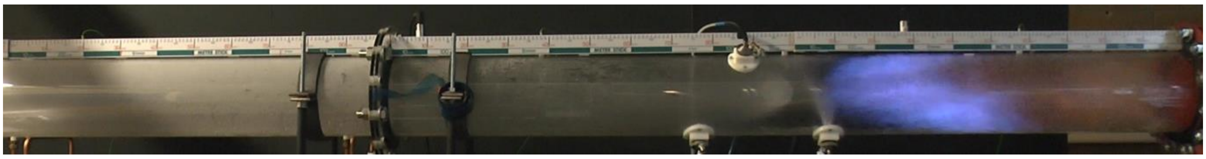

i. Flame propagating in methane-air mixture of E.R. (ϕ) 0.61 upstream of SRA

ii. Flame propagating in methane-air mixture of E.R. (ϕ) 0.61 upstream of SRA

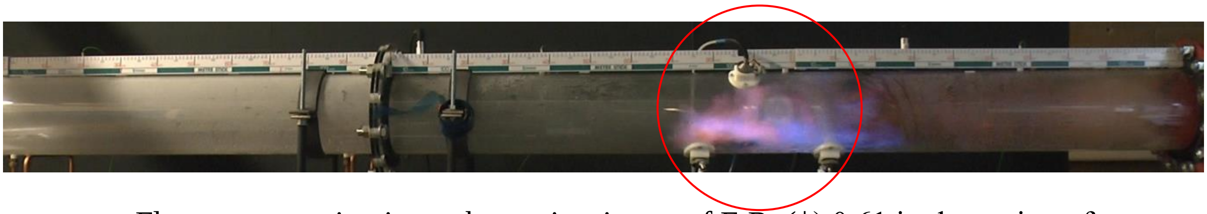

iii. Flame propagating in methane-air mixture of E.R. (ϕ) 0.61 in the region of spray

iv. Flame propagating in methane-air mixture of E.R. (ϕ) 0.61 downstream of SRA

Figure A9.179 : Flame propagating upstream and downstream of two X/F SRA Type C for a methane-air mixture (ϕ) 0.61

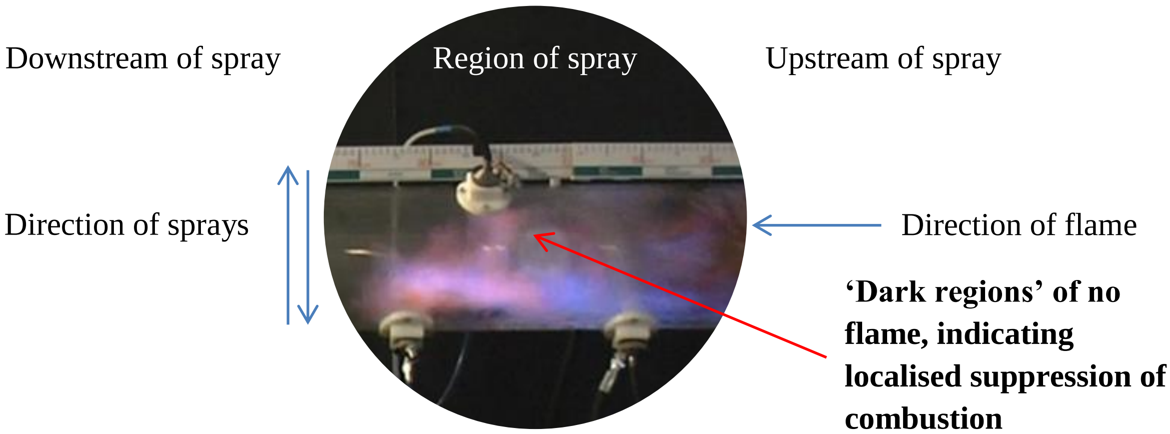

Figure A9.180 : Expanded view of region of spray highlighted in Figure A9.179(iii)

(ii) Equivalence ratio (ϕ) 0.72

i. Flame propagating in methane-air mixture of E.R. (ϕ) 0.72 upstream of SRA

ii. Flame propagating in methane-air mixture of E.R. (ϕ) 0.72 upstream of SRA

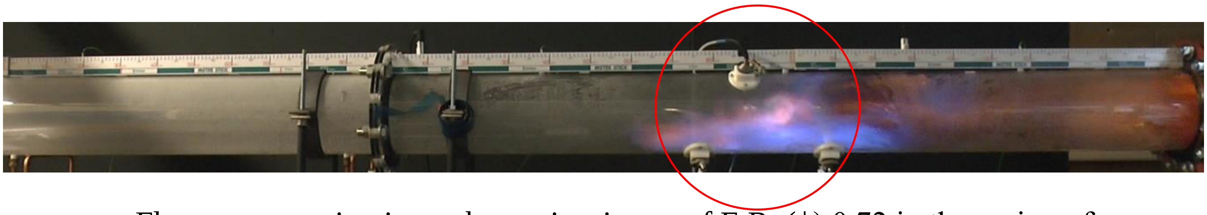

iii. Flame propagating in methane-air mixture of E.R. (ϕ) 0.72 in the region of spray

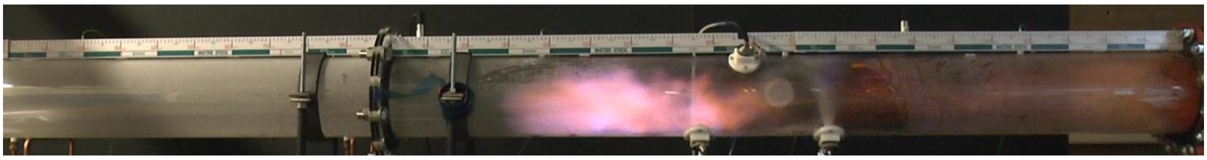

iv. Flame propagating in methane-air mixture of E.R. (ϕ) 0.72 downstream of SRA

Figure A9.181 : Flame propagating upstream and downstream of two X/F SRA Type C for a methane-air mixture (ϕ) 0.72

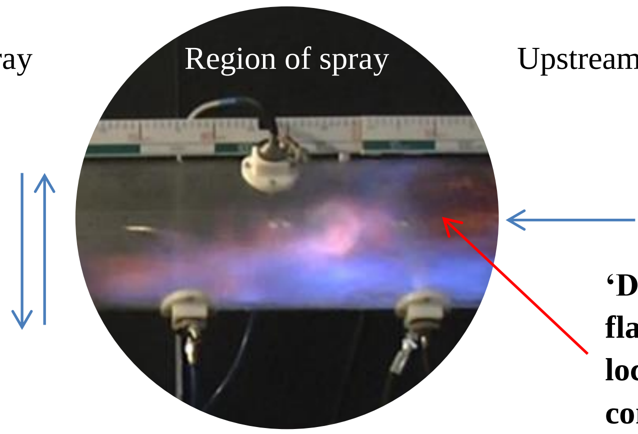

Figure A9.182 : Magnified view of region of spray highlighted in Figure A9.181(iii)

(iii) Equivalence ratio (ϕ) 0.95

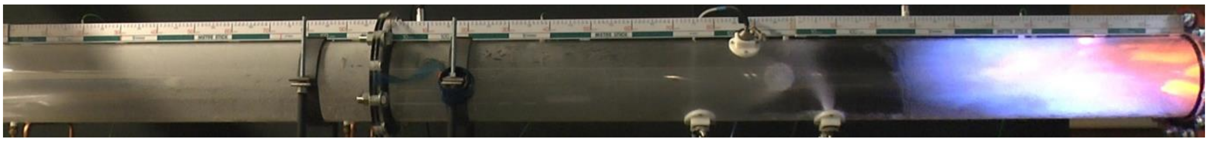

i. Flame propagating in methane-air mixture of E.R. (ϕ) 0.95 upstream of SRA

ii. Flame propagating in methane-air mixture of E.R. (ϕ) 0.95 upstream of SRA

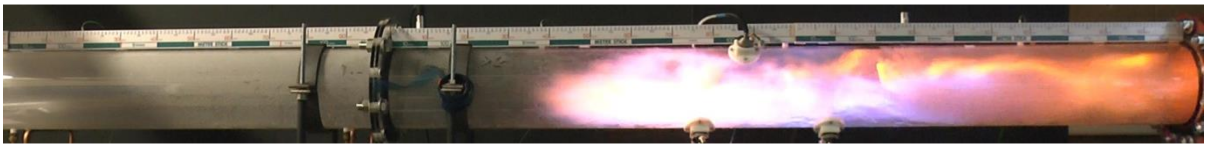

iii. Flame propagating in methane-air mixture of E.R. (ϕ) 0.95 in the region of spray

iv. Flame propagating in methane-air mixture of E.R. (ϕ) 0.95 downstream of SRA

Figure A9.183: Flame propagating upstream and downstream of two X/F SRA Type C for a methane-air mixture (ϕ) 0.95

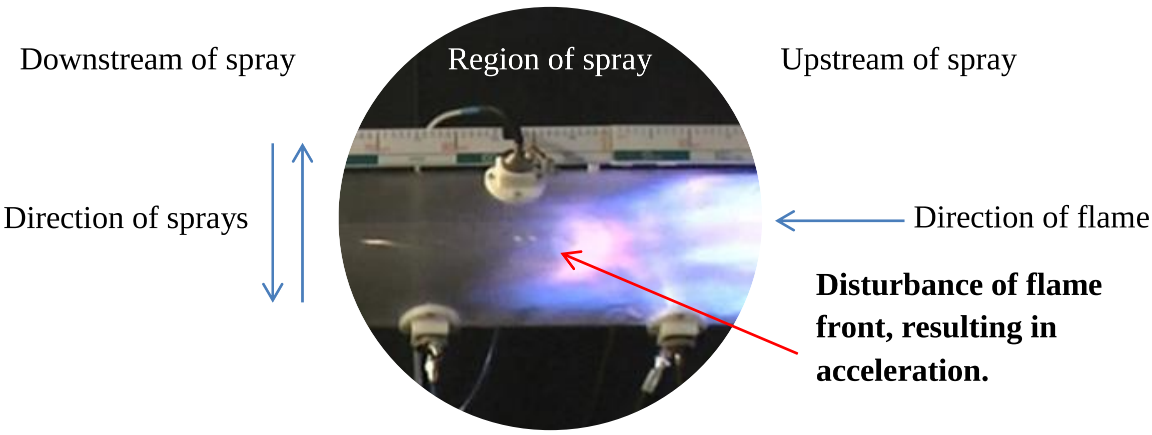

Figure A9.184 : Exploded view of region of spray highlighted in Figure A9.183(ii)

(iv) Equivalence ratio (ϕ) 1.06

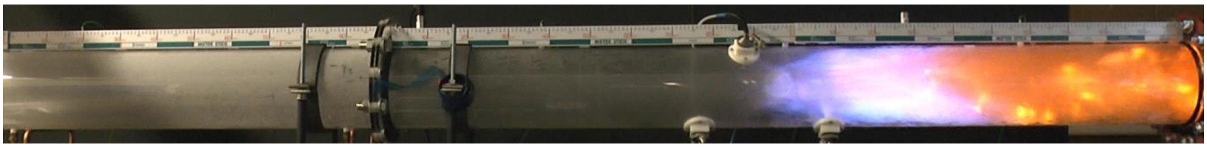

i. Flame propagating in methane-air mixture of E.R. (ϕ) 1.06 upstream of SRA

ii. Flame propagating in methane-air mixture of E.R. (ϕ) 1.06 upstream of SRA

iii. Flame propagating in methane-air mixture of E.R. (ϕ) 1.06 in the region of spray

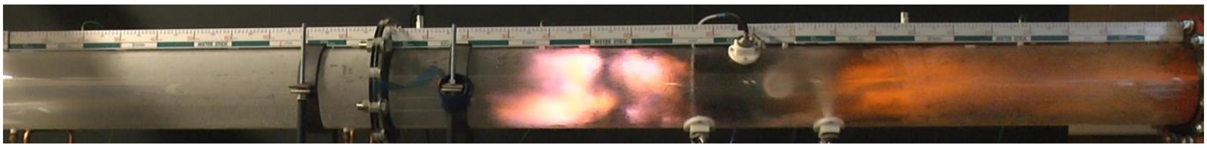

iv. Flame propagating in methane-air mixture of E.R. (ϕ) 1.06 downstream of SRA

Figure A9.185 : Flame propagating upstream and downstream of two X/F SRA Type C for a methane-air mixture (ϕ) 1.06

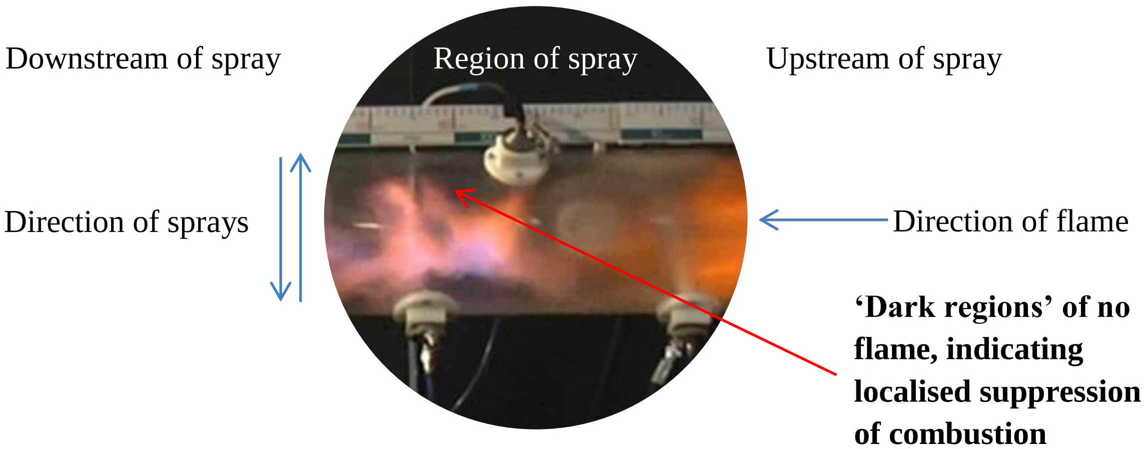

Figure A9.184 : Close up view of region of spray highlighted in Figure A9.185(iii)

A9.4.6.5 General event outcome

Table A9.25 provides a summary of the **'general event outcome'** for each trial in this current series, using the five potential 'outcome' categories offered in Chapter 5. The results of all 'hot trials' were previously given in Table 5.14 and are also shown in Table A9.45.

Trial configuration	General event outcome	Code
Two X/F SRA's : (ϕ) 0.61	No Mitigation with resulting Flame Deceleration	NMFD
Two X/F SRA's: (ϕ) 0.72	No Mitigation with resulting Flame Deceleration	NMFD
Two X/F SRA's: (ϕ) 0.95	No Mitigation with resulting Flame Acceleration	NMFA
Two X/F SRA's: (ϕ) 1.06	No Mitigation with resulting Flame Deceleration	NMFD

Table A9.25 : General event outcome (trial series A9.4.6)

A9.4.7 Three (X/F) Type C SRA's

A9.4.7.1 Trial set up

In this series of trials, three Type C SRA's were assembled and installed in position #1, #2 and #3 as previously shown in Figure A9.107 and Table A9.19. The atomisers were subjected to four trials with different methane-air mixtures of (ϕ) 0.61, 0.72, 0.95 and 1.06.

A9.4.x.2 Flame speed

Average flame speeds were measured both upstream and downstream of the spray region, which are illustrated in Figure A9.187 as flame speed reduction values. In this atomiser configuration, the propagating flame was extinguished and mitigated in the methane-air mixture of (ϕ) 0.61. This is shown in the diagram as a 100% flame speed reduction.

In the remaining three methane-mixtures all displayed a significant flame speed reduction from upstream and downstream of the spray region.

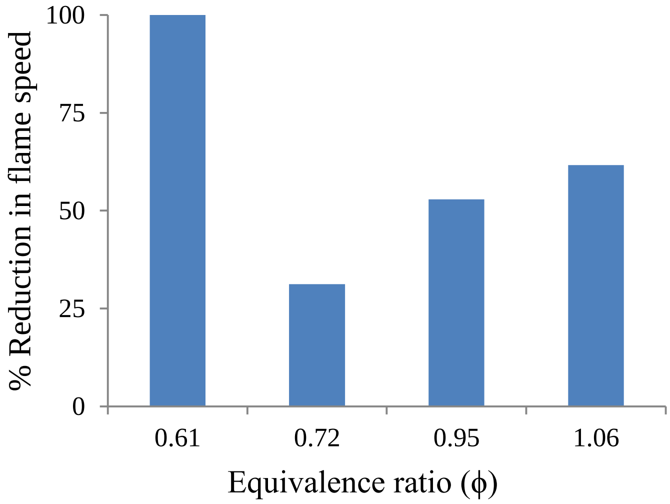

Figure A9.187 : Average flame speed reduction percentage (%) from upstream to downstream of three X/F SRA's in a various methane-air mixtures

A9.4.7.3 Time-temperature response

The representative time-temperature profiles presented in Figure A9.188 – A9.191 reinforce these flame speed reductions. In Figure A9.188, TC3, TC4 andTC5 display only display a slight increase of a ≤5˚C which indicates suspension of the combustion process. Each of the remaining time-temperature profiles reveal an initial decrease in temperature immediately downstream of the atomisers shown in the TC3 data, followed by a temperature increase at TC4 and further reduction at TC5.

(i) Equivalence ratio (ϕ) 0.61

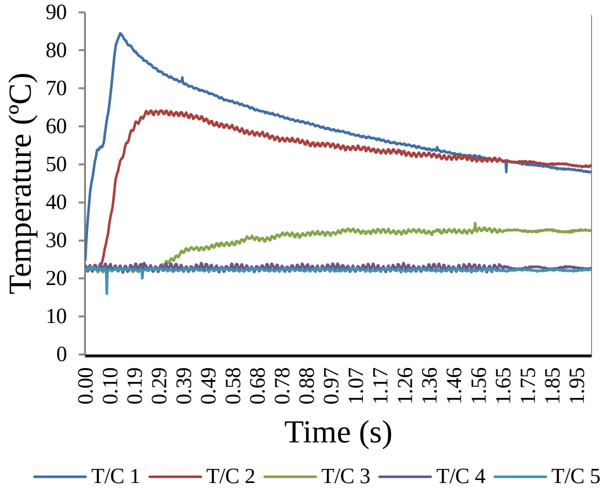

Figure A9.188 : Typical time-temperature profile for three SRA Type C in X/F arrangement with methane-air mixture of E.R. (ϕ) 0.61

(ii) Equivalence ratio (ϕ) 0.72

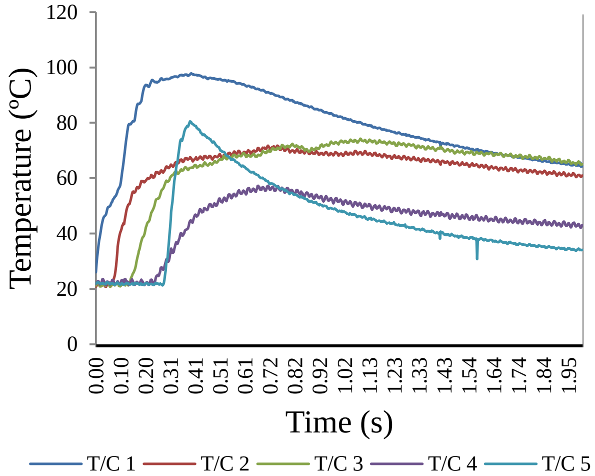

Figure A9.189 : Characteristic time-temperature profile for three SRA Type C in X/F arrangement with methane-air mixture of E.R. (ϕ) 0.72

Equivalence ratio (ϕ) 0.95

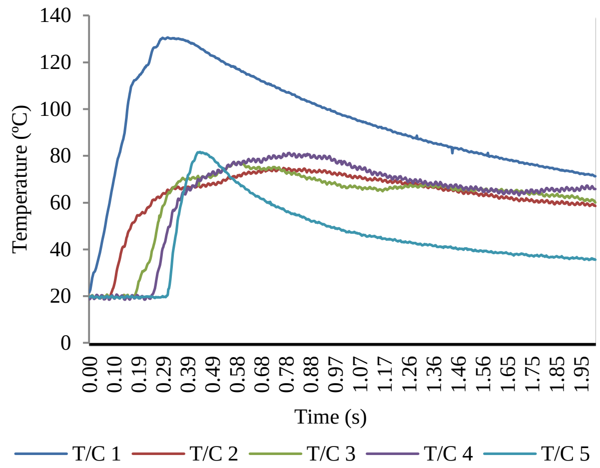

Figure A9.190 : Typical time-temperature profile for three SRA Type C in X/F arrangement with methane-air mixture of E.R. (ϕ) 0.95

(iv) Equivalence ratio (ϕ) 1.06

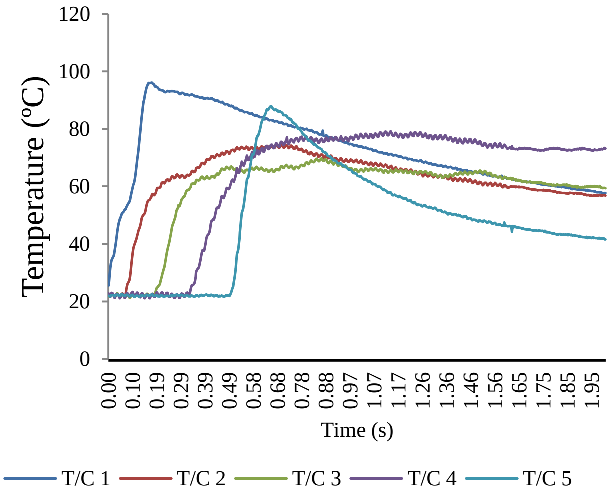

Figure A9.191 : Average time-temperature profile for three SRA Type C in X/F arrangement with methane-air mixture of E.R. (ϕ) 1.06

A9.4.7.3 Time-temperature response

In Figure A9.192 the methane-air mixture was (ϕ) 0.61. The progress of the flame can be observed in each of the frames i – iii, with no flame visible in (iv). Figure A9.188 (iii) has been highlighted and magnified in Figure A9.193 to emphasise the interaction of the sprays and reduction in flame area. There is clearly no indication of combustion beyond spray #3. The image presented in Figure A9.188 (iv) reveals the absence of any flame and global suspension of combustion.

In Figure A9.194 the methane-air mixture was (ϕ) 0.72. Figure A9.194 (iv) and Figure A9.195 show ‘dark’ regions in the flame signifying that combustion has been suspended locally.

In Figure A9.196 the methane-air mixture was (ϕ) 0.95. Figure A9.196 (iii) displays very similar behaviour to Figure A9.194, with dark areas visible in Figure A9.196 (iii) and Figure A9.197.

In Figure A9.198 the methane-air mixture was (ϕ) 1.06. Figure A9.198 (iii) also confirms localised suppression of the combustion, although the flame did continue to propagate.

It is clear that this current configuration of three cross flow Type C SRA’s is very close to the liquid volume flux threshold required for global mitigation, without relying on further droplet breakup.

The following Section will use the atomiser configuration of four cross flow Type C SRA’s, thus increasing the liquid volume flux by up to about 33%.

(i) Equivalence ratio (ϕ) 0.61

i. Flame propagating in methane-air mixture of E.R. (ϕ) 0.61 upstream of SRA

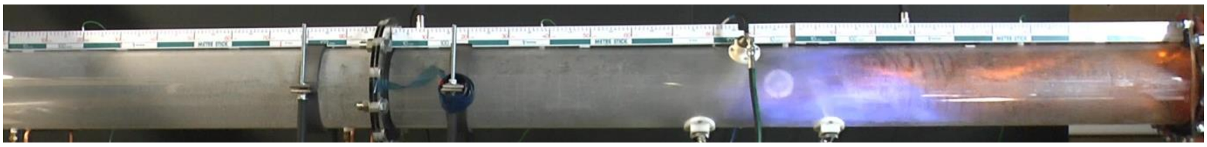

ii. Flame propagating in methane-air mixture of E.R. (ϕ) 0.61 upstream of SRA

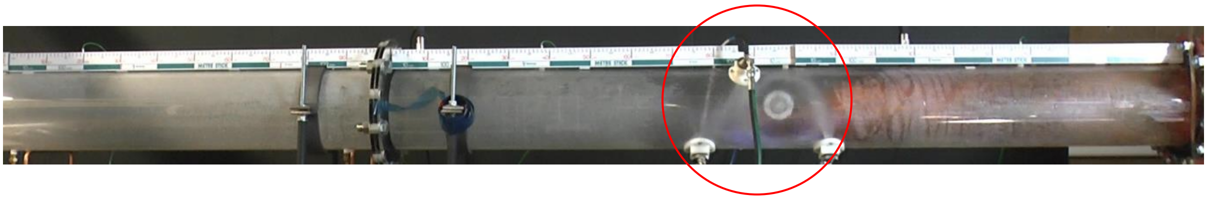

iii. **Mitigation** of flame in methane-air mixture of E.R. (ϕ) 0.61 in the region of spray

iv. **Mitigation** of flame in methane-air mixture of E.R. (ϕ) 0.61

Figure A9.192 : Flame propagating upstream of three X/F SRA Type C, with no combustion activity downstream for a methane-air mixture (ϕ) 0.61

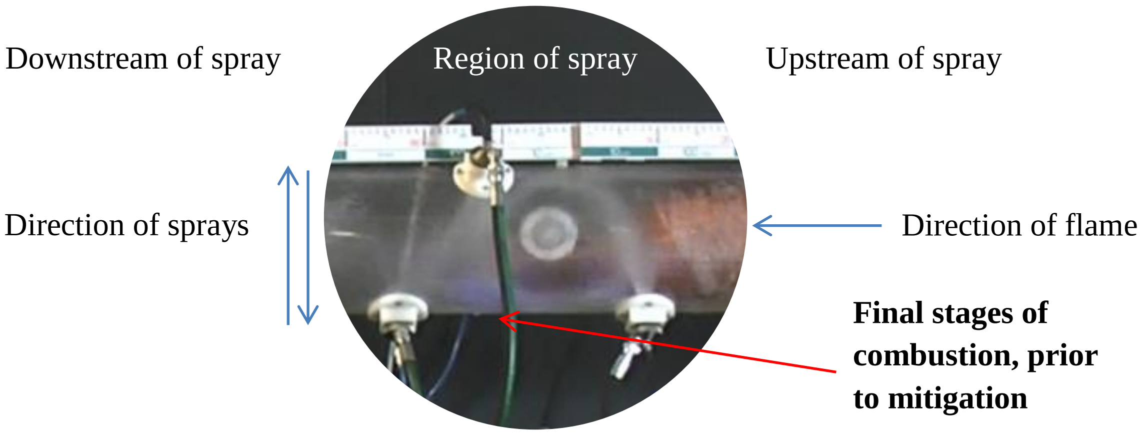

Figure A9.193 : Expanded view of region of spray highlighted in Figure A9.192(iii)

(ii) Equivalence ratio (ϕ) 0.72

i. Flame propagating in methane-air mixture of E.R. (ϕ) 0.72 upstream of SRA

ii. Flame propagating in methane-air mixture of E.R. (ϕ) 0.72 upstream of SRA

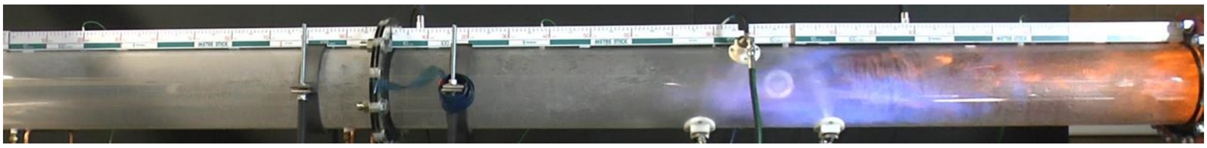

iii. Flame propagating in methane-air mixture of E.R. (ϕ) 0.72 in the region of spray

iv. Flame propagating in methane-air mixture of E.R. (ϕ) 0.72 downstream of SRA

Figure A9.194 : Flame propagating upstream and downstream of three X/F SRA Type C for a methane-air mixture (ϕ) 0.72

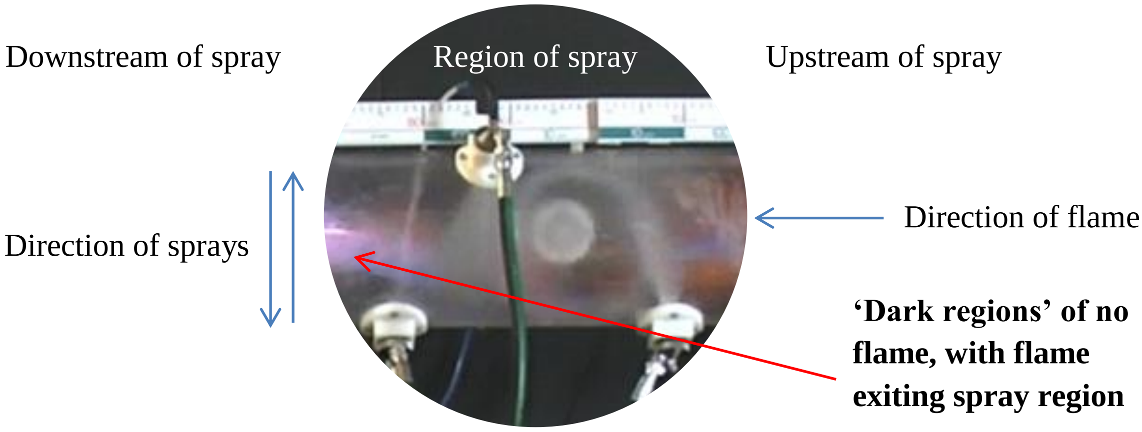

Figure A9.195 : Magnified view of region of spray highlighted in Figure A9.194(iv)

(iii) Equivalence ratio (ϕ) 0.95

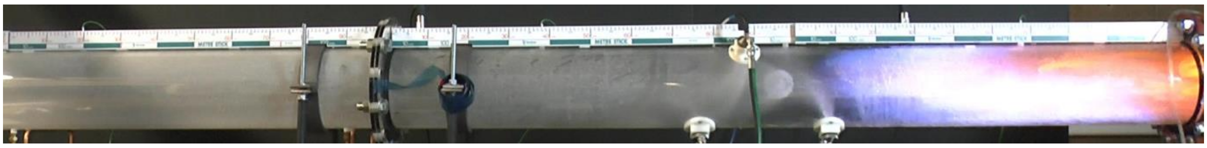

i. Flame propagating in methane-air mixture of E.R. (ϕ) 0.95 upstream of SRA

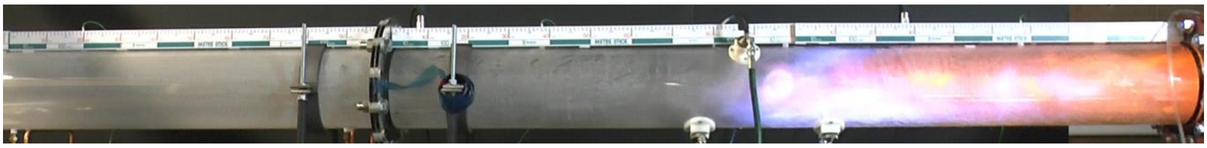

ii. Flame propagating in methane-air mixture of E.R. (ϕ) 0.95 upstream of SRA

iii. Flame propagating in methane-air mixture of E.R. (ϕ) 0.95 in the region of spray

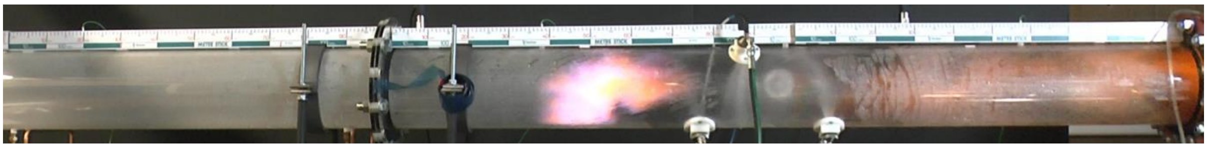

iv. Flame propagating in methane-air mixture of E.R. (ϕ) 0.95 downstream of SRA

Figure A9.196: Flame propagating upstream and downstream of three X/F SRA Type C for a methane-air mixture (ϕ) 0.95

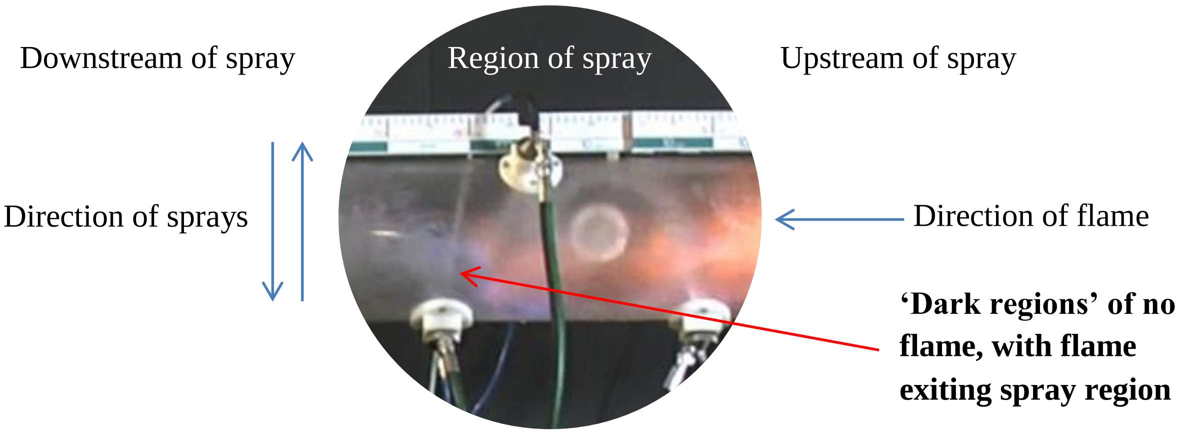

Figure A9.197 : Enlarged view of region of spray highlighted in Figure A9.196(iii)

(iv) Equivalence ratio (ϕ) 1.06

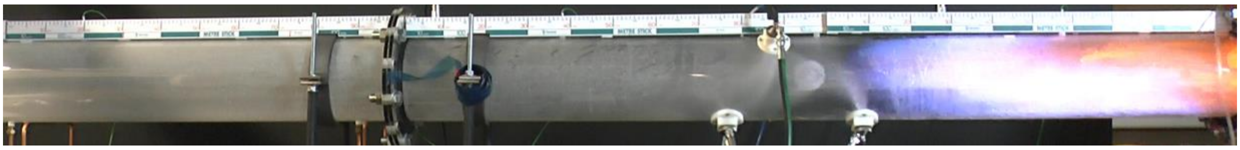

i. Flame propagating in methane-air mixture of E.R. (ϕ) 1.06 upstream of SRA

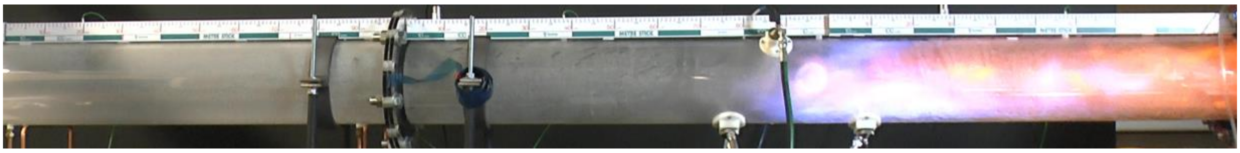

ii. Flame propagating in methane-air mixture of E.R. (ϕ) 1.06 upstream of SRA

iii. Flame propagating in methane-air mixture of E.R. (ϕ) 1.06 in the region of spray

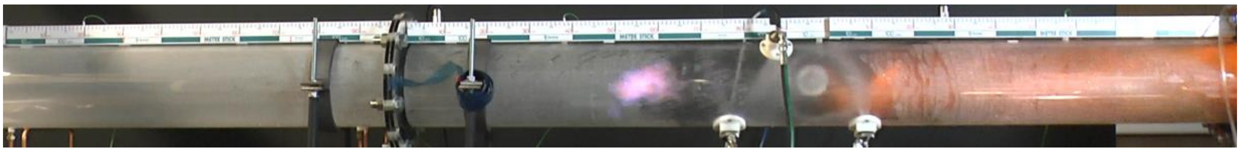

iv. Flame propagating in methane-air mixture of E.R. (ϕ) 1.06 downstream of SRA

Figure A9.198 : Flame propagating upstream and downstream of three X/F SRA Type C for a methane-air mixture (ϕ) 1.06

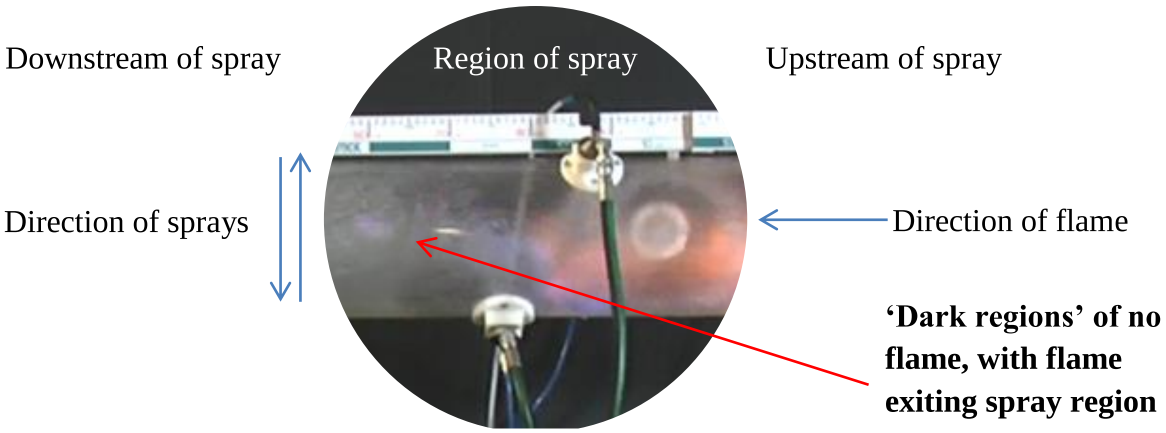

Figure A9.199: Expanded view of region of spray highlighted in Figure A9.198(iii)

A9.4.7.5 General event outcome

Table A9.26 provides a summary of the **'general event outcome'** for each trial in this current series, using the five potential 'outcome' categories offered in Chapter 5. The results of all 'hot trials' were previously given in Table 5.14 and are also shown in Table A9.45.

Trial configuration	General event outcome	Code
Three X/F SRA : (ϕ) 0.61	Full Mitigation resulting in Flame Extinguishment	FMFE
Three X/F SRA : (ϕ) 0.72	No Mitigation with resulting Flame Deceleration	NMFD
Three X/F SRA : (ϕ) 0.95	No Mitigation with resulting Flame Deceleration	NMFD
Three X/F SRA : (ϕ) 1.06	No Mitigation with resulting Flame Deceleration	NMFD

Table A9.26 : General event outcome (trial series A9.4.7)

A9.4.8 Four (X/F) Type C SRA’s

A9.4.8.1 Trial set up

In this series, of trials four Type C SRA’s were assembled and installed in position #1, #2, #3 and 4 as previously shown in Figure A9.107 and Table A9.19. The atomisers were subjected to four trials with different methane-air mixtures, of (ϕ) 0.61, 0.72, 0.95 and 1.06.

A9.4.8.2 Flame speed

Average flame speeds were measured both upstream and downstream of the spray region, which are illustrated in Figure A9.200 as flame speed reduction values. In this atomiser configuration the methane-air mixtures of (ϕ) 0.61, 0.72, 0.95 and 1.06 were fully mitigated.

The mitigation is shown in the diagram as a 100% flame speed reduction, with this being the only SRA configuration with resulting successful mitigation of all four methane-air mixtures

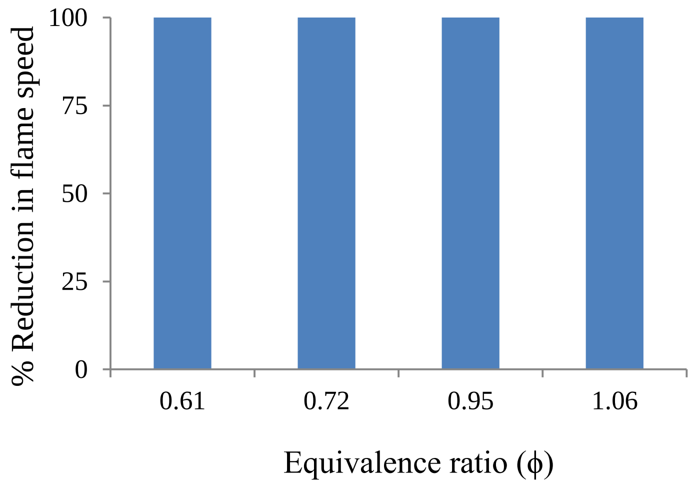

Figure A9.200 : Average flame speed reduction percentage (%) from upstream to downstream of four X/F SRA’s in a various methane-air mixtures

A9.4.8.3 Time-temperature response

The typical time-temperature profiles presented in Figure A9.201 - A9.204 reinforce the mitigation events in all four methane-air mixtures, with TC5 only indicating a slight increase of $\leq 5^{\circ}C$, thus indicating global suspension of the combustion process.

(i) Equivalence ratio (ϕ) 0.61

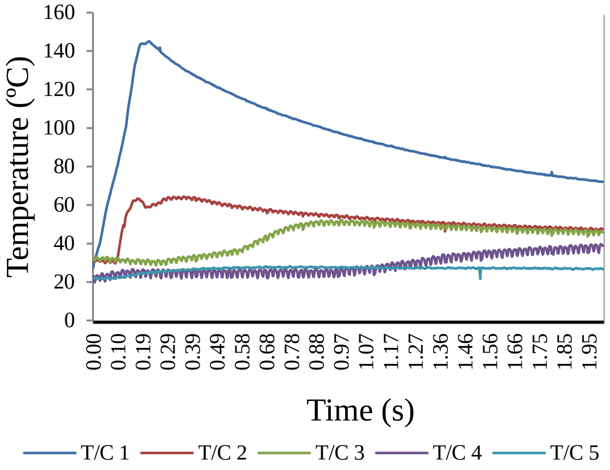

Figure A9.201 : Typical time-temperature profile for four SRA Type C in X/F arrangement with methane-air mixture of E.R. (ϕ) 0.61

(ii) Equivalence ratio (ϕ) 0.72

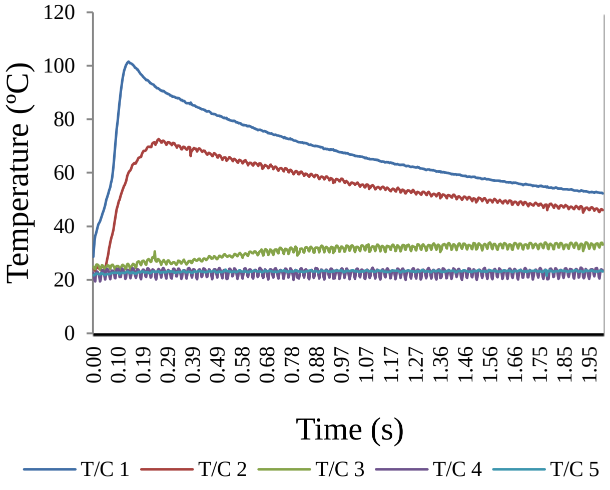

Figure A9.202 : Characteristic time-temperature profile for four SRA Type C in X/F arrangement with methane-air mixture of E.R. (ϕ) 0.72

(iii) Equivalence ratio (ϕ) 0.95

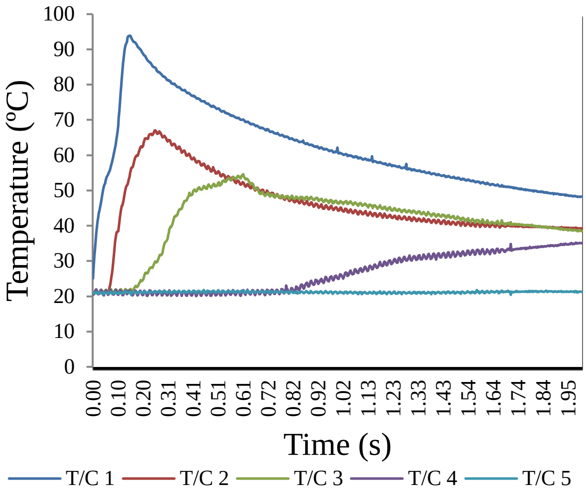

Figure A9.203 : Typical time-temperature profile for four SRA Type C in X/F arrangement with methane-air mixture of E.R. (ϕ) 0.95

(iv) Equivalence ratio (ϕ) 1.06

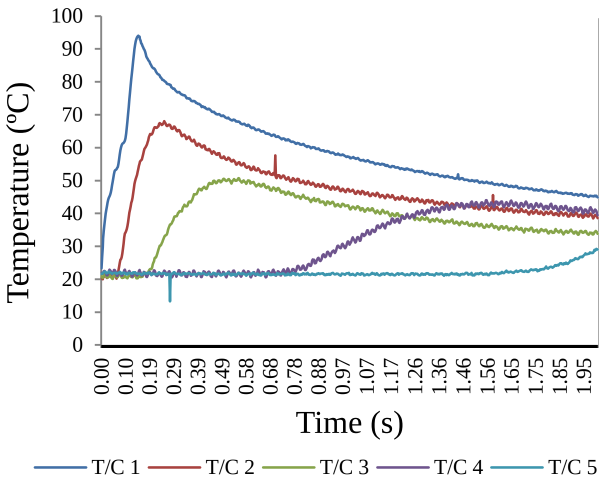

Figure A9.204 : Average time-temperature profile for four SRA Type C in X/F arrangement with methane-air mixture of E.R. (ϕ) 1.06

A9.4.8.4 Qualitative analysis

In Figure A9.205 the methane-air mixture was (ϕ) 0.61, whereby the flame is seen to approach the sprays in Figure A9.205(i) and (ii). In Figure A9.205(iii) and (iv) combustion has been mitigated.

In Figure A9.207 the methane-air mixture was (ϕ) 0.72. Figure A9.203(iv) the flame appears to exit the sprays, however it did not propagate in the downstream mixture In this case the flame was mitigated.

In Figure A9.209 the methane-air mixture was (ϕ) 0.95. The flame was mitigated in Figure A9.209 (ii - iii) and did not re-occur in the downstream mixture.

In Figure A9.211 the methane-air mixture was (ϕ) 1.06. Figure A9.207 (iii) shows the final stages of combustion prior to mitigation.

(i) Equivalence ratio (ϕ) 0.61

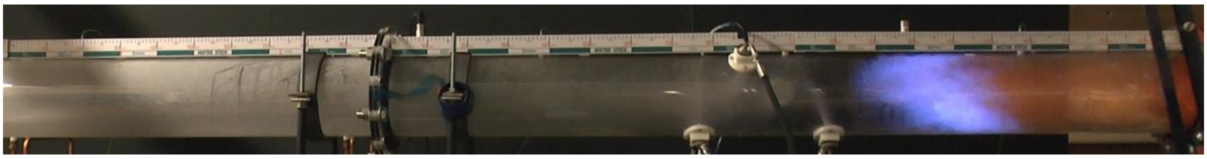

i. Flame propagating in methane-air mixture of E.R. (ϕ) 0.61 upstream of SRA

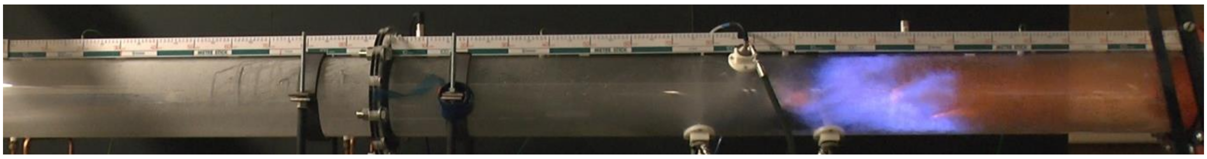

ii. Flame propagating in methane-air mixture of E.R. (ϕ) 0.61 upstream of SRA

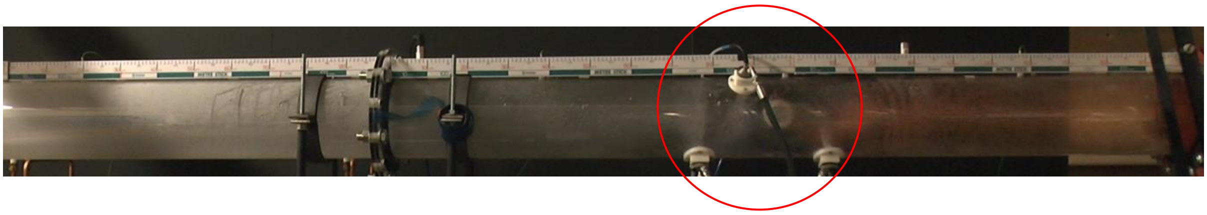

iii. **Mitigation** in methane-air mixture of E.R. (ϕ) 0.61 in the region of spray

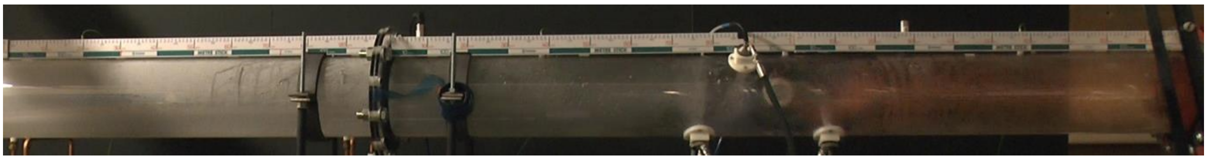

iv. **Mitigation** in methane-air mixture of E.R. (ϕ) 0.61

Figure A9.205 : Flame propagating upstream of four X/F SRA Type C, with no combustion activity downstream for a methane-air mixture (ϕ) 0.61

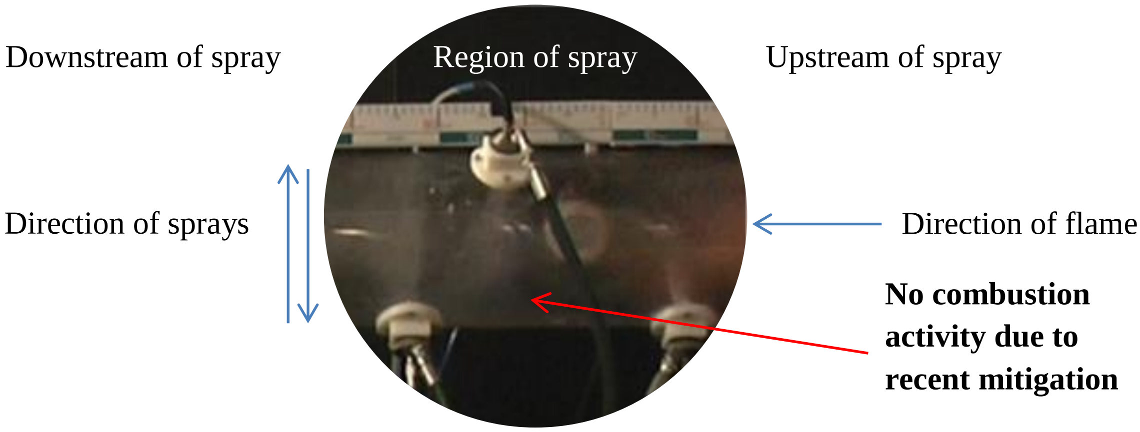

Figure A9.206: Expanded view of region of spray highlighted in Figure A9.205(iii)

(ii) Equivalence ratio (ϕ) 0.72

i. Flame propagating in methane-air mixture of E.R. (ϕ) 0.72 upstream of SRA

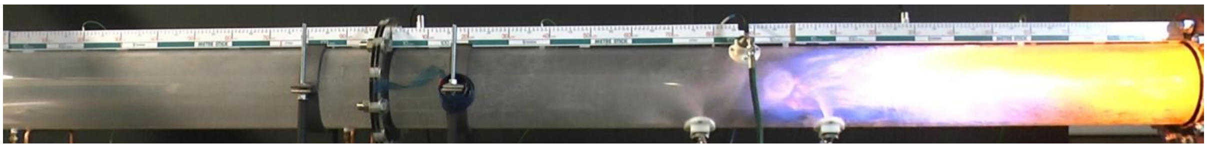

ii. Flame propagating in methane-air mixture of E.R. (ϕ) 0.72 upstream of SRA

iii. Flame propagating in methane-air mixture of E.R. (ϕ) 0.72 in the region of spray

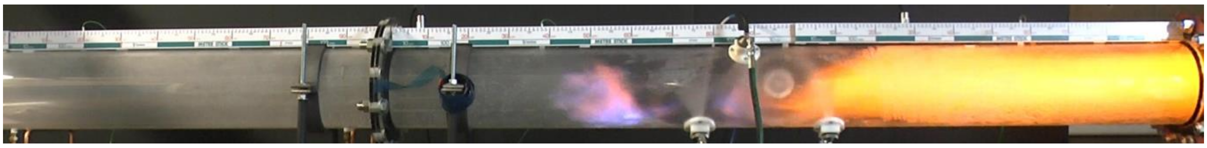

iv. Flame propagating in methane-air mixture of E.R. (ϕ) 0.72 downstream of SRA

Figure A9.207 : Flame propagating upstream of four X/F SRA Type C, with no combustion activity downstream of (iv) for a methane-air mixture (ϕ) 0.72

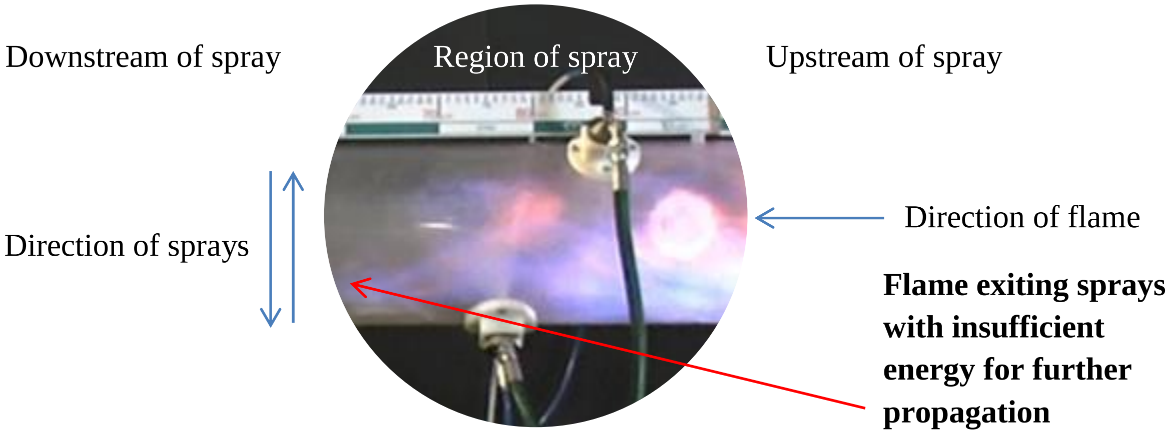

Figure A9.208 : Expanded view of region of spray highlighted in Figure A9.207(iii)

(iii) Equivalence ratio (ϕ) 0.95

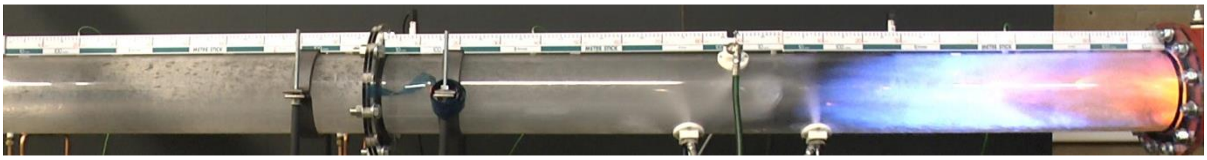

i. Flame propagating in methane-air mixture of E.R. (ϕ) 0.95 upstream of SRA

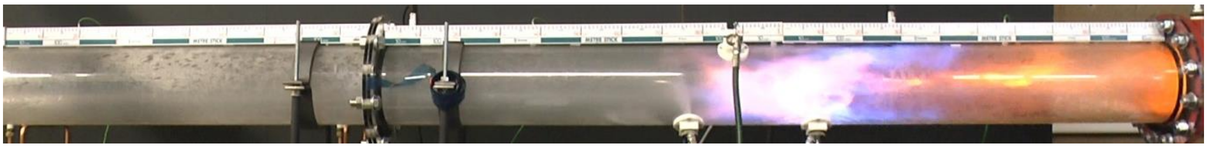

ii. Flame propagating in methane-air mixture of E.R. (ϕ) 0.95 upstream of SRA

iii. Flame propagating in methane-air mixture of E.R. (ϕ) 0.95 in the region of spray

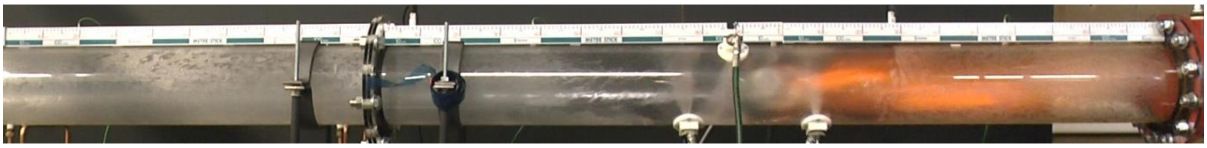

iv. **Mitigation** in methane-air mixture of E.R. (ϕ) 0.95 downstream of SRA

Figure A9.209 : Flame propagating upstream of four X/F SRA Type C, with no combustion activity downstream for a methane-air mixture (ϕ) 0.95

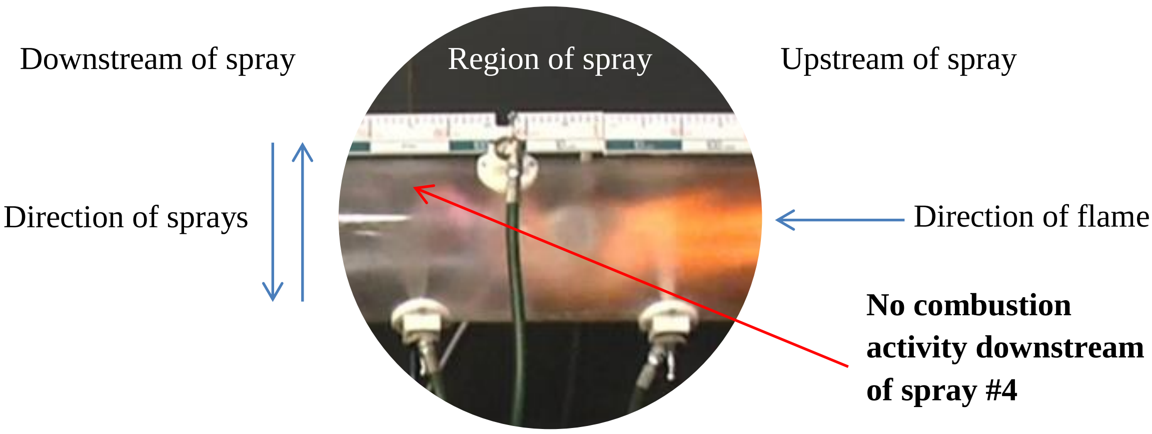

Figure A9.210 : Close up view of region of spray highlighted in Figure A9.209(iii)

(iv) Equivalence ratio (ϕ) 1.06

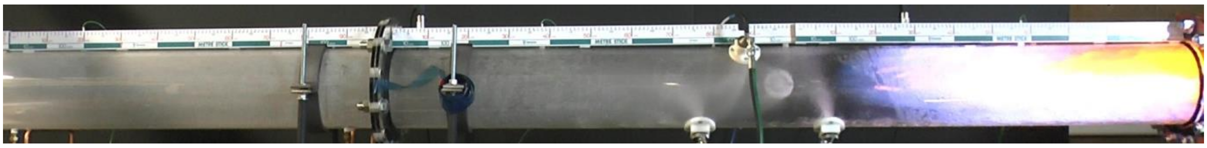

i. Flame propagating in methane-air mixture of E.R. (ϕ) 1.06 upstream of SRA

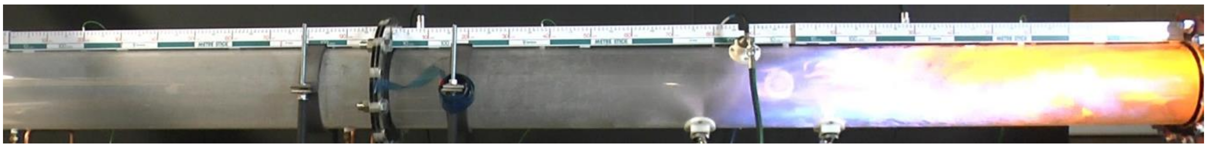

ii. Flame propagating in methane-air mixture of E.R. (ϕ) 1.06 upstream of SRA

iii. **Mitigation** in methane-air mixture of E.R. (ϕ) 1.06 in the region of spray

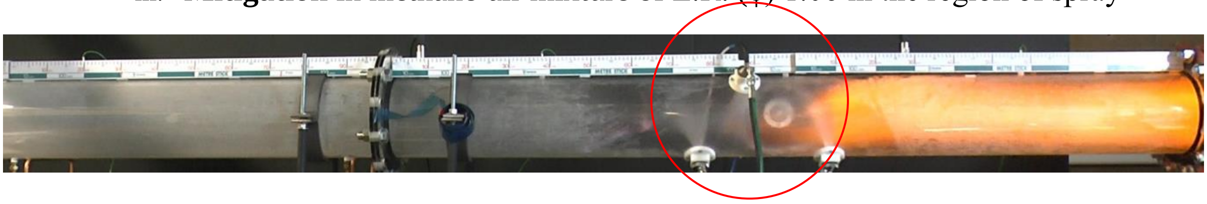

iv. **No further combustion activity** in mixture E.R. (ϕ) 1.06 downstream of SRA

Figure A9.211 : Flame propagating upstream of four X/F SRA Type C, with no combustion activity downstream for a methane-air mixture (ϕ) 1.06

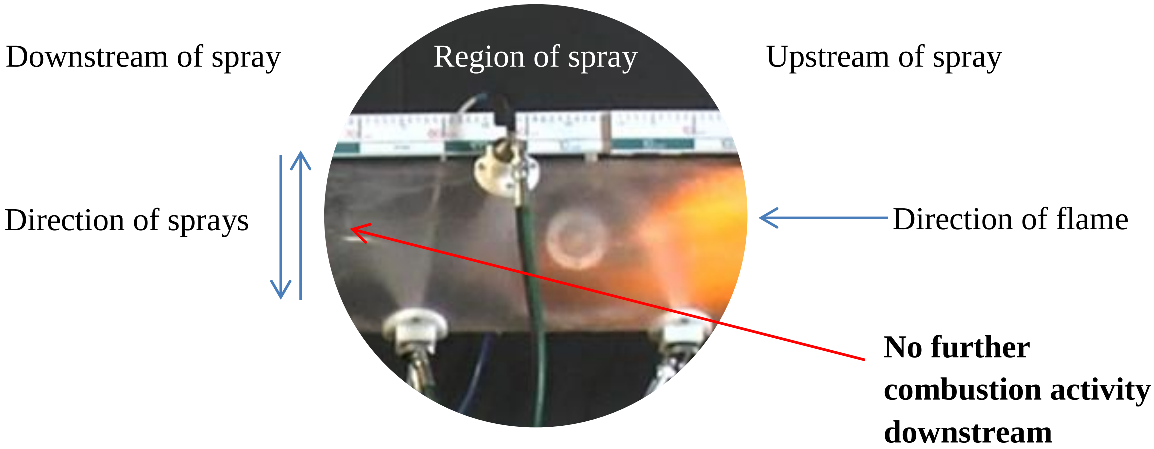

Figure A9.212 : Enlarged view of region of spray highlighted in Figure A9.211(iv)

A9.4.8.5 General event outcome

Table A9.27 provides a summary of the **'general event outcome'** for each trial in this current series, using the five potential 'outcome' categories offered in Chapter 5. The results of all 'hot trials' were previously given in Table 5.14 and are also shown in Table A9.45.

Trial configuration	General event outcome	Code
Four X/F SRA's :(ϕ) 0.61	Full Mitigation resulting in Flame Extinguishment	FMFE
Four X/F SRA's :(ϕ) 0.72	Full Mitigation resulting in Flame Extinguishment	FMFE
Four X/F SRA's :(ϕ) 0.95	Full Mitigation resulting in Flame Extinguishment	FMFE
Four X/F SRA's :(ϕ) 1.06	Full Mitigation resulting in Flame Extinguishment	FMFE

Table A9.27 : General event outcome (trial series A9.4.8)

Following the 100% mitigation success rate attributed to this 'four cross flow (X/F) Type C SRA's' arrangement, the subsequent Sections will consider the effects of four cross flow (X/F) SRA's with:-

i. SRA Type B and Type C combinations
ii. Variable water supply pressure
iii. Variable water supply temperature
iv. Methane 'rich' methane-air mixtures
v. Propane-air mixtures

A9.5 SRA Type B and C combinations using variable water temperatures and supply pressures

The pre-assembled spill return atomisers and external water feed pipework were installed in the explosion and mitigation tube, in accordance with Figure A9.213 and Table A9.28. The water pump was adjusted and set to deliver the required pressure for each particular experiment. The thermocouples were positioned in accordance with Figure A9.28 and Table A9.28.

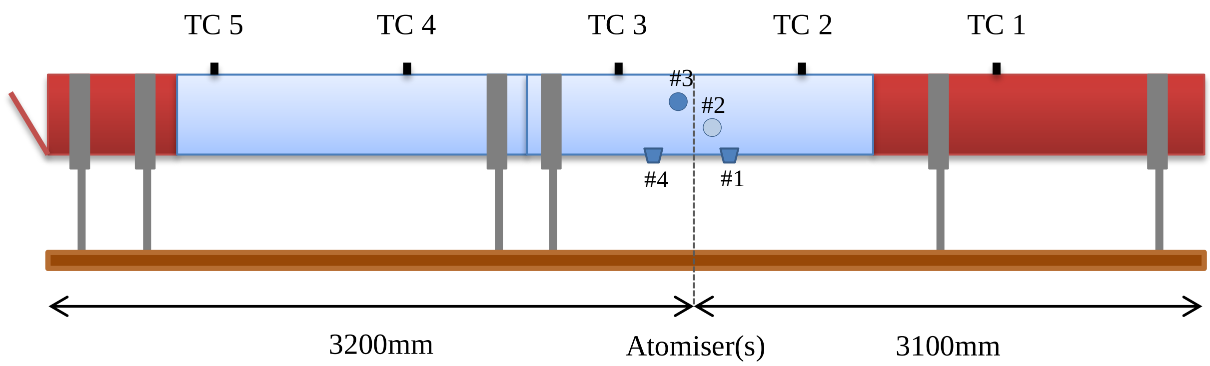

Figure A9.213 : Position of atomiser and thermocouples (relative to right hand ignition end)

Component	Position (measured from right hand end)
Thermocouple (TC1)	1200mm
Thermocouple (TC2)	2400mm
Thermocouple (TC3)	3600mm
Thermocouple (TC4)	4800mm
Thermocouple (TC5)	6000mm
Atomiser outlet orifice (cross flow)	3100mm (centre of sprays)

Table A9.28 : Measured position of thermocouples and SRA’s

A9.5.1 Four (X/F) SRA's : combination of Type B and Type C

A9.5.1.1 Trial set up

In this series of cross flow trials four atomisers consisting of an assortment of Type B and Type C SRA's were used in each case to evaluate the effect of variations in liquid volume flux and droplet size within the spray region.

In these tests four SRA's were assembled to include a:-

i. Four atomisers (#1, #2, #3 and #4) with a combination of Type B and Type C SRA's
ii. A range of operating pressures

A9.5.1.2 Flame speed

Figure A9.214 shows the typical flame speed reductions for the various multiple SRA combinations and pressures in this series. The atomiser cluster with the greatest contribution to flame speed reduction consisted of three Type C and one Type B SRA's, which affected a flame speed reduction of approximately 36% when operated at 13MPa. However, the same combination of atomisers subsequently subjected to a water operating pressure of 15MPa which resulted in an increase in average flame speed of about 28%.

The increase in water pressure and flow rate had a direct influence on the effects of induced turbulence in the unburned mixture, with the increase in water pressure from 13MPA to 15MPa causing such a dramatic effect.

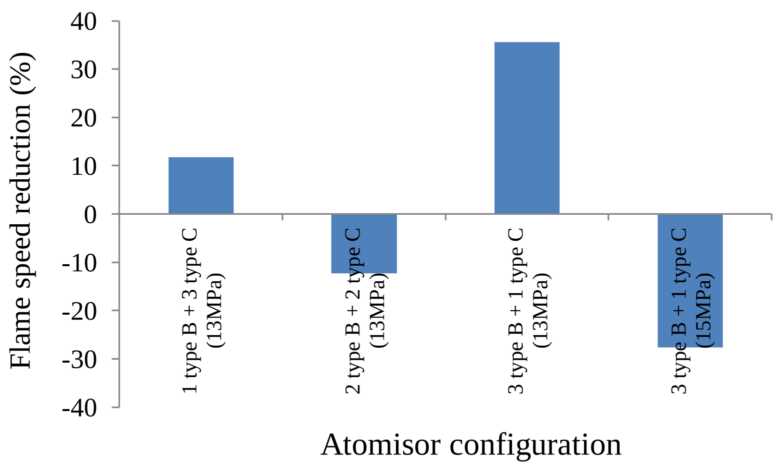

Figure A9.214 : Typical flame speed reductions for various multiple SRA combinations and pressures

As a result of this series of trials it is reasonable to suggest that small exit orifices at high operating pressures have a greater potential to disrupt unburned mixture flows and atomisers consisting of larger exit orifices at lower pressures, even though their volume flux values may be similar. Therefore in this current work, the use of Type C SRA’s is likely to favour the use of Type B SRA’s.

A9.5.1.3 Time-temperature response

The time-temperature profiles produced for each of the trials in this series are shown in Figure A9.215 – Figure A9.218. In all of the profiles the thermocouples downstream of the sprays exhibit consistent trends with respect to the flame speed reduction percentage shown previously in A9.214.

Figure A9.218 in particular demonstrates the increase in combustion activity and flame temperature with the difference in temperature observed between TC3 and TC5.

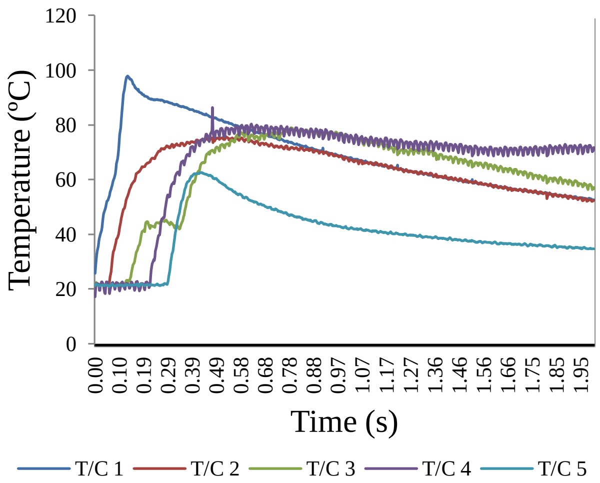

Figure A9.215 : Typical time-temperature profile for three Type C and one Type B SRA's operating at 13MPa – E.R.(ϕ) 0.95

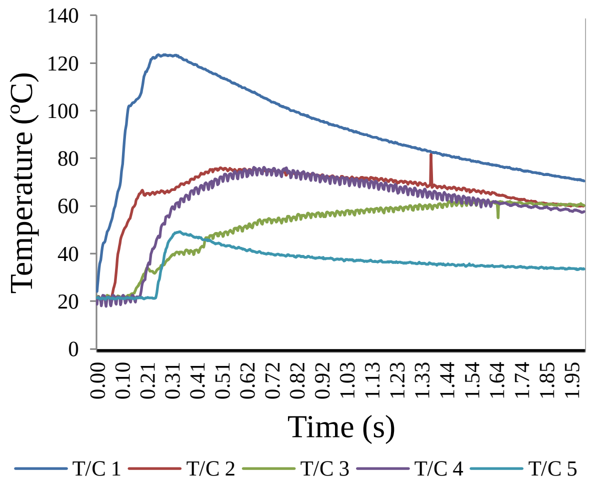

Figure A9.216 : Representative time-temperature profile for two Type C and two Type B SRA's operating at 13MPa – E.R.(ϕ) 0.95

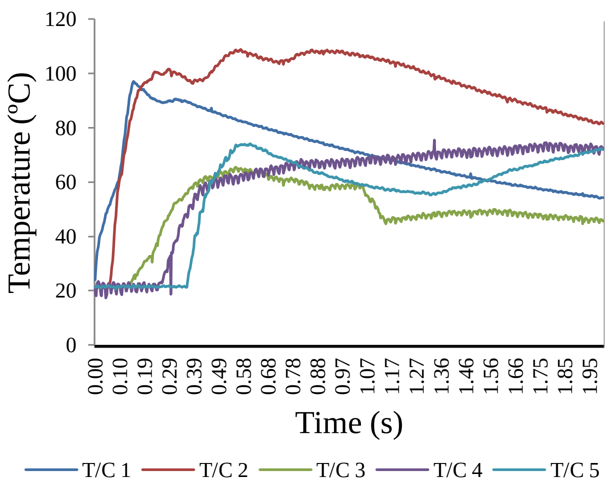

Figure A9.317 : Distinctive time-temperature profile for one Type C and three Type B SRA's operating at 13MPa – E.R.(ϕ) 0.95

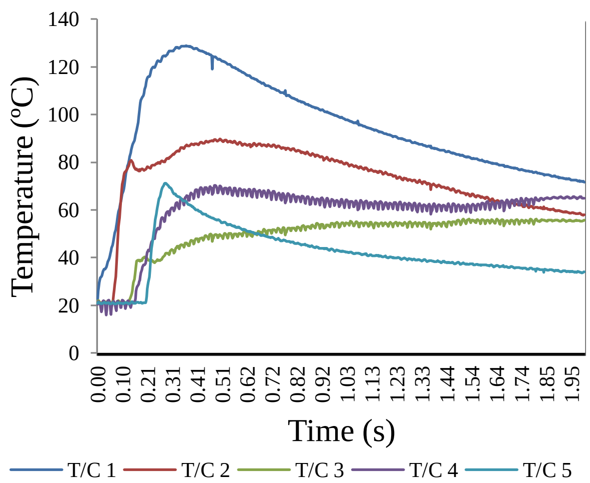

Figure A9.218 : Characteristic time-temperature profile for one Type C and three Type B SRA's operating at 14MPa – E.R 0.95

A9.5.1.4 Qualitative analysis

(i) Three Type C and one Type B SRA's – 13MPa

The still images relating to this configuration can be observed in Figure A9.219 and Figure A9.220. The flame was almost fully mitigated in the spray region, however some of the flame passed through the sprays subsequently re-establishing itself downstream. The downstream flame speed was approximately 12% less than the upstream flame speed.

(ii) Two Type C and two Type B SRA's – 13MPa

The still images relating to this configuration can be observed in Figure A9.221 and Figure A9.222. Again flame was nearly mitigated in the spray region, however some of the flame passed through the sprays consequently re-establishing itself downstream. The downstream flame speed was approximately 12% greater than the upstream flame speed.

(iii) One Type C and three Type B SRA's – 13MPa

The still images relating to this configuration can be observed in Figure A9.223 and Figure A9.224. The flame passed through the spray region, however there were large dark regions present indicating localised suspension of combustion activity. The downstream flame speed was approximately 36% less than the upstream flame speed.

(iv) One Type C and three Type B SRA's – 15MPa

The still images relating to this configuration can be observed in Figure A9.225 and Figure A9.226. As the flame passed through the spray there are dark regions of localised suspension of combustion activity, however there appears to be a high level of activity in the flame caused by the turbulent disturbance initiated by the high velocity sprays. The downstream flame speed was approximately 28% greater than the upstream flame speed.

(i) Three Type C and one Type B SRA's – 13MPa

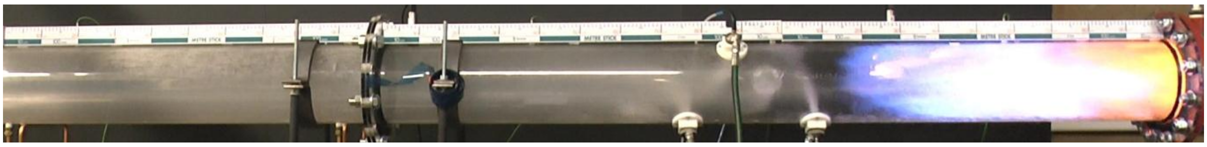

i. Flame propagating in methane-air mixture of E.R. (ϕ) 0.95upstream of SRA

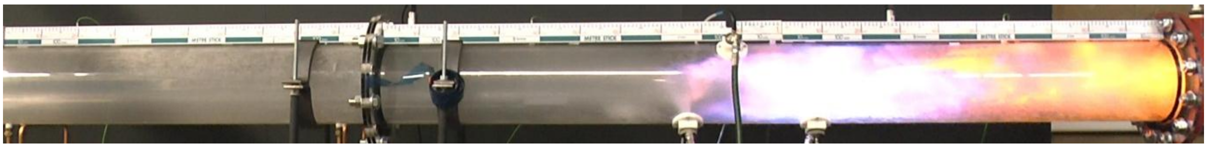

ii. Flame propagating in methane-air mixture of E.R. (ϕ) 0.95 upstream of SRA

iii. Flame propagating in methane-air mixture of E.R. (ϕ) 0.95in the region of spray

iv. Flame propagating in methane-air mixture of E.R. (ϕ) 0.95 downstream of SRA

Figure A9.219 : Flame propagating upstream and downstream of 3 Type C and 1 Type B cross flow SRA's in a methane-air mixture (ϕ) 0.95

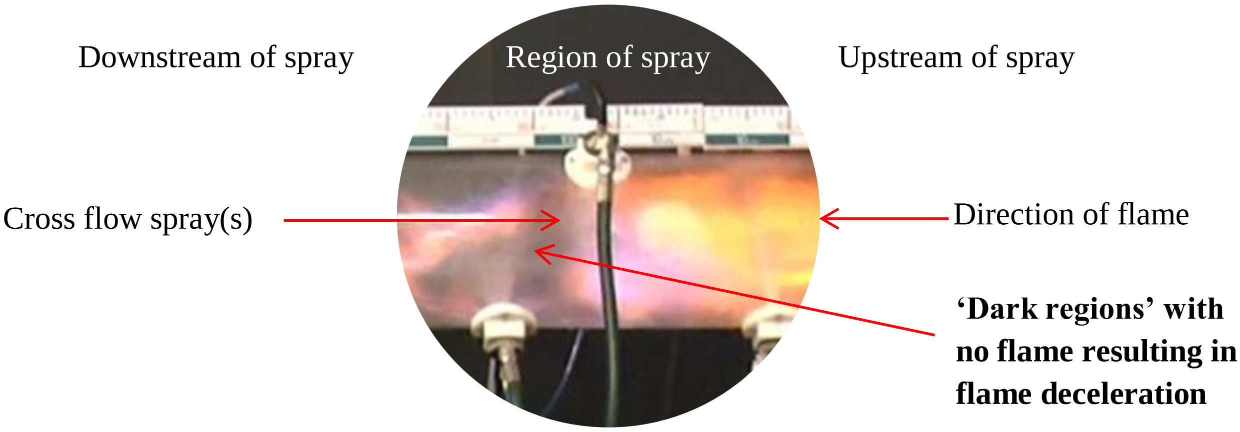

Figure A9.220 : Expanded view of region of spray highlighted in Figure A9.219(iii)

(ii) Two Type C and two Type B SRA's – 13MPa

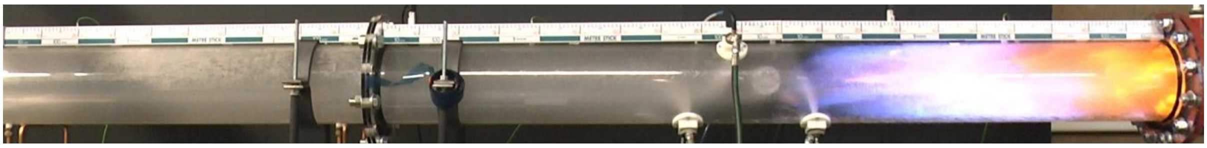

i. Flame propagating in methane-air mixture of E.R. (ϕ) 0.95upstream of SRA

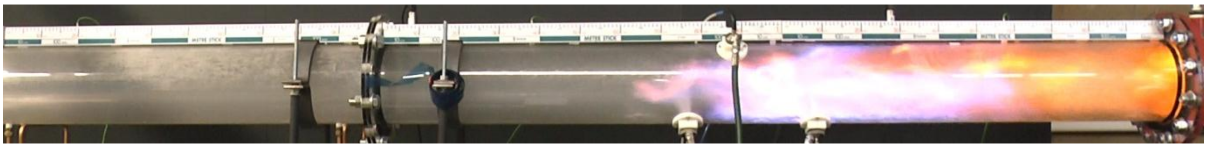

ii. Flame propagating in methane-air mixture of E.R. (ϕ) 0.95 upstream of SRA

iii. Flame propagating in methane-air mixture of E.R. (ϕ) 0.95in the region of spray

iv. Flame propagating in methane-air mixture of E.R. (ϕ) 0.95 downstream of SRA

Figure A9.221: Flame propagating upstream and downstream of 3 Type C and 1 Type B cross flow SRA's in a methane-air mixture (ϕ) 0.95

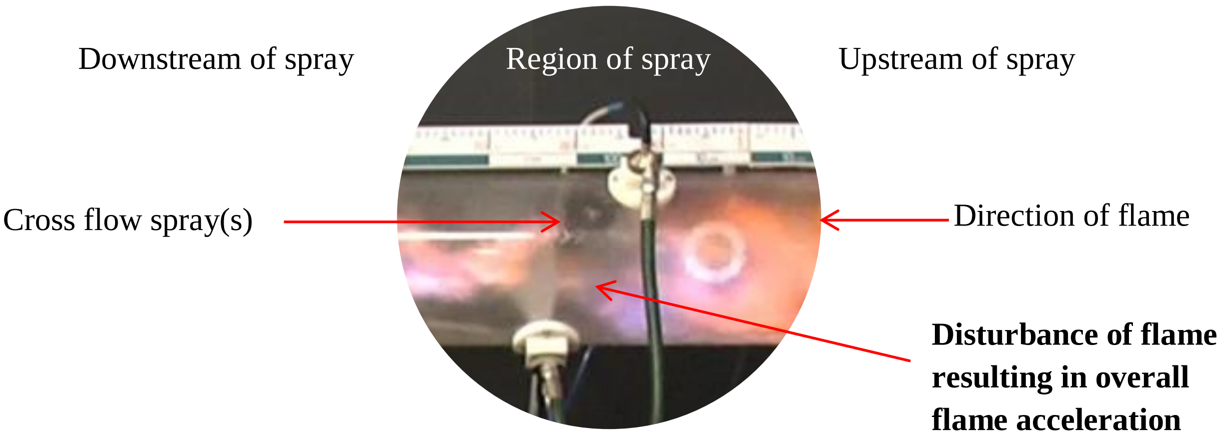

Figure A9.222 : Enlarged view of region of spray highlighted in Figure A9.221(iii)

(iii) One Type C and three Type B SRA's – 13MPa

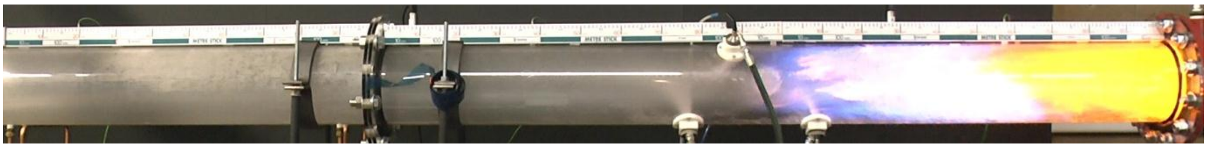

i. Flame propagating in methane-air mixture of E.R. (ϕ) 0.95upstream of SRA

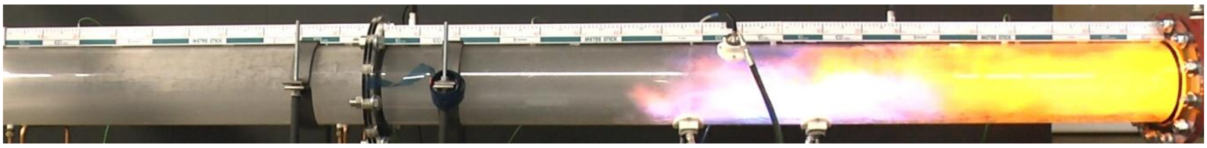

ii. Flame propagating in methane-air mixture of E.R. (ϕ) 0.95 upstream of SRA

iii. Flame propagating in methane-air mixture of E.R. (ϕ) 0.95in the region of spray

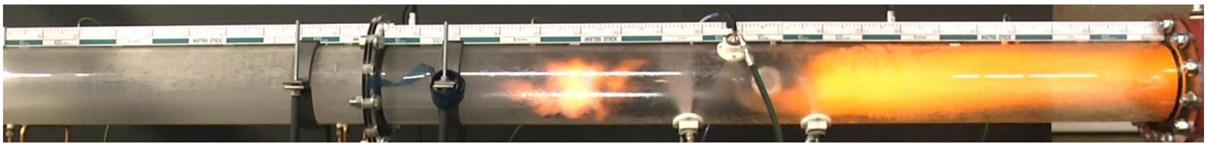

iv. Flame propagating in methane-air mixture of E.R. (ϕ) 0.95 downstream of SRA

Figure A9.223 : Flame propagating upstream and downstream of 3 Type C and 1 Type B cross flow SRA's in a methane-air mixture (ϕ) 0.95

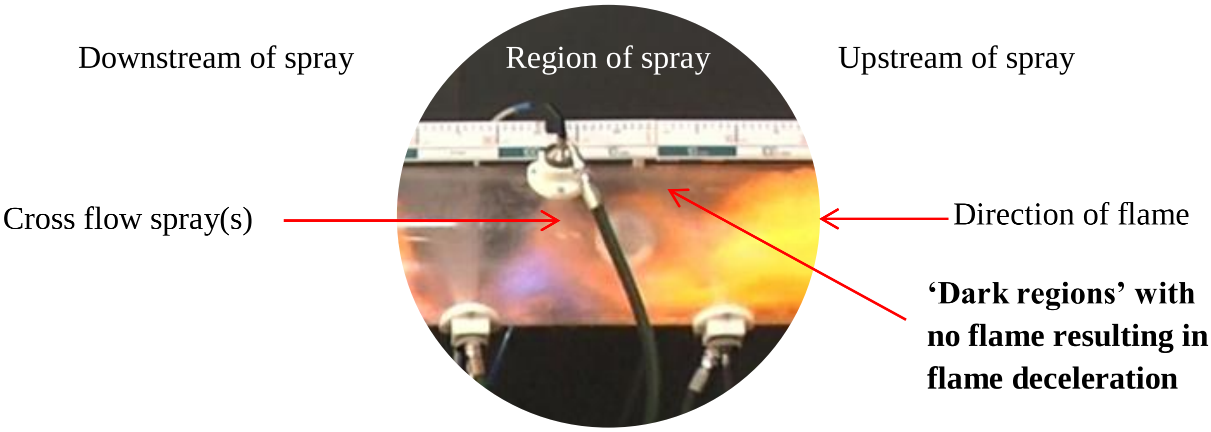

Figure A9.224: Magnified view of region of spray highlighted in Figure A9.223(iii)

(iv) One Type C and three Type B SRA's – 15MPa

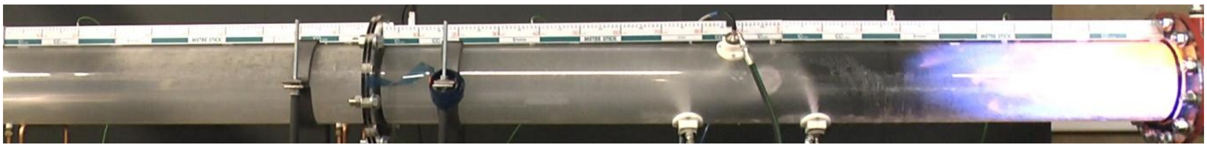

i. Flame propagating in methane-air mixture of E.R. (ϕ) 0.95upstream of SRA

ii. Flame propagating in methane-air mixture of E.R. (ϕ) 0.95 upstream of SRA

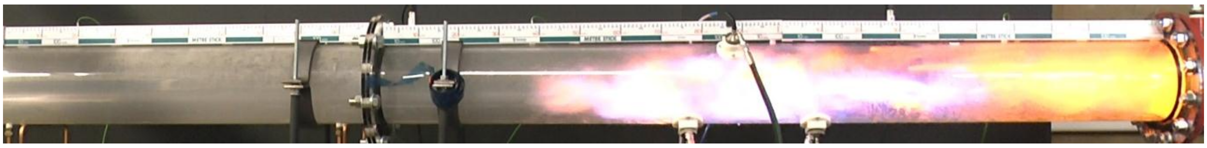

iii. Flame propagating in methane-air mixture of E.R. (ϕ) 0.95in the region of spray

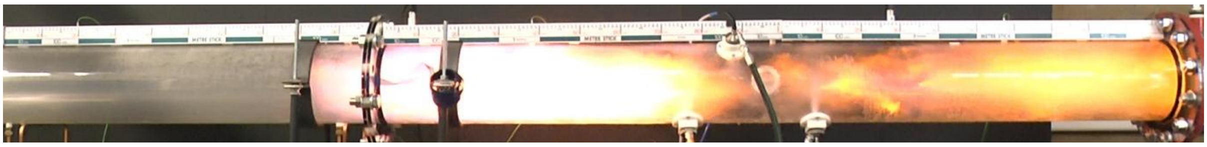

iv. Flame propagating in methane-air mixture of E.R. (ϕ) 0.95 downstream of SRA

Figure A9.225: Flame propagating upstream and downstream of 3 Type C and 1 Type B cross flow SRA's in a methane-air mixture (ϕ) 0.95

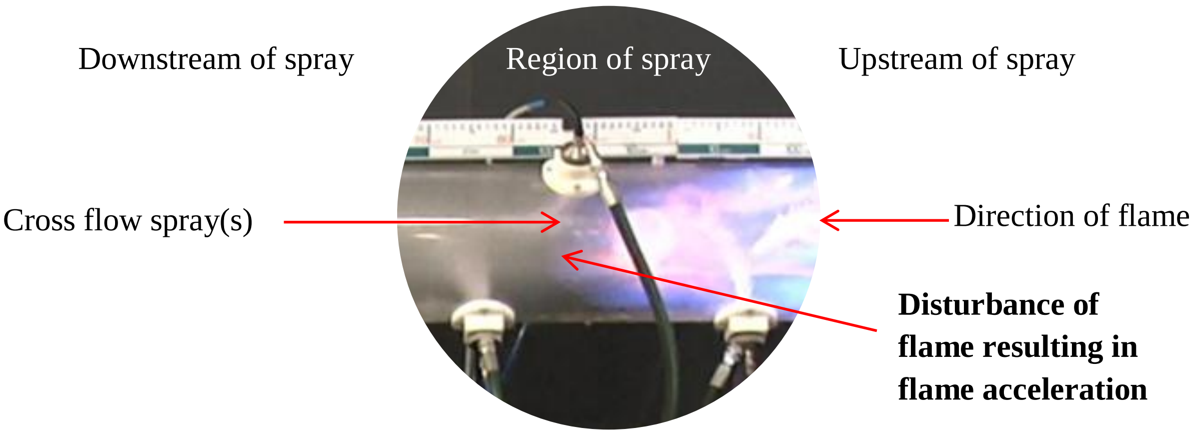

Figure A9.226 : Close up view of region of spray highlighted in Figure A9.225(ii)

A9.5.1.5 General event outcome

Table A9.29 provides a summary of the **'general event outcome'** for each trial in this current series, using the five potential 'outcome' categories offered in Chapter 5. The results of all 'hot trials' were previously given in Table 5.14 and are also shown in Table A9.45.

Trial configuration	General event outcome	Code
Single X/F SRA : (ϕ) 0.61	No Mitigation with resulting Flame Deceleration	NMFD
Single X/F SRA : (ϕ) 0.72	No Mitigation with resulting Flame Acceleration	NMFA
Single X/F SRA : (ϕ) 0.95	No Mitigation with resulting Flame Deceleration	NMFD
Single X/F SRA : (ϕ) 1.06	No Mitigation with resulting Flame Acceleration	NMFA

Table A9.29 : General event outcome (trial series A9.5.1)

A9.5.2 Three (X/F) Type C SRA's using various water supply pressures

A9.5.2.1 Trial set up

In this series of experimental trials three cross flow (X/F) Type C SRA's were assembled and supplied with de-ionised water at 20°C. The aim was to evaluate the effects of increased water pressure and whether conditions would favour those required for mitigation, or whether such an increase would contribute towards additional induced turbulence in the flammable mixture ahead of the flame in a methane-air mixture of E.R. (ϕ) 0.95. Positions of thermocouples and atomisers are illustrated in Figure A9.227 and Table A9.31.

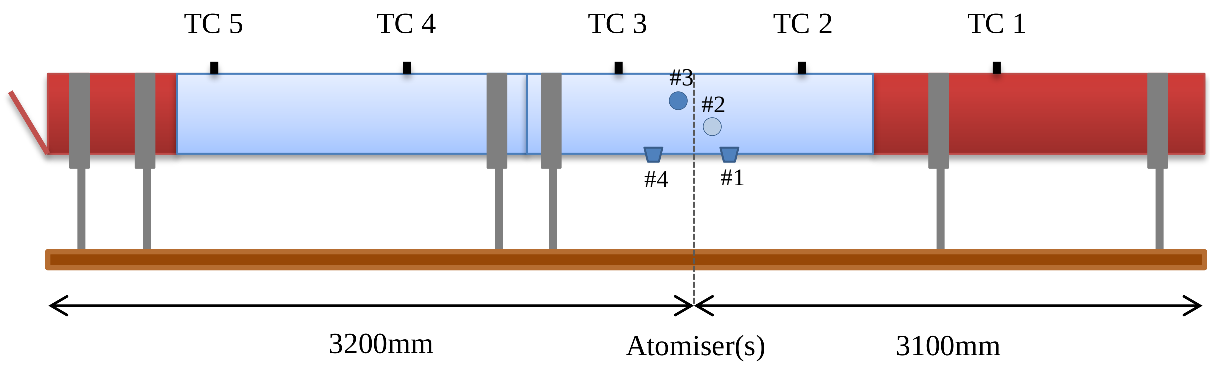

Figure A9.227 : Position of atomiser and thermocouples (relative to right hand ignition)

Component	Position (measured from right hand end)
Thermocouple (TC1)	1200mm
Thermocouple (TC2)	2400mm
Thermocouple (TC3)	3600mm
Thermocouple (TC4)	4800mm
Thermocouple (TC5)	6000mm
Atomiser outlet orifice (cross flow)	3100mm (centre of sprays)

Table A9.30 : Measured position of thermocouples and SRA's

The experimental trials included in this section are:-

(i) 13MPa
(ii) 14MPa
(iii) 15MPa
(iv) 16MPa
(v) 17MPa
(vi) 18MPa

A9.5.2.2 Flame speed

This cross flow configuration was previously tested and evaluated in Section A9.4.7 at an operating pressure of 13MPa. During the previous trial, mitigation was achieved in a methane-air mixture of E.R.(ϕ) 0.61 only. Although positive flame speed reductions were recorded during the E.R. (ϕ) 0.72, 0.95 and 1.06 tests between about 30 – 60%, the flame continued to propagate downstream of the sprays.

In this current series the a methane-air mixture of E.R. (ϕ) was 0.95 in all trials and initial operating pressure of 13MPa was selected, which resulted in a 25% reduction in flame speed from upstream to downstream as shown in Figure A9.228. The second test was conducted with a water pressure of 14MPa, resulting in a 40% reduction in flame speed.

The following experimental test was at an operating pressure of 15MPa, whereby full mitigation was achieved. Tests were also conducted at 16MPa and 18MPa which resulted in flame speed reductions of 29% and 11% respectively, followed by a 17MPa test that resulted in an increase in flame speed across the sprays of approximately 9%.

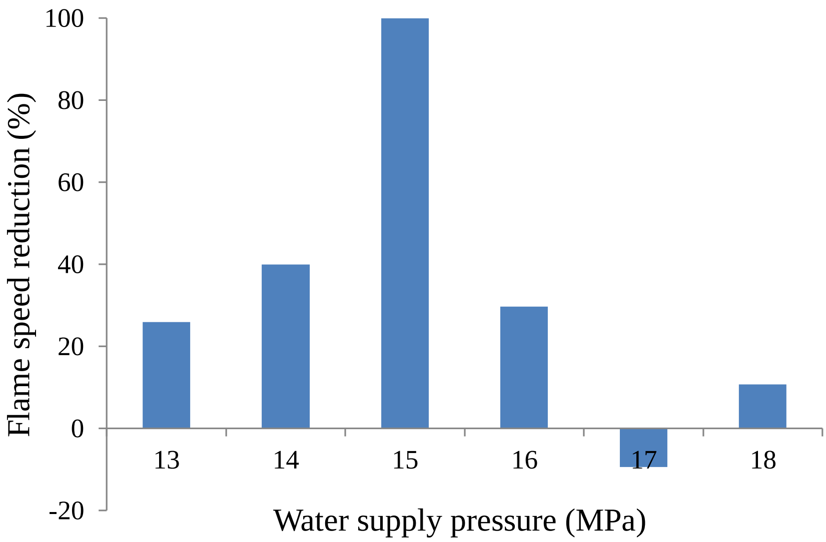

Figure A9.228 : Typical flame speed reductions for three X/F Type C SRA's at various operating pressures

Based on the results previously illustrated in Figure A9.228, there appears to be an optimum operating pressure and resulting water flow rate, whereby mitigation occurs. Below this optimum flow rate the concentration of droplets, or liquid volume flux is ineffective and above this optimum pressure and flow rate, induced turbulence and disturbance of the unburned mixture are more dominant, resulting in a continuation of flame propagation.

A9.5.2.3 Time-temperature response

Figures A9.229 – A9.235 reveal time-temperature profiles for the six trials carried out in this series. The profiles for TC5 are more or less in complete agreement with the flame speed reductions, whereby the lower the flame speed reduction, illustrated in Figure A9.229, the greater the temperature at TC5 at the flame exit end of the FPMR.

In Figure A9.231 TC5 shows virtually no increase above ambient temperature, indicating that full mitigation of the propagating flame occurred.

Figure A9.233 is of interest due to the higher initial flame temperature upstream of the sprays. This is a clear indication that the action of the sprays has caused induced turbulence in the methane-air mixture ahead of the flame, thus resulting in a higher flame speed through the sprays with less opportunity for droplet interaction in the flame front.

Inevitably faster flame speeds lead to lower droplet residence times, with less heat transfer occurring between the flame and water droplets.

(i) Water supply pressure 13MPa

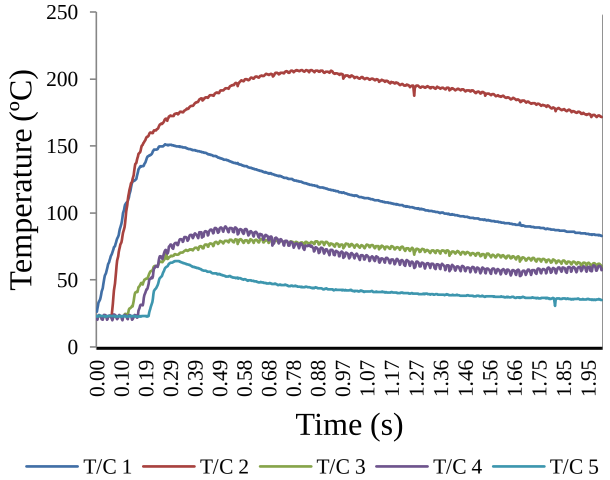

Figure A9.229 : Distinctive time-temperature profile for three Type C SRA's operating at 13MPa – E.R.(ϕ) 0.95

(ii) Water supply pressure 14MPa

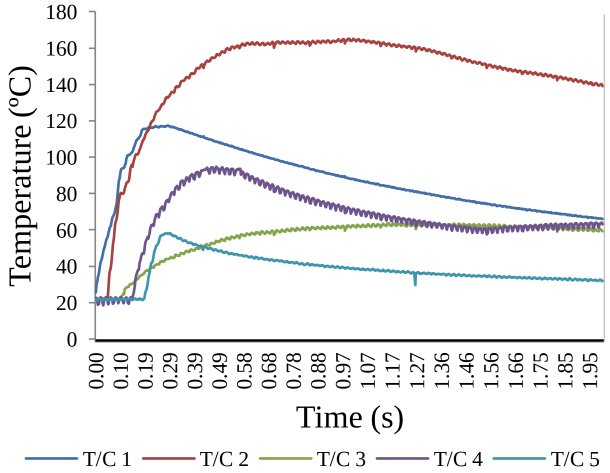

Figure A9.230 : Typical time-temperature profile for three Type C SRA's operating at 14MPa – E.R.(ϕ) 0.95

(iii) Water supply pressure 15MPa

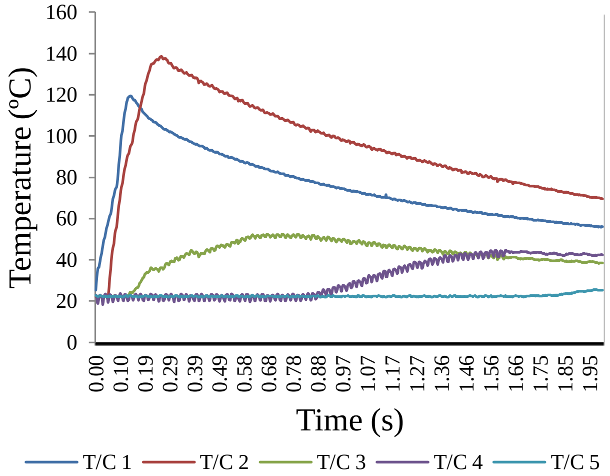

Figure A9.231 : Individual time-temperature profile for three Type C SRA's operating at 15MPa – E.R.(ϕ) 0.95

(iv) Water supply pressure 16MPa

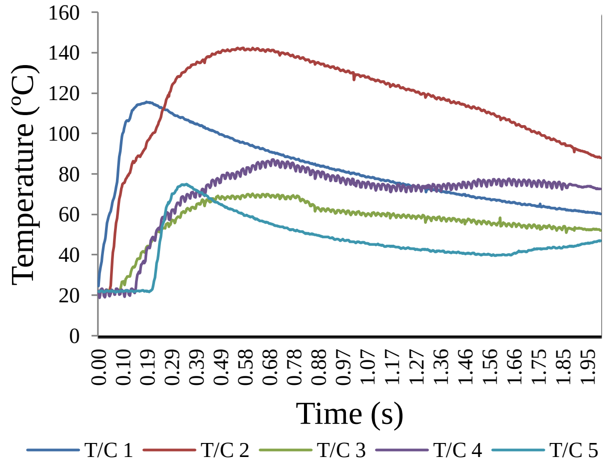

Figure A9.231 : Distinctive time-temperature profile for three Type C SRA's operating at 16MPa – E.R.(ϕ) 0.95

(v) Water supply pressure 17MPa

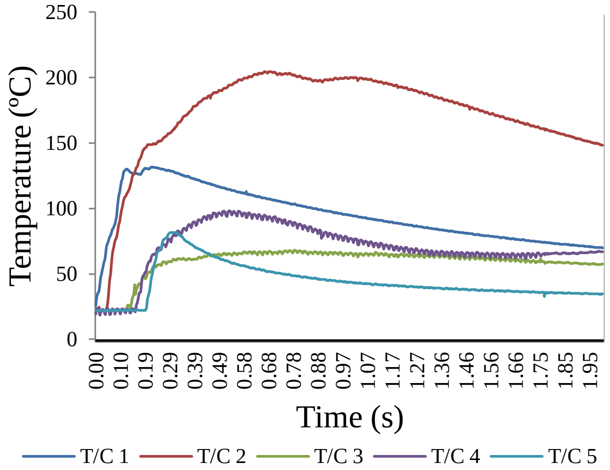

Figure A9.232 : Characteristic time-temperature profile for three Type C SRA's operating at 17MPa – E.R.(ϕ) 0.95

(vi) Water supply pressure 18MPa

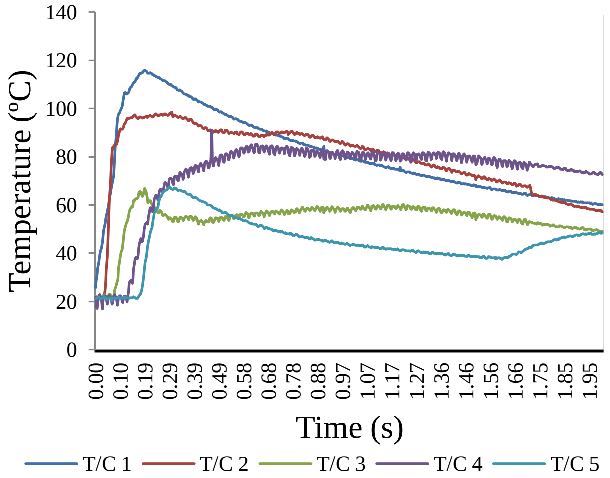

Figure A9.233 : Distinctive time-temperature profile for three Type C SRA's operating at 18MPa – E.R.(ϕ) 0.95

A9.5.2.4 Qualitative analysis

(i) and (ii) Figures A9.235 - A9.238 show the still images relating to the 13MPa and 14MPa trials. The propagating flames can be seen to pass directly through the sprays, with the sprays appearing visually to have little effect on flame suppression although flame speeds were reduced in both cases. Figure A9.236 and A9.238 highlight the spray regions and propagating flame.

(iii) In Figure A9.239 the operating pressure was 15MPa and the flame is evidently mitigated in the spray region and failed to progress into the downstream methane-air mixture. Figure A9.240 shows an enlarged section of the spray region confirming the lasting interruption of combustion.

(iv) In Figure A9.241 the operating pressure was 16MPa and the flame is seen to pass directly into and through the sprays, with the presence of dark regions in (ii) and (iii) suggesting a degree of local combustion termination. However, the flame is seen to exit the sprays with sufficient temperature to propagate through the remaining downstream combustible mixture. Figure A9.242 focuses on the region of the sprays where dark areas are magnified.

(v) Figure A9.243 reveals the 17MPa trial where the flame passed through the three sprays and in dramatically reduced. However, due to the action of the sprays the mixture was sufficiently disturbed to cause a resulting increase in average downstream flame speed.

(vi) Figure A9.245 offers the frame by frame account of the trial using 18MPa sprays. During this experimental test the flame passed through the sprays where dark regions can be observed. Figure A9.246 presents an enlarged view of the spray and flame interface.

(i) Water supply pressure 13MPa

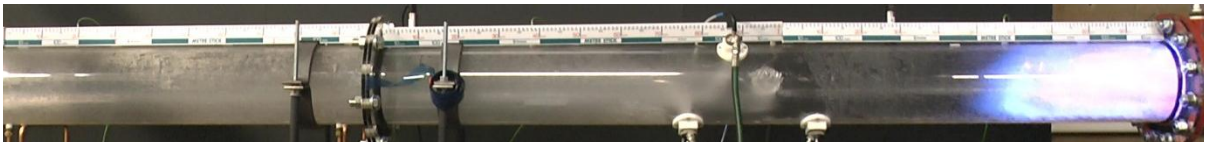

i. Flame propagating in methane-air mixture of E.R. (ϕ) 0.95 upstream of SRA

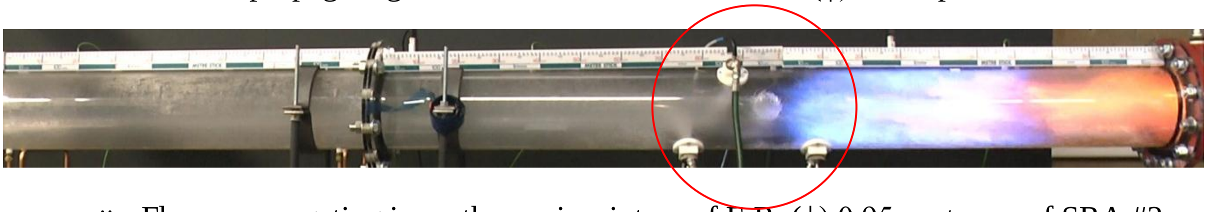

ii. Flame propagating in methane-air mixture of E.R. (ϕ) 0.95 upstream of SRA #2

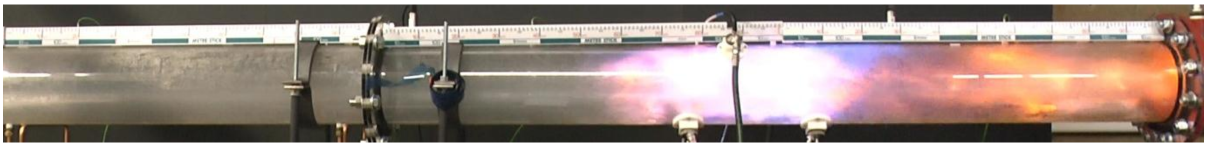

iii. Flame propagating in methane-air mixture of E.R. (ϕ) 0.95 in the region of spray

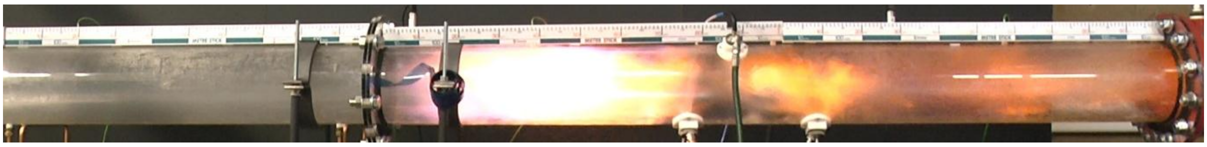

iv. Flame propagating in methane-air mixture of E.R. (ϕ) 0.95 downstream of SRA

Figure A9.235 : Flame propagating upstream and downstream of three X/F Type C SRA's with water at 20˚C and operating at 13MPa in a methane-air mixture (ϕ) 0.95

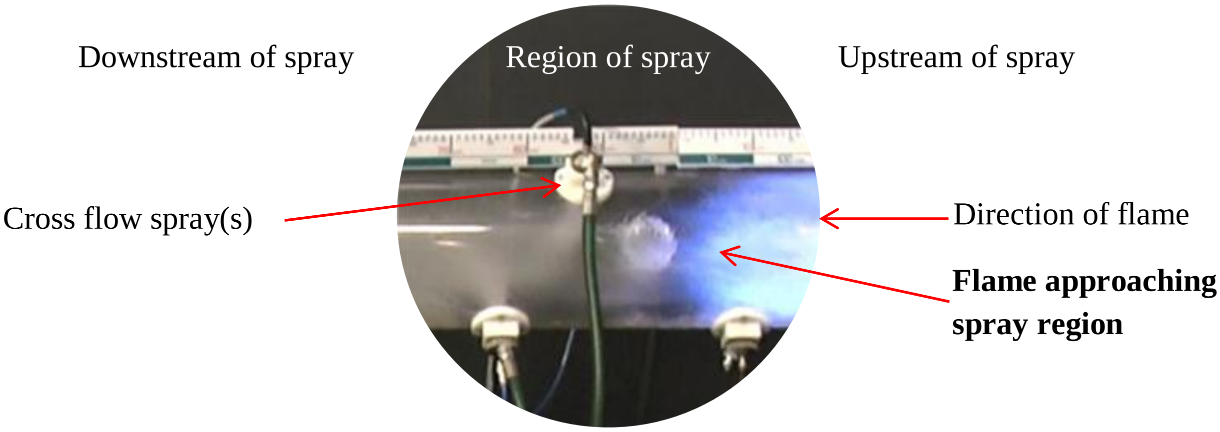

Figure A9.236 : Expanded view of region of spray highlighted in Figure A9.235(ii)

(ii) Water supply pressure 14MPa

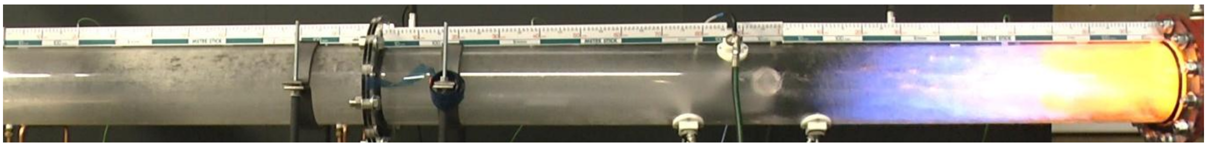

i. Flame propagating in methane-air mixture of E.R. (ϕ) 0.95 upstream of SRA

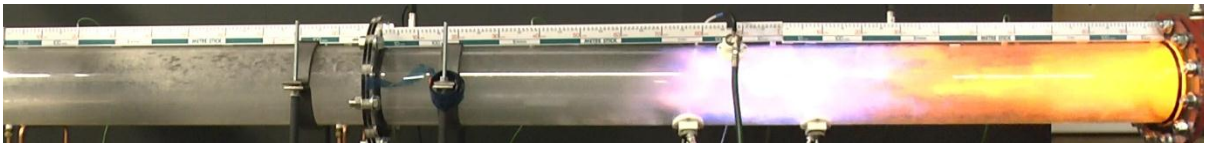

ii. Flame propagating in methane-air mixture of E.R. (ϕ) 0.95 in the region of spray

iii. Flame propagating in methane-air mixture of E.R. (ϕ) 0.95 downstream of SRA

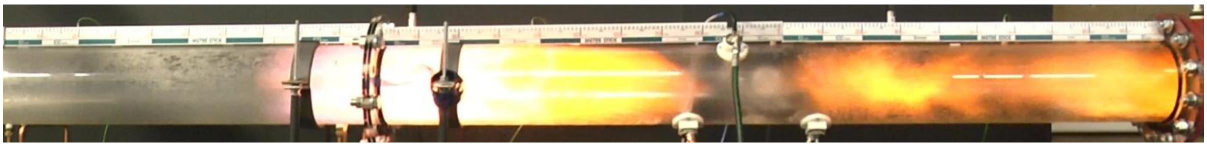

iv. Flame propagating in methane-air mixture of E.R. (ϕ) 0.95 downstream of SRA

Figure A9.237 : Flame propagating upstream and downstream of three X/F Type C SRA's with water at 20 ˚C and operating at 14MPa in a methane-air mixture (ϕ) 0.95

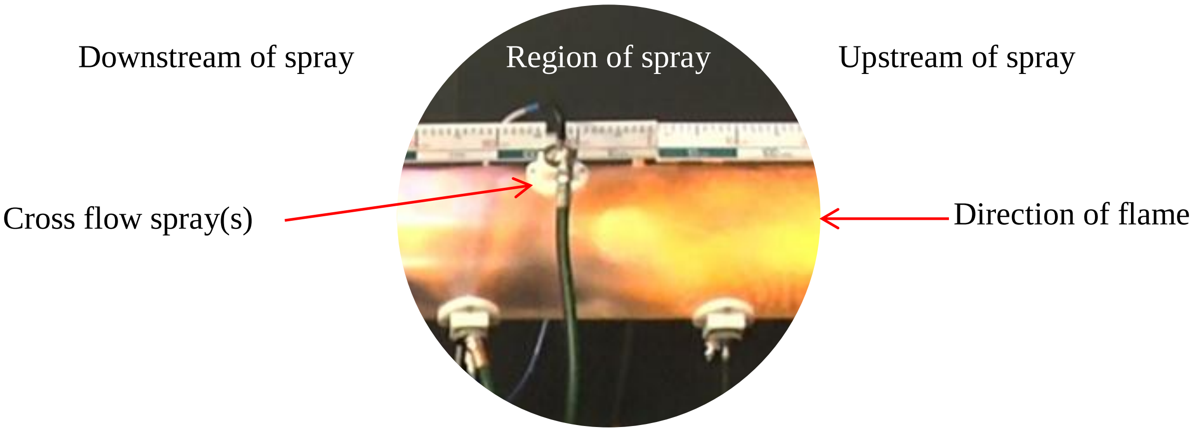

Figure A9.238 : Magnified view of region of spray highlighted in Figure A9.237(iii)

(iii) Water supply pressure 15MPa

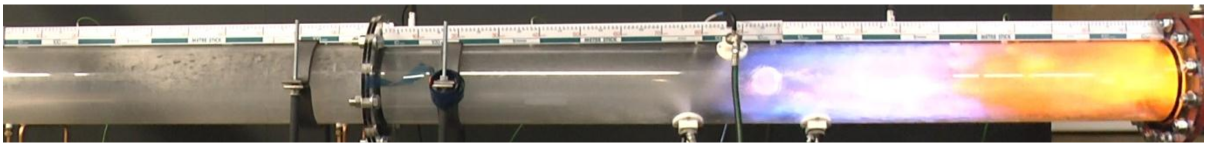

i. Flame propagating in methane-air mixture of E.R. (ϕ) 0.95upstream of SRA

ii. Flame propagating in methane-air mixture of E.R. (ϕ) 0.95 upstream of SRA

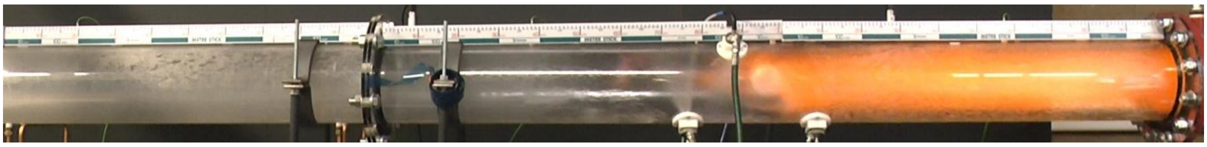

iii. Flame propagating in methane-air mixture of E.R. (ϕ) 0.95in the region of spray

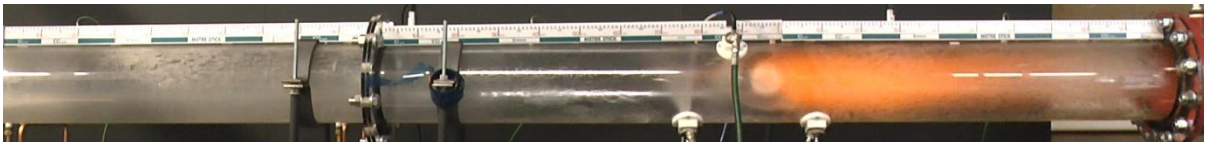

iv. **Mitigation** in methane-air mixture of E.R. (ϕ) 0.95 downstream of SRA

Figure A9.239 : Flame propagating upstream of three X/F Type C SRA's resulting in downstream mitigation with water at 20 ˚C and operating at 15MPa in a methane-air mixture (ϕ) 0.95

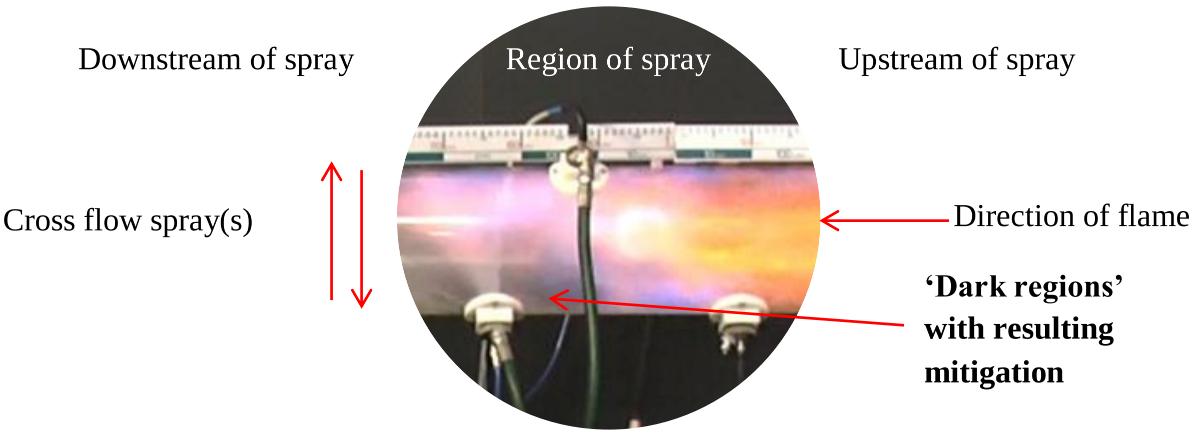

Figure A9.240 : Close up view of region of spray highlighted in Figure A9.239(ii)

(iv) Water supply pressure 16MPa

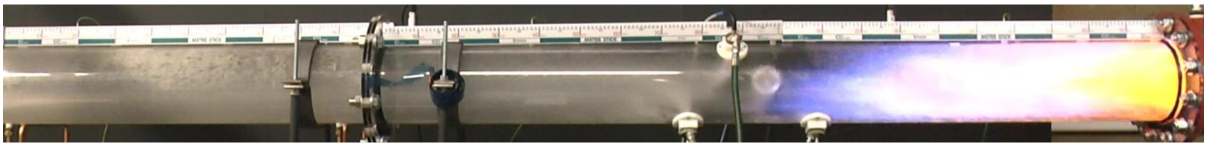

i. Flame propagating in methane-air mixture of E.R. (ϕ) 0.95upstream of SRA

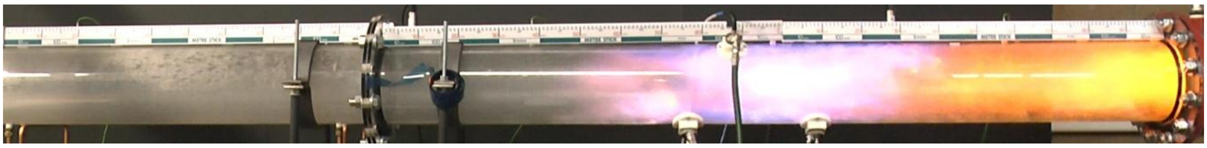

ii. Flame propagating in methane-air mixture of E.R. (ϕ) 0.95 upstream of SRA

iii. Flame propagating in methane-air mixture of E.R. (ϕ) 0.95in the region of spray

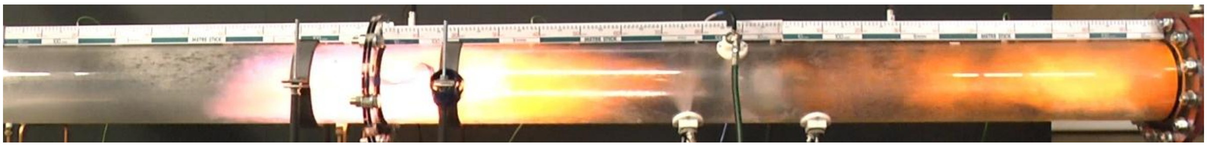

iv. Flame propagating in methane-air mixture of E.R. (ϕ) 0.95 downstream of SRA

Figure A9.241: Flame propagating upstream and downstream of three X/F Type C SRA's with water at 20 ˚C and operating at 16MPa in a methane-air mixture (ϕ) 0.95

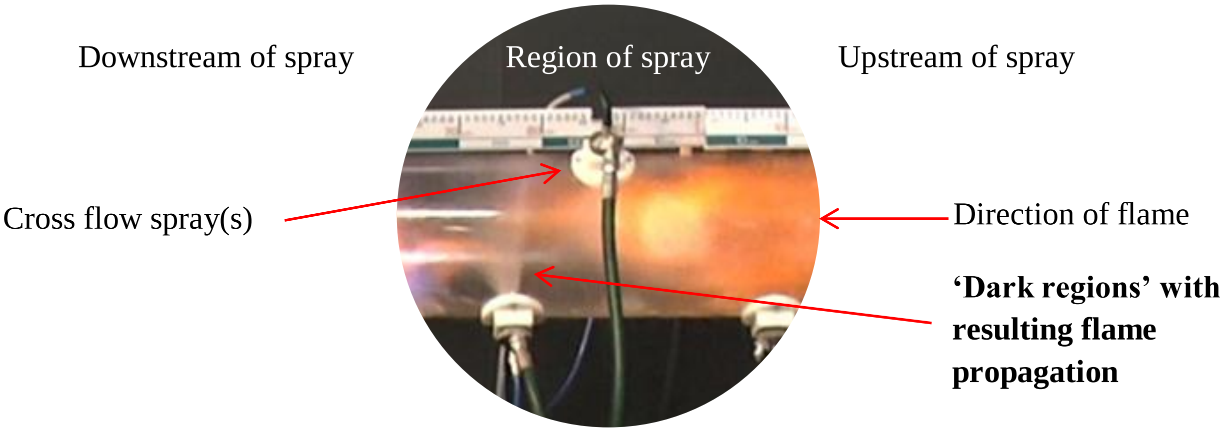

Figure A9.242 : Enlarged view of region of spray highlighted in Figure A9.241(iii)

(v) Water supply pressure 17MPa

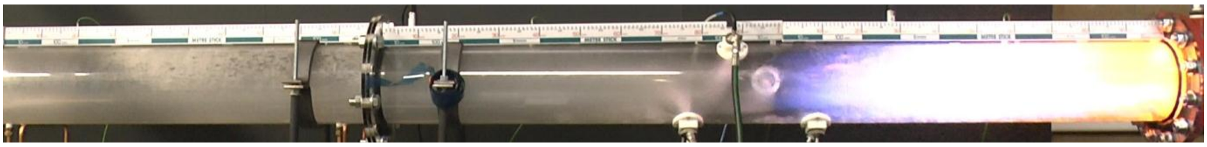

i. Flame propagating in methane-air mixture of E.R. (ϕ) 0.95upstream of SRA

ii. Flame propagating in methane-air mixture of E.R. (ϕ) 0.95 upstream of SRA

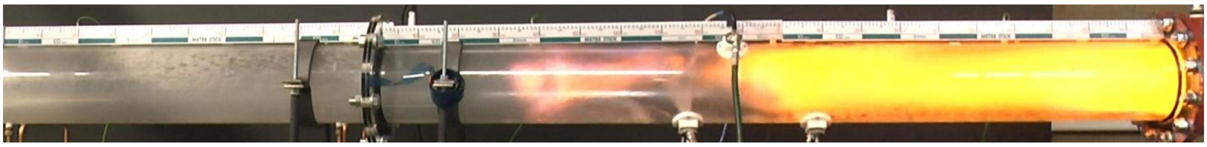

iii. Flame propagating in methane-air mixture of E.R. (ϕ) 0.95in the region of spray

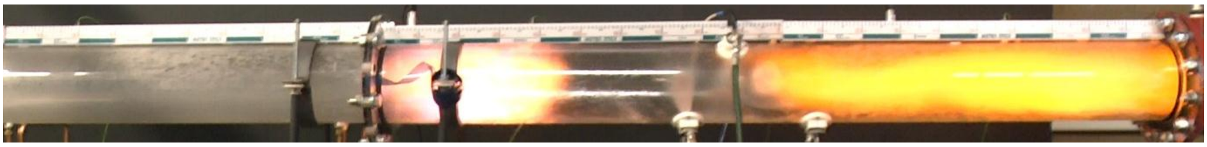

iv. Flame propagating in methane-air mixture of E.R. (ϕ) 0.95 downstream of SRA

Figure A9.243 : Flame propagating upstream and downstream of three X/F Type C SRA's with water at 20 ˚C and operating at 17MPa in a methane-air mixture (ϕ) 0.95

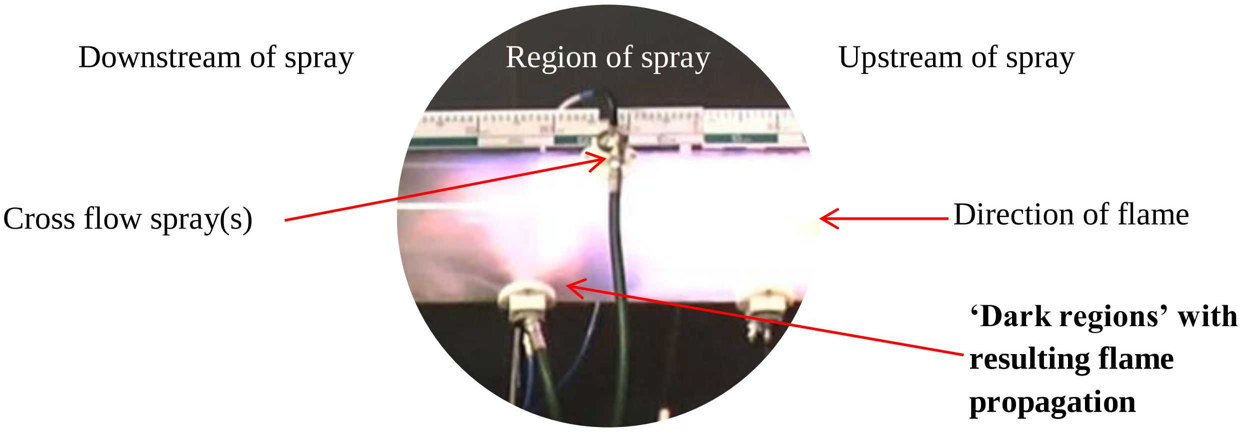

Figure A9.244 : Expanded view of region of spray highlighted in Figure A9.243(ii)

(vi) Water supply pressure 18MPa

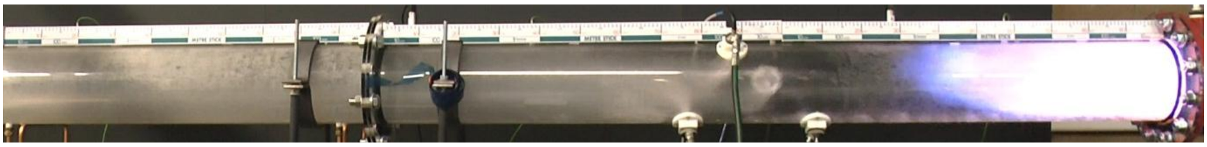

i. Flame propagating in methane-air mixture of E.R. (ϕ) 0.95upstream of SRA

ii. Flame propagating in methane-air mixture of E.R. (ϕ) 0.95 upstream of SRA

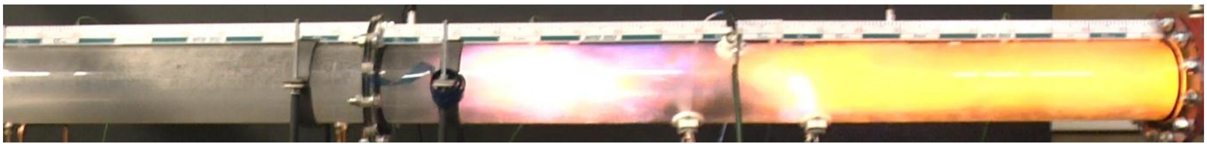

iii. Flame propagating in methane-air mixture of E.R. (ϕ) 0.95in the region of spray

iv. Flame propagating in methane-air mixture of E.R. (ϕ) 0.95 downstream of SRA

Figure A9.245 : Flame propagating upstream and downstream of three X/F Type C SRA's with water at 20 ˚C and operating at 18MPa in a methane-air mixture (ϕ) 0.95

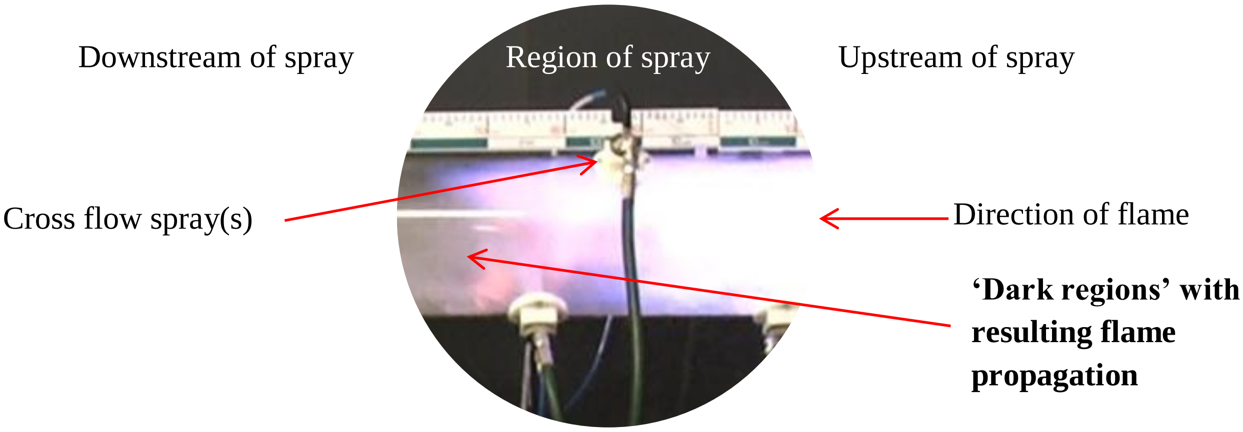

Figure A9.246 : Exploded view of region of spray highlighted in Figure A9.245(ii)

A9.5.2.5 General event outcome

Table A9.31 provides a summary of the **'general event outcome'** for each trial in this current series, using the five potential 'outcome' categories offered in Chapter 5. The results of all 'hot trials' were previously given in Table 5.14 and are also shown in Table A9.45.

Trial configuration	General event outcome	Code
3 X/F Type C : 13MPa	No Mitigation with resulting Flame Deceleration	NMFD
3 X/F Type C : 14MPa	No Mitigation with resulting Flame Deceleration	NMFD
3 X/F Type C : 15MPa	Full Mitigation resulting in Flame Extinguishment	FMFE
3 X/F Type C : 16MPa	No Mitigation with resulting Flame Deceleration	NMFD
3 X/F Type C : 17MPa	No Mitigation with resulting Flame Acceleration	NMFA
3 X/F Type C : 18MPa	No Mitigation with resulting Flame Deceleration	NMFD

Table A9.31 : General event outcome (trial series A9.5.2)

A9.5.3 Multiple (X/F) Type B SRA's using various water supply pressures

A9.5.3.1 Trial set up

In this series of experimental trials four cross flow (X/F) Type B SRA's were assembled and supplied with water at 20°C. The aim was to evaluate the effects of increased water pressure and whether conditions would favour those required for mitigation, or whether the increase in water pressure would lead towards additional induced turbulence in the flammable mixture. The positions of thermocouples and atomisers positions are illustrated in Figure A9.247 and Table A9.12.

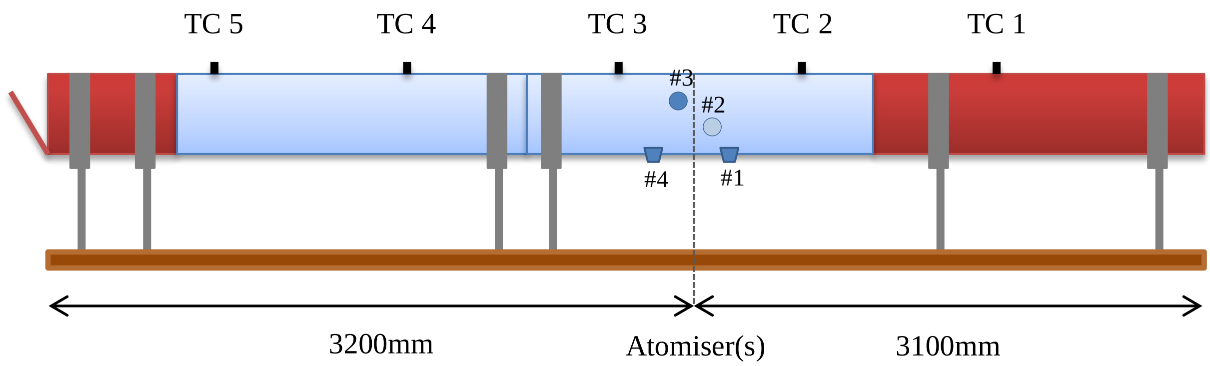

Figure A9.247 : Position of atomisers and thermocouples (relative to right hand ignition)

Component	Position (measured from right hand end)
Thermocouple (TC1)	1200mm
Thermocouple (TC2)	2400mm
Thermocouple (TC3)	3600mm
Thermocouple (TC4)	4800mm
Thermocouple (TC5)	6000mm
Atomiser outlet orifice (cross flow)	3100mm (centre of sprays)

Table A9.32 : Measured position of thermocouples and SRA's

The experimental trials included in this section are:-

(i) 14MPa
(ii) 15MPa
(iii) 16MPa
(iv) 17MPa
(v) 18MPa

A9.5.3.2 Flame speed

This cross flow configuration was previously tested and evaluated in Section A9.4.4 at an operating pressure of 13MPa. During the previous testing mitigation was achieved in methane-air mixtures of E.R.(ϕ) 0.61 and 0.72. Although a flame speed reduction was recorded during the E.R.(ϕ) 0.95 trial coupled with dark regions in the flame, the flame continued to propagate downstream.

In this current series the initial operating pressure selected was 14MPa, which resulted in a 35% reduction in flame speed from upstream to downstream as shown in Figure A9.248. The following experimental test was at an operating pressure of 15MPa, whereby full mitigation was achieved. Tests were also conducted at 16MPa and 17MPa which resulted in flame speed reductions of 38% and 11% respectively, followed by an 18MPa test that resulted in an increase in flame speed across the sprays of approximately 29%.

Based on the results illustrated in Figure A9.248 there appears to be an optimum operating pressure and resulting water flow rate, whereby mitigation occurs. Below this optimum flow rate the concentration of droplets, or flux, is ineffective and above this optimum pressure and flow rate, induced turbulence and disturbance of the unburned mixture are more dominant, resulting in a continuation of flame propagation.

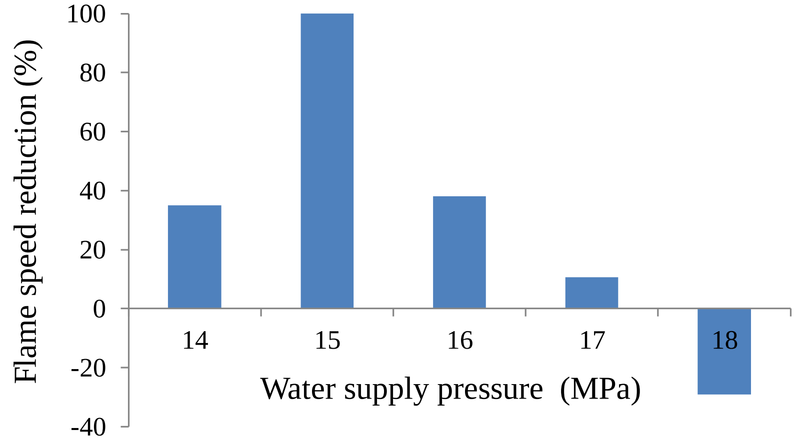

Figure A9.248 : Typical flame speed reductions for four X/F Type B SRA's at various operating pressures

The effects of induced turbulence in the unburned mixture have been reported by several authors [2]. Previous studies and finding were discussed extensively in Chapter 3.

A9.5.3.3 Time-temperature response

Figures A9.249 – A9.254 reveal time-temperature profiles for the five trials carried out in this series. The profiles for TC5 are in complete agreement with the flame speed reductions, whereby the lower the flame speed reduction, illustrated in Figure A9.248, the greater the temperature at TC5 at the flame exit end of the explosion and mitigation rig. Another important relationship is that between TC3 and TC5.

An increase in temperature between TC3 and TC5 indicates an increase in activity, resulting in higher flame temperatures and greater flame speeds. The greater difference between the peak values in these thermocouples, can be related directly to the contribution of induced turbulence caused by the increase in water flow rate.

Figure A9.250 shows the time-temperature profile for four type B SRA's operating at 15MPa, whereby mitigation occurred. The mitigation can also be seen in FiguresA9.265 and A9.257.

(i) Water supply pressure 14MPa

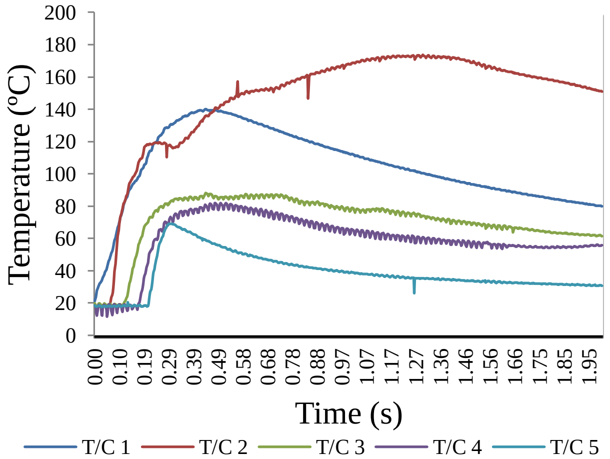

Figure A9.249 : Distinctive time-temperature profile for four type B SRA's operating at 14MPa – E.R.(ϕ) 0.95

(ii) Water supply pressure 15MPa

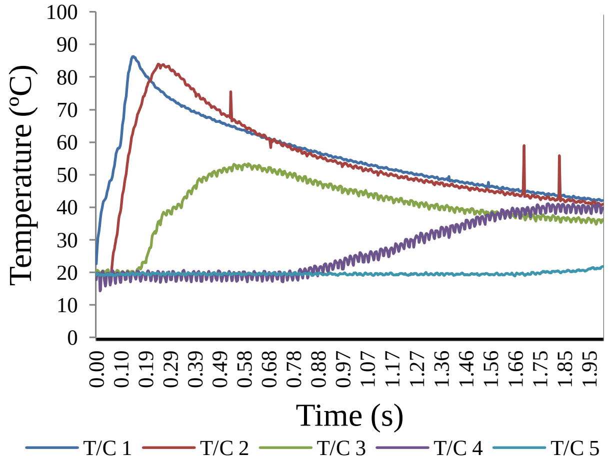

Figure A9.250 : Typical time-temperature profile for four type B SRA's operating at 15MPa – E.R.(ϕ) 0.95

(iii) Water supply pressure 16MPa

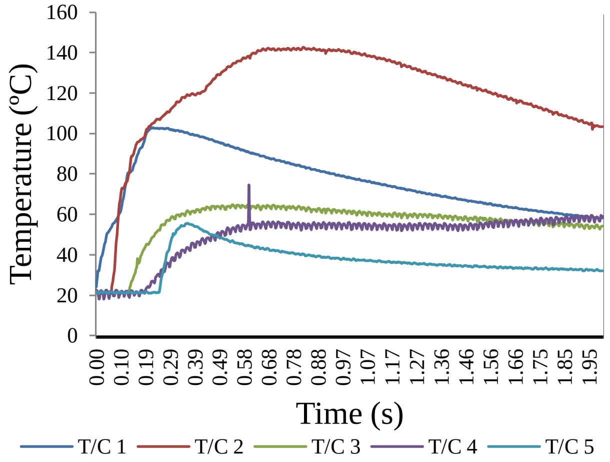

Figure A9.251 : Characteristic time-temperature profile for four type B SRA's operating at 16MPa – E.R.(ϕ) 0.95

(iv) Water supply pressure 17MPa

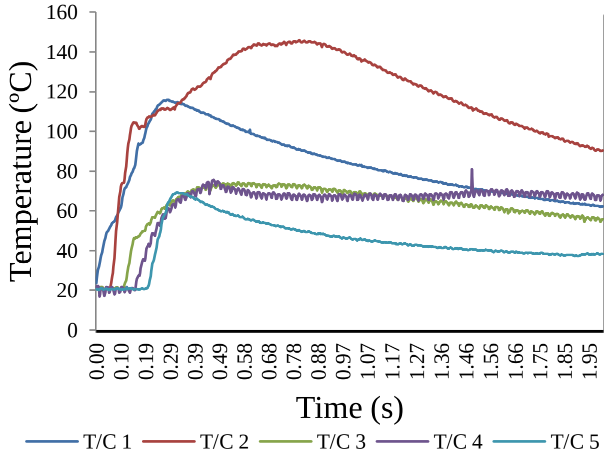

Figure A9.252 : Distinctive time-temperature profile for four type B SRA's operating at 17MPa – E.R.(ϕ) 0.95

(v) Water supply pressure 18MPa

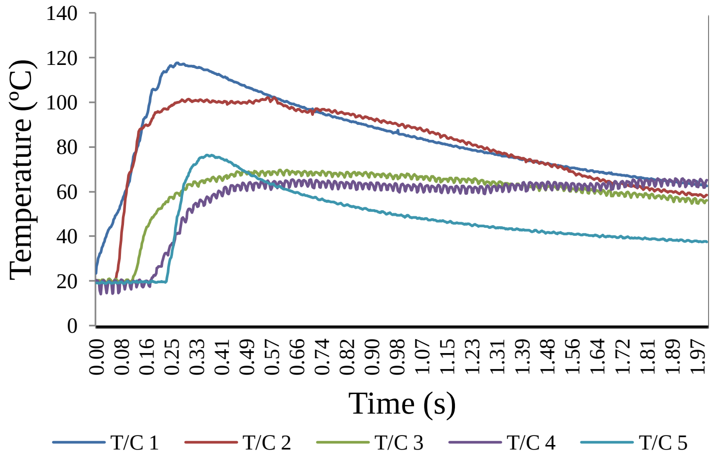

Figure A9.253 : Typical time-temperature profile for four type B SRA's operating at 18MPa – E.R.(ϕ) 0.95

A9.5.3.4 Qualitative analysis

(i) Figure A9.254 reveals four still images relating to the 14MPa trial, the propagating flame can be seen to pass directly through the sprays, with the sprays appearing visually to have little effect on flame suppression. Figure A9.255 highlights the spray downstream of the propagating flame. The spray is clearly being affected by the flow ahead of the flame front. At higher pressures the spray is less likely to be effected by the inertia downstream of the flame, however at higher pressure there becomes a greater risk of turbulence in the unburned mixture.

(ii) In Figure A9.256 the operating pressure was 15MPa and the flame is clearly mitigated in the spray region and fails to progress into the downstream combustible mixture. Figure A9.257 shows a magnified section of the spray region confirming the permanent interruption of combustion.

(iii) Figures A9.260 and A9.261 the operating pressures were 16MPa and 17MPa, reveal very similar sequences of events to those previously discussed in Figure A9.254, showing a high degree of combustion reduction caused in the spray region, followed by ignition and propagation through the downstream mixture. The spray regions are again highlighted in Figures A9.259 and A9.261.

(iv) In Figure A9.262 the operating pressure was 18MPa and the flame is seen to pass directly into the sprays, with the presence of dark regions in (ii) and (iii) suggesting a degree of flame extinguishment. The flame then exited the sprays with sufficient temperature to propagate and accelerate through the remaining downstream combustible mixture. Figure A9.263 focuses on the region of the sprays where dark areas are magnified.

(i) 14MPa

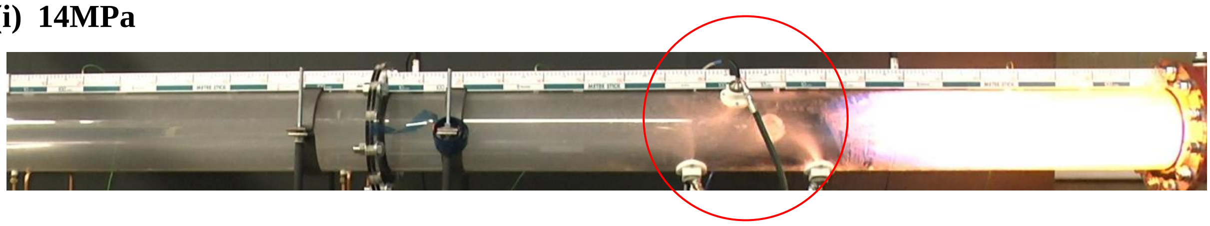

i. Flame propagating in methane-air mixture of E.R. (ϕ) 0.95upstream of SRA

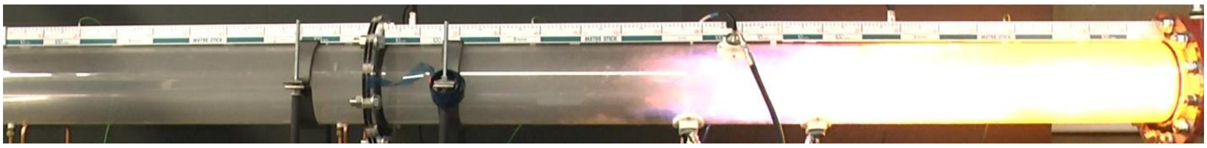

ii. Flame propagating in methane-air mixture of E.R. (ϕ) 0.95 in the region of spray

iii. Flame propagating in methane-air mixture of E.R. (ϕ) 0.95 in the region of spray

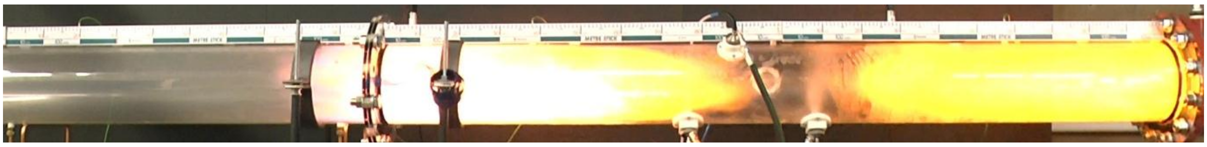

iv. Flame propagating in methane-air mixture of E.R. (ϕ) 0.95 downstream of SRA

Figure A9.254 : Flame propagating upstream and downstream of four X/F type B SRA’s with water at 20˚C and operating at 14MPa in a methane-air mixture (ϕ) 0.95

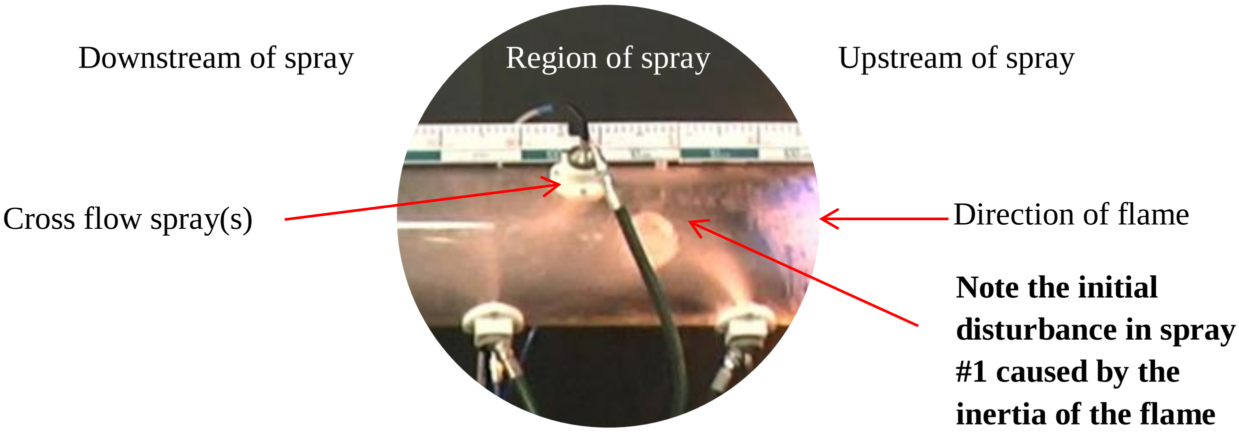

Figure A9.255 : Expanded view of region of spray highlighted in Figure A9.254(i)

(ii) 15MPa

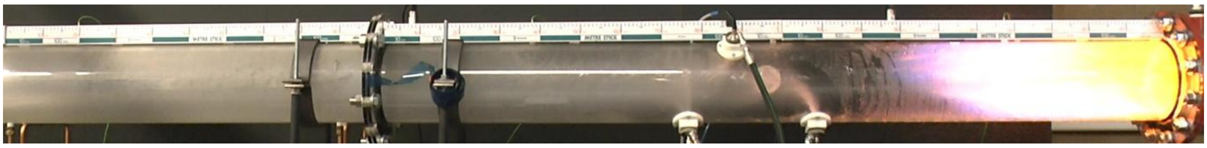

i. Flame propagating in methane-air mixture of E.R. (ϕ) 0.95upstream of SRA

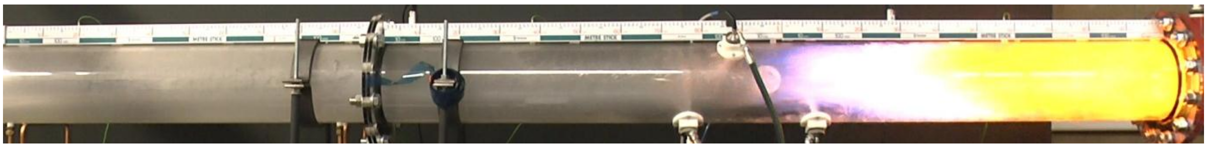

ii. Flame propagating in methane-air mixture of E.R. (ϕ) 0.95 interacting with SRA's

iii. Dark regions indicated areas where combustion has ceased

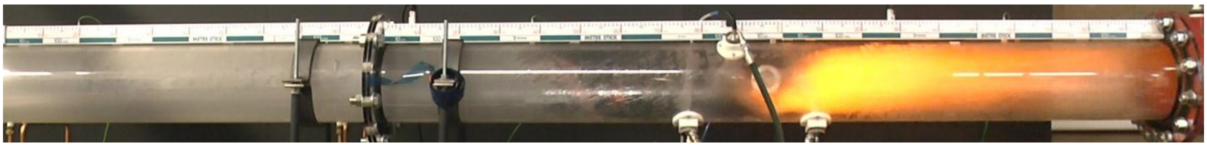

iv. **Mitigated** methane-air mixture of E.R. (ϕ) 0.95

Figure A9.256 : Flame propagating upstream and mitigation using four X/F type B SRA's with water at 20˚C and operating at 15MPa in a methane-air mixture (ϕ) 0.95

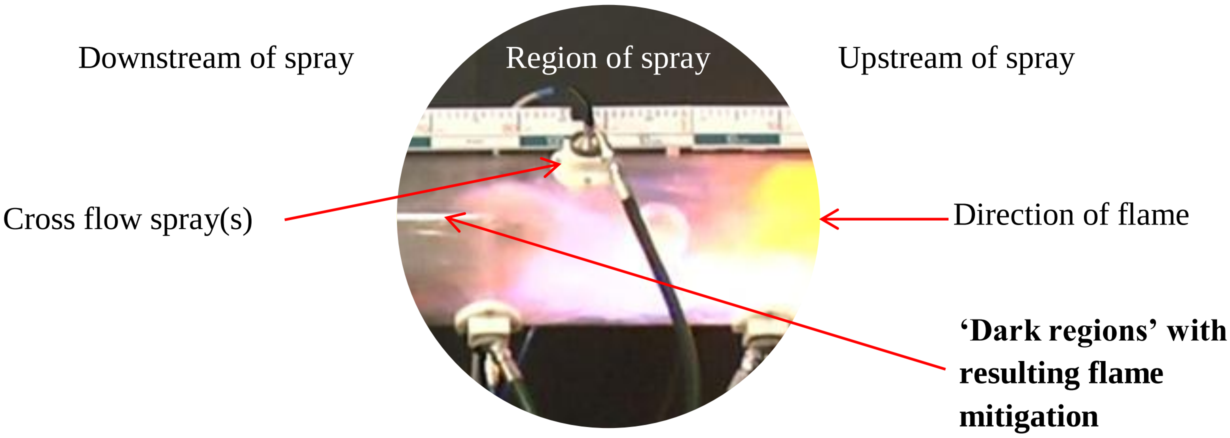

Figure A9.257 : Enlarged view of region of spray highlighted in Figure A9.256(iii)

(iii) 16MPa

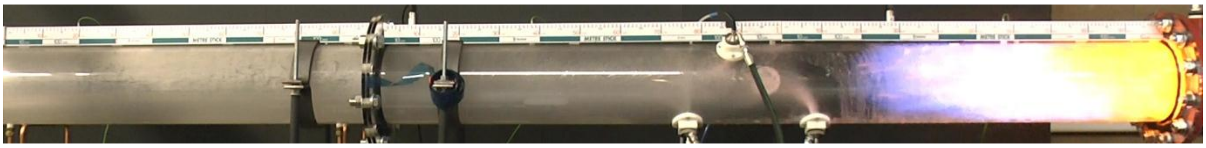

i. Flame propagating in methane-air mixture of E.R. (ϕ) 0.95upstream of SRA

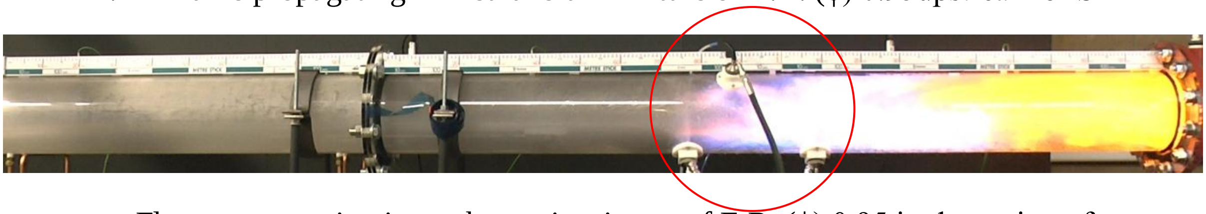

ii. Flame propagating in methane-air mixture of E.R. (ϕ) 0.95 in the region of spray

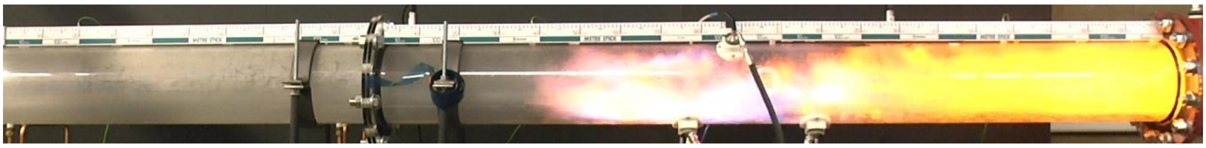

iii. Flame propagating in methane-air mixture of E.R. (ϕ) 0.95 in the region of spray

iv. Flame propagating in methane-air mixture of E.R. (ϕ) 0.95 downstream of SRA

Figure A9.258 : Flame propagating upstream and downstream of four X/F type B SRA's with water at 20˚C and operating at 16MPa in a methane-air mixture (ϕ) 0.95

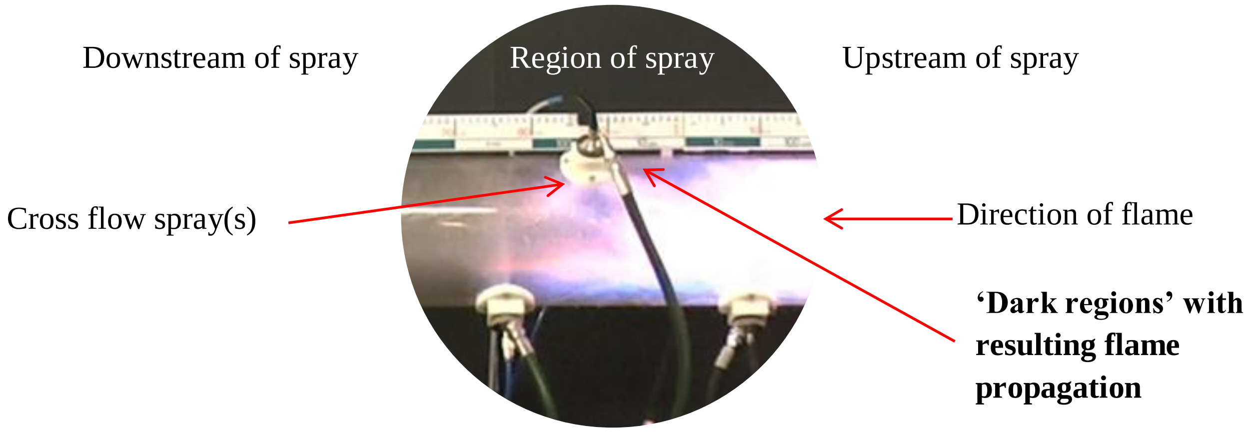

Figure A9.259 : Close up view of region of spray highlighted in Figure A9.258(ii)

(iv) 17MPa

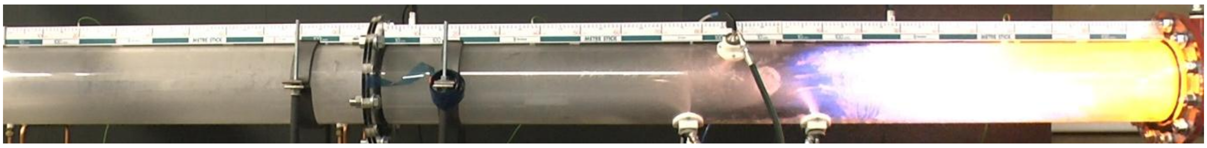

i. Flame propagating in methane-air mixture of E.R. (ϕ) 0.95 in the region of spray

ii. Flame propagating in methane-air mixture of E.R. (ϕ) 0.95 in the region of spray

iii. Flame propagating in methane-air mixture of E.R. (ϕ) 0.95 downstream of SRA

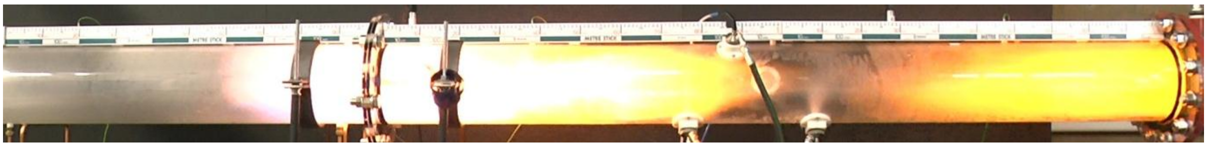

iv. Flame propagating in methane-air mixture of E.R. (ϕ) 0.95 downstream of SRA

Figure A9.260 : Flame propagating upstream and downstream of four X/F type B SRA's with water at 20˚C and operating at 17MPa in a methane-air mixture (ϕ) 0.95

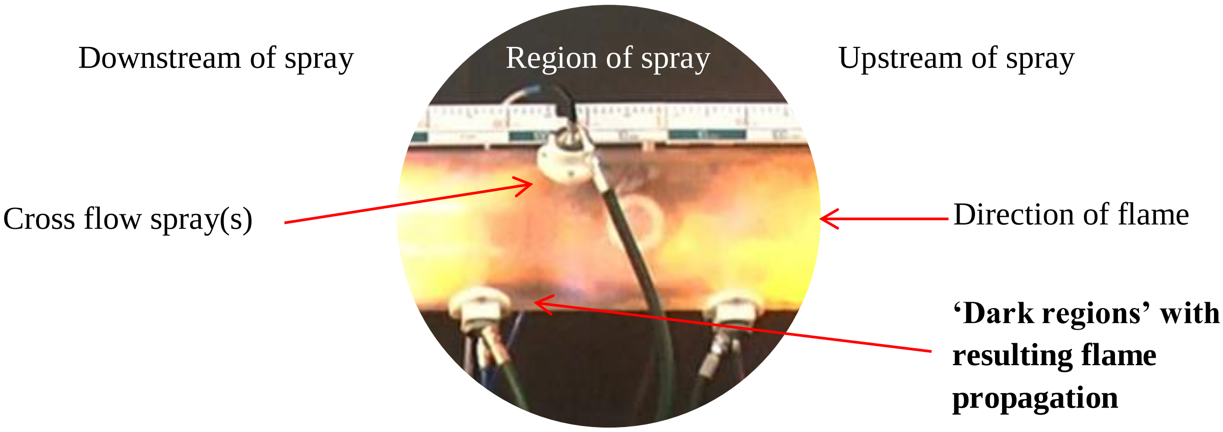

Figure A9.261 : Enlarged view of region of spray highlighted in Figure A9.260(iii)

(v)18MPa

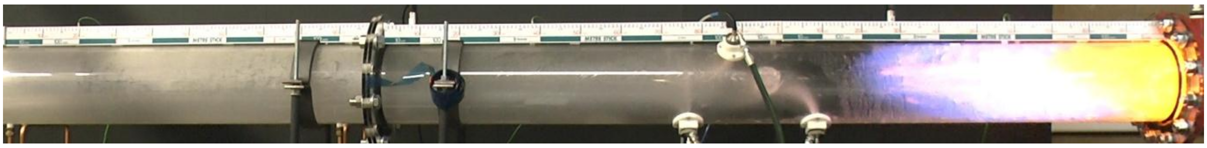

i. Flame propagating in methane-air mixture of E.R. (ϕ) 0.95upstream of SRA

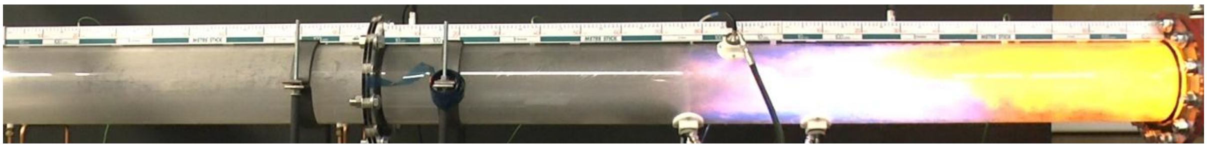

ii. Flame propagating in methane-air mixture of E.R. (ϕ) 0.95 in the region of the spray

iii. Flame propagating in methane-air mixture of E.R. (ϕ) 0.95 in the region of the spray

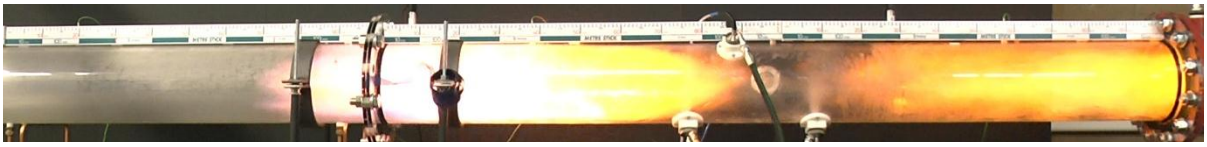

iv. Flame propagating in methane-air mixture of E.R. (ϕ) 0.95 downstream of SRA

Figure A9.262 : Flame propagating upstream and downstream of four X/F type B SRA's with water at 20˚C and operating at 18MPa in a methane-air mixture (ϕ) 0.95

Figure A9.263 : Exploded view of region of spray highlighted in Figure A9.262(iii)

A9.5.3.5 General event outcome

Table A9.33 provides a summary of the **'general event outcome'** for each trial in this current series, using the five potential 'outcome' categories offered in Chapter 5. The results of all 'hot trials' were previously given in Table 5.14 and are also shown in Table A9.45.

Trial configuration	General event outcome	Code
3 X/F Type B : 14MPa	No Mitigation with resulting Flame Deceleration	NMFD
3 X/F Type B : 15MPa	Full Mitigation resulting in Flame Extinguishment	FMFE
3 X/F Type B : 16MPa	No Mitigation with resulting Flame Deceleration	NMFD
3 X/F Type B : 17MPa	No Mitigation with resulting Flame Deceleration	NMFD
3 X/F Type B : 18MPa	No Mitigation with resulting Flame Acceleration	NMFA

Table A9.33 : General event outcome (trial series A9.5.3)

A9.5.4 Three (X/F) Type C SRA's using variable water temperatures

A9.5.4.1 Trial set up

In this series of experimental trials three cross flow Type C SRA's were supplied with water at a pressure of 13MPa at a variety of water temperatures from 30˚C to 50˚C. The aim of this set of tests was to establish the effects of an increase in water pressure combined with an increase in water temperature supplied to the sprays. The positions of thermocouples and atomisers are illustrated in Figure A9.264 and Table A9.34.

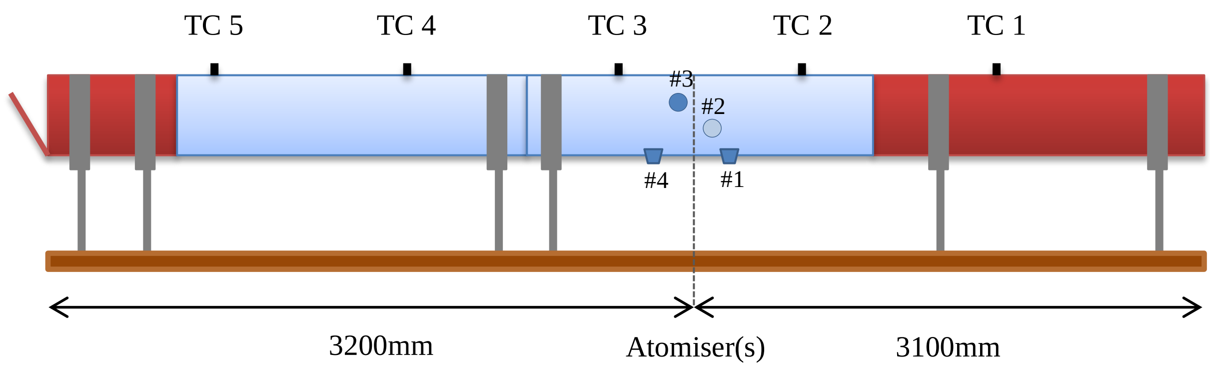

Figure A9.264 : Position of atomiser and thermocouples (relative to right hand ignition)

Component	Position (measured from right hand end)
Thermocouple (TC1)	1200mm
Thermocouple (TC2)	2400mm
Thermocouple (TC3)	3600mm
Thermocouple (TC4)	4800mm
Thermocouple (TC5)	6000mm
Atomiser outlet orifice (cross flow)	3100mm (centre of sprays)

Table 9.34 : Measured position of thermocouples and SRA's

The experimental trials included in this section are:-

(i) 30˚C

(ii) 35˚C

(iii) 40˚C

(iv) 45˚C

(v) 50˚C

A9.5.4.2 Flame speed

In this series of experimental trials the accumulative effects of an increase in operating pressure, coupled with an increase in water delivery temperature were to be examined. Average flame speeds were measure both upstream and downstream of the spray region. Figure A9.265 reveals the percentage flame speed reductions for each of the conditions tested.

In all of the trials presented in Figure A9.265 the water operating pressure water 13MPa. In the first test the water was heated to 30˚C, whereby complete mitigation of the flame occurred. However, this was the only instance in this series that instigated mitigation. All of the other trials did result in global flame speed reduction.

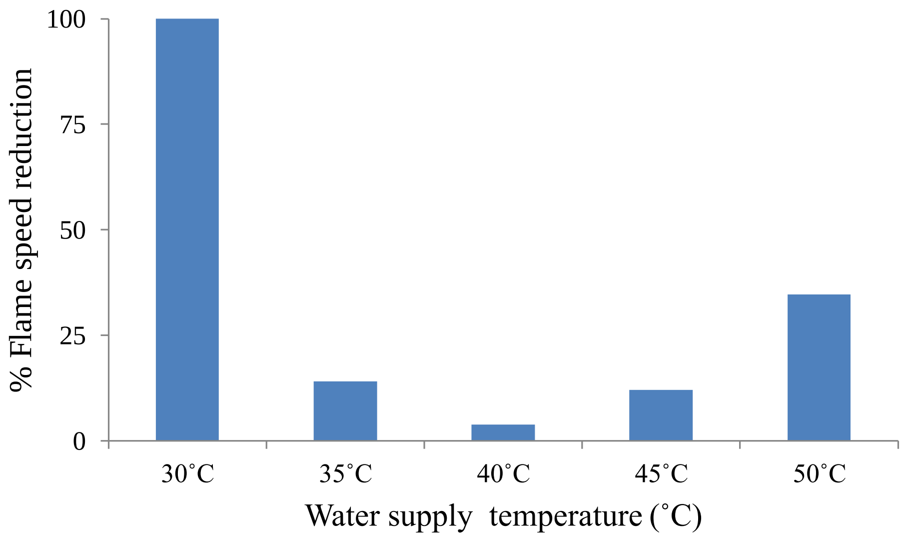

Figure A9.265 : Typical flame speed reductions for three X/F Type C SRA's operating at a pressure of 13MPa and water temperatures

A9.5.4.3 Time-temperature response

Figure A9.264 shows the typical time-temperature profile for three Type C SRA's operating at 13MPa and water temperature 30 ˚C. The thermocouple TC5 shows very little change in the final exit temperature if the rig indicating that mitigation did occur, whereas TC3 and TC5 show a small rise due to the flash vaporisation of some of the smaller droplets in the spray.

All of the other time-temperature profiles presented in this series from Figure A9.267 – A9.270 indicate that mitigation did not follow. This is shown consistently by a spike in temperature at TC5.

(i) Water supply pressure 13MPa and temperature 30 °C

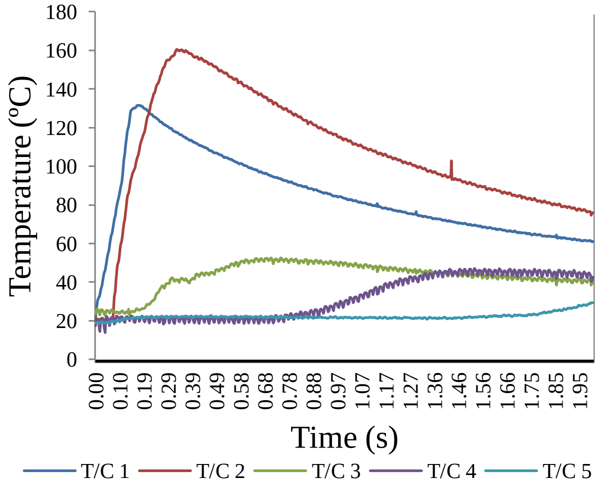

Figure A9.266 : Typical time-temperature profile for three Type C SRA's operating at 13MPa and water temperature 30 °C – E.R.(ϕ) 0.95

ii) Water supply pressure 13MPa and temperature 35 °C

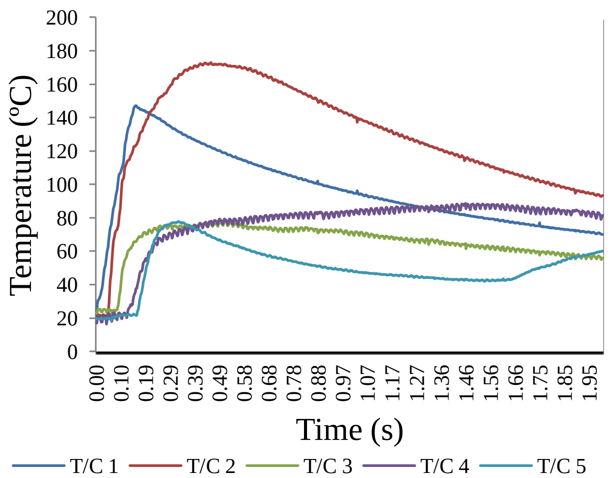

Figure A9.267 : Distinctive time-temperature profile for three Type C SRA's operating at 13MPa and water temperature 35 °C – E.R.(ϕ) 0.95

(iii) Water supply pressure 13MPa and temperature 40 °C

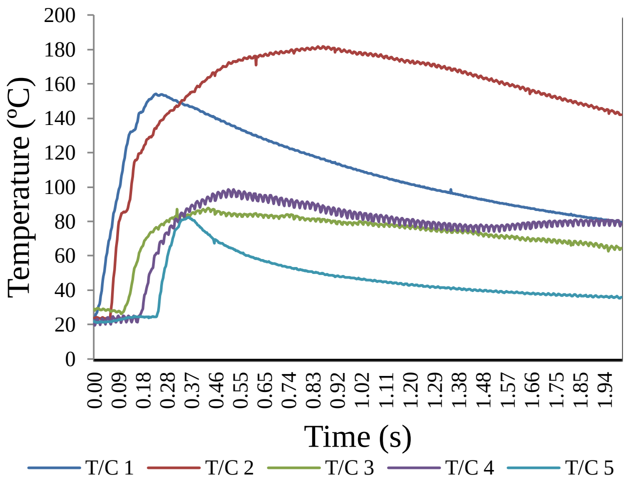

Figure A9.268 : Characteristic time-temperature profile for three Type C SRA's operating at 13MPa and water temperature 40 °C – E.R.(ϕ) 0.95

iv) Water supply pressure 13MPa and temperature 45 °C

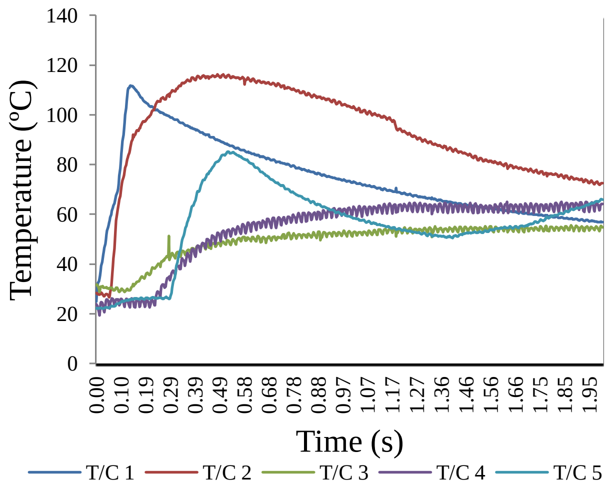

Figure A9.269 : Distinctive time-temperature profile for three Type C SRA's operating at 13MPa and water temperature 45 °C – E.R.(ϕ) 0.95

(v) Water supply pressure 13MPa and temperature 50 °C

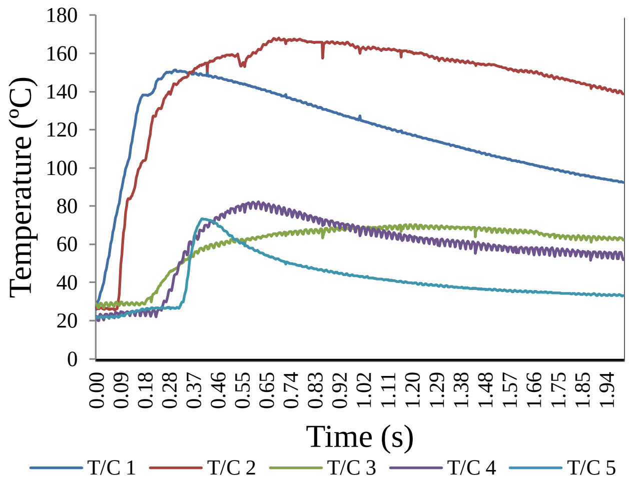

Figure A9.270 : Typical time-temperature profile for three Type C SRA's operating at 13MPa and water temperature 50 °C – E.R.(ϕ) 0.95

A9.5.4.4 Qualitative analysis

(i) Figure A9.271 reveals four still images relating to the 30 °C trial, where the flame is clearly mitigated in the spray region and fails to progress into the downstream combustible mixture. Figure A9.272 shows a magnified section of the spray region confirming cessation of combustion.

(ii) In Figure A9.273 the propagating flame can be seen to pass directly through the sprays, with the sprays appearing to have little effect on flame suppression. Figure A9.274 highlights the flame in the region of the sprays.

(iii) In Figure A9.275 the flame is seen to pass directly into the sprays, with the presence of dark regions in (ii) and (iii) suggesting a degree of flame extinguishment. However, the flame is seen to exit the sprays with sufficient temperature to propagate through the remaining downstream combustible mixture. Figure A9.276 focuses on the region of the sprays where dark areas are magnified.

(iv) and (v) Figures A9.277 and A9.279 reveal very similar sequences of events to those previously discussed in Figure A9.275, showing a high degree of combustion reduction caused in the spray region, followed by ignition and propagation through the downstream mixture. The spray regions are again highlighted in Figures A9.278 and A9.280.

(i) Water temperature 30˚C

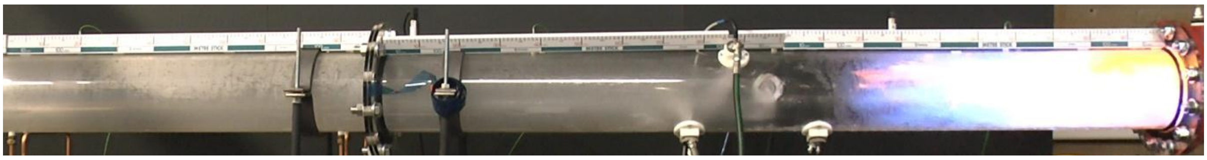

i. Flame propagating in methane-air mixture of E.R. (ϕ) 0.95upstream of SRA

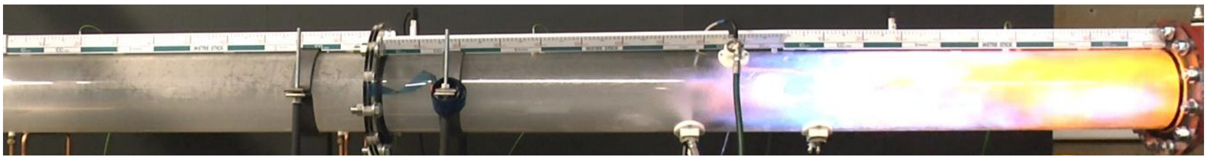

ii. Flame propagating in methane-air mixture of E.R. (ϕ) 0.95 in the region of spray

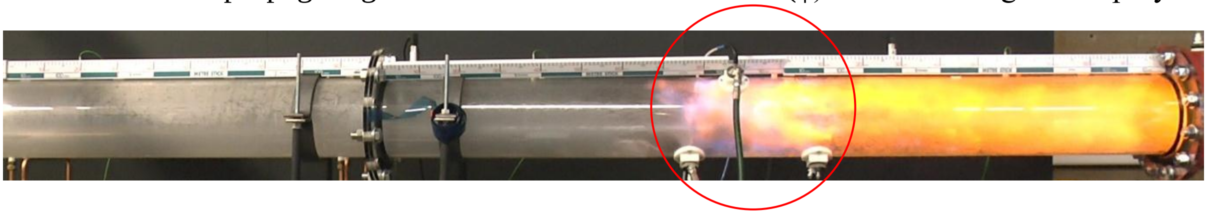

iii. Flame propagating in methane-air mixture of E.R. (ϕ) 0.95 in the region of spray

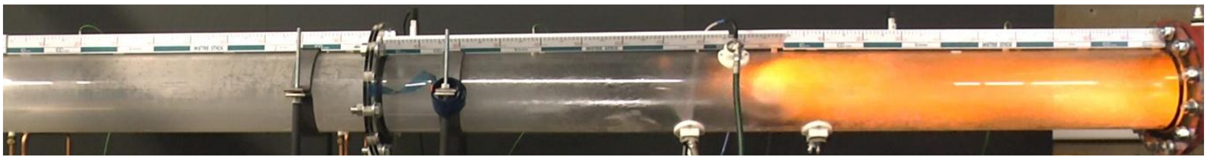

iv. **Mitigation** of flame in third spray with no further downstream combustion

Figure A9.271 : Flame propagating upstream and downstream of three X/F Type C flow SRA's with water pressure of 13MPa and 30˚C in a methane-air mixture (ϕ) 0.95

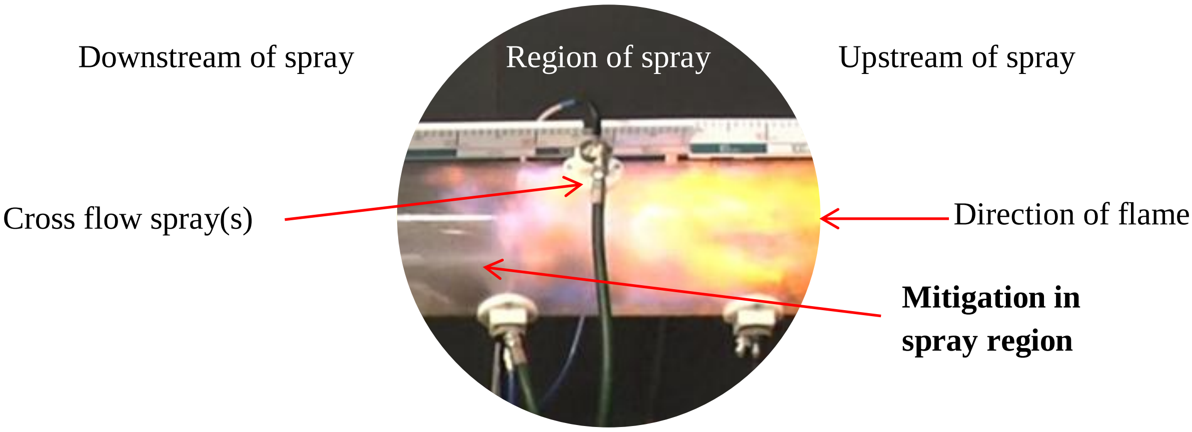

Figure A9.272 : Expanded view of region of spray highlighted in Figure A9.271(iii)

(ii) Water temperature 35°C

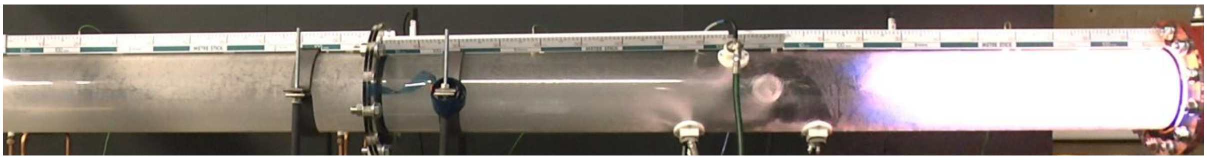

i. Flame propagating in methane-air mixture of E.R. (ϕ) 0.95upstream of SRA

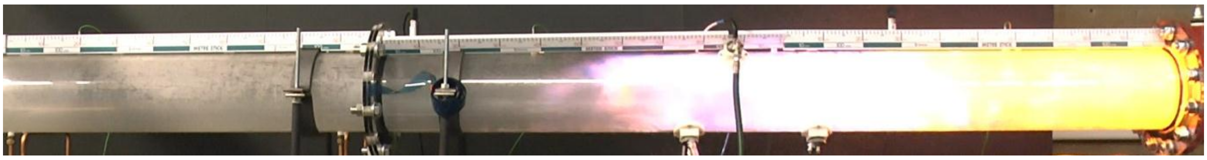

ii. Flame propagating in methane-air mixture of E.R. (ϕ) 0.95 in the region of sprays

iii. Flame propagating in downstream mixture E.R. (ϕ) 0.95

iv. Flame propagating in downstream mixture E.R. (ϕ) 0.95

Figure A9.273 : Flame propagating upstream and downstream of three X/F Type C flow SRA's with water pressure of 13MPa and 35˚C in a methane-air mixture (ϕ) 0.95

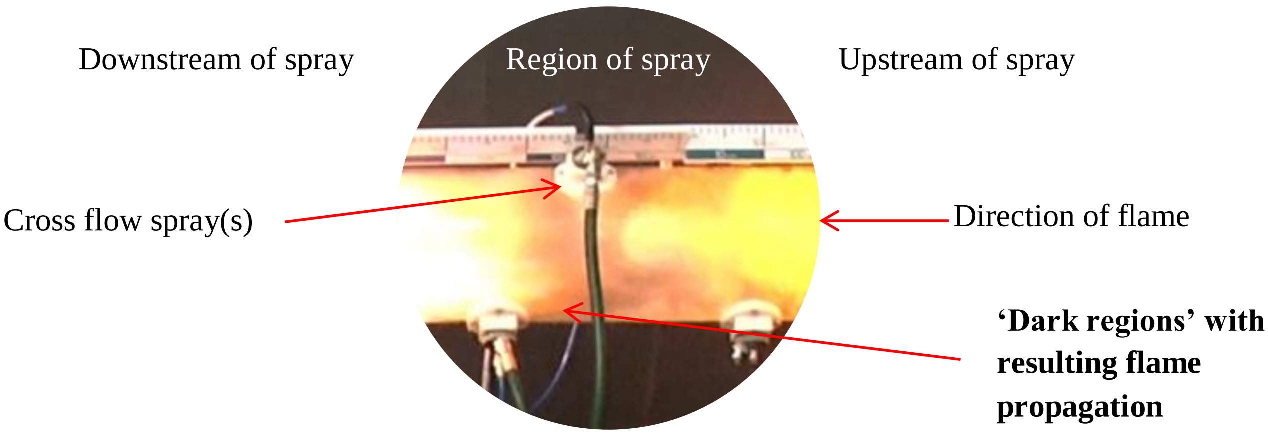

Figure A9.274 : Enlarged view of region of spray highlighted in Figure A9.273(iii)

(iii) Water temperature 40°C

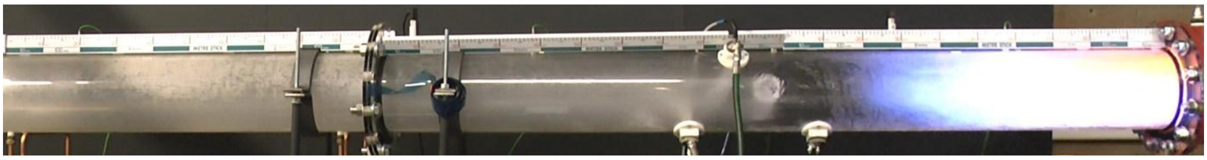

i. Flame propagating in methane-air mixture of E.R. (ϕ) 0.95upstream of SRA

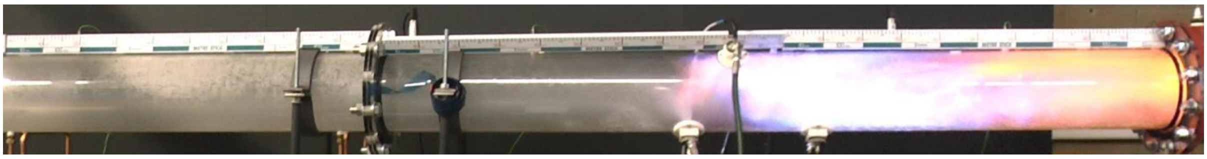

ii. Flame propagating in methane-air mixture of E.R. (ϕ) 0.95 in the region of sprays

iii. Flame propagating through spray region into downstream mixture

iv. Flame propagating through spray region into downstream mixture

Figure A9.275 : Flame propagating upstream and downstream of three X/F Type C flow SRA's with water pressure of 13MPa and 40°C in a methane-air mixture (ϕ) 0.95

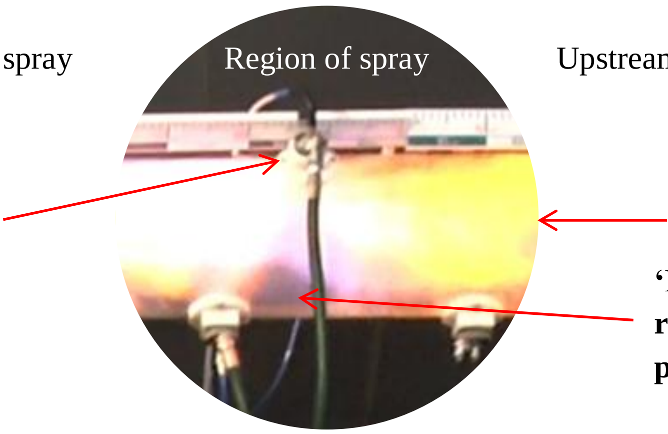

Figure A9.276 : Magnified view of region of spray highlighted in Figure A9.275(iii)

(iv) Water temperature 45°C

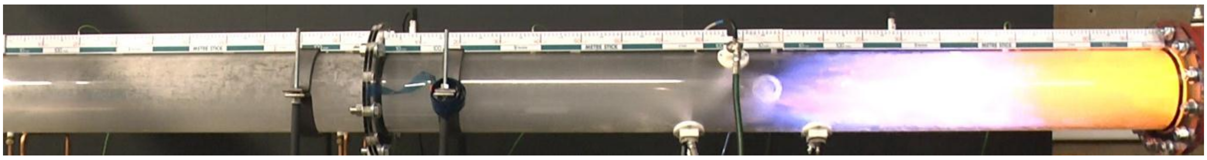

i. Flame propagating in methane-air mixture of E.R. (ϕ) 0.95 upstream of SRA

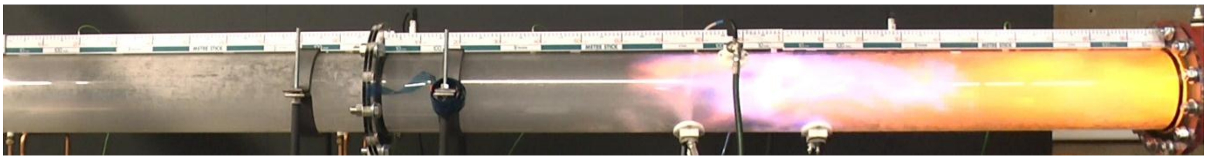

ii. Flame propagating in methane-air mixture of E.R. (ϕ) 0.95 in the region of spray

iii. Flame propagating through spray region into downstream mixture

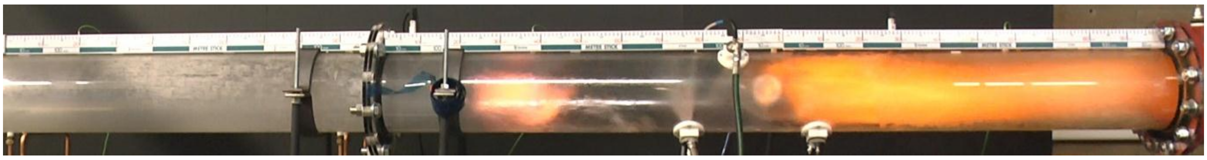

iv. Flame propagating through spray region into downstream mixture

Figure A9.277 : Flame propagating upstream and downstream of three X/F Type C flow SRA's with water pressure of 13MPa and 45°C in a methane-air mixture (ϕ) 0.95

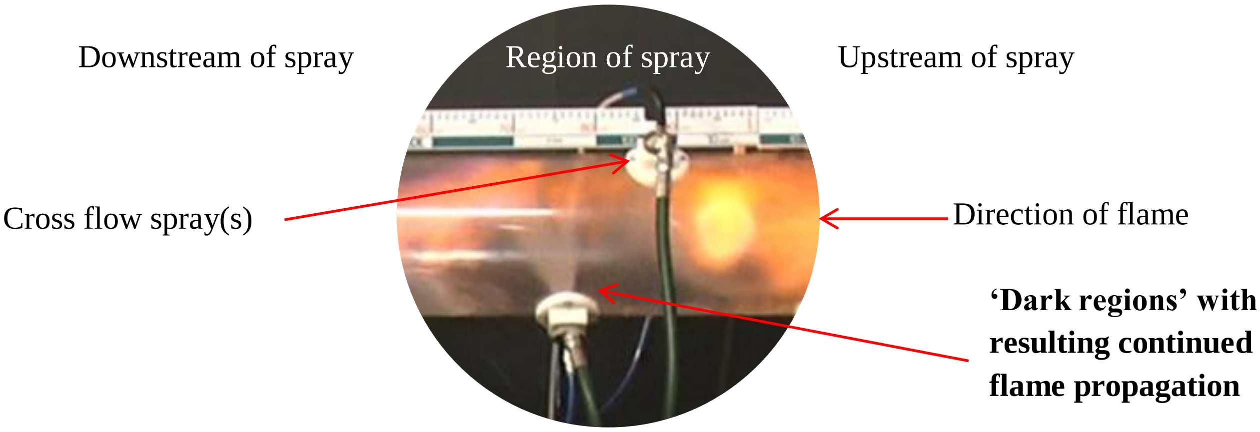

Figure A9.278 : Enlarged view of region of spray highlighted in Figure A9.277(iii)

(v) Water temperature 50˚C

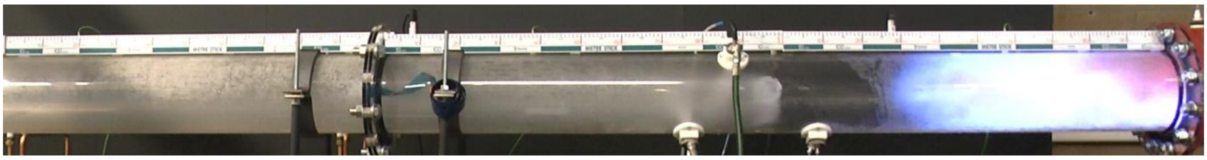

i. Flame propagating in methane-air mixture of E.R. (ϕ) 0.9 5upstream of SRA

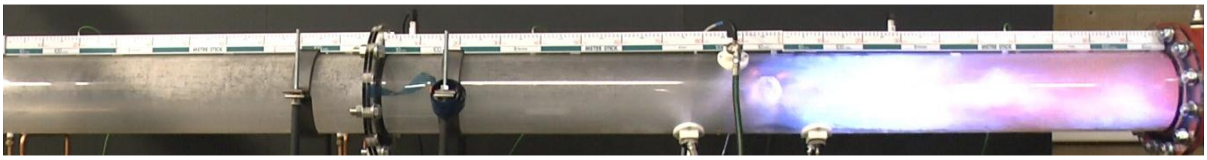

ii. Flame propagating in methane-air mixture of E.R. (ϕ) 0.95 in the region of spray

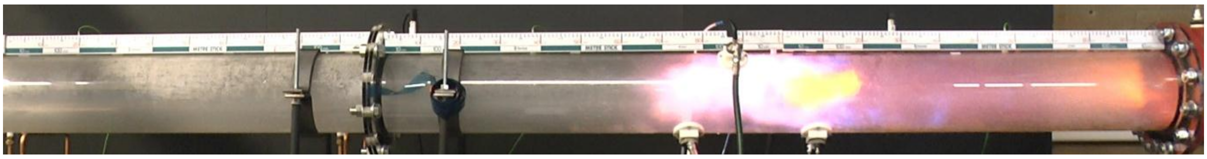

iii. Flame propagating in methane-air mixture of E.R. (ϕ) 0.95 in the region of spray

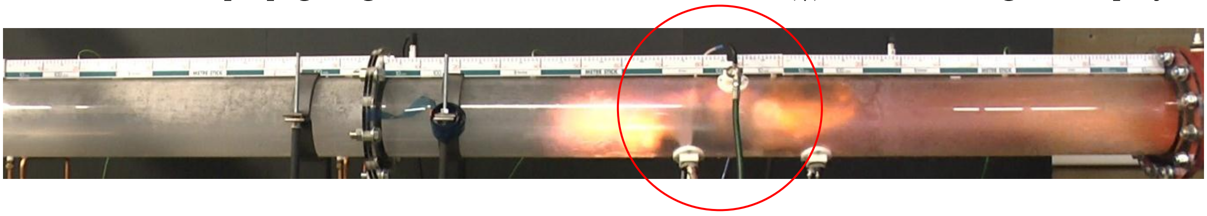

iv. Flame propagating through spray region into downstream mixture

Figure A9.279 : Flame propagating upstream and downstream of three X/F Type C flow SRA's with water pressure of 13MPa and 50˚C in a methane-air mixture (ϕ) 0.95

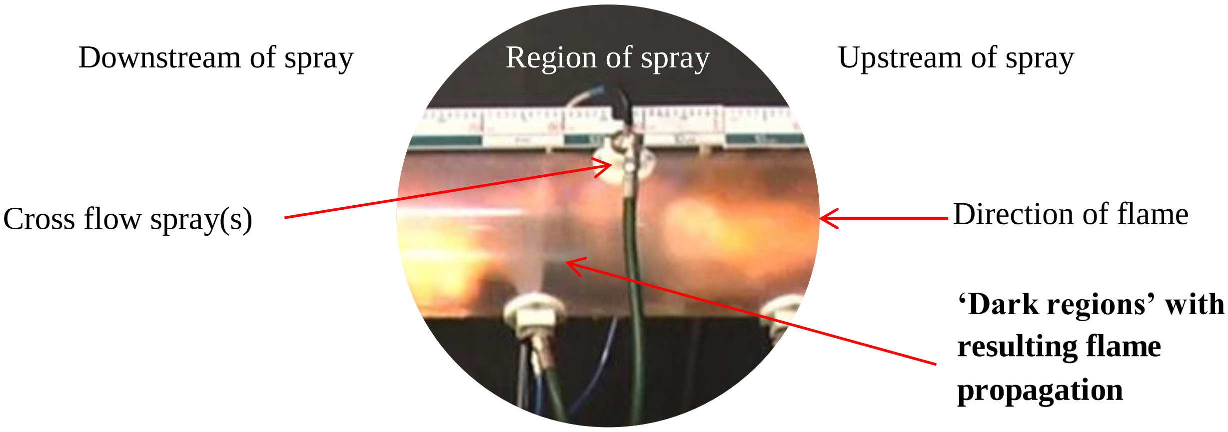

Figure A9.280 : Exploded view of region of spray highlighted in Figure A9.279(iv)

A9.5.4.5 General event outcome

Table A9.35 provides a summary of the **'general event outcome'** for each trial in this current series, using the five potential 'outcome' categories offered in Chapter 5. The results of all 'hot trials' were previously given in Table 5.14 and are also shown in Table A9.45.

Trial configuration	General event outcome	Code
3 X/F Type C : 30°C	Full Mitigation resulting in Flame Extinguishment	FMFE
3 X/F Type C : 35°C	No Mitigation with resulting Flame Deceleration	NMFD
3 X/F Type C : 40°C	No Mitigation with resulting Flame Deceleration	NMFD
3 X/F Type C : 45°C	No Mitigation with resulting Flame Deceleration	NMFD
3 X/F Type C : 50°C	No Mitigation with resulting Flame Deceleration	NMFD

Table A9.35 : General event outcome (trial series A9.5.4)

A9.5.5 Four (X/F) Type C SRA's using various water temperatures

A9.5.5.1 Trial set up

In this series of experimental trials four cross flow (X/F) Type C SRA's were supplied with water at a pressure of 13MPa at a variety of water temperatures from 25˚C to 50˚C. The aim of this run of tests was to establish the effects of an increase in water temperature supplied to the sprays. The positions of thermocouples and atomisers are illustrated in Figure A9.281 and Table A9.36.

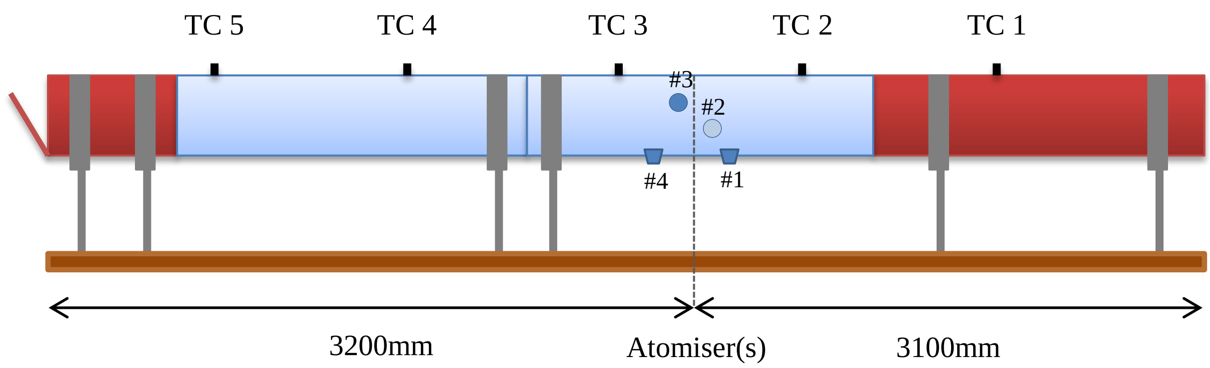

Figure A9.281 : Position of atomiser and thermocouples (relative to right hand ignition)

Component	Position (measured from right hand end)
Thermocouple no.1 (TC1)	1200mm
Thermocouple no.1 (TC2)	2400mm
Thermocouple no.1 (TC3)	3600mm
Thermocouple no.1 (TC4)	4800mm
Thermocouple no.1 (TC5)	6000mm
Atomiser outlet orifice (cross flow)	3100mm (centre of sprays)

Table A9.36 : Measured position of thermocouples and SRA's

In ensure the validity and reliability of the results in this series, two tests were performed at each of the selected temperatures and are presented as follows:-

a. Water supply temperature 25˚C : Tests (i) and (ii)
b. Water supply temperature 30˚C : Tests (i) and (ii)
c. Water supply temperature 40˚C : Tests (i) and (ii)
d. Water supply temperature 50˚C : Tests (i) and (ii)

A9.5.5.2 Flame speed

In previous studies Sapko et al [3] carried out a small scale trial with a respect to droplet temperature vaporisation and made reference to Kumm's droplet heat up and vaporisation expression. Sapko's [3] work was extensively discussed in Chapter 3.

Table A9.37 has been produced to demonstrate the conditions and temperatures considered in this series of trials. In column three the flame speed values are listed for upstream of the spray. Notably the upstream flame speed is shown to reduce with the increase in spray temperature. This relationship has not been observed in any of previous the studies offered as reference throughout this current work. The likely cause of this upstream reduction in flame speed is the interaction of droplets in the preheat zone of the flame front.

Column four of Table A9.37 shows the estimated droplet residence times for each of the tests, based on the upstream flame speed and a flame thickness of 1.05mm for the methane-air mixture E.R. .(ϕ) 0.95. Columns five, six and seven reveal the calculated residence times required to bring water droplets of various diameters to their boiling point. It is clear that in each of the scenarios offered for 10, 20 and 30μm droplets, that the actual residence time for each case is at least one or two orders of magnitude less than that required to bring the droplets to boiling point. Based on the information presented in Table A9.37 and for the D_{32} of the spray being in the order of 25 - 30 μm, the principle mode of heat transfer would favour sensible heat exchange.

Section and test number	Water temperature (˚C)	Upstream flame average speed (m/s)	Calculated droplet residence time (sec)	Calculated unsteady heat up time to bring droplet to boiling point (sec) Kumm [xx]		
				10μm	20μm	30μm
A9.5.5.1	25	27.5	3.7e-5	2.29e-4	9.14e-4	2.05e-3
(i),(ii)	25	27	3.7e-5	2.29e-4	9.14e-4	2.05e-3
A9.5.5.2	30	27.5	3.7e-5	2.28e-4	9.12e-4	2.05e-3
(i),(ii)	30	26.5	3.6e-5	2.28e-4	9.12e-4	2.05e-3
A9.5.5.3	40	23.75	4.2e-5	2.27e-4	9.07e-4	2.04e-3
(i),(ii)	40	23.5	4.2e-5	2.27e-4	9.07e-4	2.04e-3
A9.5.5.4	50	21.25	4.7e-5	2.26e-4	9.02e-4	2.03e-3
(i),(ii)	50	17.75	5.6e-5	2.26e-4	9.02e-4	2.03e-3

Table A9.37 : Flame speeds (m/s), droplet residence times (sec) and unsteady heat up time (sec) to bring droplet to boiling point

From an observational perspective, all of the experimental trials in this series produced an increasingly large volume of water vapour plume (steam) from the exit end of the flame propagation and mitigation rig as shown in Figure A9.278, thus indicating that latent heat transfer was occurring. CFD modelling was carried out in order that the mode of heat transfer could be evaluated further. This work is presented in Chapter 6.

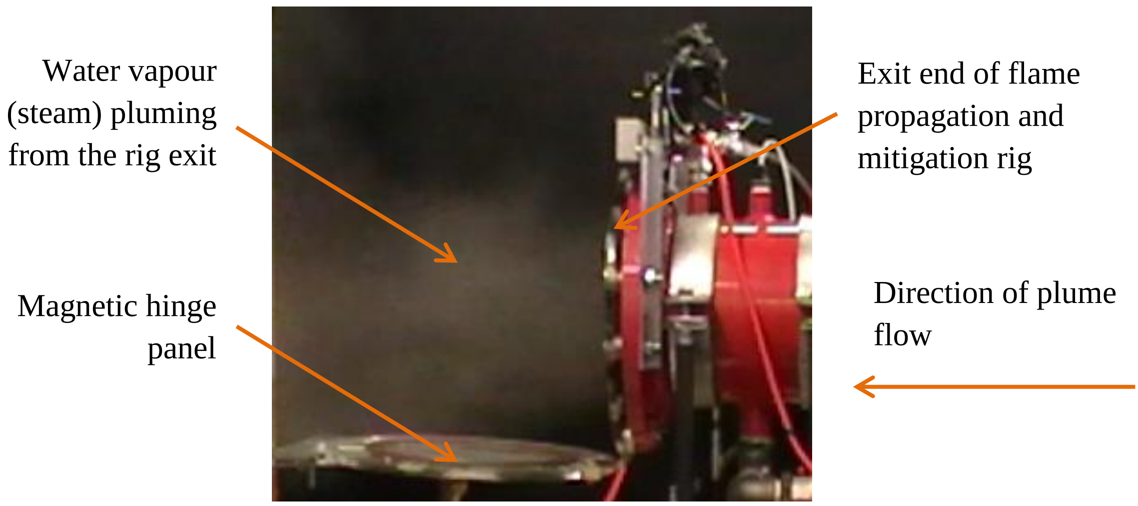

Figure A9.282 : Example of water vapour pluming from the rig exit following mitigation

Figure A9.383 shows the typical flame speed reductions (%) resulting from the eight trials in this series, whereby it is clear that all of the tests resulted in complete mitigation of the propagating methane-air flame (E.R.(ϕ) 0.95).

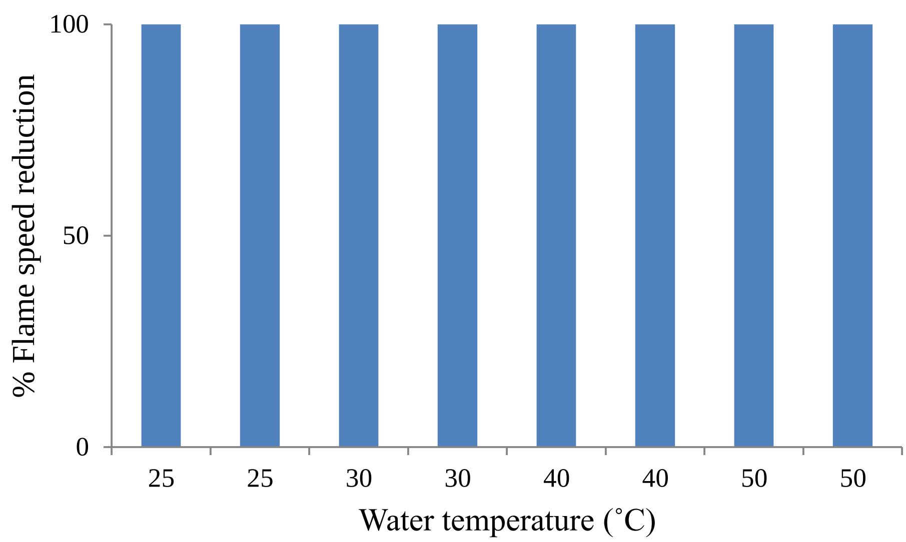

Figure A9.283 : Typical flame speed reductions for four Type C SRA’s at 13MPa

A9.5.5.3 Time-temperature response

Water supply pressure 13MPa and temperature 25°C : Tests (i) and (ii)

In Figure A9.284 and A9.285 the water supply temperature was 25°C. Each of the time-temperature profiles exhibit consistent characteristics. Thermocouples TC4 and TC5 appear approximately parallel with minimal temperature rise. The data form TC3 shows a steady increase representing a value of approximately 5 - 10°C.

Water supply pressure 13MPa and temperature 30°C : Tests (1) and (ii)

In Figure A9.286 and A9.287 the water supply temperature was 30°C. Both of the time-temperature profiles exhibit consistent appearances. Thermocouple TC5 remains more or less unaffected during each of the tests, with a marginal increase over the two seconds of data. Although mitigation occurred in both trials, TC3 and TC4 indicate an increase I temperature representing a value of about 20°C. This is consistent with the observational evidence discussed in A9.5.5, whereby a plume of vapour appeared from the rig exit point.

Water supply pressure 13MPa and temperature 40°C : Tests (1) and (ii)

In Figure A9.288 and A9.289 the water supply temperature was 40°C. Both of the time-temperature profiles exhibit similar appearances. Thermocouple TC5 remains more or less unaffected during each of the tests, with a marginal increase over the two seconds of data. Although mitigation occurred in both trials, TC3 and TC4 indicate an increase in temperature representing a value of about 20 - 25°C. This is again in agreement with the observational evidence discussed in A9.5.5, whereby a plume of vapour appeared from the exit point of the apparatus. The plume in this case appeared to be larger than that reported in A9.5.5.2.

Water supply pressure 13MPa and temperature 50°C : Tests (1) and (ii)

In Figure A9.290 and A9.291 the water supply temperature was 50°C. Both of the time-temperature profiles exhibit similar appearances. In this case thermocouple TC5 shows a much higher increase over the two seconds of data than any of the other trials in this series. Although mitigation happened in both trials, TC3 and TC4 indicate an increase in temperature representing a value of about 20 - 30°C. This being harmonious with the observational verification discussed in A9.5.5, whereby a plume of vapour appeared from the exit point of the apparatus. The plume in this case appeared to be larger than that reported in A9.5.5.2.

Water supply pressure 13MPa and temperature 25°C

(i) Water supply pressure 13MPa and temperature 25°C

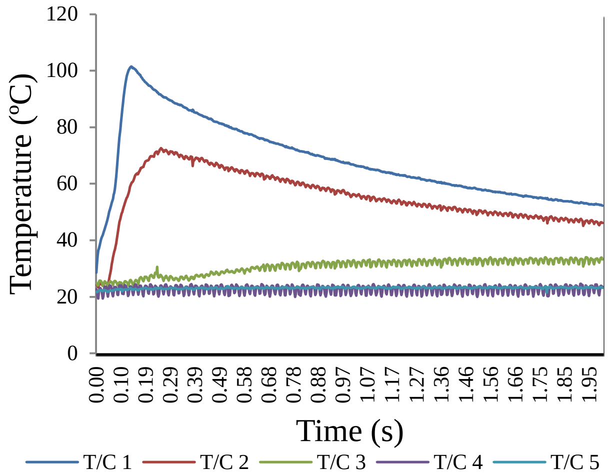

Figure A9.284 : Distinctive time-temperature profile for four Type C SRA's operating at 13MPa and water temperature 25°C – E.R.(ϕ) 0.95

(ii) Water supply pressure 13MPa and temperature 25°C

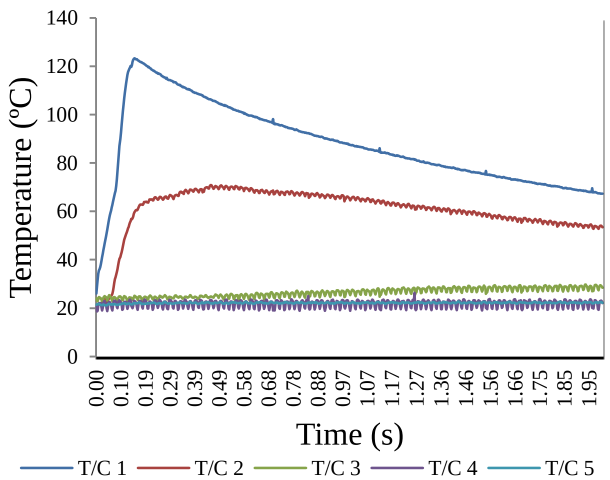

Figure A9.285 : Typical time-temperature profile for four Type C SRA's operating at 13MPa and water temperature 25°C – E.R.(ϕ) 0.95

Water supply pressure 13MPa and temperature 30°C

(i) Water supply pressure 13MPa and temperature 30 °C

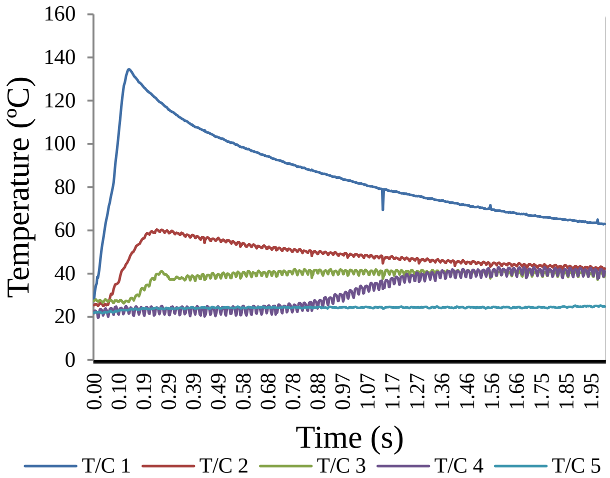

Figure A9.286 : Distinctive time-temperature profile for four Type C SRA's operating at 13MPa and water temperature 30 °C – E.R.(ϕ) 0.95

(ii) Water supply pressure 13MPa and temperature 30 °C

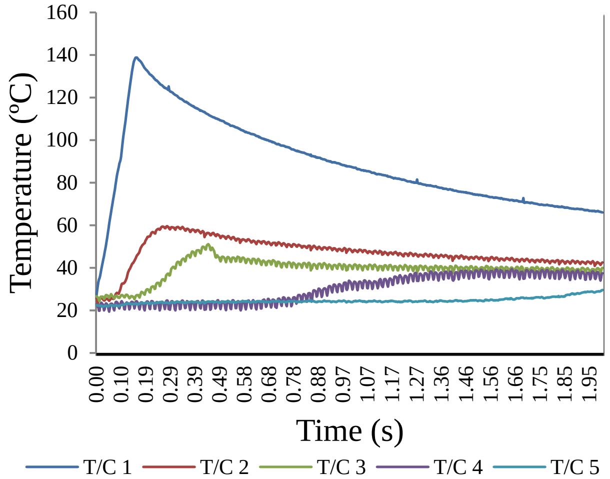

Figure A9.287 : Characteristic time-temperature profile for four Type C SRA's operating at 13MPa and water temperature 30 °C – E.R.(ϕ) 0.95

Water supply pressure 13MPa and temperature 40°C

(i) Water supply pressure 13MPa and temperature 40 °C

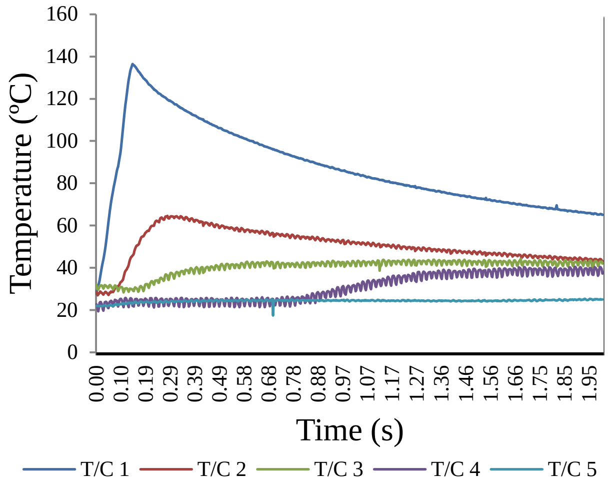

Figure A9.288 : Typical time-temperature profile for four Type C SRA's operating at 13MPa and water temperature 40 °C – E.R.(ϕ) 0.95

(ii) Water supply pressure 13MPa and temperature 40 °C

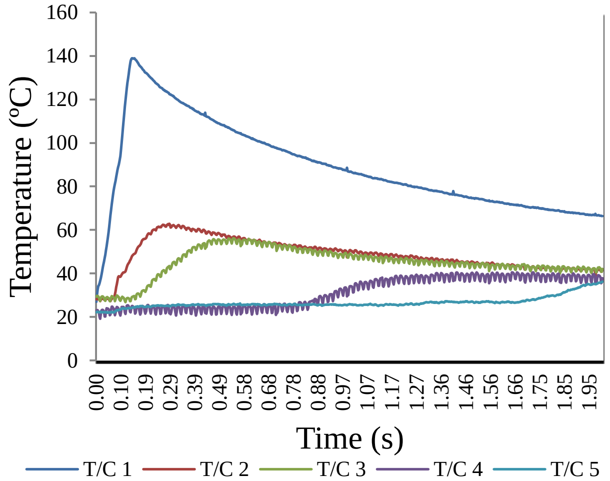

Figure A9.289 : Distinctive time-temperature profile for four Type C SRA's operating at 13MPa and water temperature 40 °C – E.R.(ϕ) 0.95

Water supply pressure 13MPa and temperature 50°C

(i) Water supply pressure 13MPa and temperature 50 °C

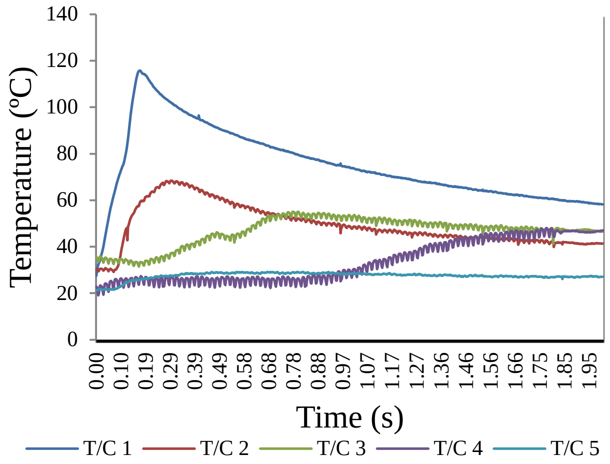

Figure A9.290 : Characteristic time-temperature profile for four Type C SRA's operating at 13MPa and water temperature 50 °C – E.R.(ϕ) 0.95

(ii) Water supply pressure 13MPa and temperature 50 °C

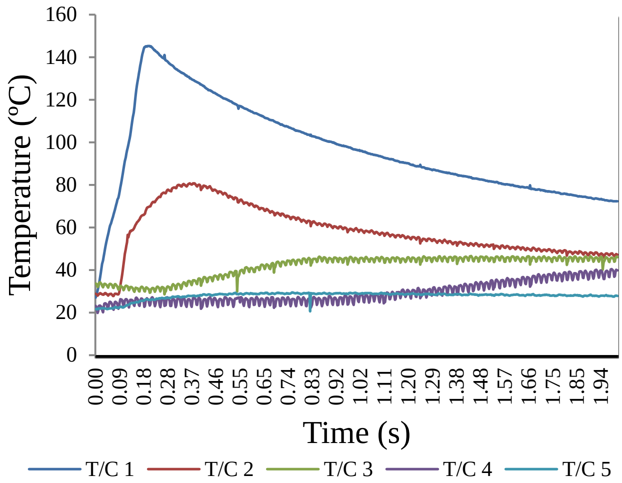

Figure A9.291 : Distinctive time-temperature profile for four Type C SRA's operating at 13MPa and water temperature 50 °C – E.R.(ϕ) 0.95

A9.5.5.4 Qualitative analysis

Water supply pressure 13MPa and temperature 25°C

Figure A9.292 the four still photographs show the initial propagation of the flame and its transition through the sprays. In this circumstance the flame did not propagate beyond spray #3. Figure A9.293 offers a magnified image of the flame being mitigated a spray #3.

The same experimental conditions were repeated and the relevant still photographs are revealed in Figure A9.294. In this test the flame did not propagate beyond spray #3 and spray #4, finally mitigated combustion. Figure A9.295 shows an expanded image of the flame being mitigated a spray #4.

Water supply pressure 13MPa and temperature 30°C

Figure A9.296 the four still photographs show the initial propagation of the flame and its transition through the sprays. On this occasion the flame did not propagate beyond spray #4. Figure A9.297 offers a magnified image of the flame being mitigated a spray #4.

The same experimental conditions were repeated and the relevant still photographs are revealed in Figure A9.298. In this instance the flame did not propagate beyond spray #4 where combustion ceased to progress. Figure A9.299 shows an expanded image of the flame being mitigated a spray #4.

Water supply pressure 13MPa and temperature 40°C

Figure A9.300 the four still photographs show the initial propagation of the flame and its transition through the sprays. In this test the flame did not propagate beyond spray #4. Figure A9.301offers a magnified image of the flame being mitigated a spray #4.

The same experimental conditions were repeated and the relevant still photographs are revealed in Figure A9.302. In this trial the flame did not propagate beyond spray #4. Figure A9.303 offers a magnified image of the flame being mitigated a spray #4.

Water supply pressure 13MPa and temperature 50°C

Figure A9.304 the still photographs show the initial propagation of the flame and its passage through the sprays. In this test the flame did not propagate beyond spray #3. Figure A9.305 offers a magnified image of the flame being mitigated a spray #3.

The same experimental conditions were repeated and the relevant still photographs are revealed in Figure A9.306. In this trial the flame did not propagate beyond spray #3. Figure A9.307 offers a magnified image of the flame being mitigated a spray #3.

Water supply pressure 13MPa and temperature 25°C (i)

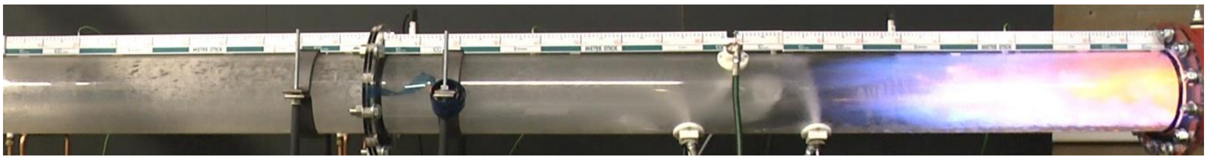

i. Flame propagating in methane-air mixture of E.R. (ϕ) 0.95upstream of SRA

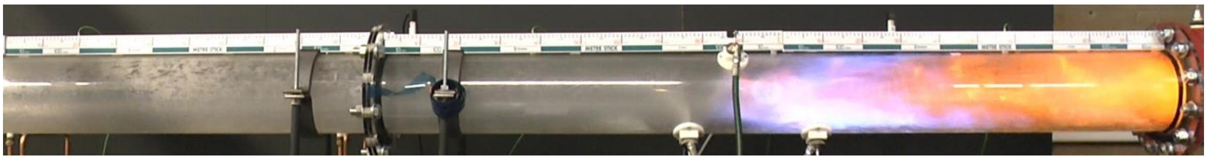

ii. Flame propagating in methane-air mixture of E.R. (ϕ) 0.95 in the region of spray

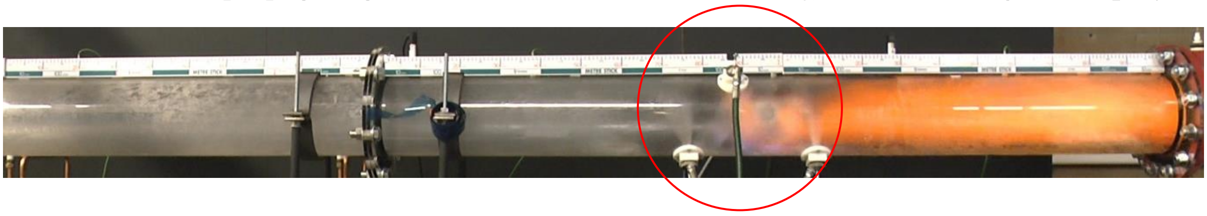

iii. Flame **propagation has been suppressed** by the sprays

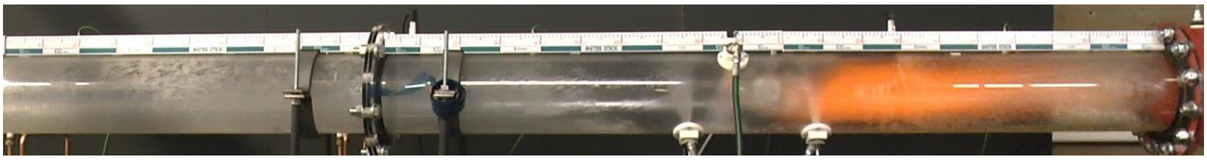

iv. Final stages and reduction of trailing combustion gases

Figure A9.292 : Flame propagating upstream and downstream of four X/F Type C SRA’s with water temperature of 25°C in a methane-air mixture (ϕ) 0.95

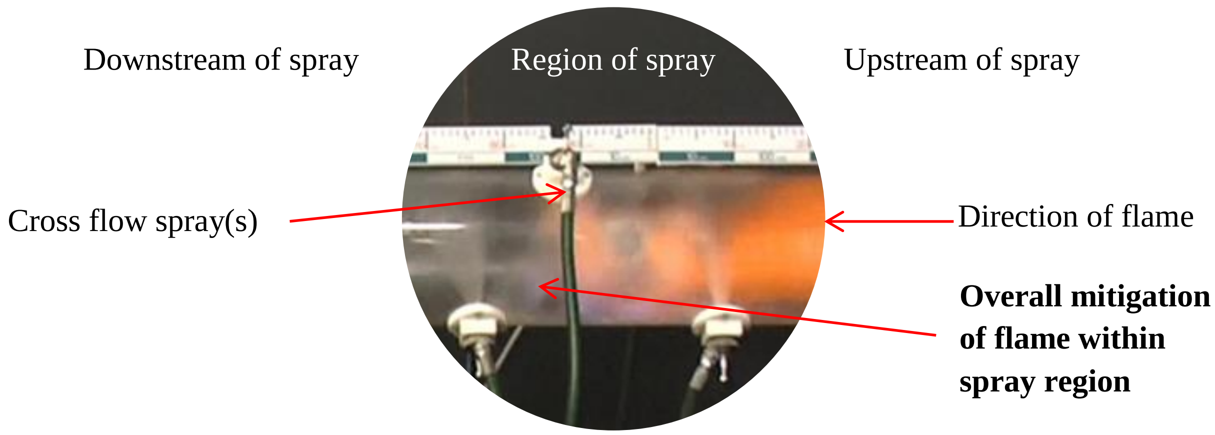

Figure A9.293 : Expanded view of region of spray highlighted in Figure A9.292(iii)

Water supply pressure 13MPa and temperature 25°C (ii)

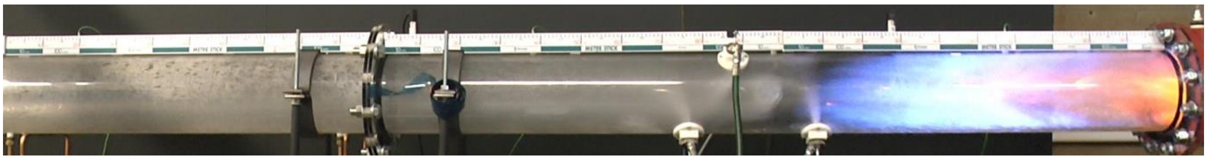

i. Flame propagating in methane-air mixture of E.R. (ϕ) 0.95upstream of SRA

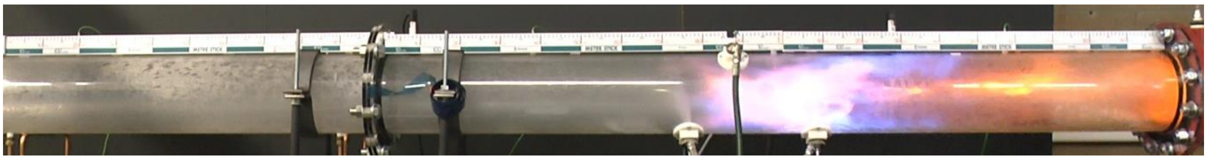

ii. Flame propagating in methane-air mixture of E.R. (ϕ) 0.95 upstream of SRA

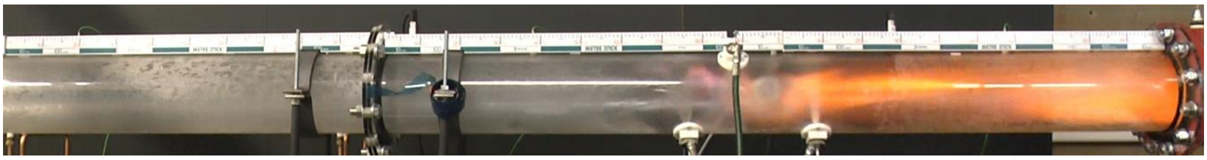

iii. **Mitigation** in methane-air mixture of E.R. (ϕ) 0.95in the region of spray

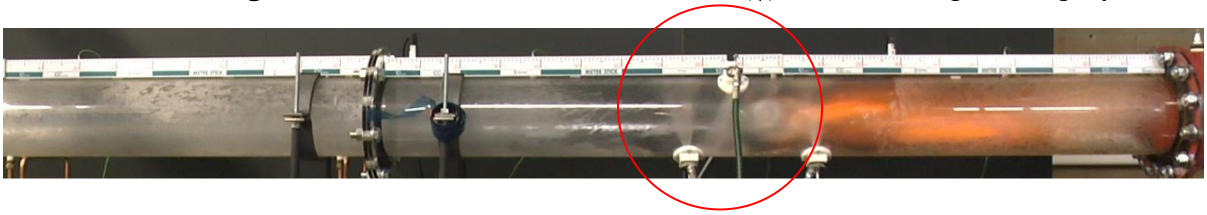

iv. Final stages and reduction of trailing combustion gases

Figure A9.294 : Flame propagating upstream and downstream of four X/F Type C SRA's with water temperature of 25°C in a methane-air mixture (ϕ) 0.95

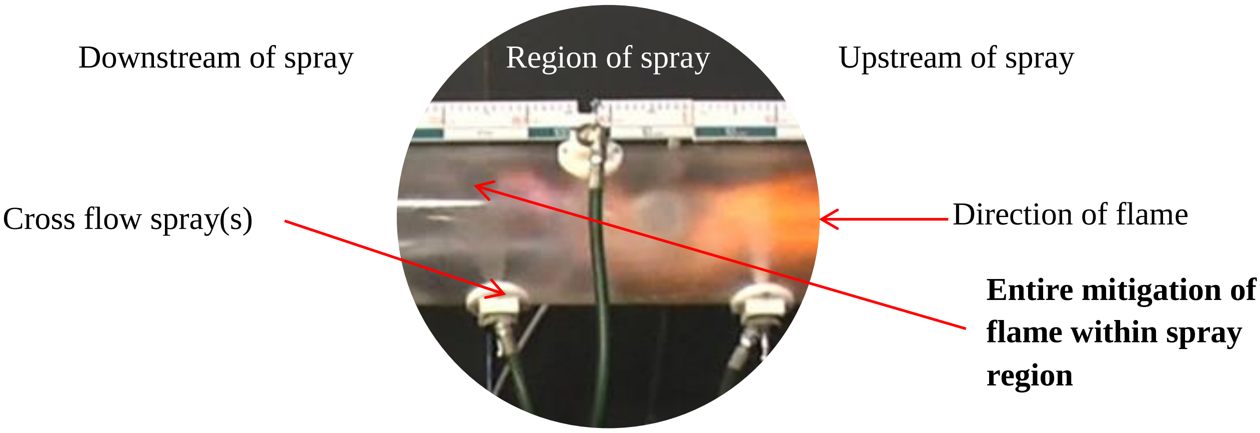

Figure A9.295 : Enlarged view of region of spray highlighted in Figure A9.294(iv)

Water supply pressure 13MPa and temperature 30°C (i)

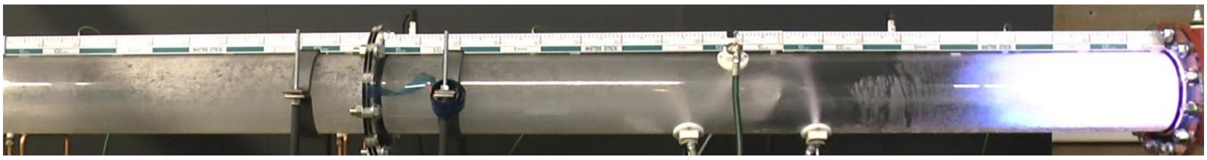

i. Flame propagating in methane-air mixture of E.R. (ϕ) 0.95 upstream of SRA

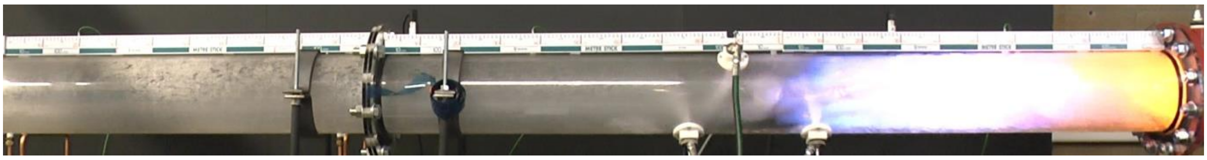

ii. Flame interacting with spray #1 in methane-air mixture of E.R. (ϕ) 0.95

iii. Flame interacting with spray region in methane-air mixture of E.R. (ϕ) 0.95

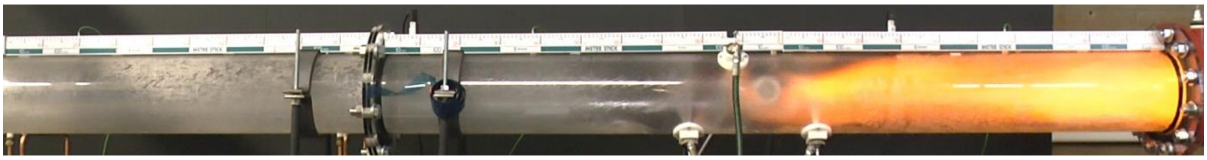

iv. Flame propagation has been terminated in methane-air mixture of E.R. (ϕ) 0.95

Figure A9.296 : Flame propagating upstream and downstream of four X/F Type C SRA's with water temperature of 30°C in a methane-air mixture (ϕ) 0.95

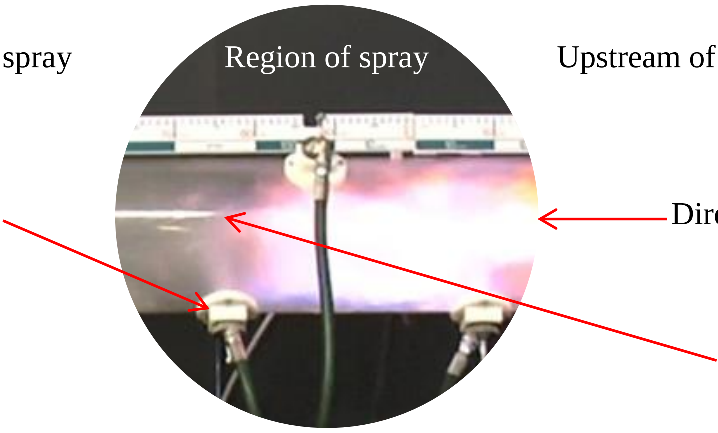

Figure A9.297 : Expanded view of region of spray highlighted in Figure A9.296(iii)

Water supply pressure 13MPa and temperature 30°C (ii)

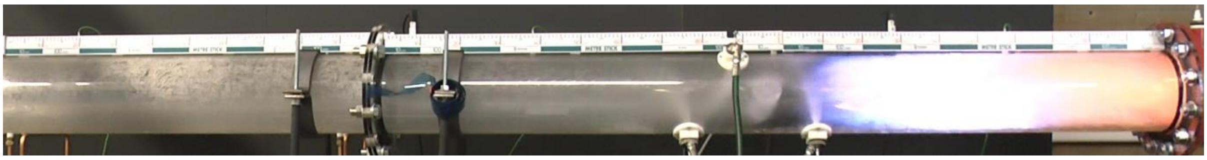

i. Flame propagating in methane-air mixture of E.R. (ϕ) 0.95 upstream of SRA

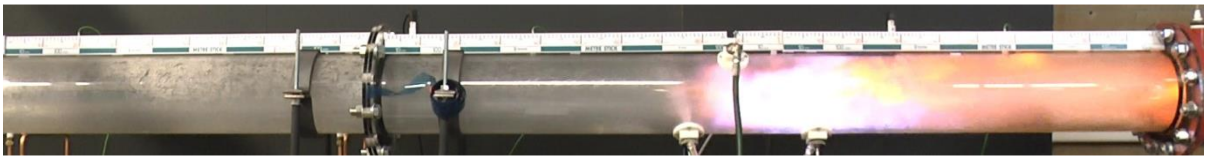

ii. Flame propagating in methane-air mixture of E.R. (ϕ) 0.95 in the region of spray

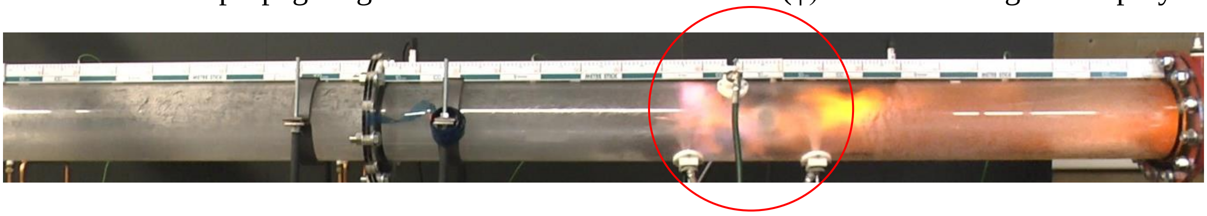

iii. **Mitigation** of flame in methane-air mixture of E.R. (ϕ) 0.95 in the region of spray

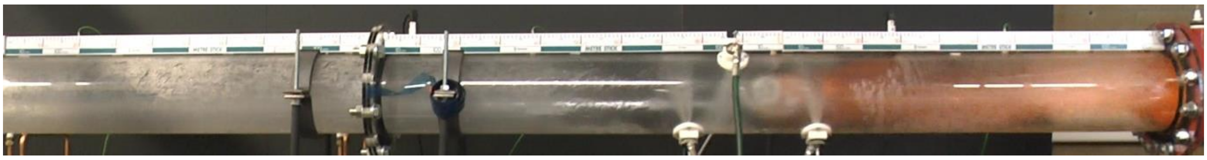

iv. Final stages of decaying combustion activity flame in methane-air mixture

Figure A9.298 : Flame propagating upstream and downstream of four X/F Type C SRA's with water temperature of 30°C in a methane-air mixture (ϕ) 0.95

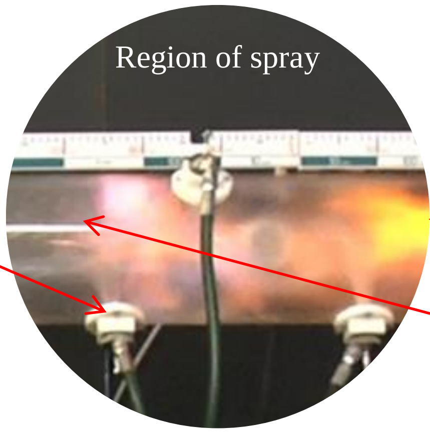

Figure A9.299 : Enlarged view of region of spray highlighted in Figure A9.298(iii)

Water supply pressure 13MPa and temperature 40°C (i)

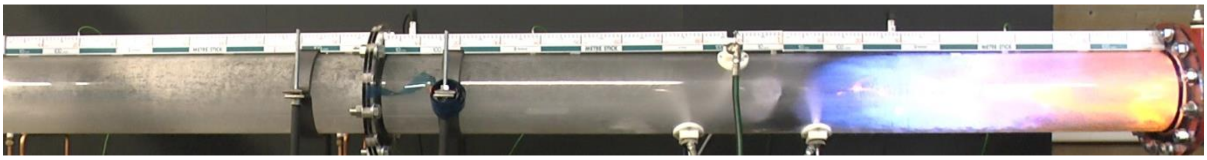

i. Flame propagating in methane-air mixture of E.R. (ϕ) 0.95upstream of SRA

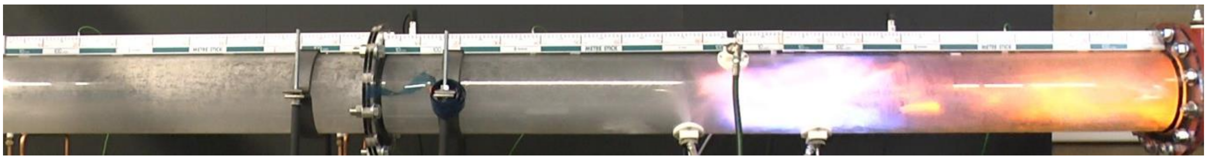

ii. Flame propagating in methane-air mixture of E.R. (ϕ) 0.95 upstream of SRA

iii. **Mitigation** in methane-air mixture of E.R. (ϕ) 0.95 in the region of spray

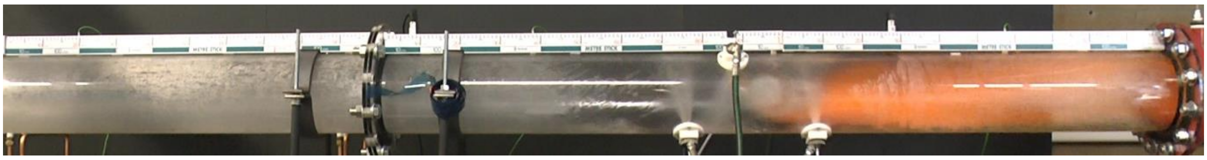

iv. Final stages of combustion in trailing gases

Figure A9.300 : Flame propagating upstream and downstream of four X/F Type C SRA's with water temperature of 40°C in a methane-air mixture (ϕ) 0.95

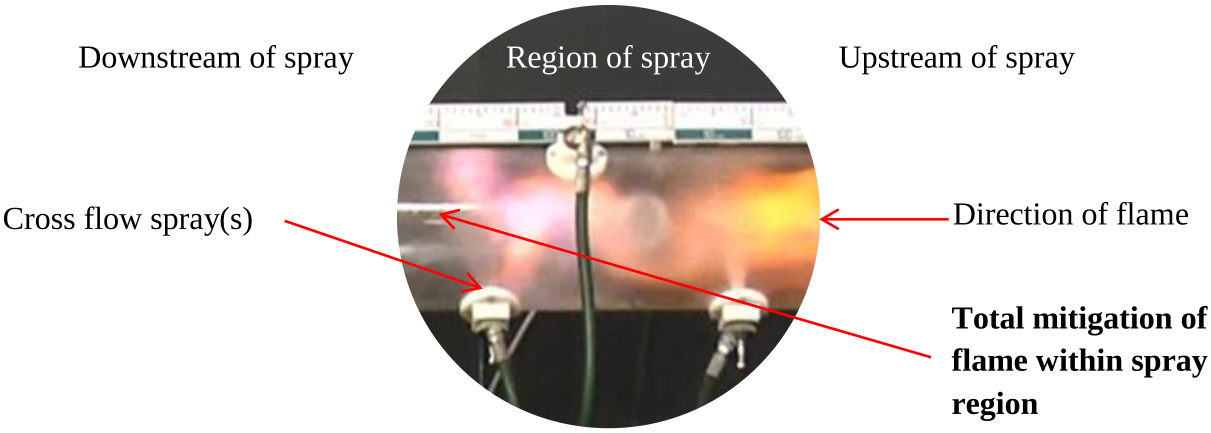

Figure A9.301 : Expanded view of region of spray highlighted in Figure A9.300(iii)

Water supply pressure 13MPa and temperature 40°C (ii)

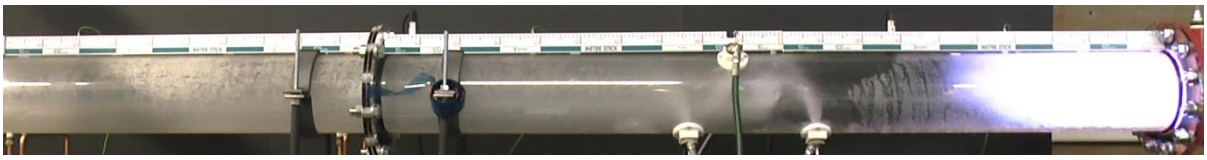

i. Flame propagating in methane-air mixture of E.R. (ϕ) 0.95upstream of SRA

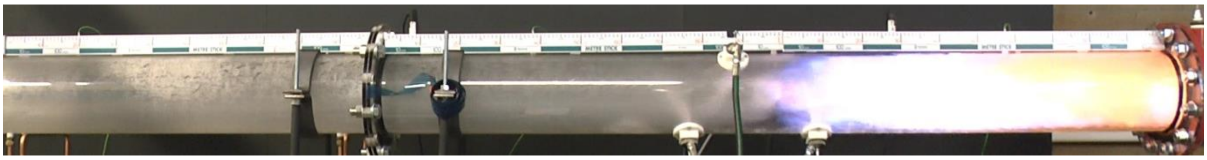

ii. Flame propagating in methane-air mixture of E.R. (ϕ) 0.95 upstream of SRA

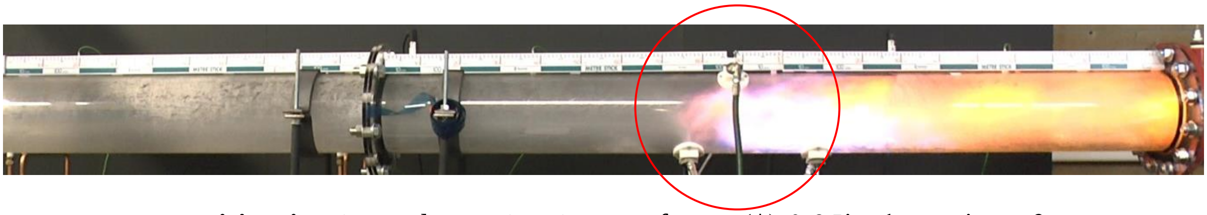

iii. **Mitigation** in methane-air mixture of E.R. (ϕ) 0.95in the region of spray

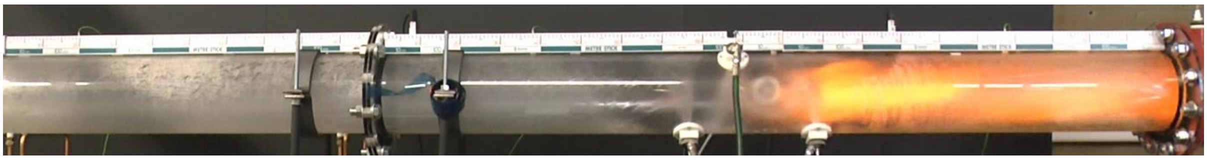

iv. **Mitigation** in methane-air mixture of E.R. (ϕ) 0.95 downstream of SRA

Figure A9.302 : Flame propagating upstream and downstream of four X/F Type C SRA's with water temperature of 40°C in a methane-air mixture (ϕ) 0.95

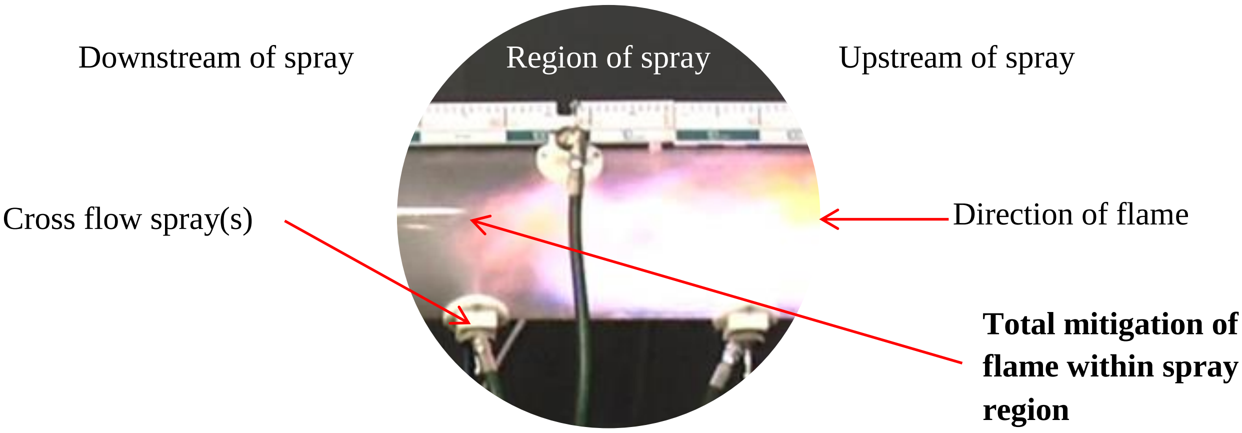

Figure A9.303 : Magnified view of region of spray highlighted in Figure A9.302(iii)

Water supply pressure 13MPa and temperature 50°C (i)

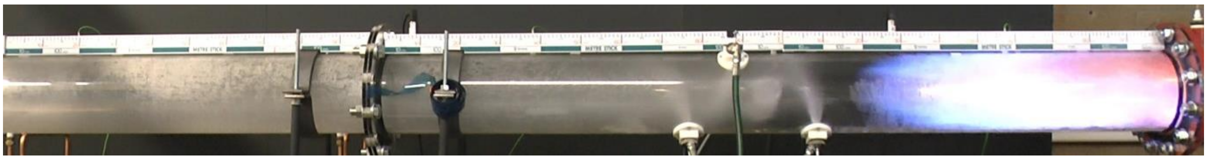

i. Flame propagating in methane-air mixture of E.R. (ϕ) 0.95upstream of SRA

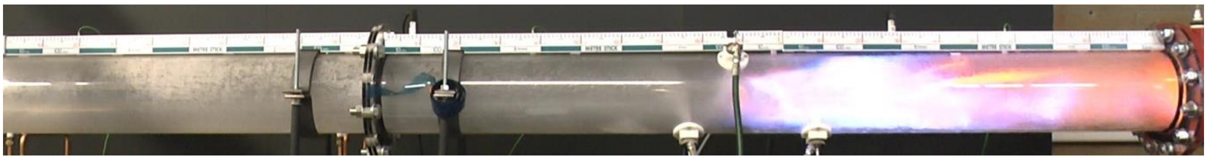

ii. Flame propagating in methane-air mixture of E.R. (ϕ) 0.95 upstream of SRA

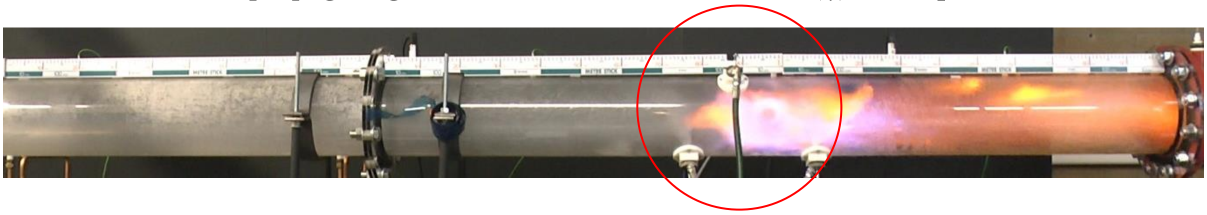

iii. **Mitigated** flame in methane-air mixture of E.R. (ϕ) 0.95in the region of spray

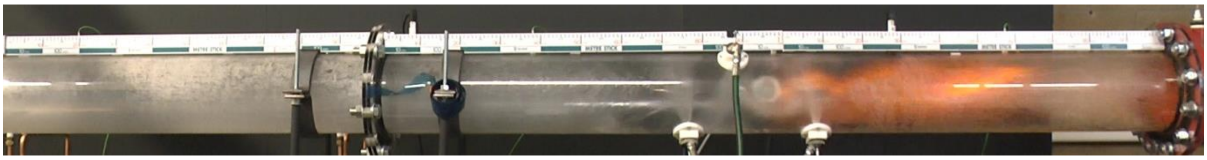

iv. Final stages of combustion occurrence

Figure A9.304 : Flame propagating upstream and downstream of four X/F Type C SRA's with water temperature of 50°C in a methane-air mixture (ϕ) 0.95

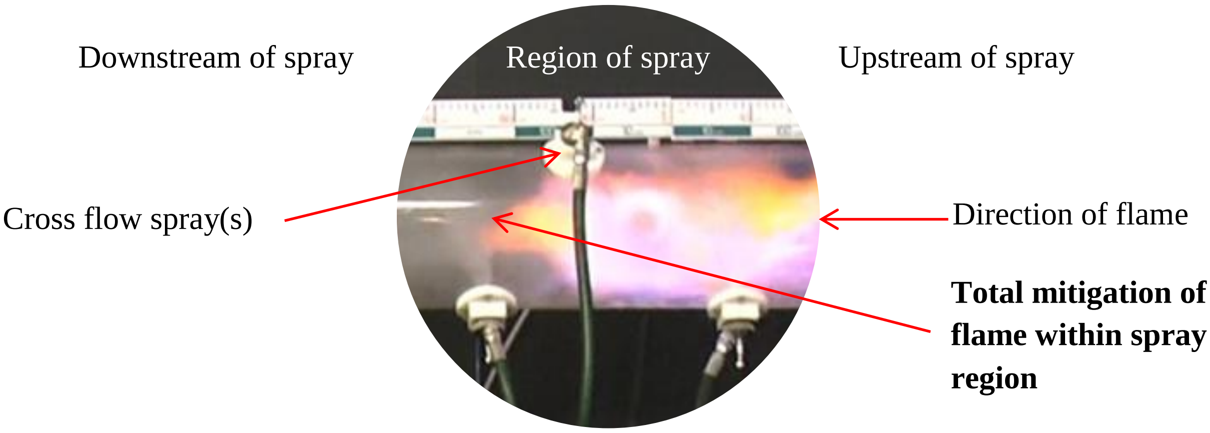

Figure A9.305 : Enlarged view of region of spray highlighted in Figure A9.304(iii)

Water supply pressure 13MPa and temperature 50°C (ii)

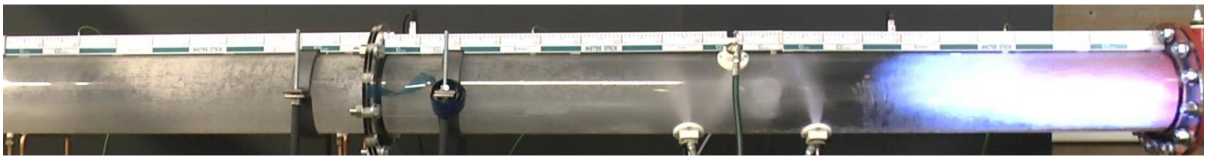

i. Flame propagating in methane-air mixture of E.R. (ϕ) 0.95upstream of SRA

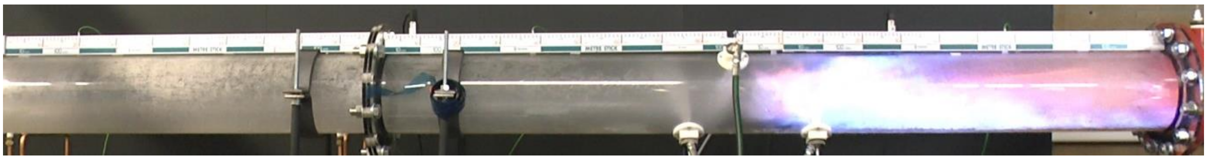

ii. Flame propagating in methane-air mixture of E.R. (ϕ) 0.95 upstream of SRA

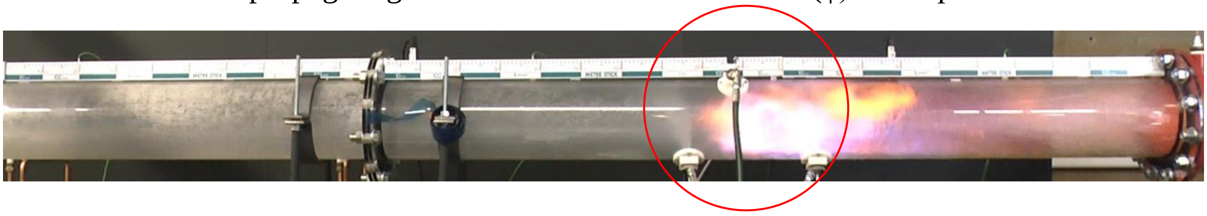

iii. **Mitigation** in methane-air mixture of E.R. (ϕ) 0.95in the region of spray

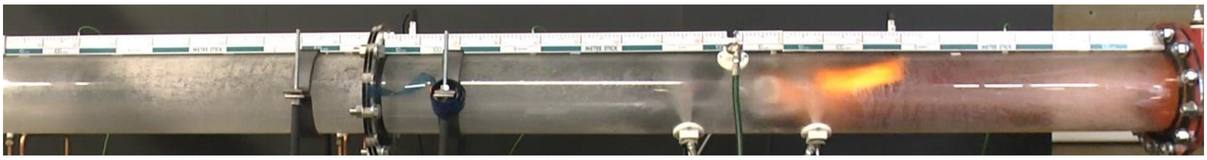

iv. Small trace of luminous flame which did not propagate any further

Figure A9.306 : Flame propagating upstream and downstream of four X/F Type C SRA's with water temperature of 50°C in a methane-air mixture (ϕ) 0.95

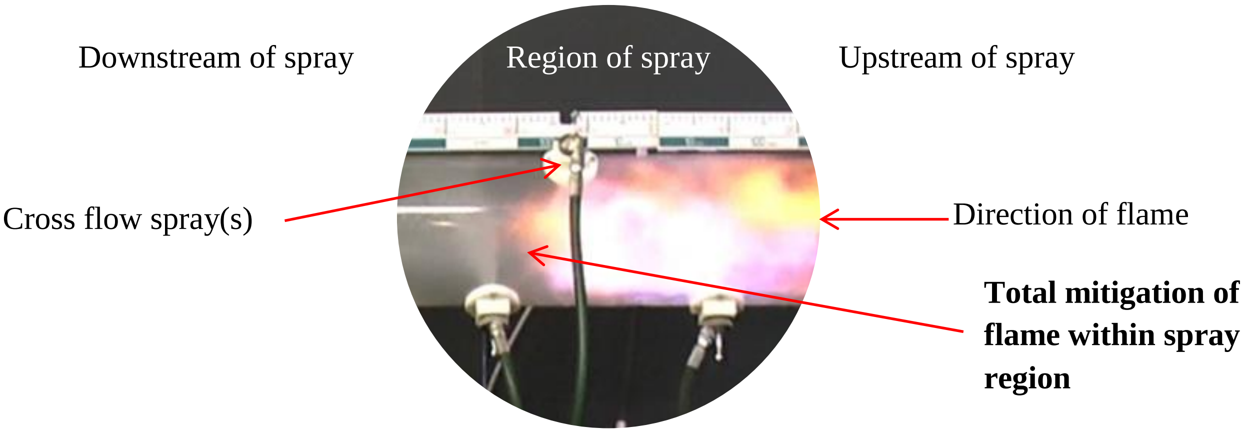

Figure A9.307 : Close up view of region of spray highlighted in Figure A9.306(iii)

A9.5.5.5 General event outcome

Table A9.38 provides a summary of the **'general event outcome'** for each trial in this current series, using the five potential 'outcome' categories offered in Chapter 5. The results of all 'hot trials' were previously given in Table 5.14 and are also shown in Table A9.45.

Trial configuration	General event outcome	Code
4 X/F Type C : 25°C (i)	Full Mitigation resulting in Flame Extinguishment	FMFE
4 X/F Type C : 25°C (ii)	Full Mitigation resulting in Flame Extinguishment	FMFE
4 X/F Type C : 30°C (i)	Full Mitigation resulting in Flame Extinguishment	FMFE
4 X/F Type C : 30°C (ii)	Full Mitigation resulting in Flame Extinguishment	FMFE
4 X/F Type C : 40°C (i)	Full Mitigation resulting in Flame Extinguishment	FMFE
4 X/F Type C : 40°C (ii)	Full Mitigation resulting in Flame Extinguishment	FMFE
4 X/F Type C : 50°C (i)	Full Mitigation resulting in Flame Extinguishment	FMFE
4 X/F Type C : 50°C (ii)	Full Mitigation resulting in Flame Extinguishment	FMFE

Table A9.38 : General event outcome (trial series A9.5.5)

A9.6 Supplementary trials

In this series of supplementary trials the performance of the four cross flow (X/F) Type C SRA's arrangement was evaluated in alternative circumstances, using the existing FPMR shown in Figure A9.308.

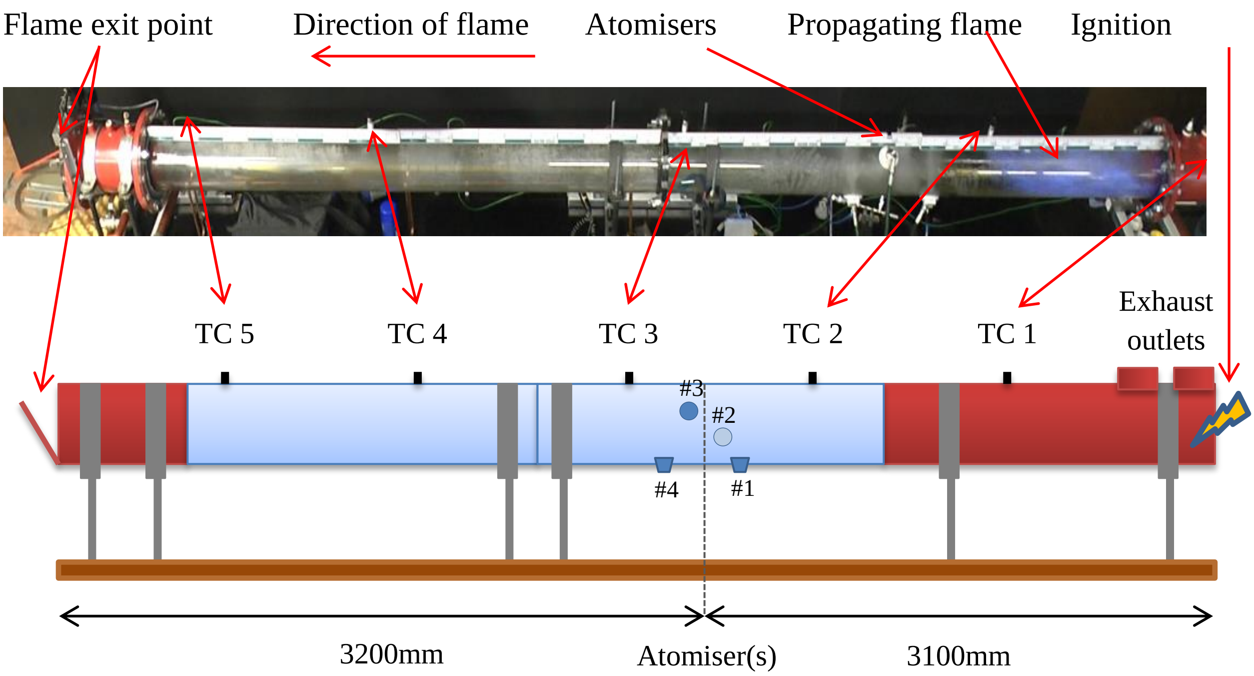

Figure A9.308 : Position of atomisers, thermocouples, exhaust outlets and ignition

Three groups of supplementary trials were conducted to evaluate the SRA performance in different situations:-

A9.6.1 Four (X/F) Type C SRA's with water at 20°C a and supply pressure of 13MPa in a methane-air flames E.R. (ϕ) 1.18, 1.30, 1.43, 1.65

A9.6.2 Four (X/F) Type C SRA's with water at 20°C a and supply pressure of 13MPa in a propane-air flame E.R. (ϕ) 0.49, 0.74, 1.00

A9.6.3 Four (X/F) Type C SRA's with water at 20°C a and supply pressure of 13MPa in a propane-air flame E.R. (ϕ) 0.95 with partial blockage of exhaust outlets in a methane-air flame

A9.6.1 Four (X/F) Type C SRA's in a methane-air E.R. (ϕ) 1.18, 1.30, 1.43, 1.65

A9.6.1.1 Trial set up

For this series of experimental trials four different methane-air mixtures of E.R. (ϕ) 1.18, 1.30, 1.43, 1.65 (11%, 12%, 13%, 14% methane in air) were used to evaluate the operation of the four cross flow Type C SRA arrangement, previously used in methane-air mixtures of E.R. (ϕ) 0.61, 0.72, 0.95, 1.06 (6%, 7%, 9%, 10% methane in air).

The relationship between equivalence ratio (ϕ) and flame thickness was previously discussed in Chapter 2 and the flame thickness for the methane-air mixtures used in these trials are summarised in Figure A9.309 and Table A9.39.

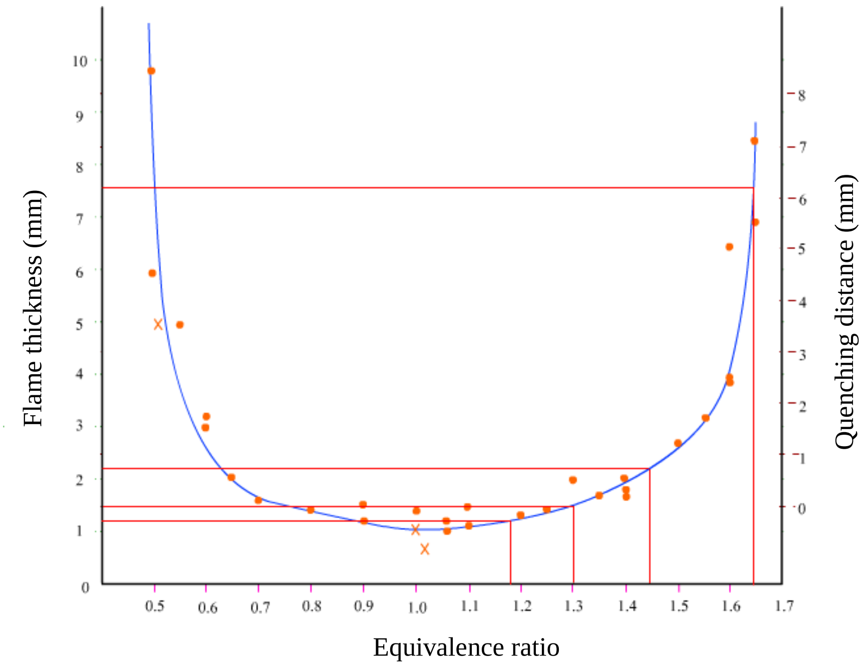

Figure A9.309 : Typical equivalence ratio-flame thickness for methane-air mixtures of E.R. (ϕ) 1.18, 1.30, 1.43, 1.65

One of the challenges encountered when igniting mixtures above stoichiometric and particularly those tending towards the upper explosive limit (UEL), is the requirement for higher ignition energy. This phenomenon was previously discussed in Chapter 2. To overcome ignition difficulties in this work several options were tested.

To ensure reliability of ignition, two spark plugs were used simultaneously via a high powered ignition transformer, normally associated with a heavy fuel oil burner system. The ignition transformer output was approximately 20,000v and produced a repetitive continuous spark which was activated by the same safety interlock system used for all other trials in this work. Average flame speeds measured upstream of the SRA position can be found in Table A9.39.

Equivalence ratio (ϕ)	Approximate flame thickness (mm)	Average upstream flame speed (m/s)
1.18	1.2	24.50
1.30	1.5	22.25
1.43	2.2	20.75
1.65	7.5	19.75

Table A9.39 : Approximate flame thickness and flame speeds

A9.6.1.2 Flame speed

All four of the methane-air mixtures tested in this series were completely mitigated by the spray. Flame speed reduction percentages are illustrated in Figure A9.310, whereas photographic images are shown in Figures A9.315 - A9.322.

The flame speeds produced in this series were predictably slower than those found in the previous trials. The combination of these slower flame speeds, together with the increased flame thickness resulting from higher equivalence ratios, provided greater residence time for the droplets to extract heat from the flame. This is evident in the photographs with the relative position to where the flame was extinguished.

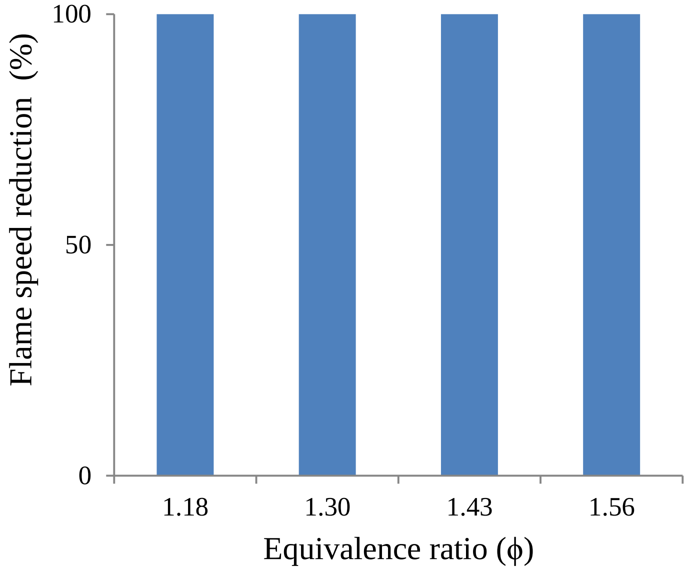

Figure A9.310 : Typical flame speed reductions (%) for four Type C SRA's at 13MPa and E.R.(ϕ)1.18, 1.30, 1.43, 1.65

Although the mitigation suitability of the spill return atomiser (SRA) has only been confirmed with respect to propagating flames in this current work, there is good reason to suggest the potential for use in fixed and portable fire mitigation equipment.

Suggestions for further research in this area are discussed in Chapter 7.

A9.6.1.3 Time-temperature response

Methane-air mixture of E.R. (ϕ) 1.18

Figure A9.311 illustrates the typical time-temperature profiles resulting from the methane-air mixture E.R. (ϕ) 1.18. The profiles for TC4 and TC5 are approximately parallel indicating that the flame did not progress. The rise in temperature in TC3 is attributed to the rapid vaporisation of droplets and subsequent production of water vapour.

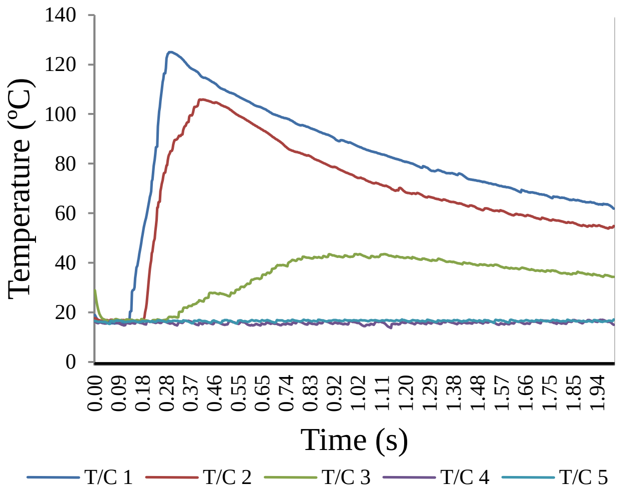

Figure A9.311 : Distinctive time-temperature profile for four SRA Type C in X/F arrangement with methane-air mixture of E.R. (ϕ) 1.18

Methane-air mixture of E.R. (ϕ) 1.30

Figure A9.312 shows the typical time-temperature profiles resulting from the methane-air mixture E.R. (ϕ) 1.30. The profiles for TC4 and TC5 are in agreement with the results discussed previously in the E.R. (ϕ) 1.18 trial and are again parallel with each other, indicating that the flame did not progress. The rise in TC3 is attributed to the rapid vaporisation of droplets is less than that exhibited by the E.R. (ϕ) 1.18 methane-air mixture.

This may be attributed to the early mitigation at spray #3 as revealed in Figure A9.311 and where less water vapour would have been produced.

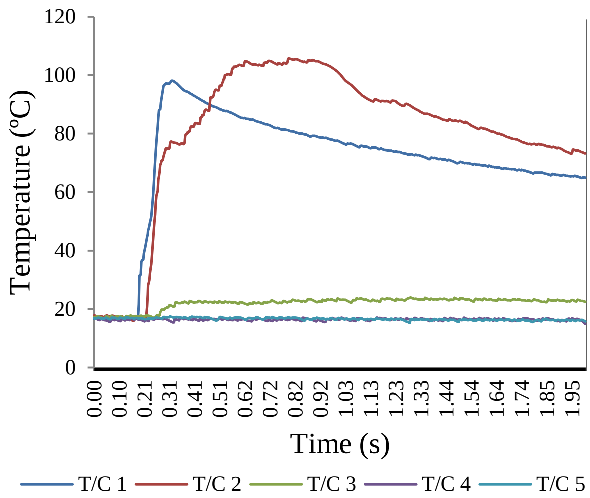

Figure A9.312 : Characteristic time-temperature profile for four SRA Type C in X/F arrangement with methane-air mixture of E.R. (ϕ) 1.30

Methane-air mixture of E.R. (ϕ) 1.43

Figure A9.313 shows the typical time-temperature profiles resulting from the methane-air mixture E.R. (ϕ) 1.43. The profiles for TC4 and TC5 are in agreement with the results discussed previously in the E.R. (ϕ) 1.18 and 1.30 trial and are again parallel with each other, indicating that the flame did not progress. The rise in TC3 is credited to be due to the rapid vaporisation of droplets is yet again less than that exhibited by the E.R. (ϕ) 1.18 methane-air mixture.

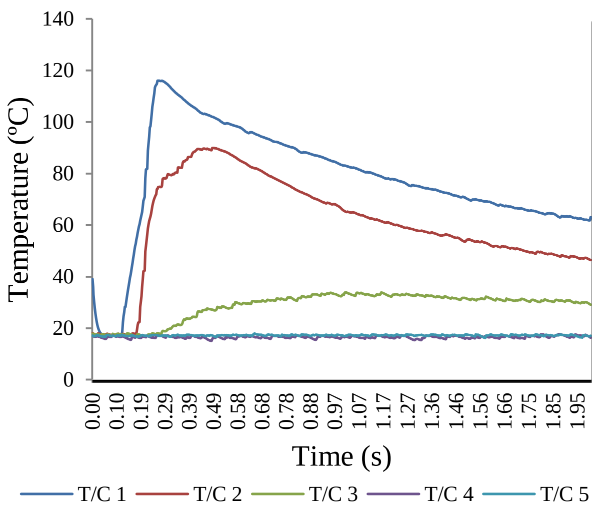

Figure A9.313 : Classic time-temperature profile for four SRA Type C in X/F arrangement with methane-air mixture of E.R. (ϕ) 1.43

Methane-air mixture of E.R. (ϕ) 1.56

Figure A9.314 shows the typical time-temperature profiles resulting from the methane-air mixture E.R. (ϕ) 1.56. The profiles for TC4 and TC5 are also in agreement with the results the E.R.(ϕ)1.18, 1.30, 1.43 trials. The rise in TC3 is ascribed to the rapid vaporisation of droplets is also less than that exhibited by the E.R. (ϕ) 1.18 methane-air mixture.

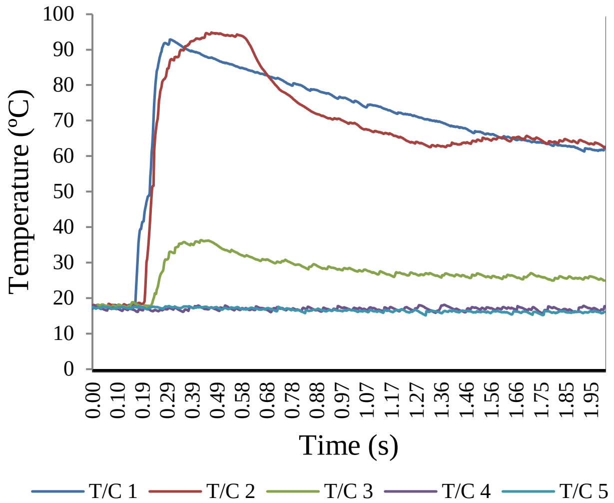

Figure A9.314 : Representative time-temperature profile for four SRA Type C in X/F arrangement with methane-air mixture of E.R. (ϕ) 1.56

A9.6.1.4 Qualitative analysis

Methane-air mixture of E.R. (ϕ) 1.18

Figure A9.315(i) reveals the flame upstream of the first spray prior to any interaction.

In Figure A9.315(ii) the flame can be seen to progress through the spray #1 with the presence of dark regions where combustion has ceased.

Figure A9.315(iii) displays further dark regions with mitigation finally occurring at spray #4.

Figure A9.315(iv) was captured 20ms after Figure A9.315(iii) and confirms that the flame did not re-establish or continue to propagate.

Methane-air mixture of E.R. (ϕ) 1.30

Figure A9.317(i) reveals the flame upstream of the first spray prior to any interaction.

In Figure A9.317(ii) displays dark regions with no flame progression beyond spray #3 which is magnified an shown in Figure A9.xxx.

Figure A9.317(iii) was captured 20ms after Figure A9.317(ii) and confirms that the flame did not re-establish or continue to propagate.

Figure A9.317(iii) was captured 40ms after Figure A9.317(ii) and shows the interaction of the trailing intermediate reactants

Methane-air mixture of E.R. (ϕ) 1.43

Figure A9.319(i) reveals the flame upstream of the first spray prior to any interaction.

In Figure A9.319(ii) displays dark regions with no flame progression beyond spray #3 which is magnified and shown in Figure A9.xxx.

Figure A9.319(iii) was captured 20ms after Figure A9.319(ii) and confirms that the flame did not re-establish or continue to propagate.

Figure A9.319(iv) was captured 40ms after Figure A9.319(ii) and confirms the suppression of the trailing intermediate reactants

A9.6.1.4 Methane-air mixture of E.R. (ϕ) 1.56

Figure A9.321(i) reveals the flame upstream of the first spray prior to any interaction.

In Figure A9.321(ii) displays dark regions with no flame progression beyond spray #3 which is magnified and shown in Figure A9.xxx.

Figure A9.321(iii) was captured 20ms after Figure A9.321(ii) and confirms that the flame did not re-establish or continue to propagate.

Figure A9.321(iv) was captured 40ms after Figure A9.321(ii) and confirms the retraction of the trailing intermediate reactants

Methane-air mixture of E.R. (ϕ) 1.18

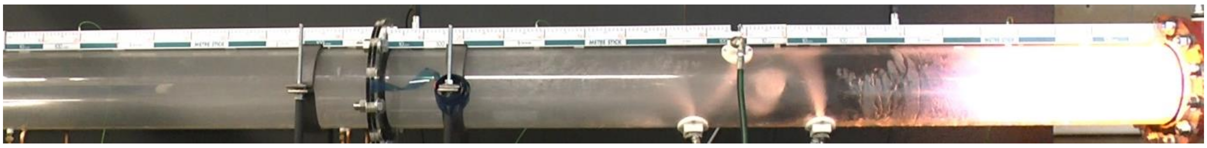

i. Flame propagating in methane-air mixture of E.R. (ϕ) 1.18 upstream of SRA

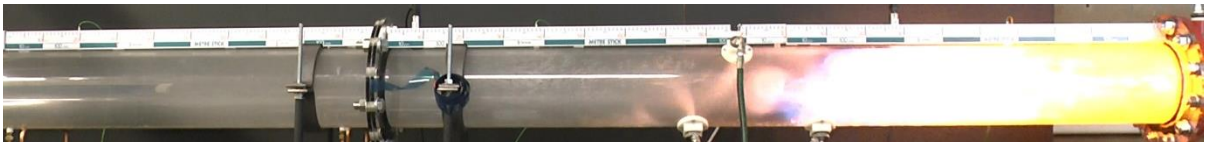

ii. Flame propagating in methane-air mixture of E.R. (ϕ) 1.18 upstream of SRA

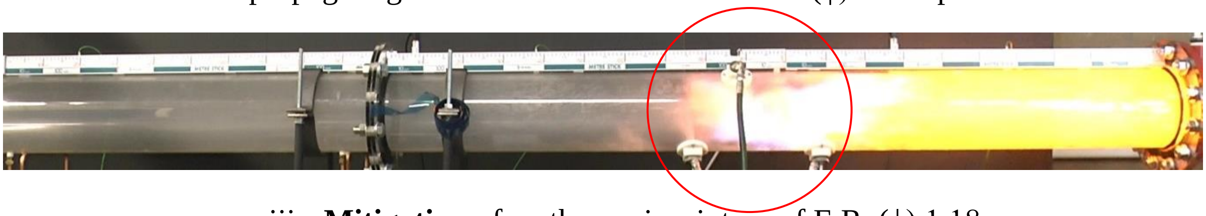

iii. **Mitigation** of methane-air mixture of E.R. (ϕ) 1.18

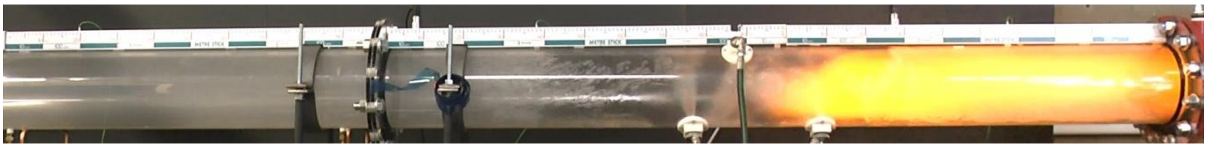

iv. 20ms after **mitigation** of methane-air mixture of E.R. (ϕ) 1.18

Figure A9.315 : Flame propagating upstream and mitigation using four Type C cross flow SRA's in a methane-air mixture (ϕ) 1.18

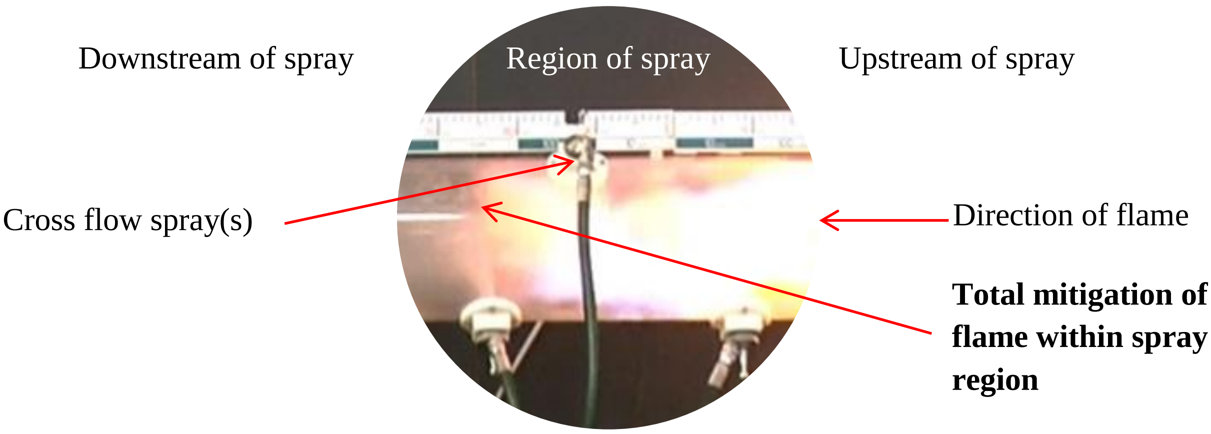

Figure A9.316: Expanded view of region of spray highlighted in Figure A9.315(iii)

Methane-air mixture of E.R. (ϕ) 1.30

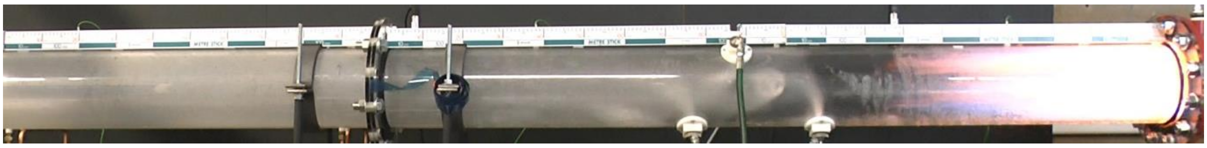

i. Flame propagating in methane-air mixture of E.R. (ϕ) 1.30 upstream of SRA

ii. Mitigation of methane-air mixture of E.R. (ϕ) 1.30

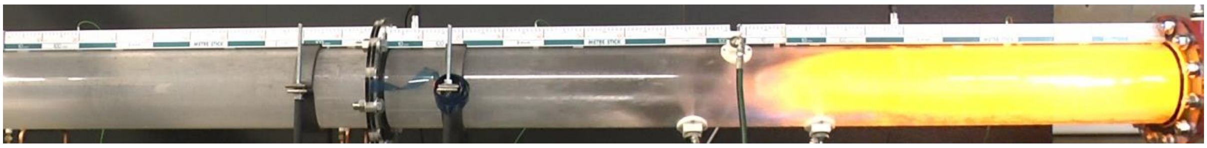

iii. 20ms after **mitigation** of methane-air mixture of E.R. (ϕ) 1.30

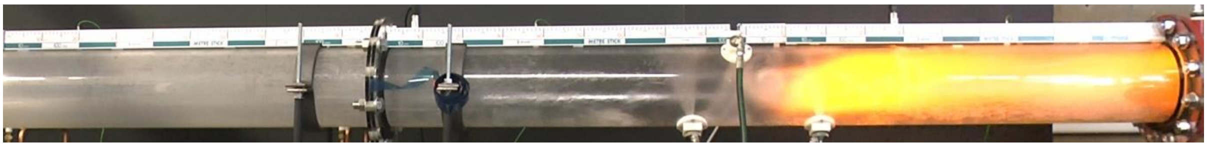

iv. 40ms after **mitigation** of methane-air mixture of E.R. (ϕ) 1.30

Figure A9.317 : Flame propagating upstream and mitigation using four Type C cross flow SRA's in a methane-air mixture (ϕ) 1.30

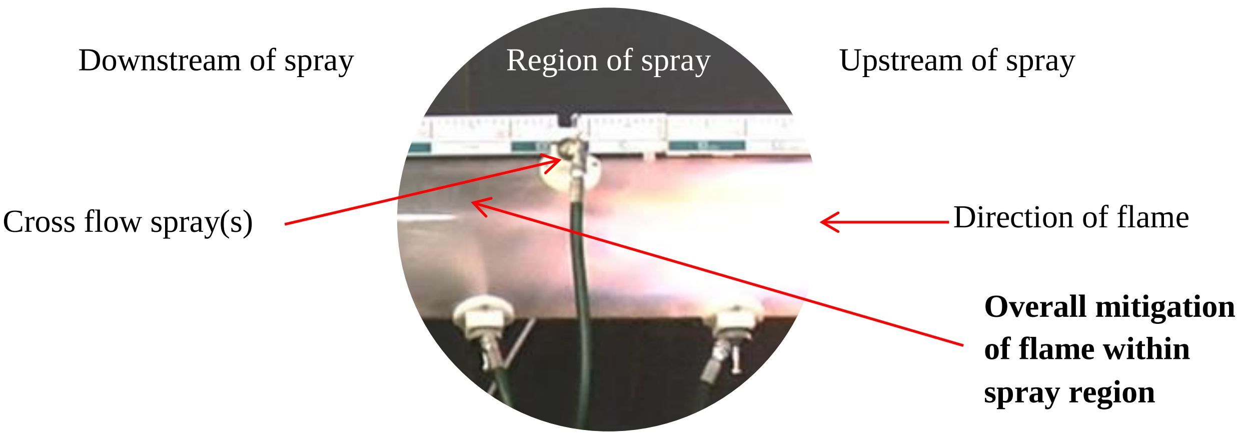

Figure A9.318 : Expanded view of region of spray highlighted in Figure A9.317(ii)

Methane-air mixture of E.R. (ϕ) 1.43

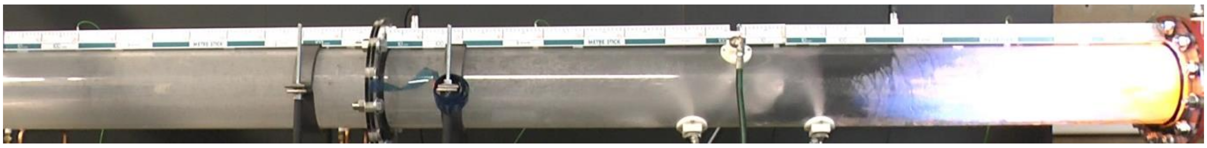

i. Flame propagating in methane-air mixture of E.R. (ϕ) 1.43 upstream of SRA

ii. Mitigation of methane-air mixture of E.R. (ϕ) 1.43 upstream of SRA

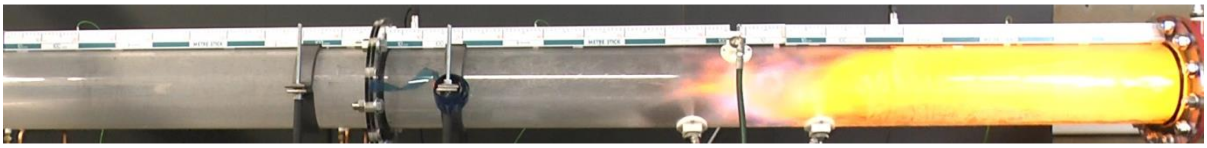

iii. 20ms after **mitigation** of methane-air mixture of E.R. (ϕ) 1.43

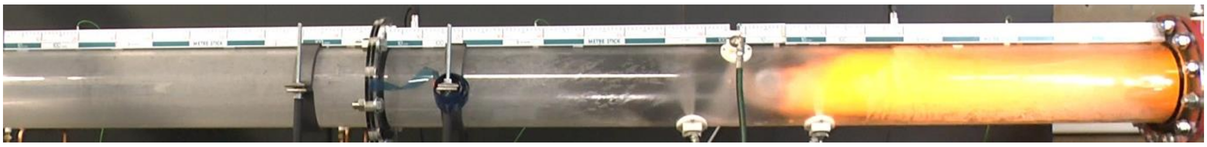

iv. 40ms after **mitigation** of methane-air mixture of E.R. (ϕ) 1.43

Figure A9.319 : Flame propagating upstream and mitigation using four Type C cross flow SRA's in a methane-air mixture (ϕ) 1.43

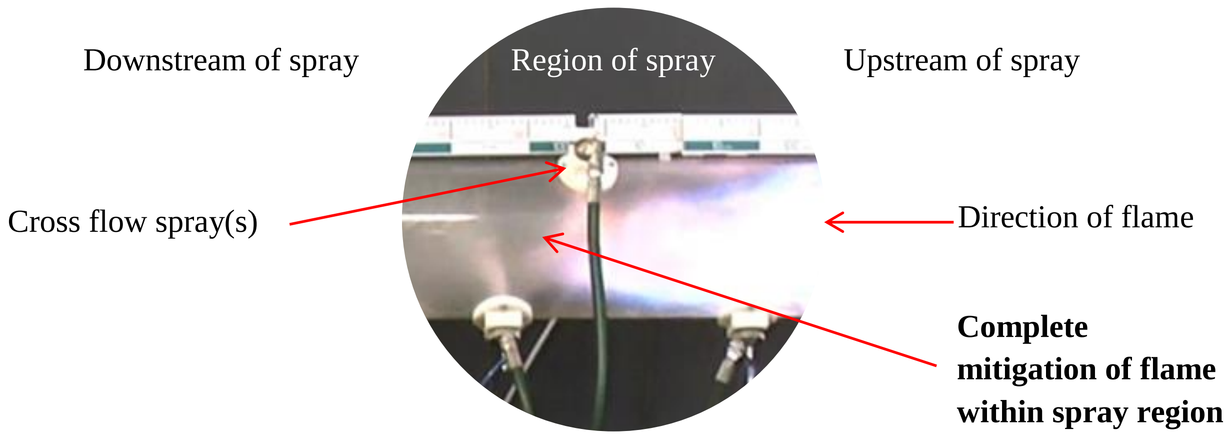

Figure A9.320 : Close up view of region of spray highlighted in Figure A9.319(ii)

Methane-air mixture of E.R. (ϕ) 1.56

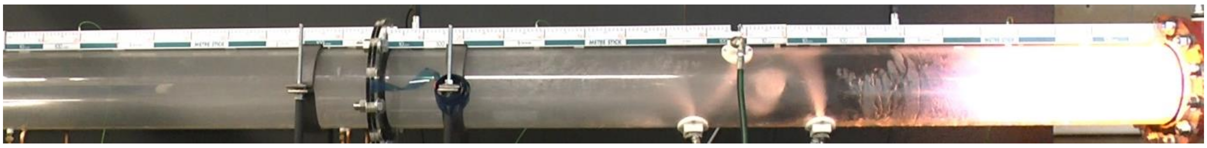

i. Flame propagating in methane-air mixture of E.R. (ϕ) 1.56 upstream of SRA

ii. Mitigation of methane-air mixture of E.R. (ϕ) 1.56 upstream of SRA

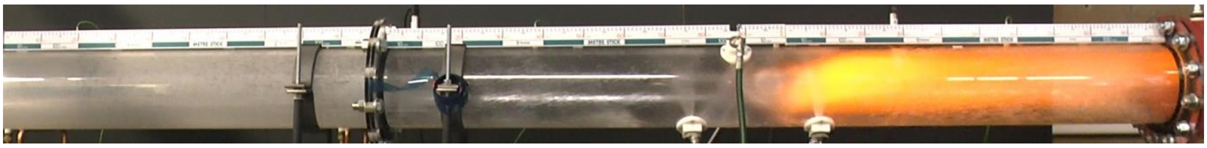

iii. 20ms after **mitigation** of methane-air mixture of E.R. (ϕ) 1.56

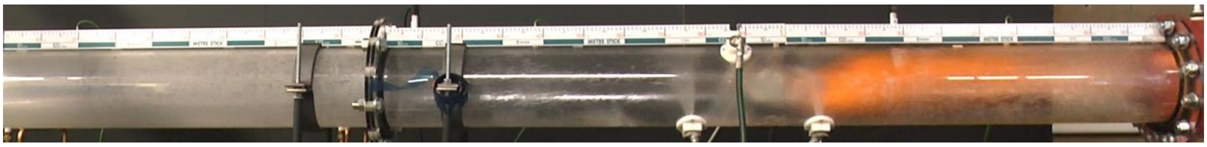

iv. 40ms after **mitigation** of methane-air mixture of E.R. (ϕ) 1.56

Figure A9.321: Flame propagating upstream and mitigation using four Type C cross flow SRA's in a methane-air mixture (ϕ) 1.56

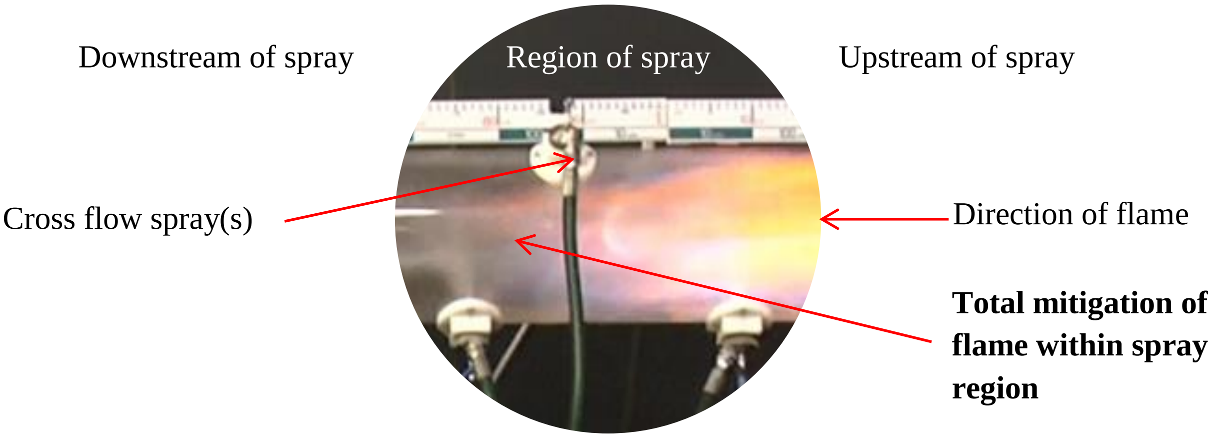

Figure A9.322 : Enlarged view of region of spray highlighted in Figure A9.317(ii)

A9.6.1.5 General event outcome

Table A9.40 provides a summary of the **'general event outcome'** for each trial in this current series, using the five potential 'outcome' categories offered in Chapter 5. The results of all 'hot trials' were previously given in Table 5.14 and are also shown in Table A9.45.

Trial configuration	General event outcome	Code
4 X/F Type C : (ϕ) 1.18	Full Mitigation resulting in Flame Extinguishment	FMFE
4 X/F Type C : (ϕ) 1.30	Full Mitigation resulting in Flame Extinguishment	FMFE
4 X/F Type C : (ϕ) 1.43	Full Mitigation resulting in Flame Extinguishment	FMFE
4 X/F Type C : (ϕ) 1.56	Full Mitigation resulting in Flame Extinguishment	FMFE

Table A9.40 : General event outcome (trial series A9.6.1)

A9.6.2 Four (X/F) Type C SRA's in a propane-air E.R. (ϕ) 0.49, 0.74, 1.00

A9.6.2.1 Trial set up

Many explosive events involve heavier than air flammable vapours, many of which are petroleum based derivatives. With the exception of this current series, all of the experimental trails and results offered in this current work where conducted using high purity methane, as previously discussed in Chapter 4.

For convenience commercial propane was used in this series of test and three different commercial propane-air mixtures of E.R. (ϕ) 0.49, 0.74, 1.00 (2%, 3%, 4% commercial propane in air) were used to evaluate the operation of the four cross flow Type C SRA arrangement.

Although commercial propane liberates approximately 2.5 times the energy by volume as methane during combustion, the lower limit of flammability is significantly less than methane. With this in mind the commercial propane-air mixtures used in this series are considered to contain similar energy content to those used in earlier methane-air trials.

A9.6.2.2 Flame speed

The average upstream flame speeds recorded in these commercial propane-air trials were very similar to the methane-air tests. Many saturated hydrocarbons exhibit very similar burning velocities. Exceptions to this include alkenes such as ethylene, which has a higher flame temperature and burning velocity as a result of its greater exothermicity, due to the presence of a double bond in the molecule. Alkynes such as acetylene contain a triple bond with even greater exothermicity and resultants higher flame temperatures and burning rates.

The average flame speed achieved upstream of the SRA position and approximate flame thickness can be found in Table A9.41 for each of the mixtures tested.

Equivalence ratio (ϕ)	Approximate flame thickness (mm)	Average upstream flame speed (m/s)
0.49	1.8	7.5
0.74	1.3	14.5
1.00	1.0	22.25

Table A9.41 : Approximate flame thickness and flame speeds

All three commercial propane-air mixtures tested in this series global mitigation was achieved by the spray configuration. Flame speed reduction percentages are illustrated in Figure A9.333, while photographic images are shown in Figures A9.327 - A9.332.

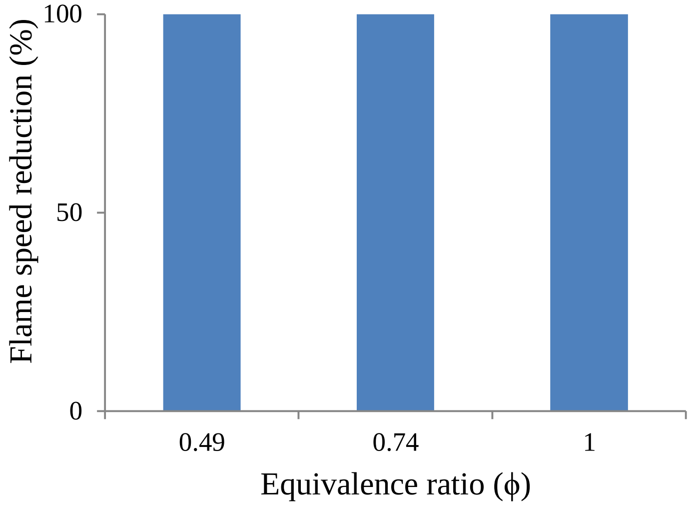

Figure A9.333: Typical flame speed reductions for four Type C SRA's at 13MPa and propane-air mixture E.R. ϕ 0.49, 0.74, 1.00

Although the majority of this current research program was conducted using laboratory grade methane-air mixtures, the inclusion of this small number of commercial propane-air trials highlight the need to expand the research to include alkenes and alkynes.

Considerations for further research are put forward in Chapter 7.

A9.6.2.3 Time-temperature response

Propane-air mixture of E.R. ϕ 0.49

Figure A9.324 shows the typical time-temperature profiles resulting from the propane-air mixture E.R. (ϕ) 0.49. The profiles for TC3, TC4 and TC5 are virtually parallel with each other, indicating that the flame did not progress. The very small rise in TC3 attributed to the rapid vaporisation of droplets.

This may be attributed to the very early mitigation between spray #1 and #2 as revealed in Figure A9.327 and where less water vapour would have been produced.

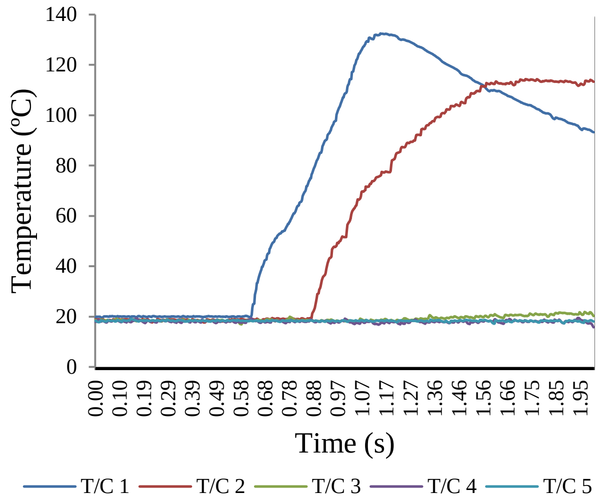

Figure A9.324 : Typical time-temperature profile for four SRA Type C in X/F arrangement with propane-air mixture of E.R. (ϕ) 0.49

Propane-air mixture of E.R. ϕ 0.74

Figure A9.325 reveals the typical time-temperature profiles resulting from the propane-air mixture E.R. (ϕ) 0.49. The profiles for TC3, TC4 and TC5 are in agreement with those presented for the propane-air mixture E.R. (ϕ) 0.49 and are almost all parallel with each other, indicating that the flame did not progress. Consequently the very small rise in TC3 in again attributed to the rapid vaporisation of droplets.

Again this is a characteristic of the very early mitigation between spray #1 and #2 as revealed in Figure A9.329 and where less water vapour would have been produced.

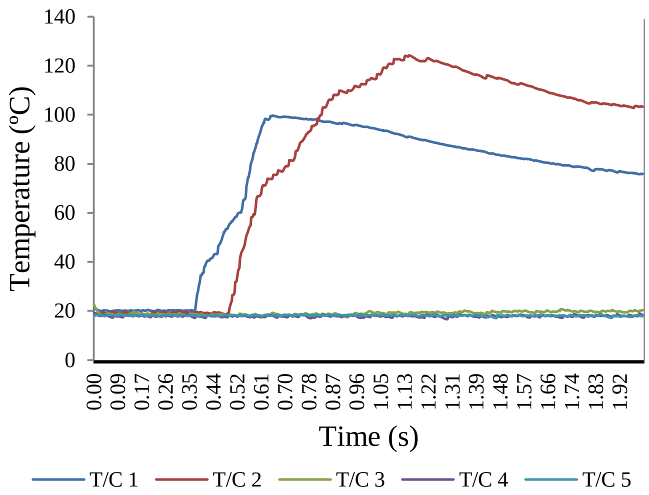

Figure A9.325 : Typical time-temperature profile for four SRA Type C in X/F arrangement with propane-air mixture of E.R. (ϕ) 0.74

Propane-air mixture of E.R. ϕ 1.00

Figure A9.326 shows the distinctive time-temperature profiles resulting from the propane-air mixture E.R. (ϕ) 0.49. The profiles for TC3, TC4 and TC5 are in agreement with those presented for the propane-air mixture E.R. (ϕ) 0.49 and 0.74, which are all approximately parallel to each other, indicating that the flame did not continue to propagate. Consequently the very small rise in TC3 in again attributed to the rapid vaporisation of droplets.

Again this is a characteristic of the very early mitigation between spray #1 and #2 as revealed in Figure A9.331 and where less water vapour would have been produced.

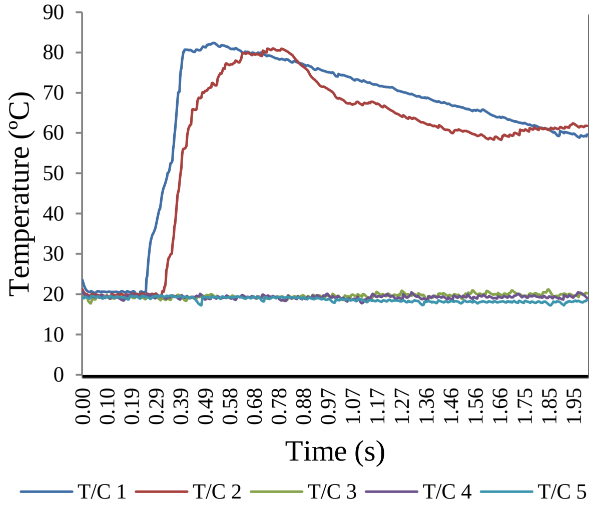

Figure A9.326 : Distinctive time-temperature profile for four SRA Type C in X/F arrangement with propane-air mixture of E.R. (ϕ) 1.00

A9.6.2.4 Qualitative analysis

Propane-air mixture of E.R. ϕ 0.49

Figure A9.327(i) reveals the flame upstream of the first spray prior to any interaction.

Figure A9.327(ii) displays the suppression of the flame and interaction with spray #1

In Figure A9.327(iii) the flame length began to shorten during its transit through spray #1 and #2.

Figure A9.327(iv) captures the final milliseconds of the flames existence.

Propane-air mixture of E.R. ϕ 0.74

In Figure A9.329(i) the flame is shown upstream of the first spray prior to any interaction.

Figure A9.329(ii) displays the suppression of the flame and interaction with spray #1

In Figure A9.329(iii) the flame length began to shorten during its transit through spray #1 and #2.

Figure A9.329(iv) captures the final milliseconds of the flames existence in the lower part of the propagation tube. This is due to the density of propane being greater than that of air.

Propane-air mixture of E.R. ϕ 1.00

In Figure A9.331(i) the flame is shown upstream of the first spray prior to any interaction.

Figure A9.331(ii) displays the suppression of the flame and interaction with spray #1

In Figure A9.331(iii) the flame length began to shorten during its transit through spray #1 and #2.

Figure A9.331(iv) captures the final milliseconds of the flames existence in the lower part of the propagation tube. This is due to the density of propane being greater than that of air.

Propane-air mixture of E.R. ϕ 0.49

i. Flame propagating in propane-air mixture of E.R. (ϕ) 0.49 upstream of SRA

ii. **Mitigation** of flame between spray #1 and #2 in propane-air mixture of E.R. (ϕ) 0.49

iii. **Shortened flame** due to interaction with spray propane-air mixture of E.R. (ϕ) 0.49

iv. Flame completely **extinguished** propane-air mixture of E.R. (ϕ) 0.49

Figure A9.327 : Flame propagating upstream and subsequent mitigation using four Type C cross flow SRA's in a propane-air mixture (ϕ) 0.49

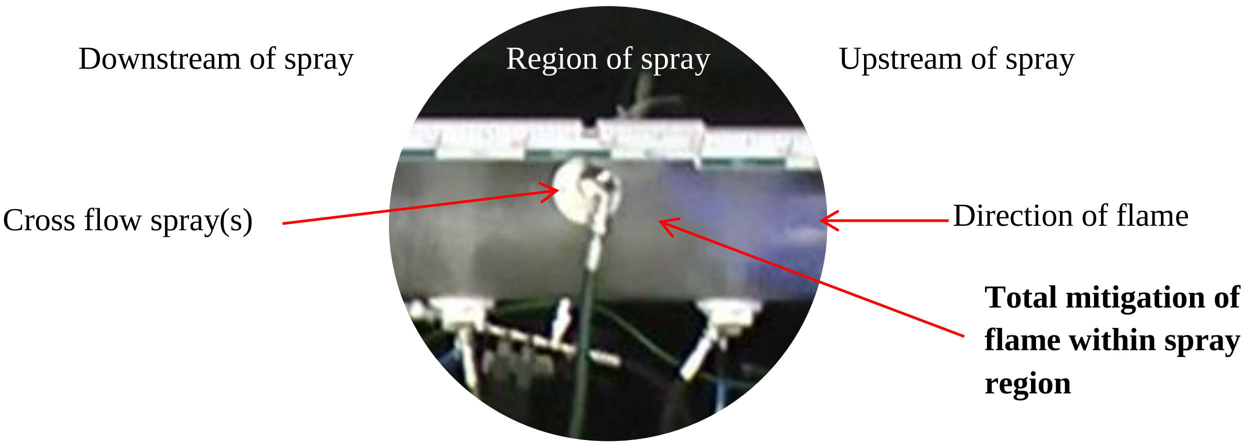

Figure A9.328 : Expanded view of region of spray highlighted in Figure A9.327(iii)

Propane-air mixture of E.R. ϕ 0.74

i. Flame propagating in propane-air mixture of E.R. (ϕ) 0.74 upstream of SRA

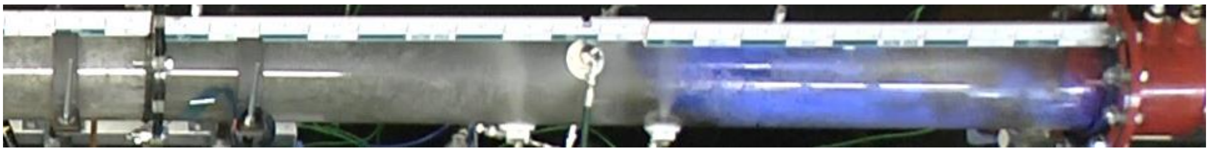

ii. **Mitigation** of flame between spray #1 and #2 in propane-air mixture of E.R. (ϕ) 0.74

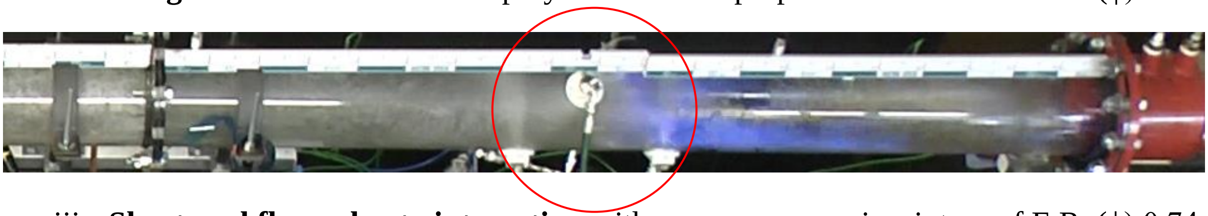

iii. **Shortened flame due to interaction** with spray propane-air mixture of E.R. (ϕ) 0.74

iv. Flame **totally extinguished** propane-air mixture of E.R. (ϕ) 0.74

Figure A9.329 : Flame propagating upstream and subsequent mitigation using four Type C cross flow SRA's in a propane-air mixture (ϕ) 0.74

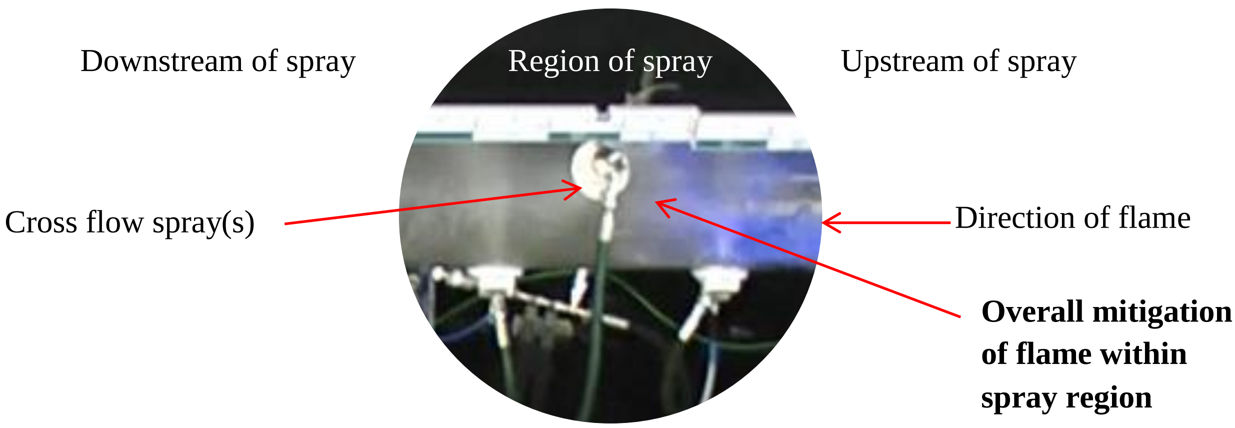

Figure A9.330 : Expanded view of region of spray highlighted in Figure A9.329(iii)

Propane-air mixture of E.R. ϕ 1.00

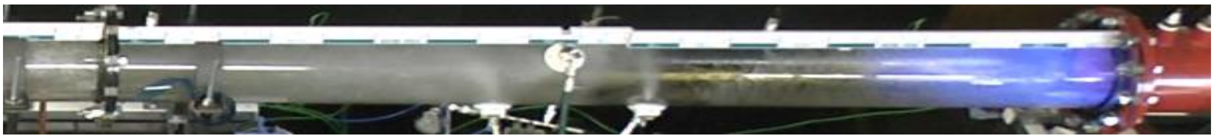

i. Flame propagating in propane-air mixture of E.R. (ϕ) 1.00 upstream of SRA

ii. Flame approaching sprays in propane-air mixture of E.R. (ϕ) 1.00 upstream of SRA

iii. **Shortened** flame due to interaction with spray propane-air mixture of E.R. (ϕ) 1.00

iv. Flame **completely extinguished** propane-air mixture of E.R. (ϕ) 1.00

Figure A9.331: Flame propagating upstream and subsequent mitigation using four Type C cross flow SRA's in a propane-air mixture (ϕ) 1.00

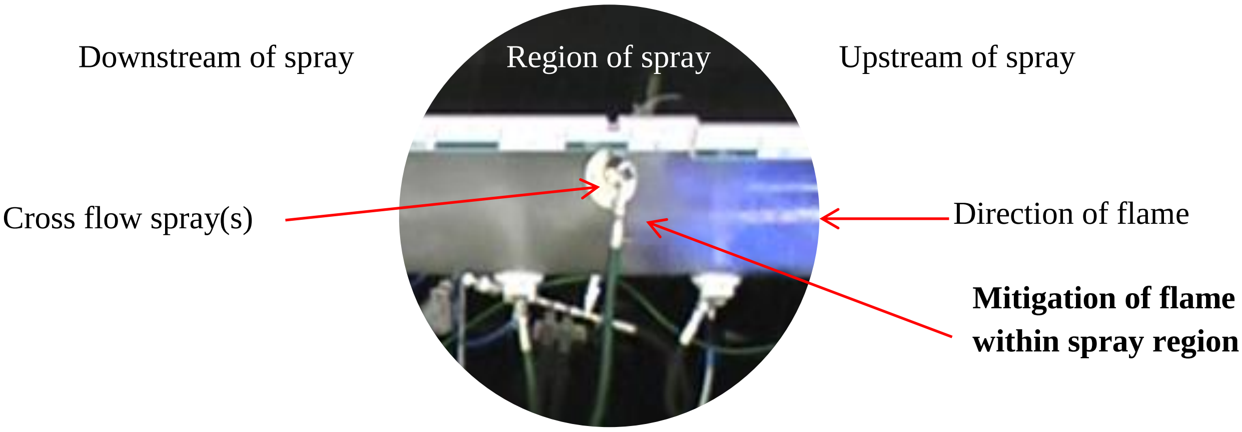

Figure A9.332 : Expanded view of region of spray highlighted in Figure A9.331(iii)

A9.6.2.5 General event outcome

Table A9.42 provides a summary of the **'general event outcome'** for each trial in this current series, using the five potential 'outcome' categories offered in Chapter 5. The results of all 'hot trials' were previously given in Table 5.14

Trial configuration	General event outcome	Code
4 X/F Type C : (ϕ) 0.49	Full Mitigation resulting in Flame Extinguishment	FMFE
4 X/F Type C : (ϕ) 0.74	Full Mitigation resulting in Flame Extinguishment	FMFE
4 X/F Type C : (ϕ) 1.00	Full Mitigation resulting in Flame Extinguishment	FMFE

Table A9.42 : General event outcome (trial series A9.6.2)

A9.6.3 Four (X/F) Type C SRA's with partial blockage of exhaust outlets

A9.6.3.1 Trial set up

With the exception of this final series of tests, all of the previous methane-air and propane-air trials were conducted in the partly confined conditions provided by the design characteristics of the FPMR. At the point of ignition the flame exit is fully opened by the magnetic hinge panel and the exhausts are vented with the rupturing of the membranes covering each of the six outlets.

The purpose of the six 80mm diameter exhaust vents was to provide a cross sectional area (CSA) greater than or equal to the diameter of the main driver section, as extensively described in Chapter 4. The temporary blockage of one or more of the six exhaust outlets would affect the explosion conditions, with the main outcome being an increase in flame speed due to the partial retardation of escaping products of combustion. As the exhaust outlets were originally manufactured with BSP threads, they were readily sealable with a standard BSP plug as illustrated in Figure A9.333

Three tests were carried out using methane-air mixtures of E.R. (ϕ) 0.95 and will the following exhaust blockages:-

i. One exhaust outlet blocked (providing relief openings of 96% of main tube CSA)
ii. Two exhaust outlets blocked (providing relief openings of 77% of main tube CSA)
iii. Three exhaust outlets blocked (providing relief openings of 58% of main tube CSA)

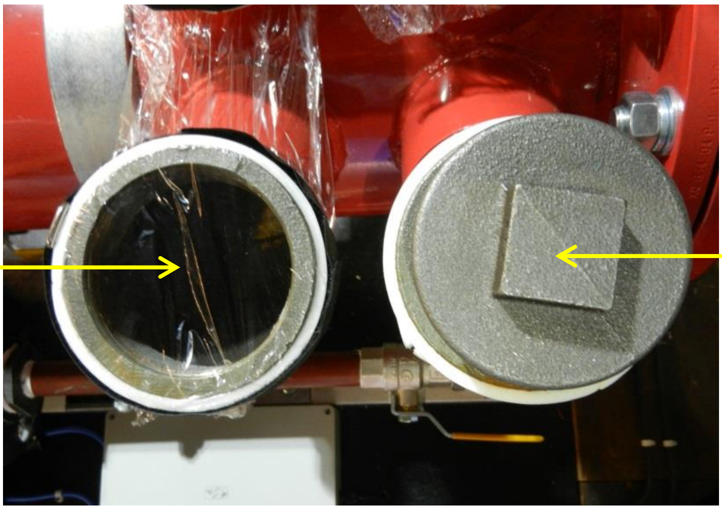

Figure A9.333 : Example of exhaust outlet preparation prior to testing

A9.6.3.2 Flame speed

The flame speeds produced in this series were predictably faster than those found in the previous trials, as revealed in Table A9.43. The combination of these greater flame speeds, in addition to the narrow band of flame thickness of 1.05mm associated with the methane-air mixture E.R. ϕ 0.95 would have had a negative effect on the residence time for the droplets to extract heat from the flame.

Although the flame speeds were faster than previous trials, each of the flames in this series were completely extinguished and mitigated by the spray configuration. Flame speed reduction percentages (%) are given in Figure A9.334.

Number of blocked exhaust ports	Equivalence ratio (ϕ)	Approximate flame thickness (mm)	Average upstream flame speed (m/s)
1	0.95	1.05	25
2	0.95	1.05	29.5
3	0.95	1.05	34.5

Table A9.43 : Approximate flame thickness and flame speeds

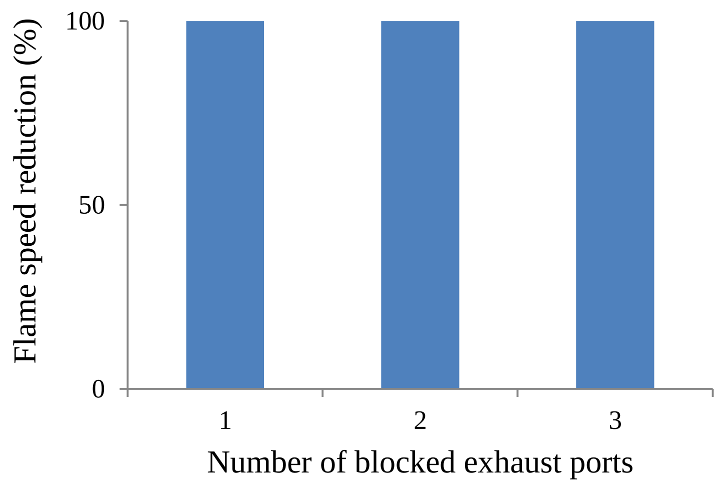

Figure A9.334 : Typical flame speed reductions for four Type C SRA's at 13MPa and methane-air flame E.R. ϕ 0.95 with various blocked exhaust ports

A9.6.3.3 Time-temperature response

One exhaust outlet blocked

In this trial one of the exhaust outlets was blocked, with the other five openings prepared with a low density polyethylene sheet ‘cling film’ bursting membranes. The blockage of the outlet resulted in exhaust relief openings of about 96% of main tube CSA.

Figure A9.335 shows the distinctive time-temperature profile for four X/F Type C SRA’s with one exhaust outlet blocked in a methane-air mixture of E.R. (ϕ) 0.95. Although downstream temperatures exhibit a small amount of activity, the rise seen in TC3 temperatures is attributed to the subsequent mitigation of combustion activity and consequential vaporisation of water droplets.

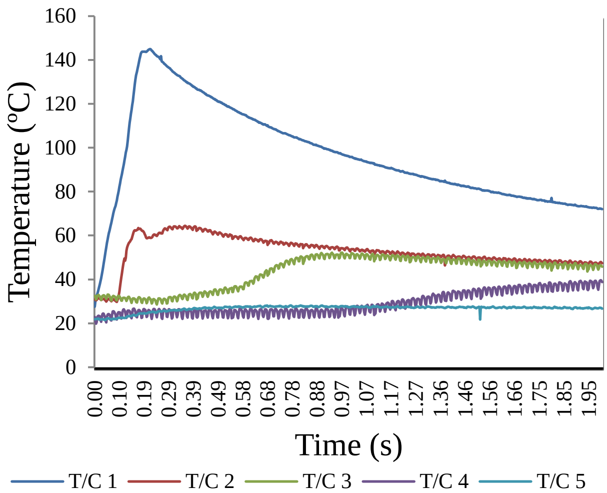

Figure A9.335 : Distinctive time-temperature profile for four X/F Type C SRA’s with on exhaust outlet blocked methane-air mixture of E.R. (ϕ) 0.95

Two exhaust outlets blocked

In this trial two of the exhaust outlets were blocked, with the other four openings primed with a low density polyethylene sheet ‘cling film’ bursting membranes. The blockage of the outlet resulted in exhaust relief openings of about 77% of main tube CSA.

Figure A9.335 shows the typical time-temperature profile for four X/F Type C SRA’s with two exhaust outlets blocked in a methane-air mixture of E.R. (ϕ) 0.95. Although downstream temperatures show some amount of activity, the rise seen in the TC3 temperatures is greater than that previously shown for one blocked exhaust. This may be credited to higher temperatures associated with a greater flame speed, giving way to vaporisation of more water droplets prior to mitigation.

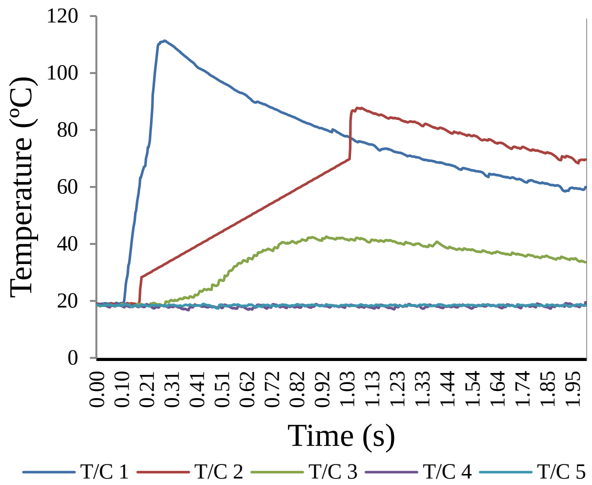

Figure A9.336 : Typical time-temperature profile for four X/F Type C SRA’s with two exhaust outlets blocked methane-air mixture of E.R. (ϕ) 0.95

Three exhaust outlets blocked.

In this trial three of the exhaust outlets were blocked, with the other three openings equipped with a low density polyethylene sheet ‘cling film’ bursting membranes. The blockage of the outlets resulted in exhaust relief openings of about 58% of main tube CSA.

Figure A9.337 shows the characteristic time-temperature profile for four X/F Type C SRA’s with three exhaust outlets blocked in a methane-air mixture of E.R. (ϕ) 0.95. In this instance the flame propagated into the sprays and was severely retarded. A small region of flame passed through the sprays, but failed to activate ignition in the remaining downstream mixture.

This scenario is unique to the trials in this study and may be attributed to the higher flame speed produced by the blocked of three exhausts. With the scope and objectives of this current study being to carry out trials on flame speeds of ≤30m/s, the use of the SRA in higher flame speed situations will be another subject for suggested further research.

Chapter 7 offers several proposals for additional research and development in this area.

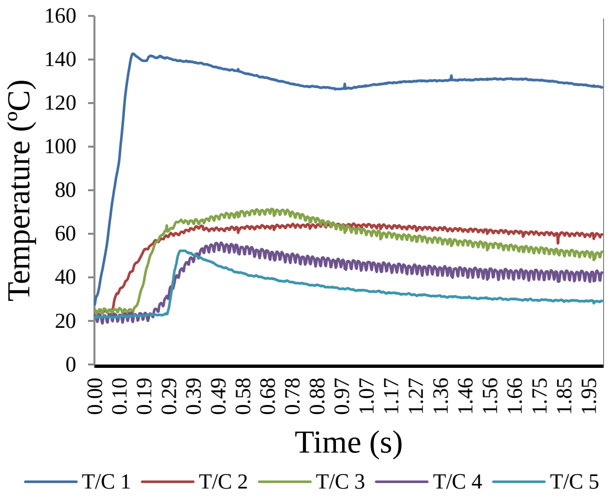

Figure A9.337 : Characteristic time-temperature profile for four X/F Type C SRA’s with three exhaust outlets blocked methane-air mixture of E.R. (ϕ) 0.95

A9.6.3.4 Qualitative analysis

One exhaust outlet blocked

In Figure A9.338(i) the flame is shown upstream of the first spray prior to any interaction.

Figure A9.338(ii) displays the flame passing through spray #1

In Figure A9.338(iii) the flame length begins to shorten during its transit through the spray region. The flame was mitigated in this frame and is magnified in In Figure A9.339.

Figure A9.338(iv) captures the subsequent cooling of the trailing intermediate gases.

Two exhaust outlets blocked

In Figure A9.340(i) the flame is shown upstream of the first spray prior to any interaction.

Figure A9.340(ii) displays the flame passing through spray #1 and #2

In Figure A9.340(iii) the flame is mitigated as it reaches spray #3. This has been magnified and is shown in Figure A9.341.

Figure A9.340(iv) captures the final traces of trailing intermediate gases in spray #1 and #2.

A9.6.3.3 Three exhaust outlets blocked.

In Figure A9.342(i) the flame is shown upstream of the first spray prior to any interaction.

In Figure A9.342(ii) the flame is approaching the final spray and exhibits dark regions and a shortening of the flame length.

Figure A9.342(iii) reveals a small luminous area of flame which has propagated beyond the sprays

Figure A9.342(iv) shows the resulting flame 20ms after the previous frame, where the flame is receding. Flame was not present in any further frames. Figure 7.343 shows an enlarged section of the spray region.

One exhaust outlet blocked

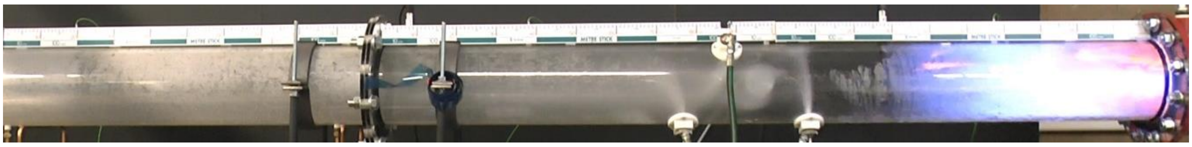

i. Flame propagating in methane-air mixture of E.R. (ϕ) 0.95 upstream of SRA

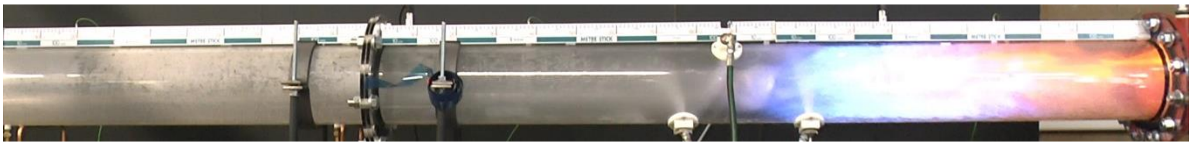

ii. Flame propagating in methane-air mixture of E.R. (ϕ) 0.95 in the region of spray #1

iii. **Mitigation** in methane-air mixture of E.R. (ϕ) 0.95in the region of spray

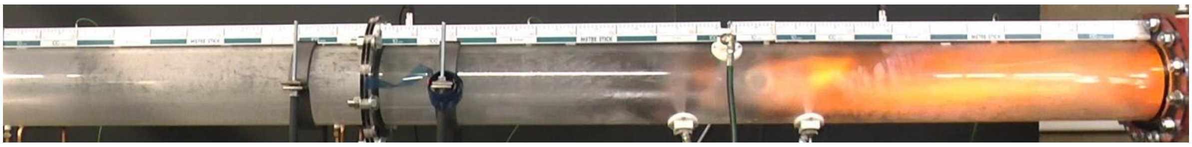

iv. Final stages of combustion in trailing gases

Figure A9.338 : Flame propagating upstream and subsequent mitigation using four X/F Type C SRA's with one exhaust outlet blocked methane-air mixture of E.R. (ϕ) 0.95

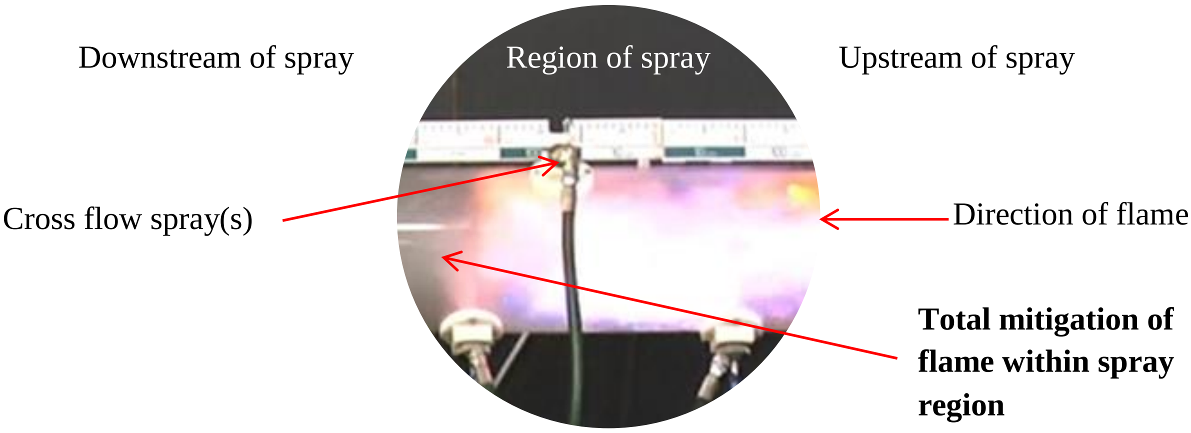

Figure A9.339 : Expanded view of region of spray highlighted in Figure A9.338(iii)

Two exhaust outlets blocked

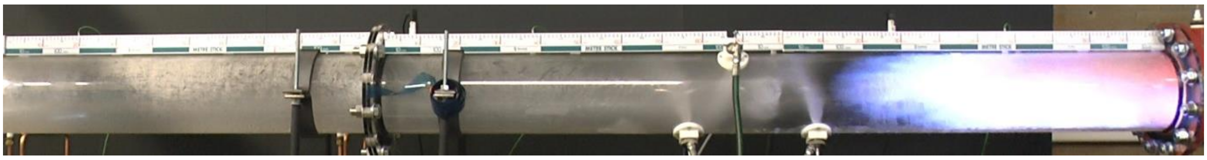

i. Flame propagating in methane-air mixture of E.R. (ϕ) 0.95upstream of SRA

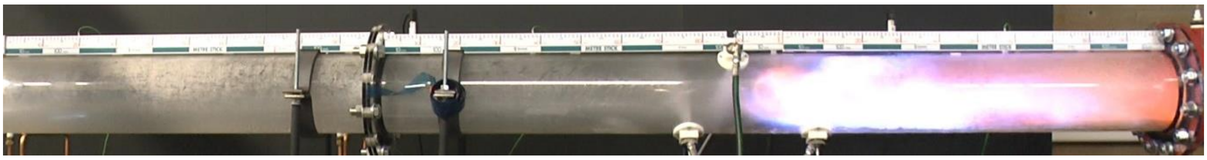

ii. Flame propagating in methane-air mixture of E.R. (ϕ) 0.95 in the spray region

iii. **Mitigation** of methane-air mixture of E.R. (ϕ) 0.95 upstream of spray #4

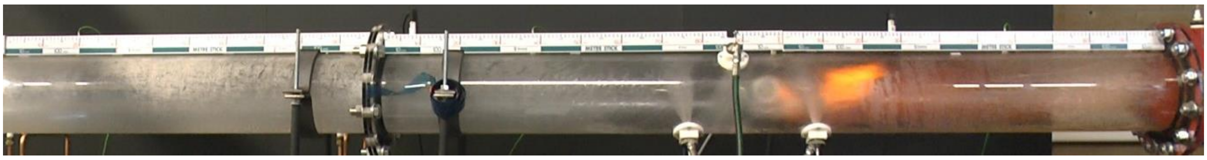

iv. 20ms after (iii) methane-air mixture of E.R. (ϕ) 0.95 downstream of SRA

Figure A9.340 : Flame propagating upstream and subsequent mitigation using four X/F Type C SRA’s with two exhaust outlets blocked methane-air mixture of E.R. (ϕ) 0.95

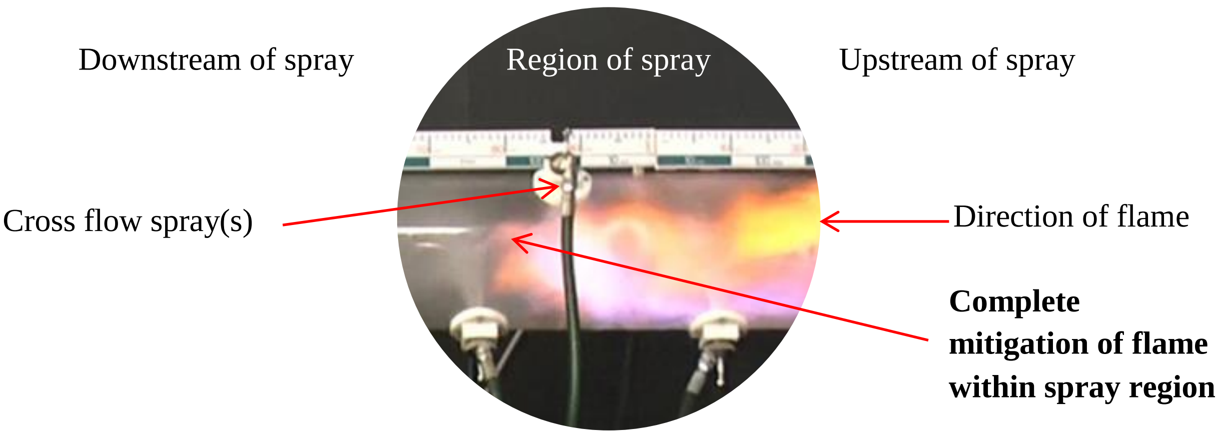

Figure A9.341 : Enlarged view of region of spray highlighted in Figure A9.340(iii)

Three exhaust outlets blocked

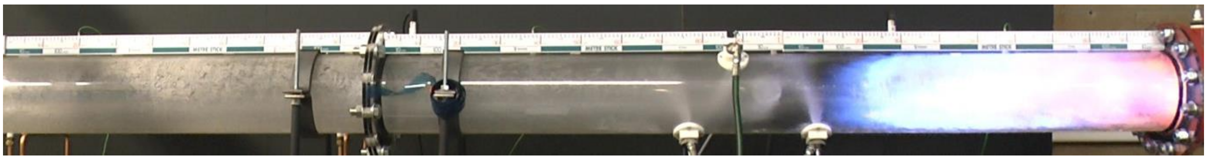

i. Flame propagating in methane-air mixture of E.R. (ϕ) 0.95 upstream of SRA

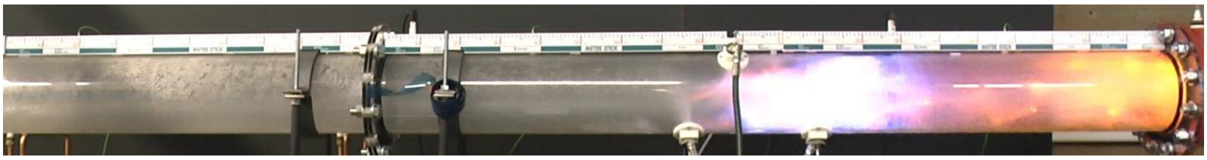

ii. Flame propagating in methane-air mixture of E.R. (ϕ) 0.95 in the region of spray

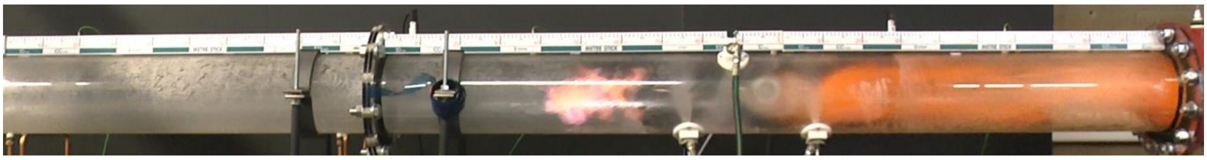

iii. A degree of combustion still occuring downstream of the sprays E.R. (ϕ) 0.95

iv. **Insufficient energy for propagation** through the remaining combustible mixture of E.R. (ϕ) 0.95 downstream of SRA

Figure A9.342 : Flame propagating upstream and subsequent mitigation using four X/F Type C SRA's with three exhaust outlet blocked methane-air mixture of E.R. (ϕ) 0.95

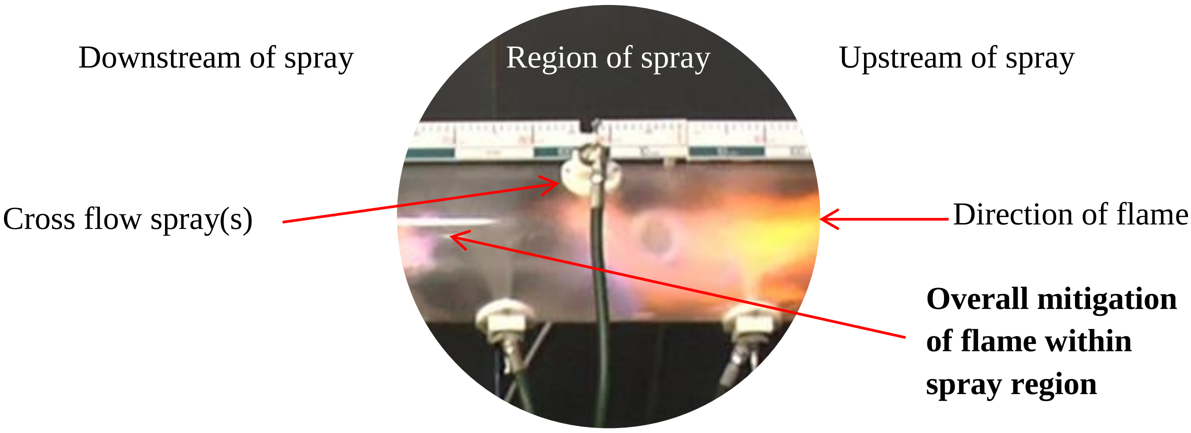

Figure A9.343 : Expanded view of region of spray highlighted in Figure A9.342(iv)

A9.6.3.5 General event outcome

Table A9.44 provides a summary of the **'general event outcome'** for each trial in this current series, using the five potential 'outcome' categories offered in Chapter 5. The results of all 'hot trials' were previously given in Table 5.14 and are also shown in Table A9.45.

Trial configuration Four (X/F) SRA's	**General event outcome**	**Code**
1 blocked exhaust	Full Mitigation resulting in Flame Extinguishment	FMFE
2 blocked exhausts	Full Mitigation resulting in Flame Extinguishment	FMFE
3 blocked exhausts	Full Mitigation resulting in Flame Extinguishment	FMFE

Table A9.44 : General event outcome (trial series A9.6.3)

A9.7 Trial results location matrix and general event outcome

<table>
<tr><th>Trial</th><th>Configuration</th><th>E.R. (ϕ)</th><th>General event outcome</th><th>Section / Appendix</th></tr>
<tr><td rowspan="12">Mitigation trials for a single water spray in counter flow (C/F) with a methane-air flame</td><td rowspan="4">SRA configuration type A
Water pressure : 13MPa
Water temperature : 20°C</td><td>0.61</td><td>NMFA</td><td>7.5.1/A9.1.1</td></tr>
<tr><td>0.72</td><td>NMFA</td><td>A9.1.1</td></tr>
<tr><td>0.95</td><td>NMFA</td><td>A9.1.1</td></tr>
<tr><td>1.06</td><td>NMFA</td><td>A9.1.1</td></tr>
<tr><td rowspan="4">SRA configuration type B
Water pressure : 13MPa
Water temperature : 20°C</td><td>0.61</td><td>NMFA</td><td>A9.1.2</td></tr>
<tr><td>0.72</td><td>NMFA</td><td>A9.1.2</td></tr>
<tr><td>0.95</td><td>NMFA</td><td>A9.1.2</td></tr>
<tr><td>1.06</td><td>NMFA</td><td>A9.1.2</td></tr>
<tr><td rowspan="4">SRA configuration type C
Water pressure : 13MPa
Water temperature : 20°C</td><td>0.61</td><td>FMFE</td><td>A9.1.3</td></tr>
<tr><td>0.72</td><td>NMFA</td><td>A9.1.3</td></tr>
<tr><td>0.95</td><td>NMFA</td><td>A9.1.3</td></tr>
<tr><td>1.06</td><td>NMFA</td><td>A9.1.3</td></tr>
<tr><td rowspan="12">Mitigation trials for a single water spray in parallel flow (P/F) with a methane-air flame</td><td rowspan="4">SRA configuration type A
Water pressure : 13MPa
Water temperature : 20°C</td><td>0.61</td><td>NMFA</td><td>7.5.2/A9.2.1</td></tr>
<tr><td>0.72</td><td>NMFA</td><td>A9.2.1</td></tr>
<tr><td>0.95</td><td>NMFA</td><td>A9.2.1</td></tr>
<tr><td>1.06</td><td>NMFA</td><td>A9.2.1</td></tr>
<tr><td rowspan="4">SRA configuration type B
Water pressure : 13MPa
Water temperature : 20°C</td><td>0.61</td><td>NMFA</td><td>A9.2.2</td></tr>
<tr><td>0.72</td><td>NMFA</td><td>A9.2.2</td></tr>
<tr><td>0.95</td><td>NMFA</td><td>A9.2.2</td></tr>
<tr><td>1.06</td><td>NMFA</td><td>A9.2.2</td></tr>
<tr><td rowspan="4">SRA configuration type C
Water pressure : 13MPa
Water temperature : 20°C</td><td>0.61</td><td>FMFE</td><td>7.5.3/A9.2.3</td></tr>
<tr><td>0.72</td><td>NMFA</td><td>A9.2.3</td></tr>
<tr><td>0.95</td><td>NMFA</td><td>A9.2.3</td></tr>
<tr><td>1.06</td><td>NMFA</td><td>A9.2.3</td></tr>
<tr><td rowspan="7">Mitigation trials for a two water sprays in parallel flow (P/F) with a methane-air flame</td><td rowspan="4">2 x Overlapping Type B SRA’s
Water pressure : 13MPa
Water temperature : 20°C</td><td>0.61</td><td>FMFE</td><td>7.5.4/A9.3.1</td></tr>
<tr><td>0.72</td><td>NMFA</td><td>A9.3.1</td></tr>
<tr><td>0.95</td><td>NMFA</td><td>A9.3.1</td></tr>
<tr><td>1.06</td><td>NMFA</td><td>A9.3.1</td></tr>
<tr><td rowspan="3">2 x Overlapping Type C SRA’s
Water pressure : 13MPa
Water temperature : 20°C</td><td>0.95</td><td>FMFE</td><td>A9.3.2</td></tr>
<tr><td>0.95</td><td>FMFE</td><td>A9.3.2</td></tr>
<tr><td>1.06</td><td>FMFE</td><td>A9.3.2</td></tr>
<tr><td rowspan="8">Mitigation trials for water sprays in cross flow (X/F) with the methane-air flames</td><td rowspan="4">Single SRA type B
Water pressure : 13MPa
Water temperature : 20°C</td><td>0.61</td><td>NMFA</td><td>A9.4.1</td></tr>
<tr><td>0.72</td><td>NMFA</td><td>A9.4.1</td></tr>
<tr><td>0.95</td><td>NMFA</td><td>A9.4.1</td></tr>
<tr><td>1.06</td><td>NMFD</td><td>A9.4.1</td></tr>
<tr><td rowspan="4">Two SRA type B
Water pressure : 13MPa
Water temperature : 20°C</td><td>0.61</td><td>NMFD</td><td>A9.4.2</td></tr>
<tr><td>0.72</td><td>NMFD</td><td>A9.4.2</td></tr>
<tr><td>0.95</td><td>NMFD</td><td>A9.4.2</td></tr>
<tr><td>1.06</td><td>NMFD</td><td>A9.4.2</td></tr>
</table>

General event outcome	Code
No Mitigation with resulting Flame Acceleration	NMFA
No Mitigation with resulting Flame Deceleration	NMFD
No Mitigation with resulting Unaffected Flame	NMUF
Partial Mitigation with resulting Flame Propagation	PMFP
Full Mitigation resulting in Flame Extinguishment	FMFE

Table A9.45 : Trial results location matrix and general event outcome

Trial	**Configuration**	**E.R. (ϕ)**	**General event outcome**	**Section / Appendix**
Mitigation trials for water sprays in **cross flow** (X/F) with the methane-air flames	Three SRA type B Water pressure : 13MPa Water temperature : 20°C	0.61	FMFE	A9.4.3
		0.72	NMFD	A9.4.3
		0.95	NMFD	A9.4.3
		1.06	NMFD	A9.4.3
	Four SRA type B Water pressure : 13MPa Water temperature : 20°C	0.61	FMFE	A9.4.4
		0.72	FMFE	7.5.5/A9.4.4
		0.95	NMFA	A9.4.4
		1.06	NMFD	A9.4.4
Mitigation trials for water sprays in **cross flow** (X/F) with the methane-air flames	Single SRA type C Water pressure : 13MPa Water temperature : 20°C	0.61	NMFD	A9.4.5
		0.72	NMFD	A9.4.5
		0.95	NMFA	A9.4.5
		1.06	NMFD	A9.4.5
	Two SRA type C Water pressure : 13MPa Water temperature : 20°C	0.61	NMFD	A9.4.6
		0.72	NMFD	A9.4.6
		0.95	NMFA	A9.4.6
		1.06	NMFD	A9.4.6
	Three SRA type C Water pressure : 13MPa Water temperature : 20°C	0.61	FMFE	A9.4.7
		0.72	NMFD	A9.4.7
		0.95	NMFD	A9.4.7
		1.06	NMFD	A9.4.7
	Four SRA type C Water pressure : 13MPa Water temperature : 20°C	0.61	FMFE	A9.4.8
		0.72	FMFE	A9.4.8
		0.95	FMFE	7.5.6/A9.4.8
		1.06	FMFE	A9.4.8
(X/F) Type B and C SRA's using variable supply pressures and water temperature : 20°C	3 type C and 1 type B:13MPa	0.95	NMFD	A9.5.1
	2 type C and 2 type B:13MPa	0.95	NMFA	A9.5.1
	1 type C and 3 type B:13MPa	0.95	NMFD	A9.5.1
	1 type C and 3 type B:15MPa	0.95	NMFA	A9.5.1
Varying number of **(X/F)**Type C SRA's using variable supply pressures and water temperature : 20°C	3 type C only:14MPa	0.95	NMFD	A9.5.2
	3 type C only:15MPa	0.95	NMFD	A9.5.2
	3 type C only:15MPa	0.95	FMFE	A9.5.2
	3 type C only:16MPa	0.95	NMFD	A9.5.2
	3 type C only:17MPa	0.95	NMFA	A9.5.2
	3 type C only:18MPa	0.95	NMFD	A9.5.2
Varying number of **(X/F)**Type B SRA's using variable supply pressures and water temperature : 20°C	4 type B only:14MPa	0.95	NMFD	A9.5.3
	4 type B only:15MPa	0.95	FMFE	A9.5.3
	4 type B only:16MPa	0.95	NMFD	A9.5.3
	4 type B only:17MPa	0.95	NMFD	A9.5.3
	4 type B only:18MPa	0.95	NMFA	A9.5.3

General event outcome	Code
No Mitigation with resulting Flame Acceleration	NMFA
No Mitigation with resulting Flame Deceleration	NMFD
No Mitigation with resulting Unaffected Flame	NMUF
Partial Mitigation with resulting Flame Propagation	PMFP
Full Mitigation resulting in Flame Extinguishment	FMFE

Table A9.45 : Trial results location matrix and general event outcome

Trial	Configuration	E.R. (ϕ)	General event outcome	Section / Appendix
Three **(X/F)**Type C SRA's using variable supply pressures and water temperatures	3 type C only:13MPa : 30°C	0.95	FMFE	A9.5.4
	3 type C only:15MPa : 35°C	0.95	NMFD	A9.5.4
	3 type C only:15MPa : 40°C	0.95	NMFD	A9.5.4
	3 type C only:16MPa : 45°C	0.95	NMFD	A9.5.4
	3 type C only:15MPa : 50°C	0.95	NMFD	A9.5.4
Three **(X/F)**Type C SRA's using variable supply pressures and water temperatures	4 type C only:13MPa : 25°C	0.95	FMFE	A9.5.5
	4 type C only:13MPa : 25°C	0.95	FMFE	A9.5.5
	4 type C only:13MPa : 30°C	0.95	FMFE	A9.5.5
	4 type C only:13MPa : 30°C	0.95	FMFE	A9.5.5
	4 type C only:13MPa : 40°C	0.95	FMFE	A9.5.5
	4 type C only:13MPa : 40°C	0.95	FMFE	A9.5.5
	4 type C only:13MPa : 50°C	0.95	FMFE	A9.5.5
	4 type C only:13MPa : 50°C	0.95	FMFE	7.5.7/A9.5.5
Supplementary trials				
Four **(X/F)**Type C SRA's trials with methane rich, methane-air flames	4 type C only:13MPa : 20°C	1.18	FMFE	A9.6.1
	4 type C only:13MPa : 20°C	1.30	FMFE	A9.6.1
	4 type C only:13MPa : 20°C	1.43	FMFE	A9.6.1
	4 type C only:13MPa : 20°C	1.56	FMFE	7.5.8/A9.6.1
Four **(X/F)**Type C SRA's trials with propane-air flames	4 type C only:13MPa : 20°C	0.49	FMFE	A9.6.2
	4 type C only:13MPa : 20°C	0.74	FMFE	A9.6.2
	4 type C only:13MPa : 20°C	1.00	FMFE	7.5.9/A9.6.2
Four **(X/F)**Type C SRA's trials with methane-air flames, with partial blockage of exhaust outlets	One exhaust outlet blocked	0.95	FMFE	A9.6.3
	Two exhaust outlets blocked	0.95	FMFE	A9.6.3
	Three exhaust outlets blocked	0.95	FMFE	7.5.10/ A9.6.3

General event outcome	Code
No Mitigation with resulting Flame Acceleration	NMFA
No Mitigation with resulting Flame Deceleration	NMFD
No Mitigation with resulting Unaffected Flame	NMUF
Partial Mitigation with resulting Flame Propagation	PMFP
Full Mitigation resulting in Flame Extinguishment	FMFE

Table A9.45 : Trial results location matrix and general event outcome

List of Figures

List of Tables

Appendix 9 - References

1 Lane, W.R. *Industrial Engineering and Chem*. 1951, 43(6), 1312 – 1317

2 Harris, R.J. and Wickens, M.J. *Understanding vapour cloud explosions – an experimental study*. The Institution of Gas Engineers, Communication 1408. 1989

3 Sapko, M., Furno, A., and Kuchta, J.M., *Quenching Methane-Air Ignitions with Water Sprays* U.S. Bureau of Mines, R.I. 8214, 1977.

APPENDIX 10

CFD Simulation

A10.1 Type B (0.5mm exit orifice) SRA

A10.2 Rig dimensions

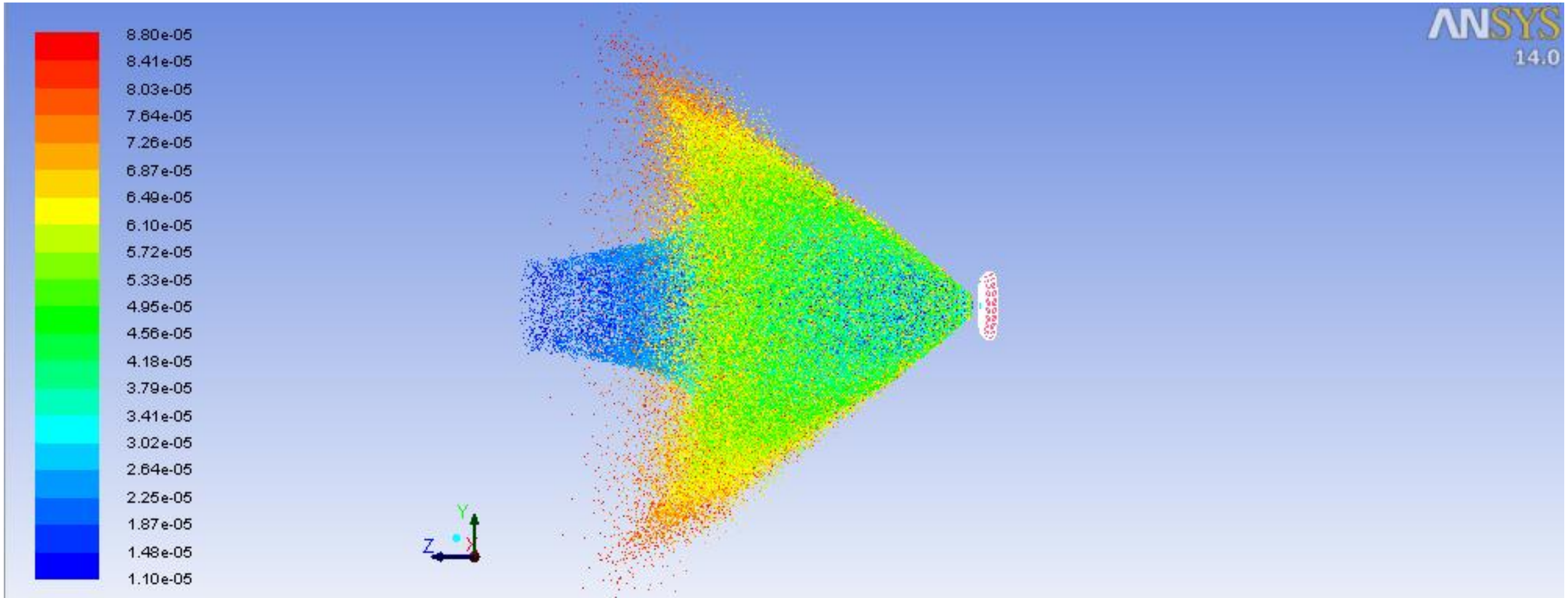
8.80e-05
8.41e-05
8.03e-05
7.64e-05
7.26e-05
6.87e-05
6.49e-05
6.10e-05
5.72e-05
5.33e-05
4.95e-05
4.56e-05
4.18e-05
3.79e-05
3.41e-05
3.02e-05
2.64e-05
2.25e-05
1.87e-05
1.48e-05
1.10e-05
ANSYS
14.0
Y
Z
X

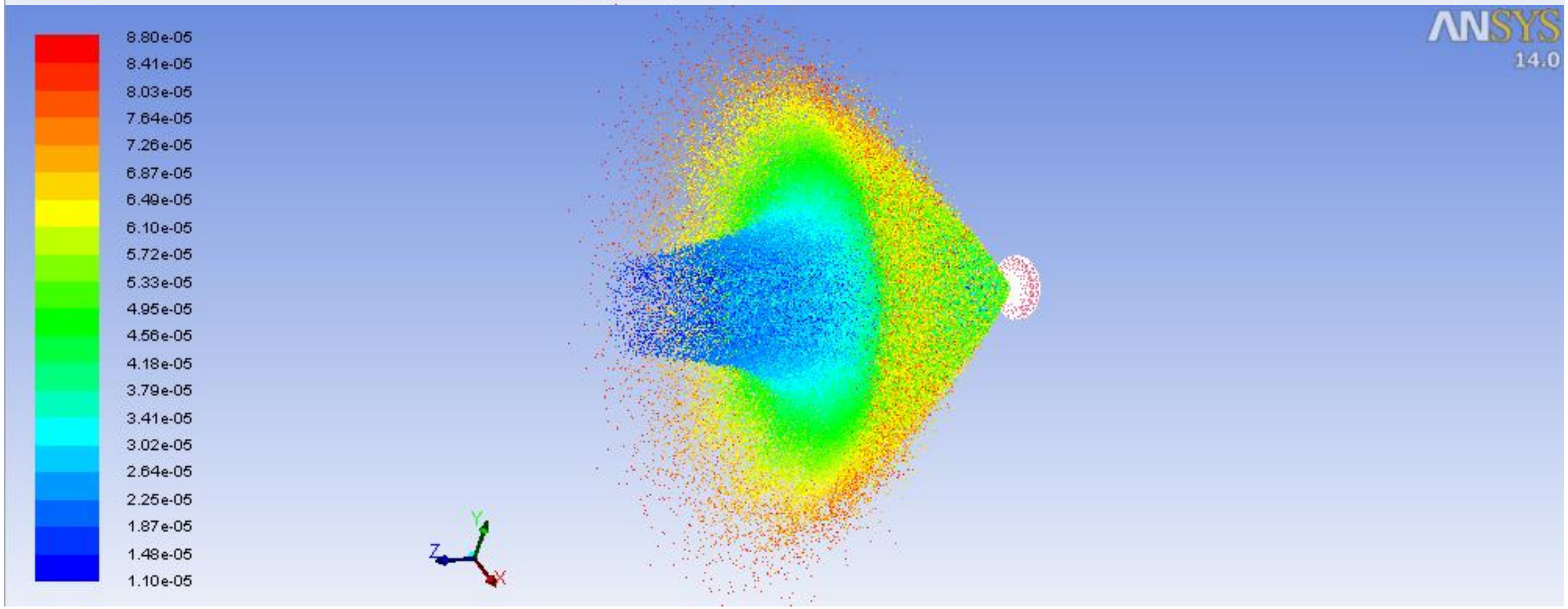
8.80e-05
8.41e-05
8.03e-05
7.64e-05
7.26e-05
6.87e-05
6.49e-05
6.10e-05
5.72e-05
5.33e-05
4.95e-05
4.56e-05
4.18e-05
3.79e-05
3.41e-05
3.02e-05
2.64e-05
2.25e-05
1.87e-05
1.48e-05
1.10e-05
ANSYS
14.0
Y
Z
X

Rig with no atomisers (open at both ends)

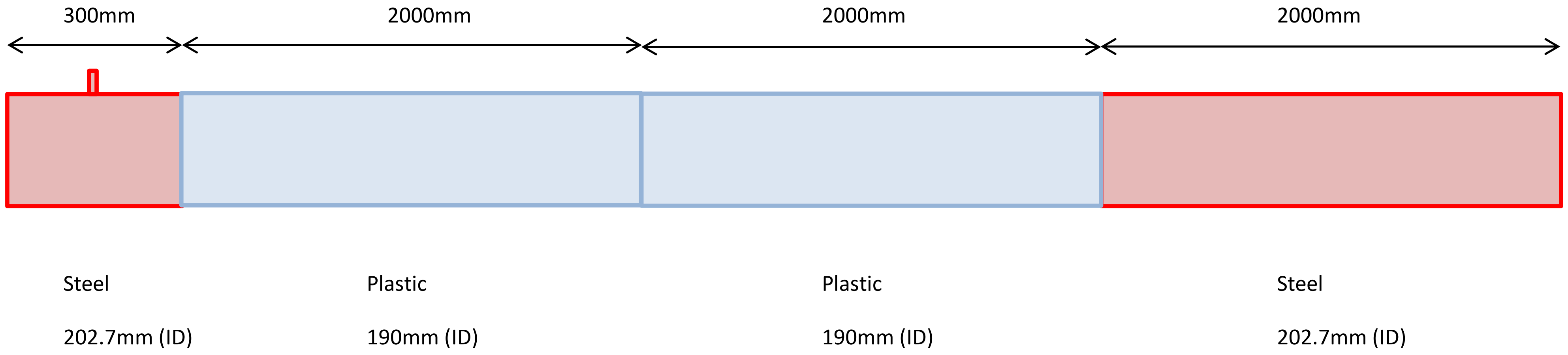

Rig with no with counterflow atomiser

Rig with no with parallel atomiser